THE PHYSICAL REVIEW

VOLUME 92 Second Series NUMBER 6

DECEMBER 15, 1953

Published for the

AMERICAN PHYSICAL SOCIETY

by the

AMERICAN INSTITUTE OF PHYSICS

Lancaster, Pa., and New York, N. Y.

THE
PHYSICAL REVIEW

A journal of experimental and theoretical physics established by E. L. Nichols in 1893

SECOND SERIES, VOL. 92, NO. 6 DECEMBER 15, 1953

The Dynamics of a Disordered Linear Chain*

FREEMAN J. DYSON
Institute for Advanced Study, Princeton, New Jersey
(Received August 17, 1953)

By a disordered chain we mean a chain of one-dimensional harmonic oscillators, each coupled to its nearest neighbors by harmonic forces, the inertia of each oscillator and the strength of each coupling being a random variable with a known statistical distribution law. A method is presented for calculating exactly the distribution-function of the frequencies of normal modes of vibration of such a chain, in the limit when the chain becomes infinitely long. For some special examples, in which the distribution law of the oscillator parameters is assumed to be of exponential form, the frequency spectra are calculated analytically. The theory applies equally well to a chain of masses connected by elastic springs and making mechanical vibrations, or to an electrical transmission line composed of alternating inductances and capacitances with random characteristics.

I. INTRODUCTION

CONSIDER a chain of N masses, each coupled to its nearest neighbors by elastic springs obeying Hooke's law. We shall study the longitudinal vibrations of the chain, all motions being supposed to take place in one dimension so that each mass is described by a single coordinate. Since the coupling forces are linear in the displacements, the most general vibration is a superposition of $(N-1)$ normal modes, each having a characteristic frequency. The object of this paper is to present a method for determining accurately the spectrum or distribution function of the characteristic frequencies of the chain, in the limit as the number of masses N becomes very large. As is well known, the knowledge of this distribution function enables all the thermodynamical properties of the chain to be deduced immediately.

In the case when the masses and the strengths of the springs are all equal, the calculation of the frequency spectrum is elementary. In Sec. IV of this paper we give explicit formulas for the frequency spectrum in the most general case when the masses and spring-constants are arbitrary. The case of equal masses and springs here serves as a check.

In Secs. V–VI we consider the physically interesting case in which the masses and springs are unequal but are distributed along the chain in a random way. This means that we know the probability that a given mass or spring-constant has a particular value, and that this probability is the same at every point in the chain. There are several different ways of defining precisely how the randomization of the masses and springs is to be understood; for example, the masses may be independent random variables with a known probability distribution, while the springs are all equal; or each mass may be correlated with the strengths of the two neighboring springs, and so on. In every case, given the probability distribution for masses and springs, our method leads to an exact determination of the spectrum of normal frequencies. To illustrate the method, one particular class of probability distributions is worked out in detail, and the corresponding frequency spectra are obtained explicitly.

These calculations were begun in response to a question of C. Kittel, who was concerned with the thermal properties of glass. Glass may be considered roughly to be a disordered array of coupled harmonic oscillators in 3 dimensions. The systems considered in this paper are models of a "one-dimensional glass," a disordered array of atoms in one dimension. It is not, of course, to be expected that the results of this paper have any immediate application to the 3-dimensional problem. But it seems to us remarkable that the 1-dimensional problem can be solved exactly, and we publish this analysis in the hope that the methods will be useful in

* Supported in part by the U. S. Office of Naval Research.

discussing other disordered systems of a less idealized character.

II. DEFINITIONS

Let particle number j in the chain have mass m_j, and let its displacement from its equilibrium position be x_j. Let the elastic modulus of the spring between particles j and $(j+1)$ be K_j. Then the equations of motion of the system are

$$m_j\ddot{x}_j=K_j(x_{j+1}-x_j)+K_{j-1}(x_{j-1}-x_j). \tag{1}$$

It is convenient to introduce new variables

$$y_j=m_j^{\frac{1}{2}}x_j \tag{2}$$

and new constants $\lambda_1, \lambda_2, \cdots, \lambda_{2N-2}$ given by

$$\lambda_{2j-1}=K_j/m_j, \quad \lambda_{2j}=K_j/m_{j+1}. \tag{3}$$

Then the equations of motion take the form

$$\ddot{y}_j=(\lambda_{2j-1}\lambda_{2j})^{\frac{1}{2}}y_{j+1}+(\lambda_{2j-3}\lambda_{2j-2})^{\frac{1}{2}}y_{j-1} -(\lambda_{2j-1}+\lambda_{2j-2})y_j, \tag{4}$$

and the coefficient-matrix is now symmetric. Next we define variables $z_1, z_2, \cdots, z_{N-1}$, by

$$\dot{z}_j=\lambda_{2j}^{\frac{1}{2}}y_{j+1}-\lambda_{2j-1}^{\frac{1}{2}}y_j, \tag{5}$$

so that (4) becomes

$$\dot{y}_j=\lambda_{2j-1}^{\frac{1}{2}}z_j-\lambda_{2j-2}^{\frac{1}{2}}z_{j-1}. \tag{6}$$

Let variables $u_1, u_2, \cdots, u_{2N-1}$ be defined by

$$u_{2j-1}=y_j, \quad u_{2j}=z_j. \tag{7}$$

Then Eqs. (5) and (6) together may be written

$$\dot{u}_j=\lambda_j^{\frac{1}{2}}u_{j+1}-\lambda_{j-1}^{\frac{1}{2}}u_{j-1}. \tag{8}$$

The characteristic frequencies ω_j of the chain are, therefore, the characteristic roots of the $(2N-1)\times(2N-1)$ matrix Λ whose elements are given by

$$\Lambda_{j+1,\,j}=-\Lambda_{j,\,j+1}=i\lambda_j^{\frac{1}{2}}, \tag{9}$$

all other elements being zero. There is one zero root corresponding to the degenerate mode in which all the x_j are equal; the remaining roots occur in $(N-1)$ pairs, the members of a pair being $+\omega_j$ and $-\omega_j$.

The spectrum of characteristic frequencies is given by the function $M(\mu)$ which is defined as the proportion of the roots ω_j for which $\omega_j^2\leq\mu$. As $N\to\infty$ we expect that $M(\mu)$ will become a smooth differentiable function, and then a density of characteristic frequencies can be defined by

$$D(\mu)=(dM/d\mu). \tag{10}$$

Our first task is to determine the $M(\mu)$ and $D(\mu)$ corresponding to given λ_j.

We study the function

$$\Omega(x)=\lim_{N\to\infty}(2N-1)^{-1}\sum_j\log(1+x\omega_j^2) =\int_0^\infty\log(1+x\mu)D(\mu)d\mu, \tag{11}$$

as a function of the complex variable x. The logarithm is defined as the branch of the function which is real for real positive x. Then the integral (11) is convergent and defines an analytic function of x over the whole x plane, the negative real axis from 0 to $(-\infty)$ being excluded. As x tends from above onto a point $(-z)$ on the negative real axis, the imaginary part of $\log(1+x\mu)$ tends to zero if $z\mu<1$ and to $i\pi$ if $z\mu>1$. Therefore, (11) gives

$$\mathrm{Re}[(i\pi)^{-1}\lim_{\epsilon\to0}\Omega(-z+i\epsilon)] =\int_{1/z}^\infty D(\mu)d\mu=1-M(1/z), \tag{12}$$

$$D(1/z)=-z^2\,\mathrm{Re}[(i\pi)^{-1}\lim_{\epsilon\to0}\Omega'(-z+i\epsilon)], \tag{13}$$

$$\Omega'(x)=(d\Omega/dx)=\int_0^\infty\mu(1+x\mu)^{-1}D(\mu)d\mu. \tag{14}$$

According to (12) or (13), the spectrum of characteristic frequencies is determined by the limiting values of $\Omega(x)$ on the negative real axis. We call $\Omega(x)$ the characteristic function of the chain.

III. CALCULATION OF THE CHARACTERISTIC FUNCTION[1]

Consider a chain for which all the ω_j^2 are less than a fixed bound B, and let $B|x|<1$; these restrictions will be removed later. Then the logarithm in (11) may be expanded in powers of x, giving

$$\Omega(x)=\lim_{N\to\infty}(2N-1)^{-1}S(x), \tag{15}$$

$$S(x)=\sum_{n=1}^\infty(-1)^{n-1}(x^n/n)\sum_j\omega_j^{2n} =\sum_{n=1}^\infty(-1)^{n-1}(x^n/n)\,\mathrm{Spur}(\Lambda^{2n}). \tag{16}$$

According to (9), the spur of Λ^{2n} is a sum of terms $Q(\sigma)$, one corresponding to each cycle σ, a cycle consisting of $2n$ integers

$$j_0, j_1, j_2, \cdots, j_{2n-1}, j_{2n}=j_0 \tag{17}$$

lying between 1 and $2N-1$ and satisfying for each m

$$j_{m+1}=j_m\pm1. \tag{18}$$

[1] The analysis of this section might have been shortened by using known results in the theory of Jacobi matrices. See A. Wintner, *Spektraltheorie der Unendlichen Matrizen* (Leipzig, 1929), pp. 69–73. For this remark the author is indebted to Professor Kac.

The term $Q(\sigma)$ is equal to the product

$$\prod_{j=1}^{2N-1} (\lambda_j)^{q(j)}, \tag{19}$$

where $q(j)$ is the number of times that the step $(j \to j+1)$ occurs in the cycle σ; the step $(j+1 \to j)$ must also occur $q(j)$ times in σ. Hence, we may write

$$\mathrm{Spur}(A^{2n}) = \sum_q R(q) \prod_j (\lambda_j)^{q(j)}, \tag{20}$$

where the summation is over all possible sets of integers $q(j)$ whose sum is n, and $R(q)$ is the number of cycles σ which exist corresponding to a given set of $q(j)$. The evaluation of $R(q)$ is carried out in Appendix I. The result is as follows. Let $q(a)$ be the first nonvanishing $q(j)$, and let $q(b)$ be the last. Then

$$R(q) = 2n[q(a)]^{-1} \left[\prod_{j=a+1}^{b} L(j) \right], \tag{21}$$

$$L(j) = (q(j)+q(j-1)-1)! / [(q(j))!(q(j-1)-1)!]. \tag{22}$$

If we substitute from (20) and (21) into (16), we find

$$S(x) = \sum_{a,b} S(a, b), \tag{23}$$

$$S(a, b) = -2 \sum_q [q(a)]^{-1} (-x\lambda_a)^{q(a)} \times \left[\prod_{j=a+1}^{b} L(j) (-x\lambda_j)^{q(j)} \right]. \tag{24}$$

In Eq. (23) the summation is over all integers a, b satisfying $1 \leq a \leq b \leq 2N-1$. In Eq. (24) the summation is over all sets of integers $q(j)$ which are nonzero for $a \leq j \leq b$. That is to say, each $q(j)$ for $a \leq j \leq b$ is summed over all positive integral values.

The summation over $q(b)$ in Eq. (24) can immediately be performed, because by Eq. (22) the sum is an elementary binomial expansion with exponent $(-q(b-1))$. Therefore,

$$S(a, b) = -2 \sum_q{}' (q(a))^{-1} (-x\lambda_a)^{q(a)} \times \left[\prod_{j=a+1}^{b-1} L(j) (-x\lambda_j)^{q(j)} \right] [(1+x\lambda_b)^{-q(b-1)} - 1], \tag{25}$$

where the summation is now over all sets of integers $q(j)$ which are nonzero on $a \leq j \leq b-1$. That is to say,

$$S(a, b) + S(a, b-1) = S_1(a, b-1), \tag{26}$$

where $S_1(a, b-1)$ is the sum $S(a, b-1)$ with the variable $x\lambda_{b-1}$ replaced by $[x\lambda_{b-1}/(1+x\lambda_b)]$. If we apply the same reduction to $S_1(a, b-1)$, we obtain

$$S(a, b) + S(a, b-1) + S(a, b-2) = S_2(a, b-2), \tag{27}$$

where $S_2(a, b-2)$ is $S(a, b-2)$ with $x\lambda_{b-2}$ replaced by $[x\lambda_{b-2}/(1+x\lambda_{b-1}/(1+x\lambda_b))]$. Continuing in this way, we find

$$\sum_{j=a}^{b} S(a, j) = S_{b-a}(a, a), \tag{28}$$

where $S_{b-a}(a, a)$ is $S(a, a)$ with $x\lambda_a$ replaced by the continued fraction

$$\xi(a, b) = x\lambda_a / (1 + x\lambda_{a+1} / [\cdots (1 + x\lambda_{b-1} / (1 + x\lambda_b)) \cdots]). \tag{29}$$

Now from (24),

$$S(a, a) = -2 \sum_{q(a)} [q(a)]^{-1} (-x\lambda_a)^{q(a)} = 2 \log(1 + x\lambda_a). \tag{30}$$

Therefore,

$$\sum_{j=a}^{b} S(a, j) = 2 \log(1 + \xi(a, b)). \tag{31}$$

We may now write $b = 2N-1$ and make $N \to \infty$ in (29) and (31). This gives

$$\sum_{j=a}^{\infty} S(a, j) = 2 \log(1 + \xi(a)), \tag{32}$$

where $\xi(a)$ is the infinite continued fraction

$$\xi(a) = x\lambda_a / (1 + x\lambda_{a+1} / (1 + x\lambda_{a+2} / (\cdots. \tag{33}$$

If we sum over all a and use (15) and (23),

$$\Omega(x) = \lim_{N \to \infty} N^{-1} \sum_{a=1}^{2N-1} \log[1 + \xi(a)]. \tag{34}$$

Equations (33) and (34) give the explicit representation of $\Omega(x)$ for an arbitrary chain with given coefficients λ_j. The result was proved only under the assumptions that all the ω_j^2 were less than a fixed bound B and that $B|x| < 1$. However, the integral (11) defining $\Omega(x)$, and the continued fractions (33), are convergent for all real positive x and for any set of positive coefficients λ_j. Since these expressions are analytic functions of x, it is easy to prove by an analytic continuation argument that Eq. (34) holds for all real positive x and without restriction on the ω_j.

IV. THE FREQUENCY SPECTRUM FOR AN ARBITRARY CHAIN

To determine the frequency spectrum for a chain with given λ_j, it is only necessary to calculate $\Omega(x)$ from Eqs. (33) and (34), and then to use (13) or (14) to find the spectrum. The second step, however, requires the analytic continuation of $\Omega(x)$ from positive to negative real values. If $\Omega(x)$ can be obtained in closed analytic form for positive x, the continuation process is usually easy. For example, consider the case of an infinite chain of equal masses m linked by springs of equal modulus K. In this case all λ_j are equal to $\lambda = (K/m)$, and all $\xi(a)$ are equal to the infinite continued fraction

$$\xi = x\lambda / (1 + x\lambda / (\cdots. \tag{35}$$

Since ξ satisfies

$$\xi = x\lambda/(1+\xi) \tag{36}$$

and is small for small x, we find

$$\xi = \tfrac{1}{2}[(1+4x\lambda)^{\frac{1}{2}}-1], \tag{37}$$

and by (34),

$$\Omega(x) = 2\log\{\tfrac{1}{2}[(1+4x\lambda)^{\frac{1}{2}}+1]\}. \tag{38}$$

If we differentiate (38) we obtain

$$\Omega'(x) = x^{-1}[1-(1+4x\lambda)^{-\frac{1}{2}}]. \tag{39}$$

This function is analytic and real for $x > -(4\lambda)^{-1}$. It can be continued analytically through the upper half plane to values $x < -(4\lambda)^{-1}$, where it becomes

$$\Omega'(x) = x^{-1}[1+i(-1-4x\lambda)^{-\frac{1}{2}}]. \tag{40}$$

Hence, Eq. (13) gives the spectrum of characteristic frequencies

$$\begin{aligned} D(\mu) &= (1/\pi)(4\lambda\mu-\mu^2)^{-\frac{1}{2}}, \quad \mu<4\lambda, \\ D(\mu) &= 0, \qquad\qquad\qquad \mu>4\lambda, \end{aligned} \tag{41}$$

a result which in this case can easily be checked by an elementary calculation.

In general we will not be able to calculate $\Omega'(x)$ in closed analytic form, and so we require an explicit formula for $D(\mu)$ in terms of the values of $\Omega'(x)$ for positive x. This formula will enable $D(\mu)$ to be calculated if $\Omega'(x)$ is only given numerically or approximately, so that a direct use of analytic continuation is impossible. The formula is

$$D(\mu) = (2\pi^2\mu)^{-1}\int_{-\infty}^{\infty}(\cosh\pi\alpha)d\alpha \times \int_0^{\infty}(x\mu)^{-\frac{1}{2}}\cos[\alpha\log(x\mu)]\Omega'(x)dx. \tag{42}$$

Its derivation is given in Appendix II. The x integration is to be carried out first and the α integration second. Taken in this order, the double integration will always be convergent for values of μ at which $D(\mu)$ exists and is continuous. With Eqs. (33), (34), and (42), we have in principle an exact determination of the frequency spectrum of an arbitrary chain.

V. DISORDERED CHAINS

We now apply the preceding theory to the case of a disordered chain, i.e., an infinite chain whose elements are distributed in a random way according to some known probability law. We consider two types of disordered chain, differing in the way in which the randomization of the elements is defined. Type I is mathematically the simpler, whereas Type II provides the closer approximation to a real chain of randomly arranged atoms.

Type I. Each of the parameters λ_j defined by Eq. (3) is an independent random variable with the probability distribution function $G(\lambda)$.

In this case each of the quantities $\xi(a)$ defined by Eq. (33) will have a probability distribution $F(\xi)$, the same for all a. Now

$$\xi(a) = x\lambda_a/(1+\xi(a+1)) \tag{43}$$

and the variables λ_a and $\xi(a+1)$ are uncorrelated, since $\xi(a+1)$ depends only on $\lambda_{a+1}, \lambda_{a+2}, \cdots$. If we equate the probability distributions of the left and right sides of Eq. (43), we find an integral equation for $F(\xi)$,

$$F(\xi) = \int_0^{\infty} F(\xi')G[\xi(1+\xi')/x]((1+\xi')/x)d\xi'. \tag{44}$$

The solution of (44) for given $G(\lambda)$ can in some cases be obtained in closed form (see Sec. VI). In all cases the solution can be obtained numerically by inserting an arbitrary trial function $F(\xi')$ on the right of (44) and iterating the equation repeatedly. The series of successive iterates will converge rapidly to the true $F(\xi)$, in consequence of the good convergence of the continued fractions (33). When we have found the solution $F(\xi)$ of (44), and have normalized it by

$$\int_0^{\infty} F(\xi)d\xi = 1, \tag{45}$$

the characteristic function of the chain is given by Eq. (34) and is

$$\Omega(x) = 2\int_0^{\infty} F(\xi)\log(1+\xi)d\xi. \tag{46}$$

From this the frequency spectrum may be found as described in Sec. IV.

The frequency spectrum determined in this way is strictly an average over a statistical ensemble of chains, each chain in the ensemble having definite values of the λ_j. But by an argument familiar in the statistical mechanics of systems containing many particles, the same frequency spectrum will be found for an arbitrary chain chosen out of the ensemble, except for an exceptional class of chains whose total probability tends to zero as the number of atoms N tends to infinity. Therefore, we may say that this frequency spectrum is the correct spectrum for a single disordered chain of infinite length.

Type II. Each mass m_j is an independent random variable with distribution function $G(m)$, the spring-constants K_j being fixed and equal.

In this case the λ_j are given by

$$\lambda_{2j-1} = \lambda_{2j-2} = Km_j^{-1}. \tag{47}$$

We introduce the variables

$$\eta_j = [\xi(2j)]^{-1}. \tag{48}$$

Then, from Eq. (33) we derive the recurrence formula

$$\eta_j = (m_{j+1}/xK)+[\eta_{j+1}/(1+\eta_{j+1})]. \tag{49}$$

The variables η_{j+1}, m_{j+1} now are uncorrelated. Hence, Eq. (49) leads to an integral equation

$$F(\eta)=xK\int_0^\infty G[xK(\eta-(\eta'/(1+\eta')))]F(\eta')d\eta', \quad (50)$$

defining the distribution function $F(\eta)$ of each of the η_j. The characteristic function (34) is given now by

$$\Omega(x)=\lim N^{-1}\sum_{j=1}^{N}\log[(1+\xi(2j))(1+\xi(2j-1))], \quad (51)$$

since $\xi(2j)$ and $\xi(2j-1)$ will have different distribution functions. From Eq. (33) we find

$$(1+\xi(2j))(1+\xi(2j-1))=1+\xi(2j)+(xK/m_j), \quad (52)$$

and here the variables $\xi(2j)$ and m_j are uncorrelated. If we insert Eq. (52) into (51), the characteristic function becomes

$$\Omega(x)=\int_0^\infty F(\eta)d\eta\int_0^\infty G(m)dm\log[1+\eta^{-1}+xKm^{-1}], \quad (53)$$

where $F(\eta)$ is defined as the solution of (50).

An interesting special case of a Type II chain is a chain composed of two kinds of atoms with masses m, M, distributed at random in the proportion p: $(1-p)$. This corresponds to the distribution function

$$G(m')=p\delta(m'-m)+(1-p)\delta(m'-M). \quad (54)$$

The equation (50) for $F(\eta)$ then reduces to a difference equation,

$$F(\eta)=p[1-\eta+(m/xK)]^{-2}F[(1-\eta+(m/xK))^{-1}-1]+(1-p)[1-\eta+(M/xK)]^{-2}\times F[(1-\eta+(M/xK))^{-1}-1], \quad (55)$$

which can be solved very rapidly by iteration since no integration is involved. The characteristic function (53) becomes

$$\Omega(x)=\int_0^\infty F(\eta)d\eta[p\log(1+\eta^{-1}+xKm^{-1})+(1-p)\log(1+\eta^{-1}+xKM^{-1})]. \quad (56)$$

Only a moderate amount of numerical work would be needed to calculate the frequency spectrum for any given values of m, M and p.

A chain in which the masses are all equal while the spring strengths are independent random variables can be treated by exactly the same method as a Type II chain. It is only necessary to interchange the roles of $\xi(2j)$ and $\xi(2j-1)$. If we go beyond Types I and II, we could consider a more general type of chain, in which the masses m_j are independent random variables, while the spring strength K_j is a known function of the two adjoining masses m_j and m_{j+1}. This would be a model for a chain composed of different kinds of atoms arranged at random, the strength of the bond between two atoms depending on the chemical nature of the two atoms. The frequency spectrum of such a chain can also be calculated by the methods of this paper, only the formulas become rather more complicated.

VI. A SPECIAL FAMILY OF DISORDERED CHAINS

In this section we calculate explicitly the spectrum of normal frequencies for a special family of disordered chains. This will serve as an illustration, to show quantitatively the effect which a given degree of disorder has upon the spectrum. We consider a chain C_n of Type I, in which each λ_j is an independent random variable with the probability distribution

$$G_n(\lambda)=[n^n/(n-1)!]\lambda^{n-1}e^{-n\lambda}. \quad (57)$$

The integer n takes the values 1, 2, 3, $\cdots$. The distribution G_n has mean value 1 and standard deviation $n^{-\frac{1}{2}}$. Thus, C_1 is a highly disordered chain, C_2 is less disordered, and in the limit as $n\to\infty$, C_n becomes the uniform chain with all $\lambda_j=1$. For large n Eq. (57) takes asymptotically the Gaussian form

$$G_n(\lambda)\sim(n/2\pi)^{\frac{1}{2}}\exp[-\tfrac{1}{2}n(\lambda-1)^2]. \quad (58)$$

We choose these C_n for the illustration for reasons of mathematical convenience only. They happen to have frequency spectra which can be calculated to the end analytically. And although they do not correspond closely to any known physical situation, they illustrate clearly enough the behavior of disordered chains in general.

If we substitute Eq. (57) into Eq. (44), we find an integral equation for $F(\xi)$ which has the exact solution

$$F_n(\xi)=K_n^{-1}\xi^{n-1}(1+\xi)^{-n}e^{-n\xi/x}, \quad (59)$$

where K_n is a function of x determined by the normalization condition (45). Hence, Eq. (46) gives

$$\Omega_n(x)=2L_n(x)/K_n(x), \quad (60)$$

$$L_n(x)=\int_0^\infty \xi^{n-1}(1+\xi)^{-n}\log(1+\xi)e^{-n\xi/x}d\xi, \quad (61)$$

$$K_n(x)=\int_0^\infty \xi^{n-1}(1+\xi)^{-n}e^{-n\xi/x}d\xi. \quad (62)$$

We next have to carry out the analytic continuation of L_n and K_n to negative x. This is done in Appendix III. Hence, if we use Eq. (12), we find the following analytic expression for the frequency spectrum of C_n,

$$M_n(z)=\frac{G_1^2-F_0G_2e^{-ns}+[F_0F_2-F_1^2+((\pi^2/6)-t_{n-1})F_0^2]e^{-2ns}}{[G_1+(F_1-(\log nz+s_{n-1}+\gamma)F_0)e^{-ns}]^2+\pi^2F_0^2e^{-2ns}}. \quad (63)$$

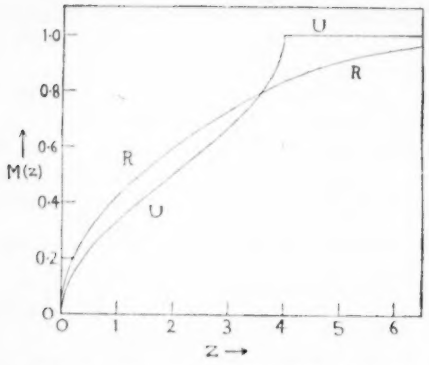

FIG. 1. Integral spectrum of characteristic frequencies for a uniform chain (curve UU) and for a random chain in which each spring-parameter λ has the distribution-function $\exp(-\lambda)$ (curve RR). $M(z)$ gives the proportion of frequencies ω for which $\omega^2 \leq z$.

Here, F_0, F_1, and F_2 are finite polynomials defined by

$$F_0 = \sum_{j=0}^{n-1} \binom{n-1}{j} (-nz)^j/j!, \tag{64}$$

$$F_1 = \sum_{j=0}^{n-1} \binom{n-1}{j} [(-nz)^j/j!]s_j, \tag{65}$$

$$F_2 = \sum_{j=0}^{n-1} \binom{n-1}{j} [(-nz)^j/j!](s_j^2+t_j), \tag{66}$$

with

$$s_j = \sum_{l=1}^{j} l^{-1}, \quad t_j = \sum_{l=1}^{j} l^{-2}. \tag{67}$$

The G_1 and G_2 are integral functions of z with power-series expansions

$$G_1 = \sum_{j=0}^{\infty} \binom{n-1+j}{j} [(-nz)^j/j!]s_j, \tag{68}$$

$$G_2 = \sum_{j=0}^{\infty} \binom{n-1+j}{j} [(-nz)^j/j!](s_j^2+t_j), \tag{69}$$

and γ is Euler's constant. Asymptotically for large z, G_1 and G_2 have semiconvergent series expansions

$$G_1 = [(-1)^n/(n-1)!] \sum_{j=n}^{\infty} (nz)^{-j} [(j-1)!]^2/(j-n)!, \tag{70}$$

$$G_2 = 2[(-1)^n/(n-1)!] \sum_{j=n}^{\infty} (nz)^{-j} \times [(j-1)!]^2 s_{j-1}/(j-n)!. \tag{71}$$

From Eq. (63) we can find at once the limiting behavior of M_n for small z,

$$M_n(z) \sim [(\pi^2/6) - t_{n-1}][\pi^2 + (\log nz + s_{n-1} + \gamma)^2]^{-1}. \tag{72}$$

This rises very rapidly as z increases from zero, showing that a disordered chain has a much greater proportion of very low characteristic frequencies than a uniform chain. The limiting behavior of M_n for large z is found from Eqs. (70) and (71) to be

$$M_n(z) \sim 1 - 2(\log nz - s_{n-1} + \gamma)e^{-nz} \times (nz)^{2n-1}[(n-1)!]^{-2}. \tag{73}$$

In Fig. 1 the numerical value of $M_1(z)$ is plotted together with the corresponding function for the uniform chain which is by Eq. (41)

$$M_\infty(z) = \pi^{-1} \arccos[1 - \tfrac{1}{2}z], \quad z<4, \qquad = 1, \quad z>4. \tag{74}$$

From Eq. (63) we can also calculate the form of the frequency spectrum for large n, i.e., for a chain composed of only slightly fluctuating elements. In this case we represent the spectrum by a complex contour integral which is evaluated by the method of steepest descent; details are given in Appendix IV. The results are the following. For any fixed z in the range $0<z<4$, we have for sufficiently large n,

$$M_n(z) \sim \pi^{-1} \arccos[1 - \tfrac{1}{2}z] + (2\pi n)^{-1}[(4/z) - 1]^{-\frac{1}{2}}. \tag{75}$$

For fixed $z>4$ and large n,

$$M_n(z) \sim 1 - \pi^{-1}\alpha \exp[-\alpha - 2n(\sinh\alpha - \alpha)], \tag{76}$$

$$\alpha = \arg\cosh[\tfrac{1}{2}z - 1]. \tag{77}$$

At the critical point $z=4$ and for large n,

$$M_n(z) \sim 1 - [\Gamma(\tfrac{1}{3})]^{-2}[12/n]^{\frac{1}{3}} = 1 - (0.32\cdots)n^{-\frac{1}{3}}. \tag{78}$$

The errors in Eqs. (75), (76), (78) are in each case of higher order in $(1/n)$ than the last term given. From these results it is seen how the spectrum approaches the limiting form (74) as $n \to \infty$.

VII. APPLICATION TO TRANSMISSION LINES

Consider an ideal loss-free transmission line composed of a series of inductances $L_1, L_2, \cdots$ with a capacitance C_j between each pair L_j and L_{j+1}. The equation of motion for the current I_j in the inductance L_j is

$$L_j d^2I_j/dt^2 = C_j^{-1}(I_{j+1} - I_j) + C_{j-1}^{-1}(I_{j-1} - I_j). \tag{79}$$

This is identical with Eq. (1), only with L_j replacing m_j and C_j^{-1} replacing K_j. Therefore, the whole of the theory of this paper applies without alteration to a transmission line whose elements L_j and C_j are statistically random variables. The function $M(z)$ gives the integrated frequency distribution of the normal modes of propagation of current in the line.

In conclusion, the author wishes to thank Professor Kittel for suggesting this problem to him, Professor Luttinger for some useful discussions, and the University of California for its hospitality during the summer of 1953 when the work was done.

APPENDIX I. EVALUATION OF $R(q)$

Define $R(q, c)$ to be the number of cycles σ corresponding to a given set of $q(j)$, and beginning and ending with a given $j_0=j_{2n}=c$. Suppose first $c<b$. From each of these σ we can derive a new cycle σ' by simply omitting from σ the steps $(b\to b+1)$ and $(b+1\to b)$, since by hypothesis the step $(b+1\to b+2)$ does not occur in σ. These σ' will all belong to the set of integers q', where $q'(b)=0$ and $q'(j)=q(j)$ for $j<b$. The number of the σ' is $R(q', c)$. From a given σ' we derive the parent σ by inserting $q(b)$ pairs of steps $(b\to b+1)$, $(b+1\to b)$ distributed in any way among the $q(b-1)$ places where the integer b occurs in σ'. So the number of σ corresponding to a given σ' is the number of ways of distributing $q(b)$ identical objects among $q(b-1)$ boxes, which is $L(b)$ defined by Eq. (22). Hence,

$$R(q, c)=L(b)R(q', c). \tag{A.1}$$

Proceeding repeatedly in the same way, we shall reduce q to the set of integers q'' defined by $q''(j)=0$ for $j>c$, $q''(j)=q(j)$ for $j\leq c$. We find

$$R(q, c)=\left[\prod_{j=c+1}^{b} L(j)\right]R(q'', c). \tag{A.2}$$

We now start reducing q'' from the other end by omitting steps $(a\to a+1)$ and $(a+1\to a)$. In this way we eventually reach q''' defined by $q'''(j)=0$ for $j>c$ or $j<c-1$, $q'''(j)=q(j)$ for $j=c$ or $j=c-1$. We find

$$R(q'', c)=\left[\prod_{j=a+1}^{c-1} L'(j)\right]R(q''', c), \tag{A.3}$$

$$L'(j)=(q(j)+q(j-1)-1)!/[(q(j)-1)!(q(j-1))!]. \tag{A.4}$$

But $R(q''', c)$ is just the number of ways of arranging $q(c)$ pairs of steps $(c\to c+1)(c+1\to c)$ and $q(c-1)$ pairs $(c\to c-1)(c-1\to c)$, beginning and ending at c. This number is

$$R(q''', c)=(q(c)+q(c-1))!/[(q(c))!(q(c-1))!]. \tag{A.5}$$

If we put together (A.2), (A.3), and (A.5), we obtain

$$R(q, c)=(q(c)+q(c-1))(q(a))^{-1}\left[\prod_{j=a+1}^{b} L(j)\right]. \tag{A.6}$$

We now sum (A.6) over all values of c from a to $b+1$. Then $\sum q(c)=\sum q(c-1)=n$, and so Eq. (21) of the text is verified.

APPENDIX II. DERIVATION OF EQUATION (42)

Consider the Fourier transform of $x^{\frac{1}{2}}\Omega'(x)$ considered as a function of the variable $\log x$, namely

$$r(\alpha)=\int_{-\infty}^{\infty} x^{\frac{1}{2}}\Omega'(x)\exp[-i\alpha\log x]d(\log x). \tag{A.7}$$

If we use Eq. (14), this becomes

$$\begin{aligned} r(\alpha)&=\int_0^\infty D(\mu)d\mu\int_{-\infty}^{\infty} dy 2\mu e^{y-2i\alpha y}[1+\mu e^{2y}]^{-1}\\ &=\int_0^\infty \mu^{\frac{1}{2}}D(\mu)d\mu e^{i\alpha\log\mu}\int_{-\infty}^{\infty} e^{-2i\alpha y}\operatorname{sech} y dy\\ &=(\pi\operatorname{sech}\pi\alpha)\int_{-\infty}^{\infty}\mu^{\frac{1}{2}}D(\mu)e^{i\alpha\log\mu}d(\log\mu). \end{aligned} \tag{A.8}$$

Thus, $[r(\alpha)\cosh\pi\alpha]$ is also the Fourier transform of $\mu^{\frac{1}{2}}D(\mu)$ as a function of $(\log\mu)$. If we invert the transform (A.8), we obtain

$$\mu^{\frac{1}{2}}D(\mu)=(2\pi^2)^{-1}\int_{-\infty}^{\infty}\exp(-i\alpha\log\mu)r(\alpha)\cosh\pi\alpha d\alpha, \tag{A.9}$$

and substitution for $r(\alpha)$ from (A.7) gives Eq. (42).

APPENDIX III. ANALYTIC CONTINUATION OF K_n AND L_n

We write

$$I(q)=I(q, n, y)=\int_0^\infty \xi^{n-1}(1+\xi)^{q-n}e^{-\xi y}d\xi, \tag{A.10}$$

where $y=n/x$. For positive y, this is an analytic function of q for every q, and in particular

$$K_n(x)=I(0), \quad L_n(x)=(dI/dq)_{q=0}. \tag{A.11}$$

We evaluate $I(q)$ assuming $q>n-1$, in which case

$$I(q)=J(q)+R(q), \tag{A.12}$$

where

$$\begin{aligned} J(q)&=\int_{-1}^{\infty}\xi^{n-1}(1+\xi)^{q-n}e^{-\xi y}d\xi\\ &=e^y\sum_{i=0}^{n-1}(-1)^i\binom{n-1}{j}\int_0^\infty z^{q-1-i}e^{-zy}dz\\ &=e^y y^{-q}\sum_{i=0}^{n-1}(-1)^i\binom{n-1}{j}\Gamma(q-j)y^i, \end{aligned} \tag{A.13}$$

$$\begin{aligned} R(q)&=-\int_0^1(-\xi)^{n-1}(1-\xi)^{q-n}e^{\xi y}d\xi\\ &=(-1)^n\sum_{j=0}^{\infty}(y^j/j!)\\ &\quad\times[\Gamma(n+j)\Gamma(q-n+1)/\Gamma(q+j+1)]. \end{aligned} \tag{A.14}$$

The series in (A.13) and (A.14) are convergent and represent functions of y which are analytic over the whole y plane except for the simple branch point at $y=0$ produced by the factor y^{-q}. As functions of q, $J(q)$ and $R(q)$ are analytic, but each has a simple pole at $q=0$ which only cancels in the sum $I(q)$. Hence, we

may evaluate K_n and L_n using (A.13) and (A.14), expanding these expressions in powers of q and retaining terms of order -1, 0 and 1. The terms in q^{-1} cancel as they should. The terms in q^0 and q^1 give, respectively,

$$K_n(x)=e^y\sum_{j=0}^{n-1}\binom{n-1}{j}(y^j/j!)(s_j-\gamma-\log y)+\sum_{j=0}^{\infty}\binom{n+j-1}{j}(y^j/j!)(s_j-s_{n-1}), \quad \text{(A.15)}$$

$$2L_n(x)=e^y\sum_{j=0}^{n-1}\binom{n-1}{j}(y^j/j!)[(s_j-\gamma-\log y)^2+t_j+\pi^2/6]-\sum_{j=0}^{\infty}\binom{n+j-1}{j}(y^j/j!)\times[(s_j-s_{n-1})^2+t_j+t_{n-1}], \quad \text{(A.16)}$$

in which γ is Euler's constant, and s_j, t_j are defined by Eq. (67). These formulas show K_n and L_n explicitly as analytic functions of $y=n/x$, with a logarithmic branch point at $y=0$. In order to obtain the analytic continuation of K_n and L_n to a point $(-x)$ on the negative real axis, going through the upper half of the x plane, we have only to replace, in Eqs. (A.15) and (A.16), y by $(-y)$ and $\log y$ by $(\log y-i\pi)$. This leads at once, by Eq. (12), to the result stated in Eq. (63).

APPENDIX IV. METHOD OF STEEPEST DESCENT

We consider the analytic continuation of the function $K_n(x)$ given by Eq. (62) through the upper half-plane to a point $x=-z^{-1}$ on the negative real axis. This continuation may be written as a contour integral

$$K_n(-z^{-1})=\int_0^{-\infty}[F(\xi)]^n\xi^{-1}d\xi, \quad \text{(A.17)}$$

$$F(\xi)=\xi(1+\xi)^{-1}e^{z\xi}, \quad \text{(A.18)}$$

and the path of integration passes from 0 to $(-\infty)$ above the singularity at $\xi=-1$. Similarly, by Eq. (61)

$$L_n(-z^{-1})=\int_0^{-\infty}[F(\xi)]^n\log(1+\xi)\xi^{-1}d\xi. \quad \text{(A.19)}$$

We choose the path of integration to pass over the lowest saddle point of $F(\xi)$ between the minima at 0 and $(-\infty)$. The saddle points η are given by the quadratic equation

$$\eta^2+\eta+z^{-1}=0. \quad \text{(A.20)}$$

Suppose first $0<z<4$. Then, there is one saddle point

$$\eta=\tfrac{1}{2}[-1+i((4/z)-1)^{\frac{1}{2}}] \quad \text{(A.21)}$$

in the upper half-plane. The path of integration crosses this saddle at an angle of 135° to the positive real axis. For large n we calculate K_n and L_n by considering contributions to the integrals from the neighborhood of the saddle only. If we use Eq. (12), this gives the result (75). Next suppose $z>4$. Then there are two saddle points on the real axis

$$\eta_+=\tfrac{1}{2}[-1+(1-(4/z))^{\frac{1}{2}}],$$
$$\eta_-=\tfrac{1}{2}[-1-(1-(4/z))^{\frac{1}{2}}]. \quad \text{(A.22)}$$

The path of integration goes along the real axis over η_+ from 0 to η_-, then breaks off at 90° to the real axis and goes from η_- to $(-\infty)$ above $\xi=-1$. For large n the real parts of K_n and L_n come from the integral near η_+, but the imaginary parts come from contributions in the neighborhood of η_-. In this way we find the result (76), which tends to 1 for large n because $|F(\eta_-)|<|F(\eta_+)|$. Finally, consider the case $z=4$. Then there is one saddle point at $\eta=-\frac{1}{2}$, at which the first two derivatives of $F(\xi)$ vanish. The path of integration goes from 0 to η along the real axis, then breaks off at an angle of 120° and goes to $(-\infty)$. The integral in the neighborhood of η now gives Eq. (78).

Determination of Thermodynamic Temperatures near 0°K without Introducing Heat below 1°K

W. F. GIAUQUE
Department of Chemistry, University of California, Berkeley, California
(Received June 29, 1953)

Various methods of introducing heat in the region of temperature and magnetic field accessible below 1°K are compared and their experimental limitations are pointed out. The fact that all thermodynamic properties can be determined in the above region without introducing heat below 1°K is discussed. This fact also applies to the use of Kelvin's equation, $dQ=TdS$, in the determination of thermodynamic temperature.

KELVIN defined thermodynamic temperature T by the expression $TdS=dQ$, where dS and dQ refer to increments of entropy and heat, respectively. Kelvin made it obvious that this general relationship can be used to determine true thermodynamic temperatures in connection with any process if the determination can be performed in a thermodynamically reversible manner. This fact is one of the reasons why considerable ingenuity and effort have been devoted to the problem of introducing heat into substances cooled to temperatures below 1°K by adiabatic demagnetization. A brief summary of the relative advantages and disadvantages of the several existing methods of adding heat will assist in showing why it will often be of importance to avoid all of them in the temperature region below 1°K.

Six methods of heating were proposed by Giauque and MacDougall[1,2] in connection with their early experiments, which made the first use of Kelvin's equation to determine true thermodynamic temperatures in the region below 1°K.

(1) Radiation from a heated filament.
(2) Radiation from ordinary temperatures.
(3) Radiation from radioactive material.
(4) The addition of a small amount of solid of known energy content.
(5) The condensation of small amounts of helium gas.
(6) Use of an induction heater.

They also reported that heat could be introduced by means of a very small magnetic irreversibility in several salts when the cooled samples were subjected to an alternating field with a frequency of 550 cps. However, this effect was not considered for use as a calorimetric procedure for reasons which will be mentioned below.

Giauque and MacDougall selected an induction heater in order to avoid electrical leads. The heater was made in the form of a circle of No. 40 gold wire containing 0.1-percent silver. It was located at one end of a sample tube which contained gadolinium phosphomolybdate tridecahydrate. An alternating field was applied by means of the surrounding solenoid magnet, and the energy input was placed on an absolute basis by means of measurements between 1 and 4°K. It was then possible to use it for absolute measurements at temperatures below 1°K. Since the wire was close to the sample, it was necessary to consider the effect of the sample on the magnetic induction through the loop.

Giauque and Stout[3] later investigated the gold-silver alloy system and showed that induction heaters could be designed to deliver a calculable amount of energy which was practically independent of temperature. They showed that gold-silver alloys of most compositions have essentially no temperature coefficient of resistance between 1 and 12°K. The heat capacities of these alloys are so low that their temperatures will rise into the region above 1° even when the sample is at a very low temperature; thus, the resistance of such a heater is known.

Giauque and MacDougall[4] also supplied heat by the condensation of small amounts of helium gas in a chamber at one end of a sample tube. However, this was used only to obtain a controlled warming rate rather than for calorimetric purposes.

Simon[5] independently proposed, and with co-workers[6] introduced the use of radioactive heating. This can be done by irradiating the sample with γ rays.

(7) Resistance thermometer-heaters.

This type of heating below 1°K was introduced by Giauque, Stout, and Clark.[7,8] They used amorphous carbon heaters of very high resistance with electrical leads made of platinized strips on glass. These leads reduced heat conductivity to almost negligible proportions and developed nearly negligible amounts of heat. The carbon had a very large negative temperature coefficient of electrical resistance, which made it very useful in thermometry; and the carbon particles were so small that the alternating fields, useful for some

[1] W. F. Giauque and D. P. MacDougall, presented at the Meeting of the American Chemical Society in affiliation with the American Association for the Advancement of Science, Berkeley, California, June 18–23, 1934 (unpublished).
[2] W. F. Giauque and D. P. MacDougall, Phys. Rev. **47**, 885 (1935).
[3] W. F. Giauque and J. W. Stout, J. Am. Chem. Soc. **60**, 358 (1938).
[4] W. F. Giauque and D. P. MacDougall, J. Am. Chem. Soc. **60**, 376 (1938).
[5] F. Simon, Nature **135**, 763 (1935).
[6] Kurti, Laine, and Simon, Compt. rend. **204**, 754 (1937).
[7] W. F. Giauque, Chandler Lecture, Columbia University, May 28, 1936; Ind. Eng. Chem. **28**, 743 (1936).
[8] Giauque, Stout, and Clark, J. Am. Chem. Soc. **60**, 1053 (1938).

types of magnetic measurements, produced negligible heating due to induction within the particles. This was shown[8] to be true even if the conductivity within the carbon particles should equal the largest value observed for a nonsuperconducting pure metal. The resistance was found to be relatively insensitive to magnetic fields.

De Haas, Casimir, and van den Berg[9] utilized a constantan wire coil heater which was typical except that it had long lead wires of impure lead. These minimized heat leak, and no heat was developed in the leads since they were superconducting. However, this would not be true in magnetic fields above the superconductivity threshold value for lead. Their measurements were concerned with an investigation of the resistances of gold and phosphorbronze cooled below 1°K by means of the demagnetization of iron ammonium alum.

(8) Heat introduction by means of paramagnetic relaxation and hysteresis.

Casimir, de Haas, and de Klerk[10] suggested that calorimetric heat could be introduced into samples below 1°K by means of the energy converted to heat by irreversible paramagnetic relaxation effects or hysteresis. They used this procedure to measure the heat capacity of $FeNH_4(SO_4)_2 \cdot 12H_2O$.

This method has also been used by de Klerk, Steenland, and Gorter[11,12] for heat introduction in determinations of thermodynamic temperatures down to 0.0029°K, with $KCr(SO_4)_2 \cdot 12H_2O$, and down to 0.0014°K with the same salt diluted with $KAl(SO_4)_2 \cdot 12H_2O$.

COMPARISON OF METHODS OF HEAT INTRODUCTION BELOW 1°K

In comparing various methods of heat introduction below 1°K, it is obvious that some methods may be satisfactory for limited conditions and useless in others. We suppose it is natural that authors should point out the advantages of a method as it applies to their particular experiment and place less emphasis on the experimental limitations they incur through the use of it.

In personal discussions we have had with many who are well informed concerning research at very low temperatures, it has been evident that no publication has given a critical evaluation of methods of introducing heat and making related observations at temperatures below 1°K. One of the purposes of this paper is to be thoroughly critical for the benefit of those who will acquire equipment for experimental investigations in the region made accessible by adiabatic demagnetization. We do not wish to imply that any one method of making some desired experimental observation will be the best method under all circumstances. It is necessary to consider simplicity, the accuracy required, the time and effort needed, and the expense. However, if time, effort, and expense are relatively equivalent in two methods, the experimenter should certainly adopt the method which has the greatest range of usefulness in as many respects as possible.

Only four of the above methods of introducing heat show much promise of usefulness as accurate methods even under very limited experimental conditions. These four may be classified in two groups.

A. External Heating:

(6) Induction heating in a conductor to avoid leads.
(7) Carbon resistance thermometer-heater or other resistors with leads.

B. Internal Heating:

(3) Radiation from radioactive material.
(8) Paramagnetic relaxation and hysteresis.

In our early experiments with an induction heater, difficulty in attaining equilibrium was encountered below 0.3°K, and in later experiments with carbon resistance thermometers, it could be shown that it was extremely difficult to obtain the degree of uniform energy distribution necessary for accurate calorimetry below 0.25°K. We believe that all experimenters are agreed on this point. The effect has usually been considered to be due to decreasing thermal conductivity of the substance, but the situation is more serious than that. Even if the thermal conductivity remained constant, an error equivalent to 0.001° in the absolute temperature might be tolerated at 1° where it is 0.1 percent, but not at 0.01° where it is 10 percent. Moreover, the heat capacity usually increases with decreasing temperature, and this increase can introduce an additional difficulty in the rate at which equilibrium is attained. These difficulties apply to the methods of Class A below about 0.25°K although they can be used with decreasing accuracy to at least 0.1°K. The methods of Class A have been used with the heater separated from the magnetic material by the wall of the sample tube. Giauque, Stout, Egan, and Clark[7,13] reported an experiment in which very rapid equilibrium was attained with a carbon thermometer at 0.13°K when some gadolinium phosphomolybdate tridecahydrate crystals were firmly attached to the glass wall. The gadolinium ions are separated by 10A in this cubic, magnetically dilute substance. Thus, they are surrounded by a very extensive lattice. In this experiment the amorphous carbon thermometer was painted on paper and attached to the outer wall of the glass sample tube by means of collodion. Preliminary demagnetizations were made to temperatures between 0.1 and 0.2°K so that the potentiometer could be set rather accurately on the reading to

[9] de Haas, Casimir, and van den Berg, Comm. Phys. Lab. Leiden (1939), 251c (1938); Physica **5**, 225 (1938).
[10] Casimir, de Haas, and de Klerk, Comm. Phys. Lab. Leiden 256b (1939); Physica **6**, 255 (1939).
[11] de Klerk, Steenland, and Gorter, Comm. Phys. Lab. Leiden, 278c (1949); Physica **15**, 649 (1949).
[12] de Klerk, Steenland, and Gorter, Comm. Phys. Lab. Leiden 282a (1950); Physica **16**, 571 (1950).
[13] Giauque, Stout, Egan, and Clark, J. Am. Chem. Soc. **63**, 405 (1941).

be expected at the final low temperature. Because of the galvanometer, a time of several seconds was required to observe that this external thermometer-heater had essentially attained equilibrium, through the glass and other material, with that fraction of the salt which adhered to the inner surface of the sample tube. Subsequent temperature measurements made with both a fluxmeter and the carbon thermometer showed that heat leak eventually caused the carbon thermometer to lead the bulk temperature by several hundredths of a degree due to spaces which acted as thermal barriers between the masses of crystal in the interior of the sample tube. Thus, at the present state of our knowledge it is possible that the problem of the external heater might be greatly reduced if the heater were attached directly to a single crystal sample.

Since our present maximum magnetic fields of 8000 oersteds have seriously limited the attainment of temperatures much below 0.1°K, we have postponed this experiment until after the installation of more powerful magnetic equipment, which is now in progress. Nevertheless, we are not optimistic concerning the attainment of equilibrium with external heating at very low temperatures. Even if so-called single crystals were to be used, there might be defects which could act as thermal barriers.

The methods of Class B have the advantage that they liberate heat uniformly throughout the sample. However, if the measurements extend over an appreciable time interval, heat leak will cause non-uniform distribution of temperature. To avoid this effect experimenters can remagnetize the sample at frequent intervals to attain equilibrium at the higher temperature before recooling for a short period of observation.

At first sight it might seem that all difficulties have been removed, but this is far from the case.

We have mentioned that Giauque and MacDougall[1,2] observed that small amounts of heat could be added to samples by means of very small irreversible magnetic effects due to an alternating field. However, they did not consider using these effects for calorimetric purposes, because it was evident that losses computed from the inductance bridge measurements were primarily due to eddy currents induced in metal parts of their apparatus and magnet.

In principal the energy loss from the bridge to surrounding metal apparatus can be evaluated experimentally in the absence of the sample; however, the small relative magnitude of the heat delivered to the sample, and the difficulty in controlling temperature and other variables in the large amounts of metal in a magnet, make evaluation of the smaller amount impracticable. This means that the sample must be removed from the magnet before there is any possibility of using bridge measurements to measure the energy converted to heat within the sample. Acceptance of the magnetic relaxation method of supplying heat essentially limits the magnetic measurements to fields of minor magnitude. Since most of the phenomena which can be studied below 1°K are field-dependent, this is a rather serious limitation to incur in order to have a method of supplying heat. It should also be pointed out that there are other complications besides those related to heat measurement, when coils utilized for inductance bridge measurements are near the metal parts of magnets. The currents induced in external metal by the ac field can produce complex effects, and measurements are certainly easier to make when the sample is separated from the metal parts of magnets. However, the realities of the situation may as well be faced; the adiabatic demagnetization method opened up an area for investigation. This area is bounded by low temperatures in one dimension and magnetic fields, consistent with the minimum entropy of the sample which is available to the experimenter, in the other dimension. If an experimenter is satisfied to investigate phenomena along a boundary line of this area, corresponding to zero field, it may be desirable to separate the sample and the magnet. We have found that static arrangements have advantages with respect to reproducibility of experimental conditions and minimum time required for measurements, quite aside from the problem of the range of investigation.

The radioactive heating employed by Simon and his co-workers raises questions concerning the rate of decay of various excited states which are known to be produced. The reliability of the radioactive heating method has been questioned by de Klerk, Steenland, and Gorter[14,15] and particularly by Platzman.[16] The method has been defended by Kurti and Simon.[17] They point out that semipermanent chemical changes due to the total radiation used cannot apply to more than the order of one in 10^6 molecules. This estimate appears to be based on the assumption that the crystal defects produced involve energy disturbances of the order of an electron volt. However, one should not overlook the fact that a crystal defect of this magnitude may have a considerable effect on a large number of surrounding molecules, whereas the kinds of cooperation involved in magnetic effects are often so energetically weak that they cannot operate until the substance is cooled to tenths or hundredths of degrees absolute, corresponding to energies of the order of 10^{-6} electron volt. Quite aside from the question of crystal defects produced by radioactivity, we have long been concerned about the possible effects of other defects which are present in most crystals. It is evident that the closer the approach to the absolute zero, the more widespread will be the effect of crystal imperfections on neighboring regions. We suspect that future investigation will show that the heat capacity and magnetic properties, especially in regions involving cooperative effects at very low tem-

[14] de Klerk, Steenland, and Gorter, Nature **161**, 678 (1948).
[15] de Klerk, Steenland, and Gorter, Physica **15**, 649 (1949).
[16] R. L. Platzman, Phil. Mag. **44**, 497 (1953).
[17] N. Kurti and F. E. Simon, Phil. Mag. **44**, 501 (1953).

peratures, will vary appreciably with crystal perfection at temperatures well below 1°K. Most of the available crystals have appreciable inclusions of impurities, electronic holes, lattice vacancies, and other assorted defects, and the consequences of producing one additional defect in 10^6 molecules (i.e., defects 100 molecules apart) must be judged by taking into consideration the perfection of the original system. It seems certain that crystal defects produced as a matter of thermodynamic equilibrium during crystal formation at ordinary temperatures would be much less serious in their long-range effects than those produced by γ rays. However, there does not appear to be any real evidence which would allow one to rule out radioactive heating on the basis of the estimated chemical changes which are produced by γ-ray heating. Nevertheless, one cannot measure the importance of possible long-range effects at extremely low temperatures by the standards appropriate to ordinary temperatures and ordinary defects, and we cannot help having reservations concerning this subject.

The evidence offered by Kurti and Simon[17] concerning the absence of delayed heat evolution from the excited states of crystals is certainly the best available but is not sufficiently detailed to be convincing. If the rate of delayed heat evolution did not change much with time, it would be included with the temperature drift due to heat leak, and the heat capacity measurements would be approximately correct. The plain facts are that no one has made very accurate measurements of heat capacity below 1°K, and we anticipate a great deal of difficulty in future measurements of this sort. Calorimetry does not become accurate until the experimenter has enough data to predict, on the basis of reproducibility, the exact amount of heat leak corresponding to the temperature difference between a calorimeter and its surroundings. At higher temperatures this makes it possible to check true equilibrium in terms of the calculable drift. The work in this laboratory has made use of the most sensitive thermometry available, but the various difficulties connected with measurements near 1°K have not enabled the use of our ordinary calorimetric procedures. One straightforward type of experiment to dispose of the question of delayed heat emission, after irradiation ceased, would be to irradiate a cooled and thermally isolated sample for a long time and arrange to stop the radiation when the sample exactly reached the temperature of a surrounding bath. Its temperature should not increase further if the excited states are stable. Platzman points out that each substance will have its own specific properties with respect to the conversion of radiation to thermal energy, and Kurti and Simon restrict their comments to the "substances employed so far." The necessity of investigating the stability of excited states in the case of each substance may not be a major handicap, but it certainly detracts somewhat from the value of the method.

Gamma-ray heating has an advantage over the magnetic relaxation method in that it can be used in strong magnetic fields. However, we believe that it has always been employed in connection with iron magnets rather than with solenoids when the sample was kept in a magnetic field. Giauque and Stout tried an unpublished experiment on γ-ray heating in their early work. The experiment was unsuccessful because they could not bring the radium source close enough to the sample which was enclosed in a solenoid magnet. Also it was not obvious how uniform irradiation could be obtained in a sample of desirable dimensions which was located within the solenoid. This latter difficulty has been minimized by experimenters using γ-ray heating by rotating samples of radium in positions which are carefully selected to improve uniformity of heating. This means that the radium must be located at an appreciable distance from the sample. This is not difficult in the case of a sample located in the pole gap of an iron magnet, but it is not obvious to us how one can afford to use the valuable volume inside a solenoid magnet in order properly to place and rotate the radioactive sources. If γ-ray heating is practicable only when the magnetized substance is in the gap of an iron magnet, the combination will seriously limit associated magnetic measurements, which are disturbed by the presence of iron.

There is another problem which can arise in the use of radioactive substances for heating. It will often, if not usually, be necessary to enclose the sample in some sort of container. Heat will be produced in the container as well as in the sample. Unless it can be arranged to make this effect of negligible proportion, the heat distribution problem will not have been avoided. If the sample and its enclosing vessel are not in equilibrium, any ordinary container material should increase considerably in temperature because of the very low heat capacity. Simon and his co-workers have so far by-passed this problem by avoiding the use of containers, but this will certainly not always be convenient or even practicable.

Many of the foregoing problems connected with γ-ray heating may be overcome, but we believe that much more work will be required before the method can be accepted as reliable.

Any conventional heater may be used to measure an increment of heat content between two low temperatures, even if the heater is not in equilibrium with a poorly conducting sample. For example, if heat is added immediately following demagnetization, and in sufficient amount to reach some temperature such as 0.5°K, then equilibrium will be attained. Similar experiments after adjacent demagnetizations will yield ΔQ at the very low temperature by difference. However, it would be experimentally inconvenient to re-establish the desired initial conditions before demagnetization after each heating to some temperature such as 0.5°K. If much time is required to add the larger increments of heat, the evaluation of heat leak may reduce the

accuracy of the small increments, determined by difference.

We consider that none of the existing methods of introducing heat below 1°K is free from objections with respect to observations on a magnetic substance over the region of field and temperature accessible in adiabatic demagnetization experiments.

DETERMINATION OF THERMODYNAMIC TEMPERATURE WITHOUT INTRODUCTION OF HEAT IN THE REGION BELOW 1°K

Many of the laboratories equipped for magnetic research have typical iron yoke magnets which were acquired prior to the introduction of adiabatic demagnetization. They are indispensable for many purposes, but after they are used for adiabatic demagnetization, the sample and magnet are ordinarily separated to enable measurements of various sorts. For this reason most of the investigations below 1°K have unfortunately been restricted to the initial field condition. Perhaps as a result of the limitations of this experimental predicament, there seems to be a somewhat prevalent feeling that the utilization of Kelvin's definition of temperature requires that heat be added at the unknown low temperature T.

Kelvin's[18] own statement: "the absolute values of two temperatures are to one another in the proportion of the heat taken in to the heat rejected in a perfect thermodynamic engine working with a source and a refrigerator at the higher and lower of the temperatures respectively," has undoubtedly often conveyed the impression that the transfer of heat at both temperatures is a physical necessity in determining the temperature by this method. For example, de Klerk,[19] referring to the determination of temperatures below 1°K states, "··· the only fundamental method to measure temperatures is to make use of Kelvin's definition of the thermodynamic temperature: $dQ=TdS$. For temperature determinations based on this formula a measured amount of heat must be supplied to the salt···."

Platzman[16] states: "In research at temperatures below about 1°K, a major problem is the conversion of readily measured 'magnetic temperatures' to true thermodynamic temperatures. In one essential stage of this conversion···it is necessary to add heat at an ascertainable rate."

In view of the rather general impression that it is necessary to add heat at temperatures below 1°K and the above-mentioned difficulties of doing this accurately, it seems desirable to point out that Kelvin's equation does not imply that heat must be added. As a matter of fact, this has been pointed out previously by Giauque[7] and by Giauque and MacDougall,[4] who state with respect to the treatment of their data on $GdPO_4(MoO_3)_{12}\cdot 30\,H_2O$: "Calculations of the type given above will permit the determination of the low temperatures without the necessity of energy input in the region below 1°K. In fact the curves through the calculated temperatures···checked the initial upper temperatures within a few hundredths of a degree···. It is evident that the lower temperatures could have been based on the measured upper temperatures and heat content data determined from the magnetic observations." They also add that "the above method should prove of importance in avoiding the slow equilibrium which accompanies energy input by means of a heater." The remarks of Giauque and MacDougall are somewhat obscured by their brevity in an otherwise rather long paper, so that it seems desirable to enlarge on this subject.

The only requirement in the application of Kelvin's equation for the determination of absolute temperature is that there should be some experimental method of measuring the heat content H and the entropy S at every point in the region investigated. $H=E-\mathbf{HI}$, where E is the internal energy and $\mathbf{H}$ and $\mathbf{I}$ are the field strength and intensity of magnetization, respectively. For a process at constant magnetic field, $dH=dQ$.

Thus

$$T=(\partial H/\partial S)_{\mathbf{H}}$$

$$TdS=dH+\mathbf{I}d\mathbf{H},$$

and since the entropy can be kept constant during demagnetization,

$$\Delta H\Big|_1^2=-\int_1^2\mathbf{I}d\mathbf{H}.$$

This means that if the relative heat content can be ascertained at temperatures above 1°K, it can be determined at any point reversibly accessible below 1°K without the introduction of heat, since the paths are all isentropies with known entropies which can be determined above 1°K. Magnetic measurements can be made in a short interval before heat leak can interfere, and if necessary the sample can be given intermediate remagnetizations to insure equilibrium before additional measurements are made. When the sample and magnet are in a static arrangement, the interval before a magnetic measurement may be made quite short, whereas the time required for the separation of magnet and sample will considerably lengthen the time of heat leak prior to a measurement. This is only one of the several reasons why iron-free solenoid magnets, rather than iron yoke magnets, should be used for most adiabatic demagnetization work. The demagnetization process must be reversible, but this is true whether heat is to be added at low temperatures or not. Fortunately most of the paramagnetic systems appear to be exceptionally reversible in the thermodynamic sense. In some cases where hysteresis effects develop at limiting low temperatures, the application of thermodynamics is of dubious value, regardless of the method.

[18] *Mathematical and Physical Papers, Thompson (Kelvin)* (Cambridge University Press, London, 1882), Vol. 1, p. 235.
[19] D. de Klerk, Phys. Today **6**, 4 (1953).

THE PLACE OF THE CARBON THERMOMETER-HEATER IN FUTURE EXPERIMENTAL WORK

The amorphous carbon thermometer-heater has been developed in this laboratory with the above facts in mind, and it is of interest to show how it fits into the experimental situation.

Any complete investigation of the magnetic substances of interest in connection with adiabatic demagnetization should provide an accurate measurement of the initial temperature and field in the region near 1°K or above. The substance will be thermally isolated prior to demagnetization, and thus only the adiabatic differential magnetic susceptibility, $(\partial \mathbf{I}/\partial \mathbf{H})_S$, can be measured. This quantity is of practically no direct use in denoting temperature,[7,20] not only because it is usually very small in large fields, but because a given value does not correspond to a specific temperature. Carbon thermometers may be designed[21] for very high sensitivity in any low-temperature range, and they have a rather small field coefficient which can be evaluated. Moreover they can be used with high accuracy for absolute entropy determinations by means of heat input near 1°K where thermal equilibrium is excellent. The entropy change during magnetization is now ordinarily calculated from assumed ideal magnetic behavior above 1°K, but this is a temporary expedient which must be replaced by actual entropy measurements before such work proceeds much further.

The values of heat content for the same initial fields and temperature may be calculated from the isothermal equation:

$$\Delta H = T\Delta S - \int_0^{\mathbf{H}} \mathbf{I} d\mathbf{H}.$$

The values of $\mathbf{I}$ may be determined by means of the relation,

$$\mathbf{I} = \int_0^{\mathbf{H}} (\partial \mathbf{I}/\partial \mathbf{H})_S d\mathbf{H},$$

since values of the adiabatic susceptibility may be measured along the magnetization paths from low temperatures. It is, of course, necessary to show that there is no remanent magnetism at the temperature where the evaluation of $\mathbf{I}$ begins. However, this may be done readily. If the remanent magnetism is present as an equilibrium state, which will probably be rare, its evaluation will give the integration constant. If non-equilibrium remanent magnetism exists, it is unlikely that reliable values of thermodynamic temperature can be determined from such a substance by any method, since the entropy will not be known.

In measuring $(\partial \mathbf{I}/\partial \mathbf{H})_S$ it is necessary that any container used should have a negligible heat capacity to prevent irreversibility, which will occur when the field is varied if this condition is not met. Fortunately, rather substantial containers of glass and other materials can be used in the region below 1°K without contributing appreciably to the heat capacity of the system. Perhaps it should be pointed out that this is a necessary condition during any demagnetization, if it is to be assumed that the process is isentropic; and, regardless of the experimental method, this is the only way in which the entropy of the material may be evaluated at very low temperatures in terms of reference points near 1°K. It is of interest to note that the values of $(\partial \mathbf{I}/\partial \mathbf{H})_S$ become so small at high fields that most of the value of the integral used to evaluate $\mathbf{I}$ results from measurements obtained at fields ranging up to a few thousand oersteds. These are within range of storage battery operation of iron-free solenoid magnets. The resultant steady field permits relatively high accuracy when a null point fluxmeter method is used. We prefer a method of this essentially static sort in connection with the application of thermodynamics since complete equilibrium is more likely to be attained. The low accuracy obtainable with conventional ballistic galvanometers is inappropriate to the methods discussed here. Iron magnets cannot be used since the presence of large masses of ferromagnetic material prevents accurate measurements of the aforementioned type.

Giauque and MacDougall[4,7] also pointed out that the entropy and heat content changes accompanying isothermal magnetization near 1°K could be obtained from the magnetic data alone, without measured additions of heat at the upper temperatures. This can be done by means of the relation

$$\Delta S\Big|_0^{\mathbf{H}} = \int_0^{\mathbf{H}} (\partial \mathbf{I}/\partial T)_{\mathbf{H}} d\mathbf{H}.$$

They showed experimentally that this could be done with satisfactory accuracy in a specially favorable case, but it is obvious that this method, which involves taking the temperature coefficient of an integral derived from the magnetic data, will be less accurate than the one suggested here. This involves the use of $\mathbf{I}$ rather than its derivative with temperature.

This paper is not particularly concerned with the cooling of one sample by means of another for some purpose such as successive demagnetizations; however, it will be evident that the problems of thermal conduction in that case are very similar to but greater than those of the external heater. A heater may be attached directly to the sample, but the superconducting thermal switch used by Darby, Hatton, Rollin, Seymour, and Silsbee[22] involves a considerable length of wire to conduct heat from the magnetized source to the previously demagnetized sink for heat. In the present early stages of work on successive demagnetizations, one can hardly

[20] W. F. Giauque, Proc. Intern. Congr. Refrig., 7th Congr., The Hague—Amsterdam **1**, 527 (1936).

[21] Geballe, Lyon, Whelan, and Giauque, Rev. Sci. Instr. **23**, 489 (1952).

[22] Darby, Hatton, Rollin, Seymour, and Silsbee, Proc. Phys. Soc. (London) **A64**, 861 (1951).

expect detailed experiments as a function of field as well as temperature on substances used in the lower stages. However, when improved technique permits such investigations, the general considerations given above will apply. Heat flow will always be necessary at the upper temperature of each demagnetization stage. If it is impracticable to make the heat flow in a reversible manner, the problem can still be solved if equilibrium values of the magnetic properties can be observed by taking a sufficient time.

In the case of single stage demagnetizations, an experimenter who has a solenoid magnet available has little reason for not making measurements in a field. The measuring equipment for making such observations is certainly not more complicated or expensive than that required in connection with heat introduction and associated magnetic observation in initial fields. Moreover, fluxmeter and bridge measurements can be made with great rapidity compared with those associated with heat input.

PHYSICAL REVIEW VOLUME 92, NUMBER 6 DECEMBER 15, 1953

Heat of Mixing of He^3 in He^4†

H. S. Sommers, Jr., W. E. Keller, and J. G. Dash
University of California, Los Alamos Scientific Laboratory, Los Alamos, New Mexico
(Received August 10, 1953)

The integral heat of mixing for an 8.6 percent solution of He^3 in He^4 at 1.0°K, measured by an adiabatic free-expansion process, is 0.17 cal/mol of solution. Combined with the free energy of mixing, obtained from vapor pressure data, this shows that at this temperature the bulk of the excess free energy of mixing is due to the heat of mixing.

WE have demonstrated the existence of a large positive heat of mixing of He^3 in He^4 by adiabatically mixing the two liquids and observing the drop in temperature. A schematic diagram of the apparatus is shown in Fig. 1. Measured amounts of the two liquids were condensed in the two liquid cells at 1.02°K. The click seals on top and bottom of the He^3 cell (inner cell) were broken by lowering a fine tungsten wire, and the temperature of the mixture measured by recording the pressure on an He^3 vapor pressure thermometer inserted in the He^4 sample. From the variation of thermometer pressure with time, Fig. 2, a minimum temperature of 0.78°K[1] was deduced. Measurement of the masses in the vapor phase showed the only process which could give a net absorption of energy on breaking the click seals was the mixing of the two liquids.

A semiquantitative measurement of the value of the heat of mixing in terms of the latent heat of vaporization of the He^3 was made by conducting the adiabatic mixing in an essentially isothermal manner. During the mixing process, the vapor pressure of the He^3 above the pure liquid drops to its partial pressure over the resulting solution; if the correct mass of He^3 is in the vapor phase at the start, the heat released by the condensation will just cancel the heat absorbed by the mixing of the liquids. Figure 3 gives a plot of the vapor pressures against time for this experiment, in which the apparatus for the first run has been modified by enlarging the vapor space above the liquid He^3. The upper curve, the pressure on the He^3 thermometer against time, shows that the liquid temperature dropped from 1.060 to 1.018°K in the first minute following mixing and then rose to its final value of 1.044 in another twenty minutes. (The final temperature is lower than the initial temperature because of a decrease of film flow on mixing.) From measurements of the pressure over the sample, shown in the lower graph, we see that by two minutes mixing is essentially complete, for after that the sample has the same warm-up rate as the He^3 thermometer.

Treating the mixing as an adiabatic constant volume process, one derives the following expression for the

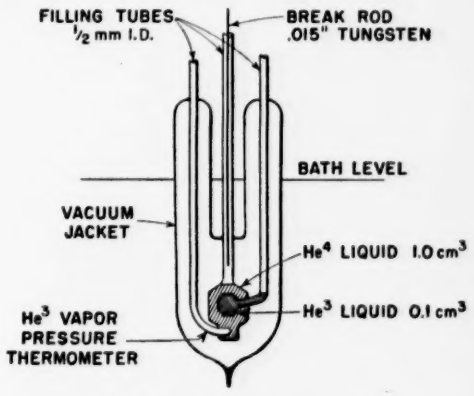

FIG. 1. He^3—He^4 sample cell.

† This paper is based on work performed under University of California contract with the U. S. Atomic Energy Commission.

[1] Abraham, Osborne, and Weinstock, Phys. Rev. **80**, 366 (1950); extrapolation of Eq. (4).

integral heat of mixing per mole,

$$\Delta H_m \equiv x\Delta\bar{H}_3+(1-x)\Delta\bar{H}_4=\frac{1}{m_3+m_4}[\Delta m_3{}^v(L_3-RT)].$$

Here x is the mole fraction of He^3 in the liquid, $\Delta\bar{H}_3$ and $\Delta\bar{H}_4$ are the partial molal heats of mixing, m_3 and m_4 the number of moles of the liquid, $\Delta m_3{}^v$ the moles of He^3 condensing, and (L_3-RT) the latent heat of vaporization per mole for a free expansion. All second-order terms, involving change of mass of He^4 in the vapor, change in temperature, or change in liquid volume, have been dropped. $\Delta m_3{}^v$ was determined from PVT measurements on the He^3 cell and filling line before the click seal was broken and on the filling line

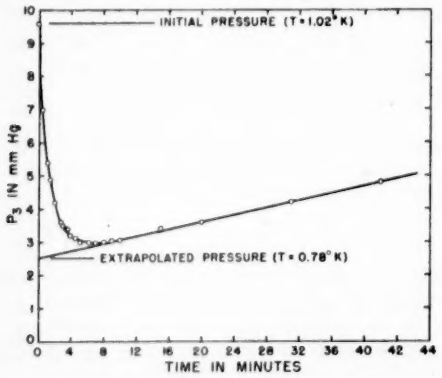

FIG. 2. Adiabatic mixing of He^3-He^4.

to the He^4 cell. A small correction was made for the volume occupied by the liquid He^3. From the change in He^3 pressure on expansion, we then deduced the mass of He^3 condensing.

The experimental values are $(m_3+m_4)=2.02\times10^{-2}$ mole, $\Delta m_3{}^v=4.8\times10^{-4}$ mole, and $(L_3-RT)=7.3$ cal/mole.[1] This gives an integral heat of mixing of 0.17

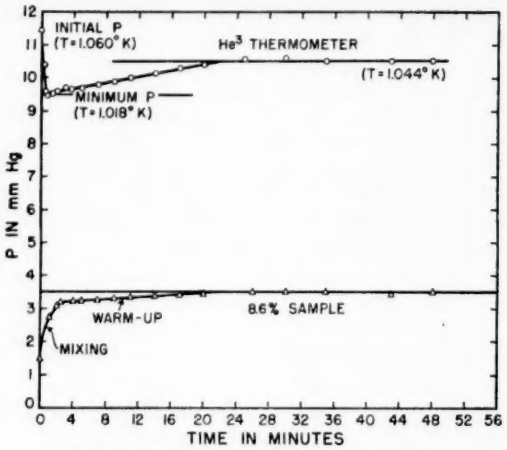

FIG. 3. Quasi-isothermal mixing of He^3-He^4.

cal/mole for an 8.6-percent solution of He^3 at 1.02°K. We have no way of estimating the accuracy of the result, but feel it is a lower limit because the principal source of error is due to the warm gas entering the cell during the initial drop in pressure of the He^3 line and thermometer. Such a discontinuous heat leak, whose presence would not be reflected in the warmup curves, would render our measured value for the heat of mixing too small.

From an extrapolation of the vapor pressure of dilute solutions of He^3 in He^4 [2] to 1.0°K, the departure of the molal free energy of mixing from that for an ideal classical solution (from $RT[x\ln x+(1-x)\ln(1-x)]$) can be deduced. This turns out to be about 0.23 cal/mole for an 8.6 percent solution at 1.02°K; combined with our heat of mixing, this shows that the departure of the molal entropy of mixing from ideality is about −0.06 cal/mole, or −10 percent of the ideal mixing entropy.

[2] H. S. Sommers, Jr., Phys. Rev. **88**, 113 (1952).

PHYSICAL REVIEW VOLUME 92, NUMBER 6 DECEMBER 15, 1953

Physical Conditions in the Initial Stages of the Expanding Universe*,†

RALPH A. ALPHER, JAMES W. FOLLIN, JR., AND ROBERT C. HERMAN
Applied Physics Laboratory, The Johns Hopkins University, Silver Spring, Maryland
(Received September 10, 1953)

The detailed nature of the general nonstatic homogeneous isotropic cosmological model as derived from general relativity is discussed for early epochs in the case of a medium consisting of elementary particles and radiation which can undergo interconversion. The question of the validity of the description afforded by this model for the very early super-hot state is discussed. The present model with matter-radiation interconversion exhibits behavior different from non-interconverting models, principally because of the successive freezing-in or annihilation of various constituent particles as the temperature in the expanding universe decreased with time. The numerical results are unique in that they involve no disposable parameters which would affect the time dependence of pressure, temperature, and density.

The study of the elementary particle reactions leads to the time dependence of the proton-neutron concentration ratio, a quantity required in problems of nucleogenesis. This ratio is found to lie in the range $\sim 4.5:1 - \sim 6.0:1$ at the onset of nucleogenesis. These results differ from those of Hayashi mainly as a consequence of the use of a cosmological model with matter-radiation interconversion and of relativistic quantum statistics, as well as a different value of the neutron half-life.

I. INTRODUCTION

THE nonstatic homogeneous isotropic cosmological model which satisfies the equations of general relativity has received a great deal of attention. However, the detailed nature of the model does not appear to have been examined at the extremely high temperatures and densities characteristic of the very early stages of the expanding universe. This question has been examined in the present paper and the dependence of the temperature and density on time has been determined for the case where the radiation density (taken to include photons, neutrinos, electrons, positrons, and mesons) is much greater than the density of matter (nucleons). For initial conditions compatible with present astrophysical observations, one can demonstrate that the radiation density exceeded the density of matter for about the first hundred million years in the expansion.

We have carried our study of this problem back to a temperature of ~ 100 Mev ($\sim 1.2\times 10^{12}$°K), corresponding to an epoch of $\sim 10^{-4}$ sec. For temperatures below this value one can treat reactions among elementary particles with some confidence. Furthermore, below ~ 100 Mev the energy stored in the gravitational field is a negligible part of the total energy so that the question of using a correct unified field theory, including the quantization of the field equations, can be avoided. Finally, at ~ 100 Mev one has a state of thermodynamic equilibrium among all the known constituent particles and radiation so that a knowledge of the previous history of the universe is not required. As part of the detailed study of the cosmological model we have examined the reactions among the elementary particles present and followed their course in the universal expansion. As will be seen, all reaction rates, except those involving the neutrino, are sufficiently high to maintain thermodynamic equilibrium. An examination of the kinetics of the reactions between nucleons and neutrinos has yielded the relative concentrations of protons and neutrons as a function of time. The only parameters involved in the cosmological model are the nucleon density and radius of curvature. At the early times prior to element formation, neither of these parameters affects the course of events because of the very high total density and because the nucleon density is neglible compared with the density of radiation. The nucleon density becomes of importance at later times in considering element formation, while the radius of curvature becomes of interest only at times of the order of a hundred million years.

The foregoing detailed considerations of the early stages of the universal expansion bear significantly on the neutron-capture theory of element formation. This theory has been concerned principally with understanding the general trend in the distribution of the cosmic abundances of the chemical elements with atomic weight.[1,2]

* This work was supported by the U. S. Bureau of Ordnance, Department of the Navy, under Contract NOrd-7386.

† Preliminary accounts of this work were presented at the Symposium on the Abundance of the Elements held at Yerkes Observatory, Williams Bay, Wisconsin, November 6–8, 1952, under the joint sponsorship of the National Science Foundation and the University of Chicago, and at the 1953 Washington Meeting of the American Physical Society, Phys. Rev. **91**, 479 (1953).

[1] R. A. Alpher and R. C. Herman, Revs. Modern Phys. **22**, 153 (1950); Phys. Rev. **84**, 60 (1951).

[2] R. A. Alpher and R. C. Herman, *Annual Review of Nuclear Science* (Annual Review of Nuclear Science, Inc., Stanford, 1953), vol. 2, p. 1. The simple-neutron capture theory has satisfactorily reproduced for all but the lightest elements the observed approximately exponential decrease in abundance with increasing atomic weight up to $A\sim 100$, as well as the approximate constancy of abundance for the heavier elements. Briefly, in the neutron-capture theory, as thus far developed, the various nuclear species were supposed to have been formed from nucleons by the successive radiative capture of fast neutrons with adjustment of nuclear charge by intervening β decay during the early stages of the expansion of the universe. The primordial material or ylem was taken to be a mixture of neutrons and radiation. As the universal expansion proceeded the neutrons underwent free decay, so that by the time the universal temperature had decreased to a value

For the lightest elements the processes of neutron capture and β decay, while adequate to explain the formation of the heavier elements, must be supplemented by thermonuclear reactions involving protons, deuterons, and other light nuclei. The very light element reactions were examined in some detail by Fermi and Turkevich,[1] using the cosmological model previously employed for the neutron-capture theory, with a finite starting time and a primordial mixture of neutrons and radiation. This improved light-element calculation did not satisfactorily resolve what remains the principle difficulty of the theory, namely, the deduction of the specific nuclear reactions and physical conditions which might carry the formation chain of reactions through and beyond atomic weight 5. To resolve this and other difficulties in the theory, it will apparently be necessary to remove many of the simplifying restrictions. In particular, the assumption of a starting time must be replaced by detailed consideration of element-building reactions increasing in importance from very early times in the universal expansion as the rates of various dissociative processes diminish with decreasing temperature. Moreover, one should include all possible reactions among the elementary particles, since these reactions, which are important at very high temperatures, may influence the physical conditions that control the element-building processes.

The elementary-particle reactions determine the ratio of the relative concentrations of protons and neutrons, a quantity which plays a vital role in predicting the general trend of abundances according to the neutron-capture theory. As has already been mentioned, in previous calculations the proton-neutron abundance ratio has been taken to be that resulting from free decay of the primordial neutrons during the period from the start of the expansion up to the starting time selected for element-building reactions. A more detailed calculation was made by Hayashi,[3] who determined the value of the proton-neutron ratio resulting from spontaneous and induced β processes among protons and neutrons in the presence of electron pairs and neutrinos in the early stages of the expansion. Whereas on the basis of the crude assumption of neutron decay only, one obtains a proton-neutron ratio of $\sim 1:7$, Hayashi's calculation gave $\sim 4:1$ by the starting time for element-building reactions. With this latter value of the ratio, it has not yet proven possible to represent the cosmic abundance distribution in atomic weight on the basis of the simple neutron-capture theory,[2] a theory which contains only one arbitrary parameter, *viz.*, the density of matter at the start of the element-building epoch, and which involves only neutron-capture reactions. In part because of this difficulty and because it seemed worth while to investigate the effect of certain modifications on Hayashi's calculation of the final value of the proton-neutron ratio, the work described in the remainder of this paper was carried out. Among the changes involved in the present study are the use of relativistic quantum statistics instead of Boltzmann statistics, a modified cosmological model for early epochs as required by the interconversion of matter and radiation, which as we have already indicated is of considerable interest for its own sake, and the use of the value of the neutron half-life recently reported by Robson[4] which differs materially from the older value employed by Hayashi.

It seems most likely that element synthesis is intimately connected with questions of cosmology. In the present work we consider the sequence of events up to the time when the rate of element formation became significant. As we shall see later in detail, all the constituents remained in thermodynamic equilibrium as the universe expanded and cooled to a temperature of ~ 10 Mev. At ~ 10 Mev the neutrinos were essentially frozen out of the equilibrium. By ~ 0.3 Mev the proton-neutron ratio was almost entirely determined by the free decay of the neutron. It remains for future study to re-examine the formation of the elements by thermonuclear reactions as a subsequent part of the picture developed here. A detailed chronology is given in a later portion of this paper [see Sec. V].

II. THE COSMOLOGICAL MODEL

The theory of element formation by non-equilibrium thermonuclear reactions has been developed as an integral part of the very early stages of the expanding universe. Detailed calculations of the necessary rate processes require a knowledge of the temporal behavior of temperature, density, and rate of expansion during these early epochs. The cosmological model that has been used previously for this purpose is the most general nonstatic model satisfying the requirements of general relativity, exhibiting homogeneity and isotropy, and which is composed of a perfect fluid with no interconversion of matter and radiation.[1,2] The rate of expansion and, implicitly, the rate of change of temperature in the expansion for this model, with no restrictions on the composition of the perfect working fluid, are given in relativistic units by the following differ-

where nuclei would be thermally stable, an appreciable number of protons had been generated. Then the capture of neutrons by protons provided the first step in the formation of the successively heavier elements. More specifically, the temperature for the beginning of building-up reactions was taken to be ~ 0.1 Mev (corresponding to a specific starting time for element building in the cosmological model used, in which $T = 1.52 \times 10^{10} t^{-\frac{1}{2}}$°K). This choice was dictated by the magnitude of the binding energy of the deuteron on the one hand and by the lack of evidence in the abundance data for any resonance neutron capture on the other hand. At the starting time, neutron decay had led to a proton-neutron ratio of $\sim 1:7$.

One of the approximations involved thus far in calculations with the neutron-capture theory has been the smoothing of available data on fast neutron radiative capture cross sections as a function of atomic weight. Moreover, reactions other than radiative neutron capture among the very lightest elements have been ignored.

[3] C. Hayashi, Progr. Theoret. Phys. (Japan) **5**, 224 (1950).

[4] J. M. Robson, Phys. Rev. **83**, 349 (1951).

ential equations:[5]

$$-\frac{e^{-g}}{R_0^2}-\frac{d^2g}{dt^2}-\frac{3}{4}\left(\frac{dg}{dt}\right)^2+\Lambda=8\pi p_0, \tag{1a}$$

$$\frac{3e^{-g}}{R_0^2}+\frac{3}{4}\left(\frac{dg}{dt}\right)^2-\Lambda=8\pi\rho_{00}, \tag{1b}$$

and

$$e^{\frac{1}{2}g(t)}=l/l_0=R/R_0, \tag{1c}$$

where l and R are proper distance and radius of curvature, respectively, given in units of l_0 and R_0, Λ is the cosmological constant, and p_0 and ρ_{00} are proper pressure and density. The quantities p_0 and ρ_{00} are functions of temperature and of l, and hence implicitly of time. Equation (1b) may also be rewritten, by using Eq. (1c), in the following form:

$$\frac{dl}{dt}=+\left(\frac{8\pi}{3}\rho_{00}l^2-\frac{l_0^2}{R_0^2}+\frac{\Lambda l^2}{3}\right)^{\frac{1}{2}}, \tag{2}$$

with the plus sign taken to indicate expansion. We have taken $\Lambda=0$ in keeping with current practice.[6] As can be easily shown, the constant term l_0^2/R_0^2 in Eq. (2) may be neglected in the application of this model to early epochs. This is equivalent to neglecting l^2e^{-g}/R_0^2 in Eq. (1). If $\rho_{00}\propto l^{-n}$ where $n>2$, then for sufficiently early times l will be so small that one has $8\pi\rho_{00}l^2/3 \propto 8\pi l^{2-n}/3\gg l_0^2/R_0^2$. Hence, for early epochs in the expansion one may replace Eq. (2) by

$$\frac{dl}{dt}=\frac{l}{2}\frac{dg}{dt}=+\left(\frac{8\pi}{3}\rho_{00}l^2\right)^{\frac{1}{2}}. \tag{3}$$

As has already been mentioned, the cosmological model, which is discussed in this paper, taken together with the presently observed smoothed-out matter density in the universe as well as the estimated age, are consistent with the supposition that during the early epochs of interest the matter density was much smaller than the radiation density (i.e., $\sim 1:10^6$). The neutron-capture theory of element formation[1] requires that the radiation density greatly exceeded the density of matter during the early epochs of the universal expansion. In this previous work it was not necessary to consider the interconversion of matter and radiation since for the epochs considered the temperature was already below that required to maintain a significant electron-pair density. Hence, the working fluid for the cosmological model was taken as black-body radiation, containing a trace of matter, and expanding adiabatically according to $T\propto 1/l$. It has been shown[1] that for early epochs Eq. (3) leads to the following expressions for the radiation density, ρ_γ, the matter density, ρ_m, the total density, ρ_{total}, the temperature, T, and proper distance, l, with $\rho_\gamma\gg\rho_m$:

$$\rho_{\text{total}}\cong\rho_\gamma\cong[3/(32\pi G)]t^{-2}=4.48\times10^5t^{-2}\ \text{g/cm}^3, \tag{4}$$

$$\rho_m=\rho_0t^{-\frac{3}{2}}\ \text{g/cm}^3, \tag{5}$$

$$T=(c^2\rho_\gamma/a_\gamma)^{\frac{1}{4}}=1.52\times10^{10}t^{-\frac{1}{2}}\text{°K}, \tag{6}$$

and

$$l=(32\pi G\rho_{\gamma''}l_0^4/3)^{\frac{1}{2}}t^{\frac{1}{2}}, \tag{7}$$

where G is the gravitational constant, c is the velocity of light, a_γ is the Stefan-Boltzmann constant, t is the time in seconds from the "start" of the expansion, $\rho_{\gamma''}$ is the density of radiation when $l=l_0$, and ρ_0 is a constant. As will be seen, the above equations are still valid in the case discussed in the present paper providing that $t\gtrsim100$ sec, ρ_γ is eliminated from Eq. (4), the constant 1.52 in Eq. (6) becomes 1.45 for Majorana neutrinos and 1.38 for Dirac neutrinos, and $\rho_{\gamma''}$ in Eq. (7) is replaced with the value of ρ_{total} when $l=l_0$. The quantity ρ_0 is the one arbitrary parameter in the simple neutron-capture theory. It has been adjusted in previous calculations[2] so that the density of matter at the start of the element-forming processes would lead to the observed cosmic abundance distribution. The cosmological model at early epochs described by Eqs. (4) and (6) was adopted by Hayashi as a basis for his calculation of the proton-neutron ratio.

While we have assumed a homogeneous and isotropic model of the universe in agreement with present astronomical evidence, it should be pointed out that this restriction is not necessary in the present considerations. Homogeneity is required only over a region of radius equal to ct since nothing further away can affect the cosmology or the elementary particle reactions to be discussed. At the universal age of $\sim$600 seconds corresponding to the end of the period of this study, the nuclear mass enclosed in the sphere of influence is $\sim10^{34}$ g, that is, $\sim$5 solar masses, and is much less at earlier epochs. Another way of looking at this result is that lengths greater than ct, in particular R_0 and any gradient of R_0, must be negligible because of the finite velocity of propagation of disturbances.

[5] R. C. Tolman, *Relativity, Thermodynamics and Cosmology* (Clarendon Press, Oxford, 1934).

[6] A very small value of Λ may be used to adjust the present age of this model, although it is of no consequence during the early epochs of interest here [see G. Gamow, Revs. Modern Phys. **21**, 367 (1949)]. In this connection it may be of interest to note that while Eqs. (1) and (2) contain a density singularity at zero time, they also implicitly contain the conclusion that the duration or age of the expansion from this singularity is finite. Taking $\Lambda=0$ and neglecting terms containing $1/R_0^3$ for early epochs, one can show that this age is given in cgs units by the following integral:

$$\mathfrak{a}=\int_0^{\mathfrak{a}}dt=\left(\frac{3}{8\pi G}\right)^{\frac{1}{2}}\int_{\rho(\mathfrak{a})}^{\infty}\frac{c^2d\rho}{\rho^{\frac{1}{2}}(p+\rho c^2)},$$

where p and ρ are total pressure and density. Since the pressure is positive,

$$\mathfrak{a}\leqq\left(\frac{3}{8\pi G}\right)^{\frac{1}{2}}\int_{\rho(\mathfrak{a})}^{\infty}\frac{d\rho}{\rho^{\frac{1}{2}}}=\left(\frac{3}{2\pi G\rho}\right)^{\frac{1}{2}}.$$

A lower bound on the duration may be obtained by noting that for a relativistic fluid $0\leqq p\leqq\rho c^2/3$. Hence

$$\mathfrak{a}\geqq\left(\frac{3}{8\pi G}\right)^{\frac{1}{2}}\int_{\rho(\mathfrak{a})}^{\infty}\frac{3d\rho}{4\rho^{\frac{1}{2}}}=\left(\frac{8}{3\pi G\rho}\right)^{\frac{1}{2}},$$

so that $\mathfrak{a}$ is bounded.

As already mentioned, the cosmological model outlined above was a sufficient approximation in previous calculations of the neutron-capture theory[1] because the temperature taken for the start of element formation was well below the electron rest mass equivalent and, therefore, reactions among elementary particles and photons could be ignored. One has only to consider that the nucleons and nuclei formed remained in thermal equilibrium with the expanding radiation field. These previous calculations, which were based on the time scale described by Eq. (6), continue to be valid provided ρ_0 is adjusted as required to fit the time scale to be described in this paper. The adjustment required is insignificant.

The study of the induced and inverse β processes involving neutrons and protons prior to any appreciable element formation concerns much earlier epochs and therefore much higher temperatures. In this case one must consider positrons, electrons, neutrinos, antineutrinos (if distinguishable from neutrinos), and radiation. The equation of state for radiation only, implicit in Eqs. (4)–(6), may no longer be an adequate approximation. We shall suppose that this mixture of elementary particles and photons is at a sufficiently high temperature for equilibrium to be maintained, but we shall not require temperatures so high as to require nucleon pairs. Furthermore, the nucleons present are assumed to have a negligible effect on pressure, density, and temperature, since even for temperatures as low as $\sim$0.1 Mev the nucleon density is many orders of magnitude less than the radiation density.

The density and pressure of the constituents of the medium may be obtained from the Fermi-Dirac and Bose-Einstein distribution laws for the number of particles in the energy range dE at E, *viz.*,

$$N(E)dE=\frac{4\pi}{h^3}\sum'|\mathbf{p}|E[\exp(E/kT)\pm1]^{-1}dE, \quad (8)$$

where $|\mathbf{p}|$ is the momentum, and the summation, $\sum'$, is over charge and spin states. In the present calculation the number of particles and photons is not conserved so that a degeneracy parameter is not required. The density and pressure, according to Eq. (8), are given by

$$\rho(T)=\frac{4\pi}{c^2h^3}\sum'\int_{mc^2}^{\infty}|\mathbf{p}|E^2[\exp(E/kT)\pm1]^{-1}dE, \quad (9a)$$

and

$$p(T)=\frac{4\pi}{3h^3}\sum'\int_{mc^2}^{\infty}|\mathbf{p}|^3[\exp(E/kT)\pm1]^{-1}dE, \quad (9b)$$

where

$$|\mathbf{p}|=(1/c)(E^2-m^2c^4)^{\frac{1}{2}}. \quad (9c)$$

In particular, for electrons and positrons one obtains, with the transformation $E=m_ec^2\cosh\theta$, the following:

$$\rho_{e^-}=\rho_{e^+}=\frac{a_e}{c^2}\int_0^{\infty}\frac{\sinh^2\theta\cosh^2\theta d\theta}{1+\exp(x\cosh\theta)}\ \text{g/cm}^3, \quad (10a)$$

$$p_{e^-}=p_{e^+}=\frac{a_e}{3}\int_0^{\infty}\frac{\sinh^4\theta d\theta}{1+\exp(x\cosh\theta)}\ \text{dynes/cm}^2. \quad (10b)$$

In these equations

$$a_e=8\pi m_e^4c^5/h^3; \quad (11a)$$

m_e and h are the electron rest mass and Planck's constant, respectively;

$$x=m_ec^2/(kT) \quad (11b)$$

defines temperature in units of the electron rest mass, and k is Boltzmann's constant. Spin states have been counted in the above expressions, and the total electron energy includes rest mass.

In order to carry out numerical calculations, it should be noted that the definite integrals in the expressions for $p_e(x)$ and $\rho_e(x)$ can be expanded in series of modified Bessel functions $K_i(nx)$. One can write

$$f_0=\int_0^{\infty}[1+\exp(x\cosh\theta)]^{-1}d\theta=\sum_{n=1}^{\infty}(-1)^{n+1}K_0(nx), \quad (12)$$

$$f_1=\int_0^{\infty}\sinh^2\theta[1+\exp(x\cosh\theta)]^{-1}d\theta$$

$$=x^{-1}\sum_{n=1}^{\infty}(-1)^{n+1}n^{-1}K_1(nx), \quad (13)$$

and

$$f_2=\int_0^{\infty}\sinh^4\theta[1+\exp(x\cosh\theta)]^{-1}d\theta$$

$$=3x^{-2}\sum_{n=1}^{\infty}(-1)^{n+1}n^{-2}K_2(nx), \quad (14)$$

so that

$$\rho_e(x)=\rho_{e^-}+\rho_{e^+}=(2a_e/c^2)(f_1+f_2), \quad (15)$$

and

$$p_e(x)=p_{e^-}+p_{e^+}=(2a_e/3)f_2. \quad (16)$$

In the high temperature limit, $kT\gg mc^2$, which is equivalent to setting $m=0$ in Eqs. (9), the density and pressure for all Bose-Einstein particles approach those for photons except for factors which depend on spin and charge states. Similarly, for Fermi-Dirac particles the density and pressure approach those for neutrinos, again except for a factor which accounts for differing charge and spin states.

For radiation, taking into account the two states of polarization, one obtains the following from the Bose-Einstein integral:

$$\rho_\gamma=\frac{a_\gamma}{c^2}T^4=\left(\frac{\pi^4a_e}{15c^2}\right)x^{-4}\ \text{g/cm}^3, \quad (17)$$

and

$$p_\gamma = \tfrac{1}{3}\rho_\gamma c^2 \text{ dynes/cm}^2, \tag{18}$$

where

$$a_\gamma = 8\pi^5 k^4/15c^3h^3. \tag{18a}$$

For neutrinos we consider two cases,[7] namely, neutrinos and antineutrinos indistinguishable ($\nu \equiv \nu^*$) and distinguishable ($\nu \not\equiv \nu^*$). For the temperature range in which the neutrinos are in thermal equilibrium with the other constitutents of the medium, the Fermi-Dirac integral gives

for $\nu \equiv \nu^*$:

$$\rho_\nu = \tfrac{7}{8}\rho_\gamma, \tag{19}$$

and

$$p_\nu = \tfrac{7}{8}p_\gamma; \tag{20}$$

for $\nu \not\equiv \nu^*$:

$$\rho_\nu = \rho_{\nu^*} = \tfrac{7}{8}\rho_\gamma, \tag{21}$$

and

$$p_\nu = p_{\nu^*} = \tfrac{7}{8}p_\gamma, \tag{22}$$

so that the neutrino pressure and density in the latter case are twice those in the former. It should be noted that the results stated in Eqs. (19)–(22) are predicated on the assumption that no type of particle is degenerate in the present problem. The simple expressions for the neutrino density and pressure given in Eqs. (19)–(22) hold for all Fermi-Dirac particles in the limit of sufficiently high temperature, i.e., there is a contribution to the density of $(7/16)\rho_\gamma$ for each degree of freedom. Similarly for Bose-Einstein particles there is a contribution to the density of $\frac{1}{2}\rho_\gamma$ for each degree of freedom.

It can be shown from Eq. (9) that for a Fermi-Dirac particle of mass, m_i,

$$\rho_i(x) \propto \left(\frac{m_i}{m_e}\right)^4 \rho_\nu[(m_i/m_e)x],$$

with the proportionality factor depending on the previously mentioned spin and charge states. Thus all Fermi-Dirac particles exhibit the same behavior provided that an appropriate shift is made in the temperature scale. A similar result can be obtained for Bose-Einstein particles. The qualitative behavior of ρ_i *versus* T after suitable normalization of the temperature scales is essentially the same for fermions and bosons.

The neutrino contribution given by Eqs. (19)–(22) to the total pressure and density requires modification for the temperature range of interest in calculating the proton-neutron ratio as a function of the time. At very high temperatures the neutrino component maintains itself in equilibrium with the other constituents of of the medium through interaction with mesons. When the medium has expanded and cooled somewhat below a temperature equivalent to the rest mass of the lightest meson, the neutrinos freeze in and continue to expand and cool adiabaticallv as would a pure radiation gas. After this freeze-in the neutrino temperature will differ from that of the other components of the medium. It will be seen that the freeze-in must have occurred at a temperature higher than is required for neutrons and protons to be very nearly in thermodynamic equilibrium. For the temperature region of interest, then, we must deal with nucleons, electrons, positrons, and radiation at one temperature, and neutrinos at another temperature. The calculation of the neutron-proton ratio does not require that a specific freeze-in temperature be given, but only that neutrinos be frozen in before an appreciable fraction of the electron pairs start to annihilate.

It is of some interest to examine in more detail the freezing in of neutrinos during the period from ~15 to ~5 Mev. Non-equilibrium reactions involving neutrinos become important only below ~5 Mev. When the temperature was well above the rest mass equivalent of mesons, the neutrinos maintained equilibrium through interaction with mesons. At such temperatures the contribution of mesons to the density was $3.25\rho_\gamma$, while the total contribution due to photons, electrons, positrons, and neutrinos was $3.625\rho_\gamma$ or $4.50\rho_\gamma$, for $\nu \equiv \nu^*$ and $\nu \not\equiv \nu^*$, respectively.[8] Since the meson rest energy is distributed uniformly among the lighter particles when the mesons annihilate, it is clear that the number of neutrinos will about double when meson annihilation occurs. Now the bulk of mesons will annihilate when the temperature in the universal expansion has dropped significantly below that equivalent to $m_\mu c^2$ (~108 Mev) or $m_\pi c^2$ (~138 Mev), down to 10 Mev. At 10 Mev the Boltzmann factors for μ and π mesons are $\sim 2\times 10^{-5}$ and $\sim 10^{-6}$, respectively. This temperature decrease, as will be seen later when the time scale for the cosmological model is calculated, requires a duration of $\sim 10^{-2}$ sec in the universal expansion.

The meson reactions $\pi^\pm \rightleftarrows \mu^\pm + \nu$ and $\mu^\pm \rightleftarrows e^\pm + 2\nu$ are very fast, even if one neglects induced decay, having lifetimes of $\sim 2\times 10^{-8}$ sec and $\sim 2\times 10^{-6}$ sec, respectively. Since the concentrations of neutrinos and mesons are comparable, the reaction rate $1/(2\times 10^{-8})$ per second per neutrino is $\sim 10^6$ times the equilibrium rate (due to annihilation) of $\sim 1/10^{-2}$ per second per neutrino. Hence between ~100- and ~10-Mev thermal equilibrium holds. By 5 Mev, however, the Boltzmann factor $\exp(-m_\mu c^2/kT) \cong \exp(-138/5)$ has reduced the reaction rate to insignificance even though there is a

[7] Recently, theoretical arguments in favor of distinguishability, i.e., against the Majorana theory of neutral particles, have been given by E. R. Caianiello, Phys. Rev. **86**, 564 (1952). However, we consider both cases throughout this paper because it does not appear to be a settled question at this time. [See also C. S. Wu, Physica **18**, 989 (1952).]

[8] As has been shown, in the high temperature limit the Fermi-Dirac μ^+ and μ^- mesons each contribute $(7/8)\rho_\gamma$, while the Bose-Einstein π^+, π^-, and π^0 mesons each contribute $(1/2)\rho_\gamma$ for a total of $3.25\rho_\gamma$. Electrons and positrons each contribute $(7/8)\rho_\gamma$, neutrinos contribute $(7/8)\rho_\gamma$ or $2(7/8)\rho_\gamma$ according as $\nu \equiv \nu^*$ or $\nu \not\equiv \nu^*$, and photons contribute ρ_γ for a total of $3.625\rho_\gamma$ or $4.50\rho_\gamma$. The numerical factors obtained here depend on the discussion following Eq. (17).

good deal more time available for reactions to take place due to the reduced rate of cooling in the universal expansion. Hence the residual mesons cannot transfer a significant amount of rest mass energy to the neutrino gas, although almost all the meson rest mass energy is uniformly distributed.

Having described the nature of the medium, we can now proceed to determine the universal expansion rate for the period of interest in this problem. The rate of expansion for early times, Eq. (3), can be written in cgs units as

$$\frac{1}{2}\frac{dg}{dt}=\frac{1}{l}\frac{dl}{dt}=\frac{d\ln l}{dt}=\left(\frac{8\pi G}{3}\right)^{\frac{1}{2}}\rho^{\frac{1}{2}}, \tag{23}$$

where ρ, the total density, may now be written

$$\rho(x,l)=\rho(x)+\rho(l), \tag{24}$$

for the following reason. The quantity

$$\rho(x)=\rho_{e^+}+\rho_{e^-}+\rho_\gamma \tag{24a}$$

depends only on the temperature, while

$$\rho(l)=\rho_\nu \text{ (or } \rho_\nu+\rho_{\nu^*}) \tag{24b}$$

depends only on the proper distance l, since the neutrinos are expanding adiabatically as a radiation gas after freeze-in. We can, in fact, write $\rho_\nu \propto l^{-4}$, so that Eq. (23) can be rewritten as follows, after differentiation with respect to time:

$$\frac{d^2g}{dt^2}=\left(\frac{8\pi G}{3\rho}\right)^{\frac{1}{2}}\left(\frac{\partial\rho}{\partial\ln x}\frac{d\ln x}{dt}+\frac{\partial\rho}{\partial\ln l}\frac{d\ln l}{dt}\right). \tag{25}$$

Substituting for $\rho^{\frac{1}{2}}$ from Eq. (23) and using Eq. (24) yields

$$\frac{d^2g}{dt^2}=\frac{8\pi G}{3}\left[\frac{d\rho(x)}{d\ln x}\frac{d\ln x}{d\ln l}-4\rho(l)\right]. \tag{26}$$

If now we add Eqs. (1a) and (1b), neglect terms containing $1/R_0^2$, and convert to cgs units, we obtain

$$\frac{d^2g}{dt^2}=-\left(\frac{8\pi G}{c^2}\right)(p+\rho c^2)$$

$$=-\left(\frac{8\pi G}{c^2}\right)[p(x)+p(l)+\rho(x)c^2+\rho(l)c^2]. \tag{27}$$

If we equate Eqs. (26) and (27) and note that $(4/3)\rho(l)c^2=p(l)+\rho(l)c^2$, then we obtain

$$\frac{d\ln l}{d\ln x}=\frac{-c^2}{3[p(x)+\rho(x)c^2]}\frac{d\rho(x)}{d\ln x}, \tag{28}$$

where

$$\frac{d\rho(x)}{d\ln x}=\frac{dp_e(x)}{d\ln x}-\frac{3}{c^2}[p_\gamma(x)+\rho_\gamma(x)c^2]. \tag{28a}$$

This result is independent of the presence of the frozen-in neutrinos. Equation (28) can now be integrated in the following manner. From Eqs. (10) one obtains

$$\frac{dp_e(x)}{d\ln x}=-(p_e+\rho_e c^2), \tag{29}$$

or, more conveniently,

$$c^2x^4\frac{d\rho_e}{d\ln x}=-3x^4(p_e+\rho_e c^2)+\frac{d}{d\ln x}[x^4(p_e+\rho_e c^2)]. \tag{29a}$$

Employing Eq. (29a) in Eqs. (28) yields the desired result, namely,

$$\frac{d\ln l}{d\ln x}=1-\frac{\dfrac{d}{d\ln x}\{x^4[p(x)+\rho(x)c^2]\}}{3x^4[p(x)+\rho(x)c^2]}. \tag{30}$$

Since the adiabatic expansion of a radiation universe leads[1] to $d\ln l/d\ln x=1$, the second term in Eq. (30) represents a correction to the description of the cosmological model previously used with the neutron-capture theory, a correction which accounts for the interconversion of matter and radiation. Equation (30) may be integrated to yield

$$\ln l=\ln x-\tfrac{1}{3}\ln\{x^4[p(x)+\rho(x)c^2]\}+\text{constant}. \tag{31}$$

Finally, using Eqs. (10)–(14), one can write Eq. (25) as

$$\frac{d\ln l}{d\ln x}=1+\frac{2a_e(f_0+2f_1)}{3[p(x)+\rho(x)c^2]}. \tag{32}$$

As will become evident, Eq. (32) is required in order to obtain the explicit time dependence of the temperature.

The neutrino temperature T_ν (or $x_\nu=m_ec^2/kT_\nu$) may be determined from Eq. (30) by recalling that during the period of interest the neutrinos expand and cool adiabatically, so that $x_\nu=f(l)$ only, and in fact, $x_\nu \propto l$. Then it follows that Eq. (31) can be written as

$$\ln x_\nu=\ln x-\tfrac{1}{3}\ln\{x^4[p(x)+\rho(x)c^2]\}+\text{constant}. \tag{33}$$

The constant of integration can be evaluated by noting that for small x (high temperatures) the neutrino temperature approaches the temperature of the rest of the medium. In fact, as $x\to 0$, $x_\nu\to x$ so that the integration constant becomes

$$\text{constant}=\tfrac{1}{3}\ln\{x^4[p(x)+\rho(x)c^2]\}\,|_{x=0}. \tag{34}$$

From the definition of p_γ and ρ_γ it is evident [see discussion following Eq. (22)] that, for any x, $\rho_\gamma c^2x^4=\text{constant}=\pi^4a_e/15$, and $p_\gamma x^4=\frac{1}{3}\rho_\gamma c^2x^4$. Since

$$\lim_{x\to 0}p_ex^4=2(7/8)p_\gamma x^4, \quad \lim_{x\to 0}\rho_ec^2x^4=2(7/8)\rho_\gamma c^2x^4,$$

TABLE I. Time scales, rate coefficients, and quantum statistical integrals.[a]

T(°K)	x	t(sec) $\nu \equiv \nu^*$	t(sec) $\nu \not\equiv \nu^*$	t(sec) rad. model[b]	$\frac{15x^4}{\pi^4} f_0$	$\frac{15x^4}{\pi^4} f_1$	$\frac{15x^4}{\pi^4} f_2$	K_n	K_p
∞	0	0	0	0	0	0	0.87500	∞	∞
5.930×10^{10}	0.1	0.04	0.04	0.06	2.2105×10^{-5}	1.2535×10^{-3}	0.87311	5.07×10^{6}	3.94×10^{6}
2.965×10^{10}	0.2	0.14	0.12	0.26	2.6866×10^{-4}	4.9011×10^{-2}	0.86754	1.91×10^{5}	1.12×10^{5}
1.482×10^{10}	0.4	0.55	0.50	1.05	2.9583×10^{-3}	1.8300×10^{-2}	0.84626	7.58×10^{3}	2.51×10^{3}
9.884×10^{9}	0.6	1.27	1.14	2.36	1.1131×10^{-2}	3.7625×10^{-2}	0.81339	1.17×10^{3}	2.34×10^{2}
7.413×10^{9}	0.8	2.26	2.02	4.20	2.6998×10^{-2}	6.0185×10^{-2}	0.77190	3.09×10^{2}	37.8
5.930×10^{9}	1.0	3.58	3.21	6.57	5.1303×10^{-2}	8.3590×10^{-2}	0.72406	1.18×10^{2}	9.37
2.965×10^{9}	2.0	15.65	14.12	26.28	0.25584	0.16512	0.46121	6.88	4.00×10^{-2}
1.977×10^{9}	3.0	39.72	36.05	59.11	0.41847	0.16423	0.25402	2.38	9.49×10^{-4}
1.482×10^{9}	4.0	78.99	72.04	105.20	0.43426	0.12227	0.12828	1.91	2.69×10^{-5}
1.186×10^{9}	5.0	134.15	122.64	164.25	0.35354	7.7674×10^{-2}	6.1253×10^{-2}	1.74	...
9.884×10^{8}	6.0	203.84	186.56	236.49	0.24783	4.4664×10^{-2}	2.8128×10^{-2}	...	...
8.472×10^{8}	7.0	285.68	261.76	321.90	0.15696	2.3982×10^{-2}	1.2552×10^{-2}	...	...
7.413×10^{8}	8.0	378.40	347.03	420.44	9.2363×10^{-2}	1.2248×10^{-2}	5.4786×10^{-3}	...	...
6.589×10^{8}	9.0	481.59	442.06	532.17	5.1402×10^{-2}	6.0209×10^{-3}	2.3499×10^{-3}	...	...
5.930×10^{8}	10.0	595.56	546.96	657.02	2.7379×10^{-2}	2.8716×10^{-3}	9.9368×10^{-4}	...	...
0	∞	∞	∞	∞	0	0	0	1.63	0

[a] The universal constants employed in these calculations are those given by J. A. Bearden and H. M. Watts, Phys. Rev. **81**, 73 (1951). Note that the limiting values at high temperatures do not include any contributions from mesons.
[b] This column gives the time scale for the pure radiation model described by Eqs. (4)–(7).

it follows that Eq. (33) can be written as

$$\left(\frac{x_\nu}{x}\right)^3=\left(\frac{T}{T_\nu}\right)^3=\frac{2.75(p_\gamma+\rho_\gamma c^2)}{p(x)+\rho(x)c^2}, \tag{35}$$

from which the neutrino temperature can be determined for any value of x. For the sake of completeness it should be noted that

$$\lim_{x\to\infty} p_e x^4=0, \quad \lim_{x\to\infty}\rho_e c^2 x^4=0,$$

while the quantities $p_\gamma x^4$ and $\rho_\gamma c^2 x^4$ are constants for all x, as just described.

One other relationship which we shall require is that between temperature and time. This is obtained by multiplying Eq. (23) by $d\ln x/d\ln l$, as evaluated from Eq. (32), with the following result:

$$\frac{d\ln x}{dt}=\frac{d\ln x}{d\ln l}\frac{d\ln l}{dt}=\left(\frac{8\pi G}{3}\rho\right)^{\frac{1}{2}}\frac{d\ln x}{d\ln l}. \tag{36}$$

The integration of Eq. (36) (performed to an accuracy better than 0.1 percent on a Maddida, a digital differential analyzer built by Northrup Aircraft, Inc.) for the two cases $\nu\equiv\nu^*$ and $\nu\not\equiv\nu^*$ gives the time in the universal expansion as a function of x, and these quantities are given in Table I. For comparison, Table I also contains the time as a function of x for the expanding cosmological model containing radiation only [see Eq. (6)]. Other quantities given in Table I are the series of modified Bessel functions f_0, f_1, and f_2, as defined in Eqs. (12)–(14), which are used in computing pressure and density. In Table II are given the total density ρ

TABLE II. Neutrino temperature; total, radiation, and electron-pair densities; and universal expansion rates.[a]

T(°K)	x	x_ν/x	ρ_γ (g/cm³)	ρ/ρ_γ $(\nu\equiv\nu^*)$	ρ/ρ_γ $(\nu\not\equiv\nu^*)$	ρ_e/ρ_γ	$\frac{d\ln}{d\ln x}$	$\frac{d\ln l}{dt}$(sec⁻¹) $(\nu\equiv\nu^*)$	$\frac{d\ln l}{dt}$(sec⁻¹) $(\nu\not\equiv\nu^*)$
∞	0	1.0000	∞	3.625	4.500	1.750	1.0000	∞	∞
5.930×10^{10}	0.1	1.0002	7.226×10^{7}	3.623	4.497	1.749	1.0005	14.51	16.17
2.965×10^{10}	0.2	1.0009	4.516×10^{6}	3.617	4.488	1.745	1.0018	3.625	4.039
1.482×10^{10}	0.4	1.0037	2.822×10^{5}	3.591	4.454	1.729	1.0073	0.9031	1.006
9.884×10^{9}	0.6	1.0082	5.575×10^{4}	3.549	4.396	1.702	1.0161	0.3990	0.4441
7.413×10^{9}	0.8	1.0145	1.764×10^{4}	3.490	4.317	1.664	1.0280	0.2226	0.2475
5.930×10^{9}	1.0	1.0224	7.226×10^{3}	3.416	4.217	1.615	1.0424	0.1409	0.1566
2.965×10^{9}	2.0	1.0821	4.516×10^{2}	2.891	3.529	1.253	1.1350	3.241×10^{-2}	3.581×10^{-2}
1.977×10^{9}	3.0	1.1616	89.20	2.317	2.798	0.836	1.2129	1.290×10^{-2}	1.417×10^{-2}
1.482×10^{9}	4.0	1.2407	28.22	1.870	2.240	0.501	1.2357	6.517×10^{-3}	7.132×10^{-3}
1.186×10^{9}	5.0	1.3044	11.56	1.580	1.882	0.278	1.2054	3.834×10^{-3}	4.184×10^{-3}
9.884×10^{8}	6.0	1.3478	5.575	1.411	1.676	0.146	1.1501	2.516×10^{-3}	2.742×10^{-3}
8.472×10^{8}	7.0	1.3736	3.009	1.319	1.564	0.073	1.0966	1.787×10^{-3}	1.946×10^{-3}
7.413×10^{8}	8.0	1.3876	1.764	1.271	1.508	0.035	1.0568	1.343×10^{-3}	1.463×10^{-3}
6.589×10^{8}	9.0	1.3947	1.101	1.248	1.479	0.017	1.0313	1.052×10^{-3}	1.145×10^{-3}
5.930×10^{8}	10.0	1.3981	0.7226	1.237	1.466	0.008	1.0165	8.480×10^{-4}	9.231×10^{-4}
0	∞	1.4010	0	1.227	1.454	0	1.0000	0	0

[a] The universal constants employed in these calculations are those given by J. A. Bearden and H. M. Watts, Phys. Rev. **81**, 73 (1951). Note that the limiting values at high temperatures do not include any contributions from mesons.

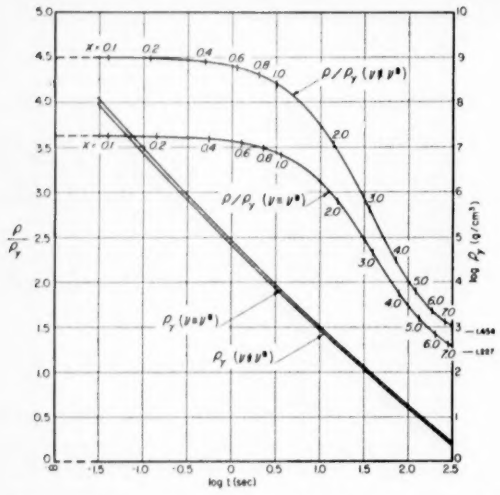

FIG. 1. Total density ρ, in units of photon density ρ_γ, and ρ_γ *versus* time during the very early epochs of the expanding universe for Majorana and Dirac neutrinos. The corresponding temperatures are given in terms of $x=m_e c^2/kT$. The ρ/ρ_γ curves are extrapolated to $t=0$ without regard to the presence of mesons and other elementary particles.

(i.e., the density of electrons, positrons, neutrinos, and radiation) and the density of electrons plus positrons, ρ_e, in units of the radiation density, ρ_γ, the neutrino temperature expressed as $x_\nu/x=T/T_\nu$, the differential quotient $d\ \mathrm{ln}l/d\ \mathrm{ln}x$, and finally the expansion rate $d\ \mathrm{ln}l/dt$.

Several interesting features of this cosmological model are evident upon examination of Tables I and II. First, the temperature drops much more rapidly in the nonstatic model with interconversion of matter and radiation than it does in the model of adiabatically expanding radiation only.[9] However the cases of distinguishable and indistinguishable neutrinos differ very little in this respect. The total density ρ does not drop off very greatly until the universe has cooled to about the electron rest mass equivalent. At this point the large density contribution of electron pairs begins to decrease sharply [see Table II] as the pairs disappear by annihilation into the radiation field which has fewer degrees of freedom. This behavior is demonstrated in Fig. 1. Next, if one recalls that the expanding model of radiation only is represented by $d\ \mathrm{ln}l/d\ \mathrm{ln}x=1$, then one can see in Table II that the maximum deviation from this model due to the interconversion of matter and radiation is $\sim$24 percent, and this occurs at 0.125 Mev ($\sim m_e c^2/4$). This deviation represents a more rapid expansion rate than in the pure radiation model and, in fact, the expansion rate $d\ \mathrm{ln}l/dt$ is higher in the model with interconversion by just the factor $(\rho/\rho_\gamma)^{\frac{1}{2}}$. Finally, it should be noted that x_ν/x (a quantity which does not depend on whether $\nu\equiv\nu^*$ or $\nu\not\equiv\nu^*$) differs from unity by less than one percent until x has increased to about 0.7 or $kT\cong 0.73$ Mev. At $x=0.1$, where $kT=5$ Mev, the deviation is 0.02 percent. It is then quite clear that selecting say 5–10 Mev as the freeze-in temperature for neutrinos is not only reasonable but quite an adequate approximation. It should be noted that the mathematical limits approached as $x\to\infty$ for all the quantities given in Tables I and II are included for the sake of completeness. However, the behavior of the cosmological model discussed changes at longer times, $x\sim 10^7$, when the density of matter exceeds the density of radiation.

In the next section we shall calculate the relative concentrations of neutrons and protons as a function of the time in the universal expansion. This ratio, it will be recalled, plays a most important role in determining the relative abundances of the nuclear species as calculated according to the simple neutron-capture theory of element formation including the effects of thermonuclear reactions. As has been stated, this theory quite clearly requires that during the early epochs in the universal expansion the density of nucleons, and of the nuclear species formed, should be negligibly small compared with the radiation density. Consequently, the physical conditions in the expanding model as described in Tables I and II, in which nucleon density is taken to be negligible, are used as a basis for examining the various non-equilibrium reactions between neutrons and protons.

III. THE NEUTRON-PROTON RATIO

In this section we shall examine the reactions which may occur among neutrinos, electrons, positrons, and nucleons in the very early stages of the cosmological model described in the previous section. In particular we shall calculate the ratio of the concentrations of protons and neutrons as a function of time, a ratio upon which the results of the neutron-capture theory of element formation strongly depend.

The nuclear reactions which must be considered in determining the proton-neutron ratio are the following:[10]

$$n+e^+\rightleftarrows p+\nu, \tag{37a}$$

$$n+\nu\rightleftarrows p+e^-, \tag{37b}$$

$$n\rightleftarrows p+e^-+\nu. \tag{37c}$$

[9] There are perhaps slight shifts in the expansion time scale, much too small to appear with the number of significant figures given in Tables I and II. These are caused by the presence of and annilation of mesons, nucleons, gravitons, etc., between $x=0$ and $x=0.1$, should such particles exist during this epoch, and should the relativistic cosmology apply at the extreme conditions existing during this very brief early period. There is, however, serious doubt that the cosmology applies and, since we are interested only in the epochs of temperature lower than $x=0.1$, we can for the present perhaps ignore this problem and accept the insignificant additive constant in the time scale. See reference 1 as well as A. Einstein, *The Meaning of Relativity* (Princeton University Press, Princeton, 1945).

[10] The question of the existence of the antineutrino is of no concern in determining the individual reaction rates (see reference 7). In the absence of charge, mass, and magnetic moment, the absorption of a neutrino from a negative energy state is in all respects equivalent to the emission of an antineutrino.

The probability per second w for these reactions may be obtained from the Fermi theory of β decay. For the reaction $n+e^+\rightarrow p+\nu$, one has, per electron

$$w_{A'}=\frac{2\pi}{\hbar}(|\psi_p(0)|\cdot|\psi_\nu(0)|\cdot|\mathfrak{M}|g)^2\frac{dn}{dE}\ \text{sec}^{-1}, \quad (38)$$

where the expectation value at the origin for the product particles, proton, and neutrino, depends on $|\psi_p(0)|^2|\psi_\nu(0)|^2$, the ψ are taken as plane wave states, $\mathfrak{M}$, the matrix element, is taken as unity for lack of a better estimate, g is the Fermi coupling constant and the quantity dn/dE is the energy density of available final states. We can, therefore, write

$$w_{A'}=\frac{2\pi g^2}{\hbar\Omega^2}\frac{dn}{dE}\ \text{sec}^{-1}, \quad (39)$$

where Ω is any finite normalization volume. For the neutrino the number of available states per unit energy in the volume Ω is the difference between the total and occupied number of states, *viz.*,

$$\frac{4\pi(2i_\nu+1)|\mathbf{p}_\nu|}{2\pi\hbar^3}\{1-[1+\exp(E_\nu/kT_\nu)]^{-1}\}\frac{d|\mathbf{p}_\nu|}{dE_\nu}, \quad (40a)$$

while for each neutron the number of available final states in this particular reaction is $(2i_p+1)$. Since all neutrons are equivalent, one may write for the total number of final states in Ω:

$$\Omega n_n(2i_p+1)=2\Omega n_n. \quad (40b)$$

In Eqs. (40) the neutrino and proton spins are denoted by i_ν and i_p, $|\mathbf{p}_\nu|$ is the neutrino momentum and n_n the number of neutrons per unit volume. Since dn/dE n Eq. (39) is the product of terms given by Eq. (40a) and Eq. (40b) one can write

$$w_{A'}=\frac{4g^2n_n|\mathbf{p}_\nu|\exp(E_\nu/kT_\nu)}{\pi\hbar^4[1+\exp(E_\nu/kT_\nu)]}\frac{d|\mathbf{p}_\nu|}{dE_\nu}\ \text{sec}^{-1}. \quad (41)$$

The number of such reactions, $n+e^+\rightarrow p+\nu$, per second per unit volume, is given by

$$A'n_nn_{e^+}=\int_{m_ec^2}^{\infty}w_{A'}n_{e^+}(E_{e^+})dE_{e^+}, \quad (42)$$

where

$$E_\nu=E_{e^+}+Q; \quad (42a)$$

$$Q=(m_n-m_p)c^2 \quad (42b)$$

is the neutron-proton energy difference and n_{e^+} is the concentration of positrons per unit energy at E_{e^+}. The lower limit of integration is the threshold energy, which in this case is the electron rest energy. Using the relation $E_\nu=|\mathbf{p}_\nu|c$ and replacing n_{e^+} by means of the Fermi-Dirac integral, *viz.*,

$$n_{e^+}(|\mathbf{p}_{e^+}|)d|\mathbf{p}_{e^+}|=\frac{8\pi|\mathbf{p}_{e^+}|^2d|\mathbf{p}_{e^+}|}{(2\pi\hbar^3)[1+\exp(E_{e^+}/kT)]}, \quad (43)$$

where $|\mathbf{p}_{e^+}|$ is given by Eq. (9c), one can write Eq. (42) in the form

$$A'n_nn_{e^+}=a_0n_n\int_{m_ec^2}^{\infty}\frac{E_{e^+}(E_{e^+}+Q)^2(E_{e^+}^2-m_e^2c^4)^{\frac{1}{2}}\exp[(E_{e^+}+Q)/kT_\nu]}{\{1+\exp[(E_{e^+}+Q)/kT_\nu]\}\{1+\exp[E_{e^+}/kT]\}}dE_{e^+}, \quad (44)$$

where Eq. (42a) has been used to eliminate E_ν, and

$$a_0=(4g^2)/(\pi^3c^6\hbar^7). \quad (44a)$$

It should be recalled that the neutrino temperature $T_\nu\neq T$, where the latter is the temperature of the remainder of the medium. Equation (44) may be rewritten by taking

$$\begin{aligned} &x=m_ec^2/(kT), \quad x_\nu=m_ec^2/(kT_\nu),\\ &q=Q/(m_ec^2), \qquad \epsilon=E_e/(m_ec^2), \end{aligned} \quad (45)$$

with the result that for the reaction $n+e^+\rightarrow p+\nu$,

$$A'n_nn_{e^+}=m_e^5c^{10}a_0n_nI_{A'}\ \text{sec}^{-1}\ \text{cm}^{-3}, \quad (46)$$

where

$$I_{A'}=\int_1^{\infty}\frac{\epsilon(\epsilon+q)^2(\epsilon^2-1)^{\frac{1}{2}}\exp[(\epsilon+q)x_\nu]d\epsilon}{\{1+\exp[\epsilon x]\}\{1+\exp[(\epsilon+q)x_\nu]\}}. \quad (46a)$$

Rates for the other reactions in Eq. (37a) and Eq. (37b) may be obtained from similar considerations, since they are all of second degree. One obtains the following:

for $p+\nu\rightarrow n+e^+$,

$$An_pn_\nu=m_e^5c^{10}a_0n_pI_A\ \text{sec}^{-1}\ \text{cm}^{-3}, \quad (47)$$

where

$$I_A=\int_1^{\infty}\frac{\epsilon(\epsilon+q)^2(\epsilon^2-1)^{\frac{1}{2}}\exp(\epsilon x)d\epsilon}{\{1+\exp[\epsilon x]\}\{1+\exp[(\epsilon+q)x_\nu]\}}, \quad (47a)$$

and where

$$E_{e^+}=E_\nu-Q; \quad (47b)$$

for $n+\nu\rightarrow p+e^+$,

$$B'n_nn_\nu=m_e^5c^{10}a_0n_nI_{B'}\ \text{sec}^{-1}\ \text{cm}^{-3}, \quad (48)$$

where

$$I_{B'}=\int_q^{\infty}\frac{\epsilon(\epsilon-q)^2(\epsilon^2-1)^{\frac{1}{2}}\exp(\epsilon x)d\epsilon}{\{1+\exp[\epsilon x]\}\{1+\exp[(\epsilon-q)x_\nu]\}}, \quad (48a)$$

and where

$$E_\nu=E_{e^-}-Q; \quad (48b)$$

for $p+e^-\rightarrow n+\nu$,

$$Bn_pn_{e^-}=m_e^5c^{10}a_0n_pI_B\ \text{sec}^{-1}\ \text{cm}^{-3}, \quad (49)$$

where

$$I_B=\int_q^\infty \frac{\epsilon(\epsilon-q)^2(\epsilon^2-1)^{\frac{1}{2}}\exp[(\epsilon-q)x_\nu]d\epsilon}{\{1+\exp[\epsilon x]\}\{1+\exp[(\epsilon-q)x_\nu]\}}, \quad (49a)$$

and where

$$E_\nu=E_{e^-}-Q. \quad (49b)$$

The reaction rates for free neutron decay and the inverse process, Eq. (37c), require a slightly different calculation. Thus for the reaction $p+e^-+\nu\rightarrow n$, we note that the quantity dn/dE in Eq. (39) is given by just the number of protons present in the volume Ω, so that

$$w_C=(2\pi g^2/\hbar)n_p(2i_n+1),$$

and

$$Cn_pn_{e^-}n_\nu=\int_{m_ec^2}^{Q} w_C(E_{e^-})n_{e^-}(E_{e^-})n_\nu(Q-E_{e^-})dE_{e^-}, \quad (50)$$

where

$$E_{e^-}=Q-E_\nu. \quad (50a)$$

In Eq. (50) $n_{e^-}(E_{e^-})$ is the concentration of electrons per unit energy at E_{e^-} and $n_\nu(Q-E_{e^-})$ is the concentration of neutrinos per unit energy at $(Q-E_{e^-})$, the argument of n_ν being that required for energy balance in this reaction. Finally, one can rewrite Eq. (50) replacing n_{e^-} and n_ν by means of the Fermi-Dirac integral [see Eq. (43)] and using Eqs. (45), as

$$Cn_pn_{e^-}n_\nu=m_e{}^5c^{10}a_0n_pI_C \text{ sec}^{-1}\text{ cm}^{-3}, \quad (51)$$

where

$$I_C=\int_1^q \frac{\epsilon(\epsilon-q)^2(\epsilon^2-1)^{\frac{1}{2}}d\epsilon}{\{1+\exp[\epsilon x]\}\{1+\exp[(q-\epsilon)x_\nu]\}}. \quad (51a)$$

For the reaction $n\rightarrow p+e^-+\nu$, we note that dn/dE in Eq. (39) is the product of three quantities, *viz.*, the available states per unit energy in the volume Ω for protons, electrons, and neutrinos. For protons the number of available states is the number of neutrons in the volume Ω, *viz.*, $\Omega n_n(2i_n+1)$, while for electrons and neutrinos one can use the form of Eq. (40a) which gives this quantity for Fermi-Dirac particles. Since formally the reaction rate for free neutron decay is

$$C'n_n=\int_{m_ec^2}^{Q} w_{C'}dE, \quad (52)$$

it follows from Eq. (39) after some manipulation that

$$C'n_n=m_e{}^5c^{10}a_0n_nI_{C'} \text{ sec}^{-1}\text{ cm}^{-3}, \quad (53)$$

where

$$I_{C'}=\int_1^q \frac{\epsilon(\epsilon-q)^2(\epsilon^2-1)^{\frac{1}{2}}\exp[(q-\epsilon)x_\nu]\exp(\epsilon x)d\epsilon}{\{1+\exp[\epsilon x]\}\{1+\exp[(q-\epsilon)x_\nu]\}}. \quad (53a)$$

The foregoing reaction rates have been used in the equations developed below which describe the time dependence of neutron and proton concentrations. Let N_j be the number of nucleons of species j in the arbitrary finite volume V. The time derivative of N_j can be expressed formally for two- and three-body processes as

$$\frac{dN_j}{dt}=\sum_{\alpha,\beta} K_{\alpha\beta}n_\alpha N_\beta+\sum_{\alpha,\beta,\gamma} K_{\alpha\beta\gamma}n_\alpha n_\beta N_\gamma, \quad (54)$$

where

$$n_\alpha=N_\alpha/V. \quad (54a)$$

We note that

$$\frac{dn_j}{dt}=\frac{1}{V}\frac{dN_j}{dt}-\frac{n_j}{V}\frac{dV}{dt}, \quad (55)$$

where, since $V\propto l^3$,

$$\frac{1}{V}\frac{dV}{dt}=\frac{3}{l}\frac{dl}{dt}. \quad (55a)$$

For the cosmological model described in Sec. II,

$$\frac{1}{l}\frac{dl}{dt}=\left(\frac{8\pi G}{3}\rho\right)^{\frac{1}{2}},$$

where ρ is the total density, so that

$$\frac{dn_j}{dt}=\sum_{\alpha,\beta} K_{\alpha\beta}n_\alpha n_\beta+\sum_{\alpha,\beta,\gamma} K_{\alpha\beta\gamma}n_\alpha n_\beta n_\gamma-3n_j(8\pi G\rho/3)^{\frac{1}{2}}. \quad (56)$$

Consequently, we can write for neutrons the following rate equation:

$$dn_n/dt=An_pn_\nu-A'n_nn_{e^-}+Bn_pn_{e^-}-B'n_nn_\nu+Cn_pn_{e^-}n_\nu-C'n_n-3n_n(8\pi G\rho/3)^{\frac{1}{2}}. \quad (57)$$

Equation (57) can be rewritten using some of Eqs. (46)–(53) as

$$dn_n/dt=m_e{}^5c^{10}a_0[n_pK_p-n_nK_n]-3n_n(8\pi G\rho/3)^{\frac{1}{2}}, \quad (58)$$

where

$$K_p=I_A+I_B+I_C, \quad (58a)$$

and

$$K_n=I_{A'}+I_{B'}+I_{C'}. \quad (58b)$$

The limits of integration in the six integrals involved in K_p and K_n make it possible to combine certain pairs, with the result that

$$K_p=\int_1^\infty \frac{\epsilon(\epsilon^2-1)^{\frac{1}{2}}}{1+\exp[\epsilon x]}\left\{\frac{(\epsilon+q)^2\exp[\epsilon x]}{1+\exp[(\epsilon+q)x_\nu]}+\frac{(\epsilon-q)^2\exp[(\epsilon-q)x_\nu]}{1+\exp[(\epsilon-q)x_\nu]}\right\}d\epsilon, \quad (59)$$

and

$$K_n=\int_1^\infty \frac{\epsilon(\epsilon^2-1)^{\frac{1}{2}}}{1+\exp[\epsilon x]}\left\{\frac{(\epsilon+q)^2\exp[(\epsilon+q)x_\nu]}{1+\exp[(\epsilon+q)x_\nu]}+\frac{(\epsilon-q)^2\exp[\epsilon x]}{1+\exp[(\epsilon-q)x_\nu]}\right\}d\epsilon. \quad (60)$$

The equation describing the time rate of change of proton concentration can be written in a manner analogous to Eq. (58) as follows:

$$dn_p/dt = m_e{}^5c^{10}a_0[n_nK_n - n_pK_p] - 3n_p(8\pi G\rho/3)^{\frac{1}{2}}. \quad (61)$$

As shall be seen below, Eqs. (58) and (61) can be combined to give a single equation for the proton-neutron ratio, with the effect of the universal expansion not appearing explicitly.

The rate coefficients K_p and K_n have been evaluated numerically using Eqs. (59) and (60) for the range of values of x of interest. The values of x_p corresponding to x have been taken from Table II, with[11]

$$q = 1 + (m_n - m_p)/m_e = 2.53.$$

It can be shown from Eqs. (59) and (60) that for small x, i.e., $x \ll 1$ where $x_p \to x$,

$$\lim_{x_p \to x} K_p = e^{-qx}K_n. \quad (62a)$$

Furthermore, for large values of x, one finds that

$$\lim_{x \to \infty} K_p = 0, \quad (62b)$$

and

$$\lim_{x \to \infty} K_n = \int_1^\infty \epsilon(\epsilon - q)^2(\epsilon^2 - 1)^{\frac{1}{2}} d\epsilon = 1.6318. \quad (62c)$$

The limit approached by K_n in Eq. (62c) for $x \to \infty$ is just the term $C'/(m_e{}^5c^{10}a_0)$ where $C'n_n = dn_n/dt$ describes free neutron decay and $C'(=\lambda)$ is the neutron-decay constant. One can, therefore, select the Fermi coupling constant g, which is the only undetermined constant in a_0 [see Eq. (44a)], so that the value of C' is the observed neutron decay constant.[12] The neutron half-life measured recently by Robson[13] is $\tau_{\frac{1}{2}} = 12.8 \pm 2.5$ minutes. The values of $m_e{}^5c^{10}a_0$ and of g corresponding to the measured half-life limits are given in Table III.

In Table I are given values of the dimensionless quantities K_n and K_p, evaluated numerically from

TABLE III. Values of Fermi constant for various neutron half-lives.

Neutron half-life (min)	10.3	12.8	15.3
$m_e{}^5c^{10}a_0(\text{sec}^{-1})$	4.627×10^{-4}	5.531×10^{-4}	6.876×10^{-4}
$g(\text{erg cm}^3)$	1.01×10^{-49}	1.11×10^{-49}	1.23×10^{-49}

[11] For $(m_n - m_p)c^2$ we have used 0.782 Mev, as given by D. M. Van Patter, Massachusetts Institute of Technology, Technical Report No. 57, January 1952 (unpublished), while m_ec^2 has been taken as 0.5110 Mev, as given by J. W. M. DuMond and E. R. Cohen, Phys. Rev. **82**, 555 (1951).

[12] Although the numerical constants in a_0 which depend on spin, etc., have been carefully evaluated in building up the rate coefficients, it may be noted that the equality $C'n_n/(m_e{}^5c^{10}a_0) = 1.6318$, with $C' = \lambda$ known from experiment, automatically yields a value for a_0, so that g, spin factors, etc., need not be separately specified.

[13] See reference 4. Recently L. M. Langer and R. J. D. Moffat, Phys. Rev. **88**, 689 (1952), obtained the value $\tau_{\frac{1}{2}} = 10.4 \pm 0.6$ min indirectly from studying tritium decay. This value and Robson's value agree within the probable errors.

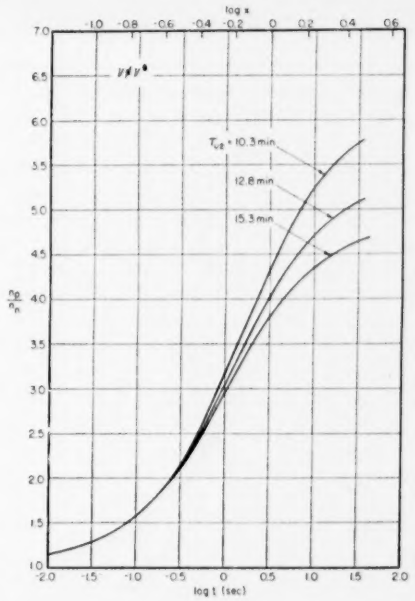

FIG. 2. The proton-neutron concentration ratio *versus* time and temperature ($x = m_ec^2/kT$) in the case of the Dirac neutrino (distinguishable neutrino and antineutrino) for the Robson neutron half-life value of 12.8 min, plus-and-minus the probable error.

Eqs. (59) and (60) in the range required for the present calculation. It may be noted that for x slightly greater than 3, K_n is close to the free decay value of 1.63 while K_p is negligibly small. Also for $x \ll 1$ the relationship $K_p \cong K_n \exp(-qx)$ holds quite closely.

Equations (58) and (61) describing neutron and proton concentrations can be combined by defining

$$\phi(t) = n_n/(n_n + n_p). \quad (63)$$

Taking the time derivative of ϕ and employing Eqs. (58) and (61) as required, one can write

$$d\phi/dt = m_e{}^5c^{10}a_0[K_p(1-\phi) - K_n\phi], \quad (64)$$

where a_0 is given by Eq. (44a). The actual integrations were done with $\ln x$ as independent variable where one writes

$$\frac{d\phi}{d\ln x} = \frac{d\phi}{dt}\frac{d\ln l}{d\ln x}\frac{dt}{d\ln l}. \quad (64a)$$

The quantity $d\ln l/d\ln x$ is given by Eq. (30) and calculated values are given in Table I, while values of $d\ln l/dt$, determined from Eq. (23), are also given in Table I

Equation (64) has been integrated numerically for the six cases of interest, *viz.*, for $\nu \equiv \nu^*$ and $\nu \not\equiv \nu^*$ taking three values of the neutron half-life, namely, the mean value and the mean value plus-and-minus the probable error, as given by Robson.[4] The integration procedure was such as to give a final accuracy in ϕ of the order

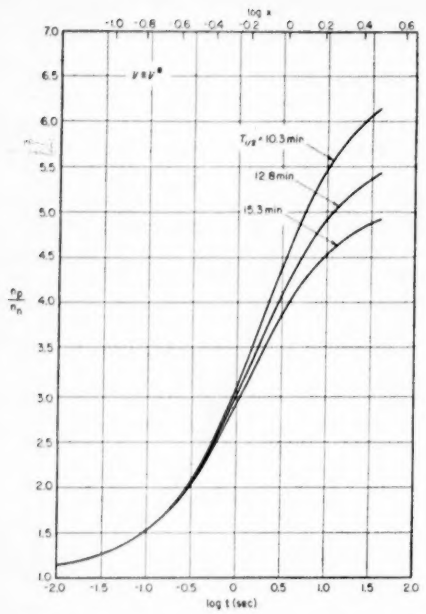

FIG. 3. The proton-neutron concentration ratio *versus* time and temperature ($x=m_ec^2/kT$) in the case of the Majorana neutrino (indistinguishable neutrino and antineutrino) for the Robson neutron half-life value of 12.8 min, plus-and-minus the probable error.

of the accuracy of the coefficients, i.e., ~1 percent. The solutions we have obtained are presented in Figs. 2 and 3, where the proton-neutron ratio is plotted *versus* x and *versus* the time scale appropriate to the type of neutrinos involved. The integrations were carried from $x=0.1$ toward larger x, the initial value of $\phi=n_n/(n_n+n_p)$ being taken as the equilibrium value, i.e., $\sim[1+\exp(qx)]^{-1}$, since at $x=0.1$ the rate coefficients K_n and K_p are large and show negligible deviation from their respective equilibrium values. The integration interval was 0.1 in $\ln x$, with the first approximation at each step being the equilibrium value which Eq. (64) would predict at the given value of x. It may be noted in Figs. 2 and 3 that by $x=4$ further change in the proton-neutron ratio is almost entirely caused by free neutron decay.

A comparison of these results with those of Hayashi indicates that the major difference between our calculation and his may arise from the difference in neutron half-life used, *viz.*, Hayashi used 20.8 min, while the remainder of the differences, amounting to perhaps 20 percent in the proton-neutron ratio, arise from the use of relativistic quantum statistics, a more detailed cosmological model, and different temperatures for neutrinos and the rest of the medium in the present calculation. The proton-neutron ratio obtained by Hayashi by the time free neutron decay predominated was ~4:1, whereas in the present calculation values from ~4.5:1 to ~6.0:1 are obtained depending on the half-life taken for the neutron and the type of neutrino considered.

It is interesting to note that if all the neutrons available at the start of element synthesis were used in making helium nuclei only, then the ratio of hydrogen to helium abundances corresponding to the range of proton-neutron ratios computed above would be from ~7:1 to ~10:1. Since some of the neutrons decay and some are involved in making the heavier elements, the above ratios would be minimum values of the initial universal H/He ratios. These values are consistent with the range of values obtained from astronomical data, *viz.*, ~5:1 to ~30:1 as found in planetary nebulae, stellar atmospheres, and theoretical stellar models.[14]

IV. DISCUSSION

In the preceding sections we have discussed quantitatively the physical conditions in the initial stages of the universal expansion. It now seems pertinent to mention some of the small physical effects whose influence on the present calculations has been neglected and also to comment on some of the limitations of the cosmological model when extrapolated to very early epochs.

The first question to be considered is whether or not the various processes, such as pair production, Compton and Coulomb scattering, etc., occur at sufficiently rapid rates to maintain equilibrium. A qualitative criterion as first described by Hayashi[3] is to compare the time required for the concentration of a constituent to change by about its own value with the time required for the universal temperature to change by about its own value. Characterizing these as relaxation times, τ, one finds from Eq. (6) and Table I that the relaxation time for temperature is given with sufficient accuracy for the present purpose by the following expression:

$$\tau_T \sim -\frac{dt}{d\ln T} = -\left(\frac{3c^2}{8\pi G a_\gamma}\right)^{\frac{1}{2}} T^{-2} = 2t. \qquad (65)$$

To take a specific example one can calculate from the equilibrium concentration of electron pairs and their rate of production by photon-photon collisions the relaxation times, τ_{pair}, for pair production-annihilation. The result for $x\ll 1$ is

$$\tau_{\text{pair}} \sim -\frac{dt}{d\ln n_{\text{pair}}} \sim \frac{144 x\hbar^3}{\pi^3 m_e e^4}, \qquad (66)$$

where e is the charge on the electron. Hence

$$\frac{\tau_{\text{pair}}}{\tau_T} \cong 10x^3\left(\frac{Gm^2}{\hbar c}\right)^{\frac{1}{2}}\left(\frac{e^2}{\hbar c}\right)^{-2} \sim 10^{-20}x^3 \ll 1. \qquad (67)$$

[14] A. Underhill, Symposium on the Abundance of Elements held at Yerkes Observatory, Williams Bay, Wisconsin, November 6–8, 1952 (unpublished), under the joint sponsorship of the National Science Foundation and the University of Chicago.

A similar result is obtained for other reactions not involving neutrinos, for which the change in the coupling coefficient $e^2/\hbar c$ does not greatly change the order of magnitude of the ratio. This is not the case for neutrino interactions. Hence all processes not involving neutrinos proceed at sufficiently rapid rates to maintain equilibrium.

The question of electron degeneracy is most easily examined by considering the requirement of electrical neutrality.[3] If one integrates Eq. (43) with a degeneracy parameter, ζ, included, then for high temperatures the electron or positron concentration can be written as

$$n_{e^\mp}\sim(2/\pi^2)(kT/\hbar c)^3 e^{\pm\zeta}, \tag{68}$$

and

$$n_{e^-}+n_{e^+}\sim(4/\pi^2)(kT/\hbar c)^3\cosh\zeta. \tag{68a}$$

If the condition of electrical neutrality is imposed then $n_{e^-}-n_{e^+}=n_p$ and

$$\sinh\zeta=\frac{\pi^2 n_p\hbar^3}{4(mc/\hbar)^3}\sim\frac{n_p}{n_{e^-}+n_{e^+}}. \tag{69}$$

As has been shown[1,2] the nucleon concentration during the early stages of the expanding universe is very small compared with the density of radiation ($1:10^6$) and, therefore, also small compared with the electron-positron pair concentration. It follows then from Eq. (69) that the parameter ζ is very small and, therefore, the degeneracy of electrons or positrons properly has been neglected.

The charge on the electrons and positrons gives rise to a Coulomb interaction energy which contributes to the total energy of the medium. The reasonableness of neglecting this interaction energy can be seen from the following. The average distance between, say, electrons is found from Eq. (68), taking $\zeta\ll 1$ as

$$(1/n_{e^-})^{\frac{1}{3}}\sim\hbar/|\mathbf{p}|, \tag{70}$$

i.e., the de Broglie wavelength. It follows that the Coulomb energy, E_c, for two electrons is

$$E_c\sim-\frac{e^2}{(\hbar/|\mathbf{p}|)}=-\left(\frac{e^2}{\hbar c}\right)|\mathbf{p}|c\sim-\frac{1}{137}E_T, \tag{71}$$

where E_T is the mean thermal energy per electron. Because of this Coulomb interaction energy there will be a slight tendency for a given charge to have more nearest neighbors with charge of opposite sign. The fractional charge excess per nearest neighbor at the distance $\hbar/|\mathbf{p}|$ may be expected to be of the order $\exp[-E_c/kT]-1\sim 1/137$. Therefore, the contribution of Coulomb energy due to nearest neighbors to the total energy of the medium is $\sim E_c/137\cong E_T/(137)^2$ times the mean number of nearest neighbors. Assuming this number to be of the order of 10, the contribution of the Coulomb energy is $<10^{-3}E_T$, and can, therefore, be neglected.

The contribution of specifically nuclear forces is negligible because the nucleon density is very small compared with nuclear density. Furthermore, the energy evolution of nuclear reactions also can be neglected because it is itself small compared with the already small contribution of the low density of nucleons.

The foregoing small effects bear mainly on the cosmological model which has been discussed in Sec. II. There are also several questions of this kind which concern the calculation of the rates of the nuclear reactions in Eq. (37) which were determined in Sec. III. An examination of these reactions shows that of the six rates only $B'n_n n_\nu$ and $C'n_n$, Eqs. (48) and (53), involve two charged product particles. For these, one should more correctly include a factor in the reaction probability, w, to take into account the effect of Coulomb forces. In general this factor is given by[15]

$$2\pi\eta[1-\exp(-2\pi\eta)]^{-1}, \tag{72}$$

where

$$\eta=Ze^2E_e(\hbar c^2|\mathbf{p}_e|)^{-1},$$

Z is the nuclear charge, and E_e and $|\mathbf{p}_e|$ are electron energy and momentum, respectively. The effect of this correction on the two integrals in $C'n_n$ and $B'n_n n_\nu$ has been estimated and found to be less than one percent. Thus the effect of the Coulomb forces can be completely neglected in these cases.

As has been mentioned the matrix elements for the nuclear reactions stated in Eqs. (37) have been taken equal to unity for lack of a better estimate.[16] There seems to be little doubt that free neutron decay is a super-allowed transition since the decay rate is consistent with those of other light element β emitters. Furthermore, it would seem likely that the matrix elements for all the reactions considered here would remain about equal in the event that one included effects such as nucleon recoil.

It should also be pointed out that in calculating reaction rates we have considered that the nucleons, i.e., the heavy particles, are at rest. This approximation, which is customarily made, leads to a negligible error.

In addition to the above questions there are a number of more general points which may bear on the validity of the theory presented in this paper. One such question concerns the extrapolation of physical theories back to extremely high temperatures and densities. For example, some quantum field theories introduce a cutoff in, say, the electric field at the value it would have on the surface of the classical electron in order to avoid high-energy difficulties. This cutoff is introduced by appropriate modification of the field equations and, therefore, of the distribution of states in momentum space. When the mean electric field is equal to the

[15] See for example, G. Gamow and C. L. Critchfield, *Theory of Atomic Nucleus and Nuclear Energy Sources* (Clarendon Press, Oxford, 1949).

[16] E. Fermi, *Nuclear Physics* (University of Chicago Press, Chicago, 1950).

TABLE IV. Timetable of events in the early epochs of the expanding universe.

Temperature (Mev)	Remarks: Neutrino ≡ antineutrino	Remarks: Neutrino ≠ antineutrino
>100	Region of doubtful validity of the field equations where ρ_γ exceeds nuclear density.	
~100	Thermodynamic equilibrium prevails.	
	$\rho_\gamma \cong 1.2\times10^{13}$ g/cm³ $\rho_\mu = (7/4)\rho_\gamma$, $\rho_\pi = (3/2)\rho_\gamma$ $\rho_\nu = (7/8)\rho_\gamma$, $\rho_e = (7/4)\rho_\gamma$ $t \cong 6.3\times10^{-6}$ sec	Same as for $\nu \equiv \nu^*$ except $\rho_\nu = (7/4)\rho_\gamma$ $t \cong 5.9\times10^{-5}$ sec
~100–~10	Mesons annihilate converting energy into photons, electrons, and neutrinos.	
~10	Neutrinos are freezing-in during this period.	
	$\rho_\gamma \cong 1.2\times10^{9}$ g/cm³ $\rho_\mu \sim 10^{-6}\rho_\gamma$, $\rho_\pi \sim 10^{-6}\rho_\gamma$ $\rho_\nu = (7/8)\rho_\gamma$, $\rho_e = (7/4)\rho_\gamma$ $t \cong 8.7\times10^{-3}$ sec	Same as for $\nu \equiv \nu^*$ except $\rho_\nu = (7/4)\rho_\gamma$ $t \cong 7.8\times10^{-2}$ sec
~10–~2	Continued adiabatic expansion of universe with $T_\nu \cong T$ despite negligible interaction of neutrinos with medium.	
~2	Start of electron-positron annihilation.	
	$\rho_\gamma \cong 1.9\times10^{6}$ g/cm³ $\rho_\mu = \rho_\pi \sim 0$ $\rho_\nu \cong (7/8)\rho_\gamma$, $\rho_e = (7/4)\rho_\gamma$ $t \cong 0.22$ sec	Same as $\nu \equiv \nu^*$ except $\rho_\nu \cong (7/4)\rho_\gamma$ $t \cong 0.20$ sec
~2–~0.05	Electron-positron annihilation, converting energy into photons. Neutrinos cool adiabatically relative to remaining particles, the latter maintaining thermodynamic equilibrium. [See Tables I and II for more details during this epoch.] The neutron-proton abundance ratio reaches the free decay value, 4.5:1–6.0:1, at $T \sim 0.2$ Mev. Nucleogenesis begins at $T \sim 0.2$ Mev.	
~0.05	Nucleogenesis is well under way.	
	$\rho_\gamma \cong 0.72$ g/cm³ $\rho_\nu \cong 0.24\rho_\gamma$, $\rho_e \sim 0$ $t \cong 600$ sec	$\rho_\gamma \cong 0.72$ g/cm³ $\rho_\nu \cong 0.47\rho_\gamma$, $\rho_e \sim 0$ $t \cong 550$ sec
~0.03	Nucleogenesis essentially complete except for charge adjustment by β decay.	
	$t \sim 30$ min	
~0.03 Mev –~1 kev	Thermonuclear reactions among some of the light elements, *viz.*, Li, Be, B, D with H, continue during this period.	
~0.015 ev	At $t \sim 10^{8}$ yr, $T \sim 170$°K and $\rho \sim 10^{-26}$ g/cm³, galaxies probably form.	

foregoing cutoff, one has

$$\sim[e/(e^2/m_e c^2)^2]^2 \cong \rho_\gamma c^2,$$

which leads to a temperature of ~15 Mev. However, recent advances in quantum field theory obviate such a high-energy cutoff. In fact, if such a cutoff exists it is probably an order of magnitude higher. This is evidenced by the quantitative agreement between theory and the observed Lamb shift, for example. Cutoffs in momentum space must be larger than present day experimental energies, i.e., $kT > 100$ Mev, since observed bremsstrahlung and pair production, etc., agree with theory quite well.

Another pertinent question is the possible contribution of equilibrium concentrations of "gravitational quanta" to the total density. Although at equilibrium the "graviton" density would be expected to be equal to the photon density, one must consider at what temperatures such equilibria can be maintained. We may apply Eq. (67) to the present situation and replace the coupling coefficient $(e^2/\hbar c)^2$ by the product of $(Gm^2/\hbar c)$ with an electronic or mesonic coupling coefficient whose value will be in the range $\sim 1 - \sim 10^{-2}$. Then, since $(Gm^2/\hbar c) \cong 10^{-45}$ with $m = m_e$, one finds $\tau_{grav}/\tau_T \sim 10^{22}$ at ~1 Mev. In order for $\tau_{grav}/\tau_T \sim 1$, i.e., for the "gravitons" to maintain equilibrium, the temperature must be $\sim 10^{4}$ Mev.[17] It is difficult to see how the introduction of many-body processes would reduce this temperature drastically. One does not know how many different kinds of particles exist in the range $\sim 10^{2} - \sim 10^{4}$ Mev but on the basis of the presently known types of particles one can determine an upper limit to the graviton contribution. We can compute the ratio of graviton density to that of neutrinos down to the temperature at which neutrinos freeze-in, since beyond this temperature the ratio remains constant. From the analog to Eq. (35) one has, if $\mathfrak{F}_i$ represents degrees of freedom for each constituent present, i.e., $\mathfrak{F}_i \to \rho_i/\rho_\gamma$ as $T \to \infty$, the following relationship:

$$\frac{\rho_{grav}}{\rho_\gamma} = \left(\frac{\sum_i \mathfrak{F}_i \text{ at } T_\nu'}{\sum_i \mathfrak{F}_i \text{ at } T_{grav}'} \right)^{4/3}, \tag{73}$$

where T_ν' and T_{grav}' are the freeze-in temperatures of neutrinos and gravitons, respectively. From the presently known elementary particles which would exist at these temperatures one can estimate from Eq. (73) that $\rho_{grav}/\rho_\gamma < 0.1$ at T_ν'. During the subsequent expansion down to $T \sim 0.1$ Mev, ρ_{grav}/ρ_γ diminishes by a factor of ~4, just as ρ_ν/ρ_γ diminishes [see Table II]. At no time does the upper bound of the graviton contribution to the density exceed 2 or 3 percent, and the total contribution is probably much smaller.

Finally, it seems pertinent to comment on the question as to whether the density of nucleons relative to the density of radiation can be calculated at some very early time on the basis of theoretical considerations with complete symmetry between nucleons and antinucleons or whether it is a free initial condition. In particular can the nucleon density be the result of a statistical fluctuation in the competition between different processes of nucleon annihilation such as

$$p^+ + p^- \rightleftharpoons 2h\nu \rightleftharpoons \pi^+ + \pi^-, \text{ etc.},$$

where p^+ and p^- are proton and antiproton, respec-

[17] It should be noted that in the coupling coefficient the quantity m must be taken to be the relativistic mass of the interacting particles, i.e., $(Gm^2/\hbar c) = (Gm_e^2/\hbar c)x^{-2}$. Also note that the numerical results given here for extreme physical conditions are at best rather crude approximations.

tively, and as yet unknown high-energy processes such as

$$p^+ \rightleftharpoons \text{mesons} + e^{\pm}, \text{ etc.?}$$

An examination of this question on statistical grounds yields a probable residual density of nucleons approximately equal to $\rho_\gamma/N^{\frac{1}{2}}$, where N is the number of nucleons initially present in any given finite volume under consideration in co-moving coordinates.[18] If we take an initial volume corresponding to the presently observable universe, the residual number of nucleons is found to be less than would be required to form the earth. It appears that the situation described above is untenable and that the initial nucleon concentration must be specified arbitrarily. This result is in agreement with present thinking in elementary particle physics which does not allow for single nucleon annihilation processes. In addition, it should be pointed out that no catalytic type of reaction (e.g., $2p^+ + p^- \rightarrow 2p^+ + \mu^-$) can vitiate the above statistical arguments because of the finite propagation velocity of disturbances noted in Sec. II.

V. CONCLUSION

The problem discussed in this paper has been concerned with the detailed nature of the general nonstatic homogeneous isotropic expanding cosmological model derived from general relativity as well as the elementary particle reactions which occur during early epochs. The study of the elementary particle reactions leads to a knowledge of the time dependence of the proton-neutron concentration ratio which is required in the problem of nucleogenesis. While the problem of element origin stimulated the present study, the results concerning the cosmological model are of interest in themselves. On the basis of the new physical conditions which have been discussed here, it would appear necessary to reexamine the specific reactions among the lighter nuclei, particularly as regards the missing species at $A=5$.

In order to summarize, we have presented the above calculations in abbreviated form as a timetable of events in the very early stages of the expanding universe, through the period of residual thermonuclear reactions[19] and galaxy formation.[20] In Table IV are given for various temperatures the corresponding epochs according to the expanding cosmological model involving the interconversion of matter and radiation, the densities of the various constituents according to the appropriate relativistic quantum statistics, as well as remarks concerning some of the principal physical phenomena that occur during these various early stages. This tabulation, it will be noted, covers both distinguishable and indistinguishable neutrinos.

Finally, we should like to point out that all of the results presented in this paper follow uniquely from general relativity, relativistic quantum statistics, and β-decay theory without the introduction of any free parameters, so long as the density of matter is very small compared with the density of radiation.

VI. ACKNOWLEDGMENTS

We wish to thank Mrs. Betty Grisamore, Mrs. Kathryn Stevenson, and Mr. Charles V. Bitterli for their assistance in some of the numerical work, Miss Shirley Thomas for typing this manuscript, and Miss Doris Rubenfeld for assistance with the illustrations.

[18] This can be seen from the following arguments. Let the numbers of protons, antiprotons, neutrons, and antineutrons in any finite co-moving volume V be equal and equal to N. Let α be the probability per particle for any of these particles to transmute to mesons at high temperature. We shall suppose that such transmutations occur first in the expansion, and that annihilation occurs later. This situation yields the largest residual density. Then on the average $4\alpha N$ particles transmute to mesons. The standard deviation σ in the number transmuting is then

$$\sigma = [4\alpha N(1-\alpha)]^{\frac{1}{2}},$$

which is a maximum of $N^{\frac{1}{2}}$ for $\alpha = \frac{1}{2}$. One may expect that in any volume V the excess of nucleons over antinucleons, or conversely, will be of the order of σ, i.e., of the order of $N^{\frac{1}{2}}$. The concentration of these residual nucleons at a later time when the initial volume V_0 has expanded to V_1 is given by $n_{\text{nuc}} = (N^{\frac{1}{2}}/V_0)(V_0/V_1)$. To a rough approximation the number of photons originally in V_0, a number approximately equal to N initially, has remained constant down to V_1, so that $V_0/V_1 \cong n_{\gamma_1}/n_{\gamma_0}$, where n_γ is photon concentration. Hence one can write

$$n_{\text{nuc}} N^{\frac{1}{2}} n_{\gamma_1}/(V_0 n_{\gamma_0}) \cong n_{\gamma_1}/N^{\frac{1}{2}}, \quad \text{or} \quad \rho_{\text{nuc}} \sim \rho_{\gamma_1}/N^{\frac{1}{2}}.$$

[19] Alpher, Herman, and Gamow, Phys. Rev. **74**, 1198 (1948).

[20] G. Gamow, Kgl. Danske Videnskab. Selskab, Mat.-fys. Medd. **27**, No. 10 (1953).

The Čerenkov Effect and the Dielectric Constant

S. M. NEAMTAN
Department of Mathematical Physics, University of Manitoba, Winnipeg, Canada
(Received August 27, 1953)

A quantum-mechanical theory of the Čerenkov radiation is developed wherein the refractive medium is treated not as a continuum but as an aggregation of atoms. The atoms and the electromagnetic field are considered as forming a single system which interacts with an incident charged particle. The Čerenkov radiation arises in first-order transitions induced by this interaction. The nature of this process suggests a quantum-mechanical definition of the dielectric constant with the aid of which the theory yields the well-known properties of the Čerenkov radiation. The definition of the dielectric constant is shown to lead to the same expression for this quantity as is given by the Kramers-Heisenberg dispersion formula.

INTRODUCTION

SINCE the discovery of the Čerenkov effect,[1] a number of theoretical treatments of this problem, both classical and quantum mechanical, have appeared in various publications.[2] These treatments all have this in common, that they are based on the assumption that the effect takes place in a continuous medium whose optical properties can be expressed in terms of a refractive index or, for a nonmagnetic material,[3] by a dielectric constant. It has been the purpose of the present investigation to develop a quantum-mechanical theory of the Čerenkov radiation wherein the refractive medium is treated not as a continuum but as an aggregation of atoms which interact with the electromagnetic field and with the incident charged particle. Such a theory demands a purely quantum-mechanical definition of the dielectric constant. It will be shown how such a definition is suggested by the nature of the Čerenkov radiation and that it leads to the well-known formula for the dielectric constant of a medium of low density.

It is to be noted at this point that there exists in the literature no completely quantum-mechanical theory of the dielectric constant. The closest approach to one is to be found in Dirac's derivation of the Kramers-Heisenberg dispersion formula.[4] In this derivation, the polarizability of an atom for a given component of the radiation is obtained by equating the spectral distribution of the radiation scattered by the atom to that which would be radiated by a classical oscillating electric dipole of the same frequency. The polarizability then appears as the ratio of the appropriate component of the amplitude of the dipole moment of the oscillator to the amplitude of the electric vector of the incident radiation. The foregoing procedure is essentially based on classical considerations; in particular, the amplitude of the electric vector is not quantum-mechanically well defined for a stationary state of the radiation field although its square is. Finally, the familiar argument invoked in expressing the dielectric constant in terms of the polarizability is a completely classical one.

THE ČERENKOV PROCESS AND THE DEFINITION OF THE DIELECTRIC CONSTANT

We consider a "zero-order system" of two noninteracting parts, *viz.*, a free charged particle and a system S, which consists of the electromagnetic field and the atoms of a refractive medium in interaction. The introduction of an interaction between the particle and S gives rise to transitions between stationary states of the zero-order system. In order to separate out the emission of Čerenkov radiation from various other processes which might occur, such as, for example, ionization, emission of bremsstrahlung, etc., we restrict our attention to first-order transitions. It will be shown that these first-order transitions give rise to the Čerenkov radiation.

Suppose that in a transition between two stationary states of the zero-order system the momentum of the particle changes from $\mathbf{p}_1$ to $\mathbf{p}_2$, while S undergoes a transition corresponding to the emission of a photon of definite momentum, frequency, and polarization.[5] In this transition let S suffer a change in energy, ΔW, and in momentum, $\Delta\mathbf{P}$. For conservation of energy and momentum we must have

$$W_1-W_2\equiv(c^2p_1^2+m^2c^4)^{\frac{1}{2}}-(c^2p_2^2+m^2c^4)^{\frac{1}{2}}=\Delta W \tag{1}$$

and

$$\mathbf{p}_1-\mathbf{p}_2=\Delta\mathbf{P}, \tag{2}$$

where m is the mass of the particle, c is the velocity of light, and p_1 and p_2 are the respective magnitudes of $\mathbf{p}_1$ and $\mathbf{p}_2$. In order that the above equations be simultaneously satisfied, ΔW and $\Delta\mathbf{P}$ must satisfy the inequality

$$\Delta W/|\Delta\mathbf{P}|<c. \tag{3}$$

[1] P. A. Čerenkov, Compt. rend. **2**, 451 (1934).
[2] I. M. Frank and I. Tamm, Compt. rend. **14**, 109 (1937); V. L. Ginsburg, J. Phys. (U.R.S.S.) **2**, 441 (1940); E. Fermi, Phys. Rev. **57**, 485 (1940); G. Beck, Phys. Rev. **74**, 795 (1948); J. M. Jauch and K. M. Watson, Phys. Rev. **74**, 950 (1948); **74**, 1485 (1948); **75**, 1249 (1949); A. Bohr, Kgl. Danske Videnskab. Selskab. Mat.-fys. Medd. **24**, Nr. 19 (1948); T. Taniuti, Progr. Theor. Phys. **6** 207 (1951); M. Schönberg, Nuovo cimento **8**, 159 (1951); **9**, 210 (1952); **9**, 372 (1952).
[3] It will be assumed in what follows that the medium is nonmagnetic.
[4] P. A. M. Dirac, Proc. Roy. Soc. (London) **A114**, 710 (1927).
[5] It is not immediately evident at this stage of the argument that S can undergo transitions which can be so interpreted. However, it will be shown below that this is indeed the case.

That a charged particle in a vacuum cannot radiate is a consequence of the fact that in the absence of the medium the inequality, (3), becomes an equality.

In the classical theory, the Čerenkov radiation is essentially made up of low-energy photons and is emitted in the motion of the charged particle through the medium at a nearly uniform relativistic velocity. We therefore consider a transition in which ΔW is small as compared to W_1. Then with the aid of (1) and (2) we can write in sufficient approximation

$$\Delta W=(c^2p_1/W_1)(p_1-p_2), \tag{4}$$

and

$$p_1-p_2=|\Delta\mathbf{P}|\cos\theta, \tag{5}$$

where θ is the angle between $\Delta\mathbf{P}$ and $\mathbf{p}_1$. Solving for $\cos\theta$, we obtain

$$\cos\theta=\Delta W/v|\Delta\mathbf{P}|, \tag{6}$$

where

$$v=c^2p_1/W_1 \tag{7}$$

is the velocity of the particle.

It will be shown below that in a first-order transition of the type here considered, the change in momentum of S is precisely the momentum of the emitted photon. Thus, we must identify θ as the angle of the Čerenkov cone. In the classical theory, this angle is given by

$$\cos\theta=u/v, \tag{8}$$

where u is the phase velocity of the emitted radiation in the medium. The corresponding dielectric constant is

$$\epsilon=c^2/u^2. \tag{9}$$

Thus, we are led to define the dielectric constant quantum-mechanically by the equation

$$\epsilon=c^2(|\Delta\mathbf{P}|/\Delta W)^2. \tag{10}$$

THE SYSTEM S: MEDIUM PLUS RADIATION

We shall consider a system S, consisting of the radiation field in interaction with a collection of atoms. For simplicity the atoms are assumed to be identical, and they will ultimately be taken to be randomly distributed. This corresponds to treating a homogeneous and isotropic medium. Box quantization in unit volume is adopted with periodic boundary conditions that permit of the Fourier expansion of the radiation field as a superposition of plane polarized progressive-plane waves. Except where otherwise indicated, the notation and formulation of the quantized field theory as given by Heitler[6] will be used. The masses, m_i, and momenta, $\mathbf{p}_i$, of the atomic particles will, however, be expressed in units of mass and momentum, respectively, and not in units of energy.

For the system S we write the Hamiltonian:

$$H_S\equiv H_r+\sum_i\frac{1}{2m_i}\left[\mathbf{p}_i-\frac{e_i}{c}\mathbf{A}(\mathbf{r}_i)\right]^2+\sum_{i\neq j}\frac{e_ie_j}{|\mathbf{r}_i-\mathbf{r}_j|}. \tag{11}$$

[6] W. Heitler, *Quantum Theory of Radiation* (Oxford University Press, London, 1944), second edition.

In the above, $\mathbf{r}_i$ represents the position vector of the i-th particle, and $\mathbf{A}(\mathbf{r}_i)$ the vector potential evaluated at $\mathbf{r}_i$. H_r is the Hamiltonian for the radiation field alone. The atomic particles are treated nonrelativistically since we are here interested only in low-energy processes.

The Hamiltonian can be rewritten

$$H_S=H_S^{(0)}+H_S^{(1)}+H_S^{(2)}, \tag{12}$$

where the terms on the right-hand side are

$$H_S^{(0)}=H_r+H_A$$
$$=H_r+\sum_i\frac{1}{2m_i}p_i^2+\sum_{i\neq j}\frac{e_ie_j}{|\mathbf{r}_i-\mathbf{r}_j|}, \tag{13a}$$

$$H_S^{(1)}=-\sum_i\frac{e_i}{m_ic}\mathbf{A}(\mathbf{r}_i)\cdot\mathbf{p}_i$$
$$=-\sum_i\sum_\lambda\frac{e_i}{m_ic}[q_\lambda\mathbf{A}_\lambda(\mathbf{r}_i)+q_\lambda^*\mathbf{A}_\lambda^*(\mathbf{r}_i)]\cdot\mathbf{p}_i, \tag{13b}$$

and

$$H_S^{(2)}=\sum_i\frac{e_i^2}{2m_ic^2}|\mathbf{A}(\mathbf{r}_i)|^2$$
$$=\sum_i\frac{e_i^2}{2m_ic^2}|\sum_\lambda\{q_\lambda\mathbf{A}_\lambda(\mathbf{r}_i)+q_\lambda^*\mathbf{A}_\lambda^*(\mathbf{r}_i)\}|^2. \tag{13c}$$

In the above expressions, the $\mathbf{A}_\lambda$ are Fourier components of the vector potential, and the q_λ and q_λ^* are the usual annihilation and creation operators. We now treat $H_S^{(1)}$ and $H_S^{(2)}$, respectively, as first- and second-order perturbations of $H_S^{(0)}$, and we wish to calculate the displacement of the energy levels of $H_S^{(0)}$ resulting from the perturbation for those states for which the atoms of the medium are unexcited. In order to avoid complications due to resonance effects, we consider only states of the radiation field for which no photons having energies close to resonance values for the atomic system exist. There will then exist no nonvanishing first-order matrix elements of the perturbation between such a state and other states of the same energy so that the perturbation vanishes in first order and the degeneracy of the system may be neglected in calculating the displacement of the energy levels to the second order of approximation.

Let a represent the ground state of the atomic system and let b represent any excited state. Let n_λ and n_λ' represent two sets of occupation numbers characterizing states of the radiation field. Then, according to perturbation theory, the second-order shift in energy of the state $(a;n_\lambda)$ is given by

$$W_{a;n_\lambda}^{(2)}=\langle a;n_\lambda|H_S^{(2)}|a;n_\lambda\rangle$$
$$+\sum_{b,n_\lambda'}\frac{|\langle a;n_\lambda|H_S^{(1)}|b;n_\lambda'\rangle|^2}{W_{a;n_\lambda}^{(0)}-W_{b;n_\lambda'}^{(0)}}, \tag{14}$$

where terms of the form $W_{a;n\lambda}{}^{(0)}$ represent eigenvalues of $H_S{}^{(0)}$.

With the aid of (13) and the familiar matrices for q_λ and $q_\lambda{}^*$, the above expression reduces to

$$W_{a;n_\lambda}{}^{(2)}=\sum_{i,\lambda}\frac{2\pi e_i^2}{m_i}\cdot\frac{(2n_\lambda+1)\hbar}{2\nu_\lambda}$$
$$+\sum_{\lambda,b}\frac{2\pi\hbar}{\nu_\lambda}\left\{(n_\lambda+1)\frac{\left|\sum_i\frac{e_i}{m_i}\langle a|\,\mathbf{e}_\lambda\cdot\mathbf{p}_i\exp(i\boldsymbol{\kappa}_\lambda\cdot\mathbf{r}_i)\,|b\rangle\right|^2}{W_a-W_b-\hbar\nu_\lambda}\right.$$
$$\left.+n_\lambda\frac{\left|\sum_i\frac{e_i}{m_i}\langle a|\,\mathbf{e}_\lambda\cdot\mathbf{p}_i\exp(-i\boldsymbol{\kappa}_\lambda\cdot\mathbf{r}_i)\,|b\rangle\right|^2}{W_a-W_b+\hbar\nu_\lambda}\right\}. \quad (15)$$

The symbols $\mathbf{e}_\lambda$, $\boldsymbol{\kappa}_\lambda$, and ν_λ here represent the polarization vector, propagation vector, and angular frequency, respectively, of a component of the radiation field, and W_a and W_b are eigenvalues of the atomic Hamiltonian, H_A, for the states a and b.

Equation (15) contains a divergent self-energy term which arises from the 1 in the factors $(2n_\lambda+1)$ and $(n_\lambda+1)$. Since, however, we shall be concerned only with changes in the energy of the system S in transitions in which one of the occupation numbers, n_λ, changes by one, the self-energy term can be dropped. Let ΔW_λ be the change in the energy of S when a particular occupation number, n_λ, increases by one, while all other quantum numbers remain unchanged. Then we can write

$$\Delta W_\lambda=(W_{a;n_\lambda+1}{}^{(0)}+W_{a;n_\lambda+1}{}^{(2)})-(W_{a;n_\lambda}{}^{(0)}+W_{a;n_\lambda}{}^{(2)})$$
$$=\hbar\nu_\lambda+\frac{2\pi\hbar}{\nu_\lambda}\left\{\sum_i\frac{e_i^2}{m_i}\right.$$
$$+\sum_b\frac{\left|\sum_i\frac{e_i}{m_i}\langle a|\,\mathbf{e}_\lambda\cdot\mathbf{p}_i\exp(i\boldsymbol{\kappa}_\lambda\cdot\mathbf{r}_i)\,|b\rangle\right|^2}{W_a-W_b-\hbar\nu_\lambda}$$
$$\left.+\sum_b\frac{\left|\sum_i\frac{e_i}{m_i}\langle a|\,\mathbf{e}_\lambda\cdot\mathbf{p}_i\exp(-i\boldsymbol{\kappa}_\lambda\cdot\mathbf{r}_i)\,|b\rangle\right|^2}{W_a-W_b+\hbar\nu_\lambda}\right\}. \quad (16)$$

It is now necessary to find the change in momentum of S that corresponds to the above energy change. The total momentum of S is

$$\mathbf{P}=\sum_\lambda 2\nu_\lambda q_\lambda{}^*q_\lambda\boldsymbol{\kappa}_\lambda+\sum_i\mathbf{p}_i. \quad (17)$$

It has the same form whether the interaction between the radiation and the atoms is taken into account or not. It is easily verified that $\mathbf{P}$ commutes with H_S, as well as with $H_S{}^{(0)}$. We therefore take as basic states of S simultaneous eigenstates of H_S and $\mathbf{P}$. If the interaction between radiation and atoms is reduced adiabatically to zero, these states reduce to simultaneous eigenstates of $H_S{}^{(0)}$ and $\mathbf{P}$ with no change in the eigenvalues of $\mathbf{P}$ to which they respectively belong.

Consider now a perturbation of S through the addition to H_S of a term proportional to $q_\lambda{}^*$ and otherwise independent of the variables of S. The commutator of $\mathbf{P}$ with $q_\lambda{}^*$ is

$$[\mathbf{P},\,q_\lambda{}^*]=\hbar\boldsymbol{\kappa}_\lambda q_\lambda{}^*, \quad (18)$$

from which it follows that the perturbation can induce only such transitions between states of S for which $\mathbf{P}$ increases by the amount

$$\Delta\mathbf{P}_\lambda=\hbar\boldsymbol{\kappa}_\lambda. \quad (19)$$

Similarly, transitions induced by a term proportional to q_λ correspond to a decrease in $\mathbf{P}$ of the same amount. This result is valid whether or not the interaction between the radiation and the atoms is taken into account. If this interaction is neglected, the energy change associated with a momentum change $\hbar\boldsymbol{\kappa}_\lambda$ is $\hbar\nu_\lambda$, corresponding to the emission (or absorption) of a photon of type λ. If the interaction is taken into account, it is clear in the light of the preceding argument that a perturbation $q_\lambda{}^*$ can induce a transiton in S, interpretable as the emission of a photon of type λ, wherein the total change in momentum of S is precisely the momentum of the photon, $\hbar\boldsymbol{\kappa}_\lambda$ and the change in energy is given to second order of approximation by (16).

THE ČERENKOV RADIATION

We consider a spin-$\frac{1}{2}$ charged particle of relativistic energy in interaction with the system S. For the combined system of particle plus S we take the Hamiltonian

$$H=H_p+H_S+H'=H^{(0)}+H', \quad (20)$$

where

$$H_p=-c\boldsymbol{\alpha}\cdot\mathbf{p}-mc^2\beta \quad (21)$$

is the relativistic Hamiltonian for the particle alone and

$$H'=e\boldsymbol{\alpha}\cdot\mathbf{A}(\mathbf{r})=e\sum_\lambda\boldsymbol{\alpha}\cdot[q_\lambda\mathbf{A}_\lambda(\mathbf{r})+q_\lambda{}^*\mathbf{A}_\lambda{}^*(\mathbf{r})]. \quad (22)$$

Here e, $\mathbf{r}$, $\mathbf{p}$, and m are respectively the charge, position, momentum, and mass of the particle, and $\boldsymbol{\alpha}$ and β are the usual Dirac matrices. The direct Coulomb interaction between the particle and the atoms of the medium has been omitted from the Hamiltonian since it can give rise to radiative transitions only in third or higher order, and we shall be concerned only with first-order transitions.

The interaction term H' is now to be considered as inducing transitions between eigenstates of $H^{(0)}$, these eigenstates being chosen to be momentum states of the particle. We consider a transition in which the momentum of the particle changes from $\mathbf{p}_1$ to $\mathbf{p}_2$, the spins

of initial and final states being in the first instance fixed, while the system undergoes a transition corresponding to the emission of a photon of type λ. Such a transition arises from the term

$$eq_\lambda^* \boldsymbol{\alpha} \cdot \mathbf{A}_\lambda^*(\mathbf{r})$$

in H', so that, as has been shown above, the momentum of S increases by $\hbar\boldsymbol{\kappa}_\lambda$. Since momentum must be conserved in the transition, we have

$$\mathbf{p}_1 - \mathbf{p}_2 = \hbar\boldsymbol{\kappa}_\lambda. \tag{23}$$

The transition matrix element is to be evaluated to the lowest order of approximation. Thus we can write for the matrix element of q_λ^* the value it would have if there were no interaction between radiation and atoms in the system S. We obtain for the transition matrix element

$$H_{12}' = e\left(\frac{2\pi\hbar c^2}{\nu_\lambda}\right)^{\frac{1}{2}} u_1^* \mathbf{e}_\lambda u \cdot \boldsymbol{\alpha}_2, \tag{24}$$

where u_1 and u_2 are, respectively, the Dirac amplitudes for the initial and final states of the particle.

In seeking the probability of transition from either initial spin state to one or other of the final spin states of the particle, we must sum the square of the above expression over the final spin states and average over the initial states. Representing the result by the symbol $|H'|_{Av}^2$, we obtain by a straightforward computation

$$|H'|_{Av}^2 = \frac{2\pi\hbar c^2 e^2}{\nu_\lambda}\left[\left(1+\frac{c^2p_1^2}{(mc^2+W_1)^2}\right)\times\left(1+\frac{c^2p_2^2}{(mc^2+W_2)^2}\right)\right]^{-1}\left\{\frac{c^2p_1^2}{(mc^2+W_1)^2}+\frac{c^2p_2^2}{(mc^2+W_2)^2}+2c^2\frac{(\mathbf{e}_\lambda\cdot\mathbf{p}_1)(\mathbf{e}_\lambda\cdot\mathbf{p}_2)-(\mathbf{e}_\lambda\times\mathbf{p}_1)\cdot(\mathbf{e}_\lambda\times\mathbf{p}_2)}{(mc^2+W_1)(mc^2+W_2)}\right\}. \tag{25}$$

In lowest order of approximation we set $\mathbf{p}_2=\mathbf{p}_1$ in the above expression and obtain, after some simplification,

$$|H'|_{Av}^2 = (2\pi\hbar e^2/\nu_\lambda)v^2\cos^2\psi, \tag{26}$$

where v is the velocity of the particle and ψ is the angle between $\mathbf{e}_\lambda$ and $\mathbf{p}_1$.

For given $\boldsymbol{\kappa}_\lambda$, we choose the two orthogonal states of polarization to correspond, respectively, to $\mathbf{e}_\lambda$ perpendicular and parallel to the plane of $\mathbf{p}_1$ and $\boldsymbol{\kappa}_\lambda$. For the perpendicular polarization $\cos^2\psi=0$. Thus we obtain the familiar result that the Čerenkov radiation is polarized parallel to the plane of $\mathbf{p}_1$ and $\boldsymbol{\kappa}_\lambda$. If θ is the angle between $\mathbf{p}_1$ and $\boldsymbol{\kappa}_\lambda$, then since $\mathbf{e}_\lambda$ is perpendicular to $\boldsymbol{\kappa}_\lambda$, we obtain for the parallel polarization

$$|H'|_{Av}^2 = (2\pi\hbar e^2/\nu_\lambda)v^2\sin^2\theta. \tag{27}$$

We now seek the probability of a transition wherein the momentum of the charged particle changes from $\mathbf{p}_1$ to $\mathbf{p}_2$ while the system S, initially in the ground state, emits a photon into solid angle $d\Omega$ with angular frequency between ν and $\nu+d\nu$. In passing to the continuum for the radiation field, subscripts λ are dropped. Let $wd\nu d\Omega$ be the probability of such a transition in a time t. Then we can write[7]

$$wd\nu d\Omega = \frac{\rho(\nu)d\nu}{t}\cdot\frac{d\Omega}{4\pi}\cdot 4|H'|_{Av}^2\frac{\sin^2(\frac{1}{2}\omega t)}{\hbar^2\omega^2}, \tag{28}$$

where

$$\hbar\omega = W_1 - W_2 - \Delta W \tag{29}$$

is the difference in energy between the initial and final state,

$$\rho(\nu) = \nu^2/2\pi^2c^3 \tag{30}$$

is the number of final states per unit volume per unit range of angular frequency,[8] $|H'|_{Av}^2$ is to have the value for the parallel polarization as given by (27), and ΔW is given by (16).

Since momentum is conserved in the transition, we can write, for $\hbar\kappa \ll p_1$,

$$W_1 - W_2 = c^2p_1(p_1-p_2)/W_1 = v(p_1-p_2) = v\hbar\kappa\cos\theta. \tag{31}$$

Thus we have

$$\omega = v\kappa\cos\theta - \Delta W/\hbar = (v\nu/c)\cos\theta - (\Delta W/\hbar), \tag{32}$$

and hence[9]

$$d\Omega = d\varphi d(\cos\theta) = (c/v\nu)d\varphi d\omega, \tag{33}$$

where θ and φ are the usual polar angles with respect to the path of the particle as polar axis.

The expression (28) is now to be integrated over all directions. After integration over φ, we obtain, with the aid of (27), (30), and (33),

$$\int wd\Omega = \frac{e^2v}{\hbar c^2}\cdot\frac{2}{\pi t}\int \sin^2\theta\frac{\sin^2(\frac{1}{2}\omega t)}{\omega^2}d\omega. \tag{34}$$

The limits of integration in (34) are

$$\omega = \pm v\kappa - \Delta W/\hbar, \tag{35}$$

while the principal maximum of the integrand, for sufficiently large t, lies essentially at $\omega=0$. If the point $\omega=0$ does not lie inside the range of integration, the right hand side of (34) will, for large t, be effectively zero. Thus, Čerenkov radiation of frequency ν will be emitted only if for that frequency the equation for θ,

$$0 = v\kappa\cos\theta - \Delta W/\hbar \tag{36}$$

---

[7] See, for example, L. I. Schiff, *Quantum Mechanics* (McGraw-Hill Book Company, Inc. New York, 1949), p. 193.

[8] The density of final states is that of the radiation field since the final momentum of the particle is determined by the momentum of the emitted photon.

[9] It is assumed that the medium is isotropic, so that ΔW is independent of the direction of $\boldsymbol{\kappa}$.

has a root θ_0, with $0<\theta_0<\pi$. If such a root exists, θ_0 is the angle of the Čerenkov cone and is given by

$$\cos\theta_0=\Delta W/v\hbar\kappa. \tag{37}$$

Recalling that $\hbar\kappa$ is the change in momentum of S in the transition, we obtain with the aid of (10),

$$\cos\theta_0=c/v\sqrt{\epsilon}. \tag{38}$$

Thus, if

$$\sqrt{\epsilon}>c/v, \tag{39}$$

Čerenkov radiation will be emitted, the angle of the Čerenkov cone being given by (38). If (39) is satisfied, the integration in (34) will extend over the principal maximum of the integrand, and one can then, for large t, write in the usual way[10]

$$\begin{aligned}\int w d\Omega&=\frac{e^2v}{\hbar c^2}\sin^2\theta_0\cdot\frac{2}{\pi t}\int_{-\infty}^{\infty}\frac{\sin^2(\frac{1}{2}\omega t)}{\omega^2}d\omega\\&=\frac{e^2v}{\hbar c^2}\sin^2\theta_0\\&=\frac{e^2v}{\hbar c^2}\left(1-\frac{c^2}{\epsilon v^2}\right),\end{aligned} \tag{40}$$

with the aid of (38). This is the number of photons emitted per unit time per unit range of angular frequency.

The above result is formally the same as is obtained in the classical theory.[10] It is however necessary now to show that the definition of the dielectric constant, (10), leads to the same expression for ϵ in a medium of low density as is given by the Kramers-Heisenberg dispersion formula.

FORMULA FOR THE DIELECTRIC CONSTANT

From the definition of the dielectric constant, (10), we obtain with the aid of (16) and (19)

$$\begin{aligned}\frac{1}{\sqrt{\epsilon}}&=\frac{\Delta W}{c|\Delta\mathbf{P}|}=\frac{\Delta W}{\hbar\nu}\\&=1+\frac{2\pi}{\nu^2}\left\{\sum_i\frac{e_i^2}{m_i}+\sum_b\frac{\left|\sum_i\frac{e_i}{m_i}\langle a|\,\mathbf{e}\cdot\mathbf{p}_i\exp(i\boldsymbol{\kappa}\cdot\mathbf{r}_i)\,|b\rangle\right|^2}{W_a-W_b-\hbar\nu}\right.\\&\quad\left.+\sum_b\frac{\left|\sum_i\frac{e_i}{m_i}\langle a|\,\mathbf{e}\cdot\mathbf{p}_i\exp(-i\boldsymbol{\kappa}\cdot\mathbf{r}_i)\,|b\rangle\right|^2}{W_a-W_b+\hbar\nu}\right\}.\end{aligned} \tag{41}$$

[10] See reference 7, p. 265.

With the assumption that the medium is of low density, the direct interaction between different atoms can be neglected. Then a matrix element such as

$$\langle a|\,\mathbf{e}\cdot\mathbf{p}_i\exp(i\boldsymbol{\kappa}\cdot\mathbf{r}_i)\,|b\rangle$$

will be different from zero only if b represents a state in which only that atom to which the ith particle belongs is excited, while all the other atoms are in their ground states. Then W_b-W_a must be the difference in energy between an excited state and the ground state of a single atom, and we can consider W_b and W_a as representing the actual energies of these states.

We now treat the atoms as being fixed. Then for radiation whose wavelength is much greater than an atomic diameter, the exponentials $\exp(i\boldsymbol{\kappa}\cdot\mathbf{r}_i)$ and $\exp(-i\boldsymbol{\kappa}\cdot\mathbf{r}_i)$ can be replaced by their values at the position of the center of the atom to which the ith particle belongs. Thus (41) can be rewritten

$$\begin{aligned}\frac{1}{\sqrt{\epsilon}}&=1+\frac{2\pi}{\nu^2}\sum_{j,k}\frac{e_k^2}{m_k}+\frac{2\pi}{\nu^2}\sum_b\left|\sum_k\frac{e_k}{m_k}\langle a|\,\mathbf{e}\cdot\mathbf{p}_k\,|b\rangle\right|^2\\&\quad\times\left[\frac{|\sum_j\exp(i\boldsymbol{\kappa}\cdot\mathbf{R}_j)|^2}{W_a-W_b-\hbar\nu}+\frac{|\sum_j\exp(-i\boldsymbol{\kappa}\cdot\mathbf{R}_j)|^2}{W_a-W_b+\hbar\nu}\right].\end{aligned} \tag{42}$$

In the foregoing expression, $\mathbf{R}_j$ is the position of the jth atom, summation over j represents summation over all of the atoms in unit volume, and summation over k represents summation over all of the particles in a single atom. For a random distribution of the atoms, we average over the phases and set

$$|\sum_j\exp(i\boldsymbol{\kappa}\cdot\mathbf{R}_j)|^2=|\sum_j\exp(-i\boldsymbol{\kappa}\cdot\mathbf{R}_j)|^2=N, \tag{43}$$

where N is the number of atoms per unit volume. We also write

$$\frac{1}{m_k}\langle a|\,\mathbf{e}\cdot\mathbf{p}_k\,|b\rangle=-i\nu_{ba}\langle a|\,\mathbf{e}\cdot\mathbf{r}_k\,|b\rangle, \tag{44}$$

where

$$\hbar\nu_{ba}=W_b-W_a. \tag{45}$$

Then (42) becomes, with the aid of (43), (44), and (45),

$$\begin{aligned}\frac{1}{\sqrt{\epsilon}}&=1+\frac{2\pi N}{\nu^2}\sum_k\frac{e_k^2}{m_k}+\frac{2\pi N}{\nu^2}\sum_b|\sum_k e_k\langle a|\,\mathbf{e}\cdot\mathbf{r}_k\,|b\rangle|^2\nu_{ba}^2\\&\quad\times\left[\frac{1}{\hbar(-\nu_{ba}-\nu)}+\frac{1}{\hbar(-\nu_{ba}+\nu)}\right].\end{aligned} \tag{46}$$

Following a procedure due to Dirac,[11] the above ex-

[11] Reference 4, p. 265.

pression can be shown to reduce to the form

$$\frac{1}{\sqrt{\epsilon}}=1-\frac{4\pi N}{\hbar}\sum_b \frac{\nu_{ba}|\langle a|\sum_k e_k \mathbf{e}\cdot\mathbf{r}_k|b\rangle|^2}{\nu_{ba}^2-\nu^2}. \quad (47)$$

Finally, recalling that we are dealing with a medium of low density for which $\epsilon-1$ is small, we can write

$$\epsilon=1+\frac{8\pi N}{\hbar}\sum_b \frac{\nu_{ba}|\langle a|\sum_k e_k \mathbf{e}\cdot\mathbf{r}_k|b\rangle|^2}{\nu_{ba}^2-\nu^2}. \quad (48)$$

This is precisely the expression for the dielectric constant given by the Kramers-Heisenberg dispersion formula.[12]

ACKNOWLEDGMENT

This investigation was carried out during the 1953 session of the Summer Research Institute of the Canadian Mathematical Congress at Queen's University, Kingston. The writer wishes to express his gratitude for the award of an Associateship with the Institute.

[12] See reference 4. Also see J. H. Van Vleck, *Electric and Magnetic Susceptibilities* (Oxford University Press, London, 1932), p. 362.

PHYSICAL REVIEW VOLUME 92, NUMBER 6 DECEMBER 15, 1953

Periodic Deviations in the Schottky Effect

S. C. MILLER, JR.,* AND R. H. GOOD, JR.†
Department of Physics, University of California, Berkeley, California

(Received August 6, 1953)

The periodic deviations in the Schottky effect are recalculated in this paper. The same basic model is taken as in the work of Guth and Mullin, and of Juenker, Colladay, and Coomes. The difference between this work and the previous treatments is that WKB-type approximations are used. It is felt that these remove some of the uncertainties in the derivation. The results are essentially the same as those of Juenker, Colladay, and Coomes, except that the amplitude of the deviations found is about twice as large and has a slightly different dependence on the field.

I. INTRODUCTION

WHEN the logarithm of the current emitted from a metal is plotted against the square root of the electric field applied, the resulting curve is very nearly a straight line over a large range of the applied field. This dependence of the current on the field is known as the Schottky[1] effect. Experimentally in the Schottky region the curve has small deviations from straightness which are roughly periodic. A summary of the experimental data has been given by Juenker, Colladay, and Coomes.[2] The period of the deviations depends primarily on the field; the amplitude depends on both the field and the temperature. The theory of Guth and Mullin,[3] based on the one-dimensional potential shown in Fig. 1 and modified by Juenker, Colladay, and Coomes,[2] predicts the correct period and it also agrees closely with the observed variation of amplitude with field and temperature. However, the amplitude itself and the phase predicted by the theory disagree with the experimental results. As one possible origin of the disagreement, Brock, Houde, and Coomes[4] have suggested that the shape of the assumed potential may be incorrect in Region II (Fig. 1). The reason for making this suggestion is that the only effect of the potential in this region is to introduce a constant factor into the amplitude and a constant term into the phase of the theoretical results. Another possible origin of the disagreement, as emphasized by Juenker, Colladay, and Coomes,[2] is that some of the approximations used in developing the theory may not be applicable.

In this paper the periodic deviations in the Schottky effect are recalculated. In accordance with the sug-

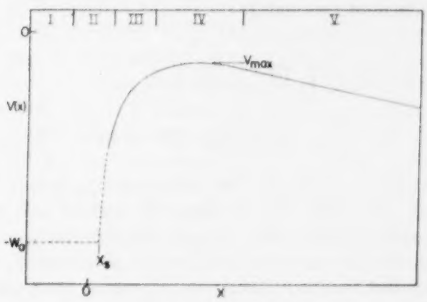

FIG. 1. The potential $V(x)$ assumed for an electron at the surface of a metal. The solid curve represents the function $-eFx-e^2(4x)^{-1}$. The dashed curve represents the same function for $x>x_s$ and the function $-W_0$ for $x<x_s$. The Roman numerals indicate special regions discussed.

* Present address: Department of Physics, University of Colorado, Boulder, Colorado.
† Present address: Department of Physics, The Pennsylvania State College, State College, Pennsylvania.
[1] W. Schottky, Physik. Z. **15**, 872 (1914).
[2] Juenker, Colladay, and Coomes, Phys. Rev. **90**, 772 (1953).
[3] E. Guth and C. J. Mullin, Phys. Rev. **59**, 575 (1941).
[4] Brock, Houde, and Coomes, Phys. Rev. **89**, 851 (1953).

gestion of Brock, Houde, and Coomes, the results are expressed in terms of a parameter μ which gives the effect of the potential in Region II; μ itself is found separately for the potential of Fig. 1. A WKB-type approximation recently proposed[5] has been used throughout; in some respects it gives improved results and it is felt that it removes some of the uncertainties in the derivation. The results obtained are essentially the same as those of Juenker, Colladay, and Coomes, except that the amplitude is about twice as large and depends in a slightly different way on the field. The details of the calculations are given in Secs. II to V; Sec. VI contains a discussion, including an estimate of the nonperiodic deviations from the Schottky effect.

II. BASIC EQUATIONS

Some of the fundamental equations needed for the study of electron emission are given in this section.[6] A model often used (in particular by Guth and Mullin, and by Juenker, Colladay, and Coomes) is that the electrons move in the one-dimensional potential, shown in Fig. 1,

$$\begin{aligned} V(x) &= -eFx - e^2(4x)^{-1}, && \text{when} \quad x > x_s, \\ &= -eFx_s - e^2(4x_s)^{-1} = -W_a, && \text{when} \quad x < x_s, \end{aligned} \tag{1}$$

where $-e^2(4x)^{-1}$ is the image potential at position x normal to the metal for an electron of charge $-e$, and $-eFx$ is the potential due to the applied field F. The value of W_a is a property of the metal. Ordinarily W_a is large compared to the amount $e^{\frac{1}{2}}F^{\frac{1}{2}}$ that the peak of the potential $V(x)$ is below zero. This is the model used below, except that in most of the calculations the shape of the potential in the neighborhood of the point x_s (the dashed part of the curve in Fig. 1) is left unspecified.

The current emitted per unit area is[7]

$$j = 4\pi mk^2eh^{-3}(1-\bar{r}_v)T^2 \exp[(\bar{\mu}-V)(kT)^{-1}], \tag{2}$$

where T is the temperature, k is Boltzmann's constant, and $\bar{\mu}$ is the electrochemical potential. The factor $(1-\bar{r}_v)$ is the average transmission coefficient through the surface of the metal,

$$(1-\bar{r}_v) = (kT)^{-1}\int_V^\infty [1-r_v(W)] \times \exp[-(W-V)(kT)^{-1}]dW, \tag{3}$$

where $[1-r_v(W)]$ is the transmission through the surface at energy W. In Eqs. (2) and (3), V is the potential at some point far outside the surface of the metal. Because of the thickness of the barrier, when the applied field is in the Schottky region, only energies near and above the peak are of importance in evaluating the integral. With these formulas the problem reduces to the calculation of $[1-r_v(W)]$. Because of its dependence on the potential V, this term gives also the final influence of the field F on the current j.

Assuming that the conventional WKB approximation applies in Regions I, III, and V (Fig. 1), Herring and Nichols[8] have shown that the transmission coefficient $[1-r_v(W)]$ can be expressed in terms of a parameter λ which depends only on the potential in Region IV and a parameter μ which depends only on the potential in Region II. The following connections between the WKB approximations to the wave functions of the electron define the parameters λ and μ;

$$\begin{aligned} &p^{-\frac{1}{2}} \exp\left(-i\hbar^{-1}\int_0^x p(\xi)d\xi\right) \text{ in Region III} \rightleftarrows \\ &\lambda c_1^* p^{-\frac{1}{2}} \exp\left(i\hbar^{-1}\int_0^x p(\xi)d\xi\right) \\ &\quad + c_1 p^{-\frac{1}{2}} \exp\left(-i\hbar^{-1}\int_0^x p(\xi)d\xi\right) \text{ in Region V}, \end{aligned} \tag{4}$$

$$\begin{aligned} &c_2 p^{-\frac{1}{2}} \exp\left(-i\hbar^{-1}\int_0^x p(\xi)d\xi\right) \text{ in Region I} \rightleftarrows \\ &\mu p^{-\frac{1}{2}} \exp\left(i\hbar^{-1}\int_0^x p(\xi)d\xi\right) \\ &\quad + p^{-\frac{1}{2}} \exp\left(-i\hbar^{-1}\int_0^x p(\xi)d\xi\right) \text{ in Region III}, \end{aligned} \tag{5}$$

where c_1 and c_2 are complex constants and

$$p(x) = \{2m[W-V(x)]\}^{\frac{1}{2}} \tag{6}$$

is the momentum of the electron. With these definitions the transmission coefficient, defined as the ratio of the current transmitted into Region I to the current incident in Region V, can be written as

$$[1-r_v(W)] = 1 - |(\lambda+\mu)(1+\lambda^*\mu)^{-1}|^2. \tag{7}$$

In terms of the abbreviation

$$\theta(W) = \arg(\lambda^*\mu) \tag{8}$$

the transmission coefficient becomes[9]

$$\begin{aligned} [1-r_v(W)] &= (1-|\lambda|^2)(1-|\mu|^2) \\ &\quad \times (1+2|\lambda\mu|\cos\theta + |\lambda\mu|^2)^{-1} \\ &= (1-|\lambda|^2)(1-|\mu|^2)(1-|\lambda\mu|^2)^{-1} \\ &\quad \times [1+2\sum_{n=1}^{\infty}(-|\lambda\mu|)^n \cos n\theta]. \end{aligned} \tag{9}$$

[5] S. C. Miller, Jr., and R. H. Good, Jr., Phys. Rev. **91**, 174 (1953).

[6] C. Herring and M. H. Nichols, Revs. Modern Phys. **21**, 185 (1949).

[7] Reference 6, p. 192.

[8] Reference 6, p. 252.

[9] This expansion is given by, for example, R. Courant and D. Hilbert, *Methoden der Mathematischen Physik* (Julius Springer, Berlin, 1937), Vol. II, p. 246.

It will be shown that the constant term in the series leads to the normal Schottky effect and that each of the terms $n \geq 1$ gives a deviation oscillatory in the field F. The frequencies of these deviations are roughly proportional to n; because of this qualitative difference, one expects to be able to separate the contributions of the various terms. Also the amplitudes decrease with increasing n because of the additional $|\lambda\mu|$ factors. In this paper only the normal Schottky effect and the first oscillatory deviation will be discussed so the series only needs to be carried as far as the $n=1$ term.

III. CALCULATION OF THE PARAMETER λ

The parameter λ, defined by Eq. (4), is to be found from a discussion of the Schrödinger equation,[10]

$$(d^2\psi/dx^2)+2[W-V(x)]\psi=0, \tag{10}$$

in the region near the peak of the potential barrier where $V(x)=-Fx-(4x)^{-1}$. A WKB-type approximation for this type of potential barrier problem has been given in reference 5. From Eq. (36) of that paper one finds easily that

$$p^{-\frac{1}{2}}\exp\left(\tfrac{1}{2}\pi E+i\,\mathrm{Re}\int_x^{x_1}p(\xi)d\xi\right)\text{ in Region III}\rightleftarrows$$

$$p^{-\frac{1}{2}}\exp\left(-\tfrac{1}{2}\pi i+i\,\mathrm{Re}\int_{x_2}^{x}p(\xi)d\xi\right)$$

$$+[(2/\pi)^{\frac{1}{2}}(|E|/2e)^{-\frac{1}{2}iE}\Gamma(\tfrac{1}{2}+\tfrac{1}{2}iE)\cosh(\tfrac{1}{2}\pi E)]$$

$$\times p^{-\frac{1}{2}}\exp\left(\tfrac{1}{4}\pi E-i\,\mathrm{Re}\int_{x_2}^{x}p(\xi)d\xi\right)\text{ in Region V,} \tag{11}$$

where x_1 and x_2 are the locations of the zeros of $p^2(x)=2[W+Fx+(4x)^{-1}]$, chosen so that $x_1<x_2$ when they are real and so that x_1 has positive imaginary part and x_2 negative imaginary part when they are complex. A branch of $p(x)$ such that $\arg p(x)$ is either 0 or $\frac{1}{2}\pi$ when x is real is to be used, and E is given by

$$E=2\pi^{-1}i\int_{x_1}^{x_2}p(\xi)d\xi. \tag{12}$$

A comparison of Connections (4) and (11) gives the parameter λ:

$$\lambda=[(2/\pi)^{\frac{1}{2}}(|E|/2e)^{\frac{1}{2}iE}\Gamma(\tfrac{1}{2}-\tfrac{1}{2}iE)\cosh(\tfrac{1}{2}\pi E)]^{-1}$$

$$\times\exp\left(-\tfrac{1}{4}\pi E-\tfrac{1}{2}\pi i-2i\,\mathrm{Re}\int_0^{x_1}p(\xi)d\xi\right). \tag{13}$$

Using the connection between the gamma and the trigonometric functions, one finds

$$|\lambda|=(1+e^{\pi E})^{-\frac{1}{2}}. \tag{14}$$

[10] Hartree units (m, e, $\hbar=1$) are used in the rest of the paper.

The expression for $\arg\lambda$ is more involved,

$$\arg\lambda=\tfrac{1}{2}E-\tfrac{1}{2}E\ln(\tfrac{1}{2}|E|)+\arg\Gamma(\tfrac{1}{2}+\tfrac{1}{2}iE)$$

$$-\tfrac{1}{2}\pi-2\,\mathrm{Re}\int_0^{x_1}p(\xi)d\xi. \tag{15}$$

The integrals in Eqs. (12) and (15) are elliptic; for $W<0$ they are

$$\int_{x_1}^{x_2}p(\xi)d\xi=\tfrac{2}{3}i|W|^{\frac{1}{2}}F^{-1}(1+a)^{\frac{1}{2}}\{\mathrm{E}[(2a)^{\frac{1}{2}}(1+a)^{-\frac{1}{2}}]$$

$$-(1-a)\mathrm{K}[(2a)^{\frac{1}{2}}(1+a)^{-\frac{1}{2}}]\}, \tag{16}$$

$$\int_0^{x_1}p(\xi)d\xi=\tfrac{2}{3}|W|^{\frac{1}{2}}F^{-1}(1+a)^{\frac{1}{2}}\{\mathrm{E}[(1-a)^{\frac{1}{2}}(1+a)^{-\frac{1}{2}}]$$

$$-a\mathrm{K}[(1-a)^{\frac{1}{2}}(1+a)^{-\frac{1}{2}}]\}, \tag{17}$$

where K and E are the complete elliptic integrals of the first and second kinds,

$$\mathrm{K}[\mathrm{k}]=\int_0^{\pi/2}(1-\mathrm{k}^2\sin^2\phi)^{-\frac{1}{2}}d\phi, \tag{18}$$

$$\mathrm{E}[\mathrm{k}]=\int_0^{\pi/2}(1-\mathrm{k}^2\sin^2\phi)^{\frac{1}{2}}d\phi, \tag{19}$$

and a is defined by

$$a=(1-FW^{-2})^{\frac{1}{2}} \tag{20}$$

(the argument of a is either 0 or $-\frac{1}{2}\pi$ and the arguments of $(1+a)^{\frac{1}{2}}$ and $(1-\mathrm{k}^2\sin^2\phi)^{\frac{1}{2}}$ are in the neighborhood of zero). A table for the evaluation of the integral in Eq. (16) when $W<-F^{\frac{1}{2}}$ has been given by Burgess, Kroemer, and Houston[11] since the same integral arose in Nordheim's discussion of field emission.[12]

IV. CALCULATION OF THE PARAMETER μ

The parameter μ, defined by Eq. (5), is to be found from a discussion of the Schrödinger equation, Eq. (10), in Regions I, II, III using the potential with the break at x_s as given in Eq. (1) and as shown in Fig. 1. Here the wave functions on the two sides of x_s are to be found separately and then are to be matched at the break. If the usual WKB method is used to approximate the wave function on the right of the break, the results obtained for $|\mu|^2$ are somewhat inaccurate, especially as W_s becomes large. This is illustrated in Fig. 27 of the review article by Herring and Nichols.[13] As W_s increases, x_s decreases and in the region just to the right of the break the $(2x)^{-1}$ term in $p^2(x)$ becomes dominant. Accordingly, one is led to use a WKB-type approximation having as basic functions the solutions

[11] Burgess, Kroemer, and Houston, Phys. Rev. **90**, 515 (1953).
[12] L. W. Nordheim, Proc. Roy. Soc. (London) **A121**, 626 (1928).
[13] Reference 6, p. 250.

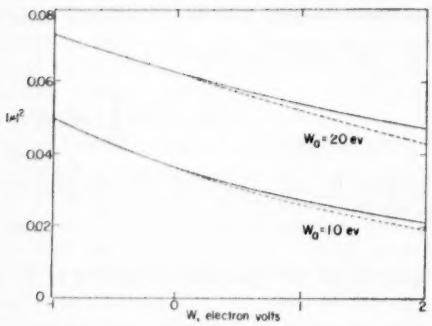

FIG. 2. The reflection coefficient $|\mu|^2$ as a function of the energy W for zero electric field. The dashed lines for $W>0$ are from the exact calculations of Nordheim and MacColl. The solid lines were found using Eq. (24).

of the Schrödinger equation,

$$(d^2\phi/dS^2)+S^{-1}\phi=0. \tag{21}$$

This gives the following approximate wave functions to the right of the break:

$$\psi\cong p^{-\frac{1}{2}}\left(\int_0^x p(\xi)d\xi\right)^{\frac{1}{2}}Z_1\left(\int_0^x p(\xi)d\xi\right), \tag{22}$$

where Z_1 indicates any Bessel function of the first order. It is convenient to take a specific wave function which has the asymptotic form appearing in Connection (5). This is

$$\psi_1=\left(\tfrac{1}{2}\pi p^{-1}\int_0^x p(\xi)d\xi\right)^{\frac{1}{2}}\left[\mu e^{\frac{1}{2}\pi i}H_1^{(1)}\left(\int_0^x p(\xi)d\xi\right)\right.$$
$$\left.+e^{-\frac{1}{2}\pi i}H_1^{(2)}\left(\int_0^x p(\xi)d\xi\right)\right]\rightarrow$$
$$\mu p^{-\frac{1}{2}}\exp\left(i\int_0^x p(\xi)d\xi\right)$$
$$+p^{-\frac{1}{2}}\exp\left(-i\int_0^x p(\xi)d\xi\right)\text{ in Region III,} \tag{23}$$

where the asymptotic forms of the Hankel functions $H_1^{(1)}(z)$, $H_1^{(2)}(z)$ for large z have been used.[14] The logarithmic derivative of the wave function must be continuous across the break x_s. Furthermore, the potential is constant to the left of the break so that the left-going wave given in Connection (5) for Region I is an exact solution of the Schrödinger equation up to the point x_s. Therefore the logarithmic derivative has the constant value $-ip=-i[2(W+W_a)]^{\frac{1}{2}}$ to the left of x_s and the condition

$$d\psi_1/dx=-i[2(W+W_a)]^{\frac{1}{2}}\psi_1, \quad \text{when} \quad x=x_s, \tag{24}$$

may be applied to determine μ. As a matter of convenience μ may be calculated in the form of an expansion on WW_a^{-1} and FW_a^{-2}, with the result that

$$\mu=\left[\frac{H_0^{(2)}(z)+iH_1^{(2)}(z)}{-H_1^{(1)}(z)+iH_0^{(1)}(z)}\right]_{z=(2W_a)^{\frac{1}{2}}}$$
$$\times\{1+O(WW_a^{-1})+O(FW_a^{-2})\}. \tag{25}$$

The value of $|\mu|^2$ for zero electric field as found from Eq. (24) is compared with the exact results of Nordheim[12] and MacColl[15] in Fig. 2. In order that other models for calculating μ may be used conveniently, the value of μ is left unspecified in the next section. For many of these models the type of approximation used above will be applicable.

V. THE PERIODIC DEVIATIONS

As a first step in finding the average transmission coefficient, Eq. (14) and Eq. (9) to order $n=1$ may be substituted into Eq. (3) yielding

$$(1-\bar{r}_v)=(kT)^{-1}\int_V^\infty(1-|\mu|^2)\left[\frac{e^{\pi E}}{1-|\mu|^2+e^{\pi E}}\right.$$
$$\left.-\frac{2e^{\pi E}|\mu|\cos\theta}{(1-|\mu|^2+e^{\pi E})(1+e^{\pi E})^{\frac{1}{2}}}\right]$$
$$\times\exp\{-(W-V)(kT)^{-1}\}dW. \tag{26}$$

An exact discussion of this integral would be difficult. A series of approximations will be applied in order to express the results in a simpler form. As a first approximation, it will be assumed that $|\mu|^2$ can be neglected compared to 1 in the range of energy W which contributes to this integral. Accordingly, $1-|\mu|^2$ will be replaced simply by 1 in the integrand.

For $E<-1$[16] the quantity in the square brackets in Eq. (26) is effectively zero (it is assumed that $e^{\pi E}$ is dominant over $\exp[-W(kT)^{-1}]$ for $E<-1$) and for $E>2$ it is effectively one. Consequently, only the functional dependence of E on W in the range $-1<E<2$ is of importance in the evaluation of the integral. From Eq. (12) one sees that E varies monotonically with W and that $E=0$ when $W=V_{\max}=-F^{\frac{1}{2}}$. Therefore one is led to expand E as given by Eqs. (12) and (16) for small ϵ, where

$$\epsilon=(|V_{\max}|)^{-1}(W-V_{\max})=1+WF^{-\frac{1}{2}}. \tag{27}$$

When ϵ is small, a is small and, using the expansions of the elliptic functions[17] for small moduli, one finds that

$$E=F^{-\frac{1}{2}}\epsilon+O(\epsilon^2). \tag{28}$$

In the Schottky region the field ranges roughly from

[14] E. Jahnke and F. Emde, *Tables of Functions* (Dover Publications, New York, 1945), fourth edition, p. 138.

[15] L. A. MacColl, Phys. Rev. **56**, 699 (1939).

[16] In what follows, $x=-\pi$ will be used uniformly as the cut-off point for e^x.

[17] Reference 14, p. 73.

10^5 to 10^6 volts/cm; therefore F ranges roughly from 2×10^{-7} to 2×10^{-4} and $F^{-\frac{1}{2}}$ from 50 to 10. Consequently, ϵ is at most 0.2 in the region $-1<E<2$ and, for the purposes of evaluating the integral, only the linear term in ϵ need be retained in Eq. (28). Then, combining Eqs. (27) and (28), one has

$$E=F^{-\frac{1}{2}}(1+WF^{-\frac{1}{2}}), \tag{29}$$

and the integration variable in Eq. (26) can conveniently be changed from W to E. Furthermore, the lower limit can be taken to be $-\infty$.

The same ideas will be used for $\arg\lambda$, given by Eqs. (15) and (17). Using the expansions of the elliptic integrals[17] about unit modulus, one finds that

$$\mathrm{Re}\int_0^{x_1} p(\xi)d\xi=F^{-\frac{1}{2}}[\tfrac{2}{3}-\tfrac{1}{4}\epsilon\ln|\epsilon| + ((5/4)\ln 2-\tfrac{3}{4})\epsilon+O(\epsilon^2\ln|\epsilon|)]. \tag{30}$$

Also the gamma function may be expanded about $E=0$,

$$\arg\Gamma(\tfrac{1}{2}+\tfrac{1}{2}iE)=-(\tfrac{1}{2}\gamma+\ln 2)E+O(E^3), \tag{31}$$

where $\gamma=0.577$ is Euler's constant. As a consequence of the arguments about the important range of E, the higher-order terms in Eq. (30) will be disregarded. The terms of order E^3 and higher in Eq. (31) will be neglected also, although this is a coarser approximation [numerical calculations indicate that, as a consequence, the amplitude of the periodic deviations in Eq. (41) is low by about 10 percent and that the phase is off by less than 3°]. Collecting Eqs. (8), (15), (30), (31), one finds

$$\theta=b+\pi cE, \tag{32}$$

where, as abbreviations,

$$b=\tfrac{1}{2}\pi+\arg\mu+(4/3)F^{-\frac{1}{2}}, \tag{33}$$

$$c=\pi^{-1}(-2+\tfrac{1}{2}\gamma+3\ln 2-\tfrac{1}{8}\ln F). \tag{34}$$

With the further abbreviation

$$d=(\pi kT)^{-1}F^{\frac{1}{2}}, \tag{35}$$

Eq. (26) in the small $|\mu|^2$ approximation becomes

$$(1-\bar{r}_v)=d\exp[(V+F^{\frac{1}{2}})(kT)^{-1}]\int_{-\infty}^{\infty}\left[\frac{e^{-\pi Ed}}{1+e^{\pi E}} - \frac{2|\mu|\ \mathrm{Re}(e^{-\pi Ed+ib+\pi iEc})}{(1+e^{\pi E})^{\frac{1}{2}}}\right]e^{\pi E}\pi dE, \tag{36}$$

where the integration variable has been changed from W to E and Eq. (32) has been used for θ. Next it will be assumed that μ does not vary appreciably with the energy W in the range of W which is important so that $|\mu|$ and b are constants for the integration. The symbol μ_p will be used for this value of μ. Then, on changing the integration variable from E to $e^{\pi E}$ it is seen that the integrals are simply beta functions, so that

$$(1-\bar{r}_v)=d\exp[(V+F^{\frac{1}{2}})(kT)^{-1}]\{\Gamma(1-d)\Gamma(d) - 4\pi^{-\frac{1}{2}}|\mu_p|\ \mathrm{Re}[e^{ib}\Gamma(1-d+ic)\Gamma(\tfrac{1}{2}+d-ic)]\}. \tag{37}$$

Here d is small; at 1500°K, d ranges from 6×10^{-4} to 10^{-1} as the field varies from 10^5 to 10^6 volts/cm. Only a first approximation for small d to each of the terms will be calculated. The dependence on d then disappears from the second term in the braces, and the connection between the gamma and trigonometric functions can be used to express the absolute values of the gamma functions simply in terms of hyperbolic functions. Then, using Eq. (2), one finds for the emitted current,

$$j=\tfrac{1}{2}\pi^{-2}(kT)^2\exp[(\bar{\mu}+F^{\frac{1}{2}})(kT)^{-1}] \times\{1-4(2\pi c)^{\frac{1}{2}}(\sinh 2\pi c)^{-\frac{1}{2}}d|\mu_p| \times\cos[b+\arg\Gamma(1+ic)+\arg\Gamma(\tfrac{1}{2}-ic)]\}. \tag{38}$$

It is seen from Eq. (34) that $2\pi c$ is greater than 3 in the Schottky region, so $2^{-\frac{1}{2}}e^{\pi c}$ can be written instead of $(\sinh 2\pi c)^{\frac{1}{2}}$. Also the Stirling approximation,

$$\Gamma(z)\cong(2\pi)^{\frac{1}{2}}e^{-z}z^{z-\frac{1}{2}}, \tag{39}$$

can be used to obtain simple expressions for the arguments of the gamma functions. Finally, the common logarithm of the current is needed for comparison with the experimental results; in taking the logarithm of the quantity in braces, the approximation $\ln(1+z)\cong z$ may be used since the second term is small compared to one. When these three operations are performed, the result is

$$\log_{10}j=\log_{10}[\tfrac{1}{2}\pi^{-2}(kT)^2] + (\log_{10}e)(kT)^{-1}(\bar{\mu}+F^{\frac{1}{2}})+F_2, \tag{40}$$

where the first terms give the normal Schottky effect and the primary contribution to the periodic deviations is given by

$$F_2=(\log_{10}e)\pi^{-\frac{1}{2}}e^{2-\frac{1}{2}\gamma}(kT)^{-1}c^{\frac{1}{2}}F^{7/8}|\mu_p| \times\sin\{(4/3)F^{-\frac{1}{2}}+\arg\mu_p+\tfrac{1}{2}\arctan c + \tfrac{1}{2}c\ln[(4+4c^2)(1+4c^2)^{-1}]\}. \tag{41}$$

In these expressions b and d have been written out explicitly to show the dependence on F and μ_p. The parameter c, given by Eq. (34), still depends on the field F but varies slowly compared to the dependences explicitly shown.

This result applies for arbitrary shapes of the potential curve in Regions I and II (Fig. 1) provided that, in agreement with the assumption made following Eq. (26), $|\mu|^2$ is small compared to one in the range $-F^{\frac{1}{2}}(1+F^{\frac{1}{2}})<W<\pi kT$ and provided that, in agreement with the assumption made following Eq. (36), μ does not vary appreciably in the range $-F^{\frac{1}{2}}(1+F^{\frac{1}{2}})<W<-F^{\frac{1}{2}}(1-2F^{\frac{1}{2}})$. The F-dependent limits here are found by translating the important range of E into terms of W according to Eq. (29).

The μ discussed in Sec. IV satisfies both these conditions, as is seen from the following argument. A

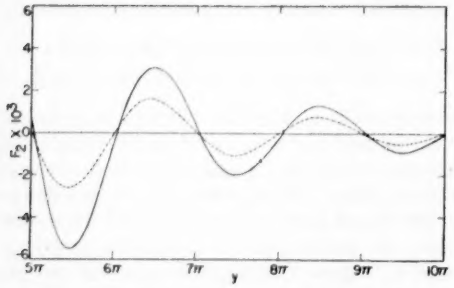

FIG. 3. The periodic deviation from the Schottky effect F_2 as a function of $y=(4/3)F^{-\frac{1}{2}}$, based on the potential shown in Fig. 1 and for $W_a=10$ electron volts and $T=1500°K$. The solid line represents the results of the present calculations; the dotted line is a plot of the results of Juenker, Colladay, and Coomes.

representative value of the temperature T is 1500°K, of W_a is 10 electron volts, and the fields are ordinarily less than 10^6 volts/cm. Therefore $FW_a^{-2}<0.001$ and also, since $|W|<0.015$ within the ranges discussed in the above paragraph, $|WW_a^{-1}|<0.04$. Accordingly the higher order terms in Eq. (25) may be disregarded. The value of $|\mu|^2$ thus never departs appreciably from its value when $W=0$ and $F=0$; from Fig. 2 it is seen that this is much less than one as required. Furthermore, μ is slowly varying with W in the required region and evidently

$$\mu_p=\left[\frac{H_0^{(2)}(z)+iH_1^{(2)}(z)}{-H_1^{(1)}(z)+iH_0^{(1)}(z)}\right]_{z=(2W_a)^{-\frac{1}{2}}}. \quad (42)$$

VI. DISCUSSION

On the basis of the model in Fig. 1, the periodic deviation predicted is given in Eqs. (41) and (42). The phase prediction agrees with that of Juenker, Colladay, and Coomes[2] as is seen from Fig. 3, in which the periodic deviations are plotted for a particular case. The only temperature dependence is the T^{-1} factor in the amplitude, and the primary field dependence of the phase is the $(4/3)F^{-\frac{1}{2}}$ term; these features agree with the results of Juenker, Colladay, and Coomes as well as with the original work of Guth and Mullin.[3] The field dependence of the amplitude is contained in the factor $c^{\frac{1}{2}}F^{7/8}$, where c is defined by Eq. (34). This differs slightly from the previous calculations which gave an $F^{\frac{1}{2}}$ dependence.

Thus, except for the difference in the amplitude, the present results are the same as those of Juenker, Colladay, and Coomes and their analysis of the agreement with experiment still applies. Especially they have re-emphasized that the predicted phase seems to differ from the experimental phase by about 90° for all metals and for all values of the field studied so far and that the difference may be due to a wrong choice of the model for calculating μ. The amplitude found here appears to be in better agreement with the experimental amplitudes. However, this improvement may not be significant because if a different model should correct the phase through the $\arg\mu_p$ term, it might also affect the amplitude through the $|\mu_p|$ factor. Also, Brock, Houde, and Coomes[4] have pointed out that, because of patch effects, measurements of the amplitude are less certain than measurements of the phase.

An estimate of the nonperiodic deviation from the Schottky effect may be obtained from a more detailed discussion of the first term in the square brackets in Eq. (26). If, as indicated by the discussion preceding Eq. (42), it may be assumed that $|\mu|^2$ may be taken constant in the range $-F^{\frac{1}{2}}(1+F^{\frac{1}{2}})<W<\pi kT$, then the nonperiodic part of the average transmission coefficient is

$$(1-\bar{r}_v)_{NP} = \frac{1-|\mu_p|^2}{kT}\int_V^{\infty}\frac{e^{\pi E}\exp\{-(W-V)(kT)^{-1}\}}{1-|\mu_p|^2+e^{\pi E}}dW. \quad (43)$$

This integral may be evaluated by the same methods as used in Sec. V; using Eq. (29) to change the integration variable from W to E, extending the lower limit to $-\infty$, and integrating on $(1-|\mu_p|^2)^{-1}e^{\pi E}$, one finds

$$(1-\bar{r}_v)_{NP}=\frac{1-|\mu_p|^2}{(1-|\mu_p|^2)^d}\frac{\pi d}{\sin\pi d}\exp\left(\frac{V+F^{\frac{1}{2}}}{kT}\right)$$
$$\cong[1-|\mu_p|^2(1-d)+\tfrac{1}{6}\pi^2d^2]$$
$$\times\exp\{(V+F^{\frac{1}{2}})(kT)^{-1}\}. \quad (44)$$

In the last step an expansion for small $|\mu_p|^2$ and d has been made and enough terms have been retained to show the primary dependence on the field regardless of whether $|\mu_p|^2$ is large or small compared to d. The final result is that the expression for $\log_{10}j$ in Eq. (40) is to be increased by the term

$$F_1=-(\log_{10}e)|\mu_p|^2[1-(\pi kT)^{-1}F^{\frac{1}{2}}]$$
$$+\tfrac{1}{6}(\log_{10}e)(kT)^{-2}F^{\frac{1}{2}}, \quad (45)$$

if the nonperiodic deviation also is required. This is smaller than the first periodic deviation and is ordinarily not observed.

Calculating of the Cohesive Energy of Diamond*

L. A. SCHMID†
Palmer Physical Laboratory, Princeton University, Princeton, New Jersey
(Received August 3, 1953)

It is well known that a satisfactory value for the binding energy of the hydrogen molecule may be calculated using a wave function which has the form of a Heitler-London (HL) function built on non-orthogonal orbitals. However, Slater has shown that a HL function built on orthogonal orbitals fails to yield any binding for the hydrogen molecule, but binding may be achieved by mixing with the HL function an ionized-molecule function which assigns two electrons to one atom and none to the other. Satisfactory results may also be achieved using a Hund-Mulliken (HM) function which may be built on either orthogonal or non-orthogonal orbitals, since the wave functions resulting in these two cases may be shown to be identical.

The present calculation shows that the situation for diamond is entirely analogous to that for the hydrogen molecule in that the usual formulation of the Slater-Pauling (SP) directional theory of valence, which is a generalization of the HL method using orthogonal orbitals, fails to yield any binding, but satisfactory results are achieved when this theory is reformulated to allow ionization to be introduced into the bonds. It is also shown that for the observed value of the lattice parameter, which is the only value for which the calculations have been performed, satisfactory results are also achieved using a wave function which is built on orthogonal HM orbitals, each of which, like its counterpart in the hydrogen molecule case, is spread out over a pair of bonded atoms.

As a by-product of the main calculation, the total exchange energy of Bloch-type functions belonging to the valence bands of diamond is calculated and found to be essentially equal to the value obtained using free-electron functions.

INTRODUCTION

THE Slater-Pauling (SP) directional theory of valence is essentially a generalization of the Heitler-London (HL) method to the case of an arbitrary molecule or crystal. However, while the HL method as applied to the problem of the hydrogen molecule employs a wave function built on one-electron functions whose space parts are not orthogonal to each other, the wave function used in the general case is built on one-electron functions whose space parts are mutually orthogonal. Until Slater[1] recently applied the general form of the theory based on orthogonal orbitals to the hydrogen molecule, it had never been subjected to a decisive analytical test because all prior applications of it, while using the energy expression appropriate to orthogonal orbitals, in one way or another made unwarranted use of the results of the HL calculation for the hydrogen molecule based on non-orthogonal orbitals. Slater's calculation shows that in the case of hydrogen, the general theory is inadequate in that it not only fails to give any binding, but also indicates that the triplet state has lower energy than the singlet state. This situation may be corrected, in the case of hydrogen, by means of a configuration interaction between a HL function which assigns one electron to each atom and an ionized-molecule wave function which assigns two electrons to one atom and none to the other. But, while the method of configuration interaction is very convenient in the case of the hydrogen molecule, it is unworkable in the case of a large molecule or crystal. A configuration interaction which mixes states of the whole molecule or crystal is also objectionable from the conceptual point of view in that it fails to give expression (or does so only in a very indirect manner) to the fact that the valence bond is a local affair involving only an atom and its immediate neighbors. It will now be shown that the SP theory may be cast into a form which emphasizes the local nature of the valence bond and which allows a generalization that permits the necessary configuration interaction between bonded orbitals to be carried out locally, rather than requiring the mixing of states of the entire molecule or crystal. This will be called the "ionized-bond" formulation of the theory.

1. IONIZED-BOND FORMULATION OF THE SLATER-PAULING THEORY

While the following discussion is in terms of the diamond lattice, it will be apparent that the methods and results may be adapted to the case of any molecule or crystal in which it is valid to assume that the bonds are localized, i.e., no resonance between different bond eigenfunctions occurs. In such a case there is a unique pairing of all the valence orbitals into bonded pairs, the two orbitals of any given pair having opposite spin. In accordance with the intuitive ideas of the SP theory which assert that the bond strength of two bonded orbitals is greater the more they overlap, we regard the orbitals as lobes which point toward their bonded partners. In the case of diamond there are four valence orbitals per atom and every atom has four nearest neighbors located at the vertices of a regular tetrahedron circumscribed about the atom. Since the diamond lattice[2]

* Part of a dissertation presented to the faculty of Princeton University in partial fulfillment of the requirements for the degree of Doctor of Philosophy.

† Now at Michigan State College, East Lansing, Michigan.

[1] J. C. Slater, J. Chem. Phys. **19**, 220 (1951).

[2] For figures illustrating the diamond lattice see, for example, C. Herring, J. Franklin Inst. **233**, 525 (1942), Fig. 3 on p. 538; or A. F. Wells, *Structural Inorganic Chemistry* (Oxford University Press, London, 1950), second edition, Fig. 166 on p. 511.

consists of two interpenetrating face-centered cubic lattices such that the four nearest neighbors of an atom belonging to one of the two interpenetrating lattices all belong to the other lattice, the lobe-like valence orbitals of atoms belonging to one lattice point toward the vertices of a tetrahedron fixed in space, while the orbitals of atoms belonging to the other lattice point in the opposite directions, i.e., toward the faces of the tetrahedron. Let the space part of a valence orbital of an atom belonging to one lattice be designated u_i and let v_j be the space part of its bonded partner which belongs to an atom of the other lattice and which points in the direction opposite to that in which u_i points so that the overlap of the two lobes is a maximum.

Instead of using these one-electron functions to construct the Slater determinants from which the electronic wave function for the crystal is formed in the usual formulation of the SP theory,[3] we shall use them to construct two-electron functions which will in turn be used to build the wave function for the crystal.‡ Let us assume that the space parts of the valence orbitals are normalized and are mutually orthogonal. Let φ_{ij} be the normalized two-electron function constructed from the two bonded lobes whose space parts are u_i and v_j. Since Slater[1] found that, in the case of the hydrogen molecule, satisfactory results could be obtained using a wave function built on orbitals with orthogonal space parts only if the wave function was taken to be a mixture of the ordinary HL function and the ionized-molecule function, we shall assume φ_{ij} to have the following form:

$$\varphi_{ij}(k,l)=\frac{1}{[2(1+A^2)]^{\frac{1}{2}}}\{[u_i(k)v_j(l)+v_j(k)u_i(l)] +A[u_i(k)u_i(l)+v_j(k)v_j(l)]\} \times\left[\frac{\alpha(k)\beta(l)-\beta(k)\alpha(l)}{\sqrt{2}}\right], \quad (1\text{-}1)$$

where α and β are spin functions, and the arguments k and l designate the kth and lth sets of electron coordinates, respectively. The quantity in the first square brackets inside the curly brackets corresponds to the HL function while that in the second square brackets may be called an "ionized-bond" function and corresponds to having two valence electrons on one bonded atom and none on the other. The adjustable parameter A which determines the relative proportions of these two functions in φ_{ij} will ultimately be adjusted so as to minimize the energy. This amounts to carrying out a configuration interaction between the two bonded orbitals having space parts u_i and v_j.

For the sake of simplicity, let us regard the two 1s orbitals belonging to any atom of the diamond lattice as constituting a bonded pair. The difference between a bonded pair of 1s orbitals and a bonded pair of valence orbitals is that, while the space parts of the bonded valence orbitals are orthogonal, the space parts of the bonded 1s orbitals are identical. If we designate the space parts of two bonded 1s orbitals by u_i^0 and u_j^0, then $u_i^0=u_j^0$ and the corresponding φ_{ij} is

$$\varphi_{ij}(k,l)=u_i^0(k)u_j^0(l)[\alpha(k)\beta(l)-\beta(k)\alpha(l)]/\sqrt{2}. \quad (1\text{-}2)$$

We note that the φ's defined by (1-1) and (1-2) are antisymmetric with respect to interchange of their electron coordinates, that is

$$\varphi_{ij}(k,l)=-\varphi_{ij}(l,k). \quad (1\text{-}3)$$

They also constitute an orthonormal system since

$$(\varphi_{ij}(k,l)\,|\,\varphi_{ij}(k,l))_{k,l}=1; \quad (\varphi_{ij}(k,l)\,|\,\varphi_{i'j'}(k,m))_k=0; \quad \text{pair } i,\ j\neq\text{pair } i',\ j',\ l\neq k, \text{ and } m\neq k; \quad (1\text{-}4)$$

where the subscripts k and l appended to the first inner product indicate that the integration is over the kth and lth sets of electron coordinates and the subscript k on the second inner product means that the integration extends only over the kth set of coordinates.

The electronic wave function of the crystal, ψ, may be written in terms of the φ's as follows:

$$\psi=2^{-N/2}\sum_P(-1)^P P\varphi_{1,2}(1,2)\varphi_{3,4}(3,4)\cdots \times\varphi_{N-1,N}(N-1,N), \quad (1\text{-}5)$$

where N is the total number of electrons (including 1s) in the crystal. The permutation operator P acts only on the electron coordinates and not on the subscripts of the φ's. Because of the antisymmetry of the φ's set forth in (1-3), if the factor $2^{-N/2}$ did not multiply the summation over all permutations, every independent term in ψ would be repeated $2^{N/2}$ times. By multiplying by $2^{-N/2}$, we obtain ψ in the form of the sum of $2^{-N/2}N!$ independent terms. Using the orthonormality conditions (1-4), we see that the norm of ψ is $2^{-N/2}N!$.

If (1-5) is to be a valid wave function for the diamond lattice, it must be an eigenfunction of total spin (assuming a spin-independent Hamiltonian for the crystal) belonging to the eigenvalue $S^2=0$, because diamond is diagmagnetic. This is obviously the case since each of the φ's as defined by (1-1) and (1-2) belongs to the eigenvalue $S^2=0$. ψ must also belong to an irreducible representation of the space group O_h^7 which describes the symmetry of the diamond lattice. ψ does, in fact, belong to the identity representation. This may easily be seen from the following argument: Any symmetry operation will result in a relabelling of the orbitals of

[3] See, for example, Eyring, Walter, and Kimball, *Quantum Chemistry* (John Wiley and Sons, New York, 1944), Chap. XIII.

‡ Note added in proof: The author's attention has been called to the brief discussion of the possibility of formulating the wave function of a crystal in terms of two-electron functions which has been given by L. Pauling, Proc. Roy. Soc. (London) **196**, 343 (1949). See p. 361 of this article.

the lattice, but a bonded pair of orbitals before the symmetry operation will be a bonded pair afterward, so the net effect on ψ will be a reordering of the factors in the terms of (1-5). But since the order of the factors in any term is completely irrelevant, ψ is unchanged. Hence it belongs to the identity representation.

It can be shown[4] that ψ as defined by (1-5) reduces for the case $A=0$ to the wave function employed in the usual formulation of the SP theory.[3] It can also be shown[4] that for the case $A\neq 0$, (1-5) is equal to a linear combination of the usual SP wave functions corresponding to all possible configurations which may be generated in the diamond lattice by shifting electrons into the orbitals of their bonded partners, that is by ionizing the bonds. Thus, if we evaluate the energy of the diamond lattice using ψ as defined in (1-5) for the case of arbitrary A, and then adjust A to minimize the energy, we are, from the point of view of the usual form of the SP theory, carrying out an immensely complicated configuration interaction, but doing it in a way which is not only computationally much more tractable, but is also intuitively more appealing because it stresses the local nature of the valence bond.

Finally, we note that for $A=1$, (1-1) may be written in the form

$$\varphi_{ij}(k,l)=\tfrac{1}{2}[u_i(k)+v_j(k)][u_i(l)+v_j(l)]\times[\alpha(k)\beta(l)-\beta(k)\alpha(l)]/\sqrt{2}, \quad (1.6)$$

which has the form of the simple Hund-Mulliken wave function for the two bonded orbitals of the hydrogen molecule. Writing all the φ's in (1-5) in this way and expanding all the products of spin functions, we obtain a sum of products of one-electron orbitals which is antisymmetric for the interchange of any pair of electron coordinates. The number of terms in this sum is $2^{N/6}2^{N/3}2^{-N/2}N!=N!$, where $N/6$ and $N/3$ are the number of pairs of $1s$ orbitals and valence orbitals, respectively, and $2^{-N/2}N!$ is the number of terms in (1-5). A typical one-electron function in this expression would have the form

$$2^{-3/4}[u_i(k)+v_j(k)]\alpha(k).$$

Thus, for $A=1$, (1-5) is identical, except for normalization, to a single Slater determinant constructed from Hund-Mulliken type orbitals, each of which is the sum of two bonded localized orbitals. This could be called a "semi-generalization" of the Hund-Mulliken method to distinguish it from the "complete generalization" represented by a wave function which is a Slater determinant of Bloch waves, which are spread out over all the atoms of the lattice, instead of just the two atoms of a bonded pair. However, it should be noted that the determinant of the semi-generalization differs only by a unitary transformation from a determinant of Bloch-type functions which are similar to Bloch waves in that they are spread out over all atoms of the lattice, but are more restricted than Bloch waves because they are prescribed linear combinations of atomic orbitals.

[4] L. A. Schmid, Thesis, Princeton University, 1953 (unpublished).

2. ENERGY EXPRESSION FOR DIAMOND LATTICE

We must next find an expression for $(\psi|H|\psi)/(\psi|\psi)$ where ψ is given by (1-5) and the spin-independent Hamiltonian H for the diamond lattice has the form

$$H=\sum_{k=1}^{N}O_1(k)+\sum_{k=1}^{N}\sum_{l<k}^{N}O_2(k,l), \quad (2\text{-}1)$$

where, in atomic units,

$$O_1(k)=-\tfrac{1}{2}\nabla_k^2-6\sum_{L}^{N/6}\frac{1}{|\mathbf{r}_k-\mathbf{R}_L|}, \quad (2\text{-}2)$$

where $\mathbf{r}_k$ and $\mathbf{R}_L$ are the vectors specifying the kth set of electron coordinates and the Lth lattice point, respectively, and ∇_k^2 is the Laplacian operating on the kth set of electron coordinates.

$$O_2(k,l)=1/r_{k,l}=1/|\mathbf{r}_k-\mathbf{r}_l|. \quad (2\text{-}3)$$

(The subscripts on the operators O_1 and O_2 indicate that they involve coordinates of one and two electrons, respectively.) The derivation of an expression for $(\psi|H|\psi)/(\psi|\psi)$ in terms of matrix elements between the one-electron orbitals is a strightforward matter and has been given elsewhere,[4] so it will be omitted here. The expression itself is made somewhat more manageable by a condensation of notation. Since the integral $(u_iu_j|O_2|u_ku_l)$ may be thought of as the Coulomb interaction between the "charge densities" u_iu_k and u_ju_l we shall denote it by $C(ik;jl)$. This notation does not indicate whether the orbitals involved are u's or v's, but no ambiguity results since the u's and v's always have different subscripts. In the expression (2-4) given below the indices i and j, when they appear in the same summation, will designate a bonded pair, and similarly for the indices k and l. If an index j appears in the summand of a summation over i this means that j is not a fixed index but is always the bonded partner of the index i which is being summed. The symbol (ij) under a summation sign means the orbitals i and j are bonded. i/k means the orbitals i and k are not bonded. An upper limit of N for a summation means that the summation is taken over all orbitals of the crystal, including the $1s$ orbitals, even if the summand is written in terms of only u_i and not both u_i and v_j, as in the first summation. An upper limit of $2N/3$ means that the summation is taken over all valence orbitals (but not $1s$ orbitals), and a limit of $N/3$ means that it is taken over all bonded *pairs* of valence orbitals.

$$
\begin{aligned}
&(\psi|H|\psi)/(\psi|\psi)\\
&=\sum_{i=1}^{N}(u_i|\overset{(1)}{O_1}|u_i)+\sum_{i=1}^{N}\sum_{k<i}^{N}C(\overset{(2)}{ii};kk)+\sum_{\substack{i\\(ij)}}^{N/3}C(\overset{(3)}{ij};ij)\\
&-\tfrac{1}{2}\sum_{\substack{i=1\\i/k}}^{N}\sum_{k<i}^{N}C(\overset{(4)}{ik};ik)+\frac{4A}{1+A^2}\sum_{\substack{i\\(ij)}}^{N/3}(u_i|\overset{(5)}{O_1}|v_j)\\
&+\frac{4A}{1+A^2}\sum_{\substack{i\\(ij)}}^{N/3}[\sum_{k=1}^{N}C(\overset{(6)}{ij};kk)\\
&-\tfrac{1}{2}C(ij;ii)-\tfrac{1}{2}C(ij;jj)]\\
&+\frac{A^2}{2(1+A^2)}\sum_{\substack{i\\(ij)}}^{2N/3}[C(ii;ii)\overset{(7)}{-}C(ii;jj)]\\
&+\frac{16A^2}{(1+A^2)^2}\sum_{\substack{i\\(ij)}}^{N/3}\sum_{\substack{k<i\\(kl)}}^{N/3}C(\overset{(8)}{ij};kl)\\
&-\frac{2A}{1+A^2}\sum_{\substack{i\\(ij)}}^{N/3}\sum_{k=1}^{N}C(\overset{(9)}{ik};jk)\\
&-\frac{4A^2}{(1+A^2)^2}\sum_{\substack{i\\(ij)}}^{N/3}\sum_{\substack{k<i\\(kl)}}^{N/3}[C(ik;jl)\overset{(10)}{+}C(il;jk)]. \qquad (2\text{-}4)
\end{aligned}
$$

It will be noted that the first four terms give the energy for the case $A=0$. This constitutes a slight generalization of the energy expression for the case of localized bonds usually cited[5] as resulting from the SP theory in that the $1s$ orbitals, as well as the valence orbitals, have been taken into account.

In the case of the terms involving A, we take the point of view that when A assumes a non-zero value, that is when ionization is introduced into the bonds, a new charge density

$$\rho_A=\sum_{\substack{i\\(ij)}}^{N/3}\rho_{ij},$$

where $\rho_{ij}=[4A/(1+A^2)]u_iv_j$, is superimposed on the charge density for $A=0$, and the terms in (2-4) involving A give the energy associated with this new charge density. Since u_i and v_j are orthogonal, the net charge of ρ_{ij}, and consequently of ρ_A, is zero.

The origin of this charge density is most easily seen for the case $A=1$. In this case we are effectively dealing with Hund-Mulliken type orbitals having space parts $(1/\sqrt{2})(u_i+v_j)$. Squaring these orbitals gives rise to the sum of the squares of the localized orbitals plus cross-product terms. These cross-product terms constitute the new charge density.

The fifth term of (2-4) gives the change in kinetic energy resulting from the ionization correction, and the energy of Coulomb interaction between the nuclear charges and the charge density ρ_A. The sixth term gives the energy of Coulomb interaction of ρ_A with the electronic charge density of the crystal. This interaction may be interpreted in the following way: The charge density ρ_{ij} interacts with the entire electronic charge density of the crystal for the case $A=0$ from which, however, is subtracted half the charge density of the orbitals u_i and v_j. Thus, if we combine the sixth term with the Coulomb part of the fifth term, we may regard the charge density ρ_{ij} as interacting with the neutral atoms of the crystal, except that the two atoms adjoining ρ_{ij} have holes cut into their electronic charge densities through which ρ_{ij} can "see" some of the nuclear charge of these two atoms which would otherwise be shielded. (Calculation[4] shows that, as far as its interaction with the nuclear charges of the two adjoining atoms is concerned, ρ_{ij} behaves like an ordinary electronic charge density; that is, the interaction is attractive.) In this way ρ_{ij} tends to bind together the two atoms adjoining it. The seventh term of (2-4) is just the increase in Coulomb energy associated with ionizing a bond, that is crowding two electrons (with opposite spins) into a single orbital. The eighth term involves the Coulomb interaction between two different charge densities of the type ρ_{ij}. Because each of these has zero net charge, the Coulomb interaction between them is negligible. The ninth and tenth terms involve exchange-type integrals which are of the same order of magnitude, or smaller than the exchange integrals between non-bonded orbitals belonging to neighboring atoms which occur in the fourth term. The approximate value of the latter integrals has been evaluated[4] and found to be completely negligible. Thus the ninth and tenth terms may also be neglected.

The expectation value of the energy of the diamond lattice as given by (2-4) has been calculated for the observed lattice parameter (1.542A) using orbitals derived from the free atom orbitals for carbon given by Torrance.[6] The details of this calculation are given elsewhere,[4] but the essential results will be presented in the following sections. First, the result given by only the first four terms of (2-4) will be discussed. This corresponds to the application of the usual form of the SP theory.[3] The effect of the ionization correction associated with the terms of (2-4) which involve the parameter A will then be discussed.

3. ENERGY OF LATTICE FOR $A=0$

For the case of infinite lattice parameter, the lobe-like u's or v's of a particular atom may be expressed as linear combinations of the single $2s$ orbital and the three $2p$ orbitals occuring in the ^5S state of the free carbon atom. If we designate the space parts of the free atom orbitals by f^s, $f_x{}^p$, $f_y{}^p$, and $f_z{}^p$ then the u's belonging to some particular atom may be written

$$
\begin{aligned}
u_1&=\tfrac{1}{2}[f^s+f_x{}^p-f_y{}^p-f_z{}^p],\\
u_2&=\tfrac{1}{2}[f^s+f_x{}^p+f_y{}^p+f_z{}^p],\\
u_3&=\tfrac{1}{2}[f^s-f_x{}^p-f_y{}^p+f_z{}^p],\\
u_4&=\tfrac{1}{2}[f^s-f_x{}^p+f_y{}^p-f_z{}^p].
\end{aligned}
\qquad (3\text{-}1)
$$

[5] See, for example, reference 3, p. 248.

[6] C. C. Torrance, Phys. Rev. **46**, 388 (1934).

The v orbitals which point in the opposite directions from the u's would be defined in a similar way except that the signs in front of f_x^p, f_y^p, and f_z^p would be changed.

If the spins of the four lobes associated with an atom were all aligned then, in the case of infinite lattice parameter, the atoms of the lattice would all be in the ^5S state because a Slater determinant written in terms of the u's of (3-1) differs only by a unitary transformation from the Slater determinant written in terms of the f's. However, for the wave function defined in (1-5), there is no correlation whatever between the spins of two lobes of an atom. For this reason the energy of the wave function (1-5) for infinite lattice parameter is not the same as the energy of an aggregate of non-interacting carbon atoms in the ^5S state. The energy difference of these two situations has been calculated[4] with the help of the Coulomb and exchange integrals for carbon in the ^5S state given by Ufford[7] and is found to be 0.127 atomic unit per atom where (1-5) is the higher energy state. (1 atomic unit of energy equals 2 Rydbergs or 27.07 ev.) Using the observed value [8] for the energy difference between the ^5S state and the ^3P ground state of the free carbon atom, which is 0.154 atomic unit, we find that the wave function (1-5) for infinite lattice parameter has an energy 0.281 atomic unit per atom above the ground state of the free carbon atom. Let us call (1-5) for infinite lattice parameter the "reference level." The energy of (1-5) for the case of finite lattice parameter must be at least 0.281 atomic unit per atom below the reference level if binding is to be achieved.

For finite lattice parameter the u's and v's may still be written in the form (3-1) except that instead of the f's which are free atom orbitals, we must use functions which belong to certain irreducible representations of the point group T_d which describes the symmetry of the diamond lattice with respect to rotations and reflections. Which of the representations of T_d are involved is determined by the condition that the functions belonging to the representations go over smoothly into free atom functions as the lattice parameter is increased to infinity. These functions may be regarded as distorted versions of the free atom functions and as such may be designated g^s, g_x^p, g_y^p, and g_z^p.

In deriving (2-4) it was assumed that the u's and v's are all mutually orthogonal. The u's or v's belonging to a given atom are mutually orthogonal because the g's belong to different rows of irreducible representations and are consequently orthogonal. (It may be seen from (3-1) that if the f's or g's constitute an orthonormal system, the u's do also.) If the g's on neighboring atoms are mutually orthogonal, then the u's and v's on neighboring atoms are also orthogonal, thus fulfilling the condition assumed in deriving (2-4). We may construct a set of mutually orthogonal g's from the non-orthogonal f's by applying the orthogonality correction which was first given by Landshoff[9] and later generalized by Löwdin.[10] In Löwdin's notation this is, for the case of real orbitals

$$\varphi_\mu=\phi_\mu-\tfrac{1}{2}\sum_\alpha \phi_\alpha S_{\alpha\mu}+\tfrac{3}{8}\sum_{\alpha,\beta}\phi_\alpha S_{\alpha\beta}S_{\beta\mu}-\cdots, \quad (3\text{-}2)$$

where the φ's are mutually orthogonal orbitals constructed from the ϕ's which are not, and

$$S_{\mu\nu}=(\phi_\mu|\phi_\nu)-\delta_{\mu\nu}; \quad \delta_{\mu\nu}=\begin{matrix}1 & \mu=\nu\\ 0 & \mu\neq\nu\end{matrix}. \quad (3\text{-}3)$$

If we neglect ϕ's in (3-2) which are multiplied by factors of order $(S_{\mu\nu})^2$ except for terms involving ϕ_μ (the leading orbital in the expansion), we obtain the form of the orthogonality correction used by Landshoff.

$$\varphi_\mu=\phi_\mu\left[1+\tfrac{3}{8}\sum_\alpha (S_{\mu\alpha})^2\right]-\tfrac{1}{2}\sum_\alpha \phi_\alpha S_{\alpha\mu}. \quad (3\text{-}4)$$

Landshoff showed that the φ's are normalized (if the ϕ's are) to terms of order $(S_{\mu\nu})^3$ and are mutually orthogonal to the extent that $\frac{3}{4}\sum_\alpha S_{\mu\alpha}S_{\alpha\nu}$ and higher order terms are negligible. In our case the φ's are to be identified with the g's and the ϕ's with the f's.

In applying (3-4), only first-nearest neighbors have been taken into account. By concentrating on a g function belonging to some particular atom, which may be called the "central atom," with the help of group theory, the orbitals entering into the orthogonality correction which belong to atoms that are first-nearest neighbors of the central atom may be expressed as a sum of products of radial and angular functions expressed in terms of coordinates centered on the central atom. Using Torrance's free atom functions for carbon,[6] the radial functions in these expansions may be plotted graphically. Thus we obtain the g's in terms of such expansions. The matrix elements of the first term of (2-4) may be expressed in terms of matrix elements involving the g's. Using the expansions for the g's, these matrix elements may then be reduced to sums of one-dimensional radial integrals which may be evaluated graphically. The details of this calculation are given in reference 4. The results show that because the orthogonality correction makes the orbitals bumpier, the kinetic energy is greatly increased. This works against binding. In partial compensation for this increase in energy, there is an increase in the magnitude of the negative energy of the Coulomb interaction of the orbitals of an atom with the nuclear charge of that atom. This comes about because the effect of the orthogonality correction on an orbital is to increase its absolute value (and consequently its charge density) in the neighborhood of the nucleus of the atom to which it belongs and in the vicinity of neighboring atoms, but to decrease it in the region in between. Because of the weighting factor $1/r$ where r is the distance from the nucleus, the net effect as far as interaction of an orbital with the nuclear charge of its own atom is concerned is that of a net shift of charge toward the nucleus.

[7] C. W. Ufford, Phys. Rev. **53**, 568 (1938).
[8] A. G. Shenstone, Phys. Rev. **72**, 411 (1947).
[9] R. Landshoff, Z. Physik **102**, 201 (1936).
[10] P. O. Löwdin, J. Chem. Phys. **18**, 365 (1950).

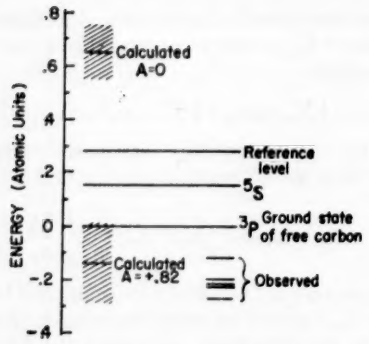

FIG. 1. Energy level diagram for diamond and free carbon. Uncertainty in calculations is indicated by cross-hatching.

The second, third, and fourth terms of (2-4) have also been evaluated by graphical means.[4] Restricting ourselves to only the most important energy contributions, we may give the following description of the situation for the case $A=0$. The orthogonality correction causes a large increase in the kinetic energy. This increase is only partially compensated for by an increase in the magnitude of the negative energy of Coulomb interaction of the orbitals with the nuclear charges of the atoms to which they belong. The Coulomb interaction between neighboring atoms contributes an appreciable negative energy which, however, is not large enough to overcome the effect of the increase in kinetic energy. The exchange integrals between bonded orbitals [third term in (2-4)] contribute a relatively small positive energy and the exchange integrals between non-bonded orbitals on neighboring atoms are found to be completely negligible. The resulting energy of the lattice for the case $A=0$ is $+0.37\pm0.1$ atomic unit per atom with respect to the reference level or $+0.65\pm0.1$ atomic unit per atom with respect to the ground state of free carbon. The uncertainty in this result arises both because of analytical approximations made in the course of the calculations, as well as from the fact that the calculations involve small differences of large numbers, particularly in the case of the Coulomb interaction between neighboring atoms.

The exact value of the observed cohesive energy with which this result is to be compared is still an open question.[11] In all, five values are defended by different workers in the field. They are 73, 125, 136, 141, and 170 kcal/mole or 0.117, 0.200, 0.218, 0.226, and 0.273 atomic unit per atom. The calculated result for $A=0$ is compared with the observed values in the energy level diagram of Fig. 1, which also shows the calculated result when allowance is made for the ionization correction ($A=0.82$).

It should be emphasized that the calculations have been carried out only for the observed lattice parameter and that, while in principle the methods used allow for a variation in the functional forms of the orbitals to minimize the energy, no such variation has actually been carried out. Rather the orthogonalized versions of Torrance's free atom orbitals[6] have been used directly in evaluating the matrix elements. However, varying the functional forms of the orbitals would have only a small effect and would do little to reduce the very large positive value for the energy of the lattice. It will now be shown, however, that the ionization correction ($A\neq0$) decreases this energy by the right amount to give agreement (within the accuracy of the calculation) with experiment.

4. IONIZATION CORRECTION

In order to apply the ionization correction, we must evaluate the matrix elements of the fifth, sixth, and seventh terms of (2-4). It has been mentioned previously that the eighth, ninth, and tenth terms are negligible. Once these matrix elements have been evaluated, we may minimize the energy with respect to A. The calculations show[4] that the energy is minimum for

$$A=+0.82\pm0.06, \tag{4-1}$$

and that the contribution to the lattice energy of the kinetic energy part of the fifth term is -0.69 atomic unit per atom while the contribution of the Coulomb part of the fifth term together with the sixth term is -0.25 and the contribution of the seventh term is $+0.15$. The total contribution of the ionization correction is thus -0.79 atomic unit per atom yielding for the energy of diamond -0.14 atomic unit per atom with respect to the ground state of the free carbon atom. Because it turns out that the calculations for the ionization correction are more sensitive to errors in the orthogonality correction than the calculations for the case $A=0$, the uncertainty in the result is correspondingly greater. However, because the various errors involved arise from independent sources, they may be combined in the manner for random errors which allows for some cancellation. The estimated uncertainty in the final result for the energy of diamond is ±0.15 atomic unit per atom. The calculated energy of diamond for the case $A=+0.82$, together with the uncertainty, is shown in the energy level diagram of Fig. 1.

For $A=1$ we find that the contribution of the ionization correction is -0.77 atomic unit per atom which differs by only a negligible amount from the minimum value of -0.79. This means that a calculation of the cohesive energy for the observed lattice parameter using the single-determinant wave function of the "semi-generalization" of the Hund-Mulliken (HM) method yields substantially the same result as a calculation based on the more general wave function (1-5). While this is true for the observed lattice parameter and probably also for smaller parameters, it is not true for

[11] The experimental situation with regard to the cohesive energy of diamond is reviewed very briefly, with references to the literature, in Appendix B of reference 4. The work prior to 1947 has also been reviewed by H. D. Hagstrum, Phys. Rev. 72, 947 (1947).

large lattice parameters. The reason for this is well known.[12] It is simply that when we use orbitals which are spread over several atoms, we are automatically introducing into the wave function ionized states, i.e., states in which some atoms have too many, and others too few electrons, but the crystal as a whole stays electrically neutral. These ionized states remain in the wave function even when the lattice parameter is increased to infinity with the result that we calculate too large an energy for the case of infinite lattice parameter. This would not happen if we were to use the more general wave function (1-5) because in this case we could remove the ionized states by setting $A=0$.

The negative sign of the kinetic energy contribution of the fifth term of (2-4) may be understood most easily in terms of the HM-type orbitals. When we go over from orbitals localized about single atoms to HM-type orbitals spread over two atoms, the orbitals necessarily become smoother with a resultant decrease in kinetic energy. The signs of the two Coulomb contributions of the ionization correction are apparent from the discussion in Sec. 2.

5. CONCLUSIONS

Since the energy for the case $A=1$ differs only by a negligible amount from that for $A=0.82$ and since it has been shown that the general wave function (1-5) reduces in the case $A=1$ to a single Slater determinant of one-electron functions similar to those employed in the HM approach to the hydrogen molecule in that each of the functions is spread over the two orbitals of a bonded pair, the following rough explanation of the nature of the binding in diamond may be given: When the free carbon atoms are brought together to form the diamond lattice, the localized orbitals become distorted in order that they might be orthogonal to orbitals on neighboring atoms. This distortion causes an increase in kinetic energy which outweighs the negative energy associated with the Coulomb interaction between neighboring atoms and the negative energy which results because the orthogonality correction brings about a net displacement of the charge of the orbitals of an atom closer to the nuclear charge of that atom. By going over from orbitals localized about single atoms to HM-type orbitals spread over two atoms a decrease in kinetic energy is brought about as well as a change in the Coulomb energy which favors binding. The two effects are of just the right magnitude to achieve the desired binding. The change in Coulomb energy may be interpreted as resulting from the redistribution of charge density associated with the transition to HM-type orbitals. In the case of HM-type orbitals the charge density tends to concentrate more between bonded atoms and, by its interaction with the nuclear charges of the atoms, hold them together. This explanation of the binding is very rough and omits many smaller contributions to the energy which are of both signs and thus tend to cancel. These contributions, however, have been taken into account in the calculations.

The most striking aspect of the calculation is its direct analogy with the corresponding calculation[1] for the hydrogen molecule which, for a HL wave function built on orthogonal orbitals, shows that an energy per atom greater than the energy of a free hydrogen atom in its ground state results. The present calculation shows that for a wave function which is the generalization of the HL function using orthogonal orbitals [(1-5) with $A=0$], the same thing happens in diamond. The calculation for hydrogen shows that satisfactory results can be obtained by mixing some of the ionized-molecule state with the HL function built on orthogonal orbitals, and it turns out that satisfactory results are also achieved when the corresponding thing is done for diamond. Finally, in the case of the hydrogen molecule, it is evident that a HM function built on orthogonal orbitals gives satisfactory results because this wave function may easily be shown to be identical with a HM function built on non-orthogonal orbitals, and the results obtained with such a function are about as satisfactory as the results obtained using a HL function built on non-orthogonal orbitals. The present calculation shows that a generalization of the HM function for hydrogen built on orthogonal orbitals also gives satisfactory results in the case of diamond.

As a by-product of the calculation, the total exchange energy per atom of the valence orbitals has been calculated for a wave function of the form of a single Slater determinant of localized HM-type orbitals. It may be shown[4] that this is equal to the exchange energy of valence orbitals for a Slater determinant of Bloch-type functions which are constructed from linear combinations of the localized HM orbitals, the valence orbitals in this case being the Bloch-type functions in the valence bands. It is found when this is compared with the exchange energy for free electrons that, to within the accuracy of the calculation, the two are equal. The exchange energy per atom for the Bloch-type functions is -1.43 ± 0.1 atomic units as against -1.39 atomic units for free electrons. Herring and Hill have shown[13] that an approximate equality of the exchange energy of Bloch waves with that of free-electron functions is to be expected in the case of monovalent metals. The present results indicate that this approximate equality is valid in much more general cases.

ACKNOWLEDGMENT

I wish to thank Professor E. P. Wigner and Dr. Conyers Herring for interesting and helpful discussions during the course of this work.

[12] See, for example, J. C. Slater, Quarterly Progress Report, Solid State and Molecular Theory Group, Massachusetts Institute of Technology, July 15, 1952 (unpublished), p. 27.

[13] C. Herring and A. G. Hill, Phys. Rev. **58**, 132 (1940).

Paramagnetic Scattering of Neutrons by Rare Earth Oxides

W. C. KOEHLER* AND E. O. WOLLAN
Oak Ridge National Laboratory, Oak Ridge, Tennessee
(Received June 1, 1953)

The magnitude and angular dependence of the paramagnetic scattering of neutrons has been studied for the trivalent ions in the rare earth oxides, Pr_2O_3, Nd_2O_3, and Er_2O_3. These rare earth ions have large angular momentum contributions to their magnetic moments and one object of the investigation was to obtain a better understanding of the magnetic scattering in such cases. The angular distribution of the scattering for samples at room temperature is compared with the theoretical results of Trammell which are given in the following paper. The calculations based on screened hydrogenic wave functions give results in reasonably good accord with the measurements when the screening constant is taken as an adjustable parameter which is then determined, within limits, by the data. Scattering measurements were also made at liquid nitrogen and liquid hydrogen temperatures, and within a few percent no changes and, hence, no crystalline field or exchange effects were observed.

INTRODUCTION

INVESTIGATIONS of the magnetic scattering of neutrons,[1] which have been carried out thus far, have been concerned, primarily, with the ions or metals of the 3*d* transition group in which the orbital contributions to the moments are wholly or partially quenched by crystalline field interactions. In the present work, the neutron technique is applied to ions of the rare earth series, in which the magnetic moments arise from the unfilled 4*f* shell in which the electrons are more deeply buried within the atom than the 3*d* electrons of the iron group, and they are thus less affected by crystalline fields. Susceptibility measurements on a variety of rare earth salts give effective magnetic moments at near room temperature which correspond closely to the values to be expected for the free ions, the orbital contributions being thus wholly operative.

The theory for the magnetic scattering of neutrons as developed by Bloch,[2] Schwinger,[3] Halpern and Johnson,[4] and others, has been limited, in the consideration of the angular dependence of the scattering, to the case of ions having spin moments only. As a consequence of the present studies on the rare earths, G. Trammell of this laboratory was led to extend the application of the theory to include the more general situation involving both spin and orbital contributions to the magnetic moments. This work appears in the following paper.[5] This problem has now also been considered by Kleiner.[6]

Only a few of the rare earths can, at the moment, be studied by the neutron-scattering technique, either because they are not available in sufficient quantities, or because in several cases they possess a prohibitively large capture cross section. Fortunately, the development of the ion exchange method in recent years has made some of them available in useable amounts. The magnetic scattering studies reported here are primarily concerned with the sesquioxides of neodymium and erbium, and in some of these measurements, separated isotopes of neodymium have been used. Some measurements are also reported for Pr_2O_3.[7] Neodymium and erbium constitute an interesting pair in that their trivalent ions have, in the ground state, the same spin and angular momentum ($L=6$, $S=3/2$). Nd^{+++} has three 4*f* electrons and according to Hund's rule the normal state is ${}^4J_{9/2}$ and Er^{+++} has three vacancies in the 4*f* shell corresponding to the state ${}^4J_{15/2}$. There is Russell-Saunders coupling with L and S combining "antiparallel" and "parallel" respectively in the two ions.

The theory of the paramagnetic susceptibility of rare earth ions has been given by Hund[8] and Van Vleck.[9] In the cases of neodymium and erbium, the multiplet spacing is large compared to kT at room temperature and to a close approximation only the normal state need be considered. The effective magnetic moment is then given by

$$\mu_{\text{eff}}^2=\beta^2\left[\mathbf{L}\cdot\frac{\mathbf{J}}{|\mathbf{J}|}+2\mathbf{S}\cdot\frac{\mathbf{J}}{|\mathbf{J}|}\right]^2 =g^2\beta^2J(J+1), \tag{1}$$

where β is the Bohr magneton and g is the Landé g-factor.

Except for a term which is independent of temperature and is negligible for this case, the susceptibility

* The work herein reported has been included as part of a dissertation submitted to the Graduate Council of the University of Tennessee in partial fulfillment of the requirements for the degree of Doctor of Philosophy.

[1] I. W. Ruderman, Phys. Rev. **76**, 1572 (1949); Shull, Strauser, and Wollan, Phys. Rev. **83**, 333 (1951); Shull, Wollan, and Koehler, Phys. Rev. **83**, 912 (1951); R. A. Erickson, Phys. Rev. **90**, 779 (1953).

[2] F. Bloch, Phys. Rev. **50**, 259 (1936); **51**, 994 (1937).

[3] J. S. Schwinger, Phys. Rev. **51**, 544 (1937).

[4] O. Halpern and M. H. Johnson, Phys. Rev. **59**, 898 (1939).

[5] G. T. Trammell, Phys. Rev. **90**, 355 (1953); Phys. Rev. (to be published).

[6] W. H. Kleiner, Phys. Rev. **90**, 168 (1953).

[7] We are indebted to Dr. F. H. Spedding of Ames Laboratory for the praseodymium and neodymium samples and to Dr. G. E. Boyd of the Oak Ridge National Laboratory Chemistry Division for the erbium sample. The separated isotopes were obtained from the Stable Isotopes Division of Oak Ridge National Laboratory.

[8] F. Hund, Z. Physik **33**, 855 (1925).

[9] J. H. Van Vleck, *The Theory of Electron and Magnetic Susceptibilities* (Oxford University Press, London, 1932).

for a free ion is related to μ_{eff} by

$$\chi = N\mu_{\text{eff}}^2/3kT. \quad (2)$$

For the rare earth oxides considered here the susceptibility has, however, been shown to follow the Curie-Weiss law over a wide range of temperature:[10-12]

$$\chi = C/(T+\Delta), \quad (3)$$

with Weiss constants Δ in the range from 10° to 50°. This indicates that there is in these compounds some effect of exchange or of crystalline field splitting or both.

Evidence for crystalline field effects has been obtained at low temperatures by Gorter and deHaas,[13] Spedding,[14] Van den Handel,[15] and Bleaney and Scovil[16] for various dilute salts of the rare earths and these experimental results have served as the basis for the theoretical calculations of Penney and Schlapp,[17] Spedding,[14] and Elliot and Stevens.[18] Presumably, similar effects should also be expected in the magnetically more concentrated oxides. Selwood[11] has investigated the effect on the Weiss constant of dilution of Nd_2O_3 with La_2O_3 and he concludes that an appreciable fraction of the Weiss constant for Nd_2O_3 may be attributed to exchange interactions. A direct measurement of the g-value for Nd_2O_3 has been carried out by Sucksmith[19] which is in good agreement with the Hund value for Nd^{+++}. This measurement, then, indicates that the effective moment at not too low temperatures is that of the free ion.

The differential cross section for the scattering of slow neutrons by a free paramagnetic ion depends also on the effective magnetic moment of the ion. There is an angular dependence of the magnetic scattering arising from the spacial distribution of the spin and orbital currents in the atom and this aspect of the problem, with which this work is primarily concerned, will be discussed in the last section of the paper. For long wavelength neutrons or for scattering in the near forward direction, the differential cross section for a free paramagnetic ion with Russell-Saunders coupling has been shown to be[3,5]

$$\sigma(k)_{k\to 0} = \frac{2}{3}\left(\frac{e^2\gamma}{2mc^2}\right)^2 g^2 J(J+1), \quad (4)$$

where $k = (4\pi/\lambda)\sin(\varphi/2)$, in which λ is the wavelength and φ the scattering angle; γ is the magnetic moment of the neutron in nuclear Bohr magnetons, and $g^2J(J+1)$ is the effective magnetic moment of the free ion in Bohr magnetons.

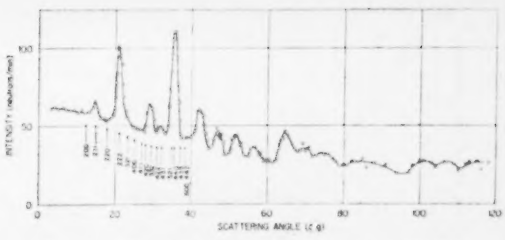

FIG. 1. Diffraction pattern for erbium oxide (Er_2O_3).

DISCUSSION OF SAMPLES

The samples were all ignited to remove any possible contamination with water and CO_2, and were stored in a desiccator until used. In every case, x-ray diffraction patterns were made to establish the crystallographic form of the materials. The diffraction cells were sealed, and weighed before and after each run. In some cases special procedures were followed and these are described for the individual samples below.

The Nd_2O_3 sample was obtained and used first in the hexagonal form. It was of high purity as determined spectroscopically at Ames, and also by C. Feldman of Oak Ridge National Laboratory. The thermal capture cross section was measured by H. Pomerance and found to have a value of 42 barns. The magnetic susceptibility was measured over the temperature range of 80°K to 300°K, by C. Nelson of this laboratory, and the results of these measurements gave a Weiss constant of $27°\pm7°$ and an effective magnetic moment of 3.8 ± 0.1 Bohr magneton.

For the measurements on the cubic form of Nd_2O_3 the sample was converted by the method of Löhberg.[20] Complete conversion was shown by an x-ray pattern as well as by the neutron pattern.

The praseodymium sample was received in the form of the black oxide, Pr_6O_{11}. The pale green sesquioxide was prepared by reducing Pr_6O_{11} in a hydrogen atmosphere at 700°C. After the reduction was complete, the sample was held at 400°C for six hours in a vacuum. Measurements of the magnetic susceptibility of this preparation were also made.

MEASUREMENTS

Erbium Oxide

The room temperature diffraction pattern of Er_2O_3 taken at a neutron wavelength of 1.16A is shown in Fig. 1. The Bragg reflections are due entirely to coherent nuclear scattering and the coherent cross section for erbium as evaluated from patterns of this type is $\sigma_{\text{coh}} = 7.8\pm0.4$ barns. In addition to the coherent contribution, there is also a considerable amount of

[10] S. Rabideau, J. Chem. Phys. **19**, 874 (1951).
[11] P. W. Selwood, J. Am. Chem. Soc. **55**, 3161 (1933).
[12] B. Cabrera and A. Duperier, Comptes rend. **188**, 1640 (1929).
[13] C. J. Gorter and W. T. de Haas, Leiden Comm. 218b (1931).
[14] F. H. Spedding, J. Chem. Phys. **5**, 316 (1937).
[15] J. Van den Handel, Thesis, Leiden, 1942 (unpublished).
[16] B. Bleaney and H. E. D. Scovil, Proc. Phys. Soc. (London) **A63**, 1369 (1950); **64**, 204 (1951).
[17] W. G. Penney and R. Schlapp, Phys. Rev. **41**, 194 (1932).
[18] R. J. Elliot and K. W. H. Stevens, Proc. Phys. Soc. (London) **A64**, 205 (1951); Proc. Roy. Soc. (London) **A215**, 437 (1952).
[19] W. Sucksmith, Proc. Roy. Soc. (London) **A135**, 276 (1932).
[20] K. Löhberg, Z. physik. Chem. (B) **28**, 402 (1935).

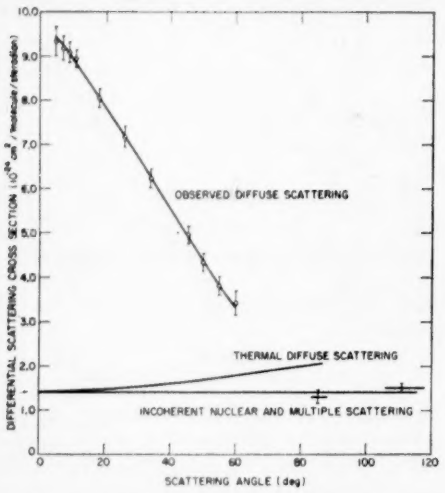

FIG. 2. Diffuse scattering by Er_2O_3. The magnetic scattering is represented by the difference between the measured curve and the other indicated contributions.

diffuse scattering arising from the presence of several isotopes in erbium and from thermal and multiple scattering effects. The decrease of the diffuse scattering with increasing angle arises from the paramagnetic scattering which predominates at small angles. The determination of both the magnitude and the angular dependence of the paramagnetic scattering requires the evaluation of the other contributions to the total scattering.

The measured total diffuse scattering standardized against the coherent scattering by nickel ($\sigma_{coh}^{Ni}=13.4 \pm 0.2$ barns) is shown by the upper curve in Fig. 2. The curve cannot be directly determined to scattering angles greater than 60° because it is then impossible to distinguish the diffuse background from the unresolved Bragg peaks. The accuracy of the measurements in the first half of the pattern is determined, primarily, by counting statistics and by the reliability of the nickel cross section used in the standardization and at scattering angles below 10° by an appreciable background arising from close proximity to the incident beam. In the region from 40° to 60°, the errors are increased by the lack of complete resolution of the Bragg peaks.

To determine what part of the total scattering is of paramagnetic origin, an evaluation must now be made of the other contributions to the diffuse scattering.

The multiple scattering for this case is small, because thin sample geometry was required by the small amount of material available and because of the large thermal capture cross section of erbium. Since this scattering has, if any, only a small dependence on angle it can be included with the other isotropic components.

The total nuclear-scattering cross section per molecule ($2\sigma_{Er}+3\sigma_O$) can best be determined in the present experiment from the scattering data at large angles, where the paramagnetic scattering can be assumed to be negligible. If it is assumed that the interference effects over the large angle region average out, as suggested by the high density of lines in this region, then the resulting total cross section can be obtained from the average scattering in this large-angle region. The isotropic background level arising from the spin and isotope effects, and to a small extent from multiple scattering, can then be evaluated by subtracting from the total scattering the average coherent scattering obtained from the known cross sections of erbium and oxygen. The background level was also evaluated by direct calculation of the intensity of the twenty-five reflections which make up the coherent part of the scattering in a five degree interval at eighty-five degrees. The value for the angularly independent scattering thus obtained is shown in Fig. 2 by the horizontal line drawn through the average of the two experimental points.

The expected thermal scattering is illustrated in Fig. 2 also, and this is based upon the temperature factor, $2w=1.0$, which was suggested by the analysis of the coherent intensities in the compounds, Er_2O_3 and cubic Nd_2O_3, of this investigation and in the isomorphous compound, Sc_2O_3, studied by Milligan *et al.*[21]

The paramagnetic scattering can now be obtained by subtracting from the total diffuse-scattering curve the contributions arising from incoherent nuclear and multiple scattering and from the thermal effect.

The results thus obtained, expressed as differential cross sections per erbium ion, are shown by the points with their respective uncertainties in Fig. 3. The para-

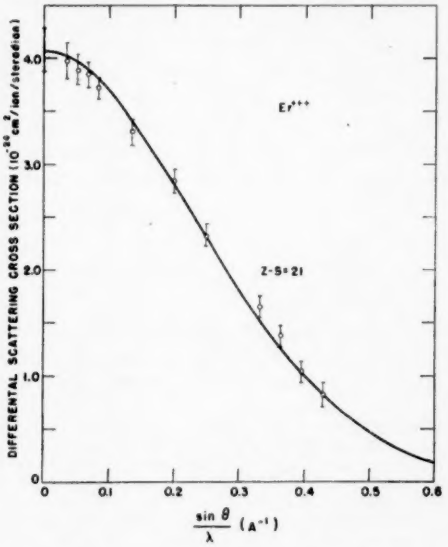

FIG. 3. Paramagnetic-scattering cross section per erbium ion in Er_2O_3.

[21] Milligan, Vernon, Levy, and Peterson, J. Phys. Chem. (to be published).

magnetic cross section in the forward direction obtained by a reasonable extrapolation of the data gives 4.1 barns per unit solid angle per erbium ion. This corresponds to an effective magnetic moment of 9.2 Bohr magnetons whereas the value for a free ion is 9.6 Bohr magnetons. If this can be considered as a real difference, it would indicate a possible small effect arising from crystalline fields. The fact that susceptibility measurements give a moment which agrees with the free ion value, does not necessarily rule out the lower value for the neutron measurements because field splitting can give rise to inelastic processes in neutron scattering. The fact that there is no observable change of the forward scattering with temperature (see later section) does, however, favor the free ion assumption for neutron scattering also. Much of the uncertainty in the forward scattering must be ascribed to the measurements of the isotropic scattering level. It is felt that apart from some unknown sources of error, the uncertainties in the forward scattering can be represented by the indicated error line, which does not quite include the 4.4 barn value which would correspond to a moment of 9.6 Bohr magnetons.

Discussion of this point in its relation to the angular dependence of the scattering, and the comparison of the data with the theoretical results of Trammell, will be given in the last section following the presentation of the other measurements.

Neodymium Oxide

A neutron diffraction pattern of hexagonal neodymium oxide taken in cylindrical cell geometry at room temperature with 1.16A neutrons is shown in Fig. 4. The several components of the scattering in this pattern are those enumerated in the preceding section which dealt with Er_2O_3, but the distribution of intensities among the components is quite different in the two cases.

The diffuse scattering is relatively high, but its angular dependence is not nearly as pronounced as in the preceding case. The calculated magnitude of the magnetic-scattering cross section in the forward direction for Nd^{+++} is smaller by a factor of about seven than that for Er^{+++}, so that an appreciable part of the diffuse scattering in the forward direction must be attributed to incoherent nuclear scattering and multiple scattering.

In measuring the total diffuse scattering, several patterns of the hexagonal neodymium oxide were taken under experimental conditions designed to favor the study of a particular component of the diffuse scattering, or a particular angular region of the pattern. The whole region was studied with cylindrical cell geometry and then to enhance the scattered intensities in the low scattering angle region (5° to 40°), in which resolution can be sacrificed, a thick sample in flat cell geometry was studied.

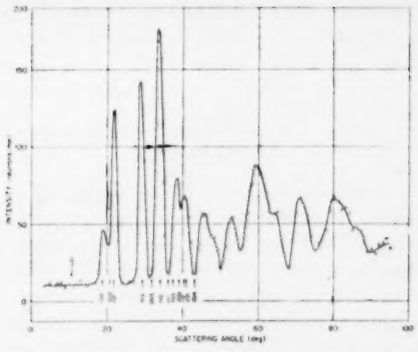

FIG. 4. Diffraction pattern for neodymium oxide (Nd_2O_3 hexagonal form).

The total measured scattering in the near forward direction was found to be somewhat greater than twice that to be expected from magnetic scattering alone. Since much of the diffuse scattering must, then, be ascribed to isotopic incoherent and multiple scattering, the procedure which was used for evaluating these contributions in the case of erbium, where they represented a relatively small part of the total, would be quite unsatisfactory for neodymium.

In view of this, another approach was made to the problem through the study of the diffuse scattering from isotopically enriched samples. Three samples of neodymium oxide enriched in Nd^{142}, Nd^{144}, and Nd^{146} were investigated, and for these samples the situation with respect to nuclear cross sections is much more favorable than for the normal isotopic mixture. The magnetic scattering, arising from the atomic electrons, should remain unchanged.

The three samples were enriched to about ninety-five percent and since their main constituents are all even-even isotopes, the incoherent nuclear scattering may be expected to be markedly reduced from that of normal neodymium. The capture cross sections for the three enriched samples were measured by Pomerance[22] and they were found to be much smaller than for normal neodymium. Thus the correction of transmission data for capture could be expected to yield reliable total scattering cross sections. The coherent scattering cross sections for the three isotopic samples were measured from the coherent reflections in the patterns.[23]

Thin sample geometry was chosen for the two purposes of minimizing multiple scattering and for making optimum use of the small quantities of isotopically enriched material available. As a consequence, the scattered intensities were low and the diffuse scattering analysis was confined to the near forward direction where the magnetic scattering is a maximum.

In each case, for the particular geometry employed, a good estimate for multiple scattering could be made.

[22] H. Pomerance, Phys. Rev. **88**, 412 (1952).
[23] W. C. Koehler and E. O. Wollan, Phys. Rev. **91**, 596 (1953).

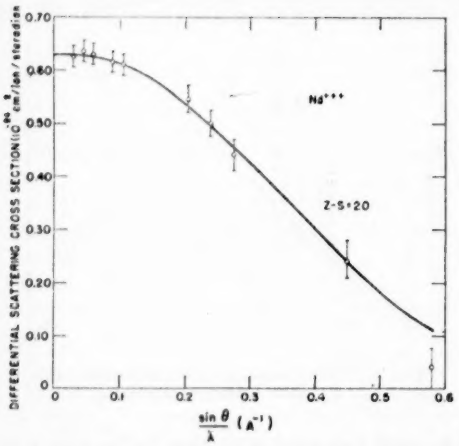

FIG. 5. Paramagnetic-scattering cross section per neodymium ion in Nd_2O_3. The forward scattering has been taken as that for the free ion.

The incoherent nuclear contribution was calculated from the measured total and coherent scattering cross sections. In the forward direction, the thermal scattering is negligible, so that the observed forward diffuse scattering must be due to the two effects mentioned above and to paramagnetic scattering. The difference between the total observed scattering and the contribution from incoherent nuclear and multiple scattering for each sample should correspond to the paramagnetic scattering.

The forward magnetic-scattering cross section, which resulted when the average of the three determinations was taken, is 1.33 ± 0.10 b/steradian molecule and the corresponding magnetic moment per neodymium ion is 3.7 Bohr magnetons. The theoretical effective moment calculated for neodymium ion in the state $^4J_{9/2}$ is 3.62 Bohr magnetons. The estimated uncertainty in the forward magnetic cross section is, thus, plus or minus seven percent corresponding to a plus or minus 3.5 percent uncertainty in the magnetic moment. Within this uncertainty, the effective magnetic moment as measured here agrees with the calculated value.

Once the forward magnetic scattering for the neodymium ion had been established, the analysis of the diffuse-scattering data of the normal neodymium samples could be made. The isotropic scattering level in the patterns was then obtained and the angularly dependent scattering as measured from this base line is composed of paramagnetic scattering and thermal scattering, for which correction can be made on the same basis as previously described for Er_2O_3. The angular dependence of the paramagnetic scattering can then be directly determined over the angular region in which the coherent peaks are reasonably well resolved. The results thus obtained are shown in Fig. 5. At scattering angles greater than 60°, where the peaks are not resolved, some information about the angular dependence of the scattering can be obtained by comparing the diffraction pattern of Nd_2O_3, Fig. 4, with that of the isomorphous and diamagnetic La_2O_3 shown in Fig. 6. This pattern is characterized by a rising trend in the large angle region which is caused by the lack of resolution among the coherent peaks and to the angular dependence of the thermal diffuse scattering. It is apparent from an inspection of the two patterns that in Nd_2O_3 the upward trend is compensated by the angular behavior of the magnetic scattering.

In order to extend the range of the observed magnetic-scattering curve for Nd_2O_3, an attempt was made to place the comparison of the two patterns on a quantitative basis. Structure factors for the two compounds were calculated for all observable reflections and the intensities to be expected for a few convenient angular intervals were computed, and these computed intensities together with the expected thermal-scattered intensities were used to estimate the background scattering in the two patterns. For the case of La_2O_3, where no magnetic scattering is to be expected, this procedure should lead to an isotropic background identical with that observed at small scattering angles. The results of these calculations did reproduce the observed forward scattering to twenty-five percent and with this sensitivity the corresponding calculation was made for Nd_2O_3 at large angles.

The points so obtained are also shown in Fig. 5. These points are of rather low precision but they indicate the behavior of the magnetic-scattering curve at those angles for which a more accurate determination cannot be made.

Praseodymium Oxide

The magnetic scattering from Pr_2O_3 was also investigated. The nuclear scattering and capture cross sections for Pr are known[23,24] and their magnitudes relative to the magnetic-scattering cross section are such that the forward magnetic-scattering cross section could be determined by the method described for the isotopic neodymium samples. For example, in the thin sample run on this oxide, the contributions from the incoherent nuclear scattering and from multiple scattering amounted to twenty-three percent of the total

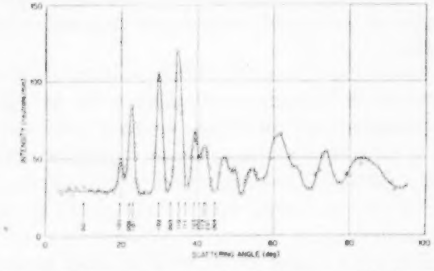

FIG. 6. Diffraction pattern for lanthanum oxide (La_2O_3).

[24] H. Pomerance, Phys. Rev. **83**, 641 (1951).

observed forward scattering. The magnetic differential scattering cross section per praseodymium ion obtained from the analysis of the data was 0.67 b/steradian as compared to the calculated value of 0.617 b/steradian.

The angular dependence of the magnetic scattering from Pr_2O_3 was determined in the manner described in the preceding section, but due to an accidental exposure of the sample to the atmosphere the data for very large angles were invalid and the magnetic scattering was obtained only for $\sin\theta/\lambda$ less than 0.3. The data accumulated over this range were, however, sufficiently extensive to demonstrate the essential features of the magnetic scattering, and the large-angle measurements were not repeated. Within the precision of the experiment, the magnetic-scattering cross section of Pr for $\sin\theta/\lambda$ less than 0.3 was scarcely distinguishable from the magnetic-scattering cross section of Nd over the same range.

That the magnetic scattering from these two ions is similar is, perhaps, not too surprising. Trivalent praseodymium is in a $^3H_4$ spectroscopic ground state and the magnetic moment calculated for this configuration is 3.58 Bohr magnetons. For Nd^{+++}, in a $^4J_{9/2}$ state, the moment is 3.62 Bohr magnetons and the calculated magnetic differential scattering cross sections for the forward direction differ, in the two cases, by slightly more than two percent.

In the praseodymium ion the cancellation of the orbital contribution to the scattering by the spin contribution is comparable to that in the neodymium ion and the resultant form factors may be expected to be quite similar. Detailed calculations for this case have not been made, but the approximate model discussed below for Nd^{+++} and Er^{+++} would predict the same general features in the angular dependence of the scattering by praseodymium ion as by neodymium ion.

Cubic Neodymium Oxide

The neutron diffraction pattern of cubic neodymium oxide, which was studied in an attempt to refine the parameters of the cubic structure, was also analyzed with respect to diffuse scattering. The analysis of the data gave results which agreed, within the experimental errors, with those for the hexagonal structure.

Low Temperature Measurements

A set of measurements on the oxides of Pr, Nd, and Er was obtained at the temperatures of liquid nitrogen and liquid hydrogen. For comparison purposes a room temperature run with the sample in the cryostat was also made. Slight changes in the coherent and diffuse scattering at the different temperatures from the several samples were observed which could be attributed to changes in the thermal effect on the scattering and to the change of sample geometry with decreasing temperature. Within the experimental uncertainties of about five percent, the magnetic scattering in the near forward direction was found to be the same at 21°K as at room temperature. There is thus no evidence for a crystalline field effect from the low-temperature measurements.

COMPARISON OF Nd^{+++} AND Er^{+++} RESULTS WITH THEORY

As we have mentioned, the derivation of the cross-section formula for magnetic scattering of neutrons by free magnetic ions as carried out by Halpern and Johnson for the case of spin only, has been extended by G. Trammell, in the following paper, to the case where there are both orbital and spin contributions in Russell-Saunders coupling and the multiplet separation is sufficiently great so that only the ground state is involved.

For the case of paramagnetic ions with no crystalline field effects, Trammell gives the cross section in the form

$$\sigma(k)d\Omega=\left(\frac{e^2\gamma}{2mc^2}\right)^2\sum_{\nu=0}^{l}[G_{2\nu,2\nu+1}{}^{L}F_{2\nu}{}^{2}(k) - G_{2\nu+2,2\nu+1}{}^{L}F_{2\nu+2}{}^{L}(k)+2G_{2\nu,2\nu+1}{}^{S}F_{2\nu}{}^{S}(k) +2G_{2\nu+2,2\nu+1}{}^{S}F_{2\nu+2}{}^{S}(k)]^2d\Omega, \quad (5)$$

where the G's and F's have been evaluated in tables for the ions Er^{+++} and Nd^{+++} pertinent to the measurements reported here. He also shows that for these ions over the range of $\sin(\frac{1}{2}\varphi)/\lambda$ included in the present experiment, the cross section can be written to within five percent in the form

$$\sigma(k)=\frac{2}{3}\left(\frac{e^2\gamma}{2mc^2}\right)^2[L_Jf_L(k)+2S_Jf_S(k)]^2, \quad (6)$$

where $L_J\equiv\mathbf{L}\cdot\mathbf{J}/|\mathbf{J}|$ and similarly $S_J\equiv\mathbf{S}\cdot\mathbf{J}/|\mathbf{J}|$, and where the quantity $f_S(k)$ can be taken within the above mentioned accuracy as the zero-order term of the general expression and, as such, represents the spherical part in the expansion of the form factor. This quantity, then, corresponds to the form factor as defined by Pauling and Sherman[25] in terms of hydrogenic wave functions; i.e., $f_S(k)=\int\langle\rho(r,\theta,\phi)\rangle_{\text{Av}}[\sin(kr)/kr]dr$, where the average is taken over the angle variables. In the case of magnetic scattering by the rare earths, the wave functions considered are those of the unpaired $4f$ electrons which are responsible for the atomic magnetic moment.

The quantity $f_L(k)$, which has been substituted for two terms $f_0{}^L(k)+\frac{1}{2}f_2{}^L(k)$ of Trammell's paper, arises from the current distributions associated with the angular momentum of the atom. It is evident from the form of Eq. (6), and it is suggested by the treatment in the Appendix of Trammell's paper, that $f_L(k)$ can be interpreted as the Fourier transform or "form factor" of the *equivalent* spherical distribution of mag-

[25] L. Pauling and J. Sherman, Z. Krist. **81**, 1 (1932).

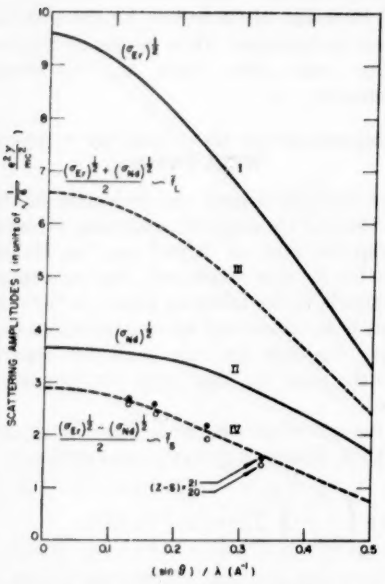

FIG. 7. Scattering amplitudes of erbium and neodymium ions, curves I and II, respectively; and the approximate resolution into average orbital and spin "form factors," curves III and IV, respectively.

netic moments, arising from the angular momentum currents, which will give the same scattering as that derived from a proper quantum mechanical averaging over the actual current distribution.

The expected magnetic scattering for Nd^{+++} and Er^{+++} can be calculated by Eq. (5) or (6) on the basis of some choice of wave function for these ions. Trammell has evaluated the scattering in terms of screened hydrogenic wave functions, and the results can be obtained from the tables given in his paper.

Although the theory applies only to free ions, we have disregarded the indication of the existence of a small crystalline field effect in Er_2O_3 and have calculated the best fitting theoretical scattering curve normalized to the measured cross section in the forward direction. This curve, calculated with $(Z-S)=21$ is shown by the solid line in Fig. 3. If the curve were to be translated upward to correspond to $\mu_{eff}=9.6$ Bohr magnetons and thus to ascribe an equivalent error to the diffuse background measurement, the best fit would be that given by Trammell with $(Z-S)=23$.

The corresponding theoretical curve for Nd^{+++} drawn for the free ion value with $(Z-S)=20$ is shown by the solid line in Fig. 5.

The screening constants given by Pauling and Sherman correspond to $(Z-S)=18$ for Nd^{+++} and 20 for Er^{+++}.

It is interesting, in connection with Eq. (6), to see how closely the effective scattering amplitudes for the erbium and neodymium ions are represented in terms of a simple interference picture involving the sum and difference of the amplitudes arising from the orbital and spin contributions. Taking the square root of both sides of Eq. (6) and evaluating L_J and $2S_J$ and disregarding the constant, one obtains

$$\begin{aligned}(\sigma_{Er})^{\frac{1}{2}} &\propto 6.40 f_L + 3.20 f_S,\\ (\sigma_{Nd})^{\frac{1}{2}} &\propto 6.35 f_L - 2.73 f_S.\end{aligned} \tag{7}$$

Taking the terms on the left as given by the experimental data, one can solve for the average orbital and spin magnetic "form factors" for the Er and Nd ions. The difference of the two equations is quite accurately proportional to $\bar{f}_S$ and as far as the interference picture is concerned we can take the sum as proportional to $\bar{f}_L$.

The experimental data which have now been normalized to the free-ion values are shown as curves I and II in Fig. 7. The sum and difference curves are shown as III and IV in the figure. The points on curve IV are those corresponding to screened hydrogenic wave functions with $(Z-S)$ as indicated now representing an average of the Nd and Er values. It can be seen, on close inspection that curve III falls off less rapidly with $\sin\theta/\lambda$ than curve IV. This is what would be expected from the following simple considerations. The moments associated with the spin are coincident with the electron positions, while the moments associated with the angular momentum currents are within the "orbits" and are hence located on the average closer to the center of the atom. The more compact distribution of the orbital moments gives rise to a slower fall-off of the "form factor" curve than that arising from the spin moments.

ACKNOWLEDGMENTS

The authors wish to express their appreciation to Dr. G. T. Trammell and Dr. T. A. Welton for their interest and help in connection with the theoretical aspects of this problem.

The assistance given by Mr. B. S. Borie and Mr. R. M. Steele in the x-ray analysis of the samples is also gratefully acknowledged.

Magnetic Scattering of Neutrons from Rare Earth Ions

G. T. TRAMMELL
Oak Ridge National Laboratory, Oak Ridge, Tennessee
(Received June 1, 1953)

The differential cross section for the magnetic scattering of thermal neutrons by paramagnetic rare earth ions is derived theoretically assuming that the ions have Russell Saunders coupling and are in the Hund ground state. Satisfactory agreement with the measured cross sections of Er_2O_3 and Nd_2O_3 is obtained using hydrogenic radial wave function with $Z-S\approx 23$ and 20 for Er^{+++} and Nd^{+++}, respectively.

THEORETICAL treatments of the magnetic scattering of slow neutrons by atomic electrons have been given by Bloch,[1] Schwinger,[2] and Halpern and Johnson.[3]

The very thorough-going paper of Halpern and Johnson was primarily concerned with scattering from the iron group atoms for which susceptibility measurements[4] and slow neutron scattering data[5] indicate that the orbital currents are nearly completely quenched by the crystalline fields.

The magnetic properties of the solid salts and oxides of the rare earths, on the other hand, clearly indicate that for these ions there is little quenching by the crystalline fields; in the preceding paper Koehler and Wollan obtain a magnetic contribution to the forward scattering from Er_2O_3 and Nd_2O_3 which is, within a few percent, equal to that which one would expect to obtain from the free rare earth ions in their ground state.

Our main purposes here are to derive a theoretical expression for the magnetic scattering of paramagnetic rare earth ions and to analyze the experimental data for Er_2O_3 and Nd_2O_3 presented in the preceding paper on this basis. In Sec. I general formulas analogous to those of Halpern and Johnson,[3] but including the effects of orbital currents, are obtained. In Sec. II the techniques for doing the integrals and sums over angular and spin variables which are involved in these calculations are discussed, the assumption being made that the magnetic electron shell is coupled according to the Russell-Saunders scheme with the Hund value for ground state. Finally, in Sec. III the results of Secs. I and II are applied to the experiments of Koehler and Wollan with Er_2O_3 and Nd_2O_3, and satisfactory agreement is obtained.

SECTION I. GENERAL FORMULAS

The term in the Hamiltonian which describes the interaction of the neutron with the atomic electrons is taken to be

$$H_{\text{int}}=-(e/c)\sum_i \boldsymbol{\alpha}_i\cdot\mathbf{A}_N(\mathbf{r}_i-\mathbf{r}_N), \tag{1}$$

where $\boldsymbol{\alpha}_i$ is the Dirac velocity operator for the ith electron and $\mathbf{A}_N(\mathbf{r})=g_N\mathbf{S}_N\times\mathbf{r}r^{-3}$, and $\mathbf{S}_N$ and g_N are, respectively, the spin operator and the Landé g factor for the neutron ($g_N=-1.9e/M_Nc$).

If a neutron of momentum $\hbar\mathbf{p}_0$ is incident on an atom, then the scattered wave will be (in the Born approximation):

$$\Psi_S=\sum_f \frac{2iMg_Ne}{\hbar^2c}(\chi_f\psi_f|\,\mathbf{S}_N\cdot\mathbf{k}k^{-2}\times\sum_i \boldsymbol{\alpha}_i e^{i\mathbf{k}\cdot\mathbf{r}_i}|\chi_0\psi_0)\times\chi_f\psi_f\frac{e^{ip_fr_N}}{r_N}, \tag{2}$$

where ψ is an energy eigenfunction of the atom; χ is the spin state of the neutron, $\mathbf{k}=\mathbf{p}_0-\mathbf{p}_f$; M is the mass of the neutron; and subscripts 0 and f serve to distinguish the quantities before and after the collision. The sum is over all possible states of the atom consistent with energy conservation. Energy conservation is given by $\hbar^2(2M)^{-1}(\mathbf{p}_0^2-\mathbf{p}_f^2)=E_f-E_0$, where E is the energy of the atom.

Schwinger,[2] using a method similar to that used below, has shown that for very small k (forward direction, elastic scattering),

$$\begin{aligned} i(e/c)(\psi_f|k^{-2}\mathbf{k}\times\textstyle\sum \boldsymbol{\alpha}_i e^{i\mathbf{k}\cdot\mathbf{r}_i}|\psi_0) &\doteq (e/2mc)(\psi_f|k^{-1}\mathbf{k}\times\textstyle\sum_i(\mathbf{L}_i+2\mathbf{S}_i)|\psi_0)\\ &=k^{-1}\mathbf{k}\times\mathbf{M}, \end{aligned} \tag{3}$$

where $\mathbf{M}$ is the atomic magnetic moment.

Upon making the Pauli non-relativistic approximation, one obtains:

$$\begin{aligned} i\mathbf{J}_{f0}(\mathbf{k})\equiv i(e/c)(\psi_f|\textstyle\sum_i\boldsymbol{\alpha}_i e^{i\mathbf{k}\cdot\mathbf{r}_i}|\psi_0)&\\ \doteq i(e/c)\sum_i\int d^3r_i\{(\hbar/2im)[\bar\psi_f\nabla\psi_0-(\nabla\bar\psi_f)\psi_0]&\\ -(1/m)\nabla\times\bar\psi_f\mathbf{S}_i\psi_0\}e^{i\mathbf{k}\cdot\mathbf{r}_i}&\\ \doteq (ie/2mc)(\psi_f|\textstyle\sum_i\mathbf{p}_i e^{i\mathbf{k}\cdot\mathbf{r}_i}+e^{i\mathbf{k}\cdot\mathbf{r}_i}\mathbf{p}_i&\\ +2i\mathbf{k}\times\mathbf{S}_i e^{i\mathbf{k}\cdot\mathbf{r}_i}|\psi_0). \end{aligned} \tag{4}$$

Halpern and Johnson[3] have used the relations (2) and (4) to discuss the scattering from atoms for which the term in (4) which represents the orbital currents, $(\psi_f|\sum_i\mathbf{p}_i e^{i\mathbf{k}\cdot\mathbf{r}_i}+e^{i\mathbf{k}\cdot\mathbf{r}_i}\mathbf{p}_i|\psi_0)$, is zero.

[1] F. Bloch, Phys. Rev. **50**, 259 (1936).
[2] J. Schwinger, Phys. Rev. **51**, 544 (1937).
[3] O. Halpern and M. Johnson, Phys. Rev. **55**, 898 (1939).
[4] J. H. Van Vleck, *Electric and Magnetic Susceptibilities* (Oxford University Press, London, 1932), Chap. IX.
[5] Shull, Strauser, and Wollan, Phys. Rev. **83**, 333 (1951).

It is convenient to transform the orbital current term in (4) as follows:

$$(\hbar/mi)[\mathbf{p}(\mathbf{k}\cdot\mathbf{r})^n+(\mathbf{k}\cdot\mathbf{r})^n\mathbf{p}]=2[H,\mathbf{r}(\mathbf{k}\cdot\mathbf{r})^n]$$
$$-(\hbar/i)(n/m)[(\mathbf{p}\cdot\mathbf{k})(\mathbf{k}\cdot\mathbf{r})^{n-1}\mathbf{r}+(\mathbf{k}\cdot\mathbf{r})^{n-1}\mathbf{r}(\mathbf{p}\cdot\mathbf{k})]$$
$$=2(n+1)^{-1}[H,\mathbf{r}(\mathbf{k}\cdot\mathbf{r})^n]-(\hbar/im)(n/n+1)\mathbf{k}$$
$$\times[\mathbf{L}(\mathbf{k}\cdot\mathbf{r})^{n-1}+(\mathbf{k}\cdot\mathbf{r})^{n-1}\mathbf{L}], \quad (5)$$

$$[\mathbf{p}e^{i\mathbf{k}\cdot\mathbf{r}}+e^{i\mathbf{k}\cdot\mathbf{r}}\mathbf{p}]=(2mi/\hbar)[H,\mathbf{r}(i\mathbf{k}\cdot\mathbf{r})^{-1}(e^{i\mathbf{k}\cdot\mathbf{r}}-1)]$$
$$-i\mathbf{k}\times[\tfrac{1}{2}\mathbf{L}f(\mathbf{k}\cdot\mathbf{r})+f(\mathbf{k}\cdot\mathbf{r})\tfrac{1}{2}\mathbf{L}], \quad (6)$$

where

$$f(\mathbf{k}\cdot\mathbf{r})=2\sum\frac{(i\mathbf{k}\cdot\mathbf{r})^n}{(n+2)n!}=\frac{2}{(i\mathbf{k}\cdot\mathbf{r})^2}\int_0^{i\mathbf{k}\cdot\mathbf{r}}xe^x dx,$$

m is the electron mass, and H is the Hamiltonian for the atomic electrons. Substituting (6) into (4), one now obtains

$$i\mathbf{J}_{f0}(\mathbf{k})=(e/2mc)(\psi_f|\mathbf{k}\times\textstyle\sum_i\{\frac{1}{2}\mathbf{L}_i f(\mathbf{k}\cdot\mathbf{r}_i)$$
$$+f(\mathbf{k}\cdot\mathbf{r}_i)\tfrac{1}{2}\mathbf{L}_i+2\mathbf{S}_i e^{i\mathbf{k}\cdot\mathbf{r}_i}\}$$
$$-2m(E_f-E_0)\hbar^{-1}\textstyle\sum_i\mathbf{r}_i(i\mathbf{k}\cdot\mathbf{r}_i)^{-1}(e^{i\mathbf{k}\cdot\mathbf{r}_i}-1)|\psi_0). \quad (7)$$

The second sum is zero if $E_f=E_0$ and indeed is always negligible for slow neutron ($E\approx 0.1$ ev) scattering.[6] With the neglection of the small term, (7) becomes[7]

$$i\mathbf{J}_{f0}(\mathbf{k})=+\mathbf{k}\times(e/2mc)(\psi_f|\textstyle\sum_i\frac{1}{2}\mathbf{L}_i f(\mathbf{k}\cdot\mathbf{r}_i)$$
$$+f(\mathbf{k}\cdot\mathbf{r}_i)\tfrac{1}{2}\mathbf{L}_i+2\mathbf{S}_i e^{i\mathbf{k}\cdot\mathbf{r}_i}|\psi_0). \quad (7')$$

Substituting (7′) into (2), one obtains

$$\Psi_S=\left(\frac{Meg_N}{2mc\hbar^2}\right)\sum_f(\chi_f\psi_f|S_{N+}P_-$$
$$+S_{N-}P_+|\chi_0\psi_0)\chi_f\psi_f\frac{e^{i\mathbf{p}_f\mathbf{r}_N}}{r_N}, \quad (2')$$

where

$$\mathbf{P}=\textstyle\sum_i[\frac{1}{2}(\mathbf{L}_i f(k\cdot r_i)+f(k\cdot r_i)\mathbf{L}_i)+2\mathbf{S}_i e^{ik\cdot r_i}],$$

and $P_\pm$, $S_{N\pm}$ are defined with respect to the direction of $\mathbf{k}=\mathbf{p}_0-\mathbf{p}_f$; namely, if $\mathbf{k}$ is taken to define the Z direction, $A_\pm=A_x\pm iA_y$, where $\mathbf{A}$ is any vector. (2′) expresses the fact that the component of $\mathbf{S}_N+\sum_i(\mathbf{L}_i+\mathbf{S}_i)$ in the $\mathbf{k}$ direction is a collision invariant. If one writes $S_{N+}P_-+S_{N-}P_+$ in the form $2\mathbf{S}_N\cdot[\mathbf{P}-k^{-2}\mathbf{k}\times(\mathbf{P}\cdot\mathbf{k})]$ in (2′), then (2′) becomes identical with Eq. (4.1) of Halpern and Johnson except for the inclusion in $\mathbf{P}$ of the orbital currents.

From (2′) one has for the differential scattering cross section (if one assumes unpolarized incident neutrons)

$$\frac{d\sigma}{d\Omega}=\left(\frac{Meg_N}{2mc\hbar}\right)^2\sum_f\frac{p_f}{2p_0}[|(\psi_f|P_-|\psi_0)|^2+|(\psi_f|P_+|\psi_0)|^2]. \quad (8)$$

Equation (8) refers to the scattering from a single ion initially in a state ψ_0; but in substances in which the effect of exchange forces acting between the magnetic shells of adjacent ions are negligible, there will be no correlation in the sense of the currents in adjacent ions and hence no net coherence in the magnetic scattering from such a substance. Now whereas gadolinium is known to become ferromagnetic at $T=16°$C and there is an indication of the possible onset of long-range magnetic order in metallic erbium at $T=70°$K, the susceptibilities[4] and neutron scattering cross sections of the rare earth salts and oxides are well accounted for on the assumption of little or no ordering of neighboring magnetic moments except possibly at very low temperatures. Thus Koehler and Wollan detected no magnetic coherent scattering from Er_2O_3 and Nd_2O_3 down to $T=20°$K. The assumption is then made that for these substances the influence of its neighbors on a given ion is representable by an effective electrostatic "crystalline field." The magnetic scattering from such a substance is then given by summing (8) over the statistically determined initial states ψ_0 of its magnetic ions.

SECTION II. THE EVALUATION OF $(\psi_f|P_\pm|\psi_0)$ FOR THE GROUND STATES OF THE RARE EARTHS, IN PARTICULAR FOR Er^{+++} AND Nd^{+++}

Russell-Saunders coupling with Hund's rule is supposed to apply to the ground state of the rare earths. The wave function for n electrons in the $4f$ shell is taken to be of the form

$$\psi_M=\phi_{4f,n}(r_1,\cdots,r_N)\Theta_{l,L,S,J,M}, \quad (9)$$

where ϕ is a symmetrical function of the radial coordinates of the n electrons, Θ a function of the angle and spin variables of the electrons which is an eigenfunction of L_i^2, with eigenvalues $\mathbf{L}_i^2=l(l+1)\hbar^2=12\hbar^2$, $\mathbf{L}^2=(\sum\mathbf{L}_i)^2$, $\mathbf{S}^2=(\sum\mathbf{S}_i)^2$, $\mathbf{J}^2=(\sum\mathbf{L}_i+\mathbf{S}_i)^2$, and some component of $\mathbf{J}$ with eigenvalue M. S has its maximum value possible, L its maximum consistent with this S, and $J=||L|-|S||$, if the shell is less than half filled, $J=||L|+|S||$, if the shell is more than half filled. We shall assume that the crystalline field may lift the M degeneracy and possibly mix states of different M's but does not cause an appreciable admixture of different J states.[8] In dealing with atoms containing more than half-filled shells we shall perform calculations for the

[6] A rough estimation of its relative magnitude may be made as follows: $\mathbf{k}\times\mathbf{L}\sim\hbar^{-1}|\Delta p_N||p_e|\bar{r}_e$, where $|\Delta p_N|$ is the change in the magnitude of the neutron's momentum as the result of the scattering process, $|p_e|$ is the average momentum of the electron, $\bar{r}_e$ is the electron's radius;

$$2m\hbar^{-1}(E_f-E_0)\mathbf{r}_e\sim m(\hbar M)^{-1}|\Delta p_N|^2\bar{r}_e.$$

Therefore,

$$|2m\hbar^{-1}(E_f-E_0)\mathbf{r}_e|\div|\mathbf{k}\times\mathbf{L}|$$
$$\sim(m/M)\cdot(|\Delta p_N|/|p_e|)\sim 10^{-2}\text{ or }10^{-3},$$

since $|\Delta p_N|\sim p_N$ and $(\hbar/p_N)\sim 1$A and $(\hbar/|p_e|)$ is $O(1$A$)$.

[7] In the appendix it is shown that

$$(e/2mc)\int\psi_f^*\tfrac{1}{2}[\mathbf{L}f(k\cdot r)+f(k\cdot r)\mathbf{L}]\psi_0 dl=\int\mathbf{M}_{fi}{}^L e^{ik\cdot r}dl,$$

where $\mathbf{M}_{fi}{}^L(r)$ is the "equivalent magnetic dipole density" of the orbital currents.

[8] Since the next J state lies some 2000–3000°K above the ground state for Er or Nd, this assumption should be valid.

magnetically equivalent model consisting of the closed-shell deficiency number of electrons. Thus Er^{+++}, which has a deficiency of three electrons from a closed $4f$ shell, is replaced by an atom containing three $4f$ electrons with, of course, the same L, S, J as Er^{+++}.

The elements $(\psi_f|P_\pm|\psi_0)$ where the ψ's are of the form (9) may now be brought to a form containing known coefficients and radial integrals only by straightforward application of the Wigner-Eckart[9] theorem and the concept of tensor operators as developed by Wigner[9] and Racah.[10] According to Racah the irreducible tensor of rank k, $T_q^{(k)}$ transforms under rotations the same as the spherical harmonics $Y_{k,q}=P_k^q(\theta)e^{iq\varphi}$, and so satisfies

$$[J_\pm, T_q^k]=[k(k+1)-q(q\pm1)]^{\frac{1}{2}}T_{q\pm1}^k,$$
$$[J_z, T_q^k]=qT_q^k. \tag{10}$$

The Wigner-Eckart theorem states

$$(\alpha'J'M'|T_q^k|\alpha JM)=(-1)^M G(\alpha'J';T^k;\alpha J)(JJ'M'-M|JJ'kq), \tag{11}$$

where G does not depend on M, M', or q, and a general expression from which the vector addition coefficient $(j_1j_2m_1m_2|j_1j_2jm)$ may be determined is given by Wigner[9] and Racah.[10] For our purposes it is convenient to introduce the special tensor $T_q^k\equiv\mathcal{Y}_{k,q}(\mathbf{J})$ such that

$$(J'M'|\mathcal{Y}_{k,q}|JM)=(-1)^M\delta_{JJ'}(JJ'M'-M|JJkq). \tag{12}$$

Defining $\mathcal{P}_k(M_J)$ by

$$(JM|\mathcal{Y}_{k,0}|JM)\equiv(JM|\mathcal{P}_k(J_z)|JM)=\mathcal{P}_k(M_J), \tag{13'}$$

we have[10,11]

$$\mathcal{P}_k(M_J)=\left[\binom{2k}{k}\binom{2J+1+k}{2k+1}\right]^{-\frac{1}{2}}\times\sum_{\nu=0}^{k}(-1)^\nu\binom{k+\nu}{k}\binom{2J-\nu}{k-\nu}\binom{J-M}{\nu}. \tag{13}$$

From (10) we have

$$\mathcal{Y}_{k,q}^+(\mathbf{J})=(-1)^q\mathcal{Y}_{k,-q}(\mathbf{J}), \tag{14}$$

and from (12),

$$\sum_{MM'}(JM|\mathcal{Y}_{k',q'}^+(\mathbf{J})|J'M')(J'M'|\mathcal{Y}_{k,q}(\mathbf{J})|JM)=\sum_M(JM|\mathcal{Y}_{k',q'}^+(J)\mathcal{Y}_{k'q}(J)|JM)=\delta_{kk'}\delta_{qq'}. \tag{15}$$

One further result which is needed is

$$J_+\mathcal{P}_k(J_z)+\mathcal{P}_k(J_z)J_+=\alpha_{k,k-1}(J)\mathcal{Y}_{k-1,+1}(J)+\alpha_{k,k+1}(J)\mathcal{Y}_{k+1,+1}(J). \tag{16}$$

Taking account of Eqs. (10) and (13), we have

$$\mathcal{P}_k(M)+\mathcal{P}_k(M+1)=[k(k-1)]^{-\frac{1}{2}}\times\alpha_{k,k-1}[\mathcal{P}_{k-1}(M)-\mathcal{P}_{k-1}(M+1)]+[(k+1)(k+2)]^{-\frac{1}{2}}\times\alpha_{k,k+1}[\mathcal{P}_{k+1}(M)-\mathcal{P}_{k+1}(M+1)]. \tag{17}$$

From (15) one may deduce

$$\mathcal{P}_n(M+1)=\mathcal{P}_n(M)+\sum_{r=0}^{n-1}C_{nr}\mathcal{P}_r(M), \tag{18}$$

where

$$C_{nr}(J)=\mathcal{P}_n(J+1)\mathcal{P}_r(J)+(-1)^{r+n+1}\mathcal{P}_n(J)\mathcal{P}_r(J+1),$$

and $\mathcal{P}_n(M)$ is the polynomial of order n in M given by the right side of (13). Substituting (18) in (17) one obtains

$$[(k+1)(k+2)]^{-\frac{1}{2}}C_{k+1,r}\alpha_{k,k+1}+[k(k+1)]^{-\frac{1}{2}}C_{k-1,r}\alpha_{k,k-1}+C_{k,r}+2\delta_{kr}=0. \tag{19}$$

Putting in (19) $r=k$ and $r=k-1$ successively one obtains

$$\alpha_{k,k+1}(J)=-2[(k+1)(k+2)]^{\frac{1}{2}}/C_{k+1,k}(J)$$
$$\alpha_{k,k-1}(J)=([k(k+1)]^{\frac{1}{2}}/C_{k-1,k-2}(J))\cdot[(2C_{k+1,k-2}(J)/C_{k+1,k}(J))-C_{k,k-2}]. \tag{20}$$

Since according to (13) the polynomial

$$\mathcal{P}_k(M)\sim\sum_{\nu=0}^{k}(-1)^\nu\binom{k+\nu}{k}\binom{2J-\nu}{k-\nu}\binom{J-M}{\nu}$$

is zero if $k>2J$, $|M|\leq J$, care must be used in interpreting (20) for $k=2J$.

From (2') we have

$$P_\pm=\sum_n\tfrac{1}{2}L_{n\pm}f(\mathbf{k}\cdot\mathbf{r}_n)+\tfrac{1}{2}f(\mathbf{k}\cdot\mathbf{r}_n)L_{n\pm}+2S_{n\pm}e^{i\mathbf{k}\cdot\mathbf{r}_n}$$
$$=\sum_n\sum_{\nu=0}^{\infty}i^\nu(2\nu+1)\{f_\nu(kr_n)\tfrac{1}{2}[L_{n\pm}P_\nu(\theta_n)+P_\nu(\theta_n)L_{n\pm}]+2g_\nu(kr_n)S_{n\pm}P_\nu(\theta_n)\}, \tag{21}$$

where

$$f_\nu(x)=2x^{-2}\int_0^x yg_\nu(y)dy,$$

$$g_\nu(x)=(\pi/2)^{\frac{1}{2}}x^{-\frac{1}{2}}J_{\nu+\frac{1}{2}}(x),$$

the subscript n refers to the nth electron, and θ is measured from the $\mathbf{k}$ direction. Now from Eqs. (10)–

[9] E. Wigner, *Gruppentheorie und ihre Anwendung auf die Quantenmechanik der Atomspectren* (J. W. Edwards, Ann Arbor, 1944).

[10] G. Racah, Phys. Rev. **62**, 438 (1942).

[11] The expression for the orthogonal-with-respect-to-summing polynomials $\mathcal{P}_k(M)$ is also given by C. Jordan, *Calculus of Finite Differences* (Chelsea Publishing Company, New York, 1950). Note that the polynomial $P_k(M_J)$ is defined for $M_J>J$ although of course it then hasn't the significance of a vector addition coefficient.

TABLE I. $G(\alpha', J'; T^\nu; \alpha, J)$ defined by Eq. (11) and evaluated for special cases by use of Eqs. (26) and (27) and reference 8.

ν	$G(l=3; Y_\nu(\theta,\phi; l=3)$	$G(L=6, J; \mathcal{Y}_\nu(\mathbf{L}); 6, J)$ $J=9/2$	$J=15/2$	$G(l_1=l_2=l_3=3, L=6; \mathcal{Y}_\nu(\mathbf{L}n); 3,3,3,6)$
0	2.645	0.877	1.108	1.365
1		0.857	1.093	0.849
2	−0.6105	0.818	1.065	0.147
3		0.758	1.011	−0.296
4	2.127	0.683	0.952	−0.226
5		0.590	0.8805	0.260
6	−0.1869	0.487	0.794	0.593
7		0.374	0.688	

(21) we have

$$\int \phi_{4f,n}{}^*\Theta^*_{l_1\cdots l_n;L;S;J;M'} P_\pm \phi_{4f,n}\Theta_{l_1\cdots l_n;L;S;J;M} d^{3n}x$$

$$= \pm(JM'|\sum_{\nu=0}^{l}(-1)^\nu\{F_{2\nu}{}^L(k)[\mathcal{G}^L{}_{2\nu,2\nu-1}\mathcal{Y}_{2\nu-1,\pm1}(\mathbf{J}) + \mathcal{G}^L{}_{2\nu,2\nu+1}\mathcal{Y}_{2\nu+1,\pm1}(\mathbf{J})] + 2F_{2\nu}{}^S(k)[\mathcal{G}^S{}_{2\nu,2\nu-1} \times \mathcal{Y}_{2\nu-1,\pm1}(\mathbf{J}) + \mathcal{G}^S{}_{2\nu,2\nu+1}\mathcal{Y}_{2\nu+1,\pm1}(J)]\}|JM), \quad (22)$$

where

$$F_\nu{}^S(k) = \int \phi_{4f,n}\phi_{4f,n} g_\nu(kr_i) d^{3n}x,$$
$$F_\nu{}^L(k) = \int \phi_{4f,n}{}^*\phi_{4f,n} f_\nu(kr_i) d^{3n}x, \quad (23)$$

where r_i is the radial coordinate of any of the n electrons, and where from (11) and (16) we have

$$\mathcal{G}_{\nu,\nu\pm1}{}^L = \frac{2\nu+1}{2} G(l; \mathcal{Y}_\nu(\theta,\phi); l)\alpha_{\nu,\nu\pm1}(l) \times G(l_1\cdots l_n, L; \textstyle\sum_n \mathcal{Y}_{\nu\pm1}(\mathbf{L}_n); l_1\cdots l_n; \mathbf{L}) \times G(L,S,J; \mathcal{Y}_{\nu\pm1}(L); L,S,J), \quad (24)$$

$$\mathcal{G}_{\nu,\nu\pm1}{}^S = (2\nu+1)G(l; Y_\nu(\theta,\varphi); l) \times G(l_1\cdots l_n, L; \mathcal{Y}_\nu(\mathbf{L}_n); l_1\cdots l_n, \mathbf{L}) \times [\alpha_{\nu,\nu\pm1}(J)G(L,S,J; \mathcal{Y}_\nu(\mathbf{L}); L,S,J) - \alpha_{\nu,\nu\pm1}(L)G(L,S,J; \mathcal{Y}_{\nu\pm1}(\mathbf{L}); L,S,J)]. \quad (25)$$

Racah has shown that

$$G(l; Y_n(\theta,\varphi); l) = (-1)^{n/2}\frac{(2l+1)}{(2n+1)^{\frac{1}{2}}}\frac{n!}{(\frac{1}{2}n!)^2} \times \frac{(l+\frac{1}{2}n)!}{(l-\frac{1}{2}n)!}\left(\frac{(2l-n)!}{(2l+n+1)!}\right)^{\frac{1}{2}} \quad n=\text{even} \quad (26)$$
$$= 0 \quad (n=\text{odd}).$$

$G(L,S,J; \mathcal{Y}_n(\mathbf{L}); L,S,J)$ is (except for a multiplying factor) the Racah function W whose values have been tabulated by Biedenharn;[12] and in virtue of the simple Hund's scheme for the coupling of the individual L_n's to give $L[L=l+(l-1)+\cdots+(l-n+1)]$,

$$G(l_1\cdots l_n, L; \mathcal{Y}_\nu(\mathbf{L}_n); l_1\cdots l_n, L) = [\mathcal{P}_\nu(l)+\mathcal{P}_\nu(l-1)+\cdots+\mathcal{P}_\nu(l-n+1)]/n\mathcal{P}_\nu(L). \quad (27)$$

In the next section the $\mathcal{G}$'s are evaluated for Nd and Er.

In (22) the $\mathcal{Y}_{\nu,q}$'s are defined with respect to axes whose z direction is along $\mathbf{k}=\mathbf{p}_0-\mathbf{p}_f$. If we call this axis S_0 and an axis rotated by Euler angles (α,β,γ) with respect to S_0, S, then we have

$$\mathcal{Y}_{\nu,q}{}^{(S_0)} = \sum_{q'=-\nu}^{\nu} \mathfrak{D}_{q,q'}{}^\nu(\alpha,\beta,\gamma)\mathcal{Y}_{\nu,q'}{}^{(S)}, \quad (28)$$

where the $\mathfrak{D}^\nu(\alpha,\beta,\gamma)$'s are the irreducible representations of the three-dimensional rotation group.

From the unitarity of the $\mathfrak{D}$ matrix and the orthogonality of the $\mathcal{Y}$'s it may be deduced that

$$\langle \mathfrak{D}_{q,q'}{}^\nu(\alpha,\beta,\gamma)\mathfrak{D}_{q'',q'''}{}^{\nu'*}(\alpha,\beta,\gamma)\rangle_{\Omega} = \delta_{\nu\nu'}\delta_{qq''}\delta_{q'q'''}/(2\nu+1), \quad (29)$$

where in (29) the average is made over all possible orientations of the rotated frame.

If the sample under consideration is a powdered crystal sample with perfectly randomly oriented microcrystals, then in virtue of (29), (28), and (22), (8) becomes

$$\frac{d\sigma}{d\Omega} = \left(\frac{Meg_N}{2mch}\right)^2 \sum_{\nu=0}^{l}\sum_{\psi_f}\frac{p_f}{p_o}[\mathcal{G}^L{}_{2\nu,2\nu+1}F^L{}_{2\nu}(k) - \mathcal{G}^L{}_{2\nu+2,2\nu+1}F^L{}_{2\nu+2}(k) + 2\mathcal{G}^S{}_{2\nu,2\nu+1}F^S{}_{2\nu}(k) - 2\mathcal{G}^S{}_{2\nu+2,2\nu+1}F^S{}_{2\nu+2}(k)]^2(4\nu+3)^{-1} \times \sum_{q=-(2\nu+1)}^{2\nu+1}|(\psi_f|\mathcal{Y}_{2\nu+1,q}|\psi_0)|^2, \quad (30)$$

where it is to be noted that in (30), k, for a given scattering angle, satisfies

$$k^2 = k_0{}^2 p_f/p_o + (p_f-p_o)^2 \doteq k_0{}^2\left(1-\frac{E_f-E_o}{2E_{N_o}}\right)+\frac{2M(E_f-E_o)}{\hbar^2}\frac{E_f-E_o}{4E_{N_o}}.$$

If we assume that $(E_f-E_0)/E_{N0}$ is sufficiently small,

TABLE II. $\alpha_{k,k\pm1}(J)$ defined by Eq. (16) and evaluated by use of Eqs. (18) and (20).

n	$\alpha_{n,n+1}(J)$ $J=3$	9/2	6	15/2	$\alpha_{n,n-1}(J)$ $J=3$	9/2	6	15/2
0	5.656	8.150	10.59	13.03	0	0	0	0
2	3.70	5.598	7.409	9.190	−2.450	−3.590	−4.694	−5.810
4	2.870	4.738	6.611	8.363	−2.941	−4.029	−5.407	−6.744
6	0	3.831	5.867	7.745	−1.645	−3.620	−5.258	−6.830

[12] L. C. Biedenharn, Oak Ridge National Laboratory Report ORNL-1098 (unpublished).

TABLE III. $\mathcal{G}_{\nu,\nu\pm1}^{L,S}(l,L,J)$ defined by Eqs. (24) and (25) and evaluated for $l=3$, $L=6$, $J=9/2$ (Nd) by use of Tables I and II.

ν	$\mathcal{G}^{L}_{2\nu,2\nu+1}(9/2)$	$\mathcal{G}^{L}_{2\nu+2,2\nu+1}(9/2)$	$\mathcal{G}^{S}_{2\nu,2\nu+1}(9/2)$	$\mathcal{G}^{S}_{2\nu+2,2\nu+1}(9/2)$
0	16.3	8.3	−7.0	−0.488
1	−3.81	−18.9	−0.465	5.83
2	12.6	0.92	2.87	−1.93
3	0	0	0.473	0

TABLE IV. $\mathcal{G}_{\nu,\nu\pm1}^{L,S}(l,L,J)$ defined by Eqs. (24) and (25) and evaluated for $l=3$, $L=6$, $J=15/2$ (Er) by use of Tables I and II.

ν	$\mathcal{G}^{L}_{2\nu,2\nu+1}(15/2)$	$\mathcal{G}^{L}_{2\nu+2,2\nu+1}(15/2)$	$\mathcal{G}^{S}_{2\nu,2\nu+1}(15/2)$	$\mathcal{G}^{S}_{2\nu+2,2\nu+1}(15/2)$
0	20.9	10.4	10.4	0.475
1	−5.08	25.2	1.03	−4.14
2	18.8	1.37	−9.3	1.14
3	0	0	3.04	0

then (30) may be approximated by expanding the expression in square brackets and (p_f/p_0) in powers of (E_f-E_0/E_{N0}), neglecting powers higher than the first; if at the same time we multiply by the statistical weight $g(E_0)=(e^{-E_0/kT}/\sum E_0 e^{-E_0/kT})$ and sum over the initial states ψ_0, we obtain

$$\frac{d\sigma}{d\Omega}=\left(\frac{Me g_N}{2mc\hbar}\right)^2\left\{\sum_{l=0}^{l}\left[\frac{B_\nu^2(k_0)}{2J+1}+\Delta_\nu\right]\right\}, \tag{31}$$

where

$$B_\nu^2(k)=[\mathcal{G}^{L}_{2\nu,2\nu+1}F^{L}_{2\nu}(k)-\mathcal{G}^{L}_{2\nu+2,2\nu+1}F^{L}_{2\nu+2}(k)+2\mathcal{G}^{S}_{2\nu,2\nu+1}F^{S}_{2\nu}(k)+2\mathcal{G}^{S}_{2\nu+2,2\nu+1}F^{S}_{2\nu+2}(k)]^2,$$

and the crystalline effects are contained in

$$\Delta_\nu=\sum_{\psi_f,\psi_0}\frac{E_f-E_o}{2E_{No}}\left\{\left(B_\nu^2(k_0)+k_0^2\frac{\partial B_\nu^2}{\partial k^2}\right)[g(E_f)-g(E_o)]+\frac{2M(E_f-E_o)}{\hbar^2}\frac{\partial B_\nu^2}{\partial k^2}[g(E_f)+g(E_o)]\right\}$$

$$\times\frac{1}{2(4\nu+3)}\sum_{q=-(2\nu+1)}^{2\nu+1}|(\psi_f|\mathcal{Y}_{2\nu+1,q}(\mathbf{J})|\psi_0)|^2. \tag{32}$$

In the next section the possibility of (32)'s explaining the possible small decrease of cross section from the free ion value for Er^{+++} is discussed.

SECTION III. CROSS SECTIONS FOR Er^{+++} AND Nd^{+++}

In Tables I and II we give the G's[13] and α's[14] for $Er(l_i=3, L=6, S=3/2, J=15/2)$ and $Nd(l_i=3, L=6, S=3/2, J=9/2)$, and in Tables III and IV the values of the $\mathcal{G}$'s[15] are given for these two cases. The figures given in Tables III and IV are not all significant; each entry should be taken to have a probable error of about 1 percent or less. The assumption has been made in deriving Eq. (31) for the powdered crystal cross section that the ground state is an eigenstate of J, that the effect of neighboring ions on a given ion can be approximated by an electrostatic field, and finally that the splitting energies due to the crystalline field is small compared to the energy of the incident neutron.

If we neglect the terms Δ_ν and substitute from Tables III and IV into (31), then we have an expression for the cross section involving the radial integrals $F_\nu(k)$'s. If we assume that charge distribution may be approximated fairly well by hydrogen-like $4f$ wave functions, $\varphi(r)\sim r^3e^{-r/2a}$, then the integrals defining the $F_\nu(k)$'s [Eq. (23)] may be done analytically and are functions of ka.

In Table V we give values of $F_\nu^{L,S}(ka)$ for a range of parameters ka. In Tables VI and VII we give the $B_\nu^2(ka)$ for Er^{+++} and Nd^{+++}. It is seen from Tables VI and VII that the differential cross section may be approximated to within 5 percent accuracy by just the first term, B_0^2, in the moment expansion given by Eq. (31) for $ka<0.4$. Since for the measurements reported on in the previous paper the values of ka for which significant accuracy could be obtained were $<ka=8\pi a_0\sin\theta/2(Z-S)^{-1}\lambda^{-1}=0.4$, we may keep only the term B_0^2 in (31).

$$\frac{d\sigma}{d\Omega}\doteq\left(\frac{Me g_N}{2mc}\right)^2(2J+1)^{-1}[\mathcal{G}_{0,1}{}^{L}F_0^{L}(ka)+\mathcal{G}_{2,1}{}^{L}F_2^{L}(ka)+\mathcal{G}_{0,1}{}^{S}F_0^{S}(ka)+\mathcal{G}_{2,1}{}^{S}F_2^{S}(ka)]^2,\quad ka<0.4. \tag{33}$$

Substituting $g_N=-1.91e/Mc$, $e^2/mc^2=2.81\ 10^{-13}$ cm,

TABLE V. $F^{L,S}$ defined by Eq. (23) and evaluated for the case $\phi^*\phi\sim r^6\exp(-r/a)$.

k^2a^2	$F_0{}^L$	$F_2{}^L$	$F_4{}^L$	$F_6{}^L$	$F_0{}^S$	$F_2{}^S$	$F_4{}^S$	$F_6{}^S$
0	1.00	0	0	0	1.00	0	0	0
0.01	0.928	0.030	0	0	0.862	0.058	0	0
0.05	0.696	0.119	0.011	0.001	0.452	0.189	0.021	0.001
0.10	0.496	0.181	0.036	0.009	0.172	0.241	0.057	0.007
0.15	0.362	0.211	0.063	0.022	0.034	0.233	0.089	0.018
0.25	0.208	0.222	0.112	0.061	−0.055	0.166	0.123	0.042
0.35	0.132	0.209	0.146	0.104	−0.058	0.101	0.126	0.062
0.5	0.0782	0.179	0.174	0.158	−0.084	0.040	0.105	0.078

[13] Equations (11), (26), and (27).
[14] Equations (16)–(20).
[15] Equations (24) and (25).

TABLE VI. B_ν^2 defined by Eq. (31) and evaluated for Er with assumptions given in Sec. III by use of Tables IV and V.

k^2a^2	B_0^2	B_1^2	B_2^2	B_3^2	ΣB_ν^2
0	978	0	0	0	978
0.05	319	0	0	0	319
0.10	103	0.2	0	0	103
0.15	31.7	1.2	0.1	0	32.9
0.25	1.92	5.61	0.7	0	8.2
0.35	0.03	10.6	1.9	0	12.5
0.50	0.35	15.8	4.0	0	20.2

we get

$$\frac{d\sigma_{Er}}{d\Omega}=\frac{7.2\times10^{-26}}{16}\text{ cm}^2[20.9F_0^L(ka)-10.4F_2^L(ka)+10.45F_0^S(ka)-0.47F_2^S(ka)]^2, \quad (34)$$

$$\frac{d\sigma_{Nd}}{d\Omega}=\frac{7.2\times10^{-26}}{10}\text{ cm}^2[16.3F_0^L(ka)-8.3F_2^L(ka)-7.0F_0^S(ka)+0.49F_2^S(ka)]^2, \quad (35)$$

for the free ion cross section for $ka<0.4$ for Er^{+++} and Nd^{+++}, respectively. We plot $F_{0,2}{}^L$, $F_{0,2}{}^S$ in Fig. 1. According to Eq. (21)

$$\begin{aligned} g_0(x)&=\sin x/x,\\ g_2(x)&=\left[\left(-1+\frac{3}{x^2}\right)\frac{\sin x}{x}-\frac{3\cos x}{x^2}\right],\\ f_0(x)&=\frac{2}{x^2}(1-\cos x),\\ f_2(x)&=\frac{2}{x^2}\left(2+\cos x-\frac{3\sin x}{x}\right), \end{aligned} \quad (36)$$

and so we get for the F's, assuming hydrogenic $4f$ wave functions,

$$\begin{aligned} F_0^S(ka)&=(8ka)^{-1}\frac{\sin 8\tan^{-1}ka}{(1+a^2k^2)^4},\\ F_2^S(ka)&=(8ka)^{-1}\left[-\frac{\sin 8\tan^{-1}ka}{(1+a^2k^2)^4}+\frac{1}{14}(ka)^-\right.\\ &\quad\left.\times\frac{\sin 6\tan^{-1}ka}{(1+a^2k^2)^3}-\frac{3}{7}(ka)^{-1}\frac{\cos 7\tan^{-1}kc}{(1+a^2k^2)^{7/2}}\right], \end{aligned} \quad (37)$$

$$\begin{aligned} F_0^L(ka)&=\frac{1}{28}(ka)^{-2}\left[1-\frac{\cos 7\tan^{-1}ka}{(1+a^2k^2)^{7/2}}\right],\\ F_2^L(ka)&=\frac{1}{28}(ka)^{-2}\left[2+\frac{\cos 7\tan^{-1}ka}{(1+k^2a^2)^{7/2}}\right.\\ &\quad\left.-\tfrac{1}{2}(ka)^{-1}\frac{\sin 6\tan^{-1}ka}{(1+a^2k^2)^3}\right]. \end{aligned}$$

Noting that the term F_2^S makes a negligibly small contribution to (34) and (35) over the region considered and that $\mathcal{G}_{0,1}{}^L$ and $\mathcal{G}_{0,1}{}^S$ are in fact $\mathbf{L}\cdot\mathbf{J}[J(J+1)]^{-1}\times[\frac{2}{3}J(J+1)(2J+1)]^{\frac{1}{2}}$ and $2\mathbf{S}\cdot\mathbf{J}[J(J+1)]^{-1}[\frac{2}{3}J(J+1)\times(2J+1)]^{\frac{1}{2}}$, respectively, Eqs. (34) and (35) may be well approximated by

$$\begin{aligned} \frac{d\sigma}{d\Omega}&=7.2\times10^{-26}\frac{2}{3}\frac{(\mathbf{L}\cdot\mathbf{J})^2}{J(J+1)}\left[F_0^L(ka)+\frac{2\mathbf{S}\cdot\mathbf{J}}{\mathbf{L}\cdot\mathbf{J}}F_0^S(ka)\right.\\ &\quad\left.-0.50F_2^L(ka)\right]^2\text{ cm}^2\\ &=1.96\times10^{-24}[F_0^L(ka)+\tfrac{1}{2}F_0^S(ka)\\ &\quad-0.50F_2^L(ka)]^2\text{ cm}^2,\quad\text{for}\quad Er^{+++}\\ &=1.94\times10^{-24}[F_0^L(ka)-0.427F_0^S(ka)\\ &\quad-0.50F_2^L(ka)]^2\text{ cm}^2\quad\text{for}\quad Nd^{+++}. \end{aligned} \quad (38)$$

In Fig. 2 a comparison of (38) with the experimental cross section obtained by Koehler and Wollan is presented; the abscissa is $\sin(\frac{1}{2}\theta)/\lambda=(8\pi a_0)^{-1}(Z-S)ka$, the best fits being obtained with $Z-S=23$ and 20 for Er and Nd, respectively. As explained in the previous paper, there is an uncertainty in the magnitude of the nuclear incoherent scattering which causes an uncertainty in the base line from which the magnetic scattering is to be measured; Koehler and Wollan estimate this to be of the order of ±6 percent of the forward magnetic scattering for Er. This is indicated in the figure by three curves derived from the experimental points having a constant difference. Curve (a) gives the free ion cross section in the forward direction which is consistent with their estimated base-line uncertainty; curve (c) is the reasonable lower bound, and curve (b) is the median of (a) and (c). The magnetic cross section for Nd as shown in Fig. 2 is small; the base line was chosen so as to give the free ion cross section in the forward direction, and it is seen that the theoretical curve fits quite well.

The free ion theoretical curve is seen to give a reasonably good fit to curve (a) for Er. On the other hand, if curve (b) represents more nearly the actual magnetic scattering, then the difference of the theoretical curve and (b) may be attributed to crystalline field splittings of the type envisaged in the last section. Considering only the term $\nu=0$ in (31), the effect of the crystalline fields will then be to add to the cross section

TABLE VII. B_ν^2 defined by Eq. (31) and evaluated for Nd with assumptions given in Sec. III by use of Tables III and V.

k^2a^2	B_0^2	B_1^2	B_2^2	B_3^2	ΣB_ν^2
0	87.2	0	0	0	87.2
0.05	53.6	0.2	0.04	0	53.8
0.10	30.4	0.2	0.4	0	31.0
0.15	16.4	0.06	1.1	0	17.6
0.25	4.1	0.2	3.2	0	7.5
0.35	0.6	1.4	5.0	0	7.0
0.50	0	3.9	6.3	0	10.2

a term

$$\delta\sigma(k^2)=\sum_{\psi_f,\psi_0}\frac{E_f-E_o}{2E_{No}}\left\{\left[\sigma_0(k^2)+k^2\frac{d\sigma_0}{dk^2}\right][g(E_f)-g(E_o)]+\frac{2M(E_f-E_o)}{\hbar^2}\frac{d\sigma_0}{dk^2}[g(E_f)+g(E_o)]\right\}\times\frac{2J+1}{6}\sum_{-1}^{1}|(\psi_f|\mathcal{Y}_{1,q}|\psi_0)|^2, \quad (39)$$

where $\sigma_0(k^2)$ is given by Eq. (34) and k^2 refers to the elastically scattered k at the given angle.

As may be seen from an inspection of the curve for σ_0, over most of the region with which we are concerned $k^2(d\sigma_0/dk^2)<\sigma_0(k^2)$; and, therefore, the expression (39) for $\delta\sigma$ is negative definite. From (39) $\delta\sigma/\sigma_0\approx(E_f-E_o)/E_{No}$; and, since crystalline field splittings of the order of 100 cm^{-1} [16,17] are expected here, it is not at all improbable that the cross section in the forward direction is actually as small as indicated by curve (b) or (c).

However, it should be pointed out that, if there is a decrease in cross section from the free ion value resulting from the above mechanism, then because of the change of the population factors $g(E, T)$ a considerable change would be generally expected in $\delta\sigma(k^2)$ in going from room temperature to 20°K; whereas, in fact, according to Koehler and Wollan's experiment only a change of a few percent which is attributed to the change in the nuclear diffuse scattering is observed. Experiments using higher energy neutrons are being considered to obtain additional information concerning this point.

The author wishes to thank Drs. E. O. Wollan and W. C. Koehler for suggesting this problem and for many interesting discussions concerning it, Dr. T. A. Welton for constructive criticisms, and Miss Nancy Givens of the ORNL Mathematics Panel for computational aid.

APPENDIX

An alternative derivation of (7′) from (4) which brings out the physical interpretation of the form (7) proceeds as follows:

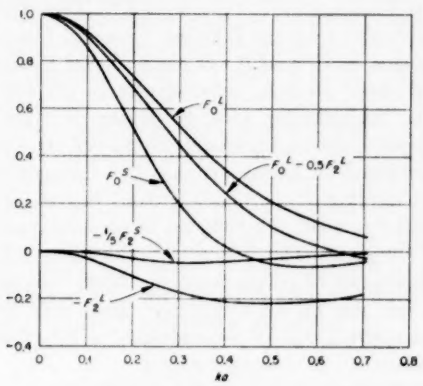

FIG. 1. $F_{0,2}^{L,S}$ defined by Eq. (23) for case $\phi^*\phi\sim r^6\exp(-r/a)$.

[16] F. A. Spedding, J. Chem. Phys. **5**, 316 (1937).
[17] B. Bleaney, Physica **17**, 175 (1951).

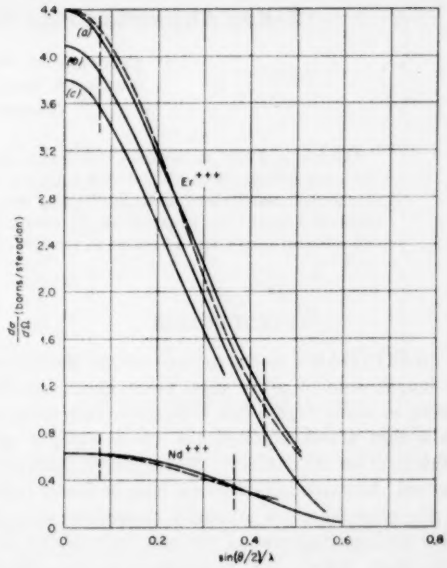

FIG. 2. The solid curves represent the measured values and the dashed curves the theoretical free ion values assuming hydrogenic radial wave function with $Z-S$ 23 and 20 for Er^{+++} and Nd^{+++}, respectively. The three curves (a), (b), and (c) for Er^{+++} represent the experimental base line uncertainty as explained in the text. The vertical dashed lines represent the regions outside of which the experimental values are uncertain.

Let ψ_0, ψ_f refer to states with the same energy; then for

$$\mathbf{j}_L=(e\hbar/2mci)[\psi_f^*\nabla\psi_0-(\nabla\psi_f^*)\psi_0],$$

we have

$$\nabla\cdot\mathbf{j}_L=0.$$

Therefore an $\mathbf{M}_L$ may be defined so that

$$\mathbf{j}_L=\nabla\times\mathbf{M}_L.$$

Therefore the term in (4)

$$\int d^3r e^{i\mathbf{k}\cdot\mathbf{r}}\mathbf{j}_L=-i\mathbf{k}\times\int\mathbf{M}_L e^{i\mathbf{k}\cdot\mathbf{r}}d^3r.$$

We may take for $\mathbf{M}_L$,

$$\mathbf{M}_L=r^{-2}\mathbf{r}\times\int_r^\infty\rho\mathbf{j}_L(r^{-1}\mathbf{r}\rho)d\rho;$$

then, integrating by parts,

$$\int\mathbf{M}_L e^{i\mathbf{k}\cdot\mathbf{r}}d^3r=\int\tfrac{1}{2}\mathbf{r}\times\mathbf{j}_L f(k\cdot r)d^3r$$

$$=(e/2mc)\int\psi_f^*\tfrac{1}{2}[\mathbf{L}f(k\cdot r)+f(k\cdot r)\mathbf{L}]\psi_0 d^3r$$

$$\therefore\int\mathbf{j}_L e^{i\mathbf{k}\cdot\mathbf{r}}d^3r$$

$$=-i\mathbf{k}\times(e/2mc)\int\psi_f^*\tfrac{1}{2}[\mathbf{L}f(k\cdot r)+f(k\cdot r)\mathbf{L}]\psi_0 d^3r,$$

in agreement with Eqs. (6) and (7′).

X-Ray Absorption Fine Structure with Polarized X-Rays*

R. KROGSTAD, W. NELSON, AND S. T. STEPHENSON
Washington State College, Pullman, Washington

(Received August 10, 1953)

The fine structure on the short wavelength side of the K x-ray absorption edge of Cl in single crystals of NaCl and KCl has been studied with polarized x-rays in a vacuum double-crystal spectrometer. The structure was obtained when the main direction of ejection of photoelectrons was perpendicular to a set of 100 planes and again when perpendicular to 110 planes. One significant difference in structure was noted for the two different directions of ejection in the case of NaCl.

INTRODUCTION

A SECONDARY fine structure on the short wavelength side of x-ray absorption edges has been observed in many crystalline materials. This structure, when within a few volts of the main edge, is quite dependent upon the character of the parent atom or ion concerned. An extended structure may be found further from the edge which is primarily dependent upon the number and arrangement of the neighbors of the atom or ion from which the photoelectron was ejected. Kronig[1] has suggested that the extended structure in solids is primarily due to the periodic potential lattice of the crystal. The ejected electron is treated as a free electron perturbed by the periodic potential of the lattice. Then the forbidden energies W_0 are found to be given by the expression,

$$W_0=\frac{h^2(\alpha^2+\beta^2+\gamma^2)}{8md^2\cos^2\theta_0},$$

for any plane of indices $\alpha\beta\gamma$ in a cubic crystal of grating space d, where θ_0 is the angle between the normal to the plane α, β, γ and the direction of motion of the electron. For the usual case of unpolarized x-rays and polycrystalline absorbers, the effect of integration over all planes and all angles is to smooth out the discontinuities to some degree so that a rather broad structure results. Many investigations have been carried out for this case. However, as Kronig points out, if one could use a single-crystal absorber and polarized x-rays, one would expect to find a more pronounced structure. Furthermore, by varying the orientation of the single crystal with respect to the electric vector of the polarized x-rays the angle θ_0 should shift for each plane, and a shift in the position of the structure should result. It is the purpose of the present work to study the fine structure resulting when polarized x-rays fall on a single-crystal absorber using different orientations of that absorber. One would expect the effects which are sought to be somewhat reduced in magnitude for the reason that, although the main direction of ejection of photoelectrons is parallel to the electric vector in a plane polarized x-ray beam, all of the electrons are not ejected in this direction.

As far as the authors are aware, only one previous investigation of this type has been made.[2] The K x-ray absorption edge of Br in a single crystal of KBr was studied using partially polarized (total deviation of 57° and 75 percent polarization) x-rays. A pronounced structure was obtained, and there was some evidence of dependence of structure on crystal orientation; but the partial polarization left much to be desired. The present availability of a vacuum x-ray spectrometer makes it possible to do a similar experiment at longer wavelengths so that the deviation in the first order is nearly 90° and the polarization is essentially complete.

EXPERIMENTAL

The vacuum double-crystal spectrometer together with the power supply and Geiger-counter means of intensity registration have been described previously.[3,4] Crystal A was a good calcite which had previously given (1, −1) rocking curves (with another calcite as Crystal B) having a full width at half-maximum of 50 seconds at 4.38A. Crystal A gave a total deviation of 92.5° for the wavelength of the K-edge of chlorine. Crystal B was used both as the absorber and as the second crystal in the double-crystal scheme; measurements were made with a single crystal of NaCl as Crystal B and later with a crystal of KCl. These crystals were obtained from the Harshaw Chemical Company. The mount for Crystal B was made so that it could be rotated about an axis, perpendicular to the 100 face used as the reflecting face, by means of a solenoid arrangement operated from outside the bell jar. Crystal B was rotated 45° between runs so that the main direction of ejection of the photoelectrons was either perpendicular to a set of 100 planes or perpendicular to a set of 110 planes. The sequence of runs was as follows: a complete set of points involving 10 000 counts per point was run for an absorption curve with photoelectric ejection mainly perpendicular to 100 planes, a

* This work was supported in part by the U. S. Office of Naval Research.

[1] R. de L. Kronig, Z. Physik **70**, 317 (1931); **75**, 191 (1932); **75**, 468 (1932).

[2] S. T. Stephenson, Phys. Rev. **44**, 349 (1933).

[3] Stephenson, Krogstad, and Nelson, Phys. Rev. **84**, 806 (1951).

[4] S. T. Stephenson and F. D. Mason, Phys. Rev. **75**, 1711 (1949).

similar complete curve for the 110 direction at 45° from the first, a similar curve for the 100 planes at 90° from the first, and so on. Spurious structure caused by imperfections in the reflecting face of the crystal would have been shown up by such a procedure. Three or more complete curves were run for the 100 and the 110 positions. A complication in taking data arose from the fact that at the long wavelengths concerned and with crystal faces of the order of 4 cm in extent it was not possible to leave Crystal A fixed while covering an adequate wavelength range with Crystal B; consequently, it was necessary to maximize Crystal A for each new setting position of Crystal B by taking the time for three or four 10 000-count points with different positions of A to determine the maximum. Intensities were of the order of 60 counts per second on the long wave side of the edge and 35 counts per second on the short wavelength side. All measurements were made at 5.5 kilovolts and 250 milliamperes with an x-ray tube having a tungsten target.

RESULTS

Typical curves are presented in Figs. 1 and 2. An absorption curve for the main direction of ejection of photoelectrons perpendicular to a set of 100 planes is labeled (100) and appears as the upper curve in each case. The lower curve is for ejection perpendicular to a set of 110 planes and is labeled (110). The ordinates of the curves are arbitrarily displaced. No displacement of the main absorption edge was observed, although the absolute accuracy of measurement would not have allowed detection of such a shift, if it had been less than about a volt. The distances in volts from the center of the main edge of the structure observed are given in Table I. The differences in position and in general shape for the feature β between the 100 curve for NaCl and the 110 curve for NaCl are considered to be significant. No other variations of significance between 100 and 110 curves were found. A search made out to 100 volts from the main edge failed to yield any repeatable structure beyond 25 volts from the edge.

TABLE I. Distances of structure features measured in volts from the center of the main edge.

Crystal	Orientation	A	α	B	β	C	γ
NaCl	(100)	3.6	9.1	15.0	21.5	...	...
NaCl	(110)	3.6	8.8	15.0	17.8	...	...
KCl	(100)	2.5	4.9	6.8	10.5	16.8	25
KCl	(110)	2.5	4.9	6.6	9.9	16.8	25

DISCUSSION

Measurements with polycrystalline absorbers and non-polarized x-rays have been made on KCl and NaCl in other laboratories.[5-7] Because of the different conditions for the present experiment one would not expect to obtain a one-to-one correspondence in structure with previous work; however, a comparison shows that the general features are similar.

A major disappointment with respect to the main objective of the present work is that no structure was found beyond 25 volts; Kronig's theory is expected to be more nearly valid at such energy distances from the edge since it concerns a small perturbation to the free electron problem. Local fields are more important as the energy becomes less until finally the energies are largely governed by semi-optical level considerations. It is currently planned to repeat the present polarization experiment with metal single crystals for which extended

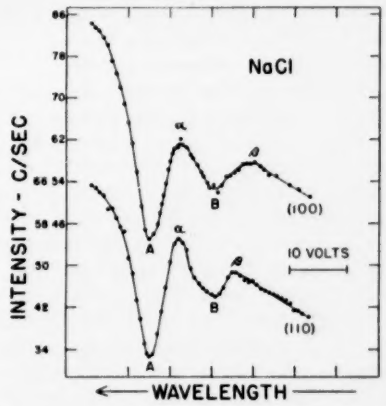

FIG. 1. K x-ray absorption edge of Cl in NaCl with main direction of photoelectron ejection perpendicular to 100 (top curve) and 110 planes (bottom curve).

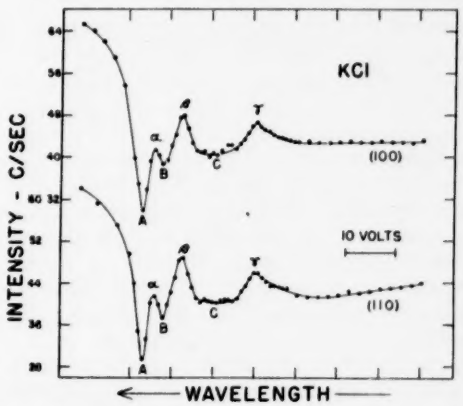

FIG. 2. K x-ray absorption edge of Cl in KCl with main direction of photoelectron ejection perpendicular to 100 (top curve) and 110 planes (bottom curve).

[5] G. P. Brewington, Phys. Rev. **46**, 861 (1934).
[6] D. Coster and G. H. Klamer, Physica **1**, 145 (1934).
[7] J. W. Trischka, Phys. Rev. **67**, 318 (1945).

structure is expected some hundreds of volts beyond the main edge. A comparative study for different directions of ejection should then be more rewarding.

It would appear that the structure for both of these ionic crystals is unaffected by the direction of photoelectron ejection within 15 volts of the main edge. No significant difference between 100 and 110 occurs for KCl throughout the entire structure range. One such difference does occur for the structure β in the Cl edge of NaCl. β is closer to the edge for 110 than 100 which, if β is caused by the same planes in each case, means that $\cos\theta_0$ is greater so that the angle with the plane is smaller. The question arises as to why there is a difference for NaCl at 18–20 volts from the edge and not for the features which are as much as 25 volts from the edge for KCl when both are ionic cubic crystals. This result implies greater symmetry of the Brillouin zones in the case of KCl. The probable explanation is that the ionic lattice for KCl contains identical numbers of scattering elements at every lattice point whereas that is not true for NaCl. Consequently KCl may be considered as a true simple cubic whereas NaCl represents an interlacing face-centered lattice network.

CONCLUSION

Pronounced structure has been observed close to the main absorption edge of chlorine using single-crystal absorbers of NaCl and KCl and polarized x-rays.

When the main direction of photoelectric ejection was changed from 100 to 110 there was a definite difference in shape and position of the feature β in NaCl. There were no significant differences for any absorption features in KCl. Thus greater symmetry of the Brillouin zones is implied for KCl, which condition may be attributed to its pure cubic structure.

PHYSICAL REVIEW VOLUME 92, NUMBER 6 DECEMBER 15, 1953

Direct Measurement of the Dielectric Constants of Silicon and Germanium

W. C. DUNLAP, JR., AND R. L. WATTERS
General Electric Research Laboratory, Schenectady, New York

(Received August 18, 1953)

Direct measurements of dielectric constants of silicon and germanium between 500 cps and 30 Mc/sec have been made. Small parallel-plate condensers were made from samples of these elements after doping with gold so as to produce high-resistivity material ($\rho \sim 10^7$ ohm cm for germanium at 77°K, $>10^{10}$ ohm cm for silicon). The dielectric constant of silicon (at 1 Mc/sec) was taken to be 11.7 ± 0.2, of germanium 15.8 ± 0.2. The dielectric constant of silicon is constant to ± 1 percent over the range 500 cps–30 Mc/sec, whereas germanium, because of its lower resistivity, has a much greater apparent variation of dielectric constant with frequency.

RECENTLY it has been found possible to produce germanium and silicon having high resistivity (above 10^6 ohm cm) at reasonable temperatures[1,2] (77°K and above). The technique of doping with the proper amount of gold leads, in the case of germanium, to samples of resistivity at 77°K, as high as 50 meg cm; in the case of silicon, greater than 10^4 meg cm. This makes it possible to do experiments on these substances that have been difficult, either because of the high conductivity or the impracticability of doing the experiment at temperatures at which ordinary germanium and silicon would have suitably high resistivity (liquid helium or hydrogen temperatures).

A case in point is the measurement of the dielectric constants. Until recently the only available precision measurements were made at infrared frequencies. Briggs,[3] working with wavelengths of the order $1–2\mu$ found values of index of refraction that extrapolate at zero frequency to dielectric constant values of 16.1 for germanium, 11.7 for silicon. Benedict and Shockley[4] have recently determined the dielectric constant of germanium by means of a wave guide method. Their value was 16.0 ± 0.5. An estimate of lesser precision has been recently made by Dacey.[5] He gives the value 16.0 ± 10 percent obtained by measurement of the "punch-through" voltage of a "unipolar" transistor.

Small parallel-plate condensers have been made of both silicon and germanium single crystals (some of the silicon wafers contained twin boundaries). A coating of aluminum-gallium paste was applied as electrodes. Fixed holders clamping the samples in a suitable position within a Dewar flask were used so that accurate correction for lead capacities would be obtained. Areas were calculated from the weight and thickness, using a density of 5.325 g/cm³ for germanium at 25°C, 2.328 for silicon.[6]

[1] W. C. Dunlap, Jr., Phys. Rev. **91**, 1282L (1953).
[2] E. A. Taft and F. H. Horn (to be published).
[3] H. B. Briggs, Phys. Rev. **77**, 287 (1950).
[4] T. S. Benedict and W. Shockley, Phys. Rev. **89**, 1152 (1953).
[5] G. C. Dacey, Phys. Rev. **90**, 759 (1953).
[6] M. E. Straumanis and E. J. Aka, J. Appl. Phys. **23**, 330 (1952).

The resistance between electrodes was sufficiently high for accurate capacity measurements to be made with ordinary precision-type capacity measuring equipment, such as the General Radio Twin-T circuit. Samples were also checked on several special laboratory equipments. Measurements were made in the frequency range 500 cps–30 Mc/sec. Generally there was an increase in apparent dielectric constant at the lower frequencies. The effect was much more pronounced for germanium than for silicon. It was also somewhat different for different samples. The effect is to be ascribed, we believe, to the inhomogeneity in resistivity that is almost unavoidable in these samples. The effects of inhomogeneity are negligible if the frequency is high enough for the capacitative admittance greatly to exceed the conductance for the most conducting region of the sample. Above this frequency, the apparent dielectric constant is found to be constant with increasing frequency. For the above reasons, dielectric constants are quoted for germanium at frequencies of 1 and 0.465 Mc/sec. For silicon the apparent dielectric constant changed, in most cases, by less than 1 percent over the entire frequency range.

Table I shows the results of measurements on a group of samples, made by a substitution method, using a parallel-connected resistance-capacity combination. A calibrated General Radio air condensor was the capacity reference. From these results the dielectric constant of germanium was taken to be 15.8 ± 0.2. The corresponding result for silicon was 11.7 ± 0.2.

The following remarks about the experimental method may be of interest.

(1) No corrections were made for edge effects, and no guard rings were used. It was felt that the dielectric constants were sufficiently high for fringing fields to affect capacity at most to the order of a few tenths of 1 percent. Detailed calculations bore out this prediction.

TABLE I. Experimental results of capacity measurements on three samples each of germanium and silicon containing traces of gold. The germanium samples were single crystalline whereas several of the silicon crystals contained a twin boundary. Measurements were made by comparison with a parallel-connected capacity-resistance combination.

Material	Sample	Area (cm^2)	Thickness cm	Freq. (Mc/sec)	Capacity ($\mu\mu f$)	d.c. Leakage (meg)	Dielectric constant
Germanium	DC-8	1.73	0.0695	1	36.31	0.25	16.0
	DC-6	1.89	0.1138	1	23.05	0.175	15.7
	DC-7	1.513	0.0475	0.465	44.98	2.0	15.8
Silicon	16	2.465	0.0696	0.465	36.88	>1000	11.68
	17	1.806	0.0539	0.465	34.09	>1000	11.76
	18	2.560	0.1181	0.465	22.43	>1000	11.70

(2) The amount of impurities present in both the silicon and germanium is so small that the dielectric constants are characteristic essentially of the pure materials. The gold content in both materials was of the order 10^{-5} percent.

(3) Since the silicon and germanium crystals were both photosensitive, measurements were made with samples in the dark. Illumination was found to have negligible effect on the dielectric constant for frequencies well below the resonant frequency of the circuit formed by leads, bridge, and capacity.

(4) The values, of course, apply strictly only at a temperature of 77°K. The error involved in their use for other temperatures is probably negligible.

The values obtained in the present work are in good agreement with others previously referred to. The data on germanium agree within experimental error with those of Benedict and Shockley and are within the expected order of agreement with Briggs' result, extrapolated to zero frequency. The value for silicon is in good agreement with Briggs' result.

We wish to thank F. H. Horn for furnishing samples of gold-doped silicon, W. N. Coffey for help with capacity measurements, and, especially, E. A. Taft for his help with all the silicon measurements.

Thermal Decay of the Luminescence of KBr

G. W. WILLIAMS, S. R. USISKIN, AND A. J. DEKKER*
Department of Physics, University of British Columbia, British Columbia, Vancouver, Canada
(Received June 29, 1953; revised manuscript received September 14, 1953)

The thermal decay of the luminescence of KBr, excited by x-rays, has been investigated over a temperature range between −77° and 250°C. The intensity of the luminescence as a function of the time after irradiation can be represented by a formula of the form:

$$I=\sum_n I_{on}\exp\left(\frac{-t}{Ae^{\epsilon_n/kT}}\right).$$

The thermal activation energies ϵ_n have been determined.

I. INTRODUCTION

A STUDY of the thermal decay of the luminescence of alkali-halides colored by irradiation with x-rays was initiated in this laboratory by Dekker and Morrish.[1,2] Essentially their technique consisted of measuring the light output in the crystals after x-ray excitation as a function of time by means of an RCA-5819 photomultiplier tube in conjunction with a scaler. The x-ray excitation and the decay measurements were carried out at the same temperature. The results obtained for KBr at room temperature could be represented by a formula of the form:

$$I\sim t^{-1.17}, \quad (1)$$

where I stands for the counting rate and t for the time measured from the instant at which the excitation was switched off. At lower temperatures the curves showed a knee, the parts above and below the knee being approximately straight lines, but of different slopes. The position of the knee could be made to shift to larger values of t by increasing the period of x-ray excitation.

In an effort to extend these preliminary investigations over a wider range of temperatures and under better controlled conditions, some serious nonlinearities were found in the apparatus. One of these was a consequence of using a 10-megohm bleeder chain to supply the dynode voltages of the RCA-5819 multiplier tube. For the relatively high initial intensities encountered, corresponding to a current in the last dynode of about 10^{-6} amp, the voltage across the first dynodes was raised as a consequence of the high resistance of the bleeder chain, resulting in an increase of gain. It was further found that the multiplier shows fatigue effects. Thus, for high, constant light intensities, the counting rate decreases as a function of time, approaching an equilibrium value (in a period of the order of minutes for collector currents of the order of 10^{-6} amp). It is interesting to note that the fatigue effect could be appreciably reduced by reducing the high voltage supply, i.e., the fatigue is related to the secondary emission surfaces rather than to the photoemissive surface. These two changes in tube gain are emphasized by the pulse-counting techniques since the discriminator is operating on a steep bias curve. Further, the finite band width of the system permits counting of two normally rejected pulses when they arrive within the resolving time of the system.

In part, the knee of the curves mentioned above could be explained as resulting from these nonlinearities. In the present circuit these effects have been eliminated by using a low impedance dynode source and a linear dc amplifier in the output. No fatigue effects have been observed for collector currents below about 10^{-6} amp, the highest value used in the experiments described below. The results have been analyzed in a different manner, leading to a number of discrete energy levels at which electrons and holes are trapped during the excitation.

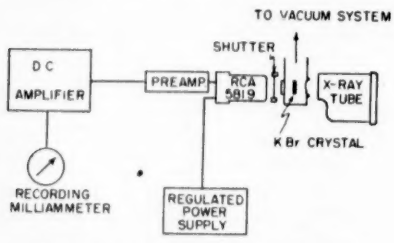

FIG. 1. Schematic diagram of the apparatus.

II. APPARATUS

An outline of the system is shown in Fig. 1. The crystal holder is placed between the x-ray machine (15 ma, 70 pkv) and the photomultiplier tube, so that the crystal is 1.5 in. from both the photomultiplier and the window of the x-ray machine. During excitation, a shutter is placed in front of the photomultiplier to cut off the relatively intense light generated in the crystal. The preamplifier, phototube, crystal holder, and x-ray machine are enclosed in a light-tight box.

The crystal holder for measurements below room

* Present address: Department of Electrical Engineering, University of Minnesota, Minneapolis, Minnesota.
[1] A. J. Dekker and A. H. Morrish, Phys. Rev. **78**, 301 (1950).
[2] A. H. Morrish and A. J. Dekker, Phys. Rev. **80**, 1030 (1950).

temperature (Fig. 2) consists of a double Dewar at the top, with a radiation shield connected to the outer Dewar and surrounding the narrow lower extension of the inner Dewar. (This makes it possible to extend future experiments to liquid helium temperatures.) For the range of temperatures investigated to date, a brass pot is fitted inside the glass system, a brass bar supplying thermal contact with the crystal. A 2-mil aluminum cup covers the side of the crystal facing the x-rays to reduce thermal gradients, and a copper-constantan thermocouple is fastened to the brass immediately beside the crystal. Temperatures from $-77°C$ to $0°C$ were obtained by placing melting mixtures in the brass pot (dry ice and acetone at $-77°C$).

The metal portion of the Dewar system has a Pyrex window facing the phototube and a 3-mil aluminum

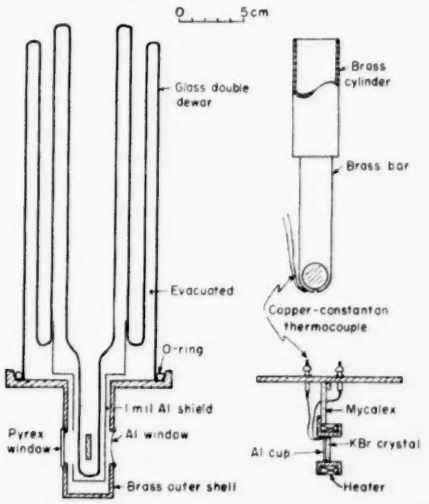

FIG. 2. Crystal holders. The holder shown at upper right is inserted in the double Dewar for measurement below 20°C. The heater shown at lower right replaces the Dewar for temperatures above 20°C. The holders are evacuated with an oil diffusion pump.

window facing the x-ray tube. This portion of the apparatus was also used for measurements above room temperature. A brass spool wound with Nichrome wire holds the crystal in its aluminum cup in the vacuum. The surfaces of the spool are entirely enclosed in an aluminium sheath, to reduce radiation. The heater current was electronically regulated. This was found sufficient to hold the temperature reasonably constant during a measurement.

The photomultiplier supply is a common regulator circuit, with an output variable from 750 to 1200 volts. The voltage divider providing the dynode voltages draws 1 ma. The last 4 sections of the divider consist of RCA-5651 voltage reference tubes which operate as voltage regulators in the current range from 0.5 to 1.2 ma, a factor which reduces the source impedance to a

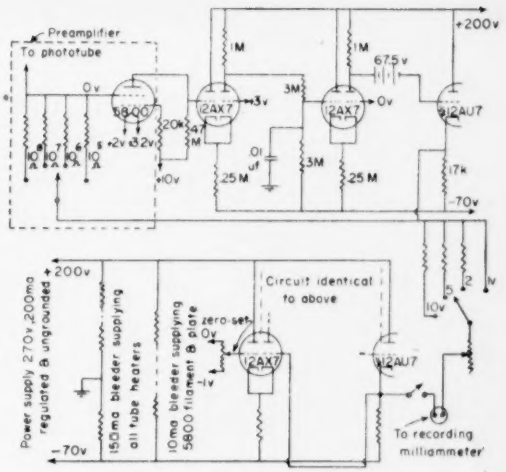

FIG. 3. Simplified diagram of the dc amplifier.

negligible value for the last dynodes where the current is appreciable.

The dc amplifier (Fig. 3) uses an electrometer tetrode (Victoreen 5800) in the input stage, followed by 2 balanced triode stages of amplification. The output stage is a cathode follower, also supplying 100 percent feedback to the grid of the input stage. The balancing voltage for the output stage is supplied by a duplicate circuit, with the exception of the input stage. This produces a zero drift of less than 1 mv per hour and an output impedance of 1 ohm. The grid resistor in the input stage is variable by factors of 10 from 10^5 to 10^8 ohms. A range switch in the output varies the meter sensitivity from 1 volt to 10 volts. The amplifier zero is unaffected by the range switches. Thus the amplifier covers a range from 10^{-8} to 10^{-4} amp driving an Esterline Angus recording milliampmeter. (The amplifier sensitivity can easily be increased to 10^{-13} amp for use with a cooled phototube.) The meter was operated at a chart speed of 6 in. per min, switching to 6 in. per hr after the faster components of the decay had disappeared. The slow response of this meter (about 1 sec) meant a time loss of about 8 sec when changing the amplifier range. However, this relatively long time constant improved the readings when the signal was less than the phototube background, integrating out the fluctuation in current.

III. RESULTS

A series of measurements of the decay of the luminescence of KBr (Harshaw) crystals has been made covering a temperature range between $-77°C$ and $240°C$. The temperature at which the decay was measured was kept constant and was always the same as that at which the crystal had been excited by x-rays. The decay curves were plotted on semi-log paper, with

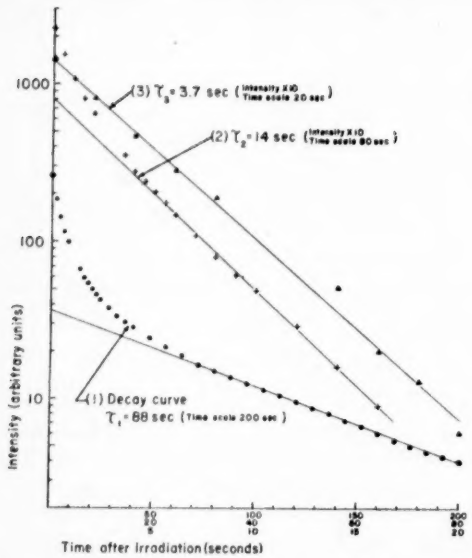

FIG. 4. Typical analysis of decay into exponential components ($T=195°C$). (1) Observed decay curve. (2) Curve replotted after subtraction of exponential of decay time 88 sec. (3) Curve replotted after subtraction of exponentials of decay times 88 sec and 14 sec.

the use of a linear time scale and a logarithmic intensity scale. It was found possible to analyze a curve corresponding to a given temperature in the form of a sum of exponential decays

$$I=\sum_n I_{on}e^{-t/\tau_n}, \tag{2}$$

where the time t was measured from the instant at which the excitation had been stopped. An example of such an analysis is given in Fig. 4. The original curve, corresponding to the decay at 195°C, in this case leads to three decay times, $\tau_1=88$ sec; $\tau_2=14$ sec; $\tau_3=3.7$ sec. At lower temperatures the analysis usually required five or six different decay times. The shortest decay time may be somewhat in doubt since it is comparable with the time constant of the meter. It may be noted that the set of τ_n's obtained for a given temperature is independent of the period of x-ray excitation. In some cases, where the slope of the decay curve for large values of t could not be determined with great accuracy, the largest decay constant was obtained from the results at the next highest temperature (see following) and its amplitude adjusted to straighten out the tail of the difference curve. This procedure is thought to be valid because the value of the longest τ affects essentially only the next shorter decay time. The other decay times are reproducible within 10 percent.

At any given temperature one thus obtains a set of different τ_n values, the logarithms of which have been plotted in Fig. 5 *vs* the reciprocal absolute temperature. The interesting feature of the analysis is that all observations can be described by a set of decay times which depend on temperature according to the relation

$$\tau_n=A_n e^{\epsilon_n/kT}, \tag{3}$$

where ϵ_n is an activation energy associated with τ_n. According to the results obtained, $A_n=10^{-9.3}$ sec and is independent of n. In general, for a single temperature, one would be hesitant to base a physical interpretation on an analysis of the type expressed by (2). However, the further analysis of the temperature dependence of the τ_n's which is possible according to Fig. 5 seems to justify the procedure.

Finally, it may be noted that at temperatures above 240°C no luminescence was observed, although the crystals showed faint luminescence after prolonged heat treatment. This phenomenon, however, has not been investigated in any detail. Another observation should be made in this connection, *viz.*, that the period of x-ray excitation measured to obtain a certain initial intensity of the luminescence is much smaller at low temperatures than it is at high temperatures. For example, between room temperature and dry ice temperature there is a factor of the order of 100 involved.

The spectrum of the emitted radiation was obtained during x-ray excitation at room temperature by means of a direct vision spectrometer, with an RCA-1P21 photomultiplier tube replacing the eye piece. The response of this tube covers a slightly wider range than the 5819, extending to 7100A instead of 6500A in the red. The maximum response occurs at 4000A instead of 4800A, but the short wavelength limit is the same. The spectrum, corrected for the response of the photo tube, is given in Fig. 6. It consists of a broad band with a peak at 5100A (2.4 ev) and a relatively sharp cutoff at 3900A (3.15 ev). At the long wavelength side it falls off more slowly, but the lack of response of the photomultiplier tube prevented measurements beyond 7100A (1.74 ev). It is important to note that by the use of optical filters it was found that the decay curves were independent of the particular wavelength region transmitted. Also, during the decay, the percentage of the

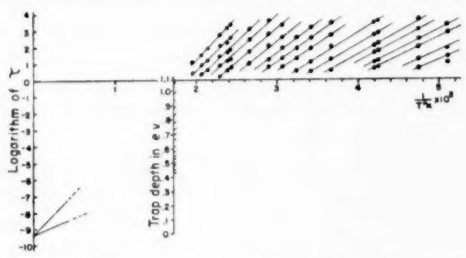

FIG. 5. Plot of $\log_{10}\tau$ *vs* $1/T$ for the temperature range −77°C to 240°C. The trap depth scale is obtained by assuming that the observed dependance on temperature is a Boltzmann function, $e^{\epsilon/kT}$. The energy ϵ is then a linear function of the slope.

total luminescence transmitted through each filter was the same as during x-ray excitation.

IV. DISCUSSION

If the foregoing analysis of the results is correct, the following conclusions can be drawn:

1. The excited crystal returns to its equilibrium state by means of a number of monomolecular processes. In fact, without reference to any particular model, consider at the instant t a number of excited centers N_n associated with a thermal activation energy ϵ_n. Assuming that these centers disappear when they absorb an energy $\geqslant \epsilon_n$, the decay of the number N_n is determined by

$$-dN_n/dt = N_n \nu_n e^{-\epsilon_n/kT}, \tag{4}$$

where ν_n is a frequency. Assuming the disappearance of a center to be associated with the emission of a photon in the visible region, the right-hand side may be identified with N_n/τ_n and thus ν_n with the reciprocal of the coefficient A_n in (3) [see, however, comment (3) below].

2. At least part of the emission spectrum is as given in Fig. 6, although it is not impossible that photons corresponding to other regions of the spectrum are emitted also.

3. The fact that the luminescence disappeared entirely above 240°C indicates that the largest thermal activation energy associated with the centers that ultimately lead to luminescence in the visible spectrum is about 1.0 ev.

4. Extrapolation of the single exponential components to $t=0$ allows an estimate of the relative populations $N_{on}=I_{on}\tau_n$ immediately after x-ray excitation. It is interesting to note that almost invariably N_{on} increases with increasing value of ϵ_n at any given temperature. Thus, the deepest traps are most densely populated at $t=0$. The very few exceptions to this rule occurred only in those cases where two N_{on} values were nearly the same and may be due to experimental errors or inaccuracy of the analysis. Unfortunately, it has not been possible to establish a quantitative law governing the initial relative populations.

5. The observation that at lower temperatures the excitation period necessary to obtain a certain luminescent intensity is much shorter than at high temperatures seems to support the idea that x-ray excitation produces color centers from incipient vacancies in the vicinity of dislocations.

Together with what is known about the properties of KBr crystals from other types of measurements, the information obtained is still too meager to permit a detailed picture of the mechanism of the decay process. Some comments may, however, be in order.

1. There are essentially three possible mechanisms for the thermal decay of the excited crystals, *viz.*, (a) by thermal release of trapped electrons into the conduction band and subsequent recombination with holes; (b) by thermal release of trapped holes into the upper filled band and subsequent recombination with electrons; (c) by a more direct recombination of trapped electrons and holes, e.g., by diffusion of color centers or tunnel effect.

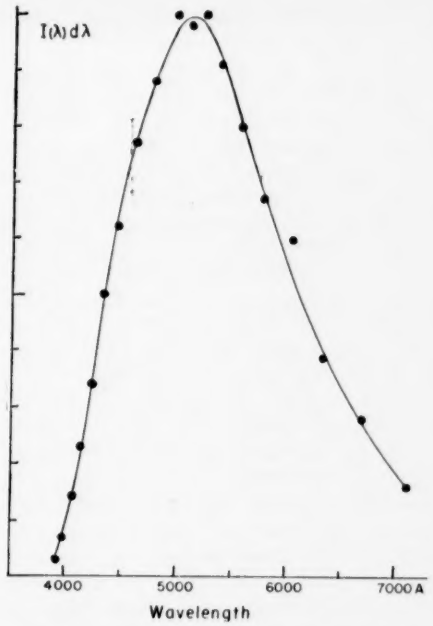

FIG. 6. Spectrum of luminescence of KBr emitted during x-ray excitation.

With regard to the latter possibility it is interesting to note that Casler, Pringsheim, and Yuster[3] have come to the conclusion that centers with the same absorption spectrum may have different thermal stability. Their measurements show that, expecially at low temperatures, a large fraction of F centers (formed by x-ray excitation) is thermally very unstable. For x-ray excitation at −185°C, the F band of KBr crystals bleaches nearly completely when kept at room temperature for one hour. When irradiated at −75°C, one hour at room temperature bleaches about $\frac{1}{3}$ of the F band and irradiation at room temperature produces hardly any F centers of the unstable kind. This effect may be a consequence of the fact that at low temperatures a relatively large number of F centers are formed from incipient vacancies in the vicinity of jogs in dislocation lines.[4] These might decay by mechanism (c) as a result of ready diffusion of color centers near jogs. The bleaching experiments just mentioned seem to indicate that for F centers at temperatures above room temperature the thermal activation energy is probably equal to that reported by Smakula,[5] *viz.*,

[3] Casler, Pringsheim, and Yuster, J. Chem. Phys. **18**, 887 (1950).
[4] See J. J. Markham, Phys. Rev. **88**, 500 (1952).
[5] A. Smakula, Gött. Nachr. **1**, 55 (1934).

0.84 ev, corresponding to excitation into the conduction band. Although this value is within the range of levels derived from the results obtained above, it is not possible to identify this level as a consequence of the qualitative nature of conclusion (4). Optically, V_1 centers and F centers should correspond to the deepest traps, but recent experiments[6] on the photoconductivity of V centers indicate that the thermal activation energy of V_1 centers is probably only a few tenths of an ev. Here again, it is possible that V_1 centers occur with different thermal stability. For a possible identification of the levels it seems that experiments on the thermal decay of the optical absorption spectrum, covering the same temperature range as used in the present experiments, may provide useful information.

2. For KBr, the optical absorption of the F band has a peak at about 2.0 ev; the V_1 band corresponds to 3.0 ev, and the gap width between the filled band and the conduction band is 8.4 ev (second maximum of the fundamental absorption). One would thus expect a free electron to combine with a V_1 center under emission of a photon of 5.4 ev, unless one assumes the existence of an intermediate state. Similarly, for a free hole recombining with an F center one would expect a photon of energy 6.4 ev. The actually observed emission spectrum ranges between about 1.8 and 3.1 ev. It is, therefore, not impossible that at least part of the light output measured in the present experiments is a result of retrapping of free electrons and holes. Whether or not this is the case may be decided by investigating crystals with a stiochiometric excess of one of the constituents: if retrapping after thermal excitation produces visible photons, the photomultiplier technique should indicate this.

3. In formula (4) one would expect $\nu_n \simeq 10^{12}$ sec^{-1} if thermal release of an electron or hole were followed by photon emission. However, the experiments give $\nu_n = 10^{9.3}$ sec^{-1}. It is not impossible that this discrepancy is a result of retrapping in such a manner that the thermally activated centers or their equivalents are restored. If the probability for a released particle to be retrapped is p, the apparent frequency factor would be reduced by a factor $(1-p)$. Agreement with experiment would then require p to be nearly unity and, moreover, to be independent of the number of filled traps to keep the process monomolecular.

[6] K. Teegarden and R. J. Mauer, Phys. Rev. **91**, 219 (1953).

ACKNOWLEDGMENTS

This investigation has been supported by the National Research Council of Canada through a Grant-in-Aid of Research to A. J. Dekker. G. W. Williams is indebted to the National Research Council for the award of a Studentship. The authors wish to acknowledge helpful comments from Mr. W. Peria.

PHYSICAL REVIEW VOLUME 92, NUMBER 6 DECEMBER 15, 1953

The Magnetic Properties of an Electronic Einstein Model Solid

M. F. M. OSBORNE AND M. C. STEELE
Naval Research Laboratory, Washington, D. C.

(Received August 31, 1953)

Following Einstein's proposal for a thermodynamic description of the ions in a solid, we propose a model for the electrons in a solid where the electrons are confined to parabolic wells and, within each well, obey Fermi statistics. The parameters of the model are ω_0, the classical frequency; m, the mass; n_e, the number of particles per well; and n_w, the number of wells per unit volume. In terms of these parameters the magnetic and caloric properties of the model can be unambiguously evaluated. This gives a satisfactory and consistent description of the thermodynamic properties of superconductors and of paramagnetic salts when appropriate values of the above parameters are determined.

I. INTRODUCTION

IT is the purpose of the present paper to devise a model of the electrons in a solid whose magnetic properties give a rough description of real materials, and by rough we mean to the same degree of approximation that an Einstein model of the lattice can be made to describe the lattice specific heat. The Einstein[1] model of the lattice consists of N identical harmonic oscillators and has the property that its specific heat approaches the Dulong-Petit value at high temperatures, whereas below some characteristic temperature it falls rapidly. The parameters of the model are fitted approximately to a real material from physical considerations (elastic constants, atomic masses, volumes, melting point) and represents roughly the behavior of the specific heat in a fairly consistent manner.

The model which we wish to propose for the electrons may therefore be expected, by analogy, to have the following properties. At large fields and high temperatures, we expect the magnetic permeability to approach 1, and the electronic specific heat to be linear, while as field and temperature diminish we would expect the permeability, μ, to approach either 0 (superconducting) or some value greater than 1 (ferromagnetic or paramagnetic). We would expect the electronic specific heat in this region to deviate considerably from a linear law. The parameters of the model would then be adjusted to fit particular real materials as well as possible (just as the Einstein model for the lattice specific heat) so that the transition fields and temperatures from $\mu\sim 1$ to $\mu\ll 1$, or $\mu>1$, would be approximately as observed.

It should be emphasized that this model as treated in this paper is essentially a thermodynamic one so that such properties as frozen-in moment, remanance, and conductivity cannot be discussed without further assumptions. However, the model itself will suggest how this might be done, just as the Einstein model of a lattice can be used to develop a theory of electrical conductivity[2] and leads to the prediction that the resistivity falls rapidly (but not like T^5 as observed) with decreasing temperature for $T<\Theta$, the Debye temperature.

The model which we propose, therefore, for the "electrons" in a solid is as follows. We imagine that there are n_w parabolic wells of potential $\frac{1}{2}B(x^2+y^2+z^2)$ per unit volume in the solid. In each well we put n_e particles. The particles are of mass m, charge e (taken as the electronic charge), and obey Fermi statistics. Thus, n_w, n_e, B, and m are the parameters of the model which we shall adjust by physical consideration to fit approximately real materials, just as in Einstein's original work. Since n_e determines E_0, the Fermi energy up to which we fill the levels (at $T=0$), we may alternatively use E_0 instead of n_e as a parameter of the model. We will find that for some considerations only the classical frequency in the well $\omega_0=(B/m)^{\frac{1}{2}}$ is the significant parameter so that B and m may not have to be determined separately (a similar situation exists for the Einstein lattice model, of the three parameters N, m, and B only N and ω_0 are needed to determine the specific heat curve). $n_e n_w=n$ is the total number of "electrons" per unit volume for the model. We shall see that fitting the model to the physical properties of a real material will either determine the above four parameters or at least give some rather interesting inequalities upon them.

We defer for the moment a justification for this model as well as an estimate on physical grounds of the values of the above parameters. Specifically, the well is not necessarily to be identified with atomic potentials. It will become apparent that the parabolic well has special properties of degeneracy not possessed by an arbitrarily chosen potential, and it is just this degeneracy which is responsible for the properties we derive. The parabolic well has, in addition, the virtue, especially valuable for the problem at hand, that the energy levels can be determined exactly for all values of the magnetic field, so that vexatious perturbation problems in the presence of degeneracy do not have to be considered.

II. SPECIFIC HEAT

A. Case for No Magnetic Field

Let us compute the electronic specific heat of one gram atom (volume A) of material on the basis of this

[1] A. Einstein, Ann. Physik **22**, 180 and 800 (1907).
[2] N. F. Mott and H. Jones, *Theory of the Properties of Metals and Alloys* (Oxford University Press, London, 1936), p. 247.

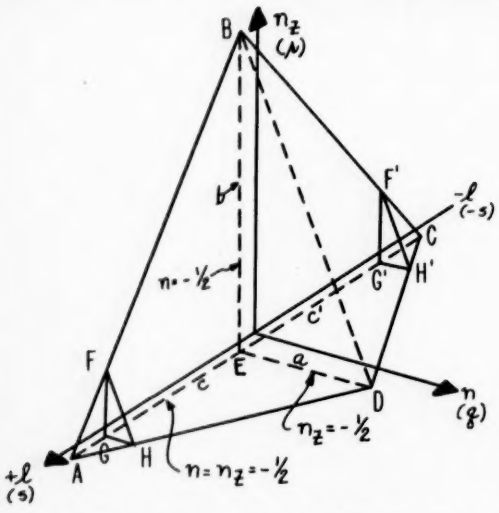

FIG. 1. Constant energy surface in quantum number space for the isotropic oscillator.

model. We shall emphasize certain aspects of this problem and go into considerable detail.

For one well we need, following the development of Seitz,[3] first to compute the number of states less than some arbitrary energy E. This is then combined with the Fermi-Dirac distribution function to compute the relation between E_0, T (temperature), and n_e.

For an isotropic oscillator whose eigenvalues are expressed in the form

$$E=\hbar\omega_0(|l|+2n+n_z+3/2), \tag{1}$$

where $l=0, \pm1, \cdots$; $n=0, 1, 2, \cdots$; $n_z=0, 1, 2, \cdots$, the surface of constant energy in quantum number space is shown in Fig. 1. We wish to compute $N(E)$, the number of points inside or on this surface. For subsequent generality we shall replace the dimensions of Fig. 1 by $ED=a$, $EB=b$, $EA=c$, $EC=c'$. With this notation we have for the isotropic oscillator in the absence of a field [Eq. (1)]

$$b=c=c'=E/\hbar\omega_0, \quad a=E/2\hbar\omega_0. \tag{2}$$

The number of points inside such a pyramid is

$$N(E)=\tfrac{1}{6}ab(c+c')+\sum_{q,r,s\neq0} e^{-\pi i(q+r)}a_{qrs}, \tag{3}$$

where the first term is the volume of Fig. 1 and a_{qrs} are the periodic terms given by

$$a_{qrs}=\int_{\text{Fig. 1}} e^{2\pi i(nq+rn_z+sl)}dndn_zdl. \tag{4}$$

Carrying out the integration gives

$$\begin{aligned} a_{qrs}=\frac{(-1)^{q+r}}{(2\pi i)^3 s}\big[&e^{2\pi irb}\{1/(q-rb/a)(r+sc'/b) \\ &-1/(q-rb/a)(r-sc/b)\} \\ &+e^{2\pi iaq}\{1/(q+sc'/a)(r-qa/b) \\ &-1/(q-sc/a)(r-qa/b)\} \\ &+e^{2\pi isc}\{1/(q-sc/a)(r-sc/b)\} \\ &-e^{-2\pi isc'}\{1/(q+sc'/a)(r+sc'/b)\}\big]. \end{aligned} \tag{5}$$

The origin of energy has been chosen at $n=-1/2$, $n_z=-1/2$.

From geometrical arguments given previously[4] it is evident that for the isotropic oscillator the principal contributions of the periodic part will be from those terms, a_{qrs}, whose indices, q, r, s, are proportional to the direction cosines of the normals to the faces ADB and DCB. This means that the four sets of principal terms will be of the form,

$$a_{2j,j,j}, \quad a_{2j,j,-j}, \quad a_{-2j,-j,-j}, \quad \text{and} \quad a_{-2j,-j,+j},$$

since these directions correspond to catching or missing an entire plane of lattice points on the faces of Fig. 1 as E increases. Substituting the four sets of indices above for q, r, s into Eq. (5) results in an indeterminacy for the isotropic oscillator. This may be resolved by a limiting process or more simply by returning to the defining Eq. (4). The latter procedure gives integrals which are quite straightforward. The resulting expression for $N(E)$ in the case of the isotropic oscillator is

$$\begin{aligned} N(E)=&\tfrac{1}{6}(E/\hbar\omega_0)^3+\textstyle\sum_j(-1)^j(E/\hbar\omega_0)^2 \\ &\times\sin[2\pi j(E/\hbar\omega_0)]/2\pi j \\ &+\text{periodic terms of } O(E/\hbar\omega_0). \end{aligned} \tag{6}$$

This expression is plotted in Fig. 2. The volume term (first term of Eqs. (3) or (6)) is given by the dotted line while the steps represent the contribution of the

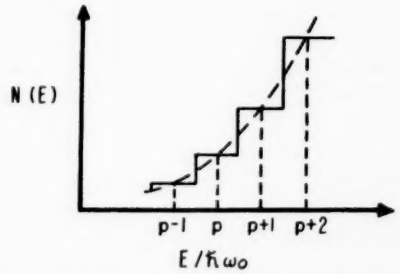

FIG. 2. Number of states within a given energy surface E for the isotropic oscillator in the absence of a field. p is an integer.

[3] F. Seitz, *The Modern Theory of Solids* (McGraw-Hill Book Company, Inc., New York, 1940), p. 150.

[4] M. F. M. Osborne, Phys. Rev. **88**, 438 (1952); M. C. Steele, Phys. Rev. **88**, 451 (1952).

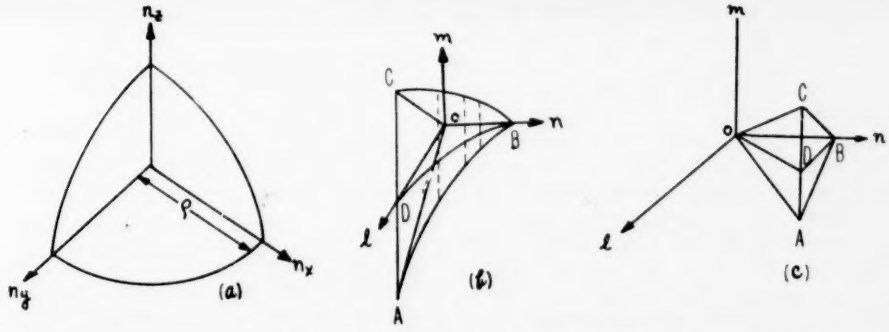

FIG. 3. Constant energy surfaces in quantum-number space for different potentials. (a) Cubical box. (b) Spherical box. ACB is a concave ruled surface and $OD \simeq DC \simeq 2OB$. (c) Coulomb potential $OB \simeq BD \simeq CA/2$.

periodic terms. The height of each riser is the number of points in the two flat faces $ADCB$ of Fig. 1, and the width of the tread is $\hbar\omega_0$.

At this point we wish to comment on the difference between the expression for $N(E)$ for the parabolic well and other types of potential. For the parabolic well the average fluctuation from a smooth curve (the volume term) is of the order of $N(E)^{\frac{1}{2}}$, or the area of a face. For a cubical box of dimension L, the average fluctuation is of order[4]

$$\rho \simeq (2mE)^{\frac{1}{2}}/\hbar L \simeq N(E)^{\frac{1}{2}},$$

where ρ is the radius of curvature in quantum number space (Fig. 3a). For a spherical container, i.e., the potential

$$V=0, \quad r<R, \quad V=\infty, \quad r>R,$$

the constant energy surface is determined by

$$\psi(R)=R^{-\frac{1}{2}}J_{l+\frac{1}{2}}[(2mE/\hbar^2)^{\frac{1}{2}}R]e^{+im\phi}P_l^m(\cos\theta)=0. \quad (7)$$

If n denotes the zeros of the Bessel function, the surface of constant energy[5] in the quantum number space l, m, n is given in Fig. 3b. The average fluctuation of $N(E)$ around a smooth curve is of order $N(E)^{\frac{1}{2}}$. For the Coulomb potential, Fig. 3c, the fluctuation around a smooth curve is of order $N(E)^{\frac{1}{2}}$ just as for the parabolic well. It will be seen that the figures for the highest degeneracy, i.e., the parabolic well and the Coulomb well, correspond to energy surfaces with flat faces whereas the cubical box with a spherical energy surface has the lowest degeneracy. The spherical box has ruled faces instead of flat faces for its constant energy surface and, therefore, falls in an intermediate degeneracy position between these two. The fluctuations for the spherical box are similarly intermediate. Since our previous work has shown that all the magnetic properties must be derivable from these fluctuations, we may expect larger and more interesting magnetic properties to arise from those wells which have the largest degeneracy (flat faces in their surfaces of constant energy in quantum number space), i.e., with the Coulomb or parabolic wells. When kT is less than the spacing of the levels, we may expect departures from the linear specific heat law of a Fermi gas. Furthermore, these departures will be more pronounced as the faces get flatter or the degeneracy increases.

Returning to the computation of the specific heat, we proceed with the condition which determines the Fermi energy, E_0, of one well as a function of T and n_e,

$$n_e=-\int_0^\infty N(E)\frac{df(E)}{dE}dE,$$

where $f(E)$ is the Fermi function. From Eq. (6) this gives

$$n_e=\tfrac{1}{6}(E_0/\hbar\omega_0)^3+\pi^2(kT)^2E_0/6(\hbar\omega_0)^3$$
$$+\mathrm{Im}\sum_{j=1}^{\infty}(-1)^j(E_0/\hbar\omega_0)^2(\exp(2\pi ijE_0/\hbar\omega_0)/2\pi j)$$
$$\times(2\pi^2jkT/\hbar\omega_0)/(\sinh 2\pi^2jkT/\hbar\omega_0)+O(E_0/\hbar\omega_0) \quad (8)$$

in which the first two terms are just those obtained by the conventional method with $N(E)=\frac{1}{6}(E/\hbar\omega_0)^3$ whereas the remaining terms represent the number theory corrections.

Evidently if $kT \gg \hbar\omega_0$, these number theory corrections become negligibly small since they are not only damped exponentially but alternate in sign. In this case the specific heat takes on the conventional expression given by Seitz. For one gram atom of volume A this is

$$C_v=An_w(\pi^2/6)k^2TE_0^2/(\hbar\omega_0)^3. \quad (9)$$

However, with diminishing temperature there must come a point where the effect of the number theory terms can no longer be neglected. In determining the dependence of E_0 on the temperature, however, it has been found impossible, to date, to assess the effect of these corrections [as they appear in Eq. (8)] on E_0 because of the great sensitivity of their contribution to how close $E_0/\hbar\omega_0$ is to an integer. From Fig. 2, which may be considered as the limit of Eq. (8) as $T \to 0$,

[5] E. Jahnke and F. Emde, *Tables of Functions* (Dover Publications, New York, 1945), p. 143.

E_0 is, within the same limits, an indeterminate function of N (or conversely). This is a consequence of degeneracy with the result that fixing E_0 and fixing the number of particles are here (at low temperatures) two different problems (see introduction).

For this reason we have chosen to abandon Eq. (8) at low temperatures ($kT<\hbar\omega_0$) and approach the problem with an approximation which succeeds best at $T=0$ and fails for larger T. This approximation fails at temperatures where the specific heat approximately agrees with the linear law, Eq. (9), so that we can compute the specific heat approximately for all T. Thus, we shall see that except at $T\equiv 0$, this indeterminacy mentioned above can, in fact, be resolved.

We, therefore, first compute by an approximation the specific heat for $kT\ll\hbar\omega_0$, where the number theory correction terms in Eq. (8) obviously dominate. Let us write the expression determining the Fermi energy, E_0, as a function of temperature in its most fundamental form. We denote by Δ_p the number of points in both faces of Fig. 1, and the energy corresponding to any point in either face by $E(p)=\hbar\omega_0(p+3/2)$. Here p is zero or a positive integer. The expression determining E_0 is

$$n_e=\sum_{p\leq p_0}\Delta_p\frac{1}{1+\exp\{[\hbar\omega_0(p+3/2)-E_0]/kT\}}+\sum_{p>p_0}\Delta_p\frac{1}{1+\exp\{[\hbar\omega_0(p+3/2)-E_0]/kT\}},\quad(10)$$

where p_0 is by definition the nearest integer smaller than or equal to $(E_0/\hbar\omega_0)-3/2$. In this form for E_0 we see that n_e is expressed as the sum of terms representing the contribution of states which are full or nearly full ($p\leqq p_0$) plus the contribution of those states which are nearly all empty ($p>p_0$). One or two layers in the immediate neighborhood of the Fermi energy ($p\sim p_0$) have a probability of occupancy near 1/2. We shall need to take explicit account of these.

Now consider in detail the number of particles n_e in one well. This can always be expressed in the form $n_e=N_E(p)+\zeta\Delta_{p+1}$. Here

$$N_E(p)=\sum_{j=0}^{p}\Delta_j$$

is the number of states up to and including the pth layer[6] and ζ is the fraction to which the next face could be filled with particles given the available number n_e. If $\zeta=0$, we speak of a filled face. $\zeta=1/2$ means that 1/2 of the next face could be filled, while $\zeta=1$ would imply that the next face, at $T=0$, would be completely filled. Thus, for the case $\zeta=1$ we could write $n_e=N_E(p+1)$. So we may write

$$n_e=N_E(p_0)+\zeta\Delta_{p_0+1}=\sum_{p\leq p_0}\Delta_p+\sum_{p\leqq p_0}\Delta_p\times\left[\frac{1}{1+\exp\{[\hbar\omega_0(p+3/2)-E_0]/kT\}}-1\right]+\sum_{p>p_0}\frac{\Delta_p}{1+\exp\{[\hbar\omega_0(p+3/2)-E_0]/kT\}}$$

or, using the definition of $N_E(p)$,

$$\zeta\Delta_{p_0+1}=-\sum_{p\leq p_0}\frac{\Delta_p}{1+\exp\{[E_0-\hbar\omega_0(p+3/2)]/kT\}}+\sum_{p>p_0}\frac{\Delta_p}{1+\exp\{[\hbar\omega_0(p+3/2)-E_0]/kT\}}.\quad(11)$$

We observe that in this form all of the terms on the right become exponentially small except for perhaps the two or three terms where p is closest to p_0, under the condition that $\hbar\omega_0/kT\gg 1$. Therefore, for sufficiently small temperatures we take into account only the larger terms which are given by those p's closest to p_0. Let us define a function of the temperature $0<\eta(T)<1$ by $(E_0/\hbar\omega_0)-3/2-p_0=\eta(T)$. Then Eq. (11) may be written approximately as

$$\begin{aligned}\zeta\Delta_{p_0+1}\cong&-\Delta_{p_0-1}\frac{1}{\exp[\hbar\omega_0(1+\eta)/kT]+1}&\text{(a)}\\&-\Delta_{p_0}\frac{1}{\exp(\hbar\omega_0\eta/kT)+1}&\text{(b)}\\&+\Delta_{p_0+1}\frac{1}{\exp[\hbar\omega_0(1-\eta)/kT]+1}&\text{(c)}\\&+\Delta_{p_0+2}\frac{1}{\exp[\hbar\omega_0(2-\eta)/kT]+1}.&\text{(d)}\end{aligned}\quad(12)$$

Equation (12) shows that at a sufficiently low temperature, where the Fermi function is sufficiently close to either 0 or 1, only terms (we have taken four) in the immediate neighborhood of the Fermi energy contribute to the temperature dependence of the Fermi energy. Let us now evaluate the specific heat for two limiting assumptions: that the face is either half filled ($\zeta=1/2$) or completely filled ($\zeta=0$).

Evidently for the case $\zeta=0$, if η is near 1/2 (Fermi energy E_0 falling halfway between lattice planes 2, 1, 1), terms (b) and (c) nearly cancel each other whereas (a) and (d) are negligible for kT sufficiently less than $\hbar\omega_0$. For the case $\zeta=0$, therefore, we have approximately, where $\eta(T)=1/2+\epsilon(T)$, $\epsilon(T)\ll 1/2$,

$$0\cong-\Delta_{p_0}/(\exp[(\hbar\omega_0/kT)(\tfrac{1}{2}+\epsilon)]+1)+\Delta_{p_0+1}/(\exp[(\hbar\omega_0/kT)(\tfrac{1}{2}-\epsilon)]+1),\quad(13)$$

[6] It can easily be shown by direct summation that $N(p)=(p^3/6)+p^2+(11p/6)+1$ whence it follows that $\Delta_p=N(p)-N(p-1)=(1/2)p^2+(5/2)p+3$.

from which we find

$$E_0=(p_0+2)\hbar\omega_0-\frac{kT}{\hbar\omega_0}\frac{1}{p_0}[1+\exp(-\hbar\omega_0/2kT)]. \quad (14)$$

The total energy is

$$U=\sum_p(p+3/2)\hbar\omega_0\Delta_p\frac{1}{\exp\{[(p+3/2)\hbar\omega_0-E_0]/kT\}+1}. \quad (15)$$

This can be evaluated in a manner similar to the above derivation for E_0, using only terms corresponding to the layers p_0 and p_0+1 closest to the Fermi energy. Ultimately one obtains for the atomic heat for the case $\zeta=0$ (filled face), using Eqs. (14) and (15),

$$C_{v,\zeta=0}=(\partial U/\partial T)_{\zeta=0}$$
$$=An_w(k/2)(\hbar\omega_0/kT)^2\Delta_{p0}\exp[-\tfrac{1}{2}(\hbar\omega_0/kT)]$$
$$\times\{1-2\exp[-\tfrac{1}{2}(\hbar\omega_0/kT)]\}. \quad (16)$$

In a similar fashion it can be shown that for the half filled face, $\zeta=1/2$, the Fermi energy lies almost directly on a lattice plane 2, 1, 1 (probability of occupancy 1/2 at $T=0$). The principal terms in Eq. (12) which have to be taken into account are (b), (c), and (d), and the atomic heat is

$$C_{v,\zeta=\frac{1}{2}}=An_w\frac{\Delta_{p0}170}{81}k(\hbar\omega_0/kT)^2\exp(-\hbar\omega_0/kT). \quad (17)$$

For any other value of ζ (except $\zeta=0$) it can be shown that the Fermi energy for $T\to0$ moves closer and closer to a lattice plane in such a way as to just give a probability of occupancy (the Fermi function) equal to the fraction ζ to which that face is filled, given the available number of particles n_e.

The three expressions for the specific heat, Eqs. (9), (16), and (17), with $p_0=E_0/\hbar\omega_0$, are plotted in dimensionless form against the dimensionless temperature variable $2\pi^2kT/\hbar\omega_0$ in Fig. 4. It will be seen that the two low-temperature approximations agree roughly with the linear law at $2\pi^2kT/\hbar\omega_0\sim3-6$, or roughly at a temperature where one expects them to begin to fail. Thus, together with the linear law they give a description of the specific heat for all temperatures. At very low temperatures the specific heat is vanishingly smaller than the linear law. The filled face case ($\zeta=0$) may rise above the linear law at intermediate temperatures.

B. Case with a Magnetic Field

Now let us consider the effect of a finite magnetic field H on the Fermi surface and its corresponding effect on the specific heat. The energy levels in this case are given[7] by

$$E=\hbar\omega[l+d|l|+d(2n+1)]+\hbar\omega_0(n_z+1/2),$$
$$\omega=eH/2mc, \quad d=(1+\omega_0^2/\omega^2)^{\frac{1}{2}}, \quad (18)$$

[7] C. G. Darwin, Proc. Cambridge Phil. Soc. **27**, 86 (1931).

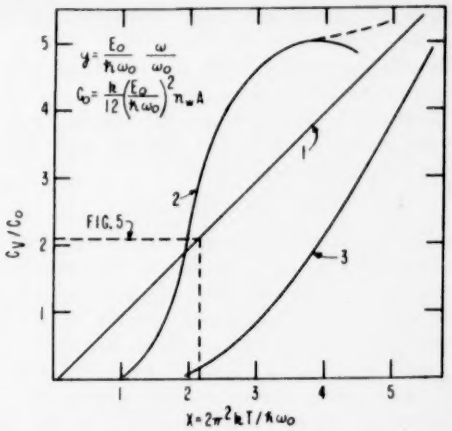

FIG. 4. Specific heat vs temperature, both in dimensionless form. (1) Equation (9), linear law, for fields such that $y>1$. (2) Equation (16), no field, filled face ($\zeta=0$, $y=0$). (3) Equation (17), no field, half-filled face ($\zeta=1/2$, $y=0$).

which for small fields, $\omega\ll\omega_0$, takes the form

$$E=\hbar\omega_0[(|l|+2n+1+n_z+1/2)+(\omega/\omega_0)l$$
$$+\tfrac{1}{2}(\omega/\omega_0)^2|l|+(2n+1)(\omega^2/2\omega_0^2)+O(\omega/\omega_0)^3]. \quad (19)$$

We see that as the magnetic field ($\sim\omega$) increases, the dimensions of Fig. 1 are modified as follows. The l_+ axis decreases linearly with H, the l_- axis increases linearly, and the n axis decreases quadratically (constant to the first order of (ω/ω_0)) in just such a way as to keep the total volume and also the area in the $l-n$ plane a constant. We also note (1) for all fields the Fermi surface is flat, since the energy is linear in the quantum numbers, and (2) that when $(E/\hbar\omega_0)(\omega/\omega_0)<1/2$, the Fermi surface can be placed in such a way as never to cross a lattice plane whereas if $(E/\hbar\omega_0)(\omega/\omega_0)>1/2$, it must do so. That is, if $(E/\hbar\omega_0)(\omega/\omega_0)=1/2$, the Fermi surface has moved by 1/2 unit in quantum number space, inward 1/2 at the end of the l_+ axis, outward 1/2 at the l_- axis (see Fig. 6).

From this we can immediately draw a conclusion about the behavior of the specific heat in a magnetic field large enough that $(E/\hbar\omega_0)(\omega/\omega_0)>1$, in contrast with its behavior in the absence of a magnetic field ($\omega=0$). The departure from the linear law displayed in Fig. 4 is primarily a consequence of the discrete intervals $\hbar\omega_0$ at which the Fermi function is evaluated. Now as soon as $(E/\hbar\omega_0)(\omega/\omega_0)>1$, these intervals are made smaller, being instead $\hbar\omega$ where $\omega\ll\omega_0$. In that case we have a return to the linear law where the specific heat is primarily determined by the volume term in $N(E)$, $\frac{1}{6}(E/\hbar\omega_0)^3$, and only when $\hbar\omega/kT\gg1$ (instead of $\hbar\omega_0/kT\gg1$) can we expect appreciable departures from the linear law, i.e., at much lower temperatures. This is indicated by the straight line (1) of Fig. 4. Thus, the effect of a magnetic field appreciably greater than a certain critical value [i.e., when $(E/\hbar\omega_0)(\omega/\omega_0)=1$] is

to make the specific heat linear to much lower temperatures.

The way in which curves (2) and (3) of Fig. 4 distort into (1) as the field increases, up to $(E/\hbar\omega_0)(\omega/\omega_0)=1$, can be evaluated approximately as follows. From Eq. (19) the energy levels within the pth layer may be written [neglecting $(\omega/\omega_0)^2$] as

$$E(p)=(p+3/2)\hbar\omega_0+l\hbar\omega. \tag{20}$$

One then evaluates the specific heat by using only the contribution of the layers nearest to the Fermi energy, exactly as in the development which led to Eq. (12), where instead of Δ_p, Δ_{p+1}, etc., we now have a summation (which can be replaced by an integral if $kT/\hbar\omega>1$), over each layer. Since the correction $l\hbar\omega$ [Eq. (20)] to the energy of a state within a given layer does not depend on n or n_z, this means that we can replace the integration over a layer by its projection on the l, n, plane. This gives for the case of a half-filled face

$$C_{v,\zeta=\frac{1}{2}}=(2\pi^2kT/\hbar\omega_0)n_wA\,(k/6)(E_0/\hbar\omega_0)^2\times(1/2)(\omega_0/\omega)(\hbar\omega_0/E_0),$$
$$\text{valid if } kT/\hbar\omega_0\ll(E_0/\hbar\omega_0)(\omega/\omega_0),$$
$$\hbar\omega\ll kT\ll\hbar\omega_0,\quad (E_0/\hbar\omega_0)(\omega/\omega_0)<1. \tag{21}$$

For the filled face case we find

$$C_{v,\zeta=0}=\pi^2(k^2T/3)n_wA\,(1/\hbar\omega)\times\left[\left(\frac{E_0}{\hbar\omega_0}\right)\left(\frac{\omega}{\omega_0}\right)-\frac{1}{2}\right](E_0/\hbar\omega_0),$$
$$\text{valid if } 1>(E_0/\hbar\omega_0)(\omega/\omega_0)>1/2 \tag{22}$$

and

$$kT\ll\left[(E_0/\hbar\omega_0)(\omega/\omega_0)-\tfrac{1}{2}\right](E_0/\hbar\omega_0)\hbar\omega.$$

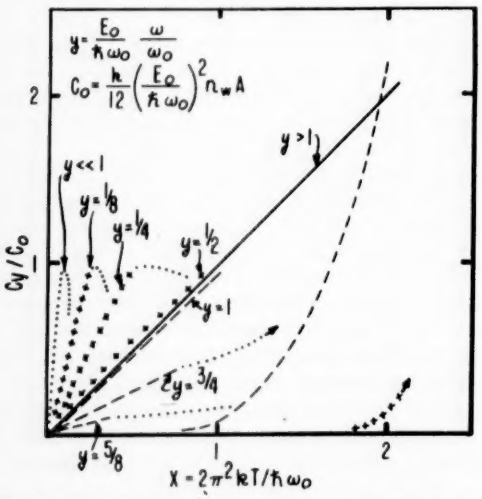

FIG. 5. Specific heat *vs* temperature, in dimensionless form, for different values of the dimensionless magnetic-field variable y. Full curve, linear law for high temperatures and $y>1$. Dashed line, filled face ($\zeta=0$). Crosses, half-filled face ($\zeta=1/2$). Dotted lines indicate estimated behavior beyond the validity range of the formulas.

These formulas essentially use the conventional expression for the specific heat, $(\pi^2/3)[k^2Tg(E_0)]$, where the density of states $g(E)$ is that "seen" by the Fermi energy (E_0) as it crosses a lattice plane, and T is so small that neither the extreme values of energy at the ends A, C of the lattice planes of Fig. 1 nor adjacent lattice planes have any contribution.

For higher temperatures both of these specific heats must approach the high-temperature linear law. However, for very weak fields there is a limited range in T over which $C_{v,\zeta=\frac{1}{2}}$ falls like $1/T^2$, corresponding to the narrow-band approximation of Mott and Jones.[2] This condition is realized when kT is much greater than $(2E_0/\hbar\omega_0)\hbar\omega$, the energy width of a single face of Fig. 1, but much less than $\hbar\omega_0$, the spacing of lattice planes. Thus, the specific heat for the case of a half-filled face develops a thin spine near $T=0$ which for increasing H broadens and flattens into the high-temperature linear law. The entropy given by the integral of $dS=C_vdT/T$ over this spine (see Sec. VI, B) is essentially constant and represents the zero-point entropy of the half-filled face case since at the absolute zero the well, considered as a single system, has a degeneracy given by the number of ways the face may be half filled.

For the filled-face case the specific heat near $T=0$ rises steadily to the linear law as the field is increased. The bump on curve (2) of Fig. 4 probably moves to lower temperatures with increasing field, although we have not been able to verify this. Figure 5 shows a dimensionless plot of Eqs. (21) and (22).

III. EVALUATION OF THE MOMENT AT $T=0°K$

Let us first consider the behavior of the Fermi energy at temperatures so small that the criterion $\hbar\omega/kT\gg1$ is observed. This is the condition for the Fermi function to drop from one to zero in the interval between adjacent energy levels [see Eq. (20)]. This will not be essentially different from the behavior as $T\to0$. For the case of a filled face we saw that for $H=0$ the Fermi energy huddled up to the plane bisecting the space between two lattice planes whereas for a partly filled face, in particular for $\zeta=1/2$, it has to huddle up to a lattice plane in just such a way as to preserve (give a probability of occupancy of) the appropriate fraction of that face.

So we can see that for $(E/\hbar\omega_0)(\omega/\omega_0)<1/2$, if we order the states in terms of increasing energy, they fall in the order indicated in Fig. 6. Each layer starts at $-l$ and increases in energy to $+l$. After a layer is filled, one starts to fill the next layer at $-l$. We now ask how the Fermi energy behaves as H increases. Evidently if at some field H the Fermi surface passes between say the points 8, 9 of Fig. 6 (face more than half full), as H increases further, E_0 must increase just enough to make the Fermi surface always pass between these same two points so that in summing the Fermi function in $n_e=\sum_i f(E_i,E_0)$, one counts essentially all the points inside and none outside in order to preserve n_e.

For a face less than half full (if E_0 passes between 5 and 6 of Fig. 6), E_0 must decrease with increasing H. Ultimately, (for $(E/\hbar\omega_0)(\omega/\omega_0)>1$) since the Fermi *volume* does not change with H, E_0 must oscillate ($\sim\hbar\omega$) with H just enough to enclose always exactly the same number of points (having the lowest energy). Precisely and only for the cases $\zeta=0$ and $\zeta=1/2$, E_0 need not change [neglecting $(\omega/\omega_0)^2$] with H at all even in the range $(E/\hbar\omega_0)(\omega/\omega_0)<1/2$, since for these two values of the face filling the Fermi surface, for fixed E_0 and changing H, either does not cut lattice planes at all ($\zeta=0$), cuts them always at the same point ($l=0$ if $\zeta=1/2$), or loses and gains lattice points in equal amounts (starting at the ends of the 1 axis) as the field varies.

With this understanding, and at extremely low temperatures ($kT\ll\hbar\omega$), we can, therefore, evaluate the magnetic moment from

$$\begin{aligned}M&=-(\partial F/\partial H)_{E_0}\\&=(\partial/\partial H)_{E_0}\textstyle\sum_i kT\ln\{1+\exp[(E_0-E_i)/kT]\}\\&=-\sum_{E_i\leq E_0}(\partial E_i/\partial H)+kT(\partial/\partial H)\\&\quad\times\sum_{E_i\leq E_0}\exp[-(E_0-E_i)/kT]\\&\quad+kT(\partial/\partial H)\sum_{E_i>E_0}\exp[(E_0-E_i)/kT]\\&\quad+\sum_{E_0\leq E_i}O\exp[\pm 2(E_0-E_i)/kT],\end{aligned}\tag{23}$$

where we understand that E_0 is so adjusted with H that the Fermi surface always encompasses exactly the same number and set of points so long as $(E_0/\hbar\omega_0)(\omega/\omega_0)<1/2$. For still larger fields E_0 can be considered as approximately constant (independent of H) since for every point lost on the $+1$ face, another will be gained on the -1 face.

If the temperature is sufficiently low ($kT\ll\hbar\omega$), we can drop all but the first term of Eq. (23) and then evaluate the summation of the first term (for some purposes an integral will here suffice). For a half-filled face we sum for finite H over the interior volume and the $-l$ face, DCB, Fig. 1, whereas for the filled face we sum over the interior volume and both faces. This procedure is valid provided we satisfy the inequality $(E/\hbar\omega_0)(\omega/\omega_0)<1/2$ if $\zeta=0$, or $(E/\hbar\omega_0)(\omega/\omega_0)<1$ for $\zeta=1/2$. This results in the following expressions for the moment per unit volume (n_w wells per cc). It should be noted that for the filled face ($\zeta=0$) summing (but not integrating) cancels exactly the $l\hbar\omega$ terms in Eq. (19) so that we must carry terms in ω^2/ω_0^2. These may be integrated. Also, for $\zeta=1/2$, we must sum the $-l$ face (or integrate it as a projected area DEC) and *not* integrate it as a thin three-dimensional wedge since a point in this face, when counted, is counted at full weight.

$$M(T=0,\zeta=0)=-n_w(1/12)(e\hbar/2mc)(\omega/\omega_0)(E_0/\hbar\omega_0)^4,$$
$$\text{valid if } (E_0/\hbar\omega_0)(\omega/\omega_0)<1/2;\tag{24}$$

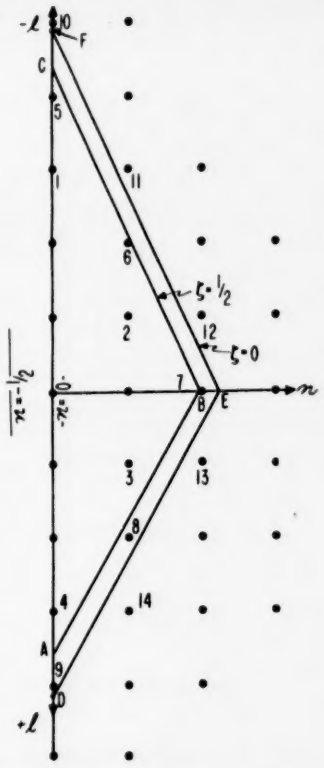

FIG. 6. Constant energy contour in n, l plane for small, finite field H. ABC corresponds to case of half-filled face, which neither loses nor gains points as long as $y=(E/\hbar\omega_0)(\omega/\omega_0)<1$. DEF corresponds to filled-face case which neither loses nor gains points for $y<1/2$.

$$M(T=0,\zeta=1/2)=+(n_w/12)(E_0/\hbar\omega_0)^3(e\hbar/2mc)$$
$$-(n_w/12)(e\hbar/2mc)(\omega/\omega_0)(E_0/\hbar\omega_0)^4,$$
$$\text{valid if } (E_0/\hbar\omega_0)(\omega/\omega_0)<1.\tag{25}$$

These are plotted in Fig. 7.

We may carry the analysis for the case of a filled face outside the range $(E_0/\hbar\omega_0)(\omega/\omega_0)<1/2$, still taking into account that the temperature is so small that the Fermi function drops from one to zero in the range ($\hbar\omega$) between points in a face and just include the contributions of the first term in Eq. (23) appropriately. We thus obtain the segment AB of Fig. 7, where the change in slope at A indicates that the Fermi surface is just catching or missing one of the lattice planes $2j$, j, $\pm j$. The range over which $\partial E_i/\partial H$ is summed is the interior and surface of Fig. 1, minus a triangular patch (points lost) AFH (projected to AGH), plus a patch $F'H'C$ (projected to $H'G'C$) of points gained in the next outer lattice plane. The dimension $AG=G'C$ is $(E/\hbar\omega_0)-(\omega_0/2\omega)$. This gives for the moment per unit volume for the case of a filled face in the range

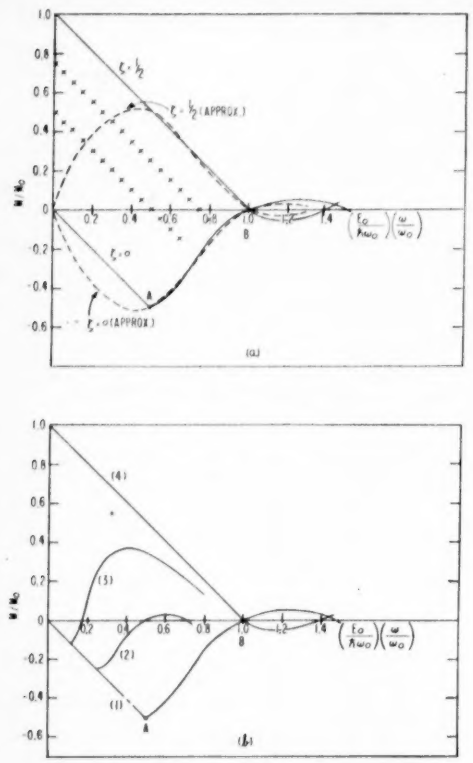

FIG. 7. Dimensionless magnetization as a function of dimensionless field at $T=0$. $M_0=n_w\beta(E_0/\hbar\omega_0)^3/12$. (a) Number of particles, n_e, fixed. Full curves, exact [Eqs. (24), (25) (26)]; ---- one term approximation [Eq. (31)]; xxxx, moment for fillings intermediate between filled and half filled. (b) Fermi energy fixed. (1) and (4) are identical with the filled and half-filled full curves of (a) and correspond to $E_0/\hbar\omega_0=p$ and $E_0/\hbar\omega_0=p+(1/2)$ (where p is an integer), respectively; (2) $E_0/\hbar\omega_0=p+(1/4)$; (3) $E_0/\hbar\omega_0=p+(3/8)$.

$$1/2<(E_0/\hbar\omega_0)(\omega/\omega_0)<1$$

$$\begin{aligned}M(T=0,\zeta=0)=-n_w[&(1/12)(eh/2mc)(\omega/\omega_0)(E_0/\hbar\omega_0)^4\\&+(1/8)(eh/2mc)(E_0/\hbar\omega_0)(\omega_0/\omega)^2\\&-(1/6)(E_0/\hbar\omega_0)^3(eh/2mc)\\&-(1/24)(eh/2mc)(\omega_0/\omega)^3].\end{aligned}\quad(26)$$

The case for face filling intermediate between half and full is indicated by the crosses in Fig. 7(a). Note that this is for fixed n_e, E_0 having been adjusted as above to preserve n_e. All of the moments shown in Fig. 7(a) reverse the sign of the moment with the sign of H so that with the exception of the filled-face case, all have a discontinuity in the moment at $H=0$. As will be shown (Fig. 8), this discontinuity is present only *at* $T=0$. For all finite T this discontinuity is removed, and the moment vanishes continuously at $H=0$.

The above developments for the moment, shown in Fig. 7(a), are essentially given by evaluating $M=-\sum\partial E_i/\partial H$, where the sum is over a constant number of states which are chosen to be the lowest ones for any given H, not necessarily the same states for all fields, as the break in OAB at A indicated. It is a calculation for an atomic Fermi-Dirac system when the central potential for all particles is given as parabolic. The results agree quite satisfactorily with what is known from atomic problems, i.e., for a filled shell (=face) the system is diamagnetic with $M\sim-(e^2H/6mc^2)\sum\langle r^2\rangle_{Av}$, which is essentially what Eq. (24) represents. For an unfilled shell the system *starts out* paramagnetic (unquenched orbital paramagnetism), to which is added Eq. (24), the above diamagnetic term. Since we have exact eigenvalues for the parabolic well, we know precisely what we have neglected and can, if we wish, estimate the validity thereof and at what point perturbation theory concepts fail.

We can extend our results to higher fields and temperatures. This we can do as follows and at the same time verify the above results in an independent manner.

The moment at $T=0$ is given by[4]

$$M_{T=0}=(\partial/\partial H)\int_0^{E_0}N(E)dE.\quad(27)$$

We recall that $N(E)$ is given by Eq. (3) with the numerical coefficients given by Eq. (4). Now in Eq. (4) we may substitute the dimensions which Fig. 1 takes on in the presence of a magnetic field. These are given

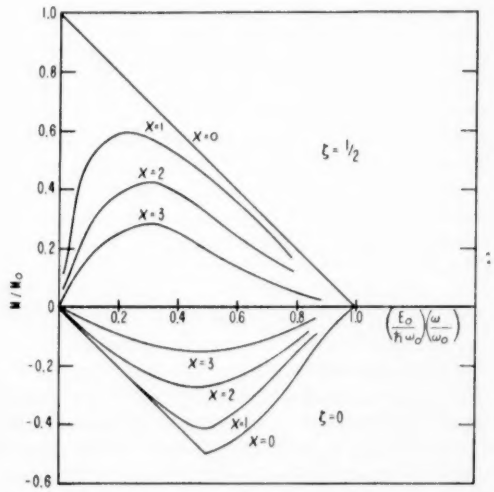

FIG. 8. Dimensionless magnetization at finite temperatures as a function of dimensionless field. The dimensionless temperature parameter for the different curves is $x=2\pi^2kT/\hbar\omega_0$. The positive values of moment are for the half-filled face whereas the negative moments are for the filled face.

exactly by Eq. (18) as

$$\begin{aligned} a&=E/2\hbar\omega,\\ b&=E/\hbar\omega_0,\\ c&=E/\hbar\omega(1+d),\\ c'&=E/\hbar\omega(1-d),\\ d&=(1+\omega^2{}_0/\omega^2)^{\frac{1}{2}}. \end{aligned} \tag{28}$$

This gives the following expressions for $N(E)$ and the moment, per unit volume (n_w wells), when one sums only the a_{qrs} corresponding to the normals (or near normals) to the principle faces of Fig. 1, i.e., only $a_{2j,j,j}$, $a_{2j,j,-j}$, $a_{-2j,-j,-j}$, $a_{-2j,-j,+j}$:

$$\begin{aligned} N(E)=&\left(\frac{n_w}{6}\right)\left(\frac{E}{\hbar\omega_0}\right)^3+2n_w\left(\frac{\omega_0}{\omega}\right)^2\sum_{j=1}^{\infty}\frac{(-1)^j}{(2\pi ij)^3}\\ &\times[-\exp(2\pi ijE/d\hbar\omega)+\tfrac{1}{2}(1+3\omega/2\omega_0)\\ &\times\exp[2\pi ijE/(d+1)\hbar\omega]+\tfrac{1}{2}(1-3\omega/2\omega_0)\\ &\times\exp(2\pi ijE/(d-1)\hbar\omega)+O(\omega^2/\omega_0^2)], \end{aligned} \tag{29}$$

$$\begin{aligned} M=&\left(\frac{\partial}{\partial H}\right)_{E_0}2n_w\hbar\omega\left(\frac{\omega_0}{\omega}\right)^2\sum_{j=1}^{\infty}\frac{1}{(2\pi j)^4}\\ &\times\left[-d\cos 2\pi j\left[\frac{E_0}{d\hbar\omega}-\frac{1}{2}\right]+\tfrac{1}{2}(d+1)\right.\\ &\times(1+3\omega/2\omega_0)\cos\left(2\pi j\left[\frac{E_0}{(d+1)\hbar\omega}-\frac{1}{2}\right]\right)\\ &+\tfrac{1}{2}(d-1)(1-3\omega/2\omega_0)\\ &\times\cos\left(2\pi j\left[\frac{E_0}{(d-1)\hbar\omega}-\frac{1}{2}\right]\right)\\ &\left.+O(\omega^2/\omega_0^2)\right]. \end{aligned} \tag{30}$$

Now this formula, Eq. (30), for the moment can be summed exactly by use of the Hurwitz formula,[8] which expresses the generalized Zeta function as a trigonometric series; and the Zeta function in turn can then be expressed as a polynomial.[9] Slightly different formulas are required for the range $0<(E_0/\hbar\omega_0)(\omega/\omega_0)<1/2$, 1/2 to 1, 1 to 3/2, etc. Different forms are also required depending on whether $E_0/\hbar\omega_0$ is an integer (filled face) or halfway between integers (half-filled face). In this way we have been able to verify exactly the expressions for the moment given in Eqs. (24), (25), (26), and have even carried them to still higher values of the field, i.e., $(E_0/\hbar\omega_0)(\omega/\omega_0)>1$. The general behavior of the moment is oscillatory, of decreasing amplitude and periodic in $(E_0/\hbar\omega_0)(\omega/\omega_0)$, as is indeed to be expected from the way in which the Fermi surface of constant energy catches and loses points in the lattice planes. Figure 7(b) gives the moment computed from Eq. (30), using the Hurwitz formula, for the somewhat artificial case for which E_0 (instead of n_e) is held fixed, so that here the "number of particles" is *not* preserved. It will be seen that *only* if $E_0/\hbar\omega_0$=an integer (filled face), or $E_0/\hbar\omega_0$ =integer+1/2 (half-filled face), is fixing E_0 equivalent to fixing n_e, as previously mentioned.

By using only the largest term ($j=1$) of Eq. (30) to evaluate the moment, one can obtain a single analytic expression for the moment for all values of $(E_0/\hbar\omega_0)\times(\omega/\omega_0)$ (ω/ω_0 still $\ll 1$) which is a quite satisfactory approximation. This approximation for the moment per unit volume is

$$\begin{aligned} M=&(4n_w/(2\pi)^4)(e\hbar/2mc)\cos(2\pi E_0/\hbar\omega_0)\\ &\times\left\{-(\omega_0/\omega)^3\left(1-\cos\left[2\pi\frac{E_0}{\hbar\omega_0}\frac{\omega}{\omega_0}\right]\right)\right.\\ &\left.+\pi(E_0/\hbar\omega_0)(\omega_0/\omega)^2\sin\left(2\pi\frac{E_0}{\hbar\omega_0}\frac{\omega}{\omega_0}\right)\right\}. \end{aligned} \tag{31}$$

In Eq. (31), $E_0/\hbar\omega_0$ is an integer for a filled face [see Eq. (14), $T\to 0$], and an integer $+1/2$ for a half-filled face. Equation (31) is also plotted in Fig. 7(a).

Equation (31) is a better approximation for the moment for the filled face than for the half-filled face since the former has no discontinuity at $H=0$. For the filled face its chief deficiency is that it has twice too large a slope in the range $(E_0/\hbar\omega_0)(\omega/\omega_0)<1/2$, but otherwise it represents the amplitude and frequency quite satisfactorily. The one term ($j=1$) approximation for $N(E)$ which led to Eq. (31) is especially useful for evaluating the moment at higher temperatures and becomes there better and better since the terms with larger j are more heavily damped with temperature.

IV. THE MOMENT FOR FINITE TEMPERATURES

The case of a finite temperature can be handled in either of two ways. For $(\hbar\omega_0/kT)\gg 1$ one may include those exponential terms, previously dropped in Eq. (23), which correspond to lattice planes closest to the Fermi energy, just as in the case of the specific heat. For $(\hbar\omega_0/kT)\ll 1$ one may compute the moment from

$$M=(\partial/\partial H)\int_0^{\infty}N(E)f(E)dE, \tag{32}$$

and for $N(E)$ use the largest term ($j=1$) of Eq. (29), a procedure analogous to that which led to Eq. (31). These procedures give the following expressions for the

[8] See, for example, C. T. Whittaker and G. N. Watson, *A Course of Modern Analysis* (Cambridge University Press, London, 1935), pp. 267–269.

[9] Reference 8, p. 127.

moment per unit volume:

$$M(\zeta=\tfrac{1}{2})=(n_w/12)(E_0/\hbar\omega_0)^3(e\hbar/2mc)-(n_w/12)(E_0/\hbar\omega_0)^4(e\hbar/2mc)(\omega/\omega_0)$$
$$+n_w(E_0/\hbar\omega_0)^3(e\hbar/2mc)\left\{\frac{\exp[-(\hbar\omega_0/kT)]}{4}\left(\frac{E_0}{\hbar\omega_0}\frac{\omega}{\omega_0}\frac{\hbar\omega_0}{2kT}\right)^{-3}\left(1-\cosh\left[\frac{E_0}{\hbar\omega_0}\frac{\omega}{\omega_0}\frac{\hbar\omega_0}{kT}\right]\right)\right.$$
$$+\frac{\exp[-(\hbar\omega_0/kT)]}{4}\left(\frac{E_0}{\hbar\omega_0}\frac{\omega}{\omega_0}\frac{\hbar\omega_0}{2kT}\right)^{-2}\sinh\left(\frac{E_0}{\hbar\omega_0}\frac{\omega}{\omega_0}\frac{\hbar\omega_0}{kT}\right)$$
$$\left.-\frac{1}{8}\left(\frac{E_0}{\hbar\omega_0}\frac{\omega}{\omega_0}\frac{\hbar\omega_0}{2kT}\right)^{-2}\left(1+\exp\left[-\frac{E_0}{\hbar\omega_0}\frac{\omega}{\omega_0}\frac{\hbar\omega_0}{kT}\right]\right)+\frac{1}{8}\left(\frac{E_0}{\hbar\omega_0}\frac{\omega}{\omega_0}\frac{\hbar\omega_0}{2kT}\right)^{-3}\left(1-\exp\left[-\frac{E_0}{\hbar\omega_0}\frac{\omega}{\omega_0}\frac{\hbar\omega_0}{kT}\right]\right)\right\}, \quad (33)$$

valid if $(\hbar\omega_0/kT)\gg 1$ and $(E_0/\hbar\omega_0)(\omega/\omega_0)<1$,

$$M(\zeta=\tfrac{1}{2})\simeq[(6n_e)^{4/3}/24](n_w/kT)(e\hbar/2mc)^2H \quad (33a)$$

provided also $(E_0/\hbar\omega_0)(\omega/\omega_0)\ll 1$, and

$$M(\zeta=0)=-(n_w/12)(e\hbar/2mc)(\omega/\omega_0)(E_0/\hbar\omega_0)^4$$
$$+n_w(E_0/\hbar\omega_0)^3(e\hbar/2mc)\exp\left(-\frac{\hbar\omega_0}{2kT}\right)\left\{\sinh\left(\frac{E_0}{\hbar\omega_0}\frac{\omega}{\omega_0}\frac{\hbar\omega_0}{kT}\right)\Big/2\left(\frac{E_0}{\hbar\omega_0}\frac{\omega}{\omega_0}\frac{\hbar\omega_0}{2kT}\right)^2\right.$$
$$\left.-\sinh^2\left(\frac{E_0}{\hbar\omega_0}\frac{\omega}{\omega_0}\frac{\hbar\omega_0}{2kT}\right)\Big/\left(\frac{E_0}{\hbar\omega_0}\frac{\omega}{\omega_0}\frac{\hbar\omega_0}{2kT}\right)^3\right\}, \quad (34)$$

valid if $(\hbar\omega_0/kT)\gg 1$ and $(E_0/\hbar\omega_0)(\omega/\omega_0)<1/2$. If $(\hbar\omega_0/kT)\ll 1$, we have

$$M=\frac{4n_w}{(2\pi)^4}\left(\frac{e\hbar}{2mc}\right)\cos(2\pi E_0/\hbar\omega_0)\left[\frac{2\pi^2kT/\hbar\omega_0}{\sinh(2\pi^2kT/\hbar\omega_0)}\right]$$
$$\times\left\{-\left(\frac{\omega_0}{\omega}\right)^3\left(1-\cos\left[2\pi\frac{E_0}{\hbar\omega_0}\frac{\omega}{\omega_0}\right]\right)+\pi\left(\frac{E_0}{\hbar\omega_0}\right)\left(\frac{\omega_0}{\omega}\right)^2\sin\left(2\pi\frac{E_0}{\hbar\omega_0}\frac{\omega}{\omega_0}\right)\right\}. \quad (35)$$

In Eq. (35) $E_0/\hbar\omega_0$ is an integer for a filled face ($\zeta=0$) and an integer $+1/2$ for a half-filled face ($\zeta=1/2$).

Equations (33), (34), and (35) are plotted in Fig. 8, using interpolated values in the range of H and T where they begin to fail. Thus, Figs. 7 and 8 give a fair picture of the behavior of the moment for all values of temperature and field (providing still $\omega/\omega_0\ll 1$). In general we see that as the fields and temperatures get larger, one may safely use Eq. (35), which indicates that the moment is heavily damped with increasing temperature; the amplitude of oscillation drops off, initially at least, like $1/H^3$. It can be shown that as the field gets still larger ($\omega/\omega_0>1$), the oscillations in moment ultimately become periodic in $1/H$ [instead of periodic in H, as in Eq. (35)] while the amplitude increases as H^3. This behavior is suggestive only of the de Haas-van Alphen effect. These conclusions are most easily reached using the general expressions for $N(E)$, Eq. (3), and the eigenvalues obtained from Eq. (18), where $\omega/\omega_0\gg 1$. Since the eigenvalues are always linear in the quantum numbers, Fig. 1 is still qualitatively applicable, and no difficulty attaches to this procedure. The principle direction is now $(j, 0, 0)$ instead of $(2j, j, \pm j)$. One can also obtain the Landau diamagnetism throughout this development, but in the range of variables in which we are interested it is smaller than the moments we have derived by $O(\hbar\omega_0/E_0)$ so that it can be safely neglected.

V. DISCUSSION

The above derivations give a fairly complete picture of the magnetic and caloric properties of our model, consisting of n_w parabolic wells per unit volume, under the assumption that the Larmor frequency, ω, is somewhat less than the natural frequency, ω_0, of the well. Further, no great difficulty attaches to deriving the properties for $\omega>\omega_0$, mentioned above. Since all of our results have been presented in dimensionless form in the figures, they could be fitted approximately to real materials by adjusting the parameters m, n_w, n_e (or E_0), ω_0, about whose numerical values nothing has as yet been said. Evidently both diamagnetic and paramagnetic materials could be described, depending on whether the face closest to the Fermi surface is filled or not and also on whether we choose (perhaps somewhat unrealistically) to keep E_0 (as opposed to n_e) fixed for

weak fields. Our model is quite impartial in that it has no preference for either diamagnetic or paramagnetic behavior. For n_e fixed (Fig. 7(a)) the initial behavior with H is paramagnetic for all fillings of a face except the unique case of one exactly full, which is diamagnetic. For E_0 fixed(Fig. 7(b)) the initial behavior is in general diamagnetic, with the exception that for an exactly half-filled face it is initially paramagnetic. Thus for $\zeta=0$ and $\zeta=1/2$, E_0 fixed and n_e fixed agree, and for these cases only.

The model has considerably more versatility than one might expect would be provided by the addition of only one more parameter to the three initially needed for an Einstein lattice model. It should be noted that this versatility depends quite intrinsically on the discreteness and degeneracy of the levels, as well as on the numbers of particles used to fill them. All this is quite in keeping with our conclusions in previous studies[4] about the significance of discreteness in energy levels for magnetic properties. The versatility of this simple and computable model also may throw some light on the diverse results[10–12] of previous calculations on the cylindrical box, especially in weak fields, since evidently by changing the numbers of particles by a relatively small amount, fixing n_e, or E_0, we get totally different results for the problem at hand.

For the purpose of clarity we would like to give one more figure which will render the comparison with real materials more illuminating.

For the filled-face case we have plotted in Fig. 9 contours of constant μ (permeability) in a dimensionless H, T plane. This figure should be studied in conjunction with the filled-face specific-heat curves of Figs. 4 and 5. drawn to the same temperature scale. Since the magnetic induction $B=\mu H=H+4\pi M$, then $\mu=1+4\pi M/H$; and since we have M as a function of H and T [Eqs. (34) and (35), or Fig. 8], we may evaluate μ for a network of dimensionless H, T values and then by interpolation draw contours of constant μ. This is done in

TABLE I. Model parameters for superconductors.

Element	H_0 gauss	T_c °K	A cc	m/m_e (lower limit)	Number of particles per atom (lower limit)	$10^{-6}\times$number of particles per well (lower limit)
Cd	28	0.56	13.0	1.5	0.023	8.9
Zn	53	0.90	9.2	1.6	0.033	6.8
Tl	170	2.4	17.2	1.6	0.20	3.7
In	275	3.4	15.7	1.7	0.32	3.0
Sn	310	3.72	16.3	1.8	0.39	3.3
Hg	420	4.17	13.9	2.2	0.55	3.4
Pb	800	7.2	18.3	2.2	1.38	2.5
Ru	46	0.47	8.3	3.7	0.061	17.8
Os	65	0.71	8.4	3.1	0.073	12.6
Al	106	1.20	10.0	2.6	0.12	8.4
Ta	980	4.4	10.9	5.9	2.71	6.2
V	1200	5.13	8.4	6.1	2.64	5.9
Nb	2600	8.0	11.0	8.2	9.16	5.3

[10] M. F. M. Osborne and M. C. Steele, Phys. Rev. **86**, 247 (1952).
[11] R. B. Dingle, Proc. Roy. Soc. (London) **A216**, 118 (1953).
[12] W. Band, Phys. Rev. **91**, 249 (1953).

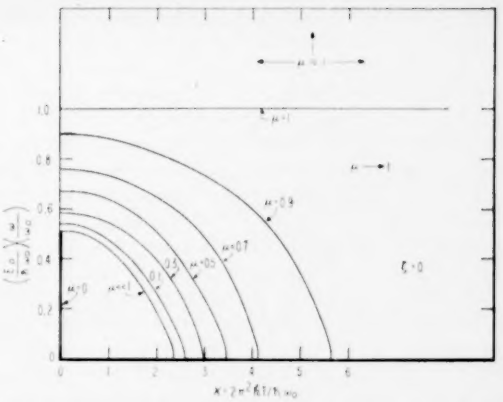

FIG. 9. Contours of constant permeability μ in a dimensionless H, T plane for the diamagnetic (filled-face) case. The parameters are adjusted so that when $x=0$, $\mu=0$ for the dimensionless field ranging from 0 to 1/2.

Fig. 9, where we have chosen $\mu=0$ as our origin at $T=0$. This corresponds to adjusting the slope OA of Fig. 7(a) [Eq. (24)] so that the material can just drive out the applied field at $T=0$. [Cf. Eq. (37).]

The similarity between the contours of constant μ and the critical field curves of superconductors is most striking. If we fit the H and T intercepts of the $\mu=1/2$ contour (inside this contour our model is strongly diamagnetic, outside essentially normal, $\mu\sim1$) to the parameters H_0 and T_c of a real superconductor, we can evaluate some of the parameters m, n_e, n_w, B of our model. Note also that this contour, $\mu\simeq1/2$, has a temperature intercept ($x=2\pi^2kT/\hbar\omega_0\sim3.5$) at approximately the same point where the corresponding specific-heat curve has an anomalous bump. If either the field or temperature is increased outside the $\mu=1/2$ contour, the diamagnetism disappears and the specific heat becomes linear, all quite in agreement with the behavior of a superconductor. If we fit the observed linear specific heat to that of our model, we obtain an additional condition on our parameters. This fitting process is carried out in the next section (Table I).

The comparison of our model to a real paramagnetic or ferromagnetic material is not so happy as is the case with superconductors. Indeed, this is not surprising, since we have nowhere introduced electron spin, conventionally regarded as essential to a description of such materials. (For superconductors on the other hand, the experiments of Kikoin and Goobar[13] on the gyromagnetic ratio of superconductors are indicative that the diamagnetism of superconductivity is not connected in any direct way with electron spin.) A description of ferro- or paramagnetic materials is nonetheless interesting, if we focus attention on certain gross properties and ignore others.

[13] I. K. Kikoin and S. V. Goobar, J. Phys. (U.S.S.R.) **3**, 333 (1940).

Let us first point out where the diamagnetic and paramagnetic contributions to our various expressions for the moment arise. Terms in ω^2 in the energy, Eq. (19) from *all* the states within the Fermi surface contribute to the diamagnetism. Paramagnetic terms arise from an unbalance in the *number* of states with negative as opposed to positive values of l [term in $lh\omega$ in Eq. (19) or (20)]. We have seen that for the filled face these balanced exactly so long as $(E_0/h\omega_0)(\omega/\omega_0)<1/2$, whereas for the half-filled face there was, for finite $H[(E_0/h\omega_0)(\omega/\omega_0)<1]$, an unbalance of one $(-l)$ face (DBC of Fig. 1), and as H increased [beyond $(E/h\omega_0)\times(\omega/\omega_0)=1$], the number of $-l$ states increased while the number of $+l$ states decreased. The net effect of the sum of pure para- and diamagnetic terms gives an oscillating moment arising from the inclusion and exclusion of states within the Fermi surface as it cuts an increasing number of lattice planes.

Now note that the paramagnetic contribution of any given state to the moment is independent of H [i.e., $(\partial/\partial H)lh\omega$] so that any *changes* in paramagnetic contribution must come from *changes* in the *occupancy* of states. Hence, in the *absence* of any small interaction (usually assumed present to permit an approach to thermodynamic equilibrium) which will allow particles to move from one state to another, the paramagnetic contribution to the moment will remain a constant.

This aspect of our model possibly gives a clue to the explanation of frozen-in moments in superconductors (for case $\zeta=0$) and to the existence of remanence on reduction of H after saturation for a paramagnetic salt which becomes ferromagnetic at $T=0$ (described on the basis of the $\zeta=1/2$ case). It can easily be seen that the unbalance of $+$ and $-l$ present in our model for large $H[(E/h\omega_0)(\omega/\omega_0)>1/2$ or 1 for $\zeta=0$ or $\zeta=1/2]$, if preserved at $H=0$ (not the state of thermodynamic equilibrium), will always give a residual moment in the absence of a field. This would correspond to moments paralleling the xxx curves of Fig. 7(a) as the field H is removed.

With this understanding of the effect of the absence of interactions which would allow states to change their occupancy, our model can have, at $H=0$, $T>0$, a remanent moment of either sign depending on the sign of the field "last seen." This is *not* a property of thermodynamic equilibrium.

We may also fit our model (with of course a different set of parameter values) at least roughly to the properties of a paramagnetic salt with zero Curie temperature. We observe that in the low temperature, low field regions of Fig. 8, or Eq. (33a), the moment for the case of a half-filled face is given by an expression of the form $M\sim CH/T$ and approaches a "saturation" value, whereas the specific heat (Fig. 5) has a thin spine which broadens with increasing field. At $T=0$ our model may develop a remanent moment, $\leq M_{\text{sat}}$ (Fig. 7). This is approximately the behavior of a paramagnetic salt with a zero Curie temperature. Thus, the parameters of our model can be evaluated by fitting the zero-point entropy, the saturation moment, and the Curie constant to a real material. Evidently the model will fail at sufficiently high fields and temperatures as the model then has a linear in T specific heat and a moment which vanishes for sufficiently large fields [Eq. (58)] in disagreement with available experiment.

Table II gives a set of values of parameters fitting this aspect of the model to a paramagnetic salt. In all of this fitting process the significant combination of parameters includes those which give the size of the well, the number of particles per well, and the numbers of particles per atom of material, rather than the parameters (B, m, n_w, n_e) with which the model was set up.

VI. EVALUATION OF THE PARAMETERS OF THE MODEL

Let us now consider the numerical problem of fitting the parameters of our model to real materials. Instead of the set B, m, n_e (or E_0), n_w we shall use equivalent sets which will perhaps provide slightly more physical insight. Superconductivity is believed to be an example of cooperative phenomena between many electrons (or atoms). Hence, the radius of the well, $R=(2E_0/B)^{\frac{1}{3}}$, or the distance from the center which corresponds to E_0, is a measure of the distance over which this cooperation is effective. The number of particles per atom, $n_e n_w A/N_{\text{Avogadro}}$, is in some sense a measure of the extent to which each atom contributes to the cooperation, whereas n_e is a measure of the effective number of cooperating particles. That elusive parameter, the ratio of the mass to the electronic mass m/m_e, is in some sense an indication of the extent to which the electrons are not free, and $\hbar\omega_0$ is a measure of the cooperative interaction energy. We shall, as far as we can, express the above in terms of observable quantities (H_0, T_c, γ_e the electronic specific heat, M_{sat}, Curie constant C, T_{Curie}, A, the atomic volume) and tabulate values for specific materials.

TABLE II. Model parameters for paramagnetic salts.

Salt	Curie constant C (molar)	M_{sat} (molar)	S_0 (molar) (ergs/mol deg)	$\frac{S_0 C}{M_s^2}$	n_w	n_e	Upper limit on λ well size (cm)	$H(M=0)$ Lower limit (gauss)
$KCr(SO_4)_2\cdot 12H_2O$ $A=273$ cc	1.86	$3N_A\beta$	1.1×10^8	0.75	2.1×10^{21}	6.7	5.0×10^{-8}	9.6×10^7
$Gd_2(SO_4)_3\cdot 8H_2O$ $A=248$ cc	7.83	$7N_A\beta$	1.7×10^8	0.89	0.90×10^{21}	38.9	6.4×10^{-8}	5.5×10^7

A. Superconductor

Consider first the case of a filled face, fitted to a superconductor. The condition for equality of the specific heats when linear is

$$\frac{\pi^2 k^2}{6}\frac{(E_0)^2}{(\hbar\omega_0)^3}n_w A=\gamma_e, \tag{36}$$

where $\gamma_e T$ is the linear term in the electron specific heat of one g atom in ergs/mol (°K). A second condition is that the permeability μ be 0 at $T=0$. From Eq. (24), setting $H+4\pi M=0$, we find

$$1=(\pi/12)(1/\omega_0)(he^2/m^2c^2)(E_0/\hbar\omega_0)^4 n_w. \tag{37}$$

Two more conditions are obtained by identifying the $\mu=1/2$ contour, Fig. 9, with the critical field curve and equating its intercepts at $H=0$ and $T=0$ to the experimental observed values for these parameters. This gives

$$(2\pi^2 kT_c/\hbar\omega_0)\simeq 3.5, \tag{38}$$

$$(E_0/\hbar\omega_0{}^2)(eH_0/2mc)\simeq 0.67. \tag{39}$$

Two additional conditions are given by the following considerations. We would like to identify the size of the well, $(2E_0/B)^{\frac{1}{2}}$ with the penetration depth, λ_0 at $T=0$. Evidently if we take a "physical sample" of our model so small that it cannot contain even one full-sized well, its diamagnetic properties will certainly be diminished if not entirely destroyed. This is also the case with a real superconductor. So we have, plausibly, at least,

$$\lambda_0=(2E_0/B)^{\frac{1}{2}}. \tag{40}$$

Finally, for the "physical consistency" of our model, since we have treated each well as not in interaction with any other well, we must have the condition that the volume occupied by each well is less than the space available $(1/n_w)$ to each well. This requires

$$(4/3)\pi(2E_0/B)^{\frac{1}{2}}<1/n_w. \tag{41}$$

The equalities (36)–(40) are *not* sufficient to determine all the parameters of our model but instead only three different combinations of them, ω_0, $n_w m^2$, and n_e/m^3. This situation is similar to that for the Einstein lattice model. Combined with the inequality Eq. (41), we can get separate inequalities on all of them. Elimination of all parameters between (36)–(40) will give conditions on the experimental observables *alone*, which are, pleasantly enough, in agreement with observation so that our model is a consistent one. ζ was a "bonus parameter" consequent to number theory since as n_e varies over a small range $(E_0/\hbar\omega_0$ from p to $p+1)$, ζ takes any value we please between 0 and 1.

Choosing as model parameters, $\omega_0=(B/m)^{\frac{1}{2}}$, $n_e=\frac{1}{6}(E_0/\hbar\omega_0)^3$, m, n_w, we can write Eqs. (36) to (41) as

$$\frac{\pi^2}{6}k^2\frac{(6n_e)^{\frac{1}{2}}}{(\hbar\omega_0)}n_w A=\gamma_e, \tag{42a}$$

$$1=(\pi/12)(\hbar/\omega_0)(e^2/m^2c^2)(6n_e)^{4/3}n_w, \tag{42b}$$

$$(2\pi^2)kT_c/\hbar\omega_0=3.5, \tag{42c}$$

$$\frac{(6n_e)^{\frac{1}{2}}}{\omega_0}(eH_0/2mc)=0.67, \tag{42d}$$

$$\lambda_0{}^2=\frac{2(6n_e)^{\frac{1}{2}}}{\omega_0 m}\hbar, \tag{42e}$$

$$(4\pi/3)(2\hbar/\omega_0 m)^{\frac{1}{2}}(6n_e)^{\frac{1}{2}}n_w<1. \tag{42f}$$

ω_0 is determined by Eq. (42c). Equations (42b, c, and d) give

$$n_w m^2=(12/\pi)(3.5\hbar/2\pi^2 kT_c)^3\frac{e^2H_0{}^4}{\hbar c^2 2^4(0.67)^4}; \tag{43}$$

(d) and (c) give

$$(n_e{}^{\frac{1}{2}}/m^2)=(0.67/6^{\frac{1}{2}})(c/eH_0)(4\pi^2 kT_c/h\,3.5)^2; \tag{44}$$

whereas (a) and (b) give

$$(n_e{}^{\frac{1}{2}}/m^2)=(2/6^{\frac{1}{2}})(c^2 A\pi k^2/\hbar^2 e^2\gamma_e). \tag{45}$$

This is as far as we can go without the use of Eq. (42f). [Equation (42e) is also a function of $n_e{}^{\frac{1}{2}}/m$.] However, equating the last two expressions [Eqs. (44) and (45)] for the combination $n_e{}^{\frac{1}{2}}/m^2$ gives

$$(T_c{}^2/H_0{}^2)(\gamma_e/A)=(3.5)^2/(0.67)^2 8\pi^3=1/9.1. \tag{46}$$

All other parameters and physical constants cancel. Equation (46) is simply the thermodynamic relation derived with the aid of the parabolic law, Rutger's equation, and the absence of a linear term in the superconducting specific heat.[14] Evidently the correct numerical coefficient 2π instead of 9.1 could be obtained by choosing a somewhat smaller permeability contour (say $\mu=0.3$) as representative of the critical field curve. Our model is evidently a consistent one thermodynamically.

A second relation in which the parameters of the model disappear can be obtained by eliminating $n_e{}^{\frac{1}{2}}/m$ between Eqs. (42d) and (e) [equivalent relations could be obtained by using Eq. (42e) with Eq. (44) or (45)]. This gives for the penetration depth

$$\lambda_0=(1.6)(\hbar c/eH_0)^{\frac{1}{2}}. \tag{47}$$

This relation is plotted in Fig. 10 as the solid curve with experimental points from the sources indicated. The trend with H_0, as well as the absolute values, is surprisingly well represented in consideration of the simplicity of the model. Evidently the theoretical coefficient in Eq. (47) is uncertain to at least a factor of 2. A relation equivalent to Eq. (47) can also be derived

[14] See, for example, D. Shoenberg, *Superconductivity* (Cambridge University Press, London, 1952), p. 64, for a derivation of the functional relation (to a numerical constant) given by Eq. (46) in the present paper.

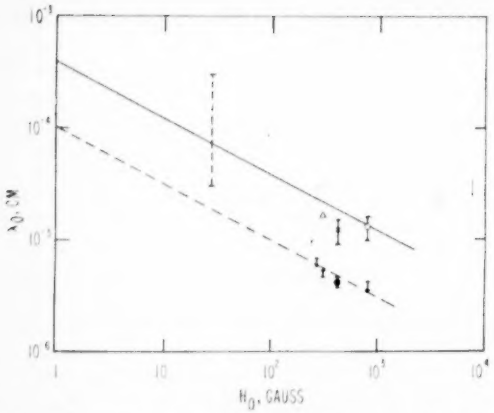

FIG. 10. Logλ_0 vs logH_0. The experimental points are taken from the following sources: I, (Pb, Sn, In) J. M. Lock, Proc. Roy. Soc. (London) **A208**, 391 (1951). ●, (Hg) E. Laurmann and D. Shoenberg, Proc. Roy. Soc. (London) **A198**, 560 (1949). ○, (Pb) M. C. Steele, Phys. Rev. **78**, 791 (1950). ×, (Hg) Appleyard, Bristow, London, and Misener, Proc. Roy. Soc. (London) **A172**, 540 (1939). △, (Sn) N. E. Alekseevsky, J. Phys. (U.S.S.R.) **4**, 401 (1941). ⁝, (Cd) M. C. Steele and R. A. Hein, Phys. Rev. **87**, 908 (1952). The dashed curve fitting the Cambridge data corresponds to a constant of 0.41 instead of 1.6 in Eq. (47).

from London's concept[15] of superficial currents whose elemental charges each carried an angular momentum of h.

An expression for the number of particles per atom $n_e n_w A/N_{\text{Avogadro}}$ can be obtained from Eqs. (43) and (44) or (45). This is

$$n_w n_e A/N_{\text{Av}} = (mA/N_{\text{Av}})(1/\pi\, 0.67)(cH_0/eh). \quad (48)$$

Finally Eq. (42f) with Eqs. (43) and either (44) or (45) can be used to obtain the following inequality on the mass,

$$m > \frac{(3.5)^{3/2}}{(0.67)^{5/4}\pi^3}\,\frac{\hbar^{7/4}e^{1/4}H_0^{5/4}}{(2)^{\frac{1}{2}}(kT_c)^{3/2}c^{1/4}}. \quad (49)$$

This in turn can be used to give lower limits on the number of electrons per atom [Eq. (48)] as well as a lower limit on n_s, and an upper limit on n_w.

Values for some typical superconductors are given in Table I.

In general it will be observed that the number of particles per atom ranges from 1/50 to 10, with masses slightly in excess of the electronic mass. Values of, or limits on, the other parameters ω_0, B, E_0, and n_w can easily be computed, but it did not seem worthwhile until their significance could be more clearly established. The three given in Table I, together with ω_0 (which is determined by T_c alone) are sufficient to determine the model completely.

[15] F. London, Revs. Modern Phys. **17**, 310 (1945); M. C. Steele and M. F. M. Osborne, Phys. Rev. **91**, 1281 (1953).

B. Paramagnetic Salt

In attempting to fit our model for $\zeta = 1/2$ to a paramagnetic salt, we observe that in the range of validity of Eq. (33a) [Fig. 8 for $(E_0/\hbar\omega_0)(\omega/\omega_0) \ll 1$], the susceptibility (per cc) is approximately

$$\chi = C/T = \eta n_w (n_e^{4/3}/k)(eh/2mc)^2/T, \quad (50)$$

where $\eta = 6^{4/3}/24$. This determines the Curie constant C. Equation (25) gives for $M_{s,0}$ the saturation moment per cc at $T=0$,

$$M_{s,0} = n_w n_e eh/4mc. \quad (51)$$

Finally, if we define an experimental quantity $S_0 = \int (Cv/T)dT$, the zero-point entropy per cc, in which the range of integration is over the experimental specific-heat peak of a paramagnetic salt, we have

$$S_0 \simeq k n_e^{\frac{1}{3}} n_w (\ln 2/2) 6^{\frac{1}{3}}. \quad (52)$$

This is obtained from[16] $S_0 = n_w k \ln G$, in which G is the number of ways a face may be half-filled according to Fermi statistics. From Eqs. (50), (51), and the inequality Eq. (41), we obtain the following expressions for our model parameters in terms of experimental quantities. $\beta = eh/2mc$ is the Bohr magneton if $m = m_e$.

$$n_w = (M_{s,0}^4 \beta^2/k^3 C^3) 2^4 \eta^3, \quad (53)$$

$$n_e = k^3 C^3/M_{s,0}^3 \beta^3 2^3 \eta^3, \quad (54)$$

$$\lambda < (3/4\pi)^{\frac{1}{2}}/n_w^{\frac{1}{2}} = (3/4\pi)^{\frac{1}{2}} kC/M_{s,0}^{4/3} \beta^{2/3} 2^{4/3} \eta. \quad (55)$$

C and $M_{s,0}$ are for 1 cc in these expressions. Moreover, we have a relation which the model requires between the observed quantities only, just as was the case for superconductors, Eq. (46). This is obtained from Eqs. (50), (51), and (52). If all experimental quantities are on a molar or cc basis, this gives

$$S_0 C/M_{s,0}^2 \simeq 2\eta 6^{\frac{1}{3}} \ln 2 = 2.1. \quad (56)$$

A free spin theory[17] of paramagnetism of N_{Av} particles of spin s, has for this numerical constant

$$S_0 C/M_{s,0}^2 = \tfrac{1}{3}[s(s+1)/s^2] \ln(2s+1). \quad (57)$$

This is a slowly varying function of s, which our crude theory has approximated by the too large constant 2.1. The disagreement is quite analogous to that found in Eq. (46) for superconductors.

There is a field $H(M=0)$ at which the moment vanishes for our paramagnetic model. We can determine a lower limit for this from the condition $(E_0/\hbar\omega_0^2) \times [eH(M=0)/2mc] = 1 = [(6n_e)^{\frac{1}{3}}/\omega_0][eH(M=0)/2mc]$, Eq. (55) and Eq. (42e) for λ^2,

$$H(M=0) > 16\eta^2 (8\pi/3)^{2/3} (ch/e)(M_{s,0})^{8/3} \beta^{4/3}/k^2 C^2. \quad (58)$$

Our model is good only at fields much less than this.

Evidently four independent parameter combinations

[16] R. C. Tolman, *Principles of Statistical Mechanics* (Clarendon Press, Oxford, 1938), p. 370.

[17] Reference 3, p. 581.

cannot be determined in this case either. A limit on the combination $\omega_0 m$ may be obtained from Eqs. (55), (54), and (42e). m is taken as the electronic mass for computing numerical values from Eqs. (52–58) in Table II, lacking other criteria to determine it. These results are tabulated below for two typical paramagnetic salts.

VII. CONCLUSION

It may appear as rather surprising that so simple a model of spinless electrons in a solid can be made to develop so great a variety of properties as those manifested by superconductors and paramagnetic salts. We should like to comment on the physical reasons underlying this versatility of the model since these comments may be suggestive of where to look for the explanation, especially of superconduction, from a more fundamental standpoint. We would first like to point out that if a system is obeying Fermi statistics and kT is greater than the spacing of electron levels, then the thermodynamic properties are essentially determined by the average density of levels in the neighborhood of the Fermi energy and are quite insensitive to the properties of the levels for larger or smaller energies. If, on the other hand, kT is less than the spacing, then the thermodynamic properties are determined by the density and degree of degeneracy of levels closest to the Fermi energy even though those levels may be more remote in energy than kT. In summary, for Fermi statistics, thermodynamic properties are determined by those levels closest to the Fermi energy; if there are levels closer than kT, specifying the properties of the levels in a range of order kT is sufficient to determine the thermodynamic properties.

Now our model has just the property that by adjusting its parameters one can vary the *average* density of levels, their degeneracy, and their spacing in an almost arbitrary manner. To show this we have plotted schematically in Fig. 11 the density of levels per cc $=n_w g(E)$ as a function of energy E and for different values of the magnetic field. Any dimension in abscissa of this figure can be made large or small compared to kT by adjusting the parameters of the model ω_0, m (or their equivalent). The ordinate can be adjusted to any size by varying, among other parameters, n_w and n_e. The area of each triangle is n_w times the number of points in the faces of Fig. 1. Their bases are in length proportional to H. The triangles begin to overlap at $(E/\hbar\omega_0)(\omega/\omega_0)=1/2$. We have seen that by half-filling a face we place the Fermi energy at the vertex of a triangle. When the face is filled, the Fermi energy falls halfway between triangles, i.e., in a region of no-energy levels if the field is weak. Hence, by adjusting the parameters of the model, we may produce any effective density, spacing, and degeneracy we please in the neighborhood of the Fermi energy and then compute unambiguously the effect of a magnetic field since the energy levels are always linear in the quantum numbers. The triangles themselves are actually composed of δ functions, spaced $\hbar\omega$ apart. This property of the model gives a flexibility we have not utilized since it becomes significant only when $kT<\hbar\omega$. We have called this condition (Sec. III) effectively $T=0$.

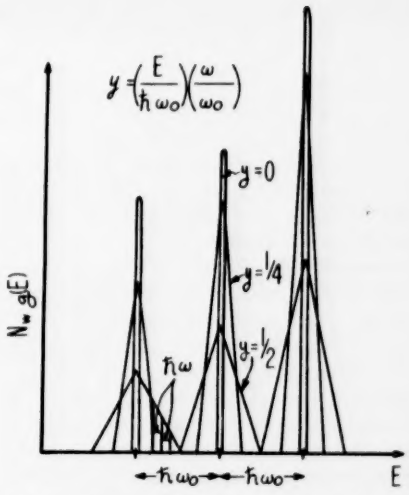

FIG. 11. Schematic density of levels per cm³ as a function of energy, for different fields.

For some of the cases we considered, not all of the dimensions of Fig. 11 are significant. This corresponds either to the fact that we could not compute all our parameters unambiguously or to the fact that our model failed when H or T exceeded certain values.

We should now like to discuss just how sensitive to imperfection are the properties of our model, especially when considered as a superconductor. We have assumed n_w isotropic wells per unit volume, each containing just the proper number of particles to fill completely the "faces" of its energy surface in quantum-number space. We have already seen that a shift from filled to half-filled face or a variation of the number of particles by 1 part in $n_e^{\frac{1}{3}}$ is sufficient to shift the properties from an intense diamagnetism to an equally intense paramagnetism. In other words, the number of particles in each well has to be fixed to better than 1 part in 10^3, judging by the figures in Table I.

Secondly, we observed that if the wells are slightly anisotropic, this condition has the effect of tilting the energy surfaces of Fig. 1 (for no field) out of parallelism with the 2, 1, 1 and 2, 1, -1 planes. If sufficient to tilt the Fermi surface enough to cut a lattice plane, it will destroy the degeneracy and spacing properties which provided the diamagnetism, or paramagnetism, and specific heat anomalies. An anisotropy (say in ω_0) as small as one part in $n_e^{\frac{1}{3}}$, ($\sim$0.1 percent by Table I) is sufficient to destroy these properties. Such an anisotropy would be equivalent to having triangles instead of δ functions, for $y=0$ in Fig. 11.

Another condition to which our model is sensitive is the degree of overlap of wave functions in one well with

neighboring wells or the extent to which the inequality (41) is obeyed. The effect of nearest neighbor interactions will be to broaden the degenerate levels in a given face into bands. If these bands overlap (broadening $>\hbar\omega_0$), the degeneracy essential to our magnetic and specific heat behavior will be destroyed.

Evidently our model is rather sensitive to physical imperfections; or, to express the idea in another way, the model must be "well ordered" to the above degree throughout the specimen.

One consequence of the above close specifications of the parabolic well model is that the moment oscillates with H and with decreasing amplitude ($\sim 1/H^3$) for fields greater than the critical field [$(E_0/\hbar\omega_0)(\omega/\omega_0)>1$, Sec. III]. The specific heat anomaly and the perfect diamagnetism were consequences of only the two degenerate faces closest to the Fermi energy, whereas the above oscillations require this high degeneracy for additional inner and outer faces.

Berlincourt and Steele[18] have performed experiments with tin to test the prediction of additional oscillations in the magnetic moment of a superconductor at fields above the critical field. Their results showed that at fields above H_0 (the critical field) the moment of tin was less than 10^{-3} times the maximum superconducting moment, whereas the above theory indicates the possibility of a paramagnetic moment 10^{-1} times the maximum superconducting moment.

The negative experimental results require the additional postulate that our wells, or their filling, are rendered imperfect by at least the small amounts specified above for fields appreciably greater than the critical field. This small modification of the well structure is quite analogous, but on a much less drastic scale, to the modification by melting of an Einstein model for a solid to a liquid.

The problem of the conductivity of our model is one which remains to be investigated. However, a few qualitative remarks as to what one should and should not ask of the model are perhaps not out of place. One could certainly compute a zone structure for n_w wells distributed in a "superlattice" by Heitler-London methods, construct progressive wave solutions from the well-type wave functions and calculate the resistance from a postulated interaction with the lattice, all along conventional lines. The problem would not be to show that the resistance $\rightarrow 0$ as $T\rightarrow 0$, since this would follow for any perfectly periodic structure. Rather one should show that in the absence of a magnetic field the resistance for the filled-face case approached zero much faster than that for the half-filled face and that both became "normal" when H and T exceeded certain values.

The behavior of the density of levels for one well and the specific heat indicate that this latter property should not be overly difficult to realize. To obtain the former would require a knowledge of the scattering between a large number of (number of points in a face of Fig. 1) overlapping zones about which we would not care to hazard a guess without further calculation.

Closely connected with the problem of resistance is that of the conservation of flux of a multiply connected superconducting body. Since this conservation of flux is also not a thermodynamic property (i.e., depends on path in H, T plane), we have not attempted to explain it in this paper.

We can also emphasize certain characteristic features which it has that should be sought from a more fundamental basis. This is its outstanding property, that the degeneracy and filling of the wells is such that no shift in population or distribution of the particles can occur until the field reaches a critical value. The merit of the model is that this field can be computed without perturbation theory. The actual size of the well is physically unimportant except in so far as it can be identified with the penetration depth. Hence, our model tells us that we must find a computable situation where the actual wave functions spread over many atoms and the energy levels are sufficiently degenerate so that the spacing between different degenerate levels is $\sim(2\pi^2 kT_c/3.5)$. As we saw from Fig. 3, boxes of the proper size[19] alone are not sufficient; the degeneracy and filling must also be taken into account. From the recent work of Slater[20] we know that certain types of exact wave functions do indeed extend over many atoms just in the range of energy of the conduction bands. Hence, the problem resolves itself if it can be shown that one can realize sufficiently extended wave functions, and at the same time with a sufficient degree of degeneracy and spacing to provide a situation equivalent to that provided by the n_w parabolic wells. When and if this is done (and in the presence of a magnetic field), one will have a theory of the superconducting state. One will *not* have a theory of the superconducting transition. The model can only tell when it (like Einstein's lattice with large oscillations) will fail and presumably be normal. Indeed the success of our model suggests that one might use as starting wave functions the wave functions of our n_w parabolic wells (certainly as complete a set as any other) and endeavor to show that these can be used with perturbation theory to represent the electronic wave functions in a lattice of atomic periodicity. Whether it can be shown that the perturbation of the electrons by the lattice, weakening with diminishing temperature, is sufficient to permit such a clumping of the electrons as our n_w wells require and Slater's exact calculations show can happen ideally, remains to be determined.

Finally, we should like to give a justification or at

[18] T. G. Berlincourt and M. C. Steele, Phys. Rev. **91**, 215 (1953).

[19] Small boxes to provide a model for a superconductor have been considered also by J. C. Slater, Phys. Rev. **52**, 214 (1937) and F. Hund, Ann. Physik **32**, 102 (1938).

[20] J. C. Slater, Phys. Rev. **87**, 807 (1952).

least a precedent for our model, not only as a superconductor but as an admittedly crude representation of magnetic solids. We have replaced the multitudinous interactions of the electrons both with each other and the lattice, including spin, by an equivalent effective potential. It is rather pleasant and encouraging that just one model is sufficient to describe approximately a rather wide variety of properties. The parabolic potential is admirably suited to the purpose although at least one other, the Coulomb well, might serve as well.

Now this assumption of an equivalent potential to replace a complex interaction has had ample precedent in the past although the path to justification is often tortuous and long delayed. The Einstein lattice model is the one we have followed. As other examples we may cite the Lennard-Jones potential for gas molecules and Hooke (and other) forces between atoms in a solid, both of which were proposed long before there was any quantum mechanical theory of their origin. Similar examples of more recent date are the Weiss internal field and theories of the heavier nuclei, justification for which is not yet complete. These examples, we hope, give some precedent for our otherwise arbitrary assumption of parabolic wells.

PHYSICAL REVIEW VOLUME 92, NUMBER 6 DECEMBER 15, 1953

Anelasticity of Quartz

RICHARD K. COOK AND ROBERT G. BRECKENRIDGE
National Bureau of Standards, Washington, D. C.
(Received March 20, 1953)

By means of the piezoelectric effect, measurements have been made of the variation with temperature of (1) the Q of quartz bars executing free acoustical oscillations in torsion, and (2) the equivalent series electrical resistance of bars driven at their natural frequencies of longitudinal acoustical oscillations. For each of the bars studied, it was found that the internal dissipation had a maximum value at a temperature between room temperature and the quartz inversion temperature of 573°C. Measurements of resistance were made on one bar at several different frequencies. These data showed that part of the dissipation was due to a relaxation effect, whose decay time varied with temperature according to an Arrhenius equation. An activation energy of 22 kcal/mole and a relaxation-time constant of 2×10^{-14} sec were deduced from the data, which showed also that the fraction of energy lost during each sinusoidal cycle of strain was independent of the frequency of vibration. Estimates of the activation energies and relaxation-time constants were deduced for the other bars measured. In one case, the dissipation was due to the migration of gold atoms from the electrodes into the quartz lattice.

I. INTRODUCTION

WHEN a solid material is set into free vibration in one of its normal modes, the amplitude of the vibration decays exponentially with time. This happens even in the absence of external losses through either acoustic radiation into the air or other medium in which the solid is immersed, or through transmission of vibrational energy through the supports of the solid. The conversion of the ordered vibrational motion into disordered thermal motions of the molecules has been called "internal friction" or "internal dissipation", and more recently has been named "anelasticity". A summary of measurements on anelastic effects in metals, and a discussion of the mechanisms which give rise to anelasticity, are given in Zener's book,[1] where many of the formal analogies to dielectric theory are pointed out.

To the best of our knowledge, there have been no previous reports on researches into anelastic effects in quartz or other piezoelectric materials. Such effects in quartz are technologically important wherever quartz crystals are used either for frequency control of oscillators, or for electric-circuit filters. Measurements of anelastic effects in quartz, and in other piezoelectric materials, are readily made with electrical techniques. This is because the mechanical motions of a piezoelectric material cause electrical effects through the electromechanical coupling in the material. The most important information concerning the mechanism in any particular piece of material can be obtained from a study of the variation of anelastic effects with temperature and frequency.

A convenient measure of the internal friction is the Q of a freely vibrating system. Suppose the vibration as a function of time t is representable by $\exp(-\alpha t)\sin(2\pi ft)$, where α=damping coefficient of the damped vibration and f=frequency. The Q is then given by $Q=\pi f/\alpha$.

Another convenient measure of the internal mechanical friction for a piezoelectric material, such as quartz, is the electrical resistance R_1 which appears in the equivalent circuit of the crystal (see Fig. 1) when it is driven electrically at frequencies near a mechanical resonance frequency. It can be readily seen from Fig. 1

[1] C. Zener, *Elasticity and Anelasticity of Metals* (University of Chicago Press, Chicago, 1948).

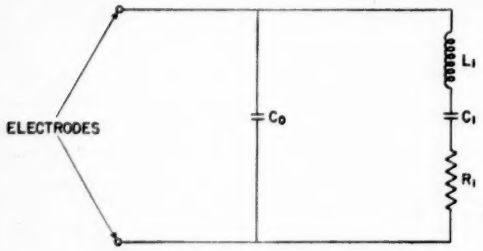

FIG. 1. Equivalent circuit of a quartz crystal bar near a natural frequency.

that the Q of a bar of quartz when it is vibrating freely with its electrodes shorted is given by $Q=2\pi fL_1/R_1$. It should be emphasized that although the quantity directly measured is an electrical resistance, R_1, the dissipation which it represents has a mechanical origin.

Measured Q's of more than 500 000 are frequently obtained for quartz bars polished and etched and vibrating in a vacuum at room temperatures. No measurements of Q, or R_1, for wide temperature ranges have been found in the literature, although Bosshard and Busch[2] found that R_1 increased linearly with temperature over a 50°C range of temperatures centered near room temperature.

II. TECHNIQUES OF MEASUREMENT AND EXPERIMENTAL RESULTS

A. Forced Vibrations of Longitudinal Bars

Measurements of the resistance R_1 were made on two quartz bars C and E described in an earlier paper,[3] which describes also the Q-meter apparatus which was used for making the measurements reported here. Briefly put, the resonant frequency of a bar was first located by the successive approximations technique, and the Q-meter was then operated at that frequency. R_1 (the series chain resistance) was deduced from the open-circuit voltage of the Q-meter, the voltage across the crystal bar when connected to the Q-meter, and the purely resistive internal impedance of the source (i.e., the Q-meter). This internal impedance, R, was adjusted both to large values, $R\gg R_1$, and to small values, $R\approx R_1$, so as to obtain checks on the measurement of R_1.

The quartz bars were placed in the holder and heated in the furnace described earlier.[3] The screening system for the crystal holder, which was devised to reduce the effects of the holder's dielectric losses on equivalent-circuit determinations at high temperatures, proved to be unnecessary when R_1 only was being determined, and was not consistently used.

The results of measurements of R_1 for bar C are plotted in Fig. 2. This bar was never heated above 555°C, and the variation of R_1 with temperature, found at the fundamental frequency of the bar, seemed to be independent of the number of heatings. R_1 was measured also at the third and fifth overtones, whose frequencies were, respectively, very near to the third and fifth harmonics of the fundamental. These results are all plotted in Fig. 2. At the fundamental frequency, the resistance R_1 had a maximum at 305°C.

The variation of the fundamental frequency with temperature is shown in Fig. 3. This latter graph shows that near the temperature (305°C) at which the dissipation is a maximum, there is no detectable anomaly in the frequency of the fundamental mode.

Figure 2 shows that the temperatures of maximum R_1 increase for the third and fifth overtones. As will be shown, these effects can be explained by a mechanical relaxation phenomenon, whose decay time is an Arrhenius function of temperature.

The assumption that a relaxation mechanism is present implies that the part of the total resistance R_1

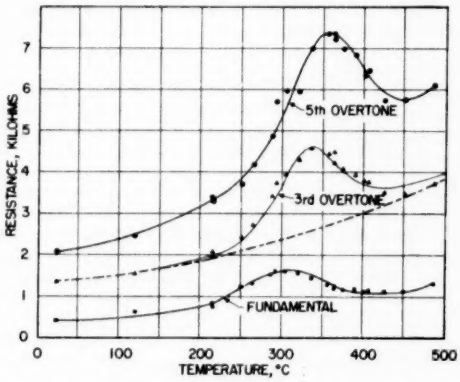

FIG. 2. R_1 *vs* temperature for bar C. For the third overtone, the solid line is computed from Eq. (1), and the open triangles are measured values.

caused by it should have its temperature variation given by

$$R_r=2R_m/(\omega\tau+1/\omega\tau)$$
$$=R_m/\cosh(\log\omega\tau_0+U/NkT), \quad (1)$$

where R_r (maximum) $=R_m$, τ is the decay time of the mechanical relaxation associated with the observed anelastic effect, and U is its activation energy.

At temperature T,

$$\tau=\tau_0e^{U/NkT}, \quad (2)$$

where Nk is the gas constant, and τ_0 is a relaxation time constant, characteristic perhaps of a defect in the quartz lattice. The location of a temperature maximum of R_r is given by

$$2\pi f\tau=\omega\tau=1, \quad (3)$$

where f is the frequency at which R_r is measured, and the corresponding pulsatance is $\omega=2\pi f$. Let $T_m=$ tem-

[2] W. Bosshard and G. Busch, Z. Physik **108**, 195 (1938).
[3] R. K. Cook and P. G. Weissler, Phys. Rev. **80**, 712 (1950).

perature of maximum R_r. Then

$$\log f = -(U/NkT_m) + \text{a constant}. \quad (4)$$

A plot of the observed $\log f$ *versus* $1/T_m$ values is shown by the open circles in Fig. 4. The circles should lie on a straight line if Eq. (4) is valid. The solid line was drawn so as to be a best fit for the open circles. From it we find $U = 22\times10^3$ cal/mole, and $\tau_0 \approx 2\times10^{-14}$ sec. This value of τ_0 is to be compared with the shortest period, τ_m, of the lattice vibrations which contribute to the specific heat. From data in the literature on quartz, cristobalite, and vitreous silica, we estimate $\tau_m \approx 5\times10^{-14}$ sec. Raman spectra and experiments with reststrahlen yield fundamental lattice periods of the same order of magnitude.

Equation (1), after addition of the "background" dissipation resistance (estimated to rise exponentially with increasing temperature, for which, however, there is no theoretical basis), is to be compared with the experi-

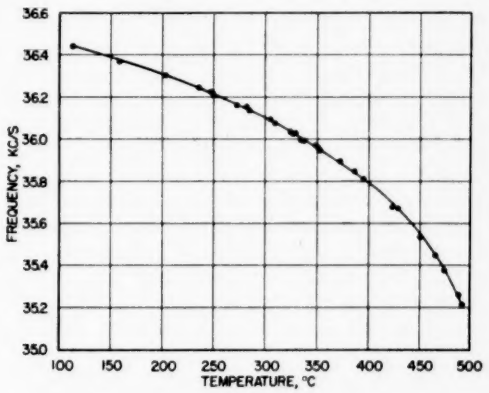

FIG. 3. Frequency *vs* temperature for the fundamental mode of bar *C*.

mentally measured values of R_1. The agreement is exemplified by the solid curve (theoretical) for the third overtone in Fig. 2. The values of U and τ_0 given above were used, and the frequency f was that of the third harmonic. The value of R_m was adjusted so that the computed curve would fit the maximum value of R_1 found experimentally. The agreement of the computed curve with the measured resistance for the third overtone (shown by the open triangles) confirms the values of U and τ_0 found from Fig. 4. Similar agreement of the computed with the measured resistance holds for the fundamental and fifth harmonics as well.

Figure 2 shows also that both R_1 at room temperature, and the maximum value of R_1 as a function of temperature, are directly proportional to the frequency. Since the inductance L_1 of a bar vibrating at a harmonic frequency is the same as the inductance at its fundamental frequency, it follows that the Q of bar C is independent of frequency. This is consistent with Mason

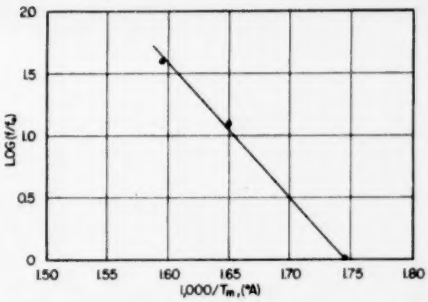

FIG. 4. $\text{Log}(f/f_0)$ *versus* $1000/T_m$ for bar *C*. Open circles are observed values derived from Fig. 2 for the fundamental, third overtone and fifth overtone. f_0 = fundamental frequency of bar.

and Fair's[4] observation that the Q (caused by internal dissipation) of a plate vibrating in thickness shear is independent of frequency.

The fractional vibrational energy lost during each cycle is $2\pi/Q$ (if $Q \gg 2\pi$). Since all measurements on bar *C* were made in air, a part of the loss must be charged to sound radiation by the vibrating bar. It is difficult to make a quantitative estimate of this loss. However, at the temperatures where R_1 is a maximum, the relaxation effect is greatest, and sound radiation is then a negligible part of the total energy loss per cycle. From the data in Fig. 2 combined with the reactance measurements reported earlier,[3] we conclude that at room temperatures the fractional energy loss of bar *C* is 0.9×10^{-4} per cycle. At the temperatures where the dissipation due to the relaxation effect is greatest (Q a minimum, maximum of $R_1 = R_m$), the fractional energy loss per cycle is 2.8×10^{-4}. This is less than one-tenth of the maximum loss found for the torsional bars *G* and *H* (see part *B* of this section and Table I).

The results of measurements of R_1 for bar *E* are plotted in Fig. 5. It is evident that after repeated heatings to about 560°C, and in one case to 571.5°C, the resistance R_1 developed a maximum value at about 380°C. Furthermore, the maximum value of R_1 increased after each heating. This remarkable behavior suggested that some change was taking place in the quartz structure. The first suggestion was that electrical (Dauphiné) twinning was setting in. Bar *E* had been originally cut from oscillator-grade quartz, free of both optical and electrical twinning. In order to determine whether or not the heating caused electrical twinning, the gold electrodes were first dissolved (after the fourth heating and cooling) by boiling in aqua regia for ten minutes. This was sufficient to remove all gold on the surface, but the bar had a reddish-purple cast which was visible only by reflected light (the bar resting on a sheet of white paper). Most remarkable was the color distribution. It appeared to be roughly "sinusoidal," that is, there was a broad flat maximum

[4] W. P. Mason and I. E. Fair, Proc. Inst. Radio Engrs. **30**, 464 (1942).

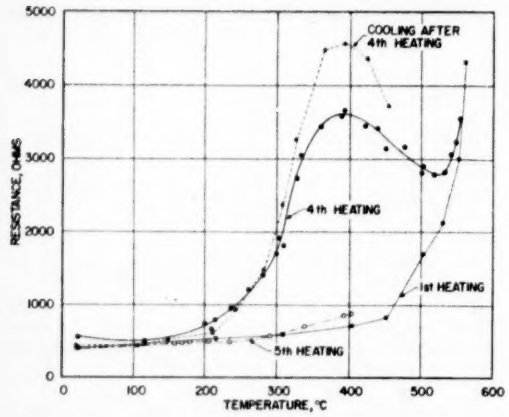

FIG. 5. R_1 *vs* temperature for bar *E*. Increase in R_1 between 1st and 4th heating is due to the migration into quartz lattice of gold atoms, which were removed by etching prior to the 5th heating (open circles).

at the middle of the bar, which shaded off to no color at the ends. We believe the coloration is due to colloidal gold, or gold atoms, which moved into the quartz lattice in the regions of greatest stress which were present during vibration of the bar at high temperatures (above 560°C). The bar was etched in order to determine whether or not twinning had occurred. Etching removed the coloration, and showed no evidence of twinning. Gold electrodes were re-applied by an evaporation technique to the bar, so as to avoid heating it. R_1 was then re-determined for the bar, and the results up to 400°C, the highest temperature used during the fifth heating, were found to be substantially the same as those shown for the first heating (see Fig. 5). The explanation of the increasing resistance R_1, therefore, is the migration of gold atoms into the quartz lattice.

Equation (1) was successful in explaining the variation of R_1 with temperature for bar *C*. This suggests that the equation can be applied to the data given for bar *E* in Fig. 5, so as to obtain estimates of U and τ_0. This was done by first subtracting the resistance R_1 during the first heating from the values for the fourth heating so as to yield the resistance R_g due to the gold atoms in the quartz. Next U and R_m in Eq. (1) were adjusted so as to yield a curve having a good fit to the measured values of R_g. Values of $U=13$ kcal/mole and $R_m=2900$ ohms were sufficient to do this. τ_0 was then computed from

$$\log 2\pi f\tau_0+U/NkT_m=0, \qquad (5)$$

where T_m = temperature of maximum R_g. We find $\tau_0\approx 10^{-10}$ sec. This is to be contrasted with the value of 10^{-14} sec found for bar *C*.

The coloration phenomena were investigated further by means of bar *F*, which had been heated to temperatures above 600°C in the earlier experiments.[3] However, no systematic measurements of its R_1 had been made. The gold electrodes were removed with aqua regia. The bar had an even more pronounced reddish-purple coloration than did bar *E*. Even more remarkable, the distribution of the color was "complementary" to that for bar *E*. That is to say, the coloration was maximum at the ends and least in the middle of the bar. No explanation can as yet be offered for these curious phenomena. Since bar *F* had been heated above 573°C (the inversion temperature of quartz), it would undoubtedly be electrically twinned on cooling down to room temperature. Etching removed the coloration, and showed that the bar was indeed twinned. It had originally been cut from quartz free of both electrical and optical twinning.

B. Free Vibrations of Torsional Bars

The decay of free vibrations of two torsional bars, *G* and *H*, has also been investigated. These bars were of identical dimensions, $5.00\times0.500\times0.500$ cm, cut with their length in the *Y* direction from untwinned quartz. Fired-on silver electrodes were applied to the bars in a configuration suitable for the excitation of torsional oscillations. The natural frequency of the bars was found to be 36.0 kc/sec at room temperature. For the measurement of the decay of free vibrations as a function of temperature, the bars were mounted on knife-edge supports in a vacuum chamber which was enclosed in a small oven. The temperatures were measured by means of a thermocouple in close proximity to the crystal. To measure the damping, the bar was forced into oscillation by an external generator and, when vibrating, was then cut off from the generator and the output of the freely oscillating crystal observed as a function of time. Since the output voltage decays exponentially, a measurement of the damping coefficient α requires a measurement of the output voltage at two

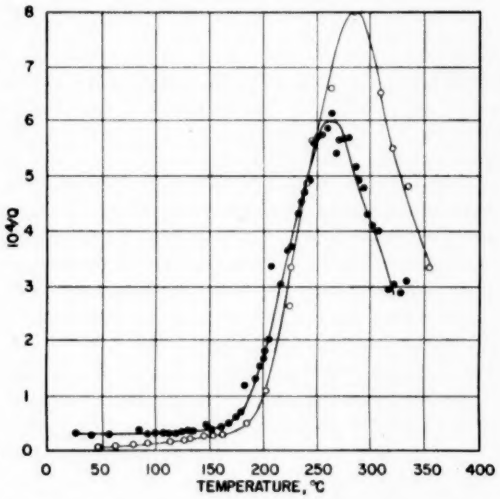

FIG. 6. $10^4/Q$ *vs* temperature for bars *G* and *H*. ● = bar *G*, ○ = bar *H*. The smooth curves are drawn through the experimental points.

times as indicated by the equation:

$$V_2/V_1=e^{\alpha(t_1-t_2)}=e^{\alpha\Delta t}. \quad (6)$$

The Q of the system is then given as

$$Q=\pi f/\alpha. \quad (7)$$

The α measured directly in this fashion depends on the circuit into which the crystal discharges and must be corrected for these effects to obtain the true crystal Q.

Two methods of measuring α have been used. In the earlier work the decaying voltage was displayed on an oscilloscope with a superposed timing signal. The trace was photographed and measured using a microscope with a vernier eyepiece. This method was used to investigate the Q of bar G. In more recent studies (bar H), an electronic instrument which allows a direct measurement of Q with improved accuracy (error $\leqq 3$ percent) was employed. This device will be described in detail elsewhere:[5] The results of these measurements are given in Fig. 6 where the Q's obtained from α's corrected for the external circuit effects are presented. In both cases a pronounced relaxation loss is observed centering at 270°C. No changes in the value of the maximum loss were noted for either bar for several temperature cycles, the highest temperature reached being about 360°C.

The data on these two bars could also be described by a relaxation expression. The values of τ_0 and U chosen to give the best agreement with experiment are given in Table I in the next section.

III. SUMMARY AND CONCLUSIONS

Measurements have been made of the Q of various quartz bars, vibrating in their fundamental acoustical modes, as a function of temperature. For bars G and H, which vibrated torsionally, and for bar E, which vibrated longitudinally, the fractional energy loss per cycle (which is approximately $2\pi/Q$) has maximum values at temperatures near 300°C. For the longitudinal bar E, the maximum loss increased with repeated heatings of the bar to temperatures near 550°C. Gold atoms from the electrodes had apparently worked into the quartz lattice, and it appears that the increased dissipation is accounted for by this lattice defect.

[5] R. D. Laughlin, J. Research Natl. Bur. Standards (to be published).

TABLE I. Activation energies and relaxation time constants for anelastic effects in quartz.

Bar	Vibration modes	Fundamental frequency (at room temp.) kc/sec	U kcal/mole	τ_0 sec	Minimum Q
C	Longitudinal	36.5	22	2×10^{-14}	22 000
E	Longitudinal	54.3	13	10^{-10}	...
G	Torsional	36.0	16	10^{-12}	1700
H	Torsional	36.0	17	10^{-13}	1200

For bar C, measurements of acoustical dissipation were made at the third and fifth overtones of the bar, as well as at its fundamental frequency. This allowed fairly accurate determinations of an activation energy and a relaxation time constant for the observed dissipation.

Table I summarizes the activation energies U and relaxation time constants τ_0 deduced from the anelastic measurements on the various bars. The values of U and τ_0 are more accurate for bar C than for bars E, G, and H.

For bar C, we suggest that the relaxation effect is due to twinning and detwinning in the quartz lattice, over a range not much greater than the size of the unit cell in quartz. For bar E, it was established that gold atoms caused the dissipation. The relaxation time constants for bars G and H are too great to be explained by the twinning-detwinning hypothesis, hence it seems likely that the losses arise from the introduction of silver atoms or ions during the firing-on of the silver electrodes. It should be noted also that if the mechanism assigned to bar C is contributing a similar amount to the losses in bars G and H, the effect would be masked by the large losses presumably due to the presence of foreign atoms or ions. Similar large dissipation effects observed in the alkali halides have been attributed to the presence of lattice imperfection.[6] Further investigations of these anomalous effects in quartz are in progress.

We are indebted to Mr. J. Upham, Mr. J. H. Wasilik, and Mr. R. D. Laughlin for assistance in the collection and reduction of data.

[6] R. G. Breckenridge, *Imperfections in Nearly Perfect Crystals*, edited by W. Shockley (John Wiley & Sons, Inc., New York, 1952), Chap. 8.

Effect of Traps on Carrier Injection in Semiconductors*

H. Y. Fan
Purdue University, Lafayette, Indiana
(Received September 9, 1953)

The effect of carrier traps on the behavior of a semiconductor with respect to injected carriers is analyzed. Two problems are considered: photoconductivity, and spread of excess carrier concentration under applied field. It is shown that trapped minority carriers, by causing an increase in majority carrier concentration, give rise to increased photoconductivity which may be nonlinear with light intensity and have a very long time constant. These conclusions are in agreement with recent experimental results. The drift of excess carriers is treated, neglecting diffusion. Expression is obtained for the time and space distribution of excess minority carriers, and the effect of traps on the apparent drift mobility is discussed.

IN a semiconductor, imperfections of the crystal may introduce in the forbidden energy gap discrete energy levels with localized wave functions. We may speak of these localized states as carrier traps. An increase in the number of electrons in these states gives trapped electrons whereas a decrease corresponds to trapped holes. Shockley and Read[1] have analyzed the hole-electron recombination rate resulting from the presence of such traps under constant perturbed electron distribution. The effect of the traps considered was that of an intermediate step for the transition of an electron from the conduction to the valence band. Recent investigations on photoconductivity[2,3] and decay of injected carriers[4] as well as experiments on drift mobility[5] indicated the necessity of considering the effect of traps in these problems where the accumulation or depletion of trapped electrons or holes has to be considered. In general there may be several different types of imperfections, and an imperfection of each kind may give several discrete levels. However, under a given condition it may be that only one set of traps is effective. In the following we shall give an analysis of this simple case. The problem of photoconductivity will be considered first, where a uniformly irradiated region of the sample is sufficiently wide and the applied field is sufficiently low that we do not have to deal with spatial variations. Then the problem of injected carriers drifting under an applied field will be discussed.

PHOTOCONDUCTIVITY

Consider a semiconductor in which the radiation of a suitable wavelength excites electrons across the energy gap, producing hole-electron pairs. The resulting photoconductivity measured by the increase of conductivity is given by

$$\Delta\sigma = e(\mu_e \Delta n + \mu_h \Delta p), \tag{1}$$

where μ_e and μ_h are electron and hole mobilities, and n and p are electron and hole concentrations. Let n_t be the concentration of electrons in the traps. When the electrons and holes deviate from their normal concentrations, n_t will also change from its normal value. We speak then of trapped electrons (Δn_t) or trapped holes ($\Delta p_t = -\Delta n_t$). Condition of electrical neutrality requires

$$\Delta n = \Delta p + \Delta p_t. \tag{2}$$

Although trapped electrons or holes do not participate in the conduction directly, their presence may change Δn and Δp, thus affecting $\Delta\sigma$.

Consider the rates of electron transition between the traps and the valence and conduction bands owing to the processes which establish thermal equilibrium. Excitation owing to the irradiation will be considered separately. Let R be the rate of transition per unit volume and let subscripts t, v, and c refer to traps, valence band, and conduction band, respectively. We can write

$$\begin{aligned} R_{tv} &= r_v n_t p, \\ R_{ct} &= r_c n (N - n_t), \end{aligned} \tag{3}$$

where N is the concentration of traps and r_c and r_v are coefficients which may depend on the temperature. According to the principle of detailed balance $R_{vt} = R_{tv}$ and $R_{tc} = R_{ct}$ in equilibrium. Furthermore, R_{vt} should be proportional to the concentration of vacant traps, and R_{tc} should be proportional to the concentration of electrons in the traps. Therefore,

$$\begin{aligned} R_{vt} &= r_v n_{t0} p_0 (N - n_t)/(N - n_{t0}) = r_v p_1 (N - n_t), \\ R_{tc} &= r_c n_0 (N - n_{t0}) n_t / n_{t0} = r_c n_1 n_t, \end{aligned} \tag{4}$$

subscript 0 referring to the normal condition. According to Fermi-Dirac statistics the ratio of empty to occupied traps is

$$(N - n_{t0})/n_{t0} = \exp[(E_t - \zeta)/kT],$$

where E_t is the energy level of traps. Thus,

$$\begin{aligned} n_1 &= n_0 \exp[(E_t - \zeta)/kT] \\ &= 2(2\pi m_e kT/h^2)^{\frac{3}{2}} \exp[(E_t - E_c)/kT], \\ p_1 &= p_0 \exp[(\zeta - E_t)/kT] \\ &= 2(2\pi m_h kT/h^2)^{\frac{3}{2}} \exp[(E_v - E_t)/kT], \end{aligned} \tag{5}$$

* Work supported by a Signal Corps Contract.
[1] W. Shockley and W. T. Read, Jr., Phys. Rev. **87**, 835 (1952).
[2] Gebbie, Nisenoff, and Fan, Phys. Rev. **91**, 230 (1953).
[3] J. R. Haynes and J. A. Hornbeck, Phys. Rev. **90**, 152 (1953).
[4] D. Navon and H. Y. Fan, Phys. Rev. **91**, 491 (1953).
[5] R. Lawrence, Phys. Rev. **89**, 1295 (1953).

where E_c is the bottom energy of the conduction band and E_v is the top energy of the valence band. We see that p_1 and n_1 are equal to the hole and electron concentrations, respectively, when $\zeta = E_t$. The net rates of transition from the traps to the two bands are

$$\begin{aligned} R_{tv} - R_{vt} &= r_v[pn_t - p_1(N-n_t)], \\ R_{tc} - R_{ct} &= r_c[n_1 n_t - n(N-n_t)]. \end{aligned} \tag{6}$$

Under thermal equilibrium both these rates are equal to zero.

(A) Steady State Under Continuous Irradiation

Under such conditions

$$(R_{tv} - R_{vt}) + (R_{tc} - R_{ct}) = 0. \tag{7}$$

It follows from (6) and (7) that the fraction of traps occupied by electrons is

$$\frac{n_t}{N} = \frac{r_c n + r_v p_1}{r_c(n+n_1) + r_v(p+p_1)}. \tag{8}$$

There is a continuous electron transition from the conduction band to the traps and from the traps to the valence band, given by

$$R_{ct} - R_{tc} = R_{tv} - R_{vt} = N r_c r_v \frac{np - n_0 p_0}{r_c(n+n_1) + r_v(p+p_1)}. \tag{9}$$

This is the hole-electron recombination rate resulting from the existence of the traps in agreement with the formula derived by Shockley and Read. Introducing

$$\eta = r_c n_0 + r_v p_1, \quad \beta = r_c(n_0+n_1) + r_v(p_0+p_1), \tag{10}$$

we get

$$n_{t0}/N = \eta/\beta, \quad \frac{\Delta n_t}{N} = \frac{r_c(\beta-\eta)\Delta n - r_v \eta \Delta p}{\beta(\beta + r_c \Delta n + r_v \Delta p)}. \tag{11}$$

Experimentally we usually have $\Delta\sigma/\sigma_0 \ll 1$. Therefore, Δn and Δp are small compared to the normal concentration of majority carriers which is n_0, assuming n-type samples; hence,

$$r_c \Delta n \ll \beta.$$

If $r_v \Delta p$ is also small compared to β, then Δn_t will vary linearly with Δn and Δp. It is found,[2] at least in germanium, that the part of photoconductivity resulting from traps saturates with increasing light intensity. This can be expected if $r_v \Delta p$ becomes large compared to β. Neglecting the terms containing $r_c \Delta n$, we get

$$\begin{aligned} -\Delta n_t/N &= (\eta/\beta)[\Delta p/(\beta/r_v) + \Delta p] \\ &= (n_{t0}/N)[\Delta p/(\beta/r_v) + \Delta p]. \end{aligned} \tag{12}$$

This approximation amounts to assuming

$$r_c \ll r_v. \tag{13}$$

For steady state under irradiation the number of electrons on the traps remains constant; therefore, Δp is determined by the rate (per unit volume) of hole-electron excitation, L, and recombination. If an excess hole has a definite rate $1/\tau_r$ of recombining with a conduction electron, then

$$\Delta p = L \tau_r. \tag{14}$$

Substituting (14) into (12), we get

$$\Delta p_t = -\Delta n_t = n_{t0} \frac{L}{\beta/r_v \tau_r + L}. \tag{15}$$

Thus we get, under irradiation trapped holes, minority carriers. Since Δp according to (14) is independent of the existence of traps, the trapped holes just cause a corresponding increase in Δn according to (2). Although the trapped minority carriers cannot conduct themselves, by increasing the excess of majority carriers they enhance the photoconductivity. Expression (14) is in agreement with observations on low temperature photoconductivity in germanium.[2] For small excitation intensity Δp_t is proportional to L. For high excitation intensities,

$$L > \beta/r_v \tau_r,$$

the trapped holes tend to saturate, approaching n_{t0}.

It has been suggested that hole-electron recombination is mainly determined by some traps present in the material.[1] It should be pointed out that if the traps considered here were also the traps determining recombination, then the photoconductivity should not show saturation. For, in that case, the recombination rate is given by (9) which should be equal to the excitation rate, L, under steady state

$$L = N r_c r_v \frac{np - n_0 p_0}{\beta + r_c \Delta n + r_v \Delta p} \simeq N r_c n_0 \frac{\Delta p}{\beta/r_v + \Delta p},$$

in view of $p_0 \ll n_0$ and $\Delta n \ll n_0$. Substituting into (12), we get

$$\Delta p_t = -\Delta n_t = (n_{t0}/r_c n_0 N) L.$$

The trapped holes, consequently the photoconductivity caused by them, are proportional to the light intensity.

For n-type material ζ should be close to the top of the energy gap. Therefore, we may expect $(\zeta - E_t) > 0$; consequently,

$$n_1 \ll n_0 \quad \text{and} \quad p_1 \gg p_0. \tag{16}$$

It follows then:

$$n_{t0}/N = \eta/\beta \sim 1, \quad \beta/r_v \simeq p_1 + r_c n_0/r_v. \tag{17}$$

Now p_1 varies exponentially with $1/T$ according to (5). At the same time, for semiconductors with low impurity activation energy, such as germanium, the majority carrier concentration n_0 remains constant over a wide temperature range. Therefore, β/r_v will be determined by p_1 if the temperature is sufficiently high. With

increasing temperature, p_1 should eventually become so high as to make Δp_t negligible according to (12). This explains the experimental observation that the photoconductivity in germanium shows the effect of traps only at low temperatures but not at room temperature.[2] On the other hand, with decreasing temperature, p_1 will become so small that very low intensity, for example, background radiation, will saturate the traps. The effect of trapping will again not be observed. Thus the effect of any set of traps should be observable only in a limited temperature range. However, the term $r_c n_0/r_v$, if not negligible, may extend the range of trapping effect to lower temperatures.

(B) Transient Condition

Let photoexcitation of hole-electron pairs begin at $t=0$ with constant rate L per unit volume. We shall assume that each excess hole has a definite rate $1/\tau_r$ of recombination with a conduction electron; τ_r may be called recombination lifetime. Furthermore, the holes also become trapped at a rate equal to the rate of decrease of electrons on the traps. The net rate of increase in hole concentration is then

$$dp/dt = L - \Delta p/\tau_r + dn_t/dt. \tag{18}$$

For the electrons on traps we find, by using (6),

$$\begin{aligned} -\frac{dn_t}{dt} &= (R_{tc} - R_{ct}) + (R_{tv} - R_{vt}) \\ &= -(r_c n + r_v p_1)N \\ &\quad + [r_c(n+n_1) + r_v(p_0+p_1)]n_t + r_v n_t \Delta p. \end{aligned} \tag{19}$$

There is also an equation for the rate of change of conduction electrons. Thus we have a set of three simultaneous equations. However, for $\Delta n \ll n_0$, n can be approximately replaced by n_0. Then we get in view of (10) and (11):

$$\begin{aligned} \frac{d(-\Delta n_t)}{dt} &= -\eta N + \beta n_t + r_v n_t \Delta p = \beta \Delta n_t + r_v n_t \Delta p \\ &= -(1/\tau_f)(-\Delta n_t) + (1/\tau_t n_{t0}) n_t \Delta p, \end{aligned} \tag{20}$$

where we have introduced

$$1/\tau_f = \beta, \quad 1/\tau_t = r_v n_{t0}.$$

Since $(-\Delta n_t)$ is the concentration of trapped holes, we see that τ_f is the time required to release a trapped hole and τ_t is the time required to trap an excess free hole if there is normal concentration n_{t0} of electrons in the traps. Now we have only to deal with Eqs. (18) and (20) with two variables Δp and Δn_t. Still (20) has a nonlinear term, involving $n_t \Delta p$, which makes the solution difficult.

We shall first limit ourselves to low intensities of light: $L \ll \beta/r_v\tau_r$. According to (15), we have in this case $-\Delta n_t \ll n_{t0}$. Putting $n_t/n_{t0} \sim 1$ in (20), we get by combining (18) and (20)

$$\begin{aligned} d^2\Delta n_t/dt^2 + (1/\tau_r + 1/\tau_f + 1/\tau_t) d\Delta n/dt \\ + (1/\tau_r\tau_f)\Delta n_t + L/\tau_t = 0. \end{aligned} \tag{21}$$

For the boundary conditions at $t=0$,

$$\Delta n_t = 0, \quad d(\Delta n_t)/dt = 0,$$

the solution is

$$\begin{aligned} \Delta p_t = -\Delta n_t = L(\tau_r\tau_f/\tau_t)[1 - (\alpha_1/\alpha_1 - \alpha_2)e^{-\alpha_2 t} \\ - (\alpha_2/\alpha_1 - \alpha_2)e^{-\alpha_1 t}] \end{aligned} \tag{22}$$

for trapped holes, and

$$\begin{aligned} \Delta p = L\tau_r\{1 - [\alpha_1/\alpha_1 - \alpha_2(1 - \tau_f\alpha_2)e^{-\alpha_2 t} \\ - \alpha_2/\alpha_1 - \alpha_2(1 - \tau_f\alpha_1)e^{-\alpha_1 t}]\} \end{aligned} \tag{23}$$

for free holes, where

$$\begin{aligned} \alpha_{1,2} = (1/2)(1/\tau_r + 1/\tau_f + 1/\tau_t) \\ \pm [(1/4)(1/\tau_r + 1/\tau_f + 1/\tau_t)^2 - 1/\tau_r\tau_f]^{\frac{1}{2}}. \end{aligned} \tag{24}$$

In the decay process after the light is cut off we get, of course, only the transient terms.

Experimentally, when the trapping effect is observed, the decay of the photoconductivity lasts much longer than τ_r, the recombination lifetime.[2,3] Since $\alpha_1 > 1/\tau_r$, this means

$$\alpha_2 \ll \alpha_1, \quad \text{or} \quad 1/\tau_r\tau_f \ll (1/4)(1/\tau_f + 1/\tau_r + 1/\tau_t)^2.$$

Therefore, $1/\tau_f \ll 1/\tau_r$ and/or $1/\tau_f \ll 1/\tau_t$. Expanding the square root in (24), we get

$$\begin{aligned} \alpha_1 &= 1/\tau_r + 1/\tau_f + 1/\tau_t \approx 1/\tau_r + 1/\tau_t, \\ \alpha_2 &= (1/\tau_r\tau_f)/(1/\tau_r + 1/\tau_f + 1/\tau_t) \approx \tau_t/\tau_f(\tau_r + \tau_t). \end{aligned} \tag{25}$$

The equation for the decay of free holes given by the transient part of (23) can be written

$$\begin{aligned} \Delta p = L\tau_r\tau_f/\tau_t[(\alpha_1/\alpha_1 - \alpha_2)\tau_t\tau_r/\tau_f(\tau_t + \tau_r)e^{-\alpha_2 t} \\ + (\alpha_2/\alpha_1 - \alpha_2)\tau_r + \tau_t/\tau_r e^{-\alpha_1 t}], \end{aligned}$$

and the decay of trapped holes is given by the transient part of (22). We see that the photoconductivity,

$$\Delta\sigma = e[(\mu_e + \mu_h)\Delta p + \mu_e \Delta p_t],$$

has a much larger slow component, with decay constant α_2, as compared to the faster component with α_1. The slow component is mainly the result of trapped holes. On the other hand, the free holes give the larger contribution to the fast component.

Consider now the case of high intensity of light: $L > \beta/r_v\tau_r$. According to (15) the steady state value of Δp_t in this case approaches the saturation value n_{t0}. Whereas the final value of Δp_t has a saturation limit, the rate of rise increases with increasing light intensity. Thus the trapped holes will be saturated faster with higher intensity. When the trapped holes are saturated, further build-up of free holes will proceed with time constant τ_r. On the other hand in the decay process the release of the trapped holes always ends

with the time constant $1/\alpha_2 > \tau_r$. Therefore, with high intensities of light the rise and decay of photoconductivity will become asymmetrical. This deduction is also in agreement with experimental observation.[2]

DRIFT OF INJECTED CARRIER UNDER APPLIED FIELD

We shall consider the one-dimensional problem. Furthermore, to get a simple solution bringing out the essential features of the problem, we shall neglect diffusion. We have then a specimen with an applied voltage giving a constant field E in the X direction. At a certain point, $x=0$, carriers are injected into the specimen. We are interested in the distribution of excess carriers in the specimen as function of time. The injection is assumed to be small so that Δn and Δp are small compared to the normal concentration of majority carriers n_0. The variation of E will then also be small, and the continuity equation for holes gives

$$\begin{aligned}\partial \Delta p/\partial t &= -\operatorname{div}(E\mu p) - \Delta p/\tau_r + \partial n_t/\partial t \\ &= -E\mu \partial \Delta p/\partial x - \Delta p/\tau_r + \partial n_t/\partial t. \end{aligned} \quad (26)$$

Assuming that hole-trapping does not approach saturation anywhere in the sample, we can use the same approximation in the expression of $\partial n_t/\partial t$ as in the analysis of transient photoconductivity. The differential equation for holes becomes

$$\begin{aligned}\partial^2 \Delta p/\partial t^2 + (1/\tau_r + 1/\tau_f + 1/\tau_t)\partial \Delta p/\partial t + E\mu \partial^2 \Delta p/\partial t \partial x \\ + E\mu/\tau_g \, \partial \Delta p/\partial x + 1/\tau_g \tau_r \Delta p = 0. \end{aligned} \quad (27)$$

Let the carrier be injected at $x=0$, beginning at $t=0$, keeping a constant hole concentration at this point. The boundary conditions are

$$\begin{aligned} &t<0: \quad \Delta p = 0 \qquad \text{for any } x, \\ &t \geqslant 0: \quad \Delta p = \Delta p_0 \quad \text{at} \quad x=0. \end{aligned} \quad (28)$$

The solution is

$$t \geqslant t_x: \quad \Delta p = P_x \left[1 + \int_0^{\Delta} e^{-(\tau_t/4t_x)\delta} \frac{I_1(\sqrt{\delta})}{2\sqrt{\delta}} d\delta \right], \quad (29)$$

$$t<t_x: \quad \Delta p = 0,$$

where

$$\begin{aligned} P_x &= \Delta p_0 \exp[-t_x(1/\tau_r + 1/\tau_t)], \\ t_x &= x/E\mu, \\ \Delta &= (4t_x/\tau_t)[(t-t_x)/\tau_g], \end{aligned} \quad (30)$$

and I_1 is the modified Bessel function. The time t_x is the transit time, the time required for the first injected carriers to reach the point x. Because we have neglected diffusion, the equation shows that at t_x there is an abrupt rise of excess holes from zero to P_x. The first holes arriving to give this abrupt rise decay during the transit time with the combined rates of recombination and trapping. The holes arriving later will be damped less and less as the accumulated trapped holes approach equilibrium with the free holes. Equation (29) gives

$$\Delta p = \Delta p_0 \exp(-t_x/\tau_r) = P_x \exp(t_x/\tau_t) \quad (31)$$

at $t=\infty$, the traps having come to an equilibrium with the valence band. The holes decay on transit only by recombination, as we would expect. If t_x/τ_t is large, the initial rise of Δp is negligible compared to the final steady state value. For a given t_x/τ_t, the time required for Δp to approach the steady state value is directly proportional to τ_g and can be very long if τ_g is large. This is in contrast to the case without traps where Δp rises immediately to the steady state value at t_x except for the smearing due to diffusion.

Consider now a pulse of injection which is often used in experiments studying drift mobility. Instead of a step function, Δp_0 at the point of injection lasts only from $t=0$ to T, the duration of the pulse. Since the differential Eq. (27) is linear, the solution in this case is simply a superposition of two solutions: one given by (29) and the other having the same form, but with $(-\Delta P_0)$ replacing Δp_0 and $(t-T)$ replacing t. Thus,

$$\begin{aligned} &t<t_x: && \Delta p = 0, \\ &t_x \leqslant t < t_x + T: && \Delta p \text{ is given by (4)}, \\ &t \geqslant t_x + T: && \Delta p = P_x \int_{\Delta_1}^{\Delta} e^{-(\tau_t/4t_x)\delta} \frac{I_1(\sqrt{\delta})}{2\sqrt{\delta}} d\delta, \end{aligned} \quad (32)$$

where

$$\Delta_1 = (4t_x/\tau_t)[(t-t_x+T)/\tau_g]$$

When the injection pulse is very short, the time variation of Δp at a given point x is very simple to calculate, e.g., for

$$\Delta - \Delta_1 = 4t_x T/\tau_t \tau_g \ll 1, \quad (33)$$

we can use for $t \geqslant (t_x+T)$, the approximation

$$\begin{aligned} \Delta p &= [(\Delta - \Delta_1) P_x I_1(\sqrt{\Delta})/2\sqrt{\Delta}] \exp[-(\tau_t/4t_x)\Delta] \\ &= (4t_x T/\tau_t \tau_g) P_x f(\Delta). \end{aligned} \quad (34)$$

Figure 1 gives the calculated curves of the function

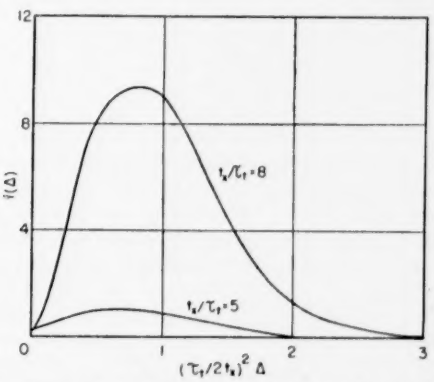

FIG. 1. Curves of the function $f(\Delta)$ plotted against $(\tau_t/2t_x)^2\Delta$, for two values of the parameter t_x/τ_t.

$f(\Delta)$ plotted against $(\tau_t/2t_x)^2\Delta$ for two values of t_x/τ_t. Starting from $f(0)=0.25$ the curves go through a maximum which rapidly increases with increasing t_x/τ_t. Differentiating $f(\Delta)$, we find that at the maximum

$$(\sqrt{\Delta})I_1(\sqrt{\Delta})/I_2(\sqrt{\Delta})=2t_x/\tau_t.$$

The function on the left-hand side increases with Δ. It approaches 4 as $\Delta\to 0$. Therefore, $f(\Delta)$ has no maximum for $t_x/\tau_t<2$. On the other hand, for large t_x/τ_t the value of Δ corresponding to the maximum of $f(\Delta)$ will be large and we have approximately

$$I_2(\sqrt{\Delta})\sim I_1(\sqrt{\Delta})\sim e^{\sqrt{\Delta}}/(2\pi\sqrt{\Delta})^{\frac{1}{2}}.$$

Therefore, the maximum of $f(\Delta)$ corresponds to

$$\sqrt{\Delta}\approx 2t_x/\tau_t. \tag{35}$$

Δ being related to t by (30), we find that the peak of pulse of excess free holes at distance x from the injection point occurs at

$$t=t_x(\tau_v+\tau_t)/\tau_t \tag{36}$$

and that the magnitude of the peak is

$$\Delta p_{\max}=[P_x/(4\pi)^{\frac{1}{2}}](T/\tau_v)(\tau_t/t_x)^{\frac{1}{2}}e^{t_x/\tau_t}. \tag{37}$$

For sufficiently large t_x/τ_t, the initial step in Δp, equal to P_x, will be negligible compared to the peak. Δp will appear to rise gradually; and it will, therefore, be impractical to determine t_x from the first arrival of the pulse. The time corresponding to the easily observable maximum is given by (36). This result is easily understood. As τ_v is the average time required for releasing a trapped hole and τ_t is the average time required for trapping a free hole, $\tau_t/(\tau_t+\tau_v)$ is the fraction of time during which the hole remains free. Therefore, the time required for most of the holes to reach the collector is $(\tau_t+\tau_v)/\tau_t$ times longer than the transit time t_x in the absence of traps. The apparent drift mobility will be $\tau_t/(\tau_t+\tau_v)$ times the true mobility. Small apparent drift mobility has been reported for silicon[3] and for germanium at low temperatures.[5]

PHYSICAL REVIEW VOLUME 92, NUMBER 6 DECEMBER 15, 1953

Generalized Variational Equations for the Scattering of Electrons by Hydrogen Atoms*

M. M. Gordon and J. G. Jones
Physics Department, University of Florida, Gainesville, Florida

(Received June 1, 1953)

Generalized variational equations are derived for calculating the elastic and inelastic scattering amplitudes associated with the scattering of electrons by hydrogen atoms. The derivation of these equations is such that no unnecessary restrictions are imposed on possible trial wave functions. Two equivalent formulations are given: one involving the use of symmetrized wave functions; the other involving wave functions of the conventional (Mott and Massey) type. For trial wave functions consisting of only the incident wave (multiplied by a hydrogen eigenfunction), these variational equations yield the same results as are obtained by the approximations of Born and Oppenheimer. Various calculation procedures are discussed.

In an appendix, it is shown that the Hulthèn variational equation for the scattering phases is a special case of the Kohn variational equation for the scattering amplitude.

I. INTRODUCTION

THE first development of a variational procedure for dealing with the scattering of electrons by hydrogen atoms was carried out by Huang.[1] His method is based on two assumptions: the wave function's asymptotic value contains only the incident and elastically scattered waves; only S-wave scattering takes place. By an extension of Hulthèn's one-body scattering variational procedure, Huang thereby obtains a variational equation for determining the S-wave phase shifts. The calculation procedure based on the Hulthèn-Huang variational equation was improved and extended by Massey and Moiseiwitsch who carried out detailed calculations for the S-wave phases.[2] Where a comparison was possible, they found that the results of their variational methods, even for very simple trial functions, are in very good agreement with the results obtained previously by direct numerical integration of the wave equation. Erskine and Massey extended this work still further by calculating variationally the $1s\to 2s$ excitation cross section at low energies.[3] Their method assumes that only S-wave scattering takes place and that a "distorted wave" approximation is valid. Moiseiwitsch has improved the variational method for dealing with the inelastic scattering processes.[4] His procedure is based on two variational equations whose

* A brief report of this work and that of reference 8 was presented at the 1952 Thanksgiving Meeting of the American Physical Society [see Phys. Rev. **89**, 913 (1953)].

[1] S. S. Huang, Phys. Rev. **76**, 477 (1949). A variational procedure for the analogous nuclear problem, n-d scattering, was developed by: W. Kohn, Phys. Rev. **74**, 1763 (1948), and M. Verde, Helv. Phys. Acta **22**, 339 (1949).

[2] H. S. W. Massey and B. L. Moiseiwitsch, Proc. Roy. Soc. (London) **A205**, 483 (1951).

[3] G. A. Erskine and H. S. W. Massey, Proc. Roy. Soc. (London) **A212**, 521 (1952).

[4] B. L. Moiseiwitsch, Phys. Rev. **82**, 753 (1951).

development involves the following assumptions: a partial wave type of wave function must be used whose asymptotic value contains the incident wave, elastically scattered wave, and only one inelastically scattered wave (the one of particular interest).

In the present paper, we shall develop generalized variational equations for dealing with the scattering of electrons by hydrogen atoms. These variational equations are such that no unnecessary restrictions are imposed on possible trial wave functions other than that they exhibit the proper asymptotic form. Our development is based on the "spatial orientation degeneracy" of the wave function and the availability of a complete set of ortho-normal eigenfunctions of the hydrogen atom. This development of the variational equations is an extension of a method devised by Kohn for a one-body scattering problem.[5] The result is a set of simultaneous variational equations for the elastic and inelastic scattering amplitudes.[6] For calculation purposes, these variational equations can be considered to displace the equivalent set of simultaneous integro-differential equations in terms of which the theory is usually formulated.[7]

Two equivalent formulations of the variational equations are presented. The first is a "symmetrized formulation" in which the wave functions display their proper symmetry character throughout. The second is a "conventional formulation" in which the asymptotic wave functions exhibit separately what might be called an "ordinary" and "exchange" type of collision.

For trial wave functions which consist of the incident wave (multiplied by a hydrogen eigenfunction) alone, our variational equations give for the scattering amplitudes the same expressions as are obtained with the usual approximation of Born and Oppenheimer.[7] Calculations have been carried out to obtain a variational improvement of the Born approximation for the elastic scattering of fast electrons by taking into account effects due to "distortion" and "polarization."[8] The results of these calculations will be presented for publication shortly.

We might note here that the existence of two separate variational equations for describing a scattering situation (e.g., our Eqs. (8) and (11)) is directly traceable to the existence of the "reciprocity" and "unitarity" properties of the S matrix. More will be said about this at some later date.

II. SYMMETRIZED FORMULATION

We consider first the eigenfunctions for both the bound and continuum states of the isolated hydrogen atom. The wave equation is taken in the form (we use Hartree atomic units throughout),

$$(\Delta+E_o+2/r)\psi_o(\mathbf{r})=0. \tag{1}$$

We designate the state o of the atom as that having the particular eigenfunction ψ_o and, incidentally, the eigenvalue E_o. We shall require here that the eigenfunctions are so chosen as to form a normalized, orthogonal set; that is, such that

$$\sum_q A_q\int\psi_p^*(\mathbf{r})\psi_q(\mathbf{r})d\tau=A_p, \tag{1a}$$

where the summation sign is used throughout to signify a sum over the discrete and integral over the continuous parts of the spectrum. For this purpose, we can consider the state o as specified entirely by E_o and the particular angular momentum quantum numbers (l_o, m_o). Now the alternative set of eigenfunctions ψ_o^* also satisfy (1) and (1a). We shall find it convenient to designate separately the state o^* of the atom as that state having the particular eigenfunction ψ_o^*. The state o^* can be entirely specified then by E_o and the particular angular momentum quantum numbers $(l_o, -m_o)$. It should be evident, then, that the two alternative sets of states, o and o^*, are merely rearrangements of each other.

The wave equation for the electron plus hydrogen atom system, with total energy E, is taken in the following form:[7]

$$[E-H(1,2)]\Psi(1,2)=[\Delta_1+\Delta_2+E+2/r_1+2/r_2-2/r_{12}]\Psi(1,2)=0, \tag{2}$$

and

$$\Psi^{(\pm)}(1,2)=\pm\Psi^{(\pm)}(2,1) \tag{2a}$$

are the two solutions; one $(+)$ symmetric, the other $(-)$ antisymmetric in the space coordinates of the two electrons, corresponding, respectively, to their antisymmetric $(S=0)$ and symmetric $(S=1)$ spin states.

Solutions of Eq. (2) are desired which represent the situation in which an electron is scattered by an atom initially in some state o (not necessarily the ground state). Hence, by way of defining this situation, these solutions must satisfy the following boundary condition:

$$\Psi_o^{(\pm)}(1,2;\mathbf{n}_a)\rightarrow\psi_o(2)\exp(ik_o\mathbf{n}_a\cdot\mathbf{r}_1)+(1/r_1)\sum_q\psi_q(2)\mathfrak{F}_{qo}^{(\pm)}(\mathbf{n}_a;\mathbf{n}_1)\exp(ik_qr_1),\quad \text{as } r_1\rightarrow\infty; \tag{3}$$

where

$$k_q^2=E-E_q, \tag{3a}$$

and the sum in (3) extends over all energetically accessible final states q of the atom (i.e., such that $k_q^2>0$). $\mathbf{n}_a$ is a unit vector in the direction of the incident electron's momentum, and is of unspecified orientation—hence the "spatial orientation degeneracy" of the wave functions.[5] $\mathbf{n}_1$ is a unit vector in the direction

[5] See W. Kohn, reference 1.

[6] It is not difficult to show that Kohn's variational equation for the scattering amplitude is equivalent, for a partial wave type of trial function, to Hulthèn's variational equation for the scattering phases. The proof of this is given in the Appendix.

[7] N. F. Mott and H. S. W. Massey, *Theory of Atomic Collisions* (Clarendon Press, Oxford, 1949), second edition, Chap. VIII.

[8] J. G. Jones, thesis, University of Florida, 1953 (unpublished).

of $\mathbf{r}_1$. $\mathfrak{F}_{qo}^{(\pm)}(\mathbf{n}_a;\mathbf{n}_1)$ is the singlet/triplet amplitude of the scattered wave (in a direction specified by the orientation of $\mathbf{n}_1$ relative to $\mathbf{n}_a$) corresponding to the $o\rightarrow q$ transition of the atom. The value of the wave function as $r_2\rightarrow\infty$ is obtained from (3) via the symmetry requirement (2a). The set of wave functions having the property (3), for all possible initial states $o(k_o^2>0)$ and all possible $\mathbf{n}_a$, form the total set of possible scattering solutions of (2) for a given total energy E.

We assume that the complete set of hydrogen eigenfunctions satisfying Eqs. (1), (1a) is given so that the only parts of (3) which must be determined from a solution of (2) are the scattered wave amplitudes. We now proceed to develop generalized variational equations which can be used to determine these $\mathfrak{F}_{qo}^{(\pm)}$.

For the first of these variational equations, we introduce an alternative set of scattering solutions of Eq. (2) for the same total energy E. These solutions represent the situation in which the electron is scattered from an atom initially in some state p^* and have then the following asymptotic form analogous to (3):

$$\Psi_{p^*}^{(\pm)}(1,2;\mathbf{n}_b)\rightarrow\psi_p^*(2)\exp(ik_p\mathbf{n}_b\cdot\mathbf{r}_1)+(1/r_1)\textstyle\sum_q\psi_q^*(2)\mathfrak{F}_{qp^*}^{(\pm)}(\mathbf{n}_b;\mathbf{n}_1)\exp(ik_qr_1)\quad\text{as}\quad r_1\rightarrow\infty;\quad(4)$$

where $\mathbf{n}_b$ has the same significance as $\mathbf{n}_a$ of (3), and $\mathfrak{F}_{qp^*}^{(\pm)}$, analogous to $\mathfrak{F}_{qo}^{(\pm)}$ of (3), is the amplitude of the scattered wave corresponding to the $p^*\rightarrow q^*$ transition of the atom. Referring to the remarks following (1a), it should be apparent that the two alternative complete sets of scattering solutions, $\Psi_{p^*}^{(\pm)}(1,2;\mathbf{n}_b)$ and $\Psi_o^{(\pm)}(1,2;\mathbf{n}_a)$, are merely rearrangements of each other.

We now define the following variational integral:

$$\mathcal{I}_{po^*}^{(\pm)}(\mathbf{n}_a;-\mathbf{n}_b)=(\tfrac{1}{2})\int\Psi_{p^*}^{(\pm)}(1,2;\mathbf{n}_b)[E-H]\times\Psi_o^{(\pm)}(1,2;\mathbf{n}_a)d\tau_1d\tau_2,\quad(5)$$

which is zero for $\Psi_o^{(\pm)}(1,2;\mathbf{n}_a)$ satisfying Eq. (2). Consider possible (physically admissable) trial wave functions, $\Psi+\delta\Psi$, which are restricted only in that their asymptotic forms differ from (3) or (4) by the replacement therein of each $\mathfrak{F}$ by $\mathfrak{F}+\delta\mathfrak{F}$; e.g.,

$$\delta\Psi_o^{(\pm)}(1,2;n_a)\rightarrow(1/r_1)\textstyle\sum_q\psi_q(2)\delta\mathfrak{F}_{qo}^{(\pm)}(\mathbf{n}_a;\mathbf{n}_1)\times\exp(ik_qr_1),\quad(6)$$

as $r_1\rightarrow\infty$. Then, if such trial wave functions are inserted into the integral (5), its resultant first-order variation is

$$\delta\mathcal{I}_{po^*}^{(\pm)}(\mathbf{n}_a;-\mathbf{n}_b)=\tfrac{1}{2}\int\Psi_{p^*}^{(\pm)}(1,2;\mathbf{n}_b)[E-H]\times\delta\Psi_o^{(\pm)}(1,2;\mathbf{n}_a)d\tau_1d\tau_2.\quad(7a)$$

Inserting the explicit value of $(E-H)$ from (2), applying Green's Theorem, and combining the two resultant surface integrals [which are equal due to the symmetry requirement (2a)], one obtains

$$\delta\mathcal{I}_{po^*}^{(\pm)}(\mathbf{n}_a;-\mathbf{n}_b)=\int[\Psi_{p^*}^{(\pm)}(1,2;\mathbf{n}_b)\nabla_1\delta\Psi_o^{(\pm)}(1,2;\mathbf{n}_a)-\delta\Psi_o^{(\pm)}(1,2;\mathbf{n}_a)\nabla_1\Psi_{p^*}^{(\pm)}(1,2;\mathbf{n}_b)]\cdot d\sigma_1d\tau_2.\quad(7b)$$

Inserting into this expression the asymptotic values of Ψ and $\delta\Psi$ from (4) and (6), carrying out first the integral over $d\tau_2$ via (1a), then the surface integral over a sphere at $r_1\rightarrow\infty$, one obtains [see Eq. (3.7) of reference 5]

$$\delta\mathcal{I}_{po^*}^{(\pm)}(\mathbf{n}_a;-\mathbf{n}_b)=-4\pi\delta\mathfrak{F}_{po^*}^{(\pm)}(\mathbf{n}_a;-\mathbf{n}_b),\quad(7c)$$

or

$$\delta[\mathcal{I}_{po^*}^{(\pm)}(\mathbf{n}_a;-\mathbf{n}_b)+4\pi\mathfrak{F}_{po^*}^{(\pm)}(\mathbf{n}_a;-\mathbf{n}_b)]=0;\quad(8)$$

that is, the quantity in the brackets is stationary.

By the same procedure as above, one also finds

$$\delta[\mathcal{I}_{op^*}^{(\pm)}(\mathbf{n}_b;-\mathbf{n}_a)+4\pi\mathfrak{F}_{op^*}^{(\pm)}(\mathbf{n}_b;-\mathbf{n}_a)]=0,\quad(9)$$

where the roles of $\Psi_{p^*}^{(\pm)}(1,2;\mathbf{n}_b)$ and $\Psi_o^{(\pm)}(1,2;\mathbf{n}_a)$ in (5) are interchanged to give

$$\mathcal{I}_{op^*}^{(\pm)}(\mathbf{n}_b;-\mathbf{n}_a)=\tfrac{1}{2}\int\Psi_o^{(\pm)}(1,2;\mathbf{n}_a)[E-H]\times\Psi_{p^*}^{(\pm)}(1,2;\mathbf{n}_b)d\tau_1d\tau_2.\quad(9a)$$

Equations (8) and (9) represent the first of the generalized variational equations for $\mathfrak{F}_{po}^{(\pm)}$.

We consider next a companion form of the above variational equations. We define as the variational integral here:

$$\mathcal{K}_{po}^{(\pm)}(\mathbf{n}_a;\mathbf{n}_b)=\tfrac{1}{2}\int\Psi_p^{(\pm)*}(1,2;\mathbf{n}_b)[E-H]\times\Psi_o^{(\pm)}(1,2;\mathbf{n}_a)d\tau_1d\tau_2,\quad(10)$$

where the left-hand wave function in the integrand differs from the corresponding member of (5) in that it it is the actual complex conjugate of the appropriate member of the set of wave functions $\Psi_o^{(\pm)}(1,2;\mathbf{n}_a)$. Applying to this integral the same considerations which led from (5) above to the variational Eq. (8), one finds

$$\delta[\mathcal{K}_{po}^{(\pm)}(\mathbf{n}_a;\mathbf{n}_b)+4\pi\mathfrak{F}_{po}^{(\pm)}(\mathbf{n}_a;\mathbf{n}_b)]=2i\textstyle\sum_q k_q\int\mathfrak{F}_{qp}^{(\pm)*}(\mathbf{n}_b;\mathbf{n})\delta\mathfrak{F}_{qo}^{(\pm)}(\mathbf{n}_a;\mathbf{n})d\Omega,\quad(11)$$

where the solid angle integration is over all orientations of $\mathbf{n}$. Equation (11) is the second of the generalized variational equations for determining the $\mathfrak{F}_{po}^{(\pm)}$.

In either of the above formulations, (8)–(9) or (11), one has available a set (generally infinite) of simultaneous variational equations for determining the required $\mathfrak{F}_{po}^{(\pm)}$. These equations can be considered to replace the equivalent set of simultaneous integro-differential equations in terms of which the theory is usually formulated.[7]

In the particular case where one uses as trial wave functions merely the first terms of (3) and (4), one obtains values for $\mathfrak{F}_{po}^{(\pm)}$ which are the same as those obtained via the Born-Oppenheimer approximation, as might be expected (see below).

III. CONVENTIONAL FORMULATION

We consider, now, the formulation of the above variational equations in their nonsymmetrized forms. These are related more directly with the conventional integro-differential equation formulation of the electron-hydrogen scattering problem as presented by Mott and Massey.[7] It must be emphasized here that this relationship is not a perfect analogy, however, since the Mott and Massey formulation is based *ab initio* on certain assumed expansions for the total wave function whose validity has recently been questioned.[9–11] The formulations of the variational equations given in this section follow directly from those of the previous section and are, therefore, free of the questionable expansions used by Mott and Massey. For purposes of comparison, however, we adopt a notation which directly parallels that of Mott and Massey. The present section introduces nothing essentially new, but serves to formulate the results of the previous section in conventional form.

If $\Psi^{(+)}(1, 2)$ and $\Psi^{(-)}(1, 2)$ are each solutions of Eq. (2), it then follows that

$$\Psi(1, 2)=\tfrac{1}{2}[\Psi^{(+)}(1, 2)+\Psi^{(-)}(1, 2)], \tag{13a}$$

$$\Psi(2, 1)=\tfrac{1}{2}[\Psi^{(+)}(1, 2)-\Psi^{(-)}(1, 2)], \tag{13b}$$

are also solutions. From this, one may write

$$\Psi^{(\pm)}(1, 2)=(1\pm X)\Psi(1, 2), \tag{13c}$$

where X is an operator which interchanges the position coordinates of the two electrons. We recognize that X is hermitian and commutes with $(E-H)$ of (2), and also that

$$(1\pm X)^2=2(1\pm X). \tag{13d}$$

We define

$$f=\tfrac{1}{2}[\mathfrak{F}^{(+)}+\mathfrak{F}^{(-)}], \tag{14a}$$

$$g=\tfrac{1}{2}[\mathfrak{F}^{(+)}-\mathfrak{F}^{(-)}], \tag{14b}$$

so that

$$\mathfrak{F}^{(\pm)}=f\pm g. \tag{14c}$$

The f and g are usually thought of as the scattering amplitudes corresponding to an "ordinary" and "exchange" type of collision, respectively.[7]

Corresponding to the asymptotic forms (3) and (4) of the two sets of wave functions considered in the previous section, we now have the following asymptotic forms of the nonsymmetrized wave function (13a):

$$\Psi_o^{(a)}(1, 2)\rightarrow\psi_o(2)\exp(ik_o\mathbf{n}_a\cdot\mathbf{r}_1)+(1/r_1)\textstyle\sum_q\psi_q(2)f_{qo}(\mathbf{n}_a;\mathbf{n}_1)\exp(ik_qr_1), \quad \text{as } r_1\rightarrow\infty;$$

and (15)

$$\Psi_o^{(a)}(1, 2)\rightarrow(1/r_2)\textstyle\sum_q\psi_q(1)g_{qo}(\mathbf{n}_a;\mathbf{n}_2)\exp(ik_qr_2), \quad \text{as } r_2\rightarrow\infty;$$

which follows directly from (3), (13a), (14); and

$$\Psi_p^{*(b)}(1, 2)\rightarrow\psi_p^*(2)\exp(ik_p\mathbf{n}_b\cdot\mathbf{r}_1)+(1/r_1)\textstyle\sum_q\psi_q^*(2)f_{qp}^*(\mathbf{n}_b;\mathbf{n}_1)\exp(ik_qr_1), \quad \text{as } r_1\rightarrow\infty;$$

and (16)

$$\Psi_p^{*(b)}(1, 2)\rightarrow(1/r_2)\textstyle\sum_q\psi_q^*(1)g_{qp}^*(\mathbf{n}_b;\mathbf{n}_2)\exp(ik_qr_2), \quad \text{as } r_2\rightarrow\infty;$$

which follows directly from (4), (13a), (14).

We define now the following two variational integrals, which are equivalent to (5):

$$I_{po}(\mathbf{n}_a;-\mathbf{n}_b)=\int\Psi_p^{*(b)}(1, 2)[E-H]\Psi_o^{(a)}(1, 2)d\tau_1d\tau_2, \tag{17a}$$

$$J_{po}(\mathbf{n}_a;-\mathbf{n}_b)=\int\Psi_p^{*(b)}(2, 1)[E-H]\Psi_o^{(a)}(1, 2)d\tau_1d\tau_2. \tag{17b}$$

One then finds, corresponding to (8),

$$\delta[I_{po}(\mathbf{n}_a;-\mathbf{n}_b)+4\pi f_{po}(\mathbf{n}_a;-\mathbf{n}_b)]=0, \tag{18a}$$

$$\delta[J_{po}(\mathbf{n}_a;-\mathbf{n}_b)+4\pi g_{po}(\mathbf{n}_a;-\mathbf{n}_b)]=0, \tag{18b}$$

which follows from (5), (8), (13c, d), (14c). The variational equations which correspond to (9) follow in similar fashion.

We define now the following two variational integrals, which correspond to (10):

$$K_{po}(\mathbf{n}_a;\mathbf{n}_b)=\int\Psi_p^{(b)*}(1, 2)[E-H]\Psi_o^{(a)}(1, 2)d\tau_1d\tau_2, \tag{19a}$$

$$L_{po}(\mathbf{n}_a;\mathbf{n}_b)=\int\Psi_p^{(b)*}(2, 1)[E-H]\Psi_o^{(a)}(1, 2)d\tau_1d\tau_2. \tag{19b}$$

[9] T. Y. Wu, Phys. Rev. **87**, 1012 (1952).
[10] S. Borowitz and B. Friedman, Phys. Rev. **89**, 441 (1953).
[11] It is not difficult to show, however, that the final results obtained by Mott and Massey from these expansions are quite valid as far as the discrete spectrum of states (excitation, but not ionization) is concerned.

One then finds, corresponding to (11),

$$\delta[K_{po}(\mathbf{n}_a;\mathbf{n}_b)+4\pi f_{po}(\mathbf{n}_a;\mathbf{n}_b)]$$
$$=2i\sum_q k_q\int[f_{qp}^*(\mathbf{n}_b;\mathbf{n})\delta f_{qo}(\mathbf{n}_a;\mathbf{n})$$
$$+g_{qp}^*(n_b;\mathbf{n})\delta g_{qo}(\mathbf{n}_a;\mathbf{n})]d\Omega; \quad (20a)$$

$$\delta[L_{po}(\mathbf{n}_a;\mathbf{n}_b)+4\pi g_{po}(\mathbf{n}_a;\mathbf{n}_b)]$$
$$=2i\sum_q k_q\int[f_{qp}^*(\mathbf{n}_b;\mathbf{n})\delta g_{qo}(\mathbf{n}_a;\mathbf{n})$$
$$+g_{qp}^*(\mathbf{n}_b;\mathbf{n})\delta f_{qo}(\mathbf{n}_a;\mathbf{n})]d\Omega. \quad (20b)$$

We now consider the results that are obtained when one uses as trial wave functions merely the first terms of (15) and (16); i.e.,

$$\Psi_o^{(a)}(1,2)=\psi_o(2)\exp(ik_o\mathbf{n}_a\cdot\mathbf{r}_1), \quad (21a)$$

$$\Psi_p^{*(b)}(1,2)=\psi_p^*(2)\exp(ik_p\mathbf{n}_b\cdot\mathbf{r}_1). \quad (21b)$$

Substituting these trial wave functions into (18a, b) or (20a, b), one finds

$$4\pi f_{po}(\mathbf{n}_a;\mathbf{n}_b)=\int[2/r_1-2/r_{12}]\psi_p^*(2)\psi_o(2)$$
$$\times\exp(ik_o\mathbf{n}_a\cdot\mathbf{r}_1-ik_p\mathbf{n}_b\cdot\mathbf{r}_1)d\tau_1d\tau_2; \quad (22a)$$

$$4\pi g_{po}(\mathbf{n}_a;\mathbf{n}_b)=\int[2/r_1-2/r_{12}]\psi_p^*(1)\psi_o(2)$$
$$\times\exp(ik_o\mathbf{n}_a\cdot\mathbf{r}_1-ik_p\mathbf{n}_b\cdot\mathbf{r}_2)d\tau_1d\tau_2. \quad (22b)$$

These expressions are equivalent to those obtained by the Born-Oppenheimer approximation. The expression for f_{po} agrees exactly with that given by Mott and Massey.[7] The expression for g_{po}, however, differs from that of Mott and Massey in that the $2/r_1$ in (22b) is $2/r_2$ according to them—a difference which is significant only in the continuous spectrum. That the above expressions are correct has been pointed out by other workers using different approaches to these same results.[9,10]

IV. CONCLUDING REMARKS

Variational equations for the scattering of electrons by hydrogen atoms which are comparable to those given above have been independently obtained by Borowitz and Friedman.[10] Their development is based on a generalization of the Schwinger (integral equation) variational formulation of the one-body scattering problem. As Kohn has shown in the one-body case, his scattering amplitude variational equation (derived from the spatial orientation degeneracy of the wave function) reduces to the comparable Schwinger variational equation when use is made of the integral equation for the wave function.[8] Hence, a similar relationship, at least in part, undoubtedly exists between the variational equations given above and those of Borowitz and Friedman.

In the Schwinger method, the integral equation for the wave function provides for a definite iteration procedure for systematically improving the trial wave function.[12] Indeed, Kato has shown that a modification of this iteration procedure will yield upper and lower bounds for the scattering coefficients.[13] For the scattering of electrons by hydrogen atoms, however, the appropriate integral equations given by Borowitz and Friedman are formidably complex so that there is little hope that such an iteration procedure (except for a one-body approximation, or the like) can be readily carried through.[14]

The procedure adopted by the London group[2,3] for applying the variational equations is simple to carry out although there is no guaranty, in general, concerning the quality of the results. This procedure involves choosing a reasonable trial wave function which is linear in all the variational parameters (scattering amplitudes included) and for which the variational integrals can be evaluated without difficulty. Two different methods are then used to determine the variational parameters: a linear (Kohn[5]) procedure; and a quadratic (Hulthèn[15]) procedure. The linear procedure leads to a value for the scattering amplitude and wave function which satisfy identically the integral equation which relates them; that is, the wave function so determined satisfies a necessary (but not sufficient) condition for its being an exact solution. In the quadratic procedure, the wave function is required, as an auxiliary condition to the variational equation, to satisfy the equation (quadratic in the variational parameters): variational integral $=0$, which is also a necessary (but not sufficient) condition for the wave function to be an exact solution. In the limit where the trial wave function approaches the exact solution, the two procedures must give the same results. Hence, the closeness of the results obtained by the two procedures is a criterion for the reliability of the results. What is lacking, of course, is a proof, if one is possible, that this criterion is sufficient for determining the reliability of the results.[16] Even so, such a criterion may be more stringent than necessary, since it serves to judge the quality of the trial wave function and one may suppose it to be possible for some relatively poor trial wave function to give fairly good results variationally for the scattering amplitudes by one or the

[12] See, e.g., J. M. Blatt and J. D. Jackson, Phys. Rev. **76**, 18 (1949).

[13] T. Kato, Progr. Theoret. Phys. **6**, 295, 394 (1951).

[14] Variational calculations for elastic electron-hydrogen scattering using the one-body approximation have been carried out by T. Kato, reference 13; L. Mower, Phys. Rev. **89**, 947 (1953); S. Altshuler, Phys. Rev. **89**, 1278 (1953).

[15] See, e.g., reference 7, page 128.

[16] For the elastic S-wave scattering case, the London group (reference 2) found that when the two procedures gave essentially the same results, these results agreed very well with those from direct numerical integrations of the wave equation.

other procedure, but not both, depending on certain factors as yet unknown.

APPENDIX: RELATIONSHIP BETWEEN KOHN'S VARIATIONAL EQUATION FOR THE SCATTERING AMPLITUDE AND HULTHÈN'S VARIATIONAL EQUATION FOR THE SCATTERING PHASES

We restrict our considerations here to a one-body scattering situation and a central force potential $V(r)$. The wave equation is

$$(E-H)\psi(\mathbf{r})=[\Delta+k^2-V(\mathbf{r})]\psi(\mathbf{r})=0; \quad \text{(A1)}$$

and a solution is desired which has the asymptotic form:

$$\psi^{(a)}(\mathbf{r})\rightarrow\exp(ik\mathbf{n}_a\cdot\mathbf{r})+f(\mathbf{n}_a;\mathbf{n})(1/r)\exp(ikr). \quad \text{(A2)}$$

The variational integral is defined as follows (see reference 5, Sec. III):

$$I(\mathbf{n}_a;-\mathbf{n}_b)=\int\psi^{(b)}[E-H]\psi^{(a)}d\tau. \quad \text{(A3)}$$

For trial functions $\psi+\delta\psi$ having the same asymptotic form as (A2), but with f replaced by $f+\delta f$, one obtains to first-order,

$$\delta I(\mathbf{n}_a;-\mathbf{n}_b)=\int\psi^{(b)}[E-H]\delta\psi^{(a)}d\tau$$

$$=-4\pi\delta f(\mathbf{n}_a;-\mathbf{n}_b), \quad \text{(A4)}$$

which is Kohn's variational equation for the scattering amplitude f.

The solution of (A1) having the asymptotic form (A2) can be expanded into partial waves and thereby written in terms of the scattering phases η_n as follows (see reference 7, Chap. II):

$$\psi^{(a)}(\mathbf{r})=(1/kr)\sum_n(2n+1)i^n \times\exp(i\eta_n)G_n(r)P_n(\mathbf{n}_a\cdot\mathbf{n}); \quad \text{(A5)}$$

where

$$\mathfrak{L}G_n=[d^2/dr^2-n(n+1)/r^2+k^2-V(r)]G_n(r)=0, \quad \text{(A5a)}$$

and

$$G_n\sim\sin(kr-\tfrac{1}{2}n\pi+\eta_n), \quad \text{(A5b)}$$

asymptotically. Then

$$f(\mathbf{n}_a;\mathbf{n})=(1/2ik)\sum_n(2n+1) \times[\exp(i2\eta_n)-1]P_n(\mathbf{n}_a\cdot\mathbf{n}). \quad \text{(A6)}$$

Now, we have from (A5):

$$\delta\psi^{(a)}=(1/kr)\sum_n(2n+1)i^n \times\exp(i\eta_n)\delta G_n(r)P_n(\mathbf{n}_a\cdot\mathbf{n}), \quad \text{(A7)}$$

plus an additional term (from $\delta\eta_n$) which gives, because of (A5a), no contribution to the integral (A4) which becomes

$$\delta I(\mathbf{n}_a;-\mathbf{n}_b)=(1/k^2)\sum_{n,m}(2n+1)(2m+1)(i)^{n+m} \times\exp(i\eta_n+i\eta_m)\int G_m(r)\,\mathfrak{L}\delta G_n(r)dr$$

$$\times\int P_m(\mathbf{n}_b\cdot\mathbf{n})P_n(\mathbf{n}_a\cdot\mathbf{n})d\Omega. \quad \text{(A8)}$$

Making use of the Addition Theorem for Legendre Polynomials, one obtains

$$\delta I(\mathbf{n}_a;-\mathbf{n}_b)=(4\pi/k^2)\sum_n(2n+1)(-1)^n \times\exp(i2\eta_n)\delta L_nP_n(\mathbf{n}_a\cdot\mathbf{n}_b), \quad \text{(A9)}$$

where

$$\delta L_n=\int_0^\infty G_n(r)\,\mathfrak{L}\delta G_n(r)dr. \quad \text{(A9a)}$$

From (A6) one has

$$4\pi\delta f(\mathbf{n}_a;-\mathbf{n}_b)=(4\pi/k)\sum_n(2n+1)(-1)^n \times\exp(i2\eta_n)\delta\eta_nP_n(\mathbf{n}_a\cdot\mathbf{n}_b). \quad \text{(A10)}$$

Hence, from (A4), (A9), it follows that

$$\delta L_n=-k\delta\eta_n, \quad \text{(A11)}$$

which is Hulthèn's variational equation for the scattering phases η_n.[15] Hence, one may conclude that Hulthèn's variational equation for the phases is a particular case of Kohn's variational equation for the scattering amplitude. Kohn[8] has already shown that his scattering amplitude variational equation reduces to the comparable Schwinger variational equation when use is made of the integral equation expression for the wave function. Hence, the above discussion serves as a further link between the various forms of the one-body scattering variational equations.[17]

[17] See also: T. Kato, Phys. Rev. **80**, 475 (1950).

Mo K and U L X-Ray Transitions from Separated Isotopes

GEORGE L. ROGOSA AND GUENTER SCHWARZ
Department of Physics, Florida State University, Tallahassee, Florida
(Received August 10, 1953)

The $K\alpha(K\rightarrow L_{III}, K\rightarrow L_{II})$ x-ray lines of Mo and the $L\beta_1(L_{II}\rightarrow M_{IV})$ and $L\alpha_1(L_{III}\rightarrow M_V)$ x-ray lines of U have been measured from separated isotopes using a double-crystal x-ray spectrometer. The x-ray transitions were induced by radiative excitation from a W target x-ray tube. Intensities were measured with a 70-cm Kr-filled Geiger counter.

No evidence of nuclear isotopic effects (hyperfine structure and isotope shift) on the x-ray levels was found in the measurement of these transitions. The $K\alpha$ transitions from the separated isotopes Mo^{92} (95.5 percent), Mo^{95} (88.0 percent), and Mo^{100} (86.65 percent) in MoO_3 and the $L\beta_1$ and $L\alpha_1$ transitions from the separated isotopes of U^{235} and U^{238} in U_3O_8 show no measurable shift in peak positions and no changes in line widths. The limit of an observable effect is 0.2 volt for the Mo transitions and 0.4 volt for the U transitions.

I. INTRODUCTION

THE high resolution available in optical spectroscopy has revealed in the spectra of many isotopes a hyperfine structure and an isotope shift. The hyperfine structure can essentially be understood by attributing to the nucleus an angular momentum I and a magnetic moment μ. The isotope shift for heavy elements results from a nuclear "volume" effect.[1] In many cases, values of nuclear moments and information on nuclear charge distribution have been obtained from spectroscopic studies. McNally[2] has pointed out the advantages of using separated isotopes for this work.

Some years ago Breit[3] considered the possible effects of nuclear spin and magnetic moment on x-ray levels, and he showed that they might cause small but presumably measurable separations of x-ray terms. Breit suggested the use of the double-crystal x-ray spectrometer for possible detection of this effect.

This suggestion of Breit was investigated by Richtmyer and Barnes[4] and by Williams[5] without success. Richtmyer and Barnes examined the $K\alpha_1$ line of W with the double crystal spectrometer and found no evidence of a hyperfine structure. Williams also used the double crystal spectrometer in a study of the width of twelve lines in the U L series. In his experiments he found no evidence for the splitting of the L levels. He suggested that the large natural width of the lines would prevent observation of hyperfine structure.

It should be pointed out that the isotopic abundances in normal U and W are not favorable for experimental detection of an x-ray hyperfine structure. W contains about 86 percent even-mass-number isotopes. The one odd-mass-number isotope of W has a nuclear spin of $\frac{1}{2}$ and a magnetic moment of only 0.09. Normal U consists of about 99.3 percent U^{238} and 0.7 percent U^{235}. Thus the measurements on W by Richtmyer and Barnes and on U by Williams depended largely on even-even nuclei for which $I=0$ and $\mu=0$.

Frilley, Gokhale, and Valadarès,[6] in an experimental attempt to observe x-ray hyperfine structure, measured the widths of the $K\alpha$ lines from $_{37}$Rb to $_{50}$Sn. Because of the high spin and magnetic moment of Nb and the two In isotopes, a measurable hyperfine broadening of the $K\alpha$ lines from these two elements was expected. However, their measurements showed no departures in these line widths from the normal variation of the line widths as a function of Z indicating no hyperfine structure. Curie[7] has discussed the results of Frilley, Gokhale, and Valadarès and has given a possible explanation of these results.

As found in optical spectroscopy, one should also expect an x-ray isotopic shift from the nuclear "volume" effect. Such an effect has also not yet been observed. Detailed calculations of this shift have been made for the optical levels but appear to be lacking for the x-ray levels. The smallness of the effect can perhaps be inferred from some calculations of Brenner and Brown[8] on K binding energies of heavy elements. They found that if the nucleus instead of being a point charge is a charged spherical shell of radius $r_0\sim 5e^2/mc^2$, then the change in the binding energy of a K electron is of the order of $Z^4\alpha^6mc^2$, which is about 0.1 Rydberg for mercury. This nuclear "volume" effect depends on the distribution of nuclear charge and should increase for an ellipsoidal shape, assuming the same volume. Large optical shifts have been measured for isotopes having a high electric quadrupole moment. The use of selected separated isotopes, now available, suggests itself for a critical study of hyperfine structure and isotope shift of x-ray levels.

In recent work, Brown[9] has reported the measurement of x-ray transitions as a result of radioactive decay

[1] J. E. Rosenthal and G. Breit, Phys. Rev. **41**, 459 (1932); M. F. Crawford and A. L. Schawlow, Phys. Rev. **76**, 1310 (1949).
[2] J. R. McNally, Jr., Am. J. Phys. **20**, 152 (1952).
[3] G. Breit, Phys. Rev. **35**, 1447 (1930).
[4] F. K. Richtmyer and S. W. Barnes, Phys. Rev. **37**, 1695 (1931).
[5] John H. Williams, Phys. Rev. **37**, 1431 (1931).
[6] Frilley, Gokhale, and Valadarès, Compt. rend. **233**, 1183 (1951).
[7] Daniel Curie, J. Phys. et radium **13**, 505 (1952).
[8] S. Brenner and G. E. Brown, Proc. Roy. Soc. (London) **A218**, 422 (1953).
[9] Charles I. Brown, Jr., University of California Radiation Laboratory Report UCRL-1764 (unpublished).

using a ten-inch bent-crystal spectrometer. He reports an apparent anomaly in the energies of the U L x-rays emitted after the β decay of Pa^{232} and Pa^{233}, the x-ray energies being uniformly higher by as much as 50 volts than the energies of the U L lines emitted after the decay of Pu^{239} or those reported by Siegbahn from conventional x-ray excitation. No explanation for this apparent effect was advanced.

We have started a program searching experimentally for x-ray isotopic effects (hyperfine structure and isotope shift) by measuring corresponding transitions from highly enriched separated isotopes. We have so far examined the $K\alpha_1$ and the $K\alpha_2$ transitions from electromagnetically enriched Mo^{92}, Mo^{95}, and Mo^{100} [10] and the $L\beta_1$ and the $L\alpha_1$ transitions from separated isotopes of U^{235} and U^{238}.[11]

II. EXPERIMENTAL

We have employed the standard techniques of double-crystal x-ray spectroscopy in the measurement of the x-ray transitions. However, the value of the enriched separated isotopes demanded a technique which would result in no loss or contamination of the samples. For this reason the transitions were not produced by electron bombardment but rather by radiative excitation.

W x-ray radiation was produced from a Machlett A-2 tube at 40 kv and 20 ma. The voltage supplied to the tube and the x-ray tube current were both stabilized to within 0.1 percent. The isotopic compound was placed in a specially constructed brass holder shown in Fig. 1. The cavity containing the material measured 4 mm×8 mm and was ½ mm deep. The compound was covered with a thin aluminum foil (0.0005 in.) which was secured to the holder with a metal frame. The 8-mm dimension of the cavity was inclined at a 30° angle with the horizontal. The isotope holder could be removed for sample change and precisely repositioned by sliding in grooved runways. The x-ray tube was clamped in a horizontal position with the tube window immediately above the isotope holder. The exciting radiation emerged downward, striking the compound and producing fluorescent radiation. The x-ray tube base and isotope holder were enclosed in a lead box to confine scattered radiation.

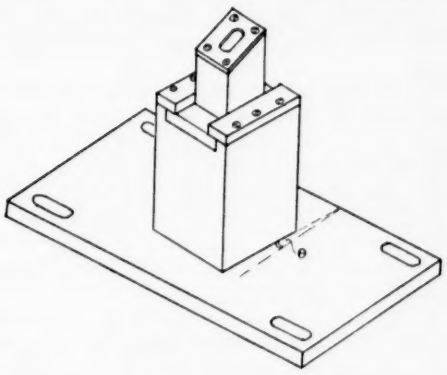

FIG. 1. Sample holder.

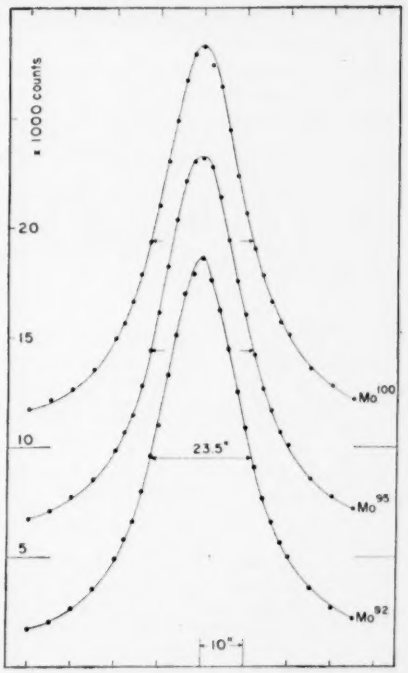

FIG. 2. Mo$K\alpha_1$ lines from Mo^{92}, Mo^{95}, and Mo^{100}. The zero line for the Mo^{95} curve is at 5000 counts, for the Mo^{100} curve at 10 000 counts.

An opening in the front of the lead box permitted the fluorescent radiation to pass through a slit system and strike the first crystal of a double-crystal spectrometer. Diffracted radiation in turn passed to the second crystal and finally entered a Geiger counter filled with krypton to a pressure of 70 cm. Data on the x-ray lines were recorded by counting for fixed time intervals, either one or two minutes, point by point through the line. Numerous runs were obtained, resetting the spectrometer and counting over at the same points.

A search for isotopic effects necessitates the highest resolution available. For the double-crystal spectrometer the physical resolving power which limits the available resolution is dependent on the crystal perfection. The calcite crystals of our spectrometer have been in use for about two years and consistently give line widths that indicate that these crystals compare favorably with the best crystals reported. The spectrometer is of the Ross type having a translating first crystal and a rotating second crystal. The rotation of the second

[10] Obtained on U. S. Atomic Energy Commission approved loan from Stable Isotope Research and Production Division, Oak Ridge National Laboratory, Oak Ridge, Tennessee.

[11] Obtained on loan through contract with the U. S. Atomic Energy Commission.

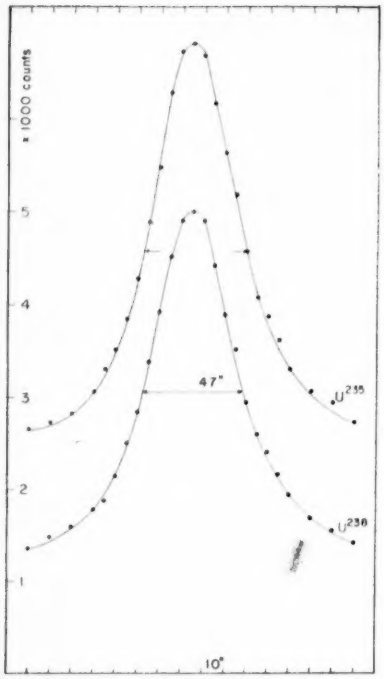

FIG. 3. U $L\beta_1$ lines from U^{235} and U^{238}. The zero line for the U^{235} curve is at 1200 counts.

crystal is performed by means of a precision micrometer screw and a lever arrangement. The micrometer head is engraved with 200 divisions, each division corresponding very closely to a crystal rotation of 1″. Absolute angles cannot be measured with this spectrometer, but angular differences are measured to better than 1″. The micrometer has been calibrated by measuring the angular difference between peaks of the $K\alpha_1$ and $K\alpha_2$ lines for Mo.

III

A. Results—Mo

The K x-ray lines of molybdenum have been measured by numerous investigators, among them Allison and Williams.[12] The $K\alpha$ lines have been found to be highly symmetrical and the lowest half-width value in the (1, +1) position has been reported to be 21″ for $K\alpha_1$. Our spectrometer gives a half-width value of 23.5″.

The separated Mo isotopes were in the chemical form MoO_3. The $K\alpha_1$ line shown in Fig. 2 was measured for normal MoO_3, $Mo^{92}O_3$, $Mo^{95}O_3$, and $Mo^{100}O_3$. Table I gives the isotopic abundance of the various samples. Five runs were made for each sample with a total peak count of about 18 000 counts for each. We find no measurable differences for this transition from separated isotopes. The peak positions and half widths for all samples agree to within 0.5″. Since the dispersion at this wavelength is close to 3″/volt, it can be stated that any existing isotopic effect on the K-transitions for Mo is less than 0.2 volt.

As a check, we have also measured the $K\alpha_2$ transition from the separated isotopes, and again we find no measurable effects on half-width or peak position. Thus, no influence on the $K\alpha$ x-ray transitions of Mo isotopes has been found either for the nuclear spin of Mo^{95} or for the nuclear "volume" difference of Mo^{92}, Mo^{95}, and Mo^{100}.

B. Results—U

The U $L\beta_1$ line which represents a transition from the $L_{II} \rightarrow M_{IV}$ state was measured from separated isotopes of U^{235} and U^{238} in the form of U_3O_8. Since the fluorescent intensity of the U L lines is much lower than that of the Mo K lines under the same excitation conditions, more runs were taken. As a further check, the line was measured twice changing the sample each time. In one case 12 runs were taken accumulating 4800 counts at the peak, and in the other case 10 runs were taken with a total peak count of 8000 counts, both for U^{235} and U^{238}. The results again indicate no measurable differences. The greater width of this line, measured to be 47″, raises the limit of an observable effect to about 1″ or 0.4 volt. The peak positions and line widths agree to within this limit.

TABLE I. Mo isotope mass analysis (in atom percent).

	92	94	95	96	97	98	100
Mo^{92}	95.5	0.8	0.8	0.8	0.4	1.3	0.5
Mo^{95}	1.1	2.2	88.0	4.2	1.2	2.7	0.7
Mo^{100}	1.70	2.02	1.93	2.35	1.32	4.04	86.65
Mo (normal)	15.86	9.12	15.7	16.5	9.45	23.75	9.62

The $L\alpha_1$ line from U^{235} and U^{238}, a $L_{III} \rightarrow M_V$ transition, has also been measured, showing no measurable difference in the x-ray transitions from the separated isotopes.

L lines originating from the L_I level are more difficult to excite and are too weak to measure with our experimental arrangement. The closeness of the U $L\beta_1$ line to the Mo $K\alpha$ lines allowed us to make a precision measurement of its wavelength with respect to the Mo $K\alpha$ doublet. We find that the angular difference between Mo $K\alpha_1$ and U $L\beta_1$ agrees to within 1″ with that calculated from the wavelength values given in the tables of Cauchois and Hulubei.[13]

IV. CONCLUSIONS

No measurable isotopic effects have been observed for the $K\alpha$ x-ray transitions of Mo^{92}, Mo^{95}, and Mo^{100} in MoO_3. The double-crystal technique would have

[12] S. K. Allison and J. H. Williams, **Phys. Rev. 35**, 1476 (1930).

[13] Y. Cauchois and H. Hulubei, *Longuers d'ondes des èmissions X et des discontinuités d'absorption X* (Hermann and Company, Paris, 1947).

shown differences of 0.2 volt for these lines. Similarly no measurable differences were found for the $L\alpha_1$ and $L\beta_1$ lines from U^{235} and U^{238} in U_3O_8. The increased width of these lines raises the limit of an observable effect to 0.4 volt. It appears that present x-ray spectroscopic techniques lack the resolution to detect nuclear isotopic influences on these x-ray levels. However, it may still be possible that somewhere in the isotopic chart a radical change in nuclear "volume," for example, may yet allow a measurable x-ray isotopic effect. It also appears of interest to make precision wavelength measurements of x-rays emitted in radioactive decay to see whether their energies really differ from x-rays produced in the conventional manner.

The authors wish to express their appreciation to Mr. Don J. Leffler, who helped much with the taking of the data. One of us (G. L. R.) wishes to acknowledge discussions with J. R. McNally, Jr., and W. Peed of the Oak Ridge National Laboratory. These discussions have stimulated this work.

PHYSICAL REVIEW VOLUME 92, NUMBER 6 DECEMBER 15, 1953

One-to-Two Millimeter Wave Spectroscopy. III. NO and DI†

C. A. BURRUS* AND WALTER GORDY
Department of Physics, Duke University, Durham, North Carolina
(Received September 14, 1953)

Pure rotational transitions of $N^{14}O^{16}$ and DI^{127} have been measured in the one-to-two millimeter wave region. For NO the $J=\frac{1}{2}\rightarrow\frac{3}{2}$ transition in the $^2\pi_{\frac{1}{2}}$ electronic ground state was observed. The transition reveals a Λ doublet with separation $\Delta\nu_{dc}=355.1$ Mc/sec. Each component of the Λ doublet is further split into five hyperfine components as a result of the nuclear magnetic coupling of N^{14}. Nuclear quadrupole coupling of N^{14} was found to be small in comparison with the magnetic interaction. Analysis of the data yields $B_0=50818.0$ Mc/sec, $r_0=1.1540$ A, $B_e=51084.8$ Mc/sec, and $r_e=1.1510$ A for the $^2\Pi_{\frac{1}{2}}$ state. For DI^{127} the following information was obtained: $B_0=97\ 537.2$ Mc/sec, $r_0=1.6165$ A, and $eQq(I^{127})=1823\pm1$ Mc/sec. Nuclear magnetic interactions of I^{127} were also detected and analyzed.

INTRODUCTION

THE opening up of the one-to-two millimeter wave region[1] has made it possible to study with the high precision of microwave methods the pure rotational spectra of such light diatomic molecules as NO and the deuterium halides, which, because of their small moments of inertia, were previously inaccessible to microwave spectroscopists. Results on NO and DI are reported here. We are searching for the lines of DBr and hope to measure DCl also.

NITRIC OXIDE

The electronic ground state of NO is $^2\Pi_{\frac{1}{2}}$, but only 120 cm^{-1} above lies the $^2\Pi_{\frac{3}{2}}$ state, also appreciably populated at room temperature. We have investigated the $J=\frac{1}{2}\rightarrow\frac{3}{2}$ rotational transition of molecules in the $^2\Pi_{\frac{1}{2}}$ state. Because of the cancellation of the orbital and spin magnetic moments the $^2\Pi_{\frac{1}{2}}$ state is supposedly nonmagnetic. Nevertheless, widely spaced magnetic hyperfine structure was found. Table I gives the pattern of 10 lines which were observed. Figure 1 shows the lower frequency group of five as they appeared on the cathode-ray scope.

Without nuclear interaction the $J=\frac{1}{2}\rightarrow\frac{3}{2}$ transition would be expected to have two components because of Λ doubling. Nuclear interaction with N^{14} would split each component of the doublet into five components, as observed. Each hyperfine multiple was found to fit an equation of the form

$$E=P\{F(F+1)-J(J+1)-I(I+1)\}+R\{(3/4)C(C+1)-J(J+1)I(I+1)\},$$

with $C=F(F+1)-J(J+1)-I(I+1)$, derived by Dr.

TABLE I. Observed and calculated components of the $J=\frac{1}{2}\rightarrow\frac{3}{2}$ transition, $^2\pi_{\frac{1}{2}}$ state, of $N^{14}O^{16}$.

Transition $F\rightarrow F'$	Frequency (Mc/sec) Observed	Calculated*	Relative intensity Observed	Calculated
Lower frequency group of Λ doublet $\nu_0{}^c=150\,195.49$ Mc/sec				
$\frac{3}{2}\rightarrow5/2$	150,176.54	150,176.52	100	100
$\frac{1}{2}\rightarrow\frac{3}{2}$	150,198.85	150,198.85	35	37.1
$\frac{3}{2}\rightarrow\frac{3}{2}$	150,218.89	150,218.89	30	29.6
$\frac{1}{2}\rightarrow\frac{1}{2}$	150,225.75	150,225.80	30	29.6
$\frac{3}{2}\rightarrow\frac{1}{2}$	150,245.69	150,245.70	5	3.7
Upper frequency group of Λ doublet $\nu_0{}^d=150\,550.60$ Mc/sec				
$\frac{3}{2}\rightarrow\frac{1}{2}$	150,375.48	150,375.47	5	3.7
$\frac{3}{2}\rightarrow\frac{3}{2}$	150,439.22	150,439.21	30	29.6
$\frac{3}{2}\rightarrow5/2$	150,546.50	150,546.46	100	100
$\frac{1}{2}\rightarrow\frac{1}{2}$	150,580.70	150,580.64	30	29.6
$\frac{1}{2}\rightarrow\frac{3}{2}$	150,644.37	150,644.32	40	37.7

* See reference 2.

† This research was supported by the United States Air Force under a contract monitored by the Office of Scientific Research, Air Research and Development Command.
* Shell Oil Company Fellow.
[1] W. C. King and W. Gordy, Phys. Rev. **90**, 319 (1953).

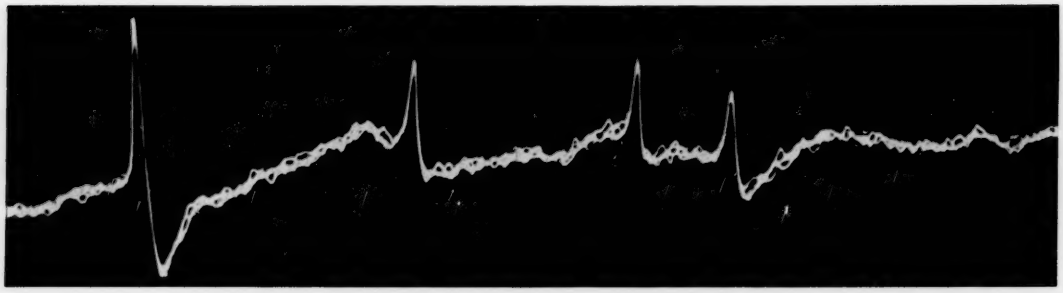

FIG. 1. Cathode-ray display of the magnetic hyperfine structure of the lower frequency component of the Λ doublet in the $J=\frac{1}{2}\rightarrow\frac{1}{2}$ transition, $^2\pi_{\frac{1}{2}}$ state, of $N^{14}O^{16}$. For frequencies see Table I.

M. Mizushima[2] of this laboratory. The parameters P and R have different values for the different levels and for the different Λ sublevels. The term in P results from the magnetic interactions and is of the form previously derived by Frosch and Foley[3] if

$$P=\{a\mp b(2J+1)\}/J(J+1),$$

in which a and b are constants, with the minus sign used for the c component and the plus sign for the d component of the Λ doublets. However, the P in Mizushima's formula includes, in addition, a small term to account for interaction of the $J=\frac{3}{2}$ level with the $^2\Pi_{\frac{1}{2}}$ electronic state. A fitting of the data[2] requires that $a=23.15$ and $b=14.07$ Mc/sec. The term in R results from nuclear quadrupole interaction. It is zero for the $J=\frac{1}{2}$ state, and in the $J=\frac{3}{2}$ state R has the values[2] 0.77 Mc/sec and 0.035 Mc/sec for the c and d components, respectively. The rather large and somewhat complicated quadrupole coupling term results mainly from the odd electron. Details will be given in a theoretical paper by Mizushima[2] to follow. In Table I the observed frequencies are compared with those calculated from the above formula.

The electronic coupling in NO is intermediate between Hund's case (a) and (b). The energy levels have been worked out by Van Vleck.[4] If we neglect centrifugal distortion (which cannot be evaluated from the one transition observed) and the structure already mentioned, the rotational lines are given by the formula

$$\nu_0{}^i=2B_{eff}{}^i(J+1)=2B_0{}^i\left(1-\frac{B_0{}^i}{A}\cdots\right)(J+1),$$

where $J=\frac{1}{2}$, $\frac{3}{2}$, 5/2, $\cdots$, and i designates the particular component, c or d, of the Λ doublet. The $D_J=0.53\times10^{-6}$ cm^{-1} for the $^2\Pi_{\frac{1}{2}}$ state obtained by Gillette and Eyster[5] from high J transitions in infrared vibration-rotation spectra indicates that centrifugal distortion shifts the $\frac{1}{2}\rightarrow\frac{3}{2}$ transition only about 0.4 Mc/sec, which is the order of our experimental error. For the $^2\Pi_{\frac{1}{2}}$ state, the doublet separation has been shown by Van Vleck[4] to be directly proportional to J. It can be expressed approximately by

$$\Delta\nu_{de}=2p(J+\tfrac{1}{2}).$$

Our measurement gives $\Delta\nu_{dc}=355.1$ Mc/sec, and with $J=\frac{1}{2}$ it is seen from the formula that $p=355.1$ Mc/sec. If it is assumed that the upper and lower components $\nu_0{}^c$ and $\nu_0{}^d$ of the Λ doublet are equally displaced from the hypothetical unsplit line, the latter has the frequency $\nu_0=(\nu_0{}^c+\nu_0{}^d)/2=150373.04$ Mc/sec, and $(B_0)_{eff}$ as determined with this frequency is 50124.4 Mc/sec or 1.67198 cm^{-1}. (Compare with Gillette and Eyster's[5] infrared value of 1.6696 cm^{-1}.) With $A=124.2$ cm^{-1} from other sources,[5] this gives $B_0=50818.0$ Mc/sec. This value of B_0 yields for the internuclear distance the value $r_0=1.1540$ A for the $^2\Pi_{\frac{1}{2}}$ state, and with $\alpha=0.0178$ cm^{-1} from infrared data[5] it yields the values $B_e=51084.8$ Mc/sec and $\gamma_e=1.1510$ A. The results are summarized in Table II.

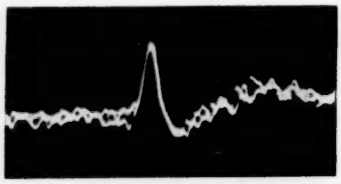

FIG. 2. Cathode-ray display of the medium strength $F=5/2\rightarrow5/2$ component of the $J=0\rightarrow1$ transition of DI^{127} at 1.5-millimeter wavelength.

DEUTERIUM IODIDE

The $J=0\rightarrow1$ rotational transition of DI has been measured with high precision. The lines were readily observed on the cathode-ray scope with a video-type spectrometer having a wide band amplifier. Figure 2 shows the medium strength $F=5/2\rightarrow5/2$ line.

The nuclear hyperfine pattern of $I^{127}(I=5/2)$ is particularly simple for the $J=0\rightarrow1$ transition since it con-

[2] M. Mizushima (to be published).
[3] R. A. Frosch and H. M. Foley, Phys. Rev. **88**, 1337 (1952).
[4] J. H. Van Vleck, Phys. Rev. **33**, 467 (1929); R. S. Mulliken and A. Cristy, Phys. Rev. **38**, 87 (1931). For convenient summary see G. Herzberg, *Spectra of Diatomic Molecules* (D. Van Nostrand Company, Inc., New York, 1950), p. 227.
[5] R. H. Gillette and E. H. Eyster, Phys. Rev. **56**, 1113 (1939).

sists of only three lines. Nevertheless, quadrupole coupling theory, even with second-order effects included, did not entirely account for the observed line spacings. It was found that the deviation could be explained as the nuclear magnetic interaction of I^{127} as given by

$$E=\tfrac{1}{2}C[F(F+1)-J(J+1)-I(I+1)],$$

with $C=0.14$ Mc/sec. (Compare with NO above, $a=23$ Mc/sec.) The molecular magnetic moment required to account for this coupling probably results from the molecular rotation. Table III gives a comparison of the observed frequencies with those calculated by use of the quadrupole coupling as $eQq=1823$ Mc/sec and the magnetic-coupling constant for I^{127} as 0.07 Mc/sec. Although the magnetic displacements in all cases are less than one megacycle, they are well outside the limits of error in the measurement of the relative differences in the frequencies of the lines.

TABLE II. Constants of $N^{14}O^{16}$ in the $^2\Pi_{\frac{1}{2}}$ state.

$\Delta\nu_{cd}=355.1$ Mc/sec,	$p=355.1$ Mc/sec
$(B_0)_{eff}=50\,124.3$ Mc/sec $=1.67198$ cm^{-1}	
$B_0=50\,818.0$ Mc/sec $=1.69512$ cm^{-1}	
$B_e=51\,084.8$ Mc/sec $=1.70402$ cm^{-1}	
$I_0=16.5082\times10^{-40}$ g cm^2,	$I_e=16.4219\times10^{-40}$ g cm^2
$r_0=1.1540$ A,	$r_e=1.1510$ A

Table IV summarizes the information obtained for the DI molecule. In calculation of B_0 we have used $D_J=1.5$ Mc/sec, as obtained from the formula $D_J=4B^3/\omega^2$.

The nuclear quadrupole coupling in atomic iodine has now been measured by Jaccarino, King, and Stroke[6] as 1146.215 Mc/sec. If one assumes that the effects of bond orbital hybridization are negligible, the nuclear quadrupole coupling should give a measure

[6] Jaccarino, King, and Stroke (private communication).

TABLE III. Observed and calculated frequencies of DI^{127}. $J=0\rightarrow1$, $\nu_0=195\,068.15\pm0.30$ Mc/sec.

Transition $F-F'$	Quadrupole splitting (Mc/sec) 1st order	2nd order	Magnetic splitting (Mc/sec)	Calculated[a] frequency (Mc/sec)	Observed frequency (Mc/sec)
$5/2\rightarrow5/2$	−291.68	0.09	−0.16	194,776.40	194,776.40 ±0.30
$5/2\rightarrow7/2$	91.15	0.07	0.38	195,159.75	195,159.68 ±0.30
$5/2\rightarrow3/2$	225.22	0.18	−0.56	195,322.99	195,323.02 ±0.30

[a] Calculated with the constants given in Table IV.

TABLE IV. Molecular constants of DI^{127}.

$eQq(I^{127})=1823\pm1$ Mc/sec	$C(I^{127})=0.14$ Mc/sec
$B_0=97\,537.2$ Mc/sec	$r_0=1.6165$ A

of the ionic character of the bond. In this case,[7]

$$\text{Ionic character}=1-\frac{\text{mol } eQq}{2\times\text{atomic } eQq}\approx\frac{x_A-x_B}{2}.$$

The electronegativity difference between I and H is 0.4, and from the above rule a coupling of

$$2290[1-(x_A-x_B)/2]=1832 \text{ Mc/sec}$$

is expected, as compared with the observed value of 1823 Mc/sec.

While these results were being prepared for publication, the note by Klein and Nethercot[8] appeared, giving results on DI. Their measurements agree with ours within their specified limits of error which, however, are some 30 times as large as our own. C. M. Johnson informs us that he is also making measurements on NO.

We wish to thank Dr. W. C. King for assistance with experimental work and Dr. M. Mizushima for helpful discussions.

[7] W. Gordy, J. Chem. Phys. **19**, 792 (1951).

[8] J. A. Klein and A. H. Nethercot, Jr., Phys. Rev. **91**, 1018 (1953).

Microwave Measurement of D_0 for CO†

F. D. BEDARD, J. J. GALLAGHER, AND C. M. JOHNSON
Radiation Laboratory, Johns Hopkins University, Baltimore, Maryland

(Received August 26, 1953)

The value of D_0 for $C^{12}O^{16}$ was determined as 189.0±0.7 kc/sec from measurements on the J=0→1 and J=1→2 rotational transitions. Also, the frequency of the J=1→2 line was determined as 230 536.59±0.52 Mc/sec.

FROM the microwave spectrum of the J=0→1 and J=1→2 transitions of $C^{12}O^{16}$ the value of D_0 for this molecule has been determined. Also, the frequency of the J=1→2 transition was determined to a high precision by combining our measurement with the previously measured frequency of the J=0→1 transition.[1]

Figure 1 shows an oscilloscope picture of the two CO absorption lines. The strong line on the right is the J=0→1 transition and the weaker line is the J=1→2 transition. This type of picture was obtained by permitting microwave energy at 1.3-mm and also at 2.6-mm wavelength to pass through the absorption cell simultaneously and be detected by one crystal. The separation between the two lines was measured by frequency modulating the klystron with a calibrated, variable-frequency oscillator to produce sidebands of the strong line. The first sideband was superimposed on the weak line, and the separation was thus given by twice the frequency of the modulating oscillator.[2] (The factor of two is due to the weak line being twice the frequency of the strong one.)

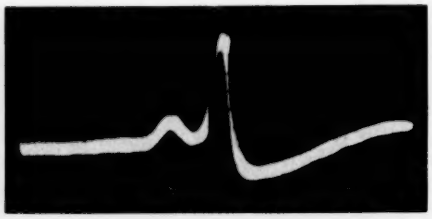

FIG. 1. Oscilloscope picture of the J=0→1 (right) and J=1→2 (left) transitions of CO at liquid air temperature. The frequencies of the lines are 115 270.56 and 230 536.59 Mc/sec, respectively.

The microwave energy at 1.3 and 2.6 mm was obtained from a crystal harmonic generator driven by a 1-cm Raytheon klystron. The absorption cell was a 7-foot length of silver waveguide 0.280×0.140 inches in cross section. The measurements were made at liquid air temperature, for which purpose the cell was encased in a brass tube insulated with two inches of styrofoam.

The frequencies of the rotational transitions of a diatomic molecule in the ground vibrational state are:

$$\nu = 2B_0(J+1) - 4D_0(J+1)^3,$$

where J=0, 1, 2, ···, $B_0 = h/8\pi^2 cI_0$, and $D_0 = 4B_0^3/\omega^2$. From this relation the frequency separation of the J=0→1 and the J=1→2 lines comes out to be $24D_0$. The measured value of $24D_0$ obtained in this experiment is 4.535±0.016 Mc/sec, thus giving a value of 189.0±0.7 kc/sec or $(6.30\pm0.03)\times10^{-6}$ cm^{-1} for D_0. This value is in fair agreement with $D_0 = 6.4_5\times10^{-6}$ cm^{-1} obtained by Herzberg and Rao[3] from infrared data.

The frequency of the J=1→2 transition was found to be 230 536.59±0.52 Mc/sec by subtracting our value for $24D_0$ from twice the measured frequency of the J=0→1 line (given as 115 270±0.25 Mc/sec in reference 1).

The measurement of D_0 is of value in the determination of the velocity of light by the method used by Rank[4] of Pennsylvania State College.

† This research was supported by the Bureau of Ordnance, U. S. Navy.

[1] Gilliam, Johnson, and Gordy, Phys. Rev. **78**, 140 (1950).

[2] Dailey, Kyhl, Strandberg, Van Vleck, and Wilson, Phys. Rev. **70**, 984 (1946).

[3] G. Herzberg and K. N. Rao, J. Chem. Phys. **17**, 1099 (1949).

[4] Rank, Ruth, and Vander Sluis, Phys. Rev. **86**, 799 (1952).

The Dissociation of H_2^+ by Electron Impact*

EDWARD H. KERNER†
Department of Physics, Iowa State College, Ames, Iowa
(Received August 3, 1953)

The collision (in Born approximation) of electrons with H_2^+, in which the molecule is raised from the ground state to the lowest lying repulsive state and is therewith dissociated, is discussed as the simplest example of a collision resulting in molecular dissociation. Both the angular distribution of dissociated protons and the excitation of the molecule to a state of definite angular momentum are investigated, and the connection between them is made clear. For the former, rules giving the dominant characteristics of the angular distribution are stated and illustrated by an example; for the latter, a detailed example is given which brings out the scope of the Franck-Condon principle and shows that near the energy of dissociation that gives the Franck-Condon maximum of the scattering amplitude there are also other sizable maxima, i.e., the Franck-Condon principle has a sort of fine structure.

INTRODUCTION

As the cross section for excitation by electron impact of a vibrational state of a diatomic molecule in a fixed electronic state is very small,[1] it is clear that dissociation of the molecule by an impinging charge must occur predominantly through an alteration of the electronic state from one which gives nuclear binding to one which gives nuclear repulsion. Roscoe[2] and Massey and Mohr[3] have examined the excitation of H_2 to various electronic states; the latter consider the dissociation of the molecule, but without regard to the angular distribution of dissociated atoms or to the details of nuclear motions that reveal details of the Franck-Condon principle. In this report we study, as the simplest example of molecular dissociation, an electron collision with H_2^+ that raises the molecule from the ground $1s\sigma\ ^2\Sigma_g^+$ state to the $2p\sigma\ ^2\Sigma_u^+$ repulsive state; we shall show in what sense the Franck-Condon principle has a structure and shall bring out the character of the angular distribution of dissociated atoms. Though several simplifying approximations will be made, the quantitative nature of the results will not be seriously forsaken. We shall treat the collision in Born approximation (neglecting electron exchange effects[4]), the molecular motions in the usual Born-Oppenheimer approximation with the simplest type of molecular-electronic wave functions, the repulsive motion of the protons in the final continuum state by means of essentially a Coulomb field, the initial vibrational motion by means of Fues's diatomic molecule model, and shall introduce some approximations of a mathematical sort.

REDUCTION OF THE SCATTERING AMPLITUDE

In Fig. 1 we label the coordinates of the protons $(\frac{1}{2}\boldsymbol{\rho}, -\frac{1}{2}\boldsymbol{\rho})$, incident electron $(\mathbf{R})$, and molecular electron $(\mathbf{r})$, reckoned from the center of mass which we place at the midpoint of the protons. The Born amplitude for scattering of the incident electron with excitation of the target from the state $\varphi_0(\mathbf{r}, \boldsymbol{\rho})$ to the state $\varphi_k(\mathbf{r}, \boldsymbol{\rho})$ is

$$f_k = -\frac{1}{4\pi}\frac{2m}{\hbar^2}\int e^{i\mathbf{K}\cdot\mathbf{R}}\varphi_k^* v\varphi_0 d\mathbf{r}d\boldsymbol{\rho}d\mathbf{R}, \tag{1}$$

$\mathbf{K}$ being the electron momentum change $\mathbf{k}_0-\mathbf{k}_k$, with $k_i^2=(2m/\hbar^2)(E-E_i)$, $E=\frac{1}{2}m\dot{R}^2+E_0$, and E_i the energy of the ith target eigenstate; v is the interaction energy

$$v=-\frac{e^2}{|\mathbf{R}-\frac{1}{2}\boldsymbol{\rho}|}-\frac{e^2}{|\mathbf{R}+\frac{1}{2}\boldsymbol{\rho}|}+\frac{e^2}{|\mathbf{R}-\mathbf{r}|}.$$

For the target eigenfunctions we write $\varphi_0=\psi_0(\rho, \mathbf{r})\chi_0(\boldsymbol{\rho})$ and $\varphi_k=\psi_k(\rho, \mathbf{r})\chi_k(\boldsymbol{\rho})$, the ψ representing electronic wave functions and depending parametrically on the nuclear separation ρ, the χ representing wave functions for the nuclear motion. Using the well-known simple linear combination of atomic orbitals for the ψ, we write (in atomic units):

$$\begin{aligned}\psi_0&=U_0[u(r_1)+u(r_2)],\\ \psi_k&=U_k[u(r_1)-u(r_2)],\\ U_k^0&=2^{-\frac{1}{2}}[1\pm e^{-\rho}(1+\rho+\tfrac{1}{3}\rho^2)]^{-\frac{1}{2}},\end{aligned} \tag{2}$$

with $u(r)=\pi^{-\frac{1}{2}}e^{-r}$; r_1 and r_2 are radial distances, measured from the protons as centers, of the molecular electron. Because of the orthogonality of φ_k and φ_0 in

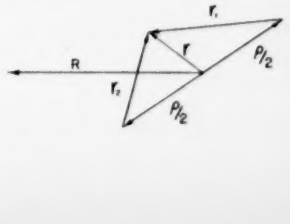

FIG. 1. Labels of the coordinates for an electron $(\mathbf{R})$ impinging on H_2^+ (molecular electron, $\mathbf{r}$; protons, $\frac{1}{2}\boldsymbol{\rho}$ and $-\frac{1}{2}\boldsymbol{\rho}$).

* The research reported in this paper has been sponsored by the Geophysics Research Directorate of the Air Force Cambridge Research Center, Air Research and Development Command.

† Present address: Physics Department, University of Buffalo, Buffalo, New York.

[1] E. H. Kerner, Phys. Rev. **91**, 1174 (1953).

[2] R. Roscoe, Phil. Mag. **31**, 349 (1941).

[3] H. S. W. Massey and C. B. O. Mohr, Proc. Roy. Soc. (London) **A135**, 258 (1932).

[4] This neglect is justifiable so long as the incident electron energy is not too low, which it mustn't be anyway for the validity of the Born results. See N. F. Mott and H. S. W. Massey, *The Theory of Atomic Collisions* (Clarendon Press, Oxford, 1949), Chaps. 8 and 11.

the coordinate $\mathbf{r}$, the terms $e^2/|\mathbf{R}\pm\frac{1}{2}\boldsymbol{\rho}|$ in v drop out. The integration over $d\mathbf{R}$ gives $(4\pi/K^2)\exp(i\mathbf{K}\cdot\mathbf{r})$, so that (using atomic units throughout now)

$$f_k=-\frac{2}{K^2}\int e^{i\mathbf{K}\cdot\mathbf{r}}[u^2(r_1)-u^2(r_2)]d\mathbf{r}U(\rho)\chi_k^*\chi_0 d\boldsymbol{\rho}, \quad (3)$$

$$U(\rho)\equiv U_0(\rho)U_k(\rho).$$

Introducing, by Fig. 1, $\mathbf{r}=\mathbf{r}_1+\frac{1}{2}\boldsymbol{\rho}=\mathbf{r}_2-\frac{1}{2}\boldsymbol{\rho}$ for the integrals in $d\mathbf{r}$ involving $u^2(r_1)$ and $u^2(r_2)$, respectively, gives, on carrying out the $\mathbf{r}$ integration,

$$f_k=\frac{-64i}{K^2(4+K^2)^2}\int \sin\tfrac{1}{2}(\mathbf{K}\cdot\boldsymbol{\rho})U(\rho)\chi_k^*\chi_0 d\boldsymbol{\rho}$$

$$=\frac{-64i}{K^2(4+K^2)^2}J(k,K). \quad (4)$$

J will be referred to as the radial integral.

We observe before going ahead that the use of the simple ψ's of Eq. (2) is probably better than might be expected at first sight. For, if better electronic wave functions of the form[5]

$$\psi_0\sim e^{-ar_1}+e^{-ar_2}, \quad \psi_k\sim e^{-br_1}-e^{-br_2},$$

(where a and b are functions of ρ) had been used one would have, instead of $u^2(r_1)-u^2(r_2)$ in Eq. (3), the $\mathbf{r}$ integral

$$\int e^{i\mathbf{K}\cdot\mathbf{r}}\{e^{-(a+b)r_1}-e^{-(a+b)r_2}+[e^{-ar_2-br_1}-e^{-ar_1-br_2}]\}d\mathbf{r}.$$

The contribution to this from the terms in square brackets will be small, at least for the range of small K that is of most importance, while $a(\rho)+b(\rho)$ stays very nearly constant at two (see Fig. 32 of reference 5) down to ρ that are of any consequence in the remaining $\boldsymbol{\rho}$ integral; the latter contains, for example, the ground state vibrational wave function which is strongly peaked at the relatively large equilibrium nuclear separation distance, and what happens at smaller ρ, where $a+b$ rises, will have negligible effects.

PROPERTIES OF THE RADIAL INTEGRAL

$J(k,K)$ contains now the desired information on the angular distribution of dissociated protons (one of which goes off bearing an electron) and of scattered electrons, and on the range of continuum states χ_k that can be significantly excited.

The χ_0 and χ_k are eigenstates of the Hamiltonians for the nuclear motions in initial and final states:

$$\left(-\frac{1}{2\mu}\nabla_\rho^2+V_{0,k}\right)\chi_{0,k}=E_{0,k}\chi_{0,k}, \quad (5)$$

where $V_{0,k}(\rho)$ are the effective nuclear potential energies in these states and μ is the reduced molecular mass. The radial parts of $\chi_{0,k}$, which describe the vibrational motions, satisfy

$$R_{0,k}''+\frac{2}{\rho}R_{0,k}'+\left(2\mu E_{0,k}-2\mu V_{0,k}-\frac{l(l+1)}{\rho^2}\right)R_{0,k}=0, \quad (6)$$

and the angular parts are spherical harmonics. For χ_0 let us take a definite rotation-vibration state,

$$\chi_0=P_{lm}(\cos\theta)e^{im\varphi}R_0(\rho), \quad (7)$$

the polar axis being taken along $\mathbf{K}$ for convenience. In order to answer the question, what is the amplitude for scattering of the incident electron into some small solid angle when the protons dissociate along a specified axis within a small solid angle and with a specified energy in a small energy range, we must normalize χ_k suitably. If the wave function Ψ for the whole problem be written in the usual way as

$$\Psi=e^{i\mathbf{k}\rho\cdot\mathbf{R}}\varphi_0(r,\rho)+\psi_{\text{scatt}},$$

the normalization of χ_k must be chosen so as to provide that ψ_{scatt} in the limit of *large rho* shall give an outward radial flux. The normalization is similar to that for the problem of the ionization of a hydrogen atom by electron impact,[6] and is such that χ_k^* (and not χ_k) has the asymptotic form

$$\chi_k^*\to e^{-ik\rho\cos\theta'}+\frac{e^{ik\rho}}{\rho}g(\theta') \quad (8)$$

$$\cos\theta'=\cos\theta\cos\theta_0+\sin\theta\sin\theta_0\cos(\varphi-\varphi_0),$$

θ_0, φ_0 being the orientation of the axis of dissociation with respect to the polar axis $\mathbf{K}$, and k^2 being $2\mu E_k$; we may place $\varphi_0=0$ by choosing the plane of $\mathbf{k}(\theta_0,\varphi_0)$ and $\mathbf{K}$ to be the xz plane.

The correctly normalized χ_k for fixed k may be built up from the radial functions $R_l(k\rho)$ of Eq. (6) as

$$\chi_k=\sum_s A_s R_s(k\rho)P_s(\cos\theta').$$

Then, using the addition theorem for Legendre functions and writing $x=\cos\theta$, $J(k,K)$ is of the form

$$J(k,K)=\sum_s\sum_{m'=-s}^{+s}\int \sin(\tfrac{1}{2}K\rho x)P_{lm}(x)e^{im\varphi}P_{sm'}(x)$$

$$\times P_{sm'}(x_0)e^{-im'\varphi}dxd\varphi A_s^*R_s^*UR_0\rho^2 d\rho, \quad (9)$$

whence only $m'=m$ in the $\sum_{m'}$ contributes. Since $\sin(\frac{1}{2}K\rho x)$ is odd in x and $P_{jm}(-x)=(-1)^{j-m}P_{jm}(x)$, we have that only those terms in $\sum_s$ contribute for which $l+s$ is odd. Hence, the scattering amplitude for scattered electrons and dissociated protons is given by a superposition of $P_{sm}(\cos\theta_0)$ that is either even or odd

[5] N. F. Mott and I. N. Sneddon, *Wave Mechanics and Its Applications* (Clarendon Press, Oxford, 1948), Sec. 33.

[6] H. S. W. Massey and C. B. O. Mohr, Proc. Roy. Soc. (London) **A140**, 613 (1933). See also reference 4, Chaps. 11 and 14.

under $\theta_0 \to \pi - \theta_0$ according as l is odd or even. This states formally what is expected from the symmetry properties of the original amplitude f_k of Eq. (1) and the symmetry of Ψ in the proton coordinates. Note that for m different from zero and for any l no dissociation occurs in the direction $\theta_0 = 0$, and that for $m = 0$ and even l (only odd s terms in $J(k, K)$) no dissociation occurs in the direction $\theta_0 = \pi/2$: thus, for excitation from the ground state there is no dissociation at right angles to **K**. Also for m different from zero there will be no dissociation in the direction $\theta_0 = \pi/2$ when m is odd and l is odd (only even s terms) and when m is even and l even (only odd s terms).

The angular distribution of dissociated protons will be dominated by the terms $P_{l\pm1,m}(\cos\theta_0)$ in $J(k, K)$, so that, for example, if the molecule is initially in the rotational ground state the dissociated protons will have mainly a $\cos^2\theta_0$ distribution; or if the initial state is an $l = 1$ state a spherically symmetric component to the distribution will be important. It is therefore relevant to ask directly for the amplitude for excitation to a state of definite l and E_k (within dE_k), understanding from the preceding discussion that we thereby find a contribution, more or less important depending on what l we select, to the angular distribution of dissociated protons. Also this amplitude will be of interest in itself, apart from questions of angular distribution in the dissociation. In what follows, the main discussion will be around this amplitude but we shall also consider the angular distribution in a little further detail.

EVALUATION OF THE RADIAL INTEGRAL

In Fig. 2 we exhibit the correct[7] potential curves A and B for the nuclear motions in initial and final states, and simple approximations thereto, F and C respectively, that are sufficient to our purposes. F is the Fues potential

$$V_0(\rho) = -D + (2\pi\nu_0)^2\mu\rho_0^2\left(\frac{1}{2} - \frac{\rho_0}{\rho} + \frac{1}{2}\frac{\rho_0^2}{\rho^2}\right),$$

where D, ν_0, ρ_0 are potential curve depth, frequency of small oscillations about equilibrium, and equilibrium nuclear separation. C is a Coulomb potential plus an additive constant chosen to make the potential agree with A near ρ_0,

$$V_k = -\epsilon_0 + \frac{1}{\rho}, \quad \epsilon_0 = 0.65.$$

We should really cut C off at $\rho_1 = (\epsilon_0 - \frac{1}{2})^{-1} = 6.67$ and continue it as C', but little harm will be done by leaving it alone, as ρ_1 is far from the interesting region immediately around ρ_0; we merely restrict the eigenvalue E_k of Eq. (6) to $E_k > -\frac{1}{2}$. V_k of course does not have the detailed structure[7] of A but nevertheless is an adequate representation of it.

[7] E. Teller, Z. Physik **61**, 458 (1930).

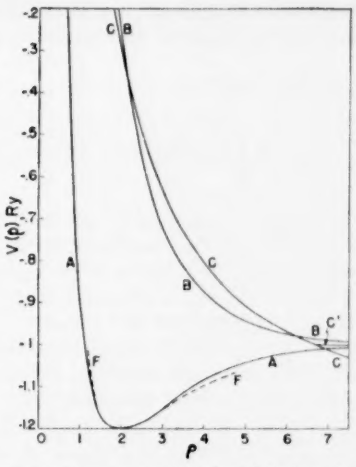

FIG. 2. Potential curves for initial and final nuclear motions. A and B are the correct curves (after Teller, reference 7), F and C, respectively, are the approximate curves that are used, F being the Fues potential, C begin the Coulomb potential $-1.3+2/\rho$ Rydberg. It suffices to use C everywhere, though, strictly, it should be cut off and continued as C'. The nuclear separation ρ is in atomic units.

The vibrational ground-state wave function $R_0(\rho)$ is

$$R_0 = N_0\rho^\lambda e^{-\alpha\rho}, \quad N_0 = \frac{(2\alpha)^{\lambda+1}}{(2\lambda+2)!^{\frac{1}{2}}}, \tag{10}$$

with $\lambda = -\frac{1}{2} + \frac{1}{2}(1+4b)^{\frac{1}{2}}$, $\alpha = (\lambda+1)^{-1}(\rho_0/2b)^{-1}$, and $b = 4\pi^2\nu_0^2\mu^2\rho_0^4/\hbar^2$. The continuum functions $R_k(\rho)$ are

$$R_{k,l} = N_k\rho^l e^{-ik\rho}F(l+1-i\beta, 2l+2, 2ik\rho) = N_k F_l(k\rho), \tag{11}$$

where $\beta = \mu/k$, $k^2 = 2\mu(E_k + \epsilon_0)$, and N_k is a suitable normalization constant; for later use we introduce also $\kappa^2 = 2(E_k + \epsilon_0)$.

The function $U(\rho) = U_0(\rho)U_k(\rho)$ that enters into $J(k, K)$ is a smooth function varying slowly and monotonically near ρ_0 and diverging for small ρ as ρ^{-1}. It can be replaced for purposes of manageability of the ρ integration by a function of the form $a + b\rho^{-1}\exp(-c\rho)$ with very good accuracy; but this is unnecessary because with respect to U, $R_0(\rho)$ is practically a delta function around ρ_0. It would be sufficient to take U outside the integral as $U(\rho_0)$, but at no extra cost we improve on this by representing $U(\rho)$ as c_0/ρ with c_0 adjusted so that $U(\rho_0) = c_0/\rho_0$; this gives $c_0 = 1.234$.

The radial integral for the transition $(0, l, m) \to (k, t, m')$, say, is now, apart from constant factors,

$$J(k, K) \sim \int \sin(\tfrac{1}{2}K\rho x)P_{lm}(x)P_{tm'}(x)e^{i(m-m')\varphi} \times dx\,d\varphi F_t(k\rho)\rho^\lambda e^{-\alpha\rho}\rho\,d\rho, \tag{12}$$

so that $m = m'$ and l and t must be of different parity. We shall discuss a special case of this, illustrative of more general cases, in order to avoid complicating the

analysis needlessly. To this end we set $l=m=0$. Expanding $\sin(\frac{1}{2}K\rho x)$ in Legendre functions then gives

$$J_t(k, K)=c_0N_0N_k(2t+1)^{\frac{1}{2}} \times\int_0^\infty j_t(\tfrac{1}{2}K\rho)\rho^{\lambda+1}e^{-\alpha\rho}F_t(k\rho)d\rho, \quad (13)$$

where j_t represents the spherical Bessel function and t is an odd integer. For the small-angle scattering of the incident electron $j_t(\frac{1}{2}K\rho)$ may be replaced by $(\pi^{\frac{1}{2}}/(t+\frac{1}{2})!\cdot 2^{2t+1})(K\rho)^t$, and it is at once clear that $t=1$ is by far the most important of all t (J has to be multiplied by K^{-2} to give the amplitude f_k); in terms of our earlier discussion, $\cos^2\theta_0$ dominates the angular distribution of dissociated protons. Reversing the roles of l and t above we obtain the scattering amplitude for the transition from different initial l states to the continuum $t=0$ state; for $l=1$ in particular we are then evaluating the important spherically symmetric contribution to the proton angular distribution for scattering of electrons off the molecule initially in the first rotational state. Detailed results will later be given for this special case as an illustrative example.

For sufficiently small K, which in practice will often cover the whole range of K of primary interest, Eq. (13) involves the integral

$$S(n, t)=\int_0^\infty \rho^n e^{-\alpha\rho}e^{-ik\rho}F(t+1-i\beta, 2t+2, 2ik\rho)d\rho, \quad (14)$$

with $n=\lambda+t+1$ for short. We evaluate S by making use of the representation of the confluent-hypergeometric and hypergeometric functions as contour integrals:[8]

$$F(a, c, x)=\frac{N\Gamma(c)}{\Gamma(a)\Gamma(c-a)} \times\int \exp\left(\frac{xz}{1+z}\right)z^{a-1}(1+z)^{-c}dz, \quad (15)$$

$$F(a, b, c, x)=\frac{N\Gamma(c)}{\Gamma(a)\Gamma(c-a)} \times\int [1+(1-x)z]^{-b}z^{a-1}(1+z)^{b-c}dz. \quad (16)$$

When the real part of $\alpha>0$, $N=1$ and the contour is a straight line from 0 to ∞. For larger K the whole spherical Bessel function must be used, and in any particular case may be written as a combination of trigonometric functions and inverse powers of $\frac{1}{2}K\rho$.

[8] W. Gordon, Ann. Physik 2, 1031 (1929).

Then Eq. (13) involves integrals of the form

$$T\left(n, t, \begin{matrix}c\\ s\end{matrix}\right)=\begin{matrix}\mathrm{Re}\\ \mathrm{Im}\end{matrix}\int_0^\infty \rho^n e^{-\alpha\rho}e^{-ik\rho}e^{\frac{1}{2}iK\rho} \times F(t+1-i\beta, 2t+2, 2ik\rho)d\rho. \quad (17)$$

The Re, Im refer to the real, imaginary parts with respect to iK as first written, but because $F_t(k\rho)$ is itself real, the real and imaginary parts of the whole final result may be taken as well.

Introducing Eq. (15) into Eq. (14) gives

$$S(n, t)=\frac{\Gamma(2t+2)}{\Gamma(t+1-i\beta)\Gamma(t+1+i\beta)}\int\int \rho^n \times\exp\left\{-\rho\left[\alpha+ik-\frac{2ikz}{1+z}\right]\right\}\frac{z^{t-i\beta}}{(1+z)^{2t+2}}dzd\rho$$

$$=\frac{\Gamma(2t+2)}{|\Gamma(t+1+i\beta)|^2}n!(\alpha+ik)^{-n-1} \times\int\frac{z^{t-i\beta}}{(1+z)^{2t+1-n}}(1+zv)^{-n-1}dz, \quad (18)$$

with

$$v=(\alpha-ik)/(\alpha+ik).$$

Using Eq. (16),

$$S(n, t)=n!(\alpha+ik)^{-n-1} \times F(1+t-i\beta, n+1, 2t+2, 1-v). \quad (19)$$

Similarly

$$T\left(n, t, \begin{matrix}c\\ s\end{matrix}\right)=\begin{matrix}\mathrm{Re}\\ \mathrm{Im}\end{matrix}n!(\alpha+ik-\tfrac{1}{2}iK)^{-n-1} F(1+t-i\beta, n+1, 2t+2, 1-u), \quad (20)$$

$$u=(\alpha-ik-\tfrac{1}{2}iK)/(\alpha+ik-\tfrac{1}{2}iK).$$

By a change of variable in Eq. (18) or by

$$F(a, b, c, x)=(1-x)^{-a}F(a, c-b, c, x/(x-1)),$$

Eq. (19) may be written

$$S(n, t)=n!(\alpha+ik)^{-n+t-i\beta}(\alpha-ik)^{-1-t+i\beta} \times F(1+t-i\beta, 2t+1-n, 2t+2, -2ik/(\alpha-ik)), \quad (21)$$

and similarly for T. Now n is in general a large number since λ is large; numerically λ is 38.10 (and α is almost exactly $\frac{1}{2}\lambda$). If we round off λ to an integral value no serious error is committed and then (except for very large t) the F function in Eq. (21) is a polynomial.

Thus S and T are expressed in closed form. However, the results are complicated and we return to Eq. (18) for a more useful approximate result. We write for

Eq. (18)

$$S(n,t)=\frac{\Gamma(2t+2)}{|\Gamma(t+1+i\beta)|^2}n!(\alpha+ik)^{-n-1}\int Q(z)\times\exp\left\{i(n+1)\left[\Omega-\frac{\beta}{n+1}\log z\right]\right\}dz, \quad (22)$$

with

$$Q(z)=\frac{z^t[\mathrm{Re}(1+zv)]^{-n-1}}{(1+z)^{2t+1-n}}=\frac{z^t}{(1+z)^{2t+1-n}}(1+z^2v_0^2+2zv_0\cos\omega)^{-(n+1)/2},$$

$$\Omega(z)=-\arg(1+zv)=\tan^{-1}\frac{zv_0\sin\omega}{1+zv_0\cos\omega},$$

where v_0 is $|v|$ and

$$\omega=-\arg v=2\tan^{-1}(k/\alpha).$$

For T one has a similar result involving u instead of v. Integrating along the real axis from 0 to ∞ we are in a position to capitalize on the largeness of n by using the method of stationary phase. What we then obtain is the asymptotic form of S (or T) in the limit of both $n(\lambda)$ and $\beta=\mu/k=\mu^{\frac{1}{2}}/\kappa$ large. This seems to place an undesirable restriction on the range of κ which we may wish to examine, but it turns out that for the κ of most interest ($\kappa\sim1$), in the Franck-Condon region, β is indeed comparable with λ and it is just here that the method of stationary phase is valuable. For small κ it is advisable to proceed differently anyway (as discussed below), and for large κ one can use the asymptotic form of $R_{k,l}$ of Eq. (11) directly in the integral for $J(k,K)$ [but already in this range of κ, $J(k,K)$ is very small].

The phase

$$\varphi(z)=\Omega-\frac{\beta}{n+1}\log z$$

is stationary for the roots z_1 and z_2 of

$$\varphi'(z)=0=\frac{v_0\sin\omega}{1+z^2v_0^2+2zv_0\cos\omega}-\frac{\beta/(n+1)}{z}.$$

Both these roots are real positive if κ is not too small. We have also $\varphi''(z_1 \text{ or } z_2)=[\beta/(n+1)]/z_1^2$ or z_2^2. For Eq. (22) we get

$$S(n,t)\simeq\frac{\Gamma(2t+2)}{|\Gamma(t+1+i\beta)|^2}n!\,\mathrm{Re}(\alpha+ik)^{-n-1}\times\left\{\left(\frac{2\pi}{\beta}\right)^{\frac{1}{2}}z_1Q(z_1)\exp[i(n+1)\varphi(z_1)+\tfrac{1}{4}\pi i]+\text{same function of } z_2\right\}. \quad (23)$$

T is to be treated the same way.

When κ is sufficiently small, the region around $\rho=\rho_0$ is a region of negative kinetic energy for the proton motions and there the Coulomb functions $R_{k,l}$ [Eq. (11)] do not oscillate but vary monotonically. We have in fact that in the limit of small κ, $R_{k,l}$ and therefore $J(k,K)$ [Eq. (12)] are small. As κ increases a point will come when $R_{k,l}$ has a first large maximum near ρ_0 and joins forces with R_0 to make $J(k,K)$ large. As κ increases further $R_{k,l}$ oscillates within the range where R_0 is large and generally $J(k,K)$ becomes small again, though not uniformly with increasing κ since $R_{k,l}$ will reinforce with R_0 when the higher extrema of $R_{k,l}$ are centered near ρ_0. Thus one expects $J(k,K)$ to rise monotonically as κ first increases, pass through a relatively large principal maximum, and then oscillate with more or less rapidly decreasing amplitude. These remarks (which are of course conditioned by the K dependence of $J(k,K)$) restate the Franck-Condon principle and endow it with a "structure" which we exhibit in the example below.

We note first that for sufficiently small κ, when $R_{k,l}$ varies monotonically in ρ near ρ_0, we can without serious error pull it (or ρ times it) outside the radial integral 13:

$$J(k,K)\simeq c_0N_0N_k(2l+1)^{\frac{1}{2}}[\rho_0F_l(k\rho_0)]\times\int_0^\infty\frac{1}{\rho}j_l(\tfrac{1}{2}K\rho)\rho^{\lambda+1}e^{-\alpha\rho}d\rho. \quad (24)$$

Further, we can use a WKB approximation for $w_l(\rho_0)=\rho_0F_l(k\rho_0)$:[9]

$$w_l(\rho_0)=(2\cos\eta)^{-\frac{1}{2}}\sin^{l+1}\left(\frac{\eta+\eta_0}{2}\right)\cos^{-l}\left(\frac{\eta-\eta_0}{2}\right)\times\exp\left\{-\beta\left(\frac{\pi}{2}-\eta\right)+(l+\tfrac{1}{2})\frac{\cos\eta}{\cos\eta_0}\right\}, \quad (25)$$

$$\sin\eta=(k\rho_0-\beta)[\beta^2+(l+\tfrac{1}{2})^2]^{-\frac{1}{2}},\quad -\tfrac{1}{2}\pi<\eta<\tfrac{1}{2}\pi,$$

$$\sin\eta_0=\beta[\beta^2+(l+\tfrac{1}{2})^2]^{-\frac{1}{2}},\quad 0<\eta_0<\tfrac{1}{2}\pi.$$

ILLUSTRATIVE EXAMPLE

As indicated before, we illustrate our general results by the example: initial state, $l=1$; final state, $l=0$. This amplitude for transition to a final state of definite angular momentum gives also the large spherically symmetric component of the angular distribution of dissociated protons resulting from the dissociation of the molecule in the assumed initial rotational state.

[9] Yost, Wheeler, and Breit, Phys. Rev. **49**, 174 (1936).

For small K we have,[10] from the discussion above,

$$J(k, K)=c_0N_0N_k(3^{\frac{1}{2}}K/6)S(\lambda, 0), \tag{26}$$

and for larger K,

$$J(k, K)=c_0N_0N_k3^{\frac{1}{2}}\left\{\frac{T(\lambda-1, 0, s)}{\frac{1}{4}K^2}-\frac{T(\lambda, 0, c)}{\frac{1}{2}K}\right\}. \tag{27}$$

For sufficiently small κ and also small K,

$$J(k, K)=c_0N_0N_k(3^{\frac{1}{2}}K/6)w_0(\rho_0)(\lambda+1)!/\alpha^{\lambda+2}, \tag{28}$$

while for small κ and larger K,

$$J(k, K)=c_0N_0N_k3^{\frac{1}{2}}w_0(\rho_0)$$
$$\times\left\{\frac{(\lambda-2)!}{\frac{1}{4}K^2(\alpha^2+\frac{1}{4}K^2)^{(\lambda-1)/2}}\sin\left(\tan^{-1}\frac{K}{2\alpha}\right)\right.$$
$$\left.-\frac{(\lambda-1)!}{\frac{1}{2}K(\alpha^2+\frac{1}{4}K^2)^{\lambda/2}}\cos\left(\tan^{-1}\frac{K}{2\alpha}\right)\right\}. \tag{29}$$

We normalize the continuum function on the $W=\frac{1}{2}k^2$ scale, for which

$$N_k=\left(\frac{2k\beta}{\sinh\beta}\right)^{\frac{1}{2}}e^{-\frac{1}{2}\pi\beta}$$

in Eq. (26) and Eq. (27) but $N_k=(2/\pi k)^{\frac{1}{2}}$ in Eqs. (28) and (29).

The differential cross section per unit solid angle of the scattered electron and per unit interval of W of the dissociated protons is

$$\frac{d\sigma}{d\omega dW}=\frac{k_k}{k_0}|f_k|^2=\frac{k_k}{k_0}\frac{64^2}{K^4(4+K^2)^4}J^2(k, K),$$

and, integrating over all angles of scattering, the total cross section per dW is

$$\frac{d\sigma}{dW}=\frac{2\pi}{k_0^2}\int_{k_0-k_k}^{k_0+k_k}KdK\frac{64^2}{K^4(4+K^2)^4}J^2(k, K).$$

The units of σ are atomic units, a_0^2.

In Fig. 3 we show $j(\kappa)=J(k, K)/(3^{\frac{1}{2}}K/6)$ in the small K limit, when this quantity is independent of K, as a function of κ (here the continuum function is normalized on the κ scale). The principal extremum is for κ very close to 1. The neighboring extrema are by no means negligible: the Franck-Condon principle clearly has a structure to it, as previously remarked. Considering the small range of κ in which $J(k, K)$ is large, this structure is to be considered a fine structure.

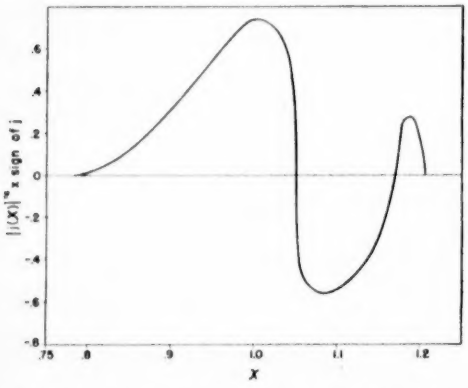

FIG. 3. Illustration of the fine structure of the Franck-Condon principle. $j(\kappa)$ is proportional to the radial integral $J(k, K)$ which gives the scattering amplitude. This example is for the dissociation of H_2 from the initial $l=1$ state to the final $l=0$ state. $j(\kappa)$ for a small region around $\kappa=0.94$ was found by interpolation; the error of the approximation used is such that $j(\kappa)$ should descend somewhat more steeply to the left of the principal maximum than is shown.

[10] The roles of l and l in the previous discussion are reversed, as remarked after Eq. (13).

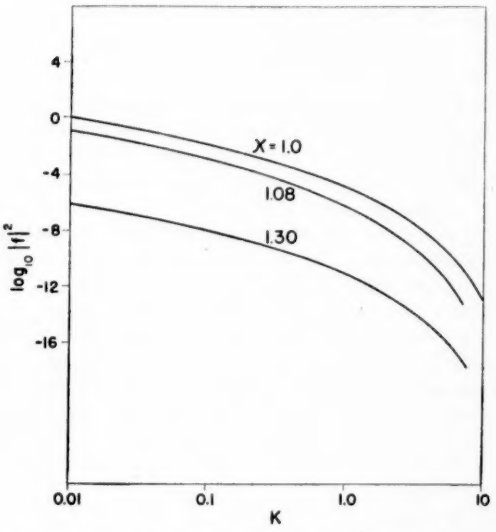

FIG. 4. The modulus of the scattering amplitude, $|f_k|^2$, which gives the differential cross section $d\sigma/d\omega dW$ for the same process as in Fig. 3, for several κ (the upper two curves belong to the κ corresponding to the first extrema of $j(\kappa)$; atomic units are used throughout.

FURTHER REMARKS ON ANGULAR DISTRIBUTION OF DISSOCIATED PROTONS

We conclude by sketching the analysis that gives the complete angular distribution of dissociated protons, leaving a fuller discussion for a later report.

In Fig. 4 we plot $|f_k|^2$ against K for several κ to show the angular distribution of scattered electrons; and in Fig. 5 we give the total cross section $d\sigma/dW$ for $\kappa=1$.

The correctly normalized final-continuum wave function[6] χ_k^* here, apart from a normalization constant, is

$$\chi_k^* = e^{ik\rho}\int_0^\infty y^{i\beta}e^{-y}J_0[2(ik\xi' y)^{\frac{1}{2}}]dy, \quad \xi' = \rho(1+\cos\theta'),$$

with $\cos\theta'$ as given in Eq. (8). Taking the initial state as the ground state, and writing $\sin(\frac{1}{2}\mathbf{K}\cdot\boldsymbol{\rho})$ $(=\sin\frac{1}{2}Kz$, $\mathbf{K}$ being the polar axis) in exponential form, the radial integral to within constant factors is

$$J(k, K) = \int\int \rho^{\lambda-1}e^{-\alpha\rho}e^{ik\rho}e^{\frac{1}{2}iK\rho}y^{i\beta}e^{-y}J_0 dt d\boldsymbol{\rho} - \text{s.f.}(-K), \quad (30)$$

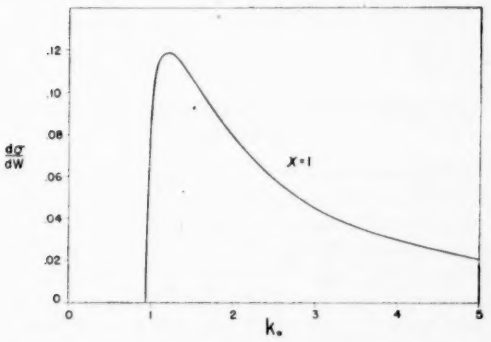

FIG. 5. Total cross section $d\sigma/dW$ for the same process as in Fig. 3, for dissociation of H_2^+ to a continuum state at $\kappa=1$ within dW near where the cross section is largest. Atomic units are used for k_0, units of πa_0^2 for σ.

where s.f.$(-K)$ means "same function of $-K$." Introducing parabolic coordinates $\xi=\rho(1+\cos\theta)$, $\eta=\rho(1-\cos\theta)$, φ, $d\boldsymbol{\rho}=\frac{1}{2}\rho d\xi d\eta d\varphi$, Eq. (30) may be written

$$J(k, K) = \tfrac{1}{2}(-1)^\lambda\frac{\partial^\lambda}{\partial\alpha^\lambda}\int \exp\{-\tfrac{1}{2}\alpha(\xi+\eta)+\tfrac{1}{4}iK(\xi-\eta) + \tfrac{1}{2}ik(\xi+\eta)\}y^{i\beta}e^{-y}J_0 dt d\xi d\eta d\varphi - \text{s.f.}(-K).$$

This integral has been treated by Massey and Mohr.[6] One uses the addition theorem for J_0, making use of the fact that

$$\xi' = \xi\cos^2\tfrac{1}{2}\theta_0 + \eta\sin^2\tfrac{1}{2}\theta_0 + 2(\xi\eta)^{\frac{1}{2}}\cos\tfrac{1}{2}\theta_0\sin\tfrac{1}{2}\theta_2\cos\varphi,$$

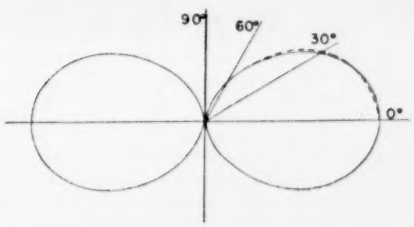

FIG. 6. Angular distribution of dissociated protons resulting from electrons impinging on H_2 in the ground state according to Eq. (32) (solid curve) in comparison with a $\cos^2\theta_0$ distribution (dotted curve) which, as discussed in the text, should dominate the distribution. The two agree everywhere to within 1½ percent. The solid curve refers to the data $\kappa=1.4$, $k_0=10$, $K=$smallest value (electron scattering in the forward direction); in this case θ_0 is measured from the axis $\mathbf{k}_0$ which is the same as $\mathbf{K}$.

and finds after reduction

$$J(k, K) = 4\pi(-1)^\lambda\frac{\partial^\lambda}{\partial\alpha^\lambda}(i\beta)! \times\frac{[(\alpha-ik-\frac{1}{2}iK)(\alpha-ik+\frac{1}{2}iK)]^{i\beta}}{[\alpha^2+k^2+\frac{1}{4}K^2-kK\cos\theta_0]^{i\beta+1}} - \text{s.f.}(-K). \quad (31)$$

This may be evaluated by writing the derivative as a Cauchy integral and choosing a suitable steepest descent contour in the complex α plane. [Actually it is better to lump $\exp(-\alpha\rho)$ and $\exp(ik\rho)$ together in Eq. (30) and take the derivatives with respect to $\alpha-ik$.]

It is apparent from Eq. (31) that, as discussed before, $J(k, K)$ vanishes for $\theta_0=\pi/2$ and there is no dissociation in the direction perpendicular to $\mathbf{K}$.

For sufficiently large k, χ_k may be adequately represented by the plane wave $\exp(i\mathbf{k}\cdot\boldsymbol{\rho})$. Then the evaluation of $J(k, K)$ is elementary and gives

$$J(k, K) = \frac{\sin(\lambda+1)\omega_0}{K_0(\alpha^2+K_0^2)^{(\lambda+1)/2}} - \frac{\sin(\lambda+1)\omega_1}{K_1(\alpha^2+K_1^2)^{(\lambda+1)/2}}, \quad (32)$$
$$K_{1,0}^2 = k^2+\tfrac{1}{4}K^2 \pm kK\cos\theta_0,$$
$$\omega_{1,0} = \tan^{-1}(K_{1,0}/\alpha).$$

Since the initial state has been taken as a state of zero angular momentum, we expect from our earlier discussion that the angular distribution of dissociated protons will be dominated by $\cos^2\theta_0$. In Fig. 6, where the distribution arising from Eq. (32) is compared with a $\cos^2\theta_0$ distribution, this is verified. The two agree to within slightly more than one percent for all θ_0.

The author is indebted to Miss Pauline Thielman for assistance with the numerical work.

Theory of the Microwave Zeeman Effect in Atomic Oxygen

A. Abragam and J. H. Van Vleck
Harvard University, Cambridge, Massachusetts
(Received August 12, 1953)

Slight deviations of the coefficient of the linear Zeeman term from the elementary Landé value arise from the following effects: (*a*) small departures from Russell-Saunders (R-S) coupling, (*b*) the motion of the nucleus, (*c*) relativity corrections, (*d*) interplay between the magnetic field and various kinds of magnetic interactions within the atom, and (*e*) the Schwinger electrodynamical corrections. In the present paper an effort is made to estimate the magnitude of the effects (*a*), (*b*), (*c*), (*d*) with the goal of examining whether the residual discrepancy between Rawson and Beringer's measurements on oxygen and the ideal Landé value is in accord with Schwinger's formula for (*e*).

The effect (*d*) may be further divided into modulation by the magnetic field, or Larmor precession, of (d_1) ordinary spin-orbit, (d_2) spin-other-orbit, and (d_3) orbit-orbit interaction. The theory for *c* and d_1 has already been developed by Margenau and Breit, and d_2 to a certain extent by Lamb, while that for *b* was first given by Phillips. The corrections (*d*) can in each case be obtained by substituting $\mathbf{p}+e\mathbf{A}/c$ for $\mathbf{p}$ in the corresponding magnetic interaction terms in the Pauli two-component Hamiltonian function, but can also be derived more fundamentally from the four-component Dirac equation. From the standpoint of the Dirac equation, the segregation of (*c*) from other magnetic effects is rather artificial, but (*c*) has the simple physical interpretation that it is tantamount to substituting the transverse mass for the rest mass in the ordinary Zeeman energy.

The numerical estimate of effects (*b*)–(*d*) requires knowing the wave functions in some detail. Certain rather crude approximations are made in the present paper, including omission of exchange terms in some places. However, the agreement between the calculated and observed Zeeman coefficients after all the corrections (*a*–*e*) are included is gratifying.

INTRODUCTION

By using quantum electrodynamics, Schwinger[1] has shown that the gyromagnetic ratio g_s of the electronic spin is $g_s=2(1+\alpha/2\pi)$, where α is the fine structure constant, rather than exactly 2, as prescribed by the one-particle Dirac theory. A higher-order approximation calculated by Karplus and Kroll[2] gives for g_s the value

$$g_s=2\left(1+\frac{\alpha}{2\pi}-2.973\frac{\alpha^2}{\pi^2}\right)\simeq 2\times 1.001145. \qquad (1)$$

These theoretical results have stimulated several very accurate measurements[3] of atomic gyromagnetic ratios or Landé factors, with microwave or molecular beam techniques to measure the Zeeman splittings of an atomic multiplet in an applied magnetic field.

From the observed values of these Landé factors one should be able in principle to deduce g_s by a straightforward calculation if the type of vector coupling prevailing in the atom is known. In practice this problem is complicated by the necessity of applying to the value of g_s obtained in this way a certain number of corrections, which take into account relativistic and diamagnetic effects, the departures from a simple vector coupling scheme, etc. The only cases considered so far have been those of a single electron outside of closed shells. The recent measurement by Rawson and Beringer[4] of the microwave Zeeman effect in atomic oxygen, which has four $2p$ electrons outside of closed shells, requires a more comprehensive treatment. The present article constitutes an attempt at such a treatment.

[1] J. Schwinger, Phys. Rev. **73**, 416 (1947).
[2] R. Karplus and N. M. Kroll, Phys. Rev. **77**, 536 (1950).
[3] P. Kusch and A. M. Foley, Phys. Rev. **74**, 250 (1948); Koenig, Prodell, and Kusch, Phys. Rev. **88**, 191 (1952).
[4] E. B. Rawson and R. Beringer, Phys. Rev. **88**, 677 (1952).

THE MICROWAVE ZEEMAN EFFECT IN ATOMIC OXYGEN

The ground state of atomic oxygen is $2p^4$. Russell-Saunders coupling is known to predominate in oxygen. From the configuration $2p^4$ the spectral terms ^3P, ^1D, ^1S can be constructed. The two singlets ^1D, ^1S are, respectively, 15 867.7 and 33 792.4 wave numbers above the ground multiplet $^3P_2$. The levels $^3P_1$ and $^3P_0$ are separated from $^3P_2$ by 158.5 and 226.5 wave numbers, respectively.

An applied magnetic field splits $^3P_1$ and $^3P_2$ into 3 and 5 magnetic sublevels, respectively. Rawson and Beringer have been able to measure the energies of the transitions *a*, *b*, *c*, *d*, *e*, *f* depicted in Fig. 1, or rather the magnetic fields at which resonances occur for a fixed oscillator frequency ν. These fields H_a, H_b, $\cdots$, H_f were measured in relative magnitude by the frequencies f_a, f_b, etc. of the proton resonance in these fields. An absolute calibration could be made from the known value of the proton moment in Bohr magnetons, $g_p/2$.

The fields used are not infinitely small and incipient Paschen-Back effect due to the off-diagonal matrix

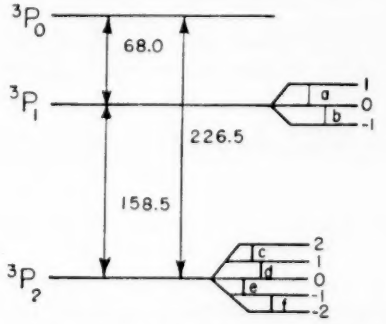

FIG. 1. Energy levels of atomic oxygen in a magnetic field.

elements of the Zeeman Hamiltonian between the different multiplets $^3P_2$, $^3P_1$, $^3P_0$ cannot be disregarded. Solving the secular equations, we find that the fields H_a, H_b, etc., are given by the following approximate equations:

$$h\nu = g_1\beta H_a + C_1 H_a^2 = g_1\beta H_b - C_1 H_b^2, \quad (2)$$

$$h\nu = g_2\beta H_c + C_2 H_c^2 = g_2\beta H_f - C_2 H_f^2, \quad (3)$$

$$h\nu = g_2\beta H_d + C_3 H_d^2 = g_2\beta H_e - C_3 H_e^2. \quad (4)$$

In these formulas β is the Bohr magneton; g_1 and g_2 the Landé factors of the multiplets $^3P_1$ and $^3P_2$; C_1, C_2, and C_3 are constants which depend on the distances between the different ^3P multiplets.

These formulas are very good approximations, for it is easily shown that terms of the third order in H are missing if Russell-Saunders coupling is assumed in the calculation of off-diagonal matrix elements, and fourth-order terms are completely negligible (smaller than one part in a million of the linear terms).

These equations have to be supplemented by the proton resonance conditions:

$$g_p\beta H_a = hf_a, \quad g_p\beta H_b = hf_b, \quad \text{etc.} \quad (5)$$

From (2) and (5) we get

$$g_1 = g_p \frac{\nu}{f_a}\left(\frac{1+f_a^2/f_b^2}{1+f_a/f_b}\right). \quad (6)$$

In the same way from (3), (4), and (5), two independent values are obtained for g_2.

It is important to notice that in (6) the Paschen-Back quadratic corrections have been eliminated experimentally rather than calculated. We can, however, calculate them by second-order perturbation theory from the known multiplet splittings. It is best to express them in terms of differences $H_a - H_b$, $H_e - H_f$, $H_d - H_e$, as is done in Table I. We see that the assumption of Russell-Saunders coupling for the calculation of the off-diagonal matrix elements works very well. (A calculation by Rawson and Beringer[4] giving 17.2 gauss for $H_b - H_a$ and indicating a very strong departure from R-S coupling was the result of an arithmetical error.)

Two other points can be made with respect to terms quadratic in H: (*a*) it follows from the agreement between the two columns of Table I that all other corrective terms in H^2, such as the quadratic diamagnetic corrections, must be small; (*b*) even if they were not small, all those corrections would be eliminated by the experimental procedure as far as determination of g_1 and g_2 are concerned.

Only corrections linear in H need to concern us.

The experimental results of Rawson and Beringer[4] are

$$g_1 = 1.500971, \quad g_2 = 1.500905, \quad (7)$$

with an uncertainty of a few parts in a million.

TABLE I. Differences between the values of magnetic fields at resonance, due to second-order effects.

	Measured	Calculated
$H_b - H_a$	10.20 gauss	10.22
$H_d - H_e$	0.581 gauss	0.580
$H_f - H_c$	1.744 gauss	1.742

On the other hand the theory for R-S coupling gives

$$g_1 = g_2 = \tfrac{1}{2}(g_l + g_s),$$

where g_l is the orbital gyromagnetic ratio. If we take g_l equal to unity and g_s as given by (1), we find

$$g_1 = g_2 = 1.501145. \quad (8)$$

The discrepancy between (7) and (8) is 174×10^{-6} for g_1 and 240×10^{-6} for g_2, which is much larger than the experimental error. These are the discrepancies which have to be explained away through the different corrections previously mentioned.

The problem of calculating these corrections can be formulated in general terms as follows: According to first-order perturbation theory, we describe the linear change in the energy of an atom, induced by an applied field H, as the expectation value of a certain operator Z (for Zeeman) taken over the unperturbed wave function ψ. Errors can result either from an incorrect choice of ψ or an incorrect Z. In the approximate theory which gave (8), we took Z to be given by $\beta\mathbf{H}\cdot(\mathbf{L}+g_s\mathbf{S})$ and ψ to be an eigenstate of L and S. Neither of these assumptions is quite correct and we shall examine them in turn.

CORRECTIONS CAUSED BY DEPARTURE FROM R-S COUPLING (WRONG ψ)

Because of magnetic interactions involving the spin, *viz.* spin-orbit, spin-other-orbit, and spin-spin interactions, L and S are not perfectly good quantum numbers. (Magnetic orbit-orbit interactions, however, do not affect R-S coupling.) Several observations are in order at this juncture.

(*a*) In the case of the $^3P_0$ and $^3P_2$ terms, perturbations by, respectively, the states ^1S and ^1D also belonging to the configuration $2p^4$ can cause deviations from Russell-Saunders coupling even if configuration interaction is neglected. In the case of the $^3P_1$ term, however, this is not the case, and here it is customarily said[5] that the departures from Russell-Saunders coupling are due to combination of magnetic (mainly spin-orbit) interactions and configuration coupling through electrostatic repulsion between electrons—for instance, a $(2p)^4\,^3P$ term may through configuration interaction get an admixture of $(2p)^3 3p\,^3P'$, and if $^3P'$ is not a pure R-S state, neither will be ^3P. It is, however, preferable to get the configuration interaction completely out of the picture by disregarding the central field approximation

[5] See, for instance, M. Phillips, Phys. Rev. **88**, 202 (1952).

from which the configuration coupling idea stems. Before spin-dependent terms are introduced L and S are good quantum numbers even though the "configuration quantum numbers" relating to individual electrons are not rigorous. For the ground state of oxygen, for instance, it is a very good approximation to say that it is ^3P, a much poorer one to say that it is $(2p^4)\,^3P$. The ideal g value is impaired only insofar as spin-dependent magnetic terms blend states of different L, S and so cause slight deviations from Russell-Saunders coupling.

(*b*) When such a blending is included, the wave function of the atom instead of being $\psi(L, S, J)$ becomes of the form

$$\psi=[\psi_0(L, S, J)+\alpha\psi'(L', S', J)](1+\alpha^2)^{-\frac{1}{2}}. \quad (9)$$

The admixture coefficient α will be of the order of magnitude $\mathfrak{M}/\Delta E$, where $\mathfrak{M}$ represents the magnetic interactions (mainly spin-orbit) and ΔE is the distance between the different R-S terms mixed together. Since the Zeeman Hamiltonian $Z=\beta H(g_l L_z+g_s S_z)$ commutes with L and S, the expectation value $\langle Z\rangle=\langle\psi|Z|\psi\rangle$, where ψ is defined by (9), will differ from $\langle\psi_0|Z|\psi_0\rangle$ only through terms quadratic in α. The correction will thus be small.

(*c*) The departure from the interval rule should not be considered as a measure of the departure from R-S coupling. In oxygen the ratio $(^3P_2-{}^3P_1)/(^3P_1-{}^3P_0)$ has the value $158.5/68=2.33$ instead of 2 exactly as required by Landé's rule. But as shown by Aller, Ufford, and Van Vleck[6] this is due mainly to the fact that the magnetic interactions which produce the Zeeman splittings are not only the spin-orbit coupling but also the spin-other-orbit and spin-spin couplings. The first-order contributions of the latter two to the intervals have no reason to, and in fact do not obey Landé's rule. The difference between 2.33 and 2.00 is in no way a measure of the admixture α from wave functions with different L and S.

The term most likely to cause any perturbation in oxygen is $^1D_2$ perturbing $^3P_2$. If we call ξ the spin-orbit coupling coefficient of a $2p$ electron, the main part of the admixture α of $^1D_2$ in $^3P_2$ is

$$\alpha=(2)^{-\frac{1}{2}}\xi/(E_D-E_P).$$

For the state $\psi=(^3P_2+\alpha\,^1D_2)(1+\alpha^2)^{-\frac{1}{2}}$, $J_z=2$, we find:

$$2g_2=\langle\psi|g_l L_z+g_s S_z|\psi\rangle=(1+\alpha^2)^{-1}(g_l+g_s+2\alpha^2 g_l)$$
$$\simeq g_l+g_s-\alpha^2(g_s-g_l),$$
$$g_2\simeq\tfrac{1}{2}(g_l+g_s)-\tfrac{1}{2}\alpha^2.$$

This gives a correction $\Delta g_2=-\frac{1}{2}\alpha^2$ to the value (8). If we take $\zeta=146.6$ (Garstang),[7] $E_D-E_P=15\,800\ \mathrm{cm}^{-1}$, we find

$$\Delta g_2\sim-21\times10^{-6}. \quad (10)$$

All other excited states in atomic oxygen which might be coupled to $^3P_1$ or $^3P_2$ through magnetic interactions, belong to different configurations (this expression has to be taken with certain reservations; the configuration is a much worse quantum number in oxygen than L or S) and are about 10^5 wave numbers away from ^3P. The nearest is $2s^2 2p^3(^4S)3p\ ^5P$, which is 86 600 wave numbers above ^3P. Although we do not know the magnitude of the matrix element of the magnetic interaction between $^3P_1$ and $3p\ ^5P_1$, there seems to be no good reason why it should be significantly larger than the one between $^3P_1$ and $^1D_1$ (the opposite is much more likely); and, the energy difference $3p\ ^5P_1-{}^3P_1$ being about 6 times larger than $^1D-{}^3P_1$, we shall expect the corresponding correction for g_1 to be smaller than 10^{-6} and disregard it.

CORRECTION TO THE ORBITAL GYROMAGNETIC RATIO CAUSED BY MOTION OF NUCLEUS

Because the nucleus has a finite rather than infinite mass, the orbital gyromagnetic ratio is not exactly unity. The general theory of the effect of the motion of the nucleus on the orbital g factor has been developed by Phillips.[8] We must make the application to the particular case of oxygen, which is somewhat more complicated than the explicit examples treated in her paper. The theory developed on the first page of her article shows that the orbital gyromagnetic factor for a neutral atom is, in general,

$$g_L=\left(1-\frac{m}{M}\right)-\frac{m}{ML_z}\langle\Phi|B_z|\Phi\rangle, \quad (11)$$

where M is the mass of the nucleus, and Φ is the wave function of the atom, inclusive of spin but exclusive of the trivial factor which depends only on the coordinates of the center of gravity and which represents a uniform translational motion of the whole atom. B_z is the z component of the vector

$$\mathbf{B}=\sum_{i<j}\mathbf{b}_{ij}, \quad (12)$$

with

$$\mathbf{b}_{ij}=\hbar^{-1}[\mathbf{r}_i\times\mathbf{p}_j+\mathbf{r}_j\times\mathbf{p}_i].$$

The quantity B_z is readily shown to be proportional in R-S coupling to the component L_z of orbital angular momentum in the direction of the applied field, and so the g factor given in (11) is independent of how the atom is oriented, as must be the case if the expression is meaningful.

In Russell-Saunders coupling the total spin S is a good quantum number and we can assume Φ to be also an eigenstate of S and S_z. We can expand Φ into a sum of Slater determinants $\Phi=\sum\alpha_p D_p$, where $D_p=(a_1, a_2, \cdots, a_z)$ and the a_i are one-electron states (spin included);

$$\langle\Phi|\mathbf{B}|\Phi\rangle=\sum_{p,p'}a_p^*a_{p'}\langle D_p|\mathbf{B}|D_{p'}\rangle. \quad (13)$$

In order to facilitate the estimate of $\langle\Phi|\mathbf{B}|\Phi\rangle$, we make the restrictive assumption that all the occupied

[6] Aller, Ufford, and Van Vleck, Astrophys. J. **109**, 42 (1949).
[7] R. H. Garstang, Monthly Notices Roy. Astron. Soc. **111**, 115 (1951).
[8] M. Phillips, Phys. Rev. **76**, 1803 (1949).

one-electron states outside of closed shells have the same parity. This is generally the case for atoms in their ground state.

It is then easy to show, by the application of the rules of calculation of Slater determinants, that because of parity and symmetry considerations, (12) reduces to

$$\langle\Phi|\mathbf{B}|\Phi\rangle_z=\sum|a_p|^2\langle D_p|\mathbf{B}|D_p\rangle_z, \tag{14}$$

and

$$\langle D_p|\mathbf{B}|D_p\rangle_z=-\sum_{i,j}\langle a_i(1)a_j(2)|\mathbf{b}_{12}|a_j(1)a_i(2)\rangle_z,$$

where a_i is an occupied one-electron state outside of closed shells and a_j is inside a closed shell and corresponds to the same spin as a_i. The existence of (14) is a consequence of the Pauli principle which establishes a correlation between electrons of the same spin.

If the expansion of the wave function in Slater determinants is known, the expression (13) can forthwith be evaluated.

We consider now the case of atomic oxygen with the electronic configuration $(2p)^4$, but all the formulas apply to the case of any atom having only s and p electrons in closed shells, and outside of closed shells p electrons only, that is, to any atom from lithium to fluorine and from aluminum to chlorine.

In that case it is easy to show that $\langle B\rangle_z/L_z$ is independent of the way in which the p electrons outside of the closed shells are coupled together (as long as it is Russell-Saunders coupling), and this quantity is given by

$$\langle B\rangle_z/L_z=-\sum_n\langle ns(1),p_+(2)|(b_{12})_z|p_+(2),ns(1)\rangle. \tag{15}$$

In (15), p_+ is the orbital state of a p electron with orbital momentum $l_z=+1$, ns is the orbital state of an s electron with principal quantum number n, and the summation is over occupied orbital s states, each orbital state being counted once only. If one uses the definition (12) of b_{ij} and the fact that for a nonrelativistic electron $p_x=mv_x=m\dot{x}$, the following alternative expressions can be given for (15):

$$\langle B\rangle_z/L_z=-(4/h)\sum_n\langle ns|x|p_+\rangle\langle p_+|p_y|ns\rangle, \tag{16}$$

$$\langle B\rangle_z/L_z=-(2/h)\sum_n\{\langle p_+|x|ns\rangle\langle ns|p_y|p_+\rangle - \langle p_+|y|ns\rangle\langle ns|p_x|p_+\rangle\}, \tag{17}$$

$$\langle B\rangle_z/L_z=-i(4m/h^2)\sum_n\langle ns|x|p_+\rangle \times\langle p_+|y|ns\rangle(E_p-E_{ns}). \tag{18}$$

In (18), E_p and E_{ns} are the total energies of the p and ns one-electron states, respectively.

If we call $f_n(r)$ and $g(r)$ the radial parts of the wave functions ns and p_+, respectively, (16) becomes

$$\langle B\rangle_z/L_z=\tfrac{2}{3}\sum_n\int_0^\infty f_n(r)g(r)r^3dr\times\int_0^\infty g(r)\frac{df_n}{dr}r^2dr. \tag{19}$$

In the same way (18) yields

$$\langle B\rangle_z/L_z=-\tfrac{2}{3}\sum_n\left(\int_0^\infty f_ngr^3dr\right)^2(E_p-E_{ns}), \tag{20}$$

where distances and energies are measured in atomic units.

Since $E_p-E_{ns}>0$, (20) shows that $\langle B\rangle_z/L_z$ is negative and therefore according to (11) the orbital gyromagnetic factor is larger than $1-(m/M)$.

In order to estimate g_L numerically for oxygen, we have evaluated (19) by using Slater's[9] analytical wave functions, and (20) by using Hartree's[10] self-consistent wave functions for oxygen. In both cases it is found that the contribution of the $1s$ orbital is negligible compared with $2s$.

Slater functions and (19) lead to

$$\langle B\rangle_z/L_z=-\tfrac{5}{6},$$

$$g_L=1-\frac{m}{M}(1-\tfrac{5}{6})=1-\frac{m}{6M}.$$

The Hartree wave functions and (20) give $\int f_2gr^3dr=1.15$ (by numerical integration or use of Lowdin's[10] analytical representation) and $E_p-E_{2s}=1.22$, thus leading to

$$\langle B\rangle_z/L_z=-\tfrac{2}{3}(1.16)^2(1.22)=-1.11.$$

Believing the Hartree functions to be a less crude approximation for this problem than the Slater wave functions, we henceforth use the formula:

$$g_L\simeq 1+0.11(m/M) \text{ for oxygen.} \tag{21}$$

RELATIVISTIC AND DIAMAGNETIC CORRECTIONS

The general problem of the relativistic and diamagnetic corrections in a complex atom like oxygen is somewhat complicated, and it is instructive to review first the previous work on the subject.

Relativistic correction.—Breit[11] and Margenau,[12] both of Yale University, have calculated the magnetic moment of a Dirac electron in a central field $V(r)$ and derived the correction to be applied to the result of the nonrelativistic calculation which uses as a nonrelativistic Zeeman Hamiltonian:

$$Z_0=\beta\mathbf{H}\cdot(\mathbf{l}+2\mathbf{s}). \tag{22}$$

For brevity we shall refer to it as the Breit-Margenau or Yale correction. In these calculations the magnetic field is taken into account by replacing $\mathbf{p}$ by $\mathbf{p}+e\mathbf{A}/c$ in the relativistic Dirac Hamiltonian,

$$\mathcal{H}=c(\mathbf{p}\cdot\boldsymbol{\alpha})+\beta mc^2+V.$$

[9] J. C. Slater, Phys. Rev. **36**, 57 (1930).
[10] Hartree, Hartree, and Swirles, Trans. Roy. Soc. (London) **A238**, 229 (1939); see also the empirical analytical representation of the Hartree results by P. O. Löwdin, Phys. Rev. **90**, 120 (1953).
[11] G. Breit, Nature **122**, 649 (1928).
[12] H. Margenau, Phys. Rev. **57**, 383 (1940).

Here and elsewhere $\mathbf{A}=\frac{1}{2}(\mathbf{H}\times\mathbf{r})$ is the vector potential from which the magnetic field is derived.

The relativistic interaction between the electron and the external magnetic field is $Z=e(\boldsymbol{\alpha}\cdot\mathbf{A})$ and the expectation value $\langle Z\rangle$ of this expression gives the change in the energy of the electron produced by the applied field $\mathbf{H}$, and is thence a measure of the magnetic moment of the electron. In the case of slow electrons with kinetic energy much smaller than the rest mass, Margenau[12] gives the following expressions for the magnetic moment of the electron expressed in Bohr magnetons:

$$\begin{aligned} l&=j-\tfrac{1}{2},\quad \mu=(j+\tfrac{1}{2})\left[1-\frac{2j+1}{j+1}\frac{\bar{T}}{2mc^2}\right],\\ l&=j+\tfrac{1}{2},\quad \mu=\frac{j}{j+1}(j+\tfrac{1}{2})\left[1-\frac{2j+1}{j}\frac{\bar{T}}{2mc^2}\right], \end{aligned} \tag{23}$$

where $\bar{T}$ is the average kinetic energy of the electron. Written in this form these formulas are not very suitable for an atom like oxygen where R-S coupling prevails. Also the physical nature of the Yale correction does not appear very clearly.

We recalculate this correction by using the well-known method of reduction of Dirac's equations to large components. In this method, a nonrelativistic operator Z' is derived such that its expectation value taken over the nonrelativistic wave function agrees with the relativistic expectation value $\langle Z\rangle$ within $(v/c)^2$.

A straightforward calculation gives

$$Z'=\beta\mathbf{H}\cdot(\mathbf{l}+2\mathbf{s})\left(1-\frac{T}{mc^2}\right)+\frac{\beta}{mc^2}\mathbf{s}\cdot(\nabla V\times\mathbf{A}). \tag{24}$$

Using integration by parts and Schrödinger's equation, one can show that the second term of (24) is equivalent to

$$-\beta\mathbf{H}\cdot\left\{\frac{(\mathbf{r}\cdot\mathbf{s})}{r^2}\mathbf{r}-\mathbf{s}\right\}\frac{T}{mc^2},$$

and (24) can be rewritten as

$$Z'=\beta\mathbf{H}\cdot(\mathbf{l}+2\mathbf{s})\left(1-\frac{T}{mc^2}\right)-\beta H\cdot\left\{\frac{(\mathbf{r}\cdot\mathbf{s})\mathbf{r}}{r^2}-\mathbf{s}\right\}\frac{T}{mc^2}. \tag{25}$$

It is easy to show that the expectation value of (25) reduces to (23).

Equation (24) admits a simple physical interpretation. If in the nonrelativistic Zeeman Hamiltonian Z_0 given by (22) we replace the mass m of the electron by its relativistic value $m(1-v^2/c^2)^{-\frac{1}{2}}$ and expand $(1-v^2/c^2)^{\frac{1}{2}}$ as $1-\frac{1}{2}v^2/c^2$, we obtain the first part of (24).

The second part is obtained as follows. In the absence of a magnetic field, there is a term in the nonrelativistic Hamiltonian of the electron representing the spin-orbit coupling which can be written as

$$(\hbar/2mc^2)(\nabla V\times\mathbf{p})\cdot\mathbf{s}. \tag{26}$$

The introduction of the magnetic field modifies the spin-orbit coupling, since it changes the velocity $\mathbf{p}/m$ of the electron by adding to it the extra velocity resulting from the Larmor precession of the electron in the magnetic field. This is equivalent to replacing $\mathbf{p}$ by $\mathbf{p}+e\mathbf{A}/c$ in (26). If we do so, we obtain the second term of (24).

We see that (24) could have been written straightaway without mentioning Dirac's equation simply using the relativistic variation of the mass with velocity and Larmor's theorem. However, we naturally feel safer with the authority and rigor of Dirac's equation behind us. We can say that the first part of the Yale correction, $-\beta\mathbf{H}\cdot(\mathbf{l}+2\mathbf{s})T/mc^2$, is the relativistic-correction proper. It depends only on the velocity of the electron and will always be there whatever the electromagnetic interactions between the electron and its surroundings, nuclei or other electrons. The second part, $(\beta/mc^2)\mathbf{s}\cdot(\nabla V\times\mathbf{A})$, is the result of velocity-dependent interactions between the electron and its surroundings (in the present case the central field gradient) which are modified by the change in the velocity of the electron due to Larmor precession. Both parts of the Yale correction are sometimes referred to in the literature as the relativity correction, as they disappear in the limit $c=\infty$; the same property also, however, applies to our remaining magnetic corrections which are superposed when there is more than one electron and which we discuss in the following sections. We therefore prefer to use the term relativity correction only in connection with the first part of (25).

Lamb's diamagnetic correction.—Lamb[13] has considered the case of an electron outside of a core formed of closed shells. In an external field a current is induced in the core, caused by the Larmor precession of the electrons in this field. It is given by $\mathbf{j}=(e^2/mc)\rho\mathbf{A}$, where ρ is the electronic density in the core. This current in turn produces a vector potential,

$$\mathbf{A}'(r)=-\frac{e^2}{mc^2}\int\frac{\mathbf{A}(\mathbf{r}')\rho(\mathbf{r}')}{|\mathbf{r}-\mathbf{r}'|}d\tau'. \tag{27}$$

Lamb then considers the interaction of the spin magnetic moment of the valence electron with the magnetic field $\mathrm{rot}\mathbf{A}'$:

$$\langle\beta\boldsymbol{\sigma}\cdot\mathrm{rot}\mathbf{A}'\rangle. \tag{28}$$

This gives an extra term in the Hamiltonian, proportional to the external field $\mathbf{H}$, which results in a correction to the magnetic moment of the electron.

Since Lamb considers s electrons only, he retains solely the spherically symmetrical part of the interaction (28). For the same reason he does not consider any diamagnetic effects resulting from orbit-orbit interaction. We shall use the term Lamb correction for (28) rather than the less general expression valid for s electrons only that Lamb derives from (28).

[13] W. Lamb, Phys. Rev. **60**, 817 (1941).

The general case.—We are now ready to tackle the general problem of the corrections to the magnetic moment of a complicated atom like oxygen.

We know that in an atom there are velocity dependent interactions between electrons, the so-called Breit interactions, as well as interactions between the electrons and the nucleus. Their contribution $\mathcal{K}$ to the non-relativistic Hamiltonian is written below:

$$(A)\quad \mathcal{K}=-\frac{Ze^2\hbar}{4m^2c^2}\sum_i\left[\nabla_i\left(\frac{1}{r_i}\right)\times\mathbf{p}_i\right]\cdot\boldsymbol{\sigma}_i \tag{29}$$

$$(B)\quad +\frac{e^2\hbar^2}{4m^2c^2}\sum_{i\neq k}\left[\nabla_i\left(\frac{1}{r_{ik}}\right)\times\mathbf{p}_i\right]\cdot\boldsymbol{\sigma}_i$$

$$(C)\quad +\frac{e^2\hbar^2}{4m^2c^2}\sum_{i\neq k}\left[\nabla_i\left(\frac{1}{r_{ik}}\right)\times\mathbf{p}_i\right]\cdot 2\boldsymbol{\sigma}_k$$

$$(D)\quad -\frac{e^2}{2m^2c^2}\sum_{i<k}\left[\frac{1}{r_{ik}}(\mathbf{p}_i\cdot\mathbf{p}_k)+\frac{1}{r_{ik}^3}(\mathbf{r}_{ik}\cdot(\mathbf{r}_{ik}\cdot\mathbf{p}_i)\cdot\mathbf{p}_k)\right].$$

(D) is written in this complicated fashion because of the noncommutability of $\mathbf{p}_i$ and $\mathbf{r}_{ik}$. These interactions which were first written by Heisenberg on a purely phenomenological basis were derived by Breit[14] by reduction to the large components of the following Hamiltonian:

$$\mathcal{H}_{\text{int}}=-Ze^2\sum_i\frac{1}{r_i}+\sum_{i<k}\frac{e^2}{r_{ik}}-\frac{e^2}{2}\sum_{i<k}\left[\frac{(\boldsymbol{\alpha}_i\cdot\boldsymbol{\alpha}_k)}{r_{ik}}+\frac{(\boldsymbol{\alpha}_i\cdot\mathbf{r}_{ik})(\boldsymbol{\alpha}_k\cdot\mathbf{r}_{ik})}{r_{ik}^3}\right]. \tag{30}$$

The last term of (30) represents the retarded velocity-dependent interactions between electrons up to the order $(v/c)^2$ and is sometimes referred to as the Möller interaction.

The reduction of the first term of (30) leads to the terms (A) in (29); the second, $\sum e^2/r_{ik}$, gives through reduction the term (B) of (29); the third or last term of (30) gives (C) and (D) of (29).

The reduction of (30) gives, of course, other terms than (29), but these are independent of velocity and do not concern us.

We will account for the presence of the magnetic field by replacing in (29) all the $\mathbf{p}$'s by $\boldsymbol{\pi}=\mathbf{p}+e\mathbf{A}/c$.

It is not obvious that this is the correct procedure. We know, for instance, that if in the nonrelativistic Hamiltonian $(\mathbf{p}^2/2m)+V$ we replace $\mathbf{p}$ by $\mathbf{p}+e\mathbf{A}/c$ we completely miss the coupling $\beta\boldsymbol{\sigma}\cdot\mathbf{H}$ of the spin with the external field. It is in the Dirac equations themselves that we must replace $\mathbf{p}$ by $\mathbf{p}+e\mathbf{A}/c$ and then carry the reduction along the lines which lead from (30) to (29).

This somewhat tedious calculation is not reproduced here. It shows that it is indeed correct to replace $\mathbf{p}$ by $\mathbf{p}+e\mathbf{A}/c$ in (29), since all extra terms resulting from the non-commutability of the $\boldsymbol{\pi}$'s (as opposed to the $\mathbf{p}$'s) cancel out.

If after replacing $\mathbf{p}$ by $\mathbf{p}+e\mathbf{A}/c$ in (29) we write out all the terms linear in $\mathbf{A}$ and add to these the relativistic correction proper, $-\beta\mathbf{H}\cdot(\mathbf{l}+2\mathbf{s})\overline{T}/mc^2$ for each electron, we find that all the relativistic and diamagnetic corrections are represented by the expectation value of the following (nonrelativistic) operator:

$$\begin{aligned}\delta Z=&-\beta\mathbf{H}\cdot\textstyle\sum_i(\mathbf{l}_i+2\mathbf{s}_i)T_i/mc^2\\&-(\beta Ze^2/2mc^2)\textstyle\sum_i[\nabla_i(1/r_i)\times\mathbf{A}_i]\cdot\boldsymbol{\sigma}_i\\&+(e^2/2mc^2)\beta\textstyle\sum_{i\neq k}[\nabla_i(1/r_{ik})\times\mathbf{A}_i]\cdot\boldsymbol{\sigma}_i\\&+(e^2/2mc^2)\beta\textstyle\sum_{i\neq k}[\nabla_i(1/r_{ik})\times\mathbf{A}_i]\cdot 2\boldsymbol{\sigma}_k\\&-(e^2/2m^2c^3)\textstyle\sum_{i\neq k}[r_{ik}^{-1}(\mathbf{A}_i\cdot\mathbf{p}_k)\\&\qquad+r_{ik}^{-3}(\mathbf{r}_{ik}\cdot\mathbf{A}_i)(\mathbf{r}_{ik}\cdot\mathbf{p}_k)].\end{aligned} \tag{31}$$

Our problem is now solved in principle. If one has a good set of atomic wave functions (self-consistent Hartree-Fock functions are available for oxygen,[10]) all one needs is to write the wave function of the whole atom as a sum of Slater determinants and take the expectation value of (31) for it. This is perfectly possible in principle and should allow a reasonably accurate estimate of the relativistic and diamagnetic corrections.

Although straightforward in principle, this calculation is lengthy because of the somewhat complicated nature of the operator (31) and of the numerical integrations involved in the use of Hartree functions. We shall introduce simplifying approximations into this calculation.

Except for the first two terms, (31) is a sum of two-particle operators, and its expectation value taken over an antisymmetric wave function involves contributions from exchange matrix elements of the type

$$\int\int\psi_i^*(1)\psi_k^*(2)W(1,2)\psi_k(1)\psi_i(2)d\tau_1d\tau_2,$$

where ψ_i and ψ_k are one-electron wave functions. For simplicity we shall drop them.

We shall then be able to show that then the expectation value of (31) reduces to the sum of the Yale correction, the Lamb correction, and an extra term coming from the orbit-orbit interaction which Lamb did not consider since he dealt with s electrons only.

Let us consider the second and third terms of (31) and in these terms focus our attention more particularly on the spin of, say, electron one.

The terms containing this spin can be written

$$\frac{\beta}{2mc^2}\left[\nabla_1\left(-\frac{Ze^2}{r_1}+\sum_{k\neq 1}\frac{e^2}{r_{1k}}\right)\times\mathbf{A}_1\right]\cdot\boldsymbol{\sigma}_1. \tag{32}$$

With our convention to disregard the exchange matrix

[14] G. Breit, Phys. Rev. **34**, 553 (1929).

elements, the expectation value of (32) can be written as

$$(\beta/2mc^2)\int \psi_1^*(1)[\nabla_1 V\times \mathbf{A}_1]\cdot\boldsymbol{\sigma}_1\psi_1(1)d\tau_1, \quad (33)$$

where

$$V(1)=-\frac{Ze^2}{r_1}+\sum_{k\neq 1}\int \psi_k^*(2)\frac{e^2}{r_{12}}\psi_k(2)d\tau_2. \quad (34)$$

We call ψ_k the wave function of the electron, spin included. Unless specified otherwise the integration over $d\tau$ includes summation over spin variables. If we observe that (34) is precisely the definition of the self-consistent potential energy of electron one, we find that (33) is the second part of the Yale correction, i.e., the expectation value of the last term of (24).

From comparison of (24), (31), and (33), it is seen that the first three terms of (31) represent the sum of the Yale corrections for all the electrons of the atom. It is, of course, obvious that only electrons outside of closed shells give a nonvanishing contribution to this correction.

(*b*) If we apply the same considerations to the fourth term of (31), its expectation value gives a sum of terms such as

$$-\frac{\beta e^2}{mc^2}\int \psi_1^*(1)\boldsymbol{\sigma}_1\cdot \mathrm{rot}\left[\int \frac{\mathbf{A}(2)\rho(2)}{|\mathbf{r}_1-\mathbf{r}_2|}d\tau_2\right]\psi_1(1)d\tau_1, \quad (35)$$

with $\rho(2)=\sum_{k\neq 1}\psi_k^*(2)\psi_k(2)$. From (27) and (28) we see that (35) is precisely the Lamb correction for electron one, which we have to sum over all the electrons of the atom. Here again only electrons outside of closed shells contribute, but the fields acting on these electrons usually come from closed shells.

(*c*) *Finally*, the expectation value of the last term of (31) gives for electron one:

$$-\frac{e^3}{2mc^3}\int \psi_1^*(1)\left\{2\int \frac{\rho(2)\mathbf{A}(2)}{|\mathbf{r}_1-\mathbf{r}_2|}d\tau_2 - \nabla_1\left[\int \frac{\{(\mathbf{r}_1-\mathbf{r}_2)\cdot\mathbf{A}(2)\}\rho(2)d\tau_2}{|\mathbf{r}_1-\mathbf{r}_2|}\right]\right\}\cdot\mathbf{p}_1\psi_1(1)d\tau_1, \quad (36)$$

and we have to add contributions from all electrons. Again only electrons outside from closed shells contribute.

CALCULATION OF RELATIVISTIC AND DIAMAGNETIC CORRECTIONS IN OXYGEN

We have now broken down our corrections into three different groups, the Breit-Margenau or Yale correction, the Lamb correction, and the orbit-orbit correction. Let us consider them in turn:

(*a*) *Breit-Margenau correction.*—The Breit-Margenau correction is the expectation value of the parts of (25) proportional to T/mc^2 for each electron. It is easy to show that for a p electron in a state defined by $l_z=m_l$, $s_z=m_s$, with the z axis along the field, this can be rewritten as the expectation value of

$$-\beta H(T/mc^2)[m_l+\tfrac{1}{3}m_s(8-2m_l^2)]. \quad (37)$$

We can calculate the expectation value of (37), summed for the four $2p$ electrons for the states $^1D_2$, $J_z=2$ and $^3P_2$, $J_z=2$. The corresponding energy corrections for $^1D_2$, $^3P_2$ for $J_z\neq 2$ then follow immediately since, with given J, general rotational transformation properties require them to be proportional to the magnetic quantum number J_z. The energy corrections for $^3P_1$ can be found by utilizing the invariance of the diagonal sum for $J_z=1$ in the same way as in Goudsmit's calculation of multiplet constants, thus avoiding the need of including nondiagonal elements omitted in passing from (25) to (37). The resulting alterations to the g factors are found to be

$$\Delta g_1=-\frac{\bar{T}}{mc^2}, \quad \Delta g_2=-\frac{12}{10}\frac{\bar{T}}{mc^2}.$$

To estimate $\bar{T}$ we can

(1) Calculate

$$-(\hbar^2/2m)\int \psi_{2p}^*\nabla^2\psi_{2p}d\tau$$

for Slater's rough analytical wave functions. The result is $\bar{T}/mc^2=1.36\times 10^{-4}$.

(2) Make the same calculation using Löwdin's quite accurate analytical representation of Hartree's wave functions. This gives 1.36×10^{-4}.

(3) Calculate the kinetic energy by subtracting the potential from the total energy, with the integrals evaluated numerically with Hartree wave functions. One thus obtains 1.24×10^{-6}.

In the light of (1), (2), and (3) we take

$$\bar{T}/mc^2=1.3\times 10^{-4}.$$

The result is then

$$\Delta g_1=-130\times 10^{-6}, \quad \Delta g_2=-156\times 10^{-6}. \quad (38)$$

This value of $\bar{T}$ is considerably higher than those considered in discussions of atomic beams experiments on alkalies. This fact is not surprising. In oxygen each $2p$ electron is imperfectly screened from the nucleus by the other three $2p$ electrons, and spends more time near the nucleus where potential and kinetic energy both have large absolute values.

(*b*) *Lamb correction.*—The Lamb correction is given for each electron by (35). We make the further simplifying assumption that

$\rho(2)=\sum_{k\neq 1}\psi_k^*(2)\psi_k(2)$ has spherical symmetry.

This is equivalent to replacing the probability distribution of all the electrons acting on the one under consideration (but not the probability density of this electron itself) by its average over the angles. Then $\rho(2)$

becomes a spherically symmetrical function $\rho(r_2)$. The expression (35) can be rewritten as

$$-\frac{\beta e^2}{mc^2}\left\langle \boldsymbol{\sigma}_1 \cdot \mathrm{rot} \int \frac{\mathbf{A}(2)}{|r_1-r_2|}\rho(2)d\tau_2 \right\rangle, \quad (39)$$

where the expectation value is to be taken over the wave function of electron one. (39) can be rewritten as

$$-(\beta e^2/mc^2)\langle \boldsymbol{\sigma}_1 \cdot \mathrm{rot}[\mathbf{A}(1)V(r_1)]\rangle,$$

where the spherically symmetrical function $V(r_1)$ is defined by:

$$V(r)=\tfrac{1}{3}[V(r)+W(r)],$$

$$V(r)=\frac{1}{r^3}\int_0^r r'^4\rho(r')dr', \quad W(r)=\int_r^\infty r'\rho(r')dr'. \quad (40)$$

If we take $\mathbf{H}$ along the z axis, (39) becomes

$$-(e^2/mc^2)\beta H\langle \sigma_z\{\tfrac{1}{6}(3\cos^2\theta-1)V(r)+\tfrac{1}{3}W(r)\}\rangle. \quad (41)$$

Here θ is the angle between $\mathbf{r}$ and the z axis. Only the second, spherically symmetrical part of (41) was considered by Lamb.

For a $2p$ wave function, (41) is equal to

$$-\beta H\langle \sigma_z\{\tfrac{1}{3}W-\tfrac{1}{5}(m_l^2-\tfrac{2}{3})V\}/(137)^2\rangle, \quad (42)$$

where V and W are to be taken in Hartree atomic units.

This leads to the following corrections:

$$\Delta g_1=-\tfrac{1}{3}\{\bar{W}-\tfrac{1}{2}\bar{V}\}/(137)^2,$$
$$\Delta g_2=-\tfrac{1}{3}\{\bar{W}+\tfrac{1}{10}\bar{V}\}/(137)^2. \quad (43)$$

In (42) and (43) all the distances are expressed in atomic units. We postpone the estimate of $\bar{V}$ and $\bar{W}$ until after the orbit-orbit correction has been considered.

(*c*) *The orbit-orbit correction.*—The orbit-orbit correction is given by (36). If the density $\rho(2)$ is spherically symmetrical the second term in the large bracket is easily seen to vanish. Then (36) yields:

$$-(e^3/2m^2c^3)\int \psi_1^*(1)[\mathbf{H}\times\mathbf{r}_1]\cdot V(r_1)\mathbf{p}_1\psi_1(r)d\tau_1, \quad (44)$$

where V is defined by (40).

The expression (44) can be rewritten as

$$-(\beta e^2/mc^2)\mathbf{H}\cdot\langle \mathbf{l}V\rangle. \quad (45)$$

This results in the following corrections for g_1 and g_2:

$$\Delta g_1=\Delta g_2=-\tfrac{1}{6}(\bar{V}+\bar{W})/(137)^2. \quad (46)$$

To estimate $\bar{V}$ and $\bar{W}$, we use Slater's wave functions. We find for $\bar{V}$ and $\bar{W}$ expressed in atomic units:

$$\bar{V}=1.27, \quad \bar{W}=2.2.$$

In Table II we recapitulate all the corrections from the beginning.

TABLE II. Corrections to g_1 and g_2.

Type of correction	Corrections in units of 10^{-6} Δg_1	Δg_2
Departures from R-S coupling	0	−21
Orbital moment (nuclear motion)	+2	+2
Breit-Margenau from (37)	−130	−156
Lamb from (43)	−28	−42
Orbit-orbit from (46)	−31	−31
Total	−187	−248

The totality of corrections added to (8) gives

$$g_1=1.500958, \quad g_2=1.500897.$$

For comparison the experimental values are [see Eq. (7)]

$$g_1=1.500971, \quad g_2=1.500905.$$

The agreement is excellent, but doubtless partly accidental. The smoothing due to the neglect of exchange matrix elements and averaging over the angles of the density ρ has probably reduced the difference between Δg_1 and Δg_2.

Beringer's experimental measurements can hence be regarded as essentially a confirmation of, or at least, in good accord with, the Schwinger electrodynamical corrections. It is instructive to express the results in the form of a theoretical g factor inclusive of only the electrodynamical correction, and experimental values correspondingly corrected for everything but the electrodynamical effect. The Schwinger theory then gives [see Eq. (8)]

$$g_1=g_2=1.501145,$$

and experiment gives

$$g_1=1.501158, \quad g_2=1.501153.$$

It is, of course, the deviations from the simple Landé value 1.5 which are significant.

The agreement could presumably be improved by more accurate numerical calculations. Notably we have omitted the exchange terms in certain places [see remarks following Eq. (31)] and we have used only crude wave functions to evaluate (40). A subtle and difficult refinement would be to base the calculations on wave functions for groups of electrons rather than simply additively from unpolarized single electron wave functions in the usual Hartree-Fock fashion.

The authors are indebted to Professors Norman Ramsey and Robert Karplus for stimulating discussions, to Professor E. R. Beringer for communication of experimental results in advance of publication and to Miss Lesley Gerould for assistance in computing. They also wish to thank the Shell Oil Company whose research grant supported one of them (A.A.) during the past year.

Energies and Angular Distributions of Neutrons from $Be^9(d,n)B^{10}$†

J. S. PRUITT,* C. D. SWARTZ, AND S. S. HANNA
Department of Physics, Johns Hopkins University, Baltimore, Maryland
(Received September 11, 1953)

The angular distributions of neutrons from $Be^9(d,n)B^{10}$, leading to the five lowest states of B^{10}, have been measured at a bombarding energy $E_d=0.945$ Mev. These distributions are compared with previous data for $Be^9(d,p)Be^{10}$. In both cases there is evidence for the deuteron stripping process. Interpretation of the distributions is discussed. Excitation energies are obtained for the B^{10} states.

I. INTRODUCTION

THE bombardment of Be^9 by deuterons, followed by emission of a neutron or proton, leads to the formation of nuclei containing ten nucleons: B^{10} states may have isotopic spin 0 or 1, Be^{10} states only isotopic spin 1. Up to an excitation energy $E_x=4$ Mev (the region studied in the present investigation) there are five states in B^{10} but only two states in Be^{10}.[1] The second excited state of B^{10} ($E_x=1.74$ Mev) and the ground state of Be^{10} have been identified as the $T_3=0$ and -1 components of a $T=1$ state. The other four states of B^{10} have $T=0$.[2]

With bombarding energies of several Mev these reactions proceed chiefly by deuteron stripping, as shown by investigations of the angular distributions.[1] The general shape of the angular distributions in stripping depends only on the orbital angular momentum l for the captured particle. It is found that $l=1$ for all the states discussed here, hence the angular distributions for stripping are all very similar.

At low bombarding energies, on the other hand, the $Be^9(d,p)Be^{10}$ reaction appears to proceed chiefly by compound nucleus formation.[3] In this case one would expect that the distributions should depend to some extent on the detailed properties of the final states.

At intermediate bombarding energies (in the neighborhood of 1 Mev) the $Be^9(d,p)Be^{10}$ distributions[3,4] appear to contain contributions from both processes.[5] Evidence for stripping can also be seen in the distributions for other (d,p) and (d,n) reactions in this energy

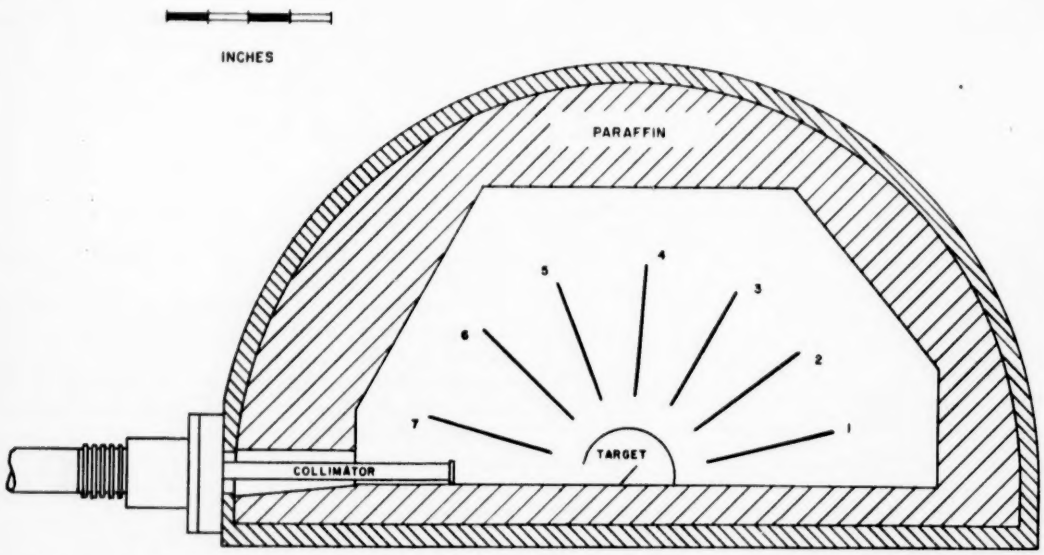

FIG. 1. Plan view of target chamber showing positions of plates 1 to 7. Deuteron beam enters through collimator from left.

† Assisted by a contract with the U. S. Atomic Energy Commission.
* Now at the National Bureau of Standards, Washington, D. C
[1] F. Ajzenberg and T. Lauritsen, Revs. Modern Phys. **24**, 321 (1952). The experimental work on these reactions is summarized in this review article.
[2] Bockelman, Browne, Sperduto, and Buechner, Phys. Rev. **90**, 340 (1953).
[3] I. Resnick and S. S. Hanna, Phys. Rev. **82**, 463 (1951).
[4] F. L. Canavan, Phys. Rev. **87**, 136 (1952).
[5] W. W. True and L. Diesendruck, Phys. Rev. **87**, 381 (1952).

range.[6] It was of interest therefore to examine the angular distributions for $Be^9(d,n)B^{10}$ at a deuteron energy $\sim$1 Mev to determine the extent to which these two processes contribute to this reaction, to investigate the dependence of the distributions on the properties of the various final states in B^{10}, and to obtain a comparison of the distributions for all seven states of Be^{10} and B^{10}.

II. EXPERIMENTAL ARRANGEMENT

A 0.1-mg/cm² beryllium target (approximately 30 kev thick for 1-Mev deuterons) evaporated on 1/64-in. copper backing was mounted in the cast-aluminum target chamber shown in Fig. 1. The target was bombarded with a 1/8-in. diameter beam of 0.96-Mev deuterons from the Van de Graaff accelerator in this department. The total exposure for this experiment was approximately 2 microampere-hours.

Neutrons from the target were detected by recoil proton tracks in Ilford C-2 nuclear plates (emulsion thickness 100 microns) placed inside the target chamber at several angles as shown in Fig. 1. The near edge of each plate was approximately 5 cm from the target.

TABLE I. Calculated Q values (Mev) for $Be^9(d,n)B^{10}$ and excitation energies E_x (Mev) for B^{10} states.

θ_{lab}	Q_1	Q_2	Q_3	Q_4	Q_5
12.4°	4.45	3.73	2.65	2.25	0.76
35.8°	4.44	3.71	2.70	2.21	0.75
60.4°	4.42	3.71	2.66	2.23	0.76
85.5°	4.43	3.70	2.64	2.24	0.80
110.8°	4.39	3.67	2.65	2.20	0.75
137.1°	4.44	3.64	2.65	2.23	0.75
Average	$Q=4.43\pm0.08$	3.69 ± 0.07	2.66 ± 0.06	2.23 ± 0.06	0.76 ± 0.05
	$E_x=0.00$	0.74 ± 0.11	1.77 ± 0.10	2.20 ± 0.10	3.67 ± 0.09

Charged particles from several competing reactions were stopped by a 0.008-in. brass shield surrounding the target. Back-scattering of neutrons from the chamber walls was minimized by a lining of paraffin, as shown.

Seven plates were exposed and then developed simultaneously to be sure that they received identical treatment. Approximately identical areas on plates 1 through 6 were scanned[7] for recoil proton tracks with a Zeiss-Winkel GF-375 binocular microscope, using a Bausch and Lomb 40× fluorite oil immersion objective, N.A. 1.00, and Bausch and Lomb 15× Hyperplane eyepieces. This equipment was very satisfactory for the present work. The field of view is about 270 microns in diameter, and depth measurements made with the fine focus adjustment (after correction for curvature of field) are reproducible to within 1/2 micron.

[6] W. Whaling and T. W. Bonner, Phys. Rev. **79**, 258 (1950); Krone, Hanna, and Inglis, Phys. Rev. **80**, 603 (1950); D. N. F. Dunbar and F. Hirst, Phys. Rev. **83**, 164 (1951); Australian J. Sci. Research **4**, 268 (1951); J. R. Risser and W. H. Burke, Phys. Rev. **85**, 742 (1952).

[7] Plate 7 was accidentally fogged and could not be scanned.

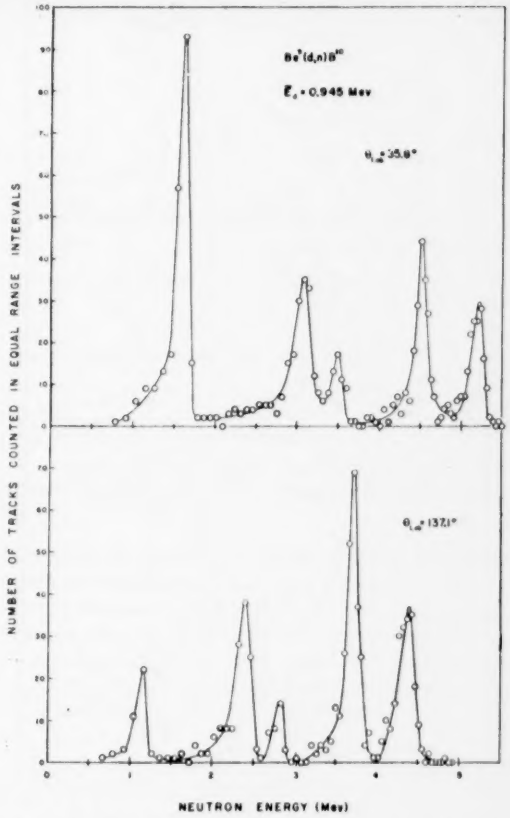

FIG. 2. Recoil proton spectra. Ordinate is the number of acceptable proton tracks counted in equal intervals of proton range. For the abscissa, proton range has been converted to neutron energy.

III. MEASUREMENT OF NEUTRON ENERGIES AND ANGULAR DISTRIBUTIONS

Neutron energies were calculated from the observed recoil proton track lengths and directions by methods similar to those described by others.[8,9] Proton tracks were accepted for measurement only if the horizontal recoil angle measured from the assumed neutron direction[10] was not more than 15° and if the dip angle in the processed emulsion was not more than 4.8°. A standard range-energy curve[11] was used to convert proton range to proton energy. Figure 2 shows two examples

[8] Johnson, Laubenstein, and Richards, Phys. Rev. **77**, 413 (1950).

[9] W. M. Gibson and D. L. Livesey, Proc. Phys. Soc. (London) **A60**, 523 (1948).

[10] Since the emulsion area scanned was only 6 cm from the target, it was not adequate to assume that all neutrons moved parallel to the center line of the plate. Instead, the plate was mapped in sectors each subtending 1½° at the center of the target. In each sector, it was assumed that neutrons moved parallel to the midline of the sector and in the plane of the emulsion.

[11] Lattes, Fowler, and Cuer, Proc. Phys. Soc. (London) **A59**, 883 (1947); N. Nereson and F. Reines, Rev. Sci. Instr. **21**, 534 (1950).

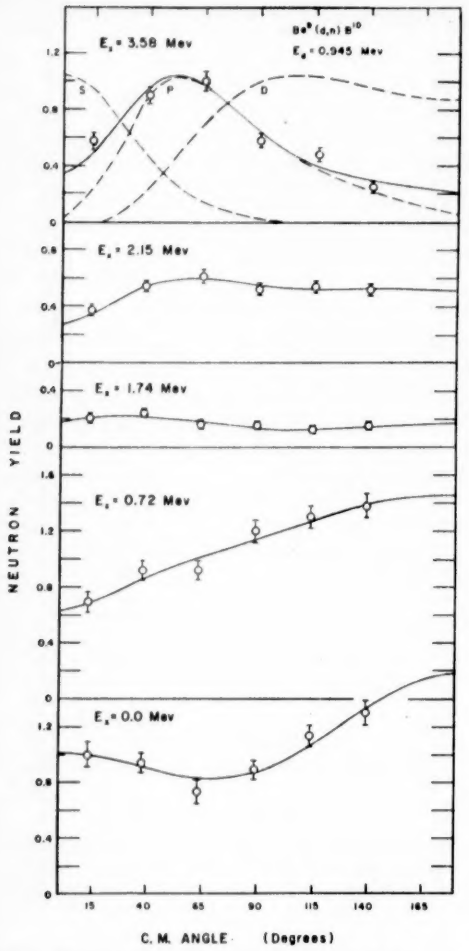

FIG. 3. Neutron angular distributions. For $E_x=3.58$ Mev, deuteron stripping curves for proton capture in s, p, and d orbits have been drawn with broken lines.

of the recoil proton spectra obtained. Five peaks are visible, corresponding to five states of the residual B^{10} nucleus.

A reaction energy Q was calculated for each peak on each plate. Table I shows these values, their averages on the six plates and estimated errors based on deviations from the average, uncertainties in the range-energy curve, and errors in measurement of the average deuteron energy ($E_d=0.945\pm0.02$ Mev) and the plate angles. Table I also shows the calculated excitation energies E_x of the B^{10} states. These measurements are in good agreement with the work of others.[2,12–14]

[12] F. Ajzenberg, Phys. Rev. **82**, 43 (1951); **88**, 298 (1952).
[13] Rasmussen, Hornyak, and Lauritsen, Phys. Rev. **76**, 581 (1949).
[14] In the following discussion the B^{10} states are labelled with the values of E_x adopted in reference 1.

To calculate the angular distribution of neutrons of a given energy group, the total number of proton tracks in the corresponding peak on each plate was counted. The usual corrections for variations of the neutron-proton scattering cross section[15] and for the varying probability that a proton stops in the emulsion[16] were applied to find the relative number of neutrons responsible for each peak. In addition, since neutron intensities on different plates were to be compared, these numbers were corrected for variations in the area scanned and in the effective solid angle subtended at the target by the emulsion which was scanned.[17]

The five angular distributions computed by this method are shown in Fig. 3. They have been normalized to unity for the most forward point in the ground-state ($E_x=0.0$ Mev) distribution. The errors indicated are only those due to counting statistics. For comparison the proton angular distributions obtained by Resnick and Hanna[3] are shown in Fig. 4, for a bombarding energy of 0.88 Mev. These two curves have the same normalization, but the relationship to the neutron curves is arbitrary.

IV. DISCUSSION

The neutron angular distribution for $E_x=3.58$ Mev shows a strong forward peak with maximum at about 50°, typical of the angular distributions for deuteron stripping discussed by Butler[18] and by Bhatia *et al.*[19] The broken lines in Fig. 3 are the angular distributions corresponding to capture of protons in s, p, and d orbits as calculated from Butler's formula with $r_0=0.5\times10^{-12}$

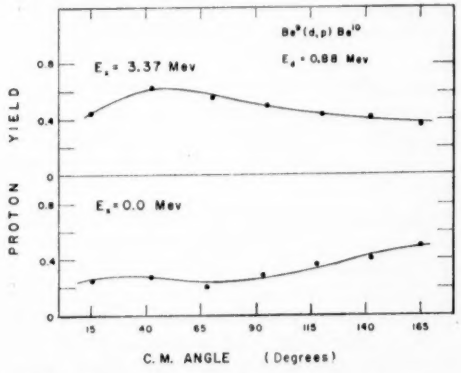

FIG. 4. Proton angular distributions, from Resnick and Hanna (reference 3).

[15] R. K. Adair, Revs. Modern Phys. **22**, 249 (1950).
[16] H. T. Richards, Phys. Rev. **59**, 796 (1941).
[17] The major contribution to this correction came from variation in emulsion thickness. The measured thicknesses of the processed emulsion on the six plates were, in order: 39.7, 50.7, 48.8, 50.3, 44.6 microns. Except for the first and last of these the uniformity is quite good. Since they were processed together, the same shrinkage factor was assumed for all plates.
[18] S. T. Butler, Proc. Roy. Soc. (London) **A208**, 36 (1951).
[19] Bhatia, Huang, Huby, and Newns, Phil. Mag. **43**, 485 (1952).

cm. The experimental points are in satisfactory agreement only with the p curve.

The remaining angular distributions do not fit the stripping theory for any angular momentum of the captured particle (Fig. 5). However, the neutron distributions for $E_x=2.15$ and 1.74 Mev and both proton distributions show some structure in the forward hemisphere suggesting the stripping maximum. The proton distribution for $E_x=0.0$ Mev has been studied by Canavan[4] at bombarding energies from 1.0 to 2.2 Mev. In this range the forward peak increases and agrees very well with stripping theory.[5] At bombarding energies below 0.88 Mev, on the other hand, the structure disappears[3] and the angular distributions can be represented by simple polynomials in $\cos\theta$.

In this transition region it seems reasonable (see reference 5) to fit the observed data by a superposition of the appropriate stripping curves calculated from Butler's theory (see Fig. 5) and simple polynomials in $\cos\theta$. (The inclusion of high powers of $\cos\theta$ in the analysis would not be warranted by the data.)

TABLE II. Values of coefficients in the expansion $Y(\theta)=A+B\cos\theta+C\cos^2\theta+DY_s(\theta)$.

E_x	A	B	C	D
		Neutrons		
0.0 Mev	0.87	−0.28	0.42	0.0
0.72	1.06	−0.56	−0.15	0.34
1.74	0.09	−0.02	0.05	0.11
2.15	0.38	−0.20	−0.06	0.37
3.58	0.10	0.09	0.11	0.83
		Protons		
0.0	0.21	−0.21	0.08	0.19
3.37	0.36	0.02	0.02	0.23

Table II lists the values found by the method of least squares for the coefficients in the expansion

$$Y(\theta)=A+B\cos\theta+C\cos^2\theta+DY_s(\theta),$$

where $Y_s(\theta)$ is the angular distribution for stripping from Fig. 5. The corresponding curves have been drawn as solid lines in Figs. 3 and 4.

The interpretation of these distributions in terms of the properties of the states of B^{10} and Be^{10} is complicated by the apparent presence of two coherent[20] processes, stripping and compound nucleus formation. The polynomial in $\cos\theta$ presumably represents the compound nucleus process plus possible interference effects. There are, however, certain features of the distributions which can be noted, as follows:

1. Wherever it can be identified,[21] the stripping maximum is located about where it is predicted by Butler's formula for capture in a p orbit.

2. The neutron yield for $E_x=1.74$ Mev is very low compared with the other neutron groups. The proton yield for $E_x=0.0$ Mev is only about 50 percent of the yield for $E_x=3.37$ Mev despite the fact that the energy available to the protons is about three times as great in the former case.

3. Except for structure which can be attributed directly to stripping, the most noticeable feature in most of the distributions is the strong asymmetry about 90°, which does not seem to be correlated with the amount of pure stripping in the distribution; thus it seems to be an effect of the compound nucleus process. In the ground state proton distribution this asymmetry extends to lower bombarding energies where there is no recognizable evidence for the stripping process. Within the accuracy of the present data, the asymmetry is adequately described by a term in $\cos\theta$.

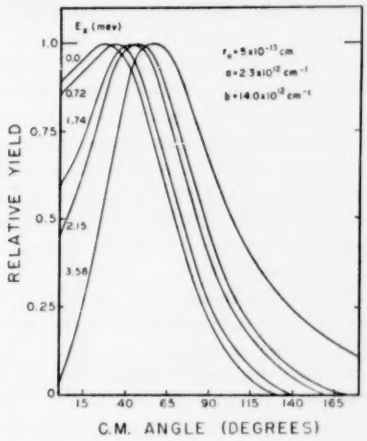

FIG. 5. Deuteron-stripping angular distributions for $Be^9(d,n)B^{10}$. Calculated from Butler's formula (reference 18) for proton capture in p orbits.

TABLE III. Allowed values of l' for various states in the compound nucleus B^{11} and final nucleus, B^{10} or Be^{10}.

B^{11}	$l_d=0$ l'	B^{10}, Be^{10}	B^{11}	$l_d=1$ l'	B^{10}, Be^{10}
$1/2^-$	1	0, 1, 2	$1/2^+$	0	0
	3	3		2	1, 2, 3
$3/2^-$	1	0, 1, 2, 3	$3/2^+$	0	1, 2
				2	0, 3
$5/2^-$	1	1, 2, 3	$5/2^+$	0	2, 3
	3	0		2	0, 1
			$7/2^+$	0	3
				2	1, 2
				4	0

[20] This is equivalent to saying that it is not possible to devise an experiment in which the two processes could be separated and studied independently.

[21] In an earlier report [Pruitt, Hanna, and Swartz, Phys. Rev. **87**, 534 (1952)] it was stated that a stripping maximum could be identified in all the neutron distributions. The additional data in the present work make this interpretation less plausible for $E_x=0.0$ and 0.72 Mev.

4. Because of the complexity introduced by the stripping process, it is not possible to establish the existence of a term in $\cos^2\theta$ in any of the distributions. In the ground-state neutron distribution, however, it is necessary to assume either that the forward maximum is a result of stripping or that a pronounced $\cos^2\theta$ dependence is present; with the present data the least-squares analysis favors the latter assumption (Table II).

5. In the neutron distributions, the relative contribution resulting from stripping seems to increase with increasing E_x (decreasing Q).

To discuss the compound-nucleus effects, we may assume that B^{11} states are formed by incoming deuterons with orbital angular momentum $l_d=0$ or 1 (we expect that higher values of l_d are improbable by considerations of penetrability). Possible B^{11} states are listed (spin and parity) in Table III, along with values of orbital angular momentum l' for the outgoing particle corresponding to various possible final states of B^{10} or Be^{10} (listed by spin; parity assumed +). On the basis of penetrability alone, one could account for a relatively low yield to the states $E_x=1.74$ Mev in B^{10} and $E_x=0.0$ Mev in Be^{10} by assuming in agreement with others[1] that these are both states of $J=0$ and that the B^{11} states involved are some combination of $5/2^-$, $3/2^+$, $5/2^+$, and $7/2^+$ or perhaps $3/2^-$ and $7/2^+$. Two B^{11} states of opposite parity are needed to account for the $\cos\theta$ terms on the basis of compound nucleus formation. A model which assumes only the B^{11} states $5/2^-$ and $3/2^+$ is in agreement with these considerations. In addition, it leads to similar angular distributions, with very little $\cos^2\theta$, for states in B^{10} and Be^{10} having spins 1 or 2 and to a more pronounced $\cos^2\theta$ term for states with spin 3 (ground state of B^{10}).

PHYSICAL REVIEW VOLUME 92, NUMBER 6 DECEMBER 15, 1953

Nuclear Quadrupole Coupling in the Li_2 Molecule*†

R. M. STERNHEIMER, *Brookhaven National Laboratory, Upton, New York*

AND

H. M. FOLEY, *Columbia University, New York, New York*

(Received August 3, 1953)

The effect of the quadrupole moment induced in the 1*s* shell on the nuclear quadrupole coupling q in the Li_2 molecule has been investigated for several wave functions. For the most accurate variational wave function of James, the inclusion of the induced moment gives $q/2e=-0.00106a_H^{-3}$. This result, together with the quadrupole coupling $eqQ=+0.060$ Mc/sec for Li^7, leads to a negative value of the quadrupole moment $Q(Li^7)$. However the value of q is so close to zero that the magnitude and even the sign of Q is uncertain. The value of $1/q$ which determines Q is very sensitive to changes in the molecular wave function, and it is shown that a small modification of the James wave function would lead to a negative $Q(Li^7)$ which agrees in order of magnitude with the prediction of the nuclear shell model. Calculations of q were also carried out for the Heitler-London and Coulson-Duncanson wave functions for the Li_2 molecule.

I. INTRODUCTION

In a recent investigation of the quadrupole coupling in the Li_2 molecule, Harris and Melkanoff[1] have shown that the sign of the electric field gradient at the Li nucleus is very sensitive to the detailed behavior of the molecular wave function, since the gradient is the difference between the nuclear and the electronic terms which nearly cancel each other. These authors confirm an earlier result of Foley[2] that the Bartlett-Furry wave function for Li_2 gives a positive quadrupole coupling q which would lead to a positive quadrupole moment Q, in view of the experimental observation[3] that eqQ is positive (+0.060 Mc/sec). However, Harris and Melkanoff[1] also carried out a calculation of q with the more accurate variational wave function obtained by James.[4] The electronic term of q as calculated with this wave function is appreciably larger than for the Bartlett-Furry function; the resultant q is negative, although small. This work does not enable one to draw a definite conclusion about the sign of q, although it shows that a negative sign of q is not excluded. This result is of interest since a positive $Q(Li^7)$ would be hard to understand on the basis of any simple model of the nucleus.[5,6]

Harris and Melkanoff[1] did not take into account the effect of the quadrupole moment induced[7] in the 1*s* shell by the nuclear Q. The induced moment around the

* The part of the work carried out at Brookhaven National Laboratory was done under the auspices of the U. S. Atomic Energy Commission.

† Supported in part by a grant from the National Science Foundation.

[1] E. G. Harris and M. A. Melkanoff, Phys. Rev. **90**, 585 (1953).
[2] P. Kusch, Phys. Rev. **76**, 138 (1949).
[3] Logan, Coté, and Kusch, Phys. Rev. **86**, 280 (1952).
[4] H. M. James, J. Chem. Phys. **2**, 794 (1934).
[5] R. D. Present, Phys. Rev. **80**, 43 (1950).
[6] R. Avery and C. H. Blanchard, Phys. Rev. **78**, 704 (1950).
[7] R. M. Sternheimer, Phys. Rev. **80**, 102 (1950); **84**, 244 (1951). The latter paper will be referred to as I.

nucleus (A), whose quadrupole coupling is considered, has two effects: (1) it shields the other nucleus (B) and the density connected with the $1s$ shell surrounding it by the amount γ_∞, where γ_∞ is the ratio of the total induced moment to Q; (2) it shields the valence electron density by an amount less than γ_∞ which depends on the extent of the penetration of the valence electrons inside the $1s$ shell. The purpose of this paper is to include the effect of the induced moment as calculated from the James and Heitler-London wave functions. For the more accurate James wave function, the inclusion of the induced moment gives $q/2e=-0.00106a_H^{-3}$. The value obtained for the Heitler-London function is $q/2e=0.00266a_H^{-3}$ as compared to $0.00390a_H^{-3}$ obtained by Harris and Melkanoff.[1] q is smaller by a factor of order $1-\gamma_\infty=0.76$ than without shielding. However, not much weight can be given to the positive sign of q as obtained with the Heitler-London function, since this function is presumably much less accurate than that of James. The difference between the Heitler-London and James results arises from the fact that the James electron distribution is concentrated more heavily for small angles θ_A with the internuclear axis at the expense of the large values of θ_A. As a result the value of $\langle(3\cos^2\theta_A-1)/2r_A^3\rangle$ is greater, increasing the electronic term. If in the actual wave function the electrons are on the average closer to the nucleus than for the James function, $\langle(3\cos^2\theta_A-1)/2r_A^3\rangle$ will be further increased and q is definitely negative.

Besides the determination of q for Li_2, a further aim of this paper is to show how the induced moment correction is calculated for the case of molecules, previous calculations[7] having been restricted to the case of free atoms. It is found that the correction to q can be obtained by simply calculating the interaction of the induced moment with the asymmetric (valence) part of the electronic density in the molecule, in the same way as for atoms.

II. CALCULATION OF THE INDUCED MOMENT

In order to obtain the correction to q for any of the wave functions considered, it is necessary to obtain the moment induced in the $1s$ shell. A complete proof that the correction for q due to the polarizability of the $1s$ shell is accurately given by the induced moment, will be presented in Sec. III.

The induced moment was calculated using the method described in I. For the unperturbed $1s$ function, we took the same function as was used by James:[4]

$$u_0=(8.82/\sqrt{2})r\exp(-2.69r), \tag{1}$$

where r is the distance from the nucleus and u_0 is r times the $1s$ function normalized according to

$$\int_0^\infty\int_0^\pi u_0^2 dr\times\sin\theta d\theta=1,$$

where θ is the angle subtended by the radius vector and the axis of the quadrupole moment. The equation to be solved is

$$(H_0-E_0)u_1=-H_1u_0, \tag{2}$$

where H_0 and H_1 are the unperturbed and the perturbed part of the Hamiltonian, respectively; u_1 is r times the d wave perturbation. We have

$$H_0=-\frac{\hbar^2}{2m}\nabla^2+V_0, \tag{3}$$

$$H_1=-e^2Q(3\cos^2\theta-1)/4r^3, \tag{4}$$

where V_0 is the spherical potential. V_0 was taken as $(-5.38/r)$ Rydbergs in order to be consistent with the wave function, Eq. (1). Similarly the energy $|E_0|$ is taken as $(2.69)^2=7.24$ ry. Upon defining the radial functions u_0' and u_1' as in I,

$$u_0\equiv 2^{-\frac{1}{2}}u_0'(r), \tag{5}$$

$$u_1\equiv Qu_1'(r)(3\cos^2\theta-1)/2\sqrt{2}, \tag{6}$$

one obtains

$$\left(-\frac{d^2}{dr^2}+\frac{6}{r^2}-\frac{5.38}{r}+7.24\right)u_1'=\frac{u_0'}{r^3}. \tag{7}$$

Equation (7) can be solved exactly because of the special form of the unperturbed function u_0' which can be written $\kappa r\exp(-Z_0r)$, with $\kappa=8.82$, $Z_0=2.69$. The solution of

$$\left(-\frac{d^2}{dr^2}+\frac{6}{r^2}-\frac{2Z_0}{r}+Z_0^2\right)u_1'=\kappa\exp(-Z_0r)/r^2 \tag{8}$$

can be shown by substitution to be

$$u_1'=\left(\frac{\kappa}{6}\right)\exp(-Z_0r)[1+(Z_0/3)r]. \tag{9}$$

As shown in I, the induced moment due to both $1s$ electrons, $Q_i(r)dr$ between r and $r+dr$ is given by

$$Q_i dr=(8/5)Qu_0'u_1'r^2dr. \tag{10}$$

Figure 1 shows u_1' together with Q_i. The total induced

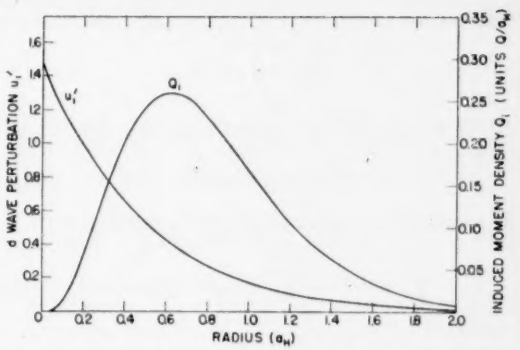

FIG. 1. Induced quadrupole density Q_i and d-wave perturbation u_1' of $1s$ function.

moment

$$Q_{iT}=\int_0^\infty Q_i dr \tag{11}$$

can be obtained by integration using Eqs. (5), (9), and (10):

$$Q_{iT}=Q\kappa^2/(6Z_0^4). \tag{11a}$$

The value of κ is determined by the requirement

$$\int_0^\infty u_0'^2 dr=\kappa^2\int_0^\infty r^2\exp(-2Z_0 r)dr=1, \tag{12}$$

whence $\kappa=2Z_0^{\frac{1}{2}}$. Upon inserting this value in (11a) one finds

$$Q_{iT}=2Q/(3Z_0). \tag{13}$$

For the present case, with $Z_0=2.69$, $Q_{iT}=0.248Q$. It may be noted that the present values of Q_i are quite close to those obtained previously in I (see Table I) using as the unperturbed u_0 the $1s$ function obtained by Fock and Petrashen.[8] The corresponding value of $|E_{\Delta Q}/E_Q|$ for the atomic $2p$ state (0.166) is somewhat smaller than Q_{iT}/Q because of the penetration of the $2p$ function into the $1s$ shell.

Equation (13) shows that the contribution to the induced moment from the $1s$ shell decreases as Z^{-1} with increasing atomic number Z. However, the number of shells increases with Z; this effect compensates the decrease for any one shell as given by Eq. (13). This result is consistent with the behavior of the Fermi-Thomas model according to which the total induced moment for the entire atom is independent of Z.

Equation (7) assumes that the perturbing potential is that of the unshielded nuclear moment Q. However, as pointed out in I, the total perturbation includes a contribution from the induced moment. In the present case each $1s$ electron experiences the perturbation due to the moment induced in the other $1s$ state, which amounts to $Q_i/2$. In order to include this effect, one defines

$$\gamma(r)\equiv(1/Q)\left[\int_0^r Q_i dr'+r^5\int_r^\infty Q_i r'^{-5}dr'\right]; \tag{14}$$

γ is 0 at $r=0$ and (Q_{iT}/Q) for large r.

The equation satisfied by the perturbation upon inclusion of the shielding, is obtained from Eq. (7) by replacing u_0'/r^3 by $(1-\gamma/2)u_0'/r^3$. The resulting equation was solved numerically for the perturbation, say $\bar{u}_1'$, using the procedure described in I [Eqs. (1)–(12)]. The effect of the $-\gamma/2$ term was found to be very small. The new induced moment $\bar{Q}_{iT}$ calculated with $\bar{u}_1'$ is $0.240Q$, only 3 percent lower than the initial value. The function γ as obtained with the induced moment $\bar{Q}_i\equiv(8/5)Qu_0'\bar{u}_1'r^2$ will be used in the calculation of the quadrupole coupling.

[8] V. Fock and M. Petrashen, Physik. Z. Sowjetunion **8**, 555 (1935).

III. THE QUADRUPOLE COUPLING FOR THE JAMES VARIATIONAL FUNCTION

The variational wave function for the Li_2 ground state obtained by James[4] is

$$\Psi_J=(1/N_J^{\frac{1}{2}})\sum_{mnjk}C_{mnjk}(\psi_{mnjk}+\psi_{nmkj}), \tag{15}$$

where the C_{mnjk} are constant coefficients, N_J is a normalization constant and ψ_{mnjk} is the following determinant:

$$\psi_{mnjk}=|(\psi_{1s}\alpha)(1)(\psi_{1s}\beta)(2)(f_{mj}\alpha)(3)\times(f_{nk}\beta)(4)(\psi_{1s}'\alpha)(5)(\psi_{1s}'\beta)(6)|, \tag{16}$$

with

$$f_{mj}=\exp(-2\lambda)\lambda^m\mu^j; \tag{17}$$

λ and μ are elliptic coordinates; $\lambda=(r_A+r_B)/R$, $\mu=(r_A-r_B)/R$, where r_A and r_B are the distances from nucleus A and B, respectively, R is the internuclear distance; ψ_{1s} and ψ_{1s}' are $1s$ wave functions centered on nucleus A and B, respectively, whose normalization is $\int\psi_{1s}^2dV=1$ (dV = volume element). α and β are the eigenfunctions for spin up and down, respectively. The notation $(\psi_{1s}\alpha)(1)$ means that the coordinates of $\psi_{1s}\alpha$ are those of electron 1. In Eq. (16), ψ_{mnjk} is a determinant whose terms include all permutations of electrons 1–6.

Instead of the original wave function obtained by James[4] which has 18 terms, Harris and Melkanoff[1] used a function composed of 12 terms. It was shown by Melkanoff[1] that the difference in the values of q obtained with the two wave functions is small. Thus, it would not affect the present considerations of the effect of shielding on q. We have used the same function as was used by Harris and Melkanoff, so that the sum in Eq. (15) has 12 terms.

We must first calculate the total electron density ρ_J for the James function. ρ_J is given by

$$\rho_J=6\int\int|\Psi_J|^2 d\sigma_1 d\tau_{2-6}, \tag{18}$$

where $d\tau_{2-6}$ indicates the space and spin coordinates of electrons 2–6 and σ_1 is the spin of 1. From (16) and (18) one finds for the density ρ_{ff} of the valence electrons,

$$\rho_{ff}=(1/N_J)\sum_{mnjk}\sum_{m'n'j'k'}C_{mnjk}C_{m'n'j'k'}\times[f_{mj}f_{m'j'}I'_{nk,n'k'}+f_{nk}f_{n'k'}I'_{mj,m'j'}+f_{nk}f_{m'j'}I'_{mj,n'k'}+f_{mj}f_{n'k'}I'_{nk,m'j'}], \tag{19}$$

where

$$I'_{mj,nk}\equiv I_{m+n,j+k}-2J_{mj}J_{nk}, \tag{20}$$

$$I_{m,j}=\int e^{-4\lambda}\lambda^m\mu^j dV, \tag{20a}$$

$$J_{mj}\equiv\int\psi_{1s}e^{-2\lambda}\lambda^m\mu^j dV. \tag{20b}$$

N_J is obtained by integrating $|\Psi_J|^2$ over all coordinates $(d\tau_{1-6})$. One finds

$$N_J=\sum_{mnjk}\sum_{m'n'j'k'}C_{mnjk}C_{m'n'j'k'}[I'_{mj,\,m'j'}I'_{nk,\,n'k'}+I'_{nk,\,m'j'}I'_{mj,\,n'k'}]. \quad (21)$$

Since ψ_{1s} and f_{mj} are not orthogonal, there are terms in ρ_J of the form $\psi_{1s}f_{mj}$. These terms contribute to the electric field gradient at nucleus A. If ρ_{sf} denotes the part of ρ_J which is linear in ψ_{1s}, one finds

$$\begin{aligned}\rho_{sf}=&-(\psi_{1s}/N_J)\sum_{mnjk}\sum_{m'n'j'k'}C_{mnjk}C_{m'n'j'k'}\\&\times\{f_{mj}[J_{m'j'}I'_{nk,\,n'k'}+J_{n'k'}I'_{nk,\,m'j'}]\\&+f_{nk}[J_{n'k'}I'_{mj,\,m'j'}+J_{m'j'}I'_{mj,\,n'k'}]\\&+f_{m'j'}[J_{mj}I'_{nk,\,n'k'}+J_{nk}I'_{mj,\,n'k'}]\\&+f_{n'k'}[J_{nk}I'_{mj,\,m'j'}+J_{mj}I'_{nk,\,m'j'}]\}. \quad (22)\end{aligned}$$

The value of q can be calculated from these expressions and from the value of the net charge concentrated at nucleus B. Because of the non-orthogonality, the coefficient of $\psi_{1s}'^2$ in ρ_J is not exactly 2, and there is also a term linear in ψ_{1s}' similar to ρ_{sf}. Upon using Harris's value[9] for the net charge due to both terms, $-1.973e$, one obtains $+1.027e$ for the charge at B which represents nucleus B and the surrounding $1s$ shell. Instead of the quadrupole coupling q, we will frequently use q', defined by $q'\equiv q/2e$, so that q' is the average of $(3\cos^2\theta_A-1)/2r_A^3$ over the charge density of the molecule excluding nucleus A.

In order to obtain the shielding effect without ambiguity, it is best to consider this effect as a result of the distortion of the $1s$ shell by the asymmetric potential caused by the other charges. The correction to q is then due to the part of the distortion which behaves as $(3\cos^2\theta_A-1)$. This picture is equivalent to the consideration of the induced moment, as will now be shown.

The distortion of the $1s$ states is caused by the asymmetric part of the potential of the charges other than the $1s$ state being considered. The density of the type ρ_{sf} with spin up (or down) is one-half of the expression given by Eq. (22). Hence, the density ρ' which produces the distortion is

$$\rho'=-\rho_{ff}-\tfrac{1}{2}\rho_{sf}+\rho_B, \quad (23)$$

where ρ_B is a charge $+1.027$ concentrated at B. Because of the potential produced by ρ', ψ_{1s} is changed to

$$\bar{\psi}_{1s}=\psi_{1s}+\psi_p+\psi_d+\cdots, \quad (24)$$

where ψ_p and ψ_d are the p and d wave perturbations, respectively. These perturbations can be obtained by solving the Schrödinger equation for the $1s$ function including the potential resulting from ρ'.

The correction to q for the polarizability of the $1s$ shell is obtained by replacing ψ_{1s} by $\bar{\psi}_{1s}$ in the James wave function [Eq. (17)]. The most important term of q which arises from this substitution is associated with ψ_{1s}^2. The ψ_{1s}^2 terms of ρ_J can be written $c\psi_{1s}^2$. Harris has given the value[9] $c=2.0268$; $c\psi_{1s}^2$ is replaced by $c\bar{\psi}_{1s}^2$, which includes a term $2c\psi_{1s}\psi_d$. This term is the only one of first order in the perturbation which has the $(3\cos^2\theta_A-1)$ dependence. The contribution to q' is

$$\Delta q'=-\int 2c\psi_{1s}\psi_d(3\cos^2\theta_A-1)/2r_A^3dV. \quad (25)$$

It can be easily shown that $\Delta q'$ as given by Eq. (25) can be expressed in terms of the function γ associated with the induced moment $\bar{Q}_i$:

$$\Delta q'=-\int[\gamma(3\cos^2\theta_A-1)/2r_A^3]\times(-\rho_{ff}-\tfrac{1}{2}\rho_{sf}+\rho_B)dV. \quad (26)$$

In order to prove Eq. (26), ρ' will be written

$$\rho'=\rho_0P_0+\rho_1P_1+\rho_2P_2+\cdots, \quad (27)$$

where $P_l(\theta_A)$ is the Legendre polynomial of order l and the ρ_l are functions of r_A only. The potential produced by ρ_2 is

$$V_2=(8\pi/5)\left[\frac{1}{r^3}\int_0^r\sigma r'^2dr'+r^2\int_r^\infty\sigma r'^{-3}dr'\right]P_2=(8\pi/5)gP_2, \quad (28)$$

where $\sigma(r')\equiv\rho_2r'^2$. The function in the square bracket is denoted by g. We note that a factor 2 arises from Rydberg units and a factor $\frac{2}{5}$ from the integration over θ_A. The d wave perturbation $\tilde{u}_1$ of the $1s$ function is determined by an equation similar to Eq. (4) of I:

$$M\tilde{u}_1=-(8\pi/5)gP_2u_0, \quad (29)$$

where M denotes the operator

$$M=-\frac{d^2}{dr^2}+\frac{6}{r^2}+V_0-E_0. \quad (30)$$

In the present case, $V_0=-5.38/r$, $E_0=-7.24$ ry. Here and in the following, the u's denote r times the corresponding parts of the $1s$ wave function. If we let $u_0=2^{-\frac{1}{2}}u_0'$ [see Eq. (5)], $\tilde{u}_1$ can be written

$$\tilde{u}_1=(-8\pi/5\sqrt{2})\tilde{u}_1'P_2, \quad (31)$$

where $\tilde{u}_1'$ satisfies

$$M\tilde{u}_1'=gu_0'. \quad (32)$$

The contribution to q' is given by

$$\Delta q'=-4\int_0^\pi\int_0^\infty(u_0\tilde{u}_1/r^3)P_2dr\sin\theta d\theta, \quad (33)$$

where the factor 4 arises from the fact that the perturbed density is $2u_0\tilde{u}_1$ for each $1s$ electron. Upon insert-

[9] E. G. Harris, thesis, University of Tennessee, 1953 (unpublished).

ing Eq. (31) into (33) one obtains

$$\Delta q' = \frac{32\pi}{25}\int_0^\infty \frac{u_0' \tilde{u}_1'}{r^3} dr. \quad (34)$$

It will be shown that the same expression is obtained, if the quadrupole energy is calculated as the interaction of the induced moment with ρ'. The perturbation u_1 due to the nuclear Q is determined by

$$M u_1 = Q P_2 u_0 / r^3. \quad (35)$$

Hence, u_1 can be written

$$u_1 = Q P_2 u_1'/\sqrt{2}, \quad (36)$$

where u_1' satisfies

$$M u_1' = u_0'/r^3. \quad (37)$$

In view of Eq. (36), the perturbed density due to u_1 is

$$\Delta\rho_{\text{ind}} = 4u_0 u_1 = 2Q u_0' u_1' P_2. \quad (38)$$

The potential due to $\Delta\rho_{\text{ind}}$ is

$$V_{\text{ind}} = (8/5)Q\left[\frac{1}{r^3}\int_0^r u_0' u_1' r'^2 dr' + r^2\int_r^\infty u_0' u_1' r'^{-3} dr'\right] P_2 = (8/5) Q g' P_2, \quad (39)$$

where g' denotes the function in the square bracket. The interaction of V_{ind} with ρ' is given by

$$2\pi\int_0^\infty\int_0^\pi V_{\text{ind}}\rho_2 P_2 r^2 dr \sin\theta d\theta = (32\pi Q/25)\int_0^\infty g'\sigma dr. \quad (40)$$

Since Eq. (40) equals $\Delta q' Q$, the two expressions for $\Delta q'$, Eqs. (34) and (40) are equivalent, provided that the radial integrals are equal; these integrals will be denoted by $\tilde{L}$ and L, respectively. Using Eq. (37) one finds

$$\tilde{L} = \int_0^\infty (u_0' \tilde{u}_1'/r^3) dr = \int_0^\infty (M u_1') \tilde{u}_1' dr = \int_0^\infty u_1' (M \tilde{u}_1') dr, \quad (41)$$

where the last step follows by partial integration. In view of Eq. (32), Eq. (41) becomes

$$L = \int_0^\infty u_0' u_1' g dr = \int_0^\infty u_0' u_1'\left[\frac{1}{r^3}\int_0^r \sigma r'^2 dr' + r^2\int_r^\infty \sigma r'^{-3} dr'\right] dr. \quad (42)$$

By partial integration $\tilde{L}$ can be transformed to

$$L = \int_0^\infty \sigma\left[\frac{1}{r^3}\int_0^r u_0' u_1' r'^2 dr' + r^2\int_r^\infty u_0' u_1' r'^{-3} dr'\right] dr, \quad (43)$$

which equals L by virtue of Eqs. (39) and (40). Thus the correction $\Delta q'$ can be calculated as the interaction of the induced moment with the charge outside the $1s$ shell. The main advantage of this method, as compared to the procedure in which $\tilde{u}_1$ is calculated, is that the distortion by the nuclear Q can be used with several external distributions without the need of solving a differential equation each time. Moreover, in the present case, u_1 can be obtained analytically, whereas this is not possible for $\tilde{u}_1$.

Aside from the term $2c\psi_{1s}\psi_d$, there are other shielding terms which arise from the lack of orthogonality of ψ_{1s} on f_{mj}. These terms arise as follows from the substitution of $\tilde{\psi}_{1s}$ for ψ_{1s} in Eq. (16): (1) there are additional terms in ρ_f caused by the fact that ψ_{1s} in ρ_{sf} [Eq. (22)] should be replaced by $\tilde{\psi}_{1s}$. The perturbation in the density arising from ψ_p is ρ_{pf}, defined as the result of replacing ψ_{1s} by ψ_p in the expression for ρ_{sf}. ψ_p was calculated by solving a differential equation similar to Eq. (29). The contribution to q' due to ρ_{pf} was found to be $\sim 10^{-5} a_H^{-3}$. An even smaller contribution is obtained from ρ_{df}, defined as the result of replacing ψ_{1s} by ψ_d in ρ_{sf}. (2) The J_{mj} [Eq. (20b)] should be calculated using $\tilde{\psi}_{1s}$ instead of ψ_{1s}. This was found to change J_{10} by ~ 0.1 percent and would result in similarly small changes for the other J_{mj}. It can be concluded that the additional shielding terms just described are negligible.

It follows from the preceding discussion that q' is given by

$$q' = -\int (1-\gamma)[(3\cos^2\theta_A - 1)/2r_A^3]\rho_{ff} dV - \int (1-\gamma/2)[(3\cos^2\theta_A - 1)/2r_A^3]\rho_{sf} dV + [1-\gamma(R)]\int [(3\cos^2\theta_A - 1)/2r_A^3]\rho_B dV + \Delta q'_{\text{exch}}. \quad (44)$$

The last term in (44) represents a small exchange contribution of the induced moment of the type which has been discussed in I. The expression for $\Delta q_{\text{exch}}'$ and its evaluation, are given in the Appendix.

The integrals in Eq. (44) involving ρ_{ff} and ρ_{sf} will be denoted by A_{ff} and A_{sf}, respectively. A_{ff} and A_{sf} were obtained by a double numerical integration. In this work, the expressions for ρ_{ff} and ρ_{sf} given by Harris[9] were used. These expressions were also checked by means of Eqs. (19)–(22), using Harris's values[9] of

the coefficients C_{mnjk}. The resulting expressions agree satisfactorily with those of Harris.

ρ_{ff} and ρ_{sf} were evaluated for the internuclear distance $5.63a_H$ for which James[4] calculated the variational function, instead of the observed $R=5.05a_H$. Therefore, the electronic term of q' will be slightly in error. Harris and Melkanoff[1] have carried out calculations for a Heitler-London wave function for various values of R, from which they showed that for this wave function the electronic part of q' is not sensitive to R. (In the range from $R=4.71a_H$ to $5.50a_H$, this part decreases by only $0.00013a_H^{-3}$.) For the term produced by ρ_B which varies more rapidly with R, the observed distance will be used.

To obtain A_{ff} and A_{sf}, the radial integration was carried out first for 11 angles θ_A. The radial integral for A_{ff} is

$$A_{ff}^{(r)}(\theta_A)=\int_0^\infty (1-\gamma)\rho_{ff}(r_A,\theta_A)/r_A dr_A. \quad (45)$$

Since ρ_{ff} is finite at $r_A=0$, a small region near $r_A=0$ must be excluded. The integral was taken from $r_A=0.2a_H$ to ∞. It can be easily shown that when the angular integration is carried out for $r_A\leqq 0.2a_H$, the contribution from this region to q' is negligible (of the order $10^{-5}a_H^{-3}$). The same considerations apply to A_{sf}. The 11 values of θ_A were taken at intervals of 11.25° for $0°\leqq\theta_A\leqq 45°$ and at intervals of 22.5° for $\theta_A\geqq 45°$.

The results are

$$A_{ff}=0.00748a_H^{-3}, \quad A_{sf}=-0.00087a_H^{-3}.$$

The term due to ρ_B is given by

$$q_B'=(0.757)(1.027)/R^3=0.00603a_H^{-3}. \quad (46)$$

The factor 1.027 is due to the charge $1.027e$ associated with nucleus B and its surrounding $1s$ shell; the factor 0.757 represents the shielding.[10] As shown in the Appendix $\Delta q_{\text{exch}}'=-0.00048a_H^{-3}$ so that the value of q' including shielding is $q_J'=-0.00106a_H^{-3}$.

As a check on the calculations, q' was evaluated without shielding by setting $\gamma=0$ in Eq. (44). The resulting values of the integrals are $A_{ff,0}=0.00984$, $A_{sf,0}=-0.00096a_H^{-3}$. Here and in the following, the subscript 0 indicates that shielding is not included. The nuclear term is $1.027/R^3=0.00797a_H^{-3}$, so that $q_{J,0}'=-0.00091a_H^{-3}$. This value is in very good agreement with that obtained by Harris,[9] $1/R^3-0.00868=-0.00092a_H^{-3}$. Although the agreement to $10^{-5}a_H^{-3}$ is fortuitous, it indicates that the integration procedure used is adequate.

As was found previously by Harris and Melkanoff,[1] the small value of q_J' makes it impossible to obtain with certainty the actual sign of the electric field gradient. We note that A_{ff} is reduced by shielding in the ratio 0.760 which is $\approx(1-Q_{sT}/Q)$. The reason this ratio is obtained is that ρ_{ff} is almost completely external to the $1s$ shell, so that the induced moment has maximum effectiveness in shielding the nucleus. The ρ_{sf} term is reduced by only a factor 0.92. Here the effect of penetration is greater and, in any case, the minimum ratio is $1-Q_{sT}/2Q=0.878$. It is seen that the inclusion of shielding does not greatly affect the total value of q_J' for the James wave function, although the individual terms are changed appreciably. The reason is that the important terms of q_J', namely q_B' and A_{ff}, are reduced by the same factor (≈ 0.76) so that one expects $q_J'\approx 0.76q_{J,0}'$. Since $q_{J,0}'$ is close to zero, the difference $0.24q_{J,0}'$ is very small.

The value of q_J' would give $Q(\text{Li}^7)=-12\times10^{-26}$ cm^2. Interpolation from the curve of quadrupole moments published by Townes, Foley, and Low[11] gives $Q(\text{Li}^7)=-1.6\times10^{-26}$ cm^2. It should be emphasized that a relatively small change of the valence density would lead to a value of q' which gives Q of the order of the predictions of the nuclear shell model. Along any line $\theta_A=$ constant, ρ_{ff} increases rapidly with increasing r_A near nucleus A. Because of the factor $1/r_A^3$, the electronic part of q' would be increased considerably if the actual density would rise faster near A than ρ_J. Thus, if the valence density ρ_{ff} were changed to a density $\tilde{\rho}_{ff}$ such that[12] $\tilde{\rho}_{ff}(r_A,\theta_A)=1.2^3\rho_{ff}(1.2r_A,\theta_A)$, A_{ff} would be increased to 1.2^3 A_{ff} and q' would be $-0.0065a_H^{-3}$ leading to $Q=-2.0\times10^{-26}$ cm^2. Moreover, A_{ff} is very sensitive to changes of the angular dependence of the density. If ρ_{ff} is increased by a factor 1.15 at $\theta_A=0°$, 1.10 at 22.5°, 1.05 at 45°, and decreased by a factor 0.80 for $\theta_A\geqq 90°$ (to ensure normalization), q' becomes $-0.00354a_H^{-3}$, so that $Q=-3.6\times10^{-26}$ cm^2. If the actual valence density should be both more internal and more peaked near the internuclear axis, in the manner just described, one finds $q'=-0.0107a_H^{-3}$ leading to $Q=-1.2\times10^{-26}$ cm^2. These considerations show that, although the value of q' obtained from the James wave function is unlikely, it is quite possible that the James wave function is still accurate enough for many purposes, since a small change of the wave function results in a considerable change of $1/q'$.

IV. THE QUADRUPOLE COUPLING FOR THE HEITLER-LONDON AND COULSON-DUNCANSON WAVE FUNCTIONS

The calculation of the shielding effect has been carried out for the Heitler-London wave function for Li_2 discussed by James.[4] This function has also been considered by Harris and Melkanoff[1] and is given by

$$\Psi_{HL}=(1/N_{HL}^{\frac{1}{2}})(\psi_{ab}+\psi_{ba}), \quad (47)$$

[10] The factor 0.757 rather than 0.760 is used because the $1s$ term of ρ_J is $2.027\,\psi_{1s}^2$, so that the induced moment is increased to $(0.240)\times(2.027/2)Q$.

[11] Townes, Foley, and Low, Phys. Rev. **76**, 1415 (1949).

[12] The factor 1.2^3 is required for normalization.

where N_{HL} is a normalization factor, ψ_{ab} is the determinant

$$\psi_{ab}=|(\psi_{1s}\alpha)(1)(\psi_{1s}\beta)(2)(a\alpha)(3)(b\beta)(4) \times(\psi_{1s}'\alpha)(5)(\psi_{1s}'\beta)(6)|, \quad (48)$$

and ψ_{ba} differs from ψ_{ab} by the interchange of a and b. Here,

$$a\equiv nr_A\exp(-0.65r_A), \quad (49)$$

$$b\equiv nr_B\exp(-0.65r_B), \quad (50)$$

are valence functions centered on nuclei A and B, respectively; n is a normalization constant to be determined below. In Eq. (48) the determinant includes all permutations of electrons 1–6.

The expressions for the density for the James wave function can be used here. Equation (47) corresponds to a single term of Ψ_J in Eq. (15) with f_{mj} and f_{nk} replaced by a and b, respectively. The valence density is given by

$$\rho_v=(1/N_{HL})[a^2I_{bb}+b^2I_{aa}+2abI_{ab}], \quad (51)$$

where

$$I_{aa}=I_{bb}=N_1-J_a^2-J_b^2,$$

$$I_{ab}=N_2-2J_aJ_b,$$

$$N_1=\int a^2dV, \qquad N_2=\int abdV, \quad (51a)$$

$$J_a=\int\psi_{1s}adV, \quad J_b=\int\psi_{1s}bdV.$$

By integrating over all coordinates one finds that N_{HL} is given by

$$N_{HL}=I_{aa}^2+I_{ab}^2. \quad (52)$$

Similarly to Eq. (22), one obtains for the density due to the overlap of ψ_{1s} with the valence functions,

$$\rho_{sv}=-(2\psi_{1s}/N_{HL})\{a[J_aI_{bb}+J_bI_{ab}] +b[J_bI_{aa}+J_aI_{ab}]\}. \quad (53)$$

The $1s$ density surrounding nucleus A is given by

$$\rho_{ss}=(\psi_{1s}^2/N_{HL})[I_{aa}(N_1+I_{aa})+I_{ab}(N_2+I_{ab})]. \quad (54)$$

The constant n in (49) and (50) was so chosen that $N_1^2+N_2^2=1$. In order to obtain n, we note that a value $n=0.111$ would give $N_1=1$ from Eq. (51a). With this normalization one obtains $N_2=0.586$ by analytic integration. Hence

$$n=0.111[1+(0.586)^2]^{-\frac{1}{2}}=0.103. \quad (55)$$

The resulting values of the integrals are: $N_1=0.863$, $N_2=0.506$, $I_{aa}=0.835$, $I_{ab}=0.487$, $J_a=0.156$, $J_b=0.0625$. In all of these calculations the actual $R=5.05a_H$ is used. With these values of the constants, the electronic density is

$$\rho_{HL}=2.035\psi_{1s}^2-0.342\psi_{1s}a-0.273\psi_{1s}b +0.894(a^2+b^2)+1.042ab-0.342\psi_{1s}'b -0.273\psi_{1s}'a+2.035\psi_{1s}'^2, \quad (56)$$

where ψ_{1s}' is the $1s$ function centered on B. The quadrupole coupling is given by

$$q'=-0.894\int(1-\gamma)[(3\cos^2\theta_A-1)/2r_A^3]b^2dV$$

$$-1.042\int(1-\gamma)[(3\cos^2\theta_A-1)/2r_A^3)abdV$$

$$+0.273\int(1-\gamma/2)[(3\cos^2\theta_A-1)/2r_A^3]\psi_{1s}bdV$$

$$+0.756e_B/R^3. \quad (57)$$

The integrals appearing in q' will be denoted by A_{bb}, A_{ab}, and $A_{1s,b}$, respectively; in the last term, e_B is the effective charge associated with nucleus B and its surrounding $1s$ shell. It is given by

$$e_B=3-2.035+0.342J_a+0.273J_b=1.035. \quad (58)$$

A_{bb}, A_{ab}, and $A_{1s,b}$ were evaluated by the same procedure as the A's of the James function. However, for the angles $\theta_A<45°$ an interval of 5.63°, rather than 11.25°, was used because the A's have a fairly pronounced variation in this region. The reason is that the closest distance of the line $\theta_A=11.25°$ to nucleus B is $\sim a_H$, and $b(r_B)$ has a maximum at $r_B=1/0.65=1.54a_H$. As a result, the radial integral $A_{bb}^{(r)}$

$$A_{bb}^{(r)}(\theta_A)=\int_\delta^\infty b^2(r_A,\theta_A)/r_Adr_A, \quad (59)$$

has a maximum at $\theta_A\approx11.25°$; here δ is a small radius introduced to give a convergent integral. A similar result holds for the integral over ab. The results of the integration are: $A_{bb}=0.00276a_H^{-3}$, $A_{ab}=0.00123a_H^{-3}$, $A_{1s,b}=0.00121a_H^{-3}$. The resulting value of q_{HL}' as obtained from Eqs. (57) and (58) is $q_{HL}'=0.00266a_H^{-3}$.

In order to check the numerical integrations, the value of q' without shielding was also calculated. By setting $\gamma=0$ in Eq. (57), one finds $A_{bb,0}=0.00357$, $A_{ab,0}=0.00159$, and $A_{1s,b,0}=0.00128a_H^{-3}$. These values of the A's are in satisfactory agreement with those of Harris and Melkanoff,[1,9] who obtain 0.00350, 0.00154, and 0.00141, respectively. The resulting value of q' is $q_{HL,0}'=0.00354a_H^{-3}$.

The fact that q_{HL}' is positive cannot be given too much weight because the Heitler-London function is only very approximate. The reason for the difference of the signs of q_{HL}' and q_J' is that the electronic part of q', q_{el}', is smaller for the Heitler-London function. By plotting both ρ_J and ρ_{HL} as a function of r_A for various θ_A, it was found that part of the difference of the q_{el}' arises from the fact that ρ_J is more peaked around $\theta_A=0°$ than ρ_{HL}.

The value of q' obtained with the Bartlett-Furry[13] function, q_{BF}', can be obtained from the preceding

[13] J. H. Bartlett, Jr., and W. H. Furry, Phys. Rev. **38**, 1615 (1931).

results by setting $J_a=J_b=0$. This procedure corresponds to the fact that the Bartlett-Furry function does not include the inner shells. One thus finds

$$q_{BF}'=0.760/R^3-N_1A_{bb}-2N_2A_{ab}=0.00227a_{\mathrm{H}}^{-3}. \quad (60)$$

Coulson and Duncanson[14] have obtained a molecular orbital type wave function for the Li_2 molecule in which the state of the valence electrons is represented by

$$\Psi_{CD}=(2N_{CD})^{-\frac{1}{2}}[\psi_{2sA}(1)+\psi_{2sB}(1)] \times[\psi_{2sA}(2)+\psi_{2sB}(2)][\alpha(1)\beta(2)-\beta(1)\alpha(2)], \quad (61)$$

where N_{CD} is a normalization constant and ψ_{2sA} is a $2s$ function centered on A, which is given by

$$\psi_{2sA}=n_{CD}(r_A-1.01)\exp(-0.81r_A), \quad (62)$$

ψ_{2sB} is obtained from ψ_{2sA} by replacing r_A by r_B; n_{CD} is a normalization constant chosen as $n_{CD}=0.301$, so that $\int\psi_{2sA}^2dV=1$. By analytic integration[15] one finds

$$\int\psi_{2sA}\psi_{2sB}dV=0.506, \quad (63)$$

so that $N_{CD}=1.506$. Because $(\psi_{2sA}+\psi_{2sB})$ is orthogonal on ψ_{1s}, no cross terms involving ψ_{1s} appear in q' which is given by

$$q_{CD}'=0.760/R^3-(1/N_{CD}) \times\left\{\int(1-\gamma)[(3\cos^2\theta_A-1)/2r_A^3]\psi_{2sB}^2dV +2\int(1-\gamma)[(3\cos^2\theta_A-1)/2r_A^3]\psi_{2sA}\psi_{2sB}dV\right\}. \quad (64)$$

By numerical integration, the integrals appearing in (64) were found to have the values 0.00367 and $0.00127a_{\mathrm{H}}^{-3}$, respectively. The result for q' is

$$q_{CD}'=0.760/R^3-0.00412=0.00178a_{\mathrm{H}}^{-3}. \quad (65)$$

Concerning the positive sign of q_{CD}', the same remark applies as for the Heitler-London result.

We would like to thank Drs. E. G. Harris and M. A. Melkanoff for sending us their results in advance of publication. We are also indebted to Dr. H. S. Snyder for several helpful discussions.

APPENDIX. EFFECT OF EXCHANGE ON THE SHIELDING CORRECTION

The exchange contribution to the shielding correction[7] arises from the fact that the field acting on the $1s$ electrons includes a term arising from the overlap of $1s$ with the valence wave function with parallel spin. The perturbation of the $1s$ function caused by this field contributes to q'. The same treatment as was given above [Eqs. (26)–(43)] shows that the change of q' can be calculated from the perturbation u_1 of the $1s$ function by the nuclear Q. The overlap of u_1 with the valence function produces a term $Q\Delta q_{\mathrm{exch}}'$ in the electrostatic energy from which $\Delta q_{\mathrm{exch}}'$ is obtained.

If one would use the actual James wave function for the valence electrons, the calculation of $\Delta q_{\mathrm{exch}}'$ would be very complicated. However, since the effect is quite small we make the approximation of replacing Ψ_J by the following wave function for the valence electrons

$$\Phi_v(1,2)=\phi_v(1)\phi_v(2), \quad (A1)$$

where

$$\phi_v=(\rho_{ff}/2)^{\frac{1}{2}}. \quad (A2)$$

Here ρ_{ff} and ϕ_v are regarded as functions of r_A and θ_A. Φ_v is a product wave function which gives the same valence density as the James function. The use of Φ_v is not expected to introduce any serious error and should give the correct order of magnitude of the exchange effect.

ϕ_v, as defined by Eq. (A2), is a superposition of s, p, d, f, $\cdots$ waves centered at A. We write

$$\phi_v=\phi_s\Theta_0+\phi_p\Theta_1+\phi_d\Theta_2+\cdots, \quad (A3)$$

where $\Theta_l=[(2l+1)/2]^{\frac{1}{2}}P_l$. ϕ_s, ϕ_p, and ϕ_d are, respectively, the radial s, p, and d, functions, and are obtained from

$$\phi_{s,p,d}(r_A)=\int_0^\pi\phi_v\Theta_{0,1,2}\sin\theta_Ad\theta_A, \quad (A4)$$

where the subscripts 0, 1, 2 correspond to s, p, d, respectively. The f and higher terms of ϕ_v make a negligible contribution to the exchange effect and will be disregarded. ϕ_s, ϕ_p, and ϕ_d were obtained by numerical integration for about 10 radii in the interval $0\leq r_A\leq 3a_{\mathrm{H}}$. For larger r_A, ψ_{1s} and u_1' are very small, so that the overlap with ϕ_v can be neglected.

It is convenient to use functions normalized to a volume element $r_A^2dr_A\sin\theta_Ad\theta_A$. We write

$$\phi_v'\equiv(2\pi)^{\frac{1}{2}}\phi_v\equiv(v_s\Theta_0+v_p\Theta_1+v_d\Theta_2)/r_A, \quad (A5)$$

so that v_s, v_p, and v_d are $(2\pi)^{\frac{1}{2}}r_A$ times ϕ_s, ϕ_p, and ϕ_d, respectively.

Consider the exchange of $\phi_v'(1)$ with the $1s$ electron of parallel spin which will be labeled $i=3$. The corresponding electron density is

$$\rho_{13}=\frac{1}{2}\left\{\frac{u_0'}{\sqrt{2}r}+\frac{Qu_1'P_2}{\sqrt{2}r}\right\}^2(1)\phi_v'^2(3) +\frac{1}{2}\left\{\frac{u_0'}{\sqrt{2}r}+\frac{Qu_1'P_2}{\sqrt{2}r}\right\}^2(3)\phi_v'^2(1) -\left\{\left[\frac{u_0'}{\sqrt{2}r}+\frac{Qu_1'P_2}{\sqrt{2}r}\right]\phi_v'\right\}(1) \times\left\{\left[\frac{u_0'}{\sqrt{2}r}+\frac{Qu_1'P_2}{\sqrt{2}r}\right]\phi_v'\right\}(3). \quad (A6)$$

[14] C. A. Coulson and W. E. Duncanson, Proc. Roy. Soc. (London) **A181**, 378 (1943).
[15] C. A. Coulson, Proc. Cambridge Phil. Soc. **38**, 210 (1942).

The last term gives the exchange effect. Upon using Eq. (A5) for ϕ_v' this term becomes

$$\rho_{\text{exch}}=-\left\{\left[\frac{u_0'}{\sqrt{2}r}+\frac{Qu_1'P_2}{\sqrt{2}r}\right]\left[\frac{v_s\Theta_0+v_p\Theta_1+v_d\Theta_2}{r}\right]\right\}(1)$$
$$\times\left\{\left[\frac{u_0'}{\sqrt{2}r}+\frac{Qu_1'P_2}{\sqrt{2}r}\right]\left[\frac{v_s\Theta_0+v_p\Theta_1+v_d\Theta_2}{r}\right]\right\}(3). \quad \text{(A7)}$$

ρ_{exch} gives rise to the following terms ΔE_i in the electrostatic energy: (1) ΔE_1 arising from the P_0 part of the potential of the density $\sim(Qu_1'v_dP_2\Theta_2)(1)$ acting on the term $\sim(u_0'v_s\Theta_0)(3)$; (2) ΔE_2 arising from the P_1 potential of $(Qu_1'P_2v_p\Theta_1)(1)$ acting on $(u_0'v_p\Theta_1)(3)$; (3) ΔE_3 arising from the P_2 potential of $(Qu_1'P_2v_s\Theta_0)(1)$ acting on $(u_0'v_d\Theta_2)(3)$; (4) ΔE_4 arising from the P_2 potential of $(Qu_1'P_2v_d\Theta_2)(1)$ acting on $(u_0'v_d\Theta_2)(3)$. In addition, there are four terms which are obtained from the preceding by interchanging electrons 1 and 3.

In order to obtain ΔE_1 one writes the density with the coordinates (1),

$$\rho_1(1)=-(2^{-\frac{1}{2}}Qu_1'v_dP_2\Theta_2/r^2)(1). \quad \text{(A8)}$$

The relevant term in the potential $2/r_{13}$ is $2P_0(1)P_0(3)/r_>$, where $r_>$ is the greater of r_1 and r_3. The potential due to $\rho_1(1)$ is

$$V_1(3)=-2^{\frac{1}{2}}Q\left[\frac{1}{r_3}\int_0^{r_3}u_1'v_dr_1+\int_{r_3}^{\infty}u_1'v_dr_1^{-1}dr_1\right]$$
$$\times\left(\int_0^{\pi}P_2\Theta_2\sin\theta_1d\theta_1\right)P_0(3)$$
$$=-(2/5^{\frac{1}{2}})QV_1'(r_3)P_0(3), \quad \text{(A9)}$$

where V_1' is the function in the square bracket; r_i and θ_i denote r and θ for electron i. $V_1(3)$ acts on the following density

$$\rho_1'(3)=2^{-\frac{1}{2}}u_0'v_s\Theta_0/r_3^2. \quad \text{(A10)}$$

This gives

$$\Delta E_1=\int_0^{\pi}\int_0^{\infty}V_1(3)\rho_1'(3)r_3^2dr_3\sin\theta_3d\theta_3$$
$$=-(2/5^{\frac{1}{2}})\int_0^{\infty}V_1'u_0'v_sdr_3. \quad \text{(A11)}$$

Equation (A7) shows that ρ_{exch} has a term $\rho_1'(1)\rho_1(3)$ which gives the same electrostatic energy as $\rho_1(1)\rho_1'(3)$. The contribution to $\Delta q_{\text{exch}}'$ from both terms is

$$\Delta q_1'=2\Delta E_1/Q=-(4/5^{\frac{1}{2}})\int_0^{\infty}V_1'u_0'v_sdr_3. \quad \text{(A12)}$$

The contributions $\Delta q_i'$ of the other terms $2\Delta E_i$ can be found in the same manner as $\Delta q_1'$. The results are as follows:

$$\Delta q_2'=-(8/15)\int_0^{\infty}V_2'u_0'v_pdr, \quad \text{(A13)}$$

where

$$V_2'(r)=(1/r^2)\int_0^{\infty}u_1'v_pr'dr'+r\int_r^{\infty}u_1'v_pr'^{-2}dr', \quad \text{(A14)}$$

$$\Delta q_3'=-(4/5^{\frac{1}{2}})\int_0^{\infty}V_3'u_0'v_ddr, \quad \text{(A15)}$$

$$V_3'(r)=r^{-3}\int_0^{r}u_1'v_sr'^2dr'+r^2\int_r^{\infty}u_1'v_sr'^{-3}dr'. \quad \text{(A16)}$$

$$\Delta q_4'=-(8/35)\int_0^{\infty}V_4'u_0'v_ddr, \quad \text{(A17)}$$

$$V_4'(r)=r^{-3}\int_0^{r}u_1'v_dr'^2dr'+r^2\int_r^{\infty}u_1'v_dr'^{-3}dr'. \quad \text{(A18)}$$

If the integrals appearing in Eqs. (A12), (A13), (A15), and (A17) are denoted by K_1, K_2, K_3, and K_4, respectively, $\Delta q_{\text{exch}}'$ can be written

$$\Delta q_{\text{exch}}'=-2[(4/5^{\frac{1}{2}})K_1+(8/15)K_2$$
$$+(4/5^{\frac{1}{2}})K_3+(8/35)K_4], \quad \text{(A19)}$$

where the factor 2 takes into account that both valence electrons contribute to the exchange.

The K_i were evaluated by numerical integration over v_s, v_p, and v_d. The values are: $K_1=11.66\times10^{-5}$, $K_2=1.87\times10^{-5}$, $K_3=5.73\times10^{-5}$, $K_4=0.25\times10^{-5}$, so that $\Delta q_{\text{exch}}'=-0.00048a_{\text{H}}^{-3}$.

Gamma-Gamma Angular Correlation in Pd^{106}

E. D. KLEMA AND F. K. MCGOWAN
Oak Ridge National Laboratory, Oak Ridge, Tennessee

(Received August 17, 1953)

The angular correlation of the 624- and 513-kev γ rays and that of the 1045- and 513-kev γ rays of Pd^{106} have been measured with a coincidence scintillation spectrometer using NaI detectors. For a dilute ruthenium chloride aqueous solution source, the correlation function of the 624–513-kev cascade is $W(\theta)=1+(0.3456\pm0.0079)P_2(\cos\theta)+(1.109\pm0.012)P_4(\cos\theta)$; that of the 1045–513-kev cascade is $W(\theta)=1+(0.0921\pm0.0027)P_2(\cos\theta)+(0.0350\pm0.0092)P_4(\cos\theta)$. In each of the above functions, the finite angular resolution of the equipment has been taken into account. The measurement on the 1045–513-kev cascade establishes the spin of the 1550-kev level as two and gives the intensity of the electric quadrupole radiation as 4.24 ± 0.14 percent relative to the intensity of the magnetic dipole radiation in the 1045-kev transition.

I. INTRODUCTION

IN a recent paper[1] Kraushaar and Goldhaber have reported a rather large discrepancy between the theoretically expected angular correlation of the 624–513-kev γ-γ cascade in Pd^{106} and the experimentally observed one. Previous measurements at Oak Ridge National Laboratory had indicated a much smaller discrepancy.[2] Since these measurements were made, the apparatus at Oak Ridge has been improved,[3] and it was decided to re-investigate the correlation with the new apparatus and to measure the angular correlation of the 1045–513-kev cascade. In addition the question of the angular resolution of the apparatus has been re-examined.

II. ANGULAR RESOLUTION CORRECTION

Finite solid angle corrections for directional angular correlation measurements have been treated in considerable detail recently by Walter,[4] Frankel,[5] Church and Kraushaar,[6] Rose,[7] and Lawson and Frauenfelder.[8] In our measurements we use the angular resolution corrections[7] which have been computed as a function of the geometry and the cross section of the NaI detector for γ radiation. Recently, Steffen[9] and Lawson and Frauenfelder[8] have indicated that the computed corrections[7] are useful as an approximation and that the corrections can only be achieved by using experimentally determined angular resolution curves. The latter statement is true for the arrangement and operation of the detectors which most other workers use in their angular correlation apparatus.

In view of this it seems appropriate to show that the computed corrections of Rose[7] are valid provided the detectors are operated under the conditions for which the calculations were made. These conditions are that the absorption of γ radiation in the NaI crystal is proportional to $(1-e^{-\tau x(\beta)})$ and that there is no radiation loss between the source and the NaI crystal. This latter condition has considerable significance in the finite angular resolution corrections.

In any practical geometrical arrangement of the source and detectors for an angular correlation apparatus, there is always degraded radiation, in addition to the undegraded radiation from the source, incident on the detectors. To shield against the degraded radiation resulting from the scattering of the primary radiation from the surroundings of the detectors, most workers have used lateral Pb shields around the NaI crystals and in some cases Pb shields on the front faces of the crystals. Unfortunately, this type of shield does not shield against degraded radiation scattered from the surroundings beyond the back face of the crystal with cylindrical symmetry. In addition, since the solid angle subtended at the source by the lateral Pb shield is usually larger than the solid angle subtended by the NaI crystal, the primary radiation scattered from the Pb shielding provides another source of degraded radiation incident on the detector. The Pb shielding in close to the detector thus increases the effective solid angle of the detector.

A differential pulse-height spectrum of 512-kev γ radiation incident on a NaI scintillation spectrometer has been measured to illustrate the points mentioned above. The solid curve of Fig. 1 is the pulse spectrum of undegraded radiation from a source of Sr^{85} located at 7 cm from the front face and on the axis of a NaI crystal 1.5 in. in diameter and 1.0 in. long. The lateral sides and front face of the crystal are covered with 30 mg/cm² of MgO and 0.010 in. of Al. The dashed curve at the lower pulse heights and the solid curve for pulse heights greater than 550 is the pulse spectrum of both the undegraded radiation and the degraded radiation resulting from scattering by the surroundings. The difference between these two curves represents the pulse spectrum of degraded radiation from the surroundings. The intensity of the degraded pulse spectrum relative to the undegraded pulse spectrum is 12 percent. The curve represented by the solid points is

[1] J. J. Kraushaar and M. Goldhaber, Phys. Rev. **89**, 1081 (1953).
[2] Arfken, Klema, and McGowan, Phys. Rev. **86**, 413 (1952).
[3] E. D. Klema and F. K. McGowan, Phys. Rev. **91**, 616 (1953).
[4] Walter, Huber, and Zünti, Helv. Phys. Acta **23**, 697 (1950).
[5] S. Frankel, Phys. Rev. **83**, 673 (1951).
[6] E. L. Church and J. J. Kraushaar, Phys. Rev. **88**, 419 (1952).
[7] M. E. Rose, Phys. Rev. **91**, 610 (1953).
[8] J. S. Lawson, Jr. and H. Frauenfelder, Phys. Rev. **91**, 649 (1953).
[9] Rolf M. Steffen, Phys. Rev. **90**, 321 (1953).

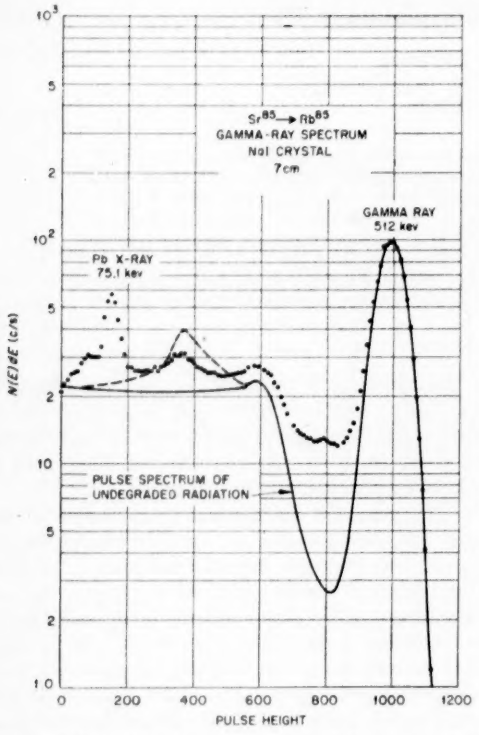

FIG. 1. Differential pulse spectrum of the Sr^{85} gamma radiation incident on a NaI scintillation spectrometer for the various experimental conditions discussed in the text.

the pulse spectrum of the γ radiation incident on the detector with 0.6 cm of Pb around the lateral sides and front face of the NaI crystal. This amount of Pb is less than that used by most workers, but is enough to attenuate the degraded radiation from the surroundings by a factor of 10^3. In this case the intensity of the degraded pulse spectrum relative to the undegraded pulse spectrum is 27 percent. In addition, the degraded spectrum is spread over a greater portion of the undegraded pulse spectrum.

In either arrangement it is desirable to operate the scintillation detector as a spectrometer rather than as a pulse counter, selecting only the full-energy peak of the pulse spectrum to insure that only undegraded radiation is counted. This method of operation immediately assures one that the solid angle subtended by the detector at the source, aside from the effect of the very small coherent scattering cross section of γ radiation by matter, is that subtended by the NaI phosphor.

In our equipment the windows of the differential pulse-height analyzers of the coincidence scintillation spectrometer in the angular-correlation apparatus are always set to include only the full-energy peak of the pulse spectrum of the γ ray in question. The full energy of the γ ray is dissipated in the phosphor by photoelectric absorption and also by multiple processes, i.e., Compton recoil electrons and the eventual absorption of the Compton-scattered γ ray. The ratio of the integral of the pulse spectrum in the full-energy peak to the integral of the total pulse spectrum of undegraded radiation is, of course, a function of the γ-ray energy incident on the NaI phosphor. Also, the peak to total ratio (ratio of the two integrals mentioned above) is expected to vary slightly over the NaI phosphor. This variation was neglected in the calculation of the corrections for finite angular resolution[7] for two reasons. The variation of the peak to total ratio over the crystal is not known, and preliminary estimates indicated that this effect on the finite angular resolution was very small.

After the computed angular resolution corrections were completed, the angular resolution was measured experimentally at $E_\gamma = 1.114$ Mev using a source of Zn^{65}. At this energy the contribution of the multiple processes to the intensity of the full-energy peak of the pulse spectrum is largest and is comparable to the photoelectric absorption contribution. If the measured and computed angular resolution corrections agree at this energy, then one is perfectly justified to use the computed corrections at all other energies.

The angular resolution curve for a collimated beam of 1.114-Mev γ rays is shown in Fig. 2. The radiation from a 2-mc source of Zn^{65} was collimated by a 0.3-cm diameter hole through a 4-in. Pb brick. To obtain the angular resolution curve in Fig. 2 one must, of course,

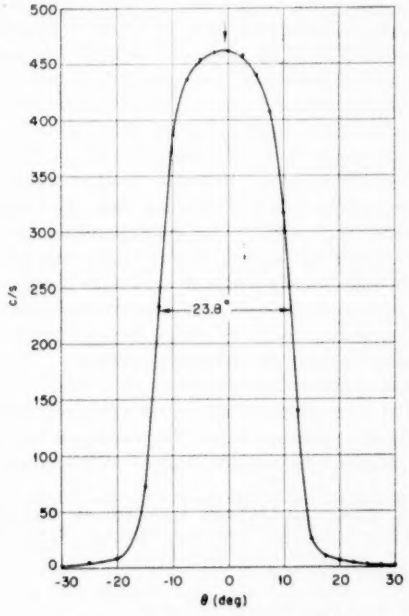

FIG. 2. Angular resolution curve for 1.114-Mev γ rays collimated onto a NaI crystal 1.5 inches in diameter by 1 inch long located at 7 cm from the axis of rotation.

measure the angular resolution with the collimator and with the collimator replaced by a solid Pb brick.

The integrals $J_l = \int_0^{\theta_{max}} P_l(\cos\theta)\epsilon(\theta)\sin\theta d\theta$ were evaluated by numerical integration for $l=0$, 2, and 4 using the observed angular resolution curve of Fig. 2 for $\epsilon(\theta)$. The results in the form J_2/J_0 and J_4/J_0 were 0.2 and 0.7 percent larger than the computed values.[7] The deviations are in the direction expected because the computed corrections are not weighted over the NaI phosphor to account for the variation of the peak to total ratio over the phosphor. Since the discrepancies are considerably smaller than the fractional standard deviations of the measured angular correlation coefficients due to statistical fluctuations, the use of the computed angular-resolution correction factors is certainly justified. To obtain the correction factors from measured angular-resolution curves, one is limited to about eight sources with a single monoenergetic γ ray having energies distributed between 279 and 1114 kev. Of these eight, only four may be obtained with sufficiently high specific activity to provide a source of well-collimated γ rays.

III. EXPERIMENTAL METHOD AND RESULTS

In the present experiments the data were obtained as discussed in the previous paper[3] and analyzed as discussed in the paper of Rose.[7] However, in the case of Pd^{106}, the energy resolution of the equipment has a very marked effect on the observed results.[2] The β^- shield for these measurements consisted of $\frac{1}{16}$ in. of Cu on the lateral sides of the crystal and $\frac{1}{2}$ in. of fluorothene on the front face. The γ-ray spectrum of the ruthenium chloride source is shown in Fig. 3. The bump on the high-energy side of the full-energy peak of the 1045-kev γ ray at about 960 pulse-height units is due mostly to sum pulses of a 513- and a 624-kev γ ray. Each point on the curve out to a pulse height of 1000 units contains 4096 counts, and the points for greater pulse heights contain 1024 counts each.

In the first set of experiments on the main cascade of Pd^{106}, the window of the differential analyzer of the fixed detector was set between the limits represented by A in Fig. 3 and the window of the moveable detector was set at B in the measurement of the correlation due to the composite 624–513, 870–513, 870–1045, 1045–513, and 870–1550 kev cascades and a source of coincidence counts due to inner and external bremsstrahlung correlated primarily with either the 513- or the 624-kev γ rays. Preliminary measurements indicate that the 870-kev γ ray is not in coincidence with the 1045. Alburger's[10] decay scheme predicts that they should be in cascade; thus the interference of the cascades other than the main one may not be as indicated above. A total of 6×10^5 coincidence counts were measured at 19 angular positions with this arrangement, and the angular correlation obtained was

[10] David E. Alburger, Phys. Rev. **88**, 339 (1952).

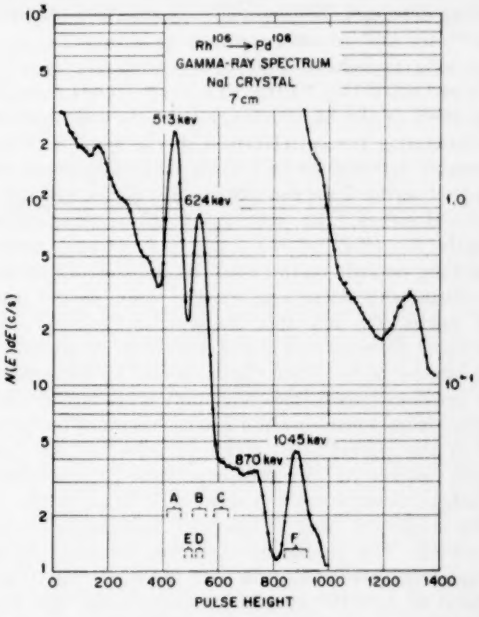

FIG. 3. Gammay-ray spectrum of the ruthenium chloride source. The right-hand section of the curve above pulse height 910 is to be referred to the scale at the right of the figure. The limits represented by A, B, C, etc. show the positions of the windows of the differential pulse-height analyzers for the various experiments described in the text.

$W(\theta)=1+0.3173\ P_2(\cos\theta)+1.058\ P_4(\cos\theta)$. The movable detector window was then set at C, and 2.5×10^4 counts were obtained at this setting, which represents the correlation due to the 1045–513-kev cascade and the bremsstrahlung correlated with the 512-kev γ ray. The position of the window at C is in the valley between the Compton distribution and the full-energy peak of the 870-kev γ ray; thus, virtually none of the cascades involving the 870-kev γ ray contribute to this measurement. The second correlation function was then subtracted from the first to give the correlation function for the 624–513-kev cascade as measured by this experiment. The function obtained is

$$W(\theta)=1+(0.3272\pm0.0047)P_2(\cos\theta)+(1.103\pm0.0025)P_4(\cos\theta).$$

Clearly, this is not quite the correct function because the correlation due to the higher energy cascades in which the 870-kev γ ray enters has not been subtracted off properly.

In order to get a better measurement of the correlation function of the main cascade, the following set of experiments was performed. The fixed analyzer was left at A and the movable one was set at D as shown in Fig. 3 in the measurement of the composite correlation. The random coincidences were not measured in this experiment, but were calculated from the known resolving time of the apparatus and the singles rates of

the two detectors. The resolving time is $(0.113\pm0.001)\times10^{-6}$ sec and remains constant to within 2 percent over long periods of time. The correlation function obtained was $W(\theta)=1+0.3310\,P_2\cos(\theta)+1.061\,P_4\cos(\theta)$. The effect of the higher-energy cascades was obtained by measuring the correlation with the window of the moveable detector set at E (both D and E are on the flat part of the Compton distribution of the 870-kev γ ray). However, the setting at E overemphasizes slightly the effect of the inner and external bremsstrahlung because of the rapid increase of the photon spectrum with decreasing energy. Also, in this case the correction for the changes in gain of the moveable detector and of the fractional acceptance of the window of its differential analyzer as discussed in the previous paper[3] does not apply since the product of the channel rates is not a good measure of the product of the individual efficiencies involved in the composite correlation. In this experiment, the windows remained constant to 1 percent with respect both to pulse height and their widths, and these data were not corrected. The correlation function obtained under these conditions in two runs with the window at D and a total of 2.8×10^5 coincidence counts and two runs with the window at E and a total of 1.2×10^5 counts is

$$W(\theta)=1+(0.3456\pm0.0079)P_2(\cos\theta)+(1.109\pm0.012)P_4(\cos\theta).$$

In the above function the standard deviations of the coefficients of P_2 and P_4 have not been calculated as discussed in the previous paper.[3] At present the standard deviation of each term in the expansion of the correlation function is calculated in the least-squares fit of the data of each run. The standard deviation of the mean of the runs is then calculated from the deviations of the individual runs. This can be done easily because the various runs of the experiment have the same number of degrees of freedom statistically and their individual variances can be combined directly.

The correlation function of the 1045–513-kev cascade was measured with one window at A and the other at F as shown in Fig. 3. Again in this case, since the counting rates were low, the correction for the random coincidence rate was calculated. The correlation obtained for four runs with a total coincidence count of 10^5 is

$$W(\theta)=1+(0.0921\pm0.0027)P_2(\cos\theta)+(0.0350\pm0.0092)P_4(\cos\theta).$$

IV. DISCUSSION

The discrepancies between the theoretical and experimental coefficients of P_2 and P_4 for the spin sequence 0–2–0 in the cleaner measurement of the present series on the main cascade are about 3 percent and are 1.5 and 2.8 times the standard deviation of the measurements. It is believed that these discrepancies are caused by interfering radiation in the windows of the differential analyzers even for the narrowest windows it was practical to use. Pound and Abragam[11] have recently attributed the considerably larger discrepancies (22.1 and 13.6 percent) found by Kraushaar and Goldhaber[1] to the interaction of the electric quadrupole moment of the intermediate state of the nucleus with the gradient of the electric field due to the electrons. The present results indicate that the attenuations of the cofficients of P_2 and P_4 by this interaction, if any, are exceedingly small. The discrepancy between the results obtained at Oak Ridge and those obtained at Brookhaven is probably to be explained in the use of differential pulse-height selection at Oak Ridge. This type of operation permits one to reduce the effect of the interfering cascades and also to measure their effect directly. This is shown by the fact that the discrepancies between the correlations uncorrected for the interfering cascades and theory were 12.5 and 7.9 percent for the coefficient of $P_2(\cos\theta)$ and 8.0 and 7.7 percent for the coefficient of $P_4(\cos\theta)$ in the two sets of experiments described in the foregoing. We have tried several different sources, both liquid and solid, and have obtained the same results with all of them. We have also used the equipment with only integral pulse-height selection, and in this case we can get correlation function similar to those obtained at Brookhaven.

The measured correlation function of the 1045–513-kev cascade allows the unambiguous assignment of spin 2 to the 1550-kev level in Pd^{106} in agreement with our previous measurements.[2] From the value of the measured coefficient of P_2 and its standard deviation, one finds that the 1045-kev transition consists of 4.24 ± 0.14-percent electric quadrupole radiation relative to magnetic dipole radiation. The value for the mixing ratio obtained from the measurement of the coefficient of P_4 is not so precise and differs from the above by about twice its standard deviation.

[11] R. V. Pound and A. Abragam, Phys. Rev. **90**, 993 (1953).

Uranium-235 Thermal Neutron Fission Yields*

GEORGE W. REED†‡ AND ANTHONY TURKEVICH
Institute for Nuclear Studies and Chemistry Department, University of Chicago, Chicago, Illinois, and Argonne National Laboratory, Lemont, Illinois

(Received September 14, 1953)

The absolute yields of six nuclides in the thermal neutron fission of U^{235} have been determined to better than 6 percent, using fission counting and radiochemical techniques. The results are in good agreement with earlier determinations of lower accuracy. They support mass spectrometric indications of fine structure in the yield-mass curve in low-energy nuclear fission.

A. INTRODUCTION

THE first techniques used to investigate quantitatively the relative yields of different masses in the slow neutron fission of U^{235} were based on radiochemistry.[1–3] These studies indicated that, to within the accuracy of the method, the yield distribution was a smooth function of the mass with rather broad maxima centering about masses 95 and 139. Although sufficiently sensitive to define the main features of the yield distribution, the radiochemical techniques have not been considered trustworthy enough to establish differences in yield of less than ten or fifteen percent, primarily because of the difficulty in absolute beta assay.§ In spite of this, the radiochemical yields are the most complete and the curve for the yields in thermal fission of U^{235} has become the standard with which many other yield curves have been compared.[4]

Recent accurate mass-spectrometric determinations[5,6] of the relative yields of stable, or relatively long-lived, isotopes of selected elements formed in the slow neutron fission of U^{235} have indicated appreciable departures from a smooth double-maximum yield curve. The conversion of relative isotopic yields of an element determined by mass spectrometry into absolute yields, as well as the comparison of the relative yields of different elements, has often involved the use of the old radiochemical results of much poorer accuracy.

The present work arose out of calibration experiments designed to determine absolute yields in the fast neutron fission of Th^{232}. In the course of this work, it was noticed that, contrary to expectation, the yield of Mo^{99} in the slow neutron fission of U^{235} appeared to be higher than that of Zr^{97}. In order to investigate this more fully, as well as attempt to provide more accurate radiochemical data to supplement current mass-spectrometric investigations, it was decided to measure the yields of several nuclides in the slow neutron fission of U^{235}.

The absolute yield of a nuclide formed in the fission of a heavy element is defined as the fraction of the fissions (usually expressed in percent) that give rise to this particular nuclide. The relative yields of two nuclides measure only the relative frequency with which they are formed. Both absolute and relative fission yields were determined in this study. In the absolute experiments, the yields of selected fission products were established in a sample of uranium that had undergone a known number of fissions. These experiments were all performed with moderated neutrons from the University of Chicago 37-in. cyclotron. In the relative experiments, the yields of various fission products in a sample of irradiated uranium were compared with each other. The irradiations for relative yield measurements were performed at the cyclotron and in a thermal column of the Argonne Heavy-Water Pile.

B. FISSION COUNTING

Counting Apparatus

The total number of fissions and the fission rate in a sample heavy enough to be used for radiochemical analyses were determined by comparison with a thin monitoring sample placed in the same neutron flux. From the relative weights of fissile material in the monitor and heavy samples, the number of fissions in the latter could be calculated from that observed in the former. The geometrical relation of the two samples is illustrated in Fig. 1.

* The University of Chicago 37-inch cyclotron, supported by the U. S. Office of Naval Research and the U. S. Atomic Energy Commission, and the Argonne National Laboratory *CP–3'* pile were used for the irradiations reported in this work.

† Submitted in partial fulfillment for the Ph.D. degree in the Department of Chemistry, University of Chicago, Chicago, Illinois.

‡ Julius Rosenwald Fellow, 1948–1949. U. S. Atomic Energy Commission Predoctoral Fellow in Chemistry, 1949–1951. Now at the Argonne National Laboratory, Lemont, Illinois.

[1] Anderson, Fermi, and Grosse, Phys. Rev. **59**, 52 (1941); see also L. A. Turner, Revs. Modern Phys. **12**, 1 (1940).

[2] *Radiochemical Studies: The Fission Products* (McGraw-Hill Book Company, Inc., New York, 1951), National Nuclear Energy Series, Plutonium Project Record, Vol. 9, Div. IV. Hereafter referred to as N.N.E.S.

[3] W. E. Grummitt and G. Wilkinson, Nature **158**, 163 (1946).

§ *Note added in proof.*—Since submission of this manuscript, a paper by S. Katcoff and W. Rubinson [Phys. Rev. **91**, 1458 (1953)] reports an accurate radiochemical determination of the yield of Xe^{133} in the thermal neutron fission of U^{235}.

[4] See, for instance, R. W. Spence and co-workers, Brookhaven Conference Report, Chemical Conference No. 3, 1949 (unpublished); A. Turkevich and J. B. Niday, Phys. Rev. **84**, 52 (1951).

[5] H. G. Thode and R. L. Graham, Can. J. Research **A25**, 1 (1947); Macnamara, Collins, and Thode, Phys. Rev. **78**, 128 (1950).

[6] Glendenin, Steinberg, Inghram, and Hess, Phys. Rev. **84**, 860 (1951).

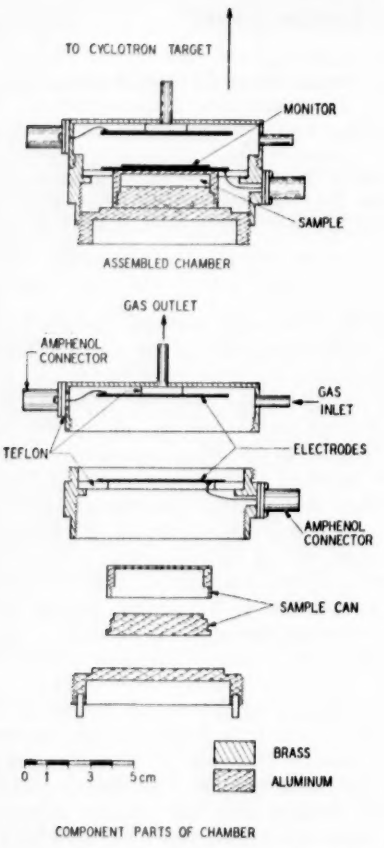

FIG. 1. Ionization chamber and sample container.

The number of fissions occurring in the monitor sample was measured by counting the fission pulses produced in an ionization chamber. The monitor sample was thin enough (6.34 $\mu g/cm^2$) so that one of the two fission fragments resulting from a fission event was quite certain to get into the active region of the ionization chamber and to produce a pulse. The ionization chamber is illustrated in Fig. 1. Teflon, a fluorocarbon plastic, was used for insulation, instead of a hydrocarbon plastic, in order to avoid the pulse resulting from pile-up of "knock-on" protons from neutrons at the cyclotron. Electron collection was used with argon continuously sweeping through the chamber.

The electronic equipment for counting the fission pulses in the chamber was fairly standard and will not be described in detail. It consisted of a phase inverter and cathode follower unit (attached directly to the ionization chamber); a preamplifier (located about five feet away from the chamber); and an amplifier, discriminator, and scaler (placed some hundred feet away in the control room of the cyclotron). The filaments of tubes in the cathode follower and preamplifier were battery heated. The over-all gain of the amplifier unit was about 5×10^3. The discriminator bias could be set to pass pulses ranging from 10 to 100 volts. The main modification from standard equipment was the insertion into the amplifier of an electronic limiter to suppress large transients caused by electrical breakdowns at the cyclotron. An oscilloscope was used at the amplifier stage of the equipment for visual observation of the behavior of the ionization chamber. The output of the scaler was put into a mechanical register and also into an Esterline-Angus recorder.

It was found that the fission pulses were at least three times larger than the alpha pulses or the noise level, even when the cyclotron was operating. Thus, electronic discrimination was easy. Likewise, the magnetic field of the cyclotron did not affect the behavior of the ionization chamber or of the close-by electronic equipment, if the latter was oriented properly.

The ionization chamber was normally operated with a collecting voltage of 250 volts; a sevenfold increase in this voltage increased the counting rate less than 1 percent. The gain plateau, corrected for background, was flat to better than 1 percent over a gain increase of 60 percent. The discriminator plateau was also satisfactory.

The main difficulty in operating near the cyclotron was caused by transients from electrical breakdown of the cyclotron which were picked up by the equipment. The effect of these on the fission counting was minimized by the "limiter" in the amplifier (see above). These spurious events were monitored visually and by comparison of the Esterline-Angus record (with its slow response time) and the beam integrator of the cyclotron with the mechanical register of the scaler. In no case was the number of spurious fissions that had to be subtracted larger than 4 percent. Usually, it was less than 1 percent.

The natural background in the chamber was negligible. In the work with thermal neutrons, however, the fission background from the chamber with the cyclotron operating was about 15 percent of monitor counting rate. This was due to contamination in the materials of the chamber. It was established that the presence of the monitor did not change this background. The background was determined separately for each experiment and was relatively constant. Since the background fission rate, like the monitor fission rate, was determined to be proportional to the beam intensity of the cyclotron, the correction for background in each run was a fractional one.

Neutron Sources

The University of Chicago 37-in. cyclotron was used as the source of neutrons for all the absolute fission yield work. A thermal column at the Argonne Heavy-Water Pile was used in some of the irradiations of uranium for relative fission yields.

At the cyclotron, neutrons were produced by 7.7-Mev deuterons impinging on a beryllium target. The

irradiations were performed by placing the ionization chamber containing the sample and monitor inside a paraffin block. There were at least 10 cm of paraffin on all sides and the monitor was 19 cm from the beryllium target. In this geometry, the fraction of fissions caused by neutrons above the cadmium cutoff was determined to be no greater than 7 percent.

Since the uranium samples used were rather large, it was important to investigate the variation in neutron flux within the heavy sample and between the sample and monitor. It was established by use of small manganese chips that this flux was uniform to better than 1 percent in the planes of the monitor and sample. The activation of manganese chips placed on the surfaces and in the interior of typical heavy U_3O_8 samples indicated that the average flux throughout the heavy sample was 1½ percent lower than that in the monitor. This self-shadowing problem was also investigated using fission recoils ejected from 6 cm^2 foils of natural uranium metal ($\sim$0.4 g/cm^2). These recoils were caught on polystyrene and counted as a measure of the fissions occurring in the foils. The results of several such experiments indicated that the flux was about 2½ percent lower in the heavy samples of U_3O_8, as compared with that in the uranium monitor. An average flux attenuation of 2 percent was used in the calculations.

Uranium Monitor and Samples

The monitor used to measure the fissions occurring in the uranium was prepared by painting several coats of a very dilute solution of uranyl nitrate in ether over an area of 12.57 cm^2 on a thin aluminum disk. The weight of uranium so deposited was determined by alpha counting in a parallel plate ionization chamber. A specific activity of 2.501×10^4 alphas/sec g was used in the calculation[7] of the mass of uranium, together with a backscattering correction of 0.85 percent.[8] The weight of uranium in the monitor was 79.2 ± 0.7 micrograms.

The heavy uranium samples used for isolation of fission products in the absolute yield experiments were U_3O_8 prepared from[9] ether extracted Mallinckrodt analytical reagent grade $UO_2(NO_3)_2\cdot6H_2O$. In the relative yield work, the nitrate itself was used. The samples were packed in sample cases 4 cm in diameter (Fig. 1) and ranged in weight from 12 to 22 g of uranium. About 0.5 percent of the fission fragments are estimated to be lost because of recoil from such samples.

In summary, the number of fissions in the heavy samples are related to the observed fissions in the monitor by the relative weights of uranium in the two samples. The computed number of fissions in the heavy sample are then reduced by 2.5 percent to correct for neutron attenuation and recoil loss. Consideration of the errors arising from the determination of weights of uranium in the monitor and sample, from the inhomogeneity of neutron flux, and from the relatively large background leads us to believe that this procedure is correct to 2.5 percent.

C. ABSOLUTE BETA DISINTEGRATION RATES. I

The problem of estimating the number of fission product atoms from their measured radioactivity involves the determination of absolute beta disintegration rates. At the time this work was started, it appeared that the use of thin end-window Geiger tubes was as good a method as any to do this for the fission products of interest.

The principle of this method, as applied to these studies, is to count samples of the radioactivity in question under conditions in which they can be compared with standard samples whose absolute disintegration rates are known. It has been shown[10–12] that this comparison is best made with weightless ($<$0.2 mg/cm^2) samples mounted on very thin films in order to reduce differences arising from variation in the backscattering and self-scattering of particles of different energies. Since the standard sample is usually a different nuclear species than the one being measured, the relative activities must be corrected for differences in the attenuation of the radiations in the air between the sample and counter tube, in the thin window of the tube, and for differences arising from complexity in decay. In addition, experimental calibration curves are prepared for each radioactivity relating the activity measured under conditions where the absolute rate can be determined by this method to that measured in the usual situation in the fission yield studies (10–30 mg samples mounted on aluminum cards).

In this work RaDEF standards were used. The use of such standards has been investigated by several workers.[10–12] Their data indicate that absolute disintegration rates of simple, moderate-energy beta emitters can be determined by comparison with RaDEF standards with an accuracy of about 2 percent.

In the last stages of this work, it was possible to check the techniques used for absolute beta assay by comparison of the results with those using a 4π beta counter.[13] Three samples of Sr^{89} measured by the two techniques agreed to 1 percent in their disintegration rates.

The RaDEF standards were prepared by the techniques described by Novey.[11] A solution of RaDEF in equilibrium was evaporated on a 1.5 cm^2 area of rubber hydrochloride film. The RaE (beta) disintegration rate in the standard was calculated from the RaF (alpha)

[7] A. F. Kovarik and N. I. Adams, J. Appl. Phys. **12**, 291 (1941).
[8] This was estimated from the theoretical work of J. A. Crawford, Paper No. 16.55, N.N.E.S., Vol. 14B, Div. IV, and by interpolation of data on Pt, Ni, and rubber hydrochloride.
[9] W. W. Scott, *Standard Methods of Analysis* (D. Van Nostrand Book Company, Inc., New York, 1939), Vol. 1, p. 1022.
[10] L. Zumwalt, U. S. Atomic Energy Commission Unclassified Report MDDC-1346 (unpublished).
[11] T. B. Novey, Rev. Sci. Instr. **21**, 280 (1950).
[12] B. P. Burtt, Nucleonics **5**, 28 (1949).
[13] This counter was made available by T. B. Novey of the Argonne National Laboratory.

activity, the alpha counter efficiency (0.5013),[11] and the disintegration constants of the RaDEF system.

The beta activities of the fission product samples and the RaDEF standards were measured in a reproducible position ~4 mm from the window of a helium-filled Geiger tube. Three different tubes were used with window thicknesses of 1.7 to 3.0 mg/cm². The measurements of the RaDEF standards were made with 9.85 mg/cm² of aluminum at the window to eliminate the soft radiations of RaD and the alphas of RaF. An absorption curve taken on RaDE samples under the same conditions, and extrapolated by an amount corresponding to the weight of air and window, indicated the factor by which the measurement through 9.85-mg/cm² aluminum should be multiplied to get the number of particles directed toward the effective part of the counter (1.29 in the case of a counter with 1.9-mg/cm² window).

D. BETA DISINTEGRATION RATES. II

The fission-product nuclides whose disintegration rates were measured in this work were 53-day Sr^{89}, 9.7-hr Sr^{91} counted through its 57-day Y^{91} daughter, the 17.0-day $Zr^{97}-Nb^{97}$ system, the 67-hr $Mo^{99}-Tc^{99m}$ system, 85-min Ba^{139}, and the 12.8-day $Ba^{140}-40.0$-hr La^{140} system.

The fission chains, as far as they are known, for the mass numbers of these nuclides are presented below. The data on half-lives and mechanism of decay of the nuclides studied in this work are primarily from the recent compilations[14,15] of nuclear data. The elements appearing in boldface are those that were isolated for observation.

Mass No.

89 $\quad Br \xrightarrow{4.5\text{-sec}} Kr \xrightarrow{2.6\text{-min}} Rb \xrightarrow{15.4\text{-min}} \mathbf{Sr} \xrightarrow{53\text{-day}} Y\ (\text{stable})$

91 $\quad Kr \xrightarrow{9.8\text{-sec}} Rb \xrightarrow{(\text{short})} \mathbf{Sr} \xrightarrow{9.7\text{-hr}} \begin{cases} Y^m \\ \downarrow\ 51\text{-min} \\ Y \xrightarrow{57\text{-day}} Zr\ (\text{stable}) \end{cases}$

97 $\quad Kr \xrightarrow{1\text{-sec}} Rb \xrightarrow{(\text{short})} Sr \xrightarrow{(\text{short})} Y \xrightarrow{(\text{short})} \mathbf{Zr} \xrightarrow{17.0\text{-hr}} Nb^m \downarrow\ 1\text{-min} \\ Nb \xrightarrow{74\text{-min}} Mo\ (\text{stable})$

99 $\quad \mathbf{Mo} \xrightarrow{67\text{-hr}} \begin{cases} Tc^m \\ \downarrow\ 6.0\text{-hr} \\ Tc \xrightarrow{2.1\times10^5\text{-yr}} Ru\ (\text{stable}) \end{cases}$

139 $\quad I \xrightarrow{2.7\text{-sec}} Xe \xrightarrow{41\text{-sec}} Cs \xrightarrow{9.5\text{-min}} \mathbf{Ba} \xrightarrow{85\text{-min}} La\ (\text{stable})$

140 $\quad Xe \xrightarrow{16\text{-sec}} Cs \xrightarrow{66\text{-sec}} \mathbf{Ba} \xrightarrow{12.8\text{-day}} La \xrightarrow{40.0\text{-hr}} Ce\ (\text{stable})$

Solutions of all the nuclides to be measured (except Y^{91}) were prepared in high purity and high specific activity from neutron irradiated uranium. Essentially weightless (<0.15 mg/cm²) samples were mounted for beta counting in exactly the same manner as were the RaDEF standards (i.e., spread over an area of 1.5 cm² on ~0.5-mg/cm² rubber hydrochloride). They were then measured in the same position as the RaDEF standards. Aluminum absorption curves were taken with the absorbers at the window of the Geiger-Mueller tube.

In order to convert the activity of samples measured in this manner to disintegration rates, there are required in addition to the geometry, which is established by comparison with the RaDEF standards, corrections for (a) the presence of isotopic radioactivity; (b) the absorption of the radiations by material present be-

[14] *Nuclear Data*, National Bureau of Standards Circular 499 (U. S. Government Printing Office, Washington, D. C., 1950) and supplements (1950–1952).

[15] Hollander, Perlman, and Seaborg, Revs. Modern Phys. **25**, 469 (1953).

tween the sample and the active volume of the counter (usually only the air and the counter window); and (c) the presence of more than one detectable particle in each disintegration (e.g., gamma rays, conversion electrons, or daughter radioactivity). Since all three factors can give rise to appreciable corrections, their estimation will be presented in some detail for each nuclide studied.

53-Day Sr^{89}

This nuclide decays with a 1.5-Mev beta and no accompanying gamma rays. The initial part of the aluminum absorption curve has a half thickness of 100 mg/cm² and the effect of the window and air (~2.4 mg/cm²) was estimated assuming exponential absorption. The only complication is the presence of the 20-yr Sr^{90}→60-hr Y^{90} chain. The effect of this was calculated assuming equal fission yields and estimating the relative counting efficiencies of the 20-yr Sr^{90} and of its 60-hr yttrium daughter. The correction was usually less than 2 percent.

57-Day Y^{91}

This nuclide has a 1.57-Mev beta and no gamma. Its beta spectrum has the same shape as that of Sr^{89}. For this reason, the same absorption corrections were used as in the case of Sr^{89}.

17.0-Hr Zr^{97}→1-Min Nb^{97m}→74-Min Nb^{97}

This system was always measured in transient equilibrium. The Zr^{97} and Nb^{97} have hard betas (1.91 Mev and 1.267 Mev, respectively). The 1-min Nb^{97m} decays by a gamma of 0.747 Mev which is 1.5 percent converted. The 74-min Nb^{97} also has a 0.665-Mev gamma ray, 0.15 percent converted. The contribution of the gamma rays was determined by absorption techniques to be 0.6 percent. The conversion electrons were assumed to contribute 0.8 percent to the equilibrium activity. The beta absorption curve of the Zr^{97} system indicate a half thickness of 100 mg/cm². This was used to correct for the effect of window and air. The contribution of the isotopic 65-day Zr^{95} and its daughter, as well as occasionally contaminating long-lived activities, were obtained after decay of the Zr^{97} chain.

67-Hr Mo^{99}

This nuclide decays partially to the 6.0-hr metastable state of Tc^{99}. A sample of Mo^{99}, freed of its daughter, was used to get an absorption curve below 21 mg/cm² aluminum. This was extrapolated by the amount of window and air absorption. Because of the presence of two beta rays in the decay of Mo^{99} (87 percent of 1.23 Mev and 13 percent of 0.5 Mev), several different methods of extrapolation were tried. These were based upon the apparent course of the actual absorption curve and on a synthetic absorption curve calculated assuming exponential absorption of the two betas and linear absorption of the conversion electrons. The results agreed to within 1 percent, indicating 95-percent transmission of the beta rays. All further samples of the Mo^{99}—Tc^{99} system were then counted in transient equilibrium with 21.0-mg/cm² added absorber. It was established that, as expected, this absorber effectively removed contributions from the 6.0-hr Tc^{99m} daughter. The total absorption correction for measurements made with this absorber was 1.47 for a tube with a window equal to 1.9 mg/cm².

The unconverted gamma rays of Mo^{99} and Tc^{99m} in equilibrium were determined experimentally to contribute 0.6 percent. In addition, a 1.4 percent contribution was assumed from the conversion of the 141-kev and 181-kev gamma rays coincident with the beta decay of Mo^{99}.

85-Min Ba^{139}

Absorption curves of the Ba^{139} samples indicated a half-thickness of 134 mg/cm² for the ~2.4-Mev beta. The reported[16] 5 percent of conversion electrons (126–159 kev) was, apparently, the cause of some scatter in the data at low absorber thicknesses. The unconverted gamma rays should contribute a negligible amount to the counting rate. After decay of this nuclide, correction for the small contribution of the 12.8-day Ba^{140} and its daughter could easily be made.

12.8-Day Ba^{140}—40.0-Hr La^{140} [17]

Neither member of this system is suitable for absolute beta assay by the techniques used in this work. Ba^{140} has 40 percent of a 0.48-Mev beta, and La^{140}, although having hard betas, has an uncertain number of conversion electrons. The chain was originally included in this study because so many fission yields in the past have been reported[18] relative to the yield of this chain. The number of disintegrations in very thin (~0.1 mg/cm²) samples of Ba^{140}—La^{140} in transient equilibrium and of pure La^{140} were determined on a 4π counter[13] and the corresponding activities were measured on an end-window Geiger counter at a known geometry. The number of Ba^{140} beta rays detected from a sample was found to be 47.5 percent of the measured Ba^{140}—La^{140} equilibrium counting rate in an end-window counter having 2.4-mg/cm² total absorber and a geometry of 19.7 percent. The results are consistent with a decay scheme involving about 6-percent conversion electrons of energy high enough to be counted by our Geiger tube in the La^{140} disintegration scheme, and very few such electrons in the decay of Ba^{140}.

In the fission yield studies, the fission products were

[16] L. R. Shepherd and J. M. Hill, Nature **162**, 566 (1948).

[17] The decay of La^{140} separated in two irradiations from fission-product barium was followed over at least seven half-lives. A half-life of 41.1±0.3 hours best represents our data.

[18] See, for example, references 2 and 3; Coryell, Sakakura, and Ross, Phys. Rev. **77**, 755 (1950); Grummitt, Guéron, Wilkinson, and Yaffe, Can. J. Research **B25**, 357 and 364 (1947).

TABLE I. Self- and backscattering factors.

Precipitate mounted	Nuclide system	Correction factor[a]	Standard error[b] (%)	Conditions under which measurements were made
$SrCO_3$	53-day Sr^{89}	1.37	1.5	...
ZrO_2	17.0-hr Zr^{97}—74-min Nb^{97}	1.43	2	In transient equilibrium
$PbMoO_4$	67-hr Mo^{99}—6.0-hr Tc^{99m}	1.40	3	In transient equilibrium; 21.0 mg/cm² absorber added
$BaCl_2 \cdot H_2O$	85-min Ba^{139}	1.30	1.5	...
$BaCl_2 \cdot H_2O$	12.8-day Ba^{140}—40.0-hr La^{140}	1.26	4	In transient equilibrium

[a] This correction factor is the factor by which the activity of a given number of atoms with less than 0.1-mg/cm² carrier and mounted on 0.5-mg/cm² rubber hydrochloride is increased by the addition of carrier and by mounting this precipitate on filter paper and an aluminum card and by covering it with rubber hydrochloride. The values in this table are applicable for a sample weight of 20 mg/cm². They were slightly different for other weights in the range 10 to 30 mg/cm².

[b] The errors were calculated from the reproducibility of the correction factors obtained in the different experiments and from the scatter of results within each experiment.

isolated with added macroscopic amounts of carrier (10–30 mg). After radiochemical purification (see below), these samples were filtered on a 1.5-cm² area, dried, weighed, mounted on $\frac{1}{16}$-in. aluminum cards, and covered with rubber hydrochloride. Their radioactivity was then measured in a standard fashion on the top shelf of the end-window Geiger tube.

For each nuclide studied (except Y^{91}), the relation between the activity measured in this way and the activity of the same number of active atoms measured under conditions where the absolute disintegration rate could be determined (see above) was established in a series of calibration experiments. In these experiments a known number of radioactive atoms (see above) was diluted with various amounts of inactive atoms and mounted and counted in the standard fashion. At least two such experiments were performed for each nuclide studied. The added carrier ranged in each experiment from about 10 to 45 mg in the final precipitate.

In all cases, as was expected,[19] the activity of a given number of atoms was enhanced by the addition of backscatterer (filter paper and aluminum) and self-scatterer (mg amounts of carrier). It was established that these self- and backscattering corrections were only slowly varying over the weight range usually encountered in the fission yield studies. In Table I are listed the chemical composition of the samples mounted (column 1), the nuclide system under consideration (column 2), the correction factor for self- and backscattering applicable for a sample weight of 20 mg/cm² (column 3), and the standard error in the determination of this factor (column 4).

E. RADIOCHEMICAL SEPARATIONS

The starting material for all the experiments was Mallinkrodt (analytical reagent) uranyl nitrate. The uranium oxide used in the absolute yield determinations was prepared by first dissolving the nitrate in ether. The ether phase was decanted and evaporated. The residue was taken up in water and precipitated as the hydroxide. This was washed, dried, and ignited to the oxide according to the procedure described by Scott.[9] The irradiated oxide was dissolved in nitric acid and diluted to volume in 1 to 3*M* HNO_3 from which aliquots were taken for analyses. Suitable amounts of carrier which had been previously standardized were added. In general, the chemical procedures used to isolate the fission products were similar to those developed on the Plutonium Project.[2] They will be only briefly outlined except where modifications were introduced.

Strontium

The procedure[20] used involved $Sr(NO_3)_2$ precipitations, $Fe(OH)_3$ scavengings using CO_2-free ammonia, and $BaCrO_4$ separations. $SrCO_3$ was the final precipitate.

The procedure for Sr^{91} was different in that strontium was separated immediately after the irradiation and weighed, and then 9.7-hr Sr^{91} was allowed to decay completely to its 57-day Y^{91} daughter. This nuclide was isolated from the remaining strontium activities (Sr^{89} and Sr^{90}) by the addition of yttrium carrier followed by a series of hydroxide and fluoride precipitations. Yttrium oxalate, the final compound, was weighed and mounted for counting.[21]

Zirconium

In the zirconium determinations there were possible contamination and exchange problems. Large amounts of Np^{239}, a 2.3-day beta emitter, are formed from U^{238} by neutron capture followed by beta decay. The neptunium was removed on LaF_3 after reduction to the lower valence states with SO_2. The rest of the procedure[22] consisted of cycles of $BaZrF_6$ precipitations and dissolution with H_3BO_3, removal of barium as the sulfate, and finally the precipitation and ignition of zirconium cupferride to zirconium oxide.

TABLE II. Absolute yield experiments.

Irradiation	Duration of irradiation (min)	Wt (g) of U in heavy sample[a]	Number of fissions in heavy sample[b]	Fission yields, % Sr^{89}	Zr^{97}	Mo^{99}
A 1	35	12.13	1.289×10^{10}	4.82	5.44	6.02
A 2	64	21.55	3.747×10^{10}	4.69	5.53	5.60
A 3	71	17.52	3.684×10^{10}	4.84	5.29	6.12
Average				4.78	5.42	5.91

[a] The heavy sample was U_3O_8. The fission monitor contained 79.2 micrograms of uranium.

[b] The number of fissions in the heavy sample was calculated from the corrected number of fissions in the monitor sample and the relative uranium contents of the monitor and heavy sample. It was then reduced by 2.5 percent to take account of recoil losses and flux attenuation.

[19] See, for instance, Engelkemeir, Seiler, Steinberg, and Winsberg, Papers No. 4 and 5, N.N.E.S., Vol. 9, Div. IV; L. Yaffe and K. M. Justus, J. Chem. Soc. **72**, Supplement 2, 342 (1949); see also references 10 and 12.

[20] L. E. Glendenin, Paper No. 236, N.N.E.S., Vol. 9, Div. IV.

[21] N. E. Ballou, Paper No. 292, N.N.E.S., Vol. 9, Div. IV.

[22] D. N. Hume, Paper No. 245, N.N.E.S., Vol. 9, Div. IV.

TABLE III. Relative yields in the thermal neutron fission of U^{235}.

Experiment[a]	Zr^{97}/Sr^{89}	Mo^{99}/Sr^{89}	Ba^{139}/Sr^{89}	Ba^{139}/Mo^{99}	Ba^{139}/Zr^{97}	Ba^{140}/Mo^{99}	Ba^{140}/Sr^{89}	Sr^{91}/Sr^{89}	Sr^{91}/Mo^{99}
A 1	1.13	1.25							
A 2	1.18	1.20							
A 3	1.09	1.27							
CR 1		1.23							
CR 3		1.25							
CR 6			1.38		1.19				
CR 7				1.11		1.09			
CR 8								1.04	
CR 9		1.23	1.27	1.03		1.06	1.31	1.05	0.85
CR 11								1.09	
PR 1	1.11								
PR 2	1.15								
PR 3		1.29							
PR 4		1.31							
PR 5	1.21	1.24							
PR 6							1.33		
PR 7							1.27		
Average	1.15	1.25							
Av. deviation	0.03	0.025							

[a] The experiments prefixed by (A) indicate absolute fission experiments at the Chicago cyclotron. (CR) indicate relative yield experiments at the Chicago cyclotron. (PR) indicate relative yield experiments at the Argonne Pile.

Concern over exchange arose from the fact that the measured zirconium fission yield was significantly lower than that expected from the reported value.[23] In one experiment irradiated uranyl nitrate was divided into two parts, one of which was dissolved in the usual way in HNO_3 and the other was introduced directly into a solution 1 *M* in KF and 3 *N* in HNO_3. The reason for the latter procedure was to have an environment of fluoride ion—for which zirconium has a great affinity—available at the instant of dissolution of the sample. The ratios of Sr^{89} to Zr^{97} activities from the two solutions were compared at a standard time and were found to be the same to within 0.2 percent.

Molybdenum

The procedure reported by Ballou[24] was modified somewhat by the addition of bromine water[25] to ensure complete oxidation of the molybdenum tracer. The usual α-benzoinoxime precipitations, $HClO_4-HNO_3$ fumings and $Fe(OH)_3$ scavengings were carried out. $PbMoO_4$ was precipitated and ignited.[26] The ignition step was introduced when it was established after many tests that the $PbMoO_4$ precipitate, in spite of careful washing, occluded enough ammonia salts to increase its weight by 3 to 5 percent.

Barium

The barium procedure[27] involved alternate $BaCl_2$ precipitations from HCl-ether solution and $Fe(OH)_3$ scavengings. The final precipitate was $BaCl_2 \cdot H_2O$.

[23] Coryell, Sakakura, and Ross, Phys. Rev. **77**, 755 (1950).
[24] N. E. Ballou, Paper No. 257, N.N.E.S., Vol. 9, Div. IV.
[25] W. W. Meinke, U. S. Atomic Energy Commission unclassified document AECD-2738 (unpublished).
[26] See reference 9, p. 589.
[27] L. E. Glendenin, Paper No. 288, N.N.E.S., Vol. 9, Div. IV.

F. RESULTS

Two types of experiments were performed. In the first set, the absolute yields of Sr^{89}, Zr^{97}, and Mo^{99} were determined using the fission counter and the general techniques described in Secs. B and D. Usually, three samples of each nuclide were isolated in each experiment. The yields calculated from these deviated from the mean by an average 1 percent. Some of the essential data pertaining to these experiments and the results obtained are collected in Table II. The yields of Sr^{89}, Zr^{97}, and Mo^{99} were determined to be 4.78, 5.42, and 5.91 percent, respectively.

In addition to the absolute yield experiments, a series of relative yield determinations on the same three nuclides and also on Sr^{91}, Ba^{139}, and Ba^{140} were performed in which the fission counter was not used. The irradiations were carried out both at the cyclotron (in the same arrangement as was used for the absolute yield experiments) and in a thermal column of the Argonne Heavy-Water Pile (CP−3′). The results of all the relative yield experiments are summarized in Table III. The Zr^{97}/Sr^{89} and Mo^{99}/Sr^{89} ratios from the absolute yield experiments are also included. It is seen that the cyclotron and pile irradiations give the same values of the Zr^{97}/Sr^{89}, Mo^{99}/Sr^{89}, and Ba^{140}/Sr^{89} ratios to within 3 percent. Hence any differences in the spectrum of the neutrons causing fission in the two irradiation arrangements were not significant in the determination of the relative fission yields.

The final results are summarized in Table IV. They were calculated in the following way. The fission yield of Sr^{89} was taken from the absolute experiments to be 4.78 percent. The average Zr^{97}/Sr^{89} and Mo^{99}/Sr^{89} ratios, 1.15 and 1.25, respectively, were used together with the absolute yield of Sr^{89} in order to calculate the yields of Zr^{97} and Mo^{99}. The results, 5.50 and 5.98, respectively, are less than 2 percent higher than those

TABLE IV. Fission yields in the thermal neutron fission of U^{235}.

	Sr^{89}	Sr^{91}	Zr^{97}	Mo^{99}	Ba^{139}	Ba^{140}
Yield, %	4.78	5.1	5.50	5.98	6.4	6.3
Standard deviation, %	1.5	2.0	3.5	3.0	3.5	2.0
Plutonium project[a] yield, %	4.6	5.0	6.2[b]	6.2	6.3	6.32[c]
Canadian project yield, %	3.2[d]				6.1[e]	5.6[e]

[a] See reference 2.
[b] See reference 23.
[c] Recalculation by E. P. Steinberg, Argonne National Laboratory, of the 6.17 value in reference 2 (private communication).
[d] See reference 3.
[e] Grummitt, Guéron, Wilkinson, and Yaffe, Can. J. Research **B25**, 371 (1947).

obtained directly from the absolute yield experiments. The Ba^{139} yield was calculated by averaging all of the results based on Ba^{139}/Sr^{89}, Ba^{139}/Mo^{99}, and Ba^{139}/Zr^{97} ratios together with the yields of Sr^{89}, Mo^{99}, and Zr^{97}. Sr^{91} and Ba^{140} were treated similarly.

The standard deviation associated with the yields calculated in this way are indicated in the table. They are consistent with an analysis of the known component errors. Consideration of the possible systematic errors (fission counting, determination of absolute disintegration rates, etc.) lead us to set an outside error of 6 percent to the absolute yields. The estimated outside error is about 3 percent for relative yields.

Table IV also compares the results of this work with literature values for the yields of these nuclides.‖ In all but two cases the agreement is much better than the 10 percent reliability generally ascribed to these older measurements. The Canadian Project[3] value of 3.2 for Sr^{89} appears much too low; the value of 6.2 for Zr^{97} reported by Coryell *et al.*[23] is much higher than our experiments would permit.

TABLE V. Combination of mass spectrometric data on relative fission yields with absolute yields from this work.

Mass No.	Relative mass spec. data[a] Zr	Mo	Absolute values this work	Combined data
89			4.78	4.78
90				
91	5.75		5.07	5.07[b]
92	5.89			5.19
93	6.31			5.56
94	6.50			5.73
95		6.55		5.80
96	6.45			5.69
97		6.21	5.50	5.50[b]
98		6.18		5.48
99			5.98	5.98
100		6.77		6.00

[a] Mass spectrometric data used by Glendenin *et al.* in constructing their fission-yield curve (see reference 6). [E. P. Steinberg, Argonne National Laboratory (private communication)].
[b] Points of normalization of mass spectrometric data to radiochemically determined absolute yields.

‖ *Note added in proof.*—Terrell, Scott, Gilmore, and Minkinen [Bull. Am. Phys. Soc. **28**, 5, 19 (1953)] report a value of 6.14±0.16 for the yield of Mo^{99} in the thermal neutron fission of U^{235}.

G. DISCUSSION

The most recently published yield curve for the thermal fission of U^{235} is that of Glendenin *et al.*[6] based upon a combination of relative mass spectrometric yields and radiochemical data. This is reproduced as the full curve in Fig. 2. Since, in general, mass spectrometric yields are measured for nuclides closer to stability than those determined radiochemically, differences in yields along a fission product chain might make a direct combination unjustified. However, consideration of the known data on this question[28] indicates that in all the chains studied in this work the expected independent yield beyond the nuclide studied radiochemically should be less than 3 percent[29] of the total chain yield. We will, therefore, assume that the radiochemical yields represent the total chain yields. The

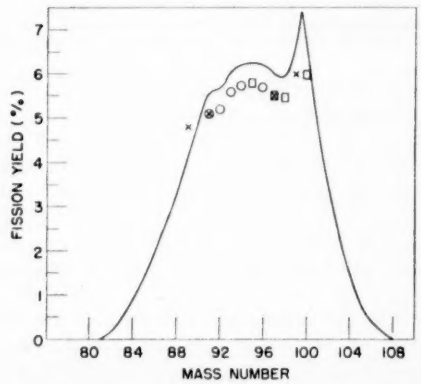

FIG. 2. Light-mass peak of the U^{235} thermal neutron fission-yield curve. Smooth curve is that of Glendenin *et al.*, reference 6. ×, absolute yields determined radiochemically in this work. ○, relative yields of zirconium isotopes determined mass-spectrometrically, normalized at mass 91. □, relative yields of molybdenum isotopes determined mass-spectrometrically, normalized at mass 97.

absolute radiochemical yields can then be used to normalize the relative yields of the isotopes of zirconium and molybdenum that have been determined mass-spectrometrically.

In Table V are presented the mass-spectrometrically determined isotopic compositions of fission zirconium and molybdenum, together with the absolute yields established in this work for nuclides in the light group of fission products. Normalizing the mass spectrometric zirconium data to give a yield of 5.07 at mass 91 and

[28] Glendenin, Coryell, and Edwards, Paper No. 52, N.N.E.S., Vol. 9, Div. IV.
[29] The yields of Sr^{91} and Y^{91} are listed in reference 2 as 5.0 and 5.8 percent. This would indicate very high direct formation of Y^{91}. Several attempts were made to check this point by determining the yield of Y^{91}. Unfortunately, the results were inconclusive presumably because of inadequate radiochemical decontamination of the Y^{91}.

the molybdenum data to give a yield of 5.50 at mass 99 determines all the yields (except one) in the light group between mass 89 and 100 inclusive. The data are also presented in Fig. 2. It is seen that the "spike" at mass 99 to 100, as well as the "shoulder" below mass 93 is confirmed by the new results. Most of the absolute yields are, however, significantly lower than the curve of Glendenin *et al.* Since even this curve integrated to less than 100 percent, higher yields than the curve of Fig. 2 are indicated for the mass region below 89 and above 100.

ACKNOWLEDGMENTS

We wish to acknowledge the assistance and cooperation of the crew of the University of Chicago 37-in. cyclotron under Mr. W. Scott and Mr. M. Fielding and of the electronics group of the Institute for Nuclear Studies under Mr. P. Shevick.

PHYSICAL REVIEW VOLUME 92, NUMBER 6 DECEMBER 15, 1953

Decay of Ga^{66}†

L. G. MANN,* W. E. MEYERHOF, AND H. I. WEST, JR.
Stanford University, Stanford, California

(Received September 15, 1953)

Scintillation equipment consisting of a three-crystal pair spectrometer, two-crystal Compton spectrometer, and single NaI(Tl) and anthracene crystals used in coincidence have been used to investigate the decay of Ga^{66}. Gamma-rays of 4.83 (2), 4.33 (4.5), 4.12 (1.5), 3.78 (2), 3.41 (3), 3.24*(2), 2.75 (22), 2.40 (2), 2.18 (6), 1.93 (3.5), 1.58 (<0.4), 1.37 (3), 1.04 (30), and 0.83 (1) Mev energy have been observed. (Intensities, given parentheses, indicate percent of Ga^{66} decay.) These are fitted into a consistent decay scheme in which Ga^{66} decays to levels in Zn^{66} at 4.83 (2), 4.33 (8), 4.12 (1.5), 3.78 (21), 3.41 (4), 3.24 (10), 2.75 (2), 2.40 (~0.5), 1.04 (<0.5) and 0 (56) Mev. (Branching intensities, given in parentheses, indicate percentages.) The beta- and gamma-ray branchings have been used to assign possible spins and parities to the states involved.

INTRODUCTION

THE decay of Ga^{66} has been investigated using scintillation detection techniques for gamma- and beta-ray spectroscopy. At the time this work was started the known features of the decay were[1–3] (1) a complex positron spectrum containing components of 4.15, 1.4, 0.9, and 0.4 Mev, and (2) gamma rays of 1.04, 2.74, 4.2, and 4.8 Mev. Since that time a more complete investigation of this problem has been carried out by Mukerji and Preiswerk,[4] more or less concurrently with our work but using for the most part different techniques. They confirmed the positron spectra reported by Langer and Moffat[1] and observed new gamma rays of 1.7, 2.2 and 3.3 Mev, and they showed that the 1.04- and 2.75-Mev gamma rays are in coincidence. They also proposed a level scheme consisting of excited states in Zn^{66} at 1.05, 2.75, 3.30, 3.80, 4.25, and 4.80 Mev to fit all the data.

The present work has improved the accuracy of the known gamma-ray energies and has shown new gamma rays requiring additional energy levels in Zn^{66}. Because of this, and because different techniques have been used, it seems worth while to describe the work in some detail. Our proposed decay scheme is shown in Fig. 1.

SOURCE PREPARATION

The Ga^{66} was produced by the $Zn(p,n)$ reaction in the University of California, Berkeley, 60-in. cyclotron.[5] Carrier free separation of the Ga was accomplished by the ether extraction process.[6] Sources were prepared either by evaporating a drop of the ether solution on a source holder (thin, weak sources for coincidence work) or by evaporating the entire ether solution and then picking up the Ga^{66} activity in a drop of HCl (for strong gamma-ray sources ~1 mc).

EQUIPMENT

Initial investigations using single iodide crystals[7] showed that better gamma-ray spectroscopy was needed. A three-crystal pair spectrometer[8] of the type originally suggested by Hofstadter[9] and subsequently built by several workers[10] was constructed for this purpose. Excellent rejection of background was achieved by the use of lead shielding and differential pulse height

† Supported in part by the joint program of the U. S. Office of Naval Research and U. S. Atomic Energy Commission.

* Now at the University of California Radiation Laboratory, Livermore, California.

[1] L. M. Langer and R. D. Moffat, Phys. Rev. **80**, 651 (1950).
[2] R. Hofstadter and J. A. McIntyre, Phys. Rev. **80**, 636 (1950).
[3] A. Mukerji and P. Preiswerk, Helv. Phys. Acta **23**, 516 (1950).
[4] A. Mukerji and P. Preiswerk, Helv. Phys. Acta **25**, 387 (1952).

[5] The staff of the Crocker Radiation Laboratory very kindly produced a number of these sources for us.
[6] See, for example, E. Bleuler and G. J. Goldsmith, *Experimental Nucleonics* (Rinehart and Company, Inc., New York, 1952), p. 196.
[7] All of our crystals were rough ground and mounted under magnesium oxide smoked aluminum covers. See, for example, W. H. Jordan, Ann. Rev. Nuc. Sci. **1**, 207 (1952).
[8] H. I. West and L. G. Mann, Rev. Sci. Instr. (to be published).
[9] R. Hofstadter and J. A. McIntyre, Phys. Rev. **79**, 389 (1950).
[10] J. K. Bair and F. C. Maienscheim, Rev. Sci. Instr. **22**, 343 (1951); S. A. E. Johansson, Nature **166**, 794 (1950); R. S. Foote and G. Kamm, Phys. Rev. **87**, 193 (1952); G. M. Griffiths and J. B. Warren, Proc. Phys. Soc. (London) **65**, 1050 (1952).

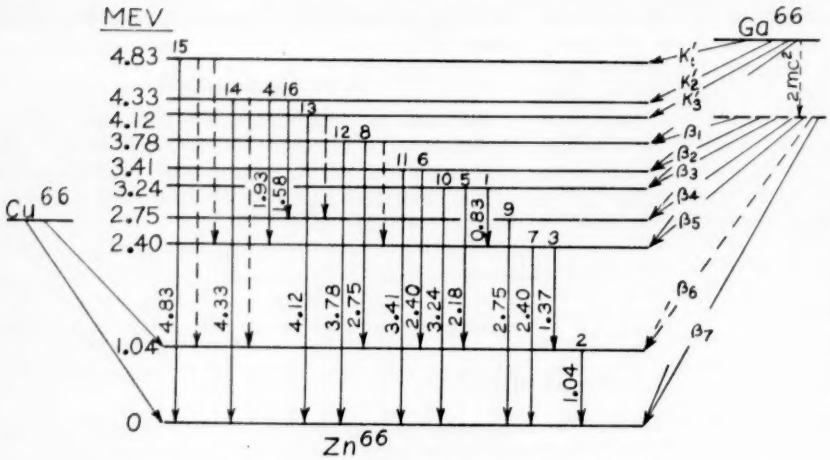

FIG. 1. Proposed decay scheme of Ga^{66}. The transitions indicated by dashed lines have energies which could not be resolved from the energies of some of the other transitions indicated. In the text all of the observed intensities have been ascribed to the solid-line transitions. The observed gamma-ray energies are shown on each transition. An order number is also given for reference to Table II. Gamma intensities, and uncertainties in energies and intensities are given in Table II. Electron capture and positron intensities are given in Table IV.

discrimination on the side crystal annihilation radiation pulses (0.51 Mev). Figure 2 shows a block diagram of the apparatus as it was used in the pair spectrometer. The discriminator is a cathode-ray tube with a mask such that only the 0.511-Mev annihilation pulses can be picked up by the 931A photomultiplier. The components were also used in double coincidence experiments (0.15 μsec resolving time) involving pulse-height discrimination on one or both crystals. The recording cathode-ray tube constitutes a multichannel discriminator, in which the height of each pulse is displayed as a dot which is photographed. The number of dots falling in a given 1-mm channel were counted and plotted as a function of the height of the channel.

The pair spectrometer was tested with the Na^{24} gamma rays from a 1-mc source collimated with a $\frac{1}{4}$-in. diameter by 6-in. hole in lead. Figure 3 shows the gamma-ray spectrum. The tail of low-energy pulses is the result of escape of bremsstrahlung and electrons from the center crystal.[8] It must be taken into account in the interpretation of all data observed with the apparatus.

For gamma rays of less than 2 Mev, the pair spectrometer efficiency was too low, and a two-crystal Compton spectrometer of the type suggested by Hofstadter[11] was constructed. An anthracene crystal was used as the Compton scatterer, to avoid pair production. A $1\frac{1}{2}$-in. by $1\frac{1}{2}$-in. sodium iodide cylinder was used for detection of the scattered radiation and was biased to reject all pulses greater than 0.3 Mev. The anthracene crystal was $\frac{1}{2}$ in. thick, capable of stopping 3-Mev electrons, and gave a resolution of 15 to 17 percent for the internal conversion electrons of Cs^{137} (0.62 Mev).

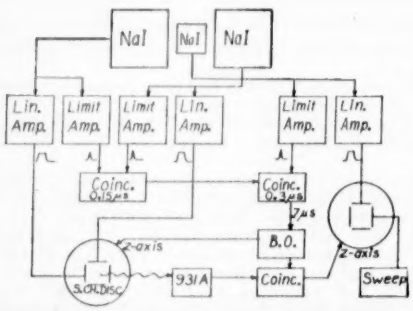

FIG. 2. Block diagram of the three-crystal pair spectrometer.

The detector arrangement for γ-γ coincidence experiments consisted of two sodium iodide crystals placed back to back with the source in between. Copper ($\frac{3}{32}$ in.) was used to absorb the beta particles. For β-γ work an anthracene crystal was used in place of one of the NaI crystals. Pulse-height discrimination, either differential or integral, was used on one crystal while the pulse-height distribution in the other crystal was photographed. Poor geometry was necessary in order to obtain sufficient detection efficiency for coincidence work on weak branches without excessive chance coincidences from the other intense radiations. As a result of this arrangement there is a (calculated) probability of about 10 percent that in the β-γ experiments an annihilation quantum was detected in coincidence with a gamma-ray.[12] These addition pulses were subtracted from all of the data (Figs. 4–6). A similar addition effect can occur due to Compton scattering between the two crystals. The copper shielding used between counters was sufficient to reduce this effect by 50 percent. However, it had to be taken into account in the γ-γ experiments (Fig. 6); in β-γ work the method of subtracting γ-γ coincidences also corrected for the Compton scattering coincidences.

EXPERIMENTS

An outline of the experiments which support the decay scheme of Fig. 1 is given in Table I.

[11] R. Hofstadter and J. A. McIntyre, Phys. Rev. **78**, 619 (1950).
[12] Jastram, Whalen, and Zinke, Rev. Sci. Instr. **23**, 648 (1952).

A. Spectrometer Measurements

The pair spectrometer results are shown in Fig. 7. A ~1-mc source was used with a $\frac{1}{4}$-in. diameter by 5-in. lead collimator hole. About six hours of running time were needed to record these data. Similar curves were taken with two other sources and confirmed all the gamma rays shown here.

The method of analysis to take account of bremsstrahlung and electron escape[8] is indicated for the two highest energy lines in the figure. A Gaussian curve has been fitted to the 4.83-Mev line and the calculated tail is indicated. Then the next highest energy line is fitted in the same way, using a Gaussian those width is reduced by the square root of the energy ratio.[13] This rule seems to be completely valid for all our data[8] (see for example the agreement in our Na^{24} results, Fig. 3, fitted in the same way). The true

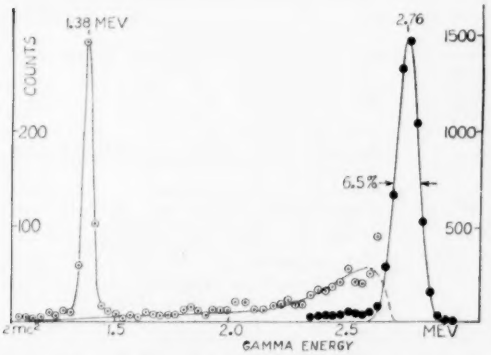

FIG. 3. The Na^{24} gamma-ray spectrum (2.76 and 1.38 Mev) observed with the three-crystal pair spectrometer. Note the change by a factor of five in the ordinate scale for the solid points. The beginning of the tail of the 2.76-Mev gamma ray is shown on both scales. The lines through the peaks are Gaussians. Elsewhere the solid line is the calculated tail of the 2.76-Mev peak, which is caused by electron and bremsstrahlung escape from the center crystal.

Gaussian widths were increased by ~5 percent at 4.83 Mev and 10 percent at 1.9 Mev to take into account the finite channel width. The curve shown in Fig. 8 was obtained by the above procedure. Of the excess counts observed in the region below 1.93 Mev, 35 percent can be accounted for by pair production of the 1.58- and 1.37-Mev gamma rays, the peaks of which are not resolved because of poor statistics. We believe that the remainder is the result of insufficient lead shielding, which caused low energy background in addition to the bremsstrahlung tail. (When more shielding was used, as in Fig. 3, the same calculational procedure gave excellent agreement with the data.)

[13] A. W. Schardt and W. Bernstein, Rev. Sci. Instr. **22**, 1020 (1951). We seem to obtain better agreement with the $E^{\frac{1}{2}}$ law than these authors. It may be that the effect of photomultiplier cathode non-uniformity was reduced because of collimation and the elimination of all secondary processes in the crystal. This tends to localize the source of light in a small region of the crystal.

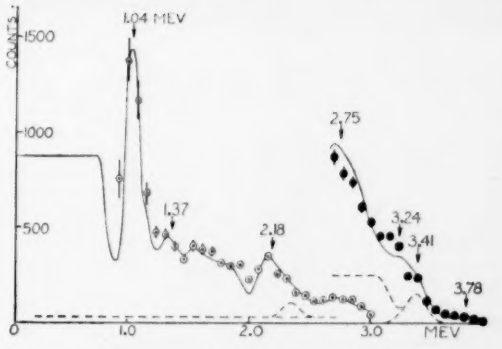

FIG. 4. Beta-gamma coincidences in Ga^{66}. The gamma-ray pulse-height distribution in a single sodium iodide crystal is shown for the pulses in coincidence with beta rays of <0.5-Mev energy. (An anthracene crystal was used as the beta spectrometer.) The points were fitted by photo, Compton, and pair distributions of the type shown for the 3.41-Mev gamma ray (dotted curve). The intensities which give the resultant curve shown are given in Table III, third column. The data for the solid points were taken with a source seven times the intensity of that used for the circled points. Experimental gamma-gamma and chance coincidences have been subtracted.

The valleys between peaks fall somewhat below the points in most cases. An effect which can partially explain this is Compton scattering of the annihilation quanta as they leave the center crystal. Recoil electrons of 100-kev energy are produced in the center crystal for scattering angles of 40°, and lower energies for smaller angles. These events can produce coincidences if the side crystal discriminator channels extend down to 0.4 Mev (as they did, to include the entire 0.511-Mev photopeak). The result is to broaden the pair peaks on the high energy side. This effect is most pronounced on low energy peaks and has been verified for Co^{60} pair peaks.[14] Using the differential Compton scattering cross

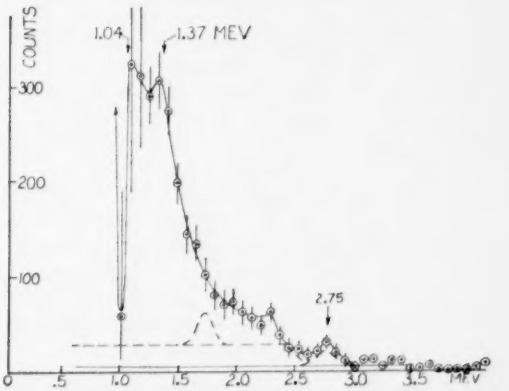

FIG. 5. Beta-gamma coincidences in Ga^{66}. Same as Fig. 4 except that the beta detector was biased so that only pulses of >1.0-Mev energy were accepted. Table III gives the intensities.

[14] H. I. West, Ph.D. thesis, in preparation, Stanford University, Stanford, California.

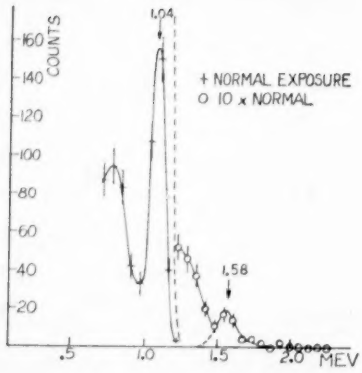

FIG. 6. Gamma-gamma coincidences in Ga^{66}. The pulse-height distribution in a single NaI(Tl) crystal is shown for the pulses in coincidence with gamma-ray pulses of >2.15 Mev in a second NaI(Tl) crystal. The 1.58-Mev peak may be entirely the result of annihilation radiation addition to the 1.04-Mev pulses. The dotted line is the Gaussian tail of the 1.04-Mev peak, shown on the scale of the 1.58-Mev peak.

section for 0.51-Mev gamma rays and the solid angles of our side crystals, and referring to the 2.75-Mev gamma-ray peak in Fig. 7, one can calculate that the 3.0-Mev point should be increased by a maximum of 40 counts and the 3.1-Mev point by 10 counts. Similarly, up to 50 percent of the discrepancy at 4.6 Mev can be removed. This effect could have been prevented by proper setting of the side crystal discriminators, but it was not expected at the time of the experiments.

In order to take into account the effect of the excess low energy pulses and the valley effect described above, the peak heights indicated in Fig. 7 for the 2.40-, 2.18-, and 1.93-Mev gamma rays were reduced by 50, 11, and 13 percent, respectively, for the intensity calculation (Table II). Although these figures cannot be very

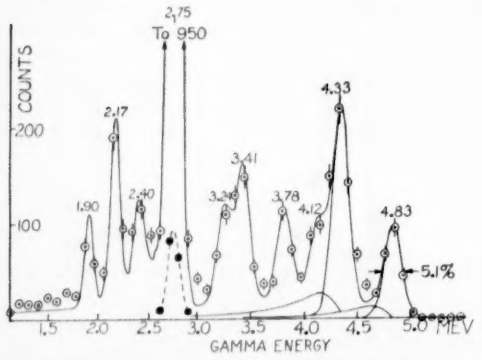

FIG. 7. Gamma-ray spectrum of Ga^{66} observed with the three-crystal pair spectrometer. The calculated bremsstrahlung and electron escape tails are shown for the two highest energy peaks. The final curve is a superposition of the Gaussian plus tail distributions of each gamma ray. The measured gamma-ray energy of each Gaussian peak is given on the diagram in Mev. The 2.76-Mev peak is shown with the ordinate scale reduced by a factor of 10 (solid points).

accurate, they are of the correct order of magnitude and are consistent with other experiments (see below).

In order to determine gamma-ray intensities the pair cross section of sodium iodide is needed as a function of gamma-ray energy. We have determined three points on this curve, at 1.17, 1.33, and 1.38 Mev, by analyzing the peaks obtained in the pair spectrometer with Co^{60} and Na^{24} sources.[14] With the help of these points the Bethe-Heitler formula was extended to low energies as shown in Fig. 8. The points of Yaeger and Hulme,[15] based on exact calculation, of Colgate,[16] based on absorption measurements and theoretical Compton, photoelectric, and Rayleigh cross sections, and of Dayton,[17] based on measured Z dependence and the Born approximation calculation at low Z, are also shown. (The Born approximation should be valid at low Z. This was veri-

TABLE I. Experimental evidence supporting the proposed decay scheme of Ga^{66} (Fig. 1).

Level (Mev)	Evidence
4.83	
4.33	γ decay to ground
4.12	
3.78	γ decay to ground 2.75−1.04 Mev γ coincidence (Mukerji,[a] present authors) 0.4 Mev β-spectrum (Mukerji[a])
3.41	γ decay to ground β-γ coincidence: β<0.5 Mev→3.41 γ β>1.0 Mev→no 3.41 γ
3.24	γ decay to ground 0.9 Mev β-spectrum (Mukerji[a]) β-γ coincidence: β<0.5 Mev→2.18, 3.24 γ β>1.0 Mev→no 2.18, 3.24 γ
2.75	1.4 Mev β-spectrum (Mukerji[a]) β-γ coincidence: β>1.0 Mev→2.75 γ
2.40	γ decay to ground β-γ coincidence: β>1.0 Mev→1.37, 1.04 γ (cascade) 1.93, 1.37, and 0.83 gammas fit this level
1.04	2.75–1.04 Mev γ coincidence (Murkerji,[a] present authors) Cu^{66} decay[b]

[a] References 3 and 4.
[b] G. Friedlander and D. E. Alburger, Phys. Rev. **84**, 231 (1951); Roderick, Meyerhof, and Mann, reference 30.

fied for anthracene.[14]) Small corrections to the resulting intensities (of the order of 10 percent) were made for counts lost due to positrons which escape from the center crystal or annihilate in flight. The final results of the energy and intensity analysis are given in the second and third columns of Table II.

For the energy region below 2 Mev the two-crystal Compton spectrometer was more useful. Figure 9 shows the gamma-ray spectrum up to the 2.75-Mev gamma-ray as observed with this instrument. Energies were obtained from a continuous photograph of the pulses, a photometer curve of which is shown in Fig. 10. The important results from these curves are that gamma rays of 0.83-, 1.37-, and 1.96-Mev energy exist in addi-

[15] J. C. Yaeger and H. R. Hulme, Nature **137**, 781 (1936); **148**, 86 (1941).
[16] S. A. Colgate, Phys. Rev. **87**, 592 (1952).
[17] I. E. Dayton, Phys. Rev. **89**, 544 (1953).

TABLE II. Ga^{66} gamma rays measured with the pair and Compton spectrometers.

Gamma-ray	Pair spectrometer Energy (Mev)	Pair spectrometer Relative intensity	Compton spectrometer Energy (Mev)	Compton spectrometer Relative intensity	Final result Energy (Mev)	Final result Intensity (percent of Ga^{66} decay)
			0.511[a]			
1			0.83±0.01	10±6	0.83	2.2±1.4
2			1.044[a]	138[b]	1.044	30.0
3			1.37±0.02	14.0±6	1.37	3.0±1.1
4	1.90±0.04	16.0±3.0	1.94±0.02	17.8±6	1.93	3.5±1.2
5	2.17±0.03	26.9±2.7	2.19±0.02	26.9	2.18	5.8±0.6
6, 7	2.40±0.04	6±4		<9	2.40	2.4±1.6[c]
8, 9	2.75[a]	100	2.75	100	2.75	21.6[d]
10	3.24±0.04	8.6±1.8			3.24	1.9±0.4
11	3.41±0.04	13.5±2.5			3.41	2.9±0.6
12	3.78±0.03	8.5±1.3			3.78	1.8±0.3
13	4.12±0.05	6.9±1.5			4.12	1.5±0.3
14	4.33±0.05	20.7±2.0			4.33	4.5±0.5
15	4.83±0.05	9.7±1.0			4.83	2.1±0.2

[a] Gamma-ray energies used for calibration are given without errors. The 1.044-Mev energy was measured by G. Friedlander and D. E. Alburger, Phys. Rev. **84**, 231 (1951).
[b] The intensities given without errors were used for intensity normalization. The value of 138 is obtained from our decay scheme by adding up all the transitions feeding the 1.04-Mev level.
[c] $\gamma_8 = 1.6_{-1.6}{}^{+0}$; $\gamma_7 = 0.8_{-0.8}{}^{+0}$. These figures are consistent with the upper limits found in the $\beta-\gamma$ coincidence experiments.
[d] $\gamma_8 = 19.4 \pm 2$; $\gamma_9 = 2.2 \pm 1$.

tion to others known from the pair spectrometer and single crystal data. No 2.40-Mev gamma ray is detectable, but we can only assign an upper limit of $\sim\frac{1}{3}$ the intensity of the 2.18-Mev gamma ray. This is the same order of magnitude that was observed in the pair spectrometer.

The Compton spectrometer curve was extended down to the 0.39- and 0.30-Mev gamma rays of Ga^{67} (78 hr half-life)[18] in order to be sure that the peak at 0.83 Mev is not caused by the 0.88-Mev transition in Ga^{67}. This transition is less than 3 percent of the 0.30-Mev intensity, whereas our observed peak was 40 percent. It is disturbing that Mukerji and Preiswerk[4] could not see this gamma-ray in their beta-ray spectrometer experiments using a lead radiator. However, the intensity that we observe is near the limit of their resolution, and it does not seem to be excluded entirely by their data.[19]

An intensity analysis was carried out using the differential Compton cross section at 135°.[20] The 2.75- and 2.18-Mev peaks were matched to the pair spectrometer results for normalization. Because of greater amounts of electron escape from the low density anthracene crystal there is considerably more background than in the pair spectrometer, making the quantitative analysis less accurate. The fourth and fifth columns in Table II show the energies and intensities obtained from the Compton spectrometer, and the last two columns show our final results expressed in terms of the total number of Ga^{66} decays (assuming our decay scheme).

These results confirm the gamma rays reported by Mukerji and Preiswerk[4] with the exception of their 1.7-Mev transition. On the basis of a re-examination of their Compton recoil data and private communication with Professor Preiswerk, we believe that this was a misinterpretation of a peak due to the 1.93-Mev gamma-ray.

B. Coincidence Measurements

In coincidence work the procedure was to isolate as far as possible certain parts of the beta- or gamma-ray spectrum, using a single crystal as a discriminator, and to observe the coincident radiations in a second crystal. This is difficult to do for a decay scheme as complicated as that shown in Fig. 1, except for favorable regions of the spectra. We have performed β-γ coincidence experiments as indicated in Table I, using beta rays >1.0 Mev, and <0.5 Mev, and analyzing the coincident gamma-ray pulse-height distributions. The gamma-ray distribution in coincidence with gamma rays of >2.15 Mev has also been analyzed.

Figure 4 shows the gamma-ray pulse heights observed in coincidence with beta rays of <0.5 Mev. This experiment was expected to enhance the radiations following the decay of the 3.78-Mev level and in particular to show the intensity of the ground-state transition from that level. However, it was not possible to put a very small upper limit on this transition because of the complexity of the spectra.

Figure 5 shows the gamma-ray pulse heights observed in coincidence with beta rays of >1.0 Mev. This eliminates completely the strong 2.75- to 1.04-Mev gamma-ray cascade and enables one to observe the decay of the 2.75- and 2.40-Mev levels (if they are fed by beta decay).

Figure 6 shows the gamma-ray pulse heights observed in coincidence with gamma-ray pulses of >2.15 Mev. In this experiment the discriminated crystal receives mainly the 2.75-Mev gamma ray, so the strong 2.75- to 1.04-Mev gamma cascade is emphasized. Any gamma

[18] Ketelle, Brosi, and Porter, Phys. Rev. **90**, 567 (1953); Meyerhof, Mann, and West, Phys. Rev. **92**, 756 (1953).
[19] Private communication from Professor Preiswerk.
[20] C. M. Davisson and R. D. Evans, Revs. Modern Phys. **24**, 79 (1952).

rays feeding the 2.75-Mev or higher levels may also be detected.

The quantitative analysis of the coincidence experiments are illustrated in Fig. 4. In this analysis the aforementioned addition of annihilation radiation must be corrected for. Also, parts of the higher energy beta spectra are detected in the beta counter. This effect is appreciable because, while only a fraction of the higher energy spectra are detected, the ratio of β^+ to K-capture decay increases with increasing energy.

The experimental points were fitted by means of Gaussian photo and pair distributions and a flat Compton distribution for each gamma ray. The three distributions are shown for the 3.41-Mev gamma ray. The number of counts in each group was adjusted according to the relative (experimental) cross sections. In order to compare these data with a given decay scheme, the absolute beta and gamma detection efficiencies are needed. We have determined our gamma detector efficiency accurately for Co^{60} gamma rays (1.33 and 1.17 Mev) by coincidence experiments. The

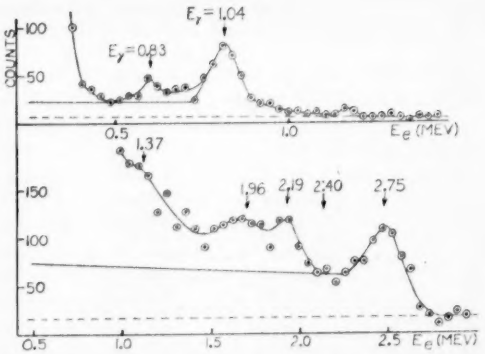

FIG. 9. Gamma-ray spectrum of Ga^{66} observed with a two-crystal Compton spectrometer. The abscissa is electron recoil energy at 135° scattering. The corresponding gamma-ray energies are indicated for the peaks. For the 2.75- and 1.04-Mev gamma-ray peaks the tails caused by electron escape from the anthracene crystal are shown.

other gamma-ray efficiencies, for energies up to 3.78 Mev, can then be calculated with sufficient accuracy because of the relatively small dependence of cross section on energy in this region. The beta-ray detection efficiency was assumed to be $[1\times(\Omega/4\pi)]$ for energies within the discriminator channel, where Ω is the solid angle subtended by the detector at the source.

The number of coincidences is given by

$$n_{\beta\gamma j}=n_{\gamma j}\sum_i\left[\alpha_i{}^j E_\beta\frac{\beta_i}{\beta_i+K_i}\times\delta_i\right],$$

where

$n_{\gamma j}=N_{\gamma j}E_{\gamma j}$=number of counts in gamma-ray counter due to a particular gamma ray,

$\alpha_i{}^j$=probability that γ_j is in coincidence with beta transition β_i (or the corresponding K-capture),

$E_\beta=1\times(\Omega_\beta/4\pi)$=beta-detector efficiency,

$\dfrac{\beta_i}{\beta_i+K_i}=\dfrac{\text{number of positrons}}{\text{number of decays}}$ for beta transition β_i,[21]

δ_i=fraction of β_i spectrum accepted by the integral discriminator (energy <0.5 Mev),

$N_{\gamma j}$=number of γ_j emitted by the source,

$E_{\gamma j}$=efficiency of the gamma-ray crystal for γ_j.

The $\alpha_i{}^j$ depend on the decay scheme, and $\beta_i/(\beta_i+K_i)$ and δ_i were obtained from theoretical curves assuming allowed beta spectra. In order to show whether or not a particular decay scheme was consistent with all the coincidence data, we calculated each N_γ, using the observed $n_{\beta\gamma}$ and the α_i for the particular scheme. For the correct scheme the N_γ must agree with the spectrometer results.

Table III shows the results for each of the coincidence experiments, using our final decay scheme (Fig. 1). The agreement with the spectrometer measurements is excellent, considering the limited accuracy with which

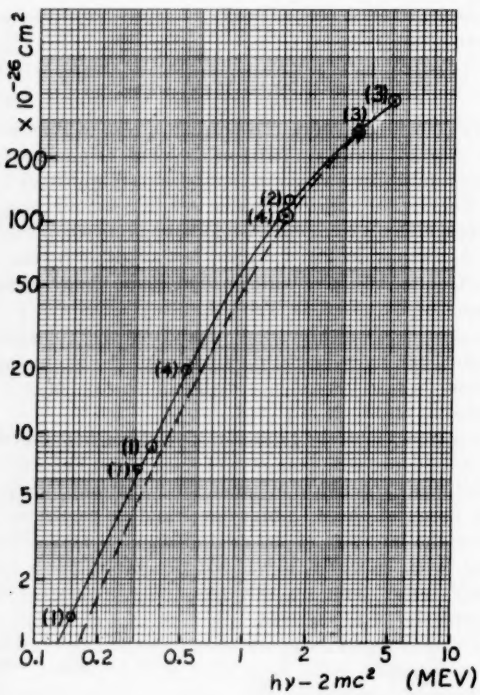

FIG. 8. Pair-production cross section in iodine as a function of gamma-ray energy above threshold. (1) West thesis (pair spectrometer); (2) Dayton (measured Z dependence and Born approximation at low Z limit); (3) Colgate (measured total cross section minus theoretical Compton, photoelectric, and Rayleigh cross sections); (4) Yaeger and Hulme (exact calculation). Experimental accuracy is given by the size of the circles. The dashed line is the Born approximation calculation. The cross section of sodium is found from Dayton's data to be 4 percent of that for iodine at 1.33 and 2.62 Mev, and the Born-approximation calculation at higher energies gives the same ratio.

[21] E. Feenberg and G. Trigg, Revs. Modern Phys. 22, 399 (1950).

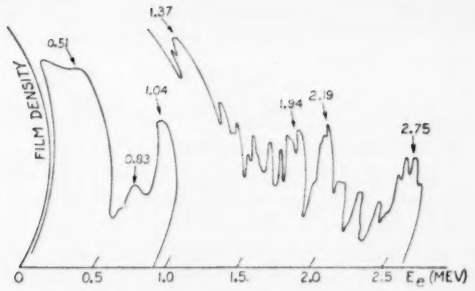

FIG. 10. Densitometer curve of a photograph of the Ga^{66} gamma-ray pulses in the two-crystal Compton spectrometer. Abscissa is recoil electron energy at 135° scattering. The corresponding gamma-ray energies are indicated on the peaks. There are about twice as many total counts as in Fig. 9. The region below 0.51 Mev consists of gamma rays in the Ga^{67} decay (unresolved by the densitometer). Note ordinate scale change by an undetermined factor.

values could be assigned to the $n_{\beta\gamma j}$ in Figs. 4–6. Because of this limited accuracy, questions about the existence of certain weak branches (indicated by dashed lines in our decay scheme) cannot be decided. On the other hand, the 0.83-Mev gamma ray is a good example of a significant result found in the $\beta<0.5-\gamma$ experiment. Without this transition feeding the 2.40-Mev level, the intensity of the 1.37-Mev gamma ray would have to be six times greater in order to explain the 1.37-Mev peak observed in this experiment. The 1.58-Mev gamma ray was observed only in the $(\gamma>2.15-\gamma)$ experiment and its actual existence must be questioned because of the amount of annihilation radiation addition that had to be corrected for. Forty percent of the 1.58-Mev peak in Fig. 6 was calculated to be due to addition to the 1.04-Mev peak of annihilation quanta from positrons feeding the 2.75–1.04 Mev gamma-ray cascade.

DECAY SCHEME

Our final decay scheme of Ga^{66} is shown in Fig. 1. The 2.75- and 2.40-Mev levels of Zn^{66} and their associated radiations require some discussion. The 2.75-Mev level was reported by Mukerji and Preiswerk[4] on the basis of an observed 1.4-Mev beta spectrum. Our $(\beta>1.0-\gamma)$ coincidence experiments confirm this conclusion. This level also offers our most satisfactory explanation for the 1.58-Mev gamma ray. There seems to be no evidence either in our work or in Mukerji's[19] for a 1.7-Mev gamma ray from this level.

The 2.40-Mev level fits the 0.83-, 1.37-, 1.93- and 2.40-Mev gamma rays observed in the spectrometers. Also, the 0.83−1.37−1.04-Mev cascade from the 3.24-Mev level proves to be the main source of the 1.37-Mev gamma ray appearing in the $(\beta<0.5-\gamma)$ experiment. Without this cascade some other way is needed to explain the 1.37-Mev peak in that experiment. The 2.40-Mev level is fed primarily by the 1.93- and 0.83-Mev gamma rays. A small amount of beta decay to that level is needed to account for the 1.37- and 1.04-Mev gamma rays seen in the $(\beta>1.0-\gamma)$ experiment.

The transitions indicated by dashed lines in Fig. 1 have energies which duplicate closely those for transitions appearing elsewhere in the decay scheme. Because of the uncertainty in assigning values to the coincidence rates we cannot say to what extent these transitions occur; they have been excluded from the scheme merely because they would change intensities in the wrong direction. The 2.75-Mev gamma ray was split between two different transitions (8 and 9) in order to agree with the results in Figs. 5 and 6 (Table II gives the amount of splitting). The 2.40-Mev gamma ray was also split between two transitions (6 and 7), because the coincidence experiments indicated an upper limit for these transitions which was too small to account for the total 2.40 intensity.

Table IV shows the intensities of the transitions from Ga^{66} to each level of Zn^{66} as calculated for our decay scheme. In this calculation we have used our observed relative gamma-ray intensities and the ratio measured by Mukerji for the ground state (4.14 Mev) beta spectrum intensity to total beta intensity. The theoretical K/β^+ ratios of Trigg[21] have been used to obtain the relative beta and K-capture intensities, as was done by Mukerji. In addition, 9 percent of the electron capture was assumed to be from the L shell.[22] Log ft values[21,23] are given in the tenth column of Table IV.

Our results are compared in Table IV with those of Mukerji (which are nearly identical with Langer and Moffat's results). Mukerji's quoted intensities are based on an assumed 4 percent electron capture to the three highest levels. We have recalculated these intensities in columns 8 and 9 of Table IV using our measured

TABLE III. Gamma-ray intensities deduced from the coincidence experiments.

Experiment	Gamma energy (Mev)	Number of coincidences	Total γ intensity (percent of Ga^{66} decays) Coincidence	Spectrometer
$\beta<0.5$ Mev$-\gamma$	1.04	7500	25.5	30.0
	1.37	1600	3.7	3.0
(Fig. 4)	2.18	4600	6.3	5.8
	2.40	<700	<2.3	2.4
	2.75	1700	21.6[a]	21.6
	3.24	1600	2.4	1.9
	3.41	1500	3.0	2.9
	3.78	<300	<4.1	1.8
$\beta>1.0$ Mev$-\gamma$	1.04	1000	31.3[b]	30.0
	1.37	960	3.9[b]	3.0
(Fig. 5)	2.40	<150	<2.3[b]	2.4
	2.75	820	21.6[a]	21.6
$\gamma>2.15-\gamma$	1.04	12 700	30.0[a]	30.0
(Fig. 6)	1.58	740	<0.4	

[a] These intensities were matched to the spectrometer results for normalization.
[b] These coincidence results are based on the decay scheme of Fig. 1, with a 1.7-Mev beta spectrum intensity of 0.5 percent.

[22] M. E. Rose and J. L. Jackson, Phys. Rev. **76**, 1540 (1949).
[23] S. A. Moszkowski, Phys. Rev. **82**, 35 (1951).

TABLE IV. Beta spectra of Ga^{66}.

Zn^{66} level (Mev)	Spectrum notation	β^+ energy (Mev)	β^+ and E.C. intensities (percent of Ga^{66} decay) Present authors β^+	Present authors E.C.	Mukerji β^+	Mukerji K-cap.	Mukerji (corrected by present authors) β^+	Mukerji (corrected by present authors) K-cap.	Log ft Present authors	Log ft Mukerji
4.83	K_1'			2.1±0.2					4.7	4.9
4.33	K_2'			7.9±0.9		4.0		11.5	4.9	5.7
4.12	K_3'	0.02		1.5±0.3					5.9	
3.78	β_1	0.36	0.7±0.1	20.7±1.7	1.1	26.2	1.0	24.2	5.1	4.9
3.41	β_2	0.73	1.3±0.3	2.9±0.5					6.2	
3.24	β_3	0.90	4.7±0.7	4.1±0.8	4.5	4.5	4.1	4.1	6.0	5.9
2.75	β_4	1.39	1.7±0.9	0.5±0.2	2.7	0.5	2.5	0.5	7.2	7.1
2.40	β_5	1.74	0.5±0.3[a]						~7.9	
1.04	β_6	3.10	<0.5						>9.3	
0	β_7	4.14	51.7±7	0.5	56.0	0.5	51.6	0.5	7.8	7.8

[a] If our measured gamma-ray intensities are used, we obtain −1.4±2.0 for this beta-decay intensity. However, the $\beta > 1.0 - \gamma$ coincidence seems to indicate that the beta spectrum does exist.

value of 11.5 percent electron capture to these three levels, but preserving Mukerji's relative beta-spectrum intensities. Agreement with our results is then very good. The failure of the beta-spectrometer workers to report the weak 0.73- and 1.74-Mev beta spectra is not a serious objection to our level scheme, because of the difficulty in separating these spectra from the other components in the beta spectrum.

The ratio of total K-capture to total beta decay in Ga^{66} has been measured by Langer and Moffat,[1] by comparison of the Auger electron intensity in a beta spectrometer with the beta spectrum intensity. They find the Auger intensity to be 28 percent of the total beta intensity. This indicates that 38 percent of the Ga^{66} decay is by orbital electron capture, if one uses the L/K capture ratio of Rose and Jackson[22] (0.09), and the best known values[24] for fluorescence yield (0.48). It is believed that this figure can be as much as 4 percent low because of unknown effects resulting from source absorption and scattering.[25] Our results based only on gamma-ray intensities are in excellent agreement (Table IV).

TABLE V. Spins and parities of Zn^{66} levels.

Zn^{66} level (Mev)	Log ft	Possible spin, parity ($Ga^{66} = 1+$) From β decay	From γ-ray branching	Best choice
4.83	4.7	0, 1, 2+	1±	1+
4.33	4.9	0, 1, 2+	1±	1+
4.12	5.9	0, 1, 2+	1±	1+
3.78	5.1	0, 1, 2+	0, 2±	0, 2+
3.41	6.2	0, 1, 2+ 1−	1±	1+
3.24	6.0	0, 1, 2+ 1−	2+ 1±	2+
2.75	7.2	0, 1, 2+ 1, 2−	1±	1+
2.40	~7.9	3, 2, 0− 0, 1, 2+	2±	2+
1.04	>9.3	3±	2+	2+
		0, 2− 0, 1, 2+		
0	7.8	3−	0+	0+
		0, 2− 0, 1, 2+		

CONCLUSIONS

The ground and first excited states of Zn^{66} have been assumed to have even parity and spins 0 and 2, respectively, in accordance with the empirical data on even-even nuclei.[26] For the other levels we have used the theoretical[27,28] and empirical [29,30] data for beta decay and gamma-ray lifetimes in order to see if reasonable spin and parity assignments could be made. This is possible, with Ga^{66} spins of either 0 or 1, for all the levels except the three lowest, where no set of assignments is found which does not have some apparent discrepancy with the existing knowledge of beta and gamma decay. It must be emphasized, though, that the use of Weisskopf's formula and ft values alone does not make possible a very accurate assignment of spins and parities in this case.

Table V shows the possible Zn^{66} assignments for Ga^{66} having spin 1 and even parity (which seems to be the least objectionable choice). The assignments based on beta decay log ft values and on gamma-ray branchings are listed in order of preference in columns 3 and 4, respectively. In most cases a change of unity in the spin of a level changes the gamma-ray branching ratio by a factor of at least 50. The fifth column gives the values which seem to be the best compromise. It is seen that the three lowest levels give poor agreement with Nordheim's classifications of log ft values.[29] The 1.04-Mev level appears to require a forbidden beta spectrum

[24] Broyles, Thomas, and Haynes, Phys. Rev. **89**, 715 (1953).

[25] Professor Langer (private communication).

[26] G. Scharff-Goldhaber, Phys. Rev. **90**, 587 (1953).

[27] E. J. Konopinski, Revs. Modern Phys. **15**, 209 (1943).

[28] V. F. Weisskopf, Phys. Rev. **83**, 1073 (1951). We have used the nomogram from R. Montalbetti, Can. J. Phys. **30**, 660 (1952).

[29] L. W. Nordheim, Revs. Modern Phys. **23**, 322 (1951).

[30] Summary Report of the Indiana Conference on Nuclear Spectroscopy and the Shell Model, Indiana University, May, 1953 (unpublished).

with a spin of 3 for the level.[31] The assignment of spin 0^+ for Ga^{66} would be more favorable in this case, but then there is a discrepancy in the beta decay to the ground state.

If Ga^{66} is 1^-, then it is possible to assign spins of 1^- to all of the Zn^{66} states above 2.40 Mev, and this would agree with Glaubman's recent proposal[32] that low lying levels of even-even nuclei have odd spin if the parity is odd, and even spin if the parity is even. The greatest objection to this would be the assignment of 1^- to the 3.78- and 3.24-Mev levels which decay predominantly to the 1.04-Mev level. Odd parity for Ga^{66} would not agree with the shell model prediction $P:P_{\frac{1}{2}}\,N:(p_{\frac{1}{2}})^4(f_{\frac{1}{2}})^3$ or $(p_{\frac{1}{2}})^3(f_{\frac{1}{2}})^4$ (P: proton configuration, N: neutron configuration).

It does not seem possible to say anything conclusive about the states above 1.04 Mev without internal conversion and angular correlation data.[33]

ACKNOWLEDGMENTS

The authors are indebted to Professor Eugene Feenberg for helpful discussions regarding the shell structure of these nuclei. We also wish to thank Professor Preiswerk and Dr. Mukerji for correspondence during the course of the work and for sending us some of their data and copies of their results prior to publication. The assistance of Lloyd Chase in taking data was greatly appreciated.

[31] It would be very unusual if this spin is not 2. Furthermore, the lifetime of this level has been found to be $<5\times10^{-9}$ sec which makes a spin >2 very unlikely. [Roderick, Meyerhof, and Mann, Phys. Rev. **84**, 887 (1951).]

[32] M. J. Glaubman, Phys. Rev. **90**, 1000 (1953).

[33] Mukerji and Preiswerk mention an (unpublished) angular correlation measurement of the 2.75–1.04-Mev gamma cascade which was inconclusive because of unknown contributions to the coincidences due to weaker components. An accurate measurement of this angular correlation could determine whether the 3.78-Mev level has spin 0 or 2. If this spin is 2 then the possibility of spin 0 for Ga^{66} must be ruled out because of the allowed beta transition to the 3.78-Mev state of Zn^{66}.

PHYSICAL REVIEW VOLUME 92, NUMBER 6 DECEMBER 15, 1953

Half-Life Determination of Po^{210} by Alpha Counting*

MARY LOU CURTIS
Mound Laboratory, Miamisburg, Ohio
(Received August 31, 1953)

A half-life of 138.374±0.032 days for polonium-210 was determined by alpha counting a sample of approximately 0.5 millicurie over a period of 328 days.

THE National Bureau of Standards[1] lists two values for the half-life of Po^{210}: 140 days as determined by Curie[2] by gamma counting, and 138.3 days as determined by Beamer and Easton[3] by calorimetry. Alpha counting affords an entirely different method of determining the half-life, and requires only a small amount of activity. Therefore, for comparison, a half-life determination by alpha counting was undertaken, with a sample of approximately 0.5 millicurie of Po^{210}.

The counting instrument chosen was the Logac,[4] a low-geometry alpha counter chosen for its stability and low-coincidence loss. It consists of a low-geometry attachment used with a methane-flow proportional alpha counter. The sample was kept in the counting chamber throughout the experiment, so that no changes in geometry could occur.

The sample was pipetted from a solution of purified Po^{210} in nitric acid onto a glass slide. Mica, weighing 0.92 mg/cm², was cemented over the sample to prevent migration of activity from the slide. Tests made by adding air to the evacuated counting chamber and counting at varying air pressures showed that the sample was sufficiently thin that no counts were lost by absorption or would be lost by diffusion into the glass.

Over a period of 328 days, 81 measurements were made. Each measurement was of sufficient duration to total at least 500,000 counts, to reduce the statistical probable error to 0.1 percent per measurement. No geometry factor was used, since the decay could be followed from the counting rate.

A least-squares analysis of the data gave a half-life of 138.374 days which compares favorably with the Beamer and Easton value. The probable error in the determination was 0.032 day or 0.02 percent, as compared with 0.1 percent by Beamer and Easton.[3]

* Operated by Monsanto Chemical Company under a U. S. Atomic Energy Commission contract.

[1] *Nuclear Data*, National Bureau of Standards Circular No. 499 (U. S. Government Printing Office, Washington, D. C., 1950), p. 247.

[2] M. Curie, J. phys. et radium (6) **1**, 12 (1920).

[3] W. H. Beamer and W. E. Easton, J. Chem. Phys. **17**, 1298 (1949).

[4] Rose, DeBenedetti, Heyd, Pittenger, Powers, Brenneman, and Curtis, Mound Laboratory Final Report No. 47, M-270, 1947 (unpublished).

The Half-Life of Am^{243}

HERBERT DIAMOND, PAUL R. FIELDS, JOSEPH MECH, MARK G. INGHRAM, AND DAVID C. HESS
Argonne National Laboratory, Lemont, Illinois

(Received August 31, 1953)

The alpha half-life of Am^{243} was found to be 8800 ± 600 years. The ratio of Am^{243} and Am^{241} masses in the sample was measured with a mass spectrometer, and the ratio of their alpha activities was measured with a differential alpha pulse analyzer. A method for preparation of thin samples of americium by electrodeposition is described.

STREET, Ghiorso, and Seaborg[1] determined a rough half-life of about 10^4 years for Am^{243} from a measurement of the amount of Np^{239} daughter in equilibrium with Am^{243}. A more accurate determination has become feasible with the acquisition of an Am^{243} sample formed in plutonium that had been extensively irradiated in the Chalk River pile.[2] The sample was chemically purified, and the mass ratio of Am^{243} to Am^{241} determined accurately with the 60°, 12-inch radius mass spectrometer, using a multiple-filament ionization source. The ratio of the alpha activities of the americium isotopes was measured with a differential alpha pulse analyzer. From these data and the known Am^{241} half-life,[3] the Am^{243} half-life was calculated.

EXPERIMENTAL

Americium, curium, and most of the fission products were separated from the bombarded plutonium by elution from an ion exchange column. Further purification from fission products was obtained by elution from two successive Dowex-50 cation exchange columns with concentrated HCl.[4] This was followed by two successive cation exchange columns of Dowex-50 at 87°C, using 0.25 *M* citric acid whose *p*H had been adjusted to 3.5 with NH_3, as the eluant.[5]

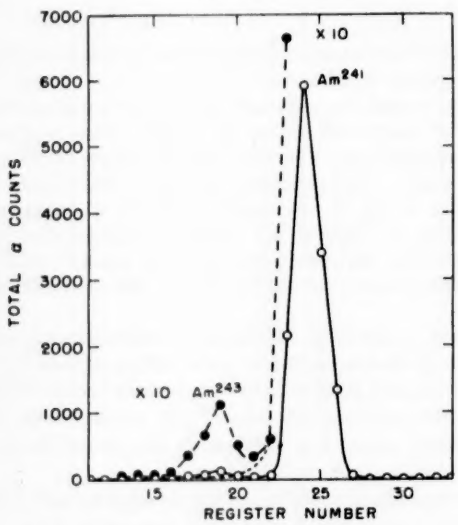

FIG. 1. Typical pulse analysis of americium fraction.

The americium and curium fractions were combined, and the mole ratio, $Am^{243}:Am^{241}=0.335\pm0.003$, was determined by mass spectrometer. The absence of fractionation of the 243 mass peak with respect to the 241 peak over a wide range of electrode temperatures, indicated that these masses were due to the same element.

Accurate pulse analyses of the americium required the removal of the curium activity. This was accomplished by three successive oxidation-reduction cycles,[6] using LaF_3 as a carrier. Three such cycles resulted in a 10^4-fold separation of americium from curium. In order to obtain the americium free from carrier and from fluoride, zirconium hydroxide was substituted for LaF_3 as a carrier, and the zirconium finally removed by thenoyltrifluoroacetone (TTA)-benzene solvent extraction.[7]

A thin, uniform deposit suitable for pulse analyses was obtained by electroplating the purified americium from 10 ml 0.2 *M* K_2CO_3 in a cell similar to the one described by Hufford and Scott.[8] The anode was a rapidly rotating carbon rod, 6 mm in diameter; the cathode was a tantalum disk, 2 cm in diameter; the emf was 11 volts; and the current 90 to 120 milliamperes. After electroplating for 100 minutes at room temperature, the cell was disassembled, and the cathode washed rapidly with dilute NH_4OH and water. The yield was about 60 percent.

The average alpha activity ratio of 5.27-Mev Am^{243}

[1] Street, Ghiorso, and Seaborg, Phys. Rev. **79**, 530 (1950).
[2] Fields, Pyle, Studier, Inghram, and Hess, Argonne National Laboratory Report ANL-4943, 1952 (unpublished).
[3] B. G. Harvey, Phys. Rev. **85**, 482 (1952).
[4] K. Street, Jr., and G. T. Seaborg, J. Am. Chem. Soc. **72**, 2790 (1950).
[5] The authors wish to acknowledge the aid of the Health Chemistry Group of the University of California Radiation Laboratory, Berkeley, California, under the direction of N. B. Garden and William G. Ruehle. This group designed and operated the remote control equipment used in the initial separations at Berkeley.
[6] Asprey, Stephanou, and Penneman, J. Am. Chem. Soc. **72**, 1425 (1950).
[7] R. E. Connick and W. H. McVey, J. Am. Chem. Soc. **71**, 3182 (1949).
[8] D. L. Hufford and B. F. Scott, Atomic Energy Commission Report MDDC-1515, 1945 (unpublished).

to Am^{241}, from five pulse analyses, was 0.0179 ± 0.0006 (Fig. 1).

RESULTS

The alpha half-life of Am^{243} was calculated from these data to be $(8.8 \pm 0.6) \times 10^3$ years, using 470_{-10}^{+5} years as the half-life of Am^{241} [3] and assuming that there is no alpha fine structure of Am^{243} that might be obscured by Am^{241} alphas. The error reported is based upon standard deviation of the alpha counting data (3 percent), the mass spectrometer error (1 percent), the error in the half-life of Am^{241} (2 percent), and the estimated error due to the uncertain correction for the Am^{241} alphas in the Am^{243} peak.

PHYSICAL REVIEW VOLUME 92, NUMBER 6 DECEMBER 15, 1953

Spin-Orbit Coupling Energy in O^{17}†

ROBERT K. ADAIR*
University of Wisconsin, Madison, Wisconsin
(Received September 8, 1953)

A proportional counter filled with carbon dioxide was irradiated with monoenergetic fast neutrons produced by bombarding thin lithium targets with protons from an electrostatic generator. Angular distributions of neutrons scattered by oxygen were deduced from the energy spectrum of recoil oxygen ions for neutron energies from 392 kev to 1412 kev, determining the parities of three spin-$\frac{3}{2}$ levels in O^{17}, 4.56, 5.08, and 5.39 Mev above the ground state. The 5.08-Mev state has even parity and appears to be the $D_{\frac{3}{2}}$ member of a $D_{\frac{1}{2}}-D_{\frac{3}{2}}$ doublet, where the $D_{\frac{3}{2}}$ level is then 5 Mev higher than the $D_{\frac{1}{2}}$ ground state of O^{17}. The other two states have odd parity and lie more than 1.5 Mev above the lowest spin-$\frac{1}{2}$ odd-parity level. This may indicate a spin-orbit splitting of the order of 2 Mev or greater in the P shell.

I. INTRODUCTION

IT might be hoped that the examination of the states of nuclei made up of a closed shell plus one "outside" nucleon would result in information which could be interpreted to help determine the source and strength of spin-orbit forces in nuclei. Various results pertaining to the spin-orbit splitting of the P states of a single nucleon outside the closed 1 S shell, that is, states of He^5 and Li^5, appear to be inconsistent and therefore inconclusive.[1] The next heavier closed shell plus one nuclei are the isobaric $O^{17}-F^{17}$ pair. According to the ordering of levels in a potential well, the lowest state of these nuclei should be either a $2S$ or $1D$ state, the integer representing the number of nodes in the radial wave function. Alder and Yu[2] have shown that the spin of the ground state of O^{17} is $\frac{5}{2}$, and it can be concluded that this state is primarily $D_{\frac{5}{2}}$, a hypothesis in good agreement with the electric quadrupole[3] and magnetic dipole[2] moments. It might, then, be expected that a $D_{\frac{3}{2}}$ state of O^{17} should exist and lie at an excitation energy determined by the strength of the spin-orbit forces acting on the added neutron. Positions of the low-energy levels of O^{17} are known from a variety of experiments,[4] and the spins and parities of all states below 4 Mev can be deduced[5-7] either from experiments on O^{17} or from measurements pertaining to the mirror nucleus F^{17}. None of these states has spin $\frac{3}{2}$, and there is no reason to believe such a state would have been missed because of selection rules or experimental limitations. However, three spin-$\frac{3}{2}$ states are known[8] between 4.5 and 5.4 Mev, and it seemed probable that one of these was the $D_{\frac{3}{2}}$ member of the doublet including the ground state. It was the purpose of these measments to determine the parity of these levels in the hope of finding the $1D_{\frac{3}{2}}$ state in O^{17}, and thus to obtain a measure of the spin-orbit splitting in the $1D$ shell.

II. THEORY OF THE MEASUREMENTS

The variation of total neutron cross section with energy at an elastic scattering resonance associated with a state of spin J is $[(2J+1)/(2I+1)]2\pi\lambda^2$, where I is the spin of the target nucleus, a result independent of the parity of either the target nucleus or the resonance level. Total cross-section measurements interpreted in this way were used to assign values of $\frac{3}{2}$ to the spin of levels in O^{17} at excitation energies of 4.56, 5.08, and 5.39 Mev.[8] If there is no interference between a resonant state and other states, the differential cross section for neutron scattering will also depend solely on J and I. However, an interpretation of the observa-

† Work supported by the U. S. Atomic Energy Commission and the Wisconsin Alumni Research Foundation.
* Now at Brookhaven National Laboratory, Upton, New York.
[1] E.g., see D. R. Inglis, Revs. Modern Phys. **25**, 390 (1953), p. 409.
[2] F. Alder and F. C. Yu, Phys. Rev. **81**, 1067 (1951).
[3] V. Low and C. H. Townes, Phys. Rev. **75**, 529 (1949).
[4] F. Ajzenberg and T. Lauritsen, Revs. Modern Phys. **24**, 321 (1952).
[5] Burrows, Powell, and Rotblat, Proc. Phys. Soc. (London) **209**, 478 (1951).
[6] R. A. Laubenstein and M. J. V. Laubenstein, Phys. Rev. **84**, 18 (1951).
[7] F. Eppling, thesis, University of Wisconsin, 1953 (unpublished).
[8] Bockelman, Miller, Adair, and Barschall, Phys. Rev. **84**, 69 (1951).

tion of the interference which occurs between the resonant state and a state of known parity will usually serve to determine the parity of the resonance level. Such interference occurs between the resonance and the continuum or potential scattering in the case of the scattering of neutrons from oxygen. At the neutron energies involved in these measurements almost all of the background scattering is the result of the interaction of S-wave neutrons with the target nucleus O^{16}. Even-parity states with spin $\frac{3}{2}$ will be formed by the interaction of D-wave neutrons, and odd-$\frac{3}{2}$ states will result in the resonant scattering of P-wave neutrons. Considering only the resonance scattering from spin-$\frac{3}{2}$ resonances and the S-wave potential scattering, the differential neutron scattering cross section in the center-of-mass system will be proportional to $A+B\times\cos\vartheta+C\times\cos^2\vartheta$ for odd-parity states and $A'+C'\times\cos^2\vartheta$ for even-parity states, where the coefficients are functions of the scattering phase shifts[9] and hence, in turn, functions of the neutron energy, and ϑ is the scattering angle in the center-of-mass system. The distributions are obviously qualitatively different inasmuch as the odd-parity resonance angular distributions are asymmetric with respect to 90° and the asymmetry varies with energy, while the even-parity resonant angular distributions are fore-and-aft symmetric.

It seemed most convenient to determine the angular distributions by measuring the recoil energy spectrum of oxygen nuclei bombarded by monoenergetic neutrons Barschall and Kanner[10] have pointed out that the distribution in energy of recoil ions in the laboratory system is proportional to the differential cross section per unit solid angle as a function of $\cos\vartheta$.

II. EXPERIMENTAL PROCEDURE

The experimental procedure was similar to that previously reported.[11] A proportional counter filled with 10 cm of carbon dioxide was irradiated with neutrons produced by bombarding a lithium target with protons from an electrostatic generator. The lithium target had a stopping power of about 16 kev for 2-Mev protons. Since it was necessary to use electron collection and gas amplification to achieve a good signal-to-noise ratio, oxygen, which attaches electrons to form negative ions, could not be used as a counter gas; and carbon dioxide, which does not attach electrons appreciably, was used instead. Carbon has no scattering resonances in the energy region under investigation; therefore the pulse-height spectrum from carbon recoils should vary quite slowly with energy and not interfere with observation of the rapidly varying oxygen-recoil spectrum. Figure 1 shows pulse-height spectra at various neutron energies as measured with a single-channel pulse-height analyser.

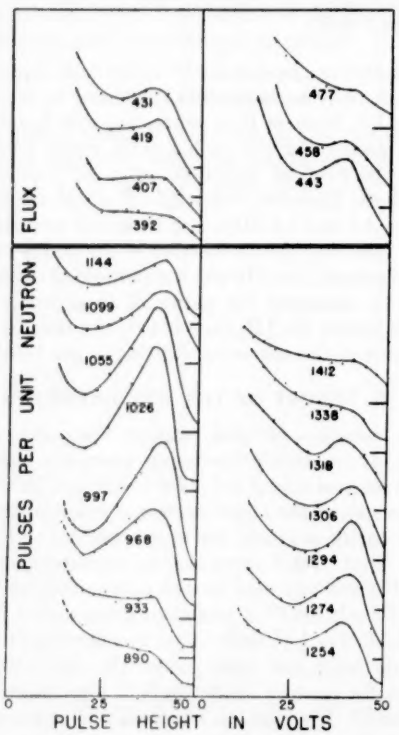

FIG. 1. Recoil-ion energy distributions resulting from the bombardment of carbon dioxide with monoenergetic neutrons of energies from 392 kev to 1412 kev. The amplifier gain was varied with neutron energy so that the maximum-energy oxygen recoil at each neutron energy produced a pulse of about 45 v. The ordinate scale is arbitrary for each distribution.

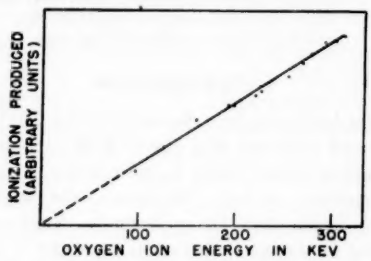

FIG. 2. Ionization produced by oxygen ions as a function of ion energy.

These pulse-height distributions are proportional to the distribution of ion recoil energies only if the number of ion pairs produced by the recoil ion is sensibly proportional to the recoil ion energy. A measurement was made which verified this proportionality within the limits required by this experiment. The maximum oxygen-recoil energy will be equal to 0.222 E_n, where E_n is the incident neutron energy, while the maximum

[9] J. A. Wheeler and H. H. Barschall, Phys. Rev. **58**, 682 (1940).

[10] H. H. Barschall and M. H. Kanner, Phys. Rev. **58**, 682 (1940).

[11] R. K. Adair, Phys. Rev. **86**, 155 (1952).

carbon-ion recoil energy will be equal to 0.28 E_n. Maximum pulse heights for carbon and for oxygen recoils could be determined for each neutron energy by inspection of the high-energy side of the pulse-height spectra, thus giving a measure of the ionization produced as a function of the recoil-ion energy. Points on Fig. 2 represent the variation in the ionization produced by oxygen ions as a function of the ion energy. Comparison of the points with the straight line drawn to pass through the origin shows that the ionization is nearly proportional to energy. This type of measurement actually pertains to the maximum ionization produced by the heavy ions, and the results do not eliminate the possibility that monoenergetic ions may produce an asymmetric pulse-height distribution with perhaps a large low-energy tail.

Aside from uncertainties concerning the effects of carbon recoils and the lack of knowledge of the ionization spectrum of the heavy ions, the measured angular distributions are affected by the rather poor energy or angular resolution of the counter and by end and wall effects. Since the evaluation of all these effects is uncertain and the corrections do not affect the qualitative features of the distributions, which are of primary physical importance, such corrections were not made.

IV. CONCLUSIONS AND DISCUSSION

From the total cross-section measurements[8] the resonant energies for the three resosnances are known to be 435, 1000, and 1311 kev. Widths of the resonances are, respectively, 42, 100, and 35 kev. It can be noted immediately upon inspection of the pulse-height distributions that the angular distributions at the 1000-kev resonance do not change in asymmetry as the neutron energy is increased through resonance. The minimum of the distribution, at about one-half of the maximum pulse height or at about 90° in the center-of-mass system, is clearly stationary with energy. This absence of a $\cos\vartheta$ term varying strongly with energy near resonance indicates that the resonance state has even parity. Distributions at the 435-kev resonance and the 1.311-Mev resonance show a strong asymmetry which varies with energy. At energies below resonance, backscattering predominates, while above the resonance, scattering is stronger in the forward direction. The minimum, therefore, moves from small angles and small pulse heights to larger angles and larger pulse heights as the neutron energy increases from below to above the resonance energy. The S-wave phase shift of neutrons scattered from oxygen must be negative from considerations of continuity, since the scattering length at zero energy is positive,[12] while the resonant P wave is expected to increase positively from near 0° below resonance to near 180° at energies above resonance. This will give a variation of angular distributions

[12] E. Fermi and L. Marshall, Phys. Rev. **71**, 666 (1947).

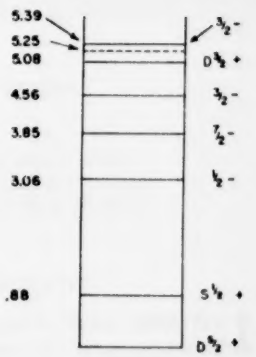

FIG. 3. Energy levels of O^{17} up to 5.5 Mev. The narrow state found in reaction experiments which may be involved in the N^{17} β decay is indicated by the dashed line. The delineation of this state by a dashed line is not meant to indicate that its presence is less certain than that of the other states.

similar to that observed near 435 kev and 1311 kev, that is, predominant backscattering below resonance and forward scattering at neutron energies above resonance. We conclude, therefore, that these resonances result from the formation of odd-parity states in the compound nucleus, O^{17}.

Though it is reasonably well established that the 5.08-Mev state is the lowest state of even parity and spin $\frac{5}{2}$, it is not obvious that it is the $D_{\frac{5}{2}}$ complement of the ground state. However, our knowledge of the width of the level gives some information concerning the wave function of the state. The reduced width of the state, defined[13] as $\Gamma/2kP$, measured in units of $\hbar^2/Ma$ (Γ is the measured width, k the neutron wave number, P the barrier penetration factor, M the reduced mass of the system, and a the nuclear radius) is likely to be approximately equal to the square of the overlap of the compound-state wave function with the initial-state wave function, which in this case consists of the O^{16} nucleus plus a $D_{\frac{5}{2}}$ neutron. The value of this quantity for the 5.08 Mev resonance is about $\frac{1}{2}$; so large a value indicates strongly that it is this level which is the $D_{\frac{5}{2}}$ single-particle state expected in this energy region.

Figure 3 shows an energy level diagram of O^{17} up to excitation energies of 5.4 Mev. Spins and parities of all states, except that shown by the dashed line,[14] are shown. States which can be represented by a single neutron outside a closed shell have the orbital angular momentum specified. The $D_{\frac{3}{2}}-D_{\frac{5}{2}}$ splitting is seen to be 5.08 Mev. It is attractive to regard the 3.07-Mev state as a $P_{\frac{1}{2}}$ hole in the P shell, with the two excess nucleons coupling to produce zero spin. we might then expect a $P_{\frac{3}{2}}$-hole state at higher energy. The energy difference would then be a measure of the strength of spin-orbit coupling in the P shell. Since the lowest $P_{\frac{3}{2}}$ states are 1.5 and 2 Mev higher, we can assume that the splitting is equal to or greater than 1.5 Mev.

[13] E. P. Wigner and L. Eisenbud, Phys. Rev. **72**, 29 (1947).

[14] Inglis points out (reference 1) that this state probably has high angular momentum and is probably the state associated with the β decay of N^{17}.

A Search for B^{13}

EDWARD L. HUBBARD, LAWRENCE RUBY, AND WARREN F. STUBBINS
Radiation Laboratory, Department of Physics, University of California, Berkeley, California
(Received September 14, 1953)

When various elements were bombarded with 340-Mev protons and 190-Mev deuterons, no neutron activity was found which would correspond to the decay of B^{13} as a delayed neutron emitter with a half-life in the range from 0.5 millisecond to 0.5 hour.

INTRODUCTION

ISOTOPES which decay by negatron emission followed promptly by a neutron are known as delayed neutron emitters. Several such isotopes have been observed as fission products, and two more have been produced in cyclotron reactions. The best identified of the fission activities,[1,2] Br^{87} and I^{137}, and the cyclotron activities,[3,4] Li^9 and N^{17}, all have in common the property that the end product of the decay contains a closed neutron shell. In addition, it has been suggested[5] that B^{13} should be a delayed neutron emitter going finally to C^{12}. Sheline,[6] using a 50-Mev betatron, has not observed B^{13} in a search for new low Z beta activities of half-life greater than 0.1 sec.

Barkas[7] predicts B^{13} to be particle stable with a mass of 13.0207. This gives a beta plus neutron excitation of 7.45 Mev. Assuming an allowed transition with $ft = 5\times10^3$, as is the case of N^{17}, one gets a minimum expected half-life of 0.2 sec. With outside limits on the mass and the ft value, one finds a minimum possible half-life of 0.002 sec.

EXPERIMENTAL PROCEDURE

Three holes were bored in a large block of paraffin, one for the targets and one on either side for a BF_3 counter. In order to reduce the background from neutrons reverberating inside the shielding, the target assembly was surrounded with $\frac{1}{16}$ inch of cadmium and three more inches of paraffin. Various low- and middle-Z targets were exposed to the deflected 340-Mev proton and 190-Mev deuteron beams of the 184-inch cyclotron.

For examination of half-lives greater than 0.1 sec, the cyclotron was turned off after a short bombardment, and the counting rate was monitored with a Brush Recorder. For half-lives shorter than 0.1 sec, the counter outputs were combined into ten scalers which were gated on and off in succession between beam pulses. The width of the gates could be varied from 80 μsec to 100 msec. In addition, the first gate could be delayed in arbitrary time from the beam pulse. The deflector was pulsed only once a second so that build up of the Li^9 activity would not obscure any other decay of shorter half-life. It was found that all targets, except those producing a high yield of Li^9 or N^{17}, exhibit neutron decay which varies with the target but whose half-life in no case exceeds 240 μsec. This is interpreted as the limit imposed by the diffusion of neutrons produced by nuclear transmutations in the target.

CONCLUSION

If B^{13} is particle stable, it should have been produced by spallation reactions; therefore, it is concluded that B^{13} is not a delayed neutron emitter with a half-life in the range from 0.5 msec to 0.5 hr.

[1] A. H. Snell *et al.*, Phys. Rev. **72**, 545 (1947).
[2] N. Sugarman, J. Chem. Phys. **15**, 544 (1947).
[3] L. Alvarez, Phys. Rev. **75**, 1127 (1949).
[4] W. L. Gardner *et al.*, Phys. Rev. **83**, 1054 (1951).
[5] A. H. Snell, Science **108**, 167 (1948).
[6] R. K. Sheline, Phys. Rev. **87**, 557 (1952).
[7] W. H. Barkas, Phys. Rev. **55**, 691 (1939).

Complex Alpha Spectra of Radiothorium (Th^{228}) and Thorium-X (Ra^{224})†

FRANK ASARO, FRANK STEPHENS, JR., AND I. PERLMAN
Radiation Laboratory and Department of Chemistry, University of California, Berkeley, California

(Received July 17, 1953)

The alpha and gamma spectra of Th^{228} have been studied with an alpha-particle spectrograph and gamma-ray scintillation counters. Thorium 228 has alpha groups of 5.421 (71 percent), 5.338_5 (28 percent), 5.208 (0.4 percent), and 5.173 Mev (0.2 percent), and gamma rays of 89 (1.6 percent), 137 (0.26 percent), 169 (0.09 percent), and 212 kev (0.27 percent). Spins and parities are assigned to the energy levels defined by the alpha groups, and the results are evaluated with respect to the developing theory and systematics of complex alpha spectra.

I. INTRODUCTION

In recent communications[1,2] we have shown that the energy levels reached by the decay of even-even alpha emitters fall into a regular pattern with respect to (1) energy level spacing, (2) spectroscopic designation of the states, and (3) the relative population of the states. Starting with the heaviest nuclei, the energy levels of the low-lying states increase progressively with decrease in charge and neutron number. The low-lying states seem to be even-spin–even-parity states, and in a limited region the relative energy spacings conform well with their assignments to even rotational states, as suggested by Bohr and Mottelson.[3] It was also shown[2] that the *second even-spin state* is populated to a much lower degree than the demands of simple alpha-decay theory, and that the degree of departure from expectation increases progressively with atomic number. As a possible explanation, it was suggested that there is a progressive change in the charge asymmetry of the nuclei, giving a spherically nonsymmetrical potential barrier, and that the alpha group in question is emitted in a direction in which it encounters a greater potential barrier than do the groups leading to the first excited state and the ground state.

Evidence already mentioned, as well as analysis of gamma-ray conversion coefficients, points to the rule that for the heaviest even-even nuclides the low-lying states all have even spin and even parity. This situation was analyzed[4] in detail for Pu^{238} (alpha-decay product of Cm^{242}), and it was also shown that the first odd-spin–odd-parity state probably lies approximately 1 Mev above the ground state. The present paper on Th^{228} alpha decay shows the existence of the low-lying even-spin states, but, in addition, an *odd-spin* state has dropped down so that it falls within the even-spin states.

The two nuclides considered here (Th^{228} and Ra^{224}) are members of the thorium decay series and, as such, have been examined a number of times in the past in other laboratories. The points of similarity and differences between the present work and earlier measurements will be brought out in the discussion of the results.

II. METHODS

The Th^{228} and Ra^{224} were obtained from a mesothorium source of ~70-mg radium gamma-ray equivalent. It will be seen that six alpha groups so far found are ascribable to these two isotopes; and, since the energies are close to each other, fairly rigorous chemical separations are required to assign the groups, particularly those in low intensity. Furthermore, possible interfering groups are at hand from the ThC(Bi^{212}) of this decay series, as well as from members of the radium (Ra^{226}) series which are present as minor contaminants in the mesothorium. The problem of analysis hinges on the growth rates of the members of the series. Th^{228} (1.9-yr half-life) can be obtained pure initially, but Ra^{224} grows in with its 3.64-day half-life. Other members rapidly follow the Ra^{224} growth, except Bi^{212} (60 min), which is held up slightly by the growth of its beta-emitting parent, 10.6-hr Pb^{212}. As may be visualized from these lifetimes, it is possible to make an alpha-spectrum analysis of Th^{228} relatively free of decay products, and of Ra^{224} with its products free of Th^{228}; but it is not possible to analyze Ra^{224} free of its decay products. If Ra^{226} is present in the mesothorium, its decay products, Em^{222} and Po^{210}, will produce alpha groups in the energy range of interest; Bi^{214} is excluded from consideration because of its extremely low alpha branching.

The method of chemical separation made use of Dowex-50 ion-exchange resin, upon which the radium and thorium fractions were adsorbed and eluted selectively. The conditions differed considerably for the different preparations and will be mentioned when the separate determinations are discussed.

After chemical separation of a sample, its solution was evaporated on a tungsten filament and then vacuum-sublimed onto a platinum plate which was masked to approximate a line source of alpha activity. The sample was then measured in the magnetic spectrograph. The techinques of source preparation and spectrograph measurements were described in earlier

† This work was performed under the auspices of the U. S. Atomic Energy Commission.

[1] F. Asaro and I. Perlman, Phys. Rev. **87**, 393 (1952).
[2] F. Asaro and I. Perlman, Phys. Rev. **91**, 763 (1953).
[3] A. Bohr and B. R. Mottelson, Phys. Rev. **89**, 316 (1953); **90**, 717 (1953).
[4] Asaro, Thompson, and Perlman, Phys. Rev. (to be published); University of California Radiation Laboratory Unclassified Report UCRL-2193, May, 1953 (unpublished).

TABLE I. Low-energy alpha group of Ra^{224} (5.445 Mev). (Main alpha group (α_0) at 5.681 Mev.)

Experiment and sample numbers	Energy reference	Energy (Mev)	Abundance relative to $Ra^{224}\alpha_0$	Abundance relative to $Th^{228}\alpha$'s
Experiment 174, sample 1	$Ra^{224}(\alpha_0)$ Em^{222}	5.441±0.005 5.445±0.005	5.6%	>600%
Experiment 226, sample 2	$Th^{228}(\alpha_{84})$	5.445±0.001	4.8%	1.6%
Experiment 241, sample 3	$Th^{228}(\alpha_{84})$	5.447±0.002		
Experiment 258, sample 4	$Ra^{224}(\alpha_0)$	5.442±0.002	5.2%	0.31%
Best value		5.445	5.2%	

TABLE II. Assignment of 5.208-Mev group as α_{217} of Th^{228}.

Experiment and sample numbers	Energy reference	Energy (Mev)	Abundance relative to $Th^{228}\alpha_0$ and α_{84} (%)	Abundance relative to $Ra^{224}\alpha_0$ (%)
Experiment 226, sample 2	$Th^{228}\alpha_{84}$	5.208±0.001	0.45	1.3
Experiment 238, sample 3	$Th^{228}\alpha_{84}$	5.21±0.10	≤0.5	≤0.2
Experiment 241, sample 3	$Th^{228}\alpha_{84}$	5.21	≤0.65	≤0.6
Experiment 258, sample 4	$Ra^{224}\alpha_0$	5.206±0.001	0.42	7.0
Experiment 230, sample 2	Po^{210}	5.209±0.001		
Best value		5.208	0.4	

publications.[5,4] An analysis was also made of the gamma-ray spectrum of Th^{228} using a sodium-iodide (thallium-activated) crystal detector and a 50-channel pulse analyzer.

III. RESULTS

The standard of reference for energy was the principal alpha group (α_0) of Ra^{224}, which had been determined as 5.681 Mev by Briggs.[6] In some instances, energies were determined more conveniently relative to Em^{222} (Rn) and Po^{210}, after these were identified in the samples. Also, other abundant groups of Ra^{224} and Th^{228} served as secondary standards. The data concerning the six alpha groups attributed to Th^{228} and Ra^{224} are shown in Tables I–III. In these, the *experiment number* refers to the spectrograph exposure, and the *sample number* identifies the particular alpha-particle source whose preparation is described in the Appendix. Pertinent data on the exposures are also summarized in Table IV.

Alpha Decay of Ra^{224}

The main alpha group of Ra^{224} (5.681 Mev) leading to the ground state of Em^{220} is readily identified and, as mentioned, has served as the energy standard for the present series of measurements. Rosenblum, Valadares, Perey, and Vial[7] have found an alpha group of Ra^{224} at 5.448 Mev in 4.6 percent abundance. Table I contains data identifying this same group. It is seen that its abundance relative to α_0 of Ra^{224} is reasonably constant in the different preparations, and it bears no relation to the amount of Th^{228} present. The energy of this group is 5.445 Mev, and its abundance (of total Ra^{224} alpha particles) is 4.9 percent; both values are in agreement with those of Rosenblum and co-workers.[7]

The energy difference between the two alpha groups of Ra^{224} as found here is 236 kev; therefore, the second group leads to an excited state of 240 kev. No measurement of the gamma-ray transition was made by us, but Rosenblum, Valadares, and Guillot[8] have observed K- and L-conversion lines of a 241-kev gamma ray and from the conversion coefficient have deduced that the transition is of the $E2$ type. This conclusion designates the 240-kev state as $2+$, the first *even-spin* state. The corresponding excited state apparently appears in each even-even nucleus, and the energies of these

TABLE III. Assignment of 5.173-Mev group to α_{253} of Th^{228}.

Experiment and sample number	Energy reference	Energy (Mev)	Abundance relative to $Th^{228}\alpha_0$ and α_{84} (%)	Abundance relative to $Ra^{224}\alpha_0$ (%)
Experiment 226, sample 2	$Th^{228}\alpha_{84}$	5.173±0.001	0.22	0.65
Experiment 238, sample 3	$Th^{228}\alpha_{84}$	5.17±0.02	≤0.2	≤0.1
Experiment 241, sample 3	$Th^{228}\alpha_{84}$	5.17	≤0.5	≤0.4
Experiment 258, sample 4	$Ra^{224}\alpha_0$	5.171±0.002	0.19	3.1
Experiment 230, sample 2	Po^{210}	5.174±0.001		
Experiment 248, sample 2	$Ra^{226}\alpha_0$	5.174±0.004		
Best value		5.173	0.2	

TABLE IV. Table showing characteristics of the various spectrograph exposures.

Sample number	Source slit[a] width—inches	Exposure number	Length of exposure	Time between preparation of sample and start of exposure
1	0.13	174	94 hr	3 days
2	0.018	225	30.0 min	1 hr
	0.018	226	19 hr	2 hr
	0.018	230	41 hr	3 days
	0.13	248	44 hr	64 days
3	0.13	238	10 hr	1 day
	0.018	241	63 hr	3 days
4	0.018	258	3¼ hr	1 hr
	0.018	259	10.0 min	4 hr

[a] This defines the width of the masking slit which is placed immediately in front of the sample to simulate a line source. The length of the slit is approximately one inch.

[5] Asaro, Reynolds, and Perlman, Phys. Rev. **87**, 277 (1952).
[6] G. H. Briggs, Proc. Roy. Soc. (London) **A157**, 183 (1936).
[7] Rosenblum, Valadares, Perey, and Vial, Compt. rend. **229**, 1009 (1949).
[8] Rosenblum, Valadares, and Guillot, Compt. rend. **234**, 1767 (1952).

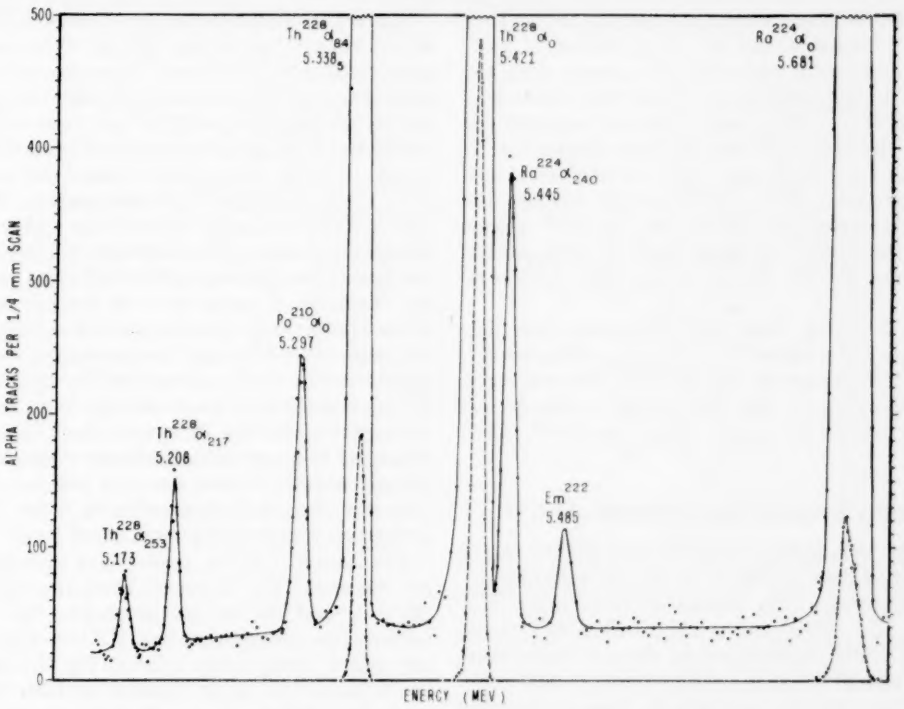

FIG. 1. Alpha spectra of Th^{228} and Ra^{224}. ———— Full scan across width of photographic plate. - - - - - About 2.4 percent of full scan.

states follow a distinct pattern from the region of lead to the heaviest elements.[1,9]

From the discussion of the Th^{228} spectrum which follows, it will be seen that no other alpha groups of Ra^{224} could be identified down to energies 884 kev below the main alpha group. This observation does not agree with the work of others.[7] On the basis of our measurements, the alpha-decay scheme of Ra^{224} consists simply of the ground-state transition in 95 percent abundance and the transition to the 240-kev 2+ state in 5-percent abundance. Any other alpha group within the range of our measurement is in <0.1 percent abundance.

Alpha Spectrum of Th^{228}

The principal alpha group of Th^{228} was measured as 5.421±0.001 Mev, using $Ra^{224}\alpha_0$ as the standard. The measurement was made on Sample 2, Experiment 225. In the same experiment, the group leading to the first excited state was observed, and its energy was found to be 5.388_5±0.001 Mev and its abundance 28 percent. The energy difference defines the first excited state at 84.3 kev. In another run (Sample 4, Experiment 259) the abundance of the group was found to be 26 percent and the energy level 84.9 kev. The data on the two principal groups of Th^{228} are in excellent agreement with those of Rosenblum, Valadares, and Perey,[10] who reported energies of 5.423 and 5.338 Mev in exactly the same relative abundances as in our Experiment 225.

Besides these two high-abundance groups, two others in low intensity were observed which we attribute to Th^{228}. Figure 1 shows one spectrum taken covering the energy range from 5.15 to 5.71 Mev (Experiment 226, Sample 2). The solid curve applies to the 19-hour exposure, and on this the groups α_0 and α_{84} of Th^{228} and α_0 of Ra^{224} were too intense to be shown on the same scale. The peaks for these groups, shown as broken lines in Fig. 1, were obtained by making partial scans of the photographic plate and represent about 2.4 percent of the total tracks registered. It will be noted that groups due to Po^{210} and Em^{222} are on the plate. Other exposures on samples, in which Po^{210} was absent and Em^{222} present in altered abundance, helped confirm their assignments. An alpha group of Bi^{212} (5.603 Mev) falls within the energy range of these measurements, but its estimated intensity would have been below our limit of detection.

Tables II and III summarize the data on the two low-intensity groups of Th^{228}. These groups at 5.173

[9] S. Rosenblum and M. Valadares, Compt. rend. **235**, 711 (1952).

[10] Rosenblum, Valadares, and Perey, Compt. rend. **228**, 385 (1949).

and 5.208 Mev bear constant relationship to the Th^{228} content of the sample and not to the amount of Ra^{224}. This observation is somewhat at variance with the results of Rosenblum and co-workers[7] who reported no groups of Th^{228} in this energy range but reported one at 5.194 Mev with Ra^{224} in 0.4-percent abundance. It will be seen that these two groups of Th^{228} fit in well with a proposed decay scheme which includes the gamma-ray transitions. Aside from the Th^{228} groups already mentioned, an upper limit of 0.04 percent could be set for any in the energy range 4.80→5.67 Mev.

It will be noted (Table III, Experiment 248) that $Ra^{226}\alpha_0$ was the standard for the energy determination of the 5.173-Mev group (α_{253}) of Th^{228}. The agreement of this energy with that using other standards was obtained using the revised energy for Ra^{226}, 4.777 Mev.[11]

Gamma Rays and Decay Scheme of Th^{228}

In order to examine the gamma rays of Th^{228} free of Ra^{224} and its decay products, a quick chemical separation was devised. The mixture in dilute nitric acid solution was placed on a Dowex-50 resin column jacketed to allow operation at an elevated temperature (in this case 87°C) which permits rapid equilibration. The radium, lead, and bismuth fractions were eluted with 4*M* nitric acid, after which the thorium was stripped with a 50-volume-percent solution of lactic acid at *p*H 3. The thorium solution was evaporated to dryness, the alpha activity measured, and then the gamma rays were analyzed with a scintillation counter coupled to a 50-channel pulse analyzer. The gamma-ray spectrum was measured within one hour of the time that the decay products of Th^{228} were separated.

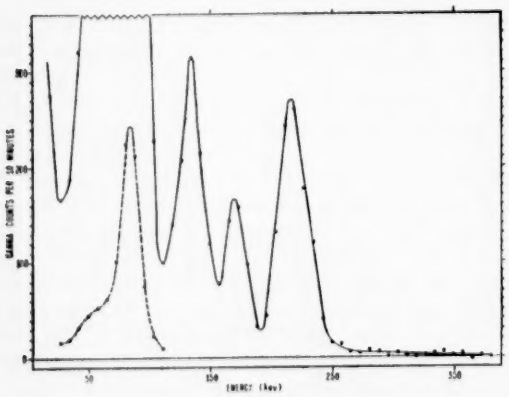

FIG. 2. Gamma-ray spectrum of Th^{228}. ———— Gamma-ray counting rate indicated by ordinate scale. – – – – – Gamma-ray counting rate equals 10 time the value indicated by ordinate scale.

[11] G. Bastin-Scoffier and Sant'ana-Dionisio, Compt. rend. **236**, 1016 (1953).

Figure 2 shows the gamma-ray spectrum of Th^{228}, in which is found a prominent peak at 89 kev and lesser peaks at 137, 169 and 212 kev.* The assignment of these gamma rays to Th^{228} seems certain, since the growth of the 238-kev gamma ray of Pb^{212} and those of Bi^{212} were readily followed, and extrapolation of their abundances to time of initial measurement showed that separation of the decay products of Th^{228} was complete. The small peak on the low-energy side of the 89-kev peak is probably its escape peak, and each of the others will also have an escape peak hidden under the next lowest one. Similarly, *K* x-rays from the internal conversion of the higher energy gamma rays will be under the 89-kev peak. For calibrating the instrument, the 60-kev gamma ray of Am^{241} and the 184-kev gamma ray of U^{235} were employed. The standards could not be run concurrently with the Th^{228}; as a result, there are uncertainties in energy because of drift of photomultiplier voltage, which has been found in practice to be less than one channel, corresponding to 8 kev. Probably the gamma energies are good to about 5 kev.

The intensities of the gamma rays were determined by correcting the observed intensities for counter efficiency and for the escape peaks. The corrected values as percentages of the total Th^{228} alpha particles are shown in the decay scheme, Fig. 3. The energy levels shown are those determined from the alpha spectrum, while the measured gamma-ray energies are indicated, along with their abundances, by the vertical arrows designating the transitions.

The 89-kev gamma ray is almost surely the same as that assigned to a pair of close-lying gamma rays[12] or, more recently, to a single gamma ray of 84 kev[13] or 83 kev.[14] The energy level of this state, according to our alpha-decay data, is 84 kev, which is closer to the aforementioned values[13,14] for the gamma-ray energy. Riou[14] measured the intensity of the gamma ray (relative to total alpha particles) as 2.1 percent, and, when this was related to the 28-percent abundance of α_{84}, the conversion coefficient was found to be twelve.[15] From our measurements (1.6-percent intensity and 28-percent population by α_{84}), the conversion coefficient is 16. These conversion coefficients, as well as the $L_I/L_{II}/L_{III}$ ratios, correspond with the assignment to *E*2 radiation (from calculated conversion coefficients of Gellman, Griffith, and Stanley[16]), as already pointed out by Rosenblum, Valadares, and Guillot.[13] Attempts

* *Note added in proof.*—Gamma rays of 84, 133, 172, and 216 kev were reported by Bouissières, Falk-Vairant, Riou, Teillac, and Victor, Compt. rend. **236**, 1874 (1953).

[12] J. Surugue and San Tsiang Tsien, Compt. rend. **213**, 172 (1941).

[13] Rosenblum, Valadares, and Guillot, Compt. rend. **235**, 238 (1952).

[14] M. Riou [cited by Victor, Teillac, Falk-Vairant, and Bouissières, J. Phys. et radium **13**, 565 (1952)].

[15] Victor, Teillac, Falk-Vairant, and Boussières, J. Phys. et radium **13**, 565 (1952).

[16] Gellman, Griffith, and Stanley, Phys. Rev. **85**, 944 (1952).

have been made[17–19] to assign the radiation uniquely by alpha-gamma angular correlations, but, although there is strong evidence[18,19] for an electric quadrupole component, the correlation is not exact.‡ Nevertheless, the preponderance of evidence in this case, as well as for even-even nuclei in general, points to 2+ for the first excited state.

We shall consider next the 169-kev gamma ray. This energy agrees well with the difference in energy between the states populated by α_{253} and α_{84}. From the population of the 253-kev state (0.2 percent) and the intensity of the 169-kev gamma ray (0.09 percent), a total conversion cofficient of 1.2 is calculated. The sum of K[20] and L[16] theoretical conversion coefficients for $E1$, $E2$, and $M1$ radiation are estimated, respectively, to be 0.1, 1.2, and 4.9. The radiation is therefore probably $E2$, and the spectroscopic state designation is 0, 2+, or 4+. Because of the absence of the crossover transition and the apparent absence of any $M1$ admixture, the most probable designation is 4+, although 0+ and 2+ are is not ruled out from these considerations alone.

The picture so far discussed for Th^{228} corresponds precisely with the spectrum of another even-even nuclide, Cm^{242}, in the appearance of two excited *even-spin* states (2+ and 4+) whose energies are in the ratio of about three.[4] The generality of this condition for the even-even nuclides of the heavy elements has been discussed[2] and shown to conform with the expectations for rotational levels for the even-spin states.[3] In the case of the excited states of Pu^{238} from alpha decay of Cm^{242} and beta decay of Np^{238}, it was deduced[4] that the low-lying states have even parity and that the first odd-parity state lies at about 1 Mev. This takes into account the aforementioned alpha-decay picture and, since Np^{238} should have odd parity, the observed division into an allowed low-energy beta transition and one or more high-energy beta transitions. To explain the other gamma rays found in Th^{228} decay, we are assuming that the first odd-parity state of Ra^{224} has decreased in energy so that it lies among the even-parity states, according to the following arguments.

The energies of the 137-kev and 212-kev gamma rays agree within experimental error with transitions from the state populated by α_{217} to the first even-spin state and to the ground state. The sum of the gamma-ray intensities is the same as the population of the 217-kev level obtained from alpha decay within experimental error (actually larger by measurement), so that the conversion coefficients for both gamma rays must be considerably less than unity. This can only be fulfilled by assigning both to E1 transitions, which makes the 217-kev level a (1−) state. All of these data are consistent with the decay scheme of Fig. 3.

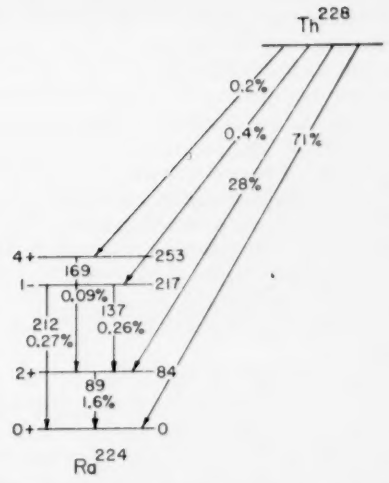

FIG. 3. Th^{228} decay scheme (energies given in kev).

Alpha-Decay Theory

It has been shown by a number of independent calculations that the half-life–energy relationships of the ground-state transitions of both Th^{228} and Ra^{224} conform substantially with simple alpha-decay theory. Similarly, the first even-spin states (2+) of both conform with the theory for their respective energies or, in our terminology, they are unhindered. However, the transitions of Th^{228} to the 1− and the 4+ states are hindered by a factor of approximately ten. The reason for this behavior is not yet clear, although in another paper[2] a suggestion is advanced.

The reason alpha groups of Ra^{224}, other than those to the ground state and to the 2+ state, are not seen must be the low energy which such groups would have. We can estimate[2] that the energy of the 4+ state would be about 600 kev above the ground state and that, even if the alpha transition were unhindered, its abundance would be less than 0.05 percent. A group of this intensity would not have been measurable even if it had not been obscured by other alpha groups in the samples. Since we cannot estimate the position of the first odd-parity state, no definite statement can be made regarding the absence of the corresponding alpha transition.

IV. SUMMARY

The present paper aims to present a link in the accumulating evidence for a high degree of regularity in the spacing of energy levels and their quantum

[17] Kul'chitsky, Latyshev, and Bulyginsky, Izvest. Akad. Nauk. S.S.S.R. Ser. Fiz. **13**, 331 (1949).
[18] Beling, Feld, and Halpern, Phys. Rev. **84**, 155 (1951).
[19] Battey, Madansky, and Rasetti, Phys. Rev. **89**, 182 (1953).
‡ *Note added in proof.*—Abragam and Pound [Phys. Rev. **89**, 1306 (1953)] have made calculations which explain the "weakening" of the 0−2−0 alpha-gamma angular correlation in terms of the interaction of the quadrupole moment of the intermediate state with the electric field gradient at the nucleus.
[20] Rose, Goertzel, and Perry, Oak Ridge National Laboratory Report ORNL-1023, June, 1951 (unpublished).

states for even-even nuclei in the heavy element region. Starting with the heaviest elements, we have as a basis a series of low-lying states $0+, 2+, 4+, 6+(?)$, with the first odd-parity state apparently lying at an elevated level. As one descends to lower elements, the same structure (at least for the lowest states) persists, but the energy spacings increase. Furthermore, the ratios of these energy levels for each nucleus follow a $J(J+1)$ dependence up to a certain point. With Th^{228}, and presumably with others in this region, an odd-parity state appears among the even-parity low-lying states. These considerations should be of value in interpreting beta spectra of the odd-odd nuclides in this region.

Alpha-decay theory for transitions to the ground state and the $2+$ state is obeyed in first approximation by the two alpha emitters considered here. However, for transitions to other states, an extension must be created. The factors to be considered are probably different from those for odd-nucleon nuclides, for which alpha-decay theory also does not apply.

V. ACKNOWLEDGMENTS

We wish to thank Mrs. J. A. Simmons for her assistance in alpha track counting.

VI. APPENDIX

Preparation of Samples for Alpha-Particle Spectrograph Exposures

Sample 1

About 10^8 disintegrations per minute of a dilute acid solution of Th^{228} were added to the top of a Dowex-50 cation-exchange resin column upon which the Th^{228} and most decay products remained. When 4-*M* nitric acid was passed through the column, the thorium fraction remained and the radium washed through. The radium fraction was concentrated and then evaporated to dryness on a tungsten filament which could function as a heater.

Heating the filament at relatively low temperature (dull red heat) removed any polonium present and also removed the lead (ThB). The Ra^{224} was then sublimed in vacuum onto a platinum plate by an increase in the filament temperature. The final sample contained 2×10^5 alpha disintegrations per minute of Ra^{224} with no detectable Th^{228}.

Sample 2

About 10^{11} disintegrations per minute of Ra^{228} (MsThI) in dilute nitric acid were placed on a Dowex-50 resin column, and the radium fraction was stripped, as mentioned previously, with 4-*M* nitric acid. The thorium was then removed with 16-*M* nitric acid. A portion of this eluate was concentrated and evaporated to dryness on a tungsten filament. The thorium and decay products which had grown in were vacuum-sublimed onto a platinum plate. The sample so prepared contained 1.4×10^5 disintegrations per minute of total alpha particles, about half of which belonged to Th^{228} and the rest to its decay products.

Sample 3

The Th^{228} residue on the filament from which Sample 2 was prepared was allowed to remain for 13 days to equilibrate with its decay products. A relatively low-temperature vacuum sublimation was carried out to concentrate the Ra^{224} on the collector plate relative to the Th^{228}. About one-sixth of the 5×10^7 alpha disintegrations caught belonged to Th^{228} and the remainder to Ra^{224} and its decay products.

Sample 4

The objective in preparing this sample was to observe groups of Th^{228} in the absence of the equilibrium amount of Ra^{224}. Thorium-228 was separated from its decay products by the rapid method outlined in the text of this paper for preparing Th^{228} for gamma-ray analysis. In this case, the separation of Th^{228} from Ra^{224} was not quantitative because macroscopic impurities interfered with the column operation. After column separation the Th^{228} solution was concentrated and evaporated to dryness on a tungsten filament. The Th^{228} was then vacuum-sublimed onto a platinum plate after a low-temperature sublimation to remove decay products. About 4×10^5 alpha disintegrations per minute were collected, about 75 percent of which were from Th^{228}.

Scattering of Deuterons in Helium

T. LAURITSEN* AND T. HUUS, *Institute for Theoretical Physics, Copenhagen, Denmark*

AND

S. G. NILSSON, *University of Lund, Lund, Sweden*

(Received September 8, 1953)

The scattering of deuterons in helium gas has been investigated at three angles in the energy range 1000 to 1200 kev. A pronounced resonance appears at $E_d=1069$ kev, of width 35 kev (lab), which corresponds to the 2.187-Mev level of Li^6. It is established that the level in question has $J=3$, even parity, and a reduced width of the order of the single-particle limit. The best fit to the observations is obtained with a channel radius of 4.0×10^{-13} cm, taking into account the effect of the ground state, $J=1^+$, which is assumed to have the same reduced width. A brief search, carried out at only one angle, revealed no further levels below $E_d=2.0$ Mev.

I. INTRODUCTION

THE scattering of alpha particles by deuterons was investigated in 1935 by Pollard and Margenau,[1] who used natural alpha-particle sources, bombarding thin targets of deuterium-containing compounds and observing the forward-projected deuterons. The alpha-particle energy was varied by means of a gas cell with adjustable pressure. Above an energy of 2.0 Mev, they found strong deviations from Coulomb scattering and in the neighborhood of 2.6 Mev, a pronounced anomaly, nearly 1 Mev broad, which they attributed to a resonance. There was also some indication of a maximum near 5 Mev. Assuming the resonance energy to be $E_\alpha=2.6$ Mev, these measurements would indicate a level of Li^6 at 2.3 Mev above the ground state. Later observations by Mohr and Pringle[2] indicated a rise in cross section in the neighborhood of 2-Mev alpha-particle energy but did not confirm the resonance. Subsequently, very careful measurements have been made of the scattering of deuterons in helium gas as a function of angle at a number of energies.[3,4] These measurements straddled the energy at which the resonance might have been expected ($E_d\simeq\frac{1}{2}E_\alpha=1.3$ Mev) and gave no indication of its existence. In the meantime, the Li^6 level in question has been well established in several other reactions, among these in connection with an alpha-particle group[5] from $Be^9(p,\alpha)Li^6$ (Fig. 1). In this measurement, carried out with a precision electrostatic analyzer, the level could be located at 2.187 ±0.008 Mev; the width was reported to be less than 8 kev. From this information and the known masses involved, it would appear that the resonance in the scattering process should lie at $E_d=1.065\pm0.040$ Mev, or $E_\alpha=2.13$ Mev.

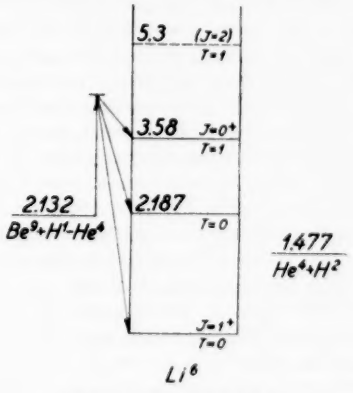

FIG. 1. Energy levels of Li^6.

No little interest attaches to this, the first excited level of Li^6, since the theory makes a rather definite prediction as to its character.[6] For a system with only two particles in the p shell, one expects levels of $J=1^+$ and 3^+, with isotopic spin $T=0$, to lie fairly low, in either $L-S$ or $j-j$ coupling. In pure $j-j$ coupling, the $(p_{\frac{1}{2}}, p_{\frac{1}{2}})$ configuration leads to states of $J=3^+$, 0^+, 1^+, and 2^+, with $T=0$, 1, 0, and 1, in order of increasing energy, while in $L-S$ coupling, the low states are $^3S_1$, $^3D_{3,2,1}$ with $T=0$, and $^1S_0$, $T=1$. Even a slight admixture of $j-j$ coupling in the latter case will separate the components of the D-triplet and tend to lower the $J=3$ member. The ground state of Li^6 has $J=1$, $T=0$, and the magnitude of the magnetic moment suggests that the character $^3S_1$ predominates for this state. The 3.58-Mev state[7] appears to have $J=0$ or $T=1$ or both, and from the mass of He^6 it is reasonably safe to conclude that this is the first $T=1$ level. A level at about 5.3 Mev, also with $T=1$ and, possibly $J=2^+$ is suggested by analogy with the first excited state of He^6. It would seem, then, that the 2.187-Mev level has $T=0$, and probably $J=3^+$. Because of the circumstance

* Fulbright Lecturer (1952–1953), on leave from California Institute of Technology, Pasadena, California.

[1] E. Pollard and H. Margenau, Phys. Rev. **47**, 833 (1935).

[2] C. B. O. Mohr and G. B. Pringle, Proc. Roy. Soc. (London) **A160**, 190 (1937).

[3] N. P. Heydenburg and R. B. Roberts, Phys. Rev. **56**, 1092 (1939).

[4] Blair, Freier, Lampi, and Sleator, Phys. Rev. **75**, 1678 (1949).

[5] Browne, Williamson, Craig, and Donahue, Phys. Rev. **83**, 179 (1951).

[6] D. R. Inglis, Phys. Rev. **87**, 915 (1952); Revs. Modern Phys. **25**, 390 (1953).

[7] R. B. Day and R. L. Walker, Phys. Rev. **85**, 582 (1952).

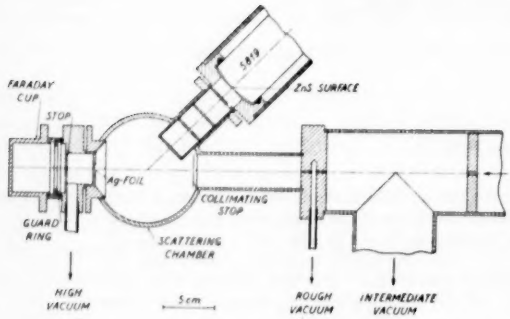

FIG. 2. Schematic diagram of the scattering chamber and differential pumping system.

that the level is unbound with respect to He^4+D^2, the scattering of deuterons in helium should provide a particularly favorable opportunity for a direct determination of the angular momentum and parity, and it was with this objective that the present experiments were undertaken. It was also hoped that a systematic search in the immediately higher excitation region might shed some light on the location of the two other D states, which would be expected if $L-S$ coupling obtains for this nucleus.

II. EXPERIMENTAL PROCEDURE

Since the resonance was expected to be only a few kev wide, a gas target at relatively low pressure, separated from the accelerator by a differential pumping system, was used. The experimental arrangement is shown in Fig. 2. Deuterons from the 2-Mev electrostatic accelerator of this Institute[8] were analyzed by a 7.5° magnetic deflection. The beam then passed through a 3-mm hole into the intermediate chamber, which was held at $\sim 10^{-4}$ mm Hg by a 3-in. diffusion pump. A 1.0-mm diameter channel 10 mm long separated this chamber from the rough-pump vacuum of $\sim 5\times 10^{-2}$ mm Hg, which was further separated from the scattering chamber, at 1- to 10-mm pressure, by an 0.8-mm diameter channel, 10 mm long. After passing through the scattering chamber, the beam entered the Faraday cage through a 7-mm hole which was covered by an 0.9-mg/cm² Ag foil. The Faraday cage was maintained at high vacuum by a direct connection to the accelerating tube.

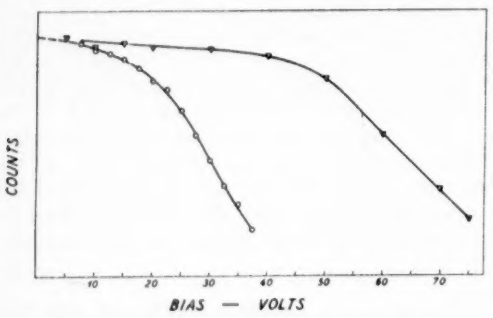

FIG. 3. Typical integral bias curves, obtained with monoenergetic protons. The upper curve refers to 260-kev protons; the lower, to 140-kev protons.

[8] Brostrom, Huus, and Tangen, Phys. Rev. **71**, 661 (1947).

An auxiliary stop, 1.2 mm in diameter, located 5 cm above the center of the scattering chamber was used in the work at low bombarding energy to reduce the effect of compound scattering in the gas and to insure that all the current actually passed through the 7-mm aperture of the Faraday cage. Rough computations, verified by direct observation of the beam, indicated that this requirement was amply met under the conditions of the present experiments. The limiting stops and guard ring of the Faraday cage were designed to accept particles diverging from the foil by angles up to 20° and should therefore have accepted more than 99 percent of protons or deuterons of 500 kev.

The scattering volume and angle were defined by two rectangular apertures $l=10$ mm high (perpendicular to the plane of the incident beam and the axis of the collector slits) and of width $2b=0.27$ and $2a=0.52$ cm, respectively. They were separated by a distance $h=7.5$ cm and the rear-most was $R=10.3$ cm from the intersection of the axis with the beam. It can readily be shown that the product (solid angle×target thickness) is given by $\int\Omega dx=4alb/(Rh\sin\theta)$, where θ is the angle of scattering, and that the effective target thickness is $2bR/(h\sin\theta)$. In the present case, for $\theta=135°$, $\int\Omega dx$ was 2.99×10^{-3} steradian cm (laboratory coordinates), and the target thickness was 0.54 cm, corresponding to an energy loss at 1.0 Mev of 0.07 kev per mm of He pressure. The angular resolution was 4.2° (lab) full width at half maximum. Three ports were available, making angles of 135.8°, 90.0°, and 63.8° with the direction of the beam.

TABLE I. Comparison of check determinations with previously published values.

	$d\sigma/d\Omega$ (barn/sterad) Standard	Present experiment
$O^{16}(p,p)O^{16}$, $E_p=0.6$ Mev, $\theta_{cm}=90°$	0.97[a]	1.00 ±0.06
$He^4(p,p)He^4$, $E_p=0.96$ Mev, $\theta_{cm}=77°$	0.112[b]	0.104±0.005
$He^4(d,d)He^4$, $E_d=1.96$ Mev, $\theta_{cm}=156°$	0.109[c]	0.11 ±0.01

[a] Rutherford cross section plus 5 percent, as estimated from curves of F. Eppling, kindly communicated by Professor H. T. Richards. See also W. Wenzel and W. Whaling, Phys. Rev. **87**, 499 (1952).
[b] Interpolated from data of Freier, Lampi, Sleator, and Williams, Phys. Rev. **75**, 1345 (1949).
[c] Interpolated from data of reference 4.

Detection of the scattered particles was accomplished by means of a thin layer of activated zinc sulfide on the end of a 5819 photomultiplier tube. Direct light from the deuteron beam was excluded by a layer of Au foil 0.2 mg/cm² thick laid directly on the ZnS surface. Residual light effects due to incomplete opacity of the

gold foil could be measured by interposing a quartz window in the path of the scattered particles.

The matter of obtaining easily interpretable bias curves occasioned some difficulty. At the back angle, where high amplification was necessary, the curve rose rapidly for low bias settings, presumably because of small pulses from electron trapping effects. It was found that the largest ratio of "true" to "spurious" pulse size, i.e., the most satisfactory plateau, was obtained with a not quite opaque layer of ZnS, corresponding to an efficiency of about 80 percent. At the forward angle, recoil alpha particles interfered to some extent. Rather than cut the alpha particles out with absorbers, which would have increased the straggling of the deuterons, we preferred to use a set of "normal curves," for matching to the curves obtained in the scattering experiment. The normal curves, of which two examples are shown in Fig. 3, were obtained with both protons and deuterons, scattered from a copper target

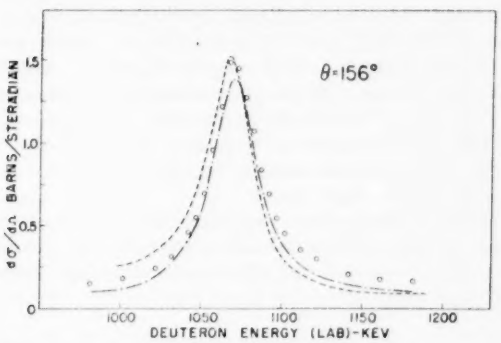

FIG. 4. Differential scattering cross section for deuterons in helium, $\theta_{cm}=156°$. Experimental points are indicated by the open circles. The dot-dashed curve is calculated for one resonance, $J=3^+$, $l=2$ with channel radius $R=4.02\times10^{-13}$ cm, whereas the dashed curve is calculated for $R=6.55\times10^{-13}$ cm.

and monochromatized with a magnetic spectrometer. The absolute efficiency was measured at a proton energy of 1.0 Mev by comparison with a proportional counter, and the relative efficiency was checked at various energies by measuring the Rutherford scattering in copper in the same instrument. The efficiency at 1.0 Mev was found to be 0.78 ± 0.03; down to the lowest energy investigated, $\sim$140 kev, it was constant within the experimental error of about 10 percent.

As a check both on the efficiency determination and on other quantities entering into the final measurement, the scattering cross sections for protons in oxygen and for protons and deuterons in helium were measured at points for which values have been given in the literature. The results, exhibited in Table I, indicate a mean deviation of the present measurements from the assumed standards of less than 5 percent.

The helium used was certified by the supplier to be 99.9 percent pure; it was further purified by prolonged

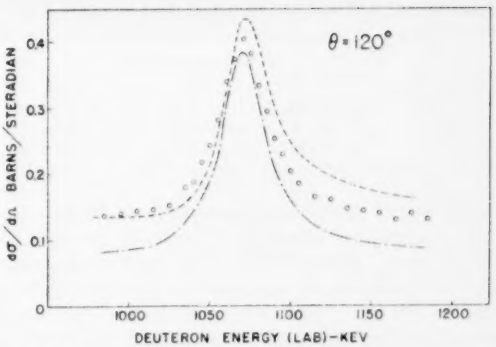

FIG. 5. Differential cross section at $\theta_{cm}=120°$. Open circles are experimental points. The dot-dashed curve is calculated for one resonance, $J=3^+$, $l=2$ with $R=4.02\times10^{-13}$ cm; the dashed curve is calculated for $R=6.55\times10^{-13}$ cm.

storage in contact with liquid-air-cooled charcoal. A similar trap directly connected to the scattering chamber prevented contamination from incidental gas sources. The oxygen was also certified to be 99.9 percent pure: it was freed of any possible condensibles by contact with a liquid-air trap.

III. RESULTS

The observed differential scattering cross section as a function of bombarding energy for three angles is exhibited by the open circles in Figs. 4, 5, and 6. It is immediately apparent that a strong resonance exists, as expected, in the neighborhood of 1070 kev bombarding energy. At the two back angles, θ (center of mass) $=156°$ and $120°$, the maximum cross section occurs at 1069 ± 2 kev and the width at half-maximum is about 35 kev. For the 90° observations (Fig. 6) the resonance is characterized by a minimum, occurring at 1075 kev. A survey run at the 156° angle, taken with 20-kev intervals, revealed no further structure at higher energies. Above the resonance, the cross section falls off to 0.11 barn/steradian at about 1300 kev and remains within 10 percent of this value to 2.0 Mev.

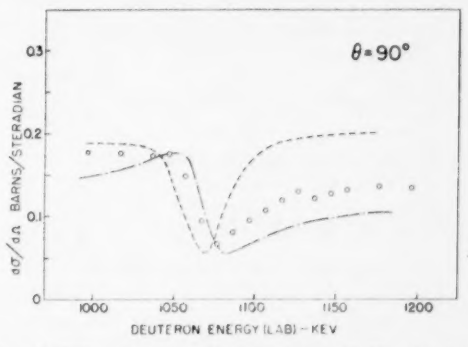

FIG. 6. Differential cross section at $\theta_{cm}=90°$. The dot-dashed curve is calculated for one resonance, $J=3^+$, $l=2$, with $R=4.02\times10^{-13}$ cm; the dashed curve is the same, with $R=6.55\times10^{-13}$ cm.

TABLE II. Absolute cross-section determinations, $He^4(d,d)He^4$.

E_d(lab) kev	$d\sigma/d\Omega$ (barns/steradian) 1000	1069	1200
$\theta_{cm}=156°$	0.15±0.03	1.49 ±0.08	0.16±0.03
$\theta_{cm}=120°$	0.14±0.01	0.40 ±0.03	0.14±0.01
$\theta_{cm}=90°$	0.18±0.02	0.062±0.006	0.14±0.02

A number of separate runs was made at the peak and in the wings of the resonance to establish the absolute cross sections. These observations were made under varying conditions of gas pressure and geometry in order to eliminate as far as possible any systematic errors. The weighted mean values so obtained are given in Table II together with the probable errors, estimated from the reproducibility of individual points and from the uncertainty in the absolute efficiency of the detector at 1 Mev. The values at maximum have been used to normalize the cross-section scale for the experimental points in the figures.

IV. DISCUSSION

The scattering formula for particles of spin 1 impinging on a spin zero nucleus can be written, in the one-level approximation:[9]

$$
\begin{aligned}
&d\sigma/d\Omega \\
&=\tfrac{2}{3}\lambda^2\big|A_e+\sum_l\{\tfrac{1}{2}(l+2)\exp(i\delta_{l,l+1}+i\psi_l)\sin\delta_{l,l+1} \\
&+\tfrac{1}{2}(2l+1)\exp(i\delta_{l,l}+i\psi_l)\sin\delta_{l,l} \\
&+\tfrac{1}{2}(l-1)\exp(i\delta_{l,l-1}+i\psi_l)\sin\delta_{l,l-1}\}P_l(\cos\theta)\big|^2 \\
&+\tfrac{1}{3}\lambda^2\big|A_e+\sum_l\{(l+1)\exp(i\delta_{l,l+1}+i\psi_l)\sin\delta_{l,l+1} \\
&+l\exp(i\delta_{l,l-1}+i\psi_l)\sin\delta_{l,l-1}\}P_l(\cos\theta)\big|^2 \\
&+\tfrac{2}{3}\lambda^2\Big|\sum_l\frac{1}{\sqrt{2}l(l+1)}\{l(l+2)\exp(i\delta_{l,l+1}+i\psi_l)\sin\delta_{l,l+1} \\
&-(2l+1)\exp(i\delta_{l,l}+i\psi_l)\sin\delta_{l,l} \\
&-(l^2-1)\exp(i\delta_{l,l-1}+i\psi_l)\sin\delta_{l,l-1}\}\sin\theta\frac{dP_l(\cos\theta)}{d\cos\theta}\Big|^2 \\
&+\tfrac{2}{3}\lambda^2\Big|\sum_l\frac{1}{\sqrt{2}l(l+1)}\{l(l+1)\exp(i\delta_{l,l+1}+i\psi_l)\sin\delta_{l,l+1} \\
&-l(l+1)\exp(i\delta_{l,l-1}+i\psi_l)\sin\delta_{l,l-1}\}\sin\theta\frac{dP_l(\cos\theta)}{d\cos\theta}\Big|^2 \\
&+\tfrac{2}{3}\lambda^2\Big|\sum_l\frac{1}{2l(l+1)}\{l\exp(i\delta_{l,l+1}+i\psi_l)\sin\delta_{l,l+1} \\
&-(2l+1)\exp(i\delta_{l,l}+i\psi_l)\sin\delta_{l,l} \\
&+(l+1)\exp(i\delta_{l,l-1}+i\psi_l)\sin\delta_{l,l-1}\}\sin^2\theta\frac{d^2P_l(\cos\theta)}{(d\cos\theta)^2}\Big|^2,
\end{aligned}
$$

where

$$A_e=-\tfrac{1}{2}\eta\csc^2(\theta/2)\exp(i\eta\ln\csc^2\theta/2);\quad \eta=e^2Z_1Z_2/\hbar v;$$

$$\exp(i\psi_l)=\frac{(1+i\eta)\cdots(l+i\eta)}{(1-i\eta)\cdots(l-i\eta)};\quad \psi_0=0;$$

$$\delta_{l,J}=\phi_l+\beta_{l,J};\quad \tan\phi_l=-(F_l/G_l)_R;$$

$$\tan\beta_{l,J}=\tfrac{1}{2}\Gamma_\lambda/(E_\lambda+\Delta_\lambda-E);$$

$$\Gamma_\lambda=2kR\gamma_\lambda/(F_l^2+G_l^2)_R;$$

$$\Delta_\lambda=-\gamma_\lambda\left[\frac{d\ln(F_l^2+G_l^2)^{\frac{1}{2}}}{d\ln kr}+l\right]_R.$$

The first two terms represent the part of the scattering in which the z component of the channel spin, m_s, is unchanged: these parts are individually coherent with the Coulomb scattering, represented by A_e. The third and fourth terms arise from the incoherent scattering with $\Delta m_s=\pm1$, while the last comes from the case $\Delta m_s=\pm2$. It is assumed that no change occurs in l, the orbital angular momentum. The adjustable parameters are the $\beta_{l,J}$, containing E_λ, Δ_λ, and Γ_λ, and R, the channel radius. As has been pointed out by Jackson and Galonsky,[10] the E_λ and Γ_λ exert their main influence in the neighborhood of the resonance, while the choice of R is essentially determined by the off-resonance behavior of the cross section.

To a sufficiently good approximation for the present case, we may expand the quantity $\Delta(E)$ as a linear function of energy[11] and rewrite the argument of the resonant term as

$$\tan\beta_{l,J}=\frac{\tfrac{1}{2}\Gamma'}{E_{res}-E}$$

where

$$\Gamma'=\frac{\Gamma}{1+\gamma b}\quad\text{and}\quad b=\left[\frac{d}{dE}\left(\frac{d\ln(F^2+G^2)^{\frac{1}{2}}}{d\ln kr}\right)\right]_{R,E_{res}}.$$

For a preliminary determination of the resonance parameters, one may use the observations at the two

TABLE III. Comparison of calculated and observed maximum cross sections for various assumed values of l and J. The calculations are based on a radius $R=4.02\times10^{-13}$ cm and include contributions from only one resonance, with no change in l, plus nonresonant scattering for all waves.

l	J,π	$d\sigma/d\Omega_{max}$ (barns/sterad) $\theta_{cm}=156°$	$\theta_{cm}=120°$
0	1^+	0.26	0.24
1	0^-	0.07	0.12
1	1^-	0.17	0.17
1	2^-	0.28	0.22
2	1^+	0.72	0.42
2	2^+	0.92	0.25
2	3^+	1.39	0.38
Observed values:		1.49	0.40

[9] We are much indebted to Mr. Kurt Alder for producing this formula for us. The present form differs from that of J. M. Blatt and L. C. Biedenharn, Revs. Modern Phys. **24**, 258 (1952), in that the scattering matrix is assumed diagonal in l; a discussion of this assumption follows in a later section.

[10] H. L. Jackson and A. I. Galonsky, Phys. Rev. **89**, 370 (1952).

[11] R. G. Thomas, Phys. Rev. **81**, 148 (1951).

back angles since here the cross-section curves are fairly symmetrical and show no pronounced distortion from interference effects. Using the observed half-width, one can estimate $\Gamma'(E=E_{res})=23$ kev (c.m.s.). One finds, then, with a channel radius $R=4.02\times10^{-13}$ cm (i.e., $1.41\times(2^{\frac{1}{2}}+4^{\frac{1}{2}})\times10^{-13}$ cm), values of $\gamma_2=1.25$ Mev and $\gamma_3=30$ Mev for the reduced widths corresponding to the assumptions of resonance formation by d and f waves, respectively. Since the Wigner limit for scattering of a single particle in a potential well is $\gamma_{SP}\sim\hbar^2/MR^2=2$ Mev, it would appear that $l>2$ are excluded.[12]

Having, at least tentatively, narrowed the field to s, p, and d waves, we proceed to compare the absolute cross sections observed with those calculated from the scattering formula, assuming that only one level contributes to the resonance but taking into account the effects of Coulomb and potential scattering from all waves. These values are exhibited in Table III. It is evident that only $l=2$, $J=3^+$ gives a reasonable account of the observations although with rather generous stretching of the experimental errors and with due regard to the uncertainties in the assumptions underlying the calculation, $l=2$, $J=2^+$ might be regarded as a possibility. This choice is, however, ruled out by the observation at $\theta_{cm}=90°$, where the calculation shows that the cross section should have a pronounced maximum for $J=2^+$ (shown by the dot-dashed curve of Fig. 9), whereas the curve for $J=3^+$ should have a minimum at this angle. The trend of the experimental points clearly excludes the former.

With the values of l and J thus established, one proceeds to attempt a more detailed fit to the cross-section data. The results of the first calculations, using $R=4.0\times10^{-13}$ cm and resonance parameters $E_{res}=1069$ kev, $\gamma=1.25$ Mev, are shown in the dot-dashed curves of Figs. 4, 5, and 6. It is evident that the agreement with the experimental points leaves much to be desired, particularly as regards the off-resonance cross section. The results of calculations with a somewhat larger channel radius, $R=6.55\times10^{-13}$ cm, in which the usual "radius" of the deuteron is used, are shown by the dashed curves of the same figures. Again, the fit to the experimental points is unsatisfactory. It may be observed that in the 156° data (Fig. 4) the larger radius actually moves the curve in the wrong direction at the high-energy end.

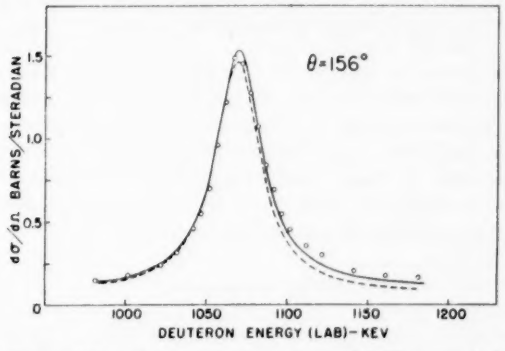

FIG. 7. Differential cross section at $\theta_{cm}=156°$. The open circles are the same experimental points as those shown in Fig. 4. The dashed curve is calculated for one resonance, $J=3^+$, $l=2$, with a channel radius $R=5.0\times10^{-13}$ cm, whereas the solid curve is calculated for $R=4.02\times10^{-13}$ cm and includes the effect of the ground state.

[12] The application of single-particle models to so loosely-bound a structure as the deuteron in the calculation of the scattering formula and in the interpretation of the reduced width must be regarded as a dubious procedure. The solution of the three-body problem appears, however, to present a number of difficulties, and the fact that a reasonably good fit to the data is obtained with the present treatment may justify the use of this simple picture here. At higher energies, where dissociation of the deuteron is possible, a rather different formalism may be necessary.

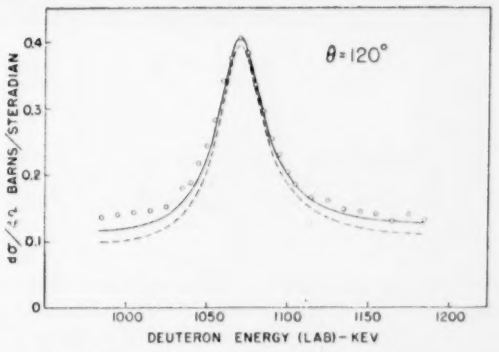

FIG. 8. Differential cross section at $\theta_{cm}=120°$. Open circles are experimental points, repeated from Fig. 5. The dashed curve is calculated for one resonance, $J=3^+$, $l=2$, with $R=5.0\times10^{-13}$ cm, whereas the solid curve is calculated for $R=4.02\times10^{-13}$ cm and includes the effect of the ground state.

The best fit which can be obtained with the assumption of a single level is given by a radius of 5.0 to 5.4 $\times10^{-13}$ cm. Calculated cross sections for a radius of 5.0×10^{-13} cm are shown in the dashed curves of Figs. 7, 8, and 9. At 90° (Fig. 9) the agreement with the experimental points is well within the estimated errors; at 120° (Fig. 8) the background both below and above resonance is low by 25 to 30 percent, or about twice the estimated error, and at 156° (Fig. 7) the background at the high end is low, again by about twice the estimated error. An increase of radius to 5.2×10^{-13} cm would improve the fit in the 120° case and would probably still be acceptable for the 90° data but would increase the discrepancy in the 156° curve.

Somewhat better agreement with the experimental data can be obtained by taking into account the effect of the ground state. The ground state of Li^6 has $J=1^+$ and can be formed by s-wave deuterons. Since it is evidently a fairly isolated state, it appears not unreasonable to assume that it has a large reduced width, and we have taken the width to be the same as for the $J=3^+$ state, $\gamma=1.25$ Mev. The characteristic energy, E_c, defined as the energy at which $f_0\equiv(Ru_0'/u_0)_R=0$ is estimated with the help of a simple square-well model, utilizing the fact that there exists a bound state with

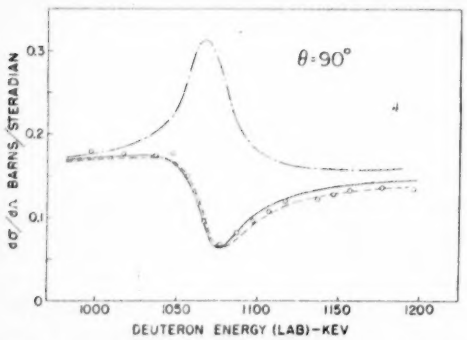

FIG. 9. Differential cross section at $\theta_{cm}=90°$. The open circles are repeated from Fig. 6. The upper (dot-dashed) curve is for $J=2^+$, $l=2$, whereas the lower is calculated for $J=3^+$, $l=2$ with $R=5.0\times10^{-13}$ cm. The solid curve is calculated for $R=4.02\times10^{-13}$ cm and includes the effect of the ground state.

$J=1^+$ at 1.477 Mev (cm) below the deuteron-alpha separation energy. It is found that $E_s=-2.9\frac{1}{4}$ Mev. With these parameters, and with the smaller channel radius, $R=4.0\times10^{-13}$ cm, one obtains the solid curves of Figs. 7, 8, and 9, which are seen to fit the experimental points well within the estimated uncertainties. The quality of the fit is, of course, rather sensitive to the choice of radius, and it is clear that the ground-state reduced width is only roughly determined by the present results. In fact, as has been shown above, the fit with the radius 5.0×10^{-13} cm, ignoring the ground state entirely, is not completely unacceptable, and it cannot be established with certainty that the effect of the ground state has been demonstrated in this experiment. It may be argued, however, that the assumption of a large reduced width for the ground state is not unreasonable and that the observations are entirely consistent with such an assumption.

The resonance energy $E_{lab}=1069\pm2$ kev for the $J=3^+$ level agrees well with the value 1065 kev calculated from the Q value of Browne *et al.*,[5] considering the uncertainty of nearly 40 kev introduced by the mass table. The width $\Gamma'=23$ kev, corresponding to the value $\gamma=1.25$ Mev used in calculating the cross-section curves, does not seem to be in so satisfactory agreement with the earlier reported value. However, we are informed by Richards[13] that the width quoted referred to the alpha-particle group width, and should be multiplied by $(\partial Q/\partial E_\alpha)=2.08$ for the existing experimental conditions. This effect, together with some uncertainty as to the target thickness, allows an upper limit for the level width which is in good agreement with the present observations.

It was pointed out earlier that the scattering formula used here presupposes that the scattering matrix is diagonal in l. This assumption does not affect the non-resonant terms, and for the resonant terms the requirement of conservation of angular momentum and parity permits a change in l only for the cases $J=1^+$, 2^-, and $3^+(J\leq3)$. Here, l may change in the course of the scattering from $l=J+1$ to $J-1$ or conversely. The error introduced by ignoring these terms may be estimated by the use of Blatt and Biedenharn's formula[9] assuming the same reduced width for both values of l. It is found that the correction amounts at most to 1.5 percent for $J=3^+$, 6 percent for $J=2^-$, and 10 percent for $J=1^+(l=0)$, for the two back angles, and accordingly has no significance for the present results.

We have also attempted in a preliminary way to account for the observations at 1.96 Mev of Blair *et al.*,[4] using the parameters found in the present experiment. It appears that the present parameters lead to a much stronger dependence on angle at the back angles than is observed, and one is forced to the conclusion that at least one more state will be required to give an account of the higher-energy data.

We are deeply indebted to Professor N. Bohr for his interest in and encouragement of the present work. Mr. Kurt Alder, Mr. Aage Bohr, and Mr. Č. Zupančič have also contributed invaluable aid in both the experimental and theoretical aspects of the problem and we are grateful to Professor T. Gustafson and Dr. G. Källén for some fruitful discussions. One of us (S.G.N.) wishes to express his thanks to the Swedish Atomic Committee for financial support. Another of us (T.L.) is indebted to the U. S. Educational Foundation in Denmark and to the California Institute of Technology for financial support during his stay in Copenhagen.

[13] H. T. Richards (private communication).

Inelastic Neutron Scattering in Al, Fe, Mg, and Cu†

RICHARD E. GARRETT,* FRANK L. HEREFORD, AND BILLY W. SLOOPE‡
Department of Physics, University of Virginia, Charlottesville, Virginia
(Received August 10 1953)

Gamma rays emitted from nuclei excited by inelastic neutron scattering were observed. Pulse-height analysis of gamma-ray scintillations which were coincident with scattered neutrons established gamma lines corresponding to excited levels in the residual nuclei. Observed levels are reported for Al, Fe, Mg, and Cu.

THE determination of nuclear energy levels through the inelastic scattering of neutrons has been the subject of several recent investigations. Discrete levels excited in residual nuclei have been established from the energy distributions of either the scattered neutrons[1] or the de-excitation gamma rays.[2,3] In the case of the latter technique, the measurements were complicated by the large background of gamma radiation inherent in most methods of fast neutron production. In the experiment described here[4] the scintillation spectrum of the de-excitation gamma rays was observed in coincidence with scattered neutrons, thereby eliminating this background.

EXPERIMENTAL METHOD

Monoenergetic 3.3-Mev neutrons from $H^2(d,n)He^3$ bombarded a scatterer as shown in Fig. 1. A 1-inch cube of stilbene (shielded from the deuterium target by 1 in. of lead and about 6 in. of paraffin) detected scattered neutrons by means of recoil proton scintillations. A 1-in. diameter by 1-in. thick NaI(Tl) crystal (shielded as shown) detected gamma rays from the scatterer. Photomultiplier pulses from this detector were amplified and differentially analyzed with respect to pulse height by a sliding-channel analyzer operating in coincidence with the pulses from the stilbene crystal.

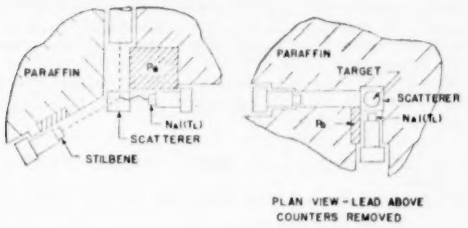

FIG. 1. Experimental arrangement. Neutrons from the target impinge upon the scatterer. The stilbene and NaI(Tl) scintillation crystals detect in coincidence scattered neutrons and de-excitation gamma rays.

The NaI(Tl) crystal was calibrated by means of the 0.51-, 0.66-, 1.28-, and (1.28+0.51)[6]-Mev peaks due to the radiations from $Na^{22}+Cs^{137}$. The curves shown and discussed below are the neutron-gamma coincidence rates (corrected for chance coincidences) *vs* gamma-ray energies (as determined from the calibration) for the indicated scatterers. A curve obtained with no scatterer showed coincidence rates which were negligible relative to those obtained with scatterers in place.

ALUMINUM

The aluminum distribution (Fig. 2) can be accounted for by levels at 0.82, 1.02, and 2.34 Mev. Photoelectric, Compton, and pair peaks fall at relative positions in good agreement with those expected from energy conservation for these three processes. The data are in good agreement with the measurements of Day[3] and with recent results on inelastic proton scattering in Al.[6]

IRON

The spectrum in this case is considerably more complex. Figure 3 shows the 0.4 to 2.2-Mev region, and

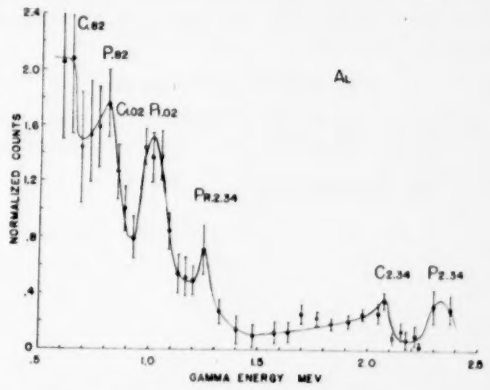

FIG. 2. The gamma-ray spectrum for an Al scatterer. In this curve and those in Figs. 3 and 4 the ordinates are coincidence counting rates normalized with respect to a BF_3-monitoring neutron counter: the abscissas are gamma-ray energies as determined from calibration of the NaI(Tl) crystal (see text).

† Supported in part by the U. S. Navy Bureau of Ordnance.
* Now at Hollins College, Hollins, Virginia.
‡ Now at Clemson Agricultural College, Clemson, South Carolina.
[1] H. F. Dunlap and R. N. Little, Phys. Rev. **60**, 693 (1941); C. E. Mandeville and C. P. Swann, Phys. Rev. **84**, 214 (1951); P. H. Stelson and W. M. Preston, Phys. Rev. **86**, 132 (1952); M. J. Poole, Phil. Mag. **43**, 1060 (1952).
[2] Grace, Beghian, Preston, and Halban, Phys. Rev. **82**, 969 (1950).
[3] R. B. Day, Phys. Rev. **89**, 908 (1953).
[4] Some preliminary results have been reported previously, Garrett, Hereford, and Sloope, Phys. Rev. **91**, 441 (1953).
[5] Jastram, Whalen, and Zinke, Rev. Sci. Instr. **23**, 648 (1952).
[6] Reilley, Allen, Arthur, Bender, Ely, and Hausman, Phys. Rev. **86**, 857 (1952).

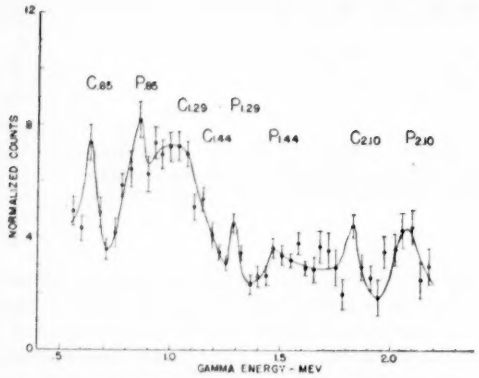

FIG. 3. The gamma ray spectrum for a Fe scatterer.

Fig. 4 shows a more detailed distribution in the 0.8- to 1.4-Mev region. In obtaining the second curve, the resolution of the scintillation spectrometer was improved and the statistical accuracy of the points increased. This curve shows a statistically doubtful peak which could be the Compton break of a 1.15-Mev gamma, the photoelectric peak of which would be obscured by the 1.44-Mev Compton distribution. Exclusive of this possible peak, others can be accounted for by levels at 0.85, 1.29, 1.44, and 2.10 Mev. The three lower levels agree with the results of Day.[3] Although he has observed a gamma line from Fe at 2.2 Mev, it was also present for other scatterers; hence, he suggests[7] that it may have originated from neutrons scattered into his NaI crystal. It is doubtful that neutron scattering in the NaI crystal could produce an appreciable coincidence rate in the experiment reported here, because of the lead and paraffin shield between the gamma and neutron detecting crystals. The fact that no level was observed in this region for Mg supports this view (see below).

MAGNESIUM AND COPPER

Among several other scatterers which were used only Mg and Cu yielded data of sufficient statistical accuracy to show well-defined gamma lines. The corresponding levels for these two elements were as follows: Mg: 1.4 Mev; Cu: 1.13, 1.53, and 2.19 Mev. The Mg level has been observed by several methods.[8] The first two levels in Cu are in fair agreement with known levels[9] in Cu^{65} determined from the beta decay of Ni^{65}. Levels in Cu at 1.1 and 2.2 Mev were reported by Grace *et al.*[2] It is doubtful that the intermediate level reported here could have been detected in their absorption measurements of the gamma-ray energy spectrum.

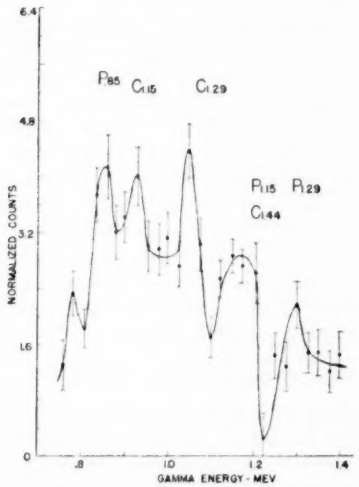

FIG. 4. The 0.8- to 1.4-Mev section of the Fe spectrum obtained with improved resolution.

Note added in proof.—In the pulse-height spectrum for Cu, the Compton break of the 1.13-Mev gamma ray was unusually pronounced and may have obscured a photoelectric peak in the vicinity of 0.9 Mev. Since preparation of this manuscript, Sherrer, Smith, Allison, and Faust [Phys. Rev. **91**, 768 (1953)] have reported a level in Cu at 0.88 Mev and a broad peak at 1.47 Mev. Their latter peak is in fair agreement with the 1.53-Mev peak (also broad) reported above.

[7] Dr. R. B. Day (private communication).

[8] D. E. Alburger and E. M. Hafner, Revs. Modern Phys. **22**, 373 (1950).

[9] K. Siegbahn and A. Ghosh, Phys. Rev. **76**, 307 (1949).

Slow Neutron Resonances in Tantalum*

R. L. CHRISTENSEN†
Brookhaven National Laboratory, Upton, New York
(Received September 3, 1953)

A crystal spectrometer has been used to investigate the total neutron cross section in tantalum in the region 0.3 to 50 ev. Resonances were detected at 4.29, 10.36, 13.9, 20.7, 24.2, 36.7, and 39.4 ev. The strengths of these resonances vary by a factor of about 35; this condition is attributed to a large variation in neutron width. The level spacing in this odd-even monoisotopic element has been estimated as 6 ev.

INTRODUCTION

THE neutron resonances of tantalum have been previously investigated in the low-energy region.[1] The results in this paper represent an attempt to approach more closely the true total cross-section spectrum between energies of 0.3 and 50 ev, using the higher resolving power of the Brookhaven crystal spectrometer.

EXPERIMENTAL METHOD

A thorough description of the spectrometer has recently been reported.[2] The samples were prepared from a number of tantalum foils obtained from the Fansteel Metallurgical Corporation. Sample purity was determined to be greater than 99.9 percent by spectrographic analysis, which precluded the possibility that any of the observed resonances might be caused by other elements. The foils were stacked to form three samples whose thicknesses were: 12.9, 2.1, and 0.09 g/cm^2. The number of nuclei per cm^2, N, was determined by weighing the foils, the areas of which were known to ± 0.1 percent. This technique yielded a value of the density of tantalum: $\rho = 16.52 \pm 0.02$ g/cm^3 (at 25°C), which is believed to be more accurate than the accepted value[3] of 16.6 g/cm^3.

RESULTS

Transmission curves were measured for each of the samples. The observed cross sections were determined from transmission values by the relationship:

$$\sigma = (1/N) \ln(1/T).$$

The resulting total cross-section curve appears as Fig. 1. The curve is a composite representation of the data from the three samples, chosen to yield best statistics. This results when T is maintained between ten and eighty percent. The probable error to be expected from statistical fluctuations is, in general, less than three percent.

From each of the resonance dips in the transmission curves, the "strength" of the resonance, $\sigma_0\Gamma^2$, was determined by area analysis.[4] In addition, the cross sections on the wings of the 4.29-ev resonance were fitted to the Breit-Wigner equation by the method of least squares. The results of this analysis indicated that the value of $\sigma_0\Gamma^2$ obtained from area analysis was too small by about one-third. This is consistent with previous results obtained with the spectrometer and may be attributed to the failure of the geometrical integration to extend far enough out on the wings of the resonance. Therefore, the values of $\sigma_0\Gamma^2$ listed in Table I are those obtained by area analysis but arbitrarily increased by one-third. Poor resolution at higher energies produces a large uncertainty in $\sigma_0\Gamma^2$ for the 36.7- and 39.4-ev resonances.

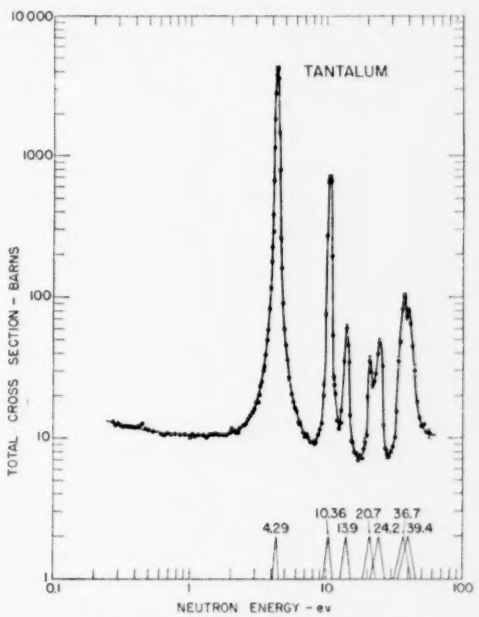

FIG. 1. The observed total neutron cross section in tantalum. The curve is derived from the transmission data of three samples of thicknesses 12.9, 2.1, and 0.09 g/cm^2. The probable error to be expected from statistical fluctuations is indicated for several representative points.

* Work carried out under contract with the U. S. Atomic Energy Commission.
† Now at Palmer Physical Laboratory, Princeton University, Princeton, New Jersey.
[1] Havens, Wu, Rainwater, and Meaker, Phys. Rev. **71**, 165 (1947).
[2] L. B. Borst and V. L. Sailor, Rev. Sci. Instr. **24**, 141 (1953).
[3] W. von Bolton, Z. Elektrochem. **11**, 45 (1905).
[4] E. Melkonian, Phys. Rev. **90**, 362 (1953).

TABLE I. Summary of total neutron cross-section resonances in tantalum. Cross sections, σ_{max}, are observed values. Level strengths, $\sigma_0\Gamma^2$, are from area analysis, increased by an arbitrary wing-fitting factor of one-third.

E(ev)	σ_{max}(barns)	$\sigma_0\Gamma^2$(barn-ev^2)	Γ_n(10^{-3} ev)	Γ_n^0(10^{-3} ev)
4.29 ±0.02	4200 ±50	59 ±5	1.9	0.9
10.36 ±0.05	710 ± 5	32 ±5	2.5	0.8
13.9 ±0.1	60 ± 3	12 ±2	1.3	0.3
20.7 ±0.2	35 ± 3	7 ±2	1.1	0.2
24.2 ±0.2	48 ± 3	27 ±5	5.0	1.0
36.7 ±0.3	100 ± 5	~250	71	11.7
39.4 ±0.5	80 ± 4	~180	54	8.6

The parameter Γ_n was determined from the relation

$$\sigma_0\Gamma^2 = 4\pi\lambda_0^2 g\Gamma_n\Gamma,$$

in which g has been set equal to 1/2. This does not lead to a significant error because $I=7/2$ for tantalum and so $g=7/16$ or $9/16$. An estimate of the total width, Γ, was made at the 4.29-ev resonance by considering the effect of instrument resolution and Doppler broadening on the transmission curve. This yielded a result $\Gamma=0.102$ ev. This value was used throughout in obtaining the tabulated values of Γ_n. Also listed is the "reduced" neutron width, Γ_n^0, defined as the width for a neutron energy of 1 ev and obtained[5] from the equation $\Gamma_n^0=\Gamma_n E^{-\frac{1}{2}}$. This parameter is useful for comparing the neutron widths of resonances at various energies. It is seen that Γ_n is considerably larger at the 36.7- and 39.4-ev resonances than elsewhere. It is usual to assume for low energies in a heavy nucleus that $\Gamma\approx\Gamma_\gamma$, i.e., that Γ_n is small. Apparently, this is not valid at these two energies. If the opposite assumption is made, i.e., $\Gamma\approx\Gamma_n$, then the measured values of $\sigma_0\Gamma^2$ yield neutron widths of 0.085 and 0.074 ev, respectively, for these resonances. That these values are not very different from the tabulated values indicates that the scattering width is at least as large as the capture width at these energies.

[5] J. M. Blatt and V. F. Weisskopf, *Theoretical Nuclear Physics* (John Wiley and Sons, Inc., New York, 1952), p. 463.

CONCLUSION

Seven resonances have been observed in the total neutron cross section of tantalum between energies of 0.3 and 50 ev. It is believed that all observed resonances belong to tantalum and that there are no other resonances of normal width within this region. The large values of the strengths of the 36.7- and 39.4-ev resonances are apparently caused by large neutron widths. From the number of resonances observed in this monoisotopic element, it is estimated that the average level spacing is 6 ev between energies of 0 and 50 ev.

The author is grateful to Dr. Vance L. Sailor and Dr. Harry H. Landon for many helpful discussions and suggestions.

Disintegration of Ca^{47}, Sc^{47}, Va^{48}, and Rh^{100}†

LUIS MARQUEZ*
Institute for Nuclear Studies, University of Chicago, Chicago, Illinois
(Received August 17, 1953)

The disintegration of four radioactive isotopes have been investigated, with the following results: Ca^{47} decays by the emission of two beta-ray groups with end-point energies and relative intensities of 685 kev, 81 percent; and 2060 kev, 19 percent. Sc^{47} decays by the emission of two beta-ray groups of end-point energies and relative intensities of 280 kev, 28 percent; and 490 kev, 72 percent. V^{48} decays by the emission of one single positron groups with end-point energy of 693 kev. Rh^{100} decays by the emission of five positron groups with end-point energies and relative intensities of 150 kev, 0.06 percent; 540 kev, 3.64 percent; 1260 kev, 12.8 percent; 2070 kev, 38.5 percent; and 2615 kev, 45.0 percent. Procedures for preparation and chemical purification of these nuclides are described; and also their other characteristics such as half-lives, conversion electrons of associated gamma rays, etc.

INTRODUCTION

THE characteristics of the yields obtained in spallation reactions when elements are irradiated with protons of a few hundred Mev show that nuclides removed from stability by several neutrons are still formed in sizeable yield.[1] This is true for both the neutron-deficient and the neutron-excess nuclides. The protons of this energy have a considerable range in matter. Since synchrocyclotrons can provide currents of protons of this energy of the order of one microampere, they are among the most suitable machines to prepare certain radioisotopes, particularly those which are far from stability.

We have used the 450-Mev synchrocyclotron at the University of Chicago to prepare several radioisotopes and to study their disintegration. The criterion in choosing the isotopes to be studied was to take those which from the available information seemed to have a large *ft* value and still could be made in sufficient yield in the synchrocyclotron.

BETA-RAY SPECTROMETER

The beta-ray spectrometer used for the experiments was the double-magnetic lens nuclear spectrometer designed by Anderson and Agnew.[2] It had also the additional helical baffle that was placed in the machine by Fan.[3] The samples were counted with an end-window Geiger counter having a mica window of 2.5-cm diameter and a thickness of 1.5 mg/cm². It had a plateau of 150 volts. All the samples were mounted on a Zapon film supported in a hard rubber frame. The thickness of the Zapon film was 0.1 mg/cm². The calibration of the spectrometer was done with the conversion line of Ba^{137m} in equilibrium with Cs^{137}. The energy of this gamma ray has been very accurately determined by Muller *et al.*[4] The line profile that this spectrometer gives has been shown by Anderson[2] and also by Bloom.[5] The resolution of the machine can be changed by varying the opening of the iris diaphragm near the detector. We carried out most of the measurements with resolutions of 5.1 percent and of 3.5 percent. We mean by resolution the full width at half-maximum of the line profile plotted as a function of current or momentum, divided by the value of the current or momentum at the maximum. In our machine the momentum of the electron being detected is proportional to the current in the coils corresponding to the maximum in the line profile.

We carried out the measurements for Ca^{47}, Sc^{47}, and V^{48} with 5.1 percent resolution and the measurements for Rh^{100} with 3.5 percent resolution.

RESULTS

The results for each isotope will be described separately. For most of the isotopes several runs were made. Some of the conditions were changed from one experiment to the other, like the length of irradiation, the weight of the target, etc. The figures quoted are then what we consider a typical run, or what is necessary to get enough activity.

The chemical procedures were derived from procedures described by Meinke[6] and from the well known books by Scott[7] and Treadwell.[8] In the description of the chemical procedures we will use terms commonly used by radiochemists, such as carriers, hold-back carriers, etc. Also, when we say 10 mg of Sc carrier is added, or some similar expression, it is understood that the Sc is dissolved and ionized and suitable precautions are taken to ensure complete exchange. In comparing our results with those of other workers, we shall refer

† This work was supported by the joint program of the U. S. Office of Naval Research and the U. S. Atomic Energy Commission.
* Now at Centro Brasileiro de Pesquisas Fisicas, Rio de Janeiro, Brazil.
[1] For a summary of spallation results see the review article by D. H. Templeton, Ann. Rev. Nuc. Sci. **2**, 93 (1953).
[2] H. L. Anderson and H. M. Agnew, Rev. Sci. Instr. **20**, 869 (1949).
[3] C. Y. Fan, Phys. Rev. **87**, 252 (1952).
[4] D. E. Muller *et al.*, Phys. Rev. **88**, 775 (1952).
[5] S. D. Bloom, Phys. Rev. **88**, 312 (1952).
[6] W. W. Meinke, University of California Radiation Laboratory Report UCRL-432, 1949 (unpublished).
[7] W. W. Scott, *Standard Methods of Chemical Analysis* (D. Van Nostrand Company, Inc., New York, 1939).
[8] F. P. Treadwell, *Analytical Chemistry* (John Wiley and Sons, New York, 1949).

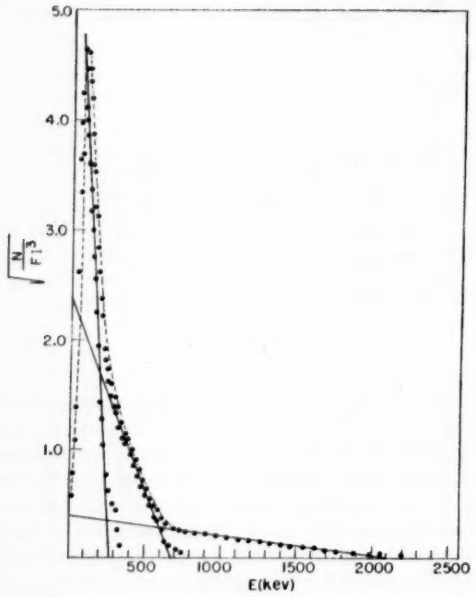

FIG. 1. The Fermi plot of the beta spectra of Ca^{45} and Ca^{47}.

only to those which appeared after the publication of the tables of Way *et al.*[9] and the table of Hollander, Perlman, and Seaborg.[10] For previous work the readers are referred to these tables.

Ca^{47}

About 10 g of $K_2Cr_2O_7$ were irradiated for two hours in the circulating beam of the synchrocyclotron at 74-inch radius, which corresponds to about 420 Mev. The $K_2Cr_2O_7$ was wrapped in an aluminum foil or placed in a thin-walled copper vial specially made for it. The $K_2Cr_2O_7$ was dissolved in hot water, one mg of Ca carrier was added, and the solution was boiled. The Ca was precipitated as $CaCO_3$ by adding NaOH and Na_2CO_3 solutions until the mixture was strongly basic. The $CaCO_3$ was centrifuged, washed with a dilute solution of Na_2CO_3, dissolved in one ml of concentrated HCl, and diluted with 20 ml of water. Hold-back carriers of the elements Ti, V, Cr, Mn, Fe, Co, Ni, and Cu were added. H_2S was passed through the solution and the sulfides were centrifuged. The excess H_2S was boiled off, the solution was oxidized with HNO_3 and the insoluble hydroxides were precipitated by adding NH_4OH until there was a slight excess and the hydroxides were centrifuged. H_2S was passed through the ammonia solution and the sulfides were centrifuged. The Ca was precipitated as $CaCO_3$ by adding an excess of NaOH and Na_2CO_3 solution and boiling; the $CaCO_3$ precipitate was washed with water, redissolved, reprecipitated, and washed with water again. Finally, a fraction of the finely divided $CaCO_3$ was transferred to a Zapon film, dried in a heat lamp, placed in the spectrometer, and measured.

The Fermi plot of the beta-spectrum obtained right after the precipitation of the $CaCO_3$ is shown in Fig. 1. As expected, the Ca^{45} activity was formed also and shows in the spectrum. The Fermi plot could be resolved into the three allowed components shown in the figure. One has an end-point energy of 685±6 kev, a relative intensity of 81 percent, and corresponds to Ca^{47}. Another has an end-point energy of 2060±20 kev, a relative intensity of 19 percent, and also corresponds to Ca^{47}. The third group is the well known beta of Ca^{45} and we find for it an end-point energy 261±4 kev, in agreement with other measurements.[9,10]

The two beta groups of Ca^{47} show allowed spectra within the limits of the experimental errors and to the extent that their overlapping will not mask it. For instance, the Fermi plot of the 2060-kev group is a straight line from about 800 kev to its end point. After subtracting the hard group, the Fermi plot of the 685-kev group shows a straight line from 320 kev to its end point. The 2060-kev group was observed to decay for several half-lives and the value obtained for its half-life was 4.3±0.2 days, which is compatible with the best value of the half-life assigned to Ca^{47} in the literature.[9,10] The group of 685-kev end point decayed and deviated from a straight line, becoming concave upward, and it was possible to resolve it into the group of 685-kev end-point energy, decaying with the half-life of Ca^{47}, and another group which was growing and corresponded to Sc^{47} and had an end-point energy of about 485±15 kev. Sc^{47} could not be studied very well in this way because of the interference of Ca^{45} and Ca^{47}, and it was investigated separately and is described in the next section.

We should mention that the conversion electrons of the 1375-kev gamma ray were not observed, probably because this gamma ray has a very small conversion coefficient and because the resolution was not good enough to detect them above the beta-spectrum. We carried out the measurement, for Ca^{47}, with a resolution of 5.1 percent.

Sc^{47}

The preparation of Sc^{47} was made by milking it from Ca^{47} in order to have it completely free from other Sc activities. Consequently, the irradiation and chemistry were the same as those described under Ca^{47}, except that the amount of Ca carrier was increased to 10 mg. After the Ca^{47} was purified, the Sc^{47} daughter was allowed to grow for about one week, 1 mg of Sc carrier was added to the solution, which was boiled, and the Sc was precipitated as the hydroxide by adding NH_4Cl and NH_4OH. The Sc was washed and dissolved in HCl, 10 mg of Ca hold-back were added, and the

[9] K. Way *et al.*, *Nuclear Data*, National Bureau of Standards Circular No. 499 (U. S. Government Printing Office, Washington, D. C., 1950).

[10] Hollander, Perlman, and Seaborg, Revs. Modern Phys. **25**, 469 (1953).

Sc was reprecipitated the same way. The Sc was washed, dissolved in HNO_3, evaporated to dryness, dissolved in a small amount of water, and a fraction of it was transferred to a Zapon film, dried, and placed in the machine for measuring. The Fermi plot of the beta spectrum of Sc^{47} is shown in Fig. 2. It can be resolved into two components having allowed shape, with end-point energies and relative intensities 280±3 kev, 28 percent; and 490±5 kev, 72 percent. There was a faint line of electrons at an energy of 218±10 kev which is the conversion electron of the gamma ray whose energy is the difference of the end-point energies of the beta rays. The conversion coefficient could not be determined with any accuracy because it is obtained by subtracting two large numbers whose difference is of the same order as the statistical error. We estimate that it is of the order of 10^{-2}. We also counted a sample of Sc^{47} with an end-window Geiger counter for more than seven half-lives to test its purity and to determine its half-life. The decay was exponential within experimental error and the half-life obtained was 3.44±0.05 days. Our results on the disintegration of Sc^{47} are in qualitative agreement, but in quantitative disagreement, with the recently reported measurements of Cheng and Pool.[11]

V^{48}

This positron emitter is known to decay to the second excited state of Ti^{48} with an energy of 690 kev. Its spectrum was investigated to see if the decay to the first excited state could be detected and also because there has been another positron group reported[12] associated with the low-intensity 2.31-Mev gamma ray.

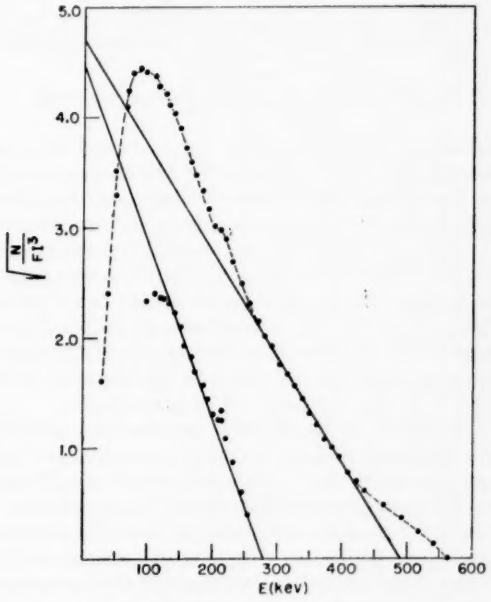

FIG. 2. The Fermi plot of the beta spectrum of Sc^{47}.

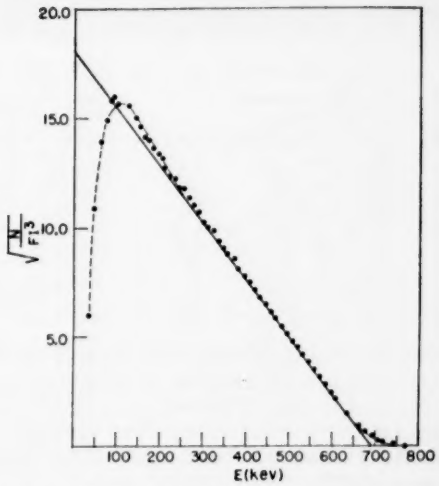

FIG. 3. The Fermi plot of the beta spectrum of V^{48}.

The activity was prepared by spallation of Cr as $K_2Cr_2O_7$ as described under Ca^{47}. The $K_2Cr_2O_7$ was dissolved in hot water, 1 mg of vanadic acid was added, the solution was boiled, 30 mg of Fe were added, and the Fe hydroxide was precipitated with ammonia and centrifuged. The hydroxide carried the vanadium; it was thoroughly washed with water, dissolved in 8*N* HCl, hold-back carriers of the elements P, S, Ca, Sc, Ti, Cr, Mn, Fe, Co, Ni, and Cu were added, and the iron was extracted in isopropyl ether. The solution was neutralized, made slightly acid with acetic acid, and the lead vanadate was precipitated by adding lead acetate. The precipitate was centrifuged, washed, and dissolved in hot HCl, diluted with water, and the lead was removed by passing H_2S. The whole procedure was repeated to get greater purity and finally the solution containing the vanadic acid was evaporated to near dryness, diluted with a few drops of water, and a fraction of that was placed in a Zapon film, dried, and placed in the machine for measurement.

The Fermi plot of the positron spectrum obtained is shown in Fig. 3. The end-point energy is 692±5 kev and the Fermi plot is straight within experimental error, and therefore the spectrum is allowed. We could not detect any other positron group; the few experimental points shown beyond the end point are due to the finite resolution of the instrument, scattering in the machine, etc. This happens in every beta spectrum. If there were a positron group of end-point energy greater than 692 kev, we could place an upper limit of its relative intensity as a function of its end-point energy under the assumption that the shape of its spectrum would be the same as the shape of the 692-kev positron.

[11] L. S. Cheng and M. L. Pool, Phys. Rev. **90**, 886 (1953).

[12] P. L. Roggenkamp *et al.*, Phys. Rev. **88**, 1262 (1952).

TABLE I. The relation between the upper limit of the relative intensity of the second positron group in V^{48}, if it exists; and its end-point energy.

End-point energy of assumed positron group (kev)	Upper limit to its relative intensity (percent)
760	1.0
780	0.6
800	0.3
820	0.2
.	.
.	.
.	.
870 or greater	0.1

The result of this calculation is shown on Table I. In the same way it was found that the transitions to the first excited state have a relative intensity of less than 0.1 percent. Our results are in excellent agreement with the results of Casson *et al.*[13] on the gamma rays following the decay of V^{48}.

Rh^{100}

This isotope was prepared by milking it from its parent Pd^{100}. Eight grams of Ag were irradiated in the circulating beam of the synchrocyclotron. The target was allowed to decay for 4 days in order to get rid of the Pd^{101}. After that the target with 10 mg of Pd was dissolved in boiling HNO_3. The solution was diluted to 500 ml and all the Ag was precipitated with HCl as AgCl. The AgCl was filtered and the Pd was precipitated as the palladium dimethylglyoxime by adding 20 ml of 1 percent alcohol solution of dimethylglyoxime and neutralizing in part the excess of acid. The precipitate was filtered, washed, and dissolved in boiling HNO_3, carriers of the elements Nb, Mo, Ru, Rh, and Cd were added, and the solution was diluted with H_2O and the Pd was precipitated again with dimethylglyoxime. The precipitate was centrifuged, washec, and dissolved again with HNO_3. The Pd was repurified by reprecipitating it with dimethylglyoxime. After dissolving it in HNO_3, 1 mg of Rh carrier was added and the solution was diluted and allowed to stand for three days. After that the Pd was precipitated with dimethylglyoxime and centrifuged, the supernatant was evaporated to dryness; the excess of dimethylglyoxime was destroyed with HNO_3. The HNO_3 was evaporated by adding 1 ml of H_2SO_4 and boiling to fumes. The solution was cooled; 20 ml of H_2O were added and the Rh was precipitated as the metal with $TiCl_3$. The Rh metal was washed with a dilute solution of H_2SO_4, then with H_2O, and then was transferred to a Zapon backing, dried in a heat lamp, and placed in the machine for measurements.

TABLE II. The end-point energy and relative intensity of the positrons from Rh^{100}.

Group	End-point energy (kev)	Relative intensity (percent)
β_1	150±30	0.06
β_2	540±25	3.64
β_3	1260±10	12.8
β_4	2070±20	38.5
β_5	2615±20	45.0

The Fermi plot of the position spectrum is shown in Fig. 4. A glance at its shape shows that it is extremely complex. We could resolve it into the five positron groups which are shown in the figure and whose properties are summarized in Table II. The relative intensity of the positrons given in the table does not take into account electron capture either to the same or to different levels.

When we started to measure the spectrum of Rh^{100} we had hoped to be able to decide whether or not the hardest beta has allowed shape; but as it turned out it could be examined only for a very narrow region, from about 2200 kev to its end-point, and probably this is not enough to make a categoric statement. If its Fermi plot is not straight, then the line shown in the figure is

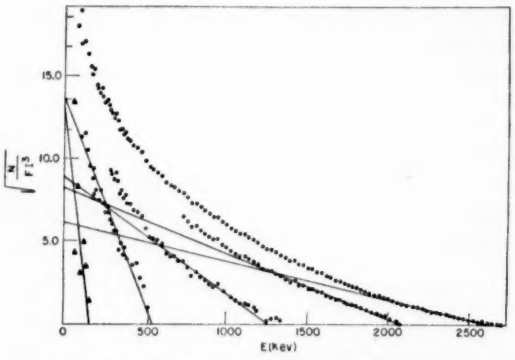

FIG. 4. The Fermi plot of the beta spectrum of Rh^{100}.

probably an average position for it. At any rate, we resolved the spectrum under the assumption that all the beta groups have allowed shape, and the three hardest beta components seem to fit the experimental spectrum quite well. The two softest betas are present in small relative intensity, and after the subtracting of the hardest groups their points scatter considerably. This is the reason for the large error in their end-point energies. We estimate that the error in their relative intensity could be as large as a factor of one-half of its value for β_1 and one-fourth of its value for β_2.

We realize that to resolve a complex beta spectrum into five components is somewhat uncertain, and perhaps one could even find another completely different set of five components fitting the data just as well.

In order to check the result of the beta-spectrum analysis, we decided to determine the energy and intensity of the conversion electrons from the gamma rays following the decay of Rh^{100}. For this prupose we prepared a very strong sample of Rh^{100} by the same technique described, but making a longer irradiation, and

[13] H. Casson *et al.*, this issue [Phys. Rev. **92**, 1517 (1953)].

we looked for the conversion electrons of the gamma rays. The spectrum obtained from the conversion electron is shown in Fig. 5. Eleven conversion lines were identified as belonging to the decay of Rh^{100} because they were observed to decay with the half-life of Rh^{100}. The only impurities observed in the electron spectrum were the K- and L-conversion lines shown at the low current of the spectrum; they decayed with 4-day half-life and probably correspond to some traces of Pd^{100} which was carried with the Rh. We found that the energy of the gamma ray originating from the decay of Pd^{100} and giving rise to these K and L electrons is 80.7 ± 0.4 kev.

The properties of the eleven conversion electrons found associated with the decay of Rh^{100} are summarized in Table III. For this run, the momentum and the current were related by the equation $\eta=5.695\times10^{-2}I$; where η is the momentum in units of mc; and I the current in the coils in amperes.

The combination of eleven gamma rays and five positron groups could be fitted into a self-consistent

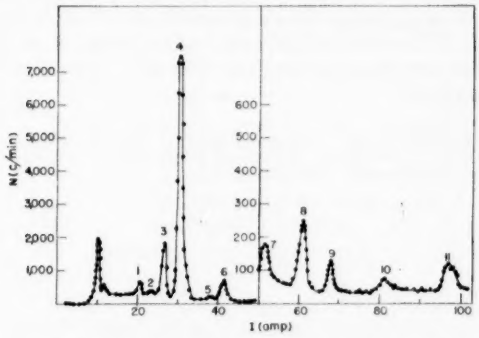

FIG. 5. The spectrum of the conversion electrons following the decay of Rh^{100}.

decay scheme on which the position of all the gamma rays and positron groups could be checked by one or more additions or subtractions applying the conservation of energy; the small residues left in these operations indicate the magnitude of the errors in the energy of the gamma rays. The only gamma ray which could not be checked this way was γ_1 which, for this reason, we placed in the top of the decay scheme, since this seemed to be the most likely place for a gamma ray with such a property.

A sample of Rh^{100} was counted with an end-window Geiger counter for ten half-lives, and we found for its half-life the value 20.8 ± 0.1 hr. In one of the runs in the spectrometer, we measured both the positron spectrum and the conversion line of the 535.3-kev gamma ray, and from the area in the plots of N/I against I we obtained the ratio of the number of electrons belonging to that gamma ray to the total number of positrons, and this was 0.062. Since the relative intensity of all the conversion electrons are given in relation to the

TABLE III. The energy and intensity of the conversion electrons of the gamma rays of Rh^{100} arising from the decay of Rh^{100}.

Current (amp)	Momentum of conversion electron (in units of mc)	Energy of conversion electron (kev)	Energy of gamma ray (kev)	Relative intensity of conversion electron ($\gamma_4=100$)	Name of gamma ray
20.70	1.1788	279.0	301.2	5.3	γ_1
23.80	1.3553	349.6	371.8	0.9	γ_2
26.75	1.5233	420.2	442.4	21.3	γ_3
30.50	1.7369	513.1	535.3	100.0	γ_4
38.50	2.1924	720.2	742.4	0.6	γ_5
41.50	2.3633	800.3	822.5	9.7	γ_6
52.0	2.9612	1085.9	1108.1	1.5	γ_7
61.0	3.4737	1336.0	1358.2	2.8	γ_8
68.1	3.8780	1535.2	1557.4	1.1	γ_9
81.4	4.6354	1911.9	1934.1	0.4	γ_{10}
97.0	5.5238	2357.1	2379.3	1.0	γ_{11}

intensity of the conversion electrons of the 535.3 gamma ray, we can relate the conversion electrons to the positron groups through the above ratio.

CONCLUSION

The disintegration characteristics of Ca^{47}, Sc^{47}, V^{48}, and Rh^{100} have been established through this work. The decay schemes of Ca^{47}, Sc^{47}, and Rh^{100} are shown in

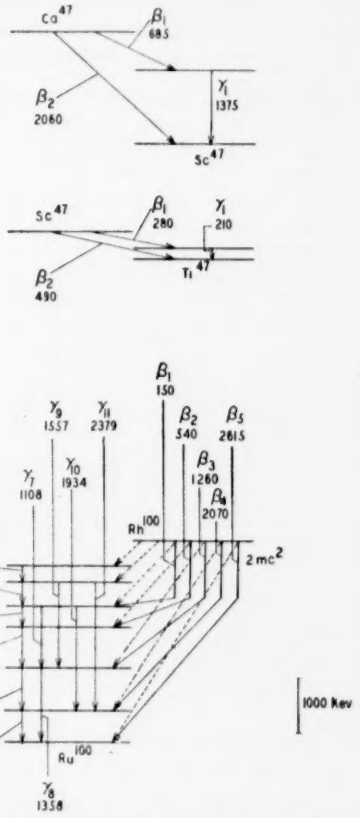

FIG. 6. The decay schemes of Ca^{47}, Sc^{47}, and Rh^{100}.

TABLE IV. The characteristics of the beta groups investigated in this work.

Isotope	Half-life	Group	End-point energy (kev)	Relative intensity (percent)	log ft
Ca^{47}	4.3 days	β_1	685	81	6.0
		β_2	2060	19	8.5
Sc^{47}	3.44 days	β_1	280	28	5.0
		β_2	490	72	5.4
V^{48}	16.0 days	β_1	692	48	6.1
		β_2	2012	0.05	11.1
Rh^{100}	20.8 hr	β_1	150	0.003	5.7
		β_2	540	0.18	6.6
		β_3	1260	0.62	7.7
		β_4	2070	1.88	8.2
		β_4	2615	2.19	8.6

Fig. 6. The relevant information for the beta decay is shown for each beta group of each isotope in Table IV. The relative intensities given in this table for positron emitters are corrected for electron capture. In order to make this correction for Rh^{100}, we assumed that γ_4 is an electric quadrupole transition (this is very likely for γ_4 according to the work of Scharff-Goldhaber[14]), and that γ_8 is either electric quadrupole or magnetic dipole. This seems to be correct from consideration of the log ft values and the competition among the gamma-ray decays; the ratio calculated from this assumption for the total number of positron emissions to the total number of electron captures is 4.9 percent and 5.0 percent, respectively; which are almost the same and in agreement with Lindner and Perlman.[15] To calculate this ratio we used the conversion coefficients of Rose *et al.*[16] As explained under the paragraph headed Rh^{100}, the spectrum of β_5 could not be explored over a region wide enough to decide definitely whether or not its Fermi plot is a straight line, although the results were compatible with a straight Fermi plot for it. The large value of logft of 8.5 for the beta decay of β_2 in Ca^{47} led us to re-examine its beta spectrum very closely and carefully. We concluded that a straight line was the best fit for the Fermi plot of its beta spectrum from 800 kev to its end-point energy; and in particular it was a much better fit than we obtained when applying the correction corresponding to the "unique" first forbidden transition.

[14] G. Scharff-Goldhaber, Phys. Rev. **90**, 587 (1953).

ACKNOWLEDGMENT

I am indebted to H. L. Anderson, who by making available to me the beta-ray spectrometer and the synchrocyclotron, made this work possible. I am also indebted to L. Kornblith, Jr., and C. A. Bordeaux and the crew of the synchrocyclotron for their help in performing the irradiations; and to H. Casson *et al.* for letting me know the results of their experiments before publication.

[15] M. Lindner and I. Perlman, Phys. Rev. **73**, 1124 (1948).

[16] Rose, Goertzel, and Perry, Oak Ridge National Laboratory Report ORNL-1023 (unpublished).

Energy Levels of Ti^{48} from the Decay of Sc^{48} and V^{48}

H. Casson, L. S. Goodman, and V. E. Krohn
Argonne National Laboratory, Lemont, Illinois

(Received August 31, 1953)

The gamma rays following the decay of Sc^{48} and V^{48} have been investigated by means of threefold coincidence techniques. In the case of Sc^{48}, it was found that within the limits of experimental error all of the decays occur via a three-gamma cascade. In V^{48}, although the decay occurs primarily via a two-gamma process, a small three gamma contribution was detected. By twofold coincidence measurements, the 2.2-Mev gamma ray of V^{48} decay was found to be in cascade with the 0.99-Mev gamma ray. Level schemes are proposed for both decays.

I. INTRODUCTION

RECENTLY the simple decay schemes which were suggested by the early work with Sc^{48} and V^{48} (both of which decay to levels in Ti^{48}) have undergone considerable modification. The previous experimental work[1–3] indicated a cascade of two gamma rays, 0.99 Mev and 1.32 Mev in each case, with a third gamma ray of low intensity observed in the V^{48} decay and believed to be the crossover (i.e., energy = 2.31 Mev). Typical pulse-height distributions, covering the region 0.3 to 1.4 Mev, are shown in Fig. 1.

In the case of the Sc^{48} decay, the first suggestion that more than two gamma rays might be involved came in 1952 from Kurath,[4] who predicted a third gamma ray of energy about 1 Mev in the cascade. Hamermesh *et al.*[5] provided experimental support for this prediction by analyzing the gamma-ray pulse-height distribution observed with a sodium-iodide scintillation spectrometer and by investigating twofold gamma-ray coincidences from a Sc^{48} source.

In the decay of V^{48}, the weak high-energy gamma ray originally thought to be the crossover for the 0.99-Mev and the 1.32-Mev gamma cascade was bracketed in energy between the thresholds for photoneutron production in deuterium and beryllium, i.e., between 1.63 and 2.23 Mev, by Fluharty and Deutsch.[6]

The work of Ticho *et al.*,[7] using a scintillation spectrometer, accurately determined the energy of this gamma ray to be 2.22 Mev and hence clearly showed that it could not be the crossover. This result was soon confirmed by other workers.[8,9] The ray described, undetected in Sc^{48} decay, has been estimated to occur in about 2 percent of the V^{48} decays.[7,8]

The Indiana group reported that they had observed coincidences between the 2.2-Mev gamma ray and annihilation radiation and, in addition, detected a weak high-energy positron by beta spectrometer measurements.[8,9] The decay schemes proposed by this group for the decay of Sc^{48} did not take into account the three-gamma cascade and involved levels whose spins and parities were difficult to reconcile with the shell model.

The present work was undertaken in an attempt to check some of the previous reports with the aim of determining more satisfactory decay schemes for these mass 48 nuclei. The results of our investigation are represented in the proposed decay scheme shown in Fig. 2.

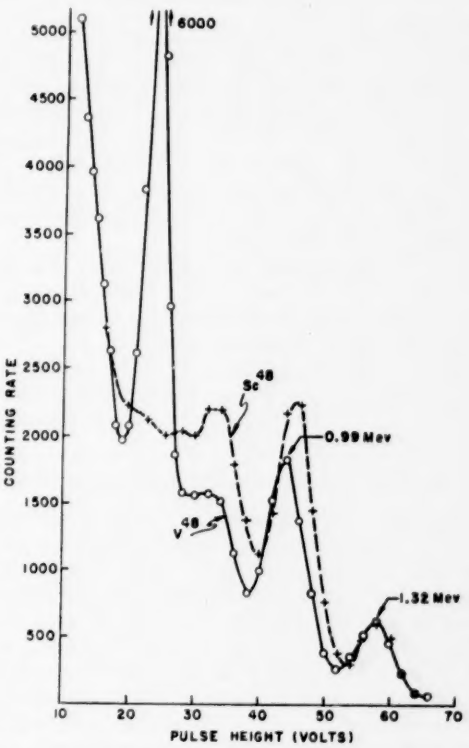

FIG. 1. Typical Sc^{48} and V^{48} gamma-ray pulse-height distributions in region 0.3–1.4 Mev. The curves have been normalized so that the 1.32-Mev photopeaks have the same height.

[1] W. C. Peacock and M. Deutsch, Phys. Rev. **69**, 306 (1946).
[2] Good, Peaslee, and Deutsch, Phys. Rev. **69**, 313 (1946).
[3] Robinson, Ter-Pogossian, and Cook, Phys. Rev. **75**, 1099 (1949).
[4] D. Kurath, Phys. Rev. **87**, 528 (1952).
[5] Hamermesh, Hummel, Goodman, and Engelkemeier, Phys. Rev. **87**, 528 (1952).
[6] R. G. Fluharty and M. Deutsch, Phys. Rev. **76**, 182 (1949).
[7] Ticho, Green, and Richardson, Phys. Rev. **86**, 422 (1952).
[8] M. M. Miller, Phys. Rev. **88**, 516 (1952).
[9] Roggenkamp, Pruett, and Wilkinson, Phys. Rev. **88**, 1262 (1952).

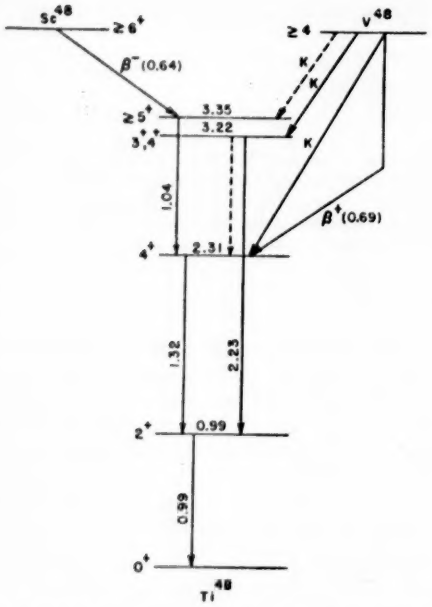

FIG. 2. Proposed decay scheme for Sc^{48} and V^{48} to levels in Ti^{48}.

II. SOURCE PREPARATION

The Sc^{48} used in this work was prepared by bombardment of Ti^{48} metal with high-energy neutrons produced in the Argonne cyclotron by bombardment of a beryllium target with 22-Mev deuterons. A few hours' bombardment supplied a sufficient amount of the desired 44-hour half-life without significant impurities. By checking the half-life and investigating the pulse-height distribution, we found the sources pure enough not to require chemical separation.

The V^{48} was produced by bombardment of a chromium-plated copper target with 22-Mev deuterons in the cyclotron. After bombardment the plating was dissolved and the V^{48} chemically separated. The V^{48} was divided into sources of various strengths, each of which was inserted in a small glass bottle whose walls were thick enough to stop the positrons without appreciably absorbing the gamma rays.

III. TRIPLE-COINCIDENCE MEASUREMENTS

The apparatus consisted of three single-crystal NaI(Tl) scintillation spectrometers employing single-channel, pulse-height analyzers whose output pulses were fed into a triple coincidence circuit. The analyzers could be operated either as differential or integral discriminators. By means of a switch, the coincidence circuit could be altered to detect twofold coincidences.

The crystals, each of diameter 1.25 in. and thickness 0.5 in. and used in conjunction with RCA-5819 photomultipliers, were mounted symmetrically with their cylindrical axes in a horizontal plane. The sources were located about 2 cm from the center of each crystal.

Since the coincidence arrangement was relatively slow (resolving time about 2 μsec) and conveniently strong sources always gave an appreciable number of accidental coincidences, the true coincidence rates were established in the following way:

The observed triple coincidence rate T can be expressed mathematically in the form $T=aS+bS^2+cS^3$. In this expression S is the singles counting rate in each detector, and a, b, and c are factors involving the detection efficiency for each gamma ray and the number of gamma rays in cascade. The term aS is associated with real triple coincidences; the term bS^2 comes from a real double coincidence combining with a third independent pulse to give an accidental triple coincidence; and the term cS^3 arises from the accidental production of a coincidence by three pulses. Since correction for the omission of the cS^3 term never exceeded a few percent for the sources used in the present work, the above relation was written in the approximate form

$$T/S=a+bS. \tag{1}$$

The triple coincidence experiments consisted of dividing the source material into sources of various convenient strengths, determining singles and coincidence counting rates for each, and plotting (T/S) *vs* S. Straight lines were observed in each case, and a non-zero intercept, a, was a measure of the occurrence of a three-gamma, or higher-order, cascade. Experiments performed with Co^{60} and Sc^{46} sources produced straight lines passing through the origin. The results for Sc^{48}, Co^{60}, and Sc^{46} are shown in Fig. 3.

The possibility that one or two pulses might occasionally feed through the electronic circuitry to produce an apparent triple-coincidence count (and hence lead to a false value for the intercept, a) was separately investigated, and a null result was obtained.

From the data taken on twofold coincidences, it was possible, in conjunction with the observed intercept, a, to estimate the number of disintegrations involving a three-gamma cascade relative to the total number of disintegrations. For Sc^{48}, a ratio of 1.05 ± 0.07 was obtained. Since beta-ray measurements on Sc^{48} decay

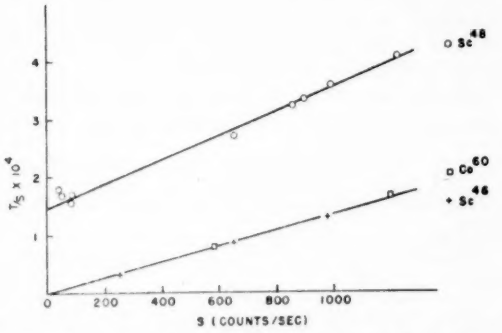

FIG. 3. Observed ratio of triples to singles counting rates as function of singles counting rate for Sc^{48}, Co^{60}, and Sc^{46}.

have detected only one branch, it seems reasonable to conclude that essentially all of the disintegrations are associated with a three-gamma cascade.

In the case of V^{48}, in which the same operating conditions were used as for Sc^{48}, it became immediately apparent from the small observed value of the intercept a, that the major mode of decay involved a two-gamma cascade.

It was found that part of this observed intercept was associated with triple coincidence pulses with one of the three component pulses produced by the combination (in one of the crystals) of an annihilation quantum and a Compton quantum escaping from one of the other crystals. An investigation of double coincidences with Na^{22} showed that this effect could be eliminated by shielding the crystals from each other with $\frac{1}{8}$ in. of lead and raising the integral discriminator bias settings to 890 kev from the previously used levels of about 720 kev.

The new bias settings reduced the detection efficiencies to the extent that a month of almost continuous counting was required in the V^{48} experiment. The stability of the equipment was checked periodically against the 890-kev photoline of a Sc^{46} source. The intercept obtained under these conditions was, as before, nonvanishing, implying the presence of a three gamma cascade. Unlike those in the Sc^{48} case, the gamma ray energies involved in the V^{48} three gamma cascade are not known unambiguously, as may be seen from the proposed decay scheme. If it is assumed that the energies are the same as the ones associated with Sc^{48} decay (i.e., involving the 3.35-, 2.31-, 0.99-, and 0.0-Mev levels of Ti^{48}), then a comparison of the V^{48} intercept with the Sc^{48} intercept gives the result that the triple cascade in V^{48} occurs in 7 ± 3 percent of the disintegrations. On the other hand, if it is assumed that the 3.22, 2.31, 0.99, and 0.0 levels are responsible for all of the threefold coincidences in V^{48}, our efficiency for detecting the cascade will be lower, and a result of 10 ± 5 percent will be obtained.

IV. POSITRON EMISSION *VS* ELECTRON CAPTURE IN V^{48}

Since 95 ± 5 percent of the decays of Na^{22} occur by positron emission[2] and all of the decays are associated with the emission of a single 1.28-Mev gamma ray, the number of positrons per 1.28-Mev gamma ray is 0.95 ± 0.05. If this number and the observed Na^{22} and V^{48} pulse-height distributions are used, an estimate can be made of the number of positrons per 1.32-Mev gamma ray in V^{48}. Comparing the annihilation and 1.28-Mev photopeaks in the one case with the annihilation and 1.32-Mev photopeaks in the other, we obtained the result 0.49 ± 0.04 positrons per 1.32-Mev gamma ray in V^{48}. An empirical correction for the variation of photopeak magnitude with energy was employed. This result is an average of the values obtained by using four different NaI(Tl) crystals: three of our standard crystals (1.25 in. in diameter and 0.5 in. thick) and one larger crystal (1.5 in. in diameter and 1.0 in. thick). It is in good agreement with the value of 0.46 ± 0.09 obtained by the same method by Sterk *et al.*[10] but only in fair agreement with the measurement of Good *et al.*[2] which gave 0.58 ± 0.04 positrons per disintegration.

V. ANALYSIS OF THE Sc^{48} GAMMA-RAY ENERGIES

By normalizing the Sc^{48} and V^{48} pulse-height distributions so that the 1.32-Mev photopeaks were of equal height and subtracting the V^{48} from the Sc^{48} distribution, Sterk *et al.*[10] determined the energy of the third gamma ray in Sc^{48} to be 1.05 Mev. By the same method we have obtained 1.04 ± 0.02 Mev.

VI. THE 2.2-MEV GAMMA RAY OF V^{48}

From V^{48} gamma-ray pulse-height distributions, we have been able to estimate the energy and relative intensity of the 2.2-Mev gamma ray, obtaining 2.23 ± 0.03 Mev for the energy and 2.3 ± 0.5 percent for the intensity relative to the 1.32-Mev gamma ray. These results are in good agreement with those obtained by others.[7,8]

The weak high-energy branch shown in the positron spectrum of the Indiana group[9] did not appear to be established with certainty but indicated an energy difference between the two branches of about 120 kev although only about 90 kev had been expected from the gamma-ray measurements. The positron spectrum has recently been reinvestigated by Marquez[11] at the University of Chicago. The high-energy branch was not visible in the positron spectra of Marquez, and an upper limit of about 1 percent was estimated for the branching ratio for an energy difference greater than 70 kev. For an energy difference of 120 kev, an upper limit of 0.3 percent was assigned. These limits are well below the 5-percent intensity estimated by the previous workers.

We have reinvestigated the pulse-height distribution in coincidence with the 2.2-Mev gamma ray using a ten-channel pulse-height analyzer[12] which was gated to register pulses in coincidences with pulses from a single-channel analyzer.

The single-channel analyzer received pulses from a NaI(Tl) crystal RCA-5819 photomultiplier tube circuit and was initially adjusted to accept gamma-ray pulses between 1.9 and 2.4 Mev in height. The ten-channel analyzer was associated with another crystal photomultiplier circuit and covered the region of pulse heights between 0.4 and 1.4 Mev. The V^{48} source was mounted a few millimeters above the ten-channel crystal and about 10 cm from the single-channel crystal in such a position that no straight line passing through the source could intersect both crystals. Studies of the singles

[10] Sterk, Wapstra, and Kropveld, Physica **19**, 135 (1953).
[11] We are indebted to Dr. L. Marquez for communicating his results in advance of publication.
[12] S. B. Burson (to be published).

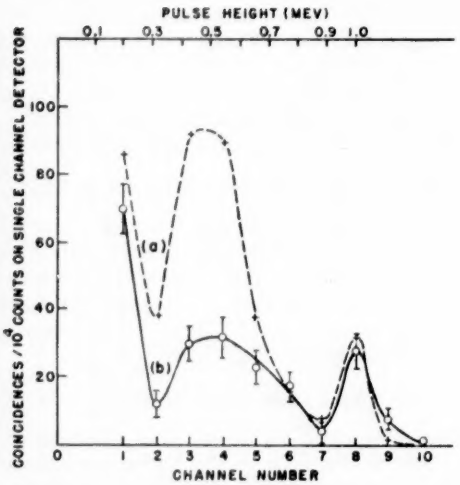

FIG. 4. Typical normalized ten-channel coincidence pulse-height distributions for V^{48} with single-channel detector counting pulses from (a) the 1.32-Mev photopeak and (b) the 2.2-Mev photopeak.

counting rate as a function of the distance between the source and the single-channel crystal indicated that about 8 percent of the counts in the 1.9–2.4 Mev window were produced by "sum-line" pulses. Since these pulses arose from the combination of pulses from the 0.99- and 1.32-Mev gamma rays, they caused the appearance of some annihilation pulses in the coincidence spectrum. Corrections were made for this effect and for accidental coincidences.

The coincidence spectra were compared with "non-coincidence" spectra and with additional coincidence spectra which had been obtained with the single-channel analyzer adjusted to count pulses from the 1.32-Mev photopeak. On normalizing the latter spectra to correspond to the same number of single-channel analyzer pulses as were obtained when the single-channel analyzer was set for the 2.2-Mev region, it was found that the 0.99-Mev photopeak was the same height in both cases within a statistical uncertainty of about 15 percent. The annihilation and 1.32-Mev photopeaks were both zero within the statistical errors in the 2.2-Mev coincidence spectrum. A typical pair of normalized distributions corrected for background, accidentals, and sum lines are plotted in Fig. 4. Three pairs of this sort were obtained in the course of the experiment. From these measurements we conclude that the 2.2-Mev gamma ray is in cascade with the 0.99-Mev gamma ray with no more than 15 percent of the 2.2-Mev gamma rays in coincidence with positrons.

The conclusion of the Indiana group[8,9] that the 2.2-Mev gamma ray is in coincidence with annihilation radiation disagrees with the present result. A calculation based on the results presented in Fig. 2 of their paper[6] indicates that the relative probability for producing a coincidence between a pulse from the annihilation channel and a 2.2-Mev gamma ray is only 20 percent of the corresponding value for a coincidence of a pulse in the annihilation channel with a 0.99-Mev gamma ray. Since it is evident that about 20 percent of the pulses in the annihilation channel were Compton pulses from the 0.99-Mev gamma ray, this part of the coincidence data of the aforementioned workers would seem to be compatible with our conclusion that the 0.99 Mev, not the annihilation radiation, is in coincidence with the 2.2-Mev gamma ray. However the null result which they obtained for 0.99–2.2 Mev coincidences is inconsistent with our result.

VII. DECAY SCHEMES

In regard to the determination of decay schemes for Sc^{48} and V^{48}, the following points, obtained from experiment, should be kept in mind: (1) Only one beta branch in Sc^{48} and one positron branch in V^{48} have been clearly established. (2) Both of these transitions are considered "allowed." (3) At least 95 percent of the disintegrations of Sc^{48} are associated with a three-gamma cascade, the gamma-ray energies being 0.99, 1.04, and 1.32 Mev, with no other gamma rays (especially the 2.2-Mev gamma ray) having been detected. (4) The decay of V^{48} is associated primarily with a two-gamma cascade, the gamma-ray energies being 0.99 and 1.32 Mev. (5) The fraction of V^{48} disintegrations which involves a three-gamma cascade is 7 ± 3 percent if the cascade starts from the 3.35 Mev level and 10 ± 5 percent if the cascade starts from the 3.22-Mev level. The present experiment does not eliminate the possibility that both of these cascades may occur. (6) About 2 percent of the V^{48} decays involve gammas of energy 2.23 Mev of which at least 85 percent are in coincidence with 0.99-Mev gamma rays. (7) Angular correlation studies[9,13] of the 0.99- and 1.32-Mev gamma rays of V^{48} give results suggesting the spin assignments 0^+, 2^+, and 4^+ for the ground and first two excited states respectively.

From the experimental evidence it is seen that the smallest number of energy levels in Ti^{48} which can account for the gamma rays observed in both the Sc^{48} and V^{48} decay is four, namely, 0.99, 2.31, 3.22, and 3.35 Mev above the Ti^{48} ground state. The V^{48} angular correlation work would then assign a spin of 2^+ to the 0.99-Mev level and 4^+ to the 2.31-Mev level. Since the Sc^{48} beta decay is allowed and goes to the 3.35-Mev level but not to the 2^+ or 4^+ levels, a lower limit of 6 is obtained for the Sc^{48} ground state and a lower limit of 5 for the 3.35-Mev level. The V^{48} decay is also allowed and goes to the 4^+ level but not the 2^+ level. Hence the V^{48} ground state must be 4^+ or 5^+. Values of 3^+ or 4^+ are assigned to the 3.22-Mev level since the transition occurs primarily to the 2^+ level and not to the ground state, 0^+. Values higher than 4^+ may be excluded since in this case transitions to the 4^+ level would be much more probable than those to the 2^+ level. (+) parities

[13] P. S. Jastram and C. E. Whittle, Phys. Rev. **87**, 1133 (1952).

are chosen for both the 3.22- and 3.35-Mev levels since shell model considerations indicate that (−) parity levels would not occur at such low energies of excitation.

We wish to thank the various members of the Laboratory, especially M. G. Mayer, D. Kurath, and B. Hamermesh, who have taken part in helpful discussions. We are indebted to S. B. Burson and W. Jordan for the use of and for assistance with their ten-channel coincidence pulse-height analyzer and to S. Wexler for performing the V^{48} chemical separations.

PHYSICAL REVIEW VOLUME 92, NUMBER 6 DECEMBER 15, 1953

Upper Limits on the Neutrino Mass from the Tritium Beta Spectrum*

DONALD R. HAMILTON, W. PARKER ALFORD,† AND LEONARD GROSS‡
Palmer Physical Laboratory, Princeton University, Princeton, New Jersey

(Received August 25, 1953)

The shape of the tritium beta spectrum near the end point has been investigated in a spherical electrostatic integral spectrograph with particular reference to the possible effects of a nonzero neutrino mass. It is shown that the source thickness of 100 micrograms/cm² may be satisfactorily taken into account in the last kilovolt of the spectrum, upon which the results are based. An upper limit to the neutrino mass of 500, 250, and 150 electron volts is found for the Dirac, Majorana, and Fermi forms, respectively, of the beta interaction.

INTRODUCTION

THE effect of a nonzero neutrino mass upon the shape of the beta spectrum is very marked within a distance of several neutrino rest masses from the end point of the spectrum,[1] and is hence best investigated with a spectrum of end point as small as possible. The present investigation uses tritium for this purpose. Since the original report on this work,[2] the results of a similar investigation by Langer and Moffat[3] have appeared; their results are in essential agreement with our mass limits, although we prefer to theirs our method of taking into account the effects of spectrograph resolution (see below). References to earlier work on tritium appear in reference 3.

The spectrograph used has been reported upon elsewhere;[4] electrons from a source at a center of hemispherical symmetry pass through a retarding field and those having more than a certain energy go to a collector thus giving an integral spectrum. The momentum resolution of 1/3 percent is an essential ingredient of the neutrino mass limits which can be set.

EFFECT OF SOURCE THICKNESS

In a spectrum of end point 18 kilovolts, source effects constitute a formidable problem which, however, diminishes if, as in the present instance, one is interested primarily in the last few kilovolts of the spectrum. It is shown in what follows that a thick source converts a differential spectrum to a simple integral spectrum near the end point, and that this process and a subsequent integration by the spectrograph do not blur the characteristic features which arise from finite neutrino mass. The source used in these measurements consisted of tritium soaked up in 100 micrograms/cm² of zirconium which in turn had been deposited on a tungsten button.[5]

We base our conclusions on the suitability of thick sources for our purpose upon two lines of evidence: the behavior of monoenergetic beams of electrons in passing through thin foils, as summarized, for example, by Klemperer;[6] and the shape of conversion lines from sources of varying thicknesses, as observed and discussed by Owen and Primakoff.[7]

As to the first line of evidence: the work of Klemperer at 7–13 kilovolts[6] and of White and Millington above 100 kilovolts[6,8] are quantitatively consistent in indicating the existence of a "universal straggling curve" for the emergent electron spectrum when monoenergetic electrons are incident upon a foil. This universal straggling curve has several noteworthy features, as follows. The energy is peaked at a value less than the incident energy by an amount ΔV proportional to the thickness of the foil; at 18 kilovolts for Al absorber and not too badly for other substances, ΔV (kilovolts) $\approx 6\times 10^3 t$ (g/cm²); the width of the peak at half maximum value is nearly equal to ΔV; the peak has a long low-energy tail, the average energy and the larger part

* This work was supported in part by the U. S. Atomic Energy Commission and The Higgins Scientific Trust Fund.
† Class of 1860 Fellow, 1949–1951.
‡ Now at Hughes Research and Development Laboratories, Culver City, California.
[1] E. Fermi, Z. Physik **88**, 161 (1934); O. Kofoed-Hansen, Phil. Mag. **42**, 1448 (1951).
[2] Hamilton, Alford, and Gross, Phys. Rev. **83**, 215 (1951).
[3] L. M. Langer and R. J. D. Moffat, Phys. Rev. **88**, 689 (1952).
[4] D. R. Hamilton and L. Gross, Rev. Sci. Instr. **21**, 912 (1950).
[5] A. B. Lillie and J. P. Conner, Rev. Sci. Instr. **22**, 210 (1951).
[6] O. Klemperer, *Einführung in die Elektronik* (Julius Springer, Berlin, 1933), especially Chap. 21.
[7] G. E. Owen and H. Primakoff, Phys. Rev. **74**, 1406 (1948); Rev. Sci. Instr. **21**, 447 (1950).
[8] P. White and G. Millington, Proc. Roy. Soc. (London) **A120**, 701 (1928).

of the half-width lying below the peak; the area under the peak is approximately constant, apparently diminishing no faster than does the most probable energy.

The above statements are based primarily on observations of electrons traveling in beams normal to the foils; but a spread of incident and emergent angles should change only the numerical value of ΔV in the above. Thus the spectrum $F(x, \epsilon)$ obtained from monochromatic electrons of energy E_1 starting at a depth x in the source and suffering an energy loss $\epsilon = E_1 - E$ in emerging will have the same general features as those just noted. We may thus write

$$F(x, \epsilon) = (x_0/x)G(x_0\epsilon/x\epsilon_0) = (x_0/x)G(y). \qquad (1)$$

Here $y \equiv x_0\epsilon/x\epsilon_0$ and ϵ_0 is the most probable energy loss for electrons coming from some arbitrary depth x_0. (The ratio ϵ_0/x_0 is significant; x_0 or ϵ_0, where they appear alone, are arbitrary normalization factors.) Since

$$\int_0^\infty F(x, \epsilon)d\epsilon = \epsilon_0 \int_0^\infty G(y)dy,$$

the right-hand integral being independent of x, it is clear that the above expression assumes no attenuation in the number of electrons coming from depth x; for $\epsilon \ll E$ this will be a fair assumption.

The spectrum, which we call $K(\epsilon)$, produced by initially monoenergetic electrons of energy E_1 coming from all depths in a source of infinite thickness, will be given by

$$K(\epsilon) = \int_0^\infty F(x, \epsilon)dx = x_0 \int_0^\infty G(y)dy/y.$$

Thus to this approximation $K(\epsilon)$ is independent of ϵ—that is,

$$K(\epsilon) = 0 \text{ for } \epsilon < 0; \quad K(\epsilon) = \text{constant for } \epsilon \gtrsim 0.$$

Of course $K(\epsilon)$ is also a function of E_1, but not to a degree relevant here.

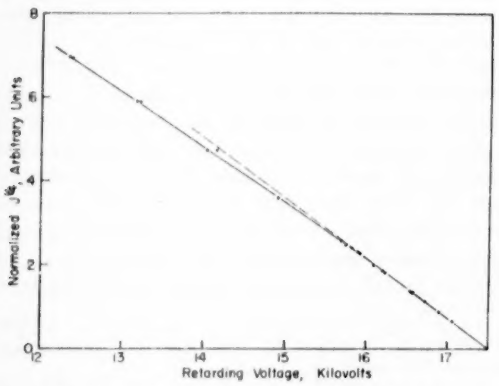

FIG. 1. Kurie-type fourth-root plot of observed collector current (as normalized for Coulomb factor and variation of electron momentum) as function of retarding voltage.

We will actually have $K(\epsilon)$ falling as ϵ increases, due to effects of electron attenuation and of noninfinite source thickness; we will expect to have $K(\epsilon) \ll K(0)$ when ϵ is of the order of the average energy loss in the source thickness (1 kilovolt for 100 micrograms/cm^2).

The feature of $K(\epsilon)$ which is most independent of approximation is the discontinuity at $\epsilon = 0$, and this is also the most relevant feature for our purposes. This behavior is borne out, for 100-microgram/cm^2 sources, by the direct observations of $K(\epsilon)$ by Owen and Primakoff[7] in measuring the shape of the conversion electron lines from sources of thickness from 40 to 840 micrograms/cm^2 for conversion lines from 50 to 500 kilovolts. For sources up to 250, but not 500, micrograms/cm^2, $K(\epsilon)$ appears in their results to be discontinuous at $\epsilon = 0$ except for the effects of spectrograph resolution; and the "width" of the lines at the base, extrapolated to 100 micrograms/cm^2 and 20 kilovolts, is about one kilovolt. As with the electron beams[6,8] discussed above, these conversion electrons were traveling normal to the source layer; as above, a spread in emergent angles should not affect the basic behavior at $\epsilon = 0$.

Electrons backscattered from the tungsten source backing produce an effect somewhat like that of an additional source thickness and will make minor modifications in $K(\epsilon)$ only for $\epsilon > 0$.

If the continuous differential beta spectrum under investigation is given, for zero neutrino mass, by $N(E_1) \sim (E_0 - E_1)^2$ (a good approximation near the end point E_0), the differential spectrum from an infinitely thick source will to the approximation that $K(\epsilon)$ is a constant for $\epsilon \gtrsim 0$ be given by

$$M(E) = \int_E^{E_0} N(E_1)K(E_1 - E)dE_1 \sim (E_0 - E)^3.$$

The spectrum observed in an integral spectrograph, that is, the collector current at retarding voltage E, will then, near the end point, be given by

$$J(E) = \int_E^{E_0} M(E)dE \sim (E_0 - E)^4. \qquad (2)$$

The spectrum $J(E)$ is referred to hereafter as the "double integral spectrum."

If $K(\epsilon)$ is replaced by a function which jumps discontinuously from zero at $\epsilon = 0$ and then falls linearly to zero at some value $\epsilon = \epsilon_1$, the error in Eq. (2) at $E_0 - E = \epsilon_1$ is only several percent. Thus, all told, for the source used in this experiment one would expect to observe a non-linearity in $J^{1/4}(E)$ at distances below the end point of the order of a kilovolt. Empirically a plot of observed $J^{1/4}(E)$ (further normalized in the manner of Kurie plots), as shown in Fig. 1 for a range 8 kilovolts below the end point, shows a fall off from a straight line beyond a point 1.5 kilovolts below the end point. On the basis of this behavior we feel justified

in interpreting the more detailed data near the end point in terms of a comparison with theoretical curves for $J^{1/4}$, which are calculated for various neutrino masses, and which are normalized to be tangent to the experimental data 1 kilovolt below the extrapolated end point. (Normalization at 1.5 kilovolts would probably have been safe and would have given smaller mass limits.)

THEORETICAL SHAPE OF DOUBLE-INTEGRAL SPECTRUM

As summarized by Langer and Moffatt,[3] various hypotheses concerning the nature of the neutrino give electron spectra which for nonzero neutrino mass differ just in the region near the end point. To an accuracy sufficient for discussion of anatomy but not for final calculation, we may neglect Coulomb effect and variation of electron momentum; the various differential spectra $N(z)$ may be represented by

$$N_0 \sim z(z^2-1)^{1/2},$$
$$N_\pm \sim (z\pm 1)(z^2-1)^{1/2},$$

where

$$z \equiv (E_0-E)/\mu c^2,$$
$$\mu \equiv \text{neutrino mass}.$$

The spectra N_0, N_+, N_- are respectively associated with the names of Majorana, Fermi, and Dirac and correspond to emission of a negatron simultaneously with emission of a Majorana neutrino (one having only positive energy states), emission of a positive-energy neutrino, and absorption of an antineutrino.

The principal features of the differential spectrum $N(z)$ and the double integral spectrum

$$J(z)=\int_0^z\int_0^z N(z)dz$$

are noted below:

$$z\gg 1, \quad N_0^{1/2}\sim J_0^{1/4}\sim z; \quad N_\pm^{1/2}\sim J_\pm^{1/4}\sim (z\pm 1/2);$$
$$z-1\ll 1, \quad N_0^{1/2}\sim N_+^{1/2}\sim (z-1)^{1/4}; \quad N_-^{1/2}\sim (z-1)^{3/4}$$
$$J_0^{1/4}\sim J_+^{1/4}\sim (z-1)^{5/8}; \quad J_-^{1/4}\sim (z-1)^{7/8}.$$

Thus Kurie-type plots of both the differential and double integral spectra (that is, plots of $N^{1/2}$ and $J^{1/4}$) have the same general features—at the end point a vertical tangent, far from the end point a straight line extrapolating to the true end point plus 1, 3/2, 1/2 neutrino masses for Majorana, Fermi, and Dirac neutrinos, respectively. It should be noted that the Dirac case (N_-) has a differential spectrum (but not $N_-^{1/2}$ or $J_-^{1/4}$ Kurie plots) with zero rather than infinite slope at the end point, hence less easily detectable mass.

But the principal conclusion from the above is that a loss of the characteristic nonzero mass behavior is not produced by going from differential to double integral spectra.

EFFECTS OF FINITE RESOLUTION

The resolution characteristic of the spectrometer is indicated in Fig. 2, which indicates the apparent differential energy distribution obtained by differentiating the integral spectrum which was observed for monoenergetic electrons. (The disappearance of the low-energy tail which appeared in the resolution characteristic of reference 4 resulted from the use, in the present resolution measurement, of a diode source which was well centered and of the same size as the tritium source.)

The problem of deducing the true beta spectrum from the observed spectrum, given the known resolution characteristics of the spectrometer, is an old one. For the purpose, procedures have been developed[7] for correcting the experimental points, the correction depending upon energy derivatives of the observed energy distribution and upon observed resolution characteristics. These procedures do not seem to be suited to the present problem, for several reasons. Thus we are interested in the region just below the end point, where the scatter of individual points is great enough to make evaluation of derivatives of the observed spectrum practically meaningless unless one wishes to prejudge the result by assuming a straight-line Kurie plot (zero neutrino mass). But what is more relevant, a correction based upon one or two observed spectrum derivatives implicitly assumes the validity of a power series expansion of the true spectrum, whereas for the finite-mass spectra N_0 and N_+ the first and higher, and for N_- the second and higher, derivatives are infinite at the true end point.

It therefore seems much preferable in the present instance to start out with a postulated spectrum $N(E)$, characterized by one of the three possible analytical forms and by a definite neutrino mass, calculate how the non-ideal resolution will distort this spectrum, and then compare the properly normalized result [say $M(E)$] with the raw experimental points.

Since it is apparent from the work of Owen and

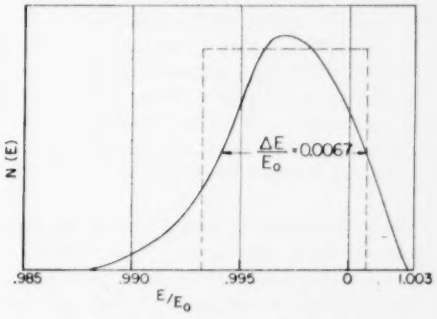

FIG. 2. Resolution characteristic of spectrograph; differential spectrum for monoenergetic electrons of energy E_0, as deduced by differentiation of observed integral spectrum. Dotted line indicates the resolution characteristic assumed for certain calculations discussed in the text.

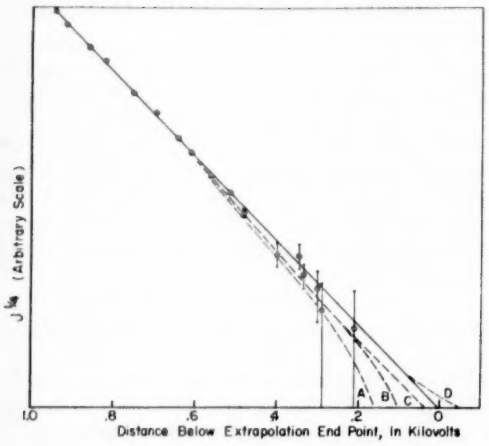

FIG. 3. Fourth root of tritium current plotted against kilovolts below end point. Dotted curves represent curves predicted on the basis of measured resolution and for various neutrino masses and interactions. Majorana, Fermi, and Dirac interactions indicated by (0) (+) (−), respectively. Neutrino mass μ in electron volts.

Curve A: $\mu=250$ (+), 350 (0).
Curve B: $\mu=150$ (+), 200 (0).
Curve C: $\mu=500$ (−).
Curve D: $\mu=0$ (0, +, −).

Primakoff[7] that the exact shape of the resolution characteristic is important, determining not only the magnitude but also the sign of the correction to be made in the usually applicable standard procedure, it appears that one needs to carry out a tedious numerical integration over the resolution characteristic, and this was done. However, in the case under consideration we are concerned primarily with the shape of $M(E)$, and not so much with displacement of $M(E)$ from $N(E)$ to higher or lower energies; for the shape of $M(E)$, the width of the resolution characteristic is the primary factor, and one may simplify things considerably by using a square characteristic of the proper width. Thus as a check, we have calculated $M(E)$ for $\mu=250$ electron volts by simple analytic procedures using a square characteristic 135 volts wide (indicated in Fig. 2 for comparison); the two methods give results indistinguishable on the scale of Fig. 3. (This latter figure shows the most relevant of the calculated double-integral spectra.) In accordance with the discussion of source thickness effects above, all these curves (as well as the experimental data, as discussed below) have been normalized to tangency with a common straight line 1 kilovolt below the end point.

For both the differential and double-integral spectra the resolution width has the effect near the end point of reversing the sign of that negative curvature of the Kurie plot which is characteristic of the nonzero neutrino mass. (This effect becomes more striking when normalization is further from the end point than in Fig. 3.) As an example, for N_- with resolution width equal to the neutrino mass and hence equal to twice the difference between true and extrapolated end points, the reversal of curvature extends for two neutrino masses from the extrapolated end point and thus destroys the most characteristic consequence of a finite mass.

In general, it would seem that one should approach with care, and with due regard to the considerations just outlined, any process of deducing upper limits to the neutrino mass which are smaller than the resolution width. (It would be more exact here to say "apparent neutrino mass," which is μ, $\mu/2$, $3\mu/2$ for the spectra N_0, N_-, N_+, respectively.) This philosophy is at variance with that of two recent neutrino-mass investigations,[3,9] in each of which the quoted upper limit on difference between true and extrapolated end point is about one-quarter of the resolution width.

EXPERIMENTAL METHOD AND RESULTS

The collector current in the spectrograph was amplified by an FP54 circuit, the output of which led to a dc photocell-galvanometer amplifier, the over-all gain of the combination being of the order of 10^{12}. The output of the second amplifier actuated an Esterline-Angus recorder. Customary procedure was to alternate ten-minute periods with the collector connected and disconnected to the amplifier inputs; in optimum operation the zero (collector disconnected) trace showed only small statistical fluctuations superimposed on a secular drift which was very constant over many hours.

Measurements made with no source in the spectrograph indicated two types of background current: a retarding voltage independent background caused by paralleling the collector resistance to ground with the FP54 grid resistor; and a strong field emission current (between the spectrograph grids) which increased slowly with voltage in a manner which could be expressed best as a quadratic increase with voltage for six kilovolts above the tritium end point, with an extrapolated zero one kilovolt below the tritium end point. At the tritium end-point voltage the strong field current was hardly perceptible. With a tritium source in the spectrograph the same strong-field current above the end point was observed, and the observed current for the last kilovolt of the spectrum was therefore corrected by subtracting the extrapolated strong field current for this region. At 300 volts below the end point the strong field current subtracted was one-third of the total, and if it had not been subtracted the points in Fig. 3 at 0.3 and 0.4 kev would have been raised by 11 and 3 percent, respectively. These amounts being small compared to the flags in the corresponding points in Fig. 3, neglect of the strong-field current would not have had a significant result.

The fourth root of the resulting current, normalized for the very small effect of the Coulomb factor and variation of electron momentum, is shown as a function

[9] G. C. Hanna and B. Pontecorvo, Phys. Rev. **75**, 983 (1949).

of voltage in Fig. 3, for the run in which the current amplifier output showed least background fluctuation. The flags on individual points represent rms fluctuations calculated from cases where the same point was repeated, and agree with rms fluctuations in recorder traces. Below 0.25 kev in the notation of Fig. 3 the fluctuations are larger than the tritium current.

The principal uncertainty in the zero neutrino mass absolute end-point value as deduced from such data as Figs. 1 and 3 arises from the uncertainty in the value of the 500-megohm resistor used for voltage measurement. This was very constant over a day's run, when corrected for the observed thermal drift due to voltage changes; but several months after the data on tritium had been taken it was discovered that the resistor possessed an instantaneous voltage coefficient, that is, a non-thermal dependence of resistance on voltage, which was an order of magnitude above the manufacturer's quoted value. (Hence the difference between the end point below and that of reference 2.) This does not give rise to any significant residual uncertainty in conclusions based on the spectrum shape near the end point; but the uncertainty in the final end-point value, 17.6 ± 0.4 kilovolts, arises primarily from the possibility of a secular drift in the voltage coefficient of the resistor.

DISCUSSION

Also shown in Fig. 3 are the $J^{1/4}$ plots predicted theoretically for various masses and interactions on the basis of the resolution characteristic of Fig. 2. As already noted, the theoretical curves are normalized to be tangent to the experimental curve one kilovolt below the end point; by choosing a point this near the end point, as seemed to be indicated by Fig. 1, the effect of any neutrino mass has unfortunately been reduced, as will be seen by the fact that the difference between true and extrapolated end points is less than that which would have resulted from extrapolation using a tangent at a greater distance below the end point.

In Fig. 3, curves *B*, *C*, *D* seem consistent with the experimental data but curve *A* seems not consistent; it therefore seems likely that the neutrino mass measured in electron volts is not greater than 500(−), 200(0), 150(+) for the Dirac, Majorana, and Fermi interactions as denoted by (−), (0), (+), respectively. The values obtained by Hanna and Pontecorvo[9] [1000(−)], and Langer and Moffat[3] [250(−)] fall in the same region and would not be increased in order of magnitude by use of the method of resolution correction which, as discussed above, we think preferable to the one which these authors used.

ACKNOWLEDGMENTS

The tritium used was obtained from the Argonne National Laboratory through the Isotopes Division of the U. S. Atomic Energy Commission. At an early stage in the experiment Dr. Dean Cowie of the Department of Terrestrial Magnetism, Carnegie Institution of Washington, was of great assistance in bombardments to make tritium; at a later stage Dr. Richard Dodson of the Brookhaven National Laboratory was of great help in connection with tritium handling and storage. One of us (D.R.H.) has benefited from the hospitality of the Institute for Advanced Study and Brookhaven National Laboratory during the period within which this work was being written up.

Nuclear Reaction Determination of the $Sn^{124}-Te^{124}$ Mass Difference*

N. S. WALL†
Laboratory for Nuclear Science and Department of Physics, Massachusetts Institute of Technology, Cambridge, Massachusetts
(Received August 7, 1953)

The Q values for the ground state (d,p) reactions on Sn^{124} and Te^{124} have been measured and found to be $Q_0=3.52\pm0.07$ Mev and $Q_0=4.25\pm0.07$ Mev, respectively. From these data and the decay energies of Sn^{125} and Sb^{125} the mass difference of $Sn^{124}-Te^{124}$ is found to be 2.4 ± 0.1 Mev.

WITH a knowledge of the neutron binding energies in Te^{125} and Sn^{125}, as well as the total decay energies of Sn^{125} and Sb^{125}, one can determine the $Sn^{124}-Te^{124}$ mass difference which is the energy available for the double beta decay of Sn^{124}. From a study of (d,p) reactions on enriched isotopes,[1] using the instrumentation available at the M.I.T. cyclotron,[2] the Q values for the appropriate reactions have been determined and hence the desired information obtained. The results of these measurements are $Q=3.52\pm0.07$ Mev for the $Sn^{124}(d,p)Sn^{125}$ reaction and $Q=4.25\pm0.07$ Mev for the $Te^{124}(d,p)Te^{125}$ reaction, yielding 5.75 Mev and 6.48 Mev, respectively, for the neutron binding energies.

Sher, Halpern, and Mann[3] have measured the (γ,n) thresholds for natural Te and obtained thresholds for two of the eight naturally occurring isotopes. On the basis that the highest odd-neutron isotope should have the lowest neutron binding energy, one can assign their 6.50 ± 0.2-Mev value to Te^{125}. Feather[4] has made this same assignment. If this is correct, the present measurement is in good agreement with the value measured in the (γ,n) experiments.

The total decay energies of Sn^{125} and Sb^{125} are 2.37 and 0.76 Mev, respectively.[5] These values, when combined with the neutron binding energies given above, yield a mass difference of 2.4 ± 0.1 Mev as the energy available for the decay of Sn^{124} by double beta decay. According to the measurements of Kalkstein and Libby[6] the minimum half-life of Sn^{124} would then be greater than 2.4×10^{17} years.

Using the negatron decay energy of Sb^{124}, 2.90 Mev,[5] one can calculate that Sb^{124} should be electron capture unstable by 0.5 Mev relative to Sn^{124}. Previous mass-spectrometer measurements of the $Sn^{124}-Te^{124}$ mass difference have given values of 1.5 ± 0.4 Mev[7] and 1.97 ± 0.13 Mev.[8] If these latter measurements are correct, then one would expect 0.9 Mev or 1.4 Mev to be available for the $Sb^{124}-Sn^{124}$ decay and it would be more probable. No electron capture or β^+ emission has been observed.[5]

* Research supported in part by the joint program of the U. S. Office of Naval Research and the U. S. Atomic Energy Commission.
† Now at Indiana University, Bloomington, Indiana.
[1] These isotopes were supplied by the Stable Isotope Division, Oak Ridge National Laboratory, Oak Ridge, Tennessee.
[2] N. S. Wall, Phys. Rev. **91**, 485 (1953).
[3] Sher, Halpern, and Mann, Phys. Rev. **84**, 387 (1951).
[4] N. Feather, Phil. Mag. Suppl. **2**, 141 (1953).
[5] Hollander, Pearlman, and Seaborg, Revs. Modern Phys. **25**, 469 (1953); M. Goldhaber and R. D. Hill, Revs. Modern Phys. **24**, 179 (1952).
[6] M. I. Kalkstein and W. F. Libby, Phys. Rev. **85**, 368 (1952).
[7] B. G. Hogg and H. E. Duckworth, Phys. Rev. **86**, 567 (1952).
[8] R. E. Halsted, Phys. Rev. **88**, 666 (1952).

Neutron Absorption and Scattering by Hafnium

L. M. BOLLINGER, S. P. HARRIS,*† C. T. HIBDON, AND C. O. MUEHLHAUSE‡
Argonne National Laboratory, Lemont, Illinois
(Received June 29, 1953)

Thermal activation, thermal absorption, resonance scattering, resonance transmission, and multiplicity of capture γ rays have been measured for the stable isotopes of hafnium. Isotopic assignments of the various resonance levels are presented which are consistent with all the data observed. Where possible, the level spacing is estimated.

INTRODUCTION

THE neutron cross-section study of a series of stable isotopes of the same atomic number provides a method for observing the changes in level density with both odd and evenness of particles and with atomic weights. A suitable example is hafnium, which has six stable isotopes: 174, 176, 177, 178, 179, and 180. One might expect to find a trend for the change of level density with mass number in the five isotopes of consecutive mass number as well as different behavior of the even-Z–even-N (176, 178, and 180) when compared with the even-Z–odd-N ones (177, 179).

The availability of hafnium isotopes from the Oak Ridge separation group[1] has made possible two investigations. The first, by Burson *et al.*,[2] covered the decay schemes resulting from neutron capture. This paper, the second, is concerned mainly with the low energy neutron cross-section behavior of hafnium. A series of preliminary experiments is first presented, and these are followed by the more definitive time-of-flight measurements.

PRELIMINARY EXPERIMENTS

A. Activation

On receipt of the enriched samples from Oak Ridge a quick search was first made for the isotope which, on thermal neutron absorption, gives rise to the 19-sec isomeric activity.[3] Known amounts of each isotope were bombarded in the pile flux of the Argonne heavy-water reactor. It was immediately obvious that Hf^{178} was the initial nucleus[4] involved in the following reactions:

$$Hf^{178}+n\rightarrow Hf^{179*}+\gamma, \quad Hf^{179*}\rightarrow Hf^{179}+\gamma.$$

"Mattauch's rule" that no metastable states of even-Z–even-N nuclei exist was obeyed. Later, however, an exception to this rule was found by Burson[2] and coworkers in their identification of the 5.6-hr hafnium activity[5] as belonging to a metastable isomer of Hf^{180}.

B. Pile Oscillator Absorption

Insufficient amounts of the enriched isotopes of hafnium were available for determining thermal-absorption cross sections <20 barns. However, since the thermal-absorption cross section of normal hafnium[6] is $\sim$105 barns, one would expect to be able to identify one or more strongly absorbing isotopes by the pile oscillator technique.[7]

Known amounts of normal and 150 mg each of enriched hafnium oxides were oscillated in the central thimble of the Argonne heavy water reactor. These were compared with a boron standard ($\sigma_B=755$ b). An analysis of the data was made in which enrichment factors and approximate resonance contributions were taken into account. Three isotopes had detectable absorption cross sections for the method and amounts of material available. The results of these measurements were in satisfactory agreement with those of Pomerance:[6]

$$\sigma_{177}=350\pm50 \text{ barns},$$
$$\sigma_{178}=90\pm20 \text{ barns}, \quad \sigma_{179}=75\pm15 \text{ barns}.$$

Hafnium 177, 178, and 179, therefore, account for $\sim$100 barns of thermal absorption in normal hafnium. Another few barns result from 180 and 176. The low abundant Hf^{174} has an absorption cross section estimated to be $\sim10^3$ barns on the basis of β spectrographic film densities of the 70-day Hf^{175} plates taken by Burson and group. It would contribute $\sim$2 barns to normal hafnium.

C. Resonance Scattering

Thin resonance-scattering detectors of the enriched oxide samples were made by causing $\sim$50 mg to adhere to a 0.3-mil aluminum foil. The detectors thus formed were round and had an area ~5 cm^2. These were placed in turn in the center of an annular 4π BF_3 proportional neutron counter.[8] A cadmium-filtered neutron beam from the Argonne heavy-water reactor was directed at the detector foils, and a neutron counting rate developed due to epi-thermal neutron scattering by the detector

* Now at Stewart-Warner Corporation, Chicago, Illinois.
† Portions of this work were presented in partial fulfillment of the requirements for the degree of Doctor of Philosophy at the Illinois Institute of Technology, Chicago, Illinois.
‡ Now at Brookhaven National Laboratory, Upton, New York.
[1] Acknowledgment is given Dr. C. P. Keim, who kindly provided the isotopically enriched samples used in this work.
[2] S. B. Burson *et al.*, Phys. Rev. **83**, 62 (1951).
[3] A. Flammersfeld, Naturwiss. **32**, 68 (1944).
[4] This result was reported privately and has appeared in various compilations.
[5] M. Goldhaber and R. D. Hill, Revs. Modern Phys. **24**, 179 (1952).
[6] H. Pomerance, Phys. Rev. **88**, 412 (1952).
[7] S. P. Harris *et al.*, Phys. Rev. **80**, 342 (1950).
[8] S. P. Harris *et al.*, Phys. Rev. **79**, 11 (1950).

TABLE I. Resonance-scattering cross sections in barns.

Isotope	Oxide (mg/cm²)	$\sigma_{\text{epi-Cd}}-\sigma_p$	Σ_{rs} (corrected)[a]
177	50	~40	~400±100
178	50	~20	~200± 50
179	50	~15	~150± 50

[a] H. Pomerance, Oak Ridge National Laboratory Report ORNL-1304, 1952 (unpublished), p. 13.

foils. Comparisons were made with both a blank aluminum foil and a graphite detector ($\bar{\sigma}_s=4.60$ b). In this manner average epi-cadmium scattering cross-sections, $\sigma_{\text{epi-Cd}}$, were obtained. Such a cross section has the following significance[7] with the particular counter employed:

$$\sigma_{\text{epi-Cd}}=\sigma_p+\frac{1}{8.4}\Sigma_{rs}, \tag{1}$$

where

$$\Sigma_{rs}=\int \sigma_{rs}d\epsilon/\epsilon \tag{2}$$

is the resonance-scattering integral, and

$$\sigma_p=\text{potential-scattering cross section.} \tag{3}$$

Therefore

$$\Sigma_{rs}=8.4(\sigma_{\text{epi-Cd}}-\sigma_p). \tag{4}$$

The resonance-scattering integral is a measure of the total resonance scattering occurring at the definite energy levels which possess a significant fraction of scattering. Equation (4) must also be slightly corrected for energy.[8]

This experiment was performed in order to ascertain which isotope possessed the significant scattering levels indicated by the authors in a previous paper.[8] An average potential scattering cross section of 23 barn for HfO_2 was subtracted from all epi-cadmium values. This had been previously determined by measuring the transmission cross-section for very thick filters of normal HfO_2. After analysis of the resulting data in terms of enrichment factors, the resonance integrals (Σ_{rs}) given in Table I were obtained. Again it may be seen that, as with thermal absorption, the principal isotopes having low-energy resonance levels are: Hf^{177}, Hf^{178}, and Hf^{179}. Hf^{177} possessed the largest resonance scattering along with the largest thermal absorption. This result is similar to one found for tungsten, in that the principal resonance scatterer[8] (W^{186}) is also the principal thermal absorber.[7]

Further experiments were carried out to determine approximate energies of the levels having significant scattering. The above-mentioned detectors enriched in 177 and 178 were again placed in turn in the center of the annular scattering counter. Filters of enriched boron were placed in the neutron beam outside the counter, and boron transmission curves of the resonant scattered neutrons were obtained. Corrections were made for the effect of the boron on the neutrons scattered by potential scattering in hafnium by use of similar boron transmission curves for neutrons scattered by graphite, for which the scattering is all potential scattering. Again the data were analyzed in terms of enrichment factors, with the following results: significant resonance-scattering levels in Hf^{177} and Hf^{178} at ~6.7 ev and ~7.6 ev, respectively.

Since Hf^{179} showed some resonance scattering, one would presume thermal energies to lie in the wing of a resonance level whose energy is <10 ev.[8] Similarly, one would expect the large thermal cross section of Hf^{177} to be the result of absorption levels lower in energy than 5 ev.

D. Capture γ-Ray Multiplicity

Following the method of one of the authors in a previous paper,[9] the neutron capture γ-ray multiplicity

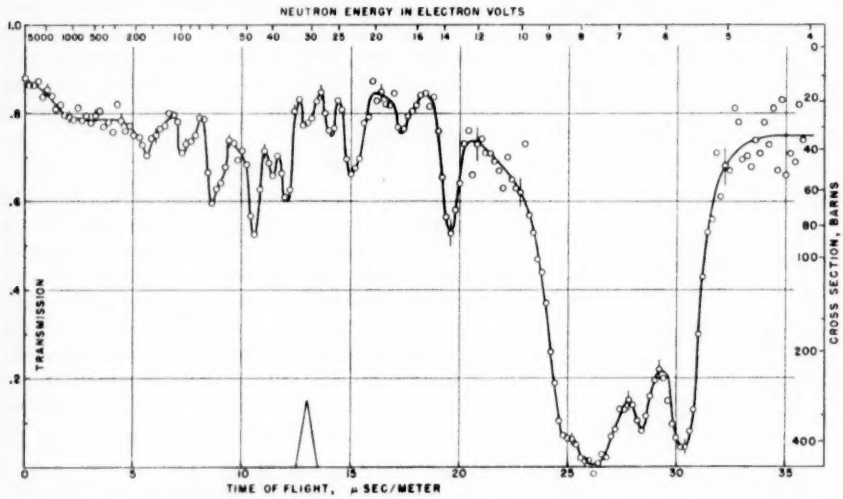

FIG. 1. The neutron transmission of a 2.45-g/cm² sample of normal HfO_2 in the energy range 4 to 5000 ev. The resolution used (full width at half maximum) was 0.5 μsec/meter for energies greater than 14.5 ev, and 0.6 μsec/meter for the remaining data.

[9] C. O. Muehlhause, Phys. Rev. **79**, 277 (1950).

($\bar{\nu}_\gamma$) was measured for Hf^{177} and Hf^{178}. Thin foils of enriched material were placed in turn between two scintillation counters in coincidence which straddled a pile neutron beam. The ratio of coincidence to single counting rates was observed, and this was compared with normal hafnium that had been measured previously ($\bar{\nu}_\gamma = 3.8$).[9]

The observed multiplicities for Hf^{177} and Hf^{178} were 4.1 ± 0.2 and 3.5 ± 0.2, respectively. This is in qualitative agreement with the observations of the following section, namely: the level density of Hf^{178} ($Hf^{177}+n$) is greater than the level density of Hf^{179} ($Hf^{178}+n$).

TIME-OF-FLIGHT MEASUREMENTS

The mechanical neutron velocity selector recently described by Selove[10] was used to investigate the transmission of hafnium oxide samples within the energy range 1 to 1000 ev. The results obtained for normal hafnium are given in Figs. 1 and 2, and those obtained for the isotopically enriched samples are given in Fig. 3. Data are not given for the enriched samples in the energy range 16 to 1000 ev because no structure was observed in that range. For the normal hafnium data, there are, in addition to the standard statistical errors indicated on the figures, possible systematic errors in the absolute level of the transmission curves, these errors being less than one percent for energies greater than 15 ev in Fig. 1 and less than three percent for the other data. The curves for the enriched samples have somewhat larger systematic errors. The transmission scales attached to the curves refer to the oxide sample, but the cross-section scales refer to the hafnium itself. The composition and thicknesses of the enriched samples that were used are listed in Table II.

In normal hafnium, transmission dips had previously been found[11] at 1.1, 2.2, 5.5, and 7.6 ev. The greater resolution used in the present work permits us to see that the pair of dips at 5.5 and 7.6 ev was caused by at least 5 resonances, at 5.6, 5.7, 6.5, 7.6, and 8.8 ev. Of these, the 6.5-, 7.6-, and 8.8-ev resonances are clearly seen in Fig. 3. An anomalous shape of the 5.5–5.7-ev transmission dip was obtained with 0.38-μsec/meter resolution (with a 20-meter neutron flight path), suggesting that it is caused by more than one resonance. Proof that this dip is caused by two resonances rests on the data obtained with the enriched samples and will be discussed in a later paragraph.

TABLE II. Composition of isotopically enriched hafnium oxide samples.

Sample	Percentage of isotope 180	179	178	177	176	174	Thickness[a] (g/cm²)
Normal	35.3	13.8	27.1	18.4	5.2	0.2	
180	94.0	3.2	2.0	0.7	0.1	0.0	1.38
179	44.2	46.6	6.7	2.1	0.4	0.0	1.0
178	6.1	6.8	80.9	5.7	0.5	0.0	0.26
177	4.0	3.7	29.2	61.7	1.3	0.1	0.195
176	5.2	3.4	14.5	28.3	48.5	0.1	0.22

[a] The thicknesses listed above apply only to time-of-flight measurements. The enrichments apply to all samples including those used in pile-oscillator and scattering experiments.

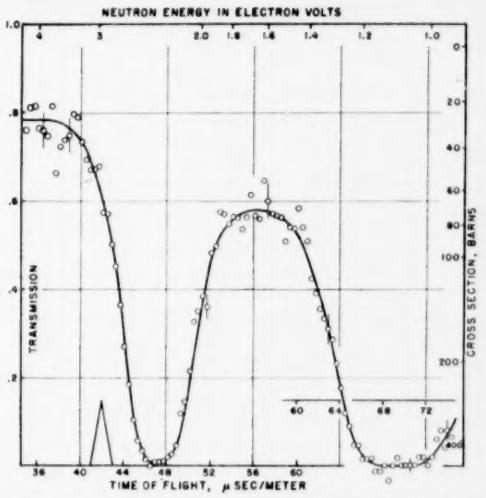

FIG. 2. The neutron transmission of normal HfO_2 in the energy range 1 to 4 ev with 1.1-μsec/meter resolution. The sample thickness is 2.45 g/cm².

A qualitative examination of the transmission curves obtained for the enriched samples seems to show that the 1.1-, 2.3-, 6.5-, 8.8-, and 13.6-ev dips are due to Hf^{177}, that the 7.6-ev dip is due to Hf^{178}, and that the 5.7-ev dip is due to Hf^{179}. A quantitative study of the isotopic assignments may be made by comparing the areas above the transmission dips obtained for the various samples. It has been shown[12] that, under favorable conditions, the area above a transmission dip provides a measure of $\sigma_0\Gamma'^2$ for the resonance causing the dip. If a particular transmission dip is caused by a resonance in a single isotope, the values of $\sigma_0\Gamma'^2$ determined for this resonance should be the same for all samples containing the isotope. In particular, the several values of $\sigma_0\Gamma'^2$ that are calculated for each transmission dip for the hafnium samples having different abundances of the isotope in question will be equal if the correct isotopic assignment for the dip has been made and will differ markedly if a wrong assignment has been made.

Table III presents an area analysis of this kind for the hafnium resonances. The first column lists the samples for which the areas were measured. Each one of the other columns gives the values of $\sigma_0\Gamma'^2$ that were obtained for a particular resonance. The number in parentheses below each value of $\sigma_0\Gamma'^2$ is an estimate as to the factor by which that value may be in error because of uncertainties in area measurement. Further errors result from the fact that $\sigma_0\Gamma'^2$ was calculated

[10] W. Selove, Rev. Sci. Instr. **23**, 350 (1952).
[11] P. A. Egelstaff and B. T. Taylor, Nature **167**, 896 (1951).
[12] W. W. Havens, Jr. and L. J. Rainwater, Phys. Rev. **83**, 1123 (1951).

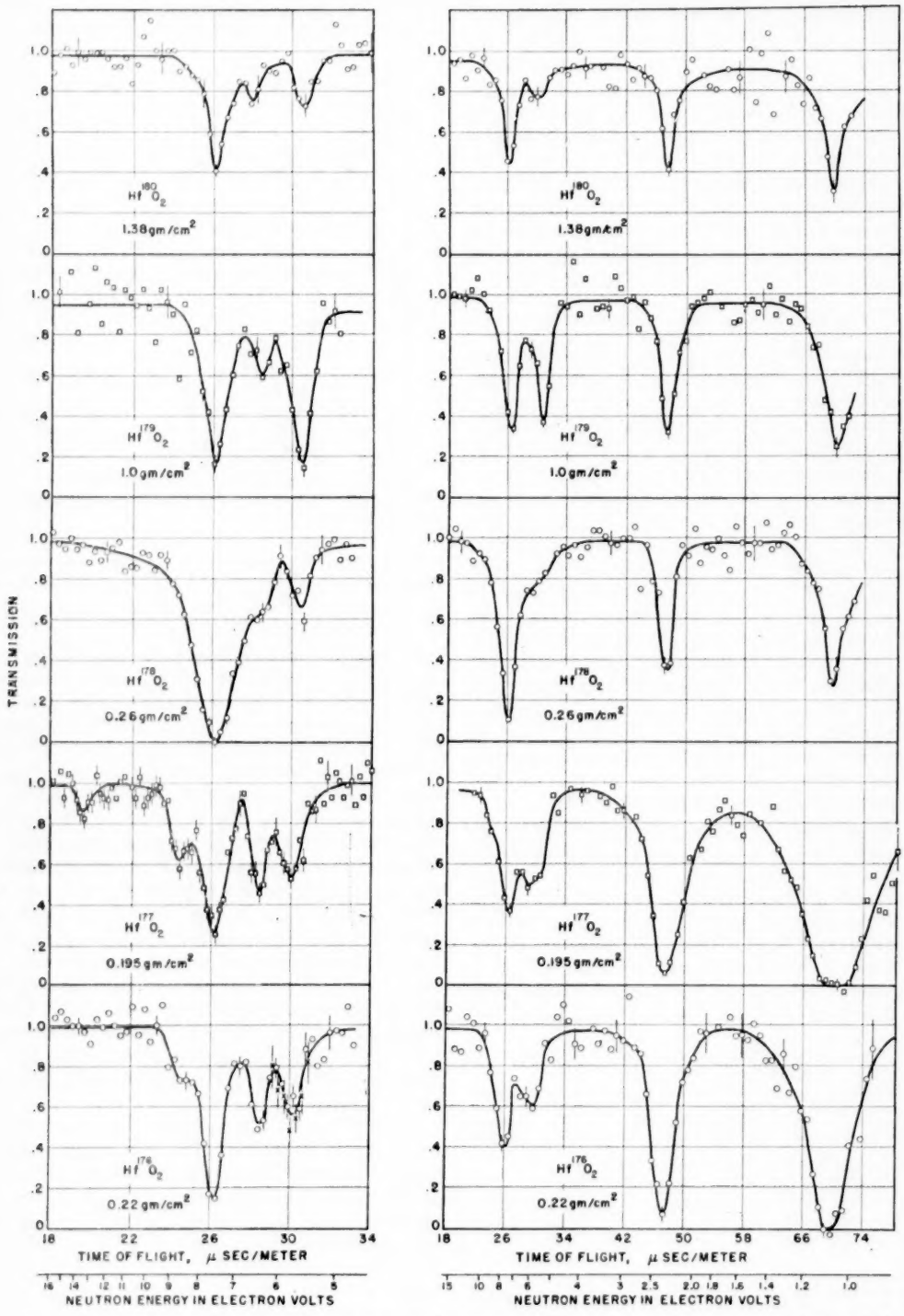

FIG. 3. The neutron transmission of isotopically enriched samples of HfO_2. The low energy data were obtained with 1.5-μsec/meter resolution and the higher energy data with 0.75-μsec/meter resolution. The isotopic composition of the samples is given in Table II.

under the assumption that we were dealing with thick samples; namely, that $n\sigma_0 \gg 1$, for which case $\sigma_0\Gamma^2 \rightarrow 4E_0^2A^2/n\pi$, where A is the "relative area" defined in reference.[12] The thick sample assumption may not be valid for all the transmission dips that were used. In particular, it is not true for the measurements on the 1.1-ev resonance in the Hf^{178}, Hf^{179}, and Hf^{180} samples. In the last row of the table is listed the isotope that was assumed to cause each resonance.

An examination of the results given in Table III for the 1.1-, 2.3-, 6.5-, 7.6-, and 13.6-ev transmission dips shows that the values of $\sigma_0\Gamma^2$ are equal within the errors listed; moreover, any other isotopic assignment fails to give satisfactory agreement. The isotopic assignment that was indicated by qualitative examination of the data is, therefore, confirmed for these resonances. For the 5.6–5.7-ev transmission dip, however, the values of $\sigma_0\Gamma^2$ that were calculated by assuming it to be due either to Hf^{179} or to Hf^{177} are clearly not equal. The data can be explained, however, by assuming that both Hf^{177} and Hf^{179} have resonances at about 5.7 ev. All the areas measured for the 5.6–5.7-ev transmission dip are in good agreement with a $\sigma_0\Gamma^2$ value of 52 barns $(ev)^2$ for the Hf^{177} resonance and 25 barns $(ev)^2$ for the Hf^{179} resonance.

Further support for the assumption that both Hf^{177} and Hf^{179} have resonances at about 5.7 ev is given by a close examination of the resonance energies observed. In the Hf^{179} and Hf^{180} samples, which contain very little Hf^{177}, the time of flight of the 5.6–5.7-ev transmission dip is 0.4 μsec/meter greater than is the corresponding time of flight for the Hf^{177} and Hf^{176} samples. We conclude, therefore, that of the 5.6–5.7-ev pair of resonances, the higher-energy one is due to Hf^{177} and the lower-energy one is due to Hf^{179}.

TABLE III. Area analysis to determine the isotopes responsible for the resonances in hafnium. The values of $\sigma_0\Gamma^2$ are given in barns·$(ev)^2$. The factor by which each value may be in error is given in parentheses.

Sample	Transmission dip (ev) 13.6	8.8	7.6	6.5	(5.6–5.7)		2.3	1.1
Normal 0.6 μsec/m		58 (2)	1430 (1.3)	106 (1.6)	330 (1.5)	250 (1.5)		
Normal 1.0 μsec/m		20 (4)	1420 (1.3)	64 (1.8)	240 (1.5)	185 (1.5)	310 (1.3)	120 (1.5)
Normal 2.45 g/cm³	31 (1.6)							
180			850 (1.6)	38 (3)	32 (2)	145 (2)	240 (1.4)	62 (1.5)
179			950 (1.5)	83 (3)	40 (1.4)	960 (1.4)	200 (1.4)	75 (1.5)
178			1640 (1.3)	69 (3)	125 (1.8)	145 (1.8)	240 (1.5)	54 (1.5)
177	20 (2)	59 (2)	830 (1.4)	52 (1.8)	1100 (1.6)	68 (1.6)	290 (1.4)	160 (1.5)
176		32 (3)	1960 (1.3)	88 (1.8)	730 (1.8)	88 (1.8)	280 (1.3)	120 (1.5)
Isotope assumed responsible	Hf^{177}	Hf^{177}	Hf^{178}	Hf^{177}	Hf^{179}	Hf^{177}	Hf^{177}	Hf^{177}

TABLE IV. Summary of analysis of hafnium resonances.

Energy (ev)	Hafnium isotope	$\sigma_0\Gamma^2$ [barn $(ev)^2$]	σ_0 (barns)	Γ (ev)
1.08±0.02	177	110± 25	55 000±15 000	0.045±0.010
2.34±0.05	177	280± 40	>30 000	<0.10
5.6 ±0.1	179	25± 10	>1400	<0.13
5.7 ±0.1	177	52± 15	>2400	<0.15
6.5 ±0.1	177	80± 30	>7200	<0.11
7.6 ±0.1	178	1400±300	>20 000	<0.26
8.8 ±0.2	177	55± 25	>3600	<0.12
13.6 ±0.4	177	28± 10	>450	<0.25

The results of the preceding paragraphs concerning the isotopic assignment of the hafnium resonances are summarized in Table IV. In addition, values of σ_0 and Γ, which have been corrected for lack of resolution, are given for the 1.1-ev resonance. Limits to the values of σ_0 and Γ are given for the other resonances.

It is gratifying to note that the results from the time-of-flight measurements are in complete agreement with the conclusions of the previous sections. The large thermal absorber, Hf^{177}, possesses most of the levels observed, and these include the two of lowest energy. In addition, Hf^{179} proved to have an observable resonance below 10 ev, as was expected on the basis of its thermal cross section. No levels were found in either Hf^{176} or Hf^{180}. This, too, is in agreement with the pile oscillator measurements.

CONCLUSION

It is evident both from the thermal cross sections and the resonance levels that the odd-N isotopes have a smaller level separation D^*, than the even-N isotopes.[8] In the case of Hf^{177} it is further evident that the mean level separation is ~3 ev. Very little may be said of any of the even-N isotopes except that their level separation is large and probably ~100 ev. An estimate of this in the case of Hf^{178} may be made on the basis of the expression,[13] $D^* \sim 10^4\Gamma_n/E_0^{\frac{1}{2}}$. To do this, one uses the following:

$$\Sigma_s = \tfrac{1}{2}\pi\sigma_0\Gamma_n/E_0 = 200 \text{ b}, \tag{5}$$

$$\sigma_0\Gamma^2 = 1400 \text{ b}\cdot\text{ev}^2, \tag{6}$$

$$\sigma_0 = \frac{2.6\times10^6}{E_0}\cdot\frac{\Gamma_n}{\Gamma}, \tag{7}$$

$$E_0 = 7.6 \text{ ev}; \tag{8}$$

these relations are not complicated by an uncertain "g" factor ($g=1$ for even-Z—even-N). The above yields a value for Γ_n of 0.023 ev, and this in turn yields $D^* \sim 85$ ev.

It may be difficult to observe additional levels in Hf^{178} in the 100 to 1000-ev region with the present instrumental resolution. Such levels should be sharp (~0.2 ev) and furthermore should be masked by the presence of the dense levels of even a little Hf^{177}.

[13] Feshbach, Peaslee, and Weisskopf, Phys. Rev. **71**, 145 (1947).

The Nuclear Moments of Se^{79}†

W. A. HARDY,* G. SILVEY, AND C. H. TOWNES, *Columbia University, New York, New York*
B. F. BURKE AND M. W. P. STRANDBERG, *Department of Physics and Research Laboratory of Electronics, Massachusetts Institute of Technology, Cambridge, Massachusetts*
GEORGE W. PARKER, *Oak Ridge National Laboratory, Oak Ridge, Tennessee*

AND

VICTOR W. COHEN, *Brookhaven National Laboratory, Upton, New York*

(Received August 24, 1953)

Microwave measurements of the $J=2\rightarrow3$ rotational transition of OCSe containing the radioactive-nucleus Se^{79} have established the Se^{79} spin as 7/2 and the Se^{79} quadrupole moment as 0.7×10^{-24} cm$^3\pm20$ percent. The quadrupole coupling constant eqQ is 752.09 ± 0.05 Mc/sec. The magnetic moment of Se^{79} has been determined as -1.015 ± 0.015 nuclear magnetons by observation of the Zeeman splitting of one hyperfine component. The 7/2 spin and the large positive Q are inconsistent with the single-particle nuclear-shell model, but suggest the configuration $(g_{9/2})^7{}_{7/2}$. This assignment is substantiated by the negative magnetic moment.

Measurement of isotopic shifts gives a value for the Se^{79} mass, and an odd-even mass difference of 2.4 millimass units for this nucleus.

(A) INTRODUCTION

IT is well known that the jj-coupling nuclear-shell model proposed by Mayer[1] and by Haxel, Jensen, and Suess[2] fails to account for the spins of several nuclei when used as a single-particle model in which the spin of a nucleus in its ground state is determined by the angular momentum of the last added odd nucleon.[1,2] For these exceptional nuclei, it is necessary to assume that several nucleons outside a closed shell contribute to the angular momentum, and that the resultant nuclear configuration is one in which the particles do not couple in pairs to give zero angular momentum for each pair. It is of especial interest to examine the configurations of these nuclei by study of their moments, or, indeed, by any other available means.

The nucleus $_{34}Se^{79}{}_{45}$ would be predicted from the single-particle version of the shell model to have the spin 9/2 or 1/2 corresponding to the assignment of the last odd neutron to a $g_{9/2}$ or possibly a $p_{1/2}$ level. The observed spin of 7/2 is a clear exception. Measurements of the magnetic dipole and electric quadrupole moments of this nucleus, discussed below, allow a fairly unique interpretation of the configuration of Se^{79}. This configuration is consistent with those found for other known exceptional nuclei, and helps to demonstrate a general favoring of states with positive quadrupole moments.

The spin and quadrupole moment of Se^{79} were measured by observation of the hyperfine pattern of the $J=2\rightarrow3$ microwave rotational transition of the molecule $OCSe^{79}$. This hyperfine structure is due to the electrostatic quadrupole interaction energy eqQ of the nuclear quadrupole moment, Q, in the molecular electric field gradient, q.[3] In the presence of an external magnetic field, there is an additional Zeeman splitting from which the nuclear magnetic moment may be determined.[4,5]

The ground state of Se^{79} is unstable, the nucleus decaying to Br^{79} with the emission of a β particle of about 160 kev with a half-life of 6.5×10^4 years. The 7/2 spin, predicted by Goldhaber and Sunyar from an analysis of this isomeric decay, was reported in an earlier note on the microwave absorption spectrum of $OCSe^{79}$.[6,7] Unfortunately, the amount of Se^{79} available in these earlier microwave measurements was less than one microgram, and hence so limited that extended measurements of high precision were difficult. A considerably enriched sample containing 270 micrograms of Se^{79}, representing an abundance of 1.2 percent, was subsequently made available by the Oak Ridge National Laboratory. This has permitted more accurate measurements of the molecular parameters of $OCSe^{79}$ and also the determination of the nuclear magnetic moment, both of which are reported here.

(B) SPECTROSCOPY ON $OCSe^{79}$ WITHOUT ZEEMAN EFFECTS

The Se^{79} sample was put into the molecular form OCSe and the previous microwave measurements were repeated. The spectrometer used was a conventional Stark modulation spectrometer of high sensitivity and good resolution. The 7/2-spin assignment was amply verified by the measurement of nine lines in the quadrupole hyperfine pattern, but only five were chosen for the determination of the molecular parameters. These five, listed in Table I, were of good intensity

† This work was supported in part by the U. S. Atomic Energy Commission, and in part by the U. S. Army Signal Corps, the Air Materiel Command, and the U. S. Office of Naval Research.

* National Research Council Pre-doctoral Fellow (1952–53).

[1] Maria Goeppert Mayer, Phys. Rev. **78**, 16 (1950).

[2] Haxel, Jensen, and Suess, Phys. Rev. **75**, 1766 (1949); Z. Physik **128**, 295 (1950).

[3] J. Bardeen and C. H. Townes, Phys. Rev. **73**, 627 (1948).

[4] Eschbach, Hillger, and Strandberg, Phys. Rev. **85**, 532 (1952).

[5] C. K. Jen, Phys. Rev. **74**, 1396 (1948).

[6] M. Goldhaber and A. W. Sunyar, Phys. Rev. **83**, 906 (1951).

[7] Hardy, Silvey, and Townes, Phys. Rev. **85**, 494 (1952).

and were not distorted by weak Stark splitting or by the Stark components of neighboring lines. The molecular parameters calculated from these lines are also listed in Table I.

Two nuclear interactions were considered in the calculations. The most important is the quadrupole interaction depending on eqQ, and this was calculated from the matrix elements given by Bardeen and Townes, including second-order corrections.[3] For refinement, the interaction $c\mathbf{I}\cdot\mathbf{J}$ was also included. This represents a perturbation on the quadrupole hyperfine structure arising from the interaction of the Se^{79} magnetic moment with the magnetic field at the nucleus due to the molecular rotation. Its effect is extremely small, being of the order of the 5-kc/sec uncertainty in the frequency measurements. In Table I the deviations between the measured line frequencies and those calculated from the quoted molecular parameters are given both for $c=-1.3$ kc/sec and for $c=0$. Although the value $c=-1.3$ kc/sec gives a minimum deviation for the data, it is clear from the size of these deviations that this value of c is not very reliable. However, the negative sign which is obtained is consistent with the negative magnetic moment of Se^{79} and the direction of the internal molecular magnetic fields observed in most molecules.

The nuclear quadrupole moment, Q, is not directly obtainable from the measured quadrupole coupling constant, eqQ, but is approximated by making a reasonable estimate of the molecular field gradient, q, following the method of Townes and Dailey.[8] In the first note on the microwave spectrum of $OCSe^{79}$, Q was estimated as 1.2×10^{-24} cm$^2\pm50$ percent.[7] However, recent work on sulfur bonds by Bird and also by Dehmelt indicates that eqQ for the nucleus S^{33} in a pure p bond would be 48 Mc/sec.[9,10] The measured eqQ for OCS^{33} is 29 Mc/sec, so the fractional importance of the pure p bond in the OCS^{33} molecular structure must be 60 percent. OCS and OCSe would be expected to have similar bonding structures, and, making only this assumption, the quadrupole moment of Se^{79} may be calculated as 0.7×10^{-24} cm^2 with a probable error of less than 20 percent.

TABLE I. Measured hyperfine lines in the $J=2\rightarrow3$ rotational spectrum of $OCSe^{79}$ and calculated frequencies using the molecular parameters determined.

Transition $F\rightarrow F'$		Measured frequency in Mc/sec	Calculated frequency in Mc/sec ($c=-1.3$ kc/sec)	Deviation in kc/sec	Calculated frequency in Mc/sec ($c=0$)	Deviation in kc/sec
7/2	7/2	24 153.204	24 153.209	−5	24 153.205	−1
11/2	13/2	24 170.194	24 170.193	1	24 170.198	−4
7/2	9/2	24 190.787	24 190.781	6	24 190.783	4
3/2	3/2	24 204.692	24 204.688	4	24 204.684	8
5/2	7/2	24 234.329	24 234.333	−4	24 234.334	−5

$\nu_0=24\,179.097\pm0.004$ Mc/sec
$eqQ=752.09\pm0.05$ Mc/sec
$c=-1.3\pm2.0$ kc/sec
$I(Se^{79})=7/2$
$\dfrac{m^{79}-m^{78}}{m^{80}-m^{78}}=0.50081\pm0.00010$

The rotational transition frequency of $OCSe^{79}$, assuming no hyperfine structure, is calculated as

$$\nu_0=24\,179.097\pm0.004\ \text{Mc/sec}.$$

From this and the rotational frequencies of other OCSe isotopic molecules the Se^{79} mass difference ratio may be determined as[11]

$$\frac{m^{79}-m^{78}}{m^{80}-m^{78}}=\frac{M^{79}}{M^{80}}\left(\frac{\nu^{80}}{\nu^{79}}\right)\left(\frac{\nu^{78}-\nu^{79}}{\nu^{78}-\nu^{80}}\right)$$
$$=0.50081\times0.00010.$$

Here m is the nuclear mass, M the molecular mass, and ν the rotational frequency. For each of these the superscript designates the isotope of selenium used. Geschwind has shown that the error in the selenium mass ratios derived from this formula is less than 0.01 percent.[11] This ratio gives the odd-even mass difference of Se^{79} as 2.4-millimass units and may be compared with the 2.0-millimass units difference of Se^{77} determined by Geschwind, Minden, and Townes.[12] These authors measured the rotational frequencies of all the naturally abundant isotopes of selenium in OCSe and express their data in terms of the masses of Se^{76} and Se^{80}, which they assume from a Bohr-Wheeler type formula. This assumption would give the mass of Se^{79} as 78.9494 ± 0.0002-mass units. The $OCSe^{78}$ rotational frequency was remeasured and found to agree within 2 kc/sec with that measured by Geschwind *et al.*

(C) THEORY OF THE ZEEMAN EFFECT

The part of the Hamiltonian giving the interaction of the molecule with an external magnetic field $\mathbf{H}$ is

$$\mathcal{H}_m=-\mu_0 g_J(\mathbf{H}\cdot\mathbf{J})-\mu_0 g_I(\mathbf{H}\cdot\mathbf{I}).$$

Here μ_0 is the nuclear magneton, g_J the molecular g factor due to the rotation of the molecule, and g_I the nuclear g factor. The nuclear term will have a negligible effect upon the observed rotational spectrum unless the nuclear spin is coupled to the molecule by an interaction energy larger than the line width. In the case of Se^{79} this interaction is provided by the quadrupole coupling. The appropriate quantum numbers when such a coupling is present are I, J, F, and M with $\mathbf{F}=\mathbf{J}+\mathbf{I}$ and M the projection of $\mathbf{F}$ on the axis of quantization. The matrix evaluation of $\mathcal{H}_m$ in this representation has been given by a number of authors.[4,5,13] We give here only the first-order diagonal terms so as to show the structure of the Zeeman pattern for the

[8] C. H. Townes and B. P. Dailey, J. Chem. Phys. **17**, 796 (1949).
[9] George Bird (private communication).
[10] H. Dehmelt, Phys. Rev. **91**, 313 (1953).
[11] S. Geschwind, thesis, Columbia University, 1951 (unpublished).
[12] Geschwind, Minden, and Townes, Phys. Rev. **78**, 174 (1950).
[13] F. Coester, Phys. Rev. **77**, 454 (1950).

case where the interaction between the nucleus and the external magnetic field is considerably less than that between its quadrupole moment and molecular electric field ($\mathcal{H}_m \ll \mathcal{H}_Q$).

$$E_m = -\mu_0 HM(g_J\alpha_J + g_I\alpha_I).$$

The α's are cosine terms (obtainable from the vector model) with

$$\alpha_J = \frac{F(F+1)-I(I+1)+J(J+1)}{2F(F+1)},$$

$$\alpha_J+\alpha_I=1.$$

For the typical case of plane polarized radiation in a rectangular wave guide, we may distinguish two types of Zeeman transitions depending on whether **H** is parallel or perpendicular to the microwave electric vector, **E**:

(a) **H** parallel to **E**: ($\Delta F=0, \pm 1$; $\Delta M=0$),

$$\Delta\nu^0 = \mu_0 HM(g_J-g_I)(\alpha_{J1}-\alpha_{J2}).$$

(b) **H** perpendicular to **E**: ($\Delta F=0, \pm 1$; $\Delta M=\pm 1$),

$$\Delta\nu^{\pm 1} = \Delta\nu^0 \mp \mu_0 H(g_J\alpha_{J2}+g_I\alpha_{I2});$$

$\Delta\nu$ is the Zeeman shift, and α_{J2} and α_{J1} are the cosines of the upper and lower states, respectively.

Because the Zeeman pattern is symmetric for either positive or negative M and ΔM, the sign of M for an individual transition cannot be determined and consequently g_J and g_I are not uniquely determined by measurements of the Zeeman splitting for the two field conditions. It is possible to determine M assignments for the pattern by the use of circularly polarized radiation to select M components, but this was not feasible in this experiment due to the poorer sensitivity of the circular polarization apparatus and the low abundance of the isotope with nuclear spin. The molecular g factor, g_J, may be determined independently of g_I by examining the Zeeman splitting in an isotopic molecule in which the substituted nucleus has no nuclear spin and hence possesses no nuclear rotational interaction. Here the Zeeman pattern simplifies and the sign of g_J may be readily determined by circular polarization techniques. When g_J is known, g_I may be completely determined by measurements of the hyperfine splitting under the two field conditions given above.

(D) MEASUREMENTS OF ZEEMAN EFFECTS

The wave-guide absorption cell used in this work consisted of a conventional Stark septum wave guide three feet in length which could be rotated with respect to a magnetic yoke running the length of the guide. Actually two identical yokes were used: one in which the wave guide was inserted, and one in which the magnetic field was measured by means of a flip-coil. These yokes were carefully calibrated so that the error due to the field measurement was of the order of 0.5 percent.

As indicated above, the molecular g factor, g_J, was determined in an isotopic molecule which did not have hyperfine structure. The magnitude of g_J was measured by the normal Zeeman splitting for the $J=2\rightarrow 3$, $\Delta M=\pm 1$ transition of the molecule $OCSe^{80}$. The separation of the two components was determined as 92 kc/sec in a field of 6300 oersteds by matching the observed line shape with that obtained by adding two lines of equal intensity and of the same shape as the unsplit line. The width of the unsplit line at half maximum intensity was 120 kc/sec. Further, the g factor was determined as negative by the use of circularly polarized microwave radiation in a special wave guide of square cross section oriented in a longitudinal magnetic field. This apparatus and the technique involved has already been described.[4,14,15] The molecular g factor is thus determined as

$$g_J = -0.019 \pm 0.002.$$

Although this is the g factor for $OCSe^{80}$, it will differ from that of $OCSe^{79}$ only by the ratio of the rotational frequencies of these molecules, and this correction is therefore not significant.

For the hyperfine lines, the dependence of the α cosines given above on F indicates the necessity for using low F transitions to insure a splitting sufficient to distinguish the Zeeman components and measure them accurately in the available fields. Of the hyperfine lines measured, the $F=3/2\rightarrow 3/2$ line was selected as best meeting this requirement, although its intensity is only 17 percent of that of the strongest hyperfine component, the $F=11/2\rightarrow 13/2$ line. The absolute absorption of the $F=3/2\rightarrow 3/2$ line in the 1.2-percent abundant sample is 7.3×10^{-9} cm^{-1}, and the strongest Zeeman component in the $\Delta M=\pm 1$ transition is only one-fifth as intense with an absorption of 1.5×10^{-9} cm^{-1}. Because of this low intensity, the 2K33 klystron frequency was stabilized with respect to a microwave frequency standard harmonic by mixing the two signals in a crystal and detecting the difference with an FM receiver. The discriminator output was then used to control the repeller voltage of the klystron and thus effect stabilization. Slow sweeping of the klystron through the line frequency was achieved simply by tuning the receiver, and the absorption line was displayed on an Esterline Angus recording meter together with frequency markers obtained from the receiver dial calibration. The observed line intensities in the three-foot wave guide were three to four times the noise level at a guide temperature of -50°C.

The separation between the components $M=-3/2\rightarrow -3/2$ and $M=3/2\rightarrow 3/2$ was determined from ten

[14] J. R. Eschbach and M. W. P. Strandberg, Rev. Sci. Instr. **23**, 623 (1952).

[15] Bernard Burke, thesis, Massachusetts Institute of Technology, 1953 (unpublished).

pairs of recorder traces at fields ranging from 3100 to 6100 oersteds. From these data,

$$|g_I - g_J| = 0.271 \pm 0.002.$$

The $\Delta M = \pm 1$ transitions must thus distinguish between the two possibilities:

$$g_I = +0.252, \quad -0.290.$$

For the $\Delta M = \pm 1$ transitions the separations were measured between the $M = -1/2 \rightarrow 1/2$ and $M = 1/2 \rightarrow -1/2$ components from three pairs of traces. Table II compares the measured separation with that calculated for the two possible values of g_I, and establishes the negative value as correct, since the positive value is outside the experimental error. Alternately, the $\Delta M = \pm 1$ data may be used to calculate g_J. For $g_I = +0.252$, $g_J = 0.016 \pm 0.016$, while for $g_I = -0.290$, $g_J = -0.016 \pm 0.016$. Again, the positive value of g_I is excluded.

The Zeeman components displaced by Stark effect as well as those which were undisplaced by Stark effect were used in the evaluation of the data. Further, independent estimates were made at both MIT and Columbia of the separations as determined from the estimated center frequencies of the weak lines on the recorder traces. Both groups obtained exactly the same average g_I, although individual line separations varied by as much as 1 percent. Second-order perturbations representing a magnetic decoupling of I from F were calculated but are of the order of magnitude of the experimental uncertainties, being about 30 kc/sec. In any case they do not affect the net separation of the observed Zeeman components. Finally, the value given for the magnetic moment has not been corrected for the molecular diamagnetic susceptibility. Such a correction would be approximately 0.3 percent, and hence appreciably less than the experimental error.[16] The values obtained from an average of all the experimental measurements are

$$g_I = -0.290 \pm 0.004,$$

$$\mu(Se^{79}) = g_I I = -1.015 \pm 0.015 \text{ nuclear magnetons.}$$

The 1.5-percent experimental error is the sum of both frequency and field calibration errors.

Recorder traces are shown in Fig. 1 for a $\Delta M = 0$ and for a $\Delta M = \pm 1$ transition, illustrating the experimental signal-to-noise ratio. The valley on the left side of the peak in each figure represents absorption by a Zeeman component during the time when the Stark field was on, and the peak represents absorption by the same Zeeman component in the zero Stark field. The calculated Zeeman pattern is shown in Fig. 2. Of ten possible lines, only the strongest pair in each type of M transition was observed. Unfortunately, the current required to establish the strong magnetic field necessary for the $\Delta M = \pm 1$ transitions heated the wave guide to the extent that the OCSe dissociated and, because the amount of $OCSe^{79}$ was limited, precluded additional measurements.

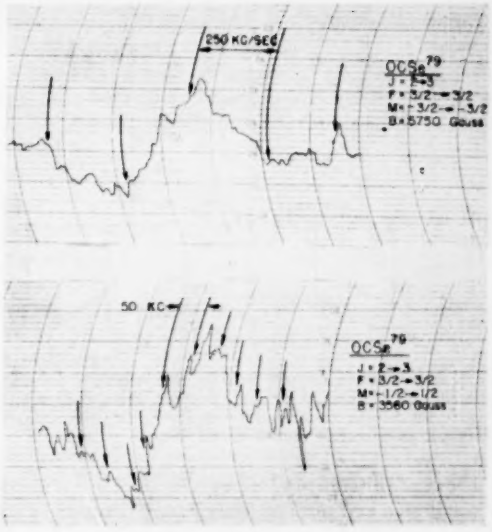

FIG. 1. Typical recording traces for a $\Delta M = 0$ and a $\Delta M = +1$ Zeeman component. The line is the positive hump on the trace and the valley at the left represents absorption during the presence of the Stark field. Frequency markers are shown above the lines.

TABLE II. Comparison of calculated and measured separations between $M = \frac{1}{2} \rightarrow -\frac{1}{2}$ and $M = -\frac{1}{2} \rightarrow \frac{1}{2}$ Zeeman components for the two possible g_I.

g_I	Calculated separation in Mc/sec	Measured separation in Mc/sec	Deviation in kc/sec
+0.252	1.956	2.144±0.050	188±50
−0.290	2.163	2.144±0.050	−19±50

[16] P. F. A. Klinkenberg, Revs. Modern Phys. **24**, 63 (1952).

(E) CHEMISTRY INVOLVED IN MAKING $OCSe^{79}$

Selenium metal containing 1.2-percent Se^{79} was converted to OCSe by introducing carbon monoxide to a pressure of one-half atmosphere into a reaction vessel containing the selenium. The vessel was sealed and heated to 500°C for fifteen minutes. The resulting OCSe was pumped into a trap cooled with liquid nitrogen and was collected.

The selenium metal was part of a larger sample isolated in June, 1949, in a search for a long-lived selenium activity in fission. It was derived from pile-irradiated uranium metal which had been subjected to the highest available neutron flux for a period of one year. The initial separation from uranyl chloride solution involved the usual reduction to elementary selenium in strong hydrochloric acid by means of SO_2 gas. Equilibration with chemical selenium was effected by the addition of the carrier at the end of the dissolution of the metal and prior to oxidation of UCl_4 to UO_2Cl_2.

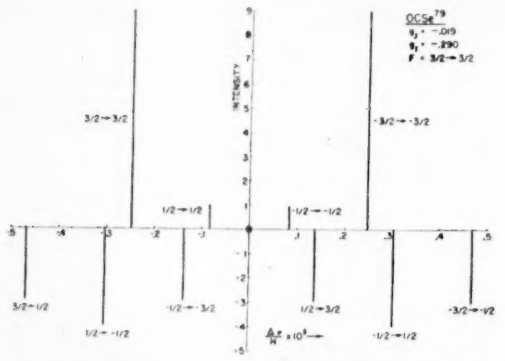

FIG. 2. Calculated Zeeman pattern for the observed $F=\frac{3}{2}\rightarrow\frac{3}{2}$ hyperfine component of $OCSe^{79}$ showing relative intensities. $\Delta M=0$ transitions extend upwards from the base line and $\Delta M=\pm 1$ transitions are indicated downwards.

The crude filtered product was dissolved in a few drops of nitric acid and purified by repeated distillations with 48-percent HBr followed by SO_2 reduction, each in the presence of hold-back carriers of As, Sb, and Tc. Finally, when the ratio of selenium activity to mass of selenium was no longer altered by chemical treatment, portions of the sample were electrolytically co-deposited with copper on platinum disks for counting. In order to obtain pure elementary selenium for this experiment, the plate was redissolved in a drop of nitric acid, fumed with HCl, reduced in 6*N* HCl with SO_2, centrifuged, dried, and weighed.

Since the mass analysis obtained was considered only qualitatively reliable, the apparent abundance in mass-79 has been estimated from the smooth-curve fission yield and the percentage of Se^{79} in the total selenium. From the known number of fissions in the uranium, a total yield of 2.7 milligrams of selenium was produced. Of this material, 10 percent or 270 micrograms was Se^{79}. When equilibrated with 20 milligrams of carrier containing no Se^{79}, this results in a final concentration of 1.2 percent.

(F) DISCUSSION

In addition to Se^{79} there are two other exceptional nuclei Na^{23} and Mn^{55}, whose spins differ from predictions of the single-particle model. All of these nuclei show a spin that is one less than that which would be expected on the single-particle version of the shell model, indicating that two nucleons fail to pair to give zero angular momentum, but give one instead.[16–18] For Se^{79} the two most reasonable configurations which would allow the 7/2 spin are thus $(p_{1/2})^2(g_{9/2})^5$ and $(g_{9/2})^7$, although it is conceivable that the 7/2 spin is due to a single $g_{7/2}$ neutron. However, while the negative sign of the measured magnetic moment is consistent with the two configurations given above, it definitely rules out the possibility of the single $g_{7/2}$ neutron. This follows because the g factor of any configuration whose moment is derived solely from $j=l+1/2$ neutrons, such as the two above, should be the same as for a single $j=l+1/2$ neutron, and hence negative. The g factor produced by a $j=l-1/2$ neutron should be positive. The measured magnetic moment, -1.015 nuclear magnetons, is in reasonable agreement with the value -1.50 nuclear magnetons calculated from a configuration of $j=l+1/2$ (and hence $g_{9/2}$) neutrons. The difference is in the same direction and of about the same magnitude as is generally found for deviations of magnetic moments from the Schmidt limits.[16]

It can be shown that there is only one properly antisymmetrized state corresponding to the configuration $(g_{9/2})^7$.[18] This state has an exceptionally large positive quadrupole moment of magnitude 1.34 times larger than the maximum quadrupole moment produced by any state conforming to the single-particle model. The configuration $(p_{1/2})^2(g_{9/2})^5$, on the other hand, is doubly degenerate and no combination of the degenerate states can produce more than a small quadrupole moment (one-seventh as large).[18] Hence, the measured large positive quadrupole moment is good evidence that the Se^{79} nucleus is best represented by a $(g_{9/2})^7$ configuration.

It is a striking fact that the quadrupole moments of the nuclei so far measured which are exceptions to the single particle version of the shell model are very large and positive. This includes Eu^{153}, as well as Na^{23}, Mn^{55}, and Se^{79} whose quadrupole moments have only recently been measured. Moszkowski and Townes discuss this and other evidence that a positive quadrupole moment tends to lower the energy of a nuclear state.[18]

Although the 7/2 spin of Se^{79} is an exception to the usual expectations, a spin of 7/2 in the $g_{9/2}$ shell is actually fairly common.[19] There is evidence[19] that it is the ground state of the odd-neutron nuclei Ge^{77}, Se^{79}, and Kr^{81}, and of the odd-proton nucleus Rh^{105}. Further, the 7/2 spin lies very close to the ground state in the odd-neutron nuclei Se^{77}, Se^{81}, Kr^{79}, Kr^{83}, and Sr^{85} and in the odd-proton nuclei Tc^{99}, Rh^{103}, Ag^{107}, and Ag^{109}. In these nuclei the 7/2 level shows strong competition with the $p_{1/2}$ level.

(G) ACKNOWLEDGMENT

The success of the above work is the result of the cooperative use of the facilities of a number of laboratories. The Se^{79} metal was prepared and purified at the Oak Ridge National Laboratory and converted to OCSe at Columbia University. The magnitude of g_J

[17] To this list Eu^{153} should probably be added. (See reference 18.)
[18] S. A. Moszkowski and C. H. Townes, Phys. Rev. (to be published).
[19] M. Goldhaber and R. D. Hill, Revs. Modern Phys. **24**, 179 (1952).

for $OCSe^{80}$ was determined at Brookhaven National Laboratory and the sign in the apparatus for circular polarization at MIT. Final Zeeman measurements on $OCSe^{79}$ were made with a Columbia University spectrometer using an MIT Zeeman cell and magnet. Certain preliminary measurements were carried out at Brookhaven. The remainder of the measurements were done at Columbia.

The authors wish to acknowledge the help of Mr. Paul Fletcher with calculations and measurements, and helpful discussions with Dr. S. Moszkowski and Dr. G. Bird.

PHYSICAL REVIEW VOLUME 92, NUMBER 6 DECEMBER 15, 1953

"Nonmesonic" Bound *V*-Particle Decay*

W. CHESTON† AND H. PRIMAKOFF
Washington University, St. Louis, Missouri
(Received June 29, 1953)

A theoretical treatment is presented of the apparent relative stability of *V* particles in nuclear matter in terms of the process of bound *V*-particle nonmesonic decay. Mean lives for nonmesonic decay of *V* particles imbedded in nuclear fragments such as He, Li, $\cdots$O, are estimated as $\approx 10^{-11}-10^{-13}$ sec. A very brief discussion is given of the bearing of such relatively long mean lives on possible mechanisms of *V*-particle production.

INTRODUCTION

RECENTLY, cosmic-ray evidence has suggested the existence of unstable nuclear fragments ($Z \geqq 2$) emitted in high-energy events.[1] These fragments are observed to come to rest in emulsions in about 10^{-12} sec and then to decay with a visible energy release of 50–150 Mev. Since the mean life for the emission of a nucleon from a nuclear fragment having an excitation energy ≈ 100 Mev is $\approx 10^{-20}$ sec, it has been assumed[2] that all the "excitation energy" in such a fragment is concentrated on a single nucleon, i.e., that one of the nucleons in the fragment is a *V* particle; it is further assumed that this *V* particle (considered as an elementary fermion) is still bound to the other nucleons in the fragment by "nuclear forces" about as strong as those acting among the nucleons themselves. It is the purpose of the present note to relate the mean life for the decay (mesonic or nonmesonic) of such a "*V*-particle nuclear fragment" to the mean life for the mesonic decay of a free (unbound) *V* particle (free $V \to p+\pi^-$ +35–40 Mev, in about 10^{-10} sec).[3] In fact, the *V* particle bound in such a fragment may decay without the emission of a π meson, the appropriate energy and momentum balance being insured by the appearance of an ejected nucleon and a recoiling, in general excited, residual fragment. It is reasonable to suppose that this nonmesonic decay of a "*V*-particle nuclear fragment" is a process formally analogous to the nonradiative deexcitation of a nucleus in an ordinary excited state (internal conversion); the general basis of the analogy may be considered by postulating an appropriate Hamiltonian density H for the system of nucleons, *V* particles, and π mesons. We take

$$H = H(\psi_n) + H(\psi_V) + H(\varphi_\alpha) + H_{\text{prod}}(\psi_n, \psi_V, \varphi_\alpha, \cdots) + \frac{g}{2\kappa_n}(\psi_n^* \boldsymbol{\sigma} \tau_\alpha \psi_n) \cdot \nabla \varphi_\alpha + \frac{g}{2\kappa_V}(\psi_V^* \boldsymbol{\sigma} \tau_\alpha \psi_V) \cdot \nabla \varphi_\alpha + \left\{ \frac{\eta}{\kappa_n + \kappa_V}(\psi_n^* \boldsymbol{\sigma} \tau_\alpha \psi_V) \cdot \nabla \varphi_\alpha + \text{h.c.} \right\}, \quad (1)$$

where

ψ_n, ψ_V, φ_α = quantized field amplitudes for the nucleon, *V* particle, and π-meson fields, respectively;

$H(\psi_n)$, $H(\psi_V)$, $H(\varphi_\alpha)$ = Hamiltonian densities for isolated nucleon, *V* particle, and π-meson fields, respectively;

κ_n, κ_V = inverse Compton wavelengths of the nucleon and *V* particle;

g = coupling constant between nucleon and π-meson fields;

η = coupling constant among nucleon, *V* particle, and π-meson fields ($\eta \ll g$ to account for the relatively long mean life of a free *V* particle against decay into a nucleon and π meson);

$H_{\text{prod}}(\psi_n, \psi_V, \varphi_\alpha, \cdots)$ = relatively large interaction term describing *V*-particle production in nucleon-nucleon and/or π-meson nucleon collisions, and contributing a major part of the *V*-particle nucleon

* Assisted by the joint program of the U. S. Office of Naval Research and the U. S. Atomic Energy Commission.

† Present address: University of Minnesota, Minneapolis, Minnesota.

[1] M. Danysz and J. Pniewski, Phil. Mag. **44**, 348 (1953); Tidman, Davis, Herz, and Tennent, Phil. Mag. **44**, 350 (1953); J. Crussard and D. Morellet, Compt. rend. **236**, 64 (1953); Freier, Anderson, and Naugle, preprint, Phys. Rev. (to be published).

[2] See M. Danysz and J. Pniewski, Phil. Mag. **44**, 348 (1953).

[3] Latest mean-life estimates in W. L. Alford and R. B. Leighton, Phys. Rev. **90**, 622 (1953); Fretter, May, and Nakada, Phys. Rev. **89**, 168 (1953); J. G. Wilson and C. C. Butler, Phil. Mag. **43**, 993 (1953); Bridge, Peyrou, Rossi, and Safford, Phys. Rev. **91**, 362 (1953).

"nuclear force." On our assumption, however, H_{prod} is necessarily of such a form that it cannot contribute appreciably to either free V-particle mesonic, or bound V-particle nonmesonic (or mesonic) decay, i.e., H_{prod} cannot be expressed in any approximation as:

$$\text{constant}\times\{(\psi_n^*\boldsymbol{\sigma}\tau_\alpha\psi_V)\cdot\nabla\varphi_\alpha+\text{h.c.}\}$$

or as

$$\text{constant}\times\{(\psi_n^*\boldsymbol{\sigma}\psi_n)\cdot(\psi_n^*\boldsymbol{\sigma}\psi_V)+\text{h.c.}\},$$

with the constants $\gtrless\eta$. It is to be noted that gradient coupling has been assumed for the (pseudoscalar) π-meson field, the here relatively small, nucleon-velocity dependent terms also present in this interaction being neglected. The assumption of direct ($\beta\gamma_5$) coupling with use of the equivalence theorem[4] leads in the nonrelativistic approximation to the Hamiltonian density of Eq. (1) together with additional interaction terms ($\sim\varphi_\alpha^2$); these latter interaction terms, however, do not alter any of the general conclusions obtained below. It should also be emphasized that if it is ever definitely established that V particles are copiously produced in the reactions:

$$\text{nucleon}+\text{nucleon}\rightarrow\text{nucleon}+V, \tag{2a}$$

or

$$\pi\text{ meson}+\text{nucleon}\rightarrow\pi\text{ meson}+V, \tag{2b}$$

it will follow that V particles cannot exist in nuclear fragments for times as long as 10^{-12} sec. For the inverse of these production reactions (with "reabsorption" by the nucleons of the fragment of any π mesons produced, e.g., $V\rightarrow$nucleon$+\pi+\bar{\pi}$; etc.) can now correspond to the nonmesonic bound V-particle decay; this decay will occur with a mean life $\ll10^{-12}$ sec if the coupling constants in the processes of Eq. (2) are adjusted to describe copious V-particle production. On the other hand, e.g., copious "pair" production of V particles via reactions of the type

$$\text{nucleon}+\text{nucleon}\rightarrow V+V, \tag{3a}$$

or

$$\pi\text{ meson}+\text{nucleon}\rightarrow V+\text{"heavy" meson} \tag{3b}$$

is not inconsistent with the relatively long mean life of bound V particles within nuclear matter.[5] At the moment, some experimental data[6] presents evidence against copious "pair" production of V particles via reactions (3a) or (3b) so that the here-adopted interpretation[2] of the behavior of the unstable nuclear fragments remains in doubt. However, very recent Brookhaven cosmotron work[6a] indicates V-particle production via reaction (3b).

CALCULATION OF PROBABILITY OF NONMESONIC BOUND V DECAY

We now assume, that the π-meson field amplitude may be written as:

$$\varphi_\alpha=\varphi_{\alpha;\,\text{quantized}}+\varphi_{\alpha;\,\text{static}}, \tag{4}$$

where

$$(\nabla^2-\kappa_\pi^2)\varphi_{\alpha;\,\text{static}}=4\pi\frac{g}{2\kappa_n}\nabla\cdot(\psi_n^*\sigma\tau_\alpha\psi_n) \tag{5}$$

or

$$\varphi_{\alpha;\,\text{static}}(\mathbf{r})=-\frac{g}{2\kappa_n}\nabla_r\cdot\int\psi_n^*(x')\boldsymbol{\sigma}'\tau_\alpha'\psi_n(x')Y(\mathbf{r}-\mathbf{r}')dx';$$

$$\text{with } x'\equiv\mathbf{r}',\ s',\ \tau';\ Y(\mathbf{r})\equiv e^{-\kappa_\pi r}/r; \tag{6}$$

and

$$\varphi_{\alpha;\,\text{quantized}}(\mathbf{r})=\sum_{\mathbf{q}}\left[\frac{2\pi\hbar c}{(q^2+\kappa_\pi^2)^{\frac{1}{2}}}\right]^{\frac{1}{2}}\times\Omega^{-\frac{1}{2}}\{a_\alpha(\mathbf{q})e^{-i\mathbf{q}\cdot\mathbf{r}}+\text{h.c.}\} \tag{7}$$

with κ_π = inverse Compton wavelength of π meson; $\mathbf{q}$ = wave-number of meson in quantized field; $a_\alpha(\mathbf{q})$ = destruction operator for mesons of wave-number $\mathbf{q}$; and Ω = hohlraum volume. The interaction term in Eq. (1) which leads to the nonmesonic decay of a V particle is then:

$$H^{\text{inter}}=\frac{\eta}{\kappa_n+\kappa_V}(\psi_n^*\boldsymbol{\sigma}\tau_\alpha\psi_V)\cdot\nabla\varphi_{\alpha;\,\text{static}}, \tag{8}$$

with $\varphi_{\alpha;\,\text{static}}$ given by Eq. (6). Passing from the quantized-field representation of the nucleons to the corresponding configuration space representation, $\varphi_{\alpha;\,\text{static}}$ is given by

$$\varphi_{\alpha;\,\text{static}}(\mathbf{r})=-\frac{g}{2\kappa_n}\nabla_r\cdot\int\sum_{j=1}^{A-1}\Psi_f^*(x_1,\cdots,x_j,\cdots x_{A-1})\times\boldsymbol{\sigma}_j\tau_{\alpha;j}Y(\mathbf{r}-\mathbf{r}_j)\Psi_i(x_1,\cdots,x_j,\cdots x_{A-1})\times dx_1\cdots dx_j\cdots dx_{A-1}, \tag{9}$$

where Ψ_i, Ψ_f are configuration space wave functions of the initial and final states of the $A-1$ "other" nucleons in the nuclear fragment. The interaction Hamiltonian matrix element for the nonmesonic decay of the bound V particle therefore becomes (setting $\kappa_n=\kappa_V=\kappa$):

$$\mathfrak{IC}_{fi}{}^{\text{inter}}=-\frac{\eta g}{(2\kappa)^2}\int\cdots dx_j\cdots\int dx_A\times\sum_{j=1}^{A-1}(\mathfrak{B}\Psi_f(\cdots x_j\cdots)\psi_n(x_A))^*[\boldsymbol{\tau}_A\cdot\boldsymbol{\tau}_j\boldsymbol{\sigma}_A\cdot\nabla_A\boldsymbol{\sigma}_j\cdot\nabla_A\times Y(\mathbf{r}_A-\mathbf{r}_j)]\psi_V(x_A)\Psi_i(\cdots x_j\cdots)=\int\cdots dx_j\cdots\Psi_f^*\mathfrak{A}\Psi_i, \tag{10a}$$

[4] Brueckner, Gell-Mann, and Goldberger, Phys. Rev. **90**, 476 (1953); L. L. Foldy, Phys. Rev. **84**, 168 (1951); F. J. Dyson, Phys. Rev. **73**, 929 (1948).

[5] Compare A. Pais' analysis [Phys. Rev. **86**, 663 (1952)] of the relative stability of the free V particle for mesonic decay which also rules out production reactions (2a) and (2b) but permits production reactions (3a) and (3b). We must assume (as does Pais) that for the "heavy" meson in question, the reactions: nucleon+nucleon→nucleon+nucleon+"heavy" meson, or, π meson+nucleon→"heavy meson"+nucleon, are very improbable.

[6] Leighton, Wanlass, and Anderson, Phys. Rev. **89**, 148 (1953); Fretter, May, and Nakada, Phys. Rev. **89**, 168 (1953).

[6a] By Fowler, Shutt, Thorndike and Whittemore, Phys. Rev. **91**, 1287 (1953).

with

$$\mathfrak{A}\equiv-\frac{\eta g}{(2\kappa)^2}\int dx_A\sum_{j=1}^{A-1}\psi_n^*(x_A)$$

$$\times\mathfrak{B}[\boldsymbol{\tau}_A\cdot\boldsymbol{\tau}_j\boldsymbol{\sigma}_A\cdot\nabla_A\boldsymbol{\sigma}_j\cdot\nabla_A Y(\mathbf{r}_A-\mathbf{r}_j)]\psi_V(x_A). \quad (10b)$$

In Eqs. (10a) and (10b) the antisymmetrization operator $\mathfrak{B}$ has been inserted to account for the Pauli exclusion principle between the nucleon into which the V particle transforms itself and the other nucleons in the residual fragment;[7] $\psi_V(x_A)$, $\psi_n(x_A)$ indicate the initial V particle and the corresponding final nucleon wave functions in configuration space.

Equation (10a) exhibits the analogy between the nonmesonic decay of a nuclear fragment containing a bound V particle and the radiationless (nonphotonic) decay of an ordinary excited nucleus (internal conversion); in the latter case Ψ_i, Ψ_f are initial and final state orbital electronic wave functions of the atom (Ψ_f contains an electron orbital corresponding to an electron ejected from the atom), $\psi_V(x)$, $\psi_n(x)$ are initial and final nucleon orbitals for the nucleon making the transition from the ordinary excited to the non-excited nuclear state ($\mathfrak{B}$, the antisymmetrization operator, is absent), $[\eta g/(2\kappa)^2]\boldsymbol{\tau}_A\cdot\boldsymbol{\tau}_j\boldsymbol{\sigma}_A\cdot\nabla_A\boldsymbol{\sigma}_j\cdot\nabla_A Y(\mathbf{r}_A-\mathbf{r}_j)$ is replaced by $e^2/|\mathbf{r}-\mathbf{r}_j|$.

In terms of $\mathcal{H}_{fi}^{\text{inter}}$, the reciprocal mean life for nonmesonic decay is given in lowest order as:

$$\frac{1}{\tau_{\text{bound; nonmesonic}}}=\frac{2\pi}{\hbar}\sum_{\epsilon_f,\,\mathbf{k}_n,\,s_n,\,\tau_n}\left|\int\cdots dx_j\cdots\Psi_f^*\mathfrak{A}\Psi_i\right|^2$$

$$\times\delta\left(\left[\frac{\hbar^2k_n^2}{2M_n}+M_nc^2+\epsilon_f+(A-1)M_nc^2\right]\right.$$

$$\left.-[\epsilon_V+M_Vc^2+\epsilon_i+(A-1)M_nc^2]\right). \quad (11)$$

Further, we may suppose that for most of the states f of the residual fragment for which $\int\cdots dx_j\cdots\Psi_f^*\mathfrak{A}\Psi_i$ is appreciable, the corresponding energy eigenvalues ϵ_f, ϵ_i satisfy $|\epsilon_f-\epsilon_i|\ll(M_V-M_n)c^2+\epsilon_V$, i.e., for most of the states f in nonmesonic bound V-particle decay, one nucleon carries off most of the available energy (see the experimental data in reference 1). Then $\hbar^2k_n^2/2M_n\approx(M_V-M_n)c^2+\epsilon_V\approx(M_V-M_n)c^2$, and, applying the closure procedure (with respect to the Ψ_f):

$$\frac{1}{\tau_{\text{bound; nonmesonic}}}=\frac{2\pi}{\hbar}\int\frac{d\omega_n}{4\pi}\sum_{s_n,\,\tau_n}$$

$$\times\left(\int\cdots dx_j\cdots\Psi_i^*\mathfrak{A}^\dagger\mathfrak{A}\Psi_i\right)\frac{4\pi k_nM_n\Omega}{\hbar^28\pi^3}, \quad (12)$$

with

$$\hbar k_n\approx[2M_n(M_V-M_n)]^{\frac{1}{2}}c\approx4\hbar\kappa_\pi.$$

[7] The mode of action of the operator $\mathfrak{B}$ may be described via the usual permutation operators.

We may now, for the sake of simplicity and without altering the order of magnitude of the result, replace the antisymmetrization operator $\mathfrak{B}$ in Eqs. (10a) and (10b) by unity. Then $\mathfrak{A}$ may be written:

$$\mathfrak{A}\approx-\frac{\eta g}{(2\kappa)^2}\int d\boldsymbol{\rho}ds_Ad\tau_A\sum_{j=1}^{A-1}\Omega^{-\frac{1}{2}}\exp[-i\mathbf{k}_n\cdot(\mathbf{r}_j+\boldsymbol{\rho})]$$

$$\times v^*(s_n,\tau_n;s_A,\tau_A)[\boldsymbol{\tau}_A\cdot\boldsymbol{\tau}_j\boldsymbol{\sigma}_A\cdot\nabla_\rho\boldsymbol{\sigma}_j\cdot\nabla_\rho Y(\boldsymbol{\rho})]$$

$$\times u(\epsilon_V;\mathbf{r}_j+\boldsymbol{\rho})v(s_V,\tau_V;s_A,\tau_A), \quad (13)$$

where, in addition, a plane wave approximation is used for $\psi_n(x_A)$ and $\psi_V(x_A)$ is factorized into its space and spin, charge parts. Since $u(\epsilon_V;\mathbf{r}_j+\boldsymbol{\rho})$ is slowly varying over spatial regions $\approx k_n^{-1}\approx(4\kappa_\pi)^{-1}$, we may effectively drop the dependence of $u(\epsilon_V)$ on $\boldsymbol{\rho}\equiv\mathbf{r}_A-\mathbf{r}_j$. The integration over $\boldsymbol{\rho}$ is then immediate if it is noted that $\nabla_\rho\nabla_\rho$ is Hermitian and so can be taken to act on

$$\exp[-i\mathbf{k}_n\cdot(\mathbf{r}_j+\boldsymbol{\rho})];$$

we obtain:

$$\mathfrak{A}\approx\int ds_Ad\tau_Av^*(s_n,\tau_n;s_A,\tau_A)\mathfrak{D}v(s_V,\tau_V;s_A,\tau_A), \quad (14a)$$

where

$$\mathfrak{D}\equiv\frac{\eta g}{(2\kappa)^2}\frac{4\pi}{k_n^2+\kappa_\pi^2}\sum_{j=1}^{A-1}\Omega^{-\frac{1}{2}}\exp(-i\mathbf{k}_n\cdot\mathbf{r}_j)$$

$$\times u(\epsilon_V;\mathbf{r}_j)\boldsymbol{\tau}_A\cdot\boldsymbol{\tau}_j\boldsymbol{\sigma}_A\cdot\mathbf{k}_n\boldsymbol{\sigma}_j\cdot\mathbf{k}_n. \quad (14b)$$

Using Eqs. (12), (14a), and (14b), we find[7a] that

$$1/\tau_{\text{bound; nonmesonic}}$$

$$=(1/\tau_0)\int\frac{d\omega_n}{4\pi}\sum_{j,l}\int\cdots dx_j\cdots dx_l\cdots$$

$$\times\Psi_i^*(\cdots x_j\cdots x_l\cdots)\exp(-i\mathbf{k}_n\cdot\mathbf{r}_{jl})\kappa_\pi^{-3}$$

$$\times u^*(\epsilon_V;\mathbf{r}_l)u(\epsilon_V;\mathbf{r}_j)\tfrac{1}{3}\boldsymbol{\tau}_j\cdot\boldsymbol{\tau}_l\boldsymbol{\sigma}_j\cdot\boldsymbol{\sigma}_l$$

$$\times\Psi_i(\cdots x_j\cdots x_l\cdots), \quad (15)$$

where

$$1/\tau_0=\pi(k_n/\kappa_\pi)(1+\kappa_\pi^2/k_n^2)^{-2}(M_\pi/M_n)^3$$

$$\times(\eta^2/\hbar c)(g^2/\hbar c)(M_\pi c^2/\hbar).$$

The terms in Eq. (15) with $j=l$ give the major contribution to the reciprocal mean life.[8] Setting $j=l$ and defining

$$\rho(\mathbf{r}_1)\equiv\int d\tau_1ds_1dx_2\cdots dx_{A-1}|\Psi_i(x_1,\cdots,x_{A-1})|^2,$$

[7a] Remembering that with the (charge-independent) H of Eq. (1), the expectation value of any linear function of $\boldsymbol{\tau}_A$ is zero in the initial V-containing nuclear fragment.

[8] The terms in $1/\tau_{\text{bound; nonmesonic}}$ for $j\neq l$ are $\approx(A-2)10^{-2}\times$terms in $1/\tau_{\text{bound; nonmesonic}}$ for $j=l$, and so are unimportant for the A of practical interest. The small factor 10^{-2} follows from the destructive interference entailed by having $k_n\langle r_{jl}\rangle\approx k_n/\kappa_\pi\approx4\gg1$.

we obtain:

$$1/\tau_{\text{bound; nonmesonic}} = (1/\tau_0)(A-1)3 \times \int d\mathbf{r}_1 \kappa_\pi^{-3} |u(\epsilon_V; \mathbf{r}_1)|^2 \rho(\mathbf{r}_1). \quad (16a)$$

Now,

$$\rho(\mathbf{r}_1) = (A-1)^{-1}\{n(s_{\frac{1}{2}})\rho(s_{\frac{1}{2}}; \mathbf{r}_1) + n(p_{\frac{1}{2}})\rho(p_{\frac{1}{2}}; \mathbf{r}_1) + n(p_{\frac{3}{2}})\rho(p_{\frac{3}{2}}; \mathbf{r}_1) + \cdots\},$$

where $n(s_{\frac{1}{2}})$ gives the number of nucleons in the lowest $s_{\frac{1}{2}}$ orbital, etc., $(n(s_{\frac{1}{2}})=4$ for $A-1 \geqq 4$, etc.), and $\rho(s_{\frac{1}{2}}; \mathbf{r}_1)$ is the space density at $\mathbf{r}_1$ caused by a nucleon in the $s_{\frac{1}{2}}$ orbital, etc. We take oscillator functions for the orbitals, i.e., $\rho(s_{\frac{1}{2}}; \mathbf{r}_1) = (\pi^{\frac{1}{2}}\alpha)^{-3} \exp(-r_1^2/\alpha^2)$, $\rho(p; \mathbf{r}_1) = \frac{2}{3}(\pi^{\frac{1}{2}}\alpha)^{-3} \times (r_1/\alpha)^2 \exp(-r_1^2/\alpha^2)$, etc.; we also take $|u(\epsilon_V; \mathbf{r}_1)|^2 = \rho(s_{\frac{1}{2}}; \mathbf{r}_1)$ (no Pauli exclusion operative between V particle and nucleon). We then obtain

$$1/\tau_{\text{bound; nonmesonic}} = (1/\tau_0)3(2^{\frac{1}{2}}\pi^{\frac{1}{2}}\kappa_\pi\alpha)^{-3} \times \{n(s_{\frac{1}{2}}) + \tfrac{1}{2}[n(p_{\frac{1}{2}}) + n(p_{\frac{3}{2}})] + \cdots\}. \quad (16b)$$

Equation (16b) can be used for all nuclear fragments with $A-1 \leqq 16$ (e.g., for $A-1=16$; $n(s_{\frac{1}{2}})=4$, $n(p_{\frac{1}{2}})=8$, $n(p_{\frac{3}{2}})=4$). For $A-1>16$, a term of the form

$$\left\{\int \rho(s_{\frac{1}{2}}, \mathbf{r}_1)\rho(d_{\frac{1}{2}}, \mathbf{r}_1)d\mathbf{r}_1 \div \int [\rho(s_{\frac{1}{2}}, \mathbf{r}_1)]^2 d\mathbf{r}_1\right\} n(d_{\frac{1}{2}})$$

must be inserted into Eq. (16b); the ("overlap") coefficient of $n(d_{\frac{1}{2}})$ will be less than $\frac{1}{2}$, etc., and it is thus seen that for large $A-1$, $1/\tau_{\text{nonmesonic}}$ ceases to increase with increasing A.

The mean life for the mesonic decay of a free V particle may now also be calculated via the term in the interaction Hamiltonian density [Eq. (1)]:

$$\frac{\eta}{\kappa_V + \kappa_n}(\psi_n^* \boldsymbol{\sigma}\tau_\alpha \psi_V)\cdot\nabla\varphi_{\alpha;\,\text{quantized}},$$

where $\varphi_{\alpha;\,\text{quantized}}$ is given in Eq. (7). One finds:

$$1/\tau_{\text{free; mesonic}} = (q/\kappa_\pi)^2[q/(q^2+\kappa_\pi^2)^{\frac{1}{2}}] \times (M_n/M_n+M_\pi)(M_\pi/M_n)^2 \times (\eta^2/\hbar c)(M_\pi c^2/\hbar) \approx 10^{10}\ \text{sec}^{-1}, \quad (17)$$

where

$$\left[\hbar^2 q^2 \Big/ 2\left(\frac{M_\pi M_n}{M_\pi + M_n}\right)\right] = (M_V - M_n - M_\pi)c^2,$$

i.e., $q \approx (5/7)\kappa_\pi$.

Thus, from Eqs. (16b) and (17),

$$\frac{1/\tau_{\text{bound; nonmesonic}}}{1/\tau_{\text{free; mesonic}}} \approx (4/3)(g^2/\hbar c)(\kappa_\pi\alpha)^{-3} \times \{n(s_{\frac{1}{2}}) + \tfrac{1}{2}[n(p_{\frac{1}{2}}) + n(p_{\frac{3}{2}})] + \cdots\} \approx 5\{n(s_{\frac{1}{2}}) + \tfrac{1}{2}[n(p_{\frac{1}{2}}) + n(p_{\frac{3}{2}})] + \cdots\}, \quad (18)$$

where we have taken $g^2/\hbar c \approx 10$ and $\alpha \approx 2\times 10^{-13}$ cm. It is obvious that the factor "5" in Eq. (18) may actually lie between, say, 5/10 and 50, since it is proportional to the rather uncertain numerical value of g^2/α^3. Whatever the exact numerical value of this factor, however, the relative stability of V particles within nuclear matter is demonstrated on our model.

DISCUSSION

The observed mean life, τ_{observed} of nuclear fragments (of a given A) containing a V particle may now be related to the mean life for the mesonic decay of a free V particle, $\tau_{\text{free; mesonic}}$, and to the nonmesonic mean life of a bound V particle, $\tau_{\text{bound; nonmesonic}}$, by the expression:

$$1/\tau_{\text{observed}} = 1/\tau_{\text{bound; mesonic}} + 1/\tau_{\text{bound; nonmesonic}} \approx 1/\tau_{\text{free; mesonic}} + 1/\tau_{\text{bound; nonmesonic}} \approx 10^{11} - 10^{12}\ \text{sec}^{-1}, \quad (19)$$

the numerical values [from Eqs. (17), (18)] applying for $A-1 \leqq 16$. From Eqs. (18), (19), we can also relate the number of such nuclear fragments which decay with the emission of a π meson to the number in which all the "excitation energy" is imparted to nucleons. We have:

$$\frac{\text{number decaying with emission of } \pi \text{ meson}}{\text{number decaying without emission of } \pi \text{ meson}} = \left(\frac{1/\tau_{\text{bound; mesonic}}}{1/\tau_{\text{bound; nonmesonic}}}\right)\cdot P \approx \left(\frac{1/\tau_{\text{free; mesonic}}}{1/\tau_{\text{bound; nonmesonic}}}\right)\cdot P \approx \tfrac{1}{5}\{n(s_{\frac{1}{2}}) + \tfrac{1}{2}[n(p_{\frac{1}{2}}) + n(p_{\frac{3}{2}})] + \cdots\}^{-1}\cdot P, \quad (20)$$

where P is the probability of a (real) π meson emitted by the V particle within the fragment, actually emerging. (P varies between 1 and $\approx (A-1)^{-\frac{1}{3}}$ according to the magnitude of the ratio: effective mean free path for π-meson absorption within nuclear matter $\div$ effective linear dimensions of fragment.) Therefore, when enough of these nuclear fragments are detected and classified according to atomic mass number, their observed mean lives and the nature of their decay products will offer a test of the present theory. So far, one example of a nuclear fragment decaying with the actual emission of a π meson[9] and three examples of nonmesonic

[9] Of course, even in such a decay of the fragment, the kinetic energy of the emitted π meson and associated nucleon need not be exactly the Q of the decay of a free V, as a consequence of the existence of V and nucleon binding energies, and since energy-momentum exchange may transpire between the emitted π and associated nucleon, and the rest of the nucleons in the fragment, as the former leave the fragment. Such energy-momentum interchanges are equivalent in our electromagnetic analogy to a radiative de-excitation of a nucleus with the emitted photon suffering a change of energy in leaving the atom in virtue, e.g., of a Compton or Raman scattering against one of the atomic electrons.

nuclear fragment decay have been observed.[1] The existence of a π meson in the decay products rules out the possibility (at least in one of these events) that the nuclear fragments are π-mesonic atoms—on the other hand, e.g., K-mesonic atoms are obviously not necessarily inconsistent with such observations. As a consequence, a more conclusive test to distinguish between the π-mesonic (or K-mesonic) atom hypothesis and the V-particle-in-a-nuclear-fragment hypothesis would involve the appearance or non-appearance of "V deuterons" among the unstable fragments produced in high energy events. Phenomenologically, "V deuterons" would ionize and scatter like deuterons, stop, and decay with the release of ≈ 175 Mev. A "V deuteron" on the mesonic atom picture would consist of a meson in a Bohr orbit about a di-proton; the latter, however, is a nuclearly unstable structure and so could not exist as a unit for a time $\approx 10^{-12}-10^{-10}$ sec. On the V-particle hypothesis, however, a "V deuteron" would be a nuclearly stable structure of a proton bound to a neutral V and would have a mean life $\approx 10^{-10}$ sec with a branching ratio of roughly one to one[10] for the two possible eventual decay schemes,

$$\text{"}V\text{ deuteron"} \begin{cases} \rightarrow p+n+\approx 175\text{ Mev} \\ \rightarrow p+p+\pi^-+\approx 35\text{ Mev} \end{cases}$$

(or, $p+n+\pi^0+\approx 35$ Mev).

Thus a "V deuteron" which comes to rest in a photographic emulsion would be seen to give rise either to a three-pronged star containing a π meson with ≈ 35 Mev kinetic energy shared among the three prongs, or to a one-pronged star with the visible particle having a kinetic energy of $\approx 175/2$ Mev. (The one-pronged star associated with the decay into $p+n+\pi^0$ would involve a visible particle with a rather small kinetic energy.)

In those events in which a π meson is not observed as a decay product, it also remains to be conclusively demonstrated that the mesonic atom hypothesis is ruled out. The nuclear fragments of this type which have been detected so far are known to live at least as long as 10^{-12} sec. Since a π meson in the lowest Bohr orbit has a mean life for nuclear absorption much shorter than 10^{-12} sec, the only way a π-mesonic atom may be expected to live as long as 10^{-12} sec is for the π meson to be originally trapped in a Bohr orbit whose principal quantum number is greater than, say, 10. On the other hand, since the fragment is formed in a high energy event, it may be assumed that it is initially completely stripped of its electrons. Then this fragment will live a considerable fraction of its slowing-down time in an almost completely stripped state, preventing many Auger transitions of the π meson from the higher Bohr orbits to the lowest; consequently the mesonic atom mean life will be determined in first approximation by radiative transition rates.[11] Such radiative transition rates between Bohr orbits of principal quantum numbers ≈ 10 are $\approx 10^{11}$ sec^{-1} for light nuclei and vary as $Z^4\sim A^4$; the apparent mean life of mesonic atom-type nuclear fragments would therefore vary as A^{-4}. On the other hand, the mean life of the nuclear fragments on the imbedded-V-particle hypothesis would vary roughly as A^{-1} [Eqs. (18) and (19)].

We wish to thank Dr. Martin Annis for very helpful discussions. Drs. M. Goldhaber and D. C. Peaslee have kindly communicated to us preprints containing brief discussions of the possible implications of the existence of the unstable nuclear fragments.

[10] The one-to-one branching ratio follows from Eqs. (16b), (18), (20) with $\alpha\approx$"deuteron radius"$\approx 3.5\times 10^{-13}$ cm; $n(s_{\frac{1}{2}})=1$, $n(p)=0$; $P\approx 1$. We have also checked it by an explicit properly antisymmetrized calculation, *ab initio*, for the deuteron. This calculation gives $1/\tau_{\text{bound; nonmesonic}}$ for the deuteron as in Eq. (16b) but with $(2^{\frac{1}{2}}\pi^{\frac{1}{2}}\kappa_\pi\alpha)^{-3}$ replaced by $2(2^{\frac{1}{2}}\kappa_\pi)^{-3}|U(0)|^2$, where $|U(0)|^2$ is the space part of the V-deuteron internal wave function evaluated at zero distance (more strictly at distances $\lesssim(3\kappa_\pi)^{-1}$) between the V and the nucleon. Thus, taking $|U(0)|^2 \approx [(\pi^{\frac{1}{2}}3.5\times 10^{-13})^{-3}/2]$ the same result is obtained; this last value of $|U(0)|^2$ is about ten times smaller than the corresponding quantity in an ordinary deuteron governed by an attractive square-well n-p potential of range κ_π^{-1}—we remark that any actually present repulsive core in the n-p and (V-p) potential could easily account for such a factor of 10.

[11] We estimate only a small probability for such a mesonic atom to lose its orbital meson (in a path length equal to its range) as a consequence of Coulomb interactions with the nuclei of the emulsion.

Electromagnetic Effects in Two-Nucleon Systems*

STANLEY DESER†
Physics Department, Harvard University, Cambridge, Massachusetts
(Received June 17, 1953)

Corrections to the electromagnetic properties of two-nucleon systems are examined by means of the relativistic two-body equation. An effective addition to the potential is derived, which describes the properties of the system in an external electromagnetic field. In particular, the correction to the deuteron's quadrupole moment is evaluated to lowest order in the meson-nucleon coupling. The result, for pseudoscalar (pseudoscalar) symmetric theory, is $\Delta Q=-1.3\times10^{-28}(g^2/4\pi)$ cm^2.

I. INTRODUCTION

IN this paper, we shall employ the relativistic two-body equation[1-3] to consider the nucleon-recoil corrections to the electromagnetic properties of a two-nucleon system coupled by a pseudoscalar (pseudoscalar) symmetric meson field. Assuming the nucleons to be bound by the instantaneous interaction, and treating retardation effects as perturbations, we shall derive an operator whose matrix elements will describe the altered properties of the system in the presence of an external electromagnetic field.

As is well known, the magnetic moment of the deuteron is not additive, that is, $\mu_D=\mu_P+1+\mu_N-0.022$ nuclear magnetons, where μ_D, μ_P+1, μ_N are the deuteron, proton, and neutron moments, respectively. Besides the admixture of D state due to the noncentral character of the binding forces, two other sources of this nonadditivity exist. On the basis of meson theory, a nucleon's magnetic moment is (apart from the proton's spin moment) attributed to its interaction with its self-mesonic field. It is, therefore, to be expected, according to this theory, that the overlapping of the self-fields of the neutron and proton in the deuteron should produce a deviation from additivity. At present, of course, it is not even possible to account for the individual moments field-theoretically. However, one can argue that in any case these overlap corrections are not as important as those coming from that part of the currents of the bound nucleons themselves, which arises from the nucleon recoils upon exchange of virtual mesons. This second source of nonadditivity is not strictly independent of the first, nor is the degree of their interaction known. Presumably, however, since the deuteron is a loose structure, the nucleons spending most of their time outside one another's range, it may be expected that the recoil effects dominate. These, as well as relativistic kinematical corrections to the moments are included in the proper relativistic equation. In any case, as we have mentioned, the theory is at present incapable of predicting either overlap[4] or individual moments, and we shall insert the latter phenomenologically. That is, we assume that the effect of the mass operators of the particles in an external electromagnetic field, $F_{\mu\nu}$, is to yield the experimental anomalous moments, in accordance with the goals of meson theory; we shall thus be able to bypass this unresolved difficulty. Further, if as has been conjectured, the self effects are of a "strong coupling" nature, while the interaction with other particles is more legitimately to be expanded in the coupling constant, this procedure will have summed up the "strong coupling" effects into the phenomenological terms, leaving only interaction terms.

II. THE EFFECTIVE ADDITION TO THE POTENTIAL

We write the two-body equation in the presence of the field $F_{\mu\nu}$, as

$$\Big\{\Big[\gamma^{(1)}\Big(p_1-e\frac{1+\tau_3^{(1)}}{2}A(1)\Big)+M-\Big(\mu_P\frac{1+\tau_3^{(1)}}{2}+\mu_N\frac{1-\tau_3^{(1)}}{2}\Big)\frac{\sigma_{\mu\nu}^{(1)}F_{\mu\nu}^{(1)}}{2}\Big]\times\Big[\gamma^{(2)}\Big(p_2-e\frac{1+\tau_3^{(2)}}{2}A(2)\Big)+M-\Big(\mu_P\frac{1+\tau_3^{(2)}}{2}+\mu_N\frac{1-\tau_3^{(2)}}{2}\Big)\frac{\sigma_{\mu\nu}^{(2)}F_{\mu\nu}^{(2)}}{2}\Big]-I_{12}[F_{\mu\nu}]\Big\}G_{12}=1_{12},\quad(1)$$

where the isotopic spin dependence of the electromagnetic terms insures that each nucleon has the appropriate coupling to the field. We assume the unperturbed problem for zero field to have been solved, and treat the electromagnetic terms as small corrections, consistent with the smallness of e. In this fashion, we shall derive an effective addition to the two-particle potential whose matrix elements will correspond to various electromagnetic effects such as quadrupole and

* Part of a doctoral thesis submitted to Harvard University.
† National Science Foundation predoctoral fellow, now at the Institute for Advanced Study, Princeton, New Jersey.
[1] J. Schwinger, Proc. Natl. Acad. Sci. U. S. **37**, 452 (1951). We shall employ the notation of this paper.
[2] E. Saltpeter and H. A. Bethe, Phys. Rev. **84**, 1232 (1951).
[3] M. Gell-Mann and F. Low, Phys. Rev. **84**, 350 (1951).
[4] See, however, H. Miyazawa, Prog. Theoret. Phys. (Japan) **7**, 207 (1952).

photodisintegration as well as magnetic moment corrections. The choice of the form of $F_{\mu\nu}$ will determine the process involved. Thus, $F_{\mu\nu}=\mathbf{H}$ will correspond to the magnetic moment problem, $F_{\mu\nu}$ an inhomogeneous electric field to quadrupole questions, while an incoming plane wave would be used for photoprocesses. In Sec. III, we shall specifically evaluate the correction to the deuteron's quadrupole moment due to the nucleon recoil currents. Only the lowest order interaction, $I_{12}[0]=-ig^2\boldsymbol{\tau}^{(1)}\cdot\boldsymbol{\tau}^{(2)}\gamma_5{}^{(1)}\gamma_5{}^{(2)}\Delta_+$, will be included here. Further, only terms linear in $F_{\mu\nu}$ and A_μ will be kept, as we are not interested in induced moments.

In order to ascertain the effects of retardation, we shall make the assumption that the static potential,

$$I_{12}{}^{(0)}=\delta(t)\int_{-\infty}^{\infty}I_{12}dt,$$

binds the deuteron, and shall treat the retardation, $I_R\equiv I_{12}-I_{12}{}^{(0)}$ as small. Incorporating the field-dependent terms in the interaction, we may write Eq. (1) as

$$(F_1F_2-I_0-I_R-I_A-I_B)G_{12}=1_{12}, \tag{2}$$

where

$$I_0=-ig^2\gamma_5{}^{(1)}\gamma_5{}^{(2)}\boldsymbol{\tau}^{(1)}\cdot\boldsymbol{\tau}^{(2)}\delta(x_0)\int_{-\infty}^{\infty}\Delta_+(x)dx_0$$

$$=-ig^2\gamma_5{}^{(1)}\gamma_5{}^{(2)}\boldsymbol{\tau}^{(1)}\cdot\boldsymbol{\tau}^{(2)}\delta(x_0)e^{-\mu r}/4\pi r, \tag{2a}$$

$$I_A=[e_1\gamma^{(1)}A(1)+\tfrac{1}{2}\mu_1\sigma_{\mu\nu}{}^{(1)}F_{\mu\nu}(1)]F_2 +[e_2\gamma^{(2)}A(2)+\tfrac{1}{2}\mu_2\sigma_{\mu\nu}{}^{(2)}F_{\mu\nu}(2)]F_1 \equiv A_1F_2+A_2F_1, \tag{2b}$$

$$I_B=I_{12}[F_{\mu\nu}]-I_{12}[0], \tag{2c}$$

and

$$e_i=\tfrac{1}{2}(1+\tau_3{}^{(i)})e, \quad \mu_i=\tfrac{1}{2}(\mu_P+\mu_N)+\tfrac{1}{2}(\mu_P-\mu_N)\tau_3{}^{(i)}.$$

I_A is thus the additional interaction due to the individual particles' coupling to the field, while I_B is due to meson current effects. We have not given the explicit form of I_B, since, as is well known, it has zero expectation value in the ground state of self-mirror nuclei such as the deuteron and will, therefore, make no contribution to the specific effect here calculated, though it will have to be taken into account in transition problems.

In order to evaluate the effects of I_A and I_B, a Green's function perturbation theory will be employed. This will yield changes of energy of the states and the appropriate coefficients of the fields and their derivatives will then be the desired moment corrections. Calling $G_{12}{}^{(0)}$ the solution of the equation,

$$(F_1F_2-I_0)G_{12}{}^{(0)}=1_{12}, \tag{3}$$

we get, formally,

$$G_{12}-G_{12}{}^{(0)}=G_{12}{}^{(0)}I_AG_{12}{}^{(0)}+G_{12}{}^{(0)}I_BG_{12}{}^{(0)} +G_{12}{}^{(0)}I_AG_{12}{}^{(0)}I_RG_{12}{}^{(0)} +G_{12}{}^{(0)}I_RG_{12}{}^{(0)}I_AG_{12}{}^{(0)}+\cdots, \tag{4}$$

keeping terms to first order in the retardation and fields. Viewing $G_{12}(x_1x_2;x_1'x_2')$ as a bilinear expansion in wave functions, which is approximately true for $t_1=t_2\to+\infty$ and $t_1'=t_2'\to-\infty$, we can get the change of energy of a state n due to the perturbation by means of the Green's function perturbation theory. In virtue of the above remarks, the equation

$$G_{12}(\mathbf{r}_1\mathbf{r}_2,T_1;\mathbf{r}_1'\mathbf{r}_2',T_2)=(\mathbf{r}_1\mathbf{r}_2T_1|G_{12}{}^{(0)}+G_{12}{}^{(0)}I'G_{12}{}^{(0)} +G_{12}{}^{(0)}I'G_{12}{}^{(0)}I'G_{12}{}^{(0)}+\cdots|\mathbf{r}_1'\mathbf{r}_2'T_2), \tag{5}$$

where I' stands for the perturbing interaction, can be rewritten as

$$-\textstyle\sum_n\psi_n(\mathbf{r}_{12})\bar{\psi}_n(\mathbf{r}_{12}')\exp[-iE_n(T_1-T_2)]$$

$$=-\textstyle\sum_n\psi_{n0}(\mathbf{r}_{12})\bar{\psi}_{n0}(\mathbf{r}_{12}')\exp[-iE_{n0}(T_1-T_2)]$$

$$+\textstyle\sum_{n,m}\psi_{n0}(\mathbf{r}_{12})\exp(-iE_{n0}T_1)\Big[\int\bar{\psi}_{n0}(x_{12}'')$$

$$\times I'(x_{12}'',x_{12}''')\psi_{m0}(x_{12}''')(dx_{12}'')(dx_{12}''')$$

$$+\int\bar{\psi}_{n0}I'G_{12}{}^{(0)}I'\psi_{m0}\Big]\exp(iE_{m0}T_2)\psi_{m0}(\mathbf{r}_{12}'), \tag{6}$$

where ψ_{n0} are the unperturbed functions, ψ_n the corrected ones, and similarly for E_{n0} and E_n. The form of the left-hand side of Eq. (6) assumes I' to be time-independent, of course.

The diagonal terms yield, as usual, the energy shifts:

$$\exp\{-iE_n(T_1-T_2)\}$$

$$=\exp\{-i(E_{n0}+\Delta E_n)(T_1-T_2)\}$$

$$\approx\exp\{-iE_{n0}(T_1-T_2)\}[1-i\Delta E_n(T_1-T_2)]$$

$$=\exp\{-iE_{n0}(T_1-T_2)\}$$

$$\times\Big[1-\int\bar{\psi}_{n0}I'\psi_{n0}-\int\bar{\psi}_{n0}I'G_{12}{}^{(0)}I'\psi_{n0}\Big], \tag{7}$$

so that

$$\Delta E_n=\Delta E_n{}^{(1)}+\Delta E_n{}^{(2)}=-i(T_1-T_2)^{-1}\int\bar{\psi}_{n0}I'\psi_{n0}$$

$$-i(T_1-T_2)^{-1}\int\bar{\psi}_{n0}I'G_{12}{}^{(0)}I'\psi_{n0}. \tag{8}$$

In the case where the external field is time-dependent, and, therefore, the system is no longer conservative, the nondiagonal matrix elements of the right-hand side of Eq. (6) will be proportional to transition amplitudes, with the time-dependences of the wave functions and

electromagnetic field amplitudes insuring that transitions take place only between energetically possible states. As we have remarked before, the expectation value of I_B vanishes in the deuteron ground state, and only contributes to transition effects. The other term in $\Delta E_n^{(1)}$ is $-i(T_1-T_2)^{-1}\int\bar{\psi}I_A\psi$. This may be shown to be approximately

$$\Delta E_n^{(1)A}=\int\bar{\psi}_{++}(\mathbf{r})(\mathbf{r}|\gamma_0\tilde{\gamma}^{(1)}A_2+\gamma_0^{(2)}A_1|\mathbf{r}')\psi_{++}(\mathbf{r}')d\mathbf{r}d\mathbf{r}', \tag{9}$$
$$\psi_{++}=\Lambda_+^{(1)}\Lambda_+^{(2)}\psi,$$

where $\mathbf{r}\equiv\mathbf{r}_1-\mathbf{r}_2$, $\Lambda_\pm(\mathbf{p})=[E(\mathbf{p})\pm H(\mathbf{p})]/2E(\mathbf{p})$ and $\psi_{++}(\mathbf{r})$ is the positive energy part of the equal times wave function with the center-of-mass time variation removed. The approximation made is that the negative energy parts of the wave functions have negligible effect.

A_1+A_2 has been assumed time-independent, as is necessary for a ΔE to be defined.[5] This is the lowest order result, as expected; that is, to this approximation the magnetic moment is the sum of the individual ones, while the quadrupole moment also reduces to the usual expression. Equation (9) may be proven either by explicit integration in momentum space, using the relative time-dependence of solutions of problems involving only instantaneous interactions, or more simply by the equivalent coordinate space statement for $G_{12}^{(0)}$,

$$G_{12}^{(0)}(x_1x_2;x_1'x_2')$$
$$=\int G_>(x_>;\mathbf{r}_>''t_<)d\mathbf{r}_>''\gamma_0{}^>G_{12}^{(0)}(\mathbf{r}_<\mathbf{r}_>''t_<;\mathbf{r}_<''\mathbf{r}_>'t_>')\gamma_0{}^<\times d\mathbf{r}_<''G_<(\mathbf{r}_<''t_>';x_<'), \tag{10}$$

and similarly for $\psi_{n0}(x_1,x_2)$,

$$\psi_{n0}(x_1,x_2)=\int G_>(x_>,\mathbf{r}_>'t_>)\gamma_0{}^>d\mathbf{r}_>'\psi_{n0}(\mathbf{r}_>',\mathbf{r}_<,t_<). \tag{11}$$

Such a reduction to equal times quantities can only be performed by virtue of the facts that $I_{12}^{(0)}$ is an instantaneous interaction, and that only $++$ components are kept.

Henceforth we shall focus on $\Delta E_n^{(2)}$ only, keeping just the two terms linear both in I_R and $F_{\mu\nu}$. In $\Delta E_n^{(2)}$ we replace the intermediate $G_{12}^{(0)}$ by G_1G_2, the product of the free-particle propagation functions.[6] We can, therefore, write the formula for $\Delta E_n^{(2)}$ as

$$\Delta E_n^{(2)}=-i(T_1-T_2)^{-1}\int\bar{\psi}_{n0}(\mathbf{r}_>,\mathbf{r}_<'',t_>)\gamma_0{}^<\times d\mathbf{r}_<'G_<(\mathbf{r}_<''t_>,x_<)(x_1x_2|I_AG_1G_2I_R+I_RG_1G_2I_A|x_1'x_2')G_>(x_>',\mathbf{r}_>'''t_<')\gamma_0{}^>\times d\mathbf{r}_>'''\psi_{n0}(\mathbf{r}_>''',\mathbf{r}_<',t_<'), \tag{12}$$

where use has been made of Eq. (11) and the adjoint equation. Since $\psi_{n0}(\mathbf{r}_1\mathbf{r}_2t)=\psi_{n0}(\mathbf{r})\exp(iP_nX)$, we may exhibit the form of the effective addition $V_{nn}(\mathbf{r},\mathbf{r}')$ to the interparticle potential, which is defined by

$$\Delta E_n=\int\bar{\psi}_{n0}(\mathbf{r})V_{nn}(\mathbf{r},\mathbf{r}')\psi_{n0}(\mathbf{r}')d\mathbf{r}d\mathbf{r}'. \tag{13}$$

We see from Eq. (12) that

$$V_{nn}(\mathbf{r},\mathbf{r}')=\int\exp(-iP_nX)G_<(I_AG_1G_2I_R+I_RG_1G_2I_A)G_>\exp(iP_nX''), \tag{14}$$

where $X=\frac{1}{2}(x_1+x_2)$.

One can similarly define a V_{mn} for transition problems where the perturbation induces jumps between states m and n. It is to be noted that, unlike the usual potentials, V_{mn} is energy dependent, being a function of the energies of the states between which it is to be taken; this is so because in removing the center-of-mass dependence, we have partially made V into a matrix element.

Comparing Eq. (13) with Eq. (9), we see that the retardation corrections to the lowest-order operator, A_1+A_2, are given by V_{nn} for the state n. V_{nn} is in general an integral operator, as is to be expected, since the effect of the recoils is to smear out the contact between the fields. Also, in the sense that V_{nn} depends on the energy of the state, it is velocity dependent; however, in practice the binding is small and V is essentially independent of it.

We now proceed to a more explicit evaluation of $\Delta E_n^{(2)}$. In momentum space, the expression for $\Delta E_n^{(2)}$ may be written as

$$\Delta E_n^{(2)}=-i\int\bar{\psi}_{n0}(p)[I_A(p,p';P)G_1(\tfrac{1}{2}P+p')\times G_2(\tfrac{1}{2}P-p')I_R(p'-p'')]\psi_{n0}(p'')(dp)(dp')(dp'')+\text{term with } I_A \text{ and } I_R \text{ interchanged}, \tag{15}$$

where we have set:

$$\psi_n(x_1,x_2)=\exp(iP_nX)(2\pi)^{-2}\int e^{ipz}\psi_n(p)(dp), \tag{16a}$$

$$\bar{\psi}_n(x_1,x_2)=\exp(-iP_nX)(2\pi)^{-2}\times\int e^{-ipz}\bar{\psi}_n(p)(dp), \tag{16b}$$

[5] We have taken the dependence of the external field operators to be purely on the relative distance; any apparent dependence of the $F_{\mu\nu}$ on the center-of-mass displacement R does not spoil our results, since we are interested only in internal structure effects, which are essentially uncoupled to the over-all center-of-mass motion. Any operator whose expectation value will be needed can be split into a part proportional to R, which is dropped, and an R-independent one.

[6] This approximation does not lead to infrared divergences in meson theory, unlike the electrodynamic case. It may also be mentioned that the dropping of the intermediate $\bar{\psi}_{n0}\psi_{n0}$ state (n_0 represents the bound state) compensates for the omission of the $\frac{1}{2}[\Delta E^{(1)}(T_1-T_2)]^2$ term, which should properly be included in the expansion of $\exp\{-i(E_{n0}+\Delta E_n)(T_1-T_2)\}$ in Eq. (7), both terms being $=-\Sigma_{n'}(\int\bar{\psi}_{n0}I'\psi_{n0})^2$.

$$I(p,p';P)=(2\pi)^{-4}\int\exp\{-iP_n(X-X')-ipx+ip'x'\}$$
$$\times I(x_1x_2;x_1'x_2')(dx)(dx')d(X-X'), \quad (16c)$$
$$G_{(i)}(p)=(\gamma^{(i)}p+M)^{-1}, \quad (16d)$$

and $P=p_1+p_2$, $p=\frac{1}{2}(p_1-p_2)$.

We transcribe Eq. (11) into momentum space in order to exhibit the explicit relative energy dependence of $\psi_{++}(p)$:

$$\psi_{++}(p)=(P-2E)(\tfrac{1}{2}P+p_0-E)^{-1}\times(\tfrac{1}{2}P-p_0-E)(2\pi)^{-4}i\phi_{++}(\mathbf{p}). \quad (17)$$

The Fourier transforms of I_A and I_R are easily seen to be

$$I_A(p,p';P)=A_1(p-p')F_2(\tfrac{1}{2}P-p)+A_2(p-p')F_1(\tfrac{1}{2}P+p), \quad (18)$$

where $A(p)$ is the transform of $A(x)$, and

$$I_R(p,p')=(2\pi)^{-4}\mathcal{O}_{12}(p_0-p_0')^2\omega^{-2}[\omega^2-(p_0-p_0')^2]^{-1}, \quad (19)$$
$$\omega=[(\mathbf{p}-\mathbf{p}')^2+\mu^2]^{\frac{1}{2}}, \quad \mathcal{O}_{12}=-ig^2\boldsymbol{\tau}^{(1)}\cdot\boldsymbol{\tau}^{(2)}\gamma_5^{(1)}\gamma_5^{(2)}.$$

We can now perform the integrations over p_0, p_0', p_0'' corresponding to setting the times equal in coordinate language. At this stage, we have

$$\Delta E_n^{(2)}=(2\pi)^{-4}i\int\phi_{++}^*(\mathbf{p})(2\pi)^{-4}i(P-2E)$$
$$\times(\tfrac{1}{2}P+p_0-E)^{-1}(\tfrac{1}{2}P-p_0-E)^{-1}\gamma_0^{(1)}\gamma_0^{(2)}\mathcal{O}_{12}$$
$$[(\tfrac{1}{2}P+p_0''-H_1')^{-1}\gamma_0^{(1)}A_1(p'-p'')$$
$$+(\tfrac{1}{2}P-p_0''-H_2')^{-1}\gamma_0^{(2)}A_2(p'-p'')]$$
$$\times(p_0-p_0'')^2\omega_{\mathbf{p}-\mathbf{p}'}^{-2}[(p_0-p_0'')^2-\omega^2]^{-2}(2\pi)^{-4}i$$
$$\times(P-2E'')(\tfrac{1}{2}P+p_0''-E'')^{-1}(\tfrac{1}{2}P-p_0''-E'')^{-1}$$
$$\times\phi_{++}(\mathbf{p}'')(dp)(dp')(dp'')$$
$$+\text{same with } p_\mu\leftrightarrow p_\mu'', \quad A(p)\leftrightarrow A(-p), \quad \text{and}$$
$$\gamma_0^{(1)}\gamma_0^{(2)}\mathcal{O}_{12}(\tfrac{1}{2}P\pm p_0''-H_i')^{-1}\gamma_0^{(i)}A_i\rightarrow$$
$$\gamma_0^{(i)}A_i(\tfrac{1}{2}P\pm p_0-H_i')^{-1}\gamma_0^{(1)}\gamma_0^{(2)}\mathcal{O}_{12}. \quad (20)$$

To arrive at Eq. (20) we have employed the fact that $A(\Delta p)=A(\Delta\mathbf{p})\delta(\Delta p_0)$. The integrations over p_0, p_0'' are carried out with the usual prescription, assigning small negative imaginary parts to the masses. The result with $P-2E$ and $P-2E''$, the binding energies, set equal to zero is:

$$\Delta E_n^{(2)}=\tfrac{1}{2}i(2\pi)^{-3}\int\phi_{++}^*(\mathbf{p})\{\gamma_0^{(1)}\gamma_0^{(2)}\mathcal{O}_{12}\omega_{\mathbf{p}-\mathbf{p}'}^{-3}$$
$$\times[\Lambda_+^{(1)}(\mathbf{p}')\gamma_0^{(1)}A_1(\mathbf{p}'-\mathbf{p}'')$$
$$+\Lambda_+^{(2)}(\mathbf{p}')\gamma_0^{(2)}A_2(\mathbf{p}'-\mathbf{p}'')]$$
$$+[\gamma_0^{(1)}A_1(\mathbf{p}-\mathbf{p}')\Lambda_+^{(1)}(\mathbf{p}')$$
$$+\gamma_0^{(2)}A_2(\mathbf{p}-\mathbf{p}')\Lambda_+^{(2)}(\mathbf{p}')]$$
$$\times\gamma_0^{(1)}\gamma_0^{(2)}\mathcal{O}_{12}\omega_{\mathbf{p}'-\mathbf{p}''}^{-3}\}\phi_{++}(\mathbf{p}'')d\mathbf{p}d\mathbf{p}'d\mathbf{p}''. \quad (21)$$

The form of this correction in coordinate space is of interest. Recalling Eq. (13), we find that

$$V_{nn}(\mathbf{r},\mathbf{r}')=\tfrac{1}{2}i(2\pi)^{-3}\{\gamma_0^{(1)}\gamma_0^{(2)}\mathcal{O}_{12}K_0(\mu r)$$
$$\times[\Lambda_+^{(1)}(\mathbf{r}-\mathbf{r}')\gamma_0^{(1)}A_1(\mathbf{r}')+\Lambda_+^{(2)}(\mathbf{r}-\mathbf{r}')\gamma_0^{(2)}A_2(\mathbf{r}')]$$
$$+[\gamma_0^{(1)}A_1(\mathbf{r})\Lambda_+^{(1)}(\mathbf{r}-\mathbf{r}')+\gamma_0^{(2)}A_2(\mathbf{r})\Lambda_+^{(2)}(\mathbf{r}-\mathbf{r}')]$$
$$\times K_0(\mu r')\gamma_0^{(1)}\gamma_0^{(2)}\mathcal{O}_{12}\}. \quad (22)$$

V is a velocity-independent integral operator, owing to the presence of the positive energy projection operators. $K_0(\mu r)$ is the usual Hankel function, which behaves logarithmically at the origin and asymptotically as $(\mu r)^{-\frac{1}{2}}\exp(-\mu r)$. If we suitably change the form of $\mathcal{O}_{12}$ in Eq. (22), we obtain the results for various other types of meson theory; further, a similar treatment may be given for the electrodynamic case to ascertain corrections to the hydrogen and positronium moments. Although the corrections to be expected are very small, they may eventually prove worth carrying out in view of the alteration of the results for such experiments as the Lamb shift, which are obtained on the assumption of an additive moment for the system. In positronium only a quadratic Zeeman effect is expected, on account of the symmetry properties of the atom.

III. CORRECTIONS TO THE DEUTERON'S QUADRUPOLE MOMENT

In what follows, we shall employ Eq. (22) to evaluate the relativistic contributions to the quadrupole moment of the deuteron. This question is of particular interest, since the recoil term effectively yields a D-state admixture. This may be seen schematically as follows: the moment Q may be written essentially as $\langle(3z^2-r^2)R\rangle$, where R is an operator expressing the various recoil effects, say after reduction to nonrelativistic wave functions. (Equivalently, the effect of R is to bring in various l states for a given j.) That part of R which is the coefficient of $P_2(\theta)$ in an expansion will then yield a contribution, since $(3z^2-r^2)=3P_2(\theta)$ and the angular averaging selects out only this term for expectation values between S states. It will be found, however, on carrying out the evaluation, that the result cannot account for the observed Q, so that a further admixture of D state is still required (as is indeed provided by the static potential).

While a similar evaluation may be carried out for the magnetic moment terms, the number obtained

would be of far less significance since magnetic moment effects, being essentially high frequency, depend strongly on the shape of the wave function at the origin where it is least known, whereas in the quadrupole calculation the asymptotic form predominates.

Equation (21) simplifies to some extent in our quadrupole calculation. In this case,

$$\gamma_0^{(i)}A_i(\Delta\mathbf{p})=-\tfrac{1}{2}e(1+\tau_3^{(i)})A_0(\Delta\mathbf{p}). \tag{23}$$

Since we are interested in the coefficient of $\partial^2A_0(R)/\partial R_i\partial R_j$, both $A_\mu(1)$ and $A_\mu(2)$ reduce to $\frac{1}{8}r_ir_j\partial^2A_0(R)/\partial R_i\partial R_j\delta(\mathbf{p}-\mathbf{p}')$ where $\mathbf{r}$ is the operator $i\nabla_p$ acting on $\delta(p-p')$. Since, further, the $\Lambda_+^{(i)}(\mathbf{p}')$ can now act directly on either $\phi_{++}^*(\mathbf{p})$ or $\phi_{++}(\mathbf{p}'')$, we can set them equal to unity with sufficient accuracy, since $\Lambda_+(\mathbf{p})\phi_+(\mathbf{p}')=1+O(M^{-2})$. We employ the fact that the deuteron is in a charge singlet state to eliminate $\tau_3^{(1)}+\tau_3^{(2)}$ terms and to set $\langle\boldsymbol{\tau}^{(1)}\cdot\boldsymbol{\tau}^{(2)}\rangle=-3$. At this stage our result reads:

$$\Delta E^{(2)}=-\tfrac{3}{2}(2\pi)^{-2}(g^2/4\pi)eq \times\int\phi_{++}^*(\mathbf{p})[(3z'^2-r'^2)\omega_{\mathbf{p}-\mathbf{p}'}^{-3}]\gamma_0^{(1)}\gamma_0^{(2)} \times\gamma_5^{(1)}\gamma_5^{(2)}\phi_{++}(\mathbf{p}')d\mathbf{p}d\mathbf{p}', \tag{24}$$

where

$$q=\tfrac{1}{6}(3\partial^2/\partial z^2-\nabla_R^2)A_0(R).$$

In the above, the z' and r' represent derivatives with respect to p' acting on ω.

Before going on with the actual evaluation, we must reduce the ϕ's and γ's to Pauli form in the usual way. This gives $\Delta E^{(2)}$ in terms of $\phi_{++}^{(++)}$, the desired nonrelativistic wave functions,

$$\Delta E^{(2)}=\tfrac{3}{2}(2\pi)^{-3}(g^2/4\pi)(2M)^{-2}eq\int\phi_{++}^{*(++)}(\mathbf{p}) \times[(3z'^2-r'^2)\omega_{\mathbf{p}-\mathbf{p}'}^{-3}]\sigma^{(1)}\cdot(\mathbf{p}-\mathbf{p}') \times\sigma^{(2)}\cdot(\mathbf{p}-\mathbf{p}')\phi_{++}^{(++)}(\mathbf{p}')d\mathbf{p}d\mathbf{p}', \tag{25}$$

or

$$\Delta E^{(2)}=-\tfrac{3}{2}\pi^{-1}(g^2/4\pi)e(2M)^{-2}q\int\phi^*(\mathbf{r}) \times[\boldsymbol{\sigma}^{(1)}\cdot\nabla\boldsymbol{\sigma}^{(2)}\cdot\nabla(3z^2-r^2)K_0(\mu r)]\phi(\mathbf{r})d\mathbf{r}. \tag{26}$$

Calling the quantity in brackets $W(\mathbf{r})$, we may write it in the following way after carrying out the differentiations:

$$\begin{aligned}W(\mathbf{r})=&[-2K_0(x)+(4/3)xK_1(x)]+6K_0\sigma_z^{(1)}\sigma_z^{(2)}\\&+(x^2K_0-xK_1)(\cos^2\theta-\tfrac{1}{3})+(4/3)xK_1S_{12}\\&+(2xK_1+x^2K_0)(\cos^2\theta-\tfrac{1}{3})S_{12}\\&-6xK_1[\sigma_z^{(1)}\cos\theta(\sigma_z^{(2)}\cos\theta+\tfrac{1}{2}(\sigma_+^{(2)}e^{-i\varphi}\\&+\sigma_-^{(2)}e^{i\varphi})\sin\theta)]-6xK_1[\sigma^{(2)}\leftrightarrow\sigma^{(1)}],\end{aligned} \tag{27}$$

where $x=\mu r$, $S_{12}=(3\boldsymbol{\sigma}^{(1)}\cdot\mathbf{r}\boldsymbol{\sigma}^{(2)}\cdot\mathbf{r}-r^2)r^{-2}$, $\sigma_\pm=\sigma_x\pm i\sigma_y$. We can now proceed to take expectation values between ground-state wave functions, which are the usual sums of $^3S_1$ and $^3D_1$ states:[7]

$$r\phi(r)=u(r)\mathcal{Y}_{101}^1+w(r)\mathcal{Y}_{121}^1. \tag{28}$$

In a spin-triplet state, $\langle\boldsymbol{\sigma}^{(1)}\cdot\boldsymbol{\sigma}^{(2)}\rangle=1$; we also employ the following spin information:

$$-\sigma_z^{(1)}\sigma_z^{(2)}\chi_{1,m_s}=(-1)^{m_s}\chi_{1,m_s}, \tag{29}$$

where χ_{1,m_s} are the usual spin functions, and

$$\begin{gathered}\sigma_+^{(i)}\alpha(i)=\sigma_-^{(i)}\beta(i)=0,\quad\sigma_+^{(i)}\beta(i)=2\alpha(i),\\\sigma_-^{(i)}\alpha(i)=2\beta(i).\end{gathered} \tag{30}$$

α, β are the spin-up and -down functions, respectively.

$$\begin{aligned}S_{12}\mathcal{Y}_{101}^1&=(8)^{\frac{1}{2}}\mathcal{Y}_{121}^1,\\S_{12}\mathcal{Y}_{121}^1&=(8)^{\frac{1}{2}}\mathcal{Y}_{101}^1-2\mathcal{Y}_{121}^1.\end{aligned} \tag{31}$$

With this information, we can reduce all terms to radial integrals:

$$\begin{aligned}&\int\phi^*(\mathbf{r})W(\mathbf{r})\phi(\mathbf{r})d\mathbf{r}\\&=\int_0^\infty dr\{u^2[4(1+x^2/15)K_0-(32/15)xK_1]\\&\quad+(2\sqrt{2}/3)uw(xK_1-x^2K_0/5)\\&\quad+w^2[(\tfrac{2}{5}+\tfrac{1}{3}x^2)K_0-(97-36(6)^{\frac{1}{2}})xK_1/105]\}.\end{aligned} \tag{32}$$

An approximate evaluation may be made, which employs the asymptotic forms of u and w throughout; this will give a slight overestimate of the actual figures. We shall keep here only the u^2 terms, which is sufficient for our accuracy.

$$u\sim(2\alpha)^{\frac{1}{2}}e^{-\alpha r}, \tag{33}$$

where $\alpha^{-1}=4.31\times10^{-13}$ cm.

The integrals occurring in Eq. (32) may be evaluated exactly to give[8]

$$I=\int_0^\infty e^{-xy}K_0(x)dx=(1-y^2)^{-\frac{1}{2}}\cos^{-1}y. \tag{34}$$

Similarly,

$$\int_0^\infty x^2K_0(x)e^{-xy}dx=d^2I/dy^2 =(1-y^2)^{-2}[(2y^2+1)I-3y], \tag{35a}$$

$$\int_0^\infty xK_1(x)e^{-xy}dx=I+ydI/dy=(1-y^2)^{-1}(I-y). \tag{35b}$$

In our case, y is the ratio of twice the meson Compton wavelength to the radius of the deuteron, and is about 0.65. The value of ΔQ is, therefore,

$$\Delta Q=-1.3\times10^{-28}(g^2/4\pi)\text{ cm}^2. \tag{36}$$

Thus, the S-state contributions to the relativistic

[7] The notation of J. M. Blatt and V. F. Weisskopf, *Theoretical Nuclear Physics* (John Wiley and Sons, Inc., New York, 1952) is used.

[8] G. N. Watson, *Theory of Bessel Functions* (Macmillan Company, New York, 1948), p. 388.

corrections to Q are of the order of $4.8\times g^2/4\pi$ percent of the experimental value,[9] and for $g^2/4\pi$ of the order of 10, about 50 percent of the actual moment and of the opposite sign. We may also note here that the corrections coming from the reduction to Pauli functions in $\Delta E^{(1)}$ are much smaller than the effect treated above. We have

$$\Delta E_{\text{quad}}{}^{(1)}=-\tfrac{1}{4}eq\int\phi_{++}{}^{*}(3z^2-r^2)\phi_{++}d\mathbf{r}$$

$$=-\tfrac{1}{4}eq\int\phi_{\text{n.r.}}{}^{*}(3z^2-r^2)\phi_{\text{n.r.}}d\mathbf{r}$$

$$-\tfrac{1}{2}eq(2M)^{-2}\int\phi_{\text{n.r.}}{}^{*}p^2(3z^2-r^2)\phi_{\text{n.r.}}d\mathbf{r}. \quad (37)$$

[9] Compare the result of F. Villars, Phys. Rev. **86**, 476 (1952) that $\Delta Q=-3.7\times10^{-29}(g^2/4\pi)$ cm². However, the two calculations differ in several respects. First, Villars did not employ the two-body equation. Second, he used the total interaction, rather than the retarded part, to compute the recoil effects. This counts the instantaneous contribution twice, since its effect is already taken into account through use of bound-state wave functions. Third, he employed different wave functions.

Any effects from the second term on the right-hand side of Eq. (37) are of the order of $(\mu/2M)^2$ of the leading term, for $p^2/(2M)^2$ represents less than the average value of $(v/c)^2$ in the deuteron, since the r^2 in Eq. (37) tends to weight the integral toward smaller p. Thus, the second term has a ratio to the first of less than 0.5 percent. The first term is the usual nonrelativistic expression for the quadrupole moment; it must now be increased to balance the negative sign of the correction term, which implies a rise in the required percentage of D state.

Although the large size of the correction obtained may be due, in part, to the particular form of the retarded interaction employed, the present considerations indicate that, in a correct treatment of the deuteron problem, the recoil effects will contribute appreciably to a calculation of the moments.

I wish to thank Professor J. Schwinger for suggesting this topic and for many stimulating comments while the work was in progress. I should also like to thank Dr. A. Klein for several enlightening conversations.

PHYSICAL REVIEW VOLUME 92, NUMBER 6 DECEMBER 15, 1953

Field Theory of Equations with Many Masses

B. T. DARLING
24 West 87 Street, New York, New York

(Received July 10, 1953; revised manuscript received September 15, 1953)

This paper develops the field theory of many mass equations with special attention to spin ½ and the operator (1) of the author's previous paper on the irreducible volume character of events. The field is assumed to interact with the electromagnetic field which is introduced in a gauge-invariant way. General expressions for the charge-current four-vector and the symmetrical energy-momentum tensor are derived and are shown to satisfy the appropriate conservation theorems. According to a theorem of Leichter, the general solution is shown to be a superposition of nonorthogonal mass states which we designate as the root fields. Nevertheless, the physical quantities, such as the current four-vector, the energy-momentum tensor, etc., are shown to decompose into a sum over those of individual mass states but with an alternation of sign for consecutive roots. The Lagrangian takes the form of an alternating sum over the individual free-field Lagrangians for the mass states, plus the usual term $+(1/c)j_\mu A_\mu$ for the interaction with the electromagnetic field. The matter field may be quantized by treating the root fields as independent anticommuting fields. The transformation to the interaction representation is obviously unaltered and the charge and mass renormalization may be treated following Schwinger. To the order of approximation in Schwinger II these renormalizations are not affected. It would seem that these methods of quantization, together with the usual treatment of the electromagnetic field, are at variance with the manifest nonlocal nature of the theory for the irreducible volume character of events.

INTRODUCTION

THE earliest multiple-mass equations arose in an attempt to circumvent the divergence difficulties in electromagnetic theory and consisted in introducing besides the photon of zero rest mass one additional nonvanishing rest mass.[1] The first considerations of equations of infinite order with a continuous or discrete spectrum of masses were those of Blokhinzev, who developed the theory for scalar neutral fields with the view of their possible application to mesons.[2] He used Bose quantization based on a set of operators which decomposed the wave field into free fields satisfying the Schrödinger-Klein-Gordon equation for the individual masses contained in the mass spectrum of the operator. Born next introduced fields involving exponential operators $[\exp(a\Box)$, where $\Box=\sum_\lambda u_\lambda{}^2]$ in connection with his method of mass quantization.[3] The present author, in connection with a theory of fundamental length, seems to be the first to propose an infinite-order differential equation for the Dirac field. In this theory

[1] F. Bopp, Ann. Physik **38**, 345 (1940); **42**, 573 (1943); A. Landé and L. H. Thomas, Phys. Rev. **60**, 121, 514 (1940); **65**, 175 (1944); B. Podolsky *et al.*, Phys. Rev. **62**, 68 (1942); **65**, 228 (1944); Revs. Modern Phys. **20**, 40 (1948); A. Green, Phys. Rev. **72**, 628 (1947); D. Montgomery, Phys. Rev. **69**, 117 (1947).

[2] D. Blokhinzev, J. Phys. (U.S.S.R.) **11**, 72 (1947).

[3] M. Born, Revs. Modern Phys. **21**, 463 (1949).

the infinite-order operator is not arbitrary but is definitely determined as a finite displacement operator associated with the introduction of a fundamental length ω, and in terms of the operator z (defined in Sec. 1), it may be written

$$D(z)=[-2J_2(z)+\bar{k}J_1(z)]/z, \tag{1}$$

where $\bar{k}=\omega k=\beta e^2/hc$, $\beta=1.6$, and J_1 and J_2 are the Bessel's functions of order one and two, respectively.[4] Pais and Uhlenbeck made an extensive investigation into operators of the form $f(\Box)$ for neutral scalar fields, where $f(x)$ is in general an integral function of x.[5] They used essentially the same quantization procedure proposed by Blokhinzev. In one short section of their paper they also applied the quantization method to a multiple-mass free Dirac field and made a few cursory remarks (without theoretical development) on the introduction of the electromagnetic potentials. However, the main conclusions which they state for the Dirac field in the presence of the electromagnetic potentials seem to be incorrect according to the results of Sec. 4 and Sec. 6 of the present paper. Finally, Heisenberg in a number of papers[6] has investigated in a general way Lagrangians with a mass spectrum and has suggested their connection with the possible existence of a fundamental length.

In this paper we present the theory of a spin-$\frac{1}{2}$ field ψ in interaction with the electromagnetic field. The field ψ will obey the gauge-invariant equation of motion,

$$D(Z)\psi=0, \tag{2}$$

where $D(z)$ is in general a real (for real argument) integral transcendental function of z with real roots (real mass spectrum). In particular, $D(z)$ may be a polynomial. The definitions of z and Z as operators are given at the beginning of Sec. 1. We shall base the quantum electromagnetics of this field on the methods of Schwinger;[7] consequently, we shall not carry along any of the electromagnetic field formulas since they will be the same as those of Schwinger. In order to conserve space we shall not give the formulas in charge-symmetric form, since these may be easily written down following Schwinger. For the same reason we also confine ourselves to the case where D has simple roots, but the method is easily extended to repeated roots; this limitation is not invoked until Sec. 4. Furthermore, if we consider the γ matrices to be those for other spins[8] (0 and 1 especially), it will be seen that up to Sec. 6 the formulas hold good. Our main concern is with our proposed theory of fundamental length, and it is for this reason that we are primarily concerned with spin $\frac{1}{2}$, as we shall explain in a later paper.

Considered as a function of z, D may be written as an everywhere convergent series:

$$D(z)=\sum_r d_r z^r, \tag{3}$$

or, according to a theorem of Weierstrass[9], as the convergent infinite product

$$D(z)=D(0)\left[\exp\frac{D'(0)}{D(0)}\right]\prod_n\left\{\left(1-\frac{z}{z_n}\right)\exp\left(\frac{z}{z_n}\right)\right\}. \tag{4}$$

We wish at this place to emphasize the importance, to the development from Sec. 4 onward, of a theorem of Leichter (cf. Sec. 4) on the nature of the solutions for operators of the form (4). We also note that these sections contain a more general solution than the usual one to the quantum mechanical superposition problem posed by Landé[10] in his papers on his anti-Gibb's paradox principle. Landé shows that this principle necessitates a superposition principle (and hence quantization) for the description of the physical states of a system; however, although he suggests that a more general solution may be of great importance, the only solution available to him was a superposition of orthogonal states after the usual pattern in quantum theory. Contrary to this usual pattern the mass states ψ_n whose superposition constitutes the complete solution [see Eq. (25), Sec. 4] are *not* orthogonal.

The source of this divergence from the usual theory may be attributed: on the one hand, to the fact that mass, like energy but unlike momentum, angular momentum, etc., cannot be determined by an instantaneous observation (Sec. 5); on the other hand, to the fact that the mass, which is conjugate to proper time, unlike the energy, which is conjugate to time, does not enter the theory as an eigenvalue problem, but rather enters with a fixed spectrum. This property of possessing a universal spectrum is one that mass shares with such other basic observables as momentum, angular momentum, etc.

We believe that the relationships mentioned in the preceding paragraph for theories based on operators of the type of Eq. (4) are in essential agreement with the nature of mass, that they imply the existence of a universal proper-time interval, and hence that the basis (see Darling and Zilsel)[4] of the special form of the operator (1) is essentially correct.

1. HAMILTON'S INTEGRAL AND THE CHARGE-CURRENT FOUR-VECTOR

We introduce the following notation: $x_\lambda(\lambda=1\cdots4)$, $x_4=ict$, $u_\lambda=\partial/\partial x_\lambda$, A_λ the electromagnetic potentials, $a_\lambda=ieA_\lambda/hc$, $U_\lambda=u_\lambda-a_\lambda$, $U_\lambda^*=u_\lambda+a_\lambda$, $z=-2\omega\gamma^\lambda u_\lambda$,

[4] B. T. Darling, Phys. Rev. **80**, 460 (1950); B. T. Darling and P. R. Zilsel, Phys. Rev. **91**, 1252 (1953).
[5] A. Pais and G. E. Uhlenbeck, Phys. Rev. **79**, 145 (1950).
[6] W. Heisenberg, Z. Naturforsch. **5**, 251, 367, 373 (1950).
[7] J. Schwinger, Phys. Rev. **74**, 1439 (1948); **75**, 651 (1949); **76**, 790 (1949).
[8] R. J. Duffin, Phys. Rev. **54**, 1114 (1938); N. Kemmer, Proc. Roy. Soc. (London) **A173**, 91 (1939); H. J. Bhabha, Revs. Modern Phys. **21**, 451 (1949); Harish-Chandra, Phys. Rev. **71**, 793 (1947).
[9] E. T. Whittaker and G. N. Watson, *Modern Analysis* (Macmillan Company, New York, 1927), fourth edition, p. 136.
[10] A. Landé, Phys. Rev. **87**, 267 (1952); Am. J. Phys. **20**, 353 (1952); Philosophy of Science **20**, 101 (1953).

$\bar{z}=-z$, $a=2\omega\gamma^\lambda a_\lambda$, $Z=-2\omega\gamma^\lambda U_\lambda=z+a$, $\bar{Z}=2\omega\gamma^\lambda U_\lambda^*=\bar{z}+a$; the summation convention on repeated index is understood throughout, ω is a constant with the dimensions of a length, and the γ^λ are the Dirac matrices.[11]

The equation of motion (2) of the field ψ in interaction with the electromagnetic field may be obtained from the variation of φ in the Hamiltonian integral:

$$I=\int_{<S}\varphi\cdot D(Z)\psi dx. \tag{5}$$

The integral is extended throughout the region of the four-dimensional space $x(x_\lambda, \lambda=1, \cdots 4)$ interior to the closed hyper-surface S, and dx is the four-dimensional volume element. The *dot* will be used throughout this paper and is such that the operators to its right act to the right while those to its left act to the left. By varying ψ we obtain the adjoint equation:

$$\varphi D(\bar{Z})=0, \tag{6}$$

which is equivalent to the Hermitian adjoint of (2) if we set $\varphi=i\psi^*\gamma^4$, where ψ^* is the Hermitian conjugate of ψ.

We shall have much use for the following transference formula for the operator Z, namely,

$$\int_{<S}\varphi\bar{Z}^m\cdot Z^n\psi dx=-2\omega\int_S\varphi\bar{Z}^m\cdot\gamma^\lambda Z^{n-1}\psi dx^\lambda+\int_{<S}\varphi\bar{Z}^{m+1}\cdot Z^{n-1}\psi dx. \tag{7}$$

This formula can be established by a simple integration by parts: φ and ψ can be any functions, and $dx^\lambda=dx/dx_\lambda$ is a component of the element of area of the hyper-surface S.

It is well known that the charge-current four-vector may be obtained by varying the potentials in the integral I. If $\delta_A Z=-i\bar{e}\gamma^\lambda\delta A_\lambda(\bar{e}=2\omega e/hc)$, then it is easy to establish that

$$\delta_A\int_{<S}\varphi\cdot Z^r\psi dx=\sum_{k=0}^{r-1}\int_{<S}\varphi\cdot Z^k\delta_A Z Z^{r-1-k}\psi dx,$$

and by repeated application of (7) we can transfer Z^k from operating to the right, so that

$$\delta_A\int_{<S}\varphi\cdot Z^r\psi dx=\int_S+\sum_{k=0}^{r-1}\int_{<S}\varphi\bar{Z}^k\cdot\delta_A Z Z^{r-1-k}\psi dx. \tag{8}$$

The surface integral may be taken zero by proper choice of δA on S. The current j_λ is the coefficient of $-i2\omega\delta A_\lambda/hc^2$ in $\delta_A I$; hence by multiplying (8) by d_r and summing over r we have $j_\lambda=ecs_\lambda$, where

$$s_\lambda=\sum_{r=1}^{\infty}d_r\sum_{k=0}^{r-1}\varphi\bar{Z}^k\cdot\gamma^\lambda Z^{r-1-k}\psi. \tag{9}$$

We shall make frequent use of expressions of the type occurring in s_λ, so it would be valuable to introduce a special notation for them.[12] If X is any operator we define $\varphi D(\bar{Z}\cdot XZ)\psi$ by

$$\varphi D(\bar{Z}\cdot XZ)\psi=\sum_{r=1}^{\infty}d_r\sum_{k=0}^{r-1}\varphi\bar{Z}^k\cdot XZ^{r-1-k}\psi. \tag{10}$$

Thus we may write:

$$s_\lambda=\varphi D(\bar{Z}\cdot\gamma^\lambda Z)\psi.$$

Through repeated application of (7) we can prove that

$$\int_{<S}\varphi\cdot D(Z)\psi dx=\int_S\varphi D(\bar{Z}\cdot\gamma^\lambda Z)\psi dx^\lambda+\int_{<S}\varphi D(\bar{Z})\cdot\psi dx. \tag{11}$$

In virtue of (2) and (6) and the arbitrariness of S, we see that s_λ satisfies the conservation theorem

$$\partial s_\lambda/\partial x_\lambda=0. \tag{12}$$

If we replace ψ by $\delta\psi$ in (11) and choose $\delta\psi$ so that the surface integral vanishes, we establish the adjoint equation (6).

2. COMPLETE VARIATION OF HAMILTON'S INTEGRAL AND THE ENERGY-MOMENTUM TENSOR FOR THE FREE FIELD

We shall make use of the method of complete variation of Hamilton's integral where we also vary the bounding surface S in order to obtain the stress-energy tensor. This method was first applied by Weiss[13] to the case of fields, but it is a generalization of a method in particle dynamics.[14] The method of Weiss has also been applied to higher order equations by de Wet.[15]

However, since the method does not seem to be generally known or used, and since we depart slightly from Weiss, we shall make a brief sketch of it. Let L be the Lagrangian of a system of particles with generalized coordinates q (we omit subscripts and summation over them since this will be understood by the reader), and let both the final time and final position as well

[11] W. Pauli, *Handbuch der Physik* (Julius Springer, Berlin, 1933), Vol. 24, p. 220.

[12] We wish to note that these expressions could just as well be written in the product form according to Eq. (4) instead of the series form according to Eq. (3) as is done here.

[13] P. Weiss, Proc. Roy. Soc. (London) **A156**, 192 (1936); **A169**, 102 (1938).

[14] E. T. Whittaker, *Analytical Dynamics* (The Macmillan Company, New York, 1937), fourth edition, p. 246.

[15] J. S. de Wet, Proc. Cambridge Phil. Soc. **44**, 546 (1948).

as the path be varied in Hamilton's integral. Then

$$\Delta\int_0^t L dt = L(t)\Delta t + \int_0^t \delta L dt$$

$$= L(t)\Delta t + \left[\frac{\partial L}{\partial \dot q}\delta q\right]_t + \int_0^t \left[\frac{\partial L}{\partial q} - \frac{d}{dt}\frac{\partial L}{\partial \dot q}\right]\delta q dt,$$

after the usual integration by parts. The last term vanishes on account of Lagrange's equations. Examination of a graph q *vs* t will show that the variation Δq of the final position is composed of the sum of $\delta q(t)$ and $\dot q(t)\Delta t$. Hence, replacing δq by its equal $\Delta q - \dot q \Delta t$, we have

$$\Delta I = \left(L - \frac{\partial L}{\partial \dot q}\dot q\right)\Delta t + \frac{\partial L}{\partial \dot q}\Delta q = -H\Delta t + p\Delta q.$$

Thus in the total variation of I the coefficient of Δt is minus the energy, and the coefficient of Δq is the momentum.

Next consider a field ψ (which may be a multi-component field such as the Dirac or Maxwell fields) possessing a quadratic Lagrangian density $L(\psi, \psi_\lambda)$, where $\psi_\lambda = u_\lambda \psi$.[16] We consider the complete variation of $I = \int L dx$ in which both ψ and the boundary is varied. Let S be a closed hyper-surface in the four-dimensional space-time continuum and let $\Delta x_\lambda(x_\sigma)$ be an infinitesimal displacement of this surface such that each point x_λ on the surface is displaced to a point $x_\lambda + \Delta x_\lambda$. Then the complete variation $\Delta\psi$ at the boundary is the sum of $\delta\psi$ and $\Delta x_\lambda \psi_\lambda$ evaluated at the boundary. For the complete variation of I we have

$$\Delta I = \int_{<S+\Delta S} (L+\delta L)dx - \int_{<S} L dx = \int_{<\Delta S} L dx + \int_{<S} \delta L dx$$

$$= \int_S L\Delta x_\sigma dx^\sigma + \int_S \frac{\partial L}{\partial \psi_\sigma}\delta\psi dx^\sigma + \int_{<S}\left(\frac{\partial L}{\partial \psi} - \frac{\partial}{\partial x_\sigma}\frac{\partial L}{\partial \psi_\sigma}\right)\delta\psi dx,$$

where the integral throughout the volume between the two surfaces has been replaced by the equivalent surface integral, the first term of the last form for ΔI. On replacing $\delta\psi$ by $\Delta\psi - \Delta x_\lambda\psi_\lambda$ and remembering that the last integral vanishes on account of Lagrangian equations, the preceding expression may be written

$$\Delta I = \int_S \frac{\partial L}{\partial \psi_\sigma}\Delta\psi dx^\sigma - \int_S \left(\psi_\lambda \frac{\partial L}{\partial \psi_\sigma} - \delta_{\lambda\sigma} L\right)\Delta x_\lambda dx^\sigma. \quad (13)$$

From these two terms we identify

$$\pi_4 = \partial L/\partial \psi_4$$

as the canonical momentum, and

$$T_{\sigma\lambda} = \psi_\lambda \partial L/\partial\psi_\sigma - \delta_{\lambda\sigma} L$$

as the canonical energy-momentum tensor.[17]

One easily deduces the conservation theorem

$$\partial T_{\sigma\lambda}/\partial x_\sigma = 0 \quad (14)$$

from (13); for if the whole space is given a constant displacement Δx_λ, then $\Delta I = 0$ and $\Delta\psi = 0$; hence

$$\Delta x_\lambda \int_S T_{\sigma\lambda} dx^\sigma = 0.$$

Since Δx_λ is arbitrary, one sees that the surface integral must vanish. Converting the surface integral to an integral throughout the volume enclosed by S, one obtains (14) since the surface S is arbitrary.

Now putting the potentials equal to zero in (5), we have for the complete variation of I:

$$\Delta I = \int_S \varphi\cdot D(z)\psi \Delta x_\sigma dx^\sigma + \int_{<S} \varphi\cdot D(z)\delta\psi dx.$$

After an integration by parts this becomes

$$\Delta I = \int_S \varphi\cdot D(z)\psi\Delta x_\sigma dx^\sigma + \int_S \varphi D(\bar z\cdot\gamma^\sigma z)\delta\psi dx^\sigma + \int_{<S}\varphi D(\bar z)\cdot\delta\psi dx.$$

Again, replacing $\delta\psi$ by $\Delta\psi - \Delta x_\lambda\psi_\lambda$ and taking account of (6) and the fact that u_λ commutes with z, the last result may be written

$$\Delta I = \int_S \varphi D(\bar z\cdot\gamma^\sigma z)\Delta\psi dx^\sigma - \int_S [\varphi D(\bar z\cdot\gamma^\sigma u_\lambda z)\Delta x_\lambda\psi - \delta_{\lambda\sigma}\varphi\cdot D(z)\psi\Delta x_\lambda]dx^\sigma.$$

On remembering that ψ satisfies (2), and on taking Δx_λ constant, we have for the canonical stress tensor:

$$T_{\sigma\lambda} = (\hbar c/i)\varphi D(\bar z\cdot\gamma^\sigma u_\lambda z)\psi, \quad (15)$$

just as in the preceding case. One may show by direct calculation that the conservation theorem (14) for $T_{\sigma\lambda}$ is a consequence of the equations of motion, but we shall not do so at this point since we shall obtain later a more general result with the potentials included. The tensor (15) is not real and may be replaced by the real tensor

$$T_{\sigma\lambda} = (\hbar c/2i)[\varphi D(\bar z\cdot\gamma^\sigma u_\lambda z)\psi - \varphi D(\bar z u_\lambda\cdot\gamma^\sigma z)\psi]. \quad (16)$$

This last form may be obtained from the complete variation of $\int[\varphi\cdot D(z)\psi + \varphi D(\bar z)\cdot\psi]dx$. It also satisfies

[16] G. Wentzel, *Quantum Theory of Fields* (Interscience Publishers, Inc., New York, 1949), first English translation, p. 1.

[17] Reference 16, p. 9.

the conservation theorem in virtue of the equations of motion.

3. INTRODUCTION OF THE ELECTROMAGNETIC POTENTIALS AND THE SYMMETRICAL ENERGY-MOMENTUM TENSOR

A gauge-invariant stress-energy tensor may be obtained by introducing the electromagnetic potentials in the usual way. Thus we replace (16) by

$$T_{\sigma\lambda}'=(hc/2i)[\varphi D(\bar{Z}\cdot\gamma^\sigma U_\lambda Z)\psi+\varphi D(\bar{Z}\tilde{U}_\lambda\cdot\gamma^\sigma Z)\psi], \quad (17)$$

where $\tilde{U}_\lambda$ stands for $-U_\lambda^*$. For the symmetrical tensor we take

$$T_{\sigma\lambda}=\tfrac{1}{2}(T_{\sigma\lambda}'+T_{\lambda\sigma}'), \quad (18)$$

and we shall verify that

$$\partial T_{\sigma\lambda}/\partial x_\sigma=-(hc/i)s_\sigma F_{\sigma\lambda}=-es_\sigma f_{\sigma\lambda}, \quad (19)$$

where s_σ is the charge-current four-vector (9) and $F_{\sigma\lambda}=u_\sigma a_\lambda-u_\lambda a_\sigma$. $F_{\sigma\lambda}=(ie/hc)f_{\sigma\lambda}$, where $f_{\sigma\lambda}$ are the electromagnetic field strengths. The conservation theorem (19) is the result that is to be expected.[18]

In order to demonstrate (19), first recall that

$$U_\sigma U_\lambda-U_\lambda U_\sigma=F_{\lambda\sigma}. \quad (20)$$

With this, one shows that

$$ZU_\lambda=U_\lambda Z+2\omega\gamma^\sigma F_{\sigma\lambda}. \quad (21)$$

One may put asterisks on the left side of (20) and change the sign of the right side and obtain a true relation. Also a bar may be put above the Z and an asterisk on the U in (21) to obtain another valid relation. Now perform u_σ on the first term of the bracket in the expression (17) for $T_{\sigma\lambda}'$ to get

$$\sum_r d_r\sum_{k=0}^{r-1}[\varphi\bar{Z}^k u_\sigma\gamma^\sigma\cdot U_\lambda Z^{r-1-k}\psi+\varphi\bar{Z}^k\cdot\gamma^\sigma u_\sigma U_\lambda Z^{r-1-k}\psi].$$

The quantity inside this bracket may be written

$$\frac{1}{2\omega}[\varphi\bar{Z}^{k+1}\cdot U_\lambda Z^{r-1-k}\psi-\varphi\bar{Z}^k\cdot ZU_\lambda Z^{r-1-k}\psi]$$

on addition of $(a/2\omega)\varphi\bar{Z}^k\cdot U_\lambda Z^{r-1-k}\psi$ to the first term and the subtraction of the same from the second term. The Z and the U may be commuted in the second term by use of (21), so that we have

$$\frac{1}{2\omega}[\varphi\bar{Z}^{k+1}\cdot U_\lambda Z^{r-1-k}\psi-\varphi\bar{Z}^k\cdot U_\lambda Z^{r-k}\psi-2\omega(\varphi\bar{Z}^k\cdot\gamma^\sigma Z^{r-1-k}\psi)F_{\sigma\lambda}].$$

On summing over k, the first two terms telescope and we have, after multiplying by d_r and summing over r,

$$\frac{1}{2\omega}[\varphi D(\bar{Z})\cdot U_\lambda\psi-\varphi\cdot U_\lambda D(Z)\psi]-s_\sigma F_{\sigma\lambda}.$$

[18] Reference 16, p. 189.

But the quantity in brackets vanishes on account of the equations of motion. Similar operations may be performed on the second term in the bracket of (17); consequently $T_{\sigma\lambda}'$ satisfies Eq. (19).

Next we show that $T_{\sigma\lambda}'-T_{\lambda\sigma}'$ has vanishing divergence. Now

$$(2i/hc)(T_{\sigma\lambda}'-T_{\lambda\sigma}')=\varphi D[\bar{Z}\cdot(\gamma^\sigma U_\lambda-\gamma^\lambda U_\sigma)Z]\psi-\varphi D[\bar{Z}(\gamma^\sigma U_\lambda^*-\gamma^\lambda U_\sigma^*)\cdot Z]\psi.$$

But the right side is equal to

$$\frac{1}{2}\frac{\partial}{\partial x_\mu}\varphi D[\bar{Z}\cdot(\gamma^\mu\gamma^\lambda\gamma^\sigma+\gamma^\lambda\gamma^\sigma\gamma^\mu)Z]\psi.$$

To prove this, one first proves by integration by parts that

$$\int_{<S}\varphi\cdot\gamma^\lambda\gamma^\sigma D(Z)\psi dx=-2\omega\int_S\varphi D(\bar{Z}\cdot\gamma^\mu\gamma^\lambda\gamma^\sigma Z)\psi dx^\mu+4\omega\int_{<S}\varphi D[\bar{Z}\cdot(\gamma^\sigma U_\lambda-\gamma^\lambda U_\sigma)Z]\psi dx+\int_{<S}\varphi D(\bar{Z})\cdot\gamma^\lambda\gamma^\sigma\psi dx,$$

in virtue of the relation

$$\gamma^\lambda\gamma^\sigma Z=Z\gamma^\lambda\gamma^\sigma+4\omega(\gamma^\sigma U_\lambda-\gamma^\lambda U_\sigma);$$

and

$$\int_{<S}\varphi D(\bar{Z})\cdot\gamma^\lambda\gamma^\sigma\psi dx=2\omega\int_S\varphi D(\bar{Z}\cdot\gamma^\lambda\gamma^\sigma\gamma^\mu Z)\psi dx^\mu+4\omega\int_{<S}\varphi D[\bar{Z}(\gamma^\sigma U_\mu^*-\gamma^\mu U_\sigma^*)\cdot Z]\psi dx+\int_{<S}\varphi\gamma^\lambda\gamma^\sigma\cdot D(Z)\psi dx,$$

in virtue of the relation

$$\bar{Z}\gamma^\lambda\gamma^\sigma=\gamma^\lambda\gamma^\sigma\bar{Z}+4\omega(\gamma^\sigma U_\lambda^*-\gamma^\lambda U_\sigma^*).$$

The surface integrals may be transformed by the divergence theorem to integrals throughout the volume. After using (2) and (6) and on subtracting the latter result from the former and remembering that the surface S is arbitrary, we obtain the above-stated expression for the difference of the tensors. We are interested in the nondiagonal terms $\sigma\neq\lambda$, in which case $\gamma^\mu\gamma^\lambda\gamma^\sigma+\gamma^\lambda\gamma^\sigma\gamma^\mu$ vanishes if $\mu=\sigma$ or λ, and is $2\gamma^\lambda\gamma^\sigma\gamma^\mu$ if $\mu\neq\sigma$, $\mu\neq\lambda$; these may be shown from the commutation properties of the γ matrices. Finally,

$$\frac{2i}{hc}\frac{\partial}{\partial x_\sigma}(T_{\sigma\lambda}'-T_{\lambda\sigma}')=\sum_{\substack{\mu\neq\sigma\\ \mu\neq\lambda}}\frac{\partial^2}{\partial x_\sigma\partial x_\mu}\varphi D(\bar{Z}\gamma^\lambda\gamma^\sigma\gamma^\mu Z)\psi$$

vanishes because of the anticommutativity of γ^σ and γ^μ.[19] This completes the demonstration of (19).

4. ROOT FIELDS AND THE DECOMPOSITION OF THE PRECEDING PHYSICAL QUANTITIES

Let z_n be a root of the equation

$$D(z_n)=0. \tag{22}$$

For the sake of simplicity in the formulas we assume that all of these roots are simple. This is true for the infinite-order operator (1) of the theory of fundamental length which holds our primary interest. The case in which the roots are not simple may be treated by a direct extension of the method. Let ψ_n and $\varphi_n=i\psi_n^*\gamma^4$ be the *root fields* defined through the equations of motion

$$(Z-z_n)\psi_n=0, \tag{23}$$

$$\varphi_n(\bar{Z}-z_n)=0. \tag{24}$$

Then these root fields are also solutions of (2) and (6) in virtue of (22).

We now make use of a general theorem due to Leichter.[20] For the special case in which $D(Z)$, whether of finite or of infinite order, has no exponential factors and has simple roots, his theorem states that the general solution of (2) is a superposition of the root fields. We write the solution in the form

$$\psi=\sum_n \frac{1}{|b_n|^{\frac{1}{2}}}\psi_n, \tag{25}$$

where b_n are constants to be chosen at our convenience later. Furthermore, the solution has the same form when exponential factors of the type in (4) are present, provided the equation

$$e^{AZ}\psi=0 \tag{26}$$

has only the solution $\psi\equiv 0$; A is a constant. He also proves that $\psi\equiv 0$ is the only solution of (26), provided the A_λ and ψ satisfy certain conditions of analyticity. Thus, for the operator (1) of the theory of fundamental length, the assumption that the A_λ and ψ are analytic except for isolated singularities in a strip obtained by surrounding each point of the space-time continuum by a region of radius 2ω in the complex space allows one to conclude that the exponential operators have no nonvanishing solutions and that the general solution is of the form (25).

Assuming then that ψ has the form (25) we may obtain the individual ψ_n. Let us define the operator $D_n(Z)$ by

$$D_n(Z)=D(Z)/(Z-z_n). \tag{27}$$

Then, if $z_m\neq z_n$, we have

$$D_n(z_m)=0,$$

whereas

$$D_n(z_n)=D'(z_n),$$

where the prime denotes the derivative of $D(z)$ with respect to z. The $D'(z_n)$ are nonvanishing real numbers (in virtue of the reality of the roots) and we choose our b_n so that $b_n=D'(z_n)$. Then,

$$D_n(Z)\psi=(b_n/|b_n|^{\frac{1}{2}})\psi_n=\beta_n|b_n|^{\frac{1}{2}}\psi_n, \tag{28}$$

where $\beta_n=$ sign of b_n.

The Lagrangian density decomposes into a sum over those for the root fields

$$\varphi\cdot D(Z)\psi=\sum_n \beta_n\varphi_n\cdot(Z-z_n)\psi_n;$$

for the left side may be written

$$\sum_n \frac{1}{|b_n|^{\frac{1}{2}}}\varphi_n\cdot D(Z)\psi=\sum_n \frac{1}{|b_n|^{\frac{1}{2}}}\varphi_n\cdot(Z-z_n)D_n(Z)\psi$$

$$=\sum_n \beta_n\varphi_n\cdot(Z-z_n)\psi_n$$

by use of (28).

The current s_λ and the stress tensor $T_{\sigma\lambda}$ also decompose, namely

$$s_\lambda=\sum_n \beta_n s_{n;\lambda}, \quad T_{\sigma\lambda}=\sum_n \beta_n T_{n;\sigma\lambda},$$

where

$$s_{n;\lambda}\equiv\varphi_n\gamma^\lambda\psi_n$$

and

$$T_{n;\sigma\lambda}\equiv(\hbar c/4i)\varphi_n[\cdot\gamma^\sigma U_\lambda+\bar{U}_\lambda\gamma^\sigma\cdot+\cdot\gamma^\lambda U_\sigma+\bar{U}_\sigma\gamma^\lambda\cdot]\psi_n$$

are just the usual expressions for the current and stress tensor for the field ψ_n.[21]

To prove these results, consider

$$\varphi D(\bar{Z}\cdot XZ)\psi$$

$$=\sum_{r,m,n}\frac{d_r}{|b_nb_m|^{\frac{1}{2}}}\sum_{k=0}^{r-1}\varphi_m\bar{Z}^k\cdot XZ^{r-1-k}\psi_n$$

$$=\sum_{r,m,n}\frac{d_r}{|b_nb_m|^{\frac{1}{2}}}\left(\sum_{k=0}^{r-1}z_m{}^k z_n{}^{r-1-k}\right)\varphi_m\cdot X\psi_n$$

$$=\sum_{r,n}\frac{rd_r z_n{}^{r-1}}{|b_n|}\varphi_n\cdot X\psi_n+\sum_{r,m\neq n}\frac{d_r}{|b_nb_m|^{\frac{1}{2}}}\frac{z_n{}^r-z_m{}^r}{z_n-z_m}\varphi_m\cdot X\psi_n$$

$$=\sum_n\frac{1}{|b_n|}D'(z_n)\varphi_n\cdot X\psi_n$$

$$+\sum_{m\neq n}\frac{1}{|b_nb_m|^{\frac{1}{2}}}\frac{D(z_n)-D(z_m)}{z_n-z_m}\varphi_m\cdot X\psi_n$$

$$=\sum_n\beta_n\varphi_n\cdot X\psi_n.$$

5. THE INITIAL VALUE PROBLEM

If the order p of (2) is finite, then at the time t_0 one may take the kth derivatives with respect to x_4, $\psi^k(t_0)$, $(k=0,\cdots p-1)$ to be given functions of $\mathbf{x}$, and then by

[19] Reference 11, p. 235.

[20] M. Leichter, doctoral thesis, Ohio State University, 1952 (unpublished). This work will be submitted for publication in the near future.

[21] Reference 16, p. 189.

use of Taylor's expansion and the differential equation obtain the solution for all time. But, alternatively, we may specify the initial values of the root fields $\psi_n(t_0)$ $(n=1, \cdots p)$, and these will determine the solution $\sum \psi_n$ (we drop the factors b_n for convenience) for all later time, since the root fields satisfy first-order equations. Inasmuch as $\psi_n{}^k(t_0)$ may be expressed in terms of $\psi_n(t_0)$ through Eqs. (23), the two modes of setting the initial conditions are equivalent, since we may solve the set of p equations:

$$\psi^k(t_0)=\psi_1{}^k+\cdots+\psi_p{}^k,$$

$k=1, \cdots p-1$, for the functions $\psi_n(t_0)(n=1, \cdots p)$.

The situation is different if the order is infinite. If we give $\psi^k(t_0)$ $(k=1, \cdots \infty)$, then Taylor's theorem determines $\psi(t)$ without any use of the differential equation. If $\psi(t)$ is to be a solution of the equation, then the quantities $\psi^k(t_0)$ cannot be arbitrary but must satisfy a complicated condition determined by the infinite-order differential equation, a condition involving not simply the time t_0 but essentially all times in view of the unspecified dependence of the electromagnetic potentials on the time. This procedure is both impractical and unphysical. The physical requirements necessitate knowing what masses are initially present and their initial states; consequently, the appropriate procedure in the infinite-order case is to specify initially the root fields $\psi_n(t_0)$ $(n=1, \cdots \infty)$. It is doubtful even in the finite case whether any physical meaning could be given to the procedure of specifying the $\psi^k(t_0)$.

Apparently the correct way to specify the initial data is to specify the individual root fields. But here we have a contradiction between the mathematical specification of initial values at a time t_0 and the physical facts. For unlike other quantum observables, such as the momentum, etc., the mass (like energy) is conjugate to a time, the proper time. Consequently, the determination of mass requires observing the system over a certain period of time. To clarify the situation, suppose we know $\psi(\mathbf{x}, t_0)=f(\mathbf{x})$ at the time t_0 [for example $f(\mathbf{x})$ might be an eigenstate of angular momentum prepared by an observation of the angular momentum], then one might pick any value of n and set $\psi_n(t_0)=f(\mathbf{x})$, or one might break $f(\mathbf{x})$ up in quite arbitrary ways and take the parts for the $\psi_n(t_0)$. How are we to determine which of the various possibilities is the correct one in a given situation? In order to answer this question, we do not have to catalog all the possible ways in which we might know the mass, such as by deflections in weak static electric and magnetic fields or by the spectral or chemical data that one uses to select, say, hydrogen gas when one wants to produce a proton beam, etc.; for these methods all seem to be equivalent from the individual particle aspect of the theory[4] to the minimum requirement of making the particle interact with an electromagnetic field of some kind for a sufficient time for us to be able to classify the associated field with respect to the individual root-field equation (23) it obeys. Once the determination of the masses has been made, it will remain unchanged for all time so long as interaction takes place only through the agency of the electromagnetic field introduced with the gauge-invariant substitution $z\rightarrow Z$. This stability of the mass is a consequence of the decomposition demonstrated in the preceding section.

6. QUANTIZATION: CHARGE AND MASS RENORMALIZATION

The decomposition of the Lagrangian derived in Sec. 4 shows that the quantization scheme for the free fields,

$$\{\psi_\alpha{}^n(x),\ \varphi_\beta{}^m(x')\}=\delta_{nm}\beta_m S_{\alpha\beta}{}^m(x-x'),$$

with all other anticommutators vanishing, is consistent with the equations of motion. The appearance of the factors β_m is necessary not only because they appear in the Lagrangian but also in order that the energy-momentum four-vector represent a displacement operator and in order that the interaction representation with $H=-(1/c)j_\mu(x)A_\mu(x)$ reduce the equations of motion of ψ^n to free-field equations. If $\bar{\psi}^m$ has its usual significance, where

$$\{\psi_\alpha{}^n(x),\ \bar{\psi}_\beta{}^m(x')\}=(1/i)\delta_{nm}S_{\alpha\beta}{}^m(x-x'),$$

we see that $\varphi^m=i\beta_m\bar{\psi}^m$ and hence that φ is not simply $i\bar{\psi}$.

Indeed,

$$\varphi=\sum_n \frac{1}{|b_n|^{\frac{1}{2}}}\varphi_n=i\sum_n \frac{\beta_n}{|b_n|^{\frac{1}{2}}}\bar{\psi}^n,$$

so that in terms of the ψ^n and $\bar{\psi}^n$ the factors β_n drop out entirely from all expressions. It is therefore clear that to the order of approximation in Schwinger II the charge and mass renormalization will not be affected, and that the vacuum is defined by

$$\psi^{n(+)}\Psi_0=0,\ \bar{\psi}^{n(+)}\Psi_0=0;$$

i.e., the positive frequency states are empty and the negative frequency states are full throughout.

From what has been said, it would seem that the quantization used by Pais and Uhlenbeck is inconsistent with their Lagrangian as well as the interaction representation, and that there is no interchange of the roles of particle and antiparticle for negative β_n.

Finally we wish to remark that the preceding results, based on the usual methods of quantization and conventional electromagnetics in which the β_n drop out of the theory and in which the charge and mass renormalization are unaffected (to the first order), seem to be at variance with the manifest nonlocal nature of the theory for the irreducible volume character of events. We intend to consider these questions later from a quite different approach.

Equivalent Mass and Other Effects of a Nonlocal Electromagnetic Field in Interaction with a Constant E, H Field*

CHRISTOPHER GREGORY
University of Hawaii, Honolulu, Hawaii
(Received April 3, 1953)

Some consequences of the interaction of a nonlocal photon with a constant E, H field are considered. The interaction is shown to vanish in the limit of local fields independently of the magnitude of the coupling constant g, so that results obtained could be traced directly to the assumption of a nonlocal field. An exact solution for the nonlocal field is obtained as a sum of a nonlocal plane waves containing the four-vector q_μ. It is shown that this four-vector in conjunction with the coupling constant plays two roles. In one it is involved in the expression for an electric dipole moment: $g\mathbf{q}$ and in the other in an expression for a magnetic dipole with moment: $g/2(\mathbf{q}\times\mathbf{k})/|k|$, where $\mathbf{k}/|k|$ is the propagation vector. This identification gives significance to the C numbers, q_μ appearing in the theory. The equivalent mass μ, averaged over orientations of $\mathbf{q}$ for which $\mu^2>0$, turns out to be of order $4.0\times10^{-12}(\gamma B/\lambda)^{\frac{1}{2}}$ electron masses, where γ is the number of Bohr magnetons; $|g\mathbf{q}|mc/he$, λ is the wavelength, and B is an upper limit to the magnitude of the external field in Gaussian units. An order of magnitude measure of the optical properties of the region containing the constant E, H field which affects the nonlocal photon is $|n-1|=3.2\times10^{-4}(\lambda\gamma B)$, where n is an upper limit to the index of refraction. For pronounced measurable effects, say, $|n-1|\approx0.1$ implies that $\langle\mu\rangle/m$ attains a value of $10^{-10}/\lambda$ electron mass.

INTRODUCTION

THE purpose of the following report is to study some consequences of the introduction of the concept of operator or nonlocal fields on current field theories. This investigation is motivated by the result of a novel feature of a variation principle for nonlocal fields[1] whereby the existence of a divergence-less four vector is shown. It was later shown that it is possible for a (real) Hermitian nonlocal field to give rise to an operator for the net number of quanta with either positive or negative eigenvalues.[2] This property suggests that even a real field in operator field theory has associated with it a four-current vector. Only for complex fields is it possible to construct four-current vectors with the customary properties for local fields in present theories. Since even real nonlocal fields imply the existence of particles with charge, one would expect that such a field could be in interaction with external local electric and magnetic fields. The structure of the interaction must be chosen in such a way as to be nonexistent in the limit of the local field case. This would imply that even a real nonlocal field has the potentiality of manifesting properties of nonreal local fields in interaction with an external E, H field. For the sake of simplicity the case for a constant external E, H field is considered, while the nonlocal field is taken to be of the electromagnetic type.

One way to introduce an interaction of the type contemplated above is to replace the displacement operator p_μ by the operator

$$P_\mu=p_\mu-(g/c)A_\mu^e, \tag{1}$$

where g is a coupling constant, c the velocity of light, and A_μ^e the external local vector potential. Such a replacement assures us that the commutator expression

$$[P_\mu, U]_-=[p_\mu, U]_--(g/c)[A_\mu^e, U]_-, \tag{2}$$

is devoid of terms containing the coupling constant g if U is a local function. As a consequence of the definition of P_μ, we find that the P_μ's do not commute among themselves:

$$\begin{aligned}[P_\mu, P_\nu]_-&=-(g/c)[p_\mu, A_\mu^e]_--(g/c)[A_\mu^e, p_\nu]\\&=-(hg/ic)F_{\mu\nu}^e,\end{aligned} \tag{3}$$

where $F_{\mu\nu}^e$ is the assymmetric external electromagnetic field strength tensor.

THE FIELD EQUATIONS

The field equations for our nonlocal electromagnetic field in interaction with a given external local E, H field may be obtained in the same manner as the commutator equations for an electromagnetic field in an earlier piece of work[3] by merely replacing the p_μ by P_μ in the commutator equations for Maxwell's equations to obtain

$$(i/h)[P_\mu, F^{\mu\nu}]=0, \tag{4}$$

$$(i/h)[P_\mu, F_{\nu\sigma}]+(i/h)[P_\nu, F_{\sigma\mu}]+(i/h)[P_\sigma, F_{\mu\nu}]=0, \tag{5}$$

where

$$F_{\mu\nu}\equiv(i/h)[P_\mu, A_\nu]-(i/h)[P_\nu, A_\mu]. \tag{6}$$

The foregoing equations reduce to the ordinary equations if the A's are local independently of the value assigned to the coupling constant.

Now let us consider the case where the A_μ^e are the vector potentials for a constant local external E, H field. For such a case the A^e's may be written as

$$A_\mu^e=c_{\mu\alpha}\chi^\alpha, \tag{7}$$

* Supported by the U. S. Office of Naval Research.
[1] C. Gregory, Phys. Rev. **78**, 449 (1950).
[2] C. Gregory, Phys. Rev. **89**, 1199 (1953).
[3] C. Gregory, Phys. Rev. **78**, 67 (1950).

where the $c_{\mu\alpha}$'s are c numbers depending upon the external field strengths E and H, and the χ's are the space-time operators. The proper identification of the $c_{\mu\nu}$'s which lead to the constant E, H field follow upon making the identication

$$\begin{aligned} &c_{\mu 0}=0, \quad \mu=0, 1, 2, 3; \\ &c_{0s}=F_{0s}{}^{e}, \quad s=1, 2, 3; \\ &c_{rs}=-c_{sr}=\tfrac{1}{2}F_{rs}{}^{e}, \quad r, s=1, 2, 3; \end{aligned} \tag{8}$$

where the F^e's are the constant external field strengths. For the case under consideration here we conclude that $[P_\mu, P_\nu]$ is a c number, as we see from (3). This observation coupled with (4) enable us to write

$$[P_\mu, [P^\mu, A^\nu]]=0, \tag{9}$$

providing we take as our supplementary condition on the A's

$$[P_\mu, A^\mu]=0. \tag{10}$$

Now let us seek a solution of (9) of the form of a nonlocal plane wave defined by

$$A_{q,k}{}^{\mu}\equiv a^\mu \exp(iq^\nu p_\nu/h) \exp(ik_\nu\chi^\nu/h), \tag{11}$$

where a^μ, q^ν, and k_ν are c numbers. The introduction of (11) in (9), (10), and (5) leads to the equations restricting the above c numbers if we make the observation that

$$\begin{aligned} &(i/h)[P_\mu, \exp(iq^\nu p_\nu/h) \exp(ik_\nu\chi^\nu/h)] \\ &\quad=[k_\mu+(g/c)c_{\mu\alpha}q^\alpha] \exp(iq^\nu p_\nu/h) \exp(ik_\nu\chi^\nu/h), \end{aligned} \tag{12}$$

which is a consequence of our fundamental commutation relationship:

$$[\chi^\mu, p_\mu]=ih\delta_\nu{}^\mu. \tag{13}$$

The result (12) implies from (10) and (9) the following relationships existing between the c numbers a^μ, q^ν, and k_ν:

$$K_\mu\equiv[k_\mu+(g/c)c_{\mu\alpha}q^\alpha], \tag{14}$$

$$a^\mu K_\mu=0, \tag{15}$$

$$K^\mu K_\mu=0. \tag{16}$$

From (6) we may write

$$F_{\mu\nu}=f_{\mu\nu} \exp(iq^\nu p_\nu/h) \exp(ik_\nu\chi^\nu/h), \tag{17}$$

where the c numbers $f_{\mu\nu}$ are given by

$$f_{\mu\nu}=K_\mu a_\nu-K_\nu a_\mu. \tag{18}$$

These results enable us to state as for the classical treatment of Maxwell's equation that upon identifying $F_{\mu\nu}$ according to the scheme

$$\begin{aligned} &F_{s0}=-F_{0s}=-cE_s, \quad s=1, 2, 3; \\ &-F_{21}=F_{12}=-H_3, \quad -F_{31}=F_{13}=H_2, \\ &F_{23}=-F_{32}=-H_1, \end{aligned} \tag{19}$$

the vector K_s $(s=1, 2, 3)$ is perpendicular to the vector E_s and H_s. Furthermore, upon using the scheme (19) with the F's replaced by f's and E_s by e_s and H_s by h_s we find that the vector e_s is perpendicular to h_s, all of which is in complete agreement with the properties of a plane-wave solution of Maxwell's equations, with the exception of the finding that the ordinary propagation four-vector k_μ is to be replaced by K_μ given by (14). The general solution of (9) will of course correspond to a sum over q and k subject to the restrictions (14), (15), and (16). The coefficient of a^μ in (9) forms a set of basic functions aside from a normalization factor.[4]

MASS EQUIVALENT OF NONLOCAL PHOTO

The results that we have obtained would enable us to consider the polarization effects of the nonlocal electromagnetic field in interaction with the constant external E^e, H^e field. It would be more interesting, however, to consider the consequences of the relationship (16). If we define the equivalent mass μ through the equation

$$\mu c^4=k_0{}^2-c^2|k|^2, \tag{20}$$

then (20) in conjunction with (14) and (16) implies that

$$\mu c^4=b_0{}^2+c^2\mathbf{b}\cdot\mathbf{b}+2c^2\mathbf{b}\cdot\mathbf{k}\pm 2cb_0|\mathbf{b}+\mathbf{k}|, \tag{21}$$

where

$$\begin{aligned} &b_0\equiv(g/c)c_{0\alpha}q^\alpha=-g\mathbf{E}^e\cdot\mathbf{q}, \\ &\mathbf{b}\equiv(g/2c)(\mathbf{H}^e\times\mathbf{q})=-(g/2c)(\mathbf{q}\times\mathbf{H}^e), \end{aligned} \tag{22}$$

in vector notation.

Equation (21), together with (20), or direct appeal to (14) yields

$$k_0=-b_0\pm|\mathbf{k}+\mathbf{b}|, \tag{23}$$

which may be interpreted to indicate that when a nonlocal photon is in an electric field, there is a contribution to the energy of the nature of a dipole term, namely $-b_0=g\mathbf{E}^e\cdot\mathbf{q}$, so that we may attribute to a nonlocal photon the electric dipole moment $g\mathbf{q}$. This identification has as a consequence given physical significance to the c numbers, q appearing in our expression for a nonlocal plane wave. It would appear then that a nonlocal photon would be subject to deflections in an inhomogeneous electric field as a consequence of its electric dipole moment and the massive properties which it would possess by virtue of (21) in the presence of a constant electric field, and consequently also in an inhomogeneous one. To consider the effect of our H^e field, we may expand k_0 given by (23) in a power series in the H^e's. Upon retaining terms which contain H^e to the first power and making use of (22), we find

$$k_0\approx g\mathbf{E}^2\cdot\mathbf{q}\pm(g/2)\mathbf{H}^e\cdot(\mathbf{q}\times\mathbf{k})/|k|\pm c|k|. \tag{24}$$

If we take $k_0>0$ in the absence of the E, H field, (24) indicates that our nonlocal photon possesses a magnetic moment: $(g/2)(\mathbf{q}\times\mathbf{k})/|k|$. Thus, we would also expect

[4] C. Gregory, Proc. Natl. Acad. Sci. U. S. **37**, 706 (1951).

a nonlocal photon to be subject to a deflection in an inhomogeneous magnetic field. We note that the dipole moment and magnetic moment are perpendicular to one another while the propagation direction $\mathbf{k}/|k|$ is perpendicular to the magnetic moment vector.

In general we will not be able to say that $\mu^2>0$ unless certain conditions are satisfied. We shall investigate the situation on the basis of the expression (24) for k_0, which provides us with first-order correction terms in terms of the first powers of our external E, H field. Upon introducing (24) into (20) we obtain to the desired order [the upper signs in (24) are taken],

$$\mu^2c^4\approx c|k|g[2\mathbf{E}^e\cdot\mathbf{q}+H^e\cdot(\mathbf{q}\times\mathbf{k})/|k|],$$
$$\approx c|k|g\mathbf{q}\cdot[2\mathbf{E}+\mathbf{k}\times\mathbf{H}^e/|k|]. \quad (26)$$

Consequently, in order that $\mu^2>0$, the dipole moment vector $g\mathbf{q}$ must be oriented in such a way as to be intermediate to those positions corresponding to the extreme cases of perpendicularity and isodirectionality to the vector $\mathbf{F}$ defined by

$$\mathbf{F}\equiv c|k|[2\mathbf{E}^e+\mathbf{k}\times\mathbf{H}^e/|k|]. \quad (27)$$

In the former case μc^2 would attain its smallest value zero, while in the latter it would have its maximum value, namely $(|g\mathbf{q}||F|)^{\frac{1}{2}}$. If we average μ over those directions for which $\mu^2>0$ we obtain

$$\langle\mu\rangle=(2/3c^2)(|g\mathbf{q}||\mathbf{F}|)^{\frac{1}{2}}$$
$$=(2/3c^2)(c|g||\mathbf{q}||\mathbf{k}||2\mathbf{E}^e+\mathbf{k}\times\mathbf{H}^e/|k||)^{\frac{1}{2}}, \quad (28)$$

which would provide us with an estimate of the equivalent mass of a nonlocal photon in an external E, H field.

Let us now make an estimate as to the order of magnitude of $\langle\mu\rangle$. Now, upon making the substitution

$$|\mathbf{F}|/c|k|=|2\mathbf{E}^e+\mathbf{k}\times\mathbf{H}^e/|k||, \quad (29)$$

in (28) to indicate the magnitude of the external effects of the field as measured in Gaussian units, we find that

$$\langle\mu\rangle/m=4/3(\pi\beta/mc^2)^{\frac{1}{2}}|g/e|^{\frac{1}{2}}|q/\lambda|^{\frac{1}{2}}(|\mathbf{F}|/|k|c)^{\frac{1}{2}}, \quad (30)$$

where e is the electron charge, m its mass, β the magnetic moment of a Bohr magneton, and λ the wavelength of our nonlocal photon. However, we must have, on the basis of the assumption of the validity of the expansion which lead to (24),

$$2\pi|g/e||q/\lambda|(\lambda/\lambda_e)^2(\beta/mc^2)(|\mathbf{F}|/|k|c)<1, \quad (31)$$

where λ_e denotes the Compton wavelength and we have assumed the rough numerical equivalence between $|\mathbf{F}|$ and $c|\mathbf{k}\times\mathbf{H}^e|$. If we take $\lambda\approx10^{-13}$, $g\approx e$, and $|\mathbf{F}|/|k|c\approx10^4$ gauss, formula (31) implies that, if $q<10\,000$ cm, the expansion (24) is valid. These results would show that, if we take q to be the order of magnitude of a Compton wavelength, $\langle\mu\rangle\approx10^{-3}$ electronic mass which would correspond ~500 ev. On the other hand, if q is of the order of an electronic radius, $\langle\mu\rangle\approx3\times10^{-5}$ electronic mass $\circ\sim15$ ev.

EQUIVALENT "INDEX OF REFRACTION" OF E, H REGION

In order to gain a rough idea as to what could be expected to occur when a nonlocal photon impinges upon a region possessing an E, H field, we may assign to the region an equivalent index of refraction:

$$n\equiv c|\mathbf{k}|/k_0\approx1-g\mathbf{q}\cdot\mathbf{F}/2c^2|k|^2. \quad (32)$$

Equation (32) is obtained by making an analogy with optical theory and using our expressions for k_0 given by (24), which in turn may be expressed in terms of $\mathbf{F}$ defined in (27). Equation (32) indicates that if $\mu^2>0$, the "wave velocity" would be greater in a region containing the E, H fields than in one devoid of such fields. Moreover, we note a dependence of n upon the direction of propagation relative to the orientation of our external E, H field and upon the wavelength which enters into our expression (32) in such a way as to show that one can expect n to deviate from unity in a manner directly proportional to the wavelength. If $\mu^2<0$, then $n>1$, which implies that the "wave velocity" is greater in a region not containing the E, H field. In this case also, the region would possess anisotropic properties, with n deviating from unity linearly with increasing wavelength.

SUMMARY

In order to indicate conveniently the order of magnitude of the effects implied by the existence of a nonlocal photon in interaction with a constant external E, H field, let us define

$$(\mathbf{q}\cdot\mathbf{F})/c|\mathbf{k}||\mathbf{q}|\equiv B, \quad (33)$$

as measured in Gaussian units and put

$$g|\mathbf{q}|/4\pi\beta\equiv\gamma, \quad (34)$$

which is the number of Bohr magnetons ($\beta\equiv he/4\pi mc$) expressed in terms of our coupling constant and the vector $\mathbf{q}$, which appears in our nonlocal plane wave (11). The inequality (31) takes on the form

$$\lambda\gamma B_{\max}<2mc^2/e, \quad (35)$$

where $B_{\max}$ denotes the value attained by B in (33) when $\mathbf{q}$ is perpendicular to $\mathbf{F}$ defined in (27). λ is the wavelength of our nonlocal photon, m the electronic mass, and e the charge. Introducing (33) and (34) into (30) and (32) we obtain

$$\langle\mu\rangle/m=(8\pi\beta/3c)(me)^{-\frac{1}{2}}(\gamma B/\lambda)^{\frac{1}{2}}, \quad (36)$$

$$|n-1|=(e/2mc^2)\lambda\gamma B. \quad (37)$$

(35), (36), and (37) become, upon introduction of the numerical values of e, m, c, and β,

$$1.7\times10^3>\lambda\gamma B_{\max},$$
$$\langle\mu\rangle/m=4.0\times10^{-12}(\gamma B/\lambda)^{\frac{1}{2}}, \quad (38)$$
$$|n-1|=3.2\times10^{-4}(\lambda\gamma B).$$

Equation (38) shows that, for pronounced measurable

optical effects, say $|n-1|\approx 0.1$, some of the nonlocal photons would have to possess an equivalent magnetic moment of the order $\gamma=300/\lambda B$ Bohr magnetons. If such were the case, then $\langle\mu\rangle/m$ would attain a value of order $10^{-10}/\lambda$ electron mass.

These effects, of course, would vanish in the limiting case of local fields: $q_s=0$, independently of the value assigned to the coupling constant g. Consequently, it would appear that nonlocal field theories could be examined in the light of experiments which are implied in this work, if we assume that our procedure for introducing an interaction is correct and that the photons existing in nature are nonlocal. In the same way, we can consider other nonlocal "particles," either "neutral" or "charged," in interaction with a constant E, H field of the type considered here.

PHYSICAL REVIEW VOLUME 92, NUMBER 6 DECEMBER 15, 1953

The Physical Basis of Gravitation

ROBERT L. KIRKWOOD
1015 Second Street, Santa Monica, California
(Received August 10, 1953)

It is shown that Einstein's principle of equivalence permits the gravitational field to be interpreted as an ether flow, and the experimentally verifiable results of the relativistic gravitational theory are deduced directly from elementary physical principles by the use of this interpretation.

I. INTRODUCTION

ALTHOUGH much of the formalism of Einstein's general theory of relativity has become widely acc pted, no method has yet been proposed by which the fundamental results of the theory can be deduced directly from elementary physical principles. It is the object of this paper to show how this can be done, although the resulting interpretation of the theory differs considerably from the one that is usually given. In particular, the postulate of special relativity will be kept separate from the gravitational theory so that the physical foundations of the special and general theories will not be confused.

In both classical physics and the special theory of relativity it is assumed that it is possible to introduce a measure of time and a measure of distance in such a way that identical physical processes will always occur in identical intervals of time and space. These measures are assumed to be defined everywhere at all instants of time, and the measured three-dimensional space is assumed to be Euclidean. With these assumptions, it is possible to describe space and time by a system of three Cartesian coordinates and a single universal time variable. In classical physics it is assumed that there is only one way to define such a time variable, except for trivial changes in origin and scale, while in the theory of special relativity is is assumed that there are many ways of introducing this variable and that all physical laws will take the same form when expressed in terms of any one of these many possible variables. There is considerable evidence to indicate that the theory of special relativity is very nearly correct, but for the purposes of this discussion it will suffice to assume that *there is at least one way of introducing a time variable, t, such that identical physical processes will always occur in identical time intervals.* If there are several completely equivalent variables of this type, then any one of them may be used, and this particular one will be denoted by t.

The three Cartesian coordinates that are introduced to describe space can be varying in any manner with time, but it is natural to let them move in such a way that the laws of nature take their simplest form when expressed in these coordinates. It is obvious that not all states of motion are equally good in this respect. For example, it is known that the motion of the planets about the sun is far more simply described in coordinates whose origin is fixed on the sun and which are rotating with the stars than in coordinates that are fixed on the earth. In fact, classical mechanics indicates the existence of a definite set of primary inertial systems in which the laws of motion of massive bodies take their simplest form. There is nothing in classical mechanics that makes it possible to distinguish between these systems, but the laws controlling the propagation of light suggest such a distinction. It is observed that light travels with a finite velocity and that there is just one frame of reference relative to which this velocity is the same in all directions. If the time variable has already been completely defined, then this preferred state of motion can be determined directly from measurements of the one-way velocity of light. If there is more than one way of introducing time, then there will be more than one way of determining this state of motion, but it will suffice here to assume that a particular time variable has already been introduced and hence that *a single preferred state of motion in which the velocity of light is the same in all directions is determined at each point in space.* Furthermore, it will be assumed that this preferred state of motion is also a primary

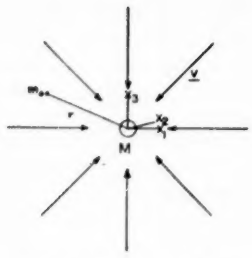

FIG. 1. The spherically symmetric gravitational field $[|\mathbf{v}| = (2KM/r)^{\frac{1}{2}}]$.

inertial system of mechanics, an assumption which is suggested by its simplicity and which at least is not contradicted by any known experimental facts. In this way the basic ideas of space, time, and motion are postulated.

There are only two results of the special theory of relativity that will be needed in this discussion. The first is that a radiating atom which is moving with velocity $\mathbf{v}_0$ relative to the preferred state of motion radiates at a frequency ν given by

$$\nu = \nu_0(1-\mathbf{v}_0^2/c^2)^{\frac{1}{2}},$$

where ν_0 is the frequency at which it radiates when at rest. The second is that the mass of a moving body varies with its velocity $\mathbf{v}_0$ relative to the preferred state of motion according to the law

$$m = m_0/(1-\mathbf{v}_0^2/c^2)^{\frac{1}{2}},$$

where m_0 is its mass when $\mathbf{v}_0=0$. Both of these conclusions have been verified directly by experiment, and, if desired, they can be considered to be only approximate statements of experimental facts. The complete and rigorous postulate of special relativity is not at all essential to the present discussion.

II. THE PRINCIPLE OF EQUIVALENCE

Now let a time variable t and a set of three Cartesian coordinates x_i $(i=1, 2, 3)$ be introduced, and let the preferred state of motion relative to these coordinates be described by a velocity field $\mathbf{v}$. In both classical physics and in special relativity it is assumed that it is possible to choose the motion of the coordinates in such a way that $\mathbf{v}=0$ everywhere. For example, Newton assumed that this would be the case if the coordinates were fixed relative to the fixed stars. However, consider for a moment the effect that is created if the chosen coordinates are moving in such a way that the preferred state of motion is accelerating past them. If a massive body is to be held at rest in such coordinates, a force must be applied to it, since the body will then be accelerating relative to the primary inertial system. Obviously, this force will be proportional to the inertial mass of the body. Hence, if it is assumed that an apparent force field is opposing this force and thereby holding the body in equilibrium, then this force field will also be proportional to the inertial mass of the body. Force fields that have this property are known to exist in nature in the form of gravitational fields, and this fact suggests that gravitational fields may be nothing more than an acceleration of the preferred state of motion past the observer's reference system. Furthermore, Einstein's principle of equivalence states that this equivalence of a gravitational field to an appropriately chosen motion applies not only to mechanics but to all other fields of physics as well. In mechanics, this principle has been tested and shown to hold to a high degree of accuracy, and in other fields of physics there are at least no known contradictions to it. Hence it will be accepted here, and *the gravitational field will be assumed to represent only an acceleration of the velocity field which describes the motion of the preferred frame of reference relative to the observer*. With this interpretation of gravity, it is apparent that it will not generally be possible to choose the coordinates in such a way that this velocity field vanishes everywhere.

The physical picture of this velocity field is so strongly suggestive of the flow of a fluid medium that the field $\mathbf{v}$ will hereafter be called the ether velocity. However, it should be emphasized that for the present purposes the ether is not endowed with any more substantial properties than just this velocity field.

As an example, the velocity field $\mathbf{v}$ about a spherically symmetric mass M will now be determined from Newton's inverse square law of gravitational atrraction. Let the coordinates x_i be fixed on the mass M and assume that $\mathbf{v}\to 0$ at great distances from M (see Fig. 1). Now let a small test mass m_0 be placed at a distance r from M. When r is very large, let the velocity of m_0 be very small, so that m_0 is fixed in the preferred frame of reference. Then, if no forces except the apparent gravitational force act on m_0, it will remain at rest in the preferred frame of reference, and hence its velocity relative to the coordinates x_i will always be $\mathbf{v}$, the ether velocity. But it is known from Newton's law of gravitational attraction that m_0 will move radially inward with a velocity determined by the energy integral:

$$\tfrac{1}{2}m_0\mathbf{v}^2 - KMm_0/r = 0,$$

where K is the gravitational constant. From this it follows that $\mathbf{v}$ is radially inward and has the radial component

$$v_r = -(2KM/r)^{\frac{1}{2}}. \tag{1}$$

This velocity field will then describe the spherically symmetric Newtonian gravitational field.

One result that follows immediately from this interpretation of the gravitational field is the gravitational red shift of spectral lines. Consider a radiating atom that is fixed on the surface of a star of radius R and mass M. Let the reference coordinates be fixed on the star so that the ether velocity is that given by Eq. (1). Since the atom is fixed on the star, it will be moving

with a velocity $-\mathbf{v}$ relative to the ether, where

$$|-\mathbf{v}| = (2KM/R)^{\frac{1}{2}}.$$

If its frequency of oscillation when it is at rest in the ether is ν_0, then its actual frequency of oscillation when moving relative to the ether with velocity $-\mathbf{v}$ is

$$\nu = \nu_0(1-\mathbf{v}^2/c^2)^{\frac{1}{2}} = \nu_0(1-2KM/c^2R)^{\frac{1}{2}}.$$

Hence the actual frequency is slightly less than it would be if the atom were at rest in the ether. This shift of spectral lines toward the red has been detected experimentally.

It might be thought that this motion of the ether past the source of radiation would cause an additional Doppler shift that would overshadow the effect just described. However, it is easily shown that this is not the case if the point of observation of the light ray is at rest relative to the star, for then the positions of the radiating atom and of the observer and the velocity field that lies between them do not change with time, and hence any sinusoidal wave crest that traverses the space between the source and the observer does so under exactly the same conditions as any other. Since the time variable is assumed to have been defined so that identical physical processes occur in equal time intervals, it follows that the time required for any one wave crest to travel this path will be the same as that required by any other. Hence the time interval separating two successive crests at the source is the same as it is at the observer, and the observed frequency is the same as the radiated frequency. Of course, if either the source or the observer had been moving relative to these coordinates, the same argument would lead to the normal Doppler shift of the frequency.

III. THE MOTION OF A RAY OF LIGHT

The next problem will be to find the orbit of a ray of light passing through an arbitrary gravitational field. The solution of this problem will be based on the following physical assumptions:

(1) Huygens' principle is assumed to hold.

(2) The velocity of light relative to the ether is assumed to be the same in all directions and is a known function, although it will not necessarily be assumed to be the same at all points.

Essentially, Huygens' principle says that each point on any surface that intersects a light wave acts as the source of a secondary spherical wavelet and that the field beyond this surface is just the resultant field produced by all these secondary wavelets. If wave crests from a given source are propagated in this way along a group of adjacent paths and arrive simultaneously at a common point, they will add constructively, and this point will be on the main lobe of the diffraction pattern produced by the source. Let x_i $(i=1, 2, 3)$ be a set of Cartesian coordinates, and let P_1 and P_2 be two points on the orbit of a ray of light (see Fig. 2). Let C_1 be a

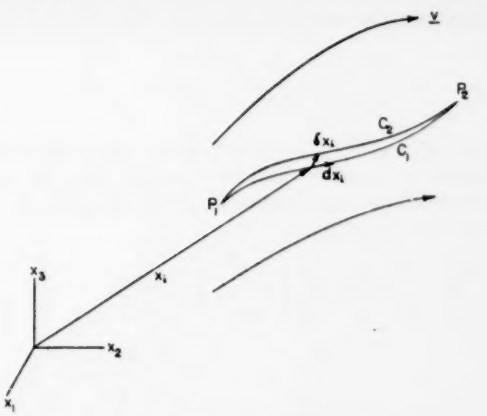

FIG. 2. The path of a ray of light in an arbitrary gravitational field.

curve connecting P_1 and P_2. It is desired to find the conditions that must be satisfied along C_1 in order that it may be the path of the ray.

If the velocity of light relative to the ether is c, then the wavelets along C_1 will move at a speed such that

$$\sum_{i=1}^{3}(\dot{x}_i - v_i)^2 = c^2, \tag{2}$$

where $\dot{x}_i = dx_i/dt$. Now let a small vector δx_i be defined at each point of C_1 such that $\delta x_i = 0$ at P_1 and P_2. Then $x_i + \delta x_i$ traces out a curve C_2 between P_1 and P_2. The secondary wavelets along C_2 must move at a speed such that Eq. (2) is also satisfied along C_2. Finally, define δt such that if a wavelet leaves P_1 along C_1 and arrives at x_i at time t, then the same wavelet leaving P_1 along C_2 will arrive at $x_i + \delta x_i$ at time $t + \delta t$. Then $\delta t = 0$ at P_1, and by Huygens' principle, the condition that C_1 should be the path of the ray is that $\delta t = 0$ at P_2 for all δx_i.

Now let

$$I(\dot{x}_i, x_i, t) = \sum_{i=1}^{3}(\dot{x}_i - v_i)^2 - c^2.$$

Then the conditions just described are the $I=0$ along C_1 and C_2, which is the same as saying that I and $I+\delta I$ vanish along C_1, or that I and δI both vanish on C_1, where

$$\delta I = \frac{\partial I}{\partial \dot{x}_i}\delta\dot{x}_i + \frac{\partial I}{\partial x_i}\delta x_i + \frac{\partial I}{\partial t}\delta t.$$

Here a repeated index is summed from 1 to 3. Furthermore, by the formula for differentiation of a quotient

$$\delta\dot{x}_i = \delta\frac{dx_i}{dt} = \frac{dt\delta dx_i - dx_i\delta dt}{dt^2} = \frac{d\delta x_i}{dt} - \dot{x}_i\frac{d\delta t}{dt}.$$

Hence δt is determined along C_1 by the condition that

$$\delta I=\frac{\partial I}{\partial \dot{x}_i}\frac{d\delta x_i}{dt}-\frac{\partial I}{\partial \dot{x}_i}\dot{x}_i\frac{d\delta t}{dt}+\frac{\partial I}{\partial x_i}\delta x_i+\frac{\partial I}{\partial t}\delta t=0.$$

When C_1 and δx_i are given, this is a first-order linear differential equation which can be solved for δt. Multiply this equation by an integrating factor $R(t)$, and it can be put in the form

$$-\frac{d}{dt}\left(R\frac{\partial I}{\partial \dot{x}_i}\dot{x}_i\delta t\right)+\left[\frac{d}{dt}\left(R\frac{\partial I}{\partial \dot{x}_i}\dot{x}_i\right)+R\frac{\partial I}{\partial t}\right]\delta t+R\frac{\partial I}{\partial \dot{x}_i}\frac{d\delta x_i}{dt}+R\frac{\partial I}{\partial x_i}\delta x_i=0.$$

Let R be chosen to be a solution of the equation

$$\frac{d}{dt}\left(R\frac{\partial I}{\partial \dot{x}_i}\dot{x}_i\right)+R\frac{\partial I}{\partial t}=0. \tag{3}$$

Since this equation does not contain δx_i, R will not depend on δx_i. Then the equation for δt becomes integrable and gives the result that

$$R\frac{\partial I}{\partial \dot{x}_i}\dot{x}_i\delta t\Big|_{P_1}^{P_2}=\int_{P_1}^{P_2}\left[R\frac{\partial I}{\partial \dot{x}_i}\frac{d\delta x_i}{dt}+R\frac{\partial I}{\partial x_i}\delta x_i\right]dt.$$

Since $\delta t=0$ at P_1 and the condition that C_1 is the path of the ray is that $\delta t=0$ at P_2 for all δx_i, this equation demands that the condition for the path of the ray is that

$$\int_{P_1}^{P_2}\left[R\frac{\partial I}{\partial \dot{x}_i}\frac{d\delta x_i}{dt}+R\frac{\partial I}{\partial x_i}\delta x_i\right]dt=0,$$

for all δx_i. Integrate once by parts, remembering that $\delta x_i=0$ at P_1 and P_2, and this becomes

$$\int_{P_1}^{P_2}\left[\frac{d}{dt}\left(R\frac{\partial I}{\partial \dot{x}_i}\right)-R\frac{\partial I}{\partial x_i}\right]\delta x_i dt=0.$$

Since R does not depend on δx_i, the condition that this should vanish for all δx_i is just that

$$\frac{d}{dt}\left(R\frac{\partial I}{\partial \dot{x}_i}\right)-R\frac{\partial I}{\partial x_i}=0. \tag{4}$$

Thus Eqs. (2), (3), and (4) are the equations that determine the path of a ray of light. However, if Eq. (4) is multiplied by $\dot{x}_i$ and summed over i, it is easily put in the form

$$\frac{d}{dt}\left(R\frac{\partial I}{\partial \dot{x}_i}\dot{x}_i\right)+R\frac{\partial I}{\partial t}-R\frac{dI}{dt}=0.$$

The last term vanishes by Eq. (2), and hence Eq. (3) has been derived from Eqs. (2) and (4), so that only Eqs. (2) and (4) need to be satisfied. If the expression for I is substituted in these equations, the final equations for the path of the light ray in vector notation are

$$\frac{d}{dt}\left[R\left(\frac{d\mathbf{r}}{dt}-\mathbf{v}\right)\right]+R(\nabla\mathbf{v})\cdot\left(\frac{d\mathbf{r}}{dt}-\mathbf{v}\right)+Rc\nabla c=0,$$

$$\left(\frac{d\mathbf{r}}{dt}-\mathbf{v}\right)^2=c^2.$$

For solving problems it is often convenient to express these equations in generalized coordinates. To do this it is only necessary to note that if x_i and R are considered to be independent variables, and if

$$L(\dot{x}_i, x_i, R, t)=RI,$$

then Eqs. (2) and (4) are just the Euler-Lagrange equations associated with the Lagrangian function L. Thus, if L is expressed in arbitrary coordinates, the equations of motion of a ray of light can be written immediately in these coordinates and known theorems concerning Lagrangian equations can be applied. For example, to find the orbit of a ray passing through a spherically symmetric Newtonian field, it is convenient to introduce polar coordinates r and θ, which lie in the plane of the ray and which are centered about the attracting mass M. Then

$$L=R[(\dot{r}-v_r)^2+r^2\dot{\theta}^2-c^2],$$

where

$$v_r=-(2KM/r)^{\frac{1}{2}}.$$

It will be assumed that c is a constant. Then L does not depend explicitly on t or on θ, and hence the system has energy and angular momentum integrals:

$$h=\frac{\partial L}{\partial \dot{r}}\dot{r}+\frac{\partial L}{\partial \dot{\theta}}\dot{\theta}-L=R[\dot{r}^2-v_r^2+r^2\dot{\theta}^2+c^2],$$

$$k=\frac{\partial L}{\partial \dot{\theta}}=2Rr^2\dot{\theta}.$$

If R is eliminated, these give

$$h=\frac{k}{2r^2\dot{\theta}}(\dot{r}^2+r^2\dot{\theta}^2+c^2-v_r^2).$$

These equations replace the Euler-Lagrange equations for r and θ, and the equation for R is

$$(\dot{r}-v_r)^2+r^2\dot{\theta}^2=c^2.$$

Let $r'=dr/d\theta=\dot{r}/\dot{\theta}$. Then $\dot{r}$ can be replaced in these last two equations by $r'\dot{\theta}$, and they can be solved to eliminate $\dot{\theta}$. The result is the equation of the orbit:

$$r'^2-\frac{h^2}{k^2c^2}r^4+r^2\left(1-\frac{v_r^2}{c^2}\right)=0.$$

Now substitute the expression for v_r and let $u=1/r$, and this becomes

$$\left(\frac{du}{d\theta}\right)^2=\frac{h^2}{k^2c^2}-u^2+\frac{2KM}{c^2}u^3.$$

This equation was first obtained by Einstein and is known to predict a deflection of a ray of light which passes a massive body. This deflection has been detected experimentally.

IV. THE MOTION OF A PARTICLE IN A GRAVITATIONAL FIELD

The next problem is that of determining the motion of a mass point through a gravitational field. Let x_i be an arbitrary system of coordinates relative to which the ether velocity is $\mathbf{v}$, and let $\mathbf{r}$ be a position vector whose end point is fixed in the ether, that is, $d\mathbf{r}/dt=\mathbf{v}$. It is known from classical hydrodynamics that the motion of a fluid at any point can be analyzed into a deformation and a pure rotation of angular velocity $\boldsymbol{\omega}=\frac{1}{2}\nabla\times\mathbf{v}$. Therefore, let x_i' be a second system of Cartesian coordinates whose origin is always at the position $\mathbf{r}$ and whose angular velocity relative to the coordinates x_i is equal to $\frac{1}{2}\nabla\times\mathbf{v}$ evaluated at the point $\mathbf{r}$ (see Fig. 3). Then if it should happen that the ether is not being deformed in a region about the point $\mathbf{r}$, the ether velocity relative to the coordinates x_i' will vanish identically in this region, and the coordinates x_i' will be a primary inertial system of classical mechanics throughout this region. In such a system of coordinates, the equation of motion of a particle is

$$\mathbf{F}=\frac{d}{dt}\left(m\frac{d\mathbf{r}_0'}{dt}\right),$$

where $\mathbf{r}_0'$ is the position vector of the particle relative to the origin of the coordinates x_i', m is the mass of the particle, and $\mathbf{F}$ is the external force acting on it. This equation will now be written relative to the coordinates x_i. Let $d'\mathbf{a}$ represent the change of any vector $\mathbf{a}$ relative to the coordinates x_i' in time dt. Then, relative to the coordinates x_i, $\mathbf{a}$ will change by an additional amount $(\boldsymbol{\omega}dt)\times\mathbf{a}$ in time dt because the coordinates x_i' are rotating with angular velocity $\boldsymbol{\omega}$ relative to x_i. Thus the vector $\mathbf{a}$ will change relative to the coordinates x_i by an amount

$$d\mathbf{a}=d'\mathbf{a}+\boldsymbol{\omega}\times\mathbf{a}dt.$$

Hence, the time rate of change of $\mathbf{a}$ relative to x_i' is given by

$$\frac{d'\mathbf{a}}{dt}=\frac{d\mathbf{a}}{dt}-\boldsymbol{\omega}\times\mathbf{a}. \tag{5}$$

With the use of this notation, the equation of motion

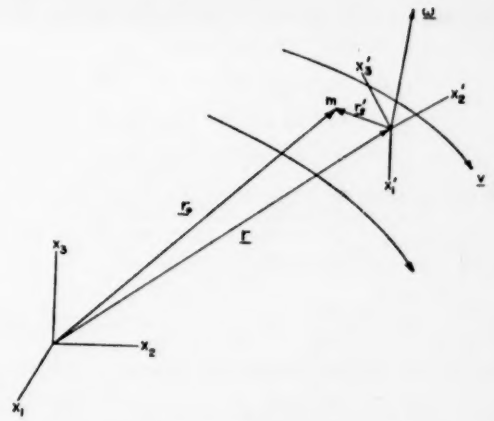

FIG. 3. Diagram for analyzing the motion of a mass point in an arbitrary gravitational field.

relative to the coordinates x_i becomes

$$\mathbf{F}=\frac{d'}{dt}\left[m\frac{d'}{dt}(\mathbf{r}_0-\mathbf{r})\right],$$

where $\mathbf{r}_0$ is the position vector of m relative to the coordinates x_i. In deriving this equation, it has been assumed that there is a region about the point $\mathbf{r}$ in which the ether is not deforming, and that $\mathbf{r}_0$ lies in this region. It will now be assumed that, even if no such region exists, this equation is still correct at the particular instant when $\mathbf{r}_0=\mathbf{r}$. Essentially, this assumes that the deformation of the ether about the point $\mathbf{r}$ has no effect on a mass which is located at $\mathbf{r}$ at the instant under consideration. The only test of this assumption is to show that it leads to a correct description of the motion of a particle in a gravitational field. With this assumption, the general equation of motion of a particle is

$$\mathbf{F}=\left\{\frac{d'}{dt}\left[m\frac{d'}{dt}(\mathbf{r}_0-\mathbf{r})\right]\right\}_{\mathbf{r}_0=\mathbf{r}}.$$

Now apply Eq. (5) twice, expand all the derivatives, and set $\mathbf{r}_0=\mathbf{r}$; this becomes

$$\mathbf{F}=m\left(\frac{d^2\mathbf{r}_0}{dt^2}-\frac{d^2\mathbf{r}}{dt^2}\right)+\frac{dm}{dt}\left(\frac{d\mathbf{r}_0}{dt}-\frac{d\mathbf{r}}{dt}\right)$$
$$-2m\boldsymbol{\omega}\times\left(\frac{d\mathbf{r}_0}{dt}-\frac{d\mathbf{r}}{dt}\right).$$

Let $\mathbf{v}_0$ be the velocity of the particle and $\mathbf{v}$ the velocity of the ether relative to the coordinates x_i. Then $d^2\mathbf{r}/dt^2$ is the time derivative of $\mathbf{v}$ evaluated at a point moving with velocity $\mathbf{v}$. However, it is customary in particle dynamics to define the total time derivative of any function of x_i and t to be the time derivative evaluated

at a point moving with the particle velocity $\mathbf{v}_0$. This notation will be used here, and hence

$$\begin{aligned} d^2\mathbf{r}/dt^2 &= \partial\mathbf{v}/\partial t + \mathbf{v}\cdot\nabla\mathbf{v} \\ &= \partial\mathbf{v}/\partial t + \mathbf{v}_0\cdot\nabla\mathbf{v} - (\mathbf{v}_0-\mathbf{v})\cdot\nabla\mathbf{v} \\ &= d\mathbf{v}/dt - (\mathbf{v}_0-\mathbf{v})\cdot\nabla\mathbf{v}, \end{aligned}$$

and the equation of motion becomes

$$\mathbf{F} = m\left[\frac{d\mathbf{v}_0}{dt} - \frac{d\mathbf{v}}{dt} + (\mathbf{v}_0-\mathbf{v})\cdot\nabla\mathbf{v}\right] + \frac{dm}{dt}(\mathbf{v}_0-\mathbf{v}) - 2m\boldsymbol{\omega}\times(\mathbf{v}_0-\mathbf{v}).$$

Now let $\boldsymbol{\omega} = \frac{1}{2}\nabla\times\mathbf{v}$ and apply the identity:

$$(\mathbf{v}_0-\mathbf{v})\times\nabla\times\mathbf{v} = (\nabla\mathbf{v})\cdot(\mathbf{v}_0-\mathbf{v}) - (\mathbf{v}_0-\mathbf{v})\cdot\nabla\mathbf{v}.$$

The equation of motion then takes its final form:

$$\mathbf{F} = \frac{d}{dt}[m(\mathbf{v}_0-\mathbf{v})] + m(\nabla\mathbf{v})\cdot(\mathbf{v}_0-\mathbf{v}). \tag{6}$$

It is assumed that the mass of a particle varies with its velocity relative to the ether according to the relation:

$$m = m_0/[1-(\mathbf{v}_0-\mathbf{v})^2/c^2]^{\frac{1}{2}}. \tag{7}$$

Equations (6) and (7) then determine the motion of a particle in a gravitational field.

Now let

$$T = -m_0c^2[1-(\mathbf{v}_0-\mathbf{v})^2/c^2]^{\frac{1}{2}}.$$

Then Eq. (6) can be written

$$F_i = \frac{d}{dt}\left(\frac{\partial T}{\partial v_{0i}}\right) - \frac{\partial T}{\partial x_i}.$$

This is the Lagrangian form of the equations, from which their form in generalized coordinates follows immediately. Furthermore, it is apparent that if the external forces vanish and if $d\tau = [1-(\mathbf{v}_0-\mathbf{v})^2/c^2]^{\frac{1}{2}}dt$, these equations are equivalent to Hamilton's principle, $\delta\int d\tau = 0$, which is the more familiar form that appears in the general theory of relativity.

The equation of the orbit of a particle moving in a spherically symmetrical gravitational field under the action of no external forces can be derived directly from the energy and angular momentum integrals of these equations when $\mathbf{v}$ is assumed to have only a radial component given by $v_r = -(2KM/r)^{\frac{1}{2}}$. However, the analogy to Einstein's theory is more apparent if $d\tau^2$ is expanded in terms of polar coordinates r and θ lying in the plane of motion of the particle and centered on the attracting mass M:

$$d\tau^2 = dt^2 - (1/c^2)\{[dr + (2KM/r)^{\frac{1}{2}}dt]^2 + r^2d\theta^2\}.$$

Now let

$$t' = t - \frac{2}{c}\left(\frac{2KMr}{c^2}\right)^{\frac{1}{2}} + \frac{4KM}{c^3}\tanh^{-1}\left(\frac{2KM}{c^2r}\right)^{\frac{1}{2}},$$

and the expression for $d\tau^2$ becomes

$$d\tau^2 = \left(1-\frac{2KM}{c^2r}\right)dt'^2 - \frac{1}{c^2}r^2d\theta^2 - \frac{1}{c^2}\frac{1}{1-2KM/c^2r}dr^2.$$

This is the customary form for the Schwarzschild line element in Einstein's theory. When it is used in the equation $\delta\int d\tau = 0$, it is known to predict the correct advance of the perihelion of Mercury. Since the oribtal equation does not depend on the time, the change of variable from t to t' does not alter this result, and hence the equations of motion given here are completely equivalent to Einstein's in this respect.

V. CONCLUSIONS

It has been shown that the verifiable results of Einstein's gravitational theory can be deduced directly from elementary physical principles without the use of the covariant formalism or of Einstein's field equations. The principle of equivalence has been used to interpret gravitational fields in terms of an ether flow, and the ether velocity in a region about a spherical mass has been determined directly from Newton's inverse square law of gravitational attraction. Finally, the principle of special relativity is not fundamental to the theory and is used only to give the equations for the variation of the mass of a particle with its velocity and for the change in frequency of radiation of a moving atom due to its motion. If desired, both of these facts can be treated as experimentally determined laws, and the complete postulate of special relativity is not needed.

ACKNOWLEDGMENTS

I am very deeply indebted to Professor H. P. Robertson of the California Institute of Technology for supervising this research and for encouraging and assisting it in many ways which space does not permit me to describe here. I am also very indebted to Mr. R. H. Dishington of The Rand Corporation. Long before I met him, Mr. Dishington had come to certain conclusions about the interpretation of electromagnetism in terms of an ether which were very close to my own ideas on this subject. Discussions of this problem with him have always been stimulating and encouraging.

Yukawa Forces with Added Attractions*

JOHN M. BLATT† AND M. H. KALOS‡
University of Illinois, Urbana, Illinois
(Received August 14, 1953)

A "Yukawa potential" is defined here as the conventional second-order potential of pseudoscalar meson theory with pseudoscalar coupling, cut off by a hard repulsive core. We have carried out many calculations of the properties of the neutron-proton system at low energies assuming that the interaction is this Yukawa potential with various additional spin independent central wells. The results indicate that interactions of this type (including the Levy potential) do not give a satisfactory fit to the low-energy data.

I. THE LÉVY POTENTIAL

WE have developed a computing program for the University of Illinois Electronic Digital Computer (The ILLIAC) which solves the differential equations for the $^3S+^3D$ ground state of the deuteron, and also computes quantities characteristic of the $^3S+^3D$ scattering state and of the ^1S scattering state. We have applied this code to a study of nuclear potentials, among them the potential suggested by Lévy.[1]

We write Lévy's potential in the form

$$\begin{aligned}(\mu ch)^{-1}V(r)&=+\infty \quad \text{for} \quad r<r_{\text{core}},\\ (\mu ch)^{-1}V(r)&=-(G^2/4\pi)^2(3/2\pi)(Mr)^{-2}K_1(2\mu r)\\ &\quad-(g^2/4\pi)(\mu/2M)^2(\mu r)^{-1}\exp(-\mu r)\\ &\quad\times\{1+S_{12}[1+(3/\mu r)+3/(\mu r)^2]\}\\ &\qquad\qquad \text{for} \quad r>r_{\text{core}}. \quad (1)\end{aligned}$$

This is essentially the form proposed by Lévy; we have introduced two coupling constants, G and g, the first for the fourth-order force, the second for the usual second-order force. Lévy imposed the condition $g=G$, but other work[2] has shown that this condition is not necessarily a consequence of the pseudoscalar meson theory of nuclear forces with pseudoscalar coupling (which underlies Lévy's treatment). We have also dropped Lévy's $V_4^{(b)}$ from the fourth-order force [the first term in (1)], following arguments presented by Drell[3] and Klein.[4]

Table I gives a list of the runs we have made so far. In each case the binding energy of the deuteron has been fitted (by adjusting g^2). Table II gives interpolated cases designed to fit the singlet state scattering length. Table III gives interpolated cases designed to fit the quadrupole moment of the deuteron.

In interpreting such results, it is necessary to know how sensitively various experimental numbers depend upon the parameters of the theory. Assuming always that we adjust things so as to fit the binding energy of the deuteron, the most sensitive experimental number is the singlet scattering length. This is because of the well-known "resonance" close to zero energy. A small change in the potential produces large changes in a_s. The next experimental number is the quadrupole moment. This is primarily determined by, and therefore fixes, the "outside" behavior of the tensor potential. This can be seen from Table III, for example, by observing that the coupling constant $g^2/4\pi$ is almost the same for all core radii. $g^2/4\pi$ determines the outside behavior of the tensor force, and the fact that $g^2/4\pi$ is nearly independent of the core radius (for cases which fit the quadrupole moment) indicates that the quadrupole moment does not depend strongly upon the close-in behavior of the tensor force. Finally, the least sensitive experimental number is the triplet effective range. It takes large changes in the potential to produce appreciable changes in the effective range. Qualitatively speaking, we may say that the following discrepancies should be considered serious: a factor of 3 in the singlet scattering length, 20 percent in the quadrupole moment, 10 percent in the triplet effective range. The singlet effective range changes rather rapidly as a function of the singlet scattering length. But if the singlet scattering length has been fitted (Table II), a 20 percent discrepancy in the singlet effective range is also serious.

Lévy's original program consisted in setting $g=G$ and adjusting r_{core} and g so that the potential fits the binding energy of the deuteron and the singlet scattering length. Table II shows that this is impossible if the fourth-order potential is taken as $V_4^{(a)}$ rather than as $V_4^{(a)}+V_4^{(b)}$. The values of $G^2/4\pi$ are systematically larger than the values of $g^2/4\pi$, for all core radii investigated by us.

Since the condition $G=g$ may well be too stringent, it is worth while to try to see how good a fit can be obtained by leaving G and g as two free parameters. Tables II and III show that the agreement is poor. In order to fit the binding energy of the deuteron, the quadrupole moment, and the singlet scattering length, the core radius must be chosen to be $r_{\text{core}}=0.189R=0.814\times10^{-13}$ cm. The triplet effective range is then $r_{0t}=0.484R=2.08\times10^{-13}$ cm. The singlet effective range is $r_{0s}=0.792R=3.41\times10^{-13}$ cm. The experimental values

* Assisted in part by the U. S. Office of Naval Research.
† Now at the University of Sydney, Sydney, Australia.
‡ Now at the Laboratory of Nuclear Studies, Cornell University, Ithaca, New York.
[1] M. M. Lévy, Phys. Rev. **88**, 72, 725 (1952).
[2] G. Wentzel, Helv. Phys. Acta **15**, 111 (1942); **25**, 569 (1952); Phys. Rev. **86**, 802 (1952).
[3] S. Drell (private communication).
[4] A. Klein, Phys. Rev. **89**, 1158 (1953); **90**, 1101 (1953).

TABLE I. This table contains the results of all runs with the Lévy potential (1). All results fit the binding energy of the deuteron. The core radius, as well as all other lengths, is measured in units of the radius of the deuteron (4.3×10^{-13} cm). s is the nondimensional well depth of the fourth-order potential. $s=1$ corresponds to a fourth-order potential which, by itself, gives rise to a scattering resonance at exactly zero energy. s is proportional to $(G^2/4\pi)^2$ for any one core radius, but the proportionality constant depends upon the core radius. $G^2/4\pi$ and $g^2/4\pi$ are defined by (1); p_D is the D-state probability, Q is the quadrupole moment, ρ_t is the triplet effective range (evaluated from the ground-state wave functions); ρ_s is the singlet effective range, and a_s is the singlet scattering length. The experimental values, in our units, are: $Q=0.0147\pm0.0002$, $\rho_t=0.395\pm0.015$, $a_s=-5.488\pm0.02$, $\rho_s=0.63\pm0.1$. The uncertainties stated here are somewhat larger than the ones claimed in the various experimental papers. Even though the machine finds the wave functions in every run, we did not ask it to print out all that information for every run. The runs for which wave functions are available are marked with an asterisk.

r_{core}	s	$G^2/4\pi$	$g^2/4\pi$	p_D	Q	ρ_t	ρ_s	a_s
0.123	0.3	6.532	13.382	0.06635	0.01484	0.4060	9.47	−0.1015
	*0.319167	6.738	13.175	0.06546	0.01470	0.4052	8.16	−0.1109
	0.6	9.238	10.020	0.05040	0.01238	0.3954	1.643	−0.3629
	0.9	11.314	6.174	0.02826	0.008863	0.3881	0.6137	−3.192
	*0.992	11.452	5.853	0.02628	0.008519	0.3877	0.5836	−5.132
	1.0	11.926	4.634	0.01879	0.007121	0.3865	0.4985	5.457
	1.170	12.899	0	0	0	...	...	...
0.140	0.3	7.570	15.894	0.07217	0.01683	0.4346	10.14	−0.1065
	*0.544	10.193	12.688	0.05907	0.01470	0.4253	2.237	−0.3075
	0.6	10.705	11.917	0.05555	0.01414	0.4234	1.737	−0.3923
	0.9	13.111	7.392	0.03203	0.01029	0.4153	0.6609	−3.760
	*0.917	13.234	7.104	0.03040	0.009998	0.4150	0.6362	−5.530
	1.0	13.820	5.600	0.02183	0.008377	0.4137	0.5396	5.183
	1.179	15.008	0	0	0	...	...	...
0.185	0.3	10.753	23.598	0.08614	0.02218	0.5000	12.27	−0.1162
	0.6	15.207	17.739	0.06822	0.01895	0.4877	1.984	−0.4635
	*0.880	18.417	11.630	0.04392	0.01467	0.4792	0.8129	−3.790
	*0.898	18.604	11.198	0.04199	0.01431	0.4788	0.7807	−5.434
	0.9	18.625	11.150	0.04177	0.01427	0.4787	0.7773	−5.702
	1.0	19.632	8.598	0.02989	0.01194	0.4769	0.6406	4.726
	1.201	21.514	0	0	0	...	...	...
0.189	*0.89698	19.142	11.601	0.04295	0.01470	0.4839	0.7924	−5.493
0.240	*0.878	26.848	17.752	0.05585	0.02008	0.5438	0.9516	−5.347
	0.9	27.182	16.980	0.05320	0.01956	0.5433	0.9073	−9.676
	1.0	28.652	13.275	0.03971	0.01676	0.5415	0.7524	4.420
	*1.057	29.458	10.950	0.03078	0.01471	0.5409	0.6893	2.610
	1.1	30.051	9.022	0.02331	0.01278	0.5406	0.6504	2.045

of the latter two are $(1.70\pm0.05)\times10^{-13}$ cm and $(2.6\pm0.4)\times10^{-13}$ cm respectively. (The effective range in proton-proton scattering is $(2.65\pm0.07)\times10^{-13}$ cm.) Conversely, if we try to fit the triplet data only (i.e., fit the binding energy, quadrupole moment, and triplet effective range), the core radius necessary is $r_{core}=0.114R=0.491\times10^{-13}$ cm, and the singlet state results are utterly unreasonable: $a_s=-0.045R=0.19\times10^{-13}$ cm compared to the experimental value $a_s=-5.49R=-23.68\times10^{-13}$ cm.

We conclude that the Lévy potential does not give an acceptable fit to the experimentally observed properties of the neutron-proton system at low energies.[5]

II. YUKAWA FORCES WITH ADDED ATTRACTIONS

Since the Lévy potential does not give an adequate fit to the neutron proton data, we have investigated to what extent the disagreement is a result of the particular form of the Lévy potential. We define a "Yukawa force with added attraction" as follows:

$$V=+\infty \quad \text{for} \quad r<r_{\text{core}};$$
$$V=V_a(r-r_{\text{core}})-(g^2/4\pi)(\mu/2M)^2(\mu ch)(\mu r)^{-1}\times\exp(-\mu r)\{1+S_{12}[1+3/\mu r+3/(\mu r)^2]\} \quad \text{for} \quad r>r_{\text{core}}. \quad (2)$$

The "added attraction" V_a is a completely arbitrary central force. It is written as a function of the difference $r-r_{\text{core}}$ in order to avoid introducing a (spurious) strong well shape dependence caused by the different ways a hard repulsive core cuts off the central attractive region of various potentials. The only conditions imposed on the potential (2) are:

(a) The singlet state force equals the central force in the triplet state (no $\sigma_1\cdot\sigma_2$ term).

(b) The quantity μ is determined from the experimental mass of the π meson, and is therefore not an adjustable parameter.

We believe that forces of this type represent a reasonable generalization of the Lévy potential.

The following well shapes have been tried for V_a: Gauss well, Yukawa well, and Morse well, in addition to the fourth-order potential of Lévy discussed in the

[5] The results of this section are in qualitative agreement with those of R. Jastrow, Phys. Rev. **91**, 749 (1953), whose procedure is similar to our own. He also examines the case $g\neq G$, but allows a different core radius for the singlet potential. Not all his numerical results agree with ours.

TABLE II. Interpolated cases which fit the singlet scattering length and the binding energy of the deuteron. Note that a core radius slightly less than 0.140, which fits ρ_t and ρ_s, gives rise to much too low a quadrupole moment Q; conversely, a core radius slightly in excess of 0.185, which fits Q, gives rise to much too large values of ρ_t and ρ_s.

r_{core}	s	$G^2/4\pi$	$g^2/4\pi$	p_D	Q	ρ_t	ρ_s	a_s
0.123	0.9244	11.478	5.818	0.02606	0.008482	0.3876	0.5804	*−5.488*
0.140	0.9167	13.232	7.108	0.03041	0.01000	0.4150	0.6366	*−5.488*
0.185	0.8984	18.615	11.188	0.04194	0.01431	0.4788	0.7800	*−5.488*
0.240	0.8792	26.867	17.709	0.05571	0.02005	0.5438	0.9490	*−5.488*

TABLE III. Interpolated cases which fit the quadrupole moment. A core radius slightly less than 0.123 fits the triplet data (binding energy, Q, ρ_t) reasonably well, but gives utter nonsense for the singlet state. Notice how nearly constant $g^2/4\pi$ is as a function of the core radius. This indicates that the quadrupole moment is determined primarily by the "exterior" behavior of the tensor force.

r_{core}	s	$G^2/4\pi$	$g^2/4\pi$	p_D	Q	ρ_t	ρ_s	a_s
0.123	0.31876	6.736	13.180	0.06548	*0.01470*	0.4053	8.185	−0.1107
0.140	0.54395	10.193	12.689	0.05908	*0.01470*	0.4253	2.238	−0.3074
0.185	0.8780	18.401	11.666	0.04408	*0.01470*	0.4792	0.8157	−3.713
0.240	1.057	29.460	10.944	0.03075	*0.01470*	0.5409	0.6892	2.607

preceding section. The Gauss and Yukawa well shapes represent extremes in well shapes: the former is highly concentrated; the latter is the most "long-tailed" of the commonly used potentials. The Yukawa shape for V_a is written as a function of $r-r_{core}$. Hence, it actually diverges at the core radius. The Morse well was employed primarily to make sure that there is nothing special about the sharply cut-off core employed for the other runs. There is not.

We cannot give a table of these runs because we ran well over 100 cases for a complete exploration. For both the Yukawa and the Gauss shape, we ran intrinsic ranges of $R/10$, $2R/10$, and $3R/10$ (R=radius of the deuteron), core radii of $0.09R$, $0.123R$, $0.140R$, $0.185R$, $0.240R$ and either 3 or 4 choices of intrinsic depths between -0.3 and 1.0; in addition we ran a large number of interpolated cases designed to fit either the quadrupole moment or the singlet state scattering length or both. Each "run" would take at least a week by hand computation (this is an extremely conservative estimate).

We shall confine ourselves to the main results here. First of all, we found, in agreement with Jastrow, that the original Yukawa potential with a repulsive core (i.e., the choice $V_a=0$) gives a good fit to the *triplet* data. Furthermore, the core radius necessary is very close to twice the Compton wavelength of the nucleon; this is a reasonable *a priori* value for r_{core}. The results for a pure Yukawa potential with repulsive core but no added attraction (interpolated to fit the quadrupole moment of the deuteron) are

$$\begin{aligned} r_{core}&=0.106R=0.456\times10^{-13}\text{ cm},\\ g^2/4\pi&=13.6,\\ p_D&=7.18\text{ percent},\\ r_{0t}&=0.386R=1.66\times10^{-13}\text{ cm}. \end{aligned} \tag{3}$$

However, the singlet data implied by the same potential are completely unreasonable ($a=-0.00411R=-1.8\times10^{-15}$ cm). This is understandable because here practically all the binding in the triplet state is due to the tensor force.

With the additional freedom associated with the introduction of V_a, one might think that it should be easy to fit all the low-energy data. We were rather surprised to find, instead, that it is not possible no matter how V_a is adjusted. Indeed, it is impossible to fit simultaneously as few as 4 experimental numbers:

(a) binding energy of deuteron,
(b) quadrupole moment of deuteron,
(c) triplet effective range,
(d) singlet scattering length. (4)

If we fit the triplet data (the first three quantities in (4)), the singlet scattering length is completely unreasonable (too low by more than a factor of 10). If we fit (a), (b), and (d), the triplet effective range is at least 15 percent too large. This 15 percent discrepancy corresponds to an (extrapolated) zero-range V_a, i.e., to an infinitely strong, zero-range attraction just outside an infinitely high repulsive core. The discrepancies for physically reasonable V_a are larger. For a range (outside the core) of V_a equal to $R/5=0.86\times10^{-13}$ cm, the triplet effective range is 21 percent too large for a Yukawa well V_a, 19 percent too large for a Gauss well V_a. Finally, if we try to fit (a), (c), and (d), the quadrupole moment is considerably less than $\frac{2}{3}$ of its experimental value in all cases.

Qualitatively speaking, the difficulty can be traced to the singular nature of the tensor force in the second-order pseudoscalar meson theory. The value of the quadrupole moment determines $g^2/4\pi$ to a first approximation (independently of the core radius and of the nature of V_a). The resulting strong tensor force contributes so much to the binding energy of the deuteron that the central force is much too weak to fit the singlet data. If we restrict ourselves to V_a with in-

trinsic ranges (outside the core) larger than $R/10$, the potentials which fit the triplet data have central forces which are too weak by more than a factor of 3 to give the required singlet state resonance.

The relativistic corrections to the magnetic moment of the deuteron are probably of the same order of magnitude as the correction due to the D state. Since these relativistic corrections cannot be computed reliably on the basis of present theory, we have taken the "experimental" D-state probability to be 4 ± 4 percent, i.e., $p_D<0.08$. All the theoretically computed values lie within that range.

The well shape of V_a makes very little difference in the results. Strong well shape dependences are spurious and arise only because usually one does not consider V_a as a function of $r-r_{\text{core}}$, but rather as a function of r. In that case a portion of V_a is "cut off" by the core, and the strength of the remaining part depends strongly on the well shape and range of V_a. This dependence was eliminated in our work by choosing to consider V_a as a function of $r-r_{\text{core}}$.

We conclude that the poor fit obtained with the Lévy potential is not a particular property of the fourth-order potential of Lévy, but applies equally to all Yukawa forces with added attractions. Of course, a good fit can be obtained to the triplet data alone (a), (b), and (c) of (4), and the singlet data can then be fitted by adding an appropriate amount of $\boldsymbol{\sigma}_1\cdot\boldsymbol{\sigma}_2$ force. However, such a fit means very little because the number of theoretical parameters used exceeds the number of experimental data.

We should like to thank the staff of the University of Illinois Digital Computer for their assistance and cooperation in this work.

PHYSICAL REVIEW VOLUME 92, NUMBER 6 DECEMBER 15, 1953

The Equations of Motion in Einstein's New Unified Field Theory

JOSEPH CALLAWAY*
Palmer Physical Laboratory, Princeton University, Princeton, New Jersey
(Received June 8, 1953)

It is shown that the field equations of Einstein's latest unified field theory do not lead to the Lorentz equations of motion for charged particles in an electromagnetic field, if these particles are considered to be singularities of the field. To a fourth-order approximation, the motion of such particles is not influenced by the electromagnetic field, no matter how much charge is placed on the particles.

INTRODUCTION

IT is well known that the field equations of general relativity (plus the Bianchi identities) lead to the correct equations of motion for a particle, represented as a point singularity. This point has been extensively discussed in the literature.[1–4] The situation is different in electromagnetism where additional hypotheses, such as the stress-energy tensor, have to be introduced before equations of motion can be obtained.[5] Here we examine the case of unified field theory, in which the use of the stress-energy tensor is abandoned, to see if the correct equations of motion for matter can be obtained. This paper is concerned only with Einstein's latest unified field theory.[6] A remark of Infeld[7] that one does not obtain the Lorentz equations of motion for a particle in an electromagnetic field in Einstein's previous unified field theory[8] is extended to apply in the latest theory. One still obtains the correct equations for the motion of an uncharged particle in a gravitational field.

We assume that particles are to be represented as singularities in the appropriate fields. We ask if the field equations place any restrictions on the motion of singularities, intending thereby to obtain the Lorentz equations of motion for the case of charged particles in an electromagnetic field. Einstein maintains,[9] however, that one must represent matter by nonsingular solutions of the field equations, and also that the fundamental nature of the Lorentz equations is open to question. He believes that in a rigorous solution of the field equations particles may interact with each other in such a way that the Lorentz equations will only represent a statistical, averaged effect. Since such solutions have not yet been obtained, we cannot comment on the possibility of obtaining equations of motion in the nonsingular case.

METHOD

The calculation is somewhat involved and will only be sketched here. An adequate discussion of details can be obtained from references 3 and 7. In particular, this calculation follows that of reference 7.

The method rests on the solution of the field equations in a quasi-static approximation. This enables us to distinguish, by means of a parameter λ, quantities involving time derivatives as of smaller size. The essential steps in the calculation are as follows:

(1) We determine the relation between the fundamental tensor g_{ik} and the affinity Γ^l_{ik} by an expansion in powers of λ. We are so far unable to determine this relation exactly, as is possible in general relativity.

(2) We identify the gravitational and electromagnetic fields by requiring that the field equations reduce to those of general relativity, and to Maxwell's equations in a suitable approximation.

(3) We calculate the field quantities in a quasi-static approximation.

(4) We ask whether any terms are added to the equations of motion of general relativity by the fact that the fundamental tensor g_{ik} is no longer symmetric. The equations of motion turn out to be given by the surface integral of certain quantities Λ_{ik}. Some elements of these Λ_{ik} appear in general relativity, and these we subtract out, since we are only interested in the additional terms. We then consider the surface integral of the remaining Λ_{ik} to see whether they contribute to the equations of motion.

One conclusion can be drawn very simply. If we make the assumption, which will later be justified, that the antisymmetric part of the fundamental tensor represents the electromagnetic field, we see that the correct equations of motion for charged matter in an electromagnetic field cannot be the geodesic equations, as is the case in general relativity. For the geodesics, the lines of shortest distance are determined from

$$\delta \int ds = 0;$$

but

$$ds^2 = g_{ik} dx^i dx^k,$$

and any antisymmetric part of the g_{ik} will cancel in the summation. Thus the geodesics are not affected by the electromagnetic field.

* National Science Foundation Predoctoral Fellow.
[1] Einstein, Infeld, and Hoffmann, Ann. Math. **39**, 66 (1938).
[2] A. Einstein and L. Infeld, Ann. Math. **41**, 797 (1940).
[3] A. Einstein and L. Infeld, Can. J. Math. **1**, 209 (1949).
[4] L. Infeld and A. Schild, Revs. Modern Phys. **21**, 408 (1949).
[5] L. Infeld and P. R. Wallace, Phys. Rev. **57**, 797 (1940).
[6] A. Einstein, *The Meaning of Relativity* (Princeton University Press, Princeton, 1953), fourth edition, pp. 133–165.
[7] L. Infeld, Acta Phys. Polonica **10**, 284 (1950).
[8] A. Einstein, *The Meaning of Relativity* (Princeton University Press, Princeton, 1950), third edition, pp 133–162.
[9] A. Einstein (private communication).

We begin with the field equations. The fundamental tensor g_{ik} has a symmetric part $g_{(ik)}$ and an antisymmetric part $g_{[ik]}$. Likewise the affinity $\Gamma^l{}_{ik}$ can be decomposed into symmetric and antisymmetric parts $\Gamma^l{}_{(ik)}$ and $\Gamma^l{}_{[ik]}$; the latter is a tensor. The tensor R_{ik} is defined as in general relativity:

$$R_{ik}\equiv(\Gamma^t{}_{ik,\,t}-\Gamma^t{}_{sk}\Gamma^s{}_{it})-(\Gamma^t{}_{it,\,k}-\Gamma^t{}_{st}\Gamma^s{}_{ik}),$$

and it can also be decomposed into symmetric and antisymmetric parts $R_{(ik)}$ and $R_{[ik]}$. The comma indicates ordinary differentiation. One defines

$$\Gamma^i{}_{[ki]}\equiv\Gamma_k.$$

This quantity is a vector. Since the affinity is nonsymmetric, there are several possibilities for covariant differentiation. For a covariant vector A_i these can be denoted as follows:

$$\begin{aligned} A_{i;k}&\equiv A_{i,k}-A_s\Gamma^s{}_{ik}, \\ A_{[i;k]}&\equiv A_{i,k}-A_s\Gamma^s{}_{ki}, \end{aligned} \qquad A_{(i;k)}\equiv A_{i;k}-\begin{Bmatrix} s \\ ik \end{Bmatrix}A_s.$$

The quantities $\begin{Bmatrix} s \\ ik \end{Bmatrix}$ are the well-known Christoffel symbols.

With these preliminaries, we can state the field equations:

$$\begin{aligned} g_{(i\ k;\,l)}&=0, \quad \Gamma_i=0, \\ R_{(ik)}&=0, \quad R_{[ik,\,l]}+R_{[kl,\,i]}+R_{[li,\,k]}=0. \end{aligned} \tag{1}$$

The equation

$$g_{(i\ k;\,l)}=\partial g_{ik}/\partial x^l-g_{sk}\Gamma^s{}_{il}-g_{is}\Gamma^s{}_{lk}=0 \tag{2}$$

relates the affinity and the metric. In general relativity, the $\Gamma^l{}_{ik}$ are replaced by the $\begin{Bmatrix} l \\ ik \end{Bmatrix}$, and the symmetry of the Christoffel symbols makes solution simple. Here we have no such pleasant properties at our disposal, and we have to solve for the affinity by successive approximations. Following Infeld, we introduce the quantities $M^l{}_{ik}$ defined by

$$M^l{}_{ik}\equiv\Gamma^l{}_{ik}-\begin{Bmatrix} l \\ ik \end{Bmatrix}$$

($M^l{}_{ik}$ is a tensor), the quantities g^{ls} defined by

$$g_{[ik]}g^{ls}=\delta_k{}^s,$$

and the tensor I_{ikl}:

$$I_{ikl}=\tfrac{1}{2}(g_{(ik,\,l)}+g_{(kl,\,i)}+g_{(li,\,k)}).$$

Then we can show that[7] that

$$M_{ik}{}^l=g^{[lt]}\{g_{(ik;\,t)}-I_{ikt}-g_{(is}M^s{}_{kt}-g_{s(k}M^s{}_{ti}\}, \tag{3}$$

where

$$g_{(ik;\,t)}\equiv g_{(ik,\,t)}-g_{(ik}\begin{Bmatrix} l \\ it \end{Bmatrix}-g_{(il}\begin{Bmatrix} l \\ kt \end{Bmatrix}.$$

If we put

$$g_{(ik)}\equiv\eta_{(ik)}+h_{(ik)},$$

where η_{ik} represent the Minkowski metric with signature $+---$; we can assume that the $h_{(ik)}$, $g_{(ik)}$, $M^l{}_{ik}$, and $\begin{Bmatrix} l \\ ik \end{Bmatrix}$ are of the same order. Thus in the first approximation those terms on the right of (3) which contain $M^l{}_{ik}$ and $\begin{Bmatrix} l \\ ik \end{Bmatrix}$ can be neglected. The $M^l{}_{ik}$ as given by the first approximation can be substituted back into (3), obtaining a second approximation, etc.

We can now discuss the identification of the symmetric and antisymmetric components of the fundamental tensor g_{ik}. Imagine a situation in which there is only a gravitational field in otherwise empty space. Then the gravitational field equations must apply, and the simplest way we can reduce our Eqs. (1) is to identify $g_{(ik)}$ with the g_{ik} of general relativity. Now consider a weak electromagnetic field in otherwise free space. In this situation, the field equations (1) must reduce to Maxwell's equations.

In order to see how this occurs, we introduce the lowest approximation of (3) into the definition of R_{ik}, and find that $R_{[ik]}$ has only one nonvanishing term, $\Gamma^t{}_{[ik,\,t]}$. Then we compute

$$R_{[ik,\,l]}+R_{[kl,\,i]}+R_{[li,\,k]}=0,$$

and obtain

$$g^{st}(g_{[ik,\,l]}+g_{[kl,\,i]}+g_{[li,\,k]})_{,\,st}=0. \tag{4}$$

It is suggested that this be considered as the D'Alembertian of one of the two Maxwell equations. The other can be obtained since the equation

$$g^{[is}{}_{,\,s}=0 \tag{5}$$

holds in this approximation. This is true since if $\mathfrak{g}^{ik}$ is the tensor density associated with g^{ik}, the equation

$$\mathfrak{g}^{[ik}{}_{,\,k}=0 \tag{6}$$

is rigorous. We want the one of Maxwell's equations which is an identity in the fields to be true in general, so we are led to identify the $\mathfrak{g}^{[ik]}$ with the dual of the electromagnetic field tensor,

$$\mathfrak{g}^{[ik]}=\epsilon^{iklm}F_{lm}, \tag{7}$$

where $\epsilon^{0123}=-1$, and F_{lm} is the ordinary electromagnetic field tensor. In our approximation, this identification gives

$$\begin{aligned} g_{[12]}&=kE_3, \quad g_{[13]}=-kE_2, \quad g_{[10]}=-kH_1, \\ g_{[23]}&=kE_1, \quad g_{[20]}=-kH_2, \quad g_{[30]}=-kH_3, \end{aligned} \tag{8}$$

where k is a constant depending on the system of units.

The quasi-static approximation in powers of λ is introduced and discussed extensively in the literature (see particularly reference 3). Through it we consider a situation in which time derivatives are an order smaller than space derivatives. The field equations are expanded as power series in λ in the following way. We distinguish time components by the index 0.

$$\begin{aligned}
g_{00} &= 1+\lambda^2\,{}_2g_{00}+\lambda^4\,{}_4g_{00}+\cdots,\\
g_{0n} &= \lambda^3\,{}_3g_{0n}+\lambda^5\,{}_5g_{0n}+\cdots,\\
g_{0\underline{n}} &= \lambda^3\,{}_3g_{0\underline{n}}+\lambda^5\,{}_5g_{0\underline{n}}+\cdots,\\
g_{mn} &= -\delta_{mn}+\lambda^2\,{}_2g_{mn}+\lambda^4\,{}_4g_{mn}+\cdots,\\
g_{m\underline{n}} &= \lambda^2\,{}_2g_{m\underline{n}}+\lambda^4\,{}_4g_{m\underline{n}}+\cdots.
\end{aligned} \tag{9}$$

The numerical subscript on the left indicates that this quantity is the coefficient of the particular power of λ; for instance, ${}_2g_{mn}$ multiplies λ^2. Reference to Eqs. (8) will show that it is appropriate to apply (9) to a system of slowly moving charged particles, where the principal interaction is electrostatic. The quantities $M^l{}_{ik}$ can be calculated using (8) and (9). We obtain

$$\begin{aligned}
&{}_3M^0{}_{00}=0, \quad {}_2M^s{}_{00}={}_2M^0{}_{s0}={}_2M^0{}_{0s}=0,\\
&{}_3M^l{}_{0k}=-{}_3g_{0\underline{k},\,l}+{}_3I_{0kl}, \quad {}_3M^0{}_{lk}=+{}_3g_{l\underline{k},\,0}-{}_3I_{lk0},\\
&{}_2M^l{}_{ik}=-{}_2g_{i\underline{k},\,l}+{}_2I_{ikl},\\
&{}_4M^0{}_{0s}={}_4M^0{}_{s0}={}_4M^s{}_{00}=0,\\
&{}_4M^l{}_{i\underline{k}}={}_4M^l{}_{\underline{k}i}=-{}_2g_{i\underline{s}}(-{}_2g_{kl,\,s}+{}_2I_{kls})\\
&\qquad\qquad -{}_2g_{s\underline{k}}(-{}_2g_{l\underline{i},\,s}+{}_2I_{lis}),\\
&{}_4M^l{}_{\underline{ik}}=-{}_4M^l{}_{\underline{ki}}=-{}_4g_{\underline{ik},\,l}+{}_4I_{ikl}+{}_2g^{n\underline{l}}({}_2g_{\underline{ik},\,n}-{}_2I_{ikn})\\
&\qquad\qquad +{}_2g_{\underline{ls}}\,{}_2\begin{Bmatrix} s \\ lk \end{Bmatrix}+{}_2g_{s\underline{k}}\begin{Bmatrix} s \\ il \end{Bmatrix}.
\end{aligned} \tag{10}$$

This analysis determines the $M^l{}_{ik}$ up to fourth order. In the above, summations run from 1 to 3 only, time being distinguished by the index 0. This convention prevails through the remainder of the paper.

We employ (9) and (10) to calculate R_{ik}. Through the second and third order, which is all we need here, the field equations split into equations of the gravitational and the electromagnetic field separately [as in (4)]. The following field equations are then obtained to second and third order:

$$\begin{aligned}
\nabla^2({}_2g_{i\underline{k}}{}_{,\,l}+{}_2g_{k\underline{l}}{}_{,\,i}+{}_2g_{l\underline{i}}{}_{,\,k})&=0,\\
\nabla^2({}_3g_{0\underline{k}}{}_{,\,l}+{}_3g_{k\underline{l}}{}_{,\,0}+{}_3g_{l\underline{0}}{}_{,\,k})&=0,
\end{aligned} \tag{11}$$

and from the equation $\Gamma^s=0$,

$$\begin{aligned}
\operatorname{div}\,{}_2g_{i\underline{k}}&={}_2g_{i\underline{k},\,k}=0,\\
\operatorname{div}\,{}_3g_{0\underline{k}}&={}_3g_{0\underline{k},\,k}=0.
\end{aligned} \tag{12}$$

Since our object is to determine the equation of motion of particles, we look for solutions of (11) and (12) which will reduce, at distances large compared to the gravitational radius of the particle, yet small compared to the wavelength of any radiation being emitted, to the ordinary electric and magnetic fields of slowly moving charges. Because the motion is assumed to be slow, however, radiative effects are assumed to be of higher order. It is true that in the immediate neighborhood of these singularities, the weak-field approximation employed above will not be valid, and it will not be possible to separate the gravitational and electromagnetic fields in such a simple fashion. But our technique in finding the equations of motion is, following Infeld, to surround each charge by a large closed surface. The distance of the surface from the particle is taken to lie within the above-mentioned limits, but is otherwise arbitrary.

Specifically, we consider the particles to be electric charges with a $1/r^2$ singularity in the electromagnetic field. The nature of the gravitational singularity is immaterial. For generality we consider n particles, and to the order of approximation in question we introduce the electric potential of these n particles:

$${}_2\varphi=\sum_{i=1}^{N}{}_2\varphi(i).$$

We have, according to electrostatics,

$${}_2\varphi(k)=e(k)/r(k),$$

where $r(k)$ is the distance (a magnitude, not a vector) from the charge to the field point, and e is a constant proportional to the charge. Thus, in accord with (8),

$${}_2g_{m\underline{n}}=\epsilon_{mns}\,{}_2\varphi_{,\,s}, \tag{13}$$

where ϵ_{mns} is a completely antisymmetric three-dimensional Cartesian tensor. This choice satisfies the field equations to the second order.

To satisfy the field equations in the third order, we let the motion of the kth singularity be given by three functions of time $\xi^m(k,t)$, velocities of order λ, $\dot{\xi}^m(k,t)$ and accelerations of order λ^2, $(\partial^2/\partial t^2)\xi(k,t)$.

Then we set

$$g_{0\underline{k}}=-\epsilon_{0kij}\Big(\sum_{l=2}^{N}{}_2\varphi(l)\dot{\xi}_i(l,t)\Big)_{,\,j}, \tag{14}$$

where ϵ_{0kij} are the components of a completely antisymmetric Cartesian tensor in four dimensions. Equation (14) satisfies the field equations in the third order.

As stated previously, we wish to compare the equations of motion obtained in unified field theory with

those from general relativity. In general relativity, the equations of motion are determined from

$$R_{ik}=0,$$

where R_{ik} is a symmetric tensor. In unified field theory, we must consider the two equations

$$\underset{\sim}{R_{ik}}=0, \quad \underset{\sim}{R_{ik,\,l}}+\underset{\sim}{R_{kl,\,i}}+\underset{\sim}{R_{li,\,k}}=0.$$

The second of these equations states that $\underset{\sim}{R_{ik}}$ can be written as the curl of a vector: there exists a vector B_i such that

$$\underset{\sim}{R_{ik}}=B_{k,\,i}-B_{i,\,k}.$$

If we form a surface integral containing (linear combinations of) $\underset{\sim}{R_{ik}}$, this integral can be transformed by Stokes' theorem into the line integral of the vector B_i around a closed path bounding the surface. But for a closed surface, this path is of zero length, and the integral must vanish. Thus the quantities $\underset{\sim}{R_{ik}}$ can play no role in determining the equations of motion. The equations of motion must be obtained from the equation

$$\underset{\sim}{R_{ik}}=0.$$

It is shown in reference 3 that the equations of motion are to be found from the surface integral of certain quantities Λ_{ik} simply related to the tensor $\underset{\sim}{R_{ik}}$. The determination of Λ_{ik} will be discussed subsequently. If

$$\Lambda_{ik,\,k}=\mathrm{div}\Lambda_{ik}=0, \tag{15}$$

then a two-dimensional surface integral over a closed surface will not depend on the shape of the surface. If we choose surfaces enclosing individual singularities at the proper distances so that (13) and (14) are good approximations, the surface integral will be independent of the surface. But then it can be a function only of the coordinates of the singularities and their time derivatives, thus giving a contribution to the equations of motion.

It can be shown[3,7] that in order to obtain additional terms in the fourth-order equations of motion, we must evaluate the surface integral of the following:

$$-{}_4\Lambda_{ik}=({}_4\underset{\sim}{R_{mn}}-{}_4P_{mn})+\tfrac{1}{2}\delta_{mn}({}_4R_{00}-{}_4P_{00})-\tfrac{1}{2}\delta_{mn}({}_4\underset{\sim}{R_{ss}}-{}_4P_{ss}), \tag{16}$$

in which P_{mn} is the Ricci tensor of general relativity (R_{mn} formed using the Christoffel symbols). In order to evaluate these quantities to the fourth order, it turns out that one needs only the second- and third-order solutions of the field equations as given by (13) and (14). The result of this computation is[7]

$$-{}_4\Lambda_{mn}=\{{}_2\underset{\sim}{g_{ms}}\,{}_2\underset{\sim}{g_{np,\,s}}+\delta_{pm}\,{}_2\varphi_{,\,rn}\,{}_2\varphi_{,\,r}-\delta_{mn}\,{}_2\varphi_{,\,pm}\,{}_2\varphi_{,\,r}\}_{,\,p}. \tag{17}$$

The quantity inside the braces is antisymmetric in n and p. Thus,

$${}_4\Lambda_{mn,\,n}=0. \tag{18}$$

We are now required to form the surface integrals[3,7]

$$\frac{1}{2\pi}\int_4\Lambda_{mk}n_k dS={}_4C_m(k), \tag{19}$$

in which n_k is the normal vector to the surface surrounding the kth singularity. The additional equation of motion is then

$${}_4C_m(k)=0. \tag{20}$$

We can write $-{}_4\Lambda_{mn}=F_{mnp,\,p}$, where $F_{mnp}=-F_{mpn}$ and $F_{mnp,\,pn}=0$. Thus we have to evaluate

$$-\frac{1}{2\pi}\int F_{mkp}n_k dS=0. \tag{21}$$

This expression is essentially the surface integral of a curl (reference 3, p. 213) and therefore vanishes. Thus we do not obtain contributions from the electromagnetic field to the equations of motion in the fourth order. We know from general relativity[3] that terms in this order should contain products of charges like $e(1)e(2)$ so that the proper equations of motion cannot be obtained.

CONCLUSIONS

Although we can make the equations of Einstein's new unified field theory reduce to something like Maxwell's equations in a sufficiently low approximation, we cannot obtain the Lorentz equation of motion, if we represent particles with charge as singularities in the field. This result is the same as that obtained by Infeld[7] for Einstein's previous unified field theory.

ACKNOWLEDGMENTS

The author would like to express his thanks to Dr. J. A. Wheeler who suggested this problem, and also to Dr. V. Bargmann and Mr. O. W. Greenberg for valuable discussions.

Note added in proof.—B. Kursunoglu [Proc. Phys. Soc. (London) **65A**, 81 (1952)] has explained the failure to obtain the correct equations of motion for a charged particle in an electromagnetic field in Einstein's 1950 theory (see reference 8) as due to the vanishing of the stress-energy tensor.

Letters to the Editor

PUBLICATION of brief reports of important discoveries in physics may be secured by addressing them to this department. The closing date for this department is five weeks prior to the date of issue. No proof will be sent to the authors. The Board of Editors does not hold itself responsible for the opinions expressed by the correspondents. Communications should not exceed 600 words in length and should be submitted in duplicate.

New Absorption Lines of Crystals in Submicrowave Region

S. KOJIMA, K. TSUKADA, S. OGAWA, AND A. SHIMAUCHI
Tokyo University of Education, Otsuka, Tokyo, Japan
(Received October 13, 1953; revised manuscript received October 30, 1953)

IN the course of studying pure quadrupole spectra of iodine nuclei in silver iodine powder, many absorption lines different from those of the nuclear quadrupole resonance have been found by the aid of a super-regenerative detector with a transmission-line tuned circuit, which was working in the frequency range between 150 Mc/sec and 350 Mc/sec. The absorption lines were not affected by a magnetic field sufficient to cause a Zeeman effect of the nuclear quadrupole resonances. The absorption appeared strongly when the sample was put in an electric radiation field, i.e., at the voltage loop of the transmission line. The first observation was made at liquid air temperature. However, after the sample was heated to 150°C, which is above the transition point of the crystals, it showed the same absorption as at room temperature. The frequency of the lines changed with temperature, having a temperature coefficient, $\nu^{-1}d\nu/dt$, of about -3×10^{-4}/°C.

A similar absorption was found in phosphorescent zinc sulfide powder in the frequency range between 24 Mc/sec and 500 Mc/sec and in barium chlorate powder (which was previously heated) between 20 Mc/sec and 500 Mc/sec at room temperature. Silver bromide at liquid air temperature and zinc oxide and cadmium sulfide at room temperature were examined, but such an absorption was not observed. In zinc sulfide it was found that the absorption disappeared when the powder was immersed in a liquid of carbon tetrachloride and that it decreased when the sample was kept in the dark for several days.

For the precise measurement of the spectra, two autodyne detectors with a *LC* tuning circuit covering the frequency range from 3 Mc/sec to 120 Mc/sec were used. About 10 cc of zinc sulfide, which were put into the gap of the condenser, yielded a spectrum composed of numerous lines with an average spacing of about 10 kc/sec.

A similar absorption was found in powders of quartz crystals and Rochelle salt. These experiments may be seen as an extension of the powder method[1] for piezoelectric materials, and some of the absorption lines may be a result of the piezoelectric vibration of individual crystals. But the absorption seems to be not completely explained by this mechanism.[2]

Single crystals of potassium bromide, thallium-activated sodium iodide, zincblende, calcites, rock salt, and Rochelle salt were examined, and the absorption appeared in only rock salt and Rochelle salt. Most of the rock salt crystals yielded a spectrum similar to that of zinc sulfide. The crystals showing no absorption became active by an irradiation of x rays.

A block of quartz with dimensions $1.305\times1.285\times4.260$ cm³, a block of Rochelle salt with dimensions $0.965\times0.525\times1.980$ cm³, and a plate of Rochelle salt with dimensions $2.015\times1.975\times0.490$ cm³ showed very strong and sharp absorption lines which accompanied "wiggles." These lines disappeared when the crystal was broken into pieces. In the case of Rochelle salt they were strongly observed outside of the ferroelectric range of temperature. These sharp lines, which were measured with the autodyne detectors, formed a spectrum composed of several series of equidistant lines with almost equal intensity. The wiggles of the lines disappeared when the crystal was immersed in oil. Furthermore, it was found in the quartz crystal that a drop of oil adhering to a special point on the surface could extinguish a series of the absorption lines. That the absorption occurred in a small region of the crystal was revealed also by the following experiment: when the crystal was cut into two parts, one of them showed exactly the same absorption as before and the other showed nothing.

Although the absorption occurs in piezoelectric crystals and may accompany mechanical vibrations, it does not seem to be caused by the higher modes of the ordinary piezoelectric vibration, in view of the intensity distribution of the lines in a wide-frequency range and of the sharpness of the lines. The absorption is characterized by the fact that it depends on crystal imperfection and occurs in a very narrow region of the crystals. In order to study the origin of the absorption, further experiments are now in progress. Irrespective of the mechanism, this absorption must be considered as an aspect of the field of radio-frequency or microwave spectroscopy of solids.

The authors wish to express their thanks to Dr. N. Bloembergen for his interest and encouragement and also to Mr. S. Annaka who carried out the x-ray irradiations.

[1] E. Geibe and A. Scheibe, Z. Physik **33**, 760 (1925); also see W. G. Cady *Piezoelectricity* (McGraw-Hill Book Company, Inc., New York, 1946).
[2] Four groups of quartz powders with dimensions of about 5 mm, 1 mm, 0.5 mm, and 0.1 mm were tested. At several Mc/sec, resonances of individual crystals were observed corresponding to the grain sizes. But all groups showed almost the same absorption in the neighborhood of 300 Mc/sec.

Liquid Helium Films

K. R. ATKINS
Department of Physics, University of Toronto, Toronto, Canada
(Received October 27, 1953)

THE Polanyi potential theory[1] is now believed to provide a satisfactory approach to the problem of multilayer adsorption.[2,3] As a first approximation, therefore, the helium film can be considered as a distribution of a continuous fluid in a potential field obtained by combining the earth's gravitational field with the field arising from the van der Waals forces between the helium and the vertical wall on which the film is formed. It follows that the hydrostatic pressure inside the film at a distance z from the wall and at a height y above the surface of the bulk liquid is[4]

$$p=p_0+\rho(\alpha/z^3-gy), \tag{1}$$

where p_0 is the vapor pressure, α depends upon the strength of the van der Waals forces, and ρ is the density of the liquid, which is assumed constant in a first approximation. At the surface of the film, $p=p_0$, and the variation of thickness d with height H is

$$H=\alpha/gd^3, \tag{2}$$

which is the result already obtained by Schiff[5] and Frenkel.[6]

Equation (1) gives a qualitative explanation of several properties of the unsaturated film.[7] The pressure p increases as the wall is approached and is equal to the solidification pressure at a distance of about 7×10^{-8} cm from the wall; this explains why the first one or two layers are solid. The entropy of liquid helium I decreases with increasing pressure, whereas the opposite is true of liquid helium II, so it is easy to see why the differential entropy of the film less the entropy of the bulk liquid should be negative above the λ point but positive below the λ point. Between 1.75°K and the λ point there is a point in the film at which the pressure crosses the λ curve, and the film must then be visualized as a solid inner portion, an intermediate portion of helium I and an outer portion of helium II. This conception may lead towards an understanding of the specific heat of the film and the flow of unsaturated films.

Arguments somewhat similar to these have already been

advanced by Mastrangelo and Aston,[8] but the pressure used by them seems to have a rather different character.

It may be necessary to supplement this picture by considering the zero-point energy, as was done by Bijl, de Boer, and Michels.[9] Although the zero-point energy is known to be much larger than the value appearing in their theory, this does not exclude the possibility of a small superimposed variation with film thickness. Using the simplifying assumptions of the Debye theory of solids, the zero-point energy of the longitudinal Debye waves in the film can be shown to be

$$Z(d)=Z(\infty)\left[1-\frac{1}{6}\frac{c}{\nu_c{}^*d}+\frac{1}{32}\left(\frac{c}{\nu_c{}^*d}\right)^2+\cdots\right], \tag{3}$$

where c is the velocity of first sound and $\nu_c{}^*$ the cut-off frequency in the bulk liquid. The resulting relationship between film thickness and height is

$$H=\alpha/gd^3+(4\times10^{-6}/d)^2. \tag{4}$$

The zero-point energy is responsible for the term in $1/d^2$, which is seen to be important for thick saturated films but less important for the thinner unsaturated films. It should be emphasized that only that part of the zero-point energy associated with the longitudinal Debye waves has been included in this treatment, and the remaining part may be equally important.

A more complete account will appear in the *Canadian Journal of Physics*.

[1] M. Polanyi, Verhandl. deut. physik. Ges. **15**, 55 (1916).
[2] T. L. Hill, *Advances in Catalysis* (Academic Press, New York, 1952), Vol. IV.
[3] W. G. McMillan and E. Teller, J. Chem. Phys. **19**, 25 (1951).
[4] K. R. Atkins, Ph.D. thesis, Cambridge University, 1948 (unpublished).
[5] L. Schiff, Phys. Rev. **59**, 838 (1941).
[6] J. Frenkel, J. Phys. (U.S.S.R.) **2**, 345 (1940).
[7] E. A. Long and L. Meyer, Advances in Physics **2**, 1 (1953).
[8] S. V. R. Mastrangelo and J. G. Aston, J. Chem. Phys. **19**, 1370 (1951).
[9] Bijl, de Boer, and Michels, Physica **8**, 655 (1941).

Anomalous Paramagnetic Resonance in Copper Propionate

HIDETARO ABE
Institute of Science and Technology, University of Tokyo, Tokyo, Japan
(Received October 26, 1953)

ANOMALOUS resonance absorption by Cu^{++} in copper acetate has been observed by Bleaney and Bowers[1,2] and in our laboratory.[3,4] In this salt, the spins of two copper ions are strongly coupled to form an equivalent spin $S=1$.

I have recently observed similar anomaly in copper propionate monohydrate $Cu(CH_3CH_2COO)_2\cdot H_2O$. This crystal is monoclinic with $a:b:c=0.874:1:0.886$ and $\beta=94°22'$.[5] The wavelength of the microwave used is 10.7 mm. When the static magnetic field H_s is applied in the ac plane, six resonance peaks are observed. Three pairs of lines can be obtained from these peaks when H_s is rotated in the ac plane. Each line observed in the ac plane splits into two lines in any plane which is perpendicular to the ac plane. In addition to these, one line is observed almost independent of the direction of H_s, at about half of the mean magnetic field for other peaks.

These observed spectra can be explained by superposition of six sets of spectral lines which are expressed by the Hamiltonian

$$\mathcal{H}=[g]\beta\mathbf{H}\cdot\mathbf{S}+DS_z{}^2+E(S_x{}^2-S_y{}^2), \tag{1}$$

under the condition that $S=1$, where x, y, and z denote the axes of the crystalline field. Values of g, D, and E for three pairs are listed in Table I, the three remaining pairs being given by mirror reflection about the ac plane. ψ in the table means the angle between the c axis and the plane containing two z axes, and α is the angle between one of the z axes and the ac plane. D^* stands for the D value to be given in order to satisfy mainly the experimental data in the x and y directions. g, D, and E for pair (3) in Table I are less reliable than the others because the resonance peaks for this pair could not be observed for some range of angle of H_s.

TABLE I. Parameters occurring in Eq. (1) for the paramagnetic spectra of copper propionate monohydrate.

	Pair (1)	Pair (2)	Pair (3)
g_x	2.34_8	2.35_6	(2.29_3)
g_z	2.09_3	2.10_0	2.09_2
g_y	2.09_6	...	2.09_8
D (in oersteds)	3460	3460	(3730)
D^*	3620	3650	3580
E	~0	~0	~0
ψ (in degrees)	106	158	174
α (in degrees)	28.5	16	52

From these results, the following conclusions may be derived: (1) The unit cell of this crystal contains six inequivalent pairs of Cu^{++} ions, whereas we have two pairs in copper acetate, so far as the microwave spectra are concerned. (2) Each pair of ions in the unit cell is in a very similar environment except that the orientations of the axes of the crystalline field are different. (3) The origin of the anomaly may be assumed to be the extraordinarily short distance between Cu^{++} ions in a pair; a distance of 2.6A between copper ions has been found in copper acetate by van Niekerk and Schoening.[6]

Single crystals of copper formate dihydrate $Cu(HCOO)_2\cdot 2H_2O$ and tetrahydrate were also examined.[7] The anomalous splitting could not be found, and only one resonance peak was observed, the g value of which ranges from 2.06 to 2.32, just as in the ordinary copper salts. Kiriyama at Ôsaka University has analyzed the structure of these salts by means of x-rays.[8] The arrangement of atoms in these crystals is quite different from that in copper acetate.

The author wishes to express his sincere thanks to Professor H. Kumagai for his continuous guidance. A more detailed report will appear in the Journal of the Physical Society of Japan.

[1] B. Bleaney and K. D. Bowers, Phil. Mag. **43**, 372 (1952).
[2] B. Bleaney and K. D. Bowers, Proc. Roy. Soc. (London) **214**, 451 (1952).
[3] Kumagai, Abe, and Shimada, Phys. Rev. **87**, 385 (1952).
[4] H. Abe and J. Shimada, Phys. Rev. **90**, 316 (1953).
[5] P. Groth, *Chemische Kristallographie* (Teubner, Leipzig, 1910), Vol. 3, p. 202.
[6] J. N. van Niekerk and F. R. L. Schoening, Acta Cryst. **6**, 227 (1953).
[7] Shimada, Abe, and Ôno, J. Phys. Soc. Japan (to be published).
[8] Kiriyama, Ibamoto, and Matsuo, Acta Cryst. (to be published).

Specific Heat of He^3 between 1.3°K and 2.3°K†

G. DE VRIES AND J. G. DAUNT
Department of Physics and Astronomy, The Ohio State University, Columbus, Ohio
(Received October 22, 1953)

PURE liquid He^3, unlike liquid He^4, has been found to show no signs of superfluidity. The experimental indications of this marked difference in behavior were evident first in the early work on solutions by Daunt and co-workers,[1] and then by the observations of the pure liquid down to 1.0°K by Osborne, Weinstock, and Abraham[2] and down to 0.2°K by Daunt and Heer.[3] Despite this established difference in the flow properties of liquid He^3 and He^4, it is known that He^3, exactly like He^4, does not become solid under its saturated vapor pressure even at the lowest possible temperatures. (See Osborne *et al.*[4] for data on the melting curve of He^3.) There consequently remains the possibility that liquid He^3 undergoes a liquid-liquid transformation at a sufficiently low temperature. Such a transformation would not be one into a superfluid phase, as in liquid He^4; but it would be, if it existed, evident from observations of the specific heat. A discussion of the many speculations by various authors regarding this possible transformation has already been given by one of us,[5] and this will not be repeated here.[6]

We have carried out calorimetric determinations of the specific heat of liquid He^3 (He^3 content 96 percent; He^4 content 4 percent) with a view to resolving this problem experimentally. Our initial

measurements have been in the temperature range 1.3°K to 2.3°K, and it is felt that the results obtained may be of interest.

8 cc at N.T.P. of He^3 (96 percent) gas, kindly supplied by the U. S. Atomic Energy Commission, were condensed in an adiabatic calorimeter of volume 16 mm^3 fed by a tube of internal diameter 0.025 cm. The temperature of the calorimeter was measured with a carbon resistance thermometer and observations of the electrical "heating cycles" were made semi-automatically using the apparatus previously developed and used in other specific heat determinations.[7,8] A copper shield, mounted in vacuum, completely surrounded the calorimeter and was maintained continuously at a temperature of approximately 0.1°K above that of the calorimeter. This shield had attached thermally to it all the electrical leads leading to the calorimeter. This shield, moreover, formed the only low-temperature anchorage for the filling tube leading to the calorimeter and by this constructional arrangement unwanted condensation of vapor in the filling tube during a heating cycle was avoided.

Our preliminary results are shown in Fig. 1. Owing to the small quantities of liquid He^3 available for these experiments, we estimate that our errors could be as large as ±10 percent. Corrections had to be made for evaporation of liquid, for the heat capacity of the vapor and for the compression of the vapor during the heating cycles. These corrections totaled approximately 14 percent of the

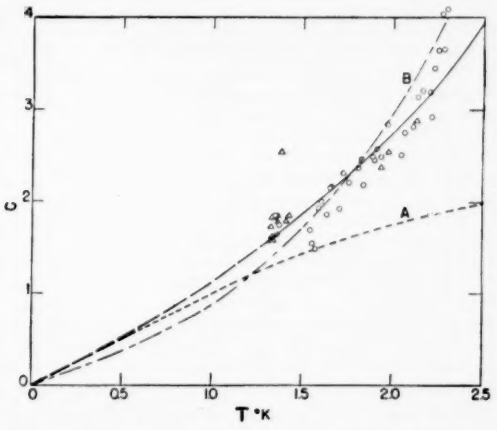

FIG. 1. The specific heat, C_{sat}, in cal/mole-deg, of liquid He^3 (96 percent He^3) as a function of the absolute temperature, T, in °K. The circles and triangles give the observed results. The full curve gives the formula (1) of this paper. The broken curve, *A*, gives the Fermi-Dirac contribution to formula (1) with $T^*=10$°K. The broken curve, *B*, gives formula: $C_{sat}=0.68T+0.27^3$ cal/mole-deg (see text).

observed heat capacities. (Measurements were made, of course, also of the heat capacity of the empty calorimeter itself, which did not amount to more than a few percent of its total heat capacity when filled. Corrections, however, also have been made for this.)

2.3°K was taken as the maximum useful temperature of observation consistent with manageable vapor corrections. The lower temperature of observation (1.3°K) was determined by initial technical considerations. We are now extending the observations to temperatures well below 1°K.

It will be seen that the observed specific heat increases monotonously from about 1.6 cal/mole-deg at 1.3°K to about 3.6 cal/mole-deg at 2.3°K. There is a singular observation at 1.38°K, giving $C_{sat}=2.53$ cal/mole-deg. We are unable, as yet, to decide whether this point represents an observational error or not.

The measured curve is convex towards the T axis and, moreover, C_{sat} at the higher temperatures is larger than $(3/2)R$. These two facts mean that it is impossible to describe the specific heat by a Fermi-Dirac function alone, no matter what degeneracy temperature T^* be chosen. As a crude first approximation our results could be described by the formula, $C_{sat}=0.68T+0.27^3$ cal/mole-deg, which was proposed earlier[9] by one of us[5] and which was based on the results of the vapor pressure measurements on liquid He^3 by Abraham *et al.*[10] This is illustrated by one broken line *B* in Fig. 1.

In interpreting our results in more detail, we have tentatively tried to use the following formulation for C_{sat}:

$$C_{sat}=F(T/T^*)+aT^3 \text{ cal/mole-deg}, \quad (1)$$

where $F(T/T^*)$ is the Fermi-Dirac specific heat function corresponding to a degeneracy temperature T^*, and where the T^3 function would be due to compressional Debye waves.[11] Putting $T^*=10.0$°K and $a=0.125$ cal/mole-deg^4, we obtain the full line of Fig. 1, which is a fair approximation of the experimental results. (One broken line *A* in Fig. 1 gives the function $F(T/10°\text{K})$ alone, which will be seen to have a slope given by 1.0 cal/mole-deg^3 at $T\to 0$.)

The apparently appropriate F-D degeneracy temperature, $T^*=10$°K, is high compared with that which can be computed for a F-D gas with the liquid He^3 number density of particles (4.85°K). The absolute magnitude of the cubic[12] term of Eq. (1) is approximately 5 times larger than that in liquid He^4, as measured by Kramers *et al.*[13]

Equation (1), if considered as an appropriate extrapolation for the specific heat *below* 1.3°K, leads to an entropy of 1.1 cal/deg^{-1} mole^{-1} at 1°K. This is 1.1 cal/deg^{-1} mole^{-1} *less* than that calculated by Abraham *et al.*[10] from the vapor pressure data if the nuclear entropy is also included. It seems peculiar that the magnitude of the discrepancy is approximately $R\ln 2$, the nuclear entropy. It seems necessary to conclude, therefore, that Eq. (1) may *not* be extrapolated below 1°K with any confidence and that at best it must be regarded as an *interpolation formula* in the temperature range covered by our measurements *only*.

† Assisted by a contract between the U. S. Atomic Energy Commission and The Ohio State University Research Foundation.

[1] Daunt, Probst, Johnston, Aldrich, and Nier, Phys. Rev. **72**, 502 (1947); Daunt, Probst, and Johnston, J. Chem. Phys. **15**, 759 (1947).

[2] Osborne, Weinstock, and Abraham, Phys. Rev. **75**, 988 (1949).

[3] J. G. Daunt and C. V. Heer, Phys. Rev. **79**, 46 (1950).

[4] Osborne, Weinstock, and Abraham, Phys. Rev. **82**, 263 (1951), and Weinstock, Abraham, and Osborne, Phys. Rev. **85**, 158 (1952).

[5] J. G. Daunt, Advances in Physics **1**, 209 (1952).

[6] The speculations have continued since the publication of our review article (reference 5), notably by K. S. Singwi [Phys. Rev. **87**, 540 (1952)], by B. Weinstock, Abraham, and Osborne [Phys. Rev. **89**, 787 (1953)], and by T. C. Chen and F. London [Phys. Rev. **89**, 1038 (1953)].

[7] Horowitz, Silvidi, Malaker, and Daunt, Phys. Rev. **88**, 1182 (1952).

[8] M. Horowitz and J. G. Daunt, Phys. Rev. **91**, 1099 (1953).

[9] In our review in Advances in Physics (reference 5), the equation noted above (formula 46 in the review) erroneously included a factor R throughout.

[10] Abraham, Osborne, and Weinstock, Phys. Rev. **80**, 366 (1950).

[11] Strictly, C_v should be used in this formulation rather than C_{sat}. In view of the relatively large possible experimental errors in the values of C_{sat} given here, it has been considered unnecessary to make the corrections for this difference.

[12] The Debye θ for compressional modes only, corresponding to the term a of Eq. (1) equal to 0.125 cal/mole-deg,[4] is 10.8°K. Strictly, therefore, the specific heat would not be exactly cubic at 2.3°K.

[13] Kramers, Wasscher, and Gorter, Physica **18**, 329 (1952).

Interpretation of Hall Effect and Resistivity Data in PbS and Similar Binary Compound Semiconductors

WAYNE W. SCANLON
U. S. Naval Ordnance Laboratory, White Oak, Maryland
(Received November 2, 1953)

THE width of the forbidden energy gap in a semiconductor is an important parameter appearing in theories of photoconductivity and other semiconductor phenomena. For the elementary semiconductors, such as germanium and silicon, there is good agreement among the various workers on the value of this energy. In the case of certain binary compound semiconductors, the values reported in the literature are not consistent. In lead sulfide, for example, values are reported ranging from 0.3 to 1.17 ev[1] for the forbidden band width (ΔE) as obtained from the slope

of the high-temperature resistivity and Hall effect data. The most recent value, 1.17 ev, based upon Hall effect data at temperatures between 700°C and 900°C, reported by Putley and Arthur,[2] is difficult to reconcile with information gained from either photoconductivity or infrared absorption studies which indicate an energy gap of about 0.4 ev.[3]

This note will point out a source of error in the interpretation of Hall effect and resistivity data on compound semiconductors which may account for the diversity of values given for the energy gap in some of these materials.

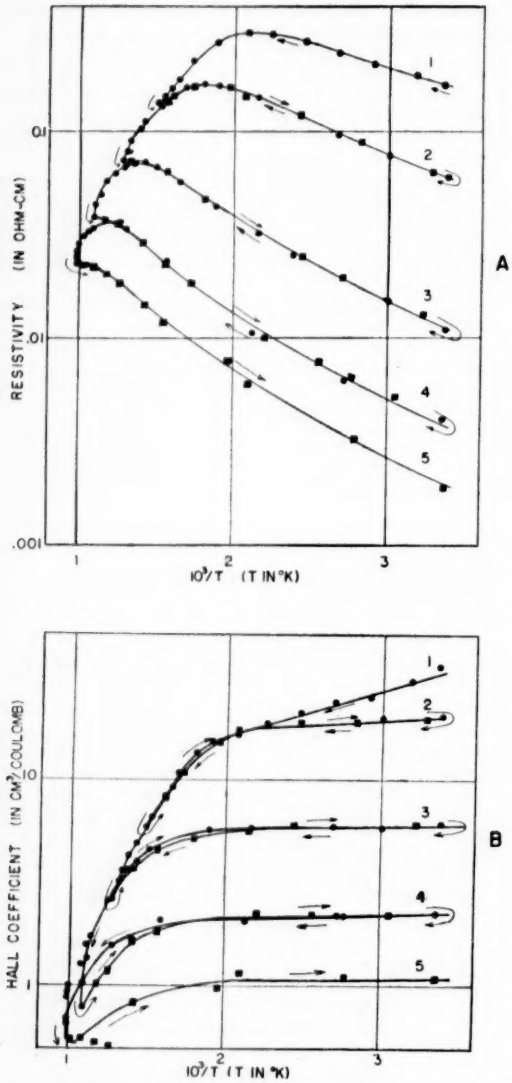

FIG. 1. (A) Resistivity, and (B) Hall effect in a PbS single crystal for heating cycles to the following maximum temperatures: Curve 1, 680°K; Curve 2, 788°K; Curve 3, 919°K; and Curve 4, 1023°K. Points on heating curve ●●●. Points on cooling curve ■■■.

The electrical properties of a binary compound semiconductor, such as PbS, are governed by deviations from stoichiometric proportions of Pb and S in the crystal. An excess of Pb results in *n*-type conductivity, while an excess of S results in *p*-type conductivity. In our experiments on single crystals of PbS, we find that the concentration of excess Pb or S atoms remains unchanged in temperature cycles up to about 500°K, as shown by the reversibility of the curves of Hall effect and resistivity. Upon heating the crystal above this temperature irreversible behavior is observed. We have observed similar irreversible behavior in single crystals of PbSe and PbTe. Effects of this type have also been noted by Chasmar and Putley in PbTe.[4]

In Fig. 1A are the curves of resistivity taken on a natural *n*-type PbS crystal for a series of temperature cycles between room temperature and maximum temperatures of about 700°, 800°, 900°, and 1000°K. The sample was in an inert atmosphere of pure argon[5] throughout the experiment. Curves 1 and 2, where the maximum temperature was about 700°K, begin to show composition changes. Curves 2 and 3, where the maximum temperature was about 800°K, show further composition changes to the extent that the cooling curve for resistivity no longer has a knee leading from the intrinsic conductivity region. At about 750°K a change in the slope of the heating curve can be seen. Curves 4 and 5 provide further evidence of changing composition of the PbS with no evidence of intrinsic conductivity appearing on the cooling curves. A series of four measurements made on the sample, while it was held at 1023°K for about an hour, show a continuous change in composition giving the resistivity curve an apparent infinite slope.

The Hall effect, which was measured at the same time as the resistivity, is plotted in Fig. 1B. The irreversible character of the data with temperature cycles can be seen. The cooling curves from the higher maximum temperatures do not show intrinsic semiconductor behavior. The data for curves 4 and 5 at high temperatures are somewhat scattered due to the small Hall effect, and they are not as reliable as the corresponding resistivity data.

As a result of the heat treatments, the composition of the PbS changed from 4×10^{17} to 7×10^{18} donor atoms/cm³. This increase in the lead concentration in the crystal may be accomplished at elevated temperatures by the loss of sulfur atoms, which leave their positions in the lattice and diffuse out through the surface. Hintenburger[6] and Eisenmann[7] have shown in similar experiments that sulfur may be added or removed from PbS by heat treatments.

The analysis of resistivity and Hall effect data from a semiconductor which undergoes composition changes is complicated by the presence of two mechanisms for increasing the concentration of electrons in the conduction band. At elevated temperatures, the loss of sulfur from PbS crystals apparently becomes so rapid as to produce changes in the concentration of electrons at a rate exceeding those produced by thermal excitation of intrinsic electrons. Furthermore, while the latter reaches an equilibrium condition rapidly, the former will proceed toward an equilibrium at a rate which depends upon the temperature of the crystal and the sulfur vapor pressure outside the crystal. In the extreme case where the sulfur pressure is maintained at zero, the PbS could eventually convert to lead. Thus, in measurements of this kind the time required to obtain a single curve becomes an important factor. Measurements carried out slowly will be more affected by the loss of sulfur than those carried out rapidly.

We believe that Putley and Arthur's[2] interpretation of the slope of the Hall effect curves, from 700° to 900°K, failed to take into account the thermal changes of composition in the material. Their published value of 1.17 ev for the width of the forbidden energy gap in lead sulfide may be due more to composition changes than to intrinsic behavior.

If, however, Hall effect data are taken on samples of relatively pure PbS only up to about 500°K, where composition changes are not observed, a calculation of the forbidden energy gap may be made using the conventional intrinsic semiconductor equation $R=AT^{-\frac{1}{2}}\exp(\Delta E/2kT)$. The value of ΔE obtained on six single crystals of PbS, with impurity concentrations from 10^{16} to 10^{17}/cc and for data taken only up to about 500°K, was found to be 0.37 ±0.01 ev. This energy gap is in better agreement with optical data and indicates that in PbS the valence band is the primary source of photoconductive electrons. This clarifies the question raised by

Smith[3] regarding the difficulty of understanding the source of primary photoconductive electrons in PbS and possibly also in PbSe and PbTe.

[1] M. C. Morton, Trans. Faraday Soc. **43**, 194 (1947); C. A. Dunaev and J. P. Maslakovtz, J. Exptl. Theoret. Phys (U.S.S.R.) **10**, 901 (1947); A. F. Gibson, Proc. Phys. Soc. (London) **B63**, 752 (1950); E. H. Putley, Proc. Phys. Soc. (London) **B65**, 993 (1952); R. A. Smith, Phil. Mag. Supplement 2, 321 (1953).
[2] E. H. Putley and J. B. Arthur, Proc. Phys. Soc. (London) **B14**, 616 (1951).
[3] R. A. Smith, Phil. Mag. Supplement 2, 321 (1953).
[4] R. P. Chasmar and E. E. Putley, *Semiconducting Materials* (Butterworth's Scientific Publications, London, 1951), p. 216.
[5] National Bureau of Standards mass spectrometer analysis gives 99.94+ percent A and 0.05 percent N_2.
[6] H. Hintenburger, Z. Physik **119**, 1 (1942).
[7] E. Eisenmann, Ann. Physik **38**, 121 (1940).

Thermal Anomalies Associated with the Antiferromagnetic Ordering of FeF_2, CoF_2, and NiF_2

J. W. Stout and Edward Catalano*
Institute for the Study of Metals and Department of Chemistry, University of Chicago, Chicago, Illinois
(Received October 28, 1953)

FROM measurements of the magnetic susceptibility of powdered materials, Bizette[1] concluded that MnF_2 and FeF_2 are antiferromagnetic, but that the isomorphous compounds CoF_2 and NiF_2 are not. The neutron diffraction studies of Erickson[2] show, however, that at low temperatures all four compounds are antiferromagnetically ordered and magnetic anisotropy measurements[3] on a single crystal of CoF_2 indicate an antiferromagnetic behavior. We have measured the heat capacity of FeF_2, CoF_2, and NiF_2 over the temperature range 12–300°K. Each of these salts shows a pronounced thermal anomaly of the lambda-shape

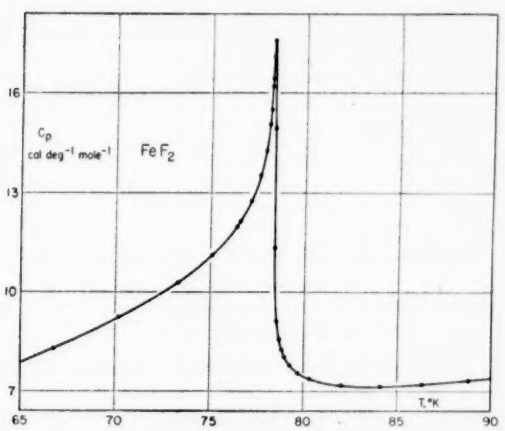

FIG. 1. Molal heat capacity of ferrous fluoride *versus* temperature.

characteristic of processes where there is cooperative ordering. The experimental heat capacity data in the neighborhood of the anomalies are shown in Figs. 1, 2, and 3 for FeF_2, CoF_2, and NiF_2, respectively. In order to determine the shape of the curves, the points in the regions of rapidly changing heat capacity were taken with small temperature increments (about 0.1°). The temperatures of the heat capacity maximum are: FeF_2, 78.3°K; CoF_2, 37.7°K; NiF_2, 73.2°K. A similar anomaly in MnF_2 with a heat capacity maximum at 66.5°K has been reported previously.[4] There seems to be no doubt that these anomalies represent the loss in entropy upon passing from the disordered paramagnetic state to the ordered antiferromagnetic state.

The antiferromagnetic Curie temperatures deduced by Erickson[2] from the temperature variation of the magnetic structure factor are higher than those of the maximum in heat capacity by factors ranging from 1.1 to 1.3. However, the neutron diffraction measurements are a relatively imprecise method for determining the Curie temperature and also it seems probable that near the Curie point the magnetic form factor is varying much more rapidly with temperature than the Brillouin function used by Erickson in his extrapolation. We do not believe, therefore, that there is a significant disagreement.

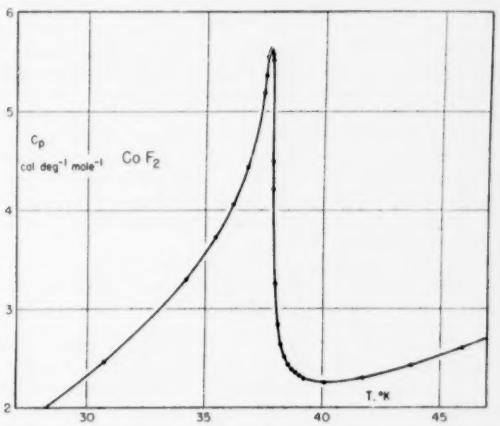

FIG. 2. Molal heat capacity of cobalt fluoride *versus* temperature.

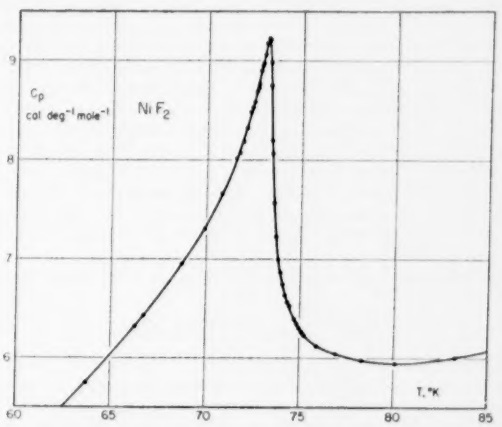

FIG. 3. Molal heat capacity of nickel fluoride *versus* temperature.

We have also made heat capacity measurements on the diamagnetic salt ZnF_2, which is isomorphous with the four antiferromagnetic fluorides. The data on ZnF_2 will permit an estimate of the entropy and heat capacity arising from lattice vibrations in the antiferromagnetic salts and thus enable the separation of the thermal effects caused by the magnetic ordering. The data and calculations will be published in detail elsewhere.

* Eastman Kodak Company Fellow 1951–52; Allied Chemical and Dye Corporation Fellow 1952–53.
[1] H. Bizette, Ann. Physik [12] **1**, 295 (1946).
[2] R. A. Erickson, Phys. Rev. **90**, 779 (1953).
[3] J. W. Stout and L. M. Matarrese, Revs. Modern Phys. **25**, 338 (1953).
[4] J. W. Stout and H. E. Adams, J. Am. Chem. Soc. **64**, 1535 (1942).

Spin-Lattice Relaxation and the Residual Width of Highly Exchange-Narrowed Paramagnetic Resonances*

J. P. Lloyd and G. E. Pake
Department of Physics, Washington University, Saint Louis, Missouri
(Received November 2, 1953)

We have investigated the saturation properties of two highly exchange-narrowed paramagnetic resonances in low magnetic fields with a view to determining the contribution of the spin-lattice relaxation mechanisms to the line width. Both samples were polycrystalline free radicals: diphenyl picryl hydrazyl or DPPH, $(C_6H_5)_2N-N-C_6H_2(NO_2)_3$, and tris-*p*-nitro-phenyl methyl or TpNPM, $C(C_6H_4(NO_2))_3$. Our experiments indicate that the limitation which spin-lattice relaxation places upon the lifetime of the odd-electron spin state contributes much, if not all, of the line width at 60 Mc/sec.

At such low frequencies, rf magnetic fields as large as 1 oersted are readily obtainable. The rf spectrometer, a variation of that designed by Schuster,[1] was used in conjunction with a Watkins-Pound calibrator[2] to make saturation measurements.

A vacuum tube voltmeter was built into the apparatus to measure the rf voltage across the coil, from which the rf field was calculated as follows. The inductance of the sample coil, wound of small flat copper strap to minimize capacitance between turns, was determined at 60 Mc/sec. Next the ratio of magnetic field to current in the coil was obtained by performing an auxiliary resonance experiment in which the sample coil carried direct current and contributed to the constant external magnetic field for a still smaller rf coil containing a free radical. The result is that $H_1=0.022V$, where V is the rms voltage at 60 Mc/sec and H_1 is the half-amplitude of the rf field, in oersteds, at the center of the coil. To the extent that the current distribution in the coil is not the same at 60 Mc/sec as for dc, this calibration may introduce some systematic error.

In the absence of a rigorous quantum treatment of the line profile as influenced by spin-lattice relaxation, dipolar spin-spin interactions, exchange, and the rf field amplitude, we use the phenomenological equations of Bloch[3] in the light of their justification from a microscopic viewpoint by Wangsness and Bloch.[4] That justification neglects spin-spin interaction and may at first seem inapplicable when both exchange and dipolar spin-spin interactions are present. However, exchange[5,6] tends to render incoherent the dipolar interactions. If this effect is pronounced, Wangsness and Bloch's analysis can apply, along with the result $T_2=T_1$ obtained for their case *d*, "isotropic molecular surroundings." The characteristic frequency ω^* of Wangsness and Bloch is then essentially the ω_e of reference 6.

The imaginary part of the Bloch susceptibility[7] is, when $T_2=T_1$,

$$\chi''=\tfrac{1}{2}\chi_0\omega_0T_1\frac{1}{1+T_1^2(\omega-\omega_0)^2+\gamma^2H_1^2T_1^2}. \quad (1)$$

Equation (1) describes a line profile of the Lorentz or damped-oscillator shape, which fits our experimental line shapes excellently and is in agreement with expectations based upon theory and other experiments.[6] The half-width $\Delta\omega_{\frac{1}{2}}$ at half-maximum intensity obtained from Eq. (1) is

$$\Delta\omega_{\frac{1}{2}}=[T_1^{-2}+\gamma^2H_1^2]^{\frac{1}{2}}. \quad (2)$$

The calibrator, which was used with a field-modulation apparatus sensitive to the derivative of the line shape, measures the saturation factor $S'=[d\chi''(H_1)/d\omega]_{max}/[d\chi''(0)/d\omega]_{max}$ which is, from Eq. (1),

$$S'=[1+\gamma^2H_1^2T_1^2]^{-\frac{1}{2}}. \quad (3)$$

Figure 1 compares a curve of S' *versus* V for $T_1=6.3\times10^{-8}$ sec with experimental values of S' for DPPH; the experimental half-width $\gamma^{-1}\Delta\omega_{\frac{1}{2}}$ is also plotted. The validity of the assumption that $T_2=T_1$ is tested by comparing $(\gamma T_1)^{-1}=0.90$ oersted with $\gamma^{-1}\Delta\omega_{\frac{1}{2}}=0.97\pm0.05$ oersted at low rf voltage.

Similarly $T_1=1.6\times10^{-7}$ sec fits the data for TpNPM, and

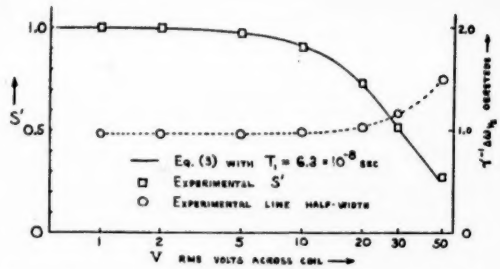

FIG. 1. Comparison of calculated and experimental values of the saturation factor S' a sa function of the rms voltage V. The experimental half-width $\gamma^{-1}\Delta\omega_{\frac{1}{2}}$ is also plotted as a function of V.

$(\gamma T_1)^{-1}=0.35$ oersted is to be compared with $\gamma^{-1}\Delta\omega_{\frac{1}{2}}=0.36\pm0.03$ oersted at low rf voltages.

These measurements indicate directly that the spin-lattice relaxation time T_1 contributes much or all of the line width in DPPH or TpNPM. In general, T_1 should depend upon the external magnetic field,[8] and one should not expect the widths of these highly exchange-narrowed resonances to be independent of the resonant frequency. Indeed, 0.97 ± 0.05 oersted for the DPPH half-width at 60 Mc/sec is to be contrasted with 1.35 ± 0.05 oersteds obtained by Professor J. Townsend of this laboratory at about 9000 Mc/sec and 1.36 ± 0.01 oersteds obtained at a similar microwave frequency by Professor R. T. Weidner at Rutgers University.[9] It should be noted, however, that this indicated decrease of T_1 with increasing field runs counter to the prediction of theory for the so-called Raman processes treated by Van Vleck.

One of us (J. P. L.) gratefully acknowledges the assistance of a Shell Fellowship held during part of this work.

* Assisted by the joint program of the U. S. Office of Naval Research and U. S. Atomic Energy Commission.
[1] N. A. Schuster, thesis, Washington University, 1951 (unpublished).
[2] G. D. Watkins and R. V. Pound, Phys. Rev. **82**, 343 (1951). We wish to thank Dr. Watkins for communicating further details of his work to us.
[3] F. Bloch, Phys. Rev. **70**, 460 (1946).
[4] R. K. Wangsness and F. Bloch, Phys. Rev. **89**, 728 (1953).
[5] J. H. Van Vleck, Phys. Rev. **74**, 1168 (1948).
[6] P. W. Anderson and P. R. Weiss, Revs. Modern Phys. **25**, 269 (1953).
[7] See, for example, G. E. Pake, Am. J. Phys. **18**, 438 (1950), the notation of which is used here.
[8] J. H. Van Vleck, Phys. Rev. **57**, 426 (1940).
[9] Rutgers University, *Fourth Annual Progress Report on Nuclear and Electronic Paramagnetism and Low Temperature Studies*, 1950 (unpublished), p. 40.

Spontaneous Hall Effect in Ferromagnetics

J. Smit and J. Volger
Philips Research Laboratories, N. V. Philips' Gloeilampenfabrieken, Eindhoven, Netherlands
(Received September 2, 1953)

The Hall voltage in ferromagnetics[1] at saturation can be expressed in the form:

$$E_y/i_x=\rho_{yx}=-\rho_{xy}=A_H\cdot B_s+\rho_{SH}. \quad (1)$$

A_H is the normal Hall coefficient and ρ_{SH} the spontaneous Hall resistivity. We have measured the Hall effect of several specimens of nickel and a number of its alloys in fields up to 14 000 gauss and, in addition, their resistivity ρ. The results are given in Table I. All samples have been annealed for 1 hr at 1000°C in pure H_2.

For our Ni sample with smallest residual resistivity, ρ_{SH} vanishes at low temperatures.[2] For alloys, however, ρ_{SH} remains finite, and, in general, ρ_{SH} varies roughly in the same way as ρ. Mostly the spontaneous Hall angle is $\frac{1}{2}$ or 1×10^{-2}.

Three possible causes for the spontaneous Hall voltage are

(a) internal real magnetic fields resulting from the dipoles,
(b) spin-orbit interaction,[3,1]
(c) the inhomogeneous magnetic field induced by the primary current i_x.[4,1]

TABLE I. Hall coefficient A_H, spontaneous Hall resistivity ρ_{SH}, and resistivity ρ of some Ni alloys.

Composition atomic %	$-A_H \times 10^{13}$ (Ω cm gauss^{-1})			$-\rho_{SH} \times 10^{8}$ (Ω cm)			$\rho \times 10^{6}$ (Ω cm)		
	20°K	77°K	290°K	20°K	77°K	290°K	20°K	77°K	290°K
Ni (carbonyl)	5.0	3.6	12.6	0.00	0.12	1.48	0.059	0.69	6.8
Ni (commercial)	5.8	5.2	6.0	0.16	0.17	3.9	0.40	0.86	7.2
Ni (cold worked)	5.1	5.1	11	0.03	0.03	2.7	0.32	0.84	7.1
Ni (annealed)	4.0	4.2	13.3	0.10	0.11	2.2	0.12		6.9
Ni 91 Cu 19	24	21	11.5	3.7	4.2	13.4	8.3	9.3	18.5
Ni 82 Cu 18	25	23	13.5	7.2	8.1	15.8	15.5	16.7	28.8
Ni 92.5 Fe 2.5 Cu 5	20.5	17	14.5	2.3	2.6	9.0	6.3	7.1	15.0
Ni 85 Fe 5 Cu 10	24	21	21	2.4	2.9	7.6			20.2
Ni 90 Co 10	12	11	22.5	0.4	0.6	5.4	2.2		11.8
Ni 80 Co 20	21	20	19	0.22	0.12	0.55	3.2		12.0
Ni 70 Co 30	29	28	13	0.32	−0.25	−1.9	3.9	4.0	11.4
Ni 89.5 Fe 10.5	4	4.5	17	1.3	1.1	1.5	3.8	4.5	13.1
Ni 84 Fe 16	23.5	22	17	−0.40	−0.65	−0.90	4.6	5.2	14.4
Ni 92 Al 8	18	18	10	11.5	13	22.5	12.4	13.1	24.8
Ni 94 Si 6	7	10	11	8.7	9.1	18.3	9.5	10.1	18.0
Ni 97 Sn 3	8.5	9	20	9.0	9.1	16.1	10.8		17.2

The mean internal field is equal to **B**, but fields alternating with distance are superposed. These fields and also the effect (b) cannot give a finite ρ_{SH} in a periodic lattice (pure metal at $T=0$°K); this may be seen as follows. Apart from the effect due to **B**, both (a) and (b) give rise to a perturbing potential[1] having the same periodicity as the lattice which is unable to change the k vector of the Bloch wave function within one band; i.e., no effective force results. The relevant integrals in reference 3 are, in fact, all zero.

The force **f**, exerted on a dipole $\boldsymbol{\mu}$, due to (c), had been based[4,1] upon the equation $\mathbf{f}=(\boldsymbol{\mu}\cdot\nabla)\mathbf{H}$, giving $f_y=\frac{1}{2}\mu_x\partial H_y/\partial z$. This formula applies only to a dumbbell dipole, whereas for a dipole generated by a circular current $\mathbf{f}=\nabla(\boldsymbol{\mu}\cdot\mathbf{H})$, giving $f_y=\mu_x\partial H_x/\partial y$. The latter model applies to electron spin and is implicitly used when stating that the mean internal field is equal to **B**. In strips, as normally used for Hall measurements, $\partial H_x/\partial y$ is negligible.

Thus, for a perfectly periodic lattice these theories do not predict a finite spontaneous Hall voltage.

[1] E. M. Pugh and N. Rostoker, Revs. Modern Phys. **25**, 151 (1953).
[2] J. Smit, Physica **17**, 612 (1951).
[3] A. G. Samolovich and B. L. Koukov, J. Exp. Theoret. Phys. (U.S.S.R.) **20**, 783 (1950).
[4] V. Rudnitsky, J. Exptl. Theoret. Phys. (U.S.S.R.) **9**, 262 (1939).

Dielectric Properties of Some Double Tartrates*

F. JONA AND R. PEPINSKY
X Ray and Crystal Analysis Laboratory, Department of Physics, Pennsylvania State College, State College, Pennsylvania
(Received October 30, 1953)

IN his excellent discussion of the dielectric anomalies of Rochelle Salt, Mueller[1] states that "the isomorphous Tl−Na[2] and Rb−Na salts also are ferroelectric, but the NH_4−Na-tartrate, although it is also an isomorph, has normal dielectric properties." Cady,[3] on the other hand, states that "pure crystals of $NH_4NaC_4H_4O_6\cdot 4H_2O$, $RbNaC_4H_4O_6\cdot 4H_2O$ or $TlNaC_4H_4O_6\cdot 4H_2O$ have quite normal dielectric behavior." Both authors quote Kourtschatov's extremely interesting observations on $Na(NH_4, K)$-$C_4H_4O_6\cdot 4H_2O$ mixed crystals.[4] That investigator found that for molar concentrations of NH_4 greater than 20 percent, with the NH_4 ions substituted for K in Rochelle Salt, the mixed crystals show a single Curie point below −70°C.

We have re-examined the dielectric constants ϵ_a, ϵ_b, and ϵ_c (along the a, the b, and the c axis, respectively) in $NaRbC_4H_4O_6\cdot 4H_2O$, over the temperature range from 4.2°K to 333°K, with a field of 10 v/cm and a frequency of 10 kc/sec. No dielectric anomaly appears in this temperature range. Table I gives values on the gently rising curves for 4.2°K, 88°K, 298°K, and 333°K. At about 333°K the crystal dehydrates rapidly, and losses and dielectric constants increase strongly.

Mueller's statement concerning the Na−Rb salt is thus not confirmed.

The dielectric behavior of the $NaNH_4$ double salt has also been re-examined. Although no *peak* appears along anyof the three axes, down to 4.2°K, confirming Mason's[5] prediction for ϵ_b, an anomaly does appear at 109°K. The dielectric constants ϵ_a, ϵ_b, and ϵ_c are 8.4, 9.3, and 9.6, respectively, at room temperature. At 110°K these values have dropped very gradually to 7.5, 8.3, and 8.6, respectively. But between this temperature and 105°K a sudden and reproducible drop of about 17 percent appears in all three values, as shown in Fig. 1. This suggests a rotational transition. The behavior is not affected by a dc biasing field of 10 kv/cm superimposed on the ac field of 10 v/cm.

TABLE I. Dielectric constants for $NaRbC_4H_4O_6\cdot 4H_2O$.

	4.2°K	88°K	298°K	333°K
ϵ_a	6.8	7.3	9.7	11.2
ϵ_b	5.8	6.0	7.6	8.4
ϵ_c	5.3	5.6	8.3	13.7

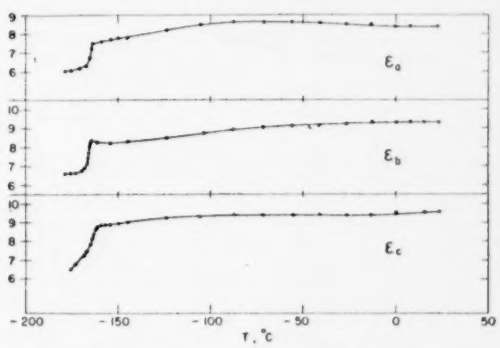

FIG. 1. Dielectric constants of $NaNH_4C_4H_4O_6\cdot 4H_2O$ vs T.

The dielectric anomaly in the $NaNH_4$ salt was discovered in a re-examination of Kourtschatov's results for mixed $NaNH_4$ and NaK salts. The complete phase diagram, explored dielectrically and thermally, will be reported shortly. An x-ray study of the mixed salts is also in progress.

* Research supported by Air Research and Development Command.
[1] H. Mueller, Ann. N. Y. Acad. Sci. **40**, 321 (1940). See p. 322.
[2] Mueller actually writes "Ta−Na," but this is obviously a typographical error.
[3] W. G. Cady, *Piezoelectricity* (McGraw-Hill Book Company, Inc., New York, 1946), p. 654.
[4] I. V. Kourtschatov, *Le Champ Moleculaire dans les Dielectriques* (Hermann et Cie, Paris, 1936).
[5] W. P. Mason, *Piezoelectric Crystals and their Applications to Ultrasonics* (D. van Nostrand Company, Inc., New York, 1950), p. 223.

The Atomic Heat and Critical Magnetic Field of Superconducting Cadmium

J. R. CLEMENT
Naval Research Laboratory, Washington, D. C.
(Received October 26, 1953)

RECENT calorimetric measurements by Samoilov[1] on cadmium below 1°K have shown an inconsistency between calorimetric data and caloric results deduced thermodynamically from a critical magnetic field equation of parabolic analytic form. Samoilov[1] notes that a rather large linear temperature term is required in the superconducting atomic heat if a parabolic equation is to give correctly the difference between the atomic heats in the normal and superconducting states; yet the calorimetric data for the superconducting state indicate that no such term is actually present. The magnitude of this discrepancy appears to be well beyond the range of experimental error. A similar inconsistency in the data for indium has recently been resolved[2] by assuming that the critical field equation is of cubic analytic form, $H_c=H_0[1-at^2+(a-1)t^3]$, where H_c is the magnetic field which just destroys superconductivity at temperature T, H_0 is the value of this field at $T=0°K$, t is the reduced temperature T/T_c, T_c is the transition temperature in zero magnetic field, and a is a dimensionless constant near unity.

If one takes $464.5T^3/(300)^3$ cal/mole deg for the lattice heat and $1.70\times10^{-4}T$ cal/mole deg for the normal electronic heat, in agreement with Samoilov's conclusions from his normal state data, and $T_c=0.555°K$, one finds, following an analysis similar to that described for indium,[2] that $a=1.20$ and $H_0=29.7$ gauss. In Fig. 1

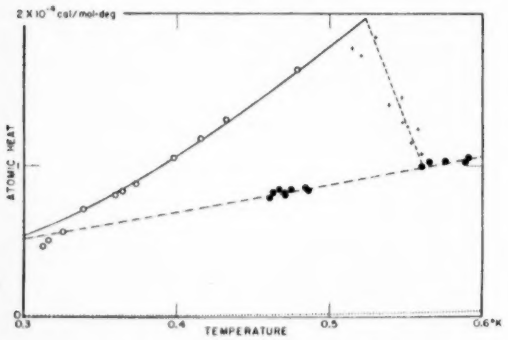

FIG. 1. Comparison of measured calorimetric data with results deduced thermodynamically from a critical magnetic field equation of cubic analytic form. Data obtained by Samoilov (reference 1): ○ in the superconducting state; ● in the normal state; + "in the transition phase." Smooth curves calculated for: —— superconducting state; -·- normal state; ···· lattice; - - - "transition phase" (approximate, assuming that the transition occurs in an earth's field of about 0.6 gauss and that the temperature rises obtained in the calorimetric measurements are always 0.04°K).

calorimetric data[1] are compared with calculated curves obtained by adding to the lattice heat, $464.5T^3/(300)^3$ cal/mole deg, electronic heats deduced from the cubic critical field equation. The electronic heat deduced for the normal state is $1.70\times10^{-4}T$ cal/mole deg, the same as that found by Samoilov[1] from his normal state calorimetric data, and that deduced for the superconducting state is $[1.70\times10^{-4}T/2a][15(a-1)^2t^4-20a(a-1)t^3+6a^2t^2+6(a-1)t]$ cal/mole deg. The lack of agreement between the curve and the three superconducting data at lowest temperatures may be due to experimental error since Samoilov notes that there was "an irregularity in the course of the resistance of the (leaded phosphor bronze) thermometer below 0.4°K." Measured critical field data[3-5] are compared with the cubic equation in Fig. 2.

A reasonably consistent description of the caloric and magnetic properties of cadmium has thus been obtained, just as for indium, by assuming that the critical magnetic field equation is of cubic analytic form rather than the simpler parabolic form. Certainly

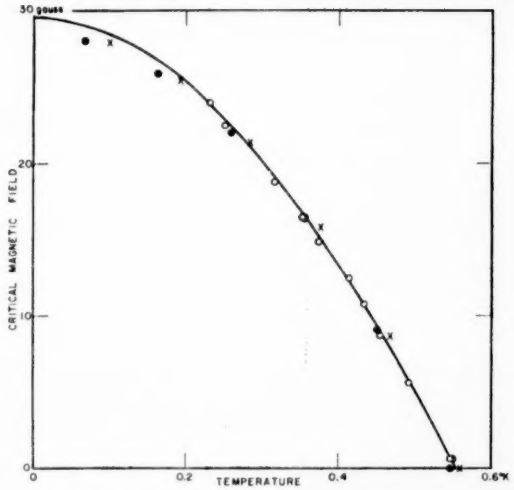

FIG. 2. Comparison of measured critical magnetic field data with a smooth curve calculated from a cubic equation with constants deduced from calorimetric data. Data of: ○ Steele and Hein (reference 3). Curve calculated from parabolic equations reported by: ● Samoilov (reference 4); × Goodman and Mendoza (reference 5).

these results are not to be interpreted as conclusive evidence that the critical field equation is of exactly cubic form. One can conclude only that the cubic equation is a sufficiently good approximation to the true equation to lead to a consistent description of caloric and magnetic properties within the limitations of experimental error, over the temperature range for which both kinds of data are now available.

[1] B. N. Samoilov, Doklady Akad. Nauk. S.S.S.R. **86**, 281 (1952).
[2] J. R. Clement and E. H. Quinnell, Phys. Rev. **92**, 258 (1953).
[3] M. C. Steele and R. A. Hein (unpublished). (The author is indebted to Dr. Steele and Dr. Hein for permission to include their data in this report.)
[4] B. N. Samoilov, Doklady Akad. Nauk. S.S.S.R. **81**, 791 (1951).
[5] B. B. Goodman and E. Mendoza, Phil. Mag. **42**, 594 (1951).

The Interaction Cross Section of Hydrogen and Heavier Elements for 450-Mev Negative and 340-Mev Positive Pions*

S. J. LINDENBAUM AND LUKE C. L. YUAN
Brookhaven National Laboratory, Upton, New York
(Received August 14, 1953)

THE hydrogen interaction cross section for pions of kinetic energies up to about 150–200 Mev have been measured by Anderson, Fermi, and others.[1-4] An investigation of the behavior of these cross sections for negative and positive ions from 150 Mev to about 700 Mev is now in progress using fast scintillation counter telescopes in the external meson beams of the 2.3-Bev Brookhaven Cosmotron.

This letter will report the cross sections obtained for 450-Mev negative and 340-Mev positive pions. The experiment was performed in two different beams using the arrangement shown in Fig. 1. First, the cross sections were determined using the negative 500-Mev π beam analyzed by the Cosmotron magnet. The beam was then analyzed a second time by a momentum selective triple monitor telescope with a deflecting magnet between the second and third counters. A fourth large liquid counter was then placed in quadruple coincidence with the monitor.

In the second arrangement, a direct beam at 32° from the forward direction diagonally through a straight section (without passing through the Cosmotron magnetic field) was defined and momentum analyzed by a similar magnetically selective quadruple telescope.

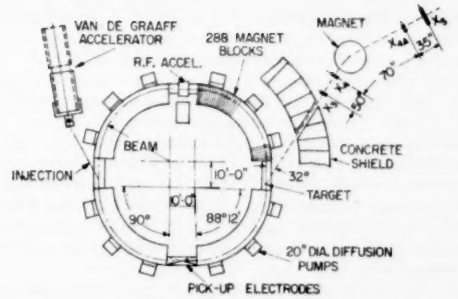

FIG. 1. The schematic arrangement of the scintillation counter telescope in the direct beam produced by the Brookhaven 2.3-Bev cosmotron. X_2 and X_3 are 2½-inch diameter diphenolacethylene crystal counters, X_{4A} is a 1½-inch crystal and X_5 is a 6-inch liquid scintillator. The beam intensity was approximately 10^{10} protons per pulse.

In order to determine the composition of the beams, copper range curves were taken, and it was found that both beams consisted of about 90 percent negative pions and 10 percent negative muons and electrons.

Transmission measurements on polyethylene, carbon, and copper yielded the cross sections,[5] shown in Table I. The results

TABLE I. Total interaction cross sections for 450-Mev negative pions.

Element	Cross section in millibarns	Percentage of geometrical cross section using $R=1.37A^{\frac{1}{3}}\times10^{-13}$ cm
Hydrogen	25±3	46± 5.7
Carbon	186±22	61± 7
Copper	730±109	77±11.5

obtained by using several lengths of absorbers came out to be the same within the errors for the two arrangements employed. In the case of hydrogen, a relatively good (6°–13° mean acceptance angle) geometry was used and varied sufficiently to show that the geometry was good enough so that the possible errors due to acceptance of secondaries were smaller than the other errors. In the case of carbon and copper the geometry was chosen to be just poor enough to avoid contributions from shadow scattering. A study of the effects of the variation of the geometry revealed an approximate plateau in the cross section as a function of geometry above the shadow and Coulomb scattering limits. Hence, these results should essentially represent the cross section for all interactions other than shadow scattering. All the listed cross sections have been corrected for the contamination of the beam.

The results show considerable transparency for carbon and copper for negative pions at 450 Mev, and one can deduce the approximate average cross section per nucleon using Serber's[6] model of the nucleus. The results thus deduced are shown in Table II, where the hydrogen result is also listed for comparison.

TABLE II. Average cross section per nucleon for 450-Mev negative pions computed from the observed transparency of carbon and copper.

Element	Computed average cross section per nucleon	Observed hydrogen cross section
Carbon	26±4	25±3
Copper	25±5	

If we compare the hydrogen result with that of Anderson, Fermi, *et al.* ($\sigma_\pi=60\pm6$ mb at 217 Mev) we see that the negative pion cross section has decreased by a factor of about 2.5 from 217 Mev to 450 Mev, indicating a fairly sharp peak in the energy dependence curve of $\sigma_{\pi^-\to p}$. Although Brueckner's resonance calculations[7] on the pion-nucleon interactions do not appear to agree with Fermi's latest data,[4] they give a calculated total cross section of about 20 mb when extended to 450 Mev, which is not in serious disagreement with our experimental result. Chew is also extending his calculations[8] to higher energies.

Also in Anderson's and Fermi's measurements[1] the hydrogen cross section for positive pions seems to be still increasing at the highest energy measured (135 Mev, $\sigma_{\pi^+\to p}=125-150$ mb) and the magnitude of the cross section was about 2.5 times that for the negative pions. In order to ascertain whether there exists a peak in the energy dependence of the hydrogen cross sections for positive pions similar to that for negative pions, we have also measured the hydrogen cross section for 340-Mev positive pions.

The second experimental arrangement in the 32° direct beam described above was used to accept all positive particles of the proper momentum emanating from the target at 32° from the forward direction. The high resolution ($2-3\times10^{-9}$ sec) circuitry normally employed in all our measurements automatically eliminated the proton component in the beam because of its longer time of flight through the telescope. The beam composition was also determined by a copper range curve.

An analysis of the range curve confirmed the elimination of the proton component by time of flight and demonstrated that the beam contained about 92 percent positive pions and about 8 percent positive muons and electrons.

Transmission measurements on the polyethylene-carbon difference were performed for a relatively good geometry (mean acceptance angle=10°). The cross section of hydrogen for 340-Mev positive pions, after corrections for muon and electron contaminations in the beam, was determined to be 48±9 mb. This value when compared to the result of Anderson, Fermi *et al.* ($\sigma_{\pi^+\to p}=125-150$ mb at 135 Mev) shows that the positive-pion cross section has decreased by a factor of close to 3 from 135 to 340 Mev. The extension of Brueckner's resonance calculations yields value of 66 mb for the positive-pion hydrogen cross section at 340 Mev.

The sharp drop in the hydrogen cross section for both positive and negative pions evidenced in these results and other preliminary measurements (not yet published) enhances the possibility of a resonance or near-resonance interaction.

A detailed description and analysis of the experiment will be presented in the near future.

The authors are greatly indebted to the entire Cosmotron staff, for their assistance and cooperation in this work. We are especially grateful to Dr. G. K. Green and Dr. J. P. Blewett for their valuable advice and cooperation in setting up the proper Cosmotron conditions for this experiment. We also wish to thank Dr. E. O. Salant for his interest and valuable discussions during the course of this experiment.

* This reaearch was performed under the auspices of the U. S. Atomic Energy Commission.

[1] Anderson, Fermi, Long, Martin, and Nagle, Phys. Rev. **85**, 934 and 936 (1952); Anderson, Fermi, Nagle, and Yodh, Phys. Rev. **86**, 793 (1952).
[2] Chedester, Isaacs, Sachs, and Steinberger, Phys. Rev. **82**, 958 (1951); Isaacs, Sachs, and Steinberger, Phys. Rev. **85**, 803 (1952).
[3] Barnes, Clark, Perry, and Angell, Phys. Rev. **87**, 669 (1952).
[4] Anderson, Fermi, Martin, and Nagle, Phys. Rev. **91**, 155 (1953).
[5] Reported before the Washington Meeting of the American Physical Society, May 2, 1953.
[6] Fernbach, Serber, and Taylor, Phys. Rev. **75**, 1352 (1949).
[7] K. A. Brueckner, Phys. Rev. **86**, 109 (1952).
[8] G. F. Chew, Phys. Rev. **89**, 591 (1953).

Internal Conversion Electrons from Coulomb Excited Ta and W

TORBEN HUUS AND JØRGEN H. BJERREGAARD
Institute for Theoretical Physics, University of Copenhagen, Copenhagen, Denmark
(Received October 26, 1953)

INTERESTING information can be obtained about the lowest-lying levels in heavier nuclei when these are excited by means of the electrical field of impinging particles which have an energy too low for barrier penetration. In recent investigations[1,2] of such

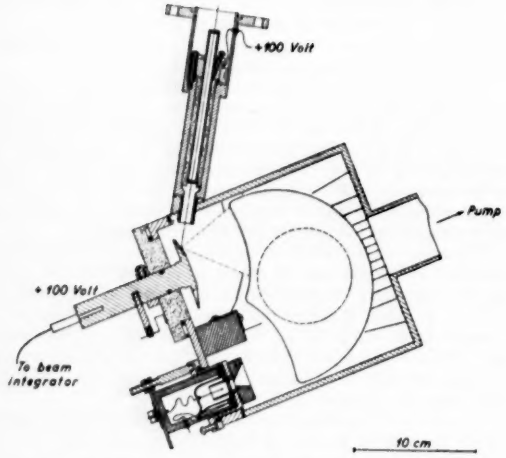

FIG. 1. Wedge-shaped magnetic beta-ray spectrometer with Geiger counter.

Coulomb-excitation processes, the gamma radiation emitted by the subsequent de-excitation was detected by means of scintillation spectrometers. However, this method gives only a relatively poor energy resolution at the low energies in question; and, therefore, the strong x-radiation from the K shell of the atoms, which are also excited by the protons, to some extent prevents measurements at the lowest energies.

In this region better results should be expected if one instead measures the spectra of the internal-conversion electrons, the yield of which is comparable to that of the gamma rays. Furthermore, the relative yields of the different conversion lines give additional information about the multipole order of the transitions.

As a test of the method we have investigated the electrons emitted by Ta and W under bombardment of protons. Our interpretation of the gamma-ray measurements[2] is confirmed by the new results.

The spectra were measured by means of the wedge-shaped magnetic spectrometer shown in Fig. 1. This spectrometer, which has been constructed by Kofoed-Hansen *et al.*,[3] proved particularly suited for the present purpose. The only change needed was the introduction of a proper set of stops at the wall opposite to the target and the Geiger counter, in order to trap the protons scattered from the target. The spectrometer was calibrated by means of the ThB lines. It was used with stops giving a solid angle of about 1.5 percent of 4π and a relative window-width $d(H\rho)/H\rho$ of about 0.7 percent.

A thin layer of Ta evaporated on a disk of graphite and a thin layer of W evaporated on a copper disk were used as targets.

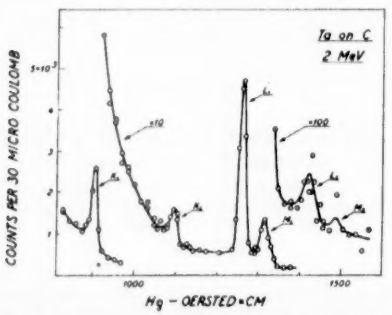

FIG. 2. Spectrum of electrons from a thin Ta target bombarded with 2.00-Mev protons.

The spectrum obtained when the Ta target was bombarded with 2-Mev protons is shown in Fig. 2. It clearly exhibits not only the lines K_1, L_1, and M_1 resulting from the internal conversion in the K, L, and M shells, of the radiation from the first excited state of Ta^{181}, but also, as expected from the gamma-ray measurements, the lines K_2 and L_2, corresponding to the first step in the cascade transition from the second excited state. The quantum energies in the two cases are found to be 137 kev and 166 kev, respectively, to an accuracy of better than 1 percent. The excitation energy for the second excited state is therefore 303 kev, which is 2.21 ± 0.02 times larger than for the first state. This is in complete agreement with the ratio 20/9 predicted for the rotational states[4] of a nucleus with ground-state spin 7/2.

One should therefore expect the first and second excited state to have the same parity as the ground state and spins 9/2 and 11/2, respectively. This means that the 137-kev and 166-kev transitions should both be mixtures mainly of the $M1$ and $E2$ types. From Fig. 2 one derives K/L ratios of about 5, showing that the two transitions are nearly pure $M1$ [about 85 percent pure, (see reference 5)].

The figure also shows that the ratio of the total number of 166-kev transitions to that of 137-kev transitions is about 1:20, when a correction is made for the difference in the conversion coefficients.[5,6] At a bombarding energy of 2 Mev it was not possible to

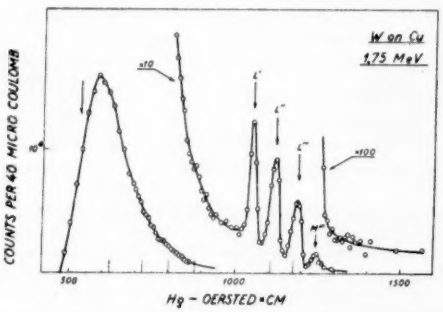

FIG. 3. Spectrum of electrons from a thin W target bombarded with 1.75-Mev protons. The marks on the $H\rho$ axis indicate where K and M conversion lines could be expected.

see any conversion lines from the weak 303-kev cross-over transitions, for which the conversion coefficients are small. However, from the gamma-ray measurements,[2] it is known that the relative number of 303-kev and 137-kev transitions is 1:80 at this energy. It therefore follows that the relative number of 303-kev and 166-kev transitions is 1:4, as also had to be assumed in the gamma-ray work in order to obtain the correct relative excitation cross sections for the two levels. This branching ratio again implies that the 166-kev radiation should correspond to about 85 percent pure $M1$ transitions. It is therefore possible by means of the conversion coefficients to determine the transition probability for the 166-kev $M1$ gamma rays relative to the transition probability for the 303-kev $E2$ gamma rays, which is known from the measurements of the absolute gamma yield. For the rotational states of a uniformly charged nucleus, one can estimate the transition probability for $M1$ gamma radiation in terms of the magnetic moment of the nucleus in the ground state.[4] On the basis of this model one finds that the experimental yield should correspond to a magnetic moment of 2.8 nuclear magnetons. The spectroscopically measured moment of Ta^{181} is 2.1 nuclear magnetons.[7]

A conversion spectrum for Ta was also measured at 1.75 Mev. Here the 166-kev transitions could barely be observed, and the yields of the 137-kev transitions decreased by a factor of 1.4, in agreement with the theoretical energy dependence.[8]

The spectrum obtained for the thin W target at a bombarding energy of 1.75 Mev is shown in Fig. 3. The curve exhibits four

sharp peaks, and from the fact that no corresponding K lines can be seen it can be concluded that the peaks are the result of $E2$ transitions in the three abundant even-A isotopes. This is also the type of transitions expected for rotational states of even-A nuclei. The M' and M'' lines cannot be resolved from the L'' and L''' lines, respectively, although they do make these peaks somewhat broader than the L' line. The three excitation energies in question are found to be 102 kev, 113 kev, and 124 kev. As the three isotopes are about equally abundant, this is in good agreement with the average energy of 115 kev found for the gamma radiation. The 124-kev line can be assigned to the isotope W^{186}, which is known to have approximately this excitation energy for the first level. It is to be expected that the 102-kev line is the result of W^{182} and the 113-kev line to W^{184}.

We are going to check these assignments on separated targets, and we also hope thereby to find the lines for the odd isotope W^{183}, which in the present case may be covered by those of the even isotopes.

The absolute cross sections have not been determined very accurately in the present measurements, but the estimates are in agreement with our previous work.[2] We intend to make more careful measurements of the total Coulomb-excitation cross sections in order to get more reliable values for the quadrupole moments as well as for the magnetic moment, which can be derived from the corresponding transition probabilities.

The large broad peak at the low energies, which can be seen in Fig. 3, was also found in the case of Ta and other elements. It is believed to be the result of stopping electrons[9] which, by means of momentum exchange with their nuclei, have acquired more energy than the maximum of about 4 kev obtainable in a free collision with a 1.75-Mev proton. The cut-off at the low-energy side is the result of the 0.9-mg/cm^2 mica window of the counter. Such peaks were found to have a shape practically independent of the proton energy and the target material, but to have thick target yields which were approximately proportional to $Z^{5/2}\cdot E^4$. Unfortunately, this process implies that the present method also is less applicable at very low excitation energies.

[1] C. L. McClelland and C. Goodman, Phys. Rev. **91**, 760 (1953).
[2] T. Huus and Č. Zupančič, Kgl. Danske Videnskab. Selskab, Mat.-fys. Medd. **28**, No. 1 (1953).
[3] Kofoed-Hansen, Lindhard, and Nielsen, Kgl. Danske Videnskab. Selskab, Mat.-fys. Medd. **25**, No. 16 (1950).
[4] A. Bohr and B. Mottelson, Kgl. Danske Videnskab. Selskab, Mat.-fys. Medd. **27**, No. 16 (1953).
[5] M. Goldhaber and A. W. Sunyar, Phys. Rev. **83**, 906 (1951).
[6] Rose, Goertzel, Spinrad, Harr, and Strong, Phys. Rev. **83**, 79 (1951).
[7] B. M. Brown and D. H. Tomboulian, Phys. Rev. **88**, 1158 (1952).
[8] K. Alder and A. Winther, Phys. Rev. **91**, 1578 (1953).
[9] W. Henneberg, Z. Physik **86**, 592 (1933).

Zeeman Splitting of Nuclear Quadrupole Resonance Lines*

YU TING, EDWARD MANRING, AND DUDLEY WILLIAMS
Ohio State University, Columbus, Ohio
(Received October 22, 1953)

THE nuclear quadrupole resonance line in sodium chlorate is a narrow intense absorption line at room temperature[1] and is, therefore, well suited for studies of the Zeeman effect.[2] The crystal lattice is a simple cube in which there are four unique directions of the gradient of the electric field at the chlorine nucleus; these four directions are along the diagonals of the unit cell.

When a single crystal of sodium chlorate is placed in an external magnetic field, the zero-field nuclear quadrupole resonance line generally splits into four components. This Zeeman pattern depends upon the external magnetic-field strength and upon the orientation of the crystal with respect to the external field. At certain orientations only two or three Zeeman components are observed. These observations are readily interpreted in terms of perturbation theory.

The theory predicts that at one orientation, in which the 111 plane is normal to the magnetic field, there should be two symmetrical Zeeman components whose frequency separation from the parent line is *strictly* proportional to the strength of the applied field. In order to verify this prediction we have studied the splitting of the Cl^{35} line in external fields in the range 0 to 8000 gauss. At the highest fields employed the separation between the Zeeman components is approximately 20 percent of the frequency of the zero-field line. The experimental results show that the splitting is indeed directly proportional to the applied field.

From the observed Zeeman pattern the nuclear magnetic moment of Cl^{35} can be calculated. The value obtained is 0.8215 $\pm$0.0010 nuclear magnetons. This result is in excellent agreement with the value 0.82180$\pm$0.00005 nuclear magnetons obtained in earlier work on magnetic resonance, in which aqueous solutions of LiCl were employed.[5] Diamagnetic corrections have not been applied in either quoted value.

Our work on sodium chlorate is being continued. Zeeman patterns for various orientations and field strengths are being investigated. Studies of line widths are also in progress. Further results will be reported in the near future.

The writers wish to express their appreciation to Mr. John Hockenberry and Mr. Carlton Brown for their assistance in parts of the experimental work.

* This work was supported by the Air Research and Development Command.
[1] Wang, Townes, Schawlow, and Holden, Phys. Rev. **86**, 809 (1952).
[2] R. Livingston, Science **118**, 61 (1953).
[5] Yu Ting and D. Williams, Phys. Rev. **89**, 595 (1953).

Hyperfine Structure and Nuclear Electric Quadrupole Moment of Boron 11

GUNTER WESSEL*
Division of Physics, National Research Council, Ottawa, Canada
(Received October 22, 1953)

THE hyperfine structures of the $^2P_{\frac{1}{2}}$ ground state and the $^2P_{\frac{3}{2}}$ metastable state of boron 11 have been measured by the atomic beam magnetic resonance method. The nuclear spin of B^{11} being $\frac{3}{2}$, the hyperfine structure of the $^2P_{\frac{1}{2}}$ state consists of two levels characterized by the total quantum numbers $F=2$ and 1, whereas that of the $^2P_{\frac{3}{2}}$ state consists of four levels characterized by $F=3$, 2, 1, and 0. Transitions between Zeeman components of the various levels have been observed at low magnetic fields and the field-free intervals obtained by extrapolation. We find:

$$^2P_{\frac{1}{2}}$$

$$\Delta\nu(F=3-F=2)=3a'+b=222.737\pm0.010 \text{ Mc/sec},$$
$$\Delta\nu(F=2-F=1)=2a'-b=144.00\pm0.02 \text{ Mc/sec},$$
$$\Delta\nu(F=1-F=0)=a'-b=70.66\pm0.20 \text{ Mc/sec},$$

$$^2P_{\frac{3}{2}}$$

$$\Delta\nu(F=2-F=1)=2a''=732.4\pm0.1 \text{ Mc/sec},$$

where we have expressed the intervals in terms of the theory of Casimir,[1,2] a', a'' being magnetic dipole interaction constants and b an electric quadrupole interaction constant. Of the three intervals of $^2P_{\frac{1}{2}}$, the smallest one has been measured less accurately than the other two. The reason for this is that it was necessary to use a two-frequency transition, in the manner described by Davis, Feld, Zabel, and Zacharias,[2] in order to observe this interval and the resulting intensity was consequently lower than that in the other cases. If we solve for a' and b from the first two relations above, we obtain

$$a'=+73.347\pm0.006 \text{ Mc/sec}, \quad b=+2.695\pm0.016 \text{ Mc/sec},$$

where the positive sign of a' is taken from the known positive magnetic moment of B^{11}. These two values are consistent with the third relation above, for we have $a'-b=70.652\pm0.022$ Mc/sec. The possibility of describing the three observed intervals of $^2P_{\frac{1}{2}}$ by the two constants a' and b indicates that, to within the accuracy of

the measurements, this state is unperturbed by the $^2P_{\frac{1}{2}}$ ground state which lies only 16 cm^{-1} away. Taking the fourth relation above into consideration, we find for the ratio of the magnetic dipole interaction constants of the $^2P_{\frac{1}{2}}$ and $^2P_{\frac{3}{2}}$ states $a''/a' = 4.993 \pm 0.001$. This ratio is to be compared with the theoretically expected one[1,2] of 5.0014. The good agreement between these two ratios suggests that the ground configuration which gives rise to the states under study is relatively free from the type of configuration interaction considered by Koster.[3] Hence, a nuclear quadrupole moment calculated from the observed constant b by the method described by Davis, Feld, Zabel, and Zacharias[2] should be fairly reliable. We find by this method

$$Q(B^{11}) = +(0.0355 \pm 0.0002) \times 10^{-24} \text{ cm}^2.$$

For this same quantity, Gordy, Ring, and Burg[4] obtained from microwave absorption spectra a value $+(0.03) \times 10^{-24}$ cm^2 whereas Dehmelt[5] obtained from pure quadrupole spectra a value $+(0.047) \times 10^{-24}$ cm^2 (without Sternheimer correction). These values are probably less reliable than ours because of the more complicated molecular fields involved. Dehmelt also obtained an accurate value for the ratio of the quadrupole moments of B^{10} and B^{11}. Using his ratio of $Q(B^{10})/Q(B^{11}) = 2.084 \pm 0.002$ and our value of $Q(B^{11})$, we find $Q(B^{10}) = +(0.0740 \pm 0.0005) \times 10^{-24}$ cm^2.

The apparatus used in the present study has been described by Wessel and Lew.[6] An attempt will be made to measure the hyperfine structure of B^{10}.

* National Research Laboratories Postdoctorate Fellow.
[1] H. B. G. Casimir, Archives du Musée Teyler, Series 3, **8**, 201 (1936).
[2] Davis, Feld, Zabel, and Zacharias, Phys. Rev. **76**, 1076 (1949).
[3] G. F. Koster, Phys. Rev. **86**, 148 (1952).
[4] Gordy, Ring, and Burg, Phys. Rev. **78**, 512 (1950).
[5] H. D. Dehmelt, Z. Physik **133**, 528 (1952); **134**, 642 (1953).
[6] G. Wessel and H. Lew, Phys. Rev. **92**, 641 (1953).

A New Quenching Effect in Liquid Scintillators

R. W. Pringle,* L. D. Black,* B. L. Funt,† and S. Sobering†
University of Manitoba, Winnipeg, Canada
(Received October 29, 1953)

LIQUID scintillator studies, initiated in connection with a C^{14} liquid-scintillator dating project, have revealed the existence of a considerable quenching effect attributable to dissolved oxygen, an effect which does not appear to have been recognized by other workers in this field. The precise nature of the quenching process is obscure, but it seems likely that photo-oxidation and photo-dimerization are involved, and each may act to reduce substantially the light output of the scintillator. In the former case a process competing with the light-emission mechanism is involved, and in the latter case the effective number of activator molecules is reduced. It must be noted that pioneer studies of fluorescence quenching had revealed effects caused by oxygen which were described in 1938.[1]

The displacement of the dissolved oxygen from the liquids was accomplished by bubbling nitrogen through a fine capillary tube sealed into the glass scintillation cell. The nitrogen was first passed through magnesium perchlorate and pyrogallol. The scintillation cell had a diffuse reflecting coating of magnesium oxide on the outside, and the light output was measured in terms of the pulse heights from a DuMont 6292 photomultiplier. The light output of an anthracene crystal, similarly mounted, was used for reference, and the scintillations were produced by gamma rays from a Cs^{137} source. It was found that nitrogen bubbling improved the pulse height in every case and that the effect could be reversed by bubbling with oxygen. A heated tube containing finely divided copper was inserted in the bubbling line to remove the last traces of oxygen but did not noticeably improve the performance.

Figure 1 illustrates the nature of the improvement for xylene solutions of 3-g/l p-terphenyl with varying concentrations of diphenyloxazole. It will be observed that the removal of oxygen *doubles* the light output of the pure p-terphenyl-xylene solution.

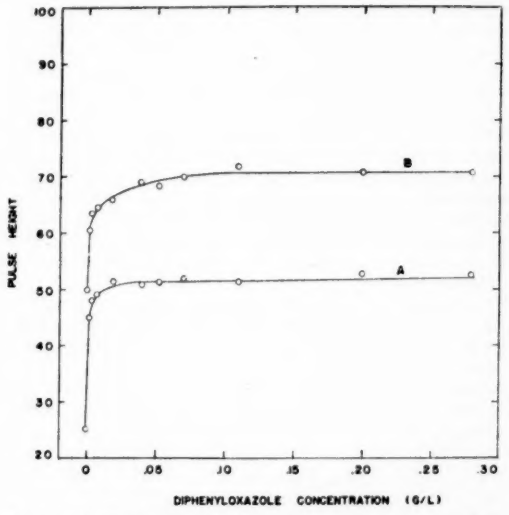

FIG. 1. Scintillation pulse height (relative to anthracene as 100) *vs* diphenyloxazole concentration for a 3-g/l terphenyl-xylene solution. Curve A: unbubbled solution. Curve B: bubbled solution.

The effect of the addition of diphenyloxazole is also most interesting, as one part in 10^6 added to the solution causes considerable enhancement of the light emission. Figure 2 illustrates a similar improvement for p-xylene, showing the effect of adding p-terphenyl to solutions with a fixed concentration of diphenyloxazole. Table I also indicates a few representative results.

It should be noted that the photomultiplier used in these experiments did not have an extended sensitivity in the ultraviolet, and so the light emission of the liquids is not measured under circumstances as favorable as for the anthracene, since the emission curve in the latter case corresponds more closely with the sensitivity curve of the photocathode. It is estimated that an ultraviolet-sensitive photomultiplier would so increase the relative light outputs of the liquids, that the best bubbled solutions would appear superior to anthracene.

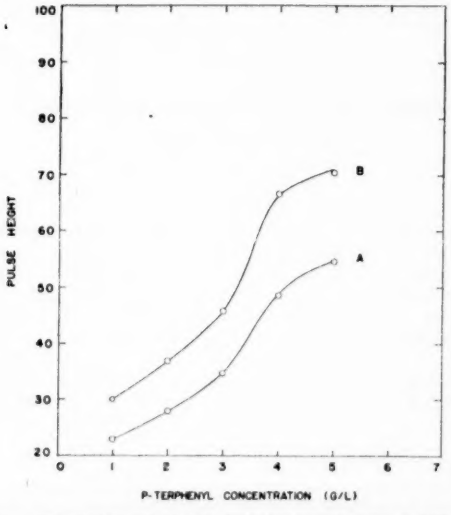

FIG. 2. Scintillation pulse height (relative to anthracene as 100) *vs* p-terphenyl concentration for a 0.1-g/l diphenyloxazole-p-xylene solution. Curve A: unbubbled solution. Curve B: bubbled solution.

TABLE I. Effect of oxygen removal on light output.[a,b]

Solvent	p-terphenyl (g/l)	Diphenyloxazole (g/l)	Light output (unbubbled)	Light output (bubbled)
xylene	3.0	0	25%	50%
xylene	3.0	0.003	48	63
xylene	3.0	0.07	52	70
xylene	3.0	3.0	52	71
p-xylene	3.0	0.10	35	46
p-xylene (refractionated)	3.0	0.10	54	72
o-xylene	4.0	0.10	38	45

[a] The materials used for this work were obtained as follows: p-terphenyl (scintillation grade) from the Pilot Chemical Company, Waltham, Massachusetts; 2,5 diphenyloxazole from Bios Chemical Laboratories, 17 West 60th Street, New York; o- and p-xylene from D.P.I., Rochester 3, New York; xylene (reagent grade) from Merck, Montreal, Canada.

[b] We are indebted to Dr. J. R. Arnold for the information that a mixture of 4-g/l diphenylonazole and 4-g/l terphenyl in toluene yields 50 percent more light than similar solutions of either solute alone.

It is evident that the removal of oxygen is necessary in all liquid-scintillator experiments, before complete reproducibility is obtainable. This fact may help to explain some of the contradictory results which have been published with respect to the light emissions of liquid scintillators. It is intended that a detailed description of the present investigations will be published soon.

Our thanks are due the Wenner-Gren Foundation for their support of this project, and the National Research Council of Canada for assistance with certain aspects of the work.

* Physics Department.
† Chemistry Department.

[1] E. J. Bowen and A. Norton, Trans. Faraday Soc. **35**, 44 (1939).

Rest Mass Energy of the Negative Pion*

R. C. CORNELIUS, C. P. SARGENT, M. C. RINEHART, L. M. LEDERMAN, AND K. ROGERS
Columbia University, New York, New York
(Received October 21, 1953)

DURING the course of a diffusion cloud-chamber study of pairs produced by the internal conversion of mesonic gamma rays, an event of particular interest was observed and is shown in Fig. 1. A slow π^- meson (A) comes to rest in hydrogen gas (19 atmospheres) and a high-energy pair (B, C) emerges from the end of the pion track. We interpret this reaction as

$$\pi^- + p \rightarrow n + e^- + e^+, \quad (1)$$

representing the internal conversion of the gamma ray produced in the radiative capture process.[1] Further results of this study and details of the measurement technique will be published soon. The point of interest in this particular event is the suitability of the tracks for accurate measurement and hence the possibility of obtaining a usefully precise determination of the rest energy of the negative pion. The tracks are about 25 cm long and have dip angles of only 1.7° and 1.3°.

The radii of curvature of the positron and electron are 21.44 ±0.05 cm and 33.47±0.12 cm. The values include corrections for ionization and radiation loss in the hydrogen gas (0.17 percent) and nonuniformity in magnetic field (0.05 percent). The errors are measurement errors. Multiple scattering and straggling contribute an additional 0.5 percent, and track distortions due to turbulence and optics contribute 0.35 percent to each uncertainty. Zero field curvatures of 60-Mev mesons were used to measure the effects of turbulence and optics. The error in our knowledge of the magnetic field at the time of the event is ±60 gauss out of a total field of 7737 gauss. Combining all of these results and employing the kinematics appropriate to reaction (1) yields for the rest energy of the π^- meson,

$$E_0 = 137.3 \pm 0.9 \text{ Mev}.$$

All uncertainties were estimated and treated as standard deviations, except the error in the final result, which is a probable error. The mass equivalent is 268.8±1.8 electron masses. This is in fair agreement with the value of $272.5 \pm 0.3 m_e$ recently reported by Smith, Birnbaum, and Barkas.[2]

We wish to thank Dr. Seymour Koenig of the Watson Laboratories for his assistance in making the proton resonance measurements of the magnetic field.

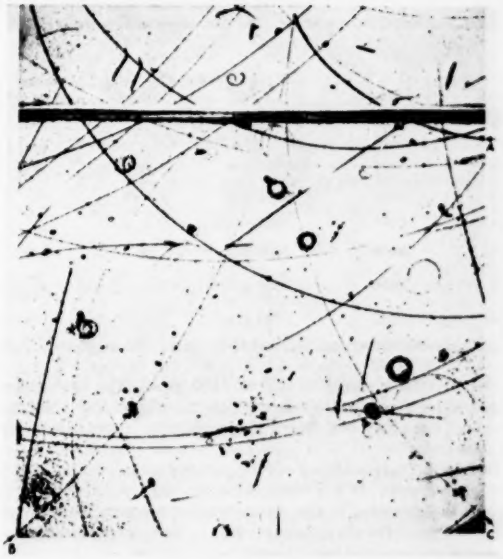

FIG. 1. Diffusion cloud-chamber photograph of the reaction $\pi^- + p \rightarrow n + e^- + e^+$. Track A is that of a low-energy π^- meson which comes to rest in the gas. Tracks C and B are the positron and electron, respectively. The horizontal plate is a sweeping field electrode and does not intercept the paths of the particles.

* This work was performed under the joint program of the U. S. Office of Naval Research and the U. S. Atomic Energy Commission.

[1] Panofsky, Aamodt, and Hadley, Phys. Rev. **81**, 565 (1951).
[2] Smith, Birnbaum, and Barkas, Phys. Rev. **91**, 765 (1953).

Mass Measurements of Primaries of S Events by a Momentum-Range Method*

W. B. FRETTER,† B. P. GREGORY, R. JOHNSTON, A. LAGARRIGUE, H. MEYER, F. MULLER, AND C. PEYROU
École Polytechnique, Paris, France
(Received October 2, 1953)

IN order to obtain further information on the newly discovered heavy particles, a large size cloud chamber (67 cm×63 cm×40 cm) equipped with eight lead (7.7 mm) and six carbon (16 mm) plates was placed below another cloud chamber (67 cm×63 cm

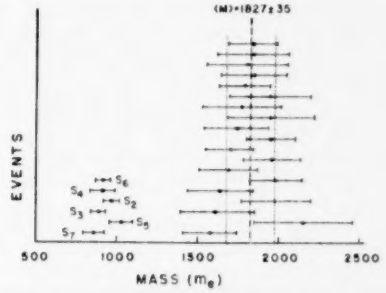

FIG. 1. Mass values for 19 protons and 6 S events. The horizontal lines represent the estimated individual errors.

TABLE I. Summary of the data on the primary and secondary particles of S events.

Event	Frame	Primary Mass	Primary Charge	Range g/cm² Pb	Observed secondary $\frac{I_{\text{final}}}{I_0}$	Observed secondary p if π Mev/c	Observed secondary p if μ Mev/c	Possible γ-ray secondary Radiation lengths	Possible γ-ray secondary γ's observed
S_1	7804	Produced in plate chamber		>60.1	<3	>185	>215	2, 2, 2	none
S_2	6307	965±50	+	13.7		98	117	1.2, 1.2	none
S_3	6192	885±50	+	>12	<2	>115	>140		
S_4	6197	915±80	+	>38	<3	>150	>177	2.3	none
S_5	8094	1030±85	+	>48.5	<3	>168	>197		
S_6	8805	918±50	+	>9.8 <20.6		>87 <115	>105 <135	1.3, 1.5	none
S_7	9231	857±70	+	>68.2	<3	>196	>227	1.8	none

×30 cm) with a magnetic field of 2500 gauss. The system was triggered by a penetrating shower detector placed above the top chamber, one particle at least being required to appear above the plate chamber.

In a preliminary scanning of 7000 pictures obtained at mountain altitude we observed 7 S events,[1] i.e., particles certainly heavier than π or μ, stopped in the plate chamber, a copunctual particle being emitted from the stopping point. In six of these, the primary particles traverse the top chamber.

The errors in our mass measurements depend in this case mainly on the precision of our momentum measurements, since the ranges are accurately known. In order to estimate our errors, we made first a rapid measurement of the mass of 63 heavy particles stopped in the bottom chamber. We found that in these individual rough measurements, protons were readily distinguishable from deuterons (of which we found 9). We then selected for a more precise measure 19 protons observed in pictures before or after the ones in which our S particles were seen. Momenta were measured by fitting circles of known radii to the tracks; this method allows an estimate of the errors of measurement. The results for the mass measurements are shown in Fig. 1. The solid lines indicate our estimated errors including errors in momentum as well as in range.

The mean standard deviation of our proton mass distribution is given by the formula:

$$\Delta M=\left[\frac{\Sigma(M_i-\langle M\rangle_{\text{Av}})^2}{n-1}\right]^{\frac{1}{2}}=\pm 150m_e,$$

where M_i are the individual mass measurements.

Since our average estimated individual error for protons is $\pm 200m_e$, we feel confident that the errors estimated in the same way for our S particles are, if anything, larger than the standard deviation. The curvature of an S-particle track is larger than that of a proton, and the relative error is therefore smaller in this case.

We have summarized in Table I our results on the primaries and secondaries of our S events. Further considerations may be made:

(1) S_2, as described at the Bagnères Conférence,[2] may well be interpreted as a τ particle that comes to rest.

(2) The secondary of S_6 is emitted at an angle of 27° with the forward direction and seems less ionizing than the primary at the point of emission. It comes to rest in the second plate after the one in which the change of direction occurred. But one may also consider that the "secondary" track is the prolongation of the primary. We would then have a K particle of mass 800 ± 60 with no visible secondary. The angle of 27° would then be a Coulomb scattering to be compared to a calculated mean square scattering angle of 10°. This event, as described in the table, can thus be either a κ or a τ but not a χ particle.

(3) S_3, S_4, S_5, and S_7 cannot be τ particles, and the behavior of their secondaries is consistent with the primary's being a κ or a χ particle, although S_7, if a χ, would have a mass $>970m_e$ from the range of the secondary. The average mass for the primaries is:

$$M=922\pm 40m_e.$$

This value is in good agreement with many of the best measurements of the masses of K particles stopping in emulsion.[2]

(4) No electronic shower was observed in the direction opposite to the secondary particle in any of the cases. The last columns of Table I indicate the number of radiation lengths that would have been traversed by the hypothetical γ ray in passing through the various lead plates. In four cases (S_1, S_4, S_6, S_7) favorable conditions for observations existed.

(5) In all six cases the particle was positive. If positive and negative particles are equally numerous, and if they decay in an identical fashion in the plate chamber, the chances for observing only positive particles is $\frac{1}{64}$.

On the other hand, if negative particles are absorbed either strongly (as the π^-) or weakly (as the μ^-), the observation in a plate chamber might be more difficult. Since four of our six events were discovered by scanning the plate chamber alone, our bias for positive particles is quite comprehensible. A systematic search for negative K particles stopping in the plate chamber is under way.

We wish to thank Professor Leprince-Ringuet for his help and interest in this work. We are very much indebted to Professor J. Rösch, director of the "Observatoire du Pic du Midi" and his staff, for their help during the construction and operation of the apparatus.

* This experiment was sponsored by the French Atomic Energy Commission and "Enseignement Supérieur."

† On leave from the University of California, Berkeley.

[1] Bridge, Peyrou, Rossi, and Safford, Phys. Rev. **90**, 921 (1953).

[2] Proceedings of Bagnères de Bigorre Conférence, July, 1953 (unpublished).

Cross Terms in Allowed-Shape β Spectra. II*

J. P. DAVIDSON, *Centro Brasileiro de Pesquisas Fisicas, Rio de Janeiro, Brazil*

AND

D. C. PEASLEE, *Columbia University, New York, New York*

(Received September 28, 1953)

THE possible mixture of (S, V) terms in the β-decay interaction is experimentally less well determined than the limits of the (T, A) mixture.[1] A major difficulty is that all the transitions certain to contain Fermi parts in the interaction ($\Delta I=0$, *no*) have very short half-lives, on the order of seconds. The recently discovered[2] isomeric transition in Cl^{34} provides a fortunate exception to this rule. The 33-minute state of Cl^{34} goes about half the time by gamma emission to a $J=0^+$ ground state of Cl^{34}; this state makes a pure Fermi $(0-0)$ transition to the ground state of S^{34}. Although this β transition has an intrinsic half-life of about 1.5 seconds, it is governed by the 33-minute half-life of the isomeric parent. Because of branching in the β-decay scheme, only the upper 2.2 Mev of the 4.5-Mev spectrum can be used.

We may also note that the spectrum shape is a more sensitive measure of the admixture terms than the electron-neutrino

correlation function,[3] provided that the admixture is small. The β-transition probability in the notation of reference 1 is

$$\frac{dP}{d\Omega dW}=C^2F_0(Z,W)(W_0-W)^2\left\{\left|\int 1\right|^2[1+R/W+Q(v/c)\cos\theta]+\left|\int\boldsymbol{\sigma}\right|^2[1+R'/W+\tfrac{1}{3}Q'(v/c)\cos\theta]\right\},\quad(1)$$

where $Q=(\lambda_V{}^2-\lambda_S{}^2)/(\lambda_V{}^2+\lambda_S{}^2)$ and $Q'=(\lambda_T{}^2-\lambda_A{}^2)/(\lambda_T{}^2+\lambda_A{}^2)$. For either Q or Q' let $\lambda_1/\lambda_2=\rho\ll 1$. Then

$$Q\approx\pm(1-2\rho^2),\quad R\approx 2\rho.\qquad(2)$$

It appears feasible experimentally to observe respective deviations of $|R|$ and $|Q|$ from 0 and 1 when these deviations exceed, say, 0.05. This observational limit would place a limit on ρ of 0.025 when determined from R, but a limit on ρ of $\sim$0.15 when determined from Q.

* Work partially supported by the research program of the U. S. Atomic Energy Commission.

[1] J. P. Davidson and D. C. Peaslee, Phys. Rev. **91**, 1232 (1953). In Eq. (10) and footnote ‡ of this paper read $\frac{1}{3}r$ in place of r.

[2] W. Arber and P. Stähelin, Helv. Phys. Acta **26**, 433 (1953).

[3] M. E. Rose, Phys. Rev. **91**, 197 (1953).

Production of Fast Lithium, Beryllium, Boron Fragments from Interactions of Primary Cosmic-Ray Nuclei*

J. H. Noon, M. F. Kaplon, and D. M. Ritson†
University of Rochester, Rochester, New York
(Received October 7, 1953)

We have studied interactions of heavy cosmic ray nuclei in a stack of 92 400-micron Ilford G-5 stripped emulsions flown at White Sands, New Mexico (41° geomagnetic). The acceptance criteria for tracks with our flight conditions restricted us to consideration of heavy nuclei with kinetic energy per nucleon $\geq$0.7 Bev. 270 heavy primary nuclei have been traced through the stack; charge determination both for the primary and collision fragments was based on delta-ray counting. The primary nuclei

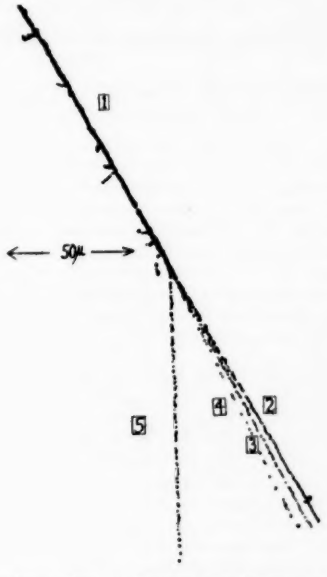

Fig. 1. A carbon nucleus (1) interacts with hydrogen of the emulsion, producing lithium (2), an alpha particle (3), a proton (4), and a recoil proton (5).

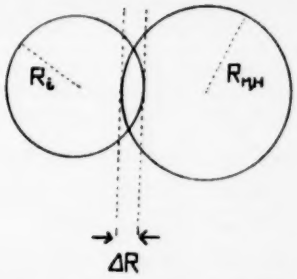

Fig. 2. Geometrical model defining overlap region ΔR effective for light element production.

have been divided into two groups: medium nuclei (M) $6\leq Z\leq 10$, and heavy nuclei (H) $Z>10$. From a study of 87 interactions occurring in emulsion, the proportion of the light elements lithium, beryllium, and boron (L nuclei) produced as fast fragments in these interactions has been determined. The probability of production of L nuclei for the two groups is

$$P_{ML}=0.36\pm0.11;\quad P_{HL}=0.34\pm0.11.$$

These probabilities refer to interactions with target nuclei of emulsion and therefore a high proportion of heavy nuclei (approximately two thirds occur in silver or bromine). Considering interactions of the type depicted in Fig. 1 as being due to hydrogen of the emulsion,[1] we find for these interactions only, the probabilities

$$P_{ML}=0.83\pm0.5;\quad P_{HL}=0.8\pm0.5.$$

The foregoing data suggest an increased probability for fragmentation into L nuclei for light target nuclei. We adopt the following geometric model (see Fig. 2) to calculate the probability of obtaining L nuclei from collisions with target nuclei of different Z. It is assumed that an overlap ΔR of target and incident nuclei is required for partial fragmentation of the incident nucleus, and for overlap greater than this more complete fragmentation into alpha particles and protons occurs. Thus it follows that light target nuclei will be more effective in producing L nuclei since the overlap ΔR represents a greater fraction of their total impact parameter than for heavy target nuclei.

Let $\Delta R_{M,H}$=overlap, $R_{M,H}$=radius of incident nucleus, R_i =radius of target nucleus, and N_i=number of atoms/cc. Then

$$P_{ML,HL}=\frac{\Sigma_i N_i(R_i+R_{M,H})^2-\Sigma_i N_i(R_i+R_{M,H}-\Delta R_{M,H})^2}{\Sigma_i N_i(R_i+R_{M,H})^2}.$$

Using the known composition of emulsion, ΔR_M and ΔR_H can be calculated to fit the experimentally observed probabilities P_{ML} and P_{HL} in emulsion. The probability for production of L nuclei in atmosphere can then be calculated for the relative amounts of nitrogen and oxygen. The figures obtained are:

$$P_{ML}=0.56\pm0.18;\quad P_{HL}=0.49\pm0.17.$$

These results are to be contrasted with the value of $P_{ML}=P_{HL}=0.23$ reported previously by Bradt and Peters.[2] Their figure was deduced by studying interactions occurring in glass and is subject to the criticism that light fragments could be missed, whereas this cannot occur with interactions in emulsion.

The results have an important bearing on experiments concerning the primary flux of light elements in cosmic rays.[2,3] These have all been performed at an appreciable depth in the atmosphere ($\geq$one mean free path) and therefore the observed flux will include secondaries arising from breakup of heavy and medium nuclei in the residual atmosphere. Since the true primary flux must be obtained by extrapolation, it is quite sensitive to the choice of P_{ML} and P_{HL}. Recent work in this laboratory[4] indicates a comparable flux of L and M nuclei at flight altitude ($\sim$24 grams) in qualitative agreement with results reported by Bristol.[3] However,

our figures suggest that a large proportion of the observed flux is not a true primary flux of light nuclei but secondary in origin.

An experiment is now in progress to test the above assumptions by observing the proportion of lithium, beryllium, and boron fragments produced by interactions of primary nuclei occurring in the plastic (cellulose acetate) layers of a stripped emulsion-plastic stack.

We wish to thank Mrs. B. Wargotz for her assistance in scanning.

* This research was supported in part by the United States Air Force under a contract monitored by the Office of Scientific Research, Air Research, and Development Command.

† Now at Massachusetts Institute of Technology, Cambridge, Massachusetts.

[1] Characterized by a recoil proton at a much greater angle than the fast fragments of the incident nucleus. Charge balance can be obtained. The proportion of hydrogen interactions observed is in agreement with that calculated from the known composition of emulsion.

[2] H. Bradt and B. Peters, Phys. Rev. **80**, 943 (1950).
[3] Dainton, Fowler, and Kent, Phil. Mag. **43**, 729 (1952).
[4] Racette, Kaplon, and Ritson (to be published).

Total Ionization of α Particles of Po in Mixtures of Gases

G. Bertolini, M. Bettoni, and A. Bisi
Istituto di Fisica Sperimentale del Politecnico, Milan, Italy
(Received August 11, 1953)

THE total ionization of α particles of Po has been measured in the following mixtures of gases: $A-N_2$, $A-H_2$, $A-CH_4$, $A-C_2H_5OH$, $A-C_6H_6$.

The experimental apparatus consisted of a gridded ionization chamber attached to a gas purifier. The purification of argon, nitrogen, and methane was done with continuous circulation of the gases over Ca−Mg turnings kept at 300–400°C. The hydrogen was circulated over Mg only. In the mixtures of argon with C_2H_5OH and C_6H_6 the previously purified argon was added to the other gas which had a purity higher than 99.9 percent. The pressure in the chamber was such that the α particles lost all of their energy in the sensitive volume and a field was produced that assured the complete collection of the electrons. The amplification chain consisted of a preamplifier and a Bell and Jordan amplifier[1] or a Model-100 amplifier.[2] The pulses were analyzed with an amplitude discriminator.

The results of our measurements are shown in Figs. 1 and 2. The ratio W_A/W_m between the average energy expended in producing an ion pair in argon and that in the mixture is plotted as a function of the parameter $z=s_1p_1/(s_1p_1+s_2p_2)$, where s_1 and s_2 are the stopping powers of the two components and p_1 and p_2 their pressures. It can be shown that the ionization in the mixtures is a linear function of z if it is assumed there is no interaction between the components of the mixture itself.[3] It is seen in Figs. 1 and 2 that the ionization rises rapidly with z and reaches a maximum at percentages of about 2 percent, 0.2 percent, and 0.2 percent for CH_4, C_2H_5OH, and C_6H_6, respectively. The ionization exceeds that in pure argon by 1.5 percent, 15 percent, and 21 percent respectively. These results can be interpreted by assuming that the

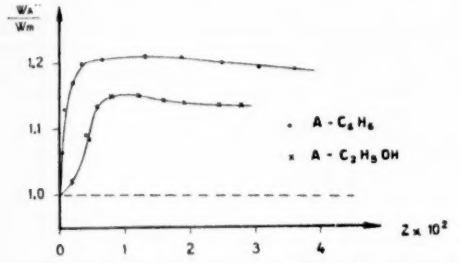

FIG. 1. Variation of W_A/W_m with z. The dotted line shows the variation of ionization in the mixture on the assumption of independent ionization of the components. The stopping powers used are: $s(A)=0.95$, $s(C_6H_6)=3.33$, $s(C_2H_5OH)=2.02$.

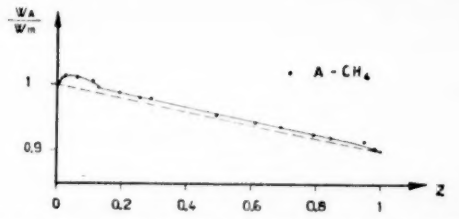

FIG. 2. Variation of W_A/W_m with z. The dotted line shows the variation of ionization in the mixture on the assumption of independent ionization of the components. The stopping powers used are: $s(A)=0.95$, $s(CH_4)=0.91$.

excited atoms of argon transfer their energy, during a collision, to atoms of foreign gas and ionize them: $A+S\rightarrow S^++A+e$, where S indicates a molecule of foreign gas (CH_4 or C_2H_5OH or C_6H_6). This process is possible because the ionization potentials of foreign gas are lower than that of argon. A, CH_4, C_2H_5OH, and C_6H_6 have ionization potentials of 15.4, 14.5, 11.5, and 9.6 volts, respectively, and it can be seen that the lower the potential of the foreign gas, the higher is the maximum ionization of the mixture.

It can further be noted that at the conditions of pressure and temperature in which the mixture was studied, the time of collision of an excited atom of argon with one of foreign gas is $\sim 5\times 10^{-11}$ sec, considering that an excited atom has a collision cross section ten times the geometrical cross section.[4]

The curves of W_A/W_m for $A-H_2$ and $A-N_2$ mixtures are in agreement with the measurements of Haeberli, Huber, and Baldinger,[3] and Valentine and Curran.[5] In these mixtures the ionization values can be understood when the ionization of δ rays is taken into account.[3]

A more detailed description of the results is to be published in *Il Nuovo cimento*.

[1] W. H. Jordan and P. R. Bell, Rev. Sci. Instr. **18**, 703 (1947).
[2] W. C. Elmore and M. Sands, *Electronic Experimental Techniques* (McGraw-Hill Book Company, Inc., New York, 1949), p. 165.
[3] Haeberli, Huber, and Baldinger, Helv. Phys. Acta **23**, 481 (1950); **26**, 145 (1953).
[4] J. P. Molnar, Phys. Rev. **83**, 940 (1951).
[5] M. Valentine and S. C. Curran, Phil. Mag. **43**, 964 (1952).

Decay-Electron Spectrum of the μ Meson*

J. H. Vilain† and R. W. Williams
Physics Department and Laboratory for Nuclear Science, Massachusetts Institute of Technology, Cambridge, Massachusetts
(Received October 14, 1953)

WE have completed an experiment to determine the shape of the energy spectrum of electrons from the decay of the μ meson. Pi mesons from a paraffin target in the gamma-ray beam of the M.I.T. synchrotron passed through an argon-filled cloud chamber, at one wall of which was an anthracene scintillation counter (see Fig. 1). The magnetic field in the cloud chamber (9000 gauss) selected a broad momentum band of positive pions which crossed the chamber and stopped in the anthracene crystal or the Lucite light-pipe behind it. The positron from the subsequent $\pi-\mu-e$ decay was then visible if it came out in a favorable direction.

Out of 4350 pictures, 830 showed clearly-associated meson and electron tracks. Rigorous selection criteria were necessary to avoid biasing the sample. The lower limit of acceptable initial kinetic energy was set at 20 Mev. Each event was reconstructed graphically and required to pass the following tests: (a) the calculated electron trajectory in the Lucite must intersect the known end point within stated limits; (b) any electron of energy between 20 Mev and 52.4 Mev having the initial direction determined from this trajectory must have a path in the Lucite plus anthracene of less than 4.2 cm; (c) any electron with this initial direction and with energy between 20 Mev and 52.4 Mev must have a visible track in the cloud chamber of more than 5 cm of arc. Consideration

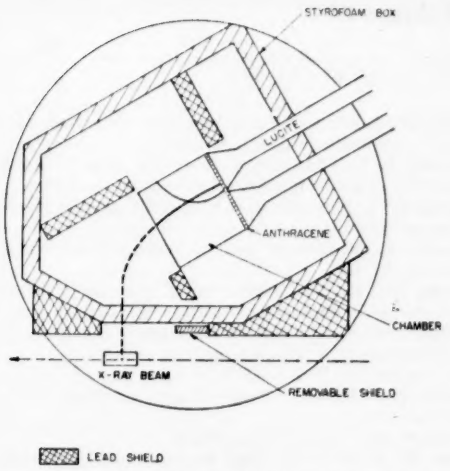

FIG. 1. Schematic plan view of the cloud chamber and scintillation counter—the large circle is the outer edge of the magnet coil.

of a number of possible effects has convinced us that there is no appreciable bias in the sample thus obtained. Of the 830 tracks, 280 satisfied these criteria.

The momentum of each track was obtained from coordinate measurements on the photographic film, plus geometric measurements on the reprojected image, taking into account the corrections for conical projection, gas motion during expansion, radial component of the magnetic field, and variation of the field along the track. The initial energy was then obtained by adding to the observed energy the collision loss of the electron in the Lucite and anthracene.

We compare our results with the energy spectrum which has been calculated from the direct-interaction theory of the decay of a muon into an electron and two neutrinos.[1] The spectrum, neglecting some small terms, may be written

$$P(E)dE=\frac{4E^2}{W^4}\left[3(W-E)+2\rho\left(\frac{4}{3}E-W\right)\right]dE,$$

where W is the maximum possible electron energy and ρ is a parameter which could have any value from 0 to 1 depending on the nature of the interaction assumed. To take account of the radiation loss of electrons in the Lucite plus anthracene (the mean path length was 0.069 radiation length), we have integrated over this spectrum with a radiation-loss distribution function.[2] This "smeared-out" set of spectra should then be directly comparable with the experimental spectrum, and indeed a good fit proves to be possible.

The value of ρ and the corresponding standard error (which includes the uncertainties in W and in individual momentum estimates) are found by the method of maximum likelihood.[3] Using the new value of the muon mass,[4] $m_\mu=207.0\pm0.6m_e$, we find $\rho=0.50\pm0.12$; that is, the spectrum does not go to zero at the end point. This agrees with Bramson, Seifert, and Havens,[5] whose result, when corrected for m_μ, is 0.48 ± 0.13.

Previous results,[6-9] when corrected for the new meson mass (and, in references 6 and 7, for radiation loss) appear to be consistent, within their statistical and estimated errors, with the value reported here.

* Supported in part by the joint program of the U. S. Office of Naval Research and the U. S. Atomic Energy Commission.

† Now at Ecole Nationale Supérieure des Télécommunications, Paris, France.

[1] Tiomno, Wheeler, and Kau, Revs. Modern Phys. **21**, 144 (1949); L. Michel, Proc. Phys. Soc. **A63**, 514 (1950).

[2] L. Eyges, Phys. Rev. **76**, 264 (1949).

[3] H. Cramèr, *Mathematical Methods of Statistics* (Princeton University Press, Princeton, 1951), p. 498. We have also computed ρ from the first four moments of the experimental distribution, and we find $\rho=0.49$, 0.47, 0.51, 0.52. The agreement of these results among themselves indicates that our sample is consistent with the assumed shape of the theoretical curve.

[4] Smith, Birnbaum, and Barkas, Phys. Rev. **91**, 765 (1953); G. Ascoli, Phys. Rev. **90**, 1079 (1953); Lederman, Booth, Byfield, and Kessler, Phys. Rev. **83**, 685 (1951). The latter measurement depended on the pion mass, and therefore now agrees with the former two.

[5] Bramson, Seifert, and Havens, Phys. Rev. **88**, 304 (1952).

[6] A. Lagarrigue and C. Peyrou, J. phys. **12**, 848 (1951); A. Lagarrigue, Compt. rend. **234**, 2060 (1952).

[7] Sagane, Gardner, and Hubbard, Phys. Rev. **82**, 557 (1951).

[8] H. W. Hubbard, thesis, University of California, 1952 (unpublished).

Errata

Unusual $\pi-\mu$ Decays in Photographic Emulsions, W. F. FRY [Phys. Rev. **86**, 418 (1952); **91**, 130 (1953)]. Because of an oversight, a reference to the work of Ioffe and Rudick[1] concerning the γ-ray emission from $\pi-\mu$ decays was not included in these publications. The results of the calculations of Ioffe and Rudick are in general agreement with the experimental observations.

[1] B. Ioffe and A. Rudick, Doklady Akad. Nauk. S.S.S.R. **82**, No. 3, 359 (1952).

Scintillation Study of As^{77} and Br^{77}, M. E. BUNKER, R. J. PRESTWOOD, AND J. W. STARNER [Phys. Rev. **91**, 1021 (1953)]. The third line in the second column on page 1021 should read "... a discriminator potential of 6 volts (~26 kev) is much too broad. . . ." The numeral 6 is missing from the printed text.

Phase-Shift Analysis of High-Energy p-p Scattering Experiments, A. GARREN [Phys. Rev. **92**, 213 (1953)]. To fit the experimental data, the value of $[\eta_A\eta_B]^{\frac{1}{2}}$ quoted in this Letter should be $\pm0.30\pm0.08$ rather than 0.40 ± 0.12. (Also, the column labeled η in Table I should have been labeled $-\eta$.) The phase shifts consistent with this value are shown in the accompanying table. Correspondingly, the shaded area in Fig. 1 should be a little lower on the diagram.

TABLE I. Some phase shifts (in degrees) at 213 Mev consistent with isotropy, $\sigma(\theta)=4.97$ mb/sterad, $\eta=-0.30\pm0.08$.

δ_1^2	δ_1^0	δ_1^1	δ_0^0	$-\eta$
− 5	70	−4.1	36	0.237
− 5	80	−0.2	31	0.256
− 5	90	5.1	28	0.267
− 5	95	10.1	23	0.275
− 5	95	16.4	5	0.297
−10	40	−6.1	55	0.251
−10	50	−5.4	46	0.340
−10	−10	29.8	36	0.249
−10	0	36.7	14	0.339
−15	30	−3.2	46	0.261
−15	35	−3.6	39	0.327
−20	20	1.9	49	0.235
−20	30	−0.6	42	0.387
−25	0	13.9	27	0.287
−25	10	7.3	33	0.256
−25	20	3.8	30	0.368

Author Index to Volume 89

References with (A) are to abstracts of papers presented at meetings of the American Physical Society, and those with (T) designate title only. References with (L) are to Letters to the Editor.

Abragam, A. and R. V. Pound. Influence of nuclear quadrupole moment on α-γ angular correlation in RaTh—1306(L)
—— (see Fields, R. E.)—908(A)
Abraham, Bernard M. (see Weinstock, Bernard)—787
Accardo, C. A. (see Lehovec, K.)—20
Adair, R. K., A. Okazaki, and M. Walt. Scattering of neutrons by deuterons—1165
Adams, E. N. II. Magnetic susceptibility of diamagnetic electron gas—role of small effective electron mass—633
Affleck, J. H. and L. V. Holroyd. Use of Ba^{140} in studies of oxide coated cathodes—893(A)
Ahrens, L. H. (see Aldrich, L. T.)—631
Alburger, D. E. and S. Thulin. Identification of 7-hr Mo^{93m}—1146(L)
—— (see Lindström, A.)—1303(L)
Aldrich, L. T., L. F. Herzog, W. K. Holyk, F. B. Whiting and L. H. Ahrens. Variations in isotopic abundances of Sr—631
Allen, James S. and W. K. Jentschke. Electron-neutrino angular correlation in β-decay of He^6—902(A)
Allis, W. P. and D. J. Rose. Transition from free to ambipolar diffusion—335(A)
Almy, G. M. (see Butler, W. A.)—893(A)
Alpert, D. Researches in ultra-high vacuum—902(T)
Alpert, Morris (see Nielsen, J. Rud)—895(A)
Altshuler, Saul. Applications of variational principles to scattering problems—1278
—— Excitation cross section for He atoms—1093(L)
Amar, Henri. General-relativistic approach to short-range forces—1298(L)
Ames, D. P., M. E. Bunker, L. M. Langer, and B. M. Sorenson. Disintegration of Sr^{91} and Y^{91m}—903(A)
Anderson, C. D. (see Leighton, R. B.)—148
Andrew, Alan and Clifton R. Davidson. Induced thermoelectric potential from radiation damage—876(L)
Andrews, Donald H. (see Haley, Floyd C.)—821
Annis, Martin, H. S. Bridge, and S. Olbert. Application of multiple scattering theory to cloud-chamber measurements—1216
Antal, J. J. and A. H. Weber. Structure of surface of glass and of Bi films deposited on glass—900(A)
Antonoff, George. Kinks in vapor pressure p *vs* temperature curves—915(A)
—— New theory of aggregates as supplement to van't Hoff's theory of solutions—915(A)
—— **and Raymond Madrazo, Jr.** Angular points in densities of water *vs* temperature—899(A)
Apker, L. Photoelectric emission from solids—902(T)
—— (see Huntington, H. B.)—352
Atkins, K. R. Heat pulses in liquid He II below 1°K—526(L)
Atkinson, W. R. and R. G. Fowler. Plane supersonic flow patterns in ionized media—906(A)
—— (see Fowler, R. G.)—336(A)
Austern, N. Validity of Born approximation in stripping—318(L)

Bair, J. K. (see Kington, J. D.)—530(L)
Bandyopadhyay, G. New equation in affine field laws—1161(L)
Barber, W. C., G. E. Becker, and E. L. Chu. Electron-electron scattering at 6.1 Mev—950
Barkas, Walter H. Range correction for electron pickup—1019
—— **and Helge Tyren.** Physical analysis of Be and C disintegration induced by 330-Mev protons—1
—— (see Wilson, H. W.)—758
Barker, W. A. and Z. V. Chraplyvy. Amplified Dirac equation and Lamb-Retherford shift—913(A)
—— **and Z. V. Chraplyvy.** Conversion of amplified Dirac equation to approximately relativistic form—446
Barnes, B. T. Electron velocity distributions in Hg-A discharge—335(A)
Baroody, E. M. Energy loss of medium-fast electrons in metals—910(A)
Barrett, Paul H., G. Cocconi, and Y. Eisenberg. Search for "T-tracks" in photographic plates—656(L)
Bartholomew, G. A. and B. B. Kinsey. Neutron capture γ-rays from Sc, V, Mn, Co, and Cu—386
—— (see Kinsey, B. B.)—375
Bartlett, J. H. and G. J. Dienes. Combined pairs of vacancies in Cu—848
Barton, R. (see Kip, A. F.)—518(L)
Battat, M. E. and F. L. Ribe. Formation of He^6 by 14-Mev neutron bombardment of Li and Be—80
Battey, James, L. Madansky, and F. Rasetti. α-γ angular correlation in RaTh—182
Becker, G. E. (see Barber, W. C.)—950
Becker, R. L., M. Walt, and A. Okazaki. Total cross sections for fast neutrons—904(A)
—— (see Fields, R. E.)—908(A)
—— (see Walt, M.)—1271
Belinfante, F. J. Special-relativistic linear gravitational theory—914(A)
Belser, Richard B. Frictional adhesion of metal to glass, quartz, and ceramic surfaces—915(A)
—— Improved techniques in aging of thin metal films—911(A)
—— Technique of soldering to thin metal films—915(A)
Bendt, Philip J. Neutron scattering by coupled paramagnetic ions—561
Benedict, T. S. and W. Shockley. Microwave observation of collision frequency of electrons in Ge—1152(L)
Bentley, W. (see Elson, R.)—320(L)
Benveniste, Jack and Bruce Cork. Inelastic events induced by 32-Mev protons on He—422
Bergmann, Peter G. and Ralph Schiller. Classical and quantum field theories in Lagrangian formalism—4
—— **and Robb Thomson.** Spin and angular momentum in general relativity—400
—— (see Goldberg, Joshua N.)—278
Berkowitz, Ami E. (see Franklin, Alan D.)—1171
Bethe, H. A. Molière's theory of multiple scattering—1256
Bhowmik, B. Negative primaries as part of cosmic radiation—327(L)
Billington, H. B. (see Roberts, J. H.)—905(A)
Biondi, Manfred A. Dissociative attachment of thermal electrons to I_2 molecules—337(A)
—— (see Chanin, Lorne M.)—337(A)
Birkhoff, R. D. (see Maerker, R. E.)—1159(L)
Birnbaum, G. and A. A. Maryott. High pressure inversion spectrum of ND_3 near 1500 Mc—895(A)
Birnbaum, Milton, Eric M. Harth, Leo Seren, and Ralph Tobin. Activity ratio method for measuring energy stability of betatrons—897(A)
Blatt, John M. β-decay interaction—83; 914(A)
—— β-decay of triton—86
Bloch, F. (see Wangsness, R. K.)—728
Bloembergen, N. and G. M. Temmer. Nuclear magnetic resonance of aligned radioactive nuclei—883(L)
Bohm, David. Causal interpretation of quantum theory—319(L)

—— Proof that probability density approaches $|\psi|^2$ in causal interpretation of quantum theory—458
Bohr, Aage and Ben R. Mottelson. Interpretation of isomeric transitions of electric quadrupole type—316(L)
Bolgiano, P., L. Madansky, and F. Rasetti. Continuous γ-ray spectrum accompanying β-decay—679
Borowitz, Sidney and Bernard Friedman. Variational principles for three-body scattering problems—441
Borsellino, A. Momentum transfer and angle of divergence of pairs produced by photons—1023
Bostick, W. H., M. A. Levine, and L. S. Combes. Photographic and spectrographic evidence of the pinch effect in N_2—339(A)
Bowell, E. (see Lockett, E. E.)—657(L)
Bozorth, R. M. and R. W. Hamming. Measurement of magnetostriction in single crystals—865
—— **and J. G. Walker.** Magnetic crystal anisotropy and magnetostriction of Fe-Ni alloys—624
Braught, Gene (see Conn, Willi M.)—898(A)
Breit, G. and R. M. Thaler. Relativistic corrections to magnetic moments of nuclear particles—1177
Bretscher, M. M. (see McFarland, C. E.)—892(A)
Brice, M. K. (see Cork, J. M.)—1291
—— (see LeBlanc, J. M.)—907(A)
Brickl, David E. (see Griffith, Wayland)—451
Bridge, H. S. (see Annis, Martin)—1216
Brix, Peter. Nuclear magnetic moment of Pr^{141} from hfs of Pr II—1245
Brock, E. G., A. L. Houde, and E. A. Coomes. Periodic deviations in Schottky effect for Mo—851
Broida, H. P. OH rotational distributions in mixtures of H_2O in high frequency discharge—336(A)
—— **and W. R. Kane.** Rotational intensity distributions of OH and OD in electrodeless discharge through water vapor—1053
Brolley, John E., Jr. Isomeric branching and threshold behavior of $Mo^{92}(n,2n)Mo^{91}$—877(L)
Bromley, D. A., J. A. Bruner, and H. W. Fulbright. Angular distributions of protons from $F^{19}(d,p)F^{20}$—396
—— (see Fulbright, H. W.)—892(A)
Broyles, C. D. and S. K. Haynes. K-fluorescence yield summary—912(A)
——, **D. A. Thomas, and S. K. Haynes.** Measurement and interpretation of the K-Auger intensities of Sn^{113}, Cs^{137}, and Au^{198}—715
Bruce, C. R. Homogeneity mapping of permanent magnet field for chemical effect studies in nuclear resonance—896(A)
Brueckner, K. A. Multiple scattering correction to impulse approximation in two-body system—834
—— Multiple scattering effects in pion-deuteron scattering—909(A)
Bruner, J. A. (see Bromley, D. A.)—396
—— (see Fulbright, H. W.)—892(A)
Budini, P. Energy loss and Čerenkov radiation of relativistic ionizing particle—1147(L)
Bunker, M. E. (see Ames, D. P.)—903(A)
Burbidge, G. R. and A. H. de Borde. Mesonic Auger effect—189
Burstein, E., J. J. Oberly, and J. W. Davisson. Infrared photoconductivity due to neutral impurities in Si—331(L)
Bushkovitch, A. B. (see Jones, L. C.)—895(A)
Butler, S. T. and E. E. Salpeter. Angular distribution of (d,t) reactions—891(A)
Butler, W. A. and G. M. Almy. Photoprotons from Mo^{100} and Mo^{92}—893(A)

Caird, R. S. and Allan C. G. Mitchell. Rb^{84m}—573; 903(A)
Callaway, Joseph (see Herman, Frank)—518(L)
Camac, M., J. B. Platt, and H. J. Schulte. Z-dependence of mesic x-ray yield—905(A)
—— (see Schulte, H. J.)—905(A)
Cameron, John R., Robert H. Davis, Ajay S. Divatia, Frederic J. Eppling, and Richard W. Hill. Elastic scattering of α-particles by O^{16}—909(A)
—— (see Jackson, H. L.)—365
Caretto, A. A., Jr., and S. Katcoff. Shortlived Ce isotopes from U fission—1267
Carlson, R. R. (see Kington, J. D.)—530(L)
Carroll, E. E., Jr. (see Stephens, W. E.)—893(A)
Carter, R. S. (see Palevsky, H.)—910(A)
Carver, J. H., R. D. Edge, and D. H. Wilkinson. Cross section for $Ta^{181}(\gamma,2n)Ta^{179}$ at 17.6 Mev—658(L)
Casson, Harvey. Nuclear γ-rays from low energy proton bombardment of Na, Mg, and Al—809
Chang, C. H., C. S. Cook, and H. Primakoff. Transmission of electrons through thin metallic foils—910(A)
Chang, W. Y., G. del Castillo, and Leon Grodzins. Sea level penetrating showers—408
Chanin, Lorne M. and Manfred A. Biondi. Mobilities of thermal ions in noble gases—337(A)
Chasson, Robert L. Effects of atmosphere on penetrating cosmic radiation—1255
Chen, Tien Chi and F. London. Entropy of liquid He^3—1038
Chew, Geoffrey F. Pion-nucleon scattering when coupling is weak and extended—591
—— Theoretical approach to pion-nucleon interaction—904(T)
Chraplyvy, Z. V. Approximate two-body relativistic wave equations—912(A)
—— (see Barker, W. A.)—446; 913(A)
Christy, R. F. Coupling of angular momenta in nuclear reactions—839
Chu, E. L. (see Barber, W. C.)—950
Clark, D. D. (see Igo, G. J.)—879(L)
Clarke, R. L. (see Paul, E. B.)—892(A)
Class, C. M. and S. S. Hanna. Angular correlation in decay of Li^8—877(L)
Cleland, Marshall R. Fast neutron scintillation spectrometer—896(A)
Clifford, R. P. Extensometer for rubber—341(A)
Cocconi, G. (see Barrett, Paul H.)—656(L)
Coester, F. Symmetry of S-matrix—619; 913(A)
Cohen, S. G. (see Jaffe, A. A.)—454
Cole, Richard W. Exchange magnetic moments of nuclei with almost closed shells of nucleons—883(L)
Colgate, S. A. and F. C. Gilbert. Electron-positron annihilation in flight—790
Colladay, G. S. (see Juenker, D. W.)—894(A)
Collins, T. L. Atomic masses of light elements—909(T)
Combes, L. S. (see Bostick, W. H.)—339(A)
Conant, F. S. (see Hall, G. L.)—342(A)
Conklin, G. L. (see Mandeville, C. E.)—559
Conn, Willi M. and Gene Braught. Separation of incident and emitted radiations in solar furnace by rotating sectors—898(A)
Conner, J. P. Cloud-chamber study of scattering of fast neutrons in O_2—712
Cook, C. F. and J. R. Smith. Cross section for $D(d,p)H^3$—785
Cook, C. J. (see Jorgensen, T.)—897(A)
Cook, C. S. (see Chang, C. H.)—910(A)
—— (see Whalen, J. A.)—902(A)
Cook, W. R., Jr., and Hans Jaffe. Ferroelectricity in oxides of face-centered cubic structure—1297(L)
Coomes, E. A., J. A. Dezoteus, and J. F. Whalen. Patch effect for thermionic emission from polycrystalline Ta—894(A)
—— (see Brock, E. G.)—851
—— (see Juenker, D. W.)—894(A)
Coor, T. (see Hafner, E. M.)—204
Cork, Bruce. Elastic scattering of protons from He^4—78
—— (see Benveniste, Jack)—422

Cork, J. M., M. K. Brice, W. H. Nester, J. M. LeBlanc, and D. W. Martin. Radioactive decay of W^{187}—2191
—— (see LeBlanc, J. M.)—907(A)
Coryell, Charles D., Pierre Lévêque, and Harold G. Richter. Isomerism for Cd^{117}, In^{117}, and In^{118}—903(A)
Cüer, P. and J. J. Jung. Angular distribution of $Be^9(d,t)Be^8$ at low energy—1151(L)
Curtis, C. D. Bremsstrahlung cross section of 60-Mev electrons in Pb—123

Damm, C. C. Secondaries of penetrating showers—826
Danielson, G. C. (see Shaw, William C.)—900(A)
—— (see Smith, J. F.)—911(A)
Dannis, Mark L. Plasticizers for polyvinyl chloride—341(A)
Darden, Sperry (see Nereson, Norris)—775
Date, Muneyuki (see Okamura, Tosihiko)—525(L)
Daunt, J. G. (see Kaplan, B.)—907(A)
—— (see Smith, T. S.)—654(L)
Davidson, Clifton R. (see Andrew, Alan)—876(L)
Davidson, J. P. and E. Feenberg. Deviations from *LS* coupling in spheroidal core nuclear model—856
Davis, Robert H. (see Cameron, John R.)—909(A)
—— (see Herb, R. G.)—897(A)
Davisson, J. W. (see Burstein, E.)—331(L)
Day, Robert B. Inelastic scattering of neutrons—908(A)
Dayhoff, Edward S., Sol Triebwasser, and Willis E. Lamb, Jr. Fine structure of the H atom—106
—— (see Triebwasser, Sol)—98
Dayton, Irving E. *Z*-dependence of pair production cross section at 1.33 and 2.62 Mev—544
de Borde, A. H. (see Burbidge, G. R.)—189
Dehmelt, H. G. (see Robinson, H. G.)—1305(L)
de Klerk, D., R. P. Hudson, and J. R. Pellam. Normal fluid concentration in liquid He II below 1°K—662(L)
——, **R. P. Hudson, and J. R. Pellam.** Second-sound velocity measurements below 1°K—326(L)
Delaney, C. F. G. and J. H. J. Poole. Half-life of Ca^{45}—529(L)
del Castillo, G. (see Chang, W. Y.)—408
del Río, C. S. and V. L. Telegdi. Inelastic nuclear scattering of photons by Rh^{103}—909(A)
Dennison, D. M. (see Ivash, E. V.)—895(A)
—— (see Gopalakrishnan, K.)—908(A)
Deverall, G. V., K. W. Meissner, and G. J. Zissis. Hfs of resonance lines of In I—895(A)
Dewdney, John W. (see Geiger, James S.)—621
Dezoteus, J. A. (see Coomes, E. A.)—894(A)
Diamond, R. M. Mo^{99}—1149(L)
Dicke, Robert H. Effect of collisions upon Doppler width of spectral lines—472
Dienes, G. J. Entropies of activation in metallic diffusion—185
—— (see Bartlett, J. H.)—848
Divatia, Ajay S. (see Cameron, John R.)—909(A)
—— (see Herb, R. G.)—897(A)
Donahue, D. J., K. W. Jones, M. T. McEllistrem, and H. T. Richards. Electrostatic analysis of nuclear reaction energies—824; 892(A)
Donaven, T. W. (see Kundu, D. N.)—1200
Donn, Bertram. Theory of interstellar grains—898(A)
Dousmanis, G. C. (see Sanders, T. M.)—1158(L)
Duckworth, Henry E. (see Geiger, James S.)—621
Dudley, J. M. (see Rosengren, J. W.)—603
Duerig, William H. and Jordan J. Markham. Rates of coloration of KCl and KBr during x-irradiation at 78°K—900(A)
Duffield, Robert B. and John R. Huizenga. Photofission and photoneutron emission in U—1040
—— **and L. M. Langer.** Decay of Zn^{69}—854
—— (see Huizenga, John R.)—893(A)
—— (see Langer, L. M.)—907(A)
Dugdale, J. S. and D. K. C. MacDonald. Thermal expansion of solids—832
DuMond, Jesse W. M. (see Henke, Burton)—1300(L)
Durbin, Richard P. (see Goodell, Warren F., Jr.)—724
Dyke, W. P. and J. K. Trolan. Field emission: Large current densities, space charge, and vacuum arc—799

Eager, R. L. and D. B. Langmuir. Self-diffusion of Ta—911(A)
Early, Harold C. (see Smith, Haldon L.)—338(A)
Easterday, Harry T. and Heinrich A. Medicus. Isomeric transitions in Tc^{93} and Tc^{96}—752
Eatherly, W. P. and J. D. McClelland. Anisotropic susceptibility of polycrystalline graphite—661(L)
Edge, R. D. (see Carver, J. H.)—658(L)
Eichholz, G. G. Characteristics of thin plastic scintillation phosphors—912(A)
—— Half-life of W^{187}—525(L)
Einstein, Albert. Unified field theory—321(L)
Eisberg, R. M. (see Igo, G. J.)—879(L)
Eisenberg, Y. (see Barrett, Paul H.)—656(L)
Ekstein, H. Multiple scattering and radiation damping—490
Elenbass, W. Similarity conditions of high pressure discharges—338(A)
Elliott, R. J. Paramagnetism of uranyl-like ions—659(L)
Elson, R., W. Bentley, A. Ghiorso, and Q. Van Winkle. Thermal neutron fission and capture cross section of U^{232}—320(L)
Enatsu, H. Mass relation of heavy particles—1304(L)
Engelkemeir, D. W. (see Wagner, F., Jr.)—502
Eppling, Frederic J. (see Cameron, John R.)—909(A)
—— (see Jackson, H. L.)—365
Epstein, Saul T. Causal interpretation of quantum mechanics—319(L)
Esaki, Leo. Properties of thermally treated Ge—1026
—— Thermal treatment of Si rectifiers—398

Faire, A. C. (see Fundingsland, O. T.)—337(A)
Falconer, John I., Jr. Irregularities in radiation along positive column of high pressure Hg arc—342(A)
Falk, C. E. (see Hafner, E. M.)—204
Falkoff, David L. Quantum-mechanical methods in classical physics—340(A)
Faust, W. R. (see Scherrer, V. E.)—1268
Feenberg, E. (see Davidson, J. P.)—856
Feingold, A. M. Ground state of N^{14}—318(L)
Feld, Bernard T. Angular and energy distributions in photomeson production—330(L)
Feldman, David. Charge independence of nuclear forces—1159(L)
Ferguson, Eldon E. Normal coordinate analysis of 1, 3, 5-trifluoro-benzene—895(A)
Fields, R. E., R. L. Becker, and R. K. Adair. Total *n-p* scattering cross section at 2.5 Mev—908(A)
—— (see Walt, M.)—1271
Firor, J. W. (see Fonger, W. H.)—891(A)
Fischer, Heinz. Hydrogen spectra from channel of spark discharge with increased energy—336(A)
Fite, Wade L. Production of negative ions and noise in negative ion beams—411
Fivel, Daniel I. (see Plass, Gilbert N.)—898(A)
Flammer, Carson. Variational methods for periodic lattices and artificial dielectrics—1298(L)
Foldy, Leslie L. New rigorous lower bound on range of triplet *n-p* interaction—1251
Fong, Peter. Asymmetric fission—332(L)
Fonger, W. H., J. W. Firor, and J. A. Simpson. Recurring daily cycles of nucleonic component intensity—891(A)
Foote, H. L., Jr. (see Sailor, V. L.)—904(A)
Fosdick, L. D. and H. M. James. Approximate treatment of order-disorder transitions in simple cubic Ising lattice—901(A)
Foster, John S., Jr., E. O. Lawrence, and E. J. Lofgren. High vacuum, high speed ion pump—338(A)

Fowler, R. G., W. R. Atkinson, and R. J. Lee. Shock waves in expansion of low pressure sparks—336(A)
—— **and H. C. Rose.** Ion concentrations in shock-type spark discharge tubes—906(A)
—— (see Atkinson, W. R.)—906(A)
Fowler, William A. (see Kraus, Alfred A., Jr.)—299
Fox, R. E., W. M. Hickam, and T. Kjeldaas, Jr. Ionization probability curves near threshold—336(A); 555
Francis, A. E., J. J. G. McCue, and Clark Goodman. Inelastic scattering of neutrons by Cd^{111}—1232
Francis, Norman C. Photoproduction of π^0-mesons in H and D—766
—— **and Kenneth M. Watson.** Relation between photoproduction and scattering cross sections for π-mesons in complex nuclei—328(L)
Frank, V. and O. Gram Jeppesen. Hall coefficient of Ca—1153(L)
Frankl, D. R. and T. A. Read. Effects of *F*-centers on internal friction of rocksalt single crystals—663(L)
Franklin, Alan D. and Ami E. Berkowitz. Approach to saturation in dilute ferromagnetics—1171
Fred, Mark, and Frank S. Tomkins. Nuclear spin of $_{95}Am^{241}$—318(L)
Freedman, Melvin S., Arthur H. Jaffey, Frank Wagner, Jr., and Jack May. Radiations of Th^{231}(UY)—302
—— (see Wagner, F., Jr.)—502
Freeman, B. E. and J. L. McHale. Barrier penetration effects for light nuclei—223
French, A. P. (see Kraus, Alfred A., Jr.)—299
Fretter, W. B., M. M. May, and M. P. Nakada. V^0 particles—168
Friedman, Bernard (see Borowitz, Sidney)—441
Frieman, E. A. and L. Motz. *p-p* reaction and energy production in sun—648
Fry, W. F. Li^9 disintegration in photographic emulsion—325(L)
Fukuda, H. Multiple meson production by high energy nucleon-nucleon collisions—842
Fulbright, H. W., D. A. Bromley, and J. A. Bruner. Angular distributions of protons from $F^{19}(d,p)F^{20}$—892(A)
—— (see Bromley, D. A.)—396
Fumi, Fausto G. and Robert G. Parr. Electronic spectra of diatomic molecules: O_2 molecule—895(A)
Fundingsland, O. T., A. C. Faire, and A. J. Penico. Microwave method for measuring mean energy transfer per collision and velocity dependence of collision cross section for slow electrons in gases—337(A)
Furst, Milton and Hartmut Kallmann. Energy transfer in complex solutions—912(A)
——, **Hartmut Kallmann, and Bernard Kramer.** Absolute light emission efficiency of crystal anthracene for γ-ray excitation—416

Gager, W. B. (see Smith, T. S.)—654(L)
Galonsky, Aaron I. (see Jackson, Herbert L.)—365; 370
Gandy, Harold W. Cathodoluminescent studies of (BaSr)O—912(A)
Gehman, S. D. Physics of rubber—341(A)
Geiger, James S., Benjamin G. Hogg, Henry E. Duckworth, and John W. Dewdney. $Zr^{92}-Mo^{92}$ and $Zr^{94}-Mo^{94}$ pairs and $Zr^{96}-Mo^{96}-Ru^{96}$ triplet—621
Gelinas, R. W. and S. S. Hanna. Magnetic analysis of *d*-Be reactions—483
Geltman, S. and H. Margenau. Theory of mobility of He_2^+ in He—337(A)
Ghiorso, A. (see Elson, R.)—320(L)
—— (see Hulet, E. K.)—878(L)
—— (see Rasmussen, J. O., Jr.)—33
Gilbert, F. C. (see Colgate, S. A.)—790
Gilley, L. W. (see Lagemann, R. T.)—906(A)
Gilvarry, J. J. Relativity precession of asteroid Icarus—1046
Gingrich, N. S., C. G. Shull, and M. K. Wilkinson. Magnetic structure of Mn antimonide—910(A)
Glauber, Roy and Verner Schomaker. Theory of electron diffraction—667
Glockler, George (see McCulloh, K. E.)—145
Golay, Marcel J. E. (see Keck, Paul H.)—1297(L)
Goldberg, E. Levels of Al^{26} from $Mg^{24}(d,n)Al^{26}$—760
—— (see Jackson, H. L.)—365
Goldberg, Joshua N. Strong conservation laws and equations of motion in covariant field theories—263
——, **John W. Trischka, and Peter G. Bergmann.** Electric resonance transitions in tapered electric field—278
Goldemberg, J. and L. Katz. Resolution of "photon difference method"—1300(L)
Goldhaber, Gerson. Elastic pion-hydrogen scattering in photographic emulsions—1187
Goldhaber, M. Core isomerism—remarks on Mo^{93m}—1146(L)
—— (see Kraushaar, J. J.)—1081
Goldman, L. M. Elastic scattering of 6.5-Mev protons from Cu—349
Goldschmidt-Clermont, Y., L. S. Osborne, and M. B. Scott. Photoproduction of neutral mesons in H—329(L)
Goldstein, Herbert, J. Ernest Wilkins, Jr., and L. V. Spencer. Systematic calculations of γ-ray penetration—1150(L)
Goldstein, Louis. Theory of liquid He II—597
Gonzales, O. D. (see White, David)—593
Goodell, Warren, F., Jr., Howard H. Loar, Richard P. Durbin, and William W. Havens, Jr. Neutron energy distribution from proton bombardment of Li, Be, and C at 375 Mev—724
Goodenough, John B. Theory of deviation from close packing in hexagonal metal crystals—282
Goodman, Clark (see Francis, A. E.)—1232
Gopalakrishnan, K., A. deShalit, and J. W. Mihelich. Neutron deficient isotopes of Hg—908(A)
Gora, E. Lower limit for interaction time in photon-photon scattering—913(A)
Gordon, M. M. and J. G. Jones. Variational procedure for electron-hydrogen scattering—913(A)
Gordy, W. (see Robinson, H. G.)—1305(L)
Goucher, F. S. and M. B. Prince. Interpretation of α-values in *p-n* junction transistors—651
Graves, Elizabeth R. and Louis Rosen. Distribution in energy of neutrons from interaction of 14-Mev neutrons with some elements—343
Green, H. S. First-order meson wave equations—965
—— (see Messel, H.)—315(L)
Gregory, Christopher. Conservation of quanta for non-local fields—1199
Griffith, Wayland and David E. Brickl. Diffraction of strong shock waves—451
Grodzins, Leon (see Chang, W. Y.)—408
Gui, K. E. New type of rubber fatigue test—341(A)
Gunst, S. B. (see Page, L. A.)—1273
Güttinger, Werner. Quantum field theory in light of distribution analysis—1004

Hafner, E. M., W. F. Hornyak, C. E. Falk, G. Snow, and T. Coor. Total *n-p* scattering cross section at 4.75 Mev—204
Hagstrum, Homer D. Effect of adsorption of common gases on electron ejection by noble gas ions—338(A)
—— Electron ejection from Mo by He^+, He^{++}, and He_2^+—244
Hales, R. W. and B. J. Moyer. Atomic number dependence of neutral meson yield from proton bombardment—1047
Haley, Floyd C. and Donald H. Andrews. Anomalous critical current effect in superconducting NbN—821
Hall, G. L. and F. S. Conant. Firestone shear flexometer—342(A)
Hall, Harry H., Daniel T. Hedden, and Thomas J. Turner. Activation energies of Se-Te alloys—340(A)

Hamermesh, Bernard. Measurement of neutron-capture γ-rays—896(T)
—— (see Kimball, Clyde)—1306(L)
Hamming, R. W. (see Bozorth, R. M.)—865
Hanna, S. S. (see Class, C. M.)—877(L)
—— (see Gelinas, R. W.)—483
Hannam, H. J. (see Lindemann, W. W.)—900(A)
Hanson, A. O. (see Whalin, E. A.)—324(L)
Hanson, H. P. Mixing of states and antiferromagnetism—1154(L)
Hardy, George F. and John K. Hulm. Superconducting silicides and germanides—884(L)
Härm, Richard (see Spitzer, Lyman, Jr.)—977
Harris, E. G. and M. A. Melkanoff. Quadrupole moment of Li^7—914(A)
Harris, Gerard G. and T. J. B. Shanley. γ-rays from μ-meson capture in Pb—983
Harris, S. P. Neutron resonances in Xe—904(A)
Harrison, F. B. (see Jackson, Jasper A.)—322(L)
Hart, Edward W. Structure of deformation bands—521(L)
Harth, Eric M. (see Birnbaum, Milton)—897(A)
Hatch, Albert J. and H. Bartel Williams. Theory of high frequency secondary electron resonance discharge mechanism—339(A)
—— (see Williams, H. Bartel)—339(A)
Havens, William W., Jr. (see Goodell, Warren F., Jr.)—724
Haxby, B. V. and P. Wargo. Effect of evaporation products from BaO coated cathode on secondary emission of MgO thin films—893(A)
Haynes, S. K. (see Broyles, C. D.)—715; 912(A)
Hedden, Daniel T. (see Hall, Harry H.)—340(A)
Hedgran, A. (see Lindström, G.)—1303(L)
Hellund, E. J. Decay of resonance radiation by spontaneous emission—919
Henke, Burton and Jesse W. M. DuMond. Low angle x-ray diffraction with long wavelengths—1300(L)
Herb, R. G., Robert H. Davis, Ajay S. Divatia, and D. Saxon. Evapor-ion pump—897(A)
Herlin, Melvin A. (see Mayper, Victor, Jr.)—523(L)
Herman, Frank and Joseph Callaway. Electronic structure of Ge crystal—518(L)
Herzog, L. F. (see Aldrich, L. T.)—631
Hickam, W. M. (see Fox, R. E.)—336(A); 555
Hildebrand, Roger H. Charge-independence in meson production—904(T)
—— Neutral meson production in n-p collisions—1090
Hill, David Lawrence and John Archibald Wheeler. Nuclear constitution and interpretation of fission phenomena—1102
Hill, R. D. and J. W. Mihelich. Probable existence of $E3+M4$ mixture in isomeric transition—323(L)
—— (see Swan, J. B.)—907(A)
Hill, Richard W. (see Cameron, John R.)—909(A)
—— (see Jackson, H. L.)—365
Hjalmar, Elis and Hilding Slätis. Q-values for $N^{14}(\alpha,p)O^{17}$—1151(L)
Hobson, J. P. and W. A. Nierenberg. Statistics of two-dimensional, hexagonal net—662(L)
Hoffman, Banesh. Relativity of size—49
—— Similarity theory of relativity and Dirac-Schrödinger theory of electrons—52
Hofstadter, Robert (see Hudson, A.)—1309(L)
—— (see Kantz, Asher)—607
Hogg, Benjamin G. (see Geiger, James S.)—621
Holmes, D. K. Application of cellular method to Si, erratum—1308(L)
Holroyd, L. V. (see Affleck, J. H.)—893(A)
Holt, J. R. and T. N. Marsham. States of S^{33} and Si^{29} from (d,p) stripping—665(L)
Holyk, W. K. (see Aldrich, L. T.)—631
Hope, J. Tensor force interaction between shell closed except for single vacancy and external nucleon—884(L)
Hornyak, W. F. (see Hafner, E. M.)—204
Horton, G. K. and R. T. Sharp. Approximate wave functions for unbound relativistic particles in Coulomb field—885(L)
Hotz, H. P. (see Porter, F. T.)—903(A); 938
Houde, A. L. (see Brock, E. G.)—851
Huddleston, Charles M. and Allan C. G. Mitchell. Nuclear spectra of Rb^{83} and Rb^{84}—903(A)
Hudson, A. and R. Hofstadter. Energy loss of cosmic-ray μ-mesons in NaI crystals, erratum—1309(L)
Hudson, D. E. (see Shaw, William C.)—900(A)
Hudson, R. P. (see de Klerk, D.)—326(L); 662(L)
Hughes, D. J. (see Palevsky, H.)—910(A)
—— (see Seidl, F. G. P.)—897(A)
Hughes, Vernon (see Perl, William)—886(L)
Huizenga, J. R. Neutron binding-energies of heavy elements and some applications—904(T)
—— **and Robert B. Duffield.** Relative photofission and photoneutron cross sections for U^{235}—893(A)
—— (see Duffield, Robert B.)—1042
—— (see Wagner, F., Jr.)—502
Hulet, E. K., S. G. Thompson, and A. Ghiorso. Spontaneous fission rate of Cf^{246}—878(L)
Hulm, John K. (see Hardy, George F.)—884(L)
—— (see Matthias, B. T.)—439
Hunt, R. Allen and Robert H. Schuler. Saturation in x-ray coloration of corundum single crystals—664(L)
Hunt, S. E. and W. M. Jones. Absolute determination of resonant energies for radiative capture of protons by B, C, F, Mg, and Al below 500 kev—1283
Huntington, H. B. Extension of Makinson's theory of photoelectric emission to periodic potential—357
—— **and L. Apker.** Transition probability for photoelectric emission from semiconductors—352
Hutchison, Clyde A., Jr., and Leonard S. Singer. Paramagnetic resonance absorption in salts of V and Mn—256
Huxford, W. S. (see Olsen, H. N.)—336(A)

Igo, G. J., D. D. Clark, and R. M. Eisberg. Statistical fluctuations in ionization by 31.5-Mev protons—879(L)
Ivash, E. V. and D. M. Dennison. Molecular constants of CH_3OH—895(A)
Ivey, Henry F. Spectral location of absorption due to color centers in alkaline earth halide crystals—322(L)

Jackson, Herbert L. and Aaron I. Galonsky. Excited states of N^{13} nucleus—370
——, **A. I. Galonsky, F. J. Eppling, R. W. Hill, E. Goldberg, and J. R. Cameron.** $C^{13}(p,p)C^{13}$ differential cross section—365
Jackson, J. David and Harry Schiff. Electron capture by protons passing through H_2—359
Jackson, Jasper A. and F. B. Harrison. Slow component in decay of scintillation phosphors—322(L)
Jacobsohn, B. A. Test for charge independence in high energy nucleon-nucleon scattering—881(L)
Jaffe, A. A. and S. G. Cohen. Disintegration of RaD—454
Jaffe, Hans (see Cook, W. R., Jr.)—1297(L)
Jaffey, Arthur H. (see Freedman, Melvin S.)—302
James, Hubert M. (see Fosdick, L. D.)—901(A)
—— (see Krieger, Theodore J.)—901(A)
Jamgochian, E. (see Lehovec, K.)—20
Jensen, Erling. Coincidence measurements with β-ray spectrometers—909(T)
Jentschke, W. K. (see Allen, James S.)—902(A)
—— (see Remley, M. E.)—1194
Jeppesen, O. Gram (see Frank, V.)—1153(L)
Johnson, C. Peter, Jr. Unified field theory—320(L)
Johnson, J. B. Experiments and thoughts on secondary emission—902(T)
Johnson, N. R. (see Sheline, R. K.)—520(L)

Johnson, Vivian A. Galvanomagnetic effects in semiconductors —910(T)
—— **and W. J. Whitesell.** Theory of magnetoresistive effect in semiconductors—941
Johnston, H. L. (see White, David)—593
Jones, E. (see Jorgensen, T.)—897(A)
Jones, J. G. (see Gordon, M. M.)—913(A)
Jones, K. W. (see Donahue, D. J.)—824; 892(A)
Jones, L. C., A. B. Bushkovitch, C. A. Potter, and A. G. Rouse. Variation of mutual collision diameters with mix ratio in binary mixtures in microwave pressure broadening —895(A)
Jones, Mark W. Respiration of plant tissue cultures as function of x-ray dose—899(A)
Jones, W. M. (see Hunt, S. E.)—1283
Jorgensen, T., E. Jones, and C. J. Cook. Extrapolated ionization ranges for 10- to 250-kv protons in various gases —897(A)
Juenker, D. W., G. S. Colladay, and E. A. Coomes. Analysis of Schottky deviation for highly refractory metals—894(A)
Jung, J. J. (see Cüer, P.)—1151(L)

Kahn, Arnold H. and C. Kittel. *F*-center wave functions and electronic *g*-values in KCl crystals—315(L)
Kallmann, Hartmut, Bernard Kramer, and Arnold Perlmutter. Induced conductivity in luminescent powders. II. Ac impedance measurements—700
—— (see Furst, Milton)—416; 912(A)
Kane, W. R. (see Broida, H. P.)—1053
Kantz, Asher and Robert Hofstadter. Electron-induced showers in Cu—607
Kaplan, B. and J. G. Daunt. Current noise in partially superconducting resistors at temperatures down to 2°K —907(A)
Katcoff, S. (see Caretto, A. A., Jr.)—1267
Katz, L. (see Goldemberg, J.)—1300(L)
Keck, Paul H. and Marcel J. E. Golay. Crystallization of Si from floating liquid zone—1297(L)
Keesom, P. H., K. Lark-Horovitz, and N. Perlman. Influence of neutron bombardment on low temperature atomic heat of Si—900(A)
Keller, Joseph B. Bohm's "interpretation of quantum theory in terms of 'hidden' variables"—1040
Kenty, Carl. Afterglow spectra observable in incandescent lamps—336(A)
—— **and D. A. Larson.** Enhancement of green continuum of Hg by rare gas—180
Kerman, R. O., W. E. Kreger, and P. G. Kruger. *p-p* scattering at 5.77 Mev using photographic techniques—908(A)
Kimball, Clyde and Bernard Hamermesh. Activation cross sections measured with Sb−Be photoneutrons—1306(L)
King, D. T., Nathan Seeman, and Maurice M. Shapiro. Mass measurements of heavy mesons—891(A)
King, J. S. and W. C. Parkinson. Angular distribution of protons from V^{52}—1080
Kington, J. D., J. K. Bair, R. R. Carlson, and H. B. Willard. Mass difference $Si^{27}-Al^{27}$—530(L)
Kinsey, B. B. and G. A. Bartholomew. Neutron capture γ-rays from Ti, Cr, Fe, Ni, and Zn—375
—— (see Bartholomew, G. A.)—386
Kip, A. F., C. Kittel, A. M. Portis, R. Barton, and F. H. Spedding. Microwave resonance absorption in Gd metal —518(L)
Kitagaki, T. Focusing method for large accelerators—1161(L)
Kittel, C. (see Kahn, Arnold H.)—315(L)
—— (see Kip, A. F.)—518(L)
Kjeldaas, T., Jr. (see Fox, R. E.)—336(A); 555
Klein, Abraham, Symmetric pseudoscalar theory of nuclear forces—1158(L)
Klick, Clifford C. Luminescence and photoconductivity in CdS at absorption edge—274
Kofoed-Hansen, O. and Aage Winther. Cross terms in β-decay —526(L)
Kofsky, Irving L. Crystal diodes in electronics laboratory —340(A)
Koster, G. F. Localized functions in molecules and crystals —67
Kramer, Bernard (see Furst, Milton)—416
—— (see Kallmann, Hartmut)—700
Kraus, Alfred A., Jr., A. P. French, William A. Fowler, and C. C. Lauritsen. Angular distribution of γ-rays and short range α-particles from $N^{15}(p,\alpha\gamma)C^{12}$—299
Kraushaar, J. J. and M. Goldhaber. Direction and polarization correlations of successive γ-rays—1081
Kreger, W. E. (see Kerman, R. O.)—908(A)
Krieger, Theodore J. and Hubert M. James. Theory of successive rotational transitions in crystals—901(A)
Krone, R. W. (see Teener, J. W.)—892(A)
Krotkov, R. V. (see Scheidegger, A. E.)—1096
Kruger, P. G. (see Kerman, R. O.)—908(A)
—— (see Remley, M. E.)—1194
Krumhansl, James A. and N. Schwartz. Calculation of *F*-center energy levels—1154(L)
—— (see Steele, Earl L.)—901(A)
Kruse, U. E., N. F. Ramsey, and B. J. Malenka. Electric scattering of deuterons—655(L)
Kruskal, Martin. Instabilities of completely ionized plasma —335(A)
Kundu, D. N., T. W. Donaven, M. L. Pool, and J. K. Long. Nuclear reactions with 21-Mev He^3 in cyclotron—1200
Kurşunoğlu, B. (see Rickayzen, G.)—522(L)

Lagemann, R. T. and L. W. Gilley. Ultrasonic velocity, density, and compressibility of supercooled H_2O and D_2O —906(A)
Lamb, Willis E., Jr. (see Dayhoff, Edward S.)—106
—— (see Triebwasser, Sol)—98
Lampert, Murray A. and Alan D. White. New microwave technique for study of discharges in gases—337(A)
Landon, H. H. (see Sailor, V. L.)—904(A)
Langer, L. M., R. B. Duffield, and C. W. Stanley. Radioactivity of Cs^{128}—907(A)
—— (see Ames, D. P.)—903(A)
—— (see Duffield, R. B.)—854
Langmuir, David B. Observations on "direct-current etch" —911(A)
—— (see Eager, R. L.)—911(A)
Larach, Simon and John Turkevich. Interaction of Mn activator ions in Zn-orthosilicate phosphors—1060
Lark-Horovitz, K. (see Keesom, P. H.)—900(A)
Larson, D. A. (see Kenty, C.)—180
Lauritsen, C. C. (see Kraus, Alfred A., Jr.)—299
Lawrance, R. Temperature dependence of drift mobility in Ge—1295(L)
Lawrence, E. O. (see Foster, John S., Jr.)—338(A)
LeBlanc, J. M., W. H. Nester, D. W. Martin, M. K. Brice, and J. M. Cork. γ-radiation from radioactive Cs^{134}—907(A)
—— (see Cork, J. M.)—1291
Lee, R. J. (see Fowler, R. G.)—336(A)
Lehovec, K., C. A. Accardo, and E. Jamgochian. Light emission produced by current injected into green SiC crystal—20
Leighton, R. B., S. D. Wanlass, and C. D. Anderson. Decay of V^0-particles—148
Lévêque, Pierre (see Coryell, Charles D.)—903(A)
Levine, M. A. (see Bostick, W. H.)—339(A)
Levinger, J. S. Effects of radioactive disintegrations on inner electrons of atom—908(A)
Levinson, Norman. Certain explicit relationships between phase shift and scattering potential—755
Lew, Hin. Ground state hfs and nuclear magnetic moment of Pr—530(L)

—— **and Günter Wessel.** Hfs of ground state of Al—894(A)
Lewis, H. W. (see Simmons, B. E.)—905(A)
Liang, C. Y. (see Nielsen, J. Rud)—895(A)
Lindemann, W. W. and H. J. Hannam. Flicker noise caused by interface layer—900(A)
Lindenfeld, P., A. Sachs, and J. Steinberger. Internal pair production of γ-rays of mesonic origin; alternate modes of π^0-decay—531
Lindner, Manfred. Heavy isotopes of Mg and Si—1150(L)
Lindström, G., A. Hedgran, and D. E. Alburger. Precision measurement of Co^{60} γ-radiation—1303(L)
Livingston, M. S. Design considerations for very high energy accelerators—339(T)
Loar, Howard H. (see Goodell, Warren F., Jr.)—724
Lockett, E. E. and E. Bowell. Thermal neutron absorption cross section of Sc—657(L)
Lofgren, E. J. (see Foster, John S., Jr.)—338(A)
Long, J. K. (see Kundu, D. N.)—1200
Luborsky, Fred E. and Stanley I. Reynolds. Frequency spectra from point-to-plane corona—338(A)
Lyon, W. S. Neutron capture cross sections for production of Sc^{46} and Sr^{85}—1307(L)
Lyons, Harold (see Nuckolls, R. G.)—1101
Lyons, W. James. Viscoelastic properties as functions of distribution of activation energies—342(A)

MacDonald, D. K. C. (see Dugdale, J. S.)—832
MacDonald, William M. (see Richardson, John M.)—913(A)
Madansky, L. (see Battey, James)—182
—— (see Bolgiano, P.)—679
Madrazo, Raymond, Jr. (see Antonoff, George)—899(A)
Maerker, R. E. and R. D. Birkhoff. Experimental K to $L+M$ ratios for internal conversion lines—1159(L)
Malenka, B. J. (see Kruse, U. E.)—655(L)
Mandeville, C. E., E. Shapiro, R. I. Mendenhall, E. R. Zucker, and G. L. Conklin. γ-radiations from Zr^{95} and Nb^{95}—559
Mapother, Dillon. Effect of x-ray irradiation on self-diffusion coefficient of Na in NaCl—1231
Margenau, H. (see Geltman, S.)—337(A)
Markham, Jordan J. Second-order acoustic fields: relations between energy and intensity—972
—— (see Duerig, William H.)—900(A)
Marsham, T. N. (see Holt, J. R.)—665(L)
Martin, André and Loup Verlet. p-p scattering at intermediate energies—519(L)
Martin, D. W. (see Cork, J. M.)—1291
—— (see LeBlanc, J. M.)—907(A)
Martin, H. C. and R. F. Taschek. (n,γ) and $(n,2n)$ reactions in I—1302(L)
Maryott, A. A. (see Birnbaum, G.)—895(A)
Matland, C. G. Quenching of Hg resonance radiation (2537A) by N_2—338(A)
Matossi, Frank and Sol Nudelman. Influence of electric fields on luminescence—660(L)
Matsuda, H. (see Ogata, K.)—27; 333(L)
Matthias, B. T. and J. K. Hulm. Superconducting properties of $CoSi_2$—439
Mattson, R. H. and A. van der Ziel. Shot noise in Ge filaments—899(A)
Max, L. W. (see Taylor, T. Smith)—899(A)
May, Jack (see Freedman, Melvin S.)—302
May, M. M. (see Fretter, W. B.)—168
Mayper, Victor, Jr., and Melvin A. Herlin. Second-sound velocity below 1°K as function of pressure—523(L)
McClelland, J. D. (see Eatherly, W. P.)—661(L)
McClure, G. W. Specific primary ionization of H_2, He, Ne, and A by high energy electrons—335(A)
McCue, J. J. G. (see Francis, A. E.)—1232
McCulloh, K. E. and George Glockler. Electronic emission spectrum of $C^{13}O^{16}$—145
McCusker, C. B. A., H. Messel, D. D. Millar, and N. A. Porter. Experimental investigation of nucleon cascade in water—1172
McEllistrem, M. T. (see Donahue, D. J.)—824; 892(A)
McFarland, Charles E., M. M. Bretscher, and F. B. Shull. Magnetic analysis of protons from $Cr^{52}(d,p)Cr^{53}$ and $Ni^{58}(d,p)Ni^{59}$—892(A)
—— **and Franklin B. Shull.** Magnetic analysis of $Sr^{88}(d,p)Sr^{89}$—489
McFarland, Robert H. and Robert E. Swanson. Sensitized fluorescence studies using photomultiplier detection method—911(A)
—— (see Swanson, Robert E.)—911(A)
McHale, J. L. (see Freeman, B. E.)—223
Medicus, G. and G. Wehner. Investigation of cathode sputtering by means of probe measurements—339(A)
—— (see Wehner, G.)—339(A)
Medicus, Heinrich A. (see Easterday, Harry T.)—752
Meinke, W. Wayne (see Schott, G. L.)—1156(L)
Meissner, K. W. (see Deverall, G. V.)—895(A)
Melkanoff, M. A. (see Harris, E. G.)—914(A)
Mendenhall, R. I. (see Mandeville, C. E.)—559
Merzbacher, E. (see Simmons, B. E.)—905(A)
Messel, H. and H. S. Green. Suggested scheme for meson production—315(L)
—— (see McCusker, C. B. A.)—1172
Meyer, D. I. and F. H. Schmidt. Precise measurement of "F" line of ThB—908(A)
Mihelich, J. W. Disintegration of Re^{188m}—907(A)
—— (see Gopalakrishnan, K.)—908(A)
—— (see Hill, R. D.)—323(L)
Millar, D. D. (see McCusker, C. B. A.)—1172
Miller, R. F. Dipole moment of β-propiolactone—341(A)
Miller, William (see Motz, J. W.)—968
Mitchell, Allan C. G. (see Caird, R. S.)—573; 903(A)
—— (see Huddleston, Charles M.)—903(A)
Mize, J. P. and D. J. Zaffarano. β-spectrum of S^{35}—902(A)
Mizushima, Masataka (see Putcha, Venkateswarlu)—896(A)
Molnar, J. P. (see Phelps, A. V.)—1202
Moore, Marvin G. Quasi-relativistic theory of gravitation—587
Moorhouse, R. G. Pair creation in intermediate coupling theory—958
Morrison, S. R. Adsorption of O_2 on ZnO—900(A)
Morrow, J. C. Vapor-liquid equilibria in He^3-He^4 solutions—1034
Moses, H. E. Canonical transformation for electron-positron field coupled to time-independent electromagnetic field—115
Moszkowski, Steven A. Lifetimes of nuclear isomers—474
Mottelson, Ben R. (see Bohr, Aage)—316(L)
Motz, J. W., William Miller, and H. O. Wyckoff. 11-Mev thick target bremsstrahlung—968
Motz, Lloyd. Gauge invariance and classical electrodynamics—60
—— (see Frieman, E. A.)—648
Mower, Lyman. Tables for second Born approximation scattering from various potential fields—947
Moyer, B. J. (see Hales, R. W.)—1047

Nakada, M. P. (see Fretter, W. B.)—168
Nakamura, Seitaro. Meson theory of β-decay and ΔL-forbidden transitions—16
Nereson, Norris and Sperry Darden. Average neutron total cross sections in 3- to 12-Mev region—775
Nester, W. H. (see Cork, J. M.)—1291
—— (see LeBlanc, J. M.)—907(A)
Newton, J. O. and B. Rose. γ-radiation from Am^{241}—1157(L)
Nicodemus, David B. and Hans H. Staub. Fission neutron spectrum of U^{235}—1288
Niday, J. B. (see Turkevich, A.)—552

Nielsen, J. Rud, C. Y. Liang, D. C. Smith, and Morris Alpert. Vibrational spectra and calculated thermodynamic properties of CCl_3CF_2Cl and CCl_3CFCl_2—895(A)
Nierenberg, W. A. (see Hobson, J. P.)—662(L)
Nomura, K. C. Secondary electron emission of MgO single crystals with excess O_2—894(A)
Novey, T. B. Experimental energy and angular distributions of inner bremsstrahlung—672
Nuckolls, R. G., L. J. Rueger, and Harold Lyons. Microwave absorption spectrum of ND_3—1101
Nudelman, Sol (see Matossi, Frank)—660
Nye, H. A. Diamagnetism of enclosed electron gas—1305(L)

Oakley, D. C. (see Walker, R. L.)—1301(L)
Oberly, J. J. (see Burstein, E.)—331(L)
Ogata, K. and H. Matsuda. Atomic mass of P^{31}—333(L)
—— **and H. Matsuda.** Masses of light atoms—27
Ohtsuka, Taiichiro (see Waniek, R. W.)—882(L);1307
Okamura, Tosihiko, Yosiharu Torizuka, and Muneyuki Date. Paramagnetic resonance in copper acetate at 47 000 Mc/sec—525(L)
Okazaki, A. (see Adair, R. K.)—1165
—— (see Becker, R. L.)—904(A)
—— (see Walt, M.)—1271
Olbert, S. (see Annis, Martin)—1216
Olsen, H. N. and W. S. Huxford. Time variation of ion concentration in flash discharge plasmas—336(A)
Olsen, K. M. (see Pfann, W. G.)—322(L)
O'Meara, F. E. Enhanced reactor—982
O'Rourke, R. C. Multiple Compton scattering of low energy γ-radiation—999
Osborne, Darrell W. (see Weinstock, Bernard)—787
Osborne, L. S. (see Goldschmidt-Clermont, Y.)—329(L)
Overhauser, Albert W. Paramagnetic relaxation in metals —689

Packard, R. G. Streaming potentials developed across porous diaphragms for sinusoidal flow—906(A)
Page, L. A., P. Stehle, and S. B. Gunst. Direct comparison of m/e for positron and electron—1273
Pake, G. E. (see Sands, R. H.)—896(A)
—— (see Townsend, J.)—606
—— (see Wilson, C. W., III)—896(A)
Palevsky, H., R. S. Carter, and D. J. Hughes. Magnetic inelastic scattering of neutrons in Fe—910(A)
—— (see Seidl, F. G. P.)—897(A)
Parkinson, W. C. (see King, J. S.)—1080
Parmenter, R. H. Acousto-electric effect—990
Parr, Robert G. (see Fumi, Fausto G.)—895(A)
Parzen, G. Electronic energy bands in metals—237
—— **and T. Wainwright.** Calculation of energy bands in crystals—901(A)
Paul, E. B. and R. L. Clarke. Yield of long-range α-particles from $F^{19}(p,\alpha)O^{16}$—892(A)
Pearlman, N. (see Keesom, P. H.)—900(A)
Peaslee, D. C. Fermi term in β-ν correlation—1148(L)
Pellam, John R. (see de Klerk, D.)—326(L); 662(L)
—— (see Weinstock, Bernard)—521(L)
Penico, A. J. (see Fundingsland, O. T.)—337(A)
Perl, William and Vernon Hughes. Non-radiative relativistic contribution to magnetic moment of $^3S_1$ He—886(L)
Perlmutter, Arnold (see Kallmann, Hartmut)—700
Petermann, A. Divergence of perturbation expansion—1160(L)
Peterson, R. W. Rate of evolution of constituents of oxide coated cathode as function of molar composition of coating —894(A)
Pfann, W. G. and K. M. Olsen. Purification and prevention of segregation in single crystals of Ge—322(L)
Phelps, A. V. and J. P. Molnar. Lifetimes of metastable states of noble gases—1202
Phillips, G. C. Accurate determination of disintegration energies—896(T)
Plass, Gilbert N. and Daniel I. Fivel. Contributions of Doppler effect to radiation exchange in stratosphere —898(A)
Platt, J. B. (see Camac, M.)—905(A)
—— (see Schulte, H. J.)—905(A)
Pool, M. L. (see Kundu, D. N.)—1200
Poole, J. H. J. (see Delaney, C. F. G.)—529(L)
Pope, N. K. Entropy of fusion of monatomic liquids—899(A)
Porter, F. T. and H. P. Hotz. Upper limit for atomic orbital electron ejection accompanying K capture in Fe^{55}—903(A); 938
—— (see Primakoff, H.)—903(A); 930
—— (see Whalen, J. A.)—902(A)
Porter, N. A. (see McCusker, C. B. A.)—1172
Portis, A. M. (see Kip, A. F.)—518(L)
Portnoy, W. M. (see Swann, J. B.)—907(A)
Potter, C. A. (see Jones, L. C.)—895(A)
Pound, R. V. (see Abragam, A.)—1306(L)
—— (see Watkins, G. D.)—658(L)
Pressly, E. C. Air mass between observer and outer space —654
Price, P. J. Macroscopic theory of superfluid He^3–He^4 mixtures—1209
Primakoff, H. and F. T. Porter. Atomic excitation and ionization accompanying orbital electron capture by nuclei —903(A); 930
—— (see Chang, C. H.)—910(A)
Prince, M. B. (see Goucher, F. S.)—651
Pruett, Charles H. (see Roggenkamp, Paul L.)—903(A)
Pugh, Emerson M. (see Schindler, Albert I.)—295
Putcha, Venkateswarlu and Masataka Mizushima. Possible microwave absorption in molecules belonging to point groups $D_{2d} = V_d$ and T_d—896(A)

Racah, G. and I. Talmi. Pairing property of nuclear interactions—913(A)
Rado, George T. Theory of microwave permeability tensor and Faraday effect in nonsaturated ferromagnetic materials —529(L)
Ramsey, Norman F. Pseudo-quadrupole effect for nuclei in molecules—527(L)
—— (see Kruse, U. E.)—655(L)
Rasetti, F. (see Battey, James)—182
—— (see Bolgiano, P.)—679
Rasmussen, J. O., Jr., S. G. Thompson, and A. Ghiorso. α-radioactivity in 82-neutron region—33
Raychaudhuri, Amalkumar. Arbitrary concentrations of matter and Schwarzschild singularity—417
Read, T. A. (see Frankl, D. R.)—663(L)
Reddan, M. J. Clean-up of He in arc discharge—339(A)
Remley, M. E., W. K. Jentschke, and P. G. Kruger. n-p scattering using organic crystal scintillation detectors—1194
Reynolds, Stanley I. (see Luborsky, Fred E.)—338(A)
Ribe, F. L. (see Battat, M. E.)—80
Rice, O. K. Irreversible processes with application to He II and Knudsen effect in gases—793
Richards, Hans Kohn. Measurement of ionizing radiation by frequency variation—897(A)
Richards, H. T. Level classification by resonance scattering of protons and alphas—909(T)
—— (see Donahue, D. J.)—824; 892(A)
Richardson, J. Reginald (see Sachs, Donald C.)—1163
Richardson, John M. and William M. MacDonald. Variation Φ^{Φ} method in quantum statistics—913(A)
Richter, Harold G. (see Coryell, Charles D.)—903(A)
Rickayzen, G. and B. Kurşunoğlu. Unified field theory and Born-Infeld electrodynamics—522(L)

Roberts, J. H., W. O. Solano, D. E. Wood, and H. B. Billington. Measurement of energy of isotropic fast neutrons with Li^6 loaded emulsions—905(A)
—— (see Solano, W. O.)—892(A)
—— (see Weddell, J. B.)—891(A)
Robinson, H. G., H. G. Dehmelt, and W. Gordy. Pure nuclear quadrupole spectrum of Bi^{209} in Bi-triphenyl—1305(L)
Roggenkamp, Paul L., Charles H. Pruett, and Roger G. Wilkinson. Excited levels of Ti^{48}—903(A)
Rose, B. (see Newton, J. O.)—1157(L)
Rose, D. J. (see Allis, W. P.)—335(A)
Rose, H. C. (see Fowler, R. G.)—906(A)
Rosen, Louis (see Graves, Elizabeth R.)—343
Rosenblum, G. (see Stephens, W. E.)—893(A)
Rosengren, J. W. and J. M. Dudley. High energy photoproton production by 322-bremsstrahlung—603
Rothstein, Jerome. Solids subjected to constant rate of generation of lattice defects—901(A)
Rouse, A. G. (see Jones, L. C.)—895(A)
Ruby, Stanley L. (see Rustad, Brice M.)—880(L)
Ruderman, M. Pseudoscalar matrix element in β-decay—1227
Rueger, L. J. (see Nuckolls, R. G.)—1101
Rustad, Brice M. and Stanley L. Ruby. Correlation between electron and recoil nucleus in He^6 decay—880(L)

Sachs, A. (see Lindenfeld, P.)—531
Sachs, Donald C. and J. Reginald Richardson. Mean excitation potentials—1163
Sailor, V. L., H. L. Foote, Jr., and H. H. Landon. Slow neutron resonances in Sm and Y—904(A)
Salpeter, E. E. Lamb shift for H and D—92
—— (see Butler, S. T.)—891(A)
Salzman, F. Photopion production from single nucleon—913(A)
Sanders, T. M., Jr., A. L. Schawlow, G. C. Dousmanis, and C. H. Townes. Microwave spectrum of free OH radical—1158(L)
Sands, R. H. and G. E. Pake. Anomalous results in attempt to determine spin of Si^{29}—896(A)
Sard, R. D. Recent research on μ-mesons—909(T)
Savitt, J. Propagation of explosive produced air shocks—906(A)
Saxon, D. (see Herb, R. G.)—897(A)
Schawlow, A. L. (see Sanders, T. M.)—1158(L)
Scheidegger, A. E. and R. V. Krotkov. Relativistic statistical thermodynamics—1096
Scherrer, V. E., R. Theus, and W. R. Faust. γ-radiation from interaction of 14-Mev neutrons with Fe—1268
Schiff, Harry (see Jackson, J. David)—359
Schiller, Ralph (see Bergmann, Peter G.)—4
Schindler, Albert I. and Emerson M. Pugh. Hall effect of Cu-Ni alloys—295
Schmidt, F. H. (see Meyer, D. I.)—908(A)
Schmitt, Roman A. and Nathan Sugarman. U photofission yields—1155(L)
Schomaker, Verner (see Glauber, Roy)—667
Schott, G. L. and W. Wayne Meinke. Assignment of Y^{92} and Y^{94}—1156(L)
Schuler, Robert H. (see Hunt, R. Allan)—664(L)
Schulte, H. J., J. B. Platt, and M. Camac. X-rays from mesic C atom—905(A)
—— (see Camac, M.)—905(A)
Schwartz, H. M. Magnetic moments of odd-odd nuclei and strong spin-orbit coupling shell model—1293
Schwartz, N. (see Krumhansl, J. A.)—1154(L)
Schwetman, Herbert D. (see Williams, Corre)—899(A)
Scott, E. J. Technique for secondary electron emission measurements—894(A)
Scott, G. G. Gyromagnetic ratio of supermalloy—618
Scott, M. B. (see Goldschmidt-Clermont, Y.)—329(L)
Seagondollar, L. W. (see Teener, J. W.)—892(A)
Seeman, Nathan (see King, D. T.)—891(A)
Seidl, F. G. P., D. J. Hughes, and H. Palevsky. Velocity spectrometer using μsec neutron shutter—897(A)
Seitz, Frederick. Generation of *F*-centers at low temperatures—1299(L)
Sengupta, S. Non-existence of stable isobars with odd mass number—1296(L)
Seren, Leo (see Birnbaum, Milton)—897(A)
Shanley, T. J. B. (see Harris, Gerard G.)—983
Shapiro, E. (see Mandeville, C. E.)—559
Shapiro, Maurice M. (see King, D. T.)—891(A)
Sharp, R. T. (see Horton, G. K.)—885(L)
Shaw, William C., D. E. Hudson, and G. C. Danielson. Electrical characteristics of crystalline B—900(A)
Sheline, R. K. and N. R. Johnson. New long-lived Mg^{28} isotope—520(L)
Sherman, Noah. Diurnal variations in intensity of cosmic rays underground—25
Shockley, W. (see Benedict, T. S.)—1152(L)
Shull, C. G. (see Gingrich, N. S.)—910(A)
Shull, Franklin B. (see McFarland, Charles E.)—489; 892(A)
Simmons, B. E., H. W. Lewis, and E. Merzbacher. Production of characteristic x-rays by proton bombardment—905(A)
Simon, A. and T. A. Welton. Production of polarized particles in nuclear reactions—886(L)
Simpson, J. A. Properties of cosmic-ray intensity variations—891(T)
—— (see Fonger, W. H.)—891(A)
Singer, Leonard S. (see Hutchison, Clyde A.)—256
Slätis, Hilding (see Hjalmar, Elis)—1151(L)
Smith, D. C. (see Nielsen, J. Rud)—895(A)
Smith, Haldon L. and Harold C. Early. Rocket measurement of upper atmosphere density by Paschen's law—338(A)
Smith, J. F. and G. C. Danielson. Diffusion of Na in sodium tungsten bronze—911(A)
Smith, J. R. (see Cook, C. F.)—785
Smith, T. S., W. B. Gager, and J. G. Daunt. Properties of superconductors below 1°K—654
Snitzer, Elias. Charge states of He beam in H_2, He_2, air, and A_2—898(A); 1237
Snow, G. (see Hafner, E. M.)—204
Solano, W. O. and J. H. Roberts. Spin of 7.4-Mev state of Li^7—892(A)
—— (see Roberts, J. H.)—905(A)
Solmitz, Frank T. *p-p* scattering for nucleon isobar model—1295(L)
Sorenson, B. M. (see Ames, D. P.)—903(A)
Spedding, F. H. (see Kip, A. F.)—518(L)
Spencer, L. V. (see Goldstein, Herbert)—1150(L)
Spitzer, Lyman, Jr., and Richard Härm. Transport phenomena in completely ionized gas—977
Stanley, C. W. (see Langer, L. M.)—907(A)
Staub, Hans H. (see Nicodemus, David B.)—1288
Steele, Earl L. and James A. Krumhansl. Cellular calculation of band structure for BaO—901(A)
Steffen, Rolf M. Angular momenta of excited states of Pt^{196}—665(L)
—— Effect of chemical binding and phase on angular correlations—903(A)
Stehle, P. (see Page, L. A.)—1273
Stehney, Andrew F. and Nathan Sugarman. Characteristics of Br^{87}, a delayed-neutron activity—194
Stein, Robert P. Electrical fields in Crookes dark space of low pressure glow discharge in air and N_2—134
Steinberger, J. (see Lindenfeld, P.)—531
Stephens, W. E., M. E. Toms, E. E. Carroll, Jr. and G. Rosenblum. Energy distributions of photoprotons from heavy elements—893(A)
Sternheimer, R. M. Density effect for ionization loss in various materials, erratum—1309(L)

—— Energy loss of fast charged particle by Čerenkov radiation—1148(L)
Stout, Virgil L. Luminescence and thermionic emission of BaO—310
Strauch, Karl. Interaction of protons with free and bound neutrons in the 100-Mev region—340(T)
Sugarman, Nathan. Genetics of $Ge^{78}-As^{78}$ fission chain—570
—— (see Schmitt, Roman A.)—1155(L)
—— (see Stehney, Andrew F.)—194
Summerfield, Mary B. Inexpensive, easily controlled process for developing 400-micron nuclear emulsions—340(A)
Swan, J. B., W. M. Portnoy, and R. D. Hill. Isomeric Pt^{193}—907(A)
Swanson, Don R. Interpretation of high energy *p-p* scattering—740
—— Polarization effects in nucleon-nucleon scattering—749
Swanson, Robert E. and Robert H. McFarland. Intensity variations in sensitized fluorescence—911(A)
—— (see McFarland, Robert H.)—911(A)
Swenson, C. A. Blocked capillary method for determining melting pressures: Melting curve of He from 1.5° to 4°K—538
Swim, Richard T. Flow of He II through narrow slits—906(A)
Synge, J. L. Primitive quantization in relativistic two-body problem—467

Talmi, Igal. Evaluation of energy matrix of tensor forces—1065
—— (see Racah, G.)—913(A)
Tannenwald, Peter E. Disintegration of He by 90-Mev neutrons—508
Taschek, R. F. (see Martin, H. C.)—1302(L)
Taylor, Norman L. and T. Smith Taylor. Design and construction of universal test mattress—899(A)
Taylor, T. Smith and L. W. Max. Research on comfort' relaxation, and quality of sleep—899(A)
—— (see Taylor, Norman L.)—899(A)
Teasdale, Tom S. Frozen moments in superconducting sphere—907(A)
Teener, J. W., L. W. Seagondollar, and R. W. Krone. γ-rays from proton bombardment of Na^{23}—892(A)
Telegdi, V. L. (see del Río, C. S.)—909(A)
Temmer, G. M. (see Bloembergen, N.)—883(L)
Thaler, R. M. (see Breit, G.)—1177
Theus, R. (see Scherrer, V. E.)—1268
Thomas, D. A. (see Broyles, C. D.)—715
Thompson, Lewis C. γ-rays produced by inelastic scattering of 14-Mev neutrons—905(A)
Thompson, S. G. (see Hulet, E. K.)—878(L)
—— (see Rasmussen, J. O., Jr.)—33
Thomson, Robb (see Bergmann, Peter G.)—400
Thulin, S. (see Alburger, D. E.)—1146(L)
Ting, Yu and Dudley Williams. Nuclear gyromagnetic ratios—595
Tobin, Ralph (see Birnbaum, Milton)—897(A)
Tollestrup, A. V. (see Walker, R. L.)—1301(L)
Tomita, Kazuhisa. States of solid CH_4 as inferred from nuclear magnetic resonance—429
Tomkins, Frank S. (see Fred, Mark)—318(L)
Tompkins, A. (see Turkevich, A.)—552
Toms, M. E. (see Stephens, W. E.)—893(A)
Torizuka, Yosiharu (see Okamura, Tosihiko)—525(L)
Townes, C. H. (see Sanders, T. M., Jr.)—1158(L)
Townsend, Jonathan. Detection of weak electron paramagnetic resonance—911(T)
——, **S. I. Weissman, and G. E. Pake.** Hfs in paramagnetic resonance of $(SO_3)_2NO^{--}$ ion—606
Trainor, L. E. H. and Ta-You Wu. Symmetry requirements in electron scattering by atom—273
Treiman, S. B. Effect of equatorial ring current on cosmic-ray intensity—130
Triebwasser, Sol, Edward S. Dayhoff, and Willis E. Lamb, Jr. Fine structure of H atom—98
—— (see Dayhoff, Edward S.)—106
Trischka, John W. (see Goldberg, Joshua N.)—278
Trolan, J. K. (see Dyke, W. P.)—799
Tunnicliffe, P. R. Differential and total neutron scattering cross sections of deuteron in energy range 0.1 to 1.0 Mev—1247
Turkevich, A., J. B. Niday, and A. Tompkins. Radiochemical studies on fission of Th^{232} with Li+D neutrons—552
Turkevich, John (see Larach, Simon)—1060
Turner, Thomas J. (see Hall, Harry H.)—340(A)
Tyler, W. W. and A. C. Wilson, Jr. Thermal conductivity, electrical resistivity, and thermoelectric power of graphite—870
Tyren, Helge (see Barkas, Walter H.)—1

Van Allen, J. A. Cosmic-ray intensity above atmosphere near geomagnetic pole—891(T)
van der Ziel, A. Shot noise in semiconductors—900(A)
—— (see Mattson, R. H.)—899(A)
Van Horn, D. D. Diffusion and motion of phase in binary alloys—910(A)
Van Hove, Leon. Occurrence of singularities in elastic frequency distribution of crystal—1189
van Kampen, N. G. *S*-matrix and causality condition. I. Maxwell field—1072
Van Winkle, Q. (see Elson, R.)—320(L)
Varney, Robert N. Drift velocity of ions in O_2, N_2, and CO_2—337(A); 708
Verlet, Loup (see Martin, André)—519(L)
von Krzywoblocki, M. Z. Boundary layer theory—906(A)

Wagner, Frank, Jr., M. S. Freedman, D. W. Engelkemeir, and J. R. Huizenga. Radiations of 6.7-day U^{237}—502
—— (see Freedman, Melvin S.)—302
Wainwright, T. (see Parzen, G.)—901(A)
Walker, J. G. (see Bozorth, R. M.)—624
Walker, R. L., D. C. Oakley, and A. V. Tollestrup. Photoproduction of neutral mesons in H at high energies—1301(L)
Walt, M., R. L. Becker, A. Okazaki, and R. E. Fields. Total fast neutron cross sections of Co, Ga, Se, Cd, Te, Pt, Au, Hg, and Th—1271
—— (see Adair, R. K.)—1165
—— (see Becker, R. L.)—904(A)
Wangsness, Roald K. Antiferromagnetic resonance above Curie temperature—142
—— **and F. Bloch.** Dynamical theory of nuclear induction—728
Waniek, R. W. and Taiichiro Ohtsuka. Angular distribution of particles from stars—1307(L)
—— **and Taiichiro Ohtsuka.** Nuclear stars in emulsions—882(L)
Wanlass, S. D. (see Leighton, R. B.)—148
Wannier, Gregory H. Threshold law for ionization of atoms by electrons—336(A)
Wargo, P. (see Haxby, B. V.)—893(A)
Watkins, G. D. and R. V. Pound. Intensities of nuclear magnetic resonances in cubic crystals—658(L)
Watson, Kenneth M. Multiple scattering and many-body problem—applications to photomeson production in complex nuclei—575
—— Photoproduction and multiple scattering of mesons within atomic nuclei—904(T)
—— (see Francis, Norman C.)—328(L)
Weaver, H. E., Jr. Magnetic moments of Si^{29}, S^{33}, Zn^{67}, As^{75}, Se^{77}, Te^{122}, and Te^{126}—923
Weber, A. H. (see Antal, J. J.)—900(A)

Weddell, J. B. and J. H. Roberts. Angular distribution and differential cross section of $Li^6(n,\alpha)H^3$—891(A)
Wehner, G. and G. Medicus. Sputtering at low ion velocities —339(A)
—— (see Medicus, G.)—339(A)
Weinstock, Bernard, Bernard M. Abraham, and Darrell W. Osborne. Nuclear alignment and entropy of liquid He^3 —787
—— **and John R. Pellam.** Thermal Rayleigh disk measurements in He^3-He^4 mixtures—521(L)
Weissman, S. I. (see Townsend, J.)—606
Welton, T. A. (see Simon, A.)—886(L)
Wentzel, G. Three-nucleon interactions in Yukawa theory —684
Werle, J. Higher order corrections in meson theory of nuclear forces—527(L)
Wessel, Günter (see Lew, Hin)—894(A)
Whalen, J. A., F. T. Porter, and C. S. Cook. High energy negatron spectrum of Sc^{46}—902(A)
Whalen, J. F. (see Coomes, E. A.)—894(A)
Whalin, E. A. and A. O. Hanson. Observation of the $(\gamma,2n)$ reaction in Ta—324(L)
Wheeler, John Archibald (see Hill, David Lawrence)—1102
White, Alan D. (see Lampert, Murray A.)—337(A)
White, David, O. D. Gonzales, and H. L. Johnson. Heat conduction of boundary layer in liquid He II—593
Whitesell, W. J. (see Johnson, V. A.)—941
Whiting, F. B. (see Aldrich, L. T.)—631
Wilkins, J. Ernest, Jr. (see Goldstein, Herbert)—1150(L)
Wilkinson, D. H. (see Carver, J. H.)—658(L)
Wilkinson, M. K. (see Gingrich, N. S.)—910(A)
Wilkinson, Roger G. (see Roggenkamp, Paul L.)—903(A)
Willard, H. B. (see Kington, J. D.)—530(L)
Williams, Corre and Herbert D. Schwetman. Analysis of bridged-T network by Laplace transformations—899(A)
Williams, Dudley (see Ting, Yu)—595
Williams, H. Bartel and Albert J. Hatch. Confirmatory measurements in high frequency secondary electron resonance discharge mechanism—339(A)
—— (see Hatch, Albert J.)—339(A)
Williams, R. W. New particles in cosmic rays—340(T)
Wilson, A. C., Jr. (see Tyler, W. W.)—870
Wilson, C. W. III and G. E. Pake. Nuclear magnetic relaxation in polytetrafluoro-ethylene and polyethylene—896(A)
Wilson, H. W. and Walter H. Barkas. Text of charge symmetry hypothesis: Positive to negative pion production ratio obtained in bombarding C with α-particles and protons—758
Winans, J. G. Possible inconsistency in customary use of vectors—914(A)
Winston, Harvey. Comparison of Slater's and Peckar's treatments of perturbed periodic potentials—317(L)
Winther, Aage (see Kofoed-Hansen, O.)—526(L)
Witmer, Enos E. Excited energy levels of nuclei as rational multiples of electron mass—905(A)
Wittels, M. Lattice expansion of quartz due to fast neutron bombardment— 656(L)
Witten, Louis. Ionizing and heating plasma—335(A)
Wood, D. E. (see Roberts, J. H.)—905(A)
Woodhouse, R. L. Effect of weak magnetic field on constricted arc in fluorescent lamp—342(A)
Worley, R. Edwin. Third Ryberg series of N_2—864
Wright, Byron T. Spectrometer measurement on high energy positrons of Na^{22}—902(A)
Wu, Ta-You. Spectrum of discrete eigenvalues in negative atomic ion—629
—— (see Trainor, L. E. H.)—273
Wyckoff, H. O. (see Motz, J. W.)—968
Wyly, L. D. and A. Zucker. Activities in light nuclei from nitrogen ion bombardment—524(L)

Zaffarano, D. J. (see Mize, J. P.)—902(A)
Zissis, G. J. (see Deverall, G. V.)—895(A)
Zucker, A. (see Wyly, L. D.)—524(L)
Zucker, E. R. (see Mandeville, C. E.)—559

Author Index to Volume 90

References with (A) are to abstracts of papers presented at meetings of the American Physical Society, and those with (T) designate title only; references with (L) are to Letters to the Editor; references to (E) are to Errata.

Aarons, M. W., J. Ashkin, F. Feiner, J. G. Gorman, and L. Smith. Nuclear cross sections of negative and positive pions—342(A)

Abe, Hidetaro and Junji Shimada. Anomalous magnetic resonance absorption of Cu acetate at 40 kMc/sec—317(L)

Abragam, A. Indirect interaction between nuclear spins in Cu acetate—358(A)

—— (see Kambe, K.)—348(A)

—— (see Pound, R. V.)—993(L)

Abraham, Bernard M., Darrell W. Osborne, and Bernard Weinstock. Nuclear alignment and entropy of liquid He^3—347(A)

Abrahams, Elihu (see Kittel, C.)—238

Acquista, N. (see Mann, D. E.)—359(A)

Adel, Arthur. Absorption line-width in infrared spectrum of atmospheric CO_2—1024

Ahrens, Tino. Pseudoscalar interaction in theory of β-decay—974

Akeley, E. S. (see Jacobs, Ira)—386(A)

Albers-Schönberg, H., F. Hänni, E. Heer, T. B. Novey, and P. Scherrer. Effect of electric quadrupole interaction on γ-γ directional correlation in Cd^{111}—322(L)

Albrecht, H. O. (see Mandeville, C. E.)—25; 364(A); 992(L)

Alford, W. L. and R. B. Leighton. Mean lifetimes of V-particles and heavy mesons—622

Allen, H. C., Jr. (see Meal, H. C.)—348(A)

Allison, Samuel K. and Harvey Casson. Scintillation response from NaI(Tl) crystals under bombardment with 60–600 kev positive ions—354(A); 880

Allred, J. C. (see Armstrong, A. H.)—340(A)

Alperovitch, E. (see Lidofsky, L.)—387(A)

Amdur, I. and W. T. Lindsay. Scattering of fast N_2 molecules by N_2—344(A)

Anderson, Carl E., George W. Wheeler, and W. W. Watson. Inner bremsstrahlung associated with K-capture in A^{37}—606

Anderson, E. C. (see Cowan, C. L., Jr.)—493(L)

Anderson, J. M. (see Goldstein, L.)—151(L); 486(L)

Anderson, James L. Use of functionals in evaluating S matrix—373(A)

Angell, C. E. and J. P. Perry. Total cross sections of 37-Mev pions in H—724(L)

Antonoff, George. Methods for advancing subject of liquid—385(A)

—— (see Madrazo, Raymond, Jr.)—385(A)

Appleton, G. L. (see Halpern, O.)—869

Arase, E., Gerson Goldhaber, and S. Goldhaber. Elastic pion-deuteron scattering—160(L)

—— (see Goldhaber, S.)—344(A)

Arfken, G. B. (see Guernsey, R. L.)—1132(A)

Armstrong, A. H., J. C. Allred, and L. Rosen. Interaction of 14-Mev neutrons with protons and deuterons—340(A)

Arnold, James R. and Thomas Sugihara. Decay scheme of natural Lu^{176}—332(L)

Artman, J. O. and J. P. Gordon. Pressure broadening of O_2 lines in mm wavelength region—338(A)

Ascoli, Giulio. Mass of cosmic-ray mesons at mountain altitudes—1079

Ashkin, J. (see Aarons, M. W.)—342(A)

Auluck, F. C. and D. S. Kothari. Fermi's theory of nucleon collisions and zero-point energy of pions—1002(L)

Austern, N. and S. T. Butler. Coulomb effects in deuteron stripping—365(A)

Baerg, A. P. Neutron capture cross section of Em^{239}—1121(L)

Bainbridge, Kenneth T., M. Goldhaber, and Elizabeth Wilson. Influence of chemical state on lifetime of nuclear isomer, Tc^{99m}—430

—— (see Kraushaar, J. J.)—610

Bair, J. K., J. D. Kington, and H. B. Willard. N^{14} level structure from $C^{13}(p,n)N^{13}$—575

—— (see Willard, H. B.)—865

Ballam, J., D. R. Harris, A. L. Hodson, R. Ronald Rau, G. T. Reynolds, and Marcello Vidale. Magnetic field cloud chamber for studying nuclear interactions in cosmic radiation. I. Equipment—369(A)

—— (see Rau, R. Ronald)—369(A)

Ballard, Stanley S. and Kathryn A. McCarthy. Thermal conductivity values for $BaTiO_3$—375(A)

Bame, S. J., Jr. (see Perry, J. E., Jr.)—380(A)

Band, William and Raymond A. Nelson. Cluster theory of saturated vapor pressure of He isotope mixtures—744

Barbour, Ian. Z-dependence of cross section and energy in cosmic-ray stars—361(A)

Barker, W. A. and Z. V. Chraplyvy. Conversion of amplified Dirac equation to approximately relativistic form, erratum—1131(E)

Barnes, R. G. (see Harrick, N. J.)—260

Barnett, C. F. (see Evans, G. E.)—825

Barnett, S. J. Gyromagnetic ratios of microcrystalline and macrocrystalline materials—315(L)

Barschall, H. H. (see Walt, M.)—714(L)

Bartell, L. S. and L. O. Brockway. Investigation of electron distribution in atoms by electron diffraction—833

Bartholomew, G. A. and B. B. Kinsey. γ-rays produced by neutron capture in Cd^{113}—355(A)

Bay, Z., V. P. Henri, and F. McLernon. Lifetimes of excited states of Ni^{60}—371(A)

—— (see Kanner, H.)—371(A)

Beach, E. H. (see King, J. S.)—381(A)

Becker, Robert A. (see Bendel, W. L.)—888

—— (see Brown, Hugh N.)—323(L)

Beers, Y. (see Weisbaum, S.)—338(A)

Beghian, L. E., H. H. Halban, T. Husain, and L. G. Sanders. Energy levels of C^{13} from $Be^9(\alpha,n)C^{13}$—1129(L)

—— (see Hicks, D.)—163(L)

Bekefi, G. Diffraction of electromagnetic waves by aperture in infinite screen—385(A)

Belinfante, F. J. and J. C. Swihart. Special-relativistic linear theory of gravitation—357(A)

Bell, George I. Capture and loss of electrons by fission fragments—548

Bell, R. E. and R. L. Graham. Time distribution of positron annihilation in liquids and solids—644

Bendel, W. L., F. J. Shore, H. N. Brown, and R. A. Becker. Disintegration of 24-min Ag^{108}—888

Benenson, R. E. Energy levels in N^{14} and C^{14} from deuteron bombardment of C^{13}—420

Bennett, Clarence and Victor H. Coffin. Molar refraction of CO_2 as function of density and age of gas—344(A)

Bennett, Willard H. Magnetically self-focusing discharges—387(A)

Bergmann, Otto. Conservation laws in classical electrodynamics—315(L)

Bergmann, Peter G. Self-consistency of Lagrangian quantization—357(A)

—— (see Thomson, Robb M.)—357(A)

Berko, Stephen and Frank L. Hereford. Deflection of high energy electrons in magnetized Fe—341(A)
Berman, Arthur I. Total Compton and pair production cross sections at 19.5 Mev—210
Bernardini, G., R. Reitz, and E. Segrè. Photomesonic fission of Bi—573
Bernstein, W. (see Chase, R. L.)—353(A)
—— (see Schardt, A. W.)—353(A)
Bethe, H. A. Sign of phase shifts in meson-nucleon scattering—994(L)
—— **and F. J. Dyson.** Asymptotic behavior and differential equation of meson wave function—372(A)
Bever, R. S. (see Sproull, R. L.)—352(A)
Beyster, J. R. (see Carter, R. E.)—389(A)
Bichsel, H. and R. F. Mozley. Range of protons in Al—354(A)
—— (see Mozley, R. F.)—354(A)
Biedenharn, L. C. and John M. Blatt. Variational principle for n-p scattering with tensor forces—365(A)
Biondi, Manfred A. Processes involving ions and metastable atoms in Hg afterglows—730
Birks, J. B. Response of organic scintillation crystals to short-range particles, erratum—1131(E)
Bitter, Francis. Magneto-resonance and magnetic optics—358(T)
Bjornerud, E. K. (see York, C. M.)—167(L)
Black, Clayton F. Angular distributions of (d,p) reactions—381(A)
Blair, J. S. and G. F. Chew. Fourth order corrections to scattering of pions by non-relativistic nucleons—1065
Blatt, John M., A. K. Stebbins, and D. J. Tendam. (α,n) and $(\alpha 2n)$ cross sections of Ag^{109}—460
—— (see Biedenharn, L. C.)—365(A)
Bleuler, E., J. W. Blue, S. A. Chowdary, A. C. Johnson, and D. J. Tendam. Isomerism of In^{110} and In^{112}—464
Blewett, J. P. Accelerators incorporating alternating-gradient focusing—347(T)
Bloom, A. L. and J. N. Shoolery. High resolution of nuclear resonance signals in flowing samples—358(A)
Bloom, Stanley. Spectral line broadening by electrons—382(A)
—— **and Henry Margenau.** Quantum theory of spectral line broadening—791
Blue, J. W. (see Bleuler, E.)—464
Bockelman, C. K., C. P. Browne, A. Sperduto, and W. W. Buechner. Inelastic scattering of protons and deuterons from B^{10}—340(A)
—— (see Browne, C. P.)—340(A)
Bodansky, D., A. Sachs, and J. Steinberger. Differential cross sections for scattering of 58-Mev π^+ mesons in H—996(L)
——, **A. M. Sachs, and J. Steinberger.** Phase-shift analysis of scattering of positive mesons at 58 Mev—997(L)
Boehm, F., D. C. Peaslee, and V. Perez-Mendez. Search for 1-Mev γ from N^{16} decay—1119(L)
—— **and C. S. Wu.** Inner bremsstrahlung and ionization of atom accompanying β-decay—369(A)
—— (see Wu, C. S.)—388(A)
Bohr, Aage and Ben R. Mottelson. Rotational states in even-even nuclei—717(L)
Boley, F. I. and D. S. Dunavan. Radioactive decay of Y^{91}—158(L)
Boorse, H. A. (see Smith, B.)—156(L)
Booth, E. C. (see Rasetti, F.)—388(A)
Borowitz, Sidney (see Boyet, Howard)—341(A)
—— (see Mostov, Philip M.)—376(A)
Borst, L. B. Resonance scattering in In—354(A); 859
Bortner, T. E. and G. S. Hurst. Energy per ion pair for 5-Mev α-particles in He—160(L)
Bots, G. J. C. and C. J. Gorter. Fountain effect in He II below 1°K—1117(L)
Boyd, A. W. (see MacKenzie, D. R.)—327(L)
Boyet, Howard and Sidney Borowitz. Scattering of electrons by H atoms—341(A)
Braams, R. and C. L. Smith. Photoneutron reaction in Ca^{40}—995(L)
Bracci, A., U. Facchini, and A. Malvicini. Spectrum of γ-radiation emitted in reaction $n+p \rightarrow d+\gamma$—162(L)
Braid, T. H. Measurements of neutron capture γ-rays with scintillation spectrometer—355(A)
Bramson, H. J. (see Seifert, A. M.)—349(A)
Branin, Franklin H., Jr. Bi-directional electronic counter for use in optical interferometry—345(A)
Brattain, W. H. (see Portis, A. M.)—988(L)
Braunstein, R. and J. W. Trischka. Nuclear-molecular interactions of Li^7F^{19}—348(A)
Bray, P. J. (see Harrick, N. J.)—260
Breckenridge, R. G. Semiconducting intermetallic compounds—488(L)
Breit, G. (see Gluckstern, R. L.)—1026
Brentano, J. C. M. and T. L. Thourson. X-ray investigation on effect of mechanical surface treatment on lattice regularity of quartz and calcite—351(A)
Brice, M. K. (see Cork, J. M.)—444; 579
Bridge, H. S., C. Peyrou, B. Rossi, and R. Safford. Cloud chamber observations of heavy charged unstable particles in cosmic rays—921
—— (see Peyrou, C.)—368(A)
—— (see Safford, R.)—369(A)
Bridgman, P. W. Recent results at high pressures—367(T)
Brockman, F. G. (see Corliss, L. M.)—1013
Brockway, L. O. (see Bartell, L. S.)—833
Broder, Jacob (see Keck, Paul H.)—521
Brolley, J. E., Jr. (see Dickinson, W. C.)—388(A)
Bronzo, Joseph (see Truell, Rohn)—152(L)
Brooks, Harvey. Diffusion of injected carriers in semiconductor of mixed conductivity type—336(A)
—— (see Ham, Frank)—383(A)
Brosi, A. R. (see Ketelle, B. H.)—567
Brower, D. (see Hinman, G.)—370(A)
Brown, Harry B. and Robert Stump. Continuous γ-radiation accompanying internal conversion in Ba^{137m}—1061
Brown, Hugh N. and Robert A. Becker. Excitation of 16-μsec state in Ta^{181} by capture of bremsstrahlung—328(L)
—— (see Bendel, W. L.)—888
Brown, L. Carlton (see Manring, Edward)—348(A)
—— (see Schwarz, Guenter)—351(A)
Brown, Laurie M. Grain density in nuclear emulsions—95
Brown, N. L. (see Cole, R. H.)—352(A)
Brown, Sanborn C. (see Goldey, James M.)—336(A)
Brown, W. L., R. C. Fletcher, and S. Machlup. Annealing of bombardment damage in solids—709(L)
—— **and W. Shockley.** n-type conduction on p-type Ge surfaces—336(A)
Browne, C. P., C. K. Bockelman, W. W. Buechner, and A. Sperduto. Inelastic scattering of protons and deuterons from N^{14} and Li^6—340(A)
—— (see Bockelman, C. K.)—340(A)
Brownell, L. E. (see Meinke, W. W.)—353(A)
Brueckner, K. A. Damping of virtual nucleon-pair formation in pseudoscalar meson theory—476
—— Elastic scattering of pions in D—715(L)
—— **and K. M. Watson.** Construction of potentials in quantum field theory—699
Brysk, Henry. Extreme single-particle model and β-decay—365(A)
Bube, Richard H. Electronic transitions in luminescence of ZnS phosphors—70

Buechner, W. W. (see Bockelman, C. K.)—340(A)
—— (see Browne, C. P.)—340(A)
Bunbury, D. StP. β-decay of Li^8—1121(L)
Burgess, R. E., H. Kroemer, and J. M. Houston. Corrected values of Fowler-Nordheim field emission functions $v(y)$ and $s(y)$—515
Burke, B. F. and M. W. P. Strandberg. Zeeman effect in rotational spectra of asymmetric-rotor molecules—303; 338(A)
Burson, S. B. (see Jordan, W. C.)—862
Buskirk, A. V., H. O. Cohn, L. R. Etter, C. J. Karzmark, R. H. Rediker, and R. W. Thompson. New magnet chamber for study of V particles—369(A)
—— (see Thompson, R. W.)—329(L)
Butler, S. T. (see Austern, N.)—365(A)
Byfield, H. (see Kessler, J.)—343(A)
—— (see Lederman, L.)—344(A)

Calhoun, B. A. Electrical conductivity of magnetite at low temperatures—374(A)
Callen, Herbert B. (see Offenbacher, Elmer L.)—401
Cameron, John R. Elastic scattering of α-particles by oxygen—839
Carlson, B. C. (see Rohrlich, F.)—378(A)
Carr, E. F. and R. D. Spence. Influence of magnetic field on microwave dielectric constant of liquid crystal—339(A)
Carr, W. J., Jr. Spin-dependent couplings in many electron system—383(A)
Carter, D. E. and M. P. Givens. Soft x-ray absorption of Fe and Fe_2O_3—379(A)
Carter, R. E. and J. R. Beyster. Inelastic collision cross sections for fission spectrum neutrons—389(A)
Caspar, D. L. and C. R. Woese. Inactivation of dysentery toxin with ionizing radiation—384(A)
Casson, Harvey (see Allison, Samuel K.)—354(A); 880
Caswell, R. S. (see Nelson, C. M.)—364(A)
Cavallo, L. (see Seliger, H. H.)—443
Chamberlain, Joseph W. and Norman J. Oliver. OH in airglow at high latitudes—1118(L)
Champion, K. S. W. Constriction of high power discharges by intense magnetic field—387(A)
Chang, C. H., C. S. Cook, and H. Primakoff. Transmission of electrons through thin metallic foils—544
Chang, W. Y., W. Bernstein, and A. W. Schardt. Versatile coincidence gray wedge pulse-height analyzer—353(A)
—— (see Grodzins, L.)—361(A)
—— (see Schardt, A. W.)—353(A)
Cheka, J. S. Fast neutron film dosimeter—353(A)
Ch'en, Shang-Yi and Donald A. Kohler. Broadening and shift of second doublet of Rb absorption series under different pressures of A and He—1019
Cheng, L. S. and M. L. Pool. Disintegration of Sc^{47}—886
Chew, G. F. (see Blair, J. S.)—1065
Chisholm, R. and B. Touschek. Spin orbit coupling and mesonic Lamb shift—763
Chou, C. N. Energy spectra of cosmic ray photons and electrons from plastic scintillation counter measurements—473
Chowdary, S. A. (see Bleuler, E.)—464
Chrapylvy, Z. V. (see Barker, W. A.)—1131(E)
Chu, Sheng To (see Tifford, Arthur N.)—377(A)
Clapp, Roger E. Elementary particle structure—356(A)
Clark, G. L. (see Goldstein, L.)—151(L); 486(L)
Clark, G. W. Scintillation counter measurements of absorption of N-component—368(A)
Clarke, R. L. (see Paul, E. B.)—381(A)
Clauser, F. H. Turbulent boundary layers having equilibrium velocity profiles in adverse pressure gradients—379(T)
Coffin, Victor (see Bennett, Clarence)—344(A)
Cohen, B. L., E. Newman, T. H. Handley, and A. Timnick. Angular distribution of deuterons from $Be^9(p,d)Be^9$—328(L)
—— (see Neidigh, R. V.)—340(A)
Cohen, M. H. Nuclear quadrupole coupling in solids—348(A)
Cohn, H. O. (see Buskirk, A. V.)—369(A)
Cole, R. H., R. W. Swenson, and N. L. Brown. Dielectric constants of solid HCl and HBr—352(A)
Coleman, E. W. (see Meinke, W. W.)—353(A)
Coleman, John W. Electron gun—386(A)
Colladay, G. S. (see Juenker, D. W.)—772
Collins, S. C. and F. J. Zimmerman. Cyclic adiabatic demagnetization—991(L)
Colton, E. T. (see Lees, S.)—346(A)
Conklin, G. L. (see Zucker, E. R.)—387(A)
Conwell, E. M. High field mobility in Ge with impurity scattering dominant—769
Cook, C. Sharp and Fred T. Porter. $Zn^{64}(d,\alpha n)Cu^{65}$—429
—— (see Chang, C. H.)—544
Cook, L. G. and K. D. Shafer. Neutron activation of Ca^{48}—1121(L)
Cook, W. R., Jr., and Hans Jaffe. Ferro-electricity in oxides of fluorite structure—375(A)
Coomes, E. A. (see Juenker, D. W.)—772
Cooper, D. I., D. H. Frisch, and R. L. Zimmerman. p-p scattering in interference minimum region—339(A)
—— (see Zimmerman, R. L.)—339(A)
Cooper, John N. (see Green, Donald W.)—1132(A)
Corey, H. E. (see Vogel, F. L.)—489(L)
Cork, Bruce, p-p scattering at 32.0 Mev—1129(L)
Cork, J. M., J. M. LeBlanc, D. W. Martin, W. H. Nester, and M. K. Brice. Nuclear levels associated with Zr^{95} and Nb^{95}—579
——, **J. M. LeBlanc, W. H. Nester, D. W. Martin, and M. K. Brice.** Radioactive decay of Cs^{134}, Os^{185}, Os^{191}, and Os^{193}—444
—— (see Jordan, W. C.)—862
Corliss, L. M., J. M. Hastings, and F. G. Brockman. Neutron diffraction study of $MgFe_2O_4$—1013
Corrsin, S. Propagation of turbulence into irrotational flow ——376(A)
Corson, Dale R. Radiation by electrons in large orbits—748
Coryell, Charles D. (see Richter, Harold G.)—389(A)
Coté, R. E. and P. Kusch. Low frequency resonances in spectra of diatomic molecules—103
Cowan, C. L., Jr., F. Reines, F. B. Harrison, E. C. Anderson, and F. N. Hayes. Large liquid scintillation detectors—493(L)
—— (see Reines, F.)—492(L)
Cowen, J. A. and R. D. Spence. Temperature dependence of ferromagnetic resonance in (Ni-Fe) alloy—359(A)
Crandall, W. E. (see Schecter, L.)—633
Crasemann, Bernd. Decay of Ga^{64} and Ga^{65}—995(L)
—— **and Harry T. Easterday.** Decay of Cr^{49}—1124(L)
Cronemeyer, D. C. (see Rank, D. H.)—202
Crosbie, Edwin A. Relative energy levels of P-shell nuclei in intermediate coupling—138
Crouch, M. F. and D. E. Diller. Method for absolute neutron source calibration—361(A)
Crussard, J., L. Leprince-Ringuet, D. Morellet, A. Orkin-Lecourtois, and J. Trembley. K-mesons—1127(L)
Culpepper, S. V. (see Seliger, H. H.)—443
Curie, Daniel. Mechanism of phosphorescence in crystal phosphors—154(L)
Cutler, M. Effect of surface states in diode rectification theory—337(A)

Dacey, G. C. Space-charge limited hole current in Ge—759
Dailey, B. P. Rotational spectrum and molecular structure of $C_3H_2Cl^{35}$—337(A)
Damm, C. C. (see Smith, Lincoln G.)—324(L)
Damon, P. E. and R. R. Edwards. Electromagnetic spectrum of RaD—280
Darlington, Lillian E., Jack Haugsnes, Harry M. Mann, and James H. Roberts. Angular distribution of $Li^6(n,\alpha)H^3$ for neutrons of 200, 270, 400, and 600 kev—1049
Dash, William C. Additive coloration of single crystals of BaO—352(A)
Daubin, Scott M. (see Pipkin, Francis M.)—353(A)
Daunt, J. G. (see Horowitz, M.)—379(A)
Davis, Marguerite. Biological determination of range of low voltage electrons—384(A)
deBretteville, A., Jr. (see Lefker, R.)—345(A)
Dehmelt, H. G. Nuclear quadrupole resonance—348(T)
Déjardin, G., J. Janin, and M. Peyron. Vibration-rotation band system of OH in near infrared—359(A)
Del Castillo, G. (see Grodzins, L.)—361(A)
del Rio, C. S. and Valentine L. Telegdi. Inelastic nuclear scattering of photons by Rh^{103}—439
Dempster, J. R. Hugh. Calculations on μ-meson capture in nuclei—349(A)
der Mateosian, E. and Luke C. L. Yuan. Surface effect of NaI scintillators—868
Deser, Stanley and Paul C. Martin. Covariant meson-nucleon equation—1075
de-Shalit, A. Effects of departure from single particle model on nuclear magnetic moments—83
Deutsch, R. W. Secondary particles resulting from 375-Mev α-bombardment of nuclei—499(L)
DeWitt, Bryce S. Pair production by curved metric—357(A)
Dexter, D. L. Small angle scattering of x-rays from cold-worked solids—1007
Dicke, R. H. Excitation of superradiant states: New technique for high resolution microwave spectroscopy—337(T)
Dickinson, W. C. and J. E. Brolley, Jr. Angular distribution of fragments from neutron-induced fission—388(A)
Dieterich, Ernest J. Excitation of light by H ions—386(A)
Diller, D. E. (see Crouch, M. F.)—361(A)
Dodd, J. S. (see Lefker, R.)—345(A)
Draper, J. E. and B. D. McDaniel. Pulsed source of fast neutrons—362(A)
Drell, S. D. (see King, William C.)—326(L)
Dudziak, Walter F. π^+ meson production cross sections from C by 341-Mev protons—342(A)
Duller, N. M. (see Walker, W. D.)—320(L)
DuMond, Jesse W. M. (see Hoyt, Harry C.)—169(L)
Dunavan, D. S. (see Boley, F. I.)—158(L)
Dunlap, W. C., Jr. (see Saby, John S.)—630; 1131(E)
Dutta, Ajit Kumar. Electrical conductivity of single crystals of graphite—187
Dutton, David and Robert Maurer. Color centers and trapped charge in KCl and KBr—126
Dvorak, H. R. and R. N. Little, Jr. Total cross sections of Cl, Na, Ti, and Br for fast neutrons—618
Dyson, Freeman J. Use of Tamm-Dancoff method in field theory—994(L)
——, **S. S. Schweber, and W. M. Visscher.** Theoretical analysis of meson-proton scattering—372(A)
—— (see Bethe, H. A.)—372(A)
—— (see Mitra, A. N.)—372(A)

Easterday, Harry T. (see Crasemann, Bernd)—1124(L)
Edwards, R. R. (See Damon, P. E.)—280
Edwards, S. F. Non-perturbation approach to quantum electrodynamics—284
Elson, R., P. A. Sellers, and E. R. John. Thermal neutron capture cross sections of Pa^{231} and Pa^{233}—102
Emrich, R. J., J. E. Mack, and R. A. Shunk. Variation with time of flow variables in shock tube—375(A)
Engelder, Theodore C. Search for short-lived nuclear isomers—259
Engelkemeir, D. W., P. R. Fields, and J. R. Huizenga. Radiations of Pu^{243}—6
Erickson, R. A. Neutron diffraction studies of antiferromagnetism in MnF_2 and some isomorphous compounds—779
Eschenfelder, A. H. and R. T. Weidner. Saturation effects in paramagnetic resonance absorption and spin-lattice relaxation time—358(A)
Eshelby, J. D. Equation of motion of a dislocation—248
Etter, L. R. (see Buskirk, A. V.)—369(A)
—— (see Thompson, R. W.)—329(L); 1122(L)
Evans, G. E., P. M. Stier, and C. F. Barnett. Stopping of heavy ions in gases—825
Evett, Arthur A. and Henry Margenau. Forces between H_2 molecules—1021

Facchini, U. (see Bracci, A.)—162(L)
Fagot, W. C. (see Simpson, J. A.)—1068
Fairbank, Henry A. (see King, J. C.)—347(A); 989(L)
Fano, U. Geometrical characterization of nuclear states and theory of angular correlations—577
Farnsworth, H. E. (see Schlier, Robert E.)—351(A)
Faust, W. R., V. E. Scherrer, and R. B. Theus. γ-radiation from interaction of 14-Mev neutrons with matter—355(A)
Feiner, F. (see Aarons, M. W.)—342(A)
Feld, B. T. Analysis of photomeson production data—342(A)
—— (see Wattenberg, A.)—380(A)
Ferguson, R. C. and E. B. Wilson, Jr. Microwave spectrum and structure of SOF_2—338(A)
Feshbach, Herman, Charles E. Porter, and Victor F. Weisskopf. Formation of compound nucleus in neutron reactions—166(L)
Feynman, R. P. λ-transition in liquid He—1116(L)
Fields, P. R. (see Engelkemeir, D. W.)—6
Findley, D. E. (see Worthington, H. R.)—899
Fiora, Verna C. (see Turner, T. E.)—338(A)
Fleming, W. H. and H. G. Thode. A^{36} in pitchblende minerals and nuclear processes in nature—857
Fletcher, R. C. (see Brown, W. L.)—709(L)
Flint, H. T. and E. Marjorie Williamson. Coordinate operators and fundamental lengths—318(L)
Fonger, W. (see Simpson, J. A.)—934
Foote, H. L., Jr., V. L. Sailor, and H. H. Landon. Low energy neutron resonance cross sections for Ho, Er, Lu, and Tm—362(A)
—— (see Landon, H. H.)—363(A)
Forbes, Stuart G. Activation cross sections for 14-Mev neutrons, erratum—1131(E)
Ford, Kenneth W. First excited states of even-even nuclei—29; 366(A)
—— (see Wilets, L.)—366(A)
Forsthoff, C. W., R. H. Goeckermann, and R. A. Naumann. Formation and decay of Mo^{99m}—1004(L)
Foss, Martyn H. Rotating condenser for synchrocyclotron oscillator—353(A)
Foster, Bruce P. (see May, John E.)—243; 370(A)
Fowler, W. B., R. P. Shutt, A. M. Thorndike, and W. L. Whittemore. Observation of V^0 particles produced at cosmotron—1126(L)
Fox, J. G. (see Grove, D. J.)—378(A)
—— (see Mott, W. E.)—712(L)
Fox, R. E. (see Hickam, W. M.)—386(A)
—— (see Kjeldaas, T., Jr.)—386(A)

Frankl, D. R. and T. A. Read. Internal friction of rocksalt single crystals—351(A)
Franklin, R., M. Friedman, and R. Setlow. Ultraviolet action spectrum of bacillus megatherium bacteriophage—384(A)
Fraser, J. S. and J. C. D. Milton. Distribution of prompt neutron emission probability for fission fragments of U^{233}—389(A)
—— (see Milton, J. C. D.)—388(A)
Friedman, M. and E. Pollard. Ionizing radiation evidence for internal structure in bacterial virus—384(A)
—— (see Franklin, R.)—384(A)
Frisch, David H. *S*-wave two-body interaction in nuclei—367(A)
—— (see Cooper, D. I.)—339(A)
—— (see Storrs, C. L.)—339(A)
—— (see Zimmerman, R. L.)—339(A)
Fry, W. F. Evidence for emission of neutrino following nuclear capture of μ-meson—999(L)
—— **and George R. White.** Range distribution of μ-mesons from π-meson decay in photographic emulsions—207
—— (see White, George R.)—349(A)
Frye, G. M. and L. Rosen. Angular distribution and energy spectrum of charged particles produced by 14-Mev neutrons on Li^6 and Li^7—381(A)
Fumi, F. G. and L. Wolfenstein. Allowed final states for annihilation into 3 photons—498(L)
Furuichi, Jiro (see Mitsui, Toshito)—193

Garwin, R. L. Search for V^0 particles produced by 450-Mev protons—274
Geller, M. (see von Hippel, A.)—364(A)
Geltman, Sydney. Mobility of He molecular ions in He—808
Gerjuoy, E. (see Saxon, David S.)—373(A)
Ghiorso, Albert (see Hyde, Earl K.)—267
Gilleo, M. A. Photoemission from Ag into AgCl, KBr, NaCl, and new bands of photosensitivity in AgCl—364(A)
Ginther, Robert J. (see Schulman, James H.)—351(A)
Givens, M. P. (see Carter, D. E.)—379(A)
Glass, Neel W., Louis K. Jensen, and J. Reginald Richardson. Short-lived radioisotopes P^{32} and Cl^{37}—320(L)
Glasser, R. G. and Marcel Schein. Energy of nucleon-nucleon collisions—218
Glaubman, Michael J. Spins and parities of excited states in even-even nuclei—1000(L)
Glazer, Herbert and Howard Reiss. Application of Fermi-Thomas model in computing dipole moment of ICl—360(A)
Gluckstern, R. L. and M. H. Hull, Jr. Polarization dependence of integrated bremsstrahlung cross section—1030
——, **M. H. Hull, Jr., and G. Breit.** Polarization of bremsstrahlung radiation—1026
Godbole, R. D. (see Wattenberg, A.)—380(A)
Goeckermann, R. H. (see Forsthoff, C. W.)—1004(L)
Goldberg, Joshua N. Gravitational radiation—356(A)
Goldberg, M. D. (see Hughes, D. J.)—497(L)
Goldemberg, J. and L. Katz. High energy γ-γ cross section of In^{115}—308
Goldey, James M. and Sanborn C. Brown. Microwave determination of electrical properties of Ge—336(A)
Goldhaber, Gerson and Leon Lederman. Positive pion scattering in H—343(A)
—— (see Arase, E.)—160(L)
—— (see Goldhaber, S.)—344(A)
Goldhaber, M. Families of fundamental particles—369(A)
—— (see Bainbridge, Kenneth T.)—430
Goldhaber, S., E. Arase, and Gerson Goldhaber. Elastic pion-deuteron scattering—344(A)
—— (see Arase, E.)—160(L)
Goldman, J. E. Theory of resistance minimum in metals—379(A)
Goldschmidt-Clermont, Y., L. S. Osborne, and M. B. Scott. Photoproduction of neutral mesons in H—350(A)
Goldstein, J. S. (see Salpeter, E. E.)—983
Goldstein, L., J. M. Anderson, and G. L. Clark. Interaction of microwaves propagated through gaseous discharge plasma—151(L)
——, **J. M. Anderson, and G. L. Clark.** Quenching of afterglow in gaseous discharge plasmas by low power microwaves—486(L)
Goldwasser, E. L., F. E. Mills, and T. R. Robillard. Direct measurement of effect of polarization on energy losses of fast electrons—378(A)
Good, R. H., Jr. Generalization of WKB method to radial wave equations—131
Goodman, Clark (see Kiehn, R. M.)—362(A)
Gordon, J. P. (see Artman, J. O.)—338(A)
Gordon, W. L. and J. A. Soules. Ross filter design for x-ray scattering experiments—346(A)
Gordy, Walter (see King, William C.)—319(L)
Gorman, J. G. (see Aarons, M. W.)—342(A)
Gorter, C. J. (see Bots, G. J. C.)—1117(L)
—— (see Kramers, H. C.)—1117(L)
Gorter, E. W. and J. A. Schulkes. Reversal of spontaneous magnetization as function of temperature in LiFeCr spinels—487(L)
Gove, H. E. p-γ angular correlations in $C^{12}(p,p'\gamma)$—370(A)
Grad, Harold (see Mostov, Philip M.)—376(A)
Graham, R. L. (see Bell, R. E.)—644
Grant, F. A. and A. D. Krumbein. Effect of temperature on duration of $^3P_2$ metastable level of Ne—59
Green, Donald W., J. C. Harris, and John N. Cooper. Method for measuring the half-lives of positron emitters—1132(A)
Green, G. K. Brookhaven cosmotron—347(T)
Green, H. S. Generalized method of field quantization—270
Green, J. B. and R. A. Loring. Zeeman effect in spectra of Te—80
Green, Melville S. Statistical mechanics of irreversible processes in fluids—376(A)
Green, Thomas A. Elastic scattering of π-mesons by deuterons—161(L)
Green, W. D. (see Lees, S.)—346(A)
Greenwald, Selma (see McGuire, T. R.)—373(A)
Greisen, K. and W. D. Walker. Ratio of neutral to charged particles in nuclear interacting component of cosmic rays—915
Grodzins, L., G. Del Castillo, and W. Y. Chang. Two-particle showers from Be—361(A)
Gross, E. P. (see von Hippel, A.)—364(A)
Grove, D. J. and J. G. Fox. e/m for 385-Mev protons—378(A)
Guernsey, R. L. and G. B. Arfken. Vector addition coefficient identity—1132(A)
Gunst, S. B. (see Page, L. A.)—377(A)
Gurney, I. D. C. Lattice sums: Validity of Evjen's method—316(L)

Haber, Agnes (see Sugarman, Nathan)—342(A)
Hahn, E. L. Spin-echo pulse technique in nuclear resonance studies—348(T)
Halban, H. H. (see Beghian, L. E.)—1129(L)
Hall, G. G. Electronic structure of diamond—316(L)
Hall, H. H. and J. L. Powell. Scattering of protons by protons—912

Halpern, O. and G. L. Appleton. Scattering of slow neutrons by O_2 molecules—869
Ham, Frank and Harvey Brooks. Effect of boundary states on free electron diamagnetism—383(A)
Hamermesh, Bernard and Clyde Kimball. Photodisintegration cross section of Be at 2.185 Mev—1063
——, **G. R. Ringo, and S. Wexler.** Thermal neutron capture cross section of H—603
Hamilton, Donald R. β-γ polarization correlations—370(A)
—— (see Pipkin, Francis M.)—353(A)
Hammer, C. L., E. C. Raka, and R. W. Pidd. Scattering of high energy electrons by nuclei—341(A)
—— (see Raka, E. C.)—341(A)
Hammond, William R., D. N. Kundu, and M. L. Pool. Activity assignment to Ti^{48}—157(L)
Handley, Thomas H. and Elmer L. Olson. Dy^{157}—500(L)
—— (see Cohen, B. L.)—323(L)
Hänni, F. (see Albers-Schönberg, H.)—322(L)
Hansen, K. F. (see Kiehn, R. M.)—362(A)
Harrick, N. J., R. G. Barnes, P. J. Bray, and N. F. Ramsey. Nuclear rf spectra of D_2 and H_2 in intermediate and strong magnetic fields—260
Harris, D. R. (see Ballam, J.)—369(A)
—— (see Rau, R. Ronald)—369(A)
Harris, Edward G. and Michel A. Melkanoff. Quadrupole moment of Li^7—585
Harris, F., B. Rossi, and I. Escobar Vallejo. East-west asymmetry for positive and negative mesons near equator—360(A)
Harris, J. C. (see Green, Donald W.)—1132(A)
Harrison, F. B. (see Cowan, C. L., Jr.)—493(L)
Harrison, G. R. Echelle spectroscopy—367(T)
Hartzler, A. J. and R. T. Siegel. Measurements with 390-Mev neutrons—362(A)
Harvey, J. A. (see Hughes, D. J.)—497(L)
Hastings, J. M. (see Corliss, L. M.)—1013
Haugsnes, Jack (see Darlington, Lillian E.)—1049
Havens, W. W., Jr. (see Seifert, A. M.)—349(A)
Hayes, F. N. (see Cowan, C. L., Jr.)—493(L)
Hayes, S., R. Smoluchowski, and R. W. Turner. Small angle x-ray scattering in deformed crystals—350(A)
Haynes, J. R. and J. A. Hornbeck. Temporary traps in Si and Ge—152(L)
Hazen, W. E., C. A. Randall, Jr., and R. W. Williams. Experiments on air showers—361(A)
—— (see Heineman, R. E.)—496(L)
—— (see Williams, R. W.)—361(A)
Heer, C. V. and C. Rauch. Magnetic susceptibility of colored KCl from 1°K to 300°K—530
Heer, E. (see Albers-Schönberg, H.)—322(L)
Heineman, R. E. and W. E. Hazen. Density distribution within 2 meters of large air shower axes—496(L)
Heller, Jack. Theory of nonhomogeneous turbulence—376(A)
Heller, W. and W. J. Pangonis. Refractive index corrections for molecular weight determined from light scattering—345(A)
—— (see Pangonis, W. J.)—345(A)
Hellund, E. J. Inner bremsstrahlung and magnetic moment of the neutrino—721(L)
Henley, E. M. and M. A. Ruderman. Recoil effects in meson-nucleon scattering—719(L)
Henri, V. P. (see Bay, Z.)—371(A)
—— (see Kanner, H.)—371(A)
Henry, Warren E. Magnetic saturation and apparent molecular fields of $MnCl_2 \cdot 4H_2O$—492(L)
Hereford, Frank L. and Jerome P. Keuper. Azimuthal distribution of photoelectrons produced by 0.5-Mev polarized photons—1043
—— **and Jerome P. Keuper.** Photoelectron ejection by 0.51-Mev polarized photons—382(A)
—— (see Berko, Stephen)—341(A)
Hermans, J. J. and Robert Ullman. Statistics of stiff chains—384(A)
Herrmann, G. (see Weisbaum, S.)—338(A)
Herschman, A. (see Hull, M. H., Jr.)—482
Heydenburg, N. P. (see Talbott, F. L.)—186
—— (see Temmer, G. M.)—340(A)
Hickam, W. M., R. E. Fox, and T. Kjeldaas, Jr. Ionization probability near threshold for formation of Xe^{++}, Kr^{++}, A^{++}, and Ne^{++}—386(A)
—— (see Kjeldaas, T., Jr.)—386(A)
Hicks, B. L. (see Turner, T. E.)—338(A)
Hicks, D. A., T. Husain, L. G. Sanders, and L. E. Beghian. Levels in N^{14} from $C^{13}(p,\gamma)N^{14}$—163(L)
—— (see Schecter, L.)—633
Hildebrand, B. Energy loss distribution of 624-kev electrons in thin foils—378(A)
Hill, David L. (see Wheeler, John A.)—366(A)
—— (see Wilets, L.)—366(A)
Hill, R. D. (see Swan, J. B.)—257
Hill, Richard William. Elastic scattering of α-particles by C—845
Hiller, Dale M. and Don S. Martin, Jr. Radiochemical studies on photofission of Th—581
Hillman, Peter and R. H. Stahl. Total cross section of He for high energy neutrons—362(A)
Hinman, G., D. Brower, and R. Leamer. Internal conversion in Na^{22} and Fe^{59}—370(A)
Hodson, A. L. (see Ballam, J.)—369(A)
—— (see Rau, R. Ronald)—369(A)
Hofmann, J. A. and K. Strauch. Interaction of 95-Mev protons with D, Li, Be, C, Al, Cu, and Pb nuclei—449
Holmes, John R. (see Parker, Lee W.)—142
Horan, John R. Non-uniform track shrinkage in nuclear emulsions—717(L)
Hornbeck, J. A. Trapping of injected carriers in semiconductors—336(T)
—— (see Haynes, J. R.)—152(L)
Horowitz, M. and J. G. Daunt. Specific heat measurements on pure metals at low temperatures—379(A)
Horton, G. K. (see Sharp, R. T.)—316(L)
Horton, J. and R. Sherr. α-γ angular correlation in ThC—388(A)
Houston, J. M. (see Burgess, R. E.)—515
Howe, Horace A. and K. R. MacKenzie. Positron-electron scattering at 1.3 Mev—678
Howling, D. H., E. Mendoza, and J. E. Zimmerman. Method of measuring specific heats at very low temperatures—347(A)
Hoyt, Harry C., Joseph J. Murray, and Jesse W. M. DuMond. Comparison of γ-ray reflections from (550) and (310) planes of quartz—169(L)
Hsiao, C. A. and V. L. Telegdi. Mechanism of $O^{16}+h\nu \rightarrow 4He^4$—494(L)
Hughes, D. J., J. A. Harvey, M. D. Goldberg, and Marilyn J. Stafne. Neutron-electron interaction—497(L)
——, **F. G. P. Seidl, H. Palevsky, and J. S. Levin.** Neutron resonance measurements with Brookhaven fast chopper—363(A)
—— (see Levin, J. S.)—363(A)
Hughes, Francis J. (see Jensen, Erling N.)—557
Hughes, Vernon W. (see Weinreich, Gabriel)—377(A)
Hugo, T. J. (see Naudé, S. M.)—318(L)
Huizenga, J. R. (see Engelkemeir, D. W.)—6
Hull, G. F., Sr. Experimental discoveries announced in programme of meeting of fifty years ago—367(T)

Hull, M. H., Jr., and A. Herschman. Effect of short range repulsion on low energy singlet nucleon-nucleon scattering —482
—— (see Gluckstern, R. L.)—1026; 1030
Hulm, J. K. Thermal resistivity of Hg in intermediate state —1116(L)
Hulthén, Lamek and Bengt C. H. Nagel. Photodisintegration of the deuteron—62
Humphrey, J. N., Frances L. Lummis, and W. W. Scanlon. Capacitance effects in thin conductive films—111
Hurst, G. S. (see Bortner, T. E.)—160(L)
Husain, T. (see Beghian, L. E.)—1129(L)
—— (see Hicks, D.)—163(L)
Hyde, Earl K. and Albert Ghiorso. α-branching of AcK and presence of As in nature—267

Ingram, D. J. E. Paramagnetic resonance in Mn formate—711(L)
Inn, Edward C. Y. (see Watanabe, K.)—155(L);—359(A)
—— (see Zelikoff, Murray)—359(A)

Jackson, J. David and D. I. Wanklyn. Disintegration of C by fast neutrons—381(A)
Jackson, J. M. and W. A. Rense. Origin of zodiacal light —345(A)
—— (see Pietenpol, W. B.)—156(L)
Jacobs, Ira and E. S. Akeley. Transverse motion of electron in constant wave speed section of linear accelerator —386(A)
Jacobs, James A. (see Schrader, Carlton D.)—159(L)
Jaffe, Hans (see Cook, W. R., Jr.)—375(A)
Jagger, John. Particle size of α-amylase—384(A)
Janes, G. S. and W. L. Kraushaar. Photoproduction of π^+ mesons from H—341(A)
Janin, J. (see Déjardin, G.)—359(A)
Jankus, V. Z. Radiative correction for collision loss of heavy particles—4
Jeffries, C. D. Spin and magnetic moment of Ca^{41}—1130(L)
Jelatis, J. G. (see von Hippel, A.)—364(A)
Jen, C. K. Classical model for rotational magnetic moments in molecules—359(A)
Jensen, Erling N., L. Jackson Laslett, Don S. Martin, Jr., Francis J. Hughes, and William W. Pratt. Radiations from Se^{75}—557
Jensen, Louis K. (see Glass, Neel W.)—320(L)
Jesse, William P. and John Sadauskis. α-particle ionization in pure gases and average energy to make ion pair—1120(L)
John, E. R. (see Elson, R.)—102
Johnson, A. C. (see Bleuler, E.)—464
Johnson, N. R. (see Sheline, R. K.)—325(L)
Johnson, P. D. Recent advances in interpretation of luminescence in solids—363(T)
Johnson, V. A. and F. M. Shipley. Adiabatic Hall effect in semiconductors—523
Jones, G. A. and D. H. Wilkinson. Purity of isotopic spin of charge parity states—722(L)
Jones, John W. and Truman P. Kohman. Synchrocyclotron production and properties of Mg^{28}—495(L)
Jongenburger, P. Extra resistivity due to vacancies in Cu—710(L)
Jordan, W. C., J. M. Cork, and S. B. Burson. Decay of Rh^{104m} (4.3-min) and Rh^{104} (44-sec)—862
Juenker, D. W., G. S. Colladay, and E. A. Coomes. Surface barrier analysis for highly refractory metals by means of Schottky deviations—772

Kahn, David. Energy loss of protons in metallic foils and mica—503
Kallmann, H. K. Continuous layer formation in atmosphere under influence of solar radiation—153(L)
Kambe, K. and A. Abragam. Line width in pure quadrupole resonance experiments in crystals—348(A)
Kane, J. A. (see Mott, W. E.)—712(L)
Kane, R. P. (see Sarabhai, V.)—204
Kanner, H., Z. Bay, and V. P. Henri. Accuracy of time measurements by delayed coincidences—371(A)
Kantrowitz, Arthur. Studies of thermally ionized gases produced by shock waves.—368(T)
Kaplon, M. F., D. M. Ritson, and W. D. Walker. High energy nuclear interactions in Pb and light elements—716(L)
—— (see Ritson, D. M.)—360(A)
Karplus, Robert, Margaret Kivelson, and Paul C. Martin. Meson-nucleon scattering—1072
Karzmark, C. J. (see Buskirk, A. V.)—369(A)
—— (see Thompson, R. W.)—329(L); 1122(L)
Kash, S. W. and D. C. Woods. Measurement of transport mean free path of thermal neutrons in D_2O by B poisoning method—564
Kasnitz, Harold L. and Kurt Sitte. Structure and composition of air shower cores—361(A)
Kato, W. Y. (see Levin, J. S.)—363(A)
Katz, L. (see Goldemberg, J.)—308
Keck, Paul H. Solubility of Si in Ga and In—379(A)
—— **and Jacob Broder.** Solubility of Si and Ge in Ga and In—521
Kellogg, D. A. Cross sections for products of 90-Mev neutrons on C—224
Kendrick, W. M. (see Turner, T. E.)—338(A)
Kessler, J., H. Byfield, L. M. Lederman, and K. Rogers. Production of high energy photons in pion collisions—343(A)
—— (see Lederman, L.)—344(A)
Ketelle, B. H., A. R. Brosi, and F. M. Porter. Gallium 67 —567
Keuffel, J. W. (see Meyer, A. J.)—349(A)
Keuper, Jerome P. (see Hereford, Frank L.)—382(A); 1043
Kiehn, R. M., Clark Goodman, and K. F. Hansen. Total neutron cross sections of Cl and C—362(A)
Kimball, Clyde (see Hamermesh, Bernard—1063
King, J. C. and Henry A. Fairbank. Second sound velocity in mixtures of He^3—He^4—347(A); 989(L)
King, J. S. and E. H. Beach. Angular distributions of (d,p) reactions on P^{31}, Cl^{35}, V^{51}, and Sc^{45}—381(A)
King, R. W. and D. C. Peaslee. Odd-odd spins and j-j coupling—1001(L)
King, William C. and Walter Gordy. One to two mm wave spectroscopy—319(L)
Kington, J. D. (see Bair, J. K.)—575
—— (see Willard, H. B.)—865
Kinsey, B. B. (see Bartholomew, G. A.)—355(A)
Kip, A. F. Paramagnetic resonance resulting from conduction-electrons in metals—348(T)
—— (see Portis, A. M.)—988(L)
Kirk, Russell D. (see Schulman, James H.)—351(A)
Kittel, C. and Elihu Abrahams. Dipolar broadening of magnetic resonance lines in magnetically-diluted crystals —238
—— (see Portis, A. M.)—988(L)
Kivel, B. Pressure broadening by electron impacts—382(A)
Kivelson, D. and E. B. Wilson, Jr. Constants of centrifugal distortion—338(A)
Kivelson, Margaret (see Karplus, Robert)—1072
Kjeldaas, T., Jr., W. M. Hickam, and R. E. Fox. Relative ionization probability of He near threshold—386(A)
—— (see Hickam, W. M.)—386(A)

Klein, Abraham. Lamb shift for spinless electrons—372(A)
—— Tamm-Dancoff formalism and symmetric pseudoscalar theory of nuclear forces—1101
Kleiner, W. H. Orbital effect in neutron-electron magnetic scattering—168(L)
Kleinman, David A. Energy distribution of slow neutrons scattered in crystals—355(A)
Klick, Clifford C. and James H. Schulman. Luminescence of divalent Mn in solids—363(A)
Koehler, W. C. and E. O. Wollan. Paramagnetic scattering of neutrons by trivalent ions of Nd and Er—354(A)
Kohler, Donald A. (see Ch'en, Shang-Yi)—1019
Kohman, Truman P. (see Jones, John W.)—495(L)
Kohn, W. Adiabatic treatment of slow atomic collisions—383(A)
Kolb, E. D. (see Slichter, W. P.)—987(L)
Kotani, M. (see Miller, S. L.)—542
Kothari, D. S. (see Auluck, F. C.)—1002(L)
Kothari, L. S. Production of heavy mesons—1087
Kramers, H. C., F. A. W. van den Burg, and C. J. Gorter. Heat pulses in He II between 0.1°K and 1.0°K—1117(L)
Kranz, A. Z. and W. W. Watson. Thermal diffusion constant of HCl—344(A)
Kraushaar, J. J., Elizabeth D. Wilson, and Kenneth T. Bainbridge. Disintegration constant of Be^7 in Be, BeO, and BeF_2—610
Kraushaar, W. L. (see Janes, G. S.)—341(A)
Kriessman, C. J. and T. R. McGuire. Magnetic susceptibilities of Hf, Gd, and Mn—374(A)
Kroemer, H. (see Burgess, R. E.)—515
Kronheimer, Erwin H. Calculation of nuclear binding energies with single-particle oscillator wave-functions—1003(L)
Kruger, Paul and Nathan Sugarman. Evidence for 25.5-day Sr—76-sec Rb chain—158(L)
Krumbein, A. D. (see Grant, F. A.)—59
Kruse, U. E. (see Malenka, B. J.)—365(A)
Kulp, J. Laurence and Herbert L. Volchok. Constancy of cosmic ray flux over past 30,000 years—713(L)
Kundu, D. N. (see Hammond, William R.)—157(L)
Kusch, P. (see Coté, R. E.)—103
Kusumoto, Osamu, Saburo Miyake, Koichi Suga, and Yuzuru Watase. Example of multiple meson production observed with high pressure H_2-filled cloud chamber—998(L)

Laitone, E. V. and Helmer Nielsen. Transonic flow past wedge profiles by hydraulic analogy—375(A)
Lakin, W. and L. Wolfenstein. Nuclear reactions involving polarized deuterons—365(A)
Lamb, Willis E., Jr. (see Yergin, Paul F.)—377(A)
Landon, H. H., V. L. Sailor, and H. L. Foote, Jr. Neutron resonance energy measurements with Brookhaven crystal spectrometer—363(A)
—— (see Foote, H. L., Jr.)—362(A)
Laslett, L. Jackson (see Jensen, Erling N.)—557
Lawson, R. D. and S. D. Drell. Double meson photoproduction—326(L)
Lax, Melvin. Transition temperatures for spherical model ferromagnets—374(A)
—— (see Levitas, Alfred)—374(A)
Leaf, Boris. Continuum in special relativity—1090
Leamer, R. (see Hinman, G.)—370(A)
LeBlanc, J. M. (see Cork, J. M.)—444; 579
Lederman, Leon, H. Byfield, J. Kessler, and K. Rogers. Pion scattering and absorption cross sections in Pb and C—344(A)
—— (see Goldhaber, Gerson)—343(A)
—— (see Kessler, J.)—343(A)
Lee, T. D., F. E. Low, and D. Pines. Motion of slow electrons in polar crystal—297
—— (see Pines, D.)—382(A)
Lees, S., W. D. Green, and E. T. Colton. Low frequency oscillator, circular sweep generator, and direct reading phase measuring instrument—346(A)
Lefker, R., A. deBretteville, Jr., and J. S. Dodd. Single crystal high temperature heater for x-ray spectrometer—345(A)
Lehovec, Kurt. Space charge layer and distribution of lattice defects at surface of ionic crystals—350(A)
Leighton, R. B. (see Alford, W. L.)—622
—— (see York, C. M.)—167(L)
Lemonick, Aaron (see Pipkin, Francis M.)—353(A)
Lenard, A. Inner bremsstrahlung in μ decay—372(A); 968
Leprince-Ringuet, L. (see Crussard, J.)—1127(L)
Levin, J. S., W. Y. Kato, N. G. Sjostrand, and D. J. Hughes. Neutron resonances in Ag, Th, and Mn—363(A)
—— (see Hughes, D. J.)—363(A)
Levinger, J. S. Effects of radioactive disintegrations on inner electrons of the atom—11
Levitas, Alfred and Melvin Lax. Improved spherical treatment of Ising model—374(A)
Lew, Hin and Günter Wessel. Hfs of $3p\ ^2P_{1/2}$ state of Al^{27}—1
Lewis, H. W. and G. H. Wannier. Spherical model of a ferromagnet, erratum—1131(E)
Li, C. W. Nuclear mass determinations from disintegration energies: O to S, erratum—1131(E)
Lidofsky, L., E. Alperovitch, and C. S. Wu. β-spectrum of Cs^{135}—387(A)
Liepmann, H. W. Skin friction in supersonic and high subsonic flow—379(T)
Lin, C. C. Stability of boundary layer at supersonic speeds—379(T)
Lindenfeld, P. (see Steinberger, J.)—343(A)
Lindsay, W. T. (see Amdur, I.)—344(A)
Lindström, Gunnar. Establishment of absolute energy scale in β-spectroscopy—369(T)
Lipworth, Edgar (see Yergin, Paul F.)—377(A)
Littauer, R. M., A. M. Perry, and W. M. Woodward. Photomesons from H—342(A)
Little, R. N., Jr. (see Dvorak, H. R.)—618
Livingston, M. S. Strong focusing synchrotron—368(T)
Livingston, Ralph and Henry Zeldes. Quadrupole moment ratio of I^{129} and I^{127} from pure quadrupole spectra—609
Locher, K. and P. Stoll. (γ,α) reaction of B^{11} and B^{10}—164(L)
Loeb, Leonard B. Current increase at constant amplification factor in steady corona with coaxial cylindrical geometry—144
Longdon, L. W. Non-central force matrix elements for nuclear d^2 configuration—1125(L)
Lönsjö, O. (see Roderick, H.)—371(A)
Loring, R. A. (see Green, J. B.)—80
Lounsbury, M. (see MacKenzie, D. R.)—327(L)
Lovberg, R. H. (see Yarnell, J. L.)—292
Low, F. E. (see Lee, T. D.)—297
—— (see Pines, D.)—382(A)
Löwdin, Per-Olov. Atomic self-consistent fields. I. Calculation of Slater functions—120
Luckey, David. Excitation curve for photomesons from Be—711(L)
Lummis, Frances L. (see Humphrey, J. N.)—111

MacDonald, J. Ross. Polarization capacitance effects in photoconductors and semiconductors—364(A)
—— (see Thickens, R. W.)—375(A)
Machlup, S. (see Brown, W. L.)—709(L)
Mack, J. E. (see Emrich, R. J.)—375(A)

MacKenzie, D. R., M. Lounsbury, and A. W. Boyd. β^- half-life of Pu^{241}—327(L)
—— (see Howe, Horace A.)—678
Madrazo, Raymond, Jr., and George Antonoff. Interpolation of vapor pressures—385(A)
Maita, J. P. (see Morin, F. J.)—337(A)
Malenka, B. J., U. E. Kruse, and N. F. Ramsey. Polarizability of deuteron—365(A)
Malkus, Willem V. R. Discrete transitions in thermal turbulence—376(A)
Malvicini, A. (see Bracci, A.)—162(L)
Mandeville, C. E. and H. O. Albrecht. α-particle induced phosphorescence of Ag-activated NaCl—25; 364(A)
—— **and H. O. Albrecht.** Phosphorescence of thoria—992(L)
—— (see Zucker, E. R.)—387(A)
Mann, D. E. and N. Acquista. Vibrational spectrum of CTFE—359(A)
Mann, Harry M. (see Darlington, Lillian E.)—1049
Mann, L. G. (see West, H. I.)—370(A)
Manring, Edward, Carlton Brown, and Dudley Williams. Nuclear quadrupole transitions in paradibromobenzene—348(A)
Marcus, Paul M. Statistical basis of 2-fluid models of superconductivity—346(A)
—— (see Maxwell, E.)—346(A)
Margenau, Henry (see Bloom, Stanley)—791
—— (see Evett, Arthur A.)—1021
Marmo, Frederick (see Watanabe, K.)—155(L)
Marquez, Luis. β-spectrum of Mg^{28}—330(L)
Marshall, John H. Liquid A ionization chamber measurement of shape of β-ray spectrum of K^{40}—371(A)
Martin, D. W. (see Cork, J. M.)—444; 579
Martin, Don S., Jr. (see Hiller, Dale M.)—581
—— (see Jensen, Erling N.)—557
Martin, Paul C. (see Deser, Stanley)—1075
—— (see Karplus, Robert)—1072
Marton, L., J. Arol Simpson, and J. A. Suddeth. Electron beam interferometer—490(L)
Matossi, Frank. Vibrational emission spectra in glow discharges—359(A)
—— (see Nudelman, Sol)—363(A)
Matthias, B. T. Superconducting compounds of non-superconducting elements—487(L)
—— (see Salam, Abdus)—690
Maurer, Robert (see Dutton, David)—126
Maxwell, E. and P. M. Marcus. Aspects of 2-fluid model of superconductivity—346(A)
May, John E. and Bruce P. Foster. γ-rays from Mg^{28}—243; 340(A)
McCarthy, John A. Search for double β-decay in Sn^{124} and Zr^{96}—853
McCarthy, Kathryn A. (see Ballard, Stanley S.)—375(A)
McClure, Gordon W. Specific primary ionization of H_2, He, Ne, and A by high energy electrons—796
McDaniel, B. D. (see Draper, J. E.)—362(A)
—— (see Weil, J. W.)—380(A)
McGruer, J. N. (see Worthington, H. R.)—899
McGuire, T. R. and Selma Greenwald. Magnetic susceptibility and x-ray diffraction measurements of VO and TiO—373(A)
—— (see Kriessman, C. J.)—374(A)
McLernon, F. (see Bay, Z.)—371(A)
Meal, H. C. and H. C. Allen, Jr. Pure quadrupole spectra of HCl and DCl—348(A)
Meinke, W. Wayne. Half-life of Pd^{109} and neutron activation cross section of Pd^{105}—410
——, **E. W. Coleman, J. V. Nehemias, and L. E. Brownell.** 10-kC Co^{60} source—353(A)
Meissner, H. (see Meissner, W.)—709(L)
Meissner, W., F. Schmeissner, and H. Meissner. Temperature, current, magnetic field phase diagram of superconductivity—709(L)
Melkanoff, Michel A. (see Harris, Edward G.)—585
Melkonian, Edward. Recent developments in methods of analysis of slow neutron transmission data in neighborhood of nuclear energy levels—362(A)
Melvin, M. Avramy. Derivation of gauge condition in new electrodynamics—389(A)
—— Generalization of new classical electrodynamics—357(A)
Mendenhall, R. I. (see Zucker, E. R.)—387(A)
Mendoza, E. (see Howling, D. H.)—347(A)
Merz, Walter J. Double hysteresis loop of $BaTiO_3$ at Curie point—375(A)
Metzger, Franz R. Spin and parity of 2.3-Mev excited state of Te^{126}—328(L)
—— (see Schiff, D.)—849
Meyer, A. J. and J. W. Keuffel. μ-meson capture probabilities for intermediate Z elements—349(A)
Meyerhof, W. E. (see Roderick, H.)—371(A)
Michaelis, R. P. and C. E. Violet. Ratio of plateau to minimum grain density for electrons—723(L)
Millburn, G. P. (see Schecter, L.)—633
Miller, Park H. (see Wahlig, Charles F.)—337(A)
Miller, S. L. and C. H. Townes. Microwave absorption spectrum of O_2^{16} and $O^{16}O^{17}$—537
—— **C. H. Townes, and M. Kotani.** Electronic structure of O_2—542
Mills, F. E. (see Goldwasser, E. L.)—378(A)
Milton, J. C. D. and J. S. Fraser. Response of NaI(Tl), KI(Tl), and stilbene phosphors to fission fragments—388(A)
—— (see Fraser, J. S.)—389(A)
Mitra, A. N. and F. J. Dyson. Evidence for direct meson-meson interaction—372(A)
Mitra, S. K. Active nitrogen—516
Mitsui, Toshito and Jiro Furuichi. Domain structure of rochelle salt and KH_2PO_4—193
Miyake, Saburo (see Kusumoto, Osamu)—998(L)
Morellet, D. (see Crussard, J.)—1127(L)
Morin, F. J. and J. P. Maita. Comparison of Cu-doped Ge with heat treated Ge—337(A)
Morita, Masato. Interference terms of electron-neutrino angular correlation—1005(L)
Morrish, A. H. Nuclear interactions of 210-Mev π^- mesons in emulsions—674
Morse, Philip M. Excitation of molecular rotation-vibration by electron impact—51
Moshinsky, Marcos. Poles of S matrix for nuclear reactions—365(A)
Moskowitz, Marvin. Apparatus for measuring thermal conductivity of metals in vacuum at high temperatures—379(A)
Mostov, Philip M., Harold Grad, and Sidney Borowitz. Moment method solution of Boltzmann equation for rough sphere molecular model—376(A)
Moszkowski, S. A. and V. L. Telegdi. Nuclear double γ-emission—366(A)
Mott, W. E. and R. B. Sutton. p-p scattering at 435 Mev—339(A)
—— **R. B. Sutton, J. G. Fox, and J. A. Kane.** Differential cross section for elastic p-p scattering at 435 Mev—712(L)
Mottelson, Ben R. (see Bohr, Aage)—717(L)
Motz, Henry T. Prompt γ-rays from slow neutron capture—355(A)
Mozley, R. F. and H. Bichsel. Analyzing magnet—354(A)
—— (see Bichsel, H.)—354(A)
Murray, Joseph J. (see Hoyt, Harry C.)—169(L)

Nagel, Bengt C. H. (see Hulthén, Lamek)—62
Nagel, E. (see Wu, C. S.)—388(A)
Naudé, S. M. and T. J. Hugo. Emission spectrum of AlF—318(L)
Naumann, R. A. (see Forsthoff, C. W.)—1004(L)
Nedzel, V. Alexander. Total cross sections for 400-Mev neutrons—169(L)
Nehemias, J. V. (see Meinke, W. W.)—353(A)
Neher, H. V. Fluctuations and latitude-effect of cosmic rays at high altitudes and latitudes—360(T)
——, **V. Z. Peterson, and E. A. Stern.** Fluctuations and latitude effect of cosmic rays at high altitudes and latitudes—655
—— **and E. A. Stern.** Energy distribution of cosmic rays—360(A)
Neidigh, R. V. and B. L. Cohen. Angular distributions of 21-Mev protons elastically scattered by various nuclei—340(A)
Nelson, C. M., R. L. Sproull, and R. S. Caswell. Conductivity changes in KCl produced by γ and n irradiation—364(A)
Nelson, Edward B. (see Schrader, Carlton D.)—159(L)
Nelson, Raymond A. (see Band, William)—744
Nergaard, L. S. Studies in oxide-coated cathodes—368(T)
Nester, W. H. (see Cork, J. M.)—444; 579
Neugebauer, H. E. J. Generalization of Kirchhoff's theorem to electromagnetic fields—385(A)
Neuman, Maurice. Radiation of a high energy electron in constant magnetic field—682
Newman, E. (see Cohen, B. L.)—323(L)
Niday, James B. (see Turkevich, A.)—342(A)
Nielsen, Helmer (see Laitone, E. V.)—375(A)
Novey, T. B. (see Albers-Schönberg, H.)—322(L)
Novick, Robert (see Yergin, Paul F.)—377(A)
Nudelman, Sol and Frank Matossi. Influence of electric fields on luminescence—363(A)

O'Day, Marcus. Electron physics in upper atmosphere—368(T)
Offenbacher, Elmer L. and Herbert B. Callen. Directional effects in electric breakdown of ionic crystals—401
Ohtsuka, T. (see Waniek, R. W.)—355(A)
Olbert, S. Atmospheric effects on cosmic-ray intensity at sea level—360(A)
Oldenberg, O. Active nitrogen, airglow—727
Oliver, Norman J. (see Chamberlain, Joseph W.)—1118(L)
Orkin-Lecourtois, A. (see Crussard, J.)—1127(L)
Olson, Elmer L. (see Handley, Thomas H.)—500(L)
O'Rourke, R. C. Deviations from Brillouin's free-spin theory in $MnSiF_6 \cdot 6H_2O$—786
Ortel, William C. G. Neutrons produced in cosmic-ray stars—368(A)
Osborne, Darrell W. (see Abraham, Bernard M.)—347(A)
Osborne, L. S. Photomeson production from H—349(T)
—— (see Goldschmidt-Clermont, Y.)—350(A)
Overhauser, Albert W. Isothermal annealing effects in irradiated Cu—393

Page, L. A., P. Stehle, and S. B. Gunst. Direct comparison of m/e for positron and electron—377(A)
Palevsky, H. (see Hughes, D. J.)—363(A)
Pangonis, W. J. and W. Heller. Solid angle corrections for light scattering measurements—345(A)
—— (see Heller, W.)—345(A)
Parker, Eugene N. Acoustical radiation from velocity field in compressible fluid—240
—— Extension of Heisenberg's model of turbulence to critical Reynolds numbers—221
Parker, Lee W. and John R. Holmes. New fine structure in neutral oxygen—142
Paul, E. B., R. L. Clarke, and W. T. Sharp. Angular distribution of long range α-particles from $F^{19}(p,\alpha)O^{16}$—381(A)
Paul, William. Pressure dependence of resistivity of Ge—336(A)
Pearson, G. L. High impedance field-effect Si transistor—336(A)
—— **and M. Tanenbaum.** Magneto-resistance effect in InSb—153(L)
Pease, Jane S. (see Pease, Robert L.)—371(A)
Pease, Robert L. and Jane S. Pease. Exact interaction of scalar and electrostatic fields—371(A)
Peaslee, D. C. (see Boehm, F.)—1119(L)
—— (see King, R. W.)—1001(L)
Pell, E. M. Recombination rate in Ge by observation of pulsed reverse characteristic—278
Perez-Mendez, V. (see Boehm, F.)—1119(L)
Perry, A. M. (see Littauer, R. M.)—342(A)
Perry, J. E., Jr., and S. J. Bame, Jr. $T(p,\gamma)$ reaction—380(A)
Perry, J. P. (see Angell, C. E.)—724(L)
Peterson, V. Z. (see Neher, H. V.)—655
Petschek, Albert G. Absorption of slow π^- mesons by He^4 nuclei—959
Peyron, M. (see Déjardin, G.)—359(A)
Peyrou, C., R. Safford, and H. Bridge. Experimental results on V^0 particles—368(A)
—— (see Bridge, H. S.)—921
—— (see Safford, R.)—369(A)
Pfann, W. G. (see Vogel, F. L.)—489(L)
Phillips, James A. Energy loss of low energy protons in some gases—532
Picus, Gerald S. Transfer rate of liquid He II film near zero level difference—719(L)
Pidd, R. W. (see Hammer, C. L.)—341(A)
—— (see Raka, E. C.)—341(A)
Pietenpol, W. B. and W. A. Rense. Observations of zodiacal light during total solar eclipse—345(A)
——, **W. A. Rense, F. C. Walz, D. S. Stacey, and J. M. Jackson.** Lyman-α line photographed in sun's spectrum—156(L)
Pines, D., F. Low, T. D. Lee, and C. N. Yang. Motion of slow electrons in polar crystals—382(A)
—— (see Lee, T. D.)—297
Pipkin, Francis M., Scott M. Daubin, Aaron Lemonick, and Donald R. Hamilton. Fast triple coincidence circuit—353(A)
Pollard, E. C. Physical studies on viruses—367(T)
—— (see Friedman, M.)—384(A)
Pool, M. L. (see Cheng, L. S.)—886
—— (see Hammond, William R.)—157(L)
Porter, Charles E. (see Feshbach, Herman)—166(L)
Porter, F. M. (see Ketelle, B. H.)—567
Porter, Fred T. (see Cook, C. Sharp)—429
—— (see Whittle, Charles E.)—498(L)
Portis, A. M., A. F. Kip, C. Kittel, and W. H. Brattain. Electron spin resonance in Si semiconductor—988(L)
Portnoy, W. M. (see Swan, J. B.)—257
Pound, R. V. and A. Abragam. Angular correlations from liquid sources—993(L)
Powell, J. L. (see Hall, H. H.)—912
Pratt, William W. (see Jensen, Erling N.)—557
Price, P. J. Macroscopic theory of superfluid He^3-He^4 mixtures, erratum—1131(E)
Prim, R. C. (see Shockley, W.)—753
Primakoff, H. (see Chang, C. H.)—544
Purcell, E. M. Nuclear magnetism—367(T)

Rainwater, James. Mesonium—349(T)
Raka, E. C., C. L. Hammer, and R. W. Pidd. Scattering of high energy electrons by nuclei—341(A)
—— (see Hammer, C. L.)—341(A)
Ramsey, Norman F. Spin interactions of accelerated nuclei in molecules—232; 382(A)
—— (see Harrick, N. J.)—260
—— (see Malenka, B. J.)—365(A)
Randall, C. A., Jr. (see Hazen, W. E.)—361(A)
Rank, D. H. and D. C. Cronemeyer. Infrared absorption characteristics of thermiated Ge—202
Raphael, R. B. and J. Schwinger. High energy nucleon scattering and isobars—373(A)
Rasetti, F. and E. C. Booth. γ-ray spectrum of ionium—388(A)
Rau, R. Ronald, Marcello Vidale, G. T. Reynolds, D. R. Harris, A. L. Hodson, and J. Ballam. Magnetic field cloud chamber for studying nuclear interactions in cosmic radiation. II. Preliminary results—369(A)
—— (see Ballam, J.)—369(A)
Rauch, C. (see Heer, C. V.)—530
Read, T. A. (see Frankl, D. R.)—351(A)
Rediker, R. H. (see Buskirk, A. V.)—369(A)
Rediker, R. H. (see Thompson, R. W.)—329(L); 1122(L)
Reines, F. and C. L. Cowan, Jr. Proposed experiment to detect free neutrino—492(L)
—— (see Cowan, C. L., Jr.)—493(L)
Reiss, Howard. Chemical equilibria involving electrons as independent chemical entities in impurity semi-conductors—336(A)
—— (see Glazer, Herbert)—360(A)
Reitz, R. (see Bernardini, G.)—573
Rense, W. A. (see Jackson, J. M.)—345(A)
—— (see Pietenpol, W. B.)—156(L); 345(A)
Reynolds, G. T. (see Ballam, J.)—369(A)
—— (see Rau, R. Ronald)—369(A)
Reynolds, John H. Isotopic constitution of Si, Ge, and Hf—1047
—— **and T. J. Ypsilantis.** Techniques in isotopic abundance measurements on elements of Group IV—378(A)
Rice, O. K. and Benjamin Widom. Thermodynamics of He film—987(L)
Richardson, J. Reginald (see Glass, Neel W.)—320(L)
Richter, Harold G. and Charles D. Coryell. Fission of U with 16-Mev x-rays—389(A)
Rinehart, M. C. (see Sargent, C. P.)—343(A)
Ringo, G. R. (see Hamermesh, B.)—603
Ritson, D. M., M. F. Kaplon, and W. D. Walker. High energy cosmic-ray interactions in photographic emulsion and Pb—360(A)
—— (see Kaplon, M. F.)—716(L)
Roberts, A., W. Spry, and J. Tinlot. Charge exchange scattering of 40-Mev π-mesons in H and D—343(A)
—— **and J. Tinlot.** Charge-exchange scattering of 34-Mev π-mesons in H and D—951
Roberts, James H. (see Darlington, Lillian E.)—1049
Roberts, Shepard. Dielectric changes of electroluminescent phosphor during illumination—364(A)
Robillard, T. R. (see Goldwasser, E. L.—378(A)
Robinson, Lawrence Baylor. Production of fissionable isotopes in thermal reactor—1054
Roderick, H., O. Lönsjö, and W. E. Meyerhof. Decay scheme of P^{33}—371(A)
Rogers, K. (see Kessler, J.)—343(A)
—— (see Lederman, L.)—344(A)
Rogosa, G. L. and Guenter Schwarz. Extent of perfect single crystal regions within imperfect single crystals—351(A)
—— (see Schwarz, Guenter)—351(A)
Rohrlich, F. and B. C. Carlson. Energy loss of positrons and electrons—378(A)
Rorschach, H. E., Jr. (see Teasdale, Tom S.)—709(L)
Rose, M. E. O^{14} β-decay and Fermi interaction—1123(L)
—— **and C. L. Terry.** Effect of finite DeBroglie wavelength in theory of β-decay—479
—— (see Armstrong, A. H.)—340(A)
—— (see Frye, G. M.)—381(A)
Rosenstock, Herbert B. Response of pulsed Geiger tube—352(A)
Ross, M. (see Sundaresan, M. K.)—372(A)
Rossi, B. (see Bridge, H. S.)—921
—— (see Harris, F.)—360(A)
—— (see Safford, R.)—369(A)
Rothstein, Jerome. Concept of physical object—356(A)
Rubin, Robert J. Propagation of "plastic" wave in material exhibiting strain-rate effect—346(A)
Ruby, Stanley L. (see Rustad, Brice M.)—370(A)
Ruderman, M. A. Nuclear forces from pseudoscalar meson theory—183
—— Pseudoscalar β-decay and RaE—366(A)
—— (see Henley, E. M.)—719(L)
Rustad, Brice M. and Stanley L. Ruby. β-recoil correlation in decay of He^6—370(A)
Ryder, E. J. Mobility of holes and electrons in high electric fields—766

Saby, John S. and W. C. Dunlap, Jr. Impurity diffusion and space charge layers in fused-impurity p-n junctions—630; 1131(E)
Sachs, A. (see Bodansky, D.)—996(L); 997(L)
—— (see Steinberger, J.)—343(A)
Sachs, Mendel. Nuclear hfs of Mn^{++}—1058
Sadauskis, John (see Jesse, William P.)—1120(L)
Safford, R., C. Peyrou, H. Bridge, and B. Rossi. Cloud-chamber observations on unstable heavy charged particles in cosmic rays—369(A)
—— (see Bridge, H. S.)—921
—— (see Peyrou, C.)—368(A)
Sagane, Ryokichi. Pion production ratios by proton bombardment—1003(L)
Sailor, V. L. (see Foote, H. L., Jr.)—362(A)
—— (see Landon, H. H.)—363(A)
Salam, Abdus and P. T. Matthews. Fredholm theory of scattering in given time-dependent field—690
Salkovitz, E. I. and P. L. Smith. Plastic deformation in ADP crystals—350(A)
Salpeter, E. E. and J. S. Goldstein. Momentum space wave functions. II. Deuteron ground state—983
—— (see Sundaresan, M. K.)—372(A)
Sanders, L. G. (see Beghian, L. E.—1129(L)
—— (see Hicks, D.)—163(L)
Sarabhai, V. and R. P. Kane. Worldwide effects of continuous emission of cosmic rays from the sun—204
Sargent, C. P. and M. C. Rinehart. Absorption of negative pions in H—343(A)
Satchler, G. R. Angular distribution of γ-rays from stripping reactions—722(L)
Saxon, David S. and E. Gerjuoy. Variational calculation of high energy scattering by Yukawa potential—373(A)
Scanlon, W. W. (see Humphrey, J. N.)—111
Schardt, A. W., W. Bernstein, and R. L. Chase. Gray wedge time delay analyzer—353(A)
—— (see Chase, R. L.)—353(A)
Scharff-Goldhaber, Gertrude. Excited states of even-even nuclei—587
Schawlow, A. L. Nuclear quadrupole resonances in Br and I compounds—348(A)

Schecter, L., W. E. Crandall, G. P. Millburn, D. A. Hicks, and A. V. Shelton. High energy charged particles from targets bombarded by 190-Mev deuterons—633
Schein, Marcel (see Glasser, R. G.)—218
Scherrer, P. (see Albers-Schönberg, H.)—322(L)
Scherrer, V. E. (see Faust, W. R.)—355(A)
Schiff, D. and F. R. Metzger. γ-γ directional correlations in Co^{58}, Xe^{133}, and Hg^{198}—849
Schlier, Robert E. and H. E. Farnsworth. Studies of gas adsorption on (100) faces of Cu and Ni crystals by low speed electron diffraction—351(A)
Schmeissner, F. (see Meissner, W.)—709(L)
Schrader, Carlton D., Edward B. Nelson, and James A. Jacobs. Angular correlation of cascade γ-rays from decay of Au^{198}—159(L)
Schubauer, G. B. Turbulent processes as observed in boundary layer and type—379(T)
Schulkes, J. A. (see Gorter, E. W.)—487(L)
Schulman, James H., Robert J. Ginther, and Russell D. Kirk. Enhancement of x-ray-induced absorption bands in alkaline-earth compounds—351(A)
—— (see Klick, Clifford C.)—363(A)
Schwarz, Guenter, L. Carlton Brown, and G. L. Rogosa. X-ray path through calcite for anomalous transmission—351(A)
—— (see Rogosa, G. L.)—351(A)
Schweber, S. S. (see Dyson, F. J.)—372(A)
Schwinger, Julian (see Raphael, R. B.)—373(A)
Scott, M. B. (see Goldschmidt-Clermont, Y.)—350(A)
Scovil, Georgiana. Hall effect in Ti—337(A)
Segrè, E. (see Bernardini, G.)—573
Seidl, F. G. P. (see Hughes, D. J.)—363(A)
Seifert, A. M., H. J. Bramson, and W. W. Havens, Jr. Photographic study of muon range spectrum from $\pi \rightarrow \mu$ decay—349(A)
Seliger, H. H., L. Cavallo, and S. V. Culpepper. Half-life of I^{131}—443
Sellers, P. A. (see Elson, R.)—102
Selove, W., K. Strauch, and F. Titus. n-p scattering near 180° at 94 Mev—339(A)
Senitzky, I. R. Transition from classical to quantum interaction between electron and high frequency field—386(A)
Setlow, Richard. Quantum yield for inactivation of dry chymotrypsin—383(A)
—— (see Franklin, R.)—384(A)
Shafer, K. D. (see Cook, L. G.)—1121(L)
Shanks, Daniel. Blasius and Weyl constants in boundary layer theory—377(A)
Shapiro, E. (see Zucker, E. R.)—387(A)
Shapiro, Mathew M. Cross sections for formation of compound nucleus by charged particles—171
Sharp, R. T. and G. K. Horton. Variational approach to uni-potential many-electron problem—316(L)
Sharp, W. T. (see Paul, E. B.)—381(A)
Sheline, R. K. and N. R. Johnson. Decay scheme of Mg^{28}—325(L)
Shelton, A. V. (see Schecter, L.)—633
Sherman, Dora F. Production of μ-mesons and their behavior in nuclear research emulsions—469
Sherr, R. (see Horton, J.)—388(A)
Shimada, Junji (see Abe, Hidetaro)—317(L)
Shipley, F. M. (see Johnson, V. A.)—523
Shockley, W. Cyclotron resonances, magnetoresistance, and Brillouin zones in semiconductors—491(L)
—— **and R. C. Prim.** Space charge limited emission in semiconductors—753
—— (see Brown, W. L.)—336(A)
Shoolery, J. N. (see Bloom, A. L.)—358(A)
Shore, F. J. (see Bendel, W. L.)—888
Shull, C. G. (see Wilkinson, M. K.)—374(A)
Shunk, R. A. (see Emrich, R. J.)—375(A)
Shutt, R. P. (see Fowler, W. B.)—1126(L)
Siegel, R. T. (see Hartzler, A. J.)—362(A)
Siegert, Arnold J. F. Theory of condensation—344(A)
—— Theory of fusion and condensation—97
Simon, Albert. Higher spin polarizations in nuclear reactions—325(L)
—— Theory of polarized particles in nuclear reactions—991(L)
—— **and T. A. Welton.** Production of polarized particles in nuclear reactions—1036
Simon, Ivan. Structure of SiO_2 and B_2O_3 glasses compacted by very high pressures—350(A)
Simons, Lennart. Existence of positronium chloride—165(L)
Simpson, J. Arol and W. C. Fagot. Properties of low energy nucleonic component at large atmospheric depths—1068
——, **W. Fonger, and S. B. Treiman.** Cosmic-ray intensity-time variations and origin. I. Neutron intensity variation method and meteorological factors—934
—— **and R. B. Uretz.** Cosmic-ray neutron production in elements as function of latitude and altitude—44
—— (see Marton, L.)—490(L)
Singer, S. F. Meteorites as cosmic-ray meters—168(L)
Sitte, Kurt (see Kasnitz, Harold L.)—361(A)
Sjostrand, N. G. (see Levin, J. S.)—363(A)
Slichter, W. P. and E. D. Kolb. Solute distribution in Ge crystals—987(L)
Smart, J. Samuel. Magnetic structure transitions—55
—— Specific heats of ferrites—374(A)
Smith, B. and H. A. Boorse. He II film transport rates over various surfaces—156(L)
Smith, Cyril L. Inactivation of desoxyribonuclease by particle bombardment and by heat—383(A)
—— (see Braams, R.)—995(L)
Smith, L. (see Aarons, M. W.)—342(A)
Smith, Lincoln G. and C. C. Damm. Mass synchrometer doublet measurement at masses 28 and 30—324(L)
Smith, P. L. (see Salkovitz, E. I.)—350(A)
Smoluchowski, R. (see Hayes, S.)—350(A)
Snowdon, S. C. and W. D. Whitehead. Total neutron cross sections of Au, Cl, and P—615
Snyder, H. S. Alternating-gradient focusing principle—347(T)
Soules, J. A. (see Gordon, W. L.)—346(A)
Spence, R. D. (see Carr, E. F.)—339(A)
—— (see Cowen, J. A.)—359(A)
Spencer, L. V. Calculation of peaked angular distributions from Legendre polynomial expansions and application to multiple scattering of charged particles—146
—— **and Charles Wolff.** Penetration and diffusion of hard x-rays: Polarization effects—510
Sperduto, A. (see Bockelman, C. K.)—340(A)
—— (see Browne, C. P.)—340(A)
Spetner, L. M. Fade-time of Rayleigh distributed random function—346(A)
Sproull, R. L. and R. S. Bever. O vacancies in BaO crystals—352(A)
—— (see Nelson, C. M.)—364(A)
Spry, W. (see Roberts, A.)—343(A)
Squires, G. L. (see Stewart, A. T.)—1125(L)
Stacey, D. S. (see Pietenpol, W. B.)—156(L)
Stafne, Marilyn J. (see Hughes, D. J.)—497(L)
Stahl, R. H. (see Hillman, Peter)—362(A)
Stebbins, A. K. (see Bleuler, E.)—460
Steffen, Rolf M. Evidence of mixed $E1+M2$ transition and angular momenta of Sr^{88} levels—321(L)

—— Interaction of electric field gradients and nuclear electric quadrupole moments in angular correlation—1119(L)
Stehle, P. (see Page, L. A.)—377(A)
Stein, Richard and John J. Keane. Scattering of light from polymer films—384(A)
Steinberger, J., A. Sachs, and P. Lindenfeld. Internal pair production of γ-rays of mesonic origin: Alternate modes of π^0 decay—343(A)
—— (see Bodansky, D.)—996(L); 997(L)
Stern, E. A. (see Neher, H. V.)—360(A); 655
Sternglass, E. J. Temperature dependence of secondary electron emission from Ta, Pt, and graphite—380(A)
Sternheimer, R. M. Double-focusing by system of two magnets with nonuniform fields—352(A)
Stewart, A. T. and G. L. Squires. Scattering of slow neutrons by ortho- and para-hydrogen—1125(L)
Stewart, John Q. Kinds of energy—356(A)
Stier, P. M. (see Evans, G. E.)—825
Stoll, P. (see Locher, K.)—164(L)
Storrs, C. L. and D. H. Frisch. Total neutron scattering cross sections of polyethylene and C at 1.32 Mev—339(A)
Strandberg, M. W. P. (see Burke, B. F.)—303; 338(A)
Stratton, W. R. (see Yarnell, J. L.)—292
Strauch, K. (see Hofmann, J. A.)—449
—— (see Selove, W.)—339(A)
Stump, Robert (see Brown, Harry B.)—1061
Suddeth, J. A. (see Marton, L.)—490(L)
Suga, Koichi (see Kusumoto, Osamu)—998(L)
Sugarman, Nathan and Agnes Haber. Interaction of negative pions with Hg—342(A)
—— (see Kruger, Paul)—158(L)
Sugihara, Thomas (see Arnold, James R.)—332(L)
Sugita, T. (see Yamaka, E.)—992(L)
Sundaresan, M. K., E. E. Salpeter, and M. Ross. Theoretical analysis of meson-proton scattering—372(A)
Sunyar, A. W. Disintegration of W^{187}: Evidence for slow $E1$ transition—387(A)
Sutton, R. B. (see Mott, W. E.)—339(A); 712(L)
Sutton, R. M. Response of Oersted medallist: Heritage of physics teacher—367(T)
Swan, J. B., W. M. Portnoy, and R. D. Hill. Radioactivity of Pt^{191} and Pt^{197m}—257
Swenson, R. W. (see Cole, R. H.)—352(A)
Swihart, J. C. (see Belinfante, F. J.)—357(A)

Talbott, F. L. and N. P. Heydenburg. γ-ray resonances in the α-particle bombardment of Be and B—186
Talmi, Igal. Spins and parities of excited states in even-even nuclei—1001(L)
Tanaka, K. Radiation emitted by uniformly moving particles—358(A)
Tanenbaum, M. (see Pearson, G. L.)—153(L)
Tchen, C. M. Transfer processes in isotropic turbulence—376(A)
Teasdale, Tom S. and H. E. Rorschach, Jr. Paramagnetic effect in superconductors—709(L)
Telegdi, Valentine L. (see del Rio, C. S.)—439
—— (see Hsiao, C. A.)—494(L)
—— (see Moszkowski, S. A.)—366(A)
Temmer, G. M. and N. P. Heydenburg. Precision α-α scattering at low energies—340(A)
Tendam, D. J. (see Bleuler, E.)—460; 464
Tenney, F. and J. Tinlot. Low energy π^+ interactions in Be—342(A)
Terry, C. L. (see Rose, M. E.)—479
Theus, R. B. (see Faust, W. R.)—355(A)
Thickens, R. W. and J. R. MacDonald. Electret-like behavior in polarized $BaTiO_3$ ceramic—375(A)
Thode, H. G. (see Fleming, W. H.)—857
—— (see Walker, W. H.)—447
Thomas, E. E. (see Vogel, F. L.)—489(L)
Thomas, L. H. (see Zondek, B.)—738
Thompson, R. W., A. V. Buskirk, L. R. Etter, C. J. Karzmark, and R. H. Rediker. Disintegration of V^0 particles—329(L)
——, **A. V. Buskirk, L. R. Etter, C. J. Karzmark, and R. H. Rediker.** Unusual example of V^0 decay—1122(L)
—— (see Buskirk, A. V.)—369(A)
Thomson, Robb M. and Peter G. Bergmann. Spin and statistics of general-relativistic Dirac field—357(A)
Thorndike, A. M. (see Fowler, W. B.)—1126(L)
Thourson, T. L. (see Brentano, J. C. M.)—351(A)
Tietz, T. Movable critical points of nonlinear wave equation—495(L)
Tifford, Arthur N. and Sheng To Chu. Boundary layer on spinning axisymmetric bodies—377(A)
Timnick, A. (see Cohen, B. L.)—323(L)
Tinlot, J. (see Roberts, A.)—343(A); 951
—— (see Tenney, F.)—342(A)
Tittman, Jay. Thermal energy relaxation length of Ra-Be neutrons in water—256
Titus, F. (see Selove, W.)—339(A)
Tolhoek, H. A. Theory of directional distribution and polarization of β- and γ-rays emitted by oriented nuclei—366(A)
Toll, John S. Radiative corrections to forward Compton scattering—372(A)
Tompkins, Althea (see Turkevich, A.)—247
Touschek, B. (see Chisholm, R.)—763
Townes, C. H. (see Miller, S. L.)—537; 542
Trammell, G. T. Elastic scattering of neutrons from paramagnetic rare earth atoms—355(A)
Trefftz, Eleanor. Energy bands in Nb metal—380(A)
Treiman, S. B. (see Simpson, J. A.)—934
Trembley, J. (see Crussard, J.)—1127(L)
Trischka, J. W. (see Braunstein, R.)—348(A)
Truell, Rohn and Joseph Bronzo. Ultrasonic attenuation measurements in Ge—152(L)
Turkevich, A. and James B. Niday. Radioactive products of interaction of π^- with As^{75}—342(A)
—— and Althea Tompkins. Search for Si^{32} in natural Si—247
Turner, R. W. (see Hayes, S.)—350(A)
Turner, T. E., Verna C. Fiora, W. M. Kendrick, and B. L. Hicks. Preliminary analysis of microwave spectrum of C_2H_4NH—338(A)

Uehling, Edwin A. (see Young, J. A., Jr.)—990(L)
Ullman, Robert (see Hermans, J. J.)—384(A)
Uretz, R. B. (see Simpson, J. A.)—44
Urey, Harold C. Abundances of elements, erratum—1131(E)

Vaidya, P. C. Spherically symmetric solutions in nonsymmetrical field theories. I. Skew symmetric tensor—695
Vallejo, I. Escobar (see Harris, F.)—360(A)
van den Burg, F. A. W. (see Kramers, H. C.)—1117(L)
Van Vleck, J. H. Two barrier phenomena—367(T)
van Wieringen, J. S. Anomalous behavior of g-factor of LiFeCr spinels as function of temperature—488(L)
Vidale, Marcello (see Ballam, J.)—369(A)
—— (see Rau, R. Ronald)—369(A)
Violet, C. E. (see Michaelis, R. P.)—723(L)
Visscher, W. M. (see Dyson, F. J.)—372(A)
Vogel, F. L., W. G. Pfann, H. E. Corey, and E. E. Thomas. Observations of dislocations in lineage boundaries in Ge—489(L)
Volchok, Herbert L. (see Kulp, J. Laurence)—713(L)

von Hippel, A., E. P. Gross, J. G. Jelatis, and M. Geller. Photocurrent space charge build-up and field emission in alkali halide crystals—364(A)

Wahlig, Charles F. and Park H. Miller. Photo-Hall-Voltaic effect—337(A)
Wakely, P. G. Binding energy calculation on He^4 with single particle wave functions—724(L)
Walchli, H. E. Nuclear magnetic resonance measurements of Se—331(L)
Walker, William D. Interactions of μ-mesons—234; 349(A)
—— **and N. M. Duller.** Unstable particles from penetrating showers—320(L)
—— (see Greisen, K.)—915
—— (see Kaplon, M. F.)—716(L)
—— (see Ritson, D. M.)—360(A)
Walker, W. H. and H. G. Thode. Relative abundances and neutron capture cross sections of Nd isotopes—447
Walt, M. and H. H. Barschall. Angular distribution of elastically scattered 1-Mev neutrons—714(L)
Walz, F. C. (see Pietenpol, W. B.)—156(L)
Waniek, R. W. and T. Ohtsuka. Stars initiated by neutrons—355(A)
Wanklyn, D. I. Fast neutron reactions in O and Ne—381(A)
—— (see Jackson, J. David)—381(A)
Wannier, Gregory H. Threshold law for single ionization of atoms or ions by electrons—817
—— (see Lewis, H. W.)—1131(E)
Watanabe, K., Edward C. Y. Inn, and Murray Zelikoff. Absorption coefficients of O_2 in vacuum uv—359(A)
——, **Frederick Marmo, and Edward C. Y. Inn.** Formation of D layer—155(L)
—— (see Zelikoff, Murray)—359(A)
Watase, Yuzuru (see Kusumoto, Osamu)—998(L)
Watson, K. M. (see Brueckner, K. A.)—699
Watson, W. W. (see Anderson, Carl E.)—606
—— (see Kranz, A. Z.)—344(A)
Wattenberg, A., B. T. Feld, and R. D. Godbole. High energy photoproton production—380(A)
Weaver, Albert B. Search for penetrating showers from H_2 at sea level using a cloud chamber—86
Weber, J. Quantum effects in noise—357(A)
—— Quantum theory of damped electrical oscillator and noise—977
Weidner, R. T. (see Eschenfelder, A. H.)—358(A)
Weil, J. W. and B. D. McDaniel. Photoproduction of protons by monoenergetic 190-Mev γ-rays—380(A)
Weinreich, Gabriel and Vernon W. Hughes. Atomic beam magnetic resonance experiments on He^3—377(A)
Weinstock, Bernard (see Abraham, Bernard M.)—347(A)
Weisbaum, S., Y. Beers, and G. Herrmann. S-band spectrum of HDO—338(A)
Weisskopf, Victor F. (see Feshbach, Herman)—166(L)
Welton, T. A. Theory of Lamb shift—373(A)
—— (see Simon, A.)—1036
Wessel, Günter (see Lew, Hin)—1
West, H. I. and L. G. Mann. Measurement of γ-ray spectra using three-crystal pair spectrometer—370(A)
Wexler, S. (see Hamermesh, B.)—603
Weyl, Peter K. Energy loss of heavy charged particles in gases—378(A)
Wheeler, George W. (see Anderson, Carl E.)—606
Wheeler, John A. and David L. Hill. Collective model of nucleus—366(A)
White, George R. and W. F. Fry. Range distribution of μ-mesons from π-meson decays in photographic emulsions—349(A)
—— (see Fry, W. F.)—207
Whitehead, W. D. (see Snowdon, S. C.)—615
Whittemore, W. L. (see Fowler, W. B.)—1126(L)
Whittle, Charles E. and Fred T. Porter. γ-ray cascade following decay of Sc^{46}—498(L)
Widgoff, M. Multiplicity of neutrons from interaction of μ^- mesons at rest in Pb, Bi, Sn, and Al—891
Widom, Benjamin (see Rice, O. K.)—987(L)
Wilets, L., D. Hill, and K. W. Ford. Contribution of nuclear distortion to isotope shifts—366(A)
Wilkinson, D. H. Possible breakdown of isotopic spin and charge parity selection rules—721(L)
—— (see Jones, G. A.)—722(L)
Wilkinson, M. K. and C. G. Shull. Neutron diffraction studies on various ferromagnetic alloys—374(A)
Willard, H. B., J. K. Bair, and J. D. Kington. $T(p,n)He^3$ and $T(p,\gamma)He^4$—865
—— (see Bair, J. K.)—575
Williams, A. O., Jr. Two-electron self-consistent field—803
Williams, Dudley (see Manring, Edward)—348(A)
Williams, R. W. and W. E. Hazen. Experiments on air showers—361(A)
—— (see Hazen, W. E.)—361(A)
Williamson, E. Marjorie (see Flint, H. T.)—318(L)
Wilson, E. B., Jr. (see Ferguson, R. C.)—338(A)
—— (see Kivelson, D.)—338(A)
Wilson, Elizabeth (see Bainbridge, Kenneth T.)—430
—— (see Kraushaar, J. J.)—610
Wilson, Robert R. Scattering of 1.3^5-Mev γ-rays by electric field—720(L)
Winsberg, Lester. Interaction of π^- mesons with I^{127}—343(A)
Woese, C. R. (see Caspar, D. L.)—384(A)
Wolfenstein, L. Tensor operators in isotopic spin space—371(A)
—— (see Fumi, F. G.)—498(L)
—— (see Lakin, W.)—365(A)
Wolff, Charles (see Spencer, L. V.)—510
Wollan, E. O. (see Koehler, W. C.)—354(A)
Woods, D. C. (see Kash, S. W.)—564
Woodward, W. M. (see Littauer, R. M.)—342(A)
Woonton, G. A. Diffraction field of circular aperture—385(A)
Worley, R. Edwin. Third Rydberg series of N_2, erratum—1131(E)
Worthington, H. R., J. N. McGruer, and D. E. Findley. p-p scattering from 1.8 to 4.2 Mev—899
Wright, Byron T. Spectrometer measurement on high energy positrons of Na^{22}—159(L)
Wu, C. S., F. Boehm, and E. Nagel. Radiations from RaD and RaE—388(A)
—— (see Boehm, F.)—369(A)
—— (see Lidofsky, L.)—387(A)

Yadoff, Oleg. Free electron emission in atmosphere—387(A)
Yamaka, E. and T. Sugita. Energy band structure in Si crystal—992(L)
Yang, C. N. (see Pines, D.)—382(A)
Yarnell, J. L., R. H. Lovberg, and W. R. Stratton. Angular distribution of $He^3(d,p)He$ between 240 kev and 3.56 Mev—292
Yergin, Paul F., Willis E. Lamb, Jr., Edgar Lipworth, and Robert Novick. Fine structure of singly ionized He—377(A)
Yevick, George J. Pines-Bohm theory of many particles with long-range forces—383(A)
York, C. M., R. B. Leighton, and E. K. Bjornerud. Direct experimental evidence for existence of heavy V^+ particle—167(L)

Young, J. A., Jr., and Edwin A. Uehling. Energy absorption in ferromagnetic resonance—990(L)
Young, R. A. (see Ziegler, W. T.)—115
Ypsilantis, T. J. (see Reynolds, J. H.)—378(A)
Yuan, Luke C. L. (see der Mateosian, E.)—868

Zeldes, Henry (see Livingston, Ralph)—609
Zeldes, Nissan. Spark spectrum of Gd II—413
—— spins of Li^8 and B^{10} in shell-model—416
Zelikoff, Murray, Edward C. Y. Inn, and K. Watanabe. Absorption coefficients of N_2O and CO_2 in vacuum uv—359(A)
—— (see Watanabe, K.)—359(A)
Ziegler, W. T. and R. A. Young. Studies of compounds for superconductivity—115
Zimmerman, F. J. (see Collins, S. C.)—991(L)
Zimmerman, J. E. (see Howling, D. H.)—347(A)
Zimmerman, R. L., D. I. Cooper, and D. H. Frisch. *n-d* and *p-d* scattering in *S*-wave region—339(A)
—— (see Cooper, D. I.)—339(A)
Zirin, Harold. Exchange potential in electron gas at nonzero temperature—795
Zondek, B. and L. H. Thomas. Stability of limiting case of plane Couette flow—738
Zucker, Alexander. Nuclear reactions with 25-Mev nitrogen nuclei—380(T)
Zucker, E. R., C. E. Mandeville, E. Shapiro, R. I. Mendenhall, and G. L. Conklin. γ-radiation from Zr^{96} and Nb^{93}—387(A)
Zucker, Francis J. Guided surface waves on lossy structures—385(A)

Author Index to Volume 91

References with (A) are to abstracts of papers presented at meetings of the American Physical Society, and those with (T) designate title only; references with (L) are to Letters to the Editor; references with (E) are to Errata.

Abragam, A. and K. Kambe. Dipolar broadening of quadrupole resonance line width in zero applied field—894

Acquista, N. (see Mann, D. E.)—464(A)

Adair, R. K. (see Fields, R. E.)—441(A)

Adam, J. S. (see Butler, J. P.)—1219

Adams, R. V. (see Whetten, N. R.)—432(A)

Ajzenberg, Fay, C. M. Braams, and W. W. Buechner. Neutrons from proton bombardment of Be^9—463(A)

—— **and W. W. Buechner.** Neutrons from proton bombardment of Be^9—674

Akers, Lawrence K. and Ernest A. Jones. Raman spectrum, force constants, and calculated thermodynamic properties of GeF_4—236(A)

Albers-Schönberg, H., K. Alder, O. Braun, E. Heer, and T. B. Novey. Effect of electric quadrupole interaction on γ-γ directional correlation in Cd^{111}—1287(L)

——, **E. Heer, T. B. Novey, and R. Rüetschi.** Effect of the electric quadruple interaction on the γ-γ directional correlation in Cd^{111}. II—199(L)

Albert, R. D. and E. R. Gaerttner. Neutron capture resonances using (n,γ) scintillation detector—451(A)

Albrecht, H. O. and C. E. Mandeville. Phosphorescence of and energy storage in Ag-activated NaCl—471(A)

—— (see Mandeville, C. E.)—219(A); 470(A); 566

Alder, K. and A. Winther. Theory of Coulomb excitation of nuclei—1578(L)

—— (see Albers-Schönberg, H.)—1287(L)

Aldrich, L. T. Natural variations in abundance of isotopes —442(T)

Alers, P. B. and R. T. Webber. Magnetoresistance of Bi crystals at low temperatures—1060

Alfrey, Turner, Jr. Opening remarks—225(T)

Allen, G. Band structures of one-dimensional crystals with square well potentials—531

—— **and Rolf Landauer.** Energy-band crossings for periodic square well potentials—471(A)

Allen, K. W. (see Almqvist, E.)—1022(L)

Allison, B. A. (see Scherrer, V. E.)—768(L)

Allison, Samuel K. Break-up energy of Be^8—882

Allred, J. C., A. H. Armstrong, and L. Rosen. Interactions of 14-Mev neutrons with protons and deuterons—90

Almqvist, E., K. W. Allen, J. T. Dewan, and T. P. Pepper. $He^3(He^3,p)Li^5$ and $T(He^3,p)He^5$—1022(L)

Almy, G. M. (see Butler, W. A.)—58

Alpher, R. A., J. W. Follin, Jr., and R. C. Herman. Initial conditions in expanding universe and element synthesis—479(A)

—— **and R. J. Rubin.** Transmission of sound pulse through shock wave—1030(A)

Althaus, E. J. and R. D. Sard. Cloud-chamber study of neutron production by sea-level cosmic rays, with particular reference to μ mesons stopped in Pb—373

Altshuler, Saul. Exchange scattering of electron by H atom—1167

Ames, D. P., M. E. Bunker, L. M. Langer, and B. M. Sorenson. Disintegration of Sr^{91} and Y^{91m}—68

Amster, Adolph B. and Quentin Van Winkle. Nucleoprotein monolayers—211(A)

Anderson, G. W., P. S. Freier, and J. E. Naugle. Time and directional study of primary heavy nuclei—431(A)

Anderson, H. L., E. Fermi, R. Martin, and D. E. Nagle. Angular distribution of pions scattered by H—155

Anderson, James L. Green's functions in S-matrix theory —479(A)

Anderson, Kinsey and John R. Winckler. High-altitude cosmic-ray investigation by means of Čerenkov counter. I. Instrumentation details—431(A)

—— (see Winckler, John R.)—431(A)

Anderson, R. L. (see Hunter, L. P.)—1315

Andrew, E. R. Nuclear magnetic resonance modulation correction—425(L)

Angell, C. E. and J. P. Perry. Total cross sections for 37-Mev pions in H—468(A)

—— (see Perry, J. P.)—1289(L)

Annis, M. (see Wilkins, H. C.)—480(A)

Anslow, Gladys A. and Irene S. White. Correlation of infrared and uv spectra of associated alcohols—241(A)

Anthony, D. J., B. Waldman, and W. C. Miller. Elastic scattering of 1.7-Mev electrons—439(A)

Armstrong, A. H. (see Allred, J. C.)—90

Arnowitt, R. Bound states of meson-nucleon system—459(A)

Aronofsky, J. S. Effect of gas slip on unsteady flow of gas through porous media—1032(A)

Artman, J. O. and P. E. Tannenwald. Measurement of permeability tensor in ferrites—1014(L)

Asaro, Frank and I. Perlman. Patterns in α spectra of even-even nuclei—763(L)

Ashkin, Julius and Seymour H. Vosko. Graphical method for obtaining phase shifts from experimental data on meson-nucleon scattering—1248

Austern, N., S. T. Butler, H. McManus, and W. T. Sharp. Angular distributions from (n,p) nuclear reactions—453(A)

Averbach, B. L. (see Warren, B. E.)—233(A)

Azumi, K. Magnetostriction in Fe-Co alloys—434(A)

Babcock, M. L., D. F. Holshouser, and H. Von Foerster. Diode characteristic of hollow cathode—755(L)

Bach, D. R. and P. V. C. Hough. (d,t) reactions and triton wave function—463(A)

Bacher, R. F. Caltech synchrotron and some experiments with high-energy photons—477(T)

Bailey, L. Evan (see Heckman, Harry H.)—1237

Balasubrahmanyam, V. K. (see Rao, A. S.)—764(L)

Balazs, N. L. Energy-momentum tensor of electromagnetic field inside matter—240(A); 408

Baldock, Russell, John R. Sites, L. O. Gilpatrick, and Howard E. Carr. Mass spectrometer analysis of UO_2F_2 in UF_4—242(A)

Ballam, J., D. R. Harris, A. L. Hodson, R. Ronald Rau, George T. Reynolds, S. B. Treiman, and M. L. Vidale. Kinetic energies of V_1^0 particles—1019(L); Momenta of V^0 particles—446(A)

Band, William. Low-temperature diamagnetism of electrons in cylinder—249

Bandtel, Kenneth C., Wilson J. Frank, and Richard Madey. Photoproduction of π^- mesons from D—487(A)

—— (see Frank, Wilson J.)—487(A)

—— (see Godfrey, Charles)—487(A)

Baranger, M. Stark shift and broadening due to electrons —436(A)

Barbour, J. P. (see Dyke, W. P.)—1043

Barkas, Walter H. Analysis of high-energy nuclear disintegrations—477(T)

—— (see Smith, F. M.)—765(L)

Barnes, C. B. (see Heer, C. V.)—412(L)

Barnes, R. G., P. J. Bray, and N. J. Harrick. Spin-orbit and spin-spin interactions in H_2—475(A)

—— (see Bray, P. J.)—475(A)
Barnes, S. W. Pion-nucleon scattering—466(T)
Barnett, C. F. Characteristics of Allen-type electron multiplier—224(A)
Barnett, S. J. Gyromagnetic ratios of microcrystalline materials, erratum—1580(E)
Barr, E. Scott. Sharp shadows as "images"—226(A)
Barr, T. A., Jr. Values of diffusion coefficients for some chain polymers computed from anomalous osmotic pressure data—211(A)
Barrett, P. H. Decay of heavy mesons in nuclear emulsion—446(A)
Barschall, H. H. (see Walt, M.)—441(A)
Bartoe, W. F. (see Protzman, T. F.)—211(A)
Baskir, E. (see Oxley, C. L.)—419(L)
Bass, J. Space and time spectra in homogeneous turbulence—1031(A)
Bassi, P., G. Clark, and B. Rossi. Time delays in air showers—432(A)
Batta, M. E. γ rays from 14-Mev neutron bombardment of C, O, Al, Fe, and Pb—441(A)
Batzel, R. E., W. W. T. Crane, and G. D. O'Kelley. Excitation function for $Al^{27}(d,\alpha p)Na^{24}$ reaction—939
Bauer, Ernst and Ta-You Wu. Origin of ionization in E layer of ionosphere—458(A)
Bauer, S. H. (see Widom, B.)—240(A)
Beams, J. W. Studies of tensile strengths and adhesion of metals by means of high centrifugal fields—239(T)
—— (see Morton, H. S., Jr.)—449(A)
—— (see Robeson, A.)—493(A)
Bearden, J. A., M. D. Earle, J. M. Minkowski, and J. S. Thomsen. Present status of fundamental atomic constants—482(A)
Beck, C. K. Raleigh research reactor—226(T)
Becker, E. W., R. Misenta, and O. Stehl. Difference in viscosity of ortho- and para-deuterium at low temperatures—414(L)
Becker, M., M. Cutler, T. Firle, R. Shulman, and W. Spitzer. Lifetime of minority carriers in localized crystal regions—491(A)
Becker, R. A. (see Shore, F. J.)—1203
Becker, R. L. (see Fields, R. E.)—441(A)
Becker, W. M. and K. Lark-Horovitz. Ge films—230(A)
Beckman, Olof, Torben Huus, and Črtomir Zupančič. Excitation curves for α particles from B^{11} bombarded with protons—606
Beer, A. C. (see Willardson, R. K.)—243(A)
Beers, Yardley and Samuel Weisbaum. Uhf rotational line of HDO—1014(L)
Beiser, Arthur. Zenith angle variation of cosmic-ray meson intensity—446(A)
Belinfante, Frederick J. Deficiency of phenomenological theory of Lamb shift—1285(L)
—— Intrinsic magnetic moment of particle of spin 3/2—477(A)
—— (see Swihart, J. C.)—500(A)
Belmont, E. (see Lehovec, K.)—492(A)
Belser, Richard B. Effect of sputtering rate on resistivity and "aging" of sputtered Ag films—221(A)
—— Versatile radiation oven—246(A)
—— **and Robert J. Raudebaugh.** Structure and aging of thin metal films—449(A); 499(A)
—— (see Raudebaugh, Robert J.)—449(A)
Benade, A. H. Mean life of μ^- mesons stopped in Fe—971
Bendel, W. L. (see Shore, F. J.)—1203
Benedict, T. S. Microwave observation of collision frequency of holes in Ge—1565(L)
—— **and W. Shockley.** Carrier contribution to dielectric constant of Ge—207(A)
Benesch, William and Tait Elder. Relative optical collision diameters from pressure broadening of individual infrared absorption lines—308
Bengston, J. and R. M. Thaler. Phase-shift analysis of high-energy p-p scattering—454(A)
—— (see Thaler, R. M.)—454(A)
Bennett, F. D. (see Bergdolt, V. E.)—1033(A)
Bennett, W. H. and E. O. Hulburt. Magnetic self-focusing of auroral protons—1562(L)
Bent, R. D., T. W. Bonner, and R. F. Sipple. γ rays from disintegration of C^{13} by deuterons—472(A)
Bergdolt, V. E. and F. D. Bennett. Preliminary drag measurements in pressurized range—1033(A)
Bergmann, Peter G. Generalized canonical ensemble in quantum mechanics—477(A)
—— **and Alice C. Thomson.** Generalized statistical mechanics and Onsager relations—180
Bergstein, J. and R. D. Birkhoff. Performance of 125-kv accelerator and spectrometer—223(A)
Berko, Stephan and Frank L. Hereford. Deflection of high-energy electrons in magnetized Fe—1127
Berkowitz, A. E. and A. D. Franklin. Approach to saturation in diluted ferromagnetic powders—206(A)
Berlincourt, Ted G. Relation between de Haas-van Alphen effect and magnetoresistance in Bi—1277(L)
—— **and M. C. Steele.** Method for measuring magnetic moments of superconductors—215(A)
Bernstein, W. (see Schwartz, Robert B.)—883
—— (see Weiss, M. M.)—483(A)
Bershader, Daniel. Shock-tube studies of transient boundary layers in compressible flow—470(A)
—— (see Bradley, L. C.)—469(A)
Bersohn, R. (see Weneser, J.)—1257
Bertaut, E. F. Electric field and energy in dipole lattices—415(L)
Bess, Leon. Possible mechanism for $1/f$ noise generation in semiconductor filaments—1569(L)
Betchov, R. Asymmetry of turbulent functions—470(A)
—— Stability of isotropic turbulence—1031(A)
Bethe, H. A., L. Maximon, and F. Low. Bremsstrahlung at high energies—417(L)
—— (see Cole, F. T.)—481(A)
Biggerstaff, J. A. (see Lafferty, D. L.)—223(A)
Billington, D. S. (see Cleland, J. W.)—238(A)
Biondi, Manfred A. Diffusion cooling of electrons in ionized gases—437(A)
Bird, George R. and Richard C. Mockler. Microwave spectrum of unstable molecule C—S—222(A)
Birkhoff, R. D. (see Bergstein, J.)—223(A)
—— (see Kalil, F.)—505
Birks, J. B. and M. E. Szendrei. Absolute scintillation efficiency of anthracene—197(L)
Birnbaum, Milton, Erich Harth, Leo Seren, and Ralph Tobin. (γ,n) thresholds of Cu^{63} and Ag^{109} based on (γ,n) thresholds of N^{14}, O^{16}, and C^{12}—474(A)
—— (see Harth, Erich)—474(A)
—— (see Seren, Leo)—474(A)
Birnbaum, W. (see Smith, F. M.)—765(L)
Biswas, S. N. Approximate solution of Heitler's integral equation—1026(L)
Bitter, F., H. Plotkin, B. Richter, A. Teviotdale, and J. E. R. Young. Magnetic scanning method for investigating hfs and isotope shift—421(L)
Blackadar, A. K. Second law of eddy thermodynamics—1031(A)
Blanchard, C. H. (see Spencer, L. V.)—240(A)
Blatt, John M. and M. H. Kalos. Ground state of deuteron with tensor forces—444(A)
—— (see Kalos, I. M. H.)—444(A)
—— (see Lustig, Harry)—453(A)

Blau, M., A. R. Oliver, and J. E. Smith. Neutron and meson stars induced in light elements of emulsion—949
Bleakney, W. (see Weimer, D.)—1032(A)
Blewett, J. P. (see Courant, E. D.)—202(L)
Blewitt, T. H. Deformation of Cu single crystals at 300° and 78°K—1115
——, **R. R. Coltman, R. E. Jamison, and J. K. Redman.** Stress-strain curves of Cu single crystal at 4.2°K—448(A)
——, **J. K. Redman, and F. A. Sherrill.** Deformation of Cu crystals at 78°K and 300°K—236(A)
—— (see Coltman, R. R.)—236(A)
—— (see Jamison, R. E.)—237(A)
—— (see Redman, J. K.)—448(A)
Bloch, Ingram and Yü-Chang Hsieh. Nuclear shell structure as many-body phenomenon—240(A)
Block, M. M., S. Passman, and W. W. Havens, Jr. Phenomenological interpretation of π^+ meson production by protons on C—210(A)
Bloembergen, N. (see Willenbrock, F. K.)—1281(L)
Bloom, S. D. and C. O. Muehlhause. Design of high-efficiency low-background fast neutron detector—494(A)
—— (see Toppel, B. J.)—473(A)
Bludman, Sidney. Hard-core interpretation of reaction $p+d \rightarrow \pi^+ + t$—487(A)
Bobb, Franklin C. (see Tipton, Isabel H.)—214(A)
Boch, A. L. and E. D. Hudson. Cyclotron efficiency and power distribution measurements—224(A)
Bockelman, C. K. (see Braams, C. M.)—474(A)
—— (see Buechner, W. W.)—1502
Bodansky, D., A. Sachs, and J. Steinberger. Differential cross sections for scattering of 48-Mev π^+ mesons in H—467(A)
Boehm, F. (see Wu, C. S.)—319
Bollinger, Lowell M., G. E. Thomas, and R. R. Palmer. Application of liquid scintillation neutron detector to time-of-flight spectroscopy—452(A)
—— (see Palmer, R. Ronald)—450(A)
—— (see Thomas, G.)—452(A)
Bömmel, H. and J. L. Olsen. Velocity of sound in superconducting Pb and Sn—1017(L)
Bonet, J. V. and A. V. Bushkovitch. Calculation of diamagnetic and paramagnetic susceptibility of N_2—433(A)
Bonner, T. W. (see Bent, R. D.)—472(A)
—— (see Cook, C. F.)—441(A)
Boorse, H. A. (see Worley, R. D.)—1567(L)
Booth, E. C. (see Rasetti, F.)—315; 1192
Borowitz, Sidney (see Mostov, Philip M.)—465(A)
Borst, L. B. (see Kunstadter, J. W.)—594
Bowen, Dwain B. Debye temperature of Cu_3Au—220(A)
Bowers, Raymond. Thickness of saturated He II film—1016(L)
Bowers, W. A. Application of Thomas-Fermi method to calculation of certain molecular vibration frequencies—242(A)
Bowman, J. C., S. Hayes, and R. Smoluchowski. X-ray study of graphitization—244(A)
Boyd, B. A. (see Domenicali, C. A.)—220(A)
Boyer, R. F. Relations between crystallization and second-order transition—225(T)
Bozorth, R. M. (see Williams, H. J.)—1107
Braams, C. M., C. K. Bockelman, C. P. Browne, and W. W. Buechner. Inelastic scattering of protons from Ca^{40}—474(A)
—— (see Ajzenberg, F.)—463(A)
Brabant, J. M., L. W. Cochran, and R. S. Caswell. Average energy of β rays of P^{32} and Ag^{111}—210(A)
Brachman, Malcolm K. and Roland E. Meyerott. Electron distributions for opacity calculations—437(A)
Bradley, L. C., C. C. Van Voorhis, and D. Bershader. Phosphorescence method for study of surface temperatures in supersonic flow field—469(A)
Braid, T. H. Neutron capture γ rays with scintillation spectrometer—442(A)
Braun, O. (see Albers-Schönberg, H.)—1287(L)
Bray, P. J. and R. G. Barnes. Nuclear shielding in H_2 and D_2—475(A)
—— (see Barnes, R. G.)—475(A)
Bray, Ralph and B. R. Gossick. Effect of transit time on Ge rectifier behavior—1011(L)
—— **and F. van der Maesen.** Thick p-n junctions in Ge—231(A)
Breckenridge, Robert G. Semiconducting intermetallic compounds—461(T)
—— **and William R. Hosler.** Electrical properties of TiO_2 semiconductors—793
——, **W. R. Hosler, and W. Oshinsky.** Electrical properties of InSb—243(A)
Breit, G. (see Thaler, R. M.)—454(A)
Breneman, Edward J. and Dudley Williams. Molecular rotation in liquids—465(A)
Brice, M. K. (see Cork, J. M.)—76; 497(A)
Bridge, H. S., H. Courant, H. DeStaebler, Jr., and B. Rossi. Recent experimental results on S particles—1024(L)
——, **C. Peyrou, B. Rossi, and R. Safford.** V^0 particles in multi-plate cloud chamber—362
Briggs, G. R., S. Singer, and W. K. Jentschke. α-α scattering at 21.8 and 22.9 Mev (proportional counter)—438(A)
Briggs, H. B. and R. C. Fletcher. Absorption of infrared light by free carriers in Ge—1342
—— (see Tanenbaum, M.)—1561(L)
Brooks, Harvey. Cohesive energy of alkali metals—1027(L)
—— 1952 NRC Conference on nature and properties of surfaces of solids—239(T)
Brown, Alexander and F. T. Reding. Infrared study of crystallization of polyethylene—226(A)
Brown, B. M. and D. H. Tomboulian. Nuclear moments of Ta^{181}, erratum—1580(E)
Brown, Fielding and George T. Reynolds. Cosmic-ray star production rates in gases—444(A)
Brown, Frank B., Jr., and A. V. Masket. Star clustering in nuclear emulsions—210(A)
Brown, H. N. (see Shore, F. J.)—1203
Brown, James B. He film flow—489(A)
Brown, R. J. S., K. F. Famularo, H. D. Holmgren, and D. M. Van Patter. Differential cross sections for elastic scattering of 1.0- to 3.25-Mev deuterons by He^3—438(A)
Brown, W. L. n-type surface conductivity on p-type Ge—518
—— **and R. C. Fletcher.** Annealing of bombardment damage in Ge: Experimental—237(A)
—— (see Fletcher, R. C.)—237(A)
Browne, C. P. (see Braams, C. M.)—474(A)
—— (see Buechner, W. W.)—1502
Brueckner, K. A. Radiative corrections to nuclear forces in pseudoscalar theory—761(L)
——, **J. Gell-Mann, and M. L. Goldberger.** Damping of virtual nucleon-pair formation in pseudoscalar meson theory—460(A)
—— (see Chappelear, J.)—480(A)
—— (see Watson, K. M.)—460(A)
Buck, Warren L. (see Swank, Robert K.)—495A; 927
Buder, E. E., J. J. Ruddick, and A. H. Weber. Photoemission of W in region of predicted Schottky deviations—561
Bueche, A. M. Reinforcement of silicone rubber—211(T)

Buechner, W. W., A. Sperduto, C. P. Browne, and C. K. Bockelman. Excited states of K^{40}—1502
—— (see Ajzenberg, Fay)—463(A); 674
—— (see Braams, C. M.)—474(A)
—— (see Sperduto, A.)—473(A)
Bunbury, D. StP. β decay of Li^8, erratum—1580(E)
Bunker, M. E., R. J. Prestwood, and J. W. Starner. Scintillation study of As^{77} and Br^{77}—1021(L)
—— (see Ames, D. P.)—68
—— (see Knight, J. D.)—889
Bunn, C. W. Molecular structure and crystallizability of polymers—225(T)
—— Recent work on structures of crystalline polymers—225(T)
Burke, Edward W. Isotope shift in B III—457(A)
Burkhardt, James L. Dipole photonuclear reactions and independent particle model—420(L)
Burrus, C. A. (see Trambarulo, R.)—222(A)
Burson, S. B. and W. C. Jordan. Argonne Laboratory scintillation coincidence spectrometer—498(A)
—— (see Jordan, W. C.)—497(A)
Burstein, Eli. Optical and photoconductive investigations of impurity levels in Ge and Si—213(T)
—— (see Lax, Melvin)—208(A); 492(A)
—— (see Sclar, N.)—215(A)
Burton, R. L. (see Cobbs, W. H., Jr.)—225(A)
Bushkovitch, A. V. (see Bonet, J. V.)—433(A)
—— (see Herbst, R. F.)—442(A)
Buskirk, A. V., L. R. Etter, C. J. Karzmark, R. H. Rediker, and R. W. Thompson. Magnetic cloud-chamber observations of V particles. I. Apparatus and reduction of data—445(A)
—— (see Thompson, R. W.)—446(A)
Butler, J. P. and J. S. Adam. Radiations of Ra^{227}—1219
Butler, S. T. Stripping and three-body system—488(T)
—— (see Austern, N.)—453(A)
—— (see Friedman, M. H.)—465(A)
Butler, W. A. and G. M. Almy. Photoprotons from Mo^{100} and Mo^{92}—58
Byatt, William J. Calculating approximate cross sections for electron scattering—240(A)
Byram, E. T., T. Chubb, H. Friedman, and N. Gailar. Lyman-α radiation in solar spectrum—1278(L)

Cabrera, N. Role of nucleation-theory in crystal growth—232(T)
Caldwell, W. C. (see Johnson, R. G.)—466(A)
Callen, Herbert B. Thermodynamics of irreversible processes—239(T)
—— (see Dank, M.)—229(A)
—— (see Harrison, Sol E.)—205(A)
—— (see Offenbacher, Elmer L.)—1580(E)
Cameron, A. G. W. and M. M. Hoffman. Angular and energy distributions of photoprotons from Al and Ta—473(A)
Cameron, J. R. (see Eppling, F. J.)—438(A)
Campbell, E. C. and F. Nelson. Chemical separation of 0.82-sec Pb^{207m} from Bi^{207}—499(A)
Campbell, R. B. (see Franklin, A. D.)—205(A)
Campbell, W. H. and J. I. Hopkins. Terphenyl-B liquid neutron detector—224(A)
Carlson, B. C. (see Gerhart, J. B.)—455(A)
Carlson, R. O. (see Fabricand, B. P.)—1403
—— (see Lee, Charles A.)—1395
Carlton, A. G. Optimum filter design for incompletely specified filter and noise processes—438(T)
Carmichael, B. M., M. B. Sampson, and O. E. Johnson. Inelastic scattering of alphas from N^{14}—473(A)
Carr, Howard E. Negative ions in gaseous phase—209(T)
—— (see Baldock, Russell)—242(A)
Carroll, Thomas J. Propagation of short radio waves well beyond horizon—458(A)
Carter, R. S., H. Palevsky, and V. W. Myers. Absorption cross section of Au and B for thermal and cold neutrons—450(A)
—— (see Myers, V. W.)—451(A)
Cartwright, W. F., C. Richman, M. N. Whitehead, and H. A. Wilcox. Production of positive pions by 341-Mev protons on protons—677
—— (see Oxley, C. L.)—419(L)
Case, K. M. and H. Mendlowitz. Measurement of gyromagnetic ratio for free electron: precession and depolarization—475(A)
—— (see Moldauer, P.)—459(A)
Caswell, R. S. (see Brabant, J. M.)—210(A)
Caulk, H. M. (see Davis, L. R.)—431(A)
Chandrasekhar, S. Thermal instability in hydrodynamics and hydromagnetics—488(T)
—— Thermonuclear reactions with light nuclei in stars—488(T)
——, **Donna Elbert, and Gerhard Herzberg.** Shift of 1^1S state of He—1172
Chang, Hung-Chi. Electric conduction at metal-semiconductor and metal-solution interfaces—214(A)
—— (see Morris, L. W.)—215(A)
Chappelear, J. and K. A. Brueckner. Photoproduction of mesons in D—480(A)
Charney, Jule. Use of high-speed computing machines in meteorological predictions—488(T)
Chase, C. E. Ultrasonic measurements in liquid He—489(A)
Chase, D. M. (see Rohrlich, F.)—454(A)
Chatterjee, Santimay and Ajit Kumar Saha. γ-γ angular correlation measurements—200(L)
Cheo, Peter (see Loh, H. Y.)—221(A)
Chiba, R. (see Takemoto, S.)—1024(L)
Chilton, A. B., J. N. Cooper, and J. C. Harris. Stopping power of several elements for protons—495(A)
Chou, C. N. Energy spectra of cosmic-ray photons and electrons from plastic scintillation counter measurements—433(A)
Chraplyvy, Zeno V. Approximate two-body relativistic wave equations—478(A)
—— Reduction of relativistic two-particle wave equations to approximate forms—388
Christian, R. S. and J. L. Gammel. Elastic scattering of protons and neutrons by deuterons—100
Christian, Russell H. and John M. Walsh. Experimental method to determine equation-of-state data for solids by shock-wave measurements—1030(A)
Chubb, T. (see Byram, E. T.)—1278(L)
Clark, A. E., R. A. Grandey, S. K. Kao, and L. Mann. Elastic scattering in nuclear emulsions—467(A)
Clark, G. (see Bassi, P.)—432(A)
Clark, L. B., Sr. Transparent, nonmetallic, electrically conducting film applications—471(A)
Clarke, Edward N. Oxygen-induced surface conductivity on Ge—756(L)
—— **and Robert L. Hopkins.** Electrical conductivity of mechanically distributed Ge surfaces—1566(L)
Clarke, R. L. (see Paul, E. B.)—463(A)
Cleland, J. W., D. S. Billington, and J. H. Crawford, Jr. Low-temperature fast-neutron bombardment of Cu-Be alloy—238(A)
—— (see Crawford, J. H., Jr.)—243(A)
Clement, J. D. (see Okazaki, A.)—440(A)
Clotfelter, B. E. Hall effect in flowing ion clouds—436(A)

Cobbs, W. H., Jr., S. B. Cole, and R. L. Burton. Orientation in polymeric films by infrared and x-ray techniques—225(A)
Cochran, J. F. (see Mapother, D. E.)—216(A)
Cochran, L. W. (see Brabant, J. M.)—210(A)
—— (see Jenkins, G. L.)—210(A); 915
Coester, F. Influence of extranuclear fields on γ-γ directional correlations—452(A)
Cohen, Bernard L. Ga^{64}—74
—— Statistical theory of nuclear reactions—241(A)
——, **R. V. Neidigh, and E. Newman.** Measurement of angular distributions of nuclear reaction products with internal cyclotron beam—486(A)
—— (see Newman, E.)—486(A)
Cohn, Hans O., L. R. Etter, and R. W. Thompson. Cluster-count determination of specific ionization of cloud-chamber tracks—445(A)
Cole, F. T. and H. A. Bethe. Capture of μ mesons in matter—481(A)
Cole, S. B. (see Cobbs, W. H., Jr.)—225(A)
Collins, F. C. Time lag in spontaneous nucleation due to non-steady-state effects—232(T)
Collins, R. J. and H. Y. Fan. Infrared absorption in n-type Ge—230(A)
—— (see Kaiser, W.)—230(A); 1380
Collins, T. L., W. H. Johnson, Jr., and A. O. Nier. Second minimum in packing fraction curve at 40 neutrons—482(A)
Coltman, R. R. and T. H. Blewitt. Effect of fast-neutron bombardment on diffusion in Cu_3Au—236(A)
—— (see Blewitt, T. H.)—448(A)
—— (see Redman, J. K.)—448(A)
Conwell, Esther M. Electrical properties of n-type Ge—208(A)
Cook, C. F. and T. W. Bonner. Scattering of 14–18 Mev neutrons in light elements—441(A)
Cook, Charles J., Emerson Jones, Jr., and Theodore Jorgensen, Jr. Range-energy relations of 10–250 kev protons and He ions in various gases—1417
Cool, R. L. (see Piccioni, O.)—433(A)
Cooper, C. Dewey. Near uv absorption spectrum of p-difluorobenzene vapor—241(A)
Cooper, J. N. (see Chilton, A. B.)—495(A)
Cooper, L. N. and E. M. Henley. μ-mesic atom—480(A)
Coor, T. (see Hornyak, W. F.)—463(A)
Corey, H. E. (see Vogel, F. L.)—230(A)
Cork, J. M., J. M. LeBlanc, W. H. Nester, and M. K. Brice. Nuclear levels in Cs^{131}—76; Radioactive decay of Ba^{131}—497(A)
—— (see Jordan, W. C.)—497(A)
Couling, L. and R. Smoluchowski. Anisotropy of grain boundary diffusion—245(A)
Coulliette, J. H. (see McCay, M. S.)—213(A)
Courant, E. D. Field inhomogeneities in alternating gradient synchrotron—456(A)
——, **M. S. Livingston, H. S. Snyder, and J. P. Blewett.** Origin of strong-focusing principle—202(L)
Courant, H. (see Bridge, H.)—1024(L)
Cowan, D. A. (see Gursky, Herbert)—209(A)
Cox, Everett F. Degeneration of shock wave into sound—1030(A)
Cox, J. T., P. B. Peyton, Jr., and Walter Gordy. Zeeman effect in microwave spectra of CH_3F and CH_3CCD—222(A)
Crane, H. R., R. W. Pidd, and W. H. Louisell. Method of measuring gyromagnetic ratio of free electron—475(A)
—— (see Louisell, W. H.)—475(A)
Crane, W. W. T. (see Batzel, R. E.)—939
Crawford, Frank S., Jr., and M. Lynn Stevenson. $p + p \rightarrow d + \pi^+$ cross section at 340 Mev and 327 Mev—468(A)
Crawford, George W. Measurement of thickness of thin films by employing electron microscope shadowcasting technique—214(A)
Crawford, J. H., Jr., J. W. Cleland, D. K. Holmes, and J. C. Pigg. Thermally unstable disorder in p-type Ge produced by fast neutron bombardment—243(A)
—— (see Cleland, J. W.)—238(A)
Crawford, M. F. and I. R. Dagg. Infrared absorption induced by static electric fields—1569(L)
Crittenden, E. C., Jr., and H. Dieckamp. Change of elastic constants resulting from annealing of Cu and Al cold worked at $-196°C$—232(A)
Croft, George T. and Foster C. Nix. de Haas-van Alphen effect in Sn-Sb alloys—212(A)
Crowell, A. D. (see Soller, T.)—1058
Cummins, William E. Forces and moments acting on body in time-varying potential stream—1029(T)
Cunningham, J. A. Multichannel pulse-height analyzer using storage tube—437(A)
Cutler, M. (see Becker, M.)—491(A)
Czyzak, S. J. (see Wessel, Walter)—986

Dagg, I. R. (see Crawford, M. F.)—1569(L)
Dailey, B. P. (see Solimene, N.)—464(A)
Dalgarno, A. Three-body scattering problems—198(L)
Daly, Richard T., Jr., and Jerrold R. Zacharias. Doppler effects in atomic-beam magnetic-resonance method—476(A)
Damm, C. C. and Lincoln G. Smith. Doublet measurements with mass synchrometer—482(A)
—— (see Smith, Lincoln G.)—481(A)
Danforth, W. E. (see Weinreich, O. A.)—231(A)
Danielson, G. C. (see Gardner, W. R.)—220(A)
—— (see Shaw, William C.)—208(A)
Dank, M. and H. B. Callen. Iteration-variation calculation of electronic structure of diamond—229(A)
Danos, Michael and Stanley Geschwind. Broadening of microwave absorption lines due to wall collisions—1159
Darden, S. E. (see Fields, R. E.)—441(A)
Darin, S. R. (see Taylor, G. R.)—211(A)
Darling, B. T. and P. R. Zilsel. Theory of finite displacement operators and fundamental length—1252
Dash, J. G. (see Goldstein, L.)—490(A)
—— (see Sommers, H. S., Jr.)—489(A)
Daunt, J. G. (see Heer, C. V.)—412(L)
—— (see Horowitz, M.)—1099
Davidson, J. P. Spectrum and half-life of κ meson—1020(L)
—— and **D. C. Peaslee.** Cross terms in allowed shape β spectra—1232
—— and **D. C. Peaslee.** $1/W$ terms in allowed β spectra—442(A)
Davies, E. B. (see Stoner, R. G.)—1032(A)
Davis, L. R., H. M. Caulk, and C. Y. Johnson. Intensity of primary protons and α particles—431(A)
Davis, Luther, Jr., Lawrence Rubin, and W. D. Straub. Recording of temperature-dependent electrical properties of semiconductors—490(A)
Davis, R. H. (see Eppling, F. J.)—438(A)
Davis, V. (see DeCarvalho, H. G.)—224(A)
Davisson, J. W. Electrical breakdown path orientation in alkali halide crystals—228(A)
—— (see Sclar, N.)—215(A)
Day, Harold R. Irradiation-induced photoconductivity in MgO—238(A); 822
Day, Robert B. (see Huus, Torben)—599
Dayton, B. and D. Willard. Decay of V^0 particle into two mesons—348

Dazai, T. (see Takemoto, S.)—1024(L)
DeBenedetti, S. (see Leipuner, L.)—198(L)
DeBretteville, A., Jr. Threshold field and free energy for antiferroelectric-ferroelectric phase transition in $PbZrO_3$—213(A)
Debye, Peter P. Hall effect and conductivity of Ge containing As or Ga as impurities—208(A)
DeCarvalho, H. G., V. Davis, and W. Tesh. Gradation development method for nuclear emulsions—224(A)
Dehmelt, H. G. Nuclear quadrupole resonance in rhombic S and quadrupole moments of S^{33} and S^{35}—313
de Klerk, D. and R. P. Hudson. Adiabatic demagnetization of chromium methylamine alum—278
DeLollis, N. J. (see Ehrlich, P.)—218(A)
DePasquali, G. (see Eby, F. S.)—495(A)
der Mateosian, E. and C. S. Wu. Decay and β spectrum of I^{129}—497(A)
de-Shalit, A. Energy levels of odd-odd nuclei—1479; Ground state of odd-odd nuclei—443(A)
—— (see Mihelich, J. W.)—78; 498(A)
Deshotels, W. J. and A. H. Weber. Effect of strong electrostatic fields on resistance of W wires—448(A)
DeStaebler, H., Jr. (see Bridge, H.)—1024(L)
Deutsch, R. W. Secondary particles resulting from high-energy bombardment—485(A)
Devaney, Joseph J. Theory of α decay—587
Deverall, G. V., K. W. Meissner, and G. J. Zissis. Hfs of resonance lines of In^{115}—297
Dewan, J. T. (see Almqvist, E.)—1022(L)
DeWire, J. (see Wolfe, B.)—446(A)
DeWitt, T. W. (see Padden, F. J.)—217(A)
—— (see Zapas, L. J.)—217(A)
Dexter, D. L. Small-angle scattering of x-rays from cold-worked crystals—448(A)
—— **and W. R. Heller.** Quantum theory of polarizability of idealized crystal—273
Dicke, R. H. (see Hawkins, W. B.)—1008(L)
Dieckamp, H. (see Crittenden, E. C., Jr.)—232(A)
Dienes, G. J. Variable activation energy and motion of lattice defects—1283(L)
—— **and D. A. Kleinman.** Nature of radiation damage in diamond—238(A)
Dillinger, J. R. (see Knudsen, W. C.)—489(A)
Ditzenberger, J. A. (see Fuller, C. S.)—193(L)
Divatia, Ajay S. (see Eppling, F. J.)—438(A)
Dixon, C. E. and C. J. Meechan. Hardness change in Cu irradiated with 1.25-Mev electrons—237(A)
Dobischek, Dietrich, Harold Jacobs, and John Freely. Mechanism of self-sustained electron emission from MgO—804
Dolan, W. W. Current density tables for field emission theory—510
——, **W. P. Dyke, and J. K. Trolan.** Field emission initiated vacuum arc. II. Resistively heated emitter—1054
Dolecek, R. L. Adiabatic magnetization of superconducting sphere—216(A); 490(A)
Domenicali, C. A. and B. A. Boyd. Thermoelectric power and electrical resistivity of dilute solid solution of Si in Cu—220(A)
Donahoe, F. J. Field and temperature dependence of de Haas-van Alphen effect in Zn alloy single crystals—212(A)
Donahue, D. J. (see Jones, K. W.)—879
Donahue, T. M. (see Foderaro, A.)—1561(L)
Douglas, C. A. Atmospheric transmission of light—459(T)
Douglas, R. A. (see Galonsky, A.)—439(A)
—— (see Haeberli, W.)—438(A)
—— (see Jones, K. W.)—482(A); 879
Doyle, Barbara (see Hutchinson, Franklin)—493(A)
—— (see Setlow, Richard)—494(A)
Drawbaugh, Donald (see Dresden, M.)—478(A)
Drell, S. D. and Kerson Huang. Many-body forces and nuclear saturation—1527
——, **K. Huang, and V. F. Weisskopf.** Many-body forces and nuclear saturation—460(A)
Dresden, M. and Donald Drawbaugh. Modified random walk problems—478(A)
Dresner, Lawrence. Spin-orbit coupling in pseudoscalar meson theory—201(L)
Duckworth, Henry E. (see Hogg, Benjamin G.)—1289(L)
DuMond, Jesse W. M. (see Hoyt, Harry C.)—1027(L)
Dunbar, D. N. F., H. K. Reynolds, W. A. Wenzel, and W. Whaling. Stopping cross section of gases for protons and deuterons—496(A)
Dungey, J. W. Origin of cosmic rays—766(L)
Dunlap, W. C., Jr. Acceptor states of Au in Ge—208(A)
—— Electrical properties of Au-Ge alloys—1282(L)
Dyke, W. P., J. K. Trolan, E. E. Martin, and J. P. Barbour. Field emission initiated vacuum arc. I. Experiments on arc initiation—1043
—— (see Dolan, W. W.)—1054
Dyson, F. J. Mass-renormalization with Tamm-Dancoff method—421(L)
—— Scattering of mesons by protons—499(T)
—— Wave function of relativistic system—1543

Earle, M. D. (see Bearden, J. A.)—482(A)
Easterday, Harry T. Radioactivity of Cu^{67}—653
Eatherly, W. P. Theoretical and experimental studies of electronic phenomena in graphite—239(T)
—— (see Rodeback, G. W.)—237(A)
Eby, F. S., W. K. Jentschke, and G. DePasquali. Response of NaI(Tl) scintillation crystals as function of Tl concentration—495(A)
Eckart, Carl. Relation between time-averages and ensemble-averages in statistical dynamics of continuous media—784
Edwards, David F. (see Green, Alex E. S.)—46; 443(A)
Eggen, D. T. and M. J. Laubenstein. Displacement energy for radiation damage in Cu—238(A)
Ehrlich, P. and N. J. DeLollis. Dielectric relaxation in styrene-acrylonitrile copolymer during and after its polymerization—218(A)
Eiland, P. F. (see Pepinsky, R.)—229(A)
Elbert, Donna (see Chandrasekhar, S.)—1172
Elder, Tait (see Benesch, William)—308
Elkind, M. M. and A. Sperduto. Energy levels of B^{11} and B^{12} by (d,p) reaction—463(A)
—— (see Sperduto, A.)—473(A)
Elliott, J. F., S. Legvold, and F. H. Spedding. Magnetic properties of Gd metal—28
Elliott, N. and M. Wolfsberg. Magnetic susceptibility of Wurster's blue between 65° and 356°K—435(A)
Engler, Nicholas A. (see Green, Alex E. S.)—40
Eppling, F. J., J. R. Cameron, R. H. Davis, Ajay S. Divatia, A. I. Galonsky, E. Goldberg, and R. W. Hill. Elastic scattering of protons—438(A)
Epstein, P. S. Absorption of sound in fogs and emulsions—458(A)
Epstein, Saul T. Causal interpretation of quantum mechanics—985
Erickson, R. A. and L. D. Roberts. Apparatus for magnetic measurements at low temperatures—216(A)
—— (see Roberts, L. D.)—488(A)
Eshelby, J. D. Tentative theory of metallic whisker growth—755(L)
Etter, L. R. (see Buskirk, A. V.)—445(A)
—— (see Cohn, Hans O.)—445(A)
—— (see Thompson, R. W.)—446(A)
Ewald, A. H. Solubility of solids in gases—215(A)
Ewald, A. W. Preparation of gray Sn filaments—244(A)

Fabricand, B. P., R. O. Carlson, C. A. Lee, and I. I. Rabi. Molecular beam investigation of rotational transitions. II. Rotational levels of KBr and their hfs—1403
—— (see Lee, Charles A.)—1395
Fader, W. J. (see Sperduto, A.)—473(A)
Fainberg, Joseph (see Schein, Marcel)—479(A); 973
Fairbank, Henry A. (see King, J. C.)—489(A)
Fairbank, W. M. (see Soller, T.)—1058
Famularo, K. F. and G. C. Phillips. Accurate determinations of nuclear reaction energies—1195
—— (see Brown, R. J. S.)—438(A)
—— (see Phillips, G. C.)—462(A)
Fan, H. Y. Infrared absorption in elementary semiconductors—213(T)
—— (see Collins, R. J.)—230(A)
—— (see Forster, J. H.)—229(A)
—— (see Gebbie, H. A.)—230(A)
—— (see Kaiser, W.)—230(A); 1380
—— (see Navon, D.)—491(A)
Fano, U. and L. V. Spencer. Energy spectrum resulting from electron slowing-down—240(A)
Farquhar, R. M. (see Russell, R. D.)—1223
Faust, W. R. (see Scherrer, V. E.)—768(L); 1476
Fechter, H. R. (see Hofstadter, R.)—422(L); 439(A)
Feld, Bernard T. Role of nucleon isobar in high-energy interactions—454(A)
Ferguson, A. J. and H. E. Gove. Resonances in $S^{32}(p,p)S^{32}$—439(A)
Fermi, Enrico. Nucleon polarization in pion-proton scattering—947
—— (see Anderson, H. L.)—155
—— (see Martin, R. L.)—467(A)
Ferry, John D. Relaxation distribution functions of polymers and their concentrated solutions and gels—218(T)
——, **Lester D. Grandine, Jr., and Edwin R. Fitzgerald.** Relaxation distribution function of polyisobutylene in transition from rubberlike to glasslike behavior and its dependence on temperature—217(A)
—— (see Fitzgerald, Edwin R.)—217(A)
Feshbach, Herman, C. E. Porter, and V. F. Weisskopf. Theory of total neutron cross sections—453(A)
—— (see Lomon, Earle)—454(A)
Feynman, R. P. Atomic theory of λ transition in He—1291; Atomic theory of liquid He near 0°K—1301
Fields, R. E., R. K. Adair, R. L. Becker, and S. E. Darden. Total n-p cross section at 1 Mev—441(A)
Fillnow, R. H., E. K. Halteman, and G. F. Mechlin. X-ray and metallurgical studies on neutron-irradiated Cu_3Au—236(A)
Fink, Richard W. and Edwin O. Wiig. Radiations of neutron-deficient Ba and Ce nuclides—194(L)
Finn, George. Evaporation of Cu from Ge—754(L)
Fireman, E. L. Measurement of (n,H^3) cross section in N and its relationship to T production in atmosphere—922
Firle, T. (see Becker, M.)—491(A)
Fisher, John C. Applications of dislocation theory to plastic deformation—205(T)
—— Strength of solid solution alloys—232(A)
Fisher, L. H. (see Kachickas, G. A.)—775
Fitzgerald, Edwin R., Lester D. Grandine, Jr., and John D. Ferry. Dynamic mechanical properties of polyisobutylene—217(A)
—— (see Ferry, John D.)—217(A)
Fleeman, Jerome. Effect of neutron irradiation on phase change in Sn—237(A)
Fletcher, R. C., W. L. Brown, and S. Machlup. Annealing of bombardment damage in Ge: Theoretical—237(A)
—— (see Briggs, H. B.)—1342
—— (see Brown, W. L.)—237(A)
Fletcher, W. H. (see Parker, F. W.)—235(A)
—— (see Shelton, R. D.)—235(A)
Flory, P. J. Equilibrium theory of crystallization—225(T)
Flowers, J. W. (see Shreckengost, R. C.)—224(A)
Floyd, J. J. (see Kunstadter, J. W.)—594
Foderaro, A. and T. M. Donahue. Production of sodium airglow excitation by imprisonment of resonance radiation—1561(L)
Foland, W. D. (see Tipton, Isabel H.)—214(A)
Foley, H. M. (see Sessler, A. M.)—444(A)
Follin, J. W., Jr. (see Alpher, R. A.)—479(A)
Foner, Simon. Hall effect in pure Ti, V, and Cr—447(A)
—— **and Emerson M. Pugh.** Hall effect in ordered and disordered Ni_3Mn—220(A); Hall effects of Co-Ni alloys and of Armco iron—20
Fonger, William H. Cosmic radiation intensity time variations and their origin. II. Energy dependence of 27-day variations—351
Foote, H. L., Jr. Low-energy neutron resonance scattering—450(A)
—— (see Sailor, V. L.)—450(A)
Foote, R. S. and Ben Petree. Operation of electromagnetic electron beam extractor—456(A)
—— (see Koch, H. W.)—455(A)
Ford, Kenneth W. (see Wilets, Lawrence)—1488
Forro, M. Method for determination of maximum energy of weak β emitters—483(A)
Forster, J. H., H. Y. Fan, and K. Lark-Horovitz. Deuteron irradiation of Ge near liquid N temperature—229(A)
Fosdick, Lloyd D. and Hubert M. James. New approximation method for order-disorder problems—1131
Fourie, D. J. Photoelectric effect of thin Bi films—803
Fowler, E. C., W. B. Fowler, R. P. Shutt, A. M. Thorndike, and W. L. Whittemore. Diffusion cloud chamber study of pion interactions in H and He—135
Fowler, J. L., C. H. Johnson, and J. R. Risser. Angular distribution of neutrons scattered from N—441(A)
Fowler, W. A. Experimental results on nuclear reactions in stars—456(T)
—— **and R. G. Thomas.** Analysis of $N^{15}(p,\alpha)C^{12}$ excitation function—473(A)
—— (see Warters, W. D.)—917
Fowler, W. B., R. P. Shutt, A. M. Thorndike, and W. L. Whittemore. Multiple pion production in n-p collisions observed at the cosmotron—758(L)
——, **R. P. Shutt, A. M. Thorndike, and W. L. Whittemore.** Pions and protons from target bombarded by 2.3-Bev protons in cosmotron—479(A)
——, **R. P. Shutt, A. M. Thorndike, and W. L. Whittemore.** Production of V_1^0 particles by π^- mesons in H—1287(L)
—— (see Fowler, E. C.)—135
Francis, Norman C. and Kenneth M. Watson. Elastic scattering of particles by atomic nuclei—454(A)
Frank, Wilson J., Kenneth C. Bandtel, Richard Madey, and Burton J. Moyer. Angular distribution of process $p+d \rightarrow t+\pi^+$—487(A)
—— (see Bandtel, Kenneth C.)—487(A)
—— (see Godfrey, Charles)—487(A)
Franklin, A. D., R. B. Campbell, and J. A. Weinman. Measurement of particle size of ultrafine ferromagnetic powders—205(A)
—— (see Berkowitz, A. E.)—206(A)
Frauenfelder, H. (see Lawson, J. S., Jr.)—484(A); 649
Frazer, B. C. Phase transition in $ND_4D_2AsO_4$—246(A)
—— **and Ray Pepinsky.** Phase transition in CsH_2AsO_4—212(A)
Frederikse, H. P. R. Thermoelectric power in Ge single crystals—491(A)

Freely, John (see Dobischek, Dietrich)—804
Freeman, A. J. Effective nuclear charges for atoms from self-consistent field calculations—1410
Freier, P. S. (see Anderson, G. W.)—431(A)
Freistadt, Hans. Electromagnetic mass in Darling's theory of elementary particles—478(A)
Fremlin, J. H. Nuclear reactions with cyclotron-accelerated He^3—488(T)
French, J. B. and Y. Shimamoto. Theory of multipole radiation—898
Fried, B. D. and R. J. Riddell, Jr. Tomonaga approximation—460(A)
Friedlander, G., Elizabeth Wilson, A. Ghiorso, and I. Perlman. Genetic relationships of 0.8-sec Pb^{207m} isómer—498(A)
—— (see Miller, J. M.)—485(A)
—— (see Welker, Joan P.)—484(A)
Friedman, H. (see Byram, E. T.)—1278(L)
Friedman, M. H. and S. T. Butler. Bose-Einstein condensation of imperfect gas—465(A)
Friedman, Murray. Influence of host in determining radiation sensitivity of bacterial virus—494(A)
Friedrich, L. W. and V. P. Jacobsmeyer. Electrical properties of elementary B—492(A)
Frisch, Harry L. Equipartition principle of generalized canonical ensembles—477(A); 791
—— (see Willis, Charles)—465(A)
Froehlich, Fritz E. and Kurt Sitte. Mean free path for shower production by high-energy π mesons—433(A)
Froman, Darol, James Kenney, and Victor H. Regener. Collision lengths of neutral, penetrating-shower-producing cosmic radiation in light and heavy water—707
Frost, Albert D., Charles R. Mingins, and Lawrence A. Howard. Electric wave filter combining piezoelectric divided electrode units—471(A)
Frost, R. T. and S. S. Hanna. $Li^6(d,t)Li^7(p)He^4$ reaction—462(A)
Frost, Robert H. and Carl E. Nielsen. Specific probable ionization of electrons observed with Wilson cloud chamber—864
Fry, W. F. Nuclear capture of μ^- mesons in photographic emulsions—481(T)
—— π^+ meson production by π^- mesons—1576(L)
—— Unusual π-μ decays in photographic emulsions—130
—— (see John, W.)—1234
Fuller, C. S. and J. A. Ditzenberger. Diffusion of Li into Ge and Si—193(L)
Fultz, Dave. Experiments in fluid mechanics for meteorological purposes—488(T)
Fung, Si Chang and A. Turkevich. Production of Cu radioactivity in interaction of negative pions and muons with Zn—480(A)
Furst, Milton and Hartmut Kallmann. Fluorescence, phosphorescence, and photostimulation of NaCl (AgCl) with high-energy irradiation—1356; Fluorescent light yields with α, β, and γ radiations—766(L)
Fusfeld, Herbert I. Comparison of resistivity and density changes in cold-worked brass—233(A)
Fuson, Nelson, Marie-Louise Josien, and Conrade C. Hinds. Infrared analysis of associated O−H and O−D stretching vibrations of simple carboxylic acids—234(A)
—— (see Josien, Marie-Louise)—235(A)

Gaerttner, E. R. (see Albert, R. D.)—451(A)
—— (see Yeater, M. L.)—451(A)
Gailar, N. (see Byram, E. T.)—1278(L)
Galonsky, A. I., W. Haeberli, E. Goldberg, and R. Douglas. Inelastic scattering of protons by Ne—439(A)
—— (see Eppling, F. J.)—438(A)
—— (see Haeberli, W.)—438(A)
Gammel, J. L. (see Christian, R. S.)—100
Gardner, W. R. and G. C. Danielson. Electron density in sodium tungsten bronze—220(A)
Garrett, R. E., F. L. Hereford, and B. W. Sloope. Inelastic scattering of *d*-*d* neutrons—441(A)
Garth, R. C. (see Hughes, D. J.)—1423
Garwin, R. L. Thermalization of positrons in metals—1571(L)
Gasiorowicz, S. Phenomenological study of meson-nucleon scattering—481(A)
Geballe, Ronald (see Harrison, Melvin A.)—1
Gebbie, H. A., M. Nisenoff, and H. Y. Fan. Photoconductivity and carrier traps in Ge—230(A)
Geisler, A. H. (see Wilson, V. C.)—494(A)
Geller, M. (see von Hippel, A.)—568
Gell-Mann, Murray and M. L. Goldberger. Formal theory of scattering—398
—— **and Valentine L. Telegdi.** Consequences of charge independence for nuclear reactions involving photons—169
—— (see Brueckner, K. A.)—460(A)
Gerhart, J. B., R. Sherr, and B. C. Carlson. Annihilation of fast positrons in flight—455(A)
—— (see Sherr, R.)—909
Gerjuoy, E. Theory of (d,p) reactions—453(A); 645
Geschwind, Stanley (see Danos, Michael)—1159
Ghiorso, A. (see Friedlander, G.)—498(A)
Ghosh, S. N. (see Trambarulo, R.)—222(A)
Gibbons, J. H. and Henry W. Newson. Neutron resonances in Bi, Tl, and Pb—209(A)
Gibbs, Julian H. Ferroelectricity in rochelle salt—447(A)
Gifford, Frank, Jr. Turbulent diffusion from volume source with nonuniform initial distribution—1031(A)
Gilleo, M. A. Photoemission from Ag into AgCl, KBr, NaCl, and new bands of photosensitivity in AgCl—534
Gillon, L. P. (see Mihelich, J. W.)—498(A)
Gilmore, F. R. Compressibility and thermal effects in cavitation—1029(T)
Gilpatrick, L. O. (see Baldock, Russell)—242(A)
Givin, H. H. (see Jenkins, G. L.)—210(A)
Glaser, Donald A. Bubble chamber tracks of penetrating cosmic-ray particles—762(L); Possible bubble chamber for study of ionizing events—496(A)
Glasser, R. G. (see Schein, Marcel)—479(A); 973
Glauber, Roy J. Potential scattering at high energies—459(A)
Glick, Harvey L. and W. F. Witzig. Resistivity of Cu_3Au during neutron irradiation—236(A)
Godfrey, Charles, Kenneth C. Bandtel, Wilson J. Frank, and Richard Madey. Production of tritons in *d*-*d* collisions—487(A)
Goertz, Matilda (see Williams, H. J.)—1107
Gokhale, G. S. (see Rao, A. S.)—764(L)
Goldberg, E. (see Eppling, F. J.)—438(A)
—— (see Galonsky, A.)—439(A)
—— (see Haeberli, W.)—438(A)
Goldberg, M. D. and J. A. Harvey. Coherent cross sections of Fe and Ni—451(A)
Goldberger, M. L. (see Brueckner, K. A.)—460(A)
—— (see Gell-Mann, M.)—398
Goldemberg, J. (see Montalbetti, R.)—659
Goldgraber, Howard D. Configuration interaction in Mo II—456(A)
Goldhaber, Gerson and S. Goldhaber. Inelastic scattering of negative pions—467(A)
Goldhaber, S. (see Goldhaber, Gerson)—467(A)
Goldman, J. E. (see Urquhart, Helen M. A.)—435(A)
Goldowski, N. Is it possible to teach physics to humanities students?—227(A)

Goldschmidt-Clermont, Y., L. S. Osborne, and A. W. Winston. Angular distribution of mesons from 320-Mev photons on protons—468(A)
Goldstein, Jack S. Properties of Salpeter-Bethe two-nucleon equation—461(A); 1516
Goldstein, L., H. S. Sommers, Jr., and J. G. Dash. Transmission of slow neutrons by liquid He—490(A)
Good, R. H., Jr. (see Miller, S. C., Jr.)—174
Good, W. M. Nuclear reactions with He^8 nuclei—226(T)
——, **W. E. Kunz, and C. D. Moak.** $He^8 + He^3$ reaction—462(A)
—— (see Kunz, W. E.)—676
Goodenough, J. B. Nucleation centers for domains of reverse magnetization—434(A)
Goodman, Clark (see Guernsey, Janet B.)—440(A)
—— (see Kay, Robert)—472(A)
—— (see Kiehn, R. M.)—66
—— (see McClelland, Clyde L.)—760(L)
Goodrich, M., J. S. Levinger, and W. Payne. Bremsstrahlung from P^{32} betas—455(A); 1225
—— (see Payne, W.)—497(A)
Gopalakrishnan, K. (see Tomlinson, E. P.)—484(A)
Gordy, Walter M. 1- to 2-mm wave spectroscopy—209(T)
—— (see Cox, J. T.)—222(A)
—— (see Hill, Robert M.)—222(A)
—— (see Mockler, Richard C.)—222(A)
—— (see Trambarulo, R.)—222(A)
—— (see Venkateswarlu, Putcha)—222(A)
Gossett, C. R. (see Phillips, G. C.)—462(A)
Gossick, B. R. Post-injection barrier emf of p-n junctions—1012(L)
—— (see Bray, R.)—1011(L)
Gouza, J. J. (see Protzman, T. F.)—211(A)
Gove, H. E. and E. B. Paul. Yield and angular distribution of γ rays from $B^{11}(p,\gamma)C^{12}$—463(A)
—— (see Ferguson, A. J.)—439(A)
Grad, Harold. Validity of Boltzmann equation—1031(T)
Graham, Irven C., David Pomeroy, W. C. McGarvey, and John G. Randall. Biophysical study of burns—214(A)
Grandey, R. A. (see Clark, A. E.)—467(A)
Grandine, Lester D., Jr. (see Ferry, John D.)—217(A)
—— (see Fitzgerald, Edwin R.)—217(A)
Green, Alex E. S. and David F. Edwards. Discontinuities in nuclear mass surface—46; 443(A)
—— **and Nicholas A. Engler.** Mass surfaces—40
Green, Farno L. Electromagnetic shims for focusing in fixed-frequency cyclotron—223(A)
Green, Louis C., Marjorie M. Mulder, and Paul C. Milner. Correlation energy in ground state of He I—35
Green, M. (see Keck, P. H.)—472(A)
Greenberg, J. Mayo. Scattering approximations for transparent nucleus model—454(A)
Gregg, E. C. (see Tucker, B. L.)—1579(L)
Gregory, Christopher. Construction of conservation equations for nonlocal field theories—770(L)
Grimes, D. M., L. W. Orr, and M. H. Winsnes. Reversible susceptibility in ferrimagnetic materials—435(A)
Gropp, Armin H. (see Letaw, Harry, Jr.)—235(A)
Grosof, Gerard M. (see Weinreich, Gabriel)—195(L)
Gross, E. P. Electron motion in polar crystals—228(A)
—— (see von Hippel, A.)—568
Grosse, A. V. (see Javan, A.)—222(A)
Grunwald, Ernest (see Marshall, Henry P.)—214(A)
Guernsey, Janet B. and Clark Goodman. Total neutron cross section of liquid A—440(A)
Gugelot, P. C. and H. A. Lauter. Inelastic scattering of 18.3-Mev protons—486(A)
Guinier, A. Possibilities of x-ray small-angle scattering for study of crystal imperfections—239(T)
Gursky, Herbert, Barbara Winnemore, and D. A. Cowan. Ranger study of Po-Be neutron spectrum—209(A)
Gursky, Judith Cassidy and P. K. S. Wang. Determination of x-ray spectrum from absorption measurements by Laplace transformation—239(A)
Gutowsky, H. S. and B. R. McGarvey. Nuclear magnetic resonance in Th compounds—81
Gutzwiller, Martin. Quantum electrodynamics in space of constant curvature—478(A)

Haeberli, W., A. Galonsky, E. Goldberg, and R. Douglas. Elastic scattering of protons by Ne—438(A)
—— (see Galonsky, A.)—439(A)
Hagstrum, Homer D. Electron ejection from Ta by He^+, He^{++}, and He_2^+—543
Hahn, Beat. Scintillations produced by α particles in CsI—772(L)
Hahn, T. M. (see Jenkins, G. L.)—210(A); 915
—— (see Lafferty, D. L.)—223(A)
Hall, R. W. (see Maxwell, L. R.)—206(A)
Halpern, J. and E. V. Weinstock. Photodisintegration of deuteron at 20 Mev—934
—— (see Weinstock, E. V.)—461(A)
Halteman, E. K. (see Fillnow, R. H.)—236(A)
Hamilton, J. Fredholm theory of S matrix—1524
Handley, T. H. (see Jones, W. H.)—486(A)
—— (see Newman, E.)—486(A)
Hanna, S. S. (see Frost, R. T.)—462(A)
—— (see Pruitt, J. S.)—463(A)
—— (see Shafroth, S. M.)—483(A)
Hansen, K. F. (see Kiehn, R. M.)—66
Hanson, H. P. and H. W. Schrader. Measurements of K edge jump ratios with linear motion x-ray spectrometer—457(A)
Harbottle, Garman. Half-life of Tl^{204}—1234
Harrick, N. J. (see Barnes, R. G.)—475(A)
Harris, D. R. (see Ballam, J.)—446(A); 1019(L)
Harris, J. C. (see Chilton, A. B.)—495(A)
Harris, S. P., C. O. Muehlhause, D. Rose, H. P. Schroeder, G. E. Thomas, Jr., and S. Wexler. Thermal n-p capture—125
Harrison, Melvin A. and Ronald Geballe. Simultaneous measurement of ionization and attachment coefficients—1
Harrison, Sol E. and Herbert B. Callen. Electronic interactions in ferromagnetic metals—205(A)
Hart, Edward W. Yield point strain—232(A)
Harth, Erich, Leo Seren, Milton Birnbaum, and Ralph Tobin. Thresholds for reactions $Cu^{63}(\gamma,n)Cu^{62}$ and $Ag^{109}(\gamma,n)Ag^{108}$—474(A)
—— (see Birnbaum, Milton)—474(A)
—— (see Seren, Leo)—474(A)
Hartman, P. L. and D. H. Tomboulian. Far uv radiation from Cornell synchrotron—1577(L)
Harvey, J. A. (see Goldberg, M. D.)—451(A)
Haskin, D. M. (see Schein, Marcel)—479(A); 973
Hastings, Samuel (see Lehnert, Richard)—1032(A)
Havas, Peter. Classical equations of motion of point particles—997
—— (see Mehl, Clarence R.)—393
Havens, W. W., Jr. (see Block, M. M.)—210(A)
—— (see Melkonian, E.)—450(A)
Hawkins, W. B. and R. H. Dicke. Polarization of Na atoms—1008(L)
Hayes, S. and R. Smoluchowski. Small-angle x-ray scattering in proton-irradiated diamond—244(A)
—— (see Bowman, J. C.)—244(A)
Haynes, C. W. and R. Smoluchowski. Grain boundary self-diffusion in body-centered lattice—245(A)
Haynes, J. R. (see Smith, Charles S.)—491(A)

Haynes, Sherwood K. (see Kerr, Robert J.)—214(A)
Heckman, Harry H. and L. Evan Bailey. Large-angle scattering of π^- mesons in Al, Cu and Pb—1237
Heckman, R. C. and H. Sponer. Near uv vapor spectrum of thianaphthene—242(A)
Heer, C. V., C. B. Barnes, and J. G. Daunt. Magnetic refrigerator for maintaining temperatures below 1°K—412(L)
Heer, E. (see Albers-Schönberg, H.)—199(L); 1287(L)
Heikes, Robert R. Magnetic properties of pyrrhotite—212(A)
Hein, R. A. (see Steele, M. C.)—490(A)
Heindl, C. (see Sheer, C.)—449(A)
Heller, W. R. (see Dexter, D. L.)—273
Hemmendinger, Arthur. Interactions of T and He^3 with light nuclei below 5 Mev—488(T)
Hemstreet, H. W. and J. M. Reynolds. Electrical resistance of graphite at low temperatures—242(A)
—— (see Reynolds, J. M.)—1152
Henisch, H. K. Transistor experiments on binary Pb compounds—213(T)
Henkels, H. W. and J. Maczuk. Anisotropic resistivities of Se crystals at high frequencies—1562(L)
Henley, E. M. and M. A. Ruderman. Nuclear forces from extended sources—480(A)
—— (see Cooper, L. N.)—480(A)
Henry, Warren E. Magnetic saturation and apparent molecular fields of $MnCl_2 \cdot 4H_2O$—435(A)
Henshaw, D. G. and D. G. Hurst. Neutron diffraction by liquid He—1222
——, **D. G. Hurst, and N. K. Pope.** Neutron diffraction by liquid O_2, N_2, and A—472(A)
Herbst, R. F. and A. V. Bushkovitch. Pauli form of β decay matrix elements—442(A)
Hereford, Frank L. Polarized photons—226(T)
—— (see Berko, Stephan)—1127
—— (see Garrett, R. E.)—441(A)
Herlin, Melvin A. (see Rogers, D. H.)—489(A)
—— (see Waldron, S.)—447(A)
Herman, Frank. Energy band structure of diamond and Ge crystals—491(A)
Herman, R. C. (see Alpher, R. A.)—479(A)
Hertzberg, Abraham and William E. Smith. C.A.L. hypersonic test facility—1029(A)
—— **and W. Squire.** Shock tube for studying chemical kinetics—469(A)
Herzberg, Gerhard (see Chandrasekhar, S.)—1172
Heydenburg, N. P. and G. M. Temmer. α-particle scattering in N—439(A)
Heyman, R. J., A. Sherman, and T. Schiffman. Pressure multiplication in reentrant corners—1032(A)
Hill, David L. (see Wilets, Lawrence)—1488
Hill, F. K. Boundary layer hypersonic flow—1029(A)
Hill, R. D. Auger electron intensities—770(L)
—— (see Swan, J. B.)—424(L)
Hill, R. W. (see Eppling, F. J.)—438(A)
Hill, Robert M. and Walter Gordy. Temperature dependence of line breadths of O_2—222(A)
Hinds, Conrade C. (see Fuson, Nelson)—234(A)
Hines, R. L. Excitation function for $Mn^{55}(\gamma,3n)Mn^{52}$—474(A)
Hobstetter, John. Nucleation of solid-solid transitions—232(T)
Hodson, A. L. (see Ballam, J.)—446(A); 1019(L)
Hoerni, Jean A. and James A. Ibers. Complex amplitudes for electron scattering by atoms—1182
Hoffmann, Banesh. Similarity theory of relativity and Dirac-Schrödinger theory of electrons—751
Hoffman, M. M. (see Cameron, A. G. W.)—473(A)
Hofstadter, R., H. R. Fechter, and J. A. McIntyre. Electron scattering from nuclei at high energies—439(A)
——, **H. R. Fechter, and J. A. McIntyre.** Scattering of high-energy electrons and method of nuclear recoil—422(L)
Hogan, C. L. Electromagnetic phenomena in ferrites—461(T)
Hoge, Harold J. Series method for comparison of resistances—493(A)
Hogg, Benjamin G. and Henry E. Duckworth. Evidence for region of extra nuclear stability between 82- and 126-neutron shells—1289(L)
Holmes, D. K. (see Crawford, J. H., Jr.)—243(A)
Holmgren, H. D. (see Brown, R. J. S.)—438(A)
Holshouser, D. F. (see Babcock, M. L.)—755(L)
Holstein, T. Electromagnetic absorptivity of metals at low temperatures—490(A)
Honig, Richard E. Mass spectrometric study of sublimation of graphite—465(A)
Hopkins, J. I. (see Campbell, W. H.)—224(A)
—— (see Porter, P. T.)—209(A)
Hopkins, Robert L. (see Clarke, Edward N.)—1566(L)
Hornyak, W. F. and T. Coor. Capture γ rays from proton bombardment of Be—463(A)
Horowitz, M. and J. G. Daunt. Electronic and lattice specific heats in W, Mo, and Re—1099
Hosler, William R. (see Breckenridge, Robert G.)—243(A); 793
Hough, P. V. C. (see Bach, D. R.)—463(A)
Howard, Lawrence A. (see Frost, Albert D.)—471(A)
Howard, Louis N. and J. Samuel Smart. Specific heat discontinuity in antiferromagnets and ferrites—17
Howland, J. J., Jr. (see Welker, Joan P.)—484(A)
Hoyt, Harry C. and Jesse W. M. DuMond. γ radiation following decay of I^{128}—1027(L)
Hsiao, C. A. and V. L. Telegdi. Mechanism of reaction $O^{16} + h\nu \rightarrow 4He^4$—473(A)
Hsieh, Yü-Chang (see Bloch, Ingram)—240(A)
Huang, Kerson (see Drell, S. D.)—460(A); 1527
Huddlestone, R. H. Compton scattering on nucleons—461(A)
Hudson, D. E. (see Johnson, R. G.)—466(A)
—— (see Shaw, William C.)—208(A)
Hudson, E. D. (see Boch, A. L.)—224(A)
Hudson, R. P. (see de Klerk, D.)—278
Huebner, W. F. (see Phelps, John)—496(A)
Hughes, D. J., R. C. Garth, and J. S. Levin. Fast-neutron cross sections and nuclear level density—1423
—— (see Kato, W. Y.)—450(A)
—— (see Palevsky, H.)—451(A)
Hughes, Raymond H. Isotope shift in arc spectrum of Li—457(A)
Hughes, Vernon W., Gardiner Tucker, Emlyn Rhoderick, and Gabriel Weinreich. Magnetic moment of He atom in metastable triplet state—828
—— **and Gabriel Weinreich.** Effect of nuclear structure on hfs of He^3—196(L)
—— (see Perl, William)—842
—— (see Weinreich, Gabriel)—195(L)
Huibregtse, E. J. and L. P. Hunter. Current carrier lifetimes deduced from Hall coefficient and resistivity measurements—208(A)
—— (see Hunter, L. P.)—1315
Hulburt, E. O. (see Bennett, W. H.)—1562(L)
Hunter, L. P. Current carrier mobility ratio in semiconductors—207(A); 579
——, **E. J. Huibregtse, and R. L. Anderson.** Current carrier lifetimes deduced from Hall coefficient and resistivity measurements—1315

—— (see Huibregtse, E. J.)—208(A)
Huntington, H. B. Mobility of interstitial atoms in face-centered metal—1092
——, **G. A. Shirn, and E. S. Wajda.** Activation entropies for diffusion mechanisms—246(A)
Hurley, J. P. (see Whittle, C. E.)—498(A)
Hurst, D. G. (see Henshaw, D. G.)—472(A); 1222
Hutchinson, Franklin and Barbara Doyle. Inactivation of bovine serum albumin with low-voltage electrons—493(A)
—— (see Phelps, John)—496(A)
Hutchison, Thomas S. Precipitation effects in Cu-Fe alloys—449(A)
—— (see Reekie, James)—490(A)
Huus, Torben and Robert B. Day. γ radiation from B^{11} bombarded by protons—599
—— (see Beckman, Olof)—606

Ibers, James A. (see Hoerni, Jean A.)—1182
Inn, Edward C. Y. Photoionization of molecules in vacuum uv—1194
—— (see Watanabe, K.)—436(A); 1155
Innes, Frederick R. Matrix elements of spin-spin interaction—31
Iwersen, Eric, W. S. Koski, and Franco Rasetti. Triton-induced activities in Mg and Al—1229

Jaccarino, V. (see King, J. G.)—209(A); 476(A)
Jacobs, Donald H., Milton E. Pugh, and Seymour Scholnick. High-accuracy, high-speed shaft position digitalizer—492(A)
Jacobs, Harold (see Dobischek, Dietrich)—804
Jacobsmeyer, V. P. (see Friedrich, L. W.)—492(A)
Jakobson, M. J., A. G. Schulz, and R. S. White. Production of charged photomesons from He. H-He ratios—695
James, Hubert M. (see Fosdick, Lloyd D.)—1131
Jamison, R. E. and T. H. Blewitt. Deformation characteristics of reactor-irradiated Cu single crystals at 78°K and 300°K—237(A)
—— (see Blewitt, T. H.)—448(A)
Jarmie, Nelson, Gordon W. Repp, and R. Stephen White. Positive photomesons from H at 0°—1023(L)
—— (see White, R. Stephen)—468(A)
Jastram, P. S. (see Robinson, J. E.)—498(A)
—— (see Whittle, C. E.)—498(A)
Jastrow, Robert. Low-energy properties of nucleon-nucleon interaction—749
—— Saturation of nuclear forces—460(A)
Jaumot, Frank E., Jr., and Leonard Muldawer. Strain and crystallite size in experimental Fe powders—232(A)
—— (see Sanville, W. W.)—220(A)
—— (see Sutcliffe, Charles H.)—221(A)
Javan, A., G. Silvey, C. H. Townes, and A. V. Grosse. Quadrupole moments of Mn^{55}, Re^{185}, and Re^{187}—222(A)
Jeffries, C. D. and P. B. Sogo. Nuclear magnetic moment of Cr^{53} and Sr^{87}—1286(L)
Jelatis, J. G. (see von Hippel, A.)—568
Jen, C. K. Zeeman effect in microwave spectroscopy—458(T)
Jenkins, G. L., L. W. Cochran, H. H. Givin, J. L. Ryan, T. M. Hahn, and B. D. Kern. Angular distribution of 12-Mev γ rays from proton bombardment of B—210(A); G. L. Jenkins, L. W. Cochran, B. D. Kern, and T. M. Hahn—915
Jenkins, T. (see Luckey, D.)—468(A)
Jentschke, W. K. (see Briggs, G. R.)—438(A)
—— (see Eby, F. S.)—495(A)
—— (see Kerman, R. O.)—438(A)
—— (see Lawson, J. S., Jr.)—484(A)
John, W. and W. F. Fry. π^- and μ^- meson-induced fission—1234
Johns, M. W. (see McMullen, C. C.)—418(L); 1580(E)
Johnson, C. H. (see Fowler, J. L.)—441(A)
—— (see Trail, Carroll C.)—474(A)
Johnson, C. Y. (see Davis, L. R.)—431(A)
Johnson, Edgar G. and Alfred O. Nier. Angular aberrations in sector-shaped electromagnetic lenses for focusing beams of charged particles—10
Johnson, F. F. (see Tittman, J.)—452(A)
Johnson, J. B. and K. G. McKay. Secondary electron emission of crystalline MgO—582
Johnson, John L. and J. L. McHale. Calculation of half-widths of one-body resonances—87
—— (see McHale, J. L.)—452(A)
Johnson, O. E. (see Carmichael, B. M.)—473(A)
Johnson, R. G., W. C. Caldwell, D. E. Hudson, and F. H. Spedding. Mass spectrometric positive ion technique for determining phase transition temperatures and heats of transformation in metals—466(A)
Johnson, T. H. Research program of AEC—442(T)
Johnson, V. A. and K. Lark-Horovitz. Theory of thermoelectric power in semiconductors—230(A)
Johnson, W. H., Jr. (see Collins, T. L.)—482(A)
Jones, Emerson, Jr. (see Cook, Charles J.)—1417
Jones, Ernest A. (see Akers, Lawrence K.)—236(A)
Jones, G. A. (see Wilkinson, D. H.)—1575(L)
Jones, K. W., D. J. Donahue, M. T. McEllistrem, R. A. Douglas, and H. T. Richards. Break-up energy of Be^8—879
——, **M. T. McEllistrem, R. A. Douglas, and H. T. Richards.** Comparison of nuclear and γ-ray absolute energy scales—482(A)
Jones, Lawrence W. and Kent M. Terwilliger. Photoneutron production excitation functions to 320 Mev—699
Jones, Royce J. Oak Ridge 44-in. cyclotron—223(A)
Jones, W. H., J. H. Paehler, T. H. Handley, and A. Timnick. Yield distribution in proton fission of U—486(A)
Jordan, W. C., J. M. Cork, and S. B. Burson. Decay scheme for $_{66}Dy^{165m}$ (1.25 min) and $_{66}Dy^{165}$ (2.3 hr)—497(A)
—— (see Burson, S. B.)—498(A)
Jorgensen, Theodore, Jr. (see Cook, Charles J.)—1417
Josien, Marie-Louise, Nelson Fuson, and Essie M. Shelton. Infrared study of influence of molecular structure on carbonyl band in polycyclic quinones—235(A)
—— (see Fuson, Nelson)—234(A)

Kachickas, G. A. and L. H. Fisher. Formative time lags of uniform field breakdown in A—775
Kahn, Bernd and W. S. Lyon. K^{42} decay—1212
Kaiser, H. F. Electron cyclotrons (microtrons) for X- and K-band operation—456(A)
—— Relativistic particle cyclotron with electrostatic focusing—499(A)
Kaiser, W., R. J. Collins, and H. Y. Fan. Infrared absorption in p-type Ge—230(A); 1380
Kalil, F. and R. D. Birkhoff. Straggling distributions for electrons in passing through thin foils—505
Kallmann, Hartmut (see Furst, Milton)—766(L); 1356
Kalos, M. H. and J. M. Blatt. Ground state of deuteron with tensor forces—444(A)
—— (see Blatt, J. M.)—444(A)
Kambe, K. (see Abragam, A.)—894
Kandel, R. J. Ionization and dissociation of nitromethane by electron impact—436(A)
Kane, R. P. (see Sarabhai, V.)—688
Kao, S. K. (see Clark, A. E.)—467(A)

Kaplon, M. F., J. Z. Klose, D. M. Ritson, and W. D. Walker. Absorption mean free path of high-energy nucleonic component of cosmic radiation—1573(L)
Karzmark, C. J. (see Buskirk, A. V.)—445(A)
—— (see Thompson R. W.)—446(A)
Kasper, J. S. (see Wilson, V. C.)—494(A)
Kastner, J. and G. N. Whyte. Half-life of Co^{60}—332
Katcoff, Seymour and William Rubinson. Yield of Xe^{133} in thermal neutron fission of U^{235}—1458
Kato, W. Y., Marilyn J. Stafne, J. S. Levin, and D. J. Hughes. Neutron resonances in Ag—450(A)
Katz, L. (see Montalbetti, R.)—659
Katz, Robert. Pairing effect in nuclei and isomerism—1487
Kay, Robert, Hans Mark, and Clark Goodman. Angular distribution of neutrons from $C^{14}(p,n)N^{14}$—472(A)
Keck, Paul H., M. Green, and M. L. Polk. Shapes of floating liquid zones between solid rods—472(A)
—— **and Wendell Van Horn.** Surface tension of liquid Si and Ge—243(A); 512
Keesom, P. H. and N. Pearlman. Atomic heat of Ge below 4°K—215(A); 1347; Heat capacity of KCl below 4°K—1354
Keffer, Frederic. Dipolar anisotropy in cubic ferromagnetic crystals—206(A)
Keister, G. L. (see Schmidt, F. H.)—483(A)
Keller, F. L. and A. H. Nielsen. Infrared spectrum and molecular constants of DBr—235(A)
Keller, W. E. (see Sommers, H. S., Jr.)—489(A)
Kendall, J. M. Compressible flow of viscous fluid in capillary connected to closed vessel—470(A)
Kenney, James (see Froman, Darol)—707
Kerman, R. O., R. Nilson, and W. K. Jentschke. α-α scattering at 21.6, 22.4, and 22.8 Mev (nuclear plate)—438(A)
Kern, B. D. (see Jenkins, G. L.)—210(A); 915
—— (see Lafferty, D. L.)—223(A)
Kerner, Edward H. Excitation of molecular rotations and vibrations in inelastic scattering processes—1174
Kerr, Robert J., Sherwood K. Haynes, and George R. Meneely. Study with NaI scintillation spectrometer of methods of estimating I^{131} contained in human thyroid—214(A)
Kevane, C. J., S. Legvold, and F. H. Spedding. Hall effect in Y, La, Ce, Pr, Nd, Gd, Dy, and Er—1372
Kiehn, R. M., Clark Goodman, and K. F. Hansen. Total neutron cross sections of Cl and C—66
Kikuchi, Ryoichi. Quantum statistical mechanics of ferromagnetism—205(A)
Kim, Y. B. Energy distribution of neutral mesons produced in cosmic-ray stars—445(A)
King, D. T. (see Seeman, Nathan)—446(A)
King, J. C. and Henry A. Fairbank. λ-point shift in He^3–He^4 mixtures—489(A)
King, J. G. and V. Jaccarino. Hfs and nuclear moment ratios of stable Br isotopes—209(A)
——, **H. H. Stroke, and V. Jaccarino.** Hfs of I—476(A)
Kip, A. F., C. Kittel, R. A. Levy, and A. M. Portis. Electronic structure of *F* centers: Hyperfine interactions in electron spin resonance—1066
—— (see Portis, A. M.)—207(A)
Kirkaldy, J. S. (see Westcott, C. H.)—495(A)
Kittel, Charles. Electronic structure of *F* centers—219(A)
—— Theory of conduction-electron spin resonance—239(T)
—— (see Kip, A. F.)—1066
Klein, Abraham. Construction of potentials in quantum field theory—1285(L); Convergence of adiabatic nuclear potential—460(A); 740
Klein, D. (see Oxley, C. L.)—419(L)
Klein, J. A. and A. H. Nethercot, Jr. Microwave spectrum of DI at 1.5-mm wavelength—1018(L)
Kleinman, D. A. (see Dienes, G. J.)—238(A)
Klema, E. D. and F. K. McGowan. γ-γ angular correlation in Ni^{60}—616
Kloepper, Robert M. Angular correlation of Ni^{60} γ-γ cascade—1026(L)
Klose, J. Z. (see Kaplon, M. F.)—1573(L)
Kmetko, E. A. Electrical properties of carbon bisulfate compounds—243(A)
—— (see Mrozowski, S.)—234(A)
Knight, J. D., M. E. Bunker, B. Warren, and J. W. Starner. Radiations of U^{240} and Np^{240}—889
Knight, W. D. Nuclear resonance line shapes at high rf fields—206(A)
Knipe, R. H. Molecular orbital treatment of contribution of π electrons to electric dipole moments of some phenyl halides—242(A)
Knudsen, W. C. and J. R. Dillinger. Linear velocity of He II film—489(A)
Kobayashi, Jinzo (see Ueda, Ryuzo)—1562(L)
Koch, H. W. X-ray spectrometer for nuclear-energy studies with betatron—477(T)
—— **and R. S. Foote.** Direct measurement of nuclear absorption of x-rays—455(A)
Koehler, J. S. Theory of initial stress strain curves in face-centered metals—233(A)
—— Work hardening in substitutional alloys—448(A)
Koehler, W. C. and E. O. Wollan. Slow-neutron scattering cross sections for rare earth nuclides—597
Koenigsberg, Ernest. Conductivity of thin films in longitudinal magnetic field—8
Kohn, Walter (see Rostoker, Norman)—234(A)
Kolsky, H. G. Low-energy properties of *n-p* system—459(A)
Korobkin, Irving. Heat transfer on hemispherical body in supersonic flow—469(A)
Koski, W. S. (see Iwersen, Eric)—1229
Koster, G. F. (see Slater, J. C.)—205(A); 1323
Kranz, A. Z. and W. W. Watson. A^{38} energy levels from $Cl(\alpha,p)$—1472
—— **and W. W. Watson.** Cl isotope separation by thermal diffusion—1469
Krishnan, K. G. (see Mihelich, J. W.)—498(A)
Krogstad, R., W. Nelson, and S. T. Stephenson. X-ray absorption fine structure with polarized x-rays—457(A)
Kroll, N. M. (see Weneser, J.)—1257
Krone, Ralph W. (see Reardon, William A.)—334; 442(A)
Kronheimer, Erwin H. Calculation of nuclear binding energies with single-particle oscillator wave functions, erratum—1580(E)
Kruse, U. E. (see Malenka, B. J.)—1165
—— (see Ramsey, N. F.)—1162
Kuhlthau, A. R. Viscous drag measurements on rarefied gas using high-rotational speed techniques—1029(A)
Kundu, D. N. H^3 and He^3 reactions with medium-heavy nuclei—488(T)
—— **and M. L. Pool.** Inverse Oppenheimer-Phillips process in $Cu^{66}(He^3,\alpha)$—417(L)
—— (see Pool, M. L.)—462(A)
Kunstadter, J. W., J. J. Floyd, and L. B. Borst. Long-lived delayed neutrons from fission—594
Kunz, W. E. Cross section of $He^3(H^3,H^1)He^4$ reaction from 100–800 kev He^3 energy—462(A)
——, **C. D. Moak, and W. M. Good.** Energy levels in Be^9 from $Li^6(He^3,p)Be^8$—676
Kupperian, J. E., Jr., and E. D. Palmatier. Ionization energy losses of relativistic μ mesons in gases—1186
Kurath, Dieter. Application of *jj*-coupling model to moderately light nuclei—1430

Kursunŏglu, Behram. Relativistic two-body equation—478(A)
Kurzweg, H. H. Physical problems encountered in high-speed flight—459(T)

Lafferty, D. L., J. A. Biggerstaff, B. D. Kern, and T. M. Hahn. High-current 120-kev positive ion accelerator—223(A)
Lamphere, R. W. Fission cross section of U^{234}—210(A); 655
Landauer, Rolf and John Swanson. Diffusion currents in Hall effect in semiconductors—207(A); 555
—— (see Allen, G.)—471(A)
Lander, J. J. Auger peaks in energy spectra of secondary electrons from various materials—1382
Landon, H. H. (see Sailor, V. L.)—450(A)
Langer, L. M., N. H. Lazar, and R. J. D. Moffat. Disintegration of Sb^{124}—338; 485(A)
—— (see Ames, D. P.)—68
—— (see Lazar, N.)—498(A)
—— (see Moffat, R. J. D.)—485(A)
Langmuir, D. B. Interpretation of "dc etch" phenomena—447(A)
Lark-Horovitz, K. (see Becker, W. M.)—230(A)
—— (see Forster, J. H.)—229(A)
—— (see Johnson, V. A.)—230(A)
Laubenstein, M. J. (see Eggen, D. T.)—238(A)
Lauritsen, C. C. (see Warters, W. D.)—917
Lauter, H. A. (see Gugelot, P. C.)—486(A)
Lawson, J. S., Jr., and H. Frauenfelder. Correction for finite angular resolution in directional correlation measurements—649
——, **H. Frauenfelder, and W. K. Jentschke.** Measurement of directional correlation of Ni^{60} γ-γ cascade—484(A)
Lax, Melvin and Eli Burstein. Broadening of impurity levels in Si—208(A)
—— **and Eli Burstein.** Lattice absorption in diamond: One-dimensional model—492(A)
Lazar, N. H., R. J. D. Moffat, and L. M. Langer. Disintegration of W^{188}—498(A)
—— (see Langer, L. M.)—338
—— (see Moffat, R. J. D.)—485(A)
Lazarus, D. (see Sonder, E.)—245(A)
—— (see Tomizuka, T.)—245(A)
Leaderman, Herbert. Rheology of polyisobutylene III. Approximation methods in linear viscoelasticity theory: Wiechert function calculations—217(A)
LeBlanc, J. M. (see Cork, J. M.)—76; 497(A)
Leddicotte, G. W. (see Reynolds, S. A.)—333
Lee, Charles A., B. P. Fabricand, R. O. Carlson, and I. I. Rabi. Molecular beam investigation of rotational transitions. I. Rotational levels of KCl and their hfs—1395
—— (see Fabricand, B. P.)—1403
Legvold, S. (see Elliott, J. F.)—28
—— (see Kevane, C. J.)—1372
Lehnert, Richard. Reynolds number effect on spheres at supersonic speeds—1033(A)
—— **and Samuel Hastings.** Spin effects on base-pressure—1032(A)
Lehovec, Kurt. Electronic energy states of impurities in nonmetallic crystals—228(A)
—— **and E. Belmont.** Preparation of junctions in single crystals by surface melting—492(A)
Leinhardt, T. E. (see Reynolds, J. M.)—1152
Leipuner, L., R. Siegel, and S. DeBenedetti. Polarization of three-photon annihilation radiation—198(L)
Leivo, W. J. Density change in proton-irradiated KCl—245(A)
—— (see Vaughan, W. H.)—245(A)
Leprince-Ringuet, L. Some unusual cases of heavy mesons (K and V_0) observed in photographic emulsions—466(T)
Letaw, Harry, Jr., and Armin H. Gropp. Infrared spectrum of amide group—235(A)
Levin, J. S. (see Hughes, D. J.)—1423
—— (see Kato, W. Y.)—450(A)
Levinger, J. S. (see Goodrich, M.)—455(A); 1225
Levy, R. A. (see Kip, A. F.)—1066
Lew, Hin. Hfs and nuclear moments of Pr^{141}—619
—— (see Wessel, Günter)—476(A)
Lewis, H. W. Search for Hall effect in superconductor—216(A)
——, **B. E. Simmons, and E. Merzbacher.** Production of characteristic x-rays by protons—943
Libby, W. F. T in nature—442(T)
Linder, E. G. and P. Rappaport. Radioactive charging through dielectric medium—202(L); erratum—1580(E)
Lindner, Manfred. New nuclides produced in Cl spallation—642
—— **and R. N. Osborne.** Cross section for $Al^{27}(\alpha,\alpha 2pn)Na^{24}$ from threshold to 380 Mev—342
—— **and R. N. Osborne.** Energy dependence of cross section for $C^{12}(\alpha,an)C^{11}$—1501
Linlor, W. I. and B. Ragent. Time-of-flight instrumentation for 100-Mev neutrons—440(A)
—— (see Ragent, B.)—440(A)
Linz, Arthur, Jr. Electrical properties of $SrTiO_3$—753(L)
Lippmann, B. A. Complementarity in angular momentum states—1213
Livingston, M. S. (see Courant, E. D.)—202(L)
Loeb, Arthur L. Free-energy model for hysteresis loop—434(A)
Loebner, E. E. Thermoelectric power of carbons—243(A)
Logan, R. A. Thermally-induced acceptors in single crystal Ge—757(L)
Loh, H. Y. and Peter Cheo. Change of optical constants of fresh thin Cu and Ag films on exposure to air—221(A)
Lomon, Earle and Herman Feshbach. n-p scattering—454(A)
London, Fritz. Theory of liquid He—209(T)
Lord, J. J. Emulsion chamber studies of high-energy cosmic-ray interactions—432(A)
—— (see Weaver, A. B.)—466(A)
Lord, Norman W. Effects of heat treatment on lattice perfection—472(A)
—— Kinetics of disorder-order transformation in Cu_3Au—221(A)
Louisell, W. H., R. W. Pidd, and H. R. Crane. Experimental measurement of gyromagnetic ratio for free electron—475(A)
—— (see Crane, H. R.)—475(A)
Lovell, Robert James. Analysis of infrared spectrum of CF_3COCl—235(A)
Low, Francis E. and David Pines. Mobility of slow electrons in polar crystals—193(L)
—— (see Bethe, H. A.)—417(L)
Luckey, D., T. Jenkins, and R. R. Wilson. Photomeson production from H and deuterium at 90° and 30°—468(A)
—— (see Palfrey, T. R.)—468(A)
Lukasiewicz, J. Shock compression in ducts and diffusers—1032(A)
Lummis, Frances L. and Richard L. Petritz. Noise in p-n junction rectifiers. II. Experiment—231(A)
Lundquist, Stig. Stability of orbits in strong-focusing synchrotron—981
Lustig, Harry and John M. Blatt. New method for calculation of nuclear phase-shifts from cross-section measurements—453(A)

Lynch, Frank J. and Clarence L. Wesenberg. Very high resistance measurement—493(A)
Lyon, W. S. (see Kahn, Bernd)—1212

Ma, S. T. Power-series expansion of unitary operator $U(t,t_0)$—392
Macdonald, J. Ross. New model for Debye dispersion equations—412(L)
Machlup, Stefan. Nyquist and Einstein relations derived from scattering model—240(A)
—— **and L. Onsager.** Fluctuations and irreversible process. II. Systems with kinetic energy—1512
—— (see Fletcher, R. C.)—237(A)
—— (see Onsager, L.)—1505
Mack, Rex C., J. J. Neuer, and M. L. Pool. $Eu^{147, 148, 149, and\ 150}$—497(A); Radioactive Eu^{150} and Gd^{150}—903
Macke, Wilhelm. Two-particle potential from Bethe-Salpeter equation—195(L); Erratum—1580(E)
MacLeod, David W. (Mingins, Charles R.)—471(A)
Maczuk, J. (see Henkels, H. W.)—1562
Madey, Richard. Short resolution time and short "dead" time coincidence counting equipment—486(A)
—— (see Bandtel, Kenneth C.)—487(A)
—— (see Frank, Wilson J.)—487(A)
—— (see Godfrey, Charles)—487(A)
Mador, I. L., J. J. Markham, and R. T. Platt, Jr. Band width of F centers in KBr—219(A); 1277(L)
—— (see Markham, J. J.)—219(A)
—— (see Platt, R. T., Jr.)—219(A)
Mahlman, H. A. (see Reynolds, S. A.)—333
Maita, J. P. (see Tanenbaum, M.)—1009(L)
Malenka, B. J., U. E. Kruse, and N. F. Ramsey. Electric scattering of polarizable deuteron—1165
—— (see Ramsey, N. F.)—1162
Mandelkern, Leo. Kinetics of crystallization—225(T)
—— (see Roberts, Donald E.)—225(A)
Mandeville, C. E. and H. O. Albrecht. Storage of energy in Ag-activated KCl—219(A); 566; Storage of energy in KCl-Tl and NaCl-Tl—470(A)
—— (see Albrecht, H. O.)—471(A)
—— (see Saraf, B. L.)—1216
Mann, D. E., N. Acquista, and Earle K. Plyler. Vibrational spectra of $F_2C{:}CF_2$ and $Cl_2C{:}CCl_2$—464(A)
Mann, L. (see Clark, A. E.)—467(A)
Mapother, D. E. and J. F. Cochran. Super-conducting transition in Al—216(A)
Marcus, Paul M. Theory of pressure effects on superconducting transition temperatures—216(A)
—— **and E. Maxwell.** Two-fluid models of superconductivity with application to isotope effects—1035
Mark, Hans (see Kay, Robert)—472(A)
Markham, Jordan J., R. T. Platt, Jr., and I. L. Mador. Bleaching properties of F centers in KBr at 5°K—219(A)
—— (see Mador, Irving L.)—219(A); 1277(L)
—— (see Platt, R. T., Jr.)—219(A)
Markovitz, H. (see Padden, F. J.)—217(A)
Marmo, Frederick (see Watanabe, K.)—436(A); 1155
Marshall, Henry P. and Ernest Grunwald. Molar activity coefficients of electrolytes from conductivity data—214(A)
Marshall, J., L. Marshall, and V. A. Nedzel. Total cross sections of 408-Mev protons for H and light elements—767(L)
Marshall, John H. Liquid A ionization chamber measurement of shape of β-ray spectrum of K^{40}—905
Marshall, L. (see Marshall, J.)—767(L)
Martin, Donald C. Graduate training for high school physics teachers and cooperation between college and high school physics departments—227(A)
Martin, E. E. (see Dyke, W. P.)—1043
Martin, J. A. Radioisotope production in ORNL 86-in. cyclotron—224(A)
Martin, R. L., E. Fermi, and D. E. Nagle. Scattering of 169- and 192-Mev pions by H—467(A)
—— (see Anderson, H. L.)—155
Marton, L., J. Arol Simpson, and J. A. Suddeth. Electron interferometer—437(A)
—— (see Simpson, J. Arol)—437(A)
—— (see Suddeth, J. A.)—437(A)
Marx, J. W. Radiation damage and rate processes—1564(L)
Masket, A. V. (see Brown, Frank B., Jr.)—210(A)
Matland, C. G. Natural lifetime of Cd 5^3P_1 state—436(A)
Matthias, B. T. Superconducting compounds—413(L)
Maurer, R. J. (see Teegarden, K.)—219(A)
Maximon, L. (see Bethe, H. A.)—417(L)
Maxwell, E. (see Marcus, Paul M.)—1035
Maxwell, L. R. Trivalent substitutions in ferrites—461(T)
——, **S. J. Pickart, and R. W. Hall.** Thermomagnetic investigations of Ni ferrite-aluminates—206(A)
Mayburg, S. and L. Rotondi. Thermal acceptors in vacuum heat-treated Ge—1015(L)
Mazenko, J. J. (see Schwertz, F. A.)—491(A)
McAfee, K. B. (see McKay, K. G.)—1079
McCay, M. S. and J. H. Coulliette. Motion of ions in perpendicular hf electric fields—213(A)
—— (see Morrison, Ray M.)—227(A)
McClelland, Clyde L. and Clark Goodman. Excitation of heavy nuclei by electric field of low-energy protons—760(L)
McClure, G. W. Upper limit on fraction of positive particles emanating from two β emitters—483(A)
—— (see Porter, W. C.)—495(A)
McCorkle, W. C. (see Tipton, Isabel H.)—214(A)
McCusker, C. B. A., N. A. Porter, and B. G. Wilson. Production of mesons above 10 Bev—384
—— **and F. C. Roesler.** Extreme energy interactions in heavy nuclei—769(L)
—— **and F. C. Roesler.** Interpretation of $0+xp$ type stars in photographic emulsions—769(L)
—— (see Roesler, Frank C.)—690
McDonald, E. W. and D. C. Ralph. 10-Mc rf ion source—223(A)
McDonald, Frank B. Cloud-chamber study of particles in primary cosmic radiation—432(A)
McEllistrem, M. T. (see Jones, K. W.)—482(A); 879
McGarvey, B. R. (see Gutowsky, H. S.)—81
McGarvey, W. C. (see Graham, Irven C.)—214(A)
McGowan, F. K. (see Klema, E. D.)—616
McGuire, T. R. Magnetic resonance absorption in Ni ferrite-aluminates—206(A)
McHale, J. L. and John L. Johnson. Half-widths and level shifts of one-body resonances—452(A)
—— (see Johnson, John L.)—87
McIntyre, J. A. (see Hofstadter, R.)—422(L); 439(A)
McKay, K. G. and K. B. McAfee. Electron multiplication in Si and Ge—1079
—— (see Johnson, J. B.)—582
McManus, H. (see Austern, N.)—453(A)
McMichael, B. D. (see Mrozowski, S.)—234(A)
McMickle, R. H., R. W. Schiessler, and W. Webb. Compressions to 150 000 psi for series of high molecular weight liquid hydrocarbons—466(A)
McMullen, C. C. and M. W. Johns. Decay of Re^{188} and lifetimes of Os^{186m} and Os^{189m}—418(L); Erratum—1580(E)
McNown, John S. Recent investigations at Iowa Institute of Hydraulic Research—1029(T)
McReynolds, Andrew W. Inelastic scattering of thermal neutrons in Pb—1368

Meadows, J. W. Excitation functions for proton-induced reactions with Cu—885
Mechlin, G. F. (see Fillnow, R. H.)—236(A)
Meckler, Alvin. Electronic energy levels of O_2—242(A)
Meechan, C. J. (see Dixon, C. E.)—237(A)
Mehl, Clarence R. and Peter Havas. Classical scattering of neutral mesons—393
Meissner, K. W. (see Deverall, G. V.)—297
Melkonian, E., W. W. Havens, Jr., and L. J. Rainwater. Doppler effect on neutron resonance levels—450(A)
Melnick, Donald A. and Leo J. Neuringer. Adsorbed O in ZnO photoconductivity—229(A)
Melvin, M. Avramy. Energy-momentum tensor in general stream electrodynamics—241(A)
Mendlowitz, H. (see Case, K. M.)—475(A)
Mendoza, E. Minimum in electrical resistance of metals at low temperatures—239(T)
Meneely, George R. (see Kerr, Robert J.)—214(A)
Meneghetti, David (see Sidhu, S. S.)—435(A)
Menyuk, Norman. Magnetization reversal of square-loop polycrystalline materials by domain growth—434(A)
Merz, Walter J. Double hysteresis loop of $BaTiO_3$ at Curie point—513
Merzbacher, E. (see Lewis, H. W.)—943
—— (see Newson, H. W.)—241(A)
Meshkov, Sydney. Theory of complex spectra—871
Metzger, F. R. and W. B. Todd. Lower limit for lifetime of 665-kev excited state of Mo^{97}—1286(L)
Meyerott, Roland E. Approximate Hartree type wave function and matrix elements for K and L shells of atoms and ions—456(A)
—— (see Brachman, Malcolm K.)—437(A)
Middleton, A. E. (see Willardson, R. K.)—243(A)
Mihelich, J. W. Successive neutron capture in Ta—427(L); Erratum—1580(E)
—— **and A. de-Shalit.** Decay of Au^{197m}—78
——, **L. P. Gillon, K. G. Krishnan, and A. de-Shalit.** Neutron-deficient isotopes of Hg—498(A)
Miller, J. M. and G. Friedlander. Nuclear reactions produced in Brookhaven cosmotron—485(A)
Miller, P. H. Infrared absorption and photoconductivity in Te—213(T)
Miller, S. C., Jr., and R. H. Good, Jr. WKB-type approximation to Schrödinger equation—174
Miller, W. C. (see Anthony, D. J.)—439(A)
Milner, Paul C. (see Green, Louis C.)—35
Mingins, Charles R., Robert W. Perry, and David W. MacLeod. Effects of grooves in piezoelectric filter plates—471(A)
—— (see Frost, Albert D.)—471(A)
Minkowski, J. M. (see Bearden, J. A.)—482(A)
Minshall, Stanley. Separation of shock wave into elastic and plastic waves, and measurement of pressure of elastic wave—1030(A)
Misenta, R. (see Becker, E. W.)—414(L)
Miskel, J. A. (see Perlman, M. L.)—899
Mitchell, F. H. Experiment with transistors for elementary electronics laboratory course—227(A)
Mittelman, Phillip S. Radiations from Zr^{95}—484(A)
Mize, J. P. and D. J. Zaffarano. β-ray spectra of C^{14} and Ni^{63}—210(A)
Mizushima, Masataka. Frequencies of microwave absorption lines of O_2—222(A)
—— Theory of rotational spectra of allene type molecules—464(A)
Moak, C. D. $H^3 + He^3$ reactions—462(A)
—— (see Kunz, W. E.)—676
Mockler, Richard C. and Walter Gordy. Microwave spectrum of $(CH_3)_3SiCl$—222(A)
—— (see Bird, George R.)—222(A)
—— (see Venkateswarlu, Putcha)—222(A)
Moffat, R. J. D. (see Langer, L. M.)—338
—— (see Lazar, N.)—498(A)
Moldauer, P. and K. M. Case. Equivalence theorems—459(A)
Mollo-Christensen, E. Separated solutions of linearized equation for unsteady transonic flow—1030(A)
Montalbetti, R., L. Katz, and J. Goldemberg. Photoneutron cross sections—659
Moore, J. (see Sheer, G.)—449(A)
Morita, Masato. Interference terms of the electron-neutrino angular correlation, erratum—1580(E)
Morowitz, Harold J. Information content of living systems—492(A)
Morris, L. W. and Hung-Chi Chang. Continuous flow cell for investigation of polarization at metal-solution interface—215(A)
Morrish, A. H. Grain density in tracks of 117- and 222-Mev π^- mesons in emulsions—423(L)
—— 210-Mev negative pion interactions—468(A)
Morrison, Ray M. and M. S. McCay. Incentive grading for basic laboratory reports—227(A)
Morton, H. S., Jr., and J. W. Beams. Tensile strength and adhesion of thin films of Ag—449(A)
Moses, Harry E. Exchange scattering in three-body problem—185
—— **and Ta-You Wu.** Dissociation and recombination of O_2 in upper atmosphere assuming three-body recombinations—458(A); 1408
Moshinsky, Marcos. Poles of S matrix for resonance reactions—984
Mostov, Philip M. and Sidney Borowitz. Radiation effects and rotational-translational relaxation time constant—465(A)
Mousuf, A. K. (see Russell, R. D.)—1223
Moyer, Burton J. (see Frank, Wilson J.)—487(A)
Mrozowski, S., B. D. McMichael, and E. A. Kmetko. New detector for infrared—234(A)
Muehlhause, Carl O. Gas scintillation counters—495(A)
—— (see Bloom, S. D.)—494(A)
—— (see Harris, S. P.)—125
Muldawer, Leonard (see Jaumot, Frank E., Jr.)—232(A)
Mulder, Marjorie M. (see Green, Louis C.)—35
Myers, V. W., R. S. Carter, and H. Palevsky. Total neutron cross sections of heavy water and glass at long wavelengths—451(A)
—— (see Carter, R. S.)—450(A)

Nagel, E. (see Wu, C. S.)—319
Nagle, D. E. (see Anderson, H. L.)—155
—— (see Martin, R. L.)—467(A)
Naugle, J. E. (see Anderson, G. W.)—431(A)
Navon, D. and H. Y. Fan. Carrier traps in Ge at low temperatures—491(A)
Nedzel, A. V. (see Marshall, J.)—767(L)
—— Total cross sections for 400-Mev neutrons—440(A)
Neidigh, R. V. (see Cohen, B. L.)—486(A)
Nelson, F. (see Campbell, E. C.)—499(A)
Nelson, W. (see Krogstad, R.)—457(A)
Nester, W. H. (see Cork, J. M.)—76; 497(A)
Nethercot, A. H., Jr. (see Klein, J. A.)—1018(L)
Neuer, J. J. (see Mack, Rex C.)—497(A); 903
Neuringer, Leo J. (see Melnick, Donald A.)—229(A)
Newell, Gordon F. Vibration spectrum of simple cubic lattice—227(A)
Newman, E., B. L. Cohen, and T. H. Handley. (p,pn) and (p,an) excitation functions—486(A)
—— (see Cohen, B. L.)—486(A)

Newman, Roger. Optical studies of injected carriers. I. Infrared absorption in Ge—1311; II. Recombination radiation in Ge—1313
Newson, Henry W. and E. Merzbacher. Magic numbers and statistical model of nucleus—241(A)
—— (see Gibbons, J. H.)—209(A)
Nichols, J. B. X-ray and infrared studies on extent of crystallization—225(T)
Nielsen, A. H. (see Keller, F. L.)—235(A)
—— (see Parker, F. W.)—235(A)
—— (see Shelton, R. D.)—235(A)
Nielsen, Carl E. (see Frost, Robert H.)—864
Nier, Alfred O. (see Collins, T. L.)—482(A)
—— (see Johnson, Edgar G.)—10
Nilson, R. (see Kerman, R. O.)—438(A)
Nisenoff, M. (see Gebbie, H. A.)—230(A)
Nix, Foster C. (see Croft, George T.)—212(A)
—— (see Sanville, W. W.)—220(A)
Novey, T. B. (see Albers-Schönberg, H.)—199(L); 1287(L)
Nowick, A. S. and A. E. Roswell. Decay of vacancies frozen into alloy by quenching—221(A)
Nozick, Seymour (see Winkler, Stanley)—492(A)

O'Dell, Francis W., Maurice M. Shapiro, and Bertram Stiller. Pellicle stacks in nuclear research—496(A)
Offenbacher, Elmer L. and Herbert B. Callen. Directional effects in the electric breakdown of ionic crystals, erratum—1580(E)
Ohtsuka, Taiichiro (see Waniek, R. W.)—445(A); 1574(L)
Okazaki, A., R. B. Walton, and J. D. Clement. Total cross sections of Nd, Er, and Hf for fast neutrons—440(A)
O'Kelley, G. D. (see Batzel, R. E.)—939
Oliver, A. R. (see Blau, M.)—949
Olsen, J. L. (see Bömmel, H.)—1017(L)
Onsager, L. and S. Machlup. Fluctuations and irreversible processes—1505
—— (see Machlup, S.)—1512
Orear, Jay. Scattering of 120-Mev π^- mesons by H—467(A)
—— (see Weaver, A. B.)—466(A)
Oriani, R. A. Thermodynamic activities in Fe-Ni alloys—465(A)
O'Rourke, R. C. Absorption of light by trapped electrons—265
Orr, L. W. (see Grimes, D. M.)—435(A)
Osborne, L. S. (see Goldschmidt-Clermont, Y.)—468(A)
Osborne, M. F. M. (see Steele, M. C.)—1281(L)
Osborne, R. N. (see Lindner, M.)—342; 1501
Osgood, T. H. Responsibilities and training of physics teachers—226(T)
Oshinsky, W. (see Breckenridge, R. G.)—243(A)
Overhauser, Albert W. Influence of impurities on diffusion in solids—246(A)
—— Polarization of nuclei in metals—476(A)
Oxley, C. L., W. F. Cartwright, J. Rouvina, E. Baskir, D. Klein, J. Ring, and W. Skillman. Double scattering of high-energy protons by H and C—419(L)

Padden, F. J., H. Markovitz, and T. W. DeWitt. Dynamic properties of concentrated polymer solutions—217(A)
Paehler, J. H. (see Jones, W. H.)—486(A)
Pai, Shih I. Hypersonic viscous flow over insulated flat plate at large angle of attack—1029(A)
Palevsky, H., N. G. Sjöstrand, and D. J. Hughes. Neutron detectors for Brookhaven fast chopper—451(A)
—— (see Carter, R. S.)—450(A)
—— (see Myers, V. W.)—451(A)
Palfrey, T. R., D. Luckey, and R. R. Wilson. Photomeson production from H and deuterium at 180°—468(A)
Palmatier, E. D. Ionization energy losses of μ mesons in gases—210(T)
—— (see Kupperian, J. E., Jr.)—1186
Palmer, R., Ronald and Lowell M. Bollinger. Neutron transmission measurements of Cd, Gd, and Hg using Argonne fast chopper—450(A)
—— (see Bollinger, L. M.)—452(A)
Parker, F. W., A. H. Nielsen, and W. H. Fletcher. Infrared grating spectrum of CH_3CN vapor—235(A)
Passman, S. (see Block, M. M.)—210(A)
Paul, E. B. and R. L. Clarke. Yield of α particles from $B^{11}(p,\alpha)Be^8$—463(A)
—— (see Gove, H. E.)—463(A)
Payne, W. and M. Goodrich. γ rays in decay of Ba^{131}—497(A)
—— (see Goodrich, M.)—455(A); 1225
Pearlman, N. (see Keesom, P. H.)—215(A); 1347; 1354
Pearlstein, E. A. Changes in conductivity of NaCl produced by bombardment with 360-Mev protons—244(A)
Pearson, G. L. (see Tanenbaum, M.)—244(A)
Peaslee, D. C. j-j coupling for $A \lesssim 50$—443(A)
—— Linear combination of invariants in β decay—1447
—— Speculation on V-spin—446(A)
—— (see Davidson, J. P.)—442(A); 1232
Peckham, D. C. (see Stoner, R. G.)—1032(A)
Pellam, J. R. Recent experiments on second sound in liquid He II—481(T)
Pepinsky, Ray and P. F. Eiland. Computations of three-dimensional structure factors on S-FAC—229(A)
—— (see Frazer, B. C.)—212(A)
—— (see Schwartz, Robert B.)—812
—— (see Shirane, Gen)—212(A)
Pepper, T. P. (see Almqvist, E.)—1022(L)
Pereira, A. W. (see Rao, A. S.)—764(L)
Perl, William. Relativistic contributions to magnetic moment of n-electron atoms—852
—— **and Vernon Hughes.** Relativistic contributions to magnetic moment of $^3S_1$ He—842
Perlman, I. (see Asaro, Frank)—763(L)
—— (see Friedlander, G.)—498(A)
Perlman, M. L. and J. A. Miskel. Average charge on daughter atoms produced in decay of A^{37} and Xe^{131m}—899
—— (see Schwartz, Robert B.)—883
Perry, J. P. and C. E. Angell. Scattering of 40-Mev π^- mesons by H—1289(L)
—— (see Angell, C. E.)—468(A)
Perry, Robert W. (see Mingins, Charles R.)—471(A)
Petree, Ben (see Foote, R. S.)—456(A)
Petritz, Richard L. Noise in p-n junction rectifiers and transistors. I. Theory—231(A)
—— (see Lummis, Frances L.)—231(A)
Peyrou, C. (see Bridge, H. S.)—362
Peyton, P. B., Jr. (see Cox, J. T.)—222(A)
Pfann, W. G. (see Vogel, F. L.)—230(A)
Phelps, Arthur V. Metastable atoms in afterglow of low-pressure He discharge—436(A)
Phelps, John, W. F. Huebner, and Franklin Hutchinson. Stopping powers of thin compound foils—496(A)
Phillips, G. C., K. F. Famularo, and C. R. Gossett. Absolute magnetic analysis of reaction energies of $Li^6(d,\alpha)He^4$, $Li^7(p,\alpha)He^4$, and $C^{13}(d,\alpha)B^{11}$—462(A)
—— (see Famularo, K. F.)—1195
Phillips, J. A. Equilibrium proton charge ratios from charge exchange in various materials—455(A)

Piccioni, O. and R. L. Cool. Altitude variation and transition effects of air showers—433(A)
Pickart, J. (see Maxwell, L. R.)—206(A)
Pidd, R. W. (see Crane, H. R.)—475(A)
—— (see Louisell, W. H.)—475(A)
Pigg, J. C. (see Crawford, J. H., Jr.)—243(A)
Pines, David (see Low, Francis E.)—193(L)
Pinnick, H. T. Crystallite size and diamagnetic susceptibility of carbons—228(A)
Plass, Gilbert N. Contribution of 15-micron CO_2 band to earth's radiation balance—458(A)
Platt, J. B. π-mesic atom—499(T)
Platt, Reuel T., Jr., I. L. Mador, and J. J. Markham. Production of F', M, and R centers in NaCl at room temperature—219(A)
—— (see Mador, Irving L.)—219(A); 1277(L)
—— (see Markham, J. J.)—219(A)
Plotkin, H. (see Bitter, F.)—421(L)
Plyler, Earle K. (see Mann, D. E.)—464(A)
Polk, M. L. (see Keck, P. H.)—472(A)
Pollard, Ernest (see Powell, W. F.)—494(A)
—— (see Schiffer, J. P.)—474(A)
Pomeroy, David. Teaching of biophysics—226(A)
—— (see Graham, Irven C.)—214(A)
Pond, T. A. Annihilation of positrons in solids—455(A)
Pool, M. L. and D. N. Kundu. He^3 reactions in Cu and Si—462(A)
—— (see Kundu, D. N.)—417(L)
—— (see Mack, Rex C.)—497(A); 903
Pope, N. K. (see Henshaw, D. G.)—472(A)
Porter, C. E. (see Feshbach, H.)—453(A)
Porter, N. A. (see McCusker, C. B. A.)—384
Porter, P. T. and J. I. Hopkins. α-particle straggling in thin foils—209(A)
Porter, W. C. and G. W. McClure. Observation of positive ion flux in GM counter—495(A)
Portis, A. M. Electronic structure of F centers: Saturation of electron spin resonance—1071
—— **and A. F. Kip.** Saturation of paramagnetic resonance from color centers in alkali halides—207(A)
—— (see Kip, A. F.)—1066
Powell, W. F. and Ernest Pollard. Radiation sensitivity of enzymes in intact cells—494(A)
Pratt, G. W., Jr. Eigenfunctions of S^2 by spin-operator method—212(A)
Preston, R. S. (see Whetten, N. R.)—432(A)
Prestwood, R. J. (see Bunker, M. E.)—1021(L)
Primakoff, H. μ^- meson nuclear capture in H and D—480(A)
Prince, M. B. Experimental confirmation of relation between pulse drift mobility and charge carrier drift mobility in Ge—271
—— Temperature variation of drift mobilities of minority carriers in semiconductors—208(A)
Pringsheim, Peter. Reversible bleaching of absorption band of diamond—220(A); 551
Protzman, T. F., J. J. Gouza, and W. F. Bartoe. Stress crazing thresholds of methyl methacrylate polymers—211(A)
Pruitt, J. S., S. S. Hanna, and C. D. Swartz. Neutrons from $Be^9(d,n)B^{10}$—463(A)
Pugh, Emerson M. (see Foner, Simon)—20; 229(A)
Pugh, Milton E. (see Jacobs, Donald H.)—492(A)
Purcell, E. M. (see Reif, F.)—631

Quimby, S. L. and Paul M. Sutton. Computation of mean Debye temperature of cubic crystals from elastic constants—1122

Rabi, I. I. (see Fabricand, B. P.)—1403
—— (see Lee, Charles A.)—1395
Ragent, B. and W. I. Linlor. Total neutron cross section of Pb from 30 to 150 Mev—440(A)
—— (see Linlor, W. I.)—440(A)
Rainwater, L. J. (see Melkonian, E.)—450(A)
Ralph, D. C. (see McDonald, E. W.)—223(A)
Ramsey, Norman F. Electron coupled interactions between nuclear spins in molecules—303
——, **B. J. Malenka, and U. E. Kruse.** Polarizability of the deuteron—1165
—— (see Malenka, B. J.)—1162
Randall, John G. (see Graham, Irven C.)—214(A)
Rao, A. S., V. K. Balasubrahmanyam, G. S. Gokhale, and A. W. Pereira. High-altitude measurements of intensity of cosmic radiation at magnetic latitudes 3°N and 19°N—764(L)
Rappaport, P. (see Lindner, E. G.)—202(L); 1580(E)
Rasetti, Franco and E. C. Booth. γ-ray spectrum of As^{77}—1192; of ionium (Th^{230})—315
—— (see Iwersen, Eric)—1229
Rau, R. Ronald (see Ballam, J.)—446(A); 1019(L)
Raudebaugh, Robert J. and Richard B. Belser. Structure and aging of thin metal films—449(A)
—— (see Belser, Richard B.)—449(A); 499(A)
Read, W. T. Recent advances in dislocation theory—205(T)
Reardon, William A., Ralph W. Krone, and Robert Stump. Neutron capture γ rays—442(A); in Cd, Co, and Cl—334
Reboul, T. Todd. Luminescent effects in chemically pure ZnO—229(A)
Redfield, Alfred G. Electronic Hall effect in NaCl—753(L)
—— Hall mobility in insulation photoconductors—244(A)
Rediker, R. H. (see Buskirk, A. V.)—445(A)
—— (see Thompson, R. W.)—446(A)
Reding, F. P. (see Brown, Alexander)—226(A)
Redlich, Martin G. Preferred ratios of energies of excited states of nuclei—328
Redman, J. K., R. R. Coltman, and T. H. Blewitt. Activation energy for recovery of reactor-irradiated Cu crystals—448(A)
—— (see Blewitt, T. H.)—236(A); 448(A)
Reekie, James and Thomas S. Hutchison. Structure of liquid He—490(A)
Reff, Israel. Nuclear photostar production—150
Regenier, Victor H. (see Froman, Darol)—707
Reif, F. and E. M. Purcell. Nuclear magnetic resonance in solid H—631
Reilly, Edith F. Electrostatic energy matrices of configuration f^4—876
Rense, William A. Intensity of Lyman-α line in solar spectrum—299
Repp, Gordon W. (see Jarmie, Nelson)—1023(L)
—— (see White, R. Stephen)—468(A)
Reynolds, George T. (see Ballam, J.)—446(A); 1019(L)
—— (see Brown, Fielding)—444(A)
Reynolds, H. K. (see Dunbar, D. N. F.)—496(A)
Reynolds, H. L. and A. Zucker. Range-energy relation of N ions in emulsion—496(A)
Reynolds, J. M., H. W. Hemstreet, and T. E. Leinhardt. Electrical resistance of graphite at low temperatures—1152
—— (see Hemstreet, H. W.)—242(A)
Reynolds, S. A., G. W. Leddicotte, and H. A. Mahlman. γ radiation from As^{77}—333
Rhoderick, Emlyn (see Hughes, Vernon)—828
Ribe, F. L. $Li^6(n,\alpha)H^3$ cross section as function of neutron energy—462(A)
Rice, O. K. Thermodynamics of stationary He films—209(T)

Richards, H. T. (see Jones, K. W.)—482(A); 879
Richman, C. (see Cartwright, W. F.)—677
Richter, B. (see Bitter, F.)—421(L)
Riddell, R. J., Jr. Number of Feynman diagrams—461(A); 1243
—— (see Fried, B. D.)—460(A)
Rider, John A. Polarization in liquids of intermediate conductivity—214(A)
Ridgway, S. L. (see Tomlinson, E. P.)—484(A)
Rieke, Foster F. (see Silber, Leo M.)—434(A)
Ring, J. (see Oxley, C. L.)—419(L)
Risser, J. R. (see Fowler, J. L.)—441(A)
Ritland, H. N. Density changes in glass during heat treatment—228(A)
Ritson, D. M. *K*-particle mass measurements—1572(L)
—— (see Kaplon, M. F.)—1573(L)
Roberts, B. W. Neutron diffraction study of BiMn alloy—435(A)
—— (see Wilson, V. C.)—494(A)
Roberts, Donald E. and Leo Mandelkern. Melting transition of natural rubber—225(A)
Roberts, Donald M. Polarization correlation of Nd^{144} γ cascade—497(A)
Roberts, L. D. and R. A. Erickson. Temperature scale in liquid He region—488(A)
—— (see Erickson, R. A.)—216(A)
Robeson, A., N. Snidow, and J. W. Beams. Improved equilibrium ultracentrifuge—493(A)
Robinson, J. E., C. E. Whittle, and P. S. Jastram. Branching ratio in Re^{186}—498(A)
Robinson, W. H. Response of anthracene crystals to monoenergetic soft x-rays—457(A)
Rodeback, G. W. and W. P. Eatherly. Electron mean free path of damaged Cu in terms of electrical resistivity and thermoelectric power—237(A)
Roesler, Frank C. and C. B. A. McCusker. Anisotropic distribution of secondaries in extreme energy cosmic-ray stars—690
—— (see McCusker, C. B. A.)—769(L); 769(L)
Rogers, D. H. and Melvin A. Herlin. Thermomechanical effect in liquid He II to 0.9°K—489(A)
Rohrlich, F. and D. M. Chase. Elastic scattering of protons by nuclei—454(A)
Rose, D. (see Harris, S. P.)—125
Rose, M. E. Analysis of angular correlation and angular distribution data—610
—— Angular correlation in allowed β transitions—197(L)
Rose, Marian. Cylindrical Couette flow—469(A)
Rosen, L. (see Allred, J. C.)—90
Rosenblatt, David B. Effects of primeval endowment of U^{235}—1474
Rosenstock, Herbert B. Lattice vibrations in graphite—233(A)
Ross, Donald. Characteristics of two-dimensional turbulent boundary layers—1031(A)
Rossi, B. (see Bassi, P.)—432(A)
—— (see Bridge, H. S.)—362; 1024(L)
Rostoker, Norman and Walter Kohn. New treatment of energy bands—234(A)
Roswell, A. E. (see Nowick, A. S.)—221(A)
Roth, W. L. (see Wilson, V. C.)—494(A)
Rotondi, L. (see Mayburg, S.)—1015(L)
Rouvina, J. (see Oxley, C. L.)—419(L)
Ruark, Arthur E. Classical neutron model—227(A)
Rubin, Lawrence (see Davis, Luther, Jr.)—490(A)
Rubin, R. J. (see Alpher, R. A.)—1030(A)
Rubinson, William (see Katcoff, Seymour)—1458
Ruddick, J. J. (see Buder, E. E.)—561
Ruderman, M. A. (see Henley, E. M.)—480(A)
Rüetschi, R. (see Albers-Schonberg, H.)—199(L)
Russell, R. D., H. A. Shillibeer, R. M. Farquhar, and A. K. Mousuf. Branching ratio of K^{40}—1223
Ryan, J. L. (see Jenkins, G. L.)—210(A)

Sachs, A. (see Bodansky, D.)—467(A)
Saénz, A. W. Changes in electrical, thermal, and thermoelectrical properties of monovalent metals by lattice distortions—1142
Safford, R. (see Bridge, H. S.)—362
Saha, Ajit Kumar (see Chatterjee, Santimay)—200(L)
Sailor, V. L. Parameters for slow neutron resonance in Rh—53
——, **H. H. Landon, and H. L. Foote, Jr.** Neutron resonances in rare earths—450(A)
Salkovitz, E. I. and A. I. Schindler. Brillouin zone structures of alloys. I. Implications of present theories—234(A)
—— (see Schindler, A. I.)—234(A); 1320
Salpeter, E. E. Repulsive core and charge independence—994
Salzman, G. and A. H. Taub. Rigid motion in special relativity—477(A)
Sampson, M. B. (see Carmichael, B. M.)—473(A)
—— (see Steigert, F. E.)—439(A)
Sanderson, J. A. Recent advances in atmospheric optics—459(T)
Sandoval, Manuel. Magnetic properties of sun and their relation to cosmic radiation—466(T)
Sanville, W. W., Foster C. Nix, and Frank E. Jaumot, Jr. Dilatometric study of order-disorder transformation in Cu-Au alloys—220(A)
Sarabhai, V. and R. P. Kane. Effects at Godhavn and lower latitudes of changes in energy and composition of solar cosmic rays—688
Saraf, B. L., J. Varma, and C. E. Mandeville. Radiations from As^{77} and Ge^{71}—1216
—— (see Varma, J.)—484(A)
Sard, R. D. (see Althaus, E. J.)—373
Sartain, Carl C. Electrolysis of water: Experiment in atomic physics—227(A)
Satten, R. A. Crystalline electric field in NdBr—471(A)
Sawada, Shozo. Thermal and electrical properties and crystal structure of tungsten oxide at high temperatures—1010(L)
Schaaf, S. A. Frictional phenomena in rarefied air—1031(T)
Schardt, A. W. (see Welker, Joan P.)—484(A)
Schein, Marcel, Joseph Fainberg, D. M. Haskin, and R. G. Glasser. High-energy pairs of particles from nuclear interactions—479(A); Production of high-energy electron pairs by negative pions in nuclear collisions—973
—— (see Yngve, Victor H.)—432(A)
Scherrer, V. E., W. L. Smith, B. A. Allison, and W. R. Faust. γ radiation from inelastic scattering of 2.7-Mev neutrons—768(L)
——, **R. B. Theus, and W. R. Faust.** γ rays from interaction of 14-Mev neutrons with various materials—1476
Schiessler, R. W. (see McMickle, R. H.)—466(A)
Schiffer, J. P. and Ernest Pollard. Limiting Q value for $K^{39}(\alpha,p)Ca^{42}$—474(A)
Schiffman, T. (see Heyman, R. J.)—1032(A)
Schindler, A. I. and E. I. Salkovitz. Brillouin zone investigation of Mg alloys. I. Hall effect and conductivity—1320
—— **and E. I. Salkovitz.** Brillouin zone structures of alloys. II. Hall constant data of dilute Mg alloys—234(A)
—— (see Salkovitz, E. I.)—234(A)
Schmidt, F. H. and G. L. Keister. Branching ratio and γ-ray order in decay of Sc^{46}—483(A)
Scholnick, Seymour (see Jacobs, Donald H.)—492(A)
Schrader, H. W. (see Hanson, H. P.)—457(A)

Schroeder, H. P. (see Harris, S. P.)—125
Schulz, A. G. (see Jakobson, M. J.)—695
Schwartz, Robert B., M. L. Perlman, and W. Bernstein. Radiations from Rb^{88} and Rb^{90m}—883
—— (see Wheeler, G. W.)—485(A)
Schwarzschild, A. (see Wu, C. S.)—483(A)
Schwertz, F. A. and J. J. Mazenko. Nonlinear semiconductor resistors—491(A)
Schwinger, Julian. Theory of quantized fields—713; 728
Sclar, N., E. Burstein, W. J. Turner, and J. W. Davisson. Low-temperature "breakdown" effect in Ge—215(A)
Scott, Allen B. (see Smith, William A.)—219(A)
Seeman, Nathan, D. T. King, and Maurice M. Shapiro. Charged ζ mesons—446(A)
Segrè, Emilio. Mesons and fission—499(T)
Seitz, F. Current status of F-center problem in alkali halides—218(T)
Senitzky, I. R. Interaction between classical electron and quantized electromagnetic field—1309
Seren, Leo, Milton Birnbaum, Erich Harth, and Ralph Tobin. Effect of magnetic flux amplitude on flux integrator energy control of betatron—474(A)
—— (see Birnbaum, Milton)—474(A)
Sessler, A. M. and H. M. Foley. Contributions to hyperfine spectrum of He^3 resulting from nuclear structure—444(A)
Setlow, Richard and Barbara Doyle. Effect of temperature and uv radiation on dry catalase—494(A)
Shafroth, S. M. and S. S. Hanna. Coincidence studies of B^{10} γ rays—483(A)
Shapiro, Maurice M. Nuclear emulsions in high-energy physics—481(T)
—— (see O'Dell, Francis W.)—496(A)
—— (see Seeman, Nathan)—446(A)
—— (see Stiller, Bertram)—496(A)
Sharp, W. T. (see Austern, N.)—453(A)
Shaw, T. M. and J. J. Windle. Dielectric dispersion of polar polymers at microwave frequencies—218(A)
Shaw, William C., D. E. Hudson, and G. C. Danielson. Mobilities of carriers in crystalline B—208(A)
Sheer, C., J. Moore, and C. Heindl. Measurement of resonant neutron scattering cross sections—449(A)
Shelton, Essie M. (see Josien, Marie-Louise)—235(A)
Shelton, R. D., A. H. Nielsen, and W. H. Fletcher. Infrared absorption spectrum of SO_2—235(A)
Sherman, A. (see Heyman, R. J.)—1032(A)
Sherr, R. and J. B. Gerhart. Experimental evidence for Fermi interaction in β decay of O^{14} and C^{10}—909
—— (see Gerhart, J. B.)—455(A)
Sherrill, F. A. (see Blewitt, T. H.)—236(A)
Shillibeer, H. A. (see Russell, R. D.)—1223
Shimamoto, Y. (see French, J. B.)—898
Shirane, Gen and Ray Pepinsky. Phase transitions in antiferroelectric $PbHfO_3$—212(A); 812
Shirn, G. A. (see Huntington, H. B.)—246(A)
Shockley, William. Dislocations and edge states in diamond crystal structure—228(A)
—— Electrons and holes in electric and magnetic fields—213(T)
—— Some predicted effects of temperature gradients on diffusion in crystals—1563(L)
—— (see Benedict, T. S.)—207(A)
Shore, F. J., W. L. Bendel, H. N. Brown, and R. A. Becker. Radiations from Zr^{89}—1203
Shreckengost, R. C., D. C. Swanson, and J. W. Flowers. Differential pulse-height discriminator—224(A)
Shufler, S. L. (see Zapas, L. J.)—217(A)
Shulman, R. (see Becker, M.)—491(A)
Shutt, R. P. (see Fowler, E. C.)—135
—— (see Fowler, W. B.)—479(A); 758(L); 1287(L)
Sidhu, S. S. and David Meneghetti. Neutron diffraction study of antiferromagnetic structure of pyrrhotite, FeS_x—435(A)
Siegel, Armand (see Wiener, Norbert)—1551
Siegel, R. (see Leipuner, L.)—198(L)
Silber, Leo M. and Foster F. Rieke. Faraday effect in metals at microwave frequencies—434(A)
Silverman, Albert. Photoproduction of neutral mesons in H and D—499(T)
—— (see Wolfe, B.)—446(A)
Silvey, G. (see Javan, A.)—222(A)
Simmons, B. E. (see Lewis, H. W.)—943
Simon, Albert. Production of polarized particles in nuclear reactions—226(T)
—— **and T. A. Welton.** Production and detection of polarized particles in nuclear reactions—453(A)
Simon, J. (see Zernow, L.)—233(A)
Simpson, J. Arol, J. A. Suddeth, and L. Marton. Observations in electron interferometer and their interpretation—437(A)
—— (see Marton, L.)—437(A)
—— (see Suddeth, J. A.)—437(A)
Singer, S. (see Briggs, G. R.)—438(A)
Sipple, R. F. (see Bent, R. D.)—472(A)
Sites, John R. and Bernard L. Strehler. Molecular weight of organic compounds by mass spectrometry—242(A)
—— (see Baldock, Russell)—242(A)
Sitte, Kurt and Don L. Stierwalt. Development of extensive showers in atmosphere—433(A)
—— (see Froehlich, Fritz E.)—433(A)
Sjöstrand, N. G. (see Palevsky, H.)—451(A)
Skillman, W. (see Oxley, C. L.)—419(L)
Sladek, Ronald J. New thermal resistivity maximum in superconducting alloys—1280(L)
Slater, J. C. Generalized self-consistent field method—528
——, **H. Statz, and G. F. Koster.** Two-electron example of ferromagnetism—205(A); 1323
Slifkin, L. (see Sonder, E.)—245(A)
—— (see Tomizuka, T.)—245(A)
Sloope, B. W. (see Garrett, R. E.)—441(A)
Smakula, Alexander. Bleaching of CaF_2 crystals colored by x-rays—1570(L)
Smart, J. Samuel (see Howard, Louis N.)—17
Smith, Charles S. and J. R. Haynes. Piezoresistance effect in Ge—491(A)
Smith, Cyril L. Inactivation of desoxyribonucleic acid by bombardment with deuterons and electrons—493(A)
Smith, F. M., W. Birnbaum, and Walter H. Barkas. Measurements of meson masses and related quantities—765(L)
Smith, H. M., Jr. (see Walbridge, N. L.)—1031(A)
Smith, J. E. (see Blau, M.)—949
Smith, Lincoln G. and C. C. Damm. Present status of mass synchrometer—481(A)
—— (see Damm, C. C.)—482(A)
Smith, R. O. (see Wildhack, W. A.)—213(A)
Smith, Thor L. Calculation of extrusion behavior of viscoelastic materials from relaxation distribution function—218(A)
Smith, W. L. (see Scherrer, V. E.)—768(L)
Smith, W. V. and R. G. Barnes. Electric field gradient of atomic p electrons—457(A)
Smith, William A. and Allen B. Scott. Electron energy levels in F centers—219(A)
Smith, William E. (see Hertzberg, Abraham)—1029(A)
Smoluchowski, R. Change of metallic conductivity through change in thermal scattering—245(A)

—— Phenomena of plastic flow—205(T)
—— (see Bowman, J. C.)—244(A)
—— (see Couling, L.)—245(A)
—— (see Hayes, S.)—244(A)
—— (see Haynes, C. W.)—245(A)
—— (see Vaughan, W. H.)—245(A)
Snidow, N. (see Robeson, A.)—493(A)
Snyder, H. S. (see Courant, E. D.)—202(L)
Sogo, P. B. (see Jeffries, C. D.)—1286(L)
Solimene, N. and B. P. Dailey. Rotational spectrum and molecular structure of CH_3SH—464(A)
Soller, T., W. M. Fairbank, and A. D. Crowell. Rapid separation of He^3 from He^4 by "heat flush" method—1058
Solomon, George E.—1030(A)
Sommers, H. S., Jr., W. E. Keller, and J. G. Dash. Heat of mixing of He^3 in He^4—489(A)
—— (see Goldstein, L.)—490(A)
Sonder, E., L. Slifkin, and D. Lazarus. Diffusion of Sb in Ag—245(A)
Sorenson, B. M. (see Ames, D. P.)—68
Spedding, F. H. (see Elliott, J. F.)—28
—— (see Johnson, R. G.)—466(A)
—— (see Kevane, C. J.)—1372
Spencer, L. V. and C. H. Blanchard. Spin-relativistic effects in multiple scattering of electrons—240(A)
—— (see Fano, U.)—240(A)
Sperduto, A., W. W. Buechner, M. M. Elkind, and W. J. Fader. Energy levels in N^{15}—473(A)
—— (see Buechner, W. W.)—1502
—— (see Elkind, M. M.)—463(A)
Spitzer, W. (see Becker, M.)—491(A)
Spohr, D. A. (see Webber, R. T.)—414(L)
Sponer, H. (see Heckman, R. C.)—242(A)
Sprague, G. and D. H. Tomboulian. Quadrupole moments of stable Sb nuclei—476(A)
Squire, W. (see Hertzberg, A.)—469(A)
Stafne, Marilyn J. (see Kato, W. Y.)—450(A)
Starner, J. W. (see Bunker, M. E.)—1021(L)
—— (see Knight, J. D.)—889
Statz, H. (see Slater, J. C.)—205(A); 1323
St. Clair, Byron W. Delayed neutrons in cosmic-ray stars—445(A)
Steele, M. C. and R. A. Hein. Superconductivity of Ti—490(A)
—— **and M. F. M. Osborne.** Penetration depth of superconductors—1281(L)
—— (see Berlincourt, Ted G.)—215(A)
Steffen, Rolf M. Reduction of $E1$ matrix element in mixed $E1+M2$ transition of Sr^{88}—443(A)
Stehl, O. (see Becker, E. W.)—414(L)
Steigert, F. E. and M. B. Sampson. Energy dependence of differential elastic scattering cross section of α-particles in He—439(A)
Steinberger, J. (see Bodansky, D.)—467(A)
Stephenson, S. T. (see Krogstad, R.)—457(A)
Sternheimer, R. M. Energy loss of fast-charged particle by Čerenkov radiation—256
Stevenson, M. Lynn (see Crawford, Frank S.)—468(A)
Stewart, John Q. Subject of social physics—493(A)
Stierwalt, Don L. (see Sitte, Kurt)—433(A)
Stiller, Bertram and Maurice M. Shapiro. Relativistic rise in ionization loss in nuclear emulsions—496(A)
—— (see O'Dell, Francis W.)—496(A)
Stix, T. H. Heavy nuclei in primary cosmic radiation—431(A)
Stoner, R. G., E. B. Davies, and D. C. Peckham. Shock refraction—1032(A)
Strandberg, M. W. P. (see Tate, P.)—464(A)
Straub, W. D. (see Davis, Luther, Jr.)—490(A)
Strehler, Bernard L. (see Sites, John R.)—242(A)
Stroke, H. H. (see King, J. G.)—476(A)
Stump, Robert (see Reardon, William A.)—334; 442(A)
Sturcken, E. F. and A. H. Weber. Internal conversion coefficients on Nb^{95} and Zn^{65} (actually Mo^{95} and Cu^{65})—484(A)
Suddeth, J. A., L. Marton, and J. Arol Simpson. Construction and operation of electron interferometer—437(A)
—— (see Marton, L.)—437(A)
—— (see Simpson, J. Arol)—437(A)
Sutcliffe, Charles H. and Frank E. Jaumot, Jr. Short-range order in Cu-Au alloy—221(A)
Sutton, Paul M. Variation of elastic constants of crystalline Al with temperature between 63°K and 773°K—816
—— (see Quimby, S. L.)—1122
Swan, J. B. and R. D. Hill. Internal conversion in L subshells—424(L)
Swank, Robert K. and Warren L. Buck. Plastic scintillators—495(A); Scintillation process in plastic solid solutions—927
Swann, W. F. G. Charged density distribution *versus* semi-permanent polarization as basis for electret behavior—447(A)
Swanson, D. C. Van de Graaff electrostatic generator—223(A)
—— (see Shreckengost, R. C.)—224(A)
Swanson, John (see Landauer, Rolf)—207(A); 555
Swartz, C. D. (see Pruitt, J. S.)—463(A)
Swihart, J. C. and F. J. Belinfante. Special-relativistic linear theory of gravitation—500(A)
Szendrei, M. E. (see Birks, J. B.)—197(L)

Takemoto, S., T. Dazai, and R. Chiba. Angular distributions of protons from $Na^{23}(d,p)Na^{24}$—1024(L)
Talmi, Igal. Matrix elements of β decay in jj-coupling—122
—— **and E. P. Wigner.** Evidence concerning spin-orbit forces from β decay—443(A)
Tanenbaum, M. and H. B. Briggs. Optical properties of InSb—1561(L)
—— **and J. P. Maita.** Hall effect and conductivity of InSb single crystals—1009(L)
—— **and G. L. Pearson.** Magneto-resistance effect in InSb—244(A)
Tannenwald, P. E. (see Artman, J. O.)—1014(L)
Tate, P. and M. W. P. Strandberg. Stark effect in high temperature microwave spectroscopy—464(A)
Taub, A. H. (see Salzman, G.)—477(A)
Tauber, G. E. and Ta-You Wu. Spin and magnetic moment of Li^8 nucleus—443(A)
Taylor, G. R. and S. R. Darin. Dependence of photoelastic properties of GR-S on degree of cross linking—211(A)
Teegarden, K. and R. J. Maurer. Photo-conductivity and V centers—219(A)
Telegdi, Valentine L. (see Gell-Mann, Murray)—169
—— (see Hsiao, C. A.)—473(A)
Temmer, G. M. (see Heydenburg, N. P.)—439(A)
ter Haar, D. Vapor pressure and entropy of liquid He^3—1018(L)
Terwillinger, Kent (see Jones, Lawrence W.)—699
Tesh, W. (see DeCarvalho, H. G.)—224(A)
Tessman, Jack R. Antiferroelectrics in applied field—447(A)
Teviotdale, A. (see Bitter, F.)—421(L)
Thaler, R. M., J. Bengston, and G. Breit. Effect of $^3P_2-{}^3F_2$ coupling on p-p scattering—454(A)
—— (see Bengston, J.)—454(A)
Theus, R. B. (see Scherrer, V. E.)—1476
Thomas, E. E. (see Vogel, F. L.)—230(A)

Thomas, G. E., Jr., and L. Bollinger. Construction and properties of liquid scintillation neutron counters—452(A)
—— (see Bollinger, L. M.)—452(A)
—— (see Harris, S. P.)—125
Thomas, L. H. Stability of plane Poiseuille flow—780
Thomas, R. G. Reduced widths in stripping processes—453(A)
—— (see Fowler, W. A.)—473(A)
Thompson, R. W., A. V. Buskirk, L. R. Etter, C. J. Karzmark, and R. H. Rediker. Magnetic cloud-chamber observations of V particles. II. V^0 particles—446(A)
—— (see Buskirk, A. V.)—445(A)
—— (see Cohn, Hans O.)—445(A)
Thomsen, John S. Logical relations among principles of statistical mechanics and thermodynamics—477(A); 1263
—— (see Bearden, J. A.)—482(A)
Thomson, Alice C. (see Bergmann, Peter G.)—180
Thorndike, A. M. (see Fowler, E. C.)—135
—— (see Fowler, W. B.)—479(A); 758(L); 1287(L)
Timnick, A. (see Jones, W. H.)—486(A)
Tinlot, J. H. Charge-exchange pion-nucleon scattering—466(T)
Tipton, Isabel H., W. D. Foland, Franklin C. Bobb, and W. C. McCorkle. Spectrographic analysis of human tissue—214(A)
Tittman, J. and F. F. Johnson. Moderation of Ra-Be neutrons in limestone—452(A)
Tobin, Ralph (see Birnbaum, Milton)—474(A)
—— (see Harth, Erich)—474(A)
—— (see Seren, Leo)—474(A)
Todd, W. B., Jr. (see Metzger, F. R.)—1286(L)
—— (see Varma, J.)—484(A)
Tomboulian, D. H. Absorption of P in neighborhood of $L_{2,3}$ edge—457(A)
—— (see Brown, B. M.)—1580(E)
—— (see Hartman, P. L.)—1577(L)
—— (see Sprague, G.)—476(A)
Tomizuka, T., L. Slifkin, and D. Lazarus. Diffusion of Cd in single crystals of Ag—245(A)
Tomlinson, E. P., S. L. Ridgway, and K. Gopalakrishnan. Conversion coefficients and spectrum shapes from Sb^{124}—484(A)
Toppel, B. J. and S. D. Bloom. $A^{36}(n,\alpha)S^{33}$ reaction—473(A)
Townes, C. H. Some recent developments in microwave spectroscopy—209(T)
—— (see Javan, A.)—222(A)
Tracy, James F. Scattering and absorption of π^+ mesons by Al—960
Trail, Carroll C. and C. H. Johnson. (p,n) thresholds of nuclei with $49 \leq A \leq 75$—474(A)
Trambarulo, R., S. N. Ghosh, C. A. Burrus, Jr., and W. Gordy. Microwave spectrum and molecular properties of O_3—222(A)
Treiman, S. B. Cosmic-ray albedo—432(A); 957
—— (see Ballam, J.)—446(A); 1019(L)
Trice, James B. Measurement of neutron energy distribution in ORNL graphite reactor—224(A)
Trolan, J. K. (see Dolan, W. W.)—1054
—— (see Dyke, W. P.)—1043
Truesdell, C. Precise hydrodynamical theory of absorption and dispersion of ultrasonic waves—1031(T)
Tucker, B. L. and E. C. Gregg. $Li^7(\gamma,p)He^6$ cross section—1579(L)
Tucker, Gardiner (see Hughes, Vernon)—828
Turkevich, A. (see Fung, Si-Chang)—480(A)
Turnbull, David. Nucleation in condensed systems—232(T)
Turner, W. J. (see Sclar, N.)—215(A)
Tweet, A. G. Small-angle scattering of x-rays from He I and He II—488(A)
Ueda, Ryuzo and Jinzo Kobayashi. Antiparallel dipole arrangement in WO_3—1562(L)
Uram, Earl M. Characteristics of axisymmetric turbulent boundary layers in adverse pressure gradient—1032(A)
Urquhart, Helen M. A. Single crystal magnetostriction constants of Fe-Co alloys—434(A)
—— **and J. E. Goldman.** Antiferromagnetostriction—435(A)

van der Maesen, F. (see Bray, Ralph)—231(A)
Van Horn, Wendell (see Keck, Paul H.)—243(A); 512
van Kampen, N. G. Causality condition and S matrix for nonrelativistic particles—459(A); 1267
Van Patter, D. M. (see Brown, R. J. S.)—438(A)
van Roosbroeck, W. Transport of added current carriers in homogeneous semiconductor—282
Van Voorhis, C. C. (see Bradley, L. C.)—469(A)
Van Winkle, Quentin (see Amster, Adolph B.)—211(A)
Varma, J., B. L. Saraf, and W. B. Todd, Jr. Angular correlation of γ rays of Sr^{88}—484(A)
—— (see Saraf, B. L.)—1216
Varnerin, L. J., Jr. Neutralization of ions and ionization of atoms near metal surfaces—859
Vaughan, W. H., W. J. Leivo, and R. Smoluchowski. Mechanical properties of proton-irradiated alkali halides—245(A)
Veenendaal, A. L. (see Wapstra, A. H.)—426(L)
Venkateswarlu, Putcha, Richard C. Mockler, and Walter Gordy. Microwave spectrum and structure of $HGeCl_3$—222(A)
Vidale, M. L. (see Ballam, J.)—446(A); 1019(L)
Villars, F. Collective modes of motion in nuclei—443(A)
Vineyard, George H. Second-order scattering correction in neutron and x-ray diffraction—239(A)
Vinti, John P. Theory of penetration of γ rays through thin barriers—345
Vogel, F. L. Dislocations in low-angle crystal boundaries—461(T)
——, **W. G. Pfann, H. E. Corey, and E. E. Thomas.** Dislocations in low-angle boundaries in Ge single crystals—230(A)
Volkin, Howard C. Effect of capture on slowing-down length of neutrons in hydrogenous mixtures—425(L)
Volkov, A. B. Magnetic moment deviations from Schmidt limits via admixed states—444(A)
von Dardel, G. and A. W. Waltner. Precision determination of n-p capture cross section—1284(L)
Von Foerster, H. (see Babcock, M. L.)—755(L)
von Hippel, A., E. P. Gross, J. G. Jelatis, and M. Geller. Photocurrent, space-charge build-up, and field emission in alkali halide crystals—568
Vosko, Seymour H. (see Ashkin, Julius)—1248

Wacker, Paul F. Matrix formulation of molecular orbital, Heitler-London, and configurational interaction computations—465(A)
Wahl, John S. Energy distributions of fission fragments—486(A)
Wajda, E. S. (see Huntington, H. B.)—246(A)
Walbridge, N. L., H. M. Smith, Jr., and L. A. Woodward. Production and measurement of surface ripples—1031(A)
Waldman, B. (see Anthony, D. J.)—439(A)
Waldron, S. and Melvin A. Herlin. Measurement of thermal diffusivity of Mg at low temperatures by variable state techniques—447(A)
Wales, M. Sedimentation rates in dilute and moderately-concentrated polymer solutions—211(A)
Walker, R. W. (see Whetten, N. R.)—432(A)

Walker, W. D. (see Kaplon, M. F.)—1573(L)
Wall, Nathan Sanders. $Bi^{209}(d,p)B^{210}$ Q value—485(A)
Walsh, Hohn M. (see Christian, Russell H.)—1030(A)
Walt, M. and H. H. Barschall. Angular distributions of elastically-scattered 1-Mev neutrons—441(A)
Walter, Lloyd W. Pressure and temperature distribution on circular cylinder in supersonic cross flow—470(A)
Waltner, A. W. (see von Dardel, G.)—1284(L)
Walton, R. B. (see Okazaki, A.)—440(A)
Wang, P. K. S. (see Gursky, Judith Cassidy)—239(A)
Wangsness, Roald K. g values of Ni ferrite-aluminates—206(A)
—— Sublattice effects in magnetic resonance—1085
Waniek, R. W. and T. Ohtsuka. Energy distribution of neutron stars—445(A)
—— **and Taiichiro Ohtsuka.** Energy spectrum of particles from stars—1574(L)
Wannier, Gregory H. Radiationless trapping of charge carriers in solids—207(A)
Wapstra, A. H. and A. L. Veenendaal. Decay of Mg^{28}—426
Warekois, E. (see Warren, B. E.)—233(A)
Warren, B. (see Knight, J. D.)—889
Warren, B. E., B. L. Averbach, and E. Warekois. X-ray measurements of cold-worked α-brass—233(A)
Warters, W. D., W. A. Fowler, and C. C. Lauritsen. Elastic scattering of protons by Li—917
Watanabe, K., Frederick Marmo, and Edward C. Y. Inn. Photoionization of NO—436(A); 1155
Watanabe, Satosi. Connection between fusion theory of bosons and non-local field theory—771(L)
Watson, Kenneth M. and K. A. Brueckner. Nuclear forces in pseudoscalar meson theory—460(A)
—— (see Francis, Norman C.)—454(A)
Watson, W. W. (see Kranz, A. Z.)—1469; 1472
—— (see Wheeler, G. W.)—485(A)
Weaver, A. B., J. J. Lord, and Jay Orear. Scattering of 43-Mev π^+ mesons by H—466(A)
Webb, W. (see McMickle, R. H.)—466(A)
Webber, R. T. Thermal conductivity of supra-conducting metals—481(T)
—— **and D. A. Spohr.** Thermal resistivity of superconducting Hg in intermediate state—414(L)
—— (see Alers, P. B.)—1060
Webeler, R. (see Welber, B.)—448(A)
Weber, A. H. (see Buder, E. E.)—561
—— (see Deshotels, W. J.)—448(A)
—— (see Sturcken, E. F.)—484(A)
Weidner, R. T. and C. A. Whitmer. Shape of exchange narrowed paramagnetic resonance lines—1279(L)
Weimer, D., W. Bleakney, and D. R. White. Inexpensive Mach Zehnder interferometer—1032(A)
Weinberg, A. M. Progress in reactor physics and reactor technology—226(T)
Weinman, J. A. (see Franklin, A. D.)—205(A)
Weinreich, Gabriel, Gerard M. Grosof, and Vernon W. Hughes. Hfs of metastable triplet state of He^3—195(L)
—— (see Hughes, Vernon)—196(L); 828
Weinreich, O. A. and W. E. Danforth. Electrical conduction and thermoelectric power in thorium oxide crystals—231(A)
Weinstock, E. V. and J. Halpern. Photodisintegration of deuteron at 20 Mev—461(A)
—— (see Halpern, J.)—934
Weisbaum, Samuel (see Beers, Yardley)—1014(L)
Weiss, M. M. and W. Bernstein. Degradation of Co^{60} γ rays in infinite water medium—483(A)
Weisskopf, V. F. (see Drell, S. D.)—460(A)
—— (see Feshbach, H.)—453(A)
Welber, B. and R. Webeler. Anomaly in heat content of metal in fatigued state—448(A)
Welker, Joan P., A. W. Schardt, J. J. Howland, Jr., and G. Friedlander. Metastable states of Ge^{73}—484(A)
Welton, T. A. (see Simon, A.)—453(A)
Weneser, J. Inner bremsstrahlung and magnetic moment of neutrino—1025(L)
——, **R. Bersohn, and N. M. Kroll.** Fourth-order radiative corrections to atomic energy levels—1257
Wentzel, Gregor. Many-nucleon forces—1573(L)
Wenzel, W. A. (see Dunbar, D. N. F.)—496(A)
Wert, C. A. Ordering in alloy system Mg-Cd—221(A)
Wesenberg, Clarence L. (see Lynch, Frank J.)—493(A)
Wessel, Günter and Hin Lew. Hfs of Ag with aid of universal ionizer for atomic beams—476(A)
Wessel, Walter and S. J. Czyzak. Interpretation and generalization of Dirac's theory of electron—986
Westcott, C. H. and J. S. Kirkaldy. Corrections for dead-time of counters in coincidence systems—495(A)
Westervelt, D. R. Z centers in alkali halides—218(A)
Wexler, S. (see Harris, S. P.)—125
Weyl, Peter K. Energy loss of H, He, N, and Ne ions in gases—289
Whaling, W. (see Dunbar, D. N. F.)—496(A)
Wheeler, G. W., R. B. Schwartz, and W. W. Watson. (d,p) reactions with separated Kr isotopes—485(A)
Whetten, N. R., R. S. Preston, R. V. Adams, and R. W. Walker. Cloud-chamber investigation of nuclear interactions—432(A)
White, D. R. (see Weimer, D.)—1032(A)
White, Irene S. (see Anslow, Gladys A.)—241(A)
White, R. Stephen, Gordon W. Repp, and Nelson Jarmie Positive photomesons from H at 0°—468(A)
—— (see Jakobson, M. J.)—695
—— (see Jarmie, Nelson)—1023(L)
White, Robert L. Quadrupole coupling of deuteron in DCCCl and DCN—1014(L)
Whitehead, M. N. (see Cartwright, W. F.)—677
Whitmer, C. A. (see Weidner, R. T.)—1279(L)
Whittemore, W. L. (see Fowler, E. C.)—135
—— (see Fowler, W. B.)—479(A); 758(L); 1287(L)
Whittle, C. E., J. P. Hurley, and P. S. Jastram. β-γ correlations in decay of Re^{186}—498(A)
—— (see Robinson, J. E.)—498(A)
Whyte, G. N. (see Kastner, J.)—332
Widom, B. and S. H. Bauer. Energy exchange in molecular collisions—240(A)
Wiedling T. Metastable state of V^{50}—767(L)
Wiener, Norbert and Armand Siegel. New form for statistical postulate of quantum mechanics—1551
Wigner, E. P. (see Talmi, I.)—443(A)
Wiig, Edwin O. (see Fink, Richard W.)—194(L)
Wilcox, H. A. (see Cartwright, W. F.)—677
Wildhack, W. A. and R. O. Smith. Effect of centrifugal force field on response of vibrating mass-spring system—213(A)
Wilets, Lawrence, David L. Hill, and Kenneth W. Ford. Isotope shift anomalies and nuclear structure—1488
Wilkins, H. C. and M. Annis. Interaction cross section of μ mesons with nuclei—480(A)
Wilkinson, D. H. and G. A. Jones. $Li^6(\alpha,\gamma)B^{10}$—1575(L)
Willard, D. (see Dayton, B.)—348
Willardson, R. K., A. C. Beer, and A. E. Middleton. Electrical properties of AlSb—243(A)
Willenbrock, F. K. and N. Bloembergen. Paramagnetic resonance in N- and P-type Si—1281(L)
Williams, Dudley (see Breneman, Edward J.)—465(A)
Williams, H. J., R. M. Bozorth, and Matilda Goertz. Mechanism of transition in magnetite at low temperatures—1107

Willis, Charles and Harry L. Frisch. Vapor-liquid transitions in closed system—465(A)
Wilson, B. G. (see McCusker, C. B. A.)—384
Wilson, Elizabeth (see Friedlander, G.)—498(A)
Wilson, R. R. (see Luckey, D.)—468(A)
—— (see Palfrey, T. R.)—468(A)
Wilson, V. C., B. W. Roberts, W. L. Roth, J. S. Kasper, and A. H. Geisler. Double crystal neutron spectrometer—494(A)
Wimett, T. F. d-p magnetic moment ratio—499(A)
—— Nuclear resonance line structure in HD and molecular shielding in HD, H_2, and D_2—476(A)
Winckler, John R. and Kinsey Anderson. High-altitude cosmic-ray investigation by means of Čerenkov counter. II. Experimental results—431(A)
—— (see Anderson, Kinsey)—431(A)
Windle, J. J. (see Shaw, T. M.)—218(A)
Winkler, Eva M. Design and calibration of total-temperature probes for use at high supersonic speeds and elevated temperatures—469(A)
Winkler, Stanley and Seymour Nozick. Noise in storage tubes—492(A)
Winnemore, Barbara (see Gursky, Herbert)—209(A)
Winsnes, M. H. (see Grimes, D. M.)—435(A)
Winston, A. W. (see Goldschmidt-Clermont, Y.)—468(A)
Winther, A. (see Alder, K.)—1578(L)
Witmer, Enos E. Excitation energies of nuclei as rational multiples of electron mass—500(A)
—— Nuclear masses as rational multiples of electron mass—482(A)
Witzig, W. F. (see Glick, Harvey L.)—236(A)
Wolfe, B., J. DeWire, and A. Silverman. Particle selection using crystal telescope—446(A)
Wolff, P. A. Plasma waves in metals—233(A)
Wolfsberg, Max. Configurational interaction in molecular orbital theory and relative energies of polar and nonpolar functions—464(A)
—— (see Elliott, N.)—435(A)
Wollan, E. O. (see Koehler, W. C.)—597
Wood, Lawrence A. Crystallization in butadiene-styrene copolymers—225(A)
Woodward, L. A. (see Walbridge, N. L.)—1031(A)
Woodward, William. Photodisintegration of deuteron—456(T)
Worley, R. D., M. W. Zemansky, and H. A. Boorse. Heat capacities of superconducting and normal Ta—1567(L)
Wright, G. T. Scintillation response of organic phosphors—1282(L)
Wrinch, Dorothy. Fourier transforms of shells and intensities from crystalline proteins—471(A)
Wu, C. S., F. Boehm, and E. Nagel. Radiations from RaD and RaE—319
—— **and A. Schwarzschild.** β spectrum of C^{14}—483(A)
—— (see der Mateosian, E.)—497(A)
Wu, Ta-You (see Bauer, Ernst)—458(A)
—— (see Moses, Harry E.)—458(A); 1408
—— (see Tauber, G. E.)—443(A)

Yagoda, Herman. Observations on stars and heavy primaries recorded in emulsions during flight of Viking rocket—445(A)
Yeater, M. L. and E. R. Gaerttner. Neutron time-of-flight spectrometer with betatron source—451(A)
Yngve, Victor H. and Marcel Schein. Time variation of cosmic-ray heavy nuclei—432(A)
Yntema, G. B. Magnetoresistance of Mg, Cu, Sb, and Al at liquid He temperatures—1388
Yokota, Ryosuke. Thermoluminescence of quartz and fused quartz colored by x-ray irradiation—1013(L)
Young, J. E. R. (see Bitter, F.)—421(L)
Yukawa, Hideki. Structure and mass spectrum of elementary particles. I. General considerations—415(L); II. Oscillator model—416(L)

Zacharias, Jerrold R. (see Daly, Richard T., Jr.)—476(A)
Zaffarano, D. J. (see Mize, J. P.)—210(A)
Zapas, L. J., S. L. Shufler, and T. W. DeWitt. Dynamic properties of unvulcanized GR-S—217(A)
Zarwyn, Berthold. Generalized theory of Mach reflection of shock waves—470(A)
Zemansky, M. W. (see Worley, R. D.)—1567(L)
Zernow, L. and J. Simon. Plastic behavior of polycrystalline metals at very high strain rates—233(A)
Zilsel, P. R. He II: Bose-Einstein condensation and two-fluid model—216(A)
—— (see Darling, B. T.)—1252
Zimm, B. H. Statistical mechanics of polymer chains in solution—232(T)
Zissis, G. J. (see Deverall, G. V.)—297
Zucker, A. (see Reynolds, H. L.)—496(A)
Zumino, Bruno. True vaccum and dressed particles in quantum field theory—478(A)
Zupančič, Črtomir (see Beckman, Olof)—606

Author Index to Volume 92

References with (A) are to abstracts of papers presented at meetings of the American Physical Society, and those with (T) designate title only. References with (L) are to Letters to the Editor. References with (E) are to Errata.

Abe, Hidetarō. Anomalous paramagnetic resonance in Cu propionate—1572(L)
—— (see Ōno, Kazuo)—551
Abragam, A. and R. V. Pound. Influence of electric and magnetic fields on angular correlations—943
—— **and J. H. Van Vleck.** Theory of microwave Zeeman effect in atomic oxygen—1448
Abrahams, Elihu and C. Kittel. Electronic spin resonance line width in metals—544(A)
Adair, Robert K. Spin-orbit coupling energy in O^{17}—1491
Adams, Edward N., II. Consequences of possible degeneracy of energy bands in Ge—1063(L)
Adel, Arthur. Seasonal trend of atmospheric ozone as revealed by solar-telluric band at 9.6 microns—1080(A)
Agogino, Mercedes M. Time variations in cosmic-ray intensity underground—1086(A)
Alburger, David E. Isomeric transition of Pb^{207} as energy standard in beta spectroscopy—1257
—— **and M. H. L. Pryce.** Isomerism in Pb^{206}—514(L)
Alford, W. L. (see Leighton, R. B.)—540(A)
Alford, W. Parker (see Hamilton, Donald R.)—1522
Allen, William A. Elastic description of high-amplitude spherical pulse in steel—1082(A)
Alley, C. L. (see Linford, L. B.)—1093(A)
Alpher, Ralph A., James W. Follin, Jr., and Robert C. Herman. Physical conditions in initial stages of expanding universe—1347
Altshuler, Saul. Binary rearrangement collision—1157
Amin, M. R. Pre-onset burst pulses in positive point to plane corona in air—536(A)
Anderson, A. B. C. Dependence of primary pfeifenton (pipe tone) frequency on pipe-orifice geometry—543(A)
—— (see Schilberg, Lloyd E.)—543(A)
Anderson, C. D. Recent results on V particles—1086(T)
——, **E. W. Cowan, R. B. Leighton, and V. A. J. van Lint.** Cascade decay of V particles—1089(A)
—— (see Cowan, E. W.)—1089(A)
Anderson, E. C., C. L. Cowan, Jr., and F. Reines. Properties of large liquid scintillation detectors—1088(A)
—— (see Schuch, R. L.)—1088(A)
Angell, C. E. and J. P. Perry. Attenuation cross sections of 37-Mev pions in H—835(L)
—— (see Barnes, S. W.)—1327(L)
Anson, John H., Kenneth A. Wright, and John G. Trump. Average energy of electrons emitted from metals under high-energy electron bombardment—843(A)
Antonoff, George. Law of equilibrium between coexisting phases—542(A)
Ard, W. B. (see Fairbank, W. M.)—208(L)
Arfken, G. B. (see Guernsey, R. L.)—1270
Arnold, James R. (see Guttman, Lester)—547
Arnowitt, R. Hfs of hydrogen—1002
—— **and S. Deser.** Solutions of meson-nucleon equation in adiabatic limit—1061(L)
Asaro, Frank, Frank Stephens, Jr., and I. Perlman. Complex α spectra of radiothorium (Th^{228}) and thorium-X (Ra^{224})—1495
——, **S. G. Thompson, and I. Perlman.** α spectra of Cm^{242}, Cm^{240}, and Cm^{241}—694
Ashburn, E. V. Measurement of light scattered from searchlight beam—534(A)
Atkins, K. R. Hydrodynamics of liquid He II—849(T)
—— Liquid He films—1571(L)
—— **and K. H. Hart.** Attenuation of second sound above 1°K—204(L)
Austern, N. Evaluation of interaction effect in n-p capture—670
——, **S. T. Butler, and H. McManus.** Angular distributions from (n,p) nuclear reactions—350.
Avery, Eugene, L. Grossweiner, and M. Matheson. Electron traps in ice—1080(A)
—— (see Smaller, Bernard)—232

Bacher, R. F., J. C. Keck, V. Z. Peterson, J. G. Teasdale, A. V. Tollestrup, R. L. Walker, and R. M. Worlock. Photoproduction of positive mesons from H: results—1090(A)
Bader, M., W. A. Wenzel, and W. Whaling. Proton stopping cross section of Li—1085(A)
Bakamjian, B. and L. H. Thomas. Relativistic particle dynamics—1300
Baldock, Russell (see Sites, John R.)—1096(A)
Balkwell, W. R. (see Litz, L. M.)—288
Ball, W. P., Burton J. Moyer, and Robert E. Richardson. Nuclear scattering of "300" Mev neutrons—539(A)
Bame, S. J., Jr. Excitation functions for $(n,2n)$ reactions in Ge, Sc, As, Tl, and Ni—1096(A)
Bandtel, Kenneth C. (see Frank, Wilson)—537(A)
—— (see Madey, Richard)—537(A)
Baños, Alfredo, Jr. Magnetic shielding produced by rotating conducting tube—1081(A)
Baranger, M., H. A. Bethe, and R. P. Feynman. Relativistic correction to Lamb shift—482
Barbour, J. P., W. W. Dolan, J. K. Trolan, E. E. Martin, and W. P. Dyke. Space charge effects in field emission—45
Barkas, Walter H. (see Deutsch, R. W.)—539(A)
—— (see Wilson, H. W.)—537(A)
Barnes, C. A. (see Neilson, G. C.)—1084(A)
Barnes, Raymond F. (see Fred, Mark)—1322(L)
Barnes, S. W., C. E. Angell, J. P. Perry, D. Miller, J. Ring, and D. Nelson. Signs of phase shifts for pion-proton scattering—1327(L)
Baroody, E. M. Role of surface barrier in secondary emission from metals—843(A)
Baskin, R. and J. R. Winckler. Relative ionization by cosmic ray μ mesons in liquid scintillator—464
Baskir, E. (see Cartwright, W. F.)—852(A)
Bassi, P., G. Clark, and B. Rossi. Distribution of arrival times of air shower particles—441
Bauer, Ernest. Vibrational spectrum and specific heat of Na—58
—— **and Ta-You Wu.** Origin of E layer of ionosphere—1101
Baumann, K. (see Halpern, O.)—1070(L)
Beach, L. A., R. B. Theus, and W. R. Faust. Penetration of gamma radiation through Fe—355
Beams, J. W. Single crystal metal rotors—502(L)
Becker, J. A. Field emission from O on W—854(T)
Bedard, F. D., J. J. Gallagher, and C. M. Johnson. Microwave measurement of D_0 for CO—1440
Belinfante, Frederik J. Intrinsic magnetic moment of elementary particles of spin $\frac{3}{2}$—997
—— Magnetic moments of neutron and proton—994
—— Pions from production of baryons by protons—145
Bell, W. A., Jr., L. O. Love, C. E. Normand, and W. K. Prater. Electromagnetic separation of Pd, Pt, and Ru isotopes—1096(A)
Bellamy, M. D. Biological studies with high-energy cathode rays—841(T)

Belser, Richard B. Effects of high sputtering rates on resistivities of sputtered Au films—1083(A)
—— In, versatile solder to metals and nonmetals—1098(A)
—— Structure and resistivities of Au films deposited by evaporation and sputtering—1098(A)
Benedict, W. S., Norman Gailar, and Earle K. Plyler. ν_1 band of D_2O in infrared—533(A)
Benedikt, E. T. Magnetoelectrostatics—1081(A)
Benjamin, Ben M. (see Livingston, Ralph)—1271
Bennett, Arthur L. Detonation in gases—543(A)
Bennett, Edgar F. (see Woods, Frank R.)—853(A)
Bergmann, Peter G. and Ezra Newman. Grand canonical ensembles, Laplace transform, and Darwin-Fowler contour integrals—856(A)
Bergström, Ingmar and R. D. Hill. Radioactivities of Tl isotopes—849(A)
—— **R. D. Hill, and G. De Pasquali.** Neutron-deficient isotopes of Tl—918
Berlin, T. H., L. Witten, and H. A. Gersch. Imperfect gas—189
Berlincourt, Ted G. deHaas-van Alphen effect in As—1068(L)
Bernstein, W. (see Perlman, M. L.)—1236
—— (see Weiss, M. M.)—1264
Bertolini, G., M. Bettoni, and A. Bisi. Total ionization of α particles of Po in mixtures of gases—1586(L)
Bethe, H. A. (see Baranger, M.)—482
Bettoni, M. (see Bertolini, G.)—1587(L)
Bever, R. S. (see Sproull, R. L.)—77
Bickford, L. R., Jr. Magnetic resonance in ferrimagnetic and antiferromagnetic systems—845(A)
—— (see Stull, J. L.)—845(A)
Birnbaum, G. and A. A. Maryott. Change in inversion spectrum of ND_3 from resonant to non-resonant absorption—270
Bisi, A. (see Bertolini, G.)—1587(L)
Bitter, Francis and Herman Feshbach. Nuclear radii—837(L)
Bjerregaard, Jørgen H. (see Huus, Torben)—1580(L)
Black, L. D. (see Pringle, R. W.)—1583(L)
Blatt, John M. and M. H. Kalos. Yukawa forces with added attractions—1563
Blau, M., M. Caulton, and J. E. Smith. Meson production by 500-Mev negative pions—516(L)
Bockelman, C. K., C. P. Browne, W. W. Buechner, and A. Sperduto. Inelastic scattering of protons and deuterons from B^{10} and N^{14}—665
Bohm, David and David Pines. Collective description of electron interactions: III. Coulomb interactions in degenerate electron gas—609
Bollinger, L. M., S. P. Harris, C. T. Hibdon, and C. O. Muehlhause. Neutron absorption and scattering by Hf—1527
Bonnor, W. B. Non-symmetric unified field theories—1067(L)
Boorse, Henry A. (see Brown, A.)—52
—— (see Smith, Bernard)—505(L)
Bourne, Henry C., Jr., Robert W. Cloud, and John G. Trump. Electron emission from metals under high-energy positive ion bombardment—847(A)
Bowen, D. B. and G. W. Rodeback. Influence of cold work and radiation damage on vibrational spectra of Cu—531(A)
Bowen, I. Gerald. Atmospheric ozone fluctuations at Albuquerque—1080(A)
Brachman, M. K. (see Hellund, E. J.)—822
Bradley, Richard C. Vacuum sputtering of metallic Na by inert gas ions—535(A)
Bratenahl, A. and B. J. Moyer. Pick-up process in proton-deuteron scattering—538(A)
Breckenridge, Robert G. (see Cook, Richard K.)—1419
Brentano, J. C. M. and I. Ladany. Recording of x-ray diffraction patterns by scintillation counter—850(A)
Brice, M. K. (see Cork, J. M.)—119; 367
Brinkman, J. Quenched vacancies in AuCu and $AuCu_3$—531(A)
Brix, P., J. T. Eisinger, H. Lew, and G. Wessel. Zeeman effect of Cr ground state—647
Brode, Robert B. North-south observations of ratio of positive to negative cosmic-ray mesons—1086(A)
—— Transition phenomena—1086(T)
Broder, J. (see Keck, P. H.)—847(A)
Brolley, J. E., Jr. (see Northrop, J. A.)—1091(A)
Brook, Marx. New studies of N_2 afterglows—1079(A)
Brousseau, A., C. L. Cowan, Jr., and F. Reines. Device for testing large numbers of photomultipliers—1088(A)
Brown, A., M. W. Zemansky, and H. A. Boorse. Superconducting and normal heat capacities of Nb—52
Brown, Frederick C. Hall effect in AgCl at low temperature—502(L)
Brown, Frederick C. Temperature dependence of electron mobility in AgCl—858(A)
Brown, H. (see Patterson, C.)—1234
Brown, Karl L. and Richard Wilson. Electrodisintegration of nuclei—540(A)
Brown, S. Leroy and John M. Norwood. Harmonic analyses of pulses and spectral analyses of transients—534(A)
Brown, W. L., R. C. Fletcher, and K. A. Wright. Annealing of bombardment damage in Ge: Experimental—591
—— (see Fletcher, R. C.)—585
Browne, C. P. (see Bockelman, C. K.)—665
Brueckner, K. A. and K. M. Watson. Nuclear forces in pseudoscalar meson theory—1023
Bryant, P. J., H. U. Rhoads, and A. H. Weber. Electrical conductance and structure studies of thin Bi films evaporated on glass—1083(A)
Bube, Richard H., Simon Larach, and Ross E. Shrader. Mechanism of impurity poisoning in luminescence of ZnS phosphors with Mn activator—1135
Buechner, W. W. (see Bockelman, C. K.)—665
Bunker, M. E., R. J. Prestwood, and J. W. Starner. Scintillation study of As^{77} and Br^{77}, erratum—1587(E)
Burcham, W. E., W. M. Gibson, A. Hossain, and J. Rotblat. Scattering of 9.5-Mev protons by C and O—1266
Burke, B. F. (see Hardy, W. A.)—1533
Burrus, Charles A., Jr., and Walter Gordy. 1–2 mm wave spectroscopy. II. H_2S—274; III. NO and DI—1437
Burson, S. B. (see Jordan, W. C.)—315; 1218
Burstein, E. and B. W. Henvis. Color-center formation in alkali halides containing $S^=$—845(A)
—— (see Sclar, N.)—858(A)
Busemann, Adolf. Steady and unsteady phenomena at transonic speeds—1087(T)
Buskirk, A. V. (see Thompson, R. W.)—209(L)
Butler, S. T. (see Austern, N.)—350
Byram, E. T., T. A. Chubb, and H. Friedman. Contribution of solar x-rays to E-layer ionization—1066(L)
Byrne, F. T. (see Dieke, G. H.)—81

Calbick, C. J., H. Christensen, and E. E. Thomas. Cleavage surfaces in Ge crystals—1082(A)
—— (see Christensen, I. H.)—1082(A)
Callaway, Joseph. Equations of motion in Einstein's new unified field theory—1567
Cameron, A. G. W. (see Hoffman, M. M.)—1184
Campbell, E. C. (see McGowan, F. K.)—523(L)
Cardwell, Alvin B. Photoelectric studies of Fe—554
Carlson, B. C. Periodic ellipse of strong-focusing equations—839(L)
Carmichael, B. M. (see Rasmussen, V. K.)—852(A)
Carothers, James Edward. Ratio of π^+ to π^- mesons produced by γ rays—538(A)
Carr, W. J., Jr. Use of non-orthogonal wave functions in treatment of solids, with applications to ferromagnetism—28
Carter, R. S., H. Palevsky, V. W. Myers, and D. J. Hughes. Thermal neutron absorption cross sections of B and Au—716

Cartwright, W. F., C. L. Oxley, J. Rouvina, E. Baskir, D. Klein, J. Ring, and W. A. Skillman. Apparatus for double scattering of 240-Mev protons—852(A)
Carver, T. R. and C. P. Slichter. Polarization of nuclear spins in metals—212(L)
Casson, H., L. S. Goodman, and V. E. Krohn. Energy level of Ti^{48} from decay of Sc^{48} and V^{48}—1517
Castle, J. G., Jr. Paramagnetic resonance absorption in graphite—1063(L)
Catalano, Edward (see Stout, J. W.)—1576(L)
Caulton, M. (see Blau, M.)—516(L)
Charbonnier, Francis M. (see Miller, Charles E.)—406
Chen, F. F. (see Shapiro, A. M.)—1073(L)
Ch'en, Shang-Yi (see Takeo, Makoto)—850(A)
Cheston, W. and H. Primakoff. "Non-mesonic" bound V-particle decay—1537
Chiang, S. F. and S. A. Schaaf. Drag on rotating cylinder at low pressures—535(A)
Chraplyvy, Zeno. Reduction of relativistic two-particle wave equations to approximate forms—1310
Christensen, H., C. J. Calbick, and E. E. Thomas. Cleavage surfaces of Ge crystals—1082(A)
—— (see Calbick, C. J.)—1082(A)
Christensen, R. L. Slow neutron resonances in Ta—1509
Christy, R. F. Coupling of angular momenta in nuclear reactions—529(A)
—— (see Liberman, D. A.)—1085(A)
Chubb, T. A. (see Byram, E. T.)—1066(L)
Clark, G. (see Bassi, P.)—441
Clement, J. R. Atomic heat and critical magnetic field of superconducting Cd—1578(L)
—— **and E. H. Quinnell.** Atomic heat of In below 20°K—258
Cloud, Robert W. (see Bourne, Henry C., Jr.)—847(A)
Cobble, J. W. (see Daunt, J. G.)—507(L)
Cohen, Bernard L. Statistical theory of nuclear reactions—1245
—— **and T. H. Handley.** Experimental search for stable dineutron—101
Cohen, Victor W. (see Hardy, W. A.)—1533
—— (see Kikuchi, C.)—109
Cole, Julian D. Slender bodies of revolution at transonic speeds—1087(T)
Conger, Robert L. Nuclear magnetic relaxation in viscous liquids—543(A)
Consolazio, George (see Sites, John R.)—1096(A)
Cook, Richard K. and Robert G. Breckenridge. Anelasticity of quartz—1419
Cooper, E. P. Water entry theory—527(T)
Cooper, L. N. and E. M. Henley. μ-mesonic atoms and electromagnetic radius of nucleus—801
Coor, T. (see Hornyak, W. F.)—675
Cork, Bruce and Emery Zajec. Quadrupole focusing lenses for charged particles—853(A)
Cork, J. M., J. M. LeBlanc, M. K. Brice, and W. H. Nester. Radioactive decay of Ca^{47}—367
——, **W. H. Nester, J. M. LeBlanc, and M. K. Brice.** Radioactive decay of W^{181}—119
—— (see Jordan, W. C.)—315; 1218
Cornelius, R. C., C. P. Sargent, M. C. Rinehart, L. M. Lederman, and K. Rogers. Rest mass energy of negative pion—1583(L)
Cowan, C. L., Jr. Experiment to detect free neutrino—1088(T)
—— (see Anderson, E. C.)—1088(A)
—— (see Brousseau, A.)—1088(A)
—— (see Harrison, F. B.)—1088(A)
—— (see Hayes, F. N.)—1088(A)
—— (see Reines, F.)—830(L)
—— (see Schuch, R. L.)—1088(A)
Cowan, E. W., C. D. Anderson, R. B. Leighton, and V. A. J. van Lint. Cascade decay of V particles—1089(A)
—— (see Anderson, C. D.)—1089(A)
Cowan, R. D. Properties of Hugoniot function—1079(A)
Cox, E. F. Atmospheric propagation of sounds from explosions—1093(T)
Cox, J. T. (see Livingston, Ralph)—1271
Cox, L. A. (see Schwager, J. E.)—102
Crandall, Walter E. and Burton J. Moyer. Characteristics of neutral meson production in proton bombardment of C nuclei—749
Crasemann, Bernd. Trochoidal analyzer for charged particles—544(A)
Crawford, J. H., Jr. (see Stevens, D. K.)—1065(L)
Crozier, W. D. (see Gourley, Mary Gaulks)—526(A)
Culp, Richard J. (see Hamermesh, Bernard)—211(L)
Cunningham, S. P. (see Dieke, G. H.)—81
Curtis, Mary Lou. Half-life determination of Po^{210} by α counting—1489

Danos, M., S. Geschwind, H. Lashinsky, and A. van Trier. Čerenkov effect at microwave frequencies—828(L)
Darling, B. T. Field theory of equations with many masses—1547
Dash, J. G. (see Sommers, H. S., Jr.)—1345
Dash, William C. Optical absorption and photoconduction in visible and near infrared in single crystals of BaO—68
Daunt, J. G. and J. W. Cobble. Superconductivity of Tc—507(L)
—— (see de Vries, G.)—1573(L)
Dauphinee, T. M. (see Preston-Thomas, H.)—844(A)
Davidson, J. P. and D. C. Peaslee. Cross terms in allowed-shape β spectra—1584(L)
Davis, William R. (see Miller, Charles E.)—406
Davisson, J. W. (see Sclar, N.)—858(A)
Day, P. (see Primak, W.)—1064(L)
Day, Robert B. and Richard L. Henkel. Neutron total cross sections at 20 Mev—358
—— (see Woodbury, H. H.)—1199
Dehmelt, H. G. Nuclear quadrupole resonance of stable Ga isotopes—1240
—— (see Fairbank, W. M.)—208(L)
De Juren, J. and H. Rosenwasser. Pulse-height measurements of recoils from $B^{10}(n,\alpha)Li^7$ in A-CO_2 mixtures—544(A)
Dekker, A. J. (see Williams, G. W.)—1398
Denney, J. M. Radiation-damage energy threshold in f.c.c. alloy—531(A)
DePangher, John. High-pressure cloud-chamber investigation of protons scattered by 300-Mev neutrons—1084(A)
De Pasquali, G. (see Bergström, I.)—918
—— (see Frauenfelder, H.)—513(L); 1241
der Mateosian, E. Scintillation spectrometer determination of L-capture to K-capture ratio in Cd^{109} and I^{126}—938
Deser, Stanley. Electromagnetic effects in two-nucleon systems—1542
—— (see Arnowitt, R.)—1061(L)
de-Shalit, A. Shell model—843(T)
—— **and M. Goldhaber.** Mixed configurations in nuclei—1211
Deutsch, Robert W. Yields of low-energy protons and alphas resulting from high-energy bombardment of Ag—515(L)
—— **and W. H. Barkas.** Secondary particles induced by 375-Mev α particles—539(A)
de Vries, G. and J. G. Daunt. Specific heat of He^3 between 1.3°K and 2.3°K—1572(L)
DeWire, J. W., A. Silverman, and B. Wolfe. Elastic photoproduction of π^0's from deuterium—520(L)
——, **A. Silverman, and B. Wolfe.** High-energy (γ,d) reactions—519(L)
Diamond, Herbert, Paul R. Fields, Joseph Mech, Mark G. Inghram, and David C. Hess. Half-life of Am^{243}—1490
Dieke, G. H., S. P. Cunningham, and F. T. Byrne. Zeeman effect in molecular spectra of H_2—81

Dingle, R. B. Low-temperature diamagnetism of electrons in cylinder—1320(L)
Ditzenberger, J. A. (see Fuller, C. S.)—846(A)
Diven, B. C. (see Martin, H. C.)—1096(A)
Dixon, C. E. and C. J. Meechan. Effect of quench temperature and cold work on ordering rates of Cu_3Au and CuAu—530(A)
Dolan, W. W. (see Barbour, J. P.)—45
Domenicali, Charles A. Irreversible thermodynamics of thermoelectric effects in inhomogeneous, anisotropic media—877
Douglas, David L., Anita C. Mewherter, and Robert P. Schuman. Long-lived activity in neutron-irradiated Nb—369; 1095(A)
Drell, S. D. (see Lawson, R. D.)—539(A)
Dresselhaus, G., A. F. Kip, and C. Kittel. Observation of cyclotron resonance in Ge crystals—827(L)
Duckworth, H. E. Mass-spectrographic studies of nuclear stability—848(T)
—— (see Hogg, B. G.)—848(A)
Dudziak, Walter (see Sagane, Ryokichi)—212(L)
DuMond, Jesse W. M., H. C. Hoyt, P. E. Marmier, and J. J. Murray. Decay of Ta^{183}—202(L)
—— (see Felt, Gaelen L.)—1160
Dunbar, D. N. F., R. E. Pixley, W. A. Wenzel, and W. Whaling. 7.68-Mev state in C^{12}—649
——, **H. K. Reynolds, W. A. Wenzel, and W. Whaling.** Stopping cross section of several gases for protons and deuterons—528(A)
—— (see Hoyle, F.)—1095(A)
—— (see Reynolds, H. K.)—528(A); 742
Dunlap, W. C., Jr., and R. L. Watters. Direct measurement of dielectric constants of Si and Ge—1396
Dunlavey, Dean C. and Glenn T. Seaborg. α activity of Sm^{146} as detected with nuclear emulsions—206(L)
Dyba, R. V. (see Lane, C. T.)—829(L)
Dyke, W. P. High-density field-emission phenomena—854(T)
—— **and J. K. Trolan.** Field emission: Large current densities, space charge, and vacuum arc—541(A)
—— (see Barbour, J. P.)—45
Dyson, Freeman J. Dynamics of disordered linear chain—1331

Easterday, Harry T. β decay of Cu^{67}—537(A)
Efremov, N. New method for approximate calculation of effective ionic radii—1081(A)
Eggen, D. T. and H. Kenworthy. NAA statitron for solid-state research—531(A)
Eggleston, R. R. Annealing of radiation damage effects in Cu—531(A)
Eisberg, Robert M. and George J. Igo. Spectrum of particles from Pb bombarded by 32-Mev protons—537(A)
Eisinger, J. T. (see Brix, P.)—647
Elkind, Mortimer M. Excited states of B^{11} and B^{12} from $B^{10}(d,p)B^{11}$ and $B^{11}(d,p)B^{12}$—127
Ellis, W. C. and E. S. Greiner. Production of acceptor centers in Ge and Si by plastic deformation—1061(L)
El-Mofty, Osman. Multiple cores in air showers—461; 1086(A)
Elsasser, W. M. and K. McDonald. Topology of magnetic fields—1081(A)
El-Sum, Hussein M. A. and Paul Kirkpatrick. Refinement and resolution in reconstructed wavefront microscopy—541(A)
Elterman, L. Stratospheric temperature profiles obtained from searchlight measurements—1080(A)
Emigh, C. R. (see Megill, L. R.)—1081(A)
English, W. N. Thermal microstructure in ocean—1087(A)
Ennis, M. E. and A. Hemmendinger. Small angle cross sections for scattering of protons by tritons—1092(A)
Ergen, W. K. Current status of theory of reactor dynamics—854(T)
Eschenfelder, A. H. and R. T. Weidner. Saturation effects in paramagnetic resonance—869
Eubank, Harold P. High-yield rf ion source—853(A)

Fagan, J. F., Jr. (see Watters, H. J.)—1248
Fagg, L. W. and S. S. Hanna. Polarization of γ rays in $F^{19}(p,\alpha\gamma)O^{16}$ reaction—372
Fairbank, W. M., W. B. Ard, H. G. Dehmelt, Walter Gordy, and S. R. Williams. Temperature dependence of the nuclear susceptibility of He^3 between 1.2°K and 4.2°K—208(L)
Fan, H. Y. Effect of traps on carrier injection in semiconductors—1424
Faneuff, C. E. (see Malich, C. W.)—1095(A)
Fano, U. Degradation and range straggling of high-energy radiations—328
Faust, W. R. (see Beach, L. A.)—355
Fechter, H. R. (see Hofstadter, R.)—978
Feldman, David. Implications of Lorentz invariance for scattering of spin $\frac{1}{2}$ particles—856(A)
—— Invariant forms of nucleon-nucleon interaction—824
Felt, Gaelen L., John N. Harris, and Jesse W. M. DuMond. Precision measurement at 24 500 volts of conversion constant λV—1160
Ferentz, M., M. Gell-Mann, and D. Pines. Giant nuclear dipole resonance—836(L)
Fermi, E. Developments in high-energy physics—1091(T)
—— Multiple production of pions in nucleon-nucleon collisions at cosmotron energies—452
—— Panel discussion on artificial mesons—1094(T)
——, **M. Glicksman, R. Martin, and D. Nagle.** Scattering of negative pions by H—161
Feshbach, Herman (see Bitter, Francis)—837(L)
Feynman, Richard P. Theoretical problems presented by V particles—536(T)
—— (see Baranger, M.)—482
Fields, Paul R. (see Diamond, Herbert)—1490
Finkelstein, R. and P. Kaus. β interaction—1316
Fisher, Philip C. Bremsstrahlung and electron scattering cross sections in Au for 247-Mev electrons and positrons—420; 853(A)
Fiske, Milan. Electrical conductivity of metals at low temperatures—841(T)
Fitch, Val L. and James Rainwater. Studies of x-rays from μ-mesonic atoms—789
Fleming, John R. and J. J. Lord. Ionization loss in nuclear emulsions—511(L); 1089(A)
Fleming, W. H. and H. G. Thode. Neutron and spontaneous fission in U ores—378
Fletcher, R. C. and W. L. Brown. Annealing of bombardment damage in diamond-type lattice: theoretical—585
—— (see Brown, W. L.)—591
Foldy, Leslie L. Matrix elements for nuclear photo-effect—178
Foley, H. M. (see Sessler, A. M.)—1321(L); 1321(L)
—— (see Sternheimer, R. M.)—1460
Follin, James W., Jr. (see Alpher, Ralph A.)—1347
Foote, H. L., Jr., H. H. Landon, and V. L. Sailor. Slow neutron resonances in Ho, Tm, and Lu—656
Ford, Franklin C. and Wilson M. Powell. π^- mesons produced in cloud chamber by high-energy neutrons—537(A)
Ford, Kenneth W. Contribution of collective motion to magnetic moments of heavy nuclei—1094(A)
Forro, M. Method for determination of end-point energy of β emitters—931
Foster, J. S. McGill, fifty years after Rutherford and Soddy—852(T)
Fowler, C. A., Jr., and E. M. Fryer. Observation of magnetic domains by longitudinal Kerr effect—532(A)
Fowler, W. B., R. M. Lea, W. D. Shephard, R. P. Shutt, A. M. Thorndike, and W. L. Whittemore. π^+-p scattering near 260 Mev—832(L)

Fowler, William A. Cross sections of proton reactions—1092(T)
—— (see Kraus, Alfred A., Jr.)—529(A)
—— (see Peterson, R. W.)—1085(A)
—— (see Webb, T. S.)—1084(A)
Francis, N. C. and K. M. Watson. Elastic scattering of particles by atomic nuclei—291
Frank, R. M. and J. L. Gammel. Inelastic scattering of protons and neutrons by deuterons—1092(A)
Frank, Wilson J., Kenneth C. Bandtel, Richard Madey, and Burton J. Moyer. Further evidence for $p+d \rightarrow t+\pi^+$—537(A)
—— (see Madey, Richard)—537(A)
Frankl, D. R. Internal friction of rocksalt single crystals—573
Frauenfelder, H., J. S. Lawson, Jr., W. Jentschke, and G. De Pasquali. Crystal structure and nuclear directional correlation. I. Pb^{204}—513(L)
——, **J. S. Lawson, Jr., W. Jentschke, and G. DePasquali.** Directional correlation of Pb^{204} γ-γ cascade—1241
Fred, Mark, Frank S. Tomkins, and Raymond F. Barnes. Nuclear spin of Bi^{210}—1324(L)
Frederikse, H. P. R. Thermoelectric power of Ge below room temperature—248
Freemantle, R. G., W. M. Gibson, D. J. Prowse, and J. Rotblat. Interaction of 19-Mev deuterons with O—1268
Freier, P. S. and J. E. Naugle. Emulsion study of large shower. I. Hard component—1086(A)
—— (see Naugle, J. E.)—1086(A)
Freistadt, Hans. Electromagnetic mass and particle model in Darling's theory of elementary particles—1015
French, A. P. (see Kraus, Alfred A., Jr.)—529(A)
Fretter, W. B. and E. W. Friesen. Charged and neutral V particles—1089(A)
——, **B. P. Gregory, R. Johnston, A. Lagarrigue, H. Meyer, F. Muller, and C. Peyrou.** Mass measurements of primaries of S events by momentum-range method—1583(L)
Friedland, S. S., H. S. Katzenstein, J. Katzenstein, D. P. Lindorff, G. S. Timoshenko, and L. E. Williams. Pulsed searchlight system for upper atmosphere density studies—1080(A)
Friedlander, G. (see Welker, Joan P.)—401
Friedman, F. L. and W. Tobocman. Approximate wave-mechanical description of deuteron stripping—93
Friedman, H. (see Byram, E. T.)—1066(L)
Friesen, E. W. (see Fretter, W. B.)—1089(A)
Fröhlich, H. and R. L. Platzman. Energy loss of moving electrons to dipolar relaxation—1152
Fry, W. F. Unusual π-μ decays in photographic emulsions, erratum—1587(E)
Frye, Glenn M. and Louis Rosen. Disintegration of C^{12}, B^{11}, and B^{10} by fast neutrons—1083(A)
Fryer, E. M. (see Fowler, C. A., Jr.)—532(A)
Fuchs, L. H. (see Primak, W.)—1064(L)
Fuller, C. S. and J. A. Ditzenberger. Diffusion of Li into Ge and Si—846(A)
—— (see Severiens, J. C.)—1322(L)
Fulton, Thomas and Robert Karplus. Bound state corrections in two-body system—1094(A)
Fung, Si Chang (see Turkevich, A.)—521(L)
Funt, B. L. (see Pringle, R. W.)—1783(L)

Gaerttner, E. R. Neutron velocity spectrometer with betatron source—841(T)
Gailar, Norman (see Benedict, W. S.)—533(A)
Gallagher, C. J. Etch pits in plastically-deformed Ge—846(A)
Gallagher, J. J., F. D. Bedard, and C. M. Johnson. Microwave measurement of D_0 for CO—1440
Gammel, J. L. Elastic scattering of protons and neutrons by deuterons at high energy—1092(A)
—— (see Frank, R. M.)—1092(A)
Gammel, Juanita H. Deuteron disintegration by 9.7-Mev protons—1092(A)
Garren, A. Phase-shift analysis of high-energy p-p scattering experiments—213(L); erratum—1587(E)
Garrett, Richard E., Frank L. Hereford, and Billy W. Sloope. Inelastic neutron scattering in Al, Fe, Mg, and Cu—1507
Garrison, Gerald R. (see Miller, Charles E.)—406
Gaydon, A. G. Spectroscopic studies of flames supported by free atoms—527(T)
Geballe, Ronald and Marvin L. Reeves. Condition on uniform field breakdown in electron-attaching gases—867
Geballe, T. H. Seebeck effect in Ge—857(A)
Gell-Mann, M. Isotopic spin and new unstable particles—833(L)
—— (see Ferentz, M.)—836(L)
Gersch, H. A. (see Berlin, T. H.)—189
Geschwind, S. (see Danos, M.)—828(L)
Giauque, W. F. Determination of thermodynamic temperatures near 0°K without introducing heat below 1°K—1339
Gibson, W. M. (see Burcham, W. E.)—1266
—— (see Freemantle, R. G.)—1268
Gilmore, J. S. (see Terrell, James)—1091(A)
Gittleman, J. Intermediate state of a hollow superconducting tin cylinder—561
—— (see Serin, B.)—566
Glicksman, M. (see Fermi, E.)—161
Godfrey, T. N. K. Negative μ-meson capture in C—512(L)
Goldemberg, J. and L. Katz. Excitation levels of Li^7 and F^{19} by betratron irradiation—852(A)
—— (see Katz, L.)—852(A)
Goldhaber, M. Hypothesis concerning relations among "new unstable particles"—1279
—— Nuclear isomers—1092(T)
—— (see de-Shalit, A.)—1211
Goldman, J. E. Electronic specific heat in relation to band structure of transition metals and alloys—528(T)
Goldstein, Louis. Theory of liquid He^3—He^4 mixtures—850(A)
Gomer, Robert. Field emission and chemisorption—854(T)
Good, Myron L. Phase-reversal focusing in linear accelerators—538(A)
Good, R. H., Jr. (see Miller, S. C., Jr.)—1367
Goodman, Clark (see Guernsey, Janet B.)—323
—— (see Hansen, K. F.)—652
—— (see Mark, Hans)—1097(A)
Goodman, L. S. (see Casson, H.)—1518
Gordon, A. S. (see Hunt, M. H.)—542(A)
Gordon, M. M. and J. G. Jones. Generalized variational equations for scattering of electrons by H atoms—1428
Gordy, Walter (see Burrus, Charles A., Jr.)—274; 1437
—— (see Fairbank, W. M.)—208(L)
—— (see Livingston, Ralph)—1271
Gourley, Mary Gaulks and W. D. Crozier. Persistent residues from ice particles—526(A)
Gove, H. E. and E. B. Paul. γ rays from $P^{31}(p,\gamma)S^{32}$—852(A)
Grant, H. L. and R. W. Stewart. Correlation studies of sound fluctuations in ocean—1087(A)
Grebe, J. J. Possible designs for an economical power reactor—854(T)
Gregory, B. P. (see Fretter, W. B.)—1089(L)
Gregory, Christopher. Equivalent mass and other effects of non-local electromagnetic field in interaction with constant E,H field—1554
Greiner, E. S. (see Ellis, W. C.)—1061(L)
Griffiths, G. M. and J. B. Warren. γ rays from $D(p,\gamma)He^3$—1084(A)
—— (see Warren, J. B.)—1084(A)
Griswold, T. W. (see Kip, A. F.)—544(A)
Gross, Leonard (see Hamilton, Donald R.)—1522
Grossweiner, L. (see Avery, E.)—1080(A)
Guderley, Gottfried. Examples of flow patterns at and near Mach one—1087(T)

Guernsey, Janet B. and Clark Goodman. Total neutron cross section of liquid A—323
Guernsey, R. L. and G. B. Arfken. Vector addition coefficient identity—1270
Guinier, Andre. Electronic x-ray probe for microanalysis of structure and composition of metallic solids—528(T)
Gunst, S. B. and L. A. Page. Compton scattering of 2.62-Mev γ rays by polarized electrons—970
Guttman, Lester and James R. Arnold. Non-participation of He^6 in superfluidity of He^4—547

Haber, Agnes (see Sugarman, Nathan)—730
Hagstrum, H. D. Theory and experiment concerning resonance transitions and Auger transitions occurring as ion approaches metal surface—847(T)
Halpern, J. (see Nathans, R.)—207(L); 940
Halpern, O. and K. Baumann. Velocity distribution of pair components in π^0 decay—1070(L)
Ham, Frank S. Effect of surface on magnetic properties of electron gas—1113
Hamermesh, Bernard and Richard J. Culp. Large NaI scintillation counter study of neutron capture γ rays from H—211(L)
Hamilton, Donald R., W. Parker Alford, and Leonard Gross. Upper limits on neutrino mass from T β spectrum—1521
——, **Aaron Lemonick, and Francis M. Pipkin.** β-γ polarization correlations—1191
—— (see Weneser, J.)—321
Hammer, C. L. (see Pidd, R. W.)—436
Handley, Thomas H. and Elmer L. Olson. Er^{163} and Tm^{165}—1260
—— (see Cohen, B. L.)—101
Hanna, S. S. (see Fagg, L. W.)—372
—— (see Pruitt, J. S.)—1456
Hansen, K. F., R. M. Kiehn, and Clark Goodman. Total neutron cross section of P—652
Hardwick, W. H. Fission yields of Ru^{103} and Ru^{106}—1072(L)
Hardy, W. A., G. Silvey, C. H. Townes, B. F. Burke, M. W. P. Strandberg, George W. Parker, and Victor W. Cohen. Nuclear moments of Sc^{79}—1532
Harris, John N. (see Felt, Gaelen L.)—1160
Harris, S. P. (see Bollinger, L. M.)—1528
Harrison, F. B., C. L. Cowan, Jr., and F. Reines. Background in neutrino experiment—1088(A)
—— (see Schuch, R. L.)—1088(A)
Hart, K. H. (see Atkins, K. R.)—204(L)
Havens, W. W., Jr. (see Melkonian, E.)—702
Haycock, O. C. (see Lien, J. R.)—508(L)
—— (see Linford, L. B.)—1093(A)
Hayes, F. N., D. L. Williams, and Betty Rogers. Liquid scintillation counting of natural C^{14}—512(L)
——, **Lloyd Williams, C. L. Cowan, Jr., and F. Reines.** Liquid scintillators for large volume detectors—1088(A)
—— (see Schuch, R. L.)—1088(A)
Haynes, S. K. (see Perkins, J. F.)—687; 1096(A)
Heidenthal, G. Experimental evidence for inheritance of radiation effects—841(T)
Hein, R. A. (see Steele, M. C.)—243
Heller, C. A. (see Hunt, M. H.)—542(A)
Hellund, E. J. and M. K. Brachman. Space-time representation in wave mechanics—822
—— **and J. M. Jauch.** Sequence of γ emission in triple correlations—203(L)
Hemmendinger, A. (see Ennis, M. E.)—1092(A)
Hemmig, P. B. and R. M. Steffen. Time-dependent quadrupole interaction in angular correlation of nuclear radiation. I. Cd^{111}—832(L)
Henderson, Joseph E. (see Miller, Charles E.)—406
Hendrick, R. W., Jr. Agreement of theoretical and experimental intensities of soft continuous x-rays—541(A)
Henke, Burton. Size-determination of submicroscopic particles by long wavelength x-ray diffraction—1079(T)
Henkel, Richard L. (see Day, Robert B.)—358
Henley, E. M. and M. A. Ruderman. Nuclear forces from *P*-wave mesons—1036
—— (see Cooper, L. N.)—801
Henry, Warren E. *H-T* antiferromagnetic boundary and apparent molecular field for $MnBr_2 \cdot 4H_2O$—844(A)
Henshaw, D. G., D. G. Hurst, and N. K. Pope. Structure of liquid N_2, O_2, and A by neutron diffraction—1229
Henvis, B. W. (see Burstein, E.)—845(A)
Hepner, W. A. and D. R. Workman. Interpretation of Bhabha's theory of particles of maximum spin 3/2—1071(L)
Hereford, Frank L. (see Garrett, Richard E.)—1508
Herman, Robert C. (see Alpher, Ralph A.)—1347
Herring, Conyers. Theory of thermoelectric power of semiconductors—857(A)
Hess, David C. (see Diamond, Herbert)—1490
Heydenburg, N. P. and G. M. Temmer. F^{18} energy levels from α-particle reactions in N—89
Hibdon, C. T. (see Bollinger, L. M.)—1528
Hickman, K. C. D. Mechanism of evaporation of liquids—854(T)
Hildebrand, Roger H. and Darragh E. Nagle. Operation of Glaser bubble chamber with liquid H_2—517(L)
Hill, R. D. (see Bergström, Ingmar)—849(A); 918
Hoffman, M. M. and A. G. W. Cameron. Angular and energy distributions of photoprotons from Al and Ta—1184
Hofstadter, Robert, H. R. Fechter, and J. A. McIntyre. High-energy electron scattering and nuclear structure determinations—978
—— **and Asher Kantz.** Electron-induced showers—536(T)
Hogg, B. G. and H. E. Duckworth. Atomic masses for Ga, Ge, As, Se, and Br—848(A)
Hollander, Jack M. Br isotopes produced by C-ion bombardment of Cu—518(L)
Holmes, John R. (see Parker, Lee W.)—532(A)
Holzer, R. E. Measurements of world-wide electrical effects—1093(T)
Honig, A., M. L. Stitch, and M. Mandel. Microwave spectra of CsF, CsCl, and CsBr—901
Horn, F. H. Crystal growth and spirals, etch-figures and holes—841(T)
Hornyak, W. F. and T. Coor. Capture γ rays from proton bombardment of Be^9—675
Horowitz, J. and A. M. L. Messiah. Mechanism of stripping reactions—1326(L)
Horton, C. W. Hydroacoustic filter networks—527(T)
Hossain, A. (see Burcham, W. E.)—1266
House, R. A. (see Lerohl, John K.)—934
Hove, J. and J. Krumhansl. Evaluation of lattice sums for cubic crystals—569
Howe, H. A. and K. R. MacKenzie. Electron positron scattering—530(A)
Howland, J. J., Jr. (see Welker, Joan P.)—401
Howland, P. R., W. E. Kreger, and R. A. Taylor. γ-ray absorption measurements—1095(A)
Hoyle, Fred. Expanding universe—536(T)
——, **D. N. F. Dunbar, W. A. Wenzel, and W. Whaling.** State in C^{12} predicted from astrophysical evidence—1095(A)
Hoyt, H. C. (see DuMond, J. W. M.)—202(L)
Hubbard, Edward L., Lawrence Ruby, and Warren F. Stubbins. Search for B^{13}—1494
Huber, Elsa. Secondary cathode action in N_2 with coaxial cylindrical geometry—536(A)
Hudson, Craig C. Acoustic approximation to weak shock diffraction—1079(A)
Hughes, D. J., W. Y. Kato, and J. S. Levin. Energy levels in Hf isotopes—1094(A)
——, **W. Y. Kato, and J. S. Levin.** Energy levels in Th—851(A)

—— **and H. Palevsky.** Formation of long-lived Bi^{210} isomer—1206
—— (see Carter, R. S.)—716
—— (see Levin, J. S.)—851(A)
—— (see Palevsky, H.)—202(L)
Hughes, D. S. and J. L. Kelly. Second order elastic deformation of solids—1145
Hulm, J. K. Low-temperature dielectric properties of Cd and Pb niobates—504(L)
Hunt, M. H., C. A. Heller, and A. S. Gordon. Surface temperature of burning double-base propellant—542(A)
Hurst, D. G. (see Henshaw, D. G.)—1229
Huster, E. β spectrum of RaD—1076(L)
Hutchison, T. S. (see Reekie, James)—827(L)
Huus, Torben and Jørgen H. Bjerregaard. Internal conversion electrons from Coulomb-excited Ta and W—1579(L)
—— (see Lauritsen, T.)—1502
Hyde, Earl K. Half-life of Zr^{88}—927

Igo, George J. (see Eisberg, Robert M.)—537(A)
Inghram, Mark G. (see Diamond, Herbert)—1490
—— (see Patterson, C.)—1234
Inglis, D. R. (see Malm, R.)—1328(L)

Jain, P. L., H. A. Moses, J. C. Lee, and R. D. Spence. Proton magnetic resonance in liquid crystals—844(A)
James, D. B. (see Neilson, G. C.)—1084(A)
Jankus, V. Z. Radiative correction to collision loss of heavy particles—540(A)
Jastram, P. S. (see Whittle, C. E.)—205(L)
Jauch, J. M. (see Hellund, E. J.)—203(L)
Jeffries, C. D. Spin and magnetic moment of Ti^{47} and Ti^{49}—1262; 1096(A)
Jentschke, W. (see Frauenfelder, H.)—513(L); 1241
Johnson, C. M. (see Gallagher, J. J.)—1440
Johnson, J. B. Secondary electron emission from diamond—843(A)
Johnson, V. A. and K. Lark-Horovitz. Theory of thermoelectric power in semiconductors with applications to Ge—226
Johnston, R. (see Fretter, W. B.)—1089(L)
Jona, F. and R. Pepinsky. Dielectric properties of some double tartrates—1577(L)
—— **and R. Pepinsky.** Transition in $LiNH_4C_4H_4O_6 \cdot H_2O$—845(A)
Jones, J. G. (see Gordon, M. M.)—1428
Jordan, W. C., J. M. Cork, and S. B. Burson. Decay of $_{66}Dy^{165m}$(1.2 min) and $_{66}Dy^{165}$(2.3 hr)—1218
——, **J. M. Cork, and S. B. Burson.** Radiations of $_{64}Gd^{159}$ (18-hr) and $_{64}Gd^{161}$(3.7-min)—315
Juretschke, Hellmut J. Exchange potential in surface region of free-electron metal—1140

Kahn, A. H. (see Tessman, Jack R.)—890
Kahn, Bernd and W. S. Lyon. Decay of Rh^{106}—902
Kallmann, H. K. Quantitative analysis of lower ionosphere—1079(A)
Kalos, M. H. (see Blatt, John M.)—1564
Kamei, Tohru (see Murakawa, Kiyoshi)—325
Kane, R. P. (see Sarabhai, V.)—415
Kantz, Asher (see Hofstadter, Robert)—536(T)
Kaplon, M. F., J. H. Noon, and D. M. Ritson. Interactions of heavy primaries of cosmic radiation—855(A)
—— (see Klose, J. Z.)—855(A)
—— (see Noon, J. H.)—1586(L)
Karplus, Robert (see Fulton, Thomas)—1094(A)
Karzmark, C. J. (see Thompson, R. W.)—209(L)
Kash, S. W. and D. C. Woods. Measurement of transport mean free path of thermal neutrons in heavy water—544(A)
Kato, W. Y. (see Hughes, D. J.)—851(A); 1094(A)
—— (see Levin, J. S.)—851(A)
Katz, L. and J. Goldemberg. Fine structure in $C^{13}(\gamma,n)C^{11}$ neutron yield—852(A)
—— (see Goldemberg, J.)—852(A)
Katz, Robert and Milford R. Lee. Radioactivity of Sm^{153}—848(A)
Katzenstein, H. S. (see Friedland, S. S.)—1080(A)
Katzenstein, J. (see Friedland, S. S.)—1080(A)
Kaufman, Allan N. Strong coupling theory of meson scattering—468
Kaus, P. (see Finkelstein, R.)—1316
Keck, J. C. (see Bacher, R. F.)—1090(A)
—— (see Tollestrup, A. V.)—1090(A)
Keck, P. H., S. B. Levin, J. Broder, and R. Lieberman. Crystal growth of Si by tip fusion process—847(A)
——, **W. Van Horn, J. Soled, and A. MacDonald.** Floating zone recrystallization—847(A)
Keller, W. E. (see Sommers, H. S., Jr.)—1345
Kelly, J. L. (see Hughes, D. S.)—1145
Kenney, James F. and Victor H. Regener. Cross section for production of penetrating cosmic-ray showers in O—1090(A)
Kent, D. W. (see Rothman, M. A.)—1097(A)
Kenworthy, H. (see Eggen, D. T.)—531(A)
Kerman, A. K. Nuclear surface oscillations—1176
Kerner, Edward H. Dissociation of H_2^+ by electron impact—1441
—— Interchange of rotational and vibrational energy in collisions of diatomic molecules—899
Kessler, Karl G. and R. E. Trees. Nuclear moments of Tc^{99}—303
Keyes, Robert W. Electrical properties of black phosphorus—580
Keywell, Frank. Sputtering in high vacuum and its relation to radiation damage as described by Seitz—535(A)
Kiehn, R. M. (see Hansen, K. F.)—652
Kikuchi, C., M. H. Sirvetz, and V. W. Cohen. Paramagnetic resonance hfs of V^{50} and V^{51}—109
King, D. T., Nathan Seeman, and Maurice M. Shapiro. Charged particles of mass intermediate between proton and deuteron—838(L)
Kip, A. F., T. W. Griswold, and A. M. Portis. Resonance absorption by conduction electrons in metals—544(A)
—— (see Dresselhaus, G.)—827(L)
Kirkpatrick, Paul (see El-Sum, Hussein M. A.)—541(A)
Kirkwood, Robert L. Physical basis of gravitation—1557
Kisliuk, P. Electrical breakdown of extremely short gaps—847(A)
Kittel, C. Microwave physics and study of solids—528(T)
—— (see Abrahams, Elihu)—544(A)
—— (see Dresselhaus, G.)—827(L)
Klein, Abraham. Convergence of adiabatic nuclear potential—1017
Klein, D. (see Cartwright, W. F.)—852(A)
Klein, Ralph. Field-emission microscope investigation of surface reactions—854(A)
Klema, E. D. and F. K. McGowan. γ-γ angular correlation in Pd^{106}—1469
Klinger, Y. Conductivity of Ge at 2.4×10^{10} cps—509(L)
Klose, J. Z., M. F. Kaplon, D. M. Ritson, and W. L. Walker. Emulsion cloud-chamber study of high-energy radiation at mountain altitude—855(A)
Knight, W. D. Nuclear resonance line broadening and quadrupole splitting in metallic Be—539(A)
Koehler, W. C. Neutron diffraction by paramagnetic substances—1088(T)
—— **and E. O. Wollan.** Paramagnetic scattering of neutrons by rare earth oxides—1380
Koehler, W. F. Multiple-beam fringes of equal chromatic order—542(A)
Kofoed-Hansen, O. Possible $0 \rightarrow 0(n\alpha)\beta$ transitions in $4n+2$ nuclei—1075(L)

Kohn, W. New method of calculating energy bands in crystal lattices—847(T)
Kojima, S., K. Tsukada, S. Ogawa, and A. Shimauchi. New absorption lines of crystals in submicrowave region—1571(L)
Konopinski, E. J. and H. M. Mahmoud. Universal Fermi interaction—1045
Kraus, Alfred A., Jr. γ rays from $Li^7(p,\gamma)Be^8$—1085(A)
——, **A. P. French, William A. Fowler, and C. C. Lauritsen.** Angular distribution of γ rays and α particles from $N^{15}(p,\alpha\gamma)C^{12}$—529(A)
Kraushaar, J. J. γ-γ directional correlation experiments with Mo^{93m}—318
—— **and R. V. Pound.** Directional correlation and electric quadrupole interaction in γ-γ cascade of 48.7-min Cd^{111m}—522(L)
Kreger, W. E. (see Howland, P. R.)—1095(A)
Kretschmar, George G. Velocity of sound apparatus for liquids at 512 kc—542(A)
Krogstad, R., W. Nelson, and S. T. Stephenson. X-ray absorption fine structure with polarized x-rays—1394
Krohn, V. E. (see Casson, H.)—1518
Krone, R. W. and L. W. Seagondollar. γ rays from proton bombardment of B^{10}—935
Krumhansl, J. (see Hove, J.)—569
Krzywoblocki, M. Z. Stability of Benard-Karman vortex street in compressible flow—527(T)
Kundu, D. N. (see Lerohl, John K.)—934
Kunkel, W. B. Short afterglow in N_2—534(A)
Kurşunoğlu, Behram. Derivation and renormalization of Tamm-Dancoff equations—1069(L)
—— Expectations from unified field theory—506(L)
Kusch, P. Sign of quadrupole interaction of Li^6 in LiCl—268
Kyhl, R. L. Stanford linear electron accelerator—536(T)

Ladany, I. (see Brentano, J. C. M.)—850(A)
Lagarrigue, A. (see Fretter, W. B.)—1089(L)
Lal, D., Yash Pal, and B. Peters. Properties of heavy unstable particles—438
Lander, J. J. Auger peaks in energy spectra of secondary electrons from various materials—843(T)
Landon, H. H. (see Foote, H. L., Jr.)—656
Lane, A. M. Intermediate coupling and nuclear reactions—839(L)
Lane, C. T. and R. V. Dyba. Capillarity in He II—829(L)
Langer, L. M. β spectra—1092(T)
Langmuir, R. V. California Institute of Technology synchrotron—536(T)
Larach, Simon (see Bube, Richard H.)—1135
Lark-Horovitz, K. (see Johnson, V. A.)—226
LaRocca, Edward W. Behavior of metals at elevated temperatures—1082(A)
Lashinsky, H. (see Danos, M.)—828(L)
Lauritsen, C. C. (see Kraus, Alfred A., Jr.)—529(A)
—— (see Peterson, R. W.)—1085(A)
Lauritsen, T., T. Huus, and S. G. Nilsson. Scattering of deuterons in He—1501
Lawson, J. S., Jr. (see Frauenfelder, H.)—513(L); 1241
Lawson, R. D. Photoproduction of π-meson pairs—1272
—— **and S. D. Drell.** Photoproduction of meson pairs—539(A)
Lawton, E. J. Apparatus for studies with cathode rays—841(T)
Lea, R. M. (see Fowler, W. B.)—832(L)
Leachman, R. B. Energy released in fission—1079(T)
—— (see Schmitt, H. W.)—1091(A)
Leavitt, C. P. (see Shapiro, A. M.)—1073(L)
—— (see Smith, L. W.)—851(A)
—— (see Widgoff, M.)—851(A)
LeBlanc, J. M. (see Cork, J. M.)—119; 367
Lederman, L. M. (see Cornelius, R. C.)—1584(L)
Lee, J. C. (see Jain, P. L.)—844(A)
Lee, Milford E. (see Katz, Robert)—848(A)
Lee, Po and G. L. Weissler. Characteristics of certain photographic plates in vacuum ultraviolet—545(A)
—— **and G. L. Weissler.** Further results on Ne and A absorption in extreme uv—533(A)
Lee, Tsung-Dao and David Pines. Interaction of non-relativistic particle with scalar field with application to slow electrons in polar crystals—883
Lehovec, Kurt. Energy of trapped electrons in ionic solids—253
Leighton, Robert B. Recent experimental evidence concerning V^0 particles—536(T)
—— **and W. L. Alford.** Mean lifetime of V^0 particles—540(A)
—— (see Anderson, C. D.)—1089(A)
—— (see Cowan, E. W.)—1089(A)
Lemonick, Aaron (see Hamilton, Donald R.)—1191
Leonard, Stanley L. Pion production at 180° by protons on C—538(A)
—— **and Donald H. Stork.** Total cross section for positive pions in hydrogen—855(A)
Leprince-Ringuet, L. and B. Rossi. Summary of K-meson data—722
Lerohl, John K., M. L. Pool, D. N. Kundu, and R. A. House. Tc of mass number 98—934
Levin, J. S., D. J. Hughes, and W. Y. Kato. Determination of level parameters for low-energy neutron resonances—851(A)
—— (see Hughes, D. J.)—851(A); 1094(A)
Levin, S. B. (see Keck, P. H.)—847(A)
Levy, H. A. (see Peterson, S. W.)—1082(A)
Levy, John L. Sensitive Hall measurements on NaCl and on photoconductive PbTe—215
Lew, Hin (see Brix, P.)—647
—— (see Wessel, Günter)—641
Lewis, H. W. Search for Hall effect in a superconductor. I. Experiment—1149
Lewis, W. B. Experience with the *NRX* reactor—854(T)
Li, C. W. γ rays from $N^{14}(p,\gamma)O^{15}$—1084(A)
—— (see Webb, T. S.)—1084(A)
Liberman, D. A. and R. F. Christy. Reactions and scattering of protons on Li^7—1085(A)
Libowitz, G. (see Sproull, R. L.)—77
Lieberman, R. (see Keck, P. H.)—847(A)
Lien, J. R., J. Marcou, J. C. Ulwick, D. R. McMorrow, L. B. Linford, and O. C. Haycock. Bifurcation of E region—508(L)
—— (see Linford, L. B.)—1093(A)
Liepmann, H. W. Effect of turbulence on linear systems—527(T)
Liller, William and F. L. Whipple. High-altitude winds by meteor-train photography—1093(T)
Lindenbaum, S. J. and Luke C. L. Yuan. Interaction cross section of H and heavier elements for 450-Mev negative pions and 340-Mev positive pions—1578(L)
Lindorff, D. P. (see Friedland, S. S.)—1080(A)
Linford, L. B., O. C. Haycock, J. I. Swigart, C. L. Alley, C. D. Westlund, and J. R. Lien. Ion density in E layer by use of sounding rocket—1093(A)
—— (see Lien, J. R.)—508(L)
Linlor, W. I. and B. Ragent. Neutron total cross section for Bi and U between 45 and 160 Mev—835(L)
Litz, L. M., S. A. Ring, and W. R. Balkwell. 1.25-min Rb^{82m} daughter of 27-day Sr^{82}—288
Livingston, Ralph, Ben M. Benjamin, J. T. Cox, and Walter Gordy. Nuclear spin and quadrupole moment of I^{131}—1271
Lloyd, J. P. and G. E. Pake. Spin-lattice relaxation and residual width of highly exchange-narrowed paramagnetic resonances—1576(L)
Lockwood, John A. (see Woods, Frank R.)—853(A)

Loebner, E. E. Time-dependent spectra of electroluminescent ZnS—846(A)
Lomont, J. S. Reformulation of solid-state electronic Boltzmann equation—1082(A)
—— Treatment of defect relaxation time of conduction electrons in crystals by tight binding approximation—532(A)
Lord, J. J. (see Fleming, John R.)—511(L); 1089(A)
Lord, Norman W. Nucleation of ordered phases in Cu_3Au—844(A)
Love, L. O. (see Bell, W. A., Jr.)—1096(A)
Love, W. F. Superconductivity in Sn-Bi and Sn-Sb alloys—238
Lynton, E. A. (see Serin, B.)—566
Lyon, W. S. (see Kahn, Bernd)—902

MacDonald, A. (see Keck, P. H.)—847(A)
MacDonald, D. K. C. and W. B. Pearson. Thermoelectricity in metals at low temperatures—844(A)
—— (see Preston-Thomas H.)—844(A)
Macdonald, J. Ross. Theory of ac space-charge polarization effects in photoconductors, semiconductors, and electrolytes—4
Macke, Wilhelm. Single-time Bethe-Salpeter equation—1072(L)
MacKenzie, K. R. (see Howe, H. A.)—530(A)
Mackin, Robert J., Jr. γ rays and internal pairs from Be^9+H^1—1084(A)
—— γ rays from $C^{12}+D^2$—529(A)
Madey, Richard, Kenneth C. Bandtel, and Wilson J. Frank. Rf fine structure of photon beam from Berkeley synchroton—537(A)
—— (see Frank, Wilson J.)—537(A)
Mador, Irving L. (see Markham, Jordan J.)—597
Mahmoud, H. M. (see Konopinski, E. J.)—1045
Malenka, B. J. Theory of high-energy deuteron pick-up—516(L)
Malich, C. W. and C. E. Faneuff. γ radiation from neutron excitation of Zr and Hf—1095(A)
Malm, R. and D. R. Inglis. Energy levels of Be^8—1326(L)
Mandel, M. (see Honig, A.)—901
Mandeville, C. E. (see Rothman, M. A.)—1097(A)
—— (see Saraf, B. L.)—848(A)
Mann, Glen A. and R. D. Spence. Rotation of microwave polarization in liquid crystals in transverse magnetic field—844(A)
Mann, L. G., W. E. Meyerhof, and H. I. West, Jr. Decay of Ga^{66}—1481
—— (see Meyerhof, W. E.)—540(A); 758
Manring, Edward (see Ting, Yu)—1582(L)
March, N. H. Exchange potential in electron gas at nonzero temperature—510(L)
—— Virial theorem for Dirac's equation—481
Marcou, J. (see Lien, J. R.)—508(L)
Mark, Hans and Clark Goodman. Angular distribution of neutrons from $O^{18}(p,n)F^{18}$—1097(A)
Markham, Jordan J., Reuel T. Platt, Jr., and Irving L. Mador. Bleaching properties of F centers in KBr at 5°K—597
—— (see Platt, Reuel T., Jr.)—40
Marmier, P. E. (see DuMond, J. W. M.)—202(L)
Marquez, Luis. Disintegration of Ca^{47}, Sc^{47}, Va^{48}, and Rh^{100}—1511
Marshall, J., L. Marshall, and V. A. Nedzel. Differential p-p elastic scattering cross section at 144, 271, and 429 Mev—834(L)
Marshall, J. F. Theory of secondary emission—843(T)
Marshall, L. (see Marshall, J.)—834(L)
Martin, E. E. (see Barbour, J. P.)—45
Martin, H. C., B. C. Diven, and R. F. Taschek. Cross sections for production of In^{115m} and Au^{197m} by inelastic scattering of neutrons—1096(A)
Martin, R. (see Fermi, E.)—161
Martinelli, E. A. (see Mather, J. W.)—780
Maryott, A. A. (see Birnbaum, G.)—270
Mather, J. W. and E. A. Martinelli. Production of neutral mesons by 340-Mev protons on H—780
Matheson, M. (see Avery, E.)—1080(A)
Matland, C. G. Quenching of Hg resonance radiation (2537A) by N_2—637
Matossi, Frank. Interpretation of some electroluminescent effects—846(A)
Matthias, B. T. Transition temperatures of superconductors—874
Maxwell, Louis R. and Stanley J. Pickart. Magnetization in Ni ferrite-aluminates and Ni ferrite-gallates—1120
McAfee, K. B. and K. G. McKay. Measurement of charge multiplication in Ge and Si p-n junctions—858(A)
McCarthy, J. T. Applications of Wigner semi-empirical mass formula to isobars—848(A)
McCarty, Robert J. Critical conditions for ice formation on silver iodide nuclei—1080(A)
McClelland, Clyde. Excitation of heavy nuclei by electric field of low-energy protons—1092(T)
McDaniel, Boyce D. (see Weil, John W.)—391
McDonald, K. (see Elsasser, W. M.)—1081(A)
McGowan, F. K. Internal conversion electron-γ directional angular correlation of Bi^{207}—524(L)
—— **and E. C. Campbell.** Internal conversion and directional angular correlation of $Bi^{207}\gamma$'s—523(L)
—— (see Klema, E. D.)—1469
McGruer, J. N. (see Rhodes, K. B.)—1328(L)
McIntyre, J. A. (see Hofstadter, R.)—978
McKay, K. G. (see McAfee, K. B.)—858(A)
McKeown, Michael (see Scharff-Goldhaber, Gertrude)—356; 1094(A)
McManus, H. (see Austern, N.)—350
McMillan, W. G. Nuclear stability curve—210(L)
McMorrow, D. R. (see Lien, J. R.)—508(L)
Mech, Joseph (see Diamond, Herbert)—1490
Meechan, C. J. (see Dixon, C. E.)—530(A)
Megill, L. R. and C. R. Emigh. Long-lived phosphorescent components of Tl-activated NaI—1081(A)
Meissner, K. W. and W. F. Miller. Influence of irradiation on characteristic of glow discharge in pure rare gases—896
Melkonian, E., W. W. Havens, Jr., and L. J. Rainwater. Slow neutron velocity spectrometer studies. V. Re, Ta, Ru, Cr, Ga—702
Messiah, A. M. L. (see Horowitz, J.)—1326(L)
Metzger, F. R. and W. B. Todd. Angular correlation of γ rays from Mn^{56}—904
Mewherter, Anita C. (see Douglas, David L.)—369; 1095(A)
Meyer, H. (see Fretter, W. B.)—1584(L)
Meyerhof, W. E., L. G. Mann, and H. I. West, Jr. Decay of Ga^{67}—540(A); 758
—— (see Mann, L. G.)—1481
Middleton, A. E. and W. W. Scanlon. Measurement of thermoelectric power of Ge at temperatures above 78°K—219
Mileikowsky, Curt and Ward Whaling. Q values of $Ne^{21}(d,\alpha)F^{19}$ and $Ne^{21}(d,p)Ne^{22}$—528(A)
Miller, Charles E., Joseph E. Henderson, David S. Potter, William R. Davis, Wayne M. Sandstrom, Gerald R. Garrison, and Francis M. Charbonnier. Search for highly-absorbable negative cosmic-ray particles at sea level—406
Miller, D. (see Barnes, S. W.)—1327(L)
Miller, D. W. (see Rasmussen, V. K.)—852(A)
Miller, R. H. and R. Sherr. K capture in Na^{22}—848(A)
Miller, S. C., Jr., and R. H. Good, Jr. Periodic deviations in Schottky effect—1367
Miller, W. F. (see Meissner, K. W.)—896
Milne, Edmund A. Elastic scattering of protons by C^{12} and C^{13}—528(A)
—— Energy levels in N^{14} from scattering of protons by C^{13}—1085(A)

Minkkinen, C. O. (see Terrell, James)—1091(A)
Moak, C. D. H^3+He^3 reactions—383
Morewitz, H. A. and M. H. Shamos. Variation of ratio of positive to negative cosmic-ray μ mesons with momentum and altitude—134
Morrison, H. L. (see Plain, G. J.)—529(A)
Morrow, J. C. λ temperatures of dilute He^3-He^4 solutions—1
Moses, H. A. (see Jain, P. L.)—844(A)
Moses, Harry E. Formulation of Kohn-Hulthén variational principle in terms of scattering operator formalism—817
Motz, H. and L. I. Schiff. Čerenkov radiation in dispersive medium—540(A)
Moyer, Burton J. (see Ball, W. P.)—539(A)
—— (see Bratenahl, A.)—538(A)
—— (see Crandall, Walter E.)—749
—— (see Frank, Wilson J.)—537(A)
Moyer, James W. (see Ruth, Ralph P.)—846(A)
Mrozowski, S. Zone structure of graphite—1320(L)
Muehlhause, C. O. (see Bollinger, L. M.)—1528
Mueller, E. W. New methods of field-emission microscopy—854(T)
Muller, F. (see Fretter, W. B.)—1584(L)
Mullin, Charles J. Solution of wave equation near extremum of potential—1323(L)
Murakawa, Kiyoshi and Tohru Kamei. Hfs of spectra of Dy, Co, V, Mn, and La—325
Murray, J. J. (see DuMond, J. W. M.)—202(L)
Myers, V. W. (see Carter, R. S.)—716

Nagle, Darragh E. (see Fermi, E.)—161
—— (see Hildebrand, Roger H.)—517(L)
Nathans, R. and J. Halpern. Excitation function for photodisintegration of Be—940
—— **and J. Halpern.** Systematics of photoneutron reactions—207(L)
Naugle, J. E. and P. S. Freier. Emulsion study of large shower. II. Soft component—1086(A)
—— (see Freier, P. S.)—1086(A)
Neal, R. B. Electron bunching in disk-loaded circular wave guide—541(A)
Neamtan, S. M. Čerenkov effect and dielectric constant—1362
Nedzel, V. A. (see Marshall, J.)—834(L)
Neilson, G. C., D. B. James, and C. A. Barnes. Angular distributions of long-range α particles from $N^{15}(p,\alpha)C^{12}$—1084(A)
Nelson, D. (see Barnes, S. W.)—1327(L)
Nelson, W. (see Krogstad, R.)—1394
Nester, W. H. (see Cork, J. M.)—119; 367
Neuman, Maurice. Green's function method for strongly interacting particles—1021
Newman, Ezra (see Bergmann, Peter G.)—856(A)
Newnham, R. E. (see Shirane, G.)—845(A)
Nicol, James and T. P. Tseng. Thermal conductivity of Cu between 0.25°K and 4.2°K—1062(L)
Nilsson, S. G. (see Lauritsen, T.)—1502
Noon, J. H., M. F. Kaplon, and D. M. Ritson. Production of fast Li, Be, B fragments from interactions of primary cosmic-ray nuclei—1585(L)
—— (see Kaplon, M. F.)—855(A)
Normand, C. E. (see Bell, W. A., Jr.)—1096(A)
Norrish, R. G. W. Ignition reactions by flash photolysis—527(T)
Northrop, J. A. and J. E. Brolley, Jr. Energy distribution of slowed fission fragments—1091(A)
Norwood, John M. (see Brown, S. Leroy)—534(A)
Nussbaum, R. H., R. van Lieshout, and A. H. Wapstra. Low-lying many-particle levels in odd-mass nuclides with 21, 23, 25, or 27 protons or neutrons—207(L)

Odencrantz, F. K. (see Rogers, Marguerite)—530(A)
Ogawa, S. (see Kojima, S.)—1572(L)
Olbert, S. Atmospheric effects on cosmic-ray intensity near sea level—454
Oleson, N. L. Probe measurements in A discharge containing running striations—848(A)
Oliver, Albert J. Variation of moisture content in nuclear track emulsion—538(A)
Olson, Elmer L. (see Handley, Thomas H.)—1260
Olson, Keith W. Variations in decay of phosphorescence with frequency of applied electric field—1323(L)
Oltman, H. George. Focusing of short electromagnetic waves by means of Fresnel half-period zone plate—1093(A)
O'Neill, G. K. Fast-neutron spectrometer using $T(d,n)\alpha$ reaction—853(A)
Ōno, Kazuo, Hidetarō Abe, and Junji Shimada. Exchange coupling in $CuK_2Cl_4\cdot 2H_2O$ by paramagnetic resonance absorption—551
Orear, Jay. Elastic scattering of 118-Mev negative pions by H—156
Osborne, M. F. M. and M. C. Steele. Magnetic properties of electronic Einstein model solid—1403
Overhauser, Albert W. Annealing effects in irradiated Cu—530(A)
—— Polarization of nuclei in metals—411
Oxley, C. L. Double scattering of protons—852(T)
—— (see Cartwright, W. F.)—852(A)

Page, L. A. (see Gunst, S. B.)—970
Pake, G. E. (see Lloyd, J. P.)—1577(L)
Pal, Yash (see Lal, D.)—438
Palevsky, H. and D. J. Hughes. Magnetic inelastic scattering of slow neutrons—202(L)
—— (see Carter, R. S.)—716
—— (see Hughes, D. J.)—1206
Papas, Charles H. Diffraction by ionized trail—542(A)
Parker, George W. (see Hardy, W. A.)—1533
Parker, James H. Secondary electron emission coefficient for low-energy positive ion bombardment of discharge-conditioned surfaces—536(A)
Parker, Lee W. and John R. Holmes. New fine structure in oxygen O I—532(A)
Parzen, George (see Wainwright, Thomas)—1129
Pattee, Howard H., Jr. Scanning x-ray microscope—541(A)
Patterson, C., H. Brown, G. Tilton, and M. Inghram. Concentration of U and Pb and isotopic composition of Pb in meteoritic material—1234
Paul, E. B. (see Gove, H. E.)—852(A)
Pearlstein, Edgar A. Change of electrical conductivity of NaCl upon bombardment with high energy protons—881
Pearson, G. L. (see Suhl, H.)—858(A)
Pearson, W. B. (see MacDonald, D. K. C.)—844(A)
Peaslee, D. C. and V. L. Telegdi. Charge independence in (γ,n) and (γ,t) reactions—126
—— (see Davidson, J. P.)—1585(L)
Pepinsky, Ray (see Jona, F.)—845(A); 1578(L)
—— (see Shirane, Gen)—504(L); 845(A)
Perkins, J. F. and S. K. Haynes. Electron and positron spectrum of Zn^{65} above 5 kev—1096(A)
—— **and S. K. Haynes.** *K*-Auger electrons, positrons, and conversion electrons of Zn^{65} above 5 kev—687
Perlman, I. (see Asaro, Frank)—694; 1496
Perlman, M. L., W. Bernstein, and R. B. Schwartz. Decay scheme of Ag^{108}—1236
Perry, J. P. (see Angell, C. E.)—835(L)
—— (see Barnes, S. W.)—1327(L)
Peters, B. (see Lal, D.)—438
Peterson, John W. Influence of electric field in contact charging—535(A)
Peterson, R. W., W. A. Fowler, and C. C. Lauritsen. Angular distributions of $F^{19}(p,\alpha)O^{16}$—1085(A)
Peterson, S. W. and H. A. Levy. Single-crystal neutron diffraction study of heavy ice—1082(A)

Peterson, V. Z. (see Bacher, R. F.)—1090(A)
—— (see Walker, R. L.)—1090(A)
Pettit, Helen B. (see Roach, F. E.)—534(A)
Peyrou, C. (see Fretter, W. B.)—1584(L)
Pickart, Stanley, J. (see Maxwell, Louis R.)—1120
Pidd, R. W., C. L. Hammer, and E. C. Raka. High-energy electron scattering by nuclei—436
Pines, David. Collective description of electron interactions: IV. Electron interaction in metals—626
—— (see Bohm, David)—609
—— (see Ferentz, M.)—836(L)
—— (see Lee, Tsung-Dao)—883
Piper, William W. Electrical and optical properties of synthetic single crystals of ZnS—23
—— Electroluminescence—841(T)
—— **and W. L. Roth.** Perfect crystals of ZnS—503(L)
Pipkin, Francis M. (see Hamilton, Donald R.)—1191
Pitkanen, Paul H. Effect of cloud-chamber geometry on β-ray studies—530(A)
—— (see Plain, G. J.)—529(A)
Pixley, R. E. (see Dunbar, D. N. F.)—649
Plain, G. J., H. L. Morrison, P. H. Pitkanen, and F. T. Rogers, Jr. β spectrum of S^{35} from $C_2H_5S^{35}H$ below 33 kev—529(A)
—— (see Rogers, Marguerite)—530(A)
Platt, Reuel T., Jr., and Jordan J. Markham. Production of F', M, and R centers in NaCl at room temperature—40
—— (see Markham, Jordan J.)—597
Platzman, R. L. (see Fröhlich, H.)—1152
Plesset, M. S. Cavitation and boiling—527(T)
Plyler, Earle K. (see Benedict, W. S.)—533(A)
Pool, M. L. (see Lerohl, John K.)—934
Pope, N. K. (see Henshaw, D. G.)—1229
Porter, G. Quantitative spectroscopic investigations of rapid gaseous reactions—527(T)
Portis, A. M. (see Kip, A. F.)—544(A)
Potter, David S. (see Miller, Charles E.)—406
Pound, R. V. (see Abragam, A.)—943
—— (see Kraushaar, J. J.)—522(L)
Powell, Wilson M. (see Ford, Franklin C.)—537(A)
Prater, W. K. (see Bell, W. A., Jr.)—1096(A)
Pratt, George W., Jr. Eigenfunctions of S^2 by spin operator method—278
Preston-Thomas, H., T. M. Dauphinee, and D. K. C. MacDonald. Measurement of specific heats of alkali metals—844(A)
Prestwood, R. J. (see Bunker, M. E.)—1588(E)
Price, E. W. Geometrical relations for solid propellant charges for rocket motors—542(A)
Primak, W., L. H. Fuchs, and P. Day. Radiation damage in insulators—1064(L)
Primakoff, H. (see Cheston, W.)—1538
Prince, M. B. Drift mobilities in semiconductors. I. Ge—681
Pringle, R. W., L. D. Black, B. L. Funt, and S. Sobering. New quenching effect in liquid scintillators—1582(L)
Prowse, D. J. (see Freemantle, R. G.)—1268
Pruitt, J. S., C. D. Swartz, and S. S. Hanna. Energies and angular distributions of neutrons from $Be^9(d,n)B^{10}$—1456
Pryce, M. H. L. (see Alburger, D. E.)—514(L)
Purcell, E. M. (see Smith, S. J.)—1069(L)

Quinnell, E. H. (see Clement, J. R.)—258

Ragent, B. (see Linlor, W. I.)—835(L)
Rainwater, L. J. (see Fitch, Val L.)—789
—— (see Melkonian, E.)—702
Raka, E. C. (see Pidd, R. W.)—436
Ramm, W. J., and M. N. Stein. Spectral distributions of filtered x-ray beams—1081(A)
Rasmussen, V. K., D. W. Miller, B. M. Carmichael, and M. B. Sampson. Preliminary results with Indiana heavy particle spectrometer—852(A)
Ravenhall, D. G. (see Yennie, D. R.)—1325(L)
Reagan, Daryl. Reaction $C^{12}(\gamma,3p)Li^9$—651
Rediker, R. H. (see Thompson, R. W.)—209(L)
Reed, George W. and Anthony Turkevich. U^{235} thermal neutron fission yields—1473
Reekie, James and T. S. Hutchison. Structure of liquid He—827(L)
Reeves, Marvin L. (see Geballe, Ronald)—867
Regener, Victor H. Automatic recording of zodiacal light—1093(A)
—— (see Kenney, James F.)—1090(A)
Reid, Walter P. Distribution of sizes of spheres in solid from study of slices of solid—1082(A)
Reines, Frederick. Experiment to detect free neutrino—1088(T)
—— **and C. L. Cowan, Jr.** Detection of free neutrino—830(L)
—— (see Anderson, E. C.)—1088(A)
—— (see Brousseau, A.)—1088(A)
—— (see Harrison, F. B.)—1088(A)
—— (see Hayes, F. N.)—1088(A)
—— (see Schuch, R. L.)—1088(A)
Rekers, R. G. and D. S. Villars. Flame zone spectroscopy of solid propellants—534(A)
Remley, M. E. and D. C. Woods. Low-power water-boiler type reactor for research use—544(A)
Rense, Wm. A. Intensity of Lyman-α line in solar spectrum—850(A)
Reynolds, H. K., D. N. F. Dunbar, W. A. Wenzel, and W. Whaling. Energy loss of low-energy protons and deuterons in gases—528(A)
——, **D. N. F. Dunbar, W. A. Wenzel, and W. Whaling.** Stopping cross section of gases for protons, 30–600 kev—742
—— (see Dunbar, D. N. F.)—528(A)
Rhoads, H. U. (see Bryant, P. J.)—1083(A)
Rhodes, K. B. and J. N. McGruer. Energy levels of Be^{10}—1328(L)
Rich, J. Čerenkov radiation—841(T)
Richardson, John M. Theory of liquid He—849(A)
Richardson, Robert E. (see Ball, W. P.)—539(A)
Rinehart, M. C. (see Cornelius, R. C.)—1584(L)
Ring, J. (see Barnes, S. W.)—1327(L)
—— (see Cartwright, W. F.)—852(A)
Ring, S. A. (see Litz, L. M.)—288
Ritson, D. M. (see Kaplon, M. F.)—855(A)
—— (see Klose, J. Z.)—855(A)
—— (see Noon, J. H.)—1586(L)
Roach, F. E., Helen B. Pettit, D. R. Williams, and P. St. Amand. Height of upper atmosphere emissions by Van Rhŷn method—534(A)
Rodeback, G. W. (see Bowen, D. B.)—531(A)
Roderick, Hilliard and Calvin Wong. Total disintegration energy of P^{29}—204(L)
Rogers, Betty (see Hayes, F. N.)—512(L)
Rogers, F. T., Jr. Variational approach to theory for critical stability of fluid—535(A)
—— (see Plain, G. J.)—529(A)
Rogers, K. (see Cornelius, R. C.)—1584(L)
Rogers, Marguerite, F. K. Odencrantz, and G. J. Plain. Thin target studies of $B^{10}(\alpha,n)N^{13}$, N^{13*}—530(A)
Rogosa, George L. and Guenter Schwarz. Mo K and U L x-ray transitions from separated isotopes—1434
—— (see Schwarz, Guenter)—88
Rose, A. and R. W. Smith. Space-charge-limited currents in insulators—857(A)
—— (see Shulman, Carl)—857(A)
—— (see Smith, R. W.)—857(A)
Rosen, Louis (see Frye, Glenn M.)—1083(A)
Rosenfeld, A. H. and S. B. Treiman. Search for V particles produced by 430-Mev protons—727
Rosenwasser, H. (see De Juren, J.)—544(A)

Ross, Marc. Tamm-Dancoff theory of pion photoproduction —855(A)
Rossi, B. (see Bassi, P.)—441
—— (see Leprince-Ringuet, L.)—722
Rotblat, J. (see Burcham, W. E.)—1266
—— (see Freemantle, R. G.)—1268
Roth, Benjamin. Two-body scattering at low energy—1250
Roth, W. L. (see Piper, William W.)—503(L)
Rothman, M. A., D. W. Kent, and C. E. Mandeville. Scattering of fast neutrons by Fe, Pb, and Cr—1097(A)
Rouvina, J. (see Cartwright, W. F.)—852(A)
Ruby, Lawrence (see Hubbard, Edward L.)—1494
Ruderman, M. A. (see Henley, E. M.)—1036
Runge, Richard J. Procedure for evaluation of automatic zodiacal light recordings—1093(A)
Ruth, Ralph P. and James W. Moyer. Efficiency of conversion from light to electric power by Ge grown junction—846(A)

Saffren, M. M. and J. C. Slater. Augmented plane-wave method for periodic potential problem—1126
Sagane, Ryokichi. π^+/π^- ratios measured with use of spiral orbit spectrometer—539(A)
—— **and Walter Dudziak.** Dependence of 33-Mev π^+ production cross section on atomic number—212(L)
Sailor, V. L. (see Foote, H. L., Jr.)—656
Sampson, M. B. (see Rasmussen, V. K.)—852(A)
—— (see Steigert, F. E.)—660
Sanders, F. H. Interference of underwater sound caused by surface reflection and upward refraction—1087(A)
Sandstrom, Wayne M. (see Miller, Charles E.)—406
Sarabhai, V. and R. P. Kane. Effects of geomagnetic field on solar cosmic rays—415
Saraf, B. L., J. Varma, and C. E. Mandeville. Radiations from As^{77} and Ge^{71}—848(A)
Sargent, C. P. (see Cornelius, R. C.)—1584(L)
Scanlon, Wayne W. Interpretation of Hall effect and resistivity data in PbS and similar binary compound semiconductors—1573(L)
—— (see Middleton, A. E.)—219
Schaaf, S. A. (see Chiang, S. F.)—535(A)
Schafroth, M. R. Spin-wave theory of antiferromagnetism for simple cubic lattices—553
Schardt, A. W. (see Welker, Joan P.)—401
Scharff-Goldhaber, Gertrude and Michael McKeown. Disintegration scheme of Br^{80} (18 min)—356
—— **and Michael McKeown.** New first excited state of even-even nucleus Kr^{80}—1094(A)
Schiff, L. I. Interpretation of electron scattering experiments —988
—— Lattice-space quantization of nonlinear field theory—766
—— (see Motz, H.)—540(A)
Schilberg, Lloyd E. and A. B. C. Anderson. Dependence of jet-tone eigenfrequencies on aerodynamic and geometrical parameters involved—543(A)
Schild, A. New modification of classical electromagnetic theory—1009
Schlegel, Richard. Inertia as consequence of wave properties —856(A)
Schmid, L. A. Calculation of cohesive energy of diamond—1373
Schmitt, H. W. and R. B. Leachman. Velocity distributions of slowed fission fragments—1091(A)
Schrader, Carlton D. Angular correlation of cascade γ rays from decay of Au^{198}—928
Schuch, R. L., E. C. Anderson, C. L. Cowan, Jr., F. B. Harrison, F. N. Hayes, and F. Reines. Liquid scintillation detectors to accommodate human subjects—1088(A)
Schuman, Robert P. (see Douglas, David L.)—369; 1095(A)
Schwager, J. E. and L. A. Cox. Magnetic analysis of $V^{51}(d,p)V^{52}$—102
Schwartz, R. B. (see Perlman, M. L.)—1236
—— (see Wheeler, G. W.)—121
Schwarz, Guenter and George L. Rogosa. Electronic excitation of L_{III} state of 5*d* elements—88
—— (see Rogosa, George L.)—1434
Schwinger, Julian. Theory of quantized fields—1283
Sclar, N., E. Burstein, and J. W. Davisson. Theory of low-temperature "breakdown" effect in Ge—858(A)
Scott, W. E. (see Terrell, James)—1091(A)
Seaborg, Glenn T. Evidence for subshell at $Z=96$—1074(L)
—— (see Dunlavey, Dean C.)—206(L)
Seagondollar, L. W. (see Krone, R. W.)—935
Seagrave, John D. Elastic scattering of fast neutrons by He^4 —1222
—— Scattering of fast neutrons by He^4—1093(A)
Seale, Robert L. Neutron spectrum from $O^{18}(d,n)F^{19}$—389
Seeman, Nathan (see King, D. T.)—838(L)
Seitz, F. Darkening of crystals of Ag halides by light—851(T)
Selove, W. Nuclear configurations inferred from high-energy pickup-deuteron distributions—1328(L)
—— Resonant effects and spin-dependence in potential scattering of slow neutrons—941
——, **K. Strauch, and F. Titus.** Neutron-proton scattering near 180° at 93 Mev—724
Sen, Hari K. Non-Maxwellian distribution in shock front and anomaly of chromospheric temperature—861
Serin, B., J. Gittleman, and E. A. Lynton. Transition into intermediate state of hollow superconducting cylinders—566
Sessler, A. M. and H. M. Foley. Relativistic correction to ground state energy of He—1321(L)
—— **and H. M. Foley.** Spin-spin interaction of electrons and ionization energy of He—1321(L)
Severiens, J. C. and C. S. Fuller. Mobility of impurity ions in Ge and Si—1322(L)
Shamos, M. H. (see Morewitz, H. A.)—134
Shapiro, A. M., C. P. Leavitt, and F. F. Chen. Total π^--p cross section at 840 and 470 Mev—1073(L)
—— (see Smith, L. W.)—851(A)
—— (see Widgoff, M.)—851(A)
Shapiro, Maurice M. (see King, D. T.)—838(L)
—— (see Stiller, Bertram)—735
Shephard, W. D. (see Fowler, W. B.)—832(L)
Sherr, R. (see Miller, R. H.)—848(A)
Shimada, Junji (see Ōno, Kazuo)—551
Shimauchi, A. (see Kojima, S.)—1572(L)
Shirane, Gen, R. E. Newnham, and R. Pepinsky. Phase transitions in $NaNbO_3$–$KNbO_3$ system—845(A)
—— **and Ray Pepinsky.** Dielectric properties and phase transitions of $Cd_2Nb_2O_7$ and $Pb_2Nb_2O_7$—504(L)
Shockley, William (see Tessman, Jack R.)—890
Shook, G. B. Propellant burning rate calculations—542(A)
Shrader, Ross E. (see Bube, Richard H.)—1135
Shulman, Carl, R. W. Smith, and A. Rose. Noise observations on CdS crystal photoconductors—857(A)
Shutt, R. P. (see Fowler, W. B.)—832(L)
Siegel, Armand (see Wiener, Norbert)—856(A)
Silverman, A. (see DeWire, J. W.)—519(L); 520(L)
Silverman, S. Infrared emission studies of some equilibrium and nonequilibrium flame reactions—527(T)
Silvey, G. (see Hardy, W. A.)—1533
Simon, Albert. Theory of polarized particles and γ rays in nuclear reactions—1050
Sirvetz, M. H. (see Kikuchi, C.)—109
Sites, John R., George Consolazio, and Russell Baldock. Isotopic abundances of Pd—1096(A)
Sitte, Kurt. Origin and propagation of air showers—1086(T)
Skillman, W. A. (see Cartwright, W. F.)—852(A)
Slater, J. C. Augmented plane wave method for periodic potential problem—603
—— (see Saffren, M. M.)—1126
Slichter, C. P. (see Carver, T. R.)—212(L)
Sloope, Billy W. (see Garrett, Richard E.)—1508.

Smaller, Bernard and Eugene Avery. Luminescence studies of KI-TlI—232
—— (see Yasaitis, E. L.)—1068(L)
Smit, J. and J. Volger. Spontaneous Hall effect in ferromagnetics—1576(L)
Smith, Bernard and Henry A. Boorse. He II film transport rates over machined metal surfaces—505(L)
Smith, J. E. (see Blau, M.)—516(L)
Smith, L. P. Present status of the electronic properties of AgCl—851(T)
Smith, L. W., C. P. Leavitt, A. M. Shapiro, C. E. Swartz, and M. Widgoff. Interactions of 2.2-Bev protons in nuclear emulsions—851(A)
—— (see Widgoff, M.)—851(A)
Smith, R. W. and A. Rose. Current-voltage characteristics of CdS crystals using ohmic contacts—857(A)
—— (see Rose, A.)—857(A)
—— (see Shulman, Carl)—857(A)
Smith, S. J. and E. M. Purcell. Visible light from localized surface charges moving across grating—1069(L)
Snodgrass, H. R. Ionization of relativistic cosmic-ray μ mesons—1089(A)
Snowdon, S. C. (see Whitehead, W. D.)—114; 1097(A)
Sobering, S. (see Pringle, R. W.)—1583(L)
Solbrig, A. W., Jr. Effects of certain three-body nuclear interactions in H^3 and He^3—855(A)
Soled, J. (see Keck, P. H.)—847(A)
Solmitz, F. T. p-p scattering for nucleon isobar model—164
Sommers, H. S., Jr., W. E. Keller, and J. G. Dash. Heat of mixing of He^3 in He^4—1345
Spence, R. D. (see Jain, P. L.)—844(A)
—— (see Mann, Glen A.)—844(A)
Spence, R. W. Fission with moderate energy neutrons—1079(T)
Sperduto, A. (see Bockelman, C. K.)—665
Sprague, G. and D. H. Tomboulian. Quadrupole moments of Sb^{121} and Sb^{123}—105
Sproull, R. L., R. S. Bever, and G. Libowitz. Oxygen vacancies in BaO—77
Stähelin, P. 0^+ states of light odd-odd nuclei—1076(L)
St. Amand, Pierre and D. R. Williams. Possible relationship between ionosphere and nightglow—534(A)
—— (see Roach, F. E.)—534(A)
—— (see Williams, D. R.)—533(A)
Stapp, H. P. Second-order electron self-energy—540(A)
Starner, J. W. (see Bunker, M. E.)—1587(E)
Steele, M. C. and R. A. Hein. Superconductivity of Ti—243
—— (see Osborne, M. F. M.)—1403
Steffen, Rolf M. Indications of the interaction of electric field gradients and nuclear electric quadrupole moments in angular correlation—849(A)
—— (see Hemmig, P. B.)—832(L)
Steigert, F. E. and M. B. Sampson. α-α scattering from 12.88 to 21.62 Mev—660
Stein, M. N. (see Ramm, W. J.)—1081(A)
Stephens, Frank, Jr. (see Asaro, Frank)—1492
Stephens, W. E. (see Toms, M. E.)—362
Stephenson, S. T. (see Krogstad, R.)—1394
Sternberg, David. Electron ejection from metals by positive ions and metastable atoms of a few electron volts—847(T)
Sternheimer, R. M. and H. M. Foley. Nuclear quadrupole coupling in Li_2 molecule—1460
Stevens, D. K. and J. H. Crawford, Jr. Magnetic susceptibility of Ge—1065(L)
Stewart, Leona. Determination of neutron spectrum and absolute yield of Pu–Be source—1095(A)
Stewart, R. W. "Lloyd mirror" interference in presence of slight uniform refraction—1087(A)
—— (see Grant, H. L.)—1087(A)
Stiller, Bertram and Maurice M. Shapiro. Ionization loss at relativistic velocities in nuclear emulsion—735
Stitch, M. L. (see Honig, A.)—901
Stookey, S. D. Effects of high-energy radiation on glass—841(T)
Stork, Donald H. Total cross sections for positive pions—538(A)
—— (see Leonard, Stanley L.)—855(A)
Stout, J. W. and Edward Catalano. Thermal anomalies associated with antiferromagnetic ordering of FeF_2, CoF_2, and NiF_2—1575(L)
Strandberg, M. W. P. (see Hardy, W. A.)—1533
Strauch, K. (see Selove, W.)—724
Straumanis, M. E. Absolute value of Avogadro's number and soundness of crystals—1155
Strickler, Thomas D. Large-angle scattering of Co^{60} γ rays—923
Stuart, Alexander Verrijn and G. B. B. M. Sutherland. Effects of H bonding on infrared spectra of alcohols—534(A)
Stubbins, Warren F. (see Hubbard, Edward L.)—1494
Stull, J. L. and L. R. Bickford, Jr. Magnetostriction of magnetite—845(A)
Sugarman, Nathan and Agnes Haber. Interaction of negative pions with Hg—730
Suhl, H. and G. L. Pearson. Faraday rotation in Ge—858(A)
Sun, H. and G. L. Weissler. Absorption coefficients of NO and NH_3 in vacuum uv—545(A)
—— (see Weissler, G. L.)—533(A)
Sutherland, G. B. B. M. (see Stuart, Alexander Verrijn)—534(A)
Swartz, C. D. (see Pruitt, J. S.)—1456
Swartz, C. E. (see Smith, L. W.)—851(A)
—— (see Widgoff, M.)—851(A)
Swigart, J. I. (see Linford, L. B.)—1093(A)
Swings, P. Comets, carbon stars, and combustion phenomena—527(T)

Takeo, Makoto and Shang-Yi Ch'en. Theory of fine structure pressure broadening of spectral lines—850(A)
Tannenwald, L. M. Linearized theory of spherical wave decay—542(A)
Taschek, R. F. Light particles reactions—1092(T)
—— (see Martin, H. C.)—1096(A)
Taylor, A. E. Total cross sections for 169-Mev neutrons—1071(L)
Taylor, R. A. (see Howland, P. R.)—1095(A)
Taylor, T. B. Nuclear scattering of high-energy neutrons—831(L)
Teasdale, J. G. (see Bacher, R. F.)—1090(A)
—— (see Walker, R. L.)—1090(A)
Telegdi, Valentine L. (see Peaslee, D. C.)—126
—— (see Thirion, Jacques)—1253
Temmer, G. M. and J. M. Wyckoff. α-γ angular correlation in ionium (Th^{230})—913; 849(A)
—— (see Heydenburg, N. P.)—89
Tenney, F. H. and J. Tinlot. Positive π-meson interactions in Be—974
Terrell, James, W. E. Scott, J. S. Gilmore, and C. O. Minkkinen. Yield of Mo^{99} from fission of U^{235} and U^{238}—1091(A)
Tessman, Jack R., A. H. Kahn, and William Shockley. Electronic polarizabilities of ions in crystals—890
Theobald, J. K. Evaluation of back diffusion for various standard gases as it affects secondary electron emission coefficients—535(A)
Theus, R. B. (see Beach, L. A.)—355
Thie, Joseph A. Semiclassical methods in meson processes—1282
Thirion, Jacques and Valentine L. Telegdi. Lifetime measurements for first excited states of O^{17} and B^{10} from recoil studies—1253
Thode, H. G. (see Fleming, W. H.)—378
Thomas, E. E. (see Calbick, C. J.)—1082(A)

—— (see Christensen, I. H.)—1082(A)
Thomas, L. H. (see Bakamijian, B.)—1300
Thomas, R. G. *R*-matrix formulation of statistical theory of nuclear reactions—1094(A)
Thomas, Roy. Cross section for production of penetrating cosmic-ray showers—1090(A)
Thompson, R. W., A. V. Buskirk, C. J. Karzmark, and R. H. Rediker. Example of a V^+ decay—209(L)
Thompson, S. G. (see Asaro, Frank)—694
Thompson, T. J. Effects of chemical structure on stopping powers for high-energy protons—1083(A)
Thorndike, A. M. (see Fowler, W. B.)—832(L)
Tilton, G. (see Patterson, C.)—1234
Timoshenko, G. S. (see Friedland, S. S.)—1080(A)
Ting, Yu, Edward Manring, and Dudley Williams. Zeeman splitting of nuclear quadrupole resonance lines—1581(L)
Tinlot, J. (see Tenney, F. H.)—974
Titus, F. (see Selove, W.)—724
Tobocman, W. (see Friedman, F. L.)—93
Todd, W. B. (see Metzger, F. R.)—904
Tollestrup, A. V., J. C. Keck, and R. M. Worlock. Angular distribution of positive photomesons from H: counter telescope method—1090(A)
—— (see Bacher, R. F.)—1090(A)
—— (see Woodbury, H. H.)—1199
Tomboulian, D. H. (see Sprague, G.)—105
Tomkins, Frank S. (see Fred, Mark)—1322(L)
Toms, M. E. and W. E. Stephens. Photoprotons from In, Ce, and Bi—362
Tonks, Lewi. Thermal test reactor at Knolls Atomic Power Laboratory—854(T)
Torrey, H. C. Nuclear spin relaxation by translation diffusion—962
Townes, C. H. (see Hardy, W. A.)—1533
—— (see White, R. L.)—1256
Townsend, John R. Solid state absorption spectra of Mg and MgO—556
Tracy, J. F. Scattering and absorption of π^+ mesons by Al—537(A)
Trammell, G. T. Magnetic scattering of neutrons from rare earth ions—1387
Trees, R. E. Hfs formulas for *LS*-coupling—308
—— (see Kessler, Karl G.)—303
Treiman, S. B. (see Rosenfeld, A. H.)—727
Trilling, G. H. (see van Lint, V. A. J.)—1089(A)
Trolan, J. K. (see Barbour, J. P.)—45
—— (see Dyke, W. P.)—541(A)
Truby, Frank K. Some electrical hysteresis properties of ice—543(A)
Trump, John G. (see Anson, John H.)—843(A)
—— (see Bourne, Henry C. Jr.)—847(A)
Tseng, T. P. (see Nicol, James)—1062(L)
Tsukada, K. (see Kojima, S.)—1572(L)
Turkevich, Anthony and Si Chang Fung. Radioactive Cu nuclides produced by slow negative pions and muons from Zn—521(L)
—— (see Reed, George W.)—1473

Ulwick, J. C. (see Lien, J. R.)—508(L)
Urbach, Franz. Fundamental approaches to problems of photographic sensitivity—851(T)
—— Long wavelength edge of photographic sensitivity and of electronic absorption of solids—1324(L)
Usiskin, S. R. (see Williams, G. W.)—1398

Valatin, J. G. Coupled-field Green's functions—522(L)
Vallarta, M. S. Evidence for general magnetic field of sun from cosmic rays—1086(T)
van der Ziel, A. Modified theory of production of secondary electrons in solids—35
—— Theory of secondary electron production for screened Coulomb interaction—843(T)
Van Horn, W. (see Keck, P. H.)—847(A)
van Lieshout, R. (see Nussbaum, R. H.)—207(L)
van Lint, V. A. J. and G. H. Trilling. Cloud-chamber observation of decay of τ meson—1089(A)
—— (see Anderson, C. D.)—1089(A)
—— (see Cowan, E. W.)—1089(A)
van Trier, A. (see Danos, M.)—828(L)
Van Vleck, J. H. (see Abragam, A.)—1448
Varma, J. (see Saraf, B. L.)—848(A)
Vilain, J. H. and R. W. Williams. Decay-electron spectrum of μ meson—1586(L)
Villars, D. S. (see Rekers, R. G.)—534(A)
Volger, J. (see Smit, J.)—1577(L)

Wada, W. W. Scattering of mesons by complex nuclei—152
Wainfan, N. and W. C. Walker. Preliminary results of direct measurements of photoionization in O_2—533(A)
—— (see Walker, W. C.)—533(A)
Wainwright, Thomas and George Parzen. Electronic energy bands in crystals—1129
Walker, R. L., J. G. Teasdale, and V. Z. Peterson. Photoproduction of positive mesons from H: magnetic spectrometer method—1090(A)
—— (see Bacher, R. F.)—1090(A)
Walker, W. C. and N. Wainfan. Photoelectric yield of Pt in vacuum uv—533(A)
—— (see Wainfan, N.)—533(A)
Walker, W. D. Recent work on penetrating showers—1086(T)
Walker, W. L. (see Klose, J. Z.)—855(A)
Wall, N. S. Nuclear reaction determination of $Sn^{124}-Te^{124}$ mass difference—1526
Wallin, W. Wave-synthesizing light chopper—543(A)
Wapstra, A. H. (see Nussbaum, R. H.)—207(L)
Warren, J. B. and G. M. Griffiths. γ rays from $T(p,\gamma)He^4$ reaction—1084(A)
—— (see Griffiths, G. M.)—1084(A)
Warters, William D. Elastic scattering of protons by Li^7—528(A)
Watanabe, Satosi. "Fusion" theory of bosons and nonlocal field—856(A)
Watson, K. M. (see Brueckner, K. A.)—1023
—— (see Francis, N. C.)—291
Watson, W. W. (see Wheeler, G. W.)—121
Watters, H. J. and J. F. Fagan, Jr. Radionuclides of As produced by deuteron bombardment of Ge—1248
Watters, R. L. (see Dunlap, W. C., Jr.)—1397
Webb, J. Low-intensity reciprocity law failure in photographic exposure and its dependence on two-quantum process—851(T)
Webb, T. S., C. W. Li, and W. A. Fowler. Elastic scattering of protons by N^{14}—1084(A)
Weber, A. H. (see Bryant, P. J.)—1083(A)
Weber, J. Vacuum fluctuation noise in electron streams—847(A)
Weidner, R. T. (see Eschenfelder, A. H.)—869
Weil, John W. and Boyce D. McDaniel. Production of protons from C by monoenergetic γ rays—391
Weiss, M. M. and W. Bernstein. Degradation of γ rays in water—1264
Weisskopf, V. F. Cloudy crystal ball model—843(T)
Weissler, G. L. and H. Sun. Absorption cross sections of CH_4 in vacuum uv—533(A)
—— (see Lee, Po)—533(A); 545(A)
—— (see Sun, H.)—545(A)
Welker, Joan P., A. W. Schardt, G. Friedlander, and J. J. Howland, Jr. Metastable states of Ge^{73}—401
Welsh, H. L. Recent developments in infrared spectroscopy of gases at very high pressures—850(T)

Weneser, J. and D. R. Hamilton. Theorem concerning angular correlations—321
Wentzel, G. Recoil corrections in strong coupling meson theory—173
Wenzel, W. A. (see Bader, M.)—1085(A)
—— (see Dunbar, D. N. F.)—528(A); 649
—— (see Hoyle, F.)—1095(A)
—— (see Reynolds, H. K.)—528(A); 742
Wessel, Günter. Hfs and nuclear electric quadrupole moment of B^{11}—1581(L)
—— **and Hin Lew.** Hfs of Ag and Au by atomic beam magnetic resonance method—641
—— (see Brix, P.)—647
West, H. I., Jr. (see Mann, L. G.)—1481
—— (see Meyerhof, W. E.)—540(A); 758
Westervelt, Donald R. Optical effects of radiation damage in alkali halides—531(A)
Westlund, C. D. (see Linford, L. B.)—1093(A)
Wetherill, George W. Spontaneous fission yields from U and Th—907
Whaling, Ward (see Bader, M.)—1085(A)
—— (see Dunbar, D. N. F.)—528(A); 649
—— (see Hoyle, F.)—1095(A)
—— (see Mileikowsky, Curt)—528(A)
—— (see Reynolds, H. K.)—528(A); 742
Wheeler, G. W., R. B. Schwartz, and W. W. Watson. Protons from deuteron bombardment of Kr^{84} and Kr^{86}—121
Wheeler, John A. Collective model—843(T)
—— Fission and nuclear models—1079(T)
—— μ meson as nuclear probe particle—812
Whipple, F. L. (see Liller, William)—1093(T)
White, R. L. and C. H. Townes. Spin of Si^{29} and mass ratios of stable Si isotopes—1256
White, William C. Suppression of AlO in wake of ultra-speed pellets—1083(A)
Whitehead, W. D. and S. C. Snowdon. Angular distribution of neutrons scattered from Al, Fe, and Pb—114; 1097(A)
Whitmore, B. G. Inelastic scattering of fast neutrons in C and Pb—654
Whittemore, W. L. (see Fowler, W. B.)—832(L)
Whittle, C. E. and P. S. Jastram. Angular correlation between the first and third γ rays in Ti^{48}—205(L)
Widgoff, M., C. P. Leavitt, A. M. Shapiro, L. W. Smith, and C. E. Swartz. Stars induced in nuclear emulsions by 2.2-Bev protons—851(A)
—— (see Smith, L. W.)—851(A)
Wiener, Norbert and Armand Siegel. Description of quantum states through distributions of observable values—856(A)
Wilkening, Marvin H. Variation of natural radioactivity in atmosphere with altitude—1080(A)
Wilkinson, M. K. Neutron diffraction by ferromagnetic and antiferromagnetic substances—1088(T)
Williams, D. L. (see Hayes, F. N.)—512(L)
Williams, D. R. and Pierre St. Amand. Multicolor photoelectric photometer for study of faint radiations—533(A)
—— (see Roach, F. E.)—534(A)
—— (see St. Amand, Pierre)—534(A)
Williams, Dudley (see Ting, Yu)—1582(L)
Williams, G. W., S. R. Usiskin, and A. J. Dekker. Thermal decay of luminescence of KBr—1398
Williams, L. E. (see Friedland, S. S.)—1080(A)
Williams, Lloyd (see Hayes, F. N.)—1088(A)
Williams, R. W. (see Vilain, J. H.)—1587(L)
Williams, S. R. (see Fairbank, W. M.)—208(L)
Wilson, H. W. and Walter H. Barkas. Test of charge symmetry hypothesis—537(A)
Wilson, R. N. (see Yennie, D. R.)—1325(L)
Wilson, Richard (see Brown, Karl L.)—540(A)
Wilson, V. C. Double-crystal neutron spectrometer—841(T)
Winckler, J. R. (see Baskin, R.)—464
Wise, Henry. Measurement of heat of dissociation of F_2 by effusion method—532(A)
Whitten, L. (see Berlin, T. H.)—189
Wolfe, B. (see DeWire, J. W.)—519(L); 520(L)
Wolfenstein, Lincoln. Use of tensor operators in nuclear collision problems—123
Wolff, G. Crystal habit of Si and Ge—847(A)
Wolff, Peter A. Theory of plasma waves in metals—18
Wolfhard, H. G. Absorption spectroscopy in stationary flames—527(T)
Wollan, E. O. (see Koehler, W. C.)—1380
Wong, Calvin. β decay of F^{17} and F^{20}—529(A)
—— (see Roderick, Hilliard)—204(L)
Woodbury, H. Hugh. Angular anisotropy of γ ray from $C^{12}(p,\gamma p')C^{12}$—529(A)
——, **R. B. Day, and A. V. Tollestrup.** γ radiation from reaction $C^{13}(p,\gamma)N^{14}$—1199
Woodruff, A. E. Phenomenological analysis of meson-nucleon scattering—855(A)
Woods, D. C. (see Kash, S. W.)—544(A)
—— (see Remley, M. E.)—544(A)
Woods, Frank R., Edgar F. Bennett, and John A. Lockwood. Temperature dependence of BF_3 proportional neutron counters—853(A)
Workman, D. R. (see Hepner, W. A.)—1071(L)
Workman, E. J. Cellular nature of ice crystals—544(A)
—— Thunderstorm electricity—1093(T)
Worlock, R. M. (see Bacher, R. F.)—1090(A)
—— (see Tollestrup, A. V.)—1090(A)
Wright, Kenneth A. (see Anson, John H.)—843(A)
—— (see Brown, W. L.)—591
Wu, Ta-You (see Bauer, Ernest)—1101
Wyckoff, J. M. (see Temmer, G. M.)—913; 849(A)

Yadoff, Oleg. Interference of waves generated by electric field—543(A)
Yasaitis, E. L. and B. Smaller. Paramagnetic resonances in irradiated glasses—1068(L)
Yennie, D. R., R. N. Wilson, and D. G. Ravenhall. Phase-shift calculation of high-energy electron scattering by nuclei—1325(L)
Yngve, Victor H. Time variation of cosmic-ray heavy nuclei—428
Yuan, Luke C. L. (see Lindenbaum, S. J.)—1579(L)

Zajec, Emery (see Cork, Bruce)—853(A)
Zemansky, M. W. (see Brown, A.)—52
Zernow, Louis. Flash radiographic studies of high-velocity metallic jets—532(A)
Zilsel, P. R. Liquid He II: Bose-Einstein condensation and two-fluid model—1106

Analytic Subject Index to Volume 92

References with (A) are to abstracts of papers presented at meetings of the American Physical Society; references with (L) are to Letters to the Editor; references with (E) are to Errata. Items are listed under the following categories:

Acoustics
Astrophysics
Atomic and Molecular Beams
Atomic Mass and Abundance
Atomic Structure and Spectra
Biophysics
Chemical Effects and Properties
Constants, Standards, Units
Cosmic Radiation
Crystalline State
Dielectrics and Dielectric Properties
Diffraction
Diffusion
Elasticity and Plasticity
Electrical Conductivity and Resistance
Electrical Discharges
Electrical Properties
Electromagnetic Theory and Electrodynamics
Electrons and Positrons
Elementary Particle Interactions
Errata
Field Theory
Films, Properties
Fluid Dynamics
Gamma Rays
Gases
Geophysics
Helium, Liquid
Imperfections in Solids
Ionization
Ions
Ions and Electrons, Mobility
Liquids
Luminescence
Magnetic Properties
Magnetic Resonance
Mathematical Methods
Mechanics
Mesons
Methods and Instruments
Microwaves
Miscellaneous
Molecular Aggregates
Molecular Structure and Spectra
Neutrino
Noise
Nuclear Fission
Nuclear Moments and Spin
Nuclear Photoeffects
Nuclear Reactions, General
Nuclear Reactions Induced by α Particles and He^3
Nuclear Reactions Induced by Deuterons and Tritons
Nuclear Reactions Induced by Mesons
Nuclear Reactions Induced by Neutrons
Nuclear Reactions Induced by Protons
Nuclear Spectra
Nuclear Structure Theory
Optical Properties
Proceedings of the American Physical Society
Quantum Electrodynamics
Quantum Mechanics
Radiation
Radioactivity
Range and Energy Loss of Particles
Relativity and Gravitation
Scattering, General
Scattering of α Particles
Scattering of Deuterons
Scattering of Electrons and Positrons
Scattering of Mesons
Scattering of Neutrons
Scattering of Protons
Semiconductors
Spectra, General
Statistical Mechanics and Thermodynamics
Superconductivity
Thermal Properties
X-Rays

Absorption of Radiation (see **Radiation**)

Acoustics

Correlation studies of sound fluctuations in ocean, H. L. Grant and R. W. Stewart—1087(A)

Dependence of jet-tone eigenfrequencies on aerodynamic and geometrical parameters involved, Lloyd E. Schilberg and A. B. C. Anderson—543(A)

Dependence of primary pfeifenton (pipe tone) frequency on pipe-orifice geometry, A. B. C. Anderson—543(A)

Interference of underwater sound caused by surface reflection and upward refraction, F. H. Sanders—1087(A)

"Lloyd mirror" interference in presence of slight uniform refraction, R. W. Stewart—1087(A)

Velocity of sound apparatus for liquids at 512 kc, George G. Kretschmar—542(A)

Adsorption (see **Gases**)

Aerodynamics (see **Fluid Dynamics**)

Afterglow (see **Electrical Discharges**)

Alloys (see **Crystalline State**)

Annihilation (see **Electrons and Positrons**)

Antiferroelectric Phenomena (see **Dielectrics and Dielectric Properties**)

Antiferromagnetism (see **Magnetic Properties**)

Arcs (see **Electrical Discharges**)

Astrophysics

Automatic recording of zodiacal light, Victor H. Regener—1093(A)

Concentration of U and Pb and isotopic composition of Pb in meteoritic material, C. Patterson, H. Brown, G. Tilton, and M. Inghram—1234

Intensity of Lyman-α line in solar spectrum, William A. Rense—850(A)

Non-Maxwellian distribution in shock front and anomaly of chromospheric temperature, Hari K. Sen—861

Physical conditions in initial stages of expanding universe, Ralph A. Alpher, James W. Follin, Jr., and Robert C. Herman—1347

Procedure for evaluation of automatic zodiacal light recordings, Richard J. Runge—1093(A)

State in C^{12} predicted from astrophysical evidence, F. Hoyle, D. N. F. Dunbar, W. A. Wenzel, and W. Whaling —1095(A)

Atmosphere (see **Geophysics**)

Atomic and Molecular Beams

Hfs of Ag and Au by atomic beam magnetic resonance method, Günter Wessel and Hin Lew—641

Sign of quadrupole interaction of Li^6 in LiCl, P. Kusch—268

Zeeman effect of Cr ground state, P. Brix, J. T. Eisinger, H. Lew, and G. Wessel—647

Atomic Mass and Abundance

Applications of Wigner semi-empirical mass formula to isobars, J. T. McCarthy—848(A)

Concentration of U and Pb and isotopic composition of Pb in meteoritic material, C. Patterson, H. Brown, G. Tilton, and M. Inghram—1234

Ga, Ge, As, Se, and Br atomic masses, B. G. Hogg and H. E. Duckworth—848(A)

Nuclear reaction determination of Sn^{124}–Te^{124} mass difference, N. S. Wall—1527

Pd isotopic abundances, John R. Sites, George Consolazio, and Russell Baldock—1096(A)

Spin of Si^{29} and mass ratios of stable Si isotopes, R. L. White and C. H. Townes—1256

Atomic Structure and Spectra
Bi^{210} spin, Mark Fred, Frank S. Tomkins, and Raymond F. Barnes—1324(L)
Hfs and nuclear electric quadrupole moment of B^{11}, Günter Wessel—1581(L)
Hfs formulas for LS-coupling, R. E. Trees—308
Hfs of H, R. Arnowitt—1002
Hfs of spectra of Dy, Co, V, Mn, and La, Kiyoshi Murakawa and Tohru Kamei—325
Intensity of Lyman-α line in solar spectrum, William A. Rense—850(A)
μ meson as nuclear probe particle, John A. Wheeler—812
μ-mesonic atoms and electromagnetic radius of nucleus, L. N. Cooper and E. M. Henley—801
Nuclear radii, Francis Bitter and Herman Feshbach—837(L)
O I new fine structure, Lee W. Parker and John R. Holmes—532(A)
Quenching of Hg resonance radiation (2537A) by N, C. G. Matland—637
Relativistic correction to ground state energy of He, A. M. Sessler and H. M. Foley—1321(L)
Relativistic correction to Lamb shift, M. Baranger, H. A. Bethe, and R. P. Feynman—482
Sb^{121} and Sb^{123} quadrupole moments, G. Sprague and D. H. Tomboulian—105
Spin-spin interaction of electrons and ionization energy of He, A. M. Sessler and H. M. Foley—1321(L)
Theory of fine structure pressure broadening of spectral lines, Makoto Takeo and Shang-Yi Ch'en—850(A)
Theory of microwave Zeeman effect in atomic oxygen, A. Abragam and J. H. Van Vleck—1448
X-rays from μ-mesonic atoms, Val L. Fitch and L. J. Rainwater—789
Zeeman effect of Cr ground state, P. Brix, J. T. Eisinger, H. Lew, and G. Wessel—647

Aurora (see **Astrophysics; Geophysics**)

Barkhausen Effect (see **Magnetic Properties**)
Biophysics
Boson Theory (see **Field Theory**)
Bremsstrahlung (see **Radiation**)
Broadening of Spectral Lines (see **Atomic Structure and Spectra; Molecular Structure and Spectra; Spectra, General**)

Capture Cross Sections (see **Electrons and Positrons; Nuclear Reactions; Radiation**)
Čerenkov Effect (see **Radiation**)
Chemical Effects and Properties
Chemical Reactions (see **Chemical Effects and Properties**)
Chemiluminescence (see **Luminescence**)
Cold Emission (see **Electrical Properties**)
Colloids (see **Chemical Effects and Properties; Molecular Aggregates**)
Compton Effect (see **Radiation**)
Conductivity, Electrical (see **Electrical Conductivity and Resistance**)
Conductivity, Thermal (see **Thermal Properties**)
Constants, Standards, Units
Absolute value of Avogadro's number and soundness of crystals, M. E. Straumanis—1155
Precision measurement at 24 500 volts of conversion constant λV, Gaelen L. Felt, John N. Harris, and Jesse W. M. DuMond—1160
Cosmic Radiation
Atmospheric effects on cosmic-ray intensity near sea level, S. Olbert—454
Cascade decay of V particles, C. D. Anderson, E. W. Cowan, R. B. Leighton, and V. A. J. van Lint—1089(A); E. W. Cowan, C. D. Anderson, R. B. Leighton, and V. A. J. van Lint—1089(A)
Charged and neutral V particles, W. B. Fretter and E. W. Friesen—1089(A)
Cloud-chamber observation of decay of τ meson, V. A. J. van Lint and G. H. Trilling—1089(A)
Cross section for production of penetrating showers, Roy Thomas—1090(A)
Cross section for production of penetrating showers in O, James F. Kenney and Victor H. Regener—1090(A)
Distribution of arrival times of air shower particles, P. Bassi, G. Clark, and B. Rossi—441
Effects of geomagnetic field on solar cosmic rays, V. Sarabhai and R. P. Kane—415
Emulsion cloud-chamber study of high-energy radiation at mountain altitude, J. Z. Klose, M. F. Kaplon, D. M. Ritson, and W. L. Walker—855(A)
Emulsion study of large shower. I. Hard component, P. S. Freier and J. E. Naugle—1086(A); II. Soft component, J. E. Naugle and P. S. Freier—1086(A)
Heavy unstable particles, D. Lal, Yash Pal, and B. Peters—438
Interactions of heavy primaries, M. F. Kaplon, J. H. Noon, and D. M. Ritson—855(A)
Ionization of relativistic cosmic-ray μ mesons, H. R. Snodgrass—1089(A)
Mass measurements of primaries of S events by momentum-range method, W. B. Fretter, B. P. Gregory, R. Johnston, A. Lagarrigue, H. Meyer, F. Muller, and C. Peyrou—1583(L)
Mean lifetime of V^0 particles, R. B. Leighton and W. L. Alford—540(A)
Multiple cores in air showers, Osman El-Mofty—461; 1086(A)
North-south observations of ratio of positive to negative cosmic-ray mesons, Robert B. Brode—1086(A)
Production of fast Li, Be, B fragments from interactions of primary cosmic-ray nuclei, J. H. Noon, M. F. Kaplon, and D. M. Ritson—1585(L)
Relative ionization by cosmic-ray μ mesons in liquid scintillator, R. Baskin and J. R. Winckler—464
Search for highly-absorbable negative cosmic-ray particles at sea level, Charles E. Miller, Joseph E. Henderson, David S. Potter, William R. Davis, Wayne M. Sandstrom, Gerald R. Garrison, and Francis M. Charbonnier—406
Time variation of cosmic-ray heavy nuclei, Victor H. Yngve—428
Time variations in cosmic-ray intensity underground, Mercedes M. Agogino—1086(A)
V^+ decay, R. W. Thompson, A. V. Buskirk, C. J. Karzmark, and R. H. Rediker—209(L)
Variation of ratio of positive to negative cosmic-ray μ mesons with momentum and altitude, H. A. Morewitz and M. H. Shamos—134
Cosmology (see **Astrophysics; Relativity and Gravitation**)
Critical Potentials (see **Atomic Structure and Spectra; Molecular Structure and Spectra**)
Cross Section (see **Electrons and Positrons; Nuclear Reactions; Radiation; Scattering**)
Crystal Counters (see **Methods and Instruments**)
Crystalline State (see also **Electrical Properties; Imperfections in Solids; Magnetic Properties; Semiconductors; etc.**)
Absolute value of Avogadro's number and soundness of crystals, M. E. Straumanis—1155
Annealing effects in irradiated Cu, Albert W. Overhauser—530(A)
Annealing of bombardment damage in diamond-type lattice: theoretical, R. C. Fletcher and W. L. Brown—585

Crystalline State (Continued)
Annealing of bombardment damage in Ge: experimental, W. L. Brown, R. C. Fletcher, and K. A. Wright—591
Annealing of radiation damage effects in Cu, R. R. Eggleston—531(A)
Augmented plane wave method for periodic potential problem, J. C. Slater—603; II, M. M. Saffren and J. C. Slater—1126
Behavior of metals at elevated temperatures, Edward W. LaRocca—1082(A)
Bleaching properties of *F* centers in KBr at 5°K, Jordan J. Markham, Reuel T. Platt, Jr., and Irving L. Mador—597
Cellular nature of ice crystals, E. J. Workman—544(A)
Cleavage surfaces in Ge crystals, C. J. Calbick, H. Christensen, and E. E. Thomas—1082(A); H. Christensen, C. J. Calbick, and E. E. Thomas—1082(A)
Collective description of electron interactions: III. Coulomb interactions in degenerate electron gas, David Bohm and David Pines—609; IV. Electron interaction in metals, David Pines—626
Color-center formation in alkali halides containing S^-, E. Burstein and B. W. Henvis—845(A)
Crystal growth of Si by tip fusion process, P. H. Keck, S. B. Levin, J. Broder, and R. Lieberman—847(A)
Crystal habit of Si and Ge, G. Wolff—847(A)
Crystal structure and nuclear directional correlation, I. Pb^{204}, H. Frauenfelder, J. S. Lawson, Jr., W. Jentschke, and G. DePasquali—513(L)
Cyclotron resonance in Ge crystals, G. Dresselhaus, A. F. Kip, and C. Kittel—827(L)
Defect relaxation time of conduction electrons in crystals by tight binding approximation, J. Lomont—532(A)
Distribution of sizes of spheres in solid from study of slices of solid, Walter P. Reid—1082(A)
Effect of quench temperature and cold work on ordering rates of Cu_3Au and CuAu, C. E. Dixon and C. J. Meechan—530(A)
Effect of surface on magnetic properties of electron gas, Frank S. Ham—1113
Electrical hysteresis properties of ice, Frank K. Truby—543(A)
Electron traps in ice, E. Avery, L. Grossweiner, and M. Matheson—1080(A)
Electronic energy bands in crystals, Thomas Wainwright and George Parzen—1129
Electronic polarizabilities of ions in crystals, Jack R. Tessman, A. H. Kahn, and William Shockley—890
Energy of trapped electrons in ionic solids, Kurt Lehovec—253
Etch pits in plastically-deformed Ge, C. J. Gallagher—846(A)
Evaluation of lattice sums for cubic crystals, J. Hove and J. Krumhansl—569
Exchange potential in electron gas at nonzero temperature, N. H. March—510(L)
Exchange potential in surface region of free-electron metal, Hellmut J. Juretschke—1140
Floating zone recrystallization, P. H. Keck, W. VanHorn, J. Soled, and A. MacDonald—847(A)
Influence of cold work and radiation damage on vibrational spectra of Cu, D. B. Bowen and G. W. Rodeback—531(A)
Interaction of nonrelativistic particle with scalar field with application to slow electrons in polar crystals, Tsung-Dao Lee and David Pines—883
Internal friction of rocksalt single crystals, D. R. Frankl—573
Long wavelength edge of photographic sensitivity and of electronic absorption of solids, Franz Urbach—1324(L)
Low-temperature diamagnetism of electrons in cylinder, R. B. Dingle—1320(L)
Magnetic properties of electronic Einstein model solid, M. F. M. Osborne and M. C. Steele—1403
NAA statitron for solid-state research, D. T. Eggen and H. Kenworthy—531(A)
Nucleation of ordered phases in Cu_3Au, Norman W. Lord—844(A)
Optical effects of radiation damage in alkali halides, Donald R. Westervelt—531(A)
Perfect crystals of ZnS, William W. Piper and W. L. Roth—503(L)
Periodic deviations in Schottky effect, S. C. Miller, Jr., and R. H. Good, Jr.—1367
Persistent residues from ice particles, Mary Goulks Gourley and W. D. Crozier—526(A)
Polarization of nuclei in metals, Albert W. Overhauser—411
Possible degeneracy of energy bands in Ge, Edward N. Adams, II—1063(L)
Production of *F'*, *M*, and *R* centers in NaCl at room temperature, Reuel T. Platt, Jr., and Jordan J. Markham—40
Proton magnetic resonance in liquid crystals, P. L. Jain, H. A. Moses, J. C. Lee, and R. D. Spence—844(A)
Quenched vacancies in AuCu and $AuCu_3$, J. Brinkman—531(A)
Radiation-damage energy threshold in f.c.c. alloy, J. M. Denney—531(A)
Radiation damage in insulators, W. Primak, L. H. Fuchs, and P. Day—1064(L)
Reformulation of solid-state electronic Boltzmann equation, J. S. Lomont—1082(A)
Rotation of microwave polarization in liquid crystals in transverse magnetic field, Glen A. Mann and R. D. Spence—844(A)
Single crystal metal rotors, J. W. Beams—502(L)
Single crystal neutron diffraction study of heavy ice, S. W. Peterson and H. A. Levy—1082(A)
Solid state absorption spectra of Mg and MgO, John R. Townsend—556
Some electrical and optical properties of synthetic single crystals of ZnS, William W. Piper—23
Theory of ac space-charge polarization effects in photoconductors, semiconductors, and electrolytes, J. Ross Macdonald—4
Theory of plasma waves in metals, Peter A. Wolff—18
Use of non-orthogonal wave functions for solids, with applications to ferromagnetism, W. J. Carr, Jr.—28
Vibrational spectrum and specific heat of Na, Ernest Bauer—58
Zone structure of graphite, S. Mrozowski—1320(L)

Diamagnetism (see **Magnetic Properties**)
Dielectrics and Dielectric Properties
Anelasticity of quartz, Richard K. Cook and Robert G. Breckenridge—1419
Čerenkov effect and dielectric constant, S. M. Neamtan—1362
Dielectric properties and phase transitions of $Cd_2Nb_2O_7$ and $Pb_2Nb_2O_7$, Gen Shirane and Ray Pepinsky—504(L)
Dielectric properties of some double tartrates, F. Jona and R. Pepinsky—1577(L)
Electrical hysteresis properties of ice, Frank K. Truby—543(A)
Electronic polarizabilities of ions in crystals, Jack R. Tessman, A. H. Kahn, and William Shockley—890
Energy loss of moving electrons to dipolar relaxation, H. Fröhlich and R. L. Platzman—1152
Low-temperature dielectric properties of Cd and Pd niobates, J. K. Hulm—504(L)
Optical absorption and photoconduction in visible and near infrared in single crystals of BaO, William C. Dash—68

Oxygen vacancies in BaO, R. L. Sproull, R. S. Bever, and G. Libowitz—77
Phase transitions in $NaNbO_3-KNbO_3$ system, Gen Shirane, R. E. Newnham, and Ray Pepinsky—845(A)
Si and Ge dielectric constants, W. C. Dunlap, Jr., and R. L. Watters—1396
Transition in $LiNH_4C_4H_4O_6 \cdot H_2O$, F. Jona and Ray Pepinsky—845(A)

Diffraction (see also **Scattering**)
Acoustic approximation to weak shock diffraction, Craig C. Hudson—1079(A)
Diffraction by ionized trail, Charles H. Papas—542(A)
Focusing of short electromagnetic waves by means of Fresnel half-period zone plate, H. George Oltman—1093(A)
"Lloyd mirror" interference in presence of slight uniform refraction, R. W. Stewart—1087(A)
Recording of x-ray diffraction patterns by scintillation counter, J. C. M. Brentano and I. Ladany—850(A)
Single-crystal neutron diffraction study of heavy ice, S. W. Peterson and H. A. Levy—1082(A)
Structure of liquid He, James Reekie and T. S. Hutchison—827(L)
Structure of liquid N_2, O_2, and A by neutron diffraction, D. G. Henshaw, D. G. Hurst, and N. K. Pope—1229
Visible light from localized surface charges moving across grating, S. J. Smith and E. M. Purcell—1069(L)
X-ray absorption fine structure with polarized x-rays, R. Krogstad, W. Nelson, and S. T. Stephenson—1394

Diffusion
Back diffusion for gases as it affects secondary electron emission coefficients, J. K. Theobald—535(A)
Diffusion of **Li** into Ge and Si, C. S. Fuller and J. A. Ditzenberger—846(A)
Nuclear spin relaxation by translation diffusion, H. C. Torrey—962

Discharge of Electricity in Gases (see **Electrical Discharges**)

Disintegration and Excitation of Nucleus (see **Nuclear Reactions**)

Dynamics (see **Mechanics**)

Elasticity and Plasticity
Anelasticity of quartz, Richard K. Cook and Robert G. Breckenridge—1419
Behavior of metals at elevated temperatures, Edward W. LaRocca—1082(A)
Elastic description of high-amplitude spherical pulse in steel, William A. Allen—1082(A)
Internal friction of rocksalt single crystals, D. R. Frankl—573
Second-order elastic deformation of solids, D. S. Hughes and J. L. Kelly—1145

Electrical Breakdown (see **Dielectrics and Dielectric Properties; Electrical Discharges**)

Electrical Conductivity and Resistance (see also **Semiconductors; Superconductors**)
Annealing effects in irradiated Cu, Albert W. Overhauser—530(A)
Annealing of radiation damage effects in Cu, R. R. Eggleston—531(A)
Change of electrical conductivity of NaCl upon bombardment with high-energy protons, Edgar A. Pearlstein—881
Effect of quench temperature and cold work on ordering rates of Cu_3Au and CuAu, C. E. Dixon and C. J. Meechan—530(A)
Effects of high sputtering rates on resistivities of sputtered Au films, Richard B. Belser—1083(A)
Electrical conductance and structure studies of thin Bi films evaporated on glass, P. J. Bryant, H. U. Rhoads, and A. H. Weber—1083(A)
Electrical hysteresis properties of ice, Frank K. Truby—543(A)
Electrical properties of black phosphorus, Robert W. Keyes—580
Hall effect in AlCl at low temperature, Frederick C. Brown—502(L)
Hall measurements on NaCl and on photoconductive PbTe, John L. Levy—215
Influence of cold work and radiation damage on vibrational spectra of Cu, D. B. Bowen and G. W. Rodeback—531(A)
Influence of electric field in contact charging, John W. Peterson—535(A)
Interpretation of Hall effect and resistivity data in PbS and similar binary compound semiconductors, Wayne W. Scanlon—1573(L)
Noise observations on CdS crystal photoconductors, Carl Shulman, R. W. Smith, and A. Rose—857(A)
Optical absorption and photoconduction in visible and near infrared in single crystals of BaO, William C. Dash—68
Search for Hall effect in superconductor. I. Experiment, H. W. Lewis—1149
Some electrical and optical properties of synthetic single crystals of ZnS, William W. Piper—23
Space-charge-limited currents in insulators, A. Rose and R. W. Smith—857(A)
Spontaneous Hall effect in ferromagnetics, J. Smit and J. Volger—1576(L)
Theory of ac space-charge polarization effects in photoconductors, semiconductors, and electrolytes, J. Ross Macdonald—4

Electrical Discharges
Condition on uniform field breakdown in electron-attaching gases, Ronald Geballe and Marvin L. Reeves—867
Electrical breakdown of extremely short gaps, P. Kisliuk—847(A)
Field emission: Large current densities, space charge, and vacuum arc, W. P. Dyke and J. K. Trolan—541(A)
Influence of irradiation on characteristic of glow discharge in pure rare gases, K. W. Meissner and W. F. Miller—896
N_2 afterglows, Marx Brook—1079(A)
Pre-onset burst pulses in positive point to plane corona in air, M. R. Amin—536(A)
Probe measurements in A discharge containing running striations, N. L. Oleson—848(A)
Secondary cathode action in N_2 with coaxial cylindrical geometry, Elsa Huber—536(A)
Secondary electron emission coefficient for low-energy positive ion bombardment of discharge-conditioned surfaces, James H. Parker—536(A)
Short afterglow in N_2, W. B. Kunkel—534(A)

Electrical Properties (see also **Dielectrics and Dielectric Properties; Electrical Conductivity and Resistance; Semiconductors; Superconductors**)
Average energy of electrons emitted from metals under high-energy electron bombardment, John H. Anson, Kenneth A. Wright, and John G. Trump—843(A)
Back diffusion for various gases as it affects secondary electron emission coefficients, J. K. Theobald—535(A)
Black phosphorus, Robert W. Keyes—580
Efficiency of conversion from light to electric power by Ge grown junction, Ralph P. Ruth and James W. Moyer—846(A)
Electron emission from metals under high-energy positive ion bombardment, Henry C. Bourne, Jr., Robert W. Cloud, and John G. Trump—847(A)
Field emission: Large current densities, space charge, and vacuum arc, W. P. Dyke and J. K. Trolan—541(A)
Field-emission microscope investigation of surface reactions, Ralph Klein—854(A)
Irreversible thermodynamics of thermoelectric effects in inhomogeneous, anisotropic media, Charles A. Domenicali—877

Electrical Properties (Continued)
Modified theory of production of secondary electrons in solids, A. van der Ziel—35
Periodic deviations in Schottky effect, S. C. Miller, Jr., and R. H. Good, Jr.—1367
Photoelectric studies of Fe, Alvin B. Cardwell—554
Photoelectric yield of Pt in vacuum uv, W. C. Walker and N. Wainfan—533(A)
Role of surface barrier in secondary emission from metals, E. M. Baroody—843(A)
Secondary electron emission coefficient for low-energy positive ion bombardment of discharge-conditioned surfaces, James H. Parker—536(A)
Secondary electron emission from diamond, J. B. Johnson—843(A)
Seebeck effect in Ge, T. H. Geballe—857(A)
Some electrical and optical properties of synthetic single crystals of ZnS, William W. Piper—23
Space-charge effects in field emission, J. P. Barbour, W. W. Dolan, J. K. Trolan, E. E. Martin, and W. P. Dyke—45
Sputtering in high vacuum and its relation to radiation damage as described by Seitz, Frank Keywell—535(A)
Thermoelectric power in semiconductors with applications to Ge, theory, V. A. Johnson and K. Lark-Horovitz—226
Thermoelectric power of Ge at temperatures above 78°K, A. E. Middleton and W. W. Scanlon—219
Thermoelectric power of Ge below room temperature, H. P. R. Frederikse—248
Thermoelectric power of semiconductors, Conyers Herring—857(A)
Thermoelectricity in metals at low temperatures, D. K. C. MacDonald and W. B. Pearson—844(A)
Vacuum sputtering of metallic Na by inert gas ions, Richard C. Bradley—535(A)
Electrodynamics (see **Electromagnetic Theory and Electrodynamics**)
Electroluminescence (see **Luminescence**)
Electrolysis (see **Chemical Effects and Properties**)
Electromagnetic Theory and Electrodynamics
Interference of waves generated by electric field, Oleg Yadoff—543(A)
Magnetoelectrostatics, E. T. Benedikt—1081(A)
New modification of classical electromagnetic theory, A. Schild—1009
Periodic ellipse of strong-focusing equations, B. C. Carlson—839(L)
Phase-reversal focusing in linear accelerators, Myron L. Good—538(A)
Topology of magnetic fields, W. M. Elsasser and K. McDonald—1081(A)
Electron Diffraction (see **Diffraction; Scattering of Electrons and Positrons**)
Electron Optics (see **Electromagnetic Theory and Electrodynamics**)
Electronic Tubes (see **Methods and Instruments**)
Electrons and Positrons (see also **Electromagnetic Theory and Electrodynamics; Elementary Particle Interactions; Scattering of Electrons and Positrons**)
Electrons, Mobility (see **Ions and Electrons, Mobility**)
Electrons, Scattering of (see **Scattering of Electrons and Positrons**)
Electrons, Secondary (see **Electrical Properties**)
Electrons, Thermionic (see **Electrical Properties**)
Electro-Optical Effects (see **Optical Properties**)
Electrostriction (see **Dielectrics and Dielectric Properties**)
Elementary Particle Interactions
Angular distribution of positive photomesons from H: counter telescope method, A. V. Tollestrup, J. C. Keck, and R. M. Worlock—1090(A)
Attenuation cross sections of 37-Mev pions in H, C. E. Angell and J. P. Perry—835(L)
β interaction, R. Finkelstein and P. Kaus—1316
Charge independence in (γ,n) and (γ,t) reactions, D. C. Peaslee and V. L. Telegdi—126
Convergence of adiabatic nuclear potential, Abraham Klein—1017
Derivation and renormalization of Tamm-Dancoff equations, Behram Kurşunoğlu—1069(L)
Detection of free neutrino, F. Reines and C. L. Cowan, Jr.—830(L)
Differential p-p elastic scattering cross section at 144, 271, and 429 Mev, J. Marshall, L. Marshall, and V. A. Nedzel—834(L)
Elastic scattering of 118-Mev negative pions by H, Jay Orear—156
Evaluation of interaction effect in n-p capture, N. Austern—670
Green's function method for strongly interacting particles, Maurice Neuman—1021
High-pressure cloud-chamber investigation of protons scattered by 300-Mev neutrons, John DePangher—1084(A)
Hypothesis concerning relations among "new unstable particles", M. Goldhaber—1279
Interaction cross section of H and heavier elements for 450-Mev negative pions and 340-Mev positive pions, S. J. Lindenbaum and Luke C. L. Yuan—1578(L)
Interaction of negative pions with Hg, Nathan Sugarman and Agnes Haber—730
Intrinsic magnetic moment of elementary particles of spin 3/2, F. J. Belinfante—997
Invariant forms of nucleon-nucleon interaction, David Feldman—824
Isotopic spin and new unstable particles, M. Gell-Mann—833(L)
Large NaI scintillation counter study of neutron-capture γ rays from H, Bernard Hamermesh and Richard J. Culp 211(L)
Magnetic moments of neutron and proton, F. J. Belinfante—994
Multiple production of pions in nucleon-nucleon collisions at cosmotron energies, E. Fermi—452
"Non-mesonic" bound V-particle decay, W. Cheston and H. Primakoff—1537
n-p scattering near 180° at 93 Mev, W. Selove, K. Strauch and F. Titus—724
Nuclear forces from P-wave mesons, E. M. Henley and M. A. Ruderman—1036
Nuclear forces in pseudoscalar meson theory, K. A. Brueckner and K. M. Watson—1023
Phase-shift analysis of high-energy p-p scattering experiments, A. Garren—213(L); erratum—1587(E)
Phenomenological analysis of meson-nucleon scattering, A. E. Woodruff—855(A)
Photoproduction of meson pairs, R. D. Lawson and S. D. Drell—539(A)
Photoproduction of π-meson pairs, R. D. Lawson—1272
Photoproduction of positive mesons from H: magnetic spectrometer method, R. L. Walker, J. G. Teasdale, and V. Z. Peterson—1090(A); results, R. F. Bacher, J. C. Keck, V. Z. Peterson, J. G. Teasdale, A. V. Tollestrup, R. L. Walker, and R. M. Worlock—1090(A)
Pions from production of baryons by protons, Frederik J. Belinfante—145
π^+-p scattering near 260 Mev, W. B. Fowler, R. M. Lea, W. D. Shephard, R. P. Shutt, A. M. Thorndike, and W. L. Whittemore—832(L)
p-p scattering for nucleon isobar model, F. T. Solmitz—164
Production of neutral mesons by 340-Mev protons on H, J. W. Mather and E. A. Martinelli—780
Scattering of negative pions by H, E. Fermi, M. Glicksman, E. Martin, and D. Nagle—161

Search for stable dineutron, B. L. Cohen and T. H. Handley —101
Semiclassical methods in meson processes, Joseph A. Thie —1282
Signs of phase shifts for pion-proton scattering, S. W. Barnes, C. E. Angell, J. P. Perry, D. Miller, J. Ring, and D. Nelson—1327(L)
Single-time Bethe-Salpeter equation, Wilhelm Macke—1072(L)
Solutions of meson-nucleon equation in adiabatic limit, R. Arnowitt and S. Deser—1061(L)
Spin-spin interaction of electrons and ionization energy of He, A. M. Sessler and H. M. Foley—1321(L)
Strong-coupling theory of meson scattering, Allan N. Kaufman—468
Tamm-Dancoff theory of pion photoproduction, Marc Ross —855(A)
Test of charge symmetry hypothesis, H. W. Wilson and Walter H. Barkas—537(A)
Total cross section for positive pions in hydrogen, Stanley L. Leonard and Donald H. Stork—855(A)
Total cross sections for 169-Mev neutrons, A. E. Taylor —1071(L)
Total π^--p cross section at 840 and 470 Mev, A. M. Shapiro, C. P. Leavitt, and F. F. Chen—1073(L)
Universal Fermi interaction, E. J. Konopinski and H. M. Mahmoud—1045
Velocity distribution of pair components in π^0 decay, O. Halpern and K. Baumann—1070(L)
Yukawa forces with added attractions, John M. Blatt and M. H. Kalos—1563

Elements (see **Atomic Mass and Abundance**)
Energy Loss of Particles (see **Range and Energy Loss of Particles**)
Energy States of Atoms (see **Atomic Structure and Spectra**)
Energy States of Molecules (see **Molecular Structure and Spectra**)
Energy States of Nucleus (see **Nuclear Reactions; Nuclear Spectra; Nuclear Structure Theory**)
Equations of State (see **Chemical Effects and Properties**)
Errata
Phase-shift analysis of high-energy $p-p$ scattering experiments, A. Garren—1588(E)
Scintillation study of As^{77} and Br^{77}, M. E. Bunker, R. J. Prestwood, and J. W. Starner—1587(E)
Unusual π-μ decays in photographic emulsions, W. F. Fry —1587(E)
Errors of Measurement (see **Methods and Instruments**)
Evaporation (see **Liquids**)
Excitation of Atoms (see **Atomic Structure and Spectra**)
Excitation of Molecules (see **Molecular Structure and Spectra**)
Excitation of Nucleus (see **Nuclear Reactions; Nuclear Spectra; Nuclear Structure Theory**)
Explosion Phenomena (see **Fluid Dynamics**)

Faraday Effect (see **Optical Properties**)
Ferroelectric Phenomena (see **Dielectrics and Dielectric Properties**)
Ferromagnetism (see **Magnetic Properties**)
Field Emission (see **Electrical Properties**)
Field Theory (see also **Quantum Electrodynamics**)
β interaction, R. Finkelstein and P. Kaus—1316
Convergence of adiabatic nuclear potential, Abraham Klein —1017
Coupled-field Green's functions, J. G. Valatin—522(L)
Derivation and renormalization of Tamm-Dancoff equations, Behram Kurşunoğlu—1069(L)
Electromagnetic effects in two-nucleon systems, Stanley Deser—1542
Electromagentic mass and particle model in Darling's theory of elementary particles, Hans Freistadt—1015
Equations of motion in Einstein's new unified theory, Joseph Callaway—1567
Equivalent mass and other effects of non-local electromagnetic field in interaction with constant E, H field, Christopher Gregory—1554
Expectations from unified field theory, Behram Kurşunoğlu —506(L)
Field theory of equations with many masses, B. T. Darling —1547
"Fusion" theory of bosons and nonlocal field, Satosi Watanabe—856(A)
Green's function method for strongly interacting particles, Maurice Neuman—1021
Implications of Lorentz invariance for scattering of spin 1/2 particles, David Feldman—856(A)
Interaction of nonrelativistic particle with scalar field with application to slow electrons in polar crystals, Tsung-Dao Lee and David Pines—883
Interpretation of Bhabha's theory of particles of maximum spin 3/2, W. A. Hepner and D. R. Workman—1071(L)
Intrinsic magnetic moment of elementary particles of spin $\frac{1}{2}$, F. J. Belinfante—997
Latticespace quantization of nonlinear field theory, L. I. Schiff—766
Nonsymmetric unified field theories, W. B. Bonnor—1067(L)
Nuclear forces in pseudoscalar meson theory, K. A. Brueckner and K. M. Watson—1023
Photoproduction of meson pairs, R. D. Lawson and S. D. Drell—539(A)
Recoil corrections in strong coupling meson theory, G. Wentzel—173
Semiclassical methods in meson processes, Joseph A. Thie —1282
Single-time Bethe-Salpeter equation, Wilhelm Macke—1072(L)
Strong-coupling theory of meson scattering, Allan N. Kaufman—468
Theory of quantized fields, Julian Schwinger—1283
Universal Fermi interaction, E. J. Konopinski and H. M. Mahmoud—1045
Yukawa forces with added attractions, John M. Blatt and M. H. Kalos—1563

Films, Properties
Effects of high sputtering rates on resistivities of sputtered gold films, Richard B. Belser—1083(A)
Electrical conductance and structure studies of thin Bi films evaporated on glass, P. J. Bryant, H. U. Rhoads, and A. H. Weber—1083(A)
Liquid He films, K. R. Atkins—1571(L)
Multiple-beam fringes of equal chromatic order, W. F. Koehler—542(A)
Structure and resistivities of Au films deposited by evaporation and sputtering, Richard B. Belser—1098(A)
Fine Structure (see **Atomic Structure and Spectra**)
Fission of Nucleus (see **Nuclear Fission**)
Fluctuation Phenomena (see **Noise**)
Fluid Dynamics
Acoustic approximation to weak shock diffraction, Craig C. Hudson—1079(A)
Dependence of jet-tone eigenfrequencies on aerodynamic and geometrical parameters, Lloyd E. Schilberg and A. B. C. Anderson—543(A)
Detonation in gases, Arthur L. Bennett—543(A)
Drag on rotating cylinder at low pressures, S. F. Chiang and S. A. Schaaf—535(A)
Flash radiographic studies of high-velocity metallic jets, Louis Zernow—532(A)
Geometical relations for solid propellant charges for rocket motors, E. W. Price—542(A)

Fluid Dynamics (Continued)
Linearized theory of spherical wave decay, L. M. Tannenwald—542(A)
Non-Maxwellian distribution in shock front and anomaly of chromospheric temperature, Hari K. Sen—861
Propellant burning rate calculations, G. B. Shook—542(A)
Properties of Hugoniot function, R. D. Cowan—1088(A)
Suppression of AlO in wake of ultra-speed pellets, William C. White—1083(A)
Surface temperature of burning double-base propellant, M. H. Hunt, C. A. Heller, and A. S. Gordon—542(A)
Variational approach to theory for critical stability of fluid, F. T. Rogers, Jr.—535(A)
Fluorescence (see **Luminescence**)
Friction (see **Mechanics**)

Galvanomagnetic Effect (see **Magnetic Properties**)
Gamma Rays (see also **Nuclear Reactions; Nuclear Spectra**)
Degradation of γ rays in water, M. M. Weiss and W. Bernstein—1269
γ-ray absorption measurements, P. R. Howland, W. E. Kreger, and R. A. Taylor—1095(A)
Penetration of gamma radiation through Fe, L. A. Beach, R. B. Theus, and W. R. Faust—355
Gases
Back diffusion for gases as it affects secondary electron emission coefficients, J. K. Theobald—535(A)
Geophysics
Atmospheric ozone fluctuations at Albuquerque, I. Gerald Bowen—1080(A)
Bifurcation of *E* region, J. R. Lien, J. Marcou, J. C. Ulwick, D. R. McMorrow, L. B. Linford, and O. C. Haycock—508(L)
Contribution of solar x-rays to *E*-layer ionization, E. T. Byram, T. A. Chubb, and H. Friedman—1066(L)
Correlation studies of sound fluctuations in ocean, H. L. Grant and R. W. Stewart—1087(A)
Critical conditions for ice formation on silver iodide nuclei, Robert J. McCarty—1080(A)
Height of upper atmosphere emissions by Van Rhŷn method, F. E. Roach, Helen B. Pettit, D. R. Williams, and P. St. Amand—534(A)
Ion density in *E* layer by use of sounding rocket, L. B. Linford, O. C. Haycock, J. I. Swigart, C. L. Alley, C. D. Westlund, and J. R. Lien—1093(A)
Origin of *E* layer of ionosphere, Ernest Bauer and Ta-You Wu—1101
Possible relationship between ionosphere and nightglow, Pierre St. Amand and D. R. Williams—534(A)
Pulsed searchlight system for upper atmosphere density studies, S. S. Friedland, H. S. Katzenstein, J. Katzenstein, D. P. Lindorff, G. S. Timoshenko, and L. E. Williams—1080(A)
Quantitative analysis of lower ionosphere, H. K. Kallmann—1079(A)
Seasonal trend of atmospheric ozone as revealed by solar-telluric band at 9.6 microns, Arthur Adel—1080(A)
Stratospheric temperature profiles obtained from searchlight measurements, L. Elterman—1080(A)
Thermal microstructure in ocean, W. N. English—1087(A)
Variation of natural radioactivity in atmosphere with altitude, Marvin H. Wilkening—1080(A)
Glasses (see **Molecular Aggregates**)
Gravitation (see **Relativity and Gravitation**)
Gyromagnetization (see **Magnetic Properties**)

Hall Effect (see **Electrical Conductivity and Resistance**)
Heat Capacity (see **Thermal Properties**)
Heat Conduction (see **Thermal Properties**)
Heat of Dissociation and Formation (see **Molecular Structure and Spectra**)
Heat of Fusion (see **Thermal Properties**)
Heat of Vaporization (see **Thermal Properties**)
Helium, Liquid
Attenuation of second sound above 1°K, K. R. Atkins and K. H. Hart—204(L)
Capillarity in He II, C. T. Lane and R. V. Dyba—829(L)
He II film transport rates over machined metal surfaces, Bernard Smith and Henry A. Boorse—505(L)
Heat of mixing of He^3 in He^4, H. S. Sommers, Jr., W. E. Keller, and J. G. Dash—1345
λ temperatures of dilute He^3–He^4 solutions, J. C. Morrow—1
Liquid He films, K. R. Atkins—1571(L)
Liquid He II: Bose-Einstein condensation and two-fluid model, P. R. Zilsel—1106
Nonparticipation of He^6 in superfluidity of He^4, Lester Guttman and James R. Arnold—547
Specific heat of He^3 between 1.3°K and 2.3°K, G. de Vries and J. G. Daunt—1572(L)
Structure of liquid He, James Reekie and T. S. Hutchison—827(L)
Temperature dependence of nuclear susceptibility of He^3 between 1.2°K and 4.2°K, W. M. Fairbank, W. B. Ard, H. G. Dehmelt, Walter Gordy, and S. R. Williams—208(L)
Theory of liquid He, John M. Richardson—849(A)
Theory of liquid He^3–He^4 mixtures, Louis Goldstein—850(A)
High Voltage Tubes and Machines (see **Methods and Instruments**)
Hydrodynamics (see **Fluid Dynamics**)
Hyperfine Structure (see **Atomic Structure and Spectra; Molecular Structure and Spectra; Nuclear Moments and Spin**)

Imperfections in Solids (see also **Crystalline State; Electrical Conductivity and Resistance; Luminescence; Semiconductors**)
Absolute value of Avogadro's number and soundness of crystals, M. E. Straumanis—1155
Anelasticity of quartz, Richard K. Cook and Robert G. Breckenridge—1419
Annealing effects in irradiated Cu, Albert W. Overhauser—530(A)
Annealing of bombardment damage in diamond-type lattice: theoretical, R. C. Fletcher and W. L. Brown—585
Annealing of bombardment damage in Ge: experimental, W. L. Brown, R. C. Fletcher, and K. A. Wright—591
Annealing of radiation damage effects in Cu, R. R. Eggleston—531(A)
Bleaching properties of *F* centers in KBr at 5°K, Jordan J. Markham, Reuel T. Platt, Jr., and Irving L. Mador—597
Cellular nature of ice crystals, E. J. Workman—544(A)
Change of electrical conductivity of NaCl upon bombardment with high-energy protons, Edgar A. Pearlstein—881
Color-center formation in alkali halides containing $S^=$, E. Burstein and B. W. Henvis—845(A)
Effect of quench temperature and cold work on ordering rates of Cu_3Au and CuAu, C. E. Dixon and C. J. Meechan—530(A)
Effect of traps on carrier injection in semiconductors, H. Y. Fan—1424
Effects of high sputtering rates on resistivities of sputtered Au films, Richard B. Belser—1083(A)
Electrical and optical properties of synthetic single crystals of ZnS, William W. Piper—23
Electrical hysteresis properties of ice, Frank K. Truby—543(A)
Electron traps in ice, E. Avery, L. Grossweiner, and M. Matheson—1080(A)

Energy of trapped electrons in ionic solids, Kurt Lehovec—253
Etch pits in plastically-deformed Ge, C. J. Gallagher—846(A)
Influence of cold work and radiation damage on vibrational spectra of Cu, D. B. Bowen and G. W. Rodeback—531(A)
Internal friction of rocksalt single crystals, D. F. Frankl—573
Interpretation of some electroluminescent effects, Frank Matossi—846(A)
Mechanism of impurity poisoning in luminescence of ZnS phosphors with Mn activator, Richard H. Bube, Simon Larach, and Ross E. Shrader—1135
NAA statitron for solid-state research, D. T. Eggen and H. Kenworthy—531(A)
Optical absorption and photoconduction in visible and near infrared in single crystals of BaO, William C. Dash—68
Optical effects of radiation damage in alkali halides, Donald R. Westervelt—531(A)
Oxygen vacancies in BaO, R. L. Sproull, R. S. Bever, and G. Libowitz—77
Paramagnetic resonances in irradiated glasses, E. L. Yasaitis and B. Smaller—1068(L)
Perfect crystals of ZnS, William W. Piper and W. L. Roth—503(L)
Production of acceptor centers in Ge and Si by plastic deformation, W. C. Ellis and E. S. Greiner—1061(L)
Production of F', M, and R centers in NaCl at room temperature, Reuel T. Platt, Jr., and Jordan J. Markham—40
Quenched vacancies in AuCu and $AuCu_3$, J. Brinkman—531(A)
Radiation-damage energy threshold in f.c.c. alloy, J. M. Denney—531(A)
Radiation damage in insulators, W. Primak, L. H. Fuchs, and P. Day—1064(L)
Space-charge-limited currents in insulators, A. Rose and R. W. Smith—857(A)
Sputtering in high vacuum and its relation to radiation damage as described by Seitz, Frank Keywell—535(A)
Thermal decay of luminescence of KBr, G. W. Williams, S. R. Usiskin, and A. J. Dekker—1398
Vacuum sputtering of metallic Na by inert gas ions, Richard C. Bradley—535(A)

Inelastic Scattering (see **Nuclear Reactions; Scattering**)
Instruments (see **Methods and Instruments**)
Internal Conversion (see **Nuclear Spectra**)
Ionization (see also **Electrical Discharges; Range and Energy Loss of Particles**)
Contribution of solar x-rays to E-layer ionization, E. T. Byram, T. A. Chubb, and H. Friedman—1066(L)
Ionization loss at relativistic velocities in nuclear emulsion, Bertram Stiller and Maurice M. Shapiro—735
Ionization loss in nuclear emulsions, John R. Fleming and J. J. Lord—511(L); 1089(A)
Ionization of relativistic cosmic-ray μ mesons, H. R. Snodgrass—1089(A)
Photoionization in O_2, N. Wainfan and W. C. Walker—533(A)
Relative ionization by cosmic-ray μ mesons in liquid scintillator, R. Baskin and J. R. Winckler—464
Total ionization of α particles of Po in mixtures of gases, G. Bertolini, M. Bettoni, and A. Bisi—1586(L)
Ionization Potentials of Atoms (see **Atomic Structure and Spectra**)
Ionization Potentials of Molecules (see **Molecular Structure and Spectra**)
Ionosphere (see **Geophysics**)
Ions (see also **Electrical Discharges**)
Effective ionic radii, N. Efremov—1081(A)
Electron emission from metals under high-energy positive ion bombardment, Henry C. Bourne, Jr., Robert W. Cloud, and John G. Trump—847(A)
Ion density in E layer by use of sounding rocket, L. B. Linford, O. C. Haycock, J. I. Swigart, C. L. Alley, and C. D. Westlund—1093(A)
Vacuum sputtering of metallic Na by inert gas ions, Richard C. Bradley—535(A)
Ions and Electrons, Mobility (see also **Semiconductors**)
Drift mobilities in semiconductors. I. Ge, M. B. Prince—681
Mobility of impurity ions in Ge and Si, J. C. Severiens and C. S. Fuller—1322(L)
Temperature dependence of electron mobility in AgCl, Frederick C. Brown—858(A)
Isobars (see **Atomic Mass and Abundance**)
Isomers, Molecular (see **Molecular Structure and Spectra**)
Isomers, Nuclear (see **Nuclear Spectra**)
Isotopes (see **Atomic Mass and Abundance; Radioactivity**)

Kerr Effect (see **Optical Properties**)
Kinetic Theory of Gases (see **Gases**)

Liquid Helium (see **Helium, Liquid**)
Liquids
Nuclear magnetic relaxation in viscous liquids, Robert L. Conger—543(A)
Proton magnetic resonance in liquid crystals, P. L. Jain, H. A. Moses, J. C. Lee, and R. D. Spence—844(A)
Rotation of microwave polarization in liquid crystals in transverse magnetic field, Glen A. Mann and R. D. Spence—844(A)
Structure of liquid N_2, O_2, and A by neutron diffraction, D. G. Henshaw, D. G. Hurst, and N. K. Pope—1229
Thermal microstructure in ocean, W. N. English—1087(A)
Velocity of sound apparatus for liquids at 512 kc, George G. Kretschmar—542(A)
Luminescence
Electron traps in ice, E. Avery, L. Grossweiner, and M. Matheson—1080(A)
Interpretation of electroluminescent effects, Frank Matossi—846(A)
Long-lived phosphorescent components of Tl-activated NaI, L. R. Megill and C. R. Emigh—1081(A)
Luminescence studies of KI-TlI, Bernard Smaller and Eugene Avery—232
Mechanism of impurity poisoning in luminescence of ZnS phosphors with Mn activator, Richard H. Bube, Simon Larach, and Ross E. Shrader—1135
New quenching effect in liquid scintillators, R. W. Pringle, L. D. Black, B. L. Funt, and S. Sobering—1582(L)
Thermal decay of luminescence of KBr, G. W. Williams, S. R. Usiskin, and A. J. Dekker—1398
Time-dependent spectra of electroluminescent zinc sulfide, E. E. Loebner—846(A)
Variations in decay of phosphorescence with frequency of applied electric field, Keith W. Olson—1323(L)

Magnetic Fields (see **Electromagnetic Theory and Electrodynamics**)
Magnetic Properties
deHaas-van Alphen effect in As, Ted G. Berlincourt—1068(L)
Effect of surface on magnetic properties of electron gas, Frank S. Ham—1113
H-T antiferromagnetic boundary and apparent molecular field for $MnBr_2 \cdot 4H_2O$, Warren E. Henry—844(A)
Low-temperature diamagnetism of electrons in cylinder, R. B. Dingle—1320(L)
Magnetic properties of electronic Einstein-model solid, M. F. M. Osborne and M. C. Steele—1403

Magnetic Properties (Continued)
Magnetic resonance in ferrimagnetic and antiferromagnetic systems, L. R. Bickford, Jr.—845(A)
Magnetic scattering of neutrons from rare earth ions, G. T. Trammell—1387
Magnetic susceptibility of Ge, D. K. Stevens and J. H. Crawford, Jr.—1065(L)
Magnetization in Ni ferrite-aluminates and Ni ferrite-gallates, Louis R. Maxwell and Stanley J. Pickart—1120
Magnetostriction of magnetite, J. L. Stull and L. R. Bickford, Jr.—845(A)
Observation of magnetic domains by longitudinal Kerr effect, C. A. Fowler, Jr., and E. M. Fryer—532(A)
Paramagnetic scattering of neutrons by rare earth oxides, W. C. Koehler and E. O. Wollan—1380
Radiation-damage energy threshold in f.c.c. alloy, J. M. Denney—531(A)
Spin-wave theory of antiferromagnetism for simple cubic lattices, M. R. Schafroth—553
Spontaneous Hall effect in ferromagnetics, J. Smit and J. Volger—1576(L)
Thermal anomalies associated with antiferromagnetic ordering of FeF_2, CoF_2, and NiF_2, J. W. Stout and Edward Catalano—1575(L)
Use of non-orthogonal wave functions for solids, with applications to ferromagnetism, W. J. Carr, Jr.—28
Magnetic Resonance (see also **Nuclear Moments and Spin**)
Anomalous paramagnetic resonance in Cu propionate, Hidetaro Abe—1572(L)
Cyclotron resonance in Ge crystals, G. Dresselhaus, A. F. Kip, and C. Kittel—827(L)
Electronic spin resonance line width in metals, Elihu Abrahams and C. Kittel—544(A)
Exchange coupling in $CuK_2Cl_4 \cdot 2H_2O$ by paramagnetic resonance absorption, Kazuo Ōno, Hidetarō Abe, and Junji Shimada—551
Hfs of Ag and Au by atomic beam magnetic resonance method, Günter Wessel and Hin Lew—641
Influence of electric and magnetic fields on angular correlations, A. Abragam and R. V. Pound—943
Magnetic resonance in ferrimagnetic and antiferromagnetic systems, L. R. Bickford, Jr.—845(A)
New absorption lines of crystals in submicrowave region, S. Kojima, K. Tsukada, S. Ogawa, and A. Shimauchi—1571(L)
Nuclear magnetic relaxation in viscous liquids, Robert L. Conger—543(A)
Nuclear quadrupole resonance of stable Ga isotopes, H. G. Dehmelt—1240
Nuclear resonance line broadening and quadrupole splitting in metallic Be, W. D. Knight—539(A)
Nuclear spin relaxation by translation diffusion, H. C. Torrey—962
Paramagnetic resonance absorption in graphite, J. G. Castle, Jr.—1063(L)
Paramagnetic resonance hfs of V^{50} and V^{51}, C. Kikuchi, M. H. Sirvetz, and V. W. Cohen—109
Paramagnetic resonances in irradiated glasses, E. L. Yasaitis and B. Smaller—1068(L)
Polarization of nuclear spins in metals, T. R. Carver and C. P. Slichter—212(L)
Polarization of nuclei in metals, Albert W. Overhauser—411
Proton magnetic resonance in liquid crystals, P. L. Jain, H. A. Moses, J. C. Lee, and R. D. Spence—844(A)
Resonance absorption by conduction electrons in metals, A. F. Kip, T. W. Griswold, and A. M. Portis—544(A)
Saturation effects in paramagnetic resonance, A. H. Eschenfelder and R. T. Weidner—869
Sign of quadrupole interaction of Li^6 in LiCl, P. Kusch—268
Spin and magnetic moment of Ti^{47} and Ti^{49}, C. D. Jeffries—1096(A); 1262
Spin-lattice relaxation and residual width of highly exchange-narrowed paramagnetic resonances, J. P. Lloyd and G. E. Pake—1576(L)
Temperature dependence of nuclear susceptibility of He^3 between 1.2°K and 4.2°K, W. M. Fairbank, W. B. Ard, H. G. Dehmelt, Walter Gordy, and S. R. Williams—208(L)
Zeeman effect of Cr ground state, P. Brix, J. T. Eisinger, H. Lew, and G. Wessel—647
Zeeman splitting of nuclear quadrupole resonance lines, Yu Ting, Edward Manring, and Dudley Williams—1581(L)
Magneto-Optical Effects (see **Optical Properties**)
Magnetoresistance (see **Electrical Conductivity and Resistance**)
Magnetostriction (see **Magnetic Properties**)
Mass Defects (see **Atomic Mass and Abundance**)
Mass Spectroscopy (see **Atomic Mass and Abundance; Methods and Instruments**)
Mathematical Methods
Distribution of sizes of spheres in solid from study of slices of solid, Walter P. Reid—1082(A)
Harmonic analyses of pulses and spectral analyses of transients, S. Leroy Brown and John M. Norwood—534(A)
Measurements (see **Methods and Instruments**)
Mechanics
Dynamics of disordered linear chain, Freeman J. Dyson—1331
Mechanics, Quantum—Atomic Structure and Spectra (see **Atomic Structure and Spectra**)
Mechanics, Quantum—General (see **Quantum Mechanics**)
Mechanics, Quantum—Molecular Structure and Spectra (see **Molecular Structure and Spectra**)
Mechanics, Quantum—Nuclear (see **Nuclear Structure Theory**)
Mechanics, Quantum—of Solid Bodies (see **Crystalline State**)
Mechanics, Statistical (see **Statistical Mechanics and Thermodynamics**)
Meson Field Theory (see **Field Theory**)
Mesons (see also **Cosmic Radiation; Elementary Particle Interactions; Nuclear Reactions Induced by Mesons; Scattering of Mesons**)
Angular distribution of positive photomesons from H: counter telescope method, A. V. Tollestrup, J. C. Keck, and R. M. Worlock—1090(A)
β interaction, R. Finkelstein and P. Kaus—1316
Cascade decay of V particles, C. D. Anderson, E. W. Cowan, R. B. Leighton, and V. A. J. van Lint—1089(A); E. W. Cowan, C. D. Anderson, R. B. Leighton, and V. A. J. van Lint—1089(A)
Charged and neutral V particles, W. B. Fretter and E. W. Friesen—1089(A)
Charged particles of mass intermediate between proton and deuteron, D. T. King, Nathan Seeman, and Maurice M. Shapiro—838(L)
Cloud-chamber observation of decay of τ meson, V. A. J. van Lint and G. H. Trilling—1089(A)
Decay-electron spectrum of μ meson, J. H. Vilain and R. W. Williams—1586(L)
Dependence of 33-Mev π^+ production cross section on atomic number, Ryokichi Sagane and Walter Dudziak—212(L)
Elastic photoproduction of π^0's from deuterium, J. W. DeWire, A. Silverman, and B. Wolfe—520(L)
Heavy unstable particles, D. Lal, Yash Pal, and B. Peters—438
High-pressure cloud-chamber investigation of protons scattered by 300-Mev neutrons, John DePangher—1084(A)
Hypothesis concerning relations among "new unstable particles", M. Goldhaber—1279

Ionization loss at relativistic velocities in nuclear emulsion, Bertram Stiller and Maurice M. Shapiro—735
Ionization loss in nuclear emulsions, John R. Fleming and J. J. Lord—511(L); 1089(A)
Ionization of relativistic cosmic-ray μ mesons, H. R. Snodgrass—1089(A)
Isotopic spin and new unstable particles, M. Gell-Mann—833(L)
Mass measurements of primaries of S events by momentum-range method, W. B. Fretter, B. P. Gregory, R. Johnston, A. Lagarrigue, H. Meyer, F. Muller, and C. Peyrou—1583(L)
Mean lifetime of V^0 particles, R. B. Leighton and W. L. Alford—540(A)
Meson production by 500-Mev negative pions, M. Blau, M. Caulton, and J. E. Smith—516(L)
Multiple production of pions in nucleon-nucleon collisions at cosmotron energies, E. Fermi—452
μ meson as nuclear probe particle, John A. Wheeler—812
μ-mesonic atoms and electromagnetic radius of nucleus, L. N. Cooper and E. M. Henley—801
Neutral meson production in proton bombardment of C, Walter E. Crandall and Burton J. Moyer—749
"Non-mesonic" bound V-particle decay, W. Cheston and H. Primakoff—1537
$p+d \rightarrow t+\pi^+$, Wilson Frank, Kenneth C. Bandtel, Richard Madey, and Burton J. Moyer—537(A)
Photoproduction of meson pairs, R. D. Lawson and S. D. Drell—539(A)
Photoproduction of π-meson pairs, R. D. Lawson—1272
Photoproduction of positive mesons from H: magnetic spectrometer method, R. L. Walker, J. G. Teasdale, and V. Z. Peterson—1090(A); results, R. F. Bacher, J. C. Keck, V. Z. Peterson, J. G. Teasdale, A. V. Tollestrup, R. L. Walker, and R. M. Worlock—1090(A)
π^- mesons produced in cloud chamber by high-energy neutrons, Franklin C. Ford and Wilson M. Powell—537(A)
π^+/π^- ratios measured with use of spiral orbit spectrometer, Ryokichi Sagane—539(A)
Pion production at 180° by protons on C, Stanley L. Leonard—538(A)
Pions from production of baryons by protons, Frederik J. Belinfante—145
Production of neutral mesons by 340-Mev protons on H, J. W. Mather and E. A. Martinelli—780
Ratio of π^+ to π^- mesons produced by γ rays, James Edward Carothers—538(A)
Relative ionization by cosmic-ray μ mesons in liquid scintillator, R. Baskin and J. R. Winckler—464
Rest mass energy of negative pion, R. C. Cornelius, C. P. Sargent, M. C. Rinehart, L. M. Lederman, and K. Rogers—1583(L)
Search for highly absorbable negative cosmic-ray particles at sea level, Charles E. Miller, Joseph E. Henderson, David S. Potter, William R. Davis, Wayne M. Sandstrom, Gerald R. Garrison, and Francis M. Charbonnier—406
Search for V particles produced by 430-Mev protons, A. H. Rosenfeld and S. B. Treiman—727
Semiclassical methods in meson processes, Joseph A. Thie—1282
Solutions of meson-nucleon equation in adiabatic limit, R. Arnowitt and S. Deser—1061(L)
Summary of K-meson data, L. Leprince-Ringuet and B. Rossi—722
Tamm-Dancoff theory of pion photoproduction, Marc Ross—855(A)
Test of charge symmetry hypothesis, H. W. Wilson and Walter H. Barkas—537(A)
Universal Fermi interaction, E. J. Konopinski and H. M. Mahmoud—1045
Unusual π-μ decays in photographic emulsions, erratum, W. F. Fry—1587(E)
V^+ decay, R. W. Thompson, A. V. Buskirk, C. J. Karzmark, and R. H. Rediker—209(L)
Variation of ratio of positive to negative cosmic-ray μ mesons with momentum and altitude, H. A. Morewitz and M. H. Shamos—134
Velocity distribution of pair components in π^0 decay, O. Halpern and K. Baumann—1070
X-rays from μ-mesonic atoms, Val L. Fitch and J. Rainwater—789

Metals (see **Crystalline State**)
Metastable Atoms (see **Atomic Structure and Spectra**)
Metastable Molecules (see **Molecular Structure and Spectra**)
Meteorology (see **Geophysics**)
Methods and Instruments
Apparatus for double scattering of 240-Mev protons, W. F. Cartwright, C. L. Oxley, J. Rouvina, E. Baskir, D. Klein, J. Ring, and W. A. Skillman—852(A)
Automatic recording of zodiacal light, Victor H. Regener—1093(A)
Characteristics of photographic plates in vacuum uv, Po Lee and G. L. Weissler—545(A)
Crystal growth of Si by tip fusion process, P. H. Keck, S. B. Levin, J. Broder, and R. Lieberman—847(A)
Device for testing large numbers of photomultipliers, A. Brousseau, C. L. Cowan, Jr., and F. Reines—1088(A)
Effect of cloud-chamber geometry on β-ray studies, Paul H. Pitkanen—530(A)
Electromagnetic separation of Pd, Pt, and Ru isotopes, W. A. Bell, Jr., L. O. Love, C. E. Normand, and W. K. Prater—1096(A)
Electron bunching in disk-loaded circular wave guide, R. B. Neal—541(A)
Fast-neutron spectrometer using $T(d,n)\alpha$ reaction, G. K. O'Neill—853(A)
Flash radiographic studies of high-velocity metallic jets, Louis Zernow—532(A)
Floating zone recrystallization, P. H. Keck, W. Van Horn, J. Soled, and A. MacDonald—847(A)
Focusing of short electromagnetic waves by means of Fresnel half-period zone plate, H. George Oltman—1093(A)
Geometrical relations for solid propellant charges for rocket motors, E. W. Price—542(A)
High-yield rf ion source, Harold P. Eubank—853(A)
In, versatile solder to metals and nonmetals, Richard B. Belser—1098(A)
Liquid scintillation counting of natural C^{14}, F. N. Hayes, D. L. Williams, and Betty Rogers—512(L)
Liquid scintillation detectors to accommodate human subjects, R. L. Schuch, E. C. Anderson, C. L. Cowan, Jr., F. B. Harrison, F. N. Hayes, and F. Reines—1088(A)
Liquid scintillators for large volume detectors, F. N. Hayes, Lloyd Williams, C. L. Cowan, Jr., and F. Reines—1088(A)
Low-power water-boiler type reactor, M. E. Remley and D. C. Woods—544(A)
Magnetic shielding produced by rotating conducting tube, Alfredo Baños, Jr.—1081(A)
Measurement of light scattered from search-light beam, E. V. Ashburn—534(A)
Measurement of specific heats of alkali metals, H. Preston-Thomas, T. M. Dauphinee, and D. K. C. MacDonald—844(A)
Method for determination of end-point energy of β emitters, M. Forro—931
Multicolor photoelectric photometer for study of faint radiations, D. R. Williams and Pierre St. Amand—533(A)
NAA statitron for solid-state research, D. T. Eggen and H. Kenworthy—531(A)

Methods and Instruments (Continued)
Neutron spectrum and absolute yield of Pu–Be source, Leona Stewart—1095(A)
New quenching effect in liquid scintillators, R. W. Pringle, L. D. Black, B. L. Funt, and S. Sobering—1582(L)
Operation of Glaser bubble chamber with liquid H_2, Roger H. Hildebrand and Darragh E. Nagle—517(L)
Perfect crystals of ZnS, William W. Piper and W. L. Roth —503(L)
Periodic ellipse of strong-focusing equations, B. C. Carlson —839(L)
Phase-reversal focusing in linear accelerators, Myron L. Good—538(A)
Procedure for evaluation of automatic zodiacal light recordings, Richard J. Runge—1093(A)
Properties of large liquid scintillation detectors, E. C. Anderson, C. L. Cowan, Jr., and F. Reines—1088(A)
Pulsed searchlight system for upper atmosphere density studies, S. S. Friedland, H. S. Katzenstein, J. Katzenstein, D. P. Lindorff, G. S. Timoshenko, and L. E. Williams—1080(A)
Quadrupole focusing lenses for charged particles, Bruce Cork and Emery Zajec—853(A)
Recording of x-ray diffraction patterns by scintillation counter, J. C. M. Brentano and I. Ladany—850(A)
Refinement and resolution in reconstructed wavefront microscopy, Hussein M. A. El-Sum and Paul Kirkpatrick —541(A)
Rf fine structure of photon beam from Berkeley synchrotron, Richard Madey, Kenneth C. Bandtel, and Wilson J. Frank—537(A)
Scanning x-ray microscope, Howard H. Pattee, Jr.—541(A)
Single crystal metal rotors, J. W. Beams—502(L)
Temperature dependence of BF_3 proportional neutron counters, Frank R. Woods, Edgar F. Bennett, and John A. Lockwood—853(A)
Trochoidal analyzer for charged particles, Bernd Crasemann —544(A)
Variation of moisture content in nuclear track emulsion, Albert J. Oliver—538(A)
Velocity of sound apparatus for liquids at 512 kc, George G. Kretschmar—542(A)
Wave-synthesizing light chopper, W. Wallin—543(A)

Microwaves (see also **Atomic Structure and Spectra; Magnetic Resonance; Molecular Structure and Spectra; Nuclear Moments and Spin**)
Čerenkov effect at microwave frequencies, M. Danos, S. Geschwind, H. Lashinsky, and A. van Trier—828(L)
1–2 mm wave spectroscopy. II. H_2S, Charles A. Burrus, Jr., and Walter Gordy—274; III. NO and DI, C. A. Burrus and Walter Gordy—1437
Rotation of microwave polarization in liquid crystals in transverse magnetic field, Glen A. Mann and R. D. Spence—844(A)
Theory of microwave Zeeman effect in atomic oxygen, A. Abragam and J. H. Van Vleck—1448

Miscellaneous

Mobility of Ions and Electrons (see **Ions and Electrons, Mobility**)

Molecular Aggregates
Paramagnetic resonances in irradiated glasses, E. L. Yasaitis and B. Smaller—1068(L)

Molecular Beams (see **Atomic and Molecular Beams**)

Molecular Structure and Spectra
Absorption coefficients of NO and NH_3 in vacuum uv, H. Sun and G. L. Weissler—545(A)
Change in inversion spectrum of ND_3 from resonant to non-resonant absorption, G. Birnbaum and A. A. Maryott —270
Dissociation of H_2^+ by electron impact, Edward H. Kerner —1441
Effects of H bonding on infrared spectra of alcohols, Alexander Verrijn Stuart and G. B. B. M. Sutherland —534(A)
Eigenfunctions of S^2 by spin operator method, George W. Pratt, Jr.—278
Heat of dissociation of F_2 by effusion method, Henry Wise —532(A)
Interchange of rotational and vibrational energy in collisions of diatomic molecules, Edward H. Kerner—899
Microwave measurement of D_0 for CO, J. J. Gallagher, F. D. Bedard, and C. M. Johnson—1440
Microwave spectra of CsF, CsCl, and CsBr, A. Honig, M. L. Stitch, and M. Mandel—901
ν_1 band of D_2O in infrared, W. S. Benedict, Norman Gailar, and Earle K. Plyler—533(A)
Nuclear moments of Se^{79}, W. A. Hardy, G. Silvey, C. H. Townes, B. F. Burke, M. W. P. Strandberg, George W. Parker, and Victor W. Cohen—1532
Nuclear quadrupole coupling in Li_2 molecule, R. M. Sternheimer and H. M. Foley—1460
Nuclear spin and quadrupole moment of I^{131}, Ralph Livingston, Ben M. Benjamin, J. T. Cox, and Walter Gordy— 1271
1–2 mm wave spectroscopy. II. H_2S, Charles A. Burrus, Jr., and Walter Gordy—274; III. NO and DI, C. A. Burrus and Walter Gordy—1437
Sign of quadrupole interaction of Li^6 in LiCl, P. Kusch—268
Spin of Si^{29} and mass ratios of stable Si isotopes, R. L. White and C. H. Townes—1256
Zeeman effect in molecular spectra of H_2, G. H. Dieke, S. P. Cunningham, and F. T. Byrne—81

Moments, Nuclear (see **Nuclear Moments and Spin**)

Moments of Molecules (see **Molecular Structure and Spectra**)

Neutrino (see also **Nuclear Spectra; Radioactivity**)
Background in neutrino experiment, F. B. Harrison, C. L. Cowan, Jr., and F. Reines—1088(A)
Detection of free neutrino, F. Reines and C. L. Cowan, Jr. —830(L)
Upper limits on neutrino mass from T β spectrum, Donald R. Hamilton, W. Parker Alford, and Leonard Gross—1521

Neutron Diffraction (see **Diffraction; Scattering of Neutrons**)

Neutrons (see **Elementary Particle Interactions**)

Noise
Noise observations on CdS crystal photoconductors, Carl Shulman, R. W. Smith, and A. Rose—857(A)
Vacuum fluctuation noise in electron streams, J. Weber —847(A)

Nuclear Fission
Energy distribution of slowed fission fragments, J. A. Northrop and J. E. Brolley, Jr.—1091(A)
Neutron and spontaneous fission in U ores, W. H. Fleming and H. G. Thode—378
Ru^{103} and Ru^{106} fission yields, W. H. Hardwick—1072(L)
Spontaneous fission yields from U and Th, George W. Wetherill—907
U^{235} thermal neutron fission yields, George W. Reed and Anthony Turkevich—1473
Velocity distributions of slowed fission fragments, H. W. Schmitt and R. B. Leachman—1091(A)
Yield of Mo^{99} from fission of U^{235} and U^{238}, James Terrell, W. E. Scott, J. S. Gilmore, and C. O. Minkkinen— 1091(A)

Nuclear Forces (see **Elementary Particle Interactions; Field Theory; Nuclear Structure Theory**)

Nuclear Induction (see **Magnetic Resonance; Nuclear Moments and Spin**)

Nuclear Isomers (see **Nuclear Spectra; Radioactivity**)

Nuclear Moments and Spin

Bi^{210} spin, Mark Fred, Frank S. Tomkins, and Raymond F. Barnes—1324(L)

Contribution of collective motion to magnetic moments of heavy nuclei, Kenneth W. Ford—1094(A)

Hfs and nuclear electric quadrupole moment of B^{11}, Günter Wessel—1581(L)

Hfs formulas for *LS*-coupling, R. E. Trees—308

Hfs of spectra of Dy, Co, V, Mn, and La, Kiyoshi Murakawa and Tohru Kamei—325

Influence of electric and magnetic fields on angular correlations, A. Abragam and R. V. Pound—943

Interaction of electric field gradients and nuclear electric quadrupole moments in angular correlation, Rolf M. Steffen—849(A)

Intrinsic magnetic moment of elementary particles of spin 3/2, F. J. Belinfante—997

Magnetic moments of neutron and proton, F. J. Belinfante—994

Nuclear moments of Se^{79}, W. A. Hardy, G. Silvey, C. H. Townes, B. F. Burke, M. W. P. Strandberg, George W. Parker, and Victor W. Cohen—1532

Nuclear quadrupole coupling in Li_2, R. M. Sternheimer and H. M. Foley—1460

Nuclear quadrupole resonance of stable Ga isotopes, H. G. Dehmelt—1240

Nuclear resonance line broadening and quadrupole splitting in metallic Be, W. D. Knight—539(A)

Nuclear spin and quadrupole moment of I^{131}, Ralph Livingston, Ben M. Benjamin, J. T. Cox, and Walter Gordy—1271

Nuclear spin relaxation by translation diffusion, H. C. Torrey—962

1–2 mm wave spectroscopy. II. H_2S, Charles A. Burrus, Jr., and Walter Gordy—274; III. NO and DI, C. A. Burrus and Walter Gordy—1437

Paramagnetic resonance hfs of V^{50} and V^{51}, C. Kikuchi, M. H. Sirvetz, and V. W. Cohen—109

Polarization of nuclear spins in metals, T. R. Carver and C. P. Slichter—212(L)

Polarization of nuclei in metals, Albert W. Overhauser—411

Sb^{121} and Sb^{123} quadrupole moments, G. Sprague and D. H. Tomboulian—105

Sign of quadrupole interaction of Li^6 in LiCl, P. Kusch—268

Spin of Si^{29} and mass ratios of stable Si isotopes, R. L. White and C. H. Townes—1256

Tc^{99} nuclear moments, Karl G. Kessler and R. E. Trees—303

Ti^{47} and Ti^{49} spin and magnetic moment, C. D. Jeffries—1096(A); 1262

Zeeman splitting of nuclear quadrupole resonance lines, Yu Ting, Edward Manring, and Dudley Williams—1581(L)

Nuclear Photoeffects

Angular and energy distributions of photoprotons from Al and Ta, M. M. Hoffman and A. G. W. Cameron—1184

Angular distribution of positive photomesons from H: counter telescope method, A. V. Tollestrup, J. C. Keck, and R. M. Worlock—1090(A)

Charge independence in (γ,π) and (γ,l) reactions, D. C. Peaslee and V. L. Telegdi—126

Elastic photoproduction of π^0's from deuterium, J. W. DeWire, A. Silverman, and B. Wolfe—520(L)

Excitation function for photodisintegration of Be, R. Nathans and J. Halpern—940

Fine structure in $C^{12}(\gamma,n)C^{11}$ neutron yield, L. Katz and J. Goldemberg—852(A)

High-energy (γ,d) reactions, J. W. DeWire, A. Silverman, and B. Wolfe—519(L)

Li^7 and F^{19} excitation levels by betatron irradiation, J. Goldemberg and L. Katz—852(A)

Matrix elements for nuclear photoeffect, Leslie L. Foldy—178

Photoproduction of meson pairs, R. D. Lawson and S. D. Drell—539(A)

Photoproduction of π-meson pairs, R. D. Lawson—1272

Photoproduction of positive mesons from H: magnetic spectrometer method, R. L. Walker, J. G. Teasdale, and V. Z. Peterson—1090(A); results, R. F. Bacher, J. C. Keck, V. Z. Peterson, J. G. Teasdale, A. V. Tollestrup, R. L. Walker, and R. M. Worlock—1090(A)

Photoprotons from In, Ce, and Bi, M. E. Toms and W. E. Stephens—362

Production of protons from C by monoenergetic γ rays, John W. Weil and Boyce D. McDaniel—391

Ratio of π^+ to π^- mesons produced by γ rays, James Edward Carothers—538(A)

Reaction $C^{12}(\gamma,3p)Li^9$, Daryl Reagan—651

Systematics of photoneutron reactions, R. Nathans and J. Halpern—207(L)

Tamm-Dancoff theory of pion photoproduction, Marc Ross—855(A)

Nuclear Reactions, General (see also **Elementary Particle Interactions; Scattering**)

Bound state corrections in two-body system, Thomas Fulton and Robert Karplus—1094(A)

Br isotopes produced by C-ion bombardment of Cu, Jack M. Hollander—518(L)

Electrodisintegration of nuclei, Karl L. Brown and Richard Wilson—540(A)

Intermediate coupling and nuclear reactions, A. M. Lane—839(L)

Internal conversion electrons from Coulomb-excited Ta and W, Torben Huus and Jørgen H. Bjerregaard—1579(L)

Invariant forms of nucleon-nucleon interaction, David Feldman—824

Multiple production of pions in nucleon-nucleon collisions at cosmotron energies, E. Fermi—452

Production of fast Li, Be, B fragments from interactions of primary cosmic-ray nuclei, J. H. Noon, M. F. Kaplon, and D. M. Ritson—1585(L)

R-matrix formulation of statistical theory of nuclear reactions, R. G. Thomas—1094(A)

Search for stable dineutron, B. L. Cohen and T. H. Handley—101

State in C^{12} predicted from astrophysical evidence, F. Hoyle, D. N. F. Dunbar, W. A. Wenzel, and W. Whaling—1095(A)

Statistical theory of nuclear reactions, Bernard L. Cohen—1245

Theory of polarized particles and γ rays in nuclear reactions, Albert Simon—1050

Use of tensor operators in nuclear collision problems, Lincoln Wolfenstein—123

Nuclear Reactions Induced by α Particles and H^3 (see also **Scattering of α Particles**)

F^{18} energy levels from α-particle reactions in N, N. P. Heydenburg and G. M. Temmer—89

H^3+He^3 reactions, C. D. Moak—383

Secondary particles induced by 375-Mev α particles, R. W. Deutsch and W. H. Barkas—539(A)

Test of charge symmetry hypothesis, H. W. Wilson and Walter H. Barkas—537(A)

Thin target studies of $B^{10}(\alpha,n)N^{13}$, N^{13*}, Marguerite Rogers, F. K. Odencrantz, and G. J. Plain—530(A)

Yields of low-energy protons and α's resulting from high-energy bombardment of Ag, Robert W. Deutsch—515(L)

Nuclear Reactions Induced by Deuterons and Tritons (see also **Scattering of Deuterons**)
Approximate wave-mechanical description of deuteron stripping, F. L. Friedman and W. Tobocman—93
Energies and angular distributions of neutrons from $Be^9(d,n)B^{10}$, J. S. Pruitt, C. D. Swartz, and S. S. Hanna—1456
Energy levels of Be^{10}, K. B. Rhodes and J. N. McGruer—1328(L)
Excited states of B^{11} and B^{12} from $B^{10}(d,p)B^{11}$ and $B^{11}(d,p)B^{12}$, Mortimer M. Elkind—127
Fast-neutron spectrometer using $T(d,n)\alpha$ reaction, G. K. O'Neill—853(A)
γ rays from $C^{12}+D^2$, R. J. Mackin, Jr.—529(A)
Inelastic scattering of protons and deuterons from B^{10} and N^{14}, C. K. Bockelman, C. P. Browne, W. W. Buechner, and A. Sperduto—665
Interaction of 19-Mev deuterons with O, R. G. Freemantle, W. M. Gibson, D. J. Prowse, and J. Rotblat—1268
Mechanism of stripping reactions, J. Horowitz and A. M. L. Messiah—1326(L)
Nuclear reaction determination of $Sn^{124}-Te^{124}$ mass difference, N. S. Wall—1526
$O^{18}(d,n)F^{19}$ neutron spectrum, Robert L. Seale—389
Protons from deuteron bombardment of Kr^{84} and Kr^{86}, G. W. Wheeler, R. B. Schwartz, and W. W. Watson—121
Q values of $Ne^{21}(d,\alpha)F^{19}$ and $Ne^{21}(d,p)Ne^{22}$, Curt Mileikowsky and Ward Whaling—528(A)
Radionuclides of As produced by deuteron bombardment of Ge, H. J. Watters and J. F. Fagan, Jr.—1248
Search for B^{13}, Edward L. Hubbard, Lawrence Ruby, and Warren F. Stubbins—1494
7.68-Mev state in C^{13}, D. N. F. Dunbar, R. E. Pixley, W. A. Wenzel, and W. Whaling—649
State in C^{13} predicted from astrophysical evidence, F. Hoyle, D. N. F. Dunbar, W. A. Wenzel, and W. Whaling—1095(A)
Theory of high-energy deuteron pick-up, B. J. Malenka—516(L)
$V^{51}(d,p)V^{52}$, magnetic analysis, J. E. Schwager and L. A. Cox—102

Nuclear Reactions Induced by Mesons (see also **Elementary Particle Interactions; Mesons; Scattering of Mesons**)
Attenuation cross sections of 37-Mev pions in H, C. E. Angell and J. P. Perry—835(L)
Interaction cross section of H and heavier elements for 450-Mev negative pions and 340-Mev positive pions, S. J. Lindenbaum and Luke C. L. Yuan—1578(L)
Interaction of negative pions with Hg, Nathan Sugarman and Agnes Haber—730
Meson production by 500-Mev negative pions, M. Blau, M. Caulton, and J. E. Smith—516(L)
Negative μ-meson capture in C, T. N. K. Godfrey—512(L)
Positive π-meson interactions in Be, F. H. Tenney and J. Tinlot—974
Radioactive Cu nuclides produced by slow negative pions and muons from Zn, A. Turkevich and Si Chang Fung—521(L)
Scattering and absorption of π^+ mesons by Al, J. F. Tracy—537(A)
Total cross section for positive pions in hydrogen, Stanley L. Leonard and Donald H. Stork—855(A)
Total cross sections for positive pions, D. Stork—538(A)

Nuclear Reactions Induced by Neutrons (see also **Elementary Particle Interactions; Scattering of Neutrons**)
Angular distributions from (n,p) nuclear reactions, N. Austern, S. T. Butler, and H. McManus—350
Cross sections for production of In^{115m} and Au^{197m} by inelastic scattering of neutrons, H. C. Martin, B. C. Diven, and R. F. Taschek—1096(A)
Disintegration of C^{13}, B^{11}, and B^{10} by fast neutrons, Glenn M. Frye and Louis Rosen—1083(A)
Energy levels in Hf isotopes, D. J. Hughes, W. Y. Kato, and J. S. Levin—1094(A)
Evaluation of interaction effect in n-p capture, N. Austern—670
Excitation functions for $(n,2n)$ reactions in Ge, Sc, As, Tl, and Ni, S. J. Bame, Jr.—1096(A)
Formation of long-lived Bi^{210} isomer, D. J. Hughes and H. Palevsky—1206
γ radiation from neutron excitation of Zr and Hf, C. W. Malich and C. E. Faneuff—1095(A)
High-pressure cloud-chamber investigation of protons scattered by 300-Mev neutrons, John DePangher—1084(A)
Inelastic neutron scattering in Al, Fe, Mg, and Cu, Richard E. Garrett, Frank L. Hereford, and Billy W. Sloope—1507
Inelastic scattering of fast neutrons in C and Pb, B. G. Whitmore—654
Inelastic scattering of protons and neutrons by deuterons, R. M. Frank and J. L. Gammel—1092(A)
Large NaI scintillation counter study of neutron-capture γ rays from H, Bernard Hamermesh and Richard J. Culp—211(L)
Level parameters for low-energy neutron resonances, J. S. Levin, D. J. Hughes, and W. Y. Kato—851(A)
Long-lived activity in neutron-irradiated Nb, David L. Douglas, Anita C. Mewherter, and Robert P. Schuman—369; 1095(A)
Magnetic inelastic scattering of slow neutrons, H. Palevsky and D. J. Hughes—202(L)
Neutron absorption and scattering by Hf, L. M. Bollinger, S. P. Harris, C. T. Hibdon, and C. O. Muehlhause—1527
Neutron total cross section for Bi and U between 45 and 160 Mev, W. I. Linlor and B. Ragent—835(L)
Neutron total cross sections at 20 Mev, Robert B. Day and Richard L. Henkel—358
Nuclear scattering of "300"-Mev neutrons, W. P. Ball, Burton J. Moyer, and Robert E. Richardson—539(A)
π^- mesons produced in cloud chamber by high-energy neutrons, Franklin C. Ford and Wilson M. Powell—537(A)
Pulse-height measurements of recoils from $B^{10}(n,\alpha)Li^7$ in A-CO_2 mixtures, J. De Juren and H. Rosenwasser—544(A)
Slow neutron resonances in Ho, Tm, and Lu, H. L. Foote, Jr., H. H. Landon, and V. L. Sailor—656
Slow neutron resonances in Ta, R. L. Christensen—1509
Slow neutron velocity spectrometer studies. V. Re, Ta, Ru, Cr, Ga, E. Melkonian, W. W. Havens, Jr., and L. J. Rainwater—702
Spin-orbit coupling energy in O^{17}, Robert K. Adair—1491
Th energy levels, D. J. Hughes, W. Y. Kato, and J. S. Levin—851(A)
Thermal neutron absorption cross sections of B and Au, R. S. Carter, H. Palevsky, V. W. Myers, and D. J. Hughes—716
Total cross sections for 169-Mev neutrons, A. E. Taylor—1071(L)
Total neutron cross section of liquid A, Janet B. Guernsey and Clark Goodman—323
Total neutron cross section of P, K. F. Hansen, R. M. Kiehn, and Clark Goodman—652

Nuclear Reactions Induced by Protons (see also **Elementary Particle Interactions; Scattering of Protons**)
Angular anisotropy of γ ray from $C^{13}(p,\gamma p')C^{12}$, H. Hugh Woodbury—529(A)
Angular distribution of γ rays and α particles from $N^{15}(p,\alpha\gamma)C^{12}$, Alfred A. Kraus, Jr., A. P. French, William A. Fowler, and C. C. Lauritsen—529(A)

Angular distribution of neutrons from $O^{18}(p,n)F^{18}$, Hans Mark and Clark Goodman—1097(A)
Angular distributions of $F^{19}(p,\alpha)O^{16}$ reaction, R. W. Peterson, W. A. Fowler, and C. C. Lauritsen—1085(A)
Angular distributions of long-range α particles from $N^{15}(p,\alpha)C^{12}$, G. C. Neilson, D. B. James, and C. A. Barnes—1084(A)
Capture γ rays from proton bombardment of Be^9, W. F. Hornyak and T. Coor—675
Dependence of 33-Mev π^+ production cross section on atomic number, Ryokichi Sagane and Walter Dudziak—212(L)
Deuteron disintegration by 9.7-Mev protons, Juanita H. Gammel—1092(A)
Energy levels of Be^8, R. Malm and D. R. Inglis—1326(L)
γ radiation from $C^{13}(p,\gamma)N^{14}$, H. H. Woodbury, R. B. Day, and A. V. Tollestrup—1199
γ rays and internal pairs from Be^9+H^1, Robert J. Mackin, Jr.—1084(A)
γ rays from $D(p,\gamma)He^3$, G. M. Griffiths and J. B. Warren—1084(A)
γ rays from $Li^7(p,\gamma)Be^8$, Alfred A. Kraus, Jr.—1085(A)
γ rays from $N^{14}(p,\gamma)O^{15}$, C. W. Li—1084(A)
γ rays from $P^{31}(p,\gamma)S^{32}$, H. E. Gove and E. B. Paul—852(A)
γ rays from proton bombardment of B^{10}, R. W. Krone and L. W. Seagondollar—935
γ rays from $T(p,\gamma)He^4$ reaction, J. B. Warren and G. M. Griffiths—1084(A)
Inelastic scattering of protons and deuterons from B^{10} and N^{14}, C. K. Bockelman, C. P. Browne, W. W. Buechner, and A. Sperduto—665
Inelastic scattering of protons and neutrons by deuterons, R. M. Frank and J. L. Gammel—1092(A)
Interactions of 2.2-Bev protons in nuclear emulsions, L. W. Smith, C. P. Leavitt, A. M. Shapiro, C. E. Swartz, and M. Widgoff—851(A)
Neutral meson production in proton bombardment of C, Walter E. Crandall and Burton J. Moyer—749
Nuclear configurations inferred from high-energy pickup-deuteron distributions, W. Selove—1328(L)
$p+d \rightarrow t+\pi^+$, Wilson Frank, Kenneth C. Bandtel, Richard Madey, and Burton J. Moyer—537(A)
π^+/π^- ratios measured with use of spiral orbit spectrometer, Ryokichi Sagane—539(A)
Pick-up process in proton-deuteron scattering, A. Bratenahl and B. J. Moyer—538(A)
Pion production at 180° by protons on C, Stanley L. Leonard—538(A)
Pions from production of baryons by protons, Frederik J. Belinfante—145
Polarization of γ rays in $F^{19}(p,\alpha\gamma)O^{16}$, L. W. Fagg and S. S. Hanna—372
Production of neutral mesons by 340-Mev protons on H, J. W. Mather and E. A. Martinelli—780
Reactions and scattering of protons on Li^7, D. A. Liberman and R. F. Christy—1085(A)
Scattering of 9.5-Mev protons by C and O, W. E. Burcham, W. M. Gibson, A. Hossain, and J. Rotblat—1266
Search for B^{13}, Edward L. Hubbard, Lawrence Ruby, and Warren F. Stubbins—1494
Search for *V* particles produced by 430-Mev protons, A. H. Rosenfeld and S. B. Treiman—727
Spectrum of particles from Pb bombarded by 32-Mev protons, Robert M. Eisberg and George J. Igo—537(A)
Stars induced in nuclear emulsions by 2.2-Bev protons, M. Widgoff, C. P. Leavitt, A. M. Shapiro, L. W. Smith, and C. E. Swartz—851(A)
Tc^{98}, John K. Lerohl, M. L. Pool, D. N. Kundu, and R. A. House—934
Test of charge symmetry hypothesis, H. W. Wilson and Walter H. Barkas—537(A)
Yields of low-energy protons and α's resulting from high-energy bombardment of Ag, Robert W. Deutsch—515(L)
Nuclear Scattering (see **Scattering**)
Nuclear Spectra (see also **Nuclear Isomers; Nuclear Reactions; Radioactivity**)
Ag^{109} decay scheme, M. L. Perlman, W. Bernstein, and R. B. Schwartz—1236
α-γ angular correlation in ionium (Th^{230}), G. M. Temmer and J. M. Wyckoff—849(A); 913
Angular correlation between first and third γ rays in Ti^{48}, C. E. Whittle and P. S. Jastram—205(L)
Angular correlation of cascade γ rays from decay of Au^{198}, Carlton D. Schrader—928
Angular correlation of γ rays from Mn^{56}, F. R. Metzger and W. B. Todd—904
As^{77} and Br^{77}, scintillation study, erratum, M. E. Bunker, R. J. Prestwood, and J. W. Starner—1587(E)
As^{77} and Ge^{71}, B. L. Saraf, J. Varma, and C. E. Mandeville—848(A)
B^{11} and B^{13} excited states from $B^{10}(d,p)B^{11}$ and $B^{11}(d,p)B^{12}$, Mortimer M. Elkind—127
Be^8 energy levels, R. Malm and D. R. Inglis—1326(L)
Be^{10} energy levels, K. B. Rhodes and J. N. McGruer—1328(L)
β-γ polarization correlations, Donald R. Hamilton, Aaron Lemonick, and Francis M. Pipkin—1191
β interaction, R. Finkelstein and P. Kaus—1316
Br^{80} disintegration scheme, Gertrude Scharff-Goldhaber and Michael McKeown—356
Ca^{47} decay, J. M. Cork, J. M. LeBlanc, M. K. Brice, and W. H. Nester—367
Ca^{47}, Sc^{47}, V^{48}, Rh^{100} disintegration, Luis Marquez—1511
Capture γ rays from proton bombardment of Be^9, W. F. Hornyak and T. Coor—675
$Cm^{242, 243, 244}$ α spectra, Frank Asaro, S. G. Thompson, and I. Perlman—694
Complex α spectra of radiothorium (Th^{228}) and thorium-X (Ra^{224}), Frank Asaro, Frank Stephens, Jr., and I. Perlman—1495
Coupling of angular momenta in nuclear reactions, R. F. Christy—529(A)
Cross terms in allowed-shape β spectra, J. P. Davidson and D. C. Peaslee—1584(L)
Crystal structure and nuclear directional correlation. I. Pb^{204}, H. Frauenfelder, J. S. Lawson, Jr., W. Jentschke, and G. DePasquali—513(L)
Cu^{67} β decay, Harry T. Easterday—537(A)
Decay of $_{66}Dy^{165m}$ (1.2 min) and $_{66}Dy^{165}$ (2.3 hr), W. C. Jordan, J. M. Cork, and S. B. Burson—1218
Directional correlation and electric quadrupole interaction in γ-γ cascade of 48.7-min Cd^{111m}, J. J. Kraushaar and R. V. Pound—522(L)
Directional correlation of Pb^{204} γ-γ cascade, H. Frauenfelder, J. S. Lawson, Jr., W. Jentschke, and G. De Pasquali—1241
Effect of cloud-chamber geometry on β-ray studies, Paul H. Pitkanen—530(A)
Er^{163} and Tm^{165}, Thomas H. Handley and Elmer L. Olson—1260
F^{17} and F^{20} β decay, Calvin Wong—529(A)
F^{18} energy levels from α-particle reactions in N, N. P. Heydenburg and G. M. Temmer—89
Formation of long-lived Bi^{210} isomer, D. J. Hughes and H. Palevsky—1206
Ga^{66} decay, L. G. Mann, W. E. Meyerhof, and H. I. West, Jr.—1481
Ga^{67} decay, W. E. Meyerhof, L. G. Mann, and H. I. West, Jr.—540(A); 758
γ-γ angular correlation in Pd^{106}, E. D. Klema and F. K. McGowan—1469

Nuclear Spectra (Continued)
γ-γ directional correlation experiments with Mo^{93m}, J. J. Kraushaar—318
γ radiation from neutron excitation of Zr and Hf, C. W. Malich and C. E. Faneuff—1095(A)
$_{64}Gd^{159}$ (18-hr) and $_{64}Gd^{161}$ (3.7-min) radiations, W. C. Jordan, J. M. Cork, and S. B. Burson—315
Ge^{73} metastable states, Joan P. Welker, A. W. Schardt, G. Friedlander, and J. J. Howland, Jr.—401
Hf isotopes, energy levels, D. J. Hughes, W. Y. Kato, and J. S. Levin—1094(A)
Influence of electric and magnetic fields on angular correlations, A. Abragam and R. V. Pound—943
Interaction of electric field gradients and nuclear electric quadrupole moments in angular correlation, Rolf M. Steffen—849(A)
Internal conversion and directional angular correlation of Bi^{207} γ's, F. K. McGowan and E. C. Campbell—523(L)
Internal conversion electron-γ directional angular correlation of Bi^{207}, F. K. McGowan—524(L)
Internal conversion electrons from Coulomb-excited Ta and W, Torben Huus and Jørgen H. Bjerregaard—1579(L)
Isomeric transition of Pb^{207} as energy standard in β spectroscopy, David E. Alburger—1257
K-Auger electrons, positrons, and conversion electrons of Zn^{65} above 5 kev, J. F. Perkins and S. K. Haynes—687
Large NaI scintillation counter study of neutron capture γ rays from H, Bernard Hamermesh and Richard J. Culp—211(L)
Li^7 and F^{19} excitation levels by betatron irradiation, J. Goldemberg and L. Katz—852(A)
Lifetime measurements for first excited states of O^{17} and B^{10} from recoil studies, Jacques Thirion and Valentine L. Telegdi—1253
Long-lived activity in neutron-irradiated Nb, David L. Douglas, Anita C. Mewherter, and Robert P. Schuman—369; 1095(A)
Low-lying many-particle levels in odd-mass nuclides with 21, 23, 25, or 27 protons or neutrons, R. H. Nussbaum, R. van Lieshout, and A. H. Wapstra—207(L)
Method for determination of end-point energy of β emitters, M. Forro—931
Na^{22} K capture, R. H. Miller and R. Sherr—848(A)
New first excited state of even-even nucleus Kr^{80}, Gertrude Scharff-Goldhaber and Michael McKeown—1094(A)
1.25-min Rb^{83m} daughter of 27-day Sr^{82}, L. M. Litz, S. A. Ring, and W. R. Balkwell—288
P^{29} total disintegration energy, Hilliard Roderick and Calvin Wong—204(L)
Pb^{206} isomerism, D. E. Alburger and M. H. L. Pryce—514(L)
Possible $0\rightarrow0$ (no) β transitions in $4n+2$ nuclei, O. Kofoed-Hansen—1075(L)
RaD β spectrum, E. Huster—1076(L)
Radionuclides of As produced by deuteron bombardment of Ge, H. J. Watters and J. F. Fagan, Jr.—1248
Rh^{106} decay, Bernd Kahn and W. S. Lyon—902
S^{35} β spectrum from $C_2H_5S^{35}H$ below 33 kev, G. J. Plain, H. L. Morrison, P. H. Pitkanen, and F. T. Rogers, Jr.—529(A)
Scintillation spectrometer determination of L-capture to K-capture ratio in Cd^{109} and I^{125}, E. der Mateosian—938
Sequence of γ emission in triple correlations, E. J. Hellund and J. M. Jauch—203(L)
7.68-Mev state in C^{13}, D. N. F. Dunbar, R. E. Pixley, W. A. Wenzel, and W. Whaling—649
Sm^{146} α activity detected with nuclear emulsions, Dean C. Dunlavey and Glenn T. Seaborg—206(L)
Sm^{153}, Robert Katz and Milford R. Lee—848(A)
Spin-orbit coupling energy in O^{17}, Robert K. Adair—1491
Ta^{183} decay, J. W. M. DuMond, H. C. Hoyt, P. E. Marmier, and J. J. Murray—202(L)
Tc^{98}, John K. Lerohl, M. L. Pool, D. N. Kundu, and R. A. House—934
Th energy levels, D. J. Hughes, W. Y. Kato, and J. S. Levin—851(A)
Theorem concerning angular correlations, J. Weneser and D. R. Hamilton—321
Theory of polarized particles and γ rays in nuclear reactions, Albert Simon—1050
Ti^{48} energy level from decay of Sc^{48} and V^{48}, H. Casson, L. S. Goodman, and V. E. Krohn—1517
Time-dependent quadrupole interaction in angular correlation of nuclear radiation. I. Cd^{111}, P. B. Hemmig and R. M. Steffen—832(L)
Tl neutron-deficient isotopes, I. Bergström, R. D. Hill, and G. DePasquali—918; Ingmar Bergström and R. D. Hill—849(A)
Universal Fermi interaction, E. J. Konopinski and H. M. Mahmoud—1045
Upper limits on neutrino mass from T β spectrum, Donald R. Hamilton, W. Parker Alford, and Leonard Gross—1521
W^{181}, J. M. Cork, W. H. Nester, J. M. LeBlanc, and M. K. Brice—119
0^+ states of light odd-odd nuclei, P. Stähelin—1076(L)
Zn^{65} electron and positron spectrum above 5 kev, J. F. Perkins and S. K. Haynes—1096(A)

Nuclear Structure Theory (see also **Nuclear Reactions; Nuclear Spectra**)
Angular distributions from (n,p) nuclear reactions, N. Austern, S. T. Butler, and H. McManus—350
Applications of Wigner semi-empirical mass formula to isobars, J. T. McCarthy—848(A)
Contribution of collective motion to magnetic moments of heavy nuclei, Kenneth W. Ford—1094(A)
Coupling of angular momenta in nuclear reactions, R. F. Christy—529(A)
Evidence for subshell at $Z=96$, Glenn T. Seaborg—1074(L)
Giant nuclear dipole resonance, M. Ferentz, M. Gell-Mann, and D. Pines—836(L)
High-energy electron scattering and nuclear structure determinations, R. Hofstadter, H. R. Fechter, and J. A. McIntyre—978
Intermediate coupling and nuclear reactions, A. M. Lane—839(L)
Interpretation of electron scattering experiments, L. I. Schiff—988
Mixed configurations in nuclei, A. de-Shalit and M. Goldhaber—1211
μ meson as nuclear probe particle, John A. Wheeler—812
μ-mesonic atoms and electromagnetic radius of nucleus, L. N. Cooper and E. M. Henley—801
Nuclear radii, Francis Bitter and Herman Feshbach—837(L)
Nuclear scattering of high-energy neutrons, T. B. Taylor—831(L)
Nuclear stability curve, W. G. McMillan—210(L)
Nuclear surface oscillations, A. K. Kerman—1176
Three-body nuclear interactions in H^3 and He^3, A. W. Solbrig, Jr.—855(A)
X-rays from μ-mesonic atoms, Val L. Fitch and L. J. Rainwater—789
0^+ states of light odd-odd nuclei, P. Stähelin—1076(L)

Optical Instruments (see **Methods and Instruments**)
Optical Properties (see also **Luminescence**)
Absorption cross sections of CH_4 in vacuum uv, G. L. Weissler and H. Sun—533(A)

Bleaching properties of *F* centers in KBr at 5°K, Jordan J. Markham, Reuel T. Platt, Jr., and Irving L. Mador —597
Čerenkov radiation in dispersive medium, H. Motz and L. I. Schiff—540(A)
Characteristics of certain photographic plates in vacuum uv, Po Lee and G. L. Weissler—545(A)
Color-center formation in alkali halides containing $S^=$, E. Burstein and B. W. Henvis—845(A)
Faraday rotation in Ge, H. Suhl and G. L. Pearson—858(A)
Long wavelength edge of photographic sensitivity and of electronic absorption of solids, Franz Urbach—1324(L)
Ne and A absorption in extreme uv, Po Lee and G. L. Weissler—533(A)
Observation of magnetic domains by longitudinal Kerr effect, C. A. Fowler, Jr., and E. M. Fryer—532(A)
Optical absorption and photoconduction in visible and near infrared in single crystals of BaO, William C. Dash —68
Optical effects of radiation damage in alkali halides, Donald R. Westervelt—531(A)
Oxygen vacancies in BaO, R. L. Sproull, R. S. Bever, and G. Libowitz—77
Solid state absorption spectra of Mg and MgO, John R. Townsend—556
Some electrical and optical properties of synthetic single crystals of ZnS, William W. Piper—23

Pair Production (see **Electrons and Positrons**)
Phosphors and Phosphorescence (see **Luminescence**)
Photoconductivity (see **Electrical Conductivity and Resistance, Optical Properties**)
Photodisintegration (see **Nuclear Photoeffects**)
Photoelasticity (see **Elasticity and Plasticity**)
Photoelectric Effect (see **Electrical Properties**)
Photography and Photographic Emulsions (see **Methods and Instruments**)
Photometry (see **Methods and Instruments**)
Photons (see **Radiation**)
Photovoltaic Effect (see **Electrical Properties**)
Piezoelectric Effect (see **Dielectrics and Dielectric Properties**)
Plasticity (see **Elasticity and Plasticity**)
Polarization, Electrical (see **Dielectrics and Dielectric Properties**)
Polymers (see **Molecular Aggregates**)
Positrons (see **Electrons and Positrons**)
Probability (see **Mathematical Methods**)
Proceedings of the American Physical Society
Inyokern-Pasadena Meeting at U. S. Naval Ordnance Test Station, Inyokern, California and the California Institute of Technology, Pasadena, California, December 26, 27, 29, and 30, 1952 [Bull. Am. Phys. Soc. **27**, No. 6 (1952)] —526
Spring Meeting of the New York State Section at the General Electric Research Laboratory, Schenectady, New York, April 10 and 11, 1953—841
Rochester Meeting at the University of Rochester, Rochester, New York, June 18–20, 1953 [Bull. Am. Phys. Soc. **28**, No. 4 (1953)]—839
New Mexico Meeting at the University of New Mexico, Albuquerque, New Mexico, September 2–5, 1953 [Bull. Am. Phys. Soc. **28**, No. 5 (1953)]—1078
Protons (see **Elementary Particle Interactions**)

Quantum Electrodynamics (see also **Field Theory**)
Bound-state corrections in two-body system, Thomas Fulton and Robert Karplus—1094(A)
Coupled-field Green's functions, J. G. Valatin—522(L)
Electromagnetic effects in two-nucleon systems, Stanley Deser—1542
Hfs of hydrogen, R. Arnowitt—1002
Radiative correction to collision loss of heavy particles, V. Z. Jankus—540(A)
Relativistic correction to Lamb shift, M. Baranger, H. A. Bethe, and R. P. Feynman—482
Second-order electron self-energy, H. P. Stapp—540(A)
Theory of quantized fields, Julian Schwinger—1283
Quantum Mechanics
Augmented plane wave method for periodic potential problem, J. C. Slater—603; H. M. M. Saffren and J. C. Slater—1126
Binary rearrangement collision, Saul Altshuler—1157
Description of quantum states through distributions of observable values, Norbert Wiener and Armand Siegel —856(A)
Eigenfunctions of S^2 by spin operator method, George W. Pratt, Jr.—278
Inertia as consequence of wave properties, Richard Schlegel —856(A)
Reduction of relativistic two-particle wave equations to approximate forms, Zeno Chraplyvy—1310
Reformulation of solid-state electronic Boltzmann equation, J. S. Lomont—1082(A)
Space-time representation in wave mechanics, E. J. Hellund and M. K. Brachman—822
Use of non-orthogonal wave functions in treatment of solids, with applications to ferromagnetism, W. J. Carr, Jr.—28
Virial theorem for Dirac's equation, N. H. March—481
Quenching of Radiation (see **Radiation**)

Radar (see **Methods and Instruments; Radiation**)
Radiation
Absorption cross sections of CH_4 in vacuum uv, G. L. Weissler and H. Sun—533(A)
Automatic recording of zodiacal light, Victor H. Regener— 1093(A)
Bremsstrahlung and electron scattering cross sections in Au for 247-Mev electrons and positrons, Philip C. Fisher —420; 853(A)
Čerenkov effect and dielectric constant, S. M. Neamtan —1362
Čerenkov effect at microwave frequencies, M. Danos, S. Geschwind, H. Lashinsky, and A. van Trier—828(L)
Čerenkov radiation in dispersive medium, H. Motz and L. I. Schiff—540(A)
Compton scattering of 2.62-Mev γ rays by polarized electrons, S. B. Gunst and L. A. Page—970
Contribution of solar x-rays to *E*-layer ionization, E. T. Byram, T. A. Chubb, and H. Friedman—1066(L)
Degradation of γ rays in water, M. M. Weiss and W. Bernstein—1264
Focusing of short electromagnetic waves by means of Fresnel half-period zone plate, H. George Oltman— 1093(A)
γ-ray absorption measurements, P. R. Howland, W. E. Kreger, and R. A. Taylor—1095(A)
Height of upper atmosphere emissions by Van Rhŷn method, F. E. Roach, Helen B. Pettit, D. R. Williams, and P. St. Amand—534(A)
Large-angle scattering of Co^{60} γ rays, Thomas D. Strickler —923
"Lloyd mirror" interference in presence of slight uniform refraction, R. W. Stewart—1087(A)
Measurement of light scattered from search-light beam, E. V. Ashburn—534(A)
Multicolor photoelectric photometer for study of faint radiations, D. R. Williams and Pierre St. Amand—533(A)
Multiple-beam fringes of equal chromatic order, W. F. Koehler—542(A)
Ne and A absorption in extreme uv, Po Lee and G. L. Weissler—533(A)

Radiation (Continued)
Penetration of gamma radiation through Fe, L. A. Beach, R. B. Theus, and W. R. Faust—355
Possible relationship between ionosphere and nightglow, Pierre St. Amand and D. R. Williams—534(A)
Procedure for evaluation of automatic zodiacal light recordings, Richard J. Runge—1093(A)
Quenching of Hg resonance radiation (2537A) by N_2, C. G. Matland—637
Rf fine structure of photon beam from Berkeley synchrotron, Richard Madey, Kenneth C. Bandtel, and Wilson J. Frank—537(A)
Visible light from localized surface charges moving across grating, S. J. Smith and E. M. Purcell—1069(L)
Wave-synthesizing light chopper, W. Wallin—543(A)
Radio Waves (see **Radiation**)
Radioactivity (see also **Nuclear Spectra**)
Am^{243} half-life, Herbert Diamond, Paul R. Fields, Joseph Mech, Mark G. Inghram, and David C. Hess—1490
$Cm^{242, 243, 244}$ α spectra, Frank Asaro, S. G. Thompson, and I. Perlman—694
Complex α spectra of radiothorium (Th^{228}) and thorium-X (Ra^{224}) Frank Asaro, Frank Stephens, Jr., and I. Perlman—1495
Er^{163} and Tm^{168}, Thomas H. Handley and Elmer L. Olson—1260
Evidence for subshell at $Z=96$, Glenn T. Seaborg—1074(L)
Formation of long-lived Bi^{210} isomer, D. J. Hughes and H. Palevsky—1206
Lifetime measurements for first excited states of O^{17} and B^{10} from recoil studies, Jacques Thirion and Valentine L. Telegdi—1253
Liquid scintillation counting of natural C^{14}, F. N. Hayes, D. L. Williams, and Betty Rogers—512(L)
Long-lived activity in neutron-irradiated Nb, David L. Douglas, Anita C. Mewherter, and Robert P. Schuman—369; 1095(A)
Method for determination of end-point energy of β emitters, M. Forro—931
1.25-min Rb^{82m} daughter of 27-day Sr^{82}, L. M. Litz, S. A. Ring, and W. R. Balkwell—288
Po^{210} half-life by α counting, Mary Lou Curtis—1489
Radionuclides of As produced by deuteron bombardment of Ge, H. J. Watters and J. F. Fagan, Jr.—1248
Sm^{146} α activity detected with nuclear emulsions, Dean C. Dunlavey and Glenn T. Seaborg—206(L)
Variation of natural radioactivity in atmosphere with altitude, Marvin H. Wilkening—1080(A)
Zr half-life, Earl K. Hyde—927
Raman Spectra (see **Molecular Structure and Spectra**)
Range and Energy Loss of Particles (see also **Scattering**)
Degradation and range straggling of high-energy radiations, U. Fano—328
Effects of chemical structure on stopping powers for high-energy protons, T. J. Thompson—1083(A)
Energy loss of low-energy protons and deuterons in gases, H. K. Reynolds, D. N. F. Dunbar, W. A. Wenzel, and W. Whaling—528(A)
Energy loss of moving electrons to dipolar relaxation, H. Fröhlich and R. L. Platzman—1152
Ionization loss at relativistic velocities in nuclear emulsion, Bertram Stiller and Maurice M. Shapiro—735
Ionization loss in nuclear emulsions, John R. Fleming and J. J. Lord—511(L); 1089(A)
Ionization of relativistic cosmic-ray μ mesons, H. R. Snodgrass—1089(A)
Proton stopping cross section of Li, M. Bader, W. A. Wenzel, and W. Whaling—1085(A)
Radiative correction to collision loss of heavy particles, V. Z. Jankus—540(A)
Stopping cross section of gases for protons, 30–600 kev, H. K. Reynolds, D. N. F. Dunbar, W. A. Wenzel, and W. Whaling—742
Stopping cross section of several gases for protons and deuterons, D. N. F. Dunbar, H. K. Reynolds, W. A. Wenzel, and W. Whaling—528(A)
Total ionization of α particles of Po in mixtures of gases, G. Bertolini, M. Bettoni, and A. Bisi—1586(L)
Recombination (see **Molecular Structure and Spectra**)
Rectifiers (see **Electrical Conductivity and Resistance; Semiconductors**)
Relativity and Gravitation
Equations of motion in Einstein's new unified field theory, Joseph Callaway—1567
Expectations from unified field theory, Behram Kurşunoğlu—506(L)
Nonsymmetric unified field theories, W. B. Bonnor—1067(L)
Physical basis of gravitation, Robert L. Kirkwood—1557
Relativistic particle dynamics, B. Bakamjian and L. H. Thomas—1300
Resistance, Electrical (see **Electrical Conductivity and Resistance**)
Resonance Radiation (see **Radiation**)

Scattering, General (see also **Diffraction; Nuclear Reactions; Range and Energy Loss of Particles**)
Binary rearrangement collision, Saul Altshuler—1157
Elastic scattering of particles by atomic nuclei, N. C. Francis and K. M. Watson—291
Formulation of Kohn-Hulthén variational principle in terms of scattering operator formalism, Harry E. Moses—817
Implications of Lorentz invariance for scattering of spin $\frac{1}{2}$ particles, David Feldman—856(A)
Interchange of rotational and vibrational energy in collisions of diatomic molecules, Edward H. Kerner—899
Two-body scattering at low energy, Benjamin Roth—1250
Use of tensor operators in nuclear collision problems, Lincoln Wolfenstein—123
Scattering of α Particles
α-α scattering from 12.88 to 21.62 Mev, F. E. Steigert and M. B. Sampson—660
Preliminary results with Indiana heavy particle spectrometer, V. K. Rasmussen, D. W. Miller, B. M. Carmichael, and M. B. Sampson—852(A)
Scattering of Atoms and Molecules (see **Atomic and Molecular Beams**)
Scattering of Deuterons
Inelastic scattering of protons and deuterons from B^{10} and N^{14}, C. K. Bockelman, C. P. Browne, W. W. Buechner, and A. Sperduto—665
Scattering of deuterons in He, T. Lauritsen, T. Huus, and S. G. Nilsson—1501
Scattering of Electrons and Positrons
Bremsstrahlung and electron scattering cross sections in Au for 247-Mev electrons and positrons, Philip C. Fisher—420; 853(A)
Dissociation of H_2^+ by electron impact, Edward H. Kerner—1441
Electron-positron scattering, H. A. Howe and K. R. MacKenzie—530(A)
Generalized variational equations for scattering of electrons by H atoms, M. M. Gordon and J. G. Jones—1428
High-energy electron scattering and nuclear structure determinations, R. Hofstadter, H. R. Fechter, and J. A. McIntyre—978
High-energy electron scattering by nuclei, R. W. Pidd, C. L. Hammer, and E. C. Raka—436
Interpretation of electron scattering experiments, L. I. Schiff—988

Phase-shift calculation of high-energy electron scattering by nuclei, D. R. Yennie, R. N. Wilson, and D. G. Ravenhall —1325(L)

Scattering of Mesons (see also **Mesons; Nuclear Reactions Induced by Mesons**)

Attenuation cross sections of 37-Mev pions in H, C. E. Angell and J. P. Perry—835(L)

Elastic scattering of 118-Mev negative pions by H, Jay Orear—156

Nuclear forces from P-wave mesons, E. M. Henley and M. A. Ruderman—1036

Phenomenological analysis of meson-nucleon scattering, A. E. Woodruff—855(A)

π^+-p scattering near 260 Mev, W. B. Fowler, R. M. Lea, W. D. Shephard, R. P. Shutt, A. M. Thorndike, and W. L. Whittemore—832(L)

Scattering and absorption of π^+ mesons by Al, J. F. Tracy —537(A)

Scattering of mesons by complex nuclei, W. W. Wada—152

Scattering of negative pions by H, E. Fermi, M. Glicksman, R. Martin, and D. Nagle—161

Signs of phase shifts for pion-proton scattering, S. W. Barnes, C. E. Angell, J. P. Perry, D. Miller, J. Ring, and D. Nelson—1327(L)

Solutions of meson-nucleon equation in adiabatic limit, R. Arnowitt and S. Deser—1061(L)

Strong-coupling theory of meson scattering, Allan N. Kaufman—468

Total π^--p cross section at 840 and 470 Mev, A. M. Shapiro, C. P. Leavitt, and F. F. Chen—1073(L)

Scattering of Neutrons

Angular distribution of neutrons scattered from Al, Fe, and Pb, W. D. Whitehead and S. C. Snowdon—114; 1097(A)

Cross sections for production of In^{115m} and Au^{197m} by inelastic scattering of neutrons, H. C. Martin, B. C. Diven, and R. F. Taschek—1096(A)

Elastic scattering of fast neutrons by He^4, John D. Seagrave—1222

Elastic scattering of protons and neutrons by deuterons at high energy, J. L. Gammel—1092(A)

High-pressure cloud-chamber investigation of protons scattered by 300-Mev neutrons, John DePangher—1084(A)

Inelastic neutron scattering in Al, Fe, Mg, and Cu, Richard E. Garrett, Frank L. Hereford, and Billy W. Sloope—1507

Inelastic scattering of fast neutrons in C and Pb, B. G. Whitmore—654

Inelastic scattering of protons and neutrons by deuterons, R. M. Frank and J. L. Gammel—1092(A)

Magnetic inelastic scattering of slow neutrons, H. Palevsky and D. J. Hughes—202(L)

Magnetic scattering of neutrons from rare earth ions, G. T. Trammell—1387

Neutron absorption and scattering by Hf, L. M. Bollinger, S. P. Harris, C. T. Hibdon, and C. O. Muehlhause—1527

n-p scattering near 180° at 93 Mev, W. Selove, K. Strauch, and F. Titus—724

Nuclear scattering of high-energy neutrons, T. B. Taylor —831(L)

Nuclear scattering of "300" Mev neutrons, W. P. Ball, Burton J. Moyer, and Robert E. Richardson—539(A)

Paramagnetic scattering of neutrons by rare earth oxides, W. C. Koehler and E. O. Wollan—1380

Resonant effects and spin-dependence in potential scattering of slow neutrons, W. Selove—941

Scattering of fast neutrons by Fe, Pb, and Cr, M. A. Rothman, D. W. Kent, and C. E. Mandeville—1097(A)

Scattering of fast neutrons by He^4, John D. Seagrave—1093(A)

Spin-orbit coupling energy in O^{17}, Robert K. Adair—1491

Structure of liquid N_2, O_2, and A by neutron diffraction, D. G. Henshaw, D. G. Hurst, and N. K. Pope—1229

Transport mean free path of thermal neutrons in heavy water, S. W. Kash and D. C. Woods—544(A)

Scattering of Protons

Apparatus for double scattering of 240-Mev protons, W. F. Cartwright, C. L. Oxley, J. Rouvina, E. Baskir, D. Klein, J. Ring, and W. A. Skillman—852(A)

Differential p-p elastic scattering cross section at 144, 271, and 429 Mev, J. Marshall, L. Marshall, and V. A. Nedzel—834(L)

Elastic scattering of protons and neutrons by deuterons at high energy, J. L. Gammel—1092(A)

Elastic scattering of protons by C^{12} and C^{13}, Edmund A. Milne—528(A)

Elastic scattering of protons by Li^7, William D. Warters —528(A)

Elastic scattering of protons by N^{14}, T. S. Webb, C. W. Li, and W. A. Fowler—1084(A)

Energy levels in N^{14} from scattering of protons by C^{13}, Edmund A. Milne—1085(A)

Inelastic scattering of protons and deuterons from B^{10} and N^{14}, C. K. Bockelman, C. P. Browne, W. W. Buechner, and A. Sperduto—665

Inelastic scattering of protons and neutrons by deuterons, R. M. Frank and J. L. Gammel—1092(A)

Phase-shift analysis of high-energy p-p scattering experiments, A. Garren—213(L); erratum—1588(E)

Pick-up process in proton-deuteron scattering, A. Bratenahl and B. J. Moyer—538(A)

p-p scattering for nucleon isobar model, F. T. Solmitz—164

Reactions and scattering of protons on Li^7, D. A. Liberman and R. F. Christy—1085(A)

Scattering of 9.5-Mev protons by C and O, W. E. Burcham, W. M. Gibson, A. Hossain, and J. Rotblat—1266

Small-angle cross sections for scattering of protons by tritons, M. E. Ennis and A. Hemmendinger—1092(A)

Scattering of Radiation (see **Radiation; X-rays**)

Scintillation Counters (see **Methods and Instruments**)

Secondary Emission (see **Electrical Properties**)

Semiconductors

Annealing of bombardment damage in diamond-type lattice: theoretical, R. C. Fletcher and W. L. Brown—585

Annealing of bombardment damage in Ge: Experimental, W. L. Brown, R. C. Fletcher, and K. A. Wright—591

Charge multiplication in Ge and Si p-n junctions, K. B. McAfee and K. B. McKay—858(A)

Cleavage surfaces in Ge crystals, C. J. Calbick, H. Christensen, and E. E. Thomas—1082(A); H. Christensen, C. J. Calbick, and E. E. Thomas—1082(A)

Conductivity of Ge at 2.4×10^{10} cps, Y. Klinger—509(L)

Crystal growth of Si by tip fusion process, P. H. Keck, S. B. Levin, J. Broder, and R. Liberman—847(A)

Crystal habit of Si and Ge, G. Wolff—847(A)

Current-voltage characteristics of CdS crystals using ohmic contacts, R. W. Smith and A. Rose—857(A)

Cyclotron resonance in Ge crystals, G. Dresselhaus, A. F. Kip, and C. Kittel—827(L)

Diffusion of Li into Ge and Si, C. S. Fuller and J. A. Ditzenberger—846(A)

Drift mobilities in semiconductors. I. Ge, M. B. Prince—681

Effect of traps on carrier injection in semiconductors, H. Y. Fan—1424

Efficiency of conversion from light to electric power by Ge grown junction, Ralph P. Ruth and James W. Moyer —846(A)

Semiconductors (Continued)
Electrical properties of black phosphorus, Robert W. Keyes —580
Etch pits in plastically-deformed Ge, C. J. Gallagher—846(A)
Faraday rotation in Ge, H. Suhl and G. L. Pearson—858(A)
Floating zone recrystallization, P. H. Keck, W. VanHorn, J. Soled, and A. MacDonald—847(A)
Interpretation of Hall effect and resistivity data in PbS and similar binary compound semiconductors, Wayne W. Scanlon—1573(L)
Magnetic susceptibility of Ge, D. K. Stevens and J. H. Crawford, Jr.—1065(L)
Mobility of impurity ions in Ge and Si, J. C. Severiens and C. S. Fuller—1322(L)
Possible degeneracy of energy bands in Ge, Edward N. Adams, II—1063(L)
Production of acceptor centers in Ge and Si by plastic deformation, W. C. Ellis and E. S. Greiner—1061(L)
Seebeck effect in Ge, T. H. Geballe—857(A)
Si and Ge dielectric constants, W. C. Dunlap, Jr., and R. L. Watters—1396
Theory of ac space-charge polarization effects in photoconductors, semiconductors, and electrolytes, J. Ross Macdonald—4
Theory of low-temperature "breakdown" effect in Ge, N. Sclar, E. Burstein, and J. W. Davisson—858(A)
Thermoelectric power in semiconductors with applications to Ge, theory, V. A. Johnson and K. Lark-Horovitz—226
Thermoelectric power of Ge at temperatures above 78°K, A. E. Middleton and W. W. Scanlon—219
Thermoelectric power of Ge below room temperature, H. P. R. Frederikse—248
Thermoelectric power of semiconductors, Conyers Herring —857(A)
Shock Waves (see **Fluid Dynamics**)
Solid State (see **Crystalline State**)
Solutions (see **Liquids**)
Sound (see **Acoustics**)
Spallation (see **Nuclear Reactions**)
Spark Discharge (see **Electrical Discharges**)
Specific Heat (see **Thermal Properties**)
Spectra, Atomic (see **Atomic Structure and Spectra**)
Spectra, General
Flame zone spectroscopy of solid propellants, R. G. Rekers and D. S. Villars—534(A)
Theory of fine structure pressure broadening of spectral lines, Makoto Takeo and Shang-Yi Ch'en—850(A)
Spectra, Molecular (see **Molecular Structure and Spectra**)
Spectra, Nuclear (see **Nuclear Spectra**)
Spectroscopy Technique (see **Methods and Instruments**)
Spinor Fields (see **Field Theory**)
Standards (see **Constants, Standards, Units**)
Stark Effect (see **Atomic Structure and Spectra**)
Statistical Mechanics and Thermodynamics
Critical conditions for ice formation on silver iodide nuclei, Robert J. McCarty—1080(A)
Determination of thermodynamic temperatures near 0°K without introducing heat below 1°K, W. F. Giauque —1339
Exchange potential in electron gas at nonzero temperature, N. H. March—510(L)
Grand canonical ensembles, Laplace transform, and Darwin-Fowler contour integrals, Peter G. Bergmann and Ezra Newman—856(A)
Imperfect gas, T. H. Berlin, L. Witten, and H. A. Gersch —189
Irreversible thermodynamics of thermoelectric effects in inhomogeneous, anisotropic media, Charles A. Domenicali —877
Law of equilibrium between coexisting phases, George Antonoff—542(A)
Liquid He II: Bose-Einstein condensation and two-fluid model, P. R. Zilsel—1106
Statistical Methods (see **Mathematical Methods**)
Superconductivity
Atomic heat and critical magnetic field of superconducting Cd, J. R. Clement—1578(L)
Intermediate state of hollow superconducting tin cylinder, J. Gittleman—561
Search for Hall effect in superconductor. I. Experiment, H. W. Lewis—1149
Sn-Bi and Sn-Sb alloys, W. F. Love—238
Superconducting and normal heat capacities of Nb, A. Brown, M. W. Zemansky, and H. A. Boorse—52
Tc superconductivity, J. G. Daunt and J. W. Cobble—507(L)
Ti superconductivity, M. C. Steele and R. A. Hein—243
Transition into intermediate state of hollow superconducting cylinders, B. Serin, J. Gittleman, and E. A. Lynton—566
Transition temperatures of superconductors, B. T. Matthias —874
Supersonics (see **Fluid Dynamics**)

Thermal Conductivity (see **Thermal Properties**)
Thermal Diffusion (see **Diffusion**)
Thermal Expansion (see **Thermal Properties**)
Thermal Properties
Atomic heat and critical magnetic field of superconducting Cd, J. R. Clement—1578(L)
Atomic heat of In below 20°K, J. R. Clement and E. H. Quinnell—258
Persistent residues from ice particles, Mary Goulks Gourley and W. D. Crozier—526(A)
Specific heat of He^3 between 1.3°K and 2.3°K, G. de Vries and J. G. Daunt—1572(L)
Specific heats of alkali metals, H. Preston-Thomas, T. M. Dauphinee, and D. K. C. MacDonald—844(A)
Superconducting and normal heat capacities of Nb, A. Brown, M. W. Zemansky, and H. A. Boorse—52
Thermal conductivity of Cu between 0.25°K and 4.2°K, James Nicol and T. P. Tseng—1062(L)
Thermal microstructure in ocean, W. N. English—1087(A)
Vibrational spectrum and specific heat of Na, Ernest Bauer—58
Thermal Radiation (see **Radiation**)
Thermionic Emission (see **Electrical Properties**)
Thermodynamics (see **Statistical Mechanics and Thermodynamics**)
Thermoelectric Effect (see **Electrical Properties**)
Thermoluminescence (see **Luminescence**)
Thermomagnetic Effect (see **Magnetic Properties**)
Total Cross Sections (see **Electrons and Positrons; Nuclear Reactions**)
Transmutation (see **Nuclear Reactions**)

Uncertainty Principle (see **Quantum Mechanics**)
Units (see **Constants, Standards, Units**)

Vacuum Tubes (see **Methods and Instruments**)
Van der Waals Forces (see **Molecular Structure and Spectra**)
Viscosity (see **Liquids**)

Wave Mechanics (see **Quantum Mechanics**)
Work Function (see **Electrical Properties**)

X-Rays

Electronic excitation of L_{III} state of 5*d* elements, Guenter Schwarz and George L. Rogosa—88

Mo *K* and U *L* x-ray transitions from separated isotopes, George L. Rogosa and Guenter Schwarz—1434

Precision measurement at 24 500 volts of conversion constant λV, Gaelen L. Felt, John N. Harris, and Jesse W. M. DuMond—1160

Recording of x-ray diffraction patterns by scintillation counter, J. C. M. Brentano and I. Ladany—850(A)

Scanning x-ray microscope, Howard H. Pattee, Jr.—541(A)

Spectral distributions of filtered x-ray beams, W. J. Ramm and M. N. Stein—1081(A)

Theoretical and experimental intensities of soft continuous x-rays, R. W. Hendrick, Jr.—541(A)

X-ray absorption fine structure with polarized x-rays, R. Krogstad, W. Nelson, and S. T. Stephenson—1394

X-rays from μ-mesonic atoms, Val L. Fitch and L. J. Rainwater—789

CONTENTS—*Continued*

Letters to the Editor:

New Absorption Lines of Crystals in Submicrowave Region . . . . . S. Kojima, K. Tsukada, S. Ogawa, and A. Shimauchi 1571

Liquid Helium Films . . . . . K. R. Atkins 1571

Anomalous Paramagnetic Resonance in Copper Propionate . . . . . Hidetaro Abe 1572

Spectra Fields of He^3 between 1.2°K and 2.4°K . . . . . G. de Vries and J. G. Daunt 1572

Interpretation of Hall Effect and Resistivity Data in PbS and Similar Binary Compound Semiconductors . . . . . Wayne W. Scanlon 1573

Thermal Anomalies Associated with the Antiferromagnetic Ordering of FeF_2, CoF_2, and NiF_2 . . . . . J. W. Stout and Edward Catalano 1575

Spin-Lattice Relaxation and the Residual Width of Highly Exchange-Narrowed Paramagnetic Resonances . . . . . J. P. Lloyd and G. E. Pake 1576

Spontaneous Hall Effect in Ferromagnetics . . . . . J. Smit and J. Volger 1576

Dielectric Properties of Some Double Titanates . . . . . F. Jona and R. Pepinsky 1577

Atomic Heat and Critical Magnetic Field of Superconducting Cadmium . . . J. R. Clement 1578

Ionization Cross Section of Hydrogen and Heavier Elements for 450-Mev Negative and 340-Mev Positive Mesons . . . . . S. J. Lindenbaum and Luke C. L. Yuan 1578

Internal Conversion Electrons from Gadolinium Excited Ta and W . . . . . Torben Huus and Jørgen H. Bjerregaard 1579

Zeeman Splitting of Nuclear Quadrupole Resonance Lines . . . . . Yu Tien, Edward Mauring, and Dudley Williams 1581

Hyperfine Structure and Nuclear Electric Quadrupole Moment of Boron 11 . Günter Wessel 1581

New Quenching Effect in Liquid Scintillators . . . . . R. W. Pringle, L. D. Black, B. L. Funt, and S. Sobering 1582

Rest Mass Energy of the Negative Pion . . . . . R. C. Cornelius, C. P. Sargent, M. C. Rinehart, L. M. Lederman, and K. Rogers 1583

Mass Measurements of Primaries of β Events by a Momentum-Range Method . W. B. Fretter, B. P. Gregory, R. Johnston, A. Lagarrigue, H. Meyer, F. Muller, and C. Peyrou 1583

Cross Terms in Allowed-Shape β Spectra. II . . . . . J. P. Davidson and D. C. Peaslee 1584

Production of Fast Lithium, Beryllium, Boron Fragments from Interactions of Primary Cosmic-Ray Nuclei . . . . . J. H. Noon, M. F. Kaplon, and D. M. Ritson 1585

Total Ionization of α Particles of Po in Mixtures of Gases . . . . . G. Bertolini, M. Bernardi, and A. Bisi 1586

Decay-Electron Spectrum of the μ Meson . . . . . J. H. Vilain and R. W. Williams 1586

Errata 1587

Author Index to Volume 89 1588

Author Index to Volume 90 1589

Author Index to Volume 91 1614

Author Index to Volume 92 1637

Analytic Subject Index to Volume 92 1652

CONTENTS

THE PHYSICAL REVIEW | SECOND SERIES, VOLUME 92, NO. 6 | DECEMBER 15, 1953

Dynamics of a Disordered Linear Chain . . . . . F. Dyson 1331
Determination of Thermoelectric Thresholds over 4π without Measuring Heat Input . . . . . P. E. 1337
Mesh of Mixing of Eu^{2+} in EuF_2 . . . . . R. S. Title, Jr., W. E. Keller, and J. C. Dash 1343
Physical Conditions in the Initial Stages of the Expanding Universe . . . . . Ralph A. Alpher, James W. Follin, Jr., and Robert C. Herman 1347
Gravitational Effects and the Relativistic Deuteron . . . . . S. M. Neamtan 1350
Periodic Perturbations in the Schottky Barrier . . . . . R. C. Miller, Jr., and R. H. Good, Jr. 1357
Calculation of the Collective Energy of Deuteron . . . . . D. Bohm 1362
Paramagnetic Scattering of Neutrons by Para-Hydrogen . . . . . W. C. Marshall and R. Wilson 1366
Magnetic Scattering of Neutrons from Rare Earth Ions . . . . . G. T. Trammell 1382
X-Ray Absorption Fine Structure from Polarized X-Rays . . . . . H. Brogersma, W. Nemetz, and R. F. Wallenstein 1386
Direct Measurement of the Dielectric Constants of Silicon and Germanium . . . . . C. Dunlap, Jr., and H. L. Watson 1396
Thermal Decay of the Antiprotons of Nb . . . . . G. W. Wheeler, S. R. Usiskin, Bob A. J. Dobbie 1398
Magnetic Properties of the Electronic Excited $^3\Sigma$ State of O_2 . . . . . E. F. M. Ogburne and H. C. Smith 1401
Anelasticity of Quartz . . . . . Richard K. Cook and Robert G. Breckenridge 1405
Effect of Traps on Carrier Injection in Semiconductors . . . . . H. Y. Fan 1424
Generalized Variational Principles for the Scattering of Electrons by Hydrogen Atoms . . . . . M. M. Gaulin and J. G. Jones 1428
Mo K and UL X-Ray Transitions from Separated Isotopes . . . . . George L. Keppel and Gladstone Salvador 1432
One-to-Two Millimeter Wave Spectroscopy. III. HCO and DCO . . . . . C. A. Burrus and Walter Gordy 1437
Microwave Measurement of D_e for CO . . . . . F. D. Shepard, J. J. Gallagher, and C. H. Johnson 1440
Dissociation of H_2^+ by Electron Impact . . . . . Edward H. Kerner 1445
Theory of the Microwave Zeeman Effect in Atomic Oxygen . . . . . A. Abragam and J. H. Van Vleck 1448
Energies and Angular Distributions of Neutrons from $Be^9(d,n)B^{10}$ . . . . . J. S. Pruitt, C. D. Swartz, and S. S. Hanna 1455
Nuclear Quadrupole Coupling in the Li_2 Molecule . . . . . R. M. Sternheimer and H. M. Foley 1460
Gamma-Gamma Angular Correlation in Fe^{57} . . . . . E. D. Klema and P. E. McGowan 1466
Uranium-235 Thermal Neutron Fission Yields . . . . . George W. Reed and Anthony Turkevich 1471
Decay of Ga^{66} . . . . . E. G. Muir, W. E. Meyerhof, and H. I. Wald, Jr. 1476
Half-Life Determination of Fe^{55} by Alpha Counting . . . . . Wing Lee Curtis 1480
Half-Life of Am^{243}. Herbert Diamond, Paul R. Fields, Joseph Mech, Mark G. Inghram, and Harold C. Hess 1481
Spin-Orbit Coupling Energy in O^{17} . . . . . Reuben K. Adair 1483
Search for B^{11} . . . . . Edward L. Hubbard, Laurence Reiss, and Warren F. Hornyak 1485
Coincident Alpha Spectra of Radiothorium (Th^{232}) and Thorium-X (Ra^{224}) . . . . . Frank Asaro, Frank Stephens, Jr., and I. Perlman 1492
Scattering of Electrons in Helium . . . . . T. Lauritsen, T. Hiza, and S. C. Wright 1499
Inelastic Neutron Scattering in Al, Fe, Mg, and Cu . . . . . Richard E. Carter, Frank L. Hereford, and Billy W. Sloope 1507
Slow Neutron Resonances in Tantalum . . . . . E. L. Carlemark 1509
Disintegration of Ca^{47}, Sc^{47}, V^{47}, and Ti^{47} . . . . . Lois Marquis 1515
Energy Levels of Ti^{48} from the Decay of Sc^{48} and V^{48} . . . . . H. Comas, L. S. Cavalcante, and V. E. Krohn 1527
Upper Limits on the Neutrino Mass from the Tritium Beta Spectrum . . . . . Donald R. Hamilton, W. Parker Alford, and Leonard Gross 1536
Nuclear Reaction Determination of the Sr^{86}—Y^{89} Mass Difference . . . . . H. E. Wall 1539
Neutron Absorption and Scattering by Hydrogen . . . . . L. M. Bollinger, R. P. Harris, C. T. Hibdon, and E. O. Hornbostel 1557
Nuclear Moments of Sr^{87} . . . . . W. A. Hardy, D. Silvey, C. H. Townes, B. F. Burke, M. W. P. Strandberg, George W. Parker, and Victor W. Cohen 1565
"Nonmesonic" Bound V-Particle Decay . . . . . W. Chinowsky and H. Primakoff 1577
Electromagnetic Effects in Two-Electron Systems . . . . . Sandoz Bhatia 1582
Field Theory of Equations with Many Masses . . . . . B. T. Darling 1590
Equivalent Mass and Other Effects of a Neutral Electromagnetic Field in Interaction with a Constant E, H Field . . . . . Christopher Gregory 1598
Physical Basis of Gravitation . . . . . Robert L. Kirkwood 1607
Tolman Forces with Added Attractions . . . . . John M. Blatt and M. H. Kalos 1612
Equations of Motion in Einstein's New Unified Field Theory . . . . . Joseph Callaway 1620

(continued on cover four)

LANCASTER PRESS, INC., LANCASTER, PA.